

Claudio Margottini
Paolo Canuti · Kyoji Sassa
Editors

Landslide Science and Practice

Volume 2
Early Warning, Instrumentation and Monitoring

Springer

Claudio Margottini • Paolo Canuti • Kyoji Sassa
Editors

Landslide Science and Practice

Volume 2: Early Warning, Instrumentation and Monitoring

Springer

Editors
Claudio Margottini
ISPRA - Italian Institute for
Environmental Protection and Research
Geological Survey of Italy
Rome, Italy

Paolo Canuti
ICL - International Consortium on Landslides
Florence, Italy

Kyoji Sassa
UNITWIN Headquarters Building
Kyoto University Uji Campus
Uji, Kyoto, Japan

Associate Editors
Filippo Catani
Department of Earth Sciences
University of Florence
Firenze, Italy

Alessandro Trigila
ISPRA - Italian Institute for
Environmental Protection and Research
Geological Survey of Italy
Rome, Italy

Additional material to Volume 1 can be downloaded from http://extras.springer.com

ISBN 978-3-642-31444-5 ISBN 978-3-642-31445-2 (eBook)
DOI 10.1007/978-3-642-31445-2
Springer Heidelberg New York Dordrecht London

Library of Congress Control Number: 2013932640

© Springer-Verlag Berlin Heidelberg 2013
This work is subject to copyright. All rights are reserved by the Publisher, whether the whole or part of the material is concerned, specifically the rights of translation, reprinting, reuse of illustrations, recitation, broadcasting, reproduction on microfilms or in any other physical way, and transmission or information storage and retrieval, electronic adaptation, computer software, or by similar or dissimilar methodology now known or hereafter developed. Exempted from this legal reservation are brief excerpts in connection with reviews or scholarly analysis or material supplied specifically for the purpose of being entered and executed on a computer system, for exclusive use by the purchaser of the work. Duplication of this publication or parts thereof is permitted only under the provisions of the Copyright Law of the Publisher's location, in its current version, and permission for use must always be obtained from Springer. Permissions for use may be obtained through RightsLink at the Copyright Clearance Center. Violations are liable to prosecution under the respective Copyright Law.
The use of general descriptive names, registered names, trademarks, service marks, etc. in this publication does not imply, even in the absence of a specific statement, that such names are exempt from the relevant protective laws and regulations and therefore free for general use.
While the advice and information in this book are believed to be true and accurate at the date of publication, neither the authors nor the editors nor the publisher can accept any legal responsibility for any errors or omissions that may be made. The publisher makes no warranty, express or implied, with respect to the material contained herein.

Printed on acid-free paper

Springer is part of Springer Science+Business Media (www.springer.com)

Preface

Landslide Science and Practice

Proceedings of the Second World Landslide Forum

The Second World Landslide Forum (**WLF**) was organized at the headquarters of the Food and Agriculture Organization of the United Nations (FAO), Rome, Italy, on 3–9 October 2011. WLF is a triennial mainstream conference of the International Programme on Landslides (**IPL**) which is jointly managed by the IPL Global Promotion Committee consisting of the International Consortium on Landslides (**ICL**), the United Nations Educational, Scientific and Cultural Organization (UNESCO), the World Meteorological Organization (WMO), the Food and Agriculture Organization of the United Nations (FAO), the United Nations International Strategy for Disaster Risk Reduction (UNISDR), the United Nations University (UNU), the International Council for Science (ICSU), and the World Federation of Engineering Organizations (WFEO).

Background to the World Landslide Forums

The International Consortium on Landslides (ICL) was established by the 2002 Kyoto Declaration "Establishment of an International Consortium on Landslides," with the Statutes adopted in January 2002. The Statutes defined the **General Assembly** of ICL: In order to report and disseminate the activities and achievements of the consortium, a General Assembly shall be convened every 3 years by inviting Members of the International Consortium on Landslides, individual members within those organizations, and all levels of cooperating organizations and individual researchers, engineers, and administrators. The General Assembly will receive reports on Consortium activities and provide a forum for open discussion and new initiatives from all participants.

The First General Assembly 2005 to the First World Landslide Forum 2008

The First General Assembly was organized at the Keck Center of the National Academy of Sciences in Washington D.C., USA, on 12–14 October 2005. At this Assembly, the first full-color book reporting consortium activities for the initial 3 years, 2002–2005, was published as "Landslides-Risk analysis and sustainable disaster management" through Springer. The 2006 Tokyo Round-Table Discussion – "Strengthening Research and Learning on Earth System Risk Analysis and Sustainable Disaster Management within UN-ISDR as Regards Landslides" – toward a dynamic global network of the International Programme on Landslides (IPL) was held at the United Nations University, Tokyo, on 18–20 January 2006. **The 2006 Tokyo**

Action Plan – *Strengthening research and learning on landslides and related earth system disasters for global risk preparedness* – was adopted. The Tokyo Action Plan established a new global International Programme on Landslides (IPL) including holding World Landslide Forums. Accordingly, the Second General Assembly 2008 was replaced by the **First World Landslide Forum** and held at the United Nations University, Tokyo, Japan, on 18–21 November 2008.

Report of the Second World Landslide Forum

The Second World Landslide Forum – *Putting Science into Practice* – was organized at the Headquarters of the Food and Agriculture Organization of the United Nations (FAO) on 3–9 October 2011. It was jointly organized by the IPL Global Promotion Committee (ICL, UNESCO, WMO, FAO, UNISDR, UNU, ICSU, WFEO) and two ICL members in Italy: the Italian Institute for Environmental Protection and Research (ISPRA) and the Earth Science Department of the University of Florence with support from the Government of Italy and many Italian landslide-related organizations.

- 864 people from 63 countries participated. Attendance was larger than expected, and twice the attendance at the First World Landslide Forum 2008 in Tokyo (430 participants: 175 from Japan and 255 from abroad).
- 25 technical sessions were held, and 465 full papers were submitted. All accepted papers were edited in 7 volumes including this volume:
  1. Landslide Inventory and Susceptibility and Hazard Zoning
  2. **Early Warning, Instrumentation and Monitoring – this volume**
  3. Spatial Analysis and Modeling
  4. Global Environmental Change
  5. Complex Environment
  6. Risk Assessment, Management and Mitigation
  7. Social and Economic Impact and Policies

Requests of Cooperation for Further Development of ICL and IPL

ICL and IPL are global multidisciplinary and cross-sectoral initiatives to promote landslide science and capacity-development to reduce landslide disasters. The core activities of ICL and IPL are ***Landslides:*** Journal of International Consortium on Landslides, World Landslide Forum, and IPL projects. Thanks to worldwide support of the journal, the Impact Factor of ***Landslides*** was 2.216 for 2011 which is the highest within 30 ISI journals in category of Engineering, Geological. The journal will develop from a quarterly journal to a bimonthly journal from Vol. 10 in 2013. The Third World Landslide Forum – Landslide risk mitigation toward a safer geo-environment – at the China National Convention Center, Beijing, China, on 2–6 June (conference) and 7–11 June (Field Trip) 2014. The ICL entered into the second decade of its activities and organized a 10th anniversary Conference on 17–20 January 2012, in Kyoto, Japan. ICL adopted the ICL Strategic Plan 2012–2021, *To create a safer geo-environment*- as an outcome of this conference.

ICL is an international nongovernmental and nonprofit scientific organization promoting landslide research and capacity-building for the benefit of society and the environment, and is

the thematic landslides platform in the UNISDR Global Platform for Disaster Risk Reduction. ICL activities are supported by voluntary efforts of ICL members and supporting organizations. All people involving in landslide research and landslide disaster mitigation activities are requested to cooperate for the development of this initiative through its second decade 2012–2021. (http://www.iplhq.org/ *and* http://icl.iplhq.org/).

We are deeply appreciative of all e Second World Landslide Forum participants and of the contributions from our UNESCO, WMO, FAO, UNISDR, UNU, ICSU, WFEO partners and all of our colleagues in ICL for the development of IPL up to now. Finally we address our sincere thanks to Filippo Catani and Alessandro Trigila (the associate editors) for their extensive efforts covering the technical sessions, and reviewing and editing the papers as well as to Patrizia Musina and Deodato Tapete for revising all the manuscripts.

Claudio Margottini
Forum Chair



Paolo Canuti
President of ICL



Kyoji Sassa
Executive Director of ICL



ICL and IPL Secretariat

IPL office: UNITWIN headquarters Buildings, Kyoto University Uji Campus,
Uji, Kyoto 611-0011, Japan
ICL office: The Association for Diaster Prevention Research,
138-1 Tanaka Asukai-cho, Sakyo-ku, Kyoto 606-8226, Japan
Email: secretariat@iclhq.org
URL: http://www.iplhq.org/ and http://icl.iplhq.org/

Organizational Structure of the Second World Landslide Forum

Organizers

IPL Global Promotion Committee including:
- International Consortium on Landslides (ICL) *
- United Nations Educational, Scientific and Cultural Organization (UNESCO)
- World Meteorological Organization (WMO)
- Food and Agriculture Organization of the United Nations (FAO)
- United Nations International Strategy for Disaster Risk Reduction (UNISDR)
- United Nations University (UNU)
- International Council for Science (ICSU)
- World Federation of Engineering Organizations (WFEO)
- Italian Institute for Environmental Protection and Research (ISPRA)

(* Members are listed in the last page of this book)

Co-sponsors

- International Union of Geological Sciences (IUGS)
- International Union of Geodesy and Geophysics (IUGG)
- International Geographical Union (IGU)
- International Flood Initiative (IFI)

Under the Auspices of

- International Association for Engineering Geology and the Environment, Italian Section (IAEG)
- Italian Association of Engineering Geologists (AIGA)
- Italian Association of Geotechnique (AGI)
- Italian Association for Mining Engineers, Environment and Territory (ANIM)
- Italian Georesources and Environment Association (GEAM)

International Organizing Board

Honorary Chairpersons

- Irina BOKOVA (UNESCO Director-General)
- Catherine BRECHIGNAC (ICSU President)
- Jacques DIOUF (FAO Director-General)

- Michel JARRAUD (WMO Secretary-General)
- Maria P. LAFFARGUE (WFEO President)
- Konrad OSTERWALDER (UNU Rector)
- Bernardo DE BERNARDINIS (ISPRA President)
- UNISDR Director

Chairpersons

- Claudio MARGOTTINI (ISPRA, Forum Chair)
- Paolo CANUTI (ICL President)
- Kyoji SASSA (ICL Executive-Director)

Deputy Chairpersons

- Peter BOBROWSKY (IUGS Secretary General)
- Deliang CHEN (ICSU Executive Director)
- Peter LYTTLE (ICL Vice President, US Geological Survey)
- Eduardo ROJAS-BRIALES (Assistant Director General of FAO)
- Badaoui ROUHBAN (Director of UNESCO's Section for Disaster Reduction)
- Yueping YIN (ICL Vice President, China Geological Survey)

Scientific Advisory Board

Representing Organisation

- Irasema ALCANTARA-AYALA (Vice President of International Geographical Union - IGU)
- Walter AMMAN (President Davos Forum)
- Michael CROZIER (President of International Association of Geomorphologists - IAG)
- Carlos DELGADO (President of International Association of Engineering Geology - IAEG)
- Luca DEMICHELI (Secretary General of EuroGeoSurveys)
- John HARDING (United Nations Secretariat to International Strategy for Disaster Reduction - UNISDR)
- Srikantha HERATH (Senior Academic Programme Officer of the United Nations University - UNU)
- Thomas HOFER (Forestry officer, Food and Agriculture Organization of the United Nations - FAO)
- Yumio ISHII (Chair of the Committee on Disaster Risk Management of The World Federation of Engineering Organizations WFEO)
- Derek MARTIN (Vice President for North America of International Society for Rock Mechanics - ISRM)
- Howard MOORE (Senior Advisor, International Council for Science - ICSU)
- Pedro SECO E PINTO (Past President of International Society for Soil Mechanics and Geotechnical Engineering - ISSMGE)
- Luciano PICARELLI (Chairperson of the Joint Technical Committee on Landslides and Engineered slopes - JTC1 of ISSMGE, ISRM, IAEG)
- Kaoru TAKARA (Vice chairperson of the Intergovernmental Council of the International Hydrological Programme of UNESCO - IHP)
- Kuniyoshi TAKEUCHI (President of GeoRisk Commission of International Union of Geodesy and Geophysics - IUGG)

Landslide Experts

- Giovanni BARLA (Politecnico di Torino, Italy)
- R.K. BHANDARI (Consultant, India)
- Christophe BONNARD (Swiss Federal Institute of Technology, Lausanne, Switzerland)
- Nicola CASAGLI (University of Florence, Italy)
- Leonardo CASCINI (University of Salerno, Italy)
- Giovanni CROSTA (University of Milano Bicocca, Milano, Italy)
- Jordi COROMINAS (Technical University of Catalonia, Barcelona, Spain)
- Dave CRUDEN (University of Alberta, Edmonton, Alberta, Canada)
- Thomas GLADE (University of Vienna, Austria)
- Jerome DE GRAFF (United States Department of Agriculture , Fresno - Ca - USA)
- Michel HERMELIN (Universidad EAFIT, Medellin, Colombia)
- Ken HO (Hong Kong Geotechnical office, Hong Kong, China)
- Jurgen KROPP (Potsdam Institute for Climate Change - PIK, Potsdam, Germany)
- Richard M. IVERSON (United States Geological Survey - Vancouver, WA , USA)
- C. F. LEE (Hong Kong University, China)
- Jacques LOCAT (University of Laval, Canada)
- Paul MARINOS (University of Athens, Greece)
- Hideaki MARUI (Niigata University, Japan)
- Hormoz MODARESSI (BRGM, Orléans, France)
- Farrouk NADIM (Norwegian Geothecnical Institute - NGI, Oslo, Norway)
- Gabriele SCARASCIA MUGNOZZA (University of Rome, Italy)
- Wang SIJING (Tsinghua University, China)
- Vern SINGHROY (Canada Centre for Remote Sensing, Ottawa, Canada)
- Alexander STROM (Institute of Geospheres Dynamics, RAS, Moscow, Russia)
- Ikuo TOWHATA (University of Tokyo, Japan)
- Keith TURNER (Emeritus Professor, Colorado School of Mines, Denver, Colorado USA)
- Keizo UGAI (Gunma University, Kiryu,Gunma, Japan)
- Roger URGELES (Institut de Ciències del Mar - CSIC, Barcelona, Spain
- Yasser el SHAYEB (Cairo University, Egypt)
- Sergio SEPULVEDA (University of Chile, Santiago)
- Mauro SOLDATI (University of Modena and Reggio Emilia, Italy)
- Pasquale VERSACE (Calabria University, Cosenza, Italy)
- Cees van WESTEN (ITC, Enschede, Netherlands)
- Kifle WOLDEAREGAY (University of Mekelle, Ethiopia)

Local Organizing Board

Forum Chairs

- Paolo CANUTI (ICL President - WLF2 Chairperson)
- Claudio MARGOTTINI (ISPRA - WLF2 Chairperson)
- Kyoji SASSA (ICL Secretary General - WLF2 Chairperson)

Scientific Programme Committee

- Luciano PICARELLI (Second University of Napoli)
- Marco AMANTI (ISPRA)
- Filippo CATANI (University of Firenze)
- Fausto GUZZETTI (CNR-IRPI)
- Javier HERVAS (JRC)

- Thomas HOFER (FAO)
- Carla IADANZA (ISPRA)
- Claudio MARGOTTINI (ISPRA - WLF2 Chairperson)
- Paolo TOMMASI (CNR-IGAG)
- Alessandro TRIGILA (ISPRA)

Editorial Committee

- Filippo CATANI (University of Firenze)
- Riccardo FANTI (University of Firenze)
- Fausto GUZZETTI (CNR-IRPI)
- Javier HERVAS (JRC)
- Irene RISCHIA (ISPRA)
- Gabriele SCARASCIA MUGNOZZA (Università di Roma "La Sapienza")
- Alessandro TRIGILA (ISPRA)

Logistic Committee

- Thomas HOFER (FAO)
- Claudio MARGOTTINI (ISPRA - WLF2 Chairperson)
- Orlando PANDOLFI (ECN)
- Luna GUBINELLI

Field Trips

- Gabriele SCARASCIA MUGNOZZA (University of Roma "La Sapienza")
- Giuseppe DELMONACO (ISPRA)
- Riccardo FANTI (University of Firenze)
- Irene RISCHIA (ISPRA)
- Daniele SPIZZICHINO (ISPRA)
- Paolo TOMMASI (CNR-IGAG)

Fund Raising and Exhibition

- Claudio MARGOTTINI (ISPRA - WLF2 Chairperson)
- Paolo FARINA (IDS SpA)
- Giorgio LOLLINO (CNR-IRPI)

Secretariat

ISPRA, Italian Institute for Environmental Protection and Research
Dept. Geological Survey of Italy, Via Vitaliano Brancati, 48-00144 Rome, Italy.

Logistics and Administration

Orlando PANDOLFI - ECN yourLIFE Foundation

Contents

Part I Landslide Instrumentation and Monitoring
Introduction by Rajenda K. Bhandari, Leonardo Cascini, and Dario Peduto

New Real-Time Landslide Monitoring System in Polish Carpathians 3
Zbigniew Bednarczyk

Application of the PS-InSAR Technique for the Post-Failure Landslide Deformation Monitoring at Lubietova Site in Central Slovakia 15
Vladimir Greif and Jan Vlcko

Monitoring of the "Razanj" Landslide in Serbia 25
Svetozar Milenkovic, Branko Jelisavac, Vladeta Vujanic, and Milovan Jotic

Terrestrial Laser Scanning for the Montaguto Landslide (Southern Italy) 33
Domenico Denora, Lia Romano, and Giulia Cecaro

Landsliding Events Triggered by Rainfalls in the Enna Area (South Italy) . . . 39
Francesco Castelli and Valentina Lentini

Assessing Volume Earthwork by Using Unconventional Photogrammetry 49
Cheng-Yang Hsiao, Pao-Shan Hsieh, and Shu-Yeong Chi

The Ancona Early Warning Centre, Instrumentation and Continuous Monitoring of the Landslides 57
Stefano Cardellini and Paolo Osimani

Slope Stability Assessment and Monitoring of a Vulnerable Site on Rishikesh-Uttarkashi Highway, India 67
Shantanu Sarkar, Amitava Ghosh, Debi Prasanna Kanungo, and Zamir Ahmad

Landslide Displacement Monitoring from Multi-Temporal Terrestrial Digital Images: Case of the Valoria Landslide Site 73
Mirco Motta, Fabio Gabrieli, Alessandro Corsini, Vinicio Manzi, Francesco Ronchetti, and Simonetta Cola

A Geosensor Network Based Monitoring and Early Warning System for Landslides 79
Kurosch Thuro, John Singer, and Judith Festl

Underground Landslide Displacement Monitoring: A New MMES Based Device 87
Andrea Segalini and Corrado Carini

Groundwater Investigations Using Optical and Microwave Remote Sensing Data in Solani Watershed, India 95
Amed Bennia, S.K. Srivastav, and R.S. Chatterjee

Application of a Multiplet-Location Coupled Technique to Microseismic Data for Identification of Rock Slope Active Surfaces 101
Cristina Occhiena, Marina Pirulli, and Claudio Scavia

Slope Disaster Monitoring System Using Battery-Operated Wireless Sensor Network 109
Keigo Koizumi, Kenji Hirata, Kazuhiro Oda, Yukishige Fujita, and Sadayuki Kamide

The Use of ERT for Investigation of Berzhita Landslide, Tirana Area, Albania 117
Hamza Reci, Ylber Muceku, and Idriz Jata

Conventional and Innovative Techniques for the Monitoring of Displacements in Landslide Affected Area 125
Loredana Antronico, Luigi Borrelli, Dario Peduto, Gianfranco Fornaro, Giovanni Gullà, Luca Paglia, and Giovanni Zeni

Spatio-Temporal Evolution of Ground Displacement of the Tena Landslide (Spain) 133
Nguyen Anh Tuan, Saillard Marianne, Darrozes José, Oliver Marc, Herrera Garcia Gerardo, Garcia Lopez-Davalillo Joan Carlos, Gonzalez Nicieza Celestino, Álvarez Fernández Inmaculada, Monod Bernard, Mulas De Peña Joaquim, Soula Jean-Claude, Guerrero Nicole, and Courjaul-Radé Pierre

Long-Term Analysis of Landslides Via SBAS-DInSAR Technique 141
Manuela Bonano, Fabiana Calò, Michele Manunta, Luca Paglia, and Giovanni Zeni

4D Monitoring of Active Landslides by Multi-Temporal Airborne LiDAR Data 147
Guido Ventura, Giuseppe Vilardo, Carlo Terranova, and Eliana Bellucci Sessa

Experiences of Debris-Flow Monitoring and Warning at Catchment Scale in the Pyrenees 153
Marcel Hürlimann, Claudia Abancó, and Jose Moya

Setup of a Landslide Monitoring System on the Philippine Island of Leyte Near the Village of Malinao (Municipality of St. Bernard) 161
Christian Arnhardt and Olaf Neussner

Application of the Newly Frequency Domain Electromagnetic Method Survey in a Landslide Area 169
Gen Furuya, Tatsuo Katayama, Akira Suemine, Takayuki Kozato, Takahiro Watanabe, and Hideaki Marui

Characterization and Study of a Complex Landslide Site in Northern Italy . . . 177
Roberto Passalacqua and Rossella Bovolenta

HR Satellite Imaging and Borehole Monitoring of Landslides in Daunia, Italy 185
Janusz Wasowski, Caterina Lamanna, Giuseppe Gigante, Domenico Casarano, and Pier Paolo Limoni

Monitoring Concepts and Requirements for Large Rockslides in Norway 193
Las Harald Blikra and Lene Kristensen

Continuous Monitoring and Near-Real Time Processing of GPS Observations for Landslide Analysis: A Methodological Framework 201
Jean-Philippe Malet, Patrice Ulrich, Aline Déprez, Frédéric Masson, Candide Lissak, and Olivier Maquaire

Retrogressive Slope Failures in Natural Slope: A Case Study 211
Che Hassandi Abdullah and Ghazali Hussin

Performance of Image Correlation Techniques for Landslide Displacement Monitoring 217
Julien Travelletti, Christophe Delacourt, Jean-Philippe Malet, Pascal Allemand, Jean Schmittbuhl, and Renaud Toussaint

A Novel Fiber Optic Sensing System for Monitoring Debris Flows 227
Chung-Ray Chu, Ching-Jer Huang, and Tsung-Mo Tien

Integrated Monitoring of Lateral Spreading Phenomena Along the North-West Coast of the Island of Malta 235
Stefano Devoto, Emanuele Forte, Matteo Mantovani, Arianna Mocnik, Alessandro Pasuto, Daniela Piacentini, and Mauro Soldati

InSAR Data for Mapping and Monitoring Landslides in Tena Valley 243
Juan-Carlos García-Davalillo, Gerardo Herrera, Davide Notti, Mario Hernández-Ruiz, Jose-Antonio Fernández-Merodo, Inmaculada Álvarez-Fernández, Celestino González-Nicieza, Tazio Strozzi, and Oscar Mora

Monitoring Displacement on the Mannen Rockslide in Western Norway 251
Lene Kristensen and Lars Harald Blikra

Multitemporal Study of the San Martino Sulla Marrucina Landslide (Central Italy) 257
Elisa Damiano, Daniele Giordan, Paolo Allasia, Marco Baldo, Nicola Sciarra, and Giorgio Lollino

Surface and Deep Displacements Evaluated by GPS and Inclinometers in a Clayey Slope 265
Caterina Di Maio, Roberto Vassallo, Margherita Vallario, Stefano Calcaterra, and Piera Gambino

A Possible Mechanism of Movement of an Ancient Clayey Landslide 273
Roberto Vassallo, Caterina Di Maio, and Margherita Vallario

Results of Geoelectrical Monitoring of Landslides Collected by the SafeLand/TEMPEL Network 281
Robert Supper, Birgit Jochum, Ivo Baroň, Alexander Römer, Mario Lovisolo, David Ottowitz, and Stefano Cardellini

Geophysical-Geotechnical Sensor Networks for Landslide Monitoring 289
Jonathan Chambers, Philip Meldrum, David Gunn, Paul Wilkinson, Andrew Merritt, William Murphy, Jared West, Oliver Kuras, Edward Haslam, Peter Hobbs, Catherine Pennington, and Chris Munro

Remedial Works on the Smrečje Landslide, Croatia 295
Željko Arbanas, Vedrana Galijašević, Petra Đomlija, and Martina Vivoda

Monitoring Slow-Moving Landslides Using Spatially Adaptive Least Squares Image Matching 301
Misganu Debella-Gilo and Andreas Kääb

Seismometric Monitoring of Hypogeous Failures Due to Slope Deformations 309
Luca Lenti, Salvatore Martino, Antonella Paciello, Alberto Prestininzi, and Stefano Rivellino

Use of Persistent Scatterer InSAR within Terrafirma Landslide Services 317
Sandro Moretti, Francesca Cigna, Federico Raspini, Geraint Cooksley, Marie-Josée Banwell, Hugo Raetzo, Gerardo Herrera, Davide Notti, and Juan Carlos García Davalillo

Detection and Characterization of Rock Slope Instabilities Using a Portable Radar Interferometer (GPRI) 325
Andrew Kos, Tazio Strozzi, Reto Stockmann, Andreas Wiesmann, and Charles Werner

Landslides and Hydro-Climatic Conditions in the Hutná Catchment Area (Central Slovakia) 331
Roberta Prokešová, Alžbeta Medveďová, and Zora Snopková

Landslide Umka: The First Automated Monitoring Project in Serbia 339
Biljana Abolmasov, Svetozar Milenković, Branko Jelisavac, and Vladeta Vujanić

Landslide-Related PS Data Interpretation by Means of Different Techniques 347
Diego Di Martire, Gabriele De Luca, Massimo Ramondini, and Domenico Calcaterra

Advanced Image Analysis for Automated Mapping of Landslide Surface Fissures 357
A. Stumpf, U. Niethhammer, S. Rothmund, A. Mathieu, J.P. Malet, N. Kerle, and M. Joswig

Portable Ring Shear Apparatus and Its Application 365
Maja Ostric, Kyoji Sassa, Bin He, Kaoru Takara, and Yosuke Yamashiki

Assessing of Spatio-Temporal Factors Influencing Landslides Using PSInSAR 371
Mateja Jemec Auflič, Magda Čarman, and Marko Komac

Methodological and Technological Advances in the Application of Spaceborne DInSAR for Landslide Monitoring 379
G. Fornaro, D.O. Nitti, R. Nutricato, F. Bovenga, D. Peduto, and L. Cascini

Freeze-Thaw Cycle and Rockfall Monitoring 385
Diego Arosio, Laura Longoni, Fabrizio Mazza, Monica Papini, and Luigi Zanzi

Rapid Assessment of Landslide Activity in Emilia Romagna Using GB-InSAR Short Surveys 391
Alessandro Corsini, Matteo Berti, Antonio Monni, Marco Pizziolo, Francesco Bonacini, Federico Cervi, Giuseppe Ciccarese, Francesco Ronchetti, Eleonora Bertacchini, Alessandro Capra, Angela Gallucci, Mauro Generali, Giampiero Gozza, Valeria Pancioli, Sara Pignone, and Giovanni Truffelli

Resolving Landslide-Bedrock Interaction by Nanoseismic Monitoring 401
Marco Walter and Manfred Joswig

SAR Interferometry for Landslides Risk Assessment at Local Scale: The Case Study of Castagnola (Northern Apennines, Italy) 407
Francesco Antolini, Veronica Tofani, Chiara Del Ventisette, Guido Luzi, Nicola Casagli, and Sandro Moretti

In Situ and Remote Long Term Real-Time Monitoring of a Large Alpine Rock Slide 415
Federico Agliardi, Giovanni B. Crosta, Rosanna Sosio, Carlo Rivolta, and Gregorio Mannucci

C/X-Band SAR Interferometry Used to Monitor Slope Instability in Daunia, Italy 423
Raffaele Nutricato, Janusz Wasowski, Fabio Bovenga, Alberto Refice, Guido Pasquariello, Davide Oscar Nitti, and Maria Teresa Chiaradia

Landslide 3D Surface Deformation Model Obtained Via RTS Measurements 431
Andrea Manconi, Paolo Allasia, Daniele Giordan, Marco Baldo, Giorgio Lollino, Angelo Corazza, and Vincenzo Albanese

Application of SqueeSAR™ to the Characterization of Deep Seated Gravitational Slope Deformations: The Berceto Case Study (Parma, Italy) 437
Andrea Tamburini, Sara Del Conte, Gianfranco Larini, Luigi Lopardo, Claudio Malaguti, and Paolo Vescovi

Use of the Seismic Dilatometer (SDMT) in Landslide Research and Practice 445
Sara Amoroso, Ferdinando Totani, and Gianfranco Totani

Gravitational Instability Analysis of the Prato Carnico Village 451
Marco Del Fabbro, Roberto Meriggi, and Nicola Stefanelli

Rockfall Full Scale Field Tests 461
Alberto Clerici, Ezio Giuriani, Danilo Cambiaghi, Antonio Isceri, Giorgio Vassena, Egidio Marchina, and Luca Cominoli

Sprinkling Tests to Understand Hydrological Behaviour of Mudslide 469
Dominika Krzeminska, Thom Bogaard, Taha-Hocine Debieche, Vincent Marc, and Jean-Philippe Malet

High Resolution InSAR Monitoring of Coastal Landslides 475
Vernon Singhroy, François Charbonneau, Junhua Li, and Rejean Couture

Evaluation of Temperature Effects on Strain Measurements with DTSS 479
Gerhard Kapeller, Rafael P.O. Rocha, Luiz Alkimin de Lacerda, and Markus Aufleger

Measurements of Hydraulic Subsurface Processes by Means of Distributed Fiber Optic Temperature Sensing (DTS) 487
Gerhard Kapeller, Thomas Etzer, and Markus Aufleger

Applying GPR and 2D ERT for Shallow Landslides Characterization: A Case Study 495
Biljana Abolmasov, Aleksandar Ristić, and Miro Govedarica

Monitoring and Modelling of Rainfall-Induced Landslide in Volcanic Soil Slope 503
Adrin Tohari, Khori Sugianti, and Katsumi Hattori

Impact Pressure Measurements in Shallow Landslides 511
Bugnion Louis and Wendeler Corinna

Application of Terrestrial Laser Scanner to the Assessment of the Evolution of Diachronic Landslides 517
José A. Palenzuela, Clemente Irigaray, Jorge D. Jiménez-Perálvarez, and José Chacón

Ground-Based Radar for Permanent Monitoring of Landslides 525
Richard Norland and Rune Gundersen

The Ganderberg Landslide (South Tyrol, Italy): Mitigation of Residual Risk by Real-Time Monitoring 531
Martina Stefani, Matteo Mantovani, Volkmar Mair, Gianluca Marcato, Alessandro Pasuto, and Ludwig Nössing

The Case History of the Bagnaschino Landslide, from Early Warning to Site Specific Rainfall Threshold 537
Corrado Faletto, Enzo Novello, and Paolo Tible

Application of Monitoring Data for the Prediction of the Time to Failure and Risk Management 543
Ziaoddin Shoaei and Karim Karamsoltani

Development of WILMS: Well Inform Landslide Monitoring System for USM Healthy Campus 549
Fauziah Ahmad, Ahmad Shukri Yahaya, Mohd Azam Osman, Wong Poh Lee, and Ahmad Badri Ismail

Integrating Landslide Monitoring into Multi-Hazard Monitoring Systems . . . 559
Guido Bernardi and Fabio Procopio

Part II Early Warnings and Emergency Plans
Introduction by Nicola Casagli and Yin Yuepin

An Appraisal on Ongoing Practices for Landslide Early Warning Systems in Selected South and East Asian Countries 573
Elmer B. Billedo, Rajinder K. Bhasin, Oddvar Kjekstad, and N.M.S.I. Arambepola

Examples of Cost Effective Practices for Landslide Monitoring for Early Warning in Developing Countries of Asia 581
R.M.S. Bandara, Rajinder K. Bhasin, Oddvar Kjekstad, and N.M.S.I. Arambepola

Validation and Interpretation of Monitored Behavior of Slopes Vulnerable to Failure 589
Taro Uchimura, Ikuo Towhata, Lin Wang, and Jianping Qiao

Overview of Some Empirical Methods to Correlate Rainfall and Shallow Landslide and Applications in Malaysia 597
Suhaimi Jamaludin and Faisal Hj Ali

Experimental Alert Model for Hydrogeological Risk: A Case Study in Sicily . . . 603
Giuseppe Basile and Marinella Panebianco

An Operational Warning System for the Forecasting of Landslide Occurrence at Regional Scale 611
Samuele Segoni, Gianluca Martelloni, Daniela Lagomarsino, Riccardo Fanti, and Filippo Catani

Radar Interferometry for Early Stage Warning on Monuments at Risk 619
Deodato Tapete, Nicola Casagli, and Riccardo Fanti

Landwarn: An Operative Early Warning System for Landslides Forecasting Based on Rainfall Thresholds and Soil Moisture 627
Francesco Ponziani, Nicola Berni, Marco Stelluti, Renato Zauri, Claudia Pandolfo, Luca Brocca, Tommaso Moramarco, Diana Salciarini, and Claudio Tamagnini

Method of Residual-State Creep Test to Understand the Creeping Behaviour of Landslide Soils 635
Deepak Raj Bhat, Netra P. Bhandary, and Ryuichi Yatabe

Operational Procedure for a Hydrogeological Warning System in Aosta Valley 643
Sara Maria Ratto, Hervé Stevenin, Evelyne Navillod, and Marco Cauduro

Defining Physically-Based Rainfall Thresholds for Early Warning Systems . . . 651
Diana Salciarini, Claudio Tamagnini, Francesco Ponziani, and Nicola Berni

Rainfall Threshold Analysis and Landslide Susceptibility Mapping in Wudu County 659
Shibiao Bai, Jian Wang, Thomas Glade, Rainer Bell, and Benni Thiebes

Cloud Monitoring: An Innovative Approach for the Prevention of Landslide Risks 665
Bigarré Pascal, Verdel Thierry, Klein Emmanuelle, and Gueniffey Yves

Landslide Triggering and Local Rainfall Thresholds in Bradanic Foredeep, Basilicata Region (Southern Italy) 671
Maurizio Lazzari, Marco Piccarreta, and Domenico Capolongo

Development of Debris Flow Early Warning System for Volcanic Rivers at Mt. Merapi Area 679
Teuku Faisal Fathani, Djoko Legono, Adam Pamudji Rahardjo, Dwikorita Karnawati, and Irawan Eko Prabowo

Part I

Landslide Instrumentation and Monitoring

Introduction by Rajenda K. Bhandari[1], Leonardo Cascini[2], and Dario Peduto[2]

1) Centre for Disaster Mitigation and Management Vellore Institute of Technology University, India
2) Department of Civil Engineering, University of Salerno, Fisciano (Salerno) 84084, Italy

Session L07 of the Second World Landslide Forum was devoted to **"Landslide instrumentation and monitoring".**

This 4-day Session attracted several researchers with diverse backgrounds in different fields of science and technology spanning from landslide numerical modelling to in situ- and laboratory instrumentations and remote sensing monitoring techniques. The success of the Session was obvious from large audience (130 participants) and the lively multi-disciplinary discussions on 75 submitted full papers, 52 oral and 28 poster presentations

The present chapter is a compendium of all the papers and well documented case studies on landslide instrumentation and monitoring contributed by landslide experts from different parts of the world.

An overview of the session papers highlights that scientific studies of landslide phenomena derive their strength from thorough analyses of multitude of factors such as subsoil geology and minor geological details, predisposing and triggering factors, physical-mechanical and engineering properties of soil, groundwater regime and piezometric characteristics, and landslide kinetics including surface/deep displacements and displacement rates. Indeed, landslide investigations and instrumentations play a fundamental role for the comprehension of the landslide mechanics, for their monitoring and for exercising a check on the efficacy and effectiveness of landslide prevention and control works. Considering the differences in landslide features, the typology of these measurements often differs according to: the geo-environmental setting and catchment characteristics; the typology of the phenomena; the scale of the analysis; the parameter to be monitored (i.e. magnitude and rate of rainfall; slope displacements; piezometric variations, etc.). The above topics addressed in the papers are briefly summarized below.

Focus on landslide modelling is found in Del Fabbro et al.; Hassandi and Ghazali, etc., whereas aspects of either fast or slow-moving landslide monitoring are analysed by Vassallo et al.; Sarkar et al.; Chambers et al.; Bugnion and Wendeler; Passalacqua and Bovolenta. Some innovative field tests for the investigation of both mechanical (Ostric et al.) and hydraulic (Krzeminska et al.; Kapeller et al.) properties of the involved soils are also presented. As far as fast-moving landslides are concerned, several case studies dealing with rockfall are presented (Clerici et al., Arosio et al.) also furnishing general concepts and requirements for their monitoring (Blikra and Kristensen). In this regard, some Authors (Lenti et al.; Amoroso et al.; Walter et al.; Occhiena et al.) show a number of applications with seismic sensor networks.

Multi-parameter (i.e. temperature, groundwater levels, displacements, etc.) monitoring systems increasingly involve wireless sensor networks (Berti et al.; Koizumu et al.), fiber-optic sensing systems (Chu et al.; Kapeller et al.) and remote sensing data which can be less expensive and time-consuming than the conventional techniques.

Changes of geo-environmental features and related information (i.e. surfacial displacements, width of surfacial cracks, variations of vegetation cover, etc.) have been

shown to be successfully detectable by optical (Debella-Gilo et al.; Wasowski et al.; Stumpf et al.; Travelletti et al.) image processing techniques over areas affected by different typologies of landslides.

With reference to deep/surfacial displacement monitoring, innovative techniques (i.e. Micro Electro-Mechanical System (MMES), Segalini et al.) as well as advanced procedures for the use of almost consolidated techniques such as GPS (Deprez et al.), total station (Manconi et al.) and LIDAR (Ventura et al.) are described.

The positive trend in the application of remote sensing data, especially when dealing with analyses over large areas, is testified in this chapter by the high number of contributions focusing on the use of synthetic aperture radar images—acquired from both spaceborne and ground-based platforms—processed via differential interferometric techniques (DInSAR). In particular, these data prove to be a valuable tool for superficial displacement monitoring over both large areas and single phenomena (Fornaro et al.; Singhroy et al.; Nutricato et al.; Moretti et al.; Antolini et al.; Tamburini et al.; Bonanno et al.; Kos et al.; Farina et al.; Norland and Gundersen; Agliardi et al.; Kristensen et al; Antronico et al.; Bozzano et al.; Tuan et al.; etc.)

Finally, some case studies reporting experiences in Europe, India and South-East Asia of either long-time working (Cardellini; Supper et al.) or recently built up (Sarkar et al., Kurosch et al.; Arnhardt et al.; Bednarczyk) early warning systems are also presented.

The overall impression gathered from the papers and poster presentations of the session has been heartening in terms of the high scientific value of the contributions made, rewarding in terms of the frontier of knowledge advanced and stimulating in terms of the limitations and problems uncovered for future research and development work. Then, referring to innovative ground-based and remote sensing techniques, a knowledge deepening appears necessary for their confident use considering that the results furnished up to now are very promising. To this end, a close cooperation among landslide experts, scientists and technologists involved in the development of advanced algorithms and instrumentations seems the most widely shared recipe to achieve more reliable data and, in turn, to foster the continuous updating of both processing algorithms and technologies.



New Real-Time Landslide Monitoring System in Polish Carpathians

Zbigniew Bednarczyk

Abstract

The first in Poland fully automated real-time landslide monitoring and warning system was implemented in Beskid Niski Mountains. Project was financed by EU funds. Investigated region was characterized by the high landslide risk. A public road, a new bridge, private buildings and important infrastructure were located in risk area. Landslides had difficult engineering geology conditions with active mass movements to the depth of 7–20 m below the natural terrain level. Observed ground movements were varied 5–180 mm in 3 years time. Lithology represented mainly soft clayey soils interbeded by stiff sandstones with shallow groundwater level. Partial stabilization of active landslide area were implemented in the end of 2009. However ground movements of 10–15 mm were observed in some parts of the landslides after that time. They have significantly accelerated in May–June 2010, because of record precipitations and a flood in southern Poland. New instrumentation completed in June 2010. It included three landslide monitoring and one meteorological field stations. Monitoring devices included 3D inclinometers, 60 sensors to the depths of 14–16 m, three uniaxial in-place IP sensors, two automatic VW pore pressure as well as groundwater level and temperature transducers. Meteorological monitoring included automatic monitoring of precipitation, air pressure, air humidity, and air temperature values. All data every hour were transferred into the Internet. It should allow recognizing of landslide processes nature and predict alarm warnings for a public road and a new bridge. Special data interpretation software will help to recognize risk conditions. It will sent early warning SMS messages. Continuous monitoring will be conducted till the end of 2012.

Keywords

Landslide monitoring • Early warning system

Landslides Localization and Characterization

The monitoring system include three field monitoring stations and meteorological station. They were installed on active landslides above a public road in Malopolskie District, southern Poland (Fig. 1). In the research area, complex of six connected landslides with active movements towards Bystrzanka River Valley were localized. In this valley over 30 % of area are landslides. Monitoring devices were localized on three landslides no 1, 5, and 6 (Fig. 2). These landslides were characterized by depths 7–20 m, areas 3.7–6 ha, lengths 350–500 m and widths 150–200 m. New monitoring system installation was preceded by the site investigations and standard monitoring measurements which were realized 2006–2010 (Fig. 3). It was detected that some parts of the landslides were active with cumulated displacements 90–180 mm to the depth of 10.8 m.

– *Landslides no 1* large active landslide altitude 300–370 m above the see level, length 355 m, width 116 m, slope

Z. Bednarczyk (✉)
Institute of Opencast Mining "Poltegor-Institute", Geotechnical Engineering Laboratory, Parkowa 25, Wroclaw, Poland
e-mail: zbyszbed@igo.wroc.pl

C. Margottini et al. (eds.), *Landslide Science and Practice*, Vol. 2,
DOI 10.1007/978-3-642-31445-2_1, © Springer-Verlag Berlin Heidelberg 2013



Fig. 1 Landslide localization map

inclination 9 °, landslide depth 6–11 m. Important public road, two private buildings, power, gas and water supply infrastructure in risk area. Real time monitoring M1 Field Station located in landslide central part including three uniaxial in-place inclinometers to the depth of 12 m, automatic pore pressure VW transducer and automatic piezometer. Fully automatic whether station located near the border of the landslide area.

– *Landslides no 2–4* small landslides, altitude 300–315 m, length/width 38/65 m, 100/154 m, 27/50 m between landslides no 1 and 5, close to the public road.
– *Landslide no 5*, very large active landslide, altitude 310–405 m, length 476 m, width 180 m, slope inclination 9–12 °, landslide depth 3–20 m, in lower parts partly stabilized. Important public road, 7 private buildings, power gas and water supply infrastructure in risk area. Real time 3D monitoring M2 Field Station (16 m depth) located in upper part of the landslide, 250 m above the standard inclinometer (18 m depth) and VW transducer (10 m depth) installed in 2005
– *Landslide no 6*, – large, active, landslide close to new bridge, altitude 315–405 m, length 561 m, width 147 m, slope inclination 6–9 °, landslide depth 6–20 m. New bridge, important public road, 10 private buildings, power, gas and water supply infrastructure in risk area. Real time 3D monitoring M3 Field Station (12 m depth) located in the lower art of the landslide 100 m above new bridge near the standard inclinometer (7.5 m depth) and piezometer installed in 2005.

Some parts of presented landslides were stabilized within the SOPO Landslide Counteraction Framework Project financed by the state budget and European Investment Bank in 2009. Stabilization works included anchors, Geobrugg high tensile wire mesh, gabion retaining walls along the river, internal and surface draining system. Anchors length of 6–15 m were drilled into the bedrock (Fig. 4). It helped to safeguard the road area however full stabilization was not possible due to landslides size and activities. Some parts of the landslides located close to road, bridge and private buildings were still active in June 2010 after the record precipitations. They caused infiltrations of groundwater's in upper parts of the landslides and movements activation (Fig. 5). New cracks, high strains in Geobrugg meshes, some destructions of drainage systems and a new cracks at buildings were observed. Previous movements depended mainly on precipitations and snow melting conditions. They were influenced by creeping processes, clayey flysch deposits strength parameters, slope inclination, infiltration processes (high pore pressure) and undercutting of landslide head during a road construction. It was confirmed by inclinometer measurements. Landslides were investigated by Poltegor-Institute in Bednarczyk (2006–2010) by the network of three standard monitoring points to the depth of 7.5, 15, and 18 m. These measurements showed that full landslide stabilization were not reached. That was caused by not fully effective landslide drainage system and difficulties in stabilization of Bystrzyca landslide lower part. Also some others landslides head parts were not stabilized due to limited financing. Displacements have accelerated mainly in periods after intensive rainfalls as in May-June 2010 (2 June 2010, 100 mm rainfall in 3 h time), when some parts of counteraction works were partly damaged (Figs. 6, 7, 8, 9, and 10). They were also intensive in some central parts of the landslides, where new ground movements and cracks occurred (Figs. 7 and 8).

Instrumentation

Five core diamond impregnated boreholes to the depth of 14–16 m, total lengths of 100 m, were used for instrumentation. At two boreholes, 3D real-time M2 and M3 inclinometer systems to the depth of 14 and 16 m were installed. At the third M1 borehole three uniaxial in-place inclinometer sensors were installed. Piezometer and vented wire transducer were located in the boreholes drilled at the distance of 2 m from the inclinometer sites. List of installed instrumentation is presented in the Table 1.

The laboratory test program included index tests, direct shear tests, IL oedometer tests and triaxial CID and CIU tests on selected soil samples. Obtained results indicated that soils to the depths of 12–15 m were characterized by low strength parameters and very high moisture content. They represented highly saturated clayey loams, clays and claystone gravel with high plasticity ratio located at the steep slopes of Bystrzanka River Valley (Figs. 1 and 2).



Fig. 2 Place of real-time monitoring system installation

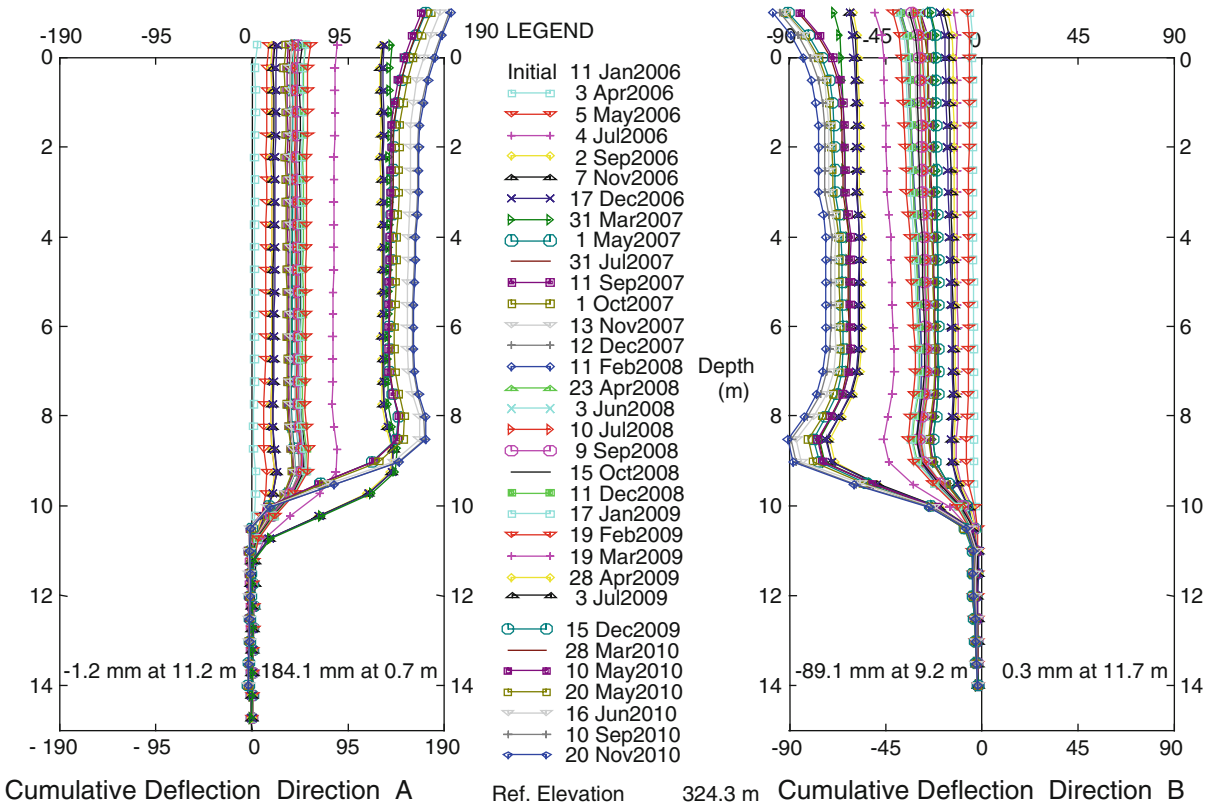


Fig. 3 Cum. displacements in stand. inclinometer at landslide no 1



Fig. 4 Partly stabilized part of the Szymbark-Szalowa public road



Fig. 5 Groundwater reservoirs in *upper part* of landslide no 1



Fig. 6 Damages in partly stabilized *lower part* of landslide no 1



Fig. 7 New cracks (May 2010) – *central part* of landslide no 5



Fig. 8 Destructions of a public road (erosion) landslide no 6

Colluviums depths recognized by boreholes varied from 10.20 at borehole M1 to 11.50 m at borehole M3. Preliminary results of 3D monitoring showed that at M2 earth station ground movements were active to the depth of 15 m, however deeper movements had lower rate than in higher, shallow parts of the colluvium profile.



Fig. 9 New cracks – land no 5



Fig. 10 Damages of drainage system – landslide no 6

Table 1 List of installed instrumentation

Earth station	Measurement type	Instrument depth [m]	Altitude [m] above see level	Landslide
M1	In-place 2D inclinometer	7–10	328.0	No 1
M1/P1	Water pore pressure temperature	11	328.3	No 1
M1/P2	Groundwater level	10	328.5	No 1
M2	3D inclinometers	0–16	359.6	No 5
M3	3D inclinometers	0–12	338.1	No 6
W	Precipitations, atmospheric pressure, air temperature and humidity	1 m above natural terrain level	320.0	No 1 PAS Research Station

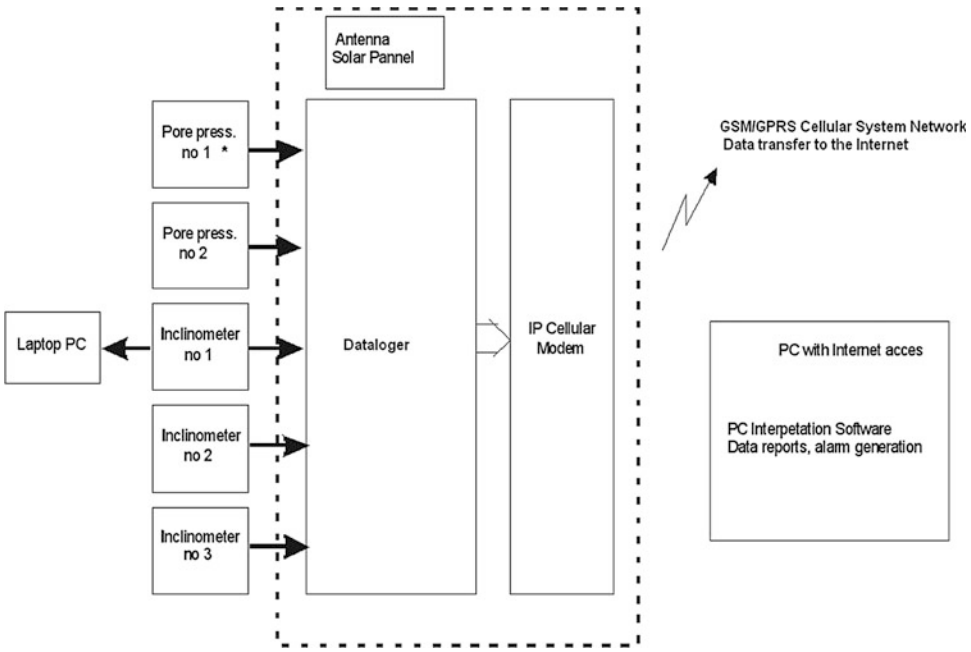


Fig. 11 Real-time landslide monitoring system scheme.* pore pressure semi-automatic transducer installed 2006 – not included in the system

System Scheme

The instrumentation was proceed by study of landslide data and input parameters. Depths of installation were chosen with respect to expected sliding surface depths and groundwater conditions. Standard inclinometer measurements and results of laboratory tests were included in the prediction. System is consisted of four stations. Three fully automated landslide monitoring field stations and the weather station. Data were stored in the loggers and transmitted using cellular GPRS network to the Internet. System was powered by batteries and solar panels (Figs. 11 and 12) (Figs. 13, 15, and 19).

The scheme of ground movement, groundwater temperature and pore pressure monitoring system is presented on Fig. 11. System were activated and calibrated in the end of May 2010. Earth stations worked separately with dataloggers and cellular data transfer to the Internet. Central points of every station were loggers collecting and transferring data by GSM/GPRS network to the Internet and then to the server. Data could be edited for risk levels predictions and exported to others software's in "txt" format. Every device were calibrated for measurement depths, number of transducers and specific calibration values. Data access could be defined for various verified users. Alarms conditions could be generated by SMS messages or emails to defined users. Data stored in the loggers could be uploaded manually to a laptop PC. Earth stations were installed in waterproof enclosures and powered by high capacity battery charged additionally by solar panels in order to ensure maintains-free operation. It allows also to control power supplies (Fig. 19) and GSM signal strength. System contains:

- Two automatic groundwater level, pore pressure and temperature transducers in piezometric boreholes to the depth of 10 and 11 m.
  Device parameters:
  – Measuring rang 1.5 Bar
  – Accuracy: 0.025 %

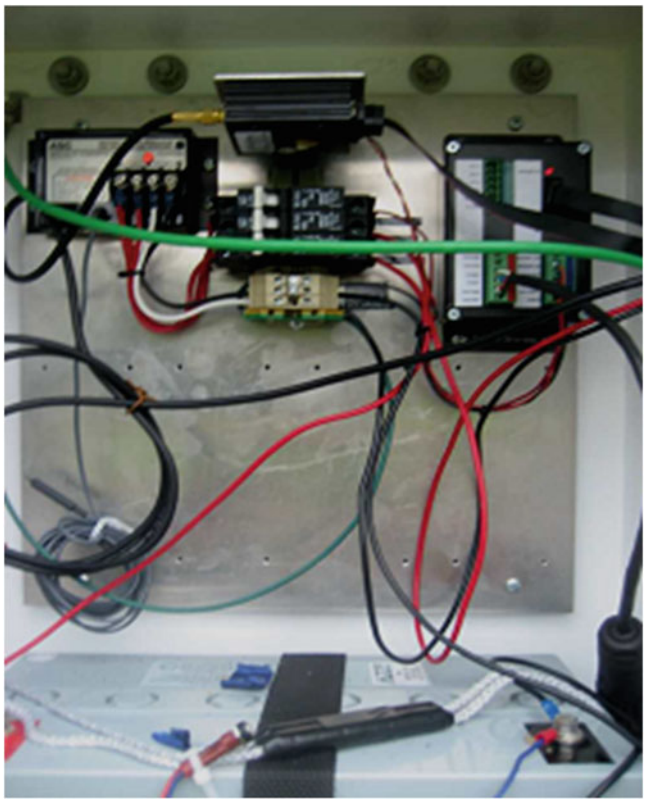


Fig. 12 Interior of M2 Field Station



Fig. 13 M2 Field Station on landslide no 5

  - Calibration accuracy: ± 0.1 %
  - Maximal pressure: 2 × range
  - Coefficient of temperature: <0.02 % for 1 °C
  - Transducer diameter <29 mm
- Three ground movement inclinometer systems:
- Inclinometer no 1 (M1) consist of three uniaxial IP sensors, every 1 m connected in rows (multiplex), pulled into inclinometer casings diam. of 70 mm to the depth of 7–10 m

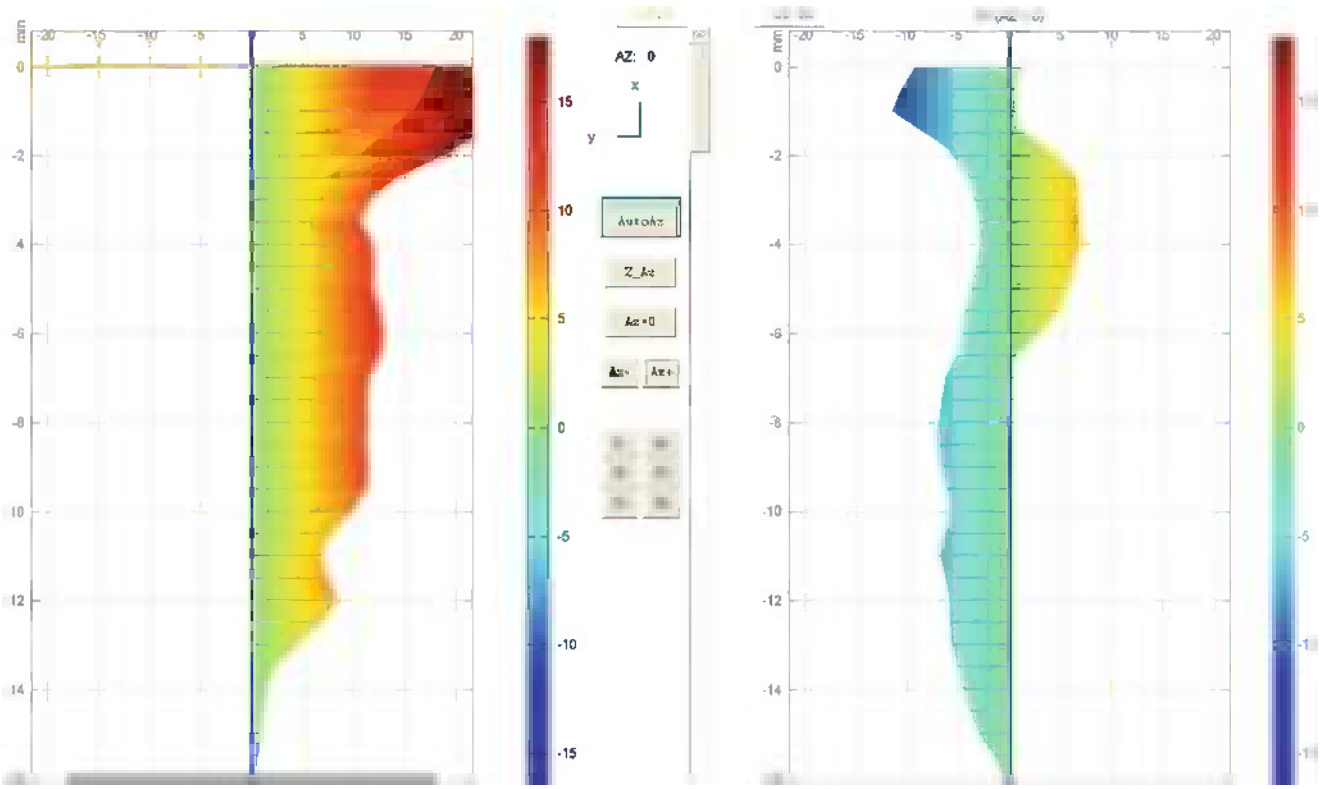


Fig. 14 2D ground movement's preliminary results M2 Field Station in *upper part* of the landslide complex

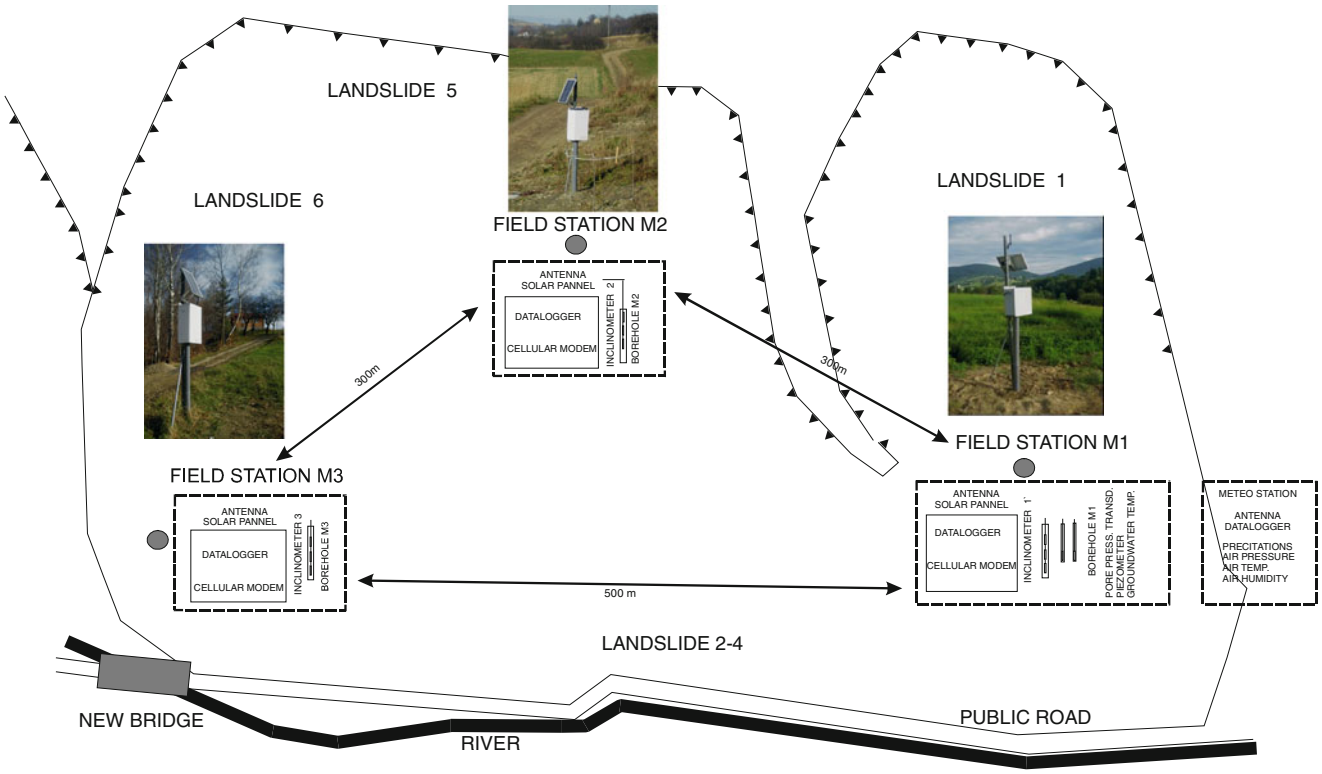


Fig. 15 Scheme of connections between monitoring devices, loggers and data transfer system

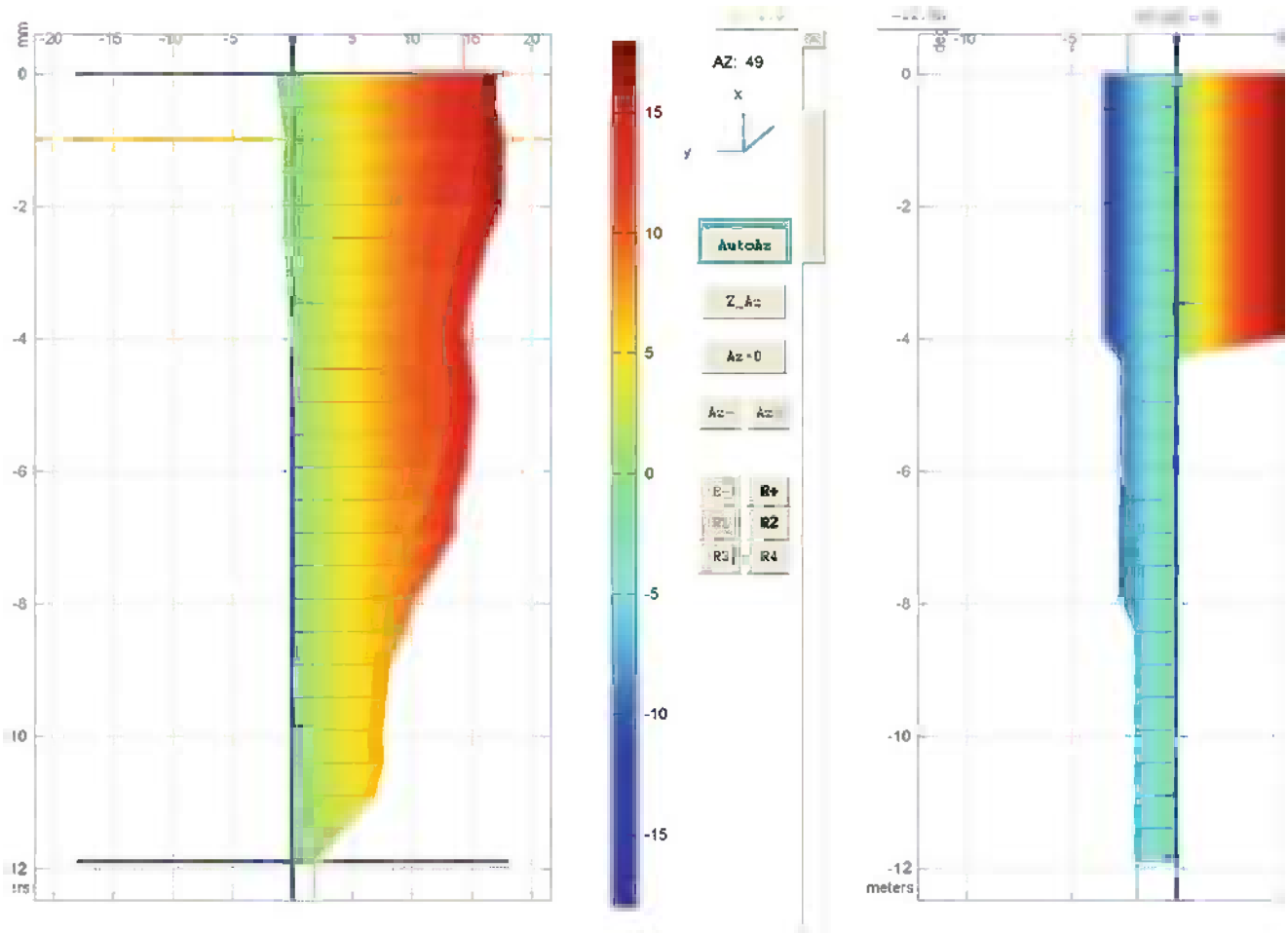


Fig. 16 2D ground movement's preliminary results, M3 Field Station located over the new bridge on Bystrzanka River

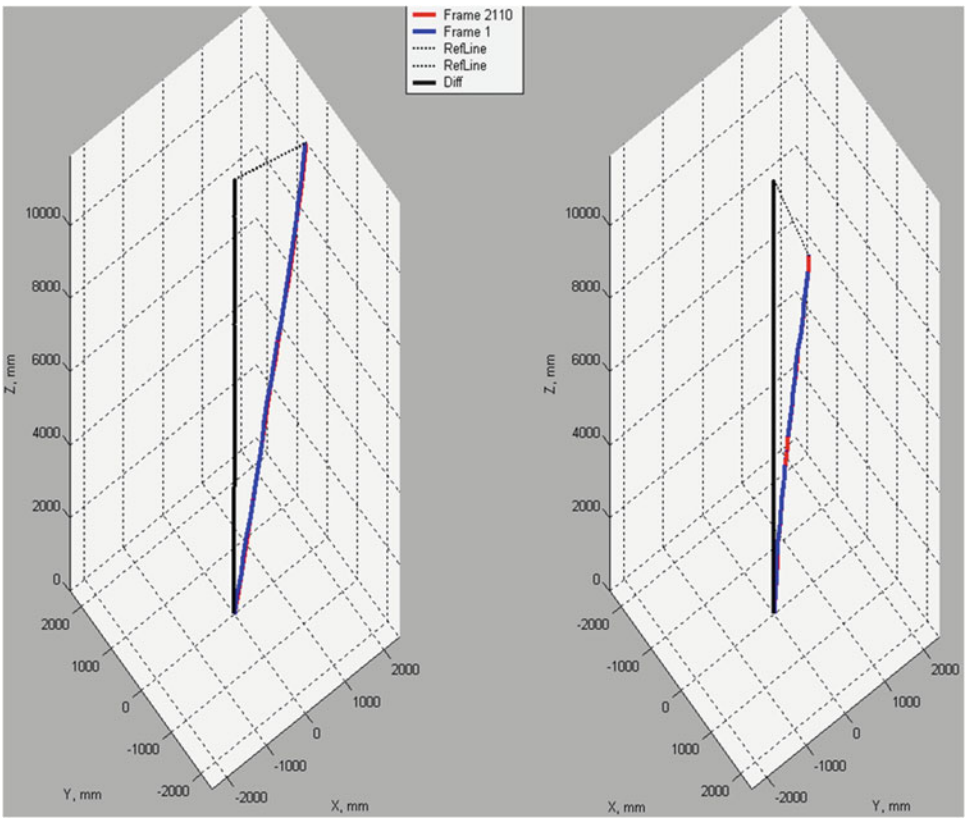


Fig. 17 3D displacements at M3 Field Station

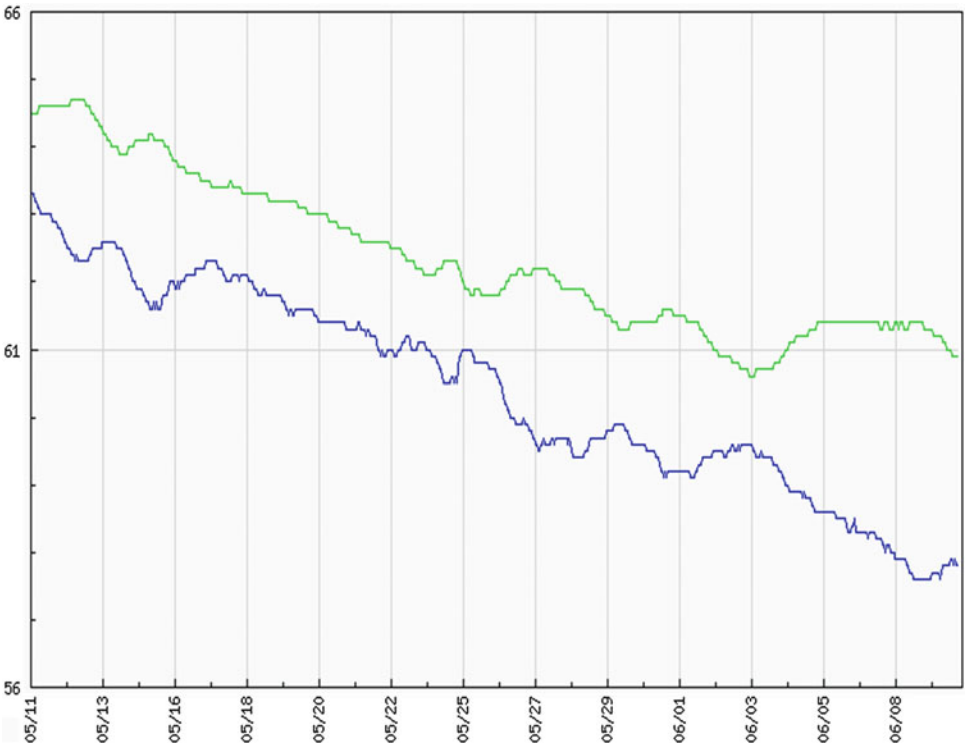


Fig. 18 Pore pressure monitoring M1 Field Station

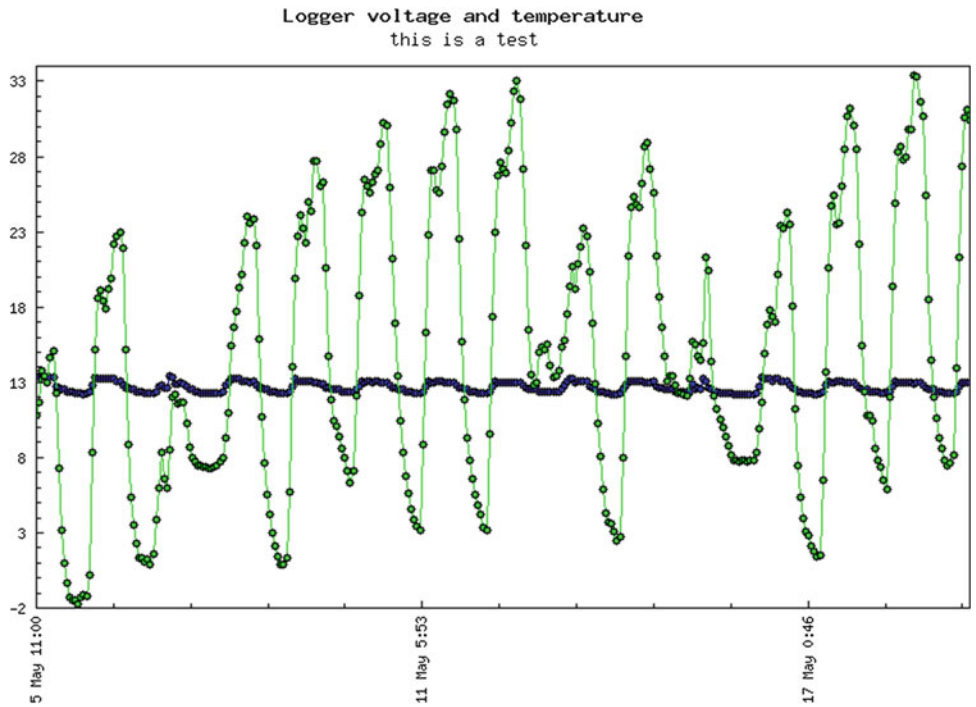


Fig. 19 M1 Field Station battery charge control

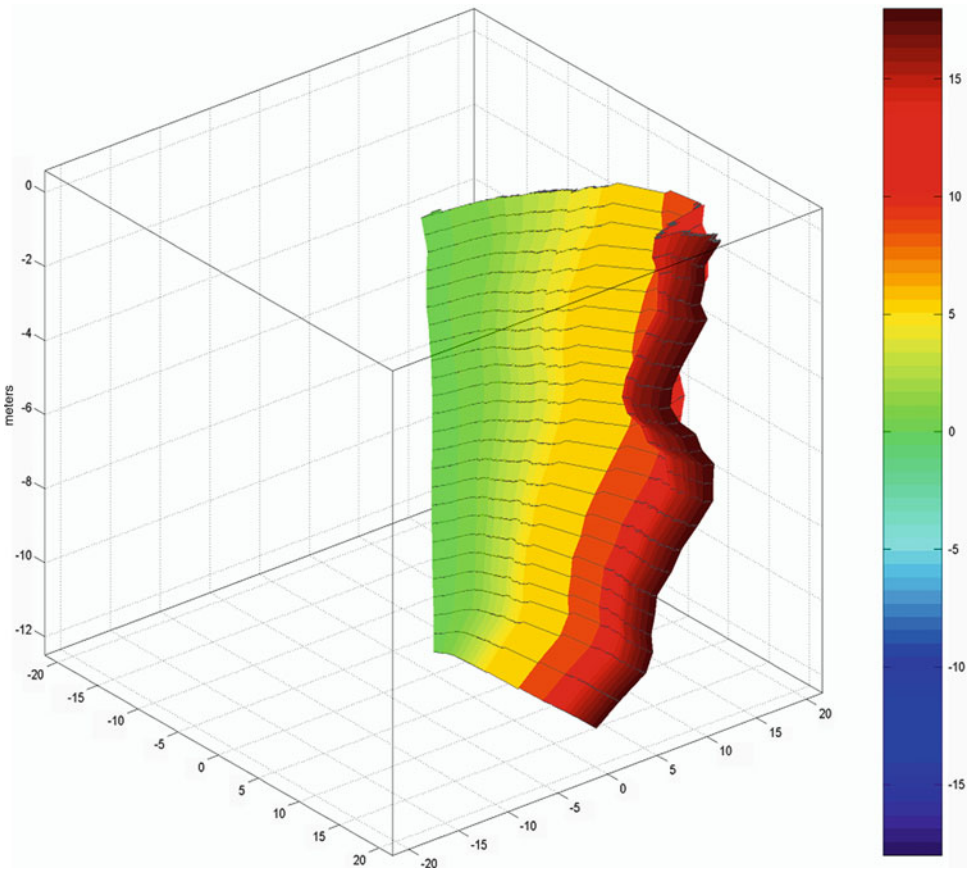


Fig. 20 3D displacement model, M3 monitoring station



Fig. 21 Automatic whether station

Device parameters (inclinometer no 1):
- Measuring range: ± 10 °.
- Accuracy: 9 s or 0.04 mm/m using datalogger,
- Accuracy: 0.04 mm/m
- Calibration: 11 calibration points in three temperatures in range 4–20 °C

- Inclinometer no 2 ÷ 3 – 3D inclinometers consist of :
  - Inclinometer 2 (M2) – four segments, eight transducers every 50 cm, total length of 16 m
  - Inclinometer 3 (M3) – three segments eight transducers every 50 cm, total length of 14 m

Device parameters (inclinometer no 2–3)
- Measuring range: ± 45 °.
- Accuracy inclination 20° from vertical 0.02 mm/m (0.029 °.).
- Mistake of joints (azimuth) <+/−0.25 °.
- Perpendicularity of segments: +/−0.1 °.

The scheme of the system components and connections is presented on Fig. 11. System consists of three field stations registering landslide data equipped with dataloggers, and multiplexers for inclinometer, groundwater level, temperature and pore pressure measurements. High capacity batteries charged by solar panels providing power supplies. The system powered by lithium batteries allowing at least 3 months of system operation without maintains. Data could be uploaded from the logger at the field manually to a laptop PC. The system is also equipped with special USB converter allowing uploading manually data to laptop PC by direct connection to the transducers (not using dataloggers). This function was valuable for zero readings and system calibration.

Real-Time Monitoring Preliminary Results

Automatic monitoring measurements started in May/June 2010 and will be performed continuously till the end of 2012. Displacements will be compared with groundwater level, temperature and pore pressure readings. This measurements will be analyzed using whether station data including precipitations, temperature, air humidity and air pressure. Obtained correlations will be used for designing of early warning system and prediction of alarm stages. Preliminary results of monitoring measurements presented on Figs. 14, 16, 17, 18, 20 showed that variable displacements were registered up to 11–15 m. At M3 field station, between 24 May and 10 June 2010 displacements reached value of 1.3 cm. Sliding zone depth at that point was 12.4 m bellow natural terrain level. At M2 field station between 18 May till 7 September displacements reached 18 mm and were activated to 15 m depth, however, the largest were registered at depth of 2 m. The values of pore pressure at the landslides were very high 57–63.9 kPa. The interpretation software allowed 3D presentation of measured displacements (Figs. 17–20 and 22). It showed that displacements at M3 Field Station were rotated towards a new bridge on Bystrzanka River (Figs. 15–17).

Real Time Weather Conditions Monitoring

The weather conditions were investigated using automatic station installed near the border of landslide no 1 (Fig. 21). Measurements were stored in the logger and transmitted every 60 min to the Internet using GPRS network. Station enabled continuous observation of precipitations, air pressure, air temperature and air humidity values. The battery voltage and GSM signal level were also continuously controlled. This allowed prevention of data loosing. Obtained data could be exported as "txt" files or edited as a plots (Fig. 22). Since April 2011 the station is additionally powered by the solar panel.

The meteorological parameters measurements has been started in May 2010 air pressure in August 2010. Exemplar daily values of precipitations are presented on Fig. 22. It allowed registration of record monthly precipitations in

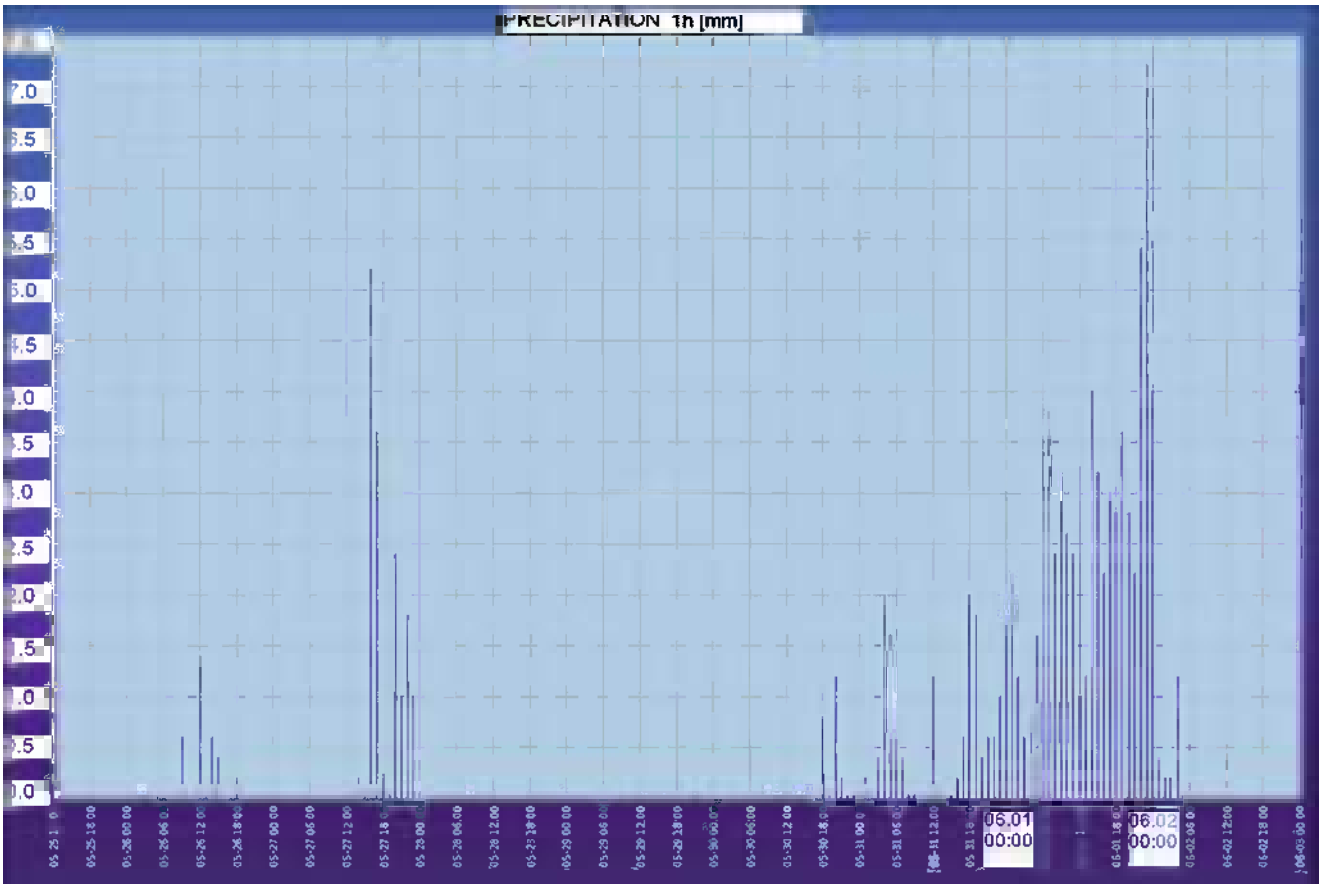


Fig. 22 Precipitation values May/June2010

May–June 2010. Detected record precipitations between June the 1 and June the 2 reached 100 mm (Fig. 22). Meteorlogical parameters will correlated with displacements and pore pressure data.

Conclusions

Implementation of new real-time monitoring system in the Polish Carpathians was presented in the paper. Preliminary monitoring results has been shortly described. On three active and dangerous landslides modern field monitoring stations were installed. They included 3 inclinometers, total length of 50 m and 3 groundwater level, pore pressure and temperature transducers. New geological and geotechnical engineering data were obtained. Detailed recognition of landslides depths and activities will be possible after a longer period of time but preliminary results indicated that ground movements occurred to the depth of 0–15 m. Colluviums were characterized by variable mechanical parameters to the depths of 11–15 m bellow the natural terrain level. The highly saturated (20–40 %) mixtures of weathered, disintegrated claystones and clays with very high plasticity index were recognized to the depths of 3–7 m. Landslides located above Szymbark-Bystra public road were still active despite of partly stabilization works. They had influence road area what was seen on tightening of Geobrugg meshes and new cracks in head landslides parts. It was also visible near the new bridge over the Bystrzanka River. Record precipitations in May and June 2010 indicated that some parts of counteraction works were not fully effective in extreme whether conditions. New system allowed monitoring these of risk sites. Obtained data should be used for correction of counteraction works and early warning messages.

References

Bednarczyk Z (2006) Landslide monitoring and instrumentation for Sekowa landslide stabilization project. EU Centre of Excellence (REA), Warsaw, PGI Special Paper 24, pp 7–10

Bednarczyk Z (2008) Landslide geotechnical monitoring network for mitigation measures in chosen locations inside the SOPO Landslide Counteraction Framework Project Carpathian Mountains, Poland. The First World Landslide Forum, Tokyo International Consortium of Landslides (ICL), United Nations University Tokyo (UNU), pp 71–75

Bednarczyk Z (2008) Flysch landslides geotechnical monitoring in Beskidy. In: A-B Huang, P Mayne (eds) The carpathian mountains

Poland. ISC-3 Conference, ISSMGE Taipei, Taylor and Francis, Balkema, pp 269–274

Bednarczyk Z (2009) Landslide risk and mitigation measures in Poland. In: 17th conference on Engineering Geology University Zittau/Gorlitz, DGGT Deutsche Gess. fur Geotechnik., DGG Deutsche Ges. fur Geowis, pp 121–126

Bednarczyk Z (2009) Ground penetrating radar (GPR) scanning in geological and geotechnical recognition of mountain site. In: 22 SAGEEP symposium on the application of geophysics to engineering and environmental problems, Fort Worth, EEGS, US Army Texas USA, pp 731–738

Bednarczyk Z (2010) Soil-structure interaction on three stabilized flysch landslides in polish carpathians. In: Proceedings of the first international conference on advances in multiscale mechanics AIMM'10. Korea Advertisement Institute KAIST, National Taiwan University U.S. Air Force T-Press, pp 1389–1397



Application of the PS-InSAR Technique for the Post-Failure Landslide Deformation Monitoring at Lubietova Site in Central Slovakia

Vladimir Greif and Jan Vlcko

Abstract

The interferometric synthetic aperture radar data from ERS and ENVISAT sensors were utilized in the analysis of the post-failure deformations in the area of Lubietova town in Central Slovakia. The catastrophic landslide of 1977 together with surrounding landslides in the Lubietova area were analysed with the help of persistent scatterers (PS) technique in order to evaluate recent and past deformations of the unstable slopes. Although long-term precise geodetic monitoring of the 1977 landslide revealed differential deformations inside the sliding mass, due to the lack of the PS located inside the landside caused by temporal decorrelation, unfortunately these records could not be directly compared. The adjacent landslides with sufficient number of PS were analysed by transformation of the line of sight displacements recorded by the sensors to the slope vector direction. This procedure allowed identification of the precise boundaries of the actively moving landslide parts and the updating of the landslide inventory for the Lubietova area.

Keywords

Landslide monitoring • PS-InSAR • Radar interferometry • Lubietova

Introduction

Slow-moving landslides pose a challenge for the engineer, due to the difficulty of distinguishing their mechanism and simultaneously the inability to determine the exact area which will be affected by these phenomena. Prediction of displacement rate increase is very problematic and thus the assessment of future behaviour is almost impossible.

Remote satellite techniques have been routinely used for landslide mapping and monitoring for some time, and optical imagery and GPS techniques are well established methods in studying the geomorphology and topography of landslides including monitoring slope deformation (Malet et al. 2002).

In comparison, the idea of the exploitation of satellite-born radar sensors is quite new. The practical use of radar techniques in landslide study originated in 1989 when differential interferometric synthetic aperture radar technique (DInSAR) was described by Gabriel et al. (1989). Early attempts used few interferograms which provided flexibility in assessing the ground deformations even in conditions of limited SAR data availability. The original DInSAR consisted of only two SAR data acquisitions and it contained at least two inherent errors in interferogram creation. Firstly atmospheric variations affected radar wave phase delay and secondly, the digital elevation model used for cancellation of the topography created from two-pass signal interference was inaccurate. Following analysis of a multitemporal and multibaseline stack of interferograms, Ferretti et al. (1999, 2001) came up with the idea of using longer acquisition sequences to overcome this limitation. This technique was called Permanent Scatterers (PS) and it mitigated the Atmospheric Phase Delay (APD) via statistical filtering oflong-term radar sequences. It also provided residual

V. Greif (✉) • J. Vlcko
Department of Engineering Geology, Faculty of Natural Sciences, Comenius University in Bratislava, Mlynska Dolina G, Bratislava, Slovakia
e-mail: greif@fns.uniba.sk

C. Margottini et al. (eds.), *Landslide Science and Practice*, Vol. 2,
DOI 10.1007/978-3-642-31445-2_2, © Springer-Verlag Berlin Heidelberg 2013

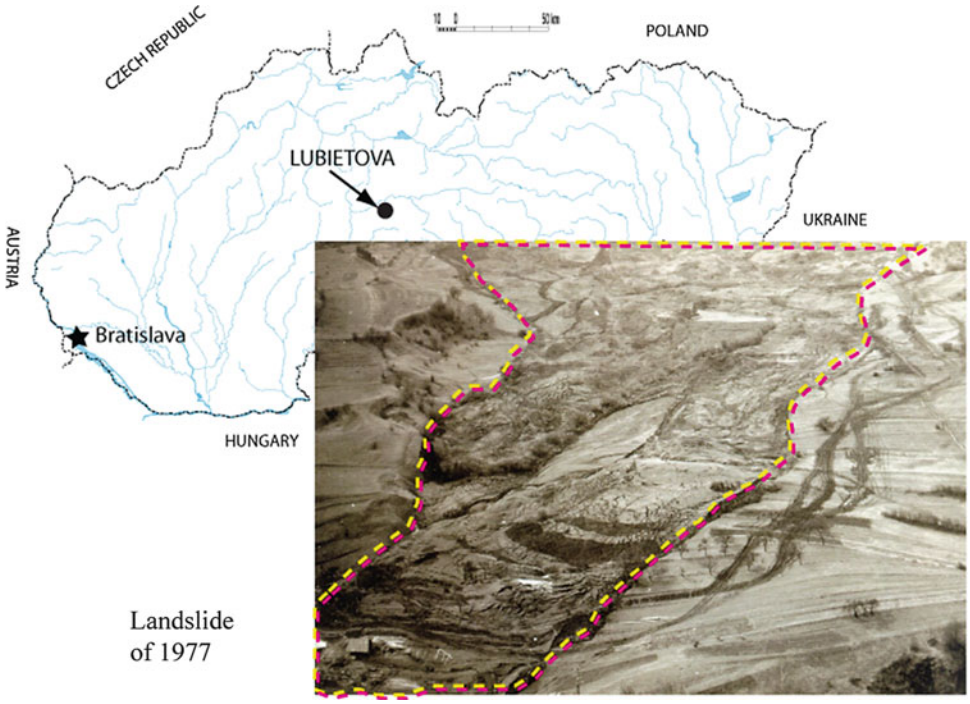


Fig. 1 Localization of the study site with the photo of the catastrophic Lubietova landslide taken shortly after the event

topography estimates with very high accuracy on stable targets. More recently intensive research and development in the field of algorithms and procedures for PS analysis was introduced (Berardino et al. 2002; Mora et al. 2003; Wegmüller et al. 2005; Kampes and Adam 2005; Fornaro et al. 2007; Guarnieri and Tebaldini 2008).

The DInSAR technique has detailed description in scientific literature (Rott and Nagler 2006; Colesanti and Wasowski 2006), and it has been successfully used in subsidence study (Ferretti et al. 2000; Henry et al. 2004; Amelung et al. 1999; Rott et al. 2002,2003), co-earthquake deformation analysis, volcano monitoring and for other purposes.

The first application of DInSAR in landslide study was reported from France (Fruneau et al. 1996), followed by Canada (Singhroy et al. 1998), Austria (Rott et al 1999) and other areas (Vietmeier et al. 1999; Crosetto et al. 2005). The improved PS-InSAR is especially useful in landslide monitoring where the deformation rates are less than approx. 1.4 cm/month and long term series of SAR data is available (Colesanti et al. 2003; Colesanti and Wasowski 2004; Hilley et al. 2004; Bovenga et al. 2006; Farina et al. 2006, 2008; Herrera et al. 2009). PS-InSAR is capable of detecting deformations of individual objects from "small" individual houses to objects only about 1 m^2 in size. A certain density of stable objects (about 5 per km^2) is needed to enable accurate correction of APD (Singhroy 2009). One significant advantage beside the price per sq. km, is the existence of an archive of SAR data allowing monitoring of favourably oriented landslides or other phenomena as far back as July 1991 (Hasager et al. 2002) However, the following challenges remain to be solved, according to Colesanti and Wasowski 2006; Rocca 2003; Manzo et al. 2006:

1. PS data represent a one-demensional line of sight (1D LOS) projection of a deformation occurring in a 3D world. Some attempts to resolve horizontal displacements from 1D LOS were carried out by Cascini et al. (2010);
2. Deformation greater than $\lambda/4$ between two following visits of the satellite are difficult to track due to the ambiguity of radar phase measurements;
3. The measurements are limited due to the positioning of PS and the re-appearance time intervals of the satellite;
4. While it is possible to obtain high density PS in urban areas, it is very difficult to obtain coherent density of pixels in rural areas where most landslides occur. This was addressed by the use of artificial corner reflectors (Ye et al. 2004; Novali et al. 2005), which had the accompanying shortcoming of loss of availability of archive SAR data.

Herein, the authors adopt the PS-InSAR technique in the study of post-failure behaviour in the landslide area near Lubietova in Central Slovakia.

Geological Settings

Lubietova village is located in Central Slovakia about 16 km east of the third largest Slovak city Banska Bystrica (Fig. 1).

During the middle ages, the town of Lubietova was one of the seven most important mining towns in the Upper Hungarian monarchy. The town was famous for its rich abundance of copper ore mined there in fourteenth and fifteenth Centuries, with the mineral Libethenite being a rare secondary copper phosphate hydroxide which derived its name from the formal German name of this town – Libethen.

The studied site is situated in the narrow valley of the Hutna River between the two ranges of the Slovenske Stredohorie Mountains on the west and the Slovenske Rudohorie Mountains on the east. The hillsides dip at gentle slopes at altitudes from 450 to 700 m a.s.l. The eastern aspect slopes are composed of Lower Triassic quartzites, conglomerates and sandstones, and also dolomitic breccias and dolomites. The upper horizons consist of Quaternary clays and slope detritic loams. The bedrock of the opposite slopes of the valley is formed by the Inner-Carpatian Paleogene flysh strata consisting mainly of highly weathered claystones with occasional interbeds of sandy layers. Andesitic epiclastic breccias and conglomerates of Neogene age outcrop at the higher altitudes of the western facing slopes and these form the geomorphologically active parts of the mountain ridge. They rest on a Paleogene clay strata which forms favourable conditions for slow slope deformations. From the geodynamic point of view, these slopes are prone to sliding and this is in stark comparison to the eastern slopes of quartzite and dolomite rocks where stable conditions prevail.

Catastrophic Landslide of Lubietova in 1977

Lubietova landslide (L1) (Fig. 1) occurred in the spring of 1977 (February-April), following a precipitation anomaly lasting from December 1976 to the end of February 1977, when the average monthly precipitation recorded 150–220 % of the long-term average. This precipitation combined with melting snow and triggered an earth flow of asymmetric shape covering an area of approximately 30 ha. The detachment area consisted of three separate detachment zones which merged into an earth flow with the deposition zone partly damming the Hutna River. The altitude difference between the detachment and accumulation zones was 170 m while the length of the earth flow was 1,230 m. The largest width of 400 m in the detachment zone narrowed to 100 m where the river obstruction occurred. Velocities measured during the first days after the occurrence of the landslide reached 2.5 m/day and total recorded displacements were about 9 m, 42.9 m, and 3–6 m in the detachment, transportation and accumulation zones respectively. The sliding surface depths varied dependent on the location from 30 m near the landslide scarp, 15–20 m in the transportation area and 6–8 m in the deposition zone. The total displaced mass measured about 4.5 million cubic metres of deluvial clays (Nemčok 1982). The recent study carried out by Prokesova et al. (2010) using sequential sets of high resolution aerial photographs of this area estimeated the displaced mass balance between 1969–1977 and −111,400/+91,500 m^3. In order to minimize the risk of the river damming during the landslide's maximal activity, several large diameter steel pipes were placed in the river bed allowing the river to flow unobstructed by sliding masses.

The bedrock geology in the vicinity of the landslide is rather complex, with Lower Triassic massive quartzite rocks found in the accumulation zone and Paleogene Flysch-like sediments overlain by slope sediments in the transportation and detachment zones. The Paleogene claystones and shales dip 5–15° towards the northeast creating predisposing shear planes. In the close vicinity of the catastrophic landslide there were several displaced huge blocks of Neogene vulcanoclastics in the form of lateral spreads giving the potential for extremely slow slides.

Shortly after this catastrophic event stabilization works were recommended and applied. Surface drainage and subhorizontal drainage boreholes to decrease the water level inside the sliding body together with buttress-fill grading were installed at the accumulation zone in order to stabilise the area. Following this event a deeper study was carried out by Malgot (1978), who identified several landslides on the western slopes and classified them according to their type and activity. This catastrophic landslide has been continuously monitored since 1988 by precise geodetic measurements and by recording the water level inside the boreholes located within the landslide boundaries.

In a more recent study, Vlcko et al. (2001) adopted a different approach in landslide hazard assessment of the studied area. In the first stage, a traditional landslide distribution map was compiled and this served for further landslide risk map elaboration based on quantitative analysis using the geotechnical approach. This geotechnical, or deterministic, approach was based on the calculation of the safety factor of each landslide body in relation to the designed type of buildings on the urban plan. Since the majority of residential houses were located in the accumulation part of the currently dormant landslides, the calculation was based on foundation dimensions of 12 × 12 × 3 m. The final landslide risk zones in the map were delineated according to the factor of safety (FOS) calculated for each landslide separately. The FOS for the L1 landslide using the soil parameters from a previous survey carried out by Jadroň et al. 1975 was 1.023 when stabilization measures were not taken into account. This illustrates the susceptibility to sliding of the western-facing slopes of the valley formed of clays, clayey loams and shales, which were overlain by Neovolcanic rock caps in some areas. Subsequent

deformations inside the landslide body had a negative effect on the stabilization measures. This particularly applied to the surface drainage channels which were displaced, thus losing functionality. The effectiveness of the subsurface drainage boreholes was limited due to this same reason and re-activation of the landslide is merely a matter of time according to Míka (1999).

Post-Failure Geodetic Monitoring

In 1988, the Geological Survey of Slovakia installed a geodetic monitoring network of more than 30 geodetic points (GP) located inside the L1 landslide body to track the post-failure development of the failure to discover if the sliding body posed a threat to the inhabitants and their property. The geodetic points were monitored by precise geodetic surveys beginning in 1988 and carried out at irregular time intervals. The survey still continues and the results for the period 1988–2006 are shown in Fig. 2. The displacement rates for 30 GP's were calculated from the changes of their coordinates over time by calculating the slopes of the linear regression lines for each X, Y, and Z coordinates separately. Figure 2 shows the projection of the displacement rates in an XY plane.

Higher post-failure velocities were recorded in the northern part of the landslide body reaching values up the 10 mm/year, while the southern parts are moving at slower rates from 1 to 3 mm/year. This shows a differential distribution of the deformation within one sliding mass. The results of this monitoring campaign were intended to be a benchmark to compare results of the PS-InSAR monitoring, in order to evaluate the displacement rates of PS.

PS Technique Results

Three datasets were used for the PS analysis consisting of 50 scenes (track 451) from ERS 1, 2 acquired between 1993–2000 and 58 scenes (track 415, 451) from the ENVISAT two satellite, acquired between the 2002 and 2009. The ENVISAT scenes were from both ascending and descending acquisition orbits, while the ERS1, 2 images were taken only from the descending orbit. The number of derived PS targets for the 4.5 km^2 area of interest was 1683 (455 PS – ENVISAT/Asc., 787 PS – ENVISAT/Desc. and 441 PS – ERS/Desc.). The PS processing was performed by Telerilevamento Europa and satellite images were provided under EC/ESA GSC-DA within the FP7 GMES SAFER project. The three data stacks were processed by means of PSInSAR technique using PSI approach developed by Polytechnic University of Milan and licensed to TRE Europa. A simple linear model of phase variation through time was used for estimation of phase components related to deformations. For the DEM (Digital Elevation Model) correction a SRTM (Shuttle Radar Topography Mission) DEM with 3 arc seconds resolution produced by NASA was used. For each data set a reference point exhibiting no displacement located in the presumably stable area in the fluvial sediments near the town centre was selected. All PS displacements in the data set were referred to this point.

The average density of PS is approx. 374 PS/km^2, which represents a rather high density considering that the studied site is a rural area. Most of the PS targets were located, as expected, on man-made structures such as steel roofs, houses, and bridges in the town, while the landslides were unfortunately lacking scatter points due to temporal de-correlation. The catastrophic landslide of 1977, located in the northwestern part of the town does not contain any reflection points, while the other two, landslides 2 and 3, have the PS located mainly in the accumulation zone. The distributions of the PS and their LOS displacement rates from both satellites are shown in Fig. 3. The hilly parts of the area had PS located on rocky outcrops, showing very slow movements in the LOS direction and mainly corresponding to deep seated deformations of a creep character.

The 1D LOS displacement rates in the studied area vary in range from −5 to +5 mm/year, with the negative values indicating displacements away from the radar sensor along the line of sight direction. From the PS located in the area of the landslides 2 (L2) and 3 (L3) most of the targets are located in the accumulation zone with gentle slope. These targets have an LOS displacement rate below the 2 mm/year, which some authors such as Colesanti and Wasowski (2006); and Righini et al. 2009 consider to be the threshold between stable and unstable states of sliding. Nevertheless, it is possible to trace the boundary between the slowly creeping areas and the stable parts of the landslide mass.

Discussion and Conclusions

The use of the PS-InSAR technique for the identification of unstable areas proved to be a very cost-efficient method in large areas, where sufficient number of PS can be found (Van der Kooij 1999). Such areas mainly represent urban sites, slope outcrops or rocky ranges, where the intensity of the scattered radiation is higher compared to rural areas wherein vegetated areas, meadows and crop fields suffer from temporal de-correlation of the radar signal. Furthermore, the applicability of this technique to landslide monitoring has further limitations, particularly the slope aspect which further limits applicability of the data for the analysis. This is also in addition to the previously mentioned lack of PS on vegetated and soil covered land.

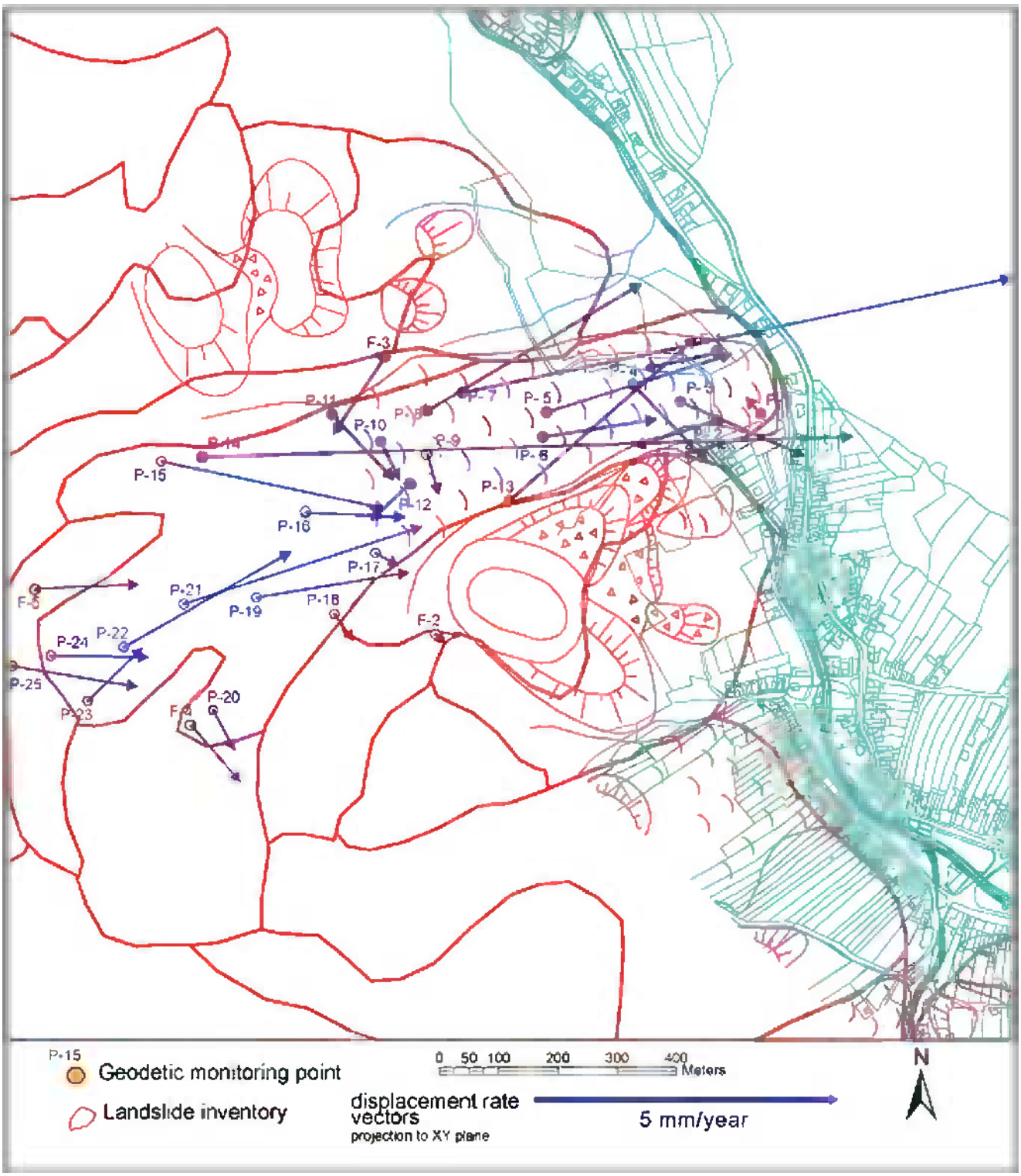


Fig. 2 Displacement rate vectors derived from the geodetic monitoring system of the catastrophic Lubietova landslide projected onto the horizontal plane showing differential deformation rates inside the landslide mass

The influence of atmospheric conditions on the accuracy of the PS results is well known, and to certain extent the error can be removed using a statistical approach where there is availability of long-term data.

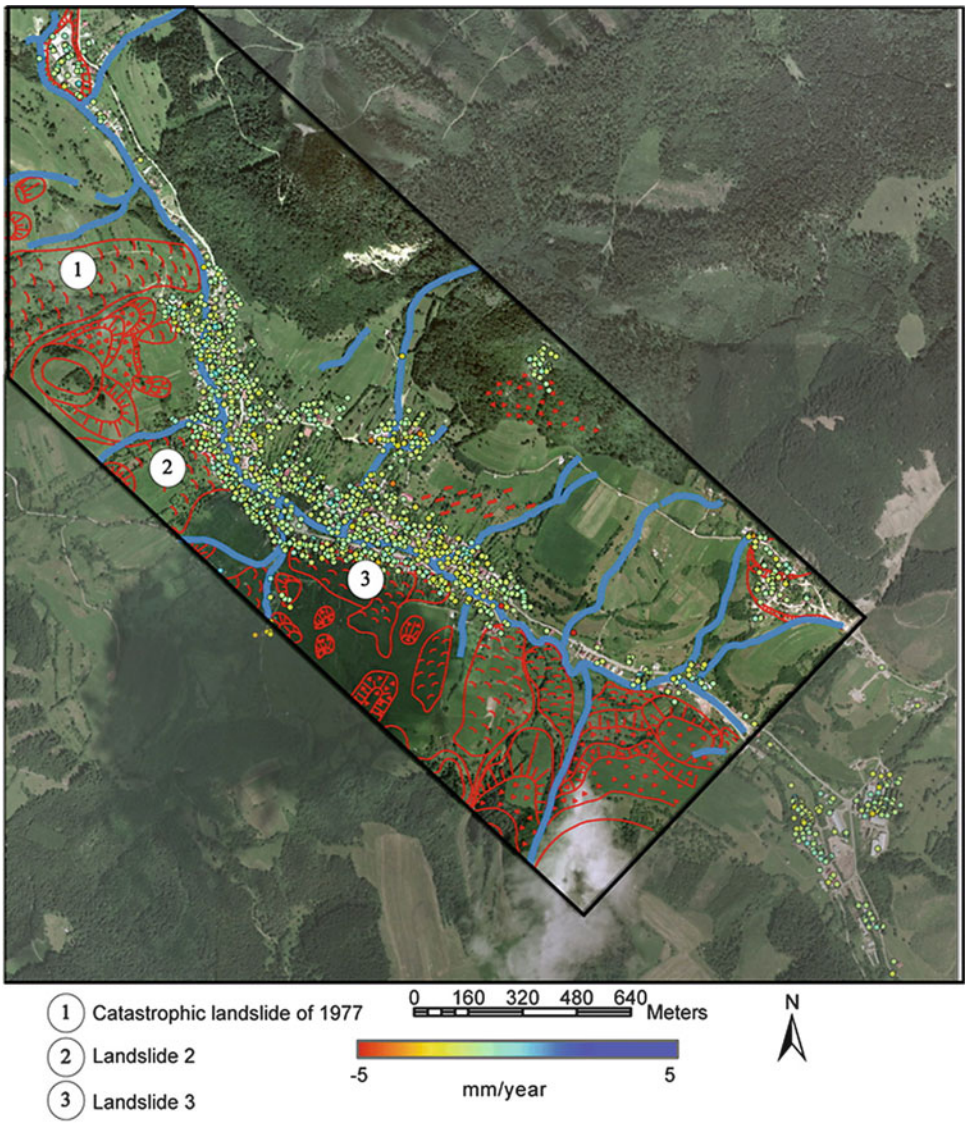


Fig. 3 Combined ERSd, ENVISATa,d LOS PS velocities in the Lubietova area showing the landslides in the vicinity of the town

The most important data for landslide monitoring are the displacement vectors derived from various sensors indicating the amplitude and direction of the deformations. The PS data represents the displacements in the line of sight direction of the radar sensor, and this is of limited use for the detection of the orientation in which the deformation progresses. In order to extract the horizontal component of the deformation along the line of the slope, a transformation of 1D LOS data has to take place, and this also further limits the applicable data mainly due to relative orientation of radar vision vector toward the slope orientation. The aspect angle and slope dip angle particularly affect the utility of the PS-InSAR data (Cascini et al. 2010).

Moduli of displacement rates in the slope direction were determined by the transformation of 1D LOS PS velocity rates in the accumulation zones of landslides L2 and L3. The velocities for the active areas of the L2 landslide were less than 3 mm/year while in the L3 landslides it reached less than 20 mm/year. The later displacement rates must be approached with caution, since these were based only on ERS and ENVISAT descending orbits data with a scaling factor near 7. The data from the ascending ENVISAT acquisitions were discarded due to the high value of the scaling factor. Even though the PS-InSAR technique did not produce any usable targets within the L1 catastrophic landslide of 1977, the measured displacement rates for the L2 and L3 landslides in the immediate vicinity of the L1 landslide are comparable in magnitude to the results obtained by long-term geodetic monitoring recorded within the L1 landslide.

Furthermore, it was possible to redraw the boundaries of the L2 and L3 landslides based on the slope direction velocity

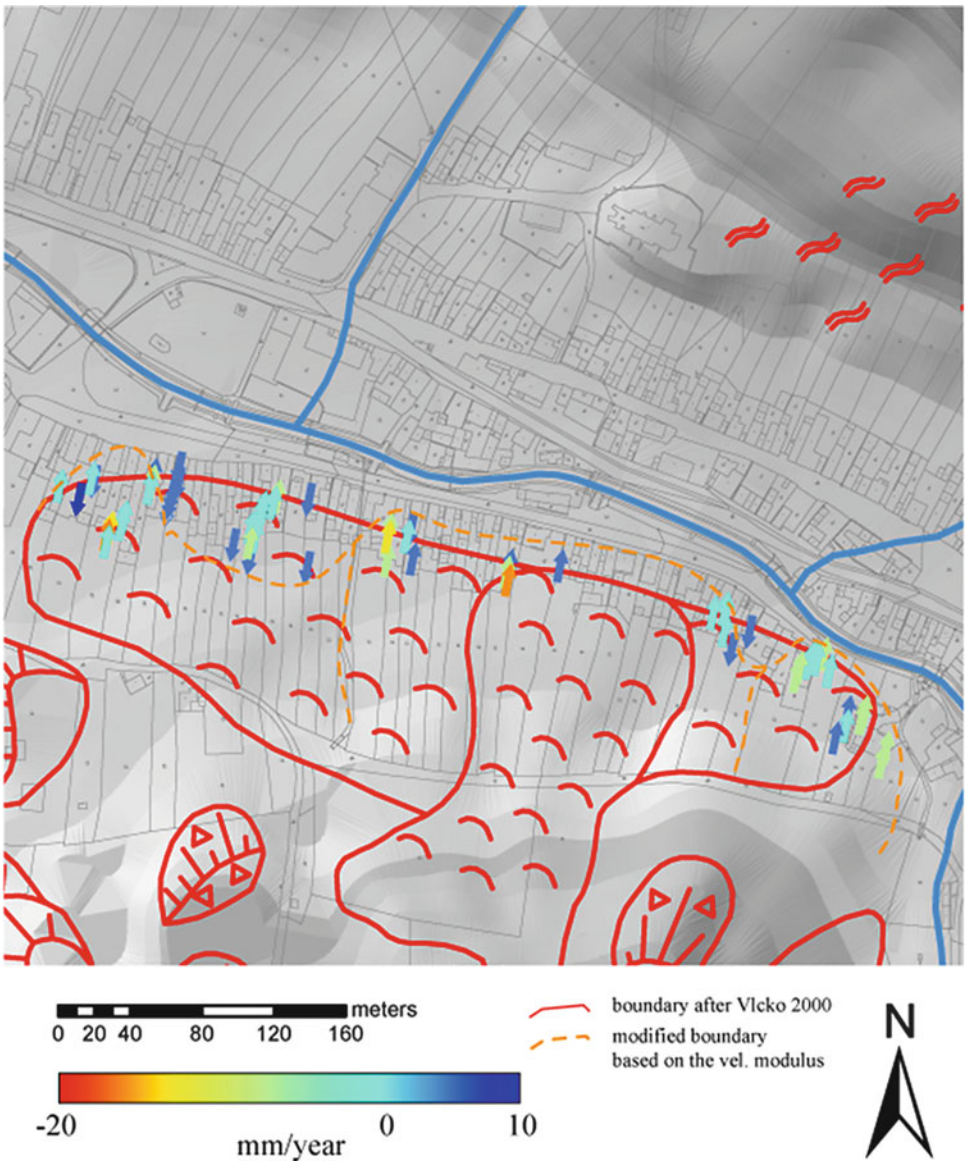


Fig. 4 Displacement rates transformed to the deepest slope orientation for the landslide L3 with the modified accumulation part of the landslide boundary according to the moduli of the displacement rates at the PS locations

moduli of displacements indicating different deformation rates within one sliding body (Fig. 4).

The PS-InSAR technique proved to be a valuable help in cases where it succeeds in producing sufficient densities of targets within the landslide mass.

An attempt to extract slope direction displacement rates from 1D LOS data was carried out, and this proved to have greater value in the landslide monitoring. However, it also indicated the limits for useful transformation of PS LOS displacement rates, with the slope aspect particularly heavily affecting successful application of this method. It would be beneficial to further automate the transformation procedure within the GIS in order to have the results to hand more rapidly. This could be an area for future development of the PS technique in landslide monitoring practice.

All results obtained either with precise geodetic monitoring and with satellite interferometry indicate that the landslides located on the western bank of the Hutna River are in continuous slow creep movement, and they require constant monitoring even though the current threat to people and property is not considered to be very high.

Acknowledgments This work was supported by a grant from the Slovak Ministry of Education VEGA (contract no. 1/0331/09) and partly by the EU FP7 project "SAFER" (contract no. 218802) and Grant of the Slovak Research and Development Agency (contract no. DO7RP-0012-09, **APVV – 0330–10** and APVV-0641-10).

References

Amelung F, Galloway DL, Bell JW, Zebker HA, Laczniak RJ (1999) Sensing the ups and downs of Las Vegas: InSAR reveals structural control of land subsidence and aquifer-system deformation. Geology 27(6):483–486

Berardino P, Fornaro G, Lanari R, Sansosti E (2002) A new algorithm for surface deformationmonitoring based on small baseline differential SAR interferograms. IEEE Trans Geosci Remot Sen 40(11):2375–2383

Bovenga F, Nutricato R, Refice A, Wasowski J (2006) Application of multi-temporal differential interferometry to slope instability detection in urban/peri-urban areas. Eng Geol 88:219–240

Cascini L, Fornaro G, Peduto D (2010) Advanced low- and full-resolution DInSAR map generation for slow-moving landslide analysis at different scales. Eng Geol 112(1–4):29–42

Colesanti C, Wasowski J (2004) Satellite SAR interferometry for wide-area slope hazard detection and site-specific monitoring of slow landslides. In: Proceedings ninth international symposium on landslides, June 28–July 2 2004, Rio de Janeiro, pp 795–802

Colesanti C, Wasowski J (2006) Investigating landslides with spaceborne synthetic aperture radar (SAR) interferometry. Eng Geol 88:173–199

Colesanti C, Ferretti A, Prati C, Rocca F (2003) Monitoring landslides and tectonic motion with the Permanent Scatterers Technique. Eng Geol 68:1–14

Crosetto M, Crippa B, Biescas E (2005) Early detection and in-depth analysis of deformation phenomena by radar interferometry. Eng Geol 79(1–2):81–91

Farina P, Colombo D, Fumagalli A, Marks F, Moretti S (2006) Permanent scatterers for landslide investigations: outcomes from the ESA-SLAM project. Eng Geol 88:200–217

Farina P, Casagli N, Ferretti A (2008) Radar-interpretation of InSAR measurements for landslide investigations in civil protection practices. In: Proceedings of the 1st North American landslide conference, Vail, 3–7 June 2007, pp 272–283

Ferretti A, Prati C, Rocca F (1999) Multibaseline InSAR DEM reconstruction: the wavelet approach. IEEE Trans Geosci Remot Sen 37(2):705–715

Ferretti A, Prati C, Rocca F (2000) Non-linear subsidence rate estimation using permanent scatterers in differential SAR interferometry. IEEE Trans Geosci Remot Sen 38(5):2202–2212

Ferretti A, Prati C, Rocca F (2001) Permanent scatterers in SAR interferometry. IEEE Trans Geosci Remot Sen 39(1):8–20

Fornaro G, Pauciullo A, Serafino F (2007) Multipass SAR processing for urbanized areas imaging and deformation monitoring at small and large scales. In: Proceedings of urban remote sensing joint event URS 2007 Paris, 11–13 April

Fruneau B, Achache J, Delacourt C (1996) Observation and modelling of the Saint-E' tienne-de-Tine'e landslide using SAR interferometry. Tectonophysics 265:181–190

Gabriel AK, Goldstein RM, Zebker HA (1989) Mapping small elevation changes over large areas: differential radar interferometry. J Geophys Res 94(B7):9183–9191

Guarnieri AM, Tebaldini S (2008) On the exploitation of target statistics for SAR interferometry applications. IEEE Trans Geosc Remot Sen 46(11):3436–3443

Hasager CHB, Jensen NO, Nielsen M, Furevik B (2002) SAR satellite image derived wind speed maps validated with in-situ meteorological observations and footprint theory for offshore wind resource mapping. In: 2002 global windpower proceedings 2–5 April 2002, CNIT – La Défense – Paris – France. Available also online: http://sitecoremedia.risoe.dk/research/vea/Documents/globalwindpower2002_proceedings.pdf. Accessed 4 May 2010

Henry E, Mayer C, Rott H (2004) Mapping mining-induced subsidence from space in a hard rock mine: example of SAR interferometry application at Kiruna mine. CIM Bull 97(1083):1–5

Herrera G, Davalillo JC, Cooksley G, Monserrat O, Pancioli V (2009) Mapping and monitoring geomorphological processes in mountainous areas using PSI data: Central pyrenees case study. Nat Hazards Earth Syst 9:1587–1598

Hilley GE, Bürgmann R, Ferretti A, Novali F, Rocca F (2004) Dynamics of slow-moving landslides from permanent scatterer analysis. Science 304:1952–1955

Jadroň D, Fussgänger E, Banský M, Tyleček B, Malgot J, Fekeč J, Frnčo M (1975) Lubietova landslide – detailed survey. Final report, 106 p (in Slovak)

Kampes BM, Adam N (2005) The STUN algorithm for persistent scatterer interferometry. In: Fringe 2005 Workshop, Frascati. http://earth.esa.int/fringe2005/proceedings/papers/58_kampes.pdf. Accessed 19 Jan 2009

Malet JP, Maquaire O, Calais E (2002) The use of global positioning system techniques for the continuous monitoring of landslides – application to the super – sauze earth flow (Alpes de Haute-Provence, France). Geomorphology 43:33–54

Malgot J (1978) Slope deformations in the vicinity of Lubietova. Geol Průzkum 20(1):11–14 (in Slovak)

Manzo M, Ricciardi GP, Casu F, Ventura G, Zeni G, Borgstrom S, Berardino P, Del Gaudio C, Lanari R (2006) Surface deformation analysis in the Ischia Island (Italy) based on spaceborne radar interferometry. J Volcanol Geoth Res 151(4):399–416

Míka R (1999) Assessment of the Lubietova landslide stability. In: Klukanová A (ed) in Slovak. GSSR, Bratislava, pp 54–58, in Slovak

Mora O, Mallorqui JJ, Broquetas A (2003) Linear and nonlinear terrain deformation maps from a reduced set of interferometric SAR images. IEEE Trans Geosci Remot Sen 41(10):2243–2253

Nemčok A (1982) Landslides in slovak carpathians. Veda, vyd SAV, Bratislava, p 319, in Slovak

Novali F, Ferretti A, Prati C, Rocca F, Savio G, Musazzi S (2005) PSInSAR validation by means of a blind experiment using dihedral reflectors. In: Proceedings FRINGE 2005, Frascati, 28 Nov–2 Dec 2005, ESASP-610. Available also online: http://earth.esa.int/workshops/fringe2005/proceedings/papers/253_novali.pdf. Accessed 9 Dec 2009

Prokesova R, Kardos M, Medvedova A (2010) Landslide dynamics from high-resolution aerial photographs: a case study from the Western Carpathians, Slovakia. Geomorphology 115:90–101

Righini G, Del Ventisette C, Constantini M, Malvarosa F, Minati F (2009) Spaceborne SAR analysis for landslides mapping in the framework of the PREVIEW project. In: Sassa K, Canuti P (eds) Landslides: disaster risk reduction. Springer, Berlin, pp 299–301

Rocca F (2003) 3D motion recovery with multi-angle and/or left right Interferometry. In: Proceedings 3rd international workshop on ERS SAR interferometry, FRINGE 2003, Frascati, 2–5 Dec 2003. ESA SP-550. Available also online: http://earth.esa.int/fringe03/proceedings/posters/62_roca.pdf. Accessed 6 Mar 2009

Rott H, Nagler T (2006) The contribution of radar interferometry to the assessment of landslide hazards. Adv Space Res 37(4):710–719

Rott H, Scheuchl B, Siegel A, Grasemann B (1999) Monitoring very slow slope movements by means of SAR interferometry: a case study from a mass waste above a reservoir in the Ötztal Alps, Austria. Geophys Res Lett 26:1629–1632

Rott H, Nagler T, Rocca F, Prati C, Mazzotti A, Keusen HR, Liener, Tarchi D (2002) MUSCL – monitoring urban subsidence, cavities and landslides by remote sensing. Final Report, EC Project EVG1-CT-1999-00008, Institute for Meteorology and Geophysics, University of Innsbruck, Austria

Rott H, Nagler T, Rocca F, Prati C, Mazzotti A, Keusen HR, Liener, Tarchi D (2003) InSAR techniques and applications for monitoring

landslides and subsidence. In: Benes (ed) Geoinformation for European-wide integration, proceedings of EARSeL assembly, Prague, June 2002, Millpress, Rotterdamp 25–31

Singhroy V (2009) Satellite remote sensing applications for landslide detection and monitoring. In: Sassa K, Canuti P (eds) Landslides: disaster risk reduction. Springer, Berlin, pp 143–158

Singhroy V, Mattar KE, Gray AL (1998) Landslide characteristics in Canada using interferometric SARand combined SAR and TM images. Adv Space Res 3:465–476

Van der Kooij M (1999) Engineering geology landslide investigations and SAR Interferometry. In: Proceedings of FRINGE'99, Liege

Vietmeier J, Wagner W, Dikau R (1999) Monitoring moderate slope movements (landslides) in the southern French Alps using differential SAR interferometry. In: Proceedings of Fringe '99, Lieges

Vlcko J, Maas P, Ayele T (2001) Assessment of the engineering geological conditions of Lubietova village for the urbanization purposes. Final report, p 20 (in Slovak)

Wegmüller U, Werner C, Strozzi T, Wiesmann A (2005) ERS – ASAR integration in the interferometric point target analysis. In: Proceedings Fringe 2005 workshop, Frascati, 28 Nov–2 Dec. http://earth.esa.int/workshops/fringe05/proceedings/papers/196_wegmuller.pdf. Accessed 6 Mar 2009

Ye X, Kaufmann H, Guo XF (2004) Landslide monitoring in the three gorges area using D-InSAR and corner reflectors. Photogramm Eng Rem S 70(10):1167–1172



Monitoring of the "Razanj" Landslide in Serbia

Svetozar Milenkovic, Branko Jelisavac, Vladeta Vujanic, and Milovan Jotic

Abstract

Serbia is quite known for its conspicuous number of landslides. Unstable slopes with great number of landslides capture very large areas. Detailed engineering-geological investigations of these slides were carried out in the previous period meant for repair works. Unfortunately, the works thereof were carried out within the budgetary constraints, so that the majority of landslides are still active. Highly precise data on the mechanism and depth of sliding processes and cause and effect links of soil water-saturation and landslide activity level have been obtained through long-standing monitoring of landslides.

Keywords

Road network • Landslide • Monitoring

Introduction

Serbia is well known for its conspicuous number of various landslides, formed prevailingly in the weathering crust, of neogene age, wherein the clays, marls, and sands alternate each other. Unstable slopes created along the river banks of Danube and Sava are particularly known, with great number of landslides which capture very large areas. Basic cause of such numerous occurrences, most frequently spacious and deep landslides, is attributed to complex geological and morphological evolution of the terrain.

Immediate pretext, however, in our time is quite often the consequence of human building and economic activity such as construction of E-75 motorway within the corridor 10. The most complex landslides are as follows: Beska, Begaljicko Brdo, Kolari, Bracin, and Razanj (Fig. 1). These landslides were a calm phenomenons untill the construction of motorway. From then and onwards their activity was growing gradually, and thus causing more and more complex problems which were often culminating even with overall traffic break-down along motorway. The most significant example for such activities is Razanj landslide.

This paper presents the results of the most recent, essential monitoring results, which among other things included as well the inclinometers, piezometers, survey points and triaxes deformeters. Highly precise data on the mechanism and depth of sliding processes and cause-effect links of soil water-saturation and landslide activity level have been obtained through long-lasting monitoring. More objective assessment of hazards and risks has been made possible by this operation, along with the establishment of rating and prioritization for repairs. Moreover, certain stages of repair implementation are being checked-up by monitoring.

Engineering Geological Review of the Landslide Razanj

The area of the "Razanj" landslide is made of deluvial and deluvial-proluvial quaternary clayey-silty sediments, of thickness being 2–6 m in the wider zone. Landslide body is prevailingly made of silty and marly clay, covered with a 5–10 m of filling material (motorway embankment). The thickness of the mass set in motion is the greatest within the landslide peak, in motorway zone (landslide head scarp)

S. Milenkovic (✉) • B. Jelisavac • V. Vujanic • M. Jotic
The Highway Institute, Geotechnical Department, Kumodraska 257, Belgrade, Serbia
e-mail: tozony@gmail.com

C. Margottini et al. (eds.), *Landslide Science and Practice*, Vol. 2,
DOI 10.1007/978-3-642-31445-2_3, © Springer-Verlag Berlin Heidelberg 2013

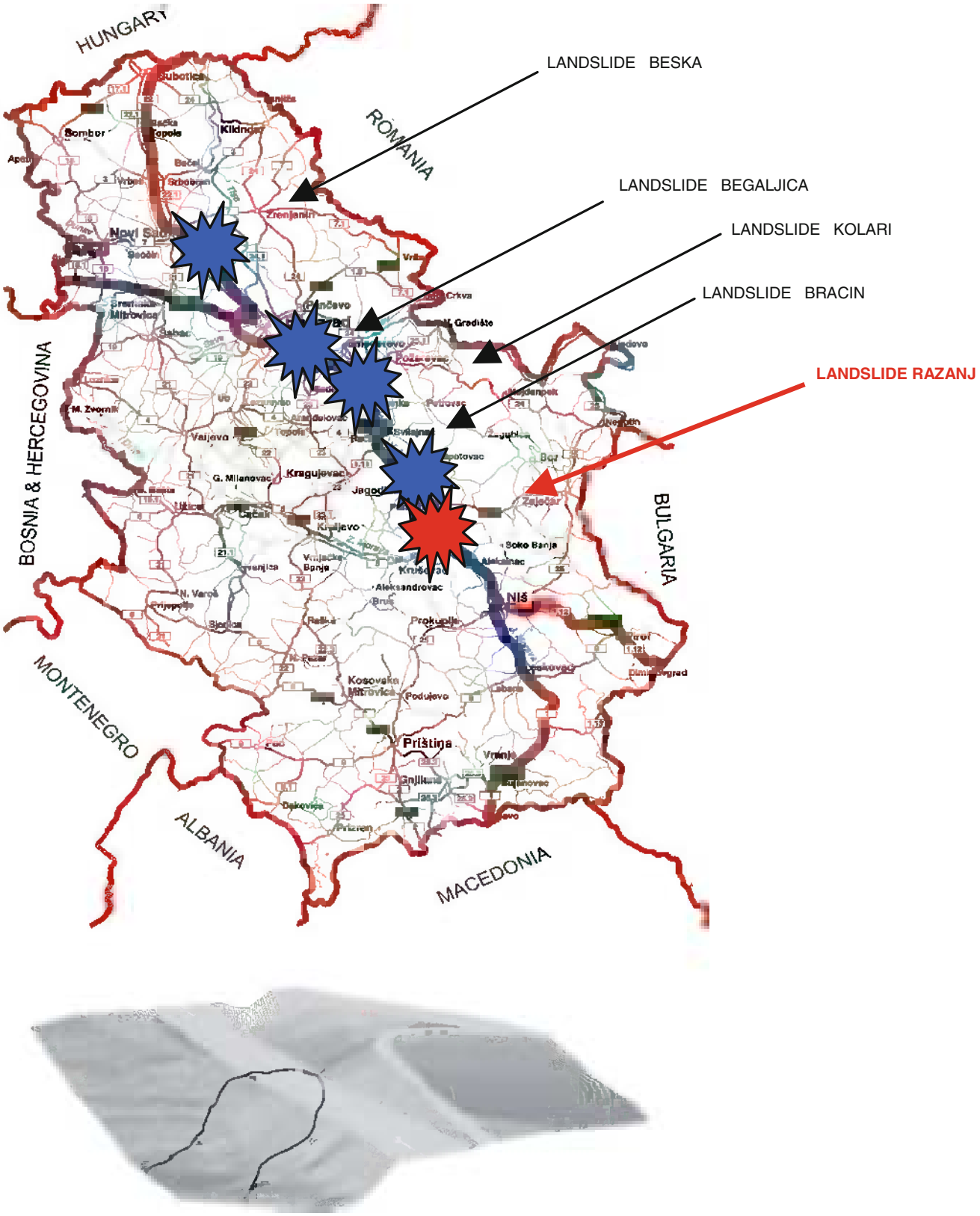


Fig. 1 Geographic location of the major landlides on corridor 10 through Serbia with 3D terrain model of the landslide Razanj

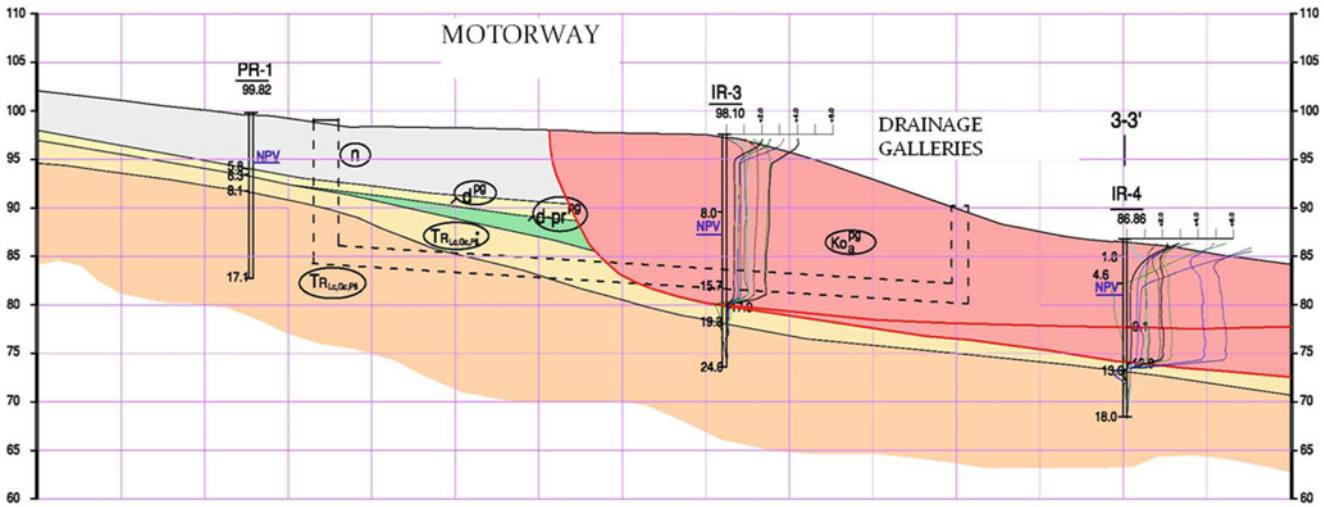


Fig. 2 Engineering geological cross section

and amounts to 16–17 m. Within the motorway embankment toe the landslide depth in the central part is about 10 m. Residual values of the shear strength, as defined under direct shear test are φ = 8.5–10.0 with C = 0 kPa. Other values of physical characteristics are: natural moisture content w = 14–22 %, consistency features Wp = 19–35 %, WI =39–70 %, Ip = 19–30 %, and Ic = 1.0–1.3.

Within the interaction zone, lower sediments consists of miocene clay and marly clay with thin interlayers and lenticular sand.

These deposits are quite degraded (weathering crust), with thickness being 5–10 m, and are located directly below the landslide main body. They represent the product of surface physical-chemical alterations of miocene marls, which are found in the underlying stratum.

Basically they feature considerable weakness of specific physical-chemical properties, and as such prone to sliding. Laboratory testing on representative samples established residual values of the shear strengthtance are φ = 8–14 along with C = 0 kPa. Besides, these samples had specific consistence features Wp = 24–38 %, WI = 37–85 %, Ip = 18–58 %, and Ic = 0.9–1,2. Natural moisture content w = 20–32 %.

Miocene marls are located below the complex of clays and marly clays and are sandy here and there with thickness reaching several tens of meters (The Highway Institute documentation 2008–2010).

Recent Investigations and Previous Remedial Works

In order to point to overall complexity of this landslide, it is worth stressing that the investigations as regards the origins of appearance, depth, mechanism and dynamics of sliding were carried out by various specialized institutions in the period from 1979 till 1997. Previous geotechnical and design documentation has limited possibilities of utilization and application due to differing investigation approaches to the issue of deformation causes.

In view of the threat of traffic break-down on the right carriageway of motorway Belgrade – Nis due to the sliding process, the Highway Institute carried out additional geotechnical investigations of soils involved in the sliding zone and prepared the Project of risk mitigation control works during 1989–1990. In order to prevent further movements of landslide, by the above mentioned Project, two drainage galleries (Fig. 2) were made (about 100 and 60 m long). Since then, landslide displacement rates are in the trend of decreasing, but as one can observe from further text, certainly not completelly stopped. A great contribution in the perception of causes, dynamics, geometry and particularly future activity of the landslide was given by systematic observations from year 2002 till nowadays as follows: geodetic, inclinometric, hydrogeological and deformation measurements in drainage galleries.

Additional geotechnical works were carried out in order to define mechanism and dynamics of sliding (Hunt 1984; Leonards et al. 1993; Lollino & Wasowski 1994; Leroueil et al. 1996; Baldassarre et al. 1996; DeGraff 2002; Haberler-Weber 2005). They encompassed: detailed engineering-geological mapping of terrain on a very narrow location around the landslide; nine exploratory holes were drilled with overall length of 150 m and besides the mapping, the sampling was done as well; within the framework of four exploratory hole four inclinometers were set in total length of 58 m; within five exploratory holes piezometers were set in total length of about 16 m; observations as regards ground water level were performed (total of 30 measuring cycles); observations were carried out within the four installed inclinometers (also 12 measuring cycles); 10 surveying marks were set and

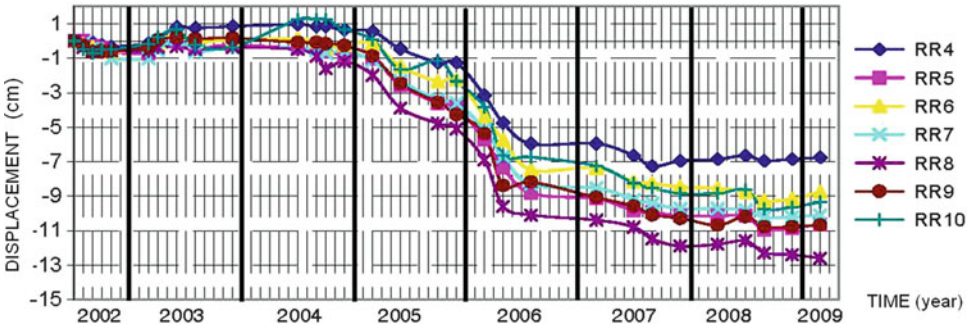


Fig. 3 Overall downhill displacement of landslide

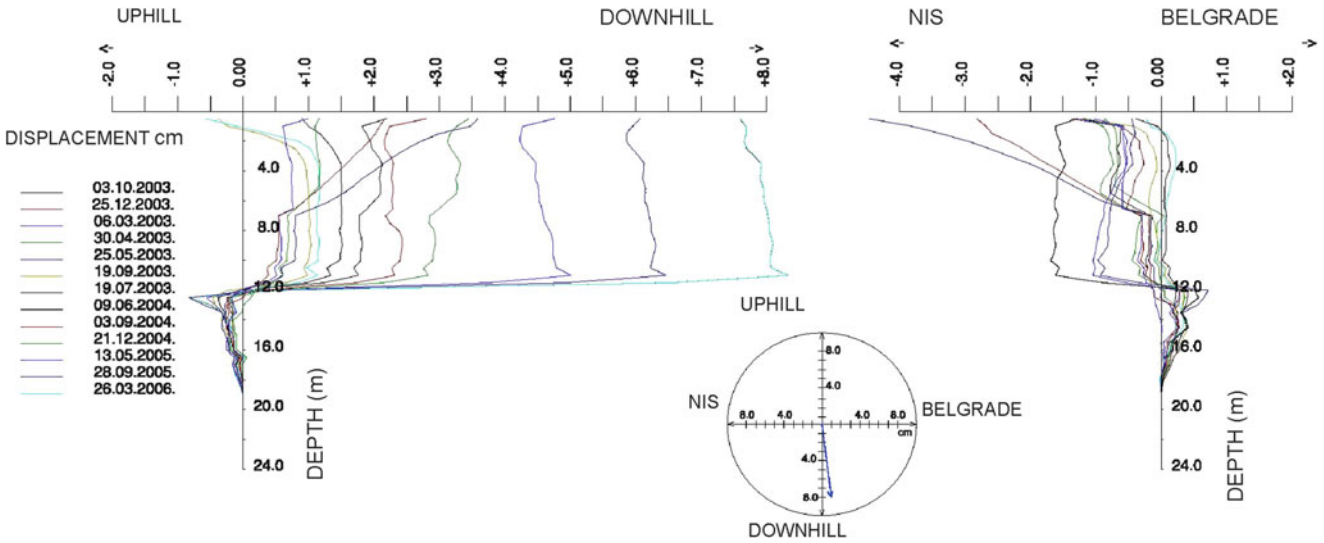


Fig. 4 Displacement profiles and vector of overall inclination (BI-2)

observations of their shifting were carried out on the supporting structure set in motion; various laboratory soil mechanics investigations were carried out on 12 samples from the slide main body. Also, observations of eight triaxial mechanical deformeters, installed in drainage galleries were carried out.

Monitoring of the Landslide

Geodetic Data

Geodetic survey was carried out on the net of 19 survey points established on July 2002, and during 32 measuring cycles, surface displacements in the range of centimeters were recorded within the sliding body.

All of the points which are situated within the sliding body are shifted vertically from a range 0.5 to 1.0 cm, and horizontally from 7.0 to 13.0 cm (Fig. 3). In comparison with displacements observed during previous stages of investigations, general tendency of displacement rates decreasing is significant. In spite of that fact, and one may expect that after longer observations these displacements will be more pronounced.

Installation and Monitoring of Inclinometers

After the installation and protection, the initial measurement has been carried out in two orthogonal planes defined by the position of internal grooves: one normal onto the motorway (AB) and the other one parallel to the motorway (CD). Other measurements have been carried out as relation to zero point, so disregarding the original position of the structure within spatial considerations, each landslide motion is recorded as the discrepancy from upright vertical. A total of seven series of measurements have been carried out, whereas the monitoring results have been presented as diagrams of differences of cumulative displacements for two measuring planes and vectors of overall displacements (Fig. 4).

In the period from July 2002 till nowadays, a series of 32 measurements in both measuring planes have been

carried out on seven installed inclinometers within the landslide body.

Measurement results are presented in diagrams of overall motions whereby one was in a position to define the depth of sliding, landslide body motion dynamics, as well as the vectors of overall motions. Maximum displacement is carried out within the zone of weathered tertiary sediments, and within its scope during the mapping procedure one was able to record clear and numerous shearing cracks. Overall shifting of the landslide body within AB plane, i.e. along the embankment towards the stream amounts to 8 cm.

Installation and Monitoring of Triaxial Orthogonal Deformeter

Mechanical displacement measuring device – triaxial orthogonal deformeter (Fig. 5) is used to measure relative motions of cracks within three orthogonal directions. These are practically installed in concrete or masonry structures, or even to follow-up the discontinuity in hard rock masses.

It is composed of two crank type profiles which are bifurcating in three parts under a right angle. Profiles are made of stainless metal, with consistent thermal properties. Every profile thereof has three reference bolts each being utilized to measure relative motions within three orthogonal directions. Measurements are facilitated by micrometer. Eight triaxial measuring devices have been installed four each in both drainage galleries (Fig. 6), and one inch within the stable terrain. By analyzing the motions measured by triaxial deformeter one is obtaining the data on spatial motions of concrete centerings which make the structural foundation of drainage galleries.

Deformation devices are installed in both galleries, on the spots where one can observe visually the largest deformations of structure, i.e. the cracks with the width ranging from 3 to 7 cm, which appeared in previous 20 years. Total motions measured during 8 years amount to 6 cm. Displacement vectors reflect actual motion intensity, while their spatial position is relative one. The rationale for this is the impossibility of installing the deformation devices in a position which is coinciding with the absolute orientation of spatial axes.

Installation and Monitoring of Piezometers

In order to perceive the conditions and regime of ground waters within the terrain, a monitoring network of piezometers was established in June 2002. Five standard piezometers have been installed, out of which one within the stable backing, while four within the landslide body.

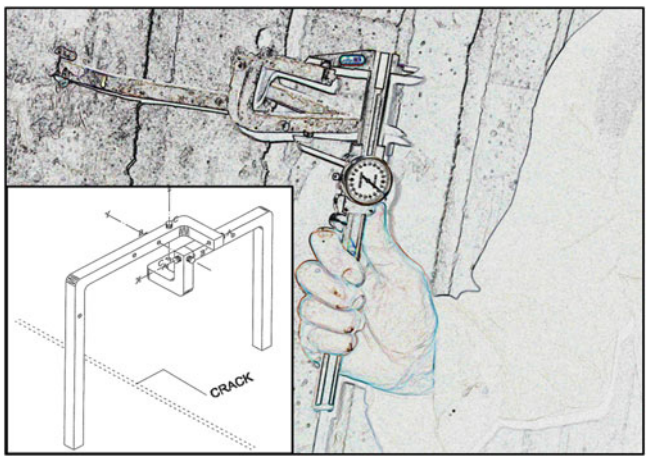


Fig. 5 Triaxial measuring device

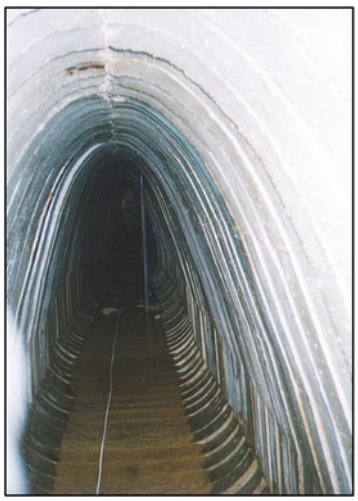


Fig. 6 Drainage gallery

The analysis of results arising from systematic monitoring with piezometers network provided for the conclusion pertaining the ground waters in the area under study.

Fourteen series of measurements for ground waters level on all installed piezometers and inclinometers have been carried out in the course of monitoring period (July 2002 – March 2005). The results indicate onto the seasonal variations with somewhat more pronounced maximums in the spring months, i.e. the minimums by the end of autumn. These variations are within the range of 1 m, which are obviously below the anticipated values. This fact can be corroborated by the functionality of constructed drainage system, whereby the entire surplus of infiltrated water from precipitations is brought down to rather uniform level.

By interpolation of results regarding the ground waters measured level, one may draw a conclusion that within the sliding body an aquifer has been formed with relatively stable static level. This aquifer is inclined along the slope

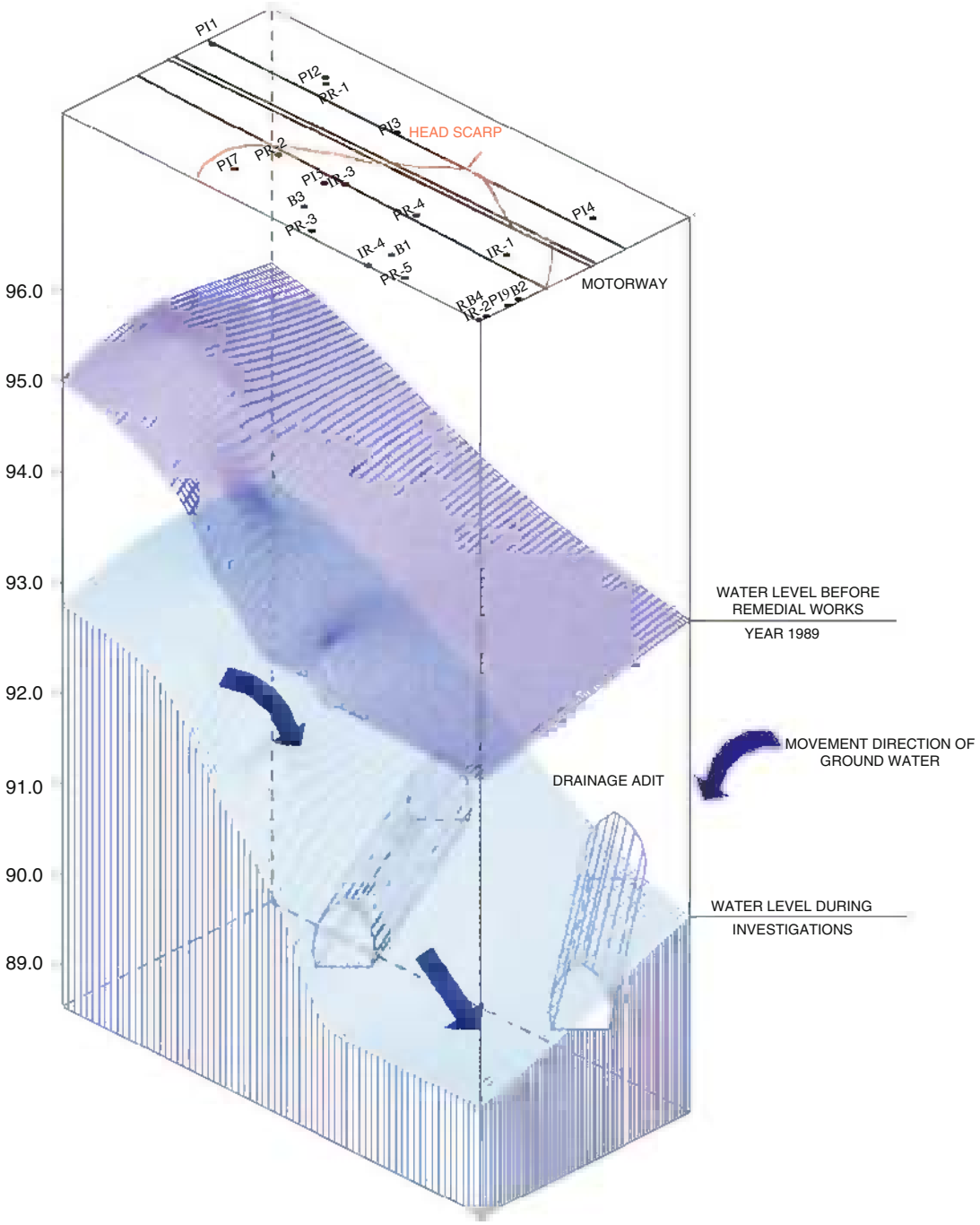


Fig. 7 3D review of ground waters level lowering

towards Nis township, which perfectly matches to the displacement vectors.

These results are of exceptional relevance, since one can compare them with the ground waters levels prior to the construction of drainage galleries/drifts, i.e. to establish the effect of the drainage itself. Namely, Fig. 7 is showing 3D review of ground waters level lowering after putting two drainage galleries into operation. It is obvious that the basic cause of slowing down the sliding process is the fact that ground water level within the short period has been lowered for 4–5 m and mostly within the zone of activity performed by drainage facilities (Fig. 6).

Conclusion

Terrain deformations caused by the landslide appearance, not only exert the influence directly onto the stability and security of road traffic operations, but also endanger the security of the population living nearby. Road improvement works and reestablishment of previous conditions call for extensive financial funds. That is why it is

necessary to recognize all potential (active and calmed) landslides, at an early stage of appearance, through their recording, investigation and monitoring in order to prevent the sliding processes phenomena of larger proportions.

Since this is the most rational way of investigations, monitoring on the landslide should be continued as it was the case in the past, while the attained results are of high relevance, and thereby the effects of previous repair measures are evaluated and remaining works directed towards further implementation.

The remote location of many landslides has also created an urgent need for systems that can be monitored automaticaly and remotely in order to provide immediate warnings in the case of failure signs. Due to widely availability of modern electronic instrumentation it is possible to monitor landslides more effectively and economically. This is the dirrection the monitoring programs in Serbia should evolve to.

Acknowledgments The authors wish to acknowledge authorities from the Public Enterprise – Roads of Serbia for funding the monitoring programs for all large landslides along the major road corridors in Serbia.

References

Baldassarre G et al (1996) A contribution to a geotechnical knowledge of the Varicoloured Clays of Italy's Basilicata Region, with specific reference to a test slope. In: Landslides-international symposium, Trondhaim

DeGraff J (2002) A perspective for achieving improved landslide monitoring. Geol Soc Amer With Programs 34(6):47, Denver, USA

Haberler-Weber M (2005) Analysis and interpretation of geodetic landslide monitoring data based on fuzzy systems. Nat Hazard Earth Sys Sci 5:755–760

Hunt R (1984) Geotechnical engineering investigation manual. McGraw-Hill, London

Leonards GA et al (1993) Two case studies of slope instability in soft rock, Geotechnical Engineering of Hard Soils-Soft Rocks, Athens

Leroueil S, Locat J, Vaunat J, Picarelli L, Faure R (1996) Geotechnical characterisation of slope movements. In: Proceedings, seventh international symposium on landslides, (Senneset ed.), vol 1. Trondheim, Balkema, pp 53–74

Lollino G, Wasowski J (1994) Deep inklinometer monitoring of partially remobilished old landslide complex: case of Caramanico Terme, South-central Italy. In: 7th international IAEG congress, Lisboa

The Highway Institute documentation (1988–2010) Landslide monitoring – landslide Liberty bridge in Novi Sad, Landslide Umka, Landslides Begaljicko Brdo, Kolari and Razanj



Terrestrial Laser Scanning for the Montaguto Landslide (Southern Italy)

Domenico Denora, Lia Romano, and Giulia Cecaro

Abstract

The evaluation of the landslide surface movements is often difficult because of the inaccessibility of these impervious areas. For this reason, a powerful tool for monitoring is the laser scanning technology (TLS). The landslide monitoring by TLS is complementary to terrestrial SAR interferometry and traditional monitoring techniques. While SAR interferometry is useful for rapid detection of the displacement velocity of monitored points, laser scanning technology also allows the displacement volume quantification (Schwalbe et al. 2008). These analysis provide important information for planning hazard management actions. Experimental surveys were performed for the Montaguto landslide (Campania, Italy), the greatest of Europe, by means of laser scanner Riegl LPM-321 (Alba et al. 2005), with measurement range up to 6,000 m. Differential volume maps from different surveys were obtained. The complex morphology of the Montaguto landslide, located in the Cervaro river valley, had required a viewshed analysis for the selection of the base station locations. Detailed laser scanner acquisitions were conducted on the tip landslide zone, because of the presence of strategic mobility.

Keywords

Terrestrial laser scanning • TLS • Landslide monitoring • Displacement volume quantification • GPS • Montaguto

Introduction

The landslide of Montaguto is one of the most important landslide in Europe. It is located in South Italy, in Campania Region. The landslide concerns an hillslope on the hydraulic left of Cervaro river – that in this section drains about 135 km^2 – from 956 m s.l.m. to the river bed at 400 m s.l.m. The geological formation are related to the Faeto flysch, the Marne Argillose del 'Toppo Capuana' (clay and clayey blue-grey marls, layered with rare sandy layers; Tortonian) and the Altavilla Unit (Tortonian Middle Pleistocene) (Guadagno 2010).

The landslide is activated in the upper part by several roto-translational mechanisms and develops into an earth flow, moving along a deep and extending on the whole over a length of 3 km for a variable width of 400 m in the upper and lower parts to 100 m in the medium part (Fig. 1). The movement has involved in the last years a mass of about one milion cubic meters (Cascini and Di Nocera 2009).

Between the tip of the landslide and the Cervaro river there are two important transport infrastructures, that connected Apulia and Campania – the federal road 90 and a strategic railway – which requires a constant monitoring, carried out by the Civil Protection Department by means of SAR interferometry. In this activities, the Apulia Basin Authority (AdBP) has tested the use of modern technologies in topographic data acquisition and modelling, with particular attention to the tip zone.

D. Denora (✉) • L. Romano • G. Cecaro
Autorità di Bacino della Puglia (AdBP), 70010 Valenzano (Bari), Italy
e-mail: domenico.denora@adb.puglia.it; lia.romano@adb.puglia.it; giulia.cecaro@adb.puglia.it

C. Margottini et al. (eds.), *Landslide Science and Practice*, Vol. 2,
DOI 10.1007/978-3-642-31445-2_4, © Springer-Verlag Berlin Heidelberg 2013

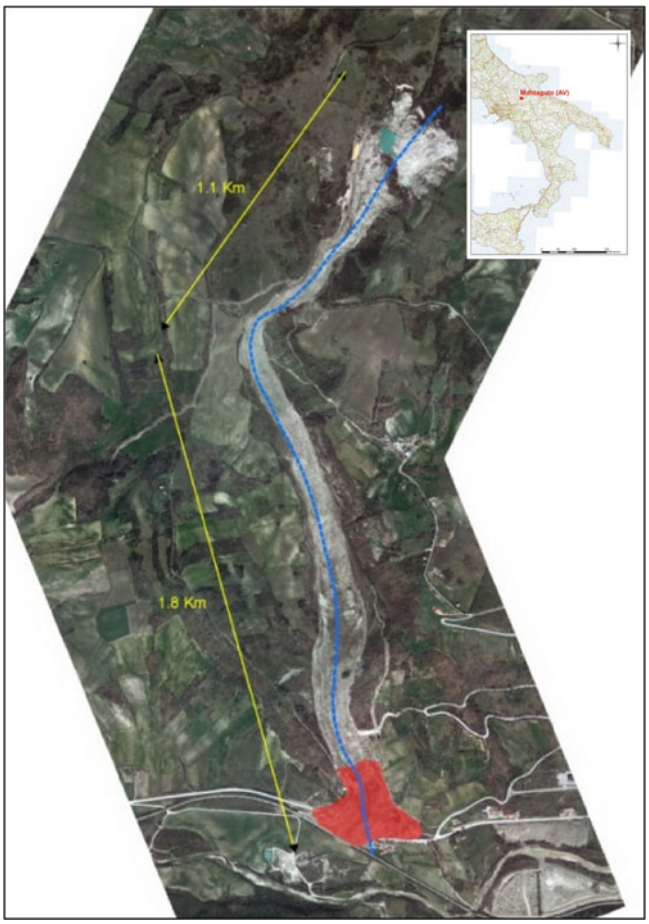


Fig. 1 The Montaguto landslide longitudinal extension with the tip zone in *red*

Table 1 RIEGL LPM-321 technical characteristics (Bornaz et al. 2008)

Max measurement range	@ rate 1,000 Hz	@ rate 100 Hz	@ rate 10 Hz
For natural targets, $\rho > 80$ %	≥1,500 m	≥2,500 m	6,000 m
For natural targets, $\rho > 10$ %	≥500 m	≥850 m	≥1,500 m
Meas. accuracy	25 mm		
Precision	15 mm		
Laser beam diverg	typ. 0.8 mrad		
Laser wavelength	Near infrared		
Meas. rate	10–1,000 points/s		

The Landslide Analysis

The Surveying Equipment

The instruments used are the Laser Profile Measuring System LPM-321 (Table 1) with a continuous electrical generator for the data acquisition system, the GPS Leica System 1200, and several 10 cm cylindrical and 50 cm flat circular retroreflectors.



Fig. 2 The viewshed analysis for LS1 scan position with a range of 3 km

A viewshed analysis (Fig. 2) based on the digital terrain model had showed the need to locate the acquisition point on the opposite hillslope of the Cervaro valley, in the LS1 scan position, for covering the whole lower part of the landslide. The distance of the landslide surface, which starts on about 1 km from LS1, detects in the LPM-321, having a range up to 6 km and a measurement accuracy of 25 mm, the suitable instrument for this long range 3D profiling, considering moreover that the acquisition range is strictly influenced by the measurement rate, by the reflectivity of materials and by the atmospheric conditions. In particular, the tip of the landslide from LS1 is totally covered by the laser scanner, from the railway to the next 1 km, with about 47 ° horizontal range and 7 ° vertical range. For time optimization, the measurement rate has been set to 100 Hz.

The Leica System 1200 is a geodetic GPS receiver (GPS GLONASS), which allows the communication through RTCM 3.0 transmission protocol to the permanent stations for differential correction data for reducing the systematic errors that decrease the accuracy of GPS positions.

3D Georeferenced Terrestrial Laser Scanning

Since may 2010, when the landslide closed the railway, four measurement campaigns were performed on the tip of the Montaguto landslide (Table 2). A great work to clear the landslide from the railway and the federal road was made, despite the continuous movement of the landslide.

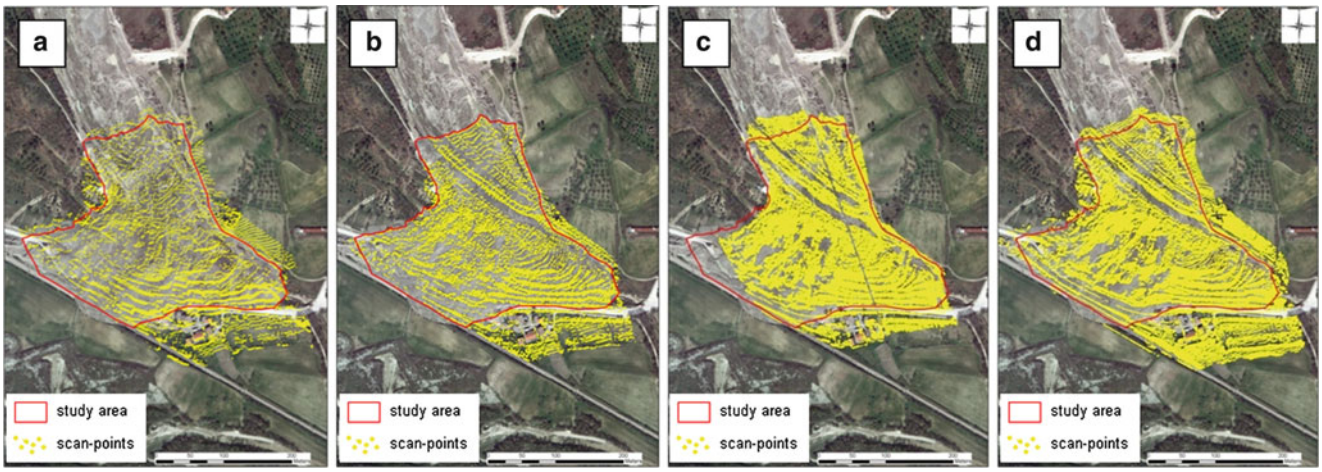


Fig. 3 The point clouds acquired for the four measurement campaigns: (**a**) May 27, 2010 (the landslide invades the railway); (**b**) November 4, 2010 (trench cut for opening the railway, cut-off drain excavation and benching); (**c**) December 1, 2010 (progression of landslide movement on the west side); (**d**) March 31, 2011 (stability conditions)

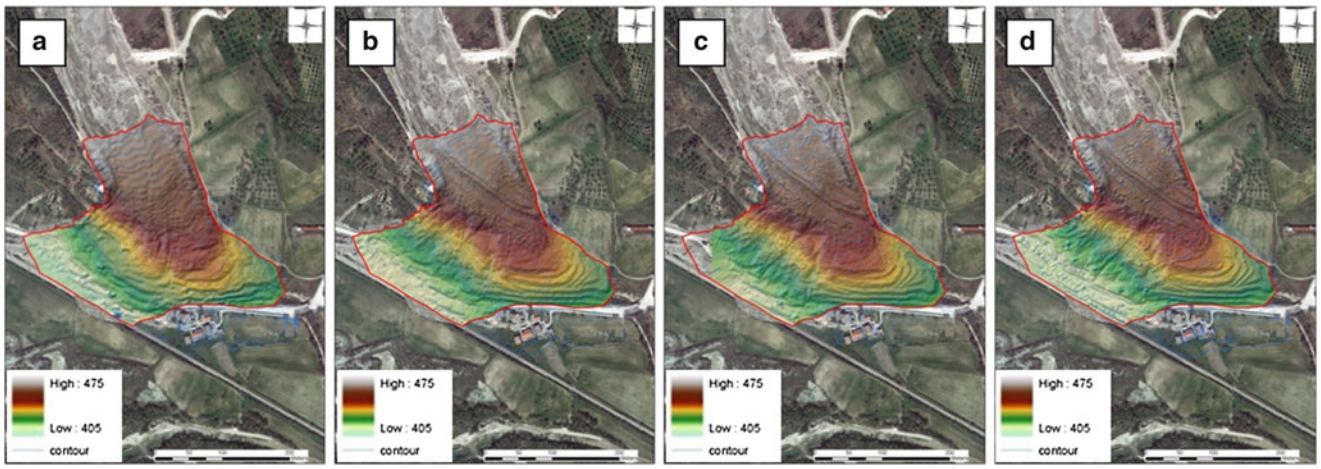


Fig. 4 The digital model terrain of the landslide tip related to previous scan acquisition

Table 2 Technical parameters of scan acquisitions

Date	T (°C)	Press (mbar)	RH (%)	N. points	Resolution (m)
05-27-10	22.0	1,020	49.1	28,796	1
11-4-10	14.7	1,000	88.4	13,460	1
12-1-10	6.4	921	77	20,777	0.4
03-31-11	13	1,016	60	189,302	0.35

For controlling the landslide, a cut-off drain was excavated in the upper part of the tip for intercepting subsurface ground-water flowing down in the main body of the landslide and a stable benching system was realized.

The laser scanning was managed by the software 'Riprofile', which allows the scan setting, the georeferencing of the point cloud acquired (Fig. 3), the post-processing of data and the export to ASCII format for GIS applications.

In particular, the scan was georeferenced in WGS84-ETRF89 projection UTM zone 33 N, placing at least four reflector-tiepoints, which coordinates were identified by the GPS receiver in RTK mode with differential correction data provided by the Grottaminarda (AV) permanent station of the smartNET ITALPOS national network. The ellipsoidical heights were processed by using Verto 3 K software (IGMI) for the geoidal heights calculation, based on the standard geoid 'ITALGEO2005', characterized by an average deviation of ± 0.04 m referred to the geometric levelling lines. About the altitude values, an appropriate data table of IGMI was analyzed taking into account the differences between the national geoid and the GRS80 ellipsoid (in the ETRS89 system), in order to convert the ellipsoid records WGS84 (ETRS89) in geoidal data, based on national altimetric networks. The roto-translation matrix was calculated for obtaining georeferenced scan acquisitions.

Due to the presence vegetation placed in the borders of the landslide, the data was firstly cleaned by filtering techniques in RISCANPRO software for obtaining a bare

Table 3 Volume analysis of reprofiling works related to three different observation periods

Period	Volume (m^3)	
	Accumulation	Emptying
May 2010	5,8076.48	3,7383.09
November 2010		
November 2010	5,3903.99	21,245.05
December 2010		
December 2010	6,445.93	169,109.92
March 2011		

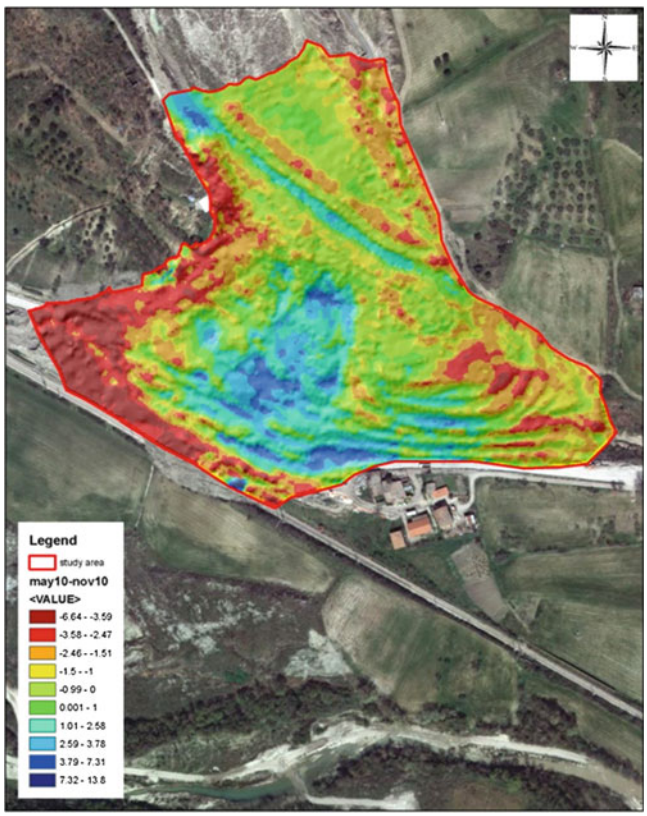


Fig. 5 Volumetric analysis from May to November 2010

ground surface. Then the scan points were interpolated by ordinary kriging method for generating DTM (Fig. 4) (Scaioni et al. 2004).

Volumetric Analysis

Since the landslide movement was in progress and works for cleaning the railway and defining stable profile were executed during the months of observation, it's not possible to quantify the slide down materials or the removal one by volumetric analysis at the landslide tip. The comparison between the terrain surfaces of different dates defines just reprofiling of landslide for anthropic or natural causes (Table 3).

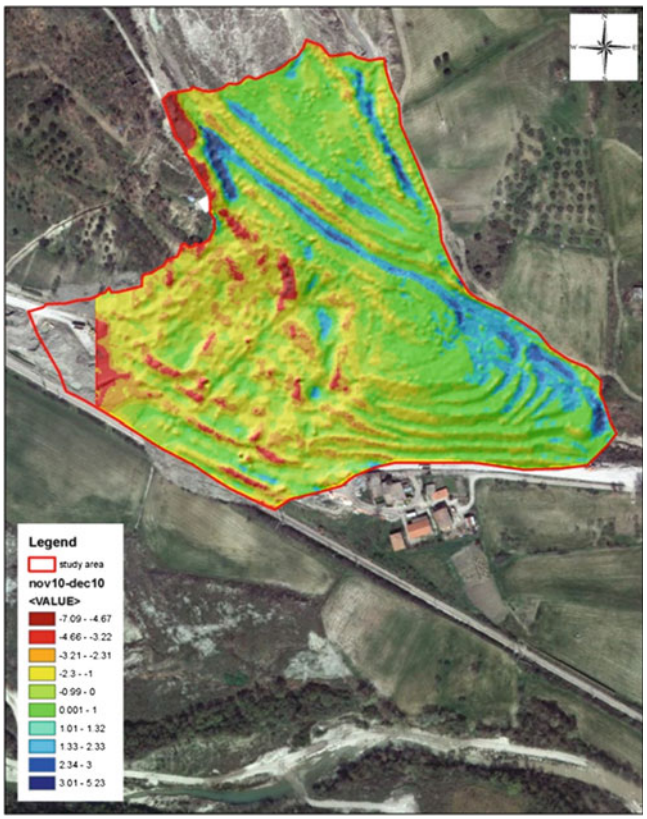


Fig. 6 Volumetric analysis from November to December 2010

Every comparison is obtained subtracting terrain elevation of the newer scan from terrain elevation of the older scan. Consequently the negative values represent material accumulation (red colors), while the positive ones represent emptying (blue colors). Anyway the range of value from −1 to +1 m is considered a no-change condition (green colors), according to the scan resolution. The hillshade effect is related to the newest digital terrain model (Guarnieri et al. 2009).

During the period from May to November 2010, works for restoring the traffic on the transport infrastructures have been realized. On the west side of landslide there's a wide emptying area that attested the reprofiling works for cleaning the federal road and the railway from the landslide material, while on the east side the benching has been reshaped. In the upper zone of the tip the cut-off drain is visible (Fig. 5). From November to December 2010, there are not substantial differences of the landslide surfaces, showing a general stable condition, although the west side continues to show landslide movement with material accumulation at the tip. On the east side there's an excavation caused by sediment transport of the drain flows (Fig. 6). In March 2011 it's clear the stop of the landslide movement in the previous months that has allowed to reprofile the hillslope for a stable setting with excavations even over 10 m (Fig. 7).

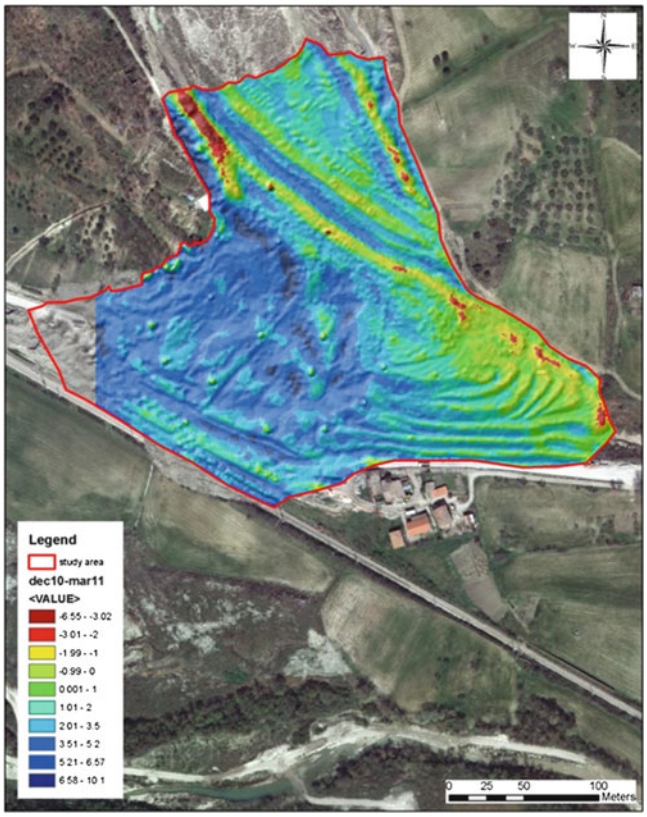


Fig. 7 Volumetric analysis from December 2010 to March 2011

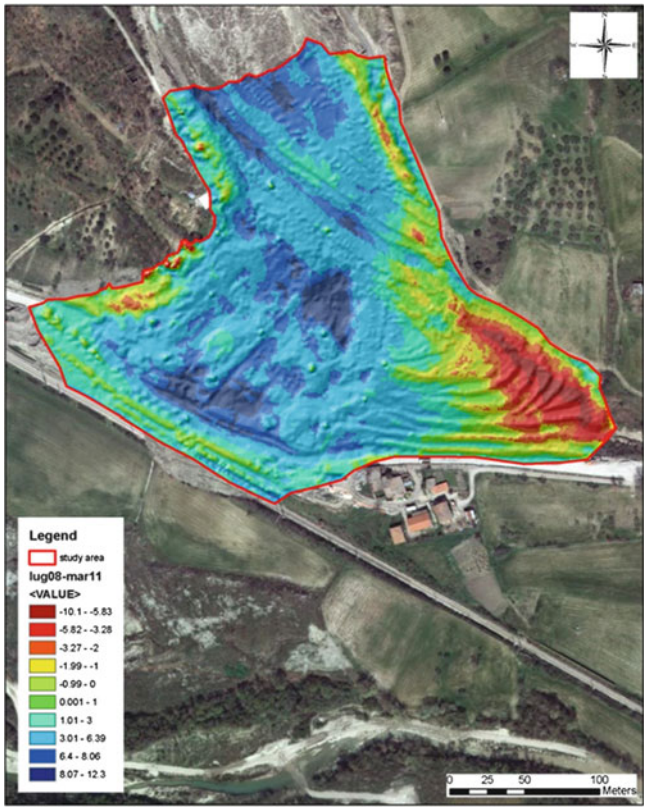


Fig. 8 Volumetric analysis from July 2008 to March 2011

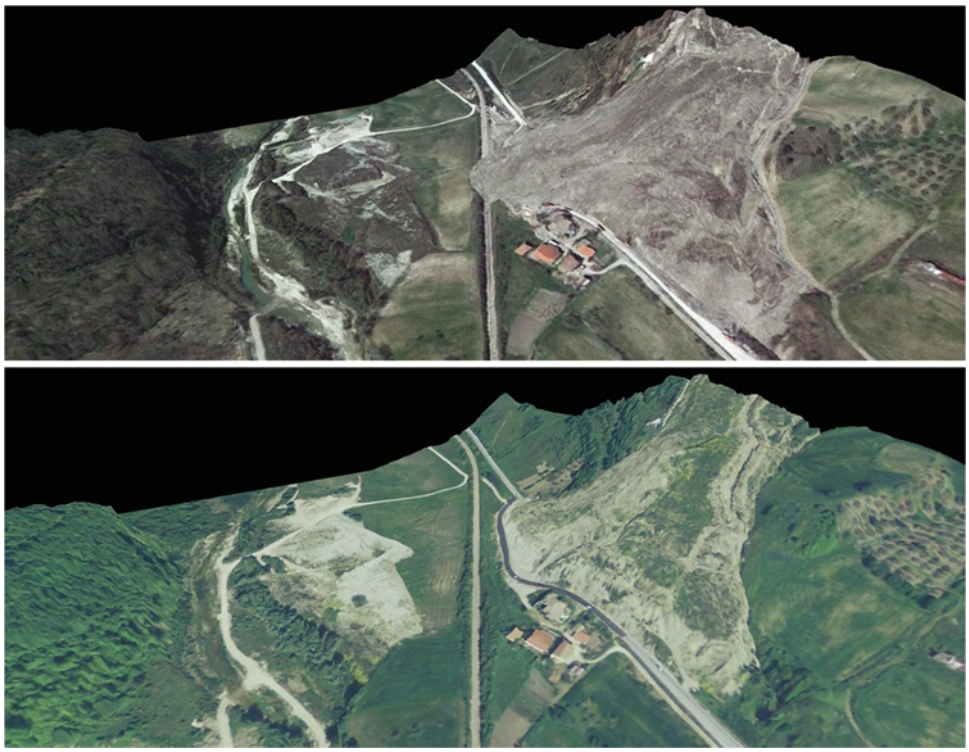


Fig. 9 3D Representation of the landslide tip in the Cervaro valley. May 2010 (*up*) and March 2011 (*down*)

Conclusion

At last, comparing the newest scan with the surface derived from the airborne laser scanning of July 2008, it's possible to mark the settlement works for reducing the slope. While on the east side the benching has given to the surface a stable assessment, the landslide movement has flowed on the west side, causing the need of continuous materials removal works. The open-cut for railway and federal road in the lower part of the tip and for draining the water in the upper part are clearly evident (Fig. 8).

The applications previously showed demonstrate the potentialities of the terrestrial laser scanner technologies for landslide monitoring. The instrument allows the high resolution DTM generation and related contour lines, the survey of impervious area.

The results of the analysis are strictly consistent with the information given by then Civil Protection Department. Moreover the combination of this technologies with SAR interferometry could provide an excellent monitoring system, that not only detects the landslide movements, but also shows where these are placed, useful in this case for transport infrastructures security (Fig. 9).

References

Alba M, Longoni L, Papini M, Roncoroni F, Scaioni M (2005) Feasibility and problems of TLS in modeling rock faces for hazard mapping. ISPRS WG III/3, III/4, V/3 workshop Laser scanning 2005

Bornaz L, Marenchino D, Nex F, Rinaudo F (2008) Riegl LPM-321 uno strumento Laser Scanner a lunga portata per i rilievi ambientali. Atti 12a Conferenza Nazionale ASITA

Cascini L, Di Nocera S (2009) Consulenza specialistica alla progettazione degli interventi di somma urgenza relativi al sistema franoso di Montaguto. Soggetto Attuatore: Struttura Commissariale Unificata ex. Art. 15 dell'OPCM n. 3591/2007

Giussani A, Scaioni M (2004) Application of TLS to support landslides study: survey planning, operational issues and data processing. In: IAPRSSIS, vol 36(8/W2). Freiburg, Germany, pp 318–323

Guadagno FM (2010) Relazione geologica tecnica allegata ai Progetti della Struttura Commissariale ex. Art. 1 OPCM 3868/2010

Guarnieri A, Milan N, Pirotti F, Tarolli P (2009) Integrazione dei dati ALS e TLS per la produzione di DTM in zone alpine. Atti 13a Conferenza Nazionale ASITA

Scaioni M, Giussani A, Roncoroni F, Sgrenzaroli M, Vassena G, (2004) Monitoring of Geological Sites by Laser Scanning Techniques. IAPRS, Istanbul, Turkey, Vol. 35(7/WG5)

Schwalbe E, Maa HG, Dietrich R, Ewert H (2008) Glacier velocity determination from multi temporal terrestrial long range laser scanner point clouds. In: XXIst ISPRS congress: commission V, WG 3, Beijing, pp 457–462



Landsliding Events Triggered by Rainfalls in the Enna Area (South Italy)

Francesco Castelli and Valentina Lentini

Abstract

The factors affecting slope stability are various, and virtually most are closely interconnected. Among these, meteoric events (or rather, the effects induced by these) are of primary importance, both as predisposing elements, and above all, as triggering factors. Detailed models describing hydrological phenomena at hill-slope scale are complex and expensive. Alternatively, simpler conceptual or empirical models can be used. These models directly correlate rainfall and landslide occurrence and may give satisfactory results both in hazard analysis and real-time forecast. Empirical thresholds are defined collecting rainfall data for landslide meteoric events and for events without landslides. In this paper, the results of a hydrological model correlating the rainfall amount and the landslide occurrences in the Enna area (South Italy) are reported and discussed.

Keywords

Landslides • Rainfall • Hydrological models

Introduction

In Italy rainfall is the primary trigger of landslides that frequently cause fatalities and large economic damage.

A number of case studies have been published describing the effects of rainfall on landslides in Italy, most important for a national system of the real-time prediction of hydrogeological hazards (floods and landslides).

D'Amato Avanzi et al. (2004) report a series of rainfall induced shallow landslides which occurred on 9 June 1996 in the Apuan Alps in north western Tuscany, Italy. The associated rainstorm was concentrated over a 150 km^2 area and 474 mm the rainfall corresponded to 21 % of the annual mean. Some 647 main landslides were recorded and were estimated to have caused damages for the value of hundreds of millions of Euros, in addition to causing the deaths of 14 people. At Pomezzana 474 mm of rain was recorded in about 12 h, with a maximum intensity of 158 mm/h, whilst at Fornovolasco 420 mm of rain fell in about 10 h, before the instrument was destroyed by either a flood or a landslide.

Frattini et al. (2004) describe a series of more than 400 landslides which occurred in May 1998 near Sarno, to the east of Naples and Vesuvius, in pyroclastic soils. The landslides were triggered by a storm event and destroyed houses and infrastructure in addition to killing a total of 159 people. Cumulative rainfall for 4–5 May 1998 were recorded by rainfall gauges at Lauro, S. Pietro, Ponte Camerelle, S. Mauro, and Sarno. Data from the Lauro gauge was considered to be the most relevant: the cumulative rainfall recorded during the 48 h event was 173 mm.

Sirangelo and Braca (2004) studied the same area as Frattini et al. (2004). The authors proposed a hydrological model, based upon a back analysis of the May 1998 events. The model includes two parts: *Rainfall-Landslide* for correlating precipitation and landslide occurrence, intended for model calibration through the reproduction of historic

F. Castelli (✉)
University "Kore" of Enna, Faculty of Engineering and Architecture, University Campus, Enna, Italy
e-mail: francesco.castelli@unikore.it

V. Lentini
Department of Civil and Environmental Engineering, University of Catania, Catania, Italy

C. Margottini et al. (eds.), *Landslide Science and Practice*, Vol. 2,
DOI 10.1007/978-3-642-31445-2_5, © Springer-Verlag Berlin Heidelberg 2013

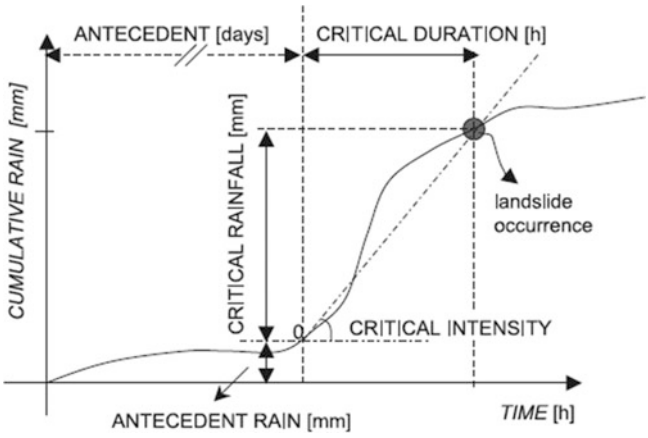


Fig. 1 Definition of rainfall parameters

events and *Stochastic Rainfall* for real-time forecasting of landslide events.

From mid-October to 22 November 2000, the Western Liguria Region experienced prolonged and intense rainfall. This was followed on 23 November by a high intensity storm of 180 mm of rain in 24 h. The landslides started between 8 and 10 h after the beginning of the storm and the most intense areal landslide activity occurred as a consequence of rainfall intensities of 8–10 mm/h (Guzzetti et al. 2004).

In dealing with debris flows and soil slips triggered by short intensity storms in the Piedmont Region Italy, Aleotti (2004) proposed an equation to correlate the rainfall intensity I calculated in mm/h and the duration D of critical rainfall event expressed in hour. Moreover, it is possible to define a value of "critical rainfall" (Fig. 1), as the rainfall measured from the time when rainfall intensity increases sharply to the time of the occurrence of the first landslide (Aleotti 2004).

On October 1, 2009 a heavy rainfall hit the limited area on the N-E part of Sicily (Italy) near the town of Messina. At the station of St. Stefano di Briga a rainfall of 223 mm occurred in 7 h with a peak of 10.6 mm in 5 min. During the event many landslides such as sliding, debris flows and mud flows occurred in 14 villages, caused 37 victims, mainly in the villages of Giampilieri and Scaletta Zanclea (Maugeri and Motta 2011).

Rainfall Thresholds

The identification of thresholds for the beginning of slope movements may play an important role in helping mitigating geo-hydrological risk.

The monitoring of meteorological, hydrological or geotechnical parameters, coupled with initial threshold values

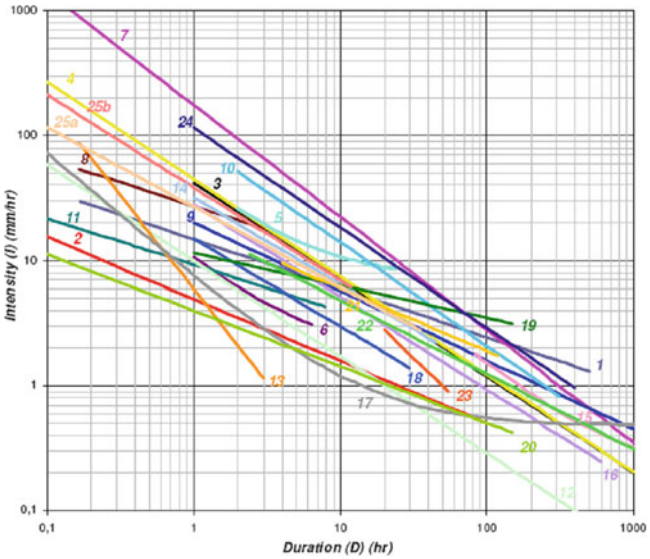


Fig. 2 Intensity-duration thresholds for landslide occurrence. Numbers refer to references listed in Guzzetti et al. (2005)

defined in different fashions, may allow for the identification of potentially hazardous conditions and to issue warning or alarm messages to civil protection authorities and the population.

The main operational advantage of rainfall thresholds, that justify their definition and application in warning systems, lays in the fact that rainfall is relatively simple and inexpensive to measure over large areas. Indeed, at several places rainfall is being forecasted with increasing accuracy.

Different approaches were proposed to determine global and local rainfall thresholds. The most commonly investigated rainfall parameters are: cumulative rainfall, antecedent rainfall, rainfall intensity and rainfall duration. Various combinations of the listed parameters have been attempted. Most of the proposed thresholds perform reasonably well in the region where they were developed, and cannot be exported to neighbouring areas. Also, their temporal accuracy remains largely untested.

The availability of data has a key role in the definition of rainfall thresholds as well the quality (proximity to study area, spatial and temporal resolution, etc.) and the quantity (number of historical information, covered period, etc.) of the data, which influence the results of the analysis.

The empirical relationship between rainfall intensity, rainfall duration, and slope instability has been thoroughly documented, and many authors have put a great deal of work estimating rainfall thresholds, also as a part of landslide warning systems.

Figure 2 (Guzzetti et al. 2005) represents the empirical relationships between rainfall intensity and rainfall duration

obtained by different authors, taking into account the area for which thresholds can be applied, the extent of the area, the type of triggered landslides, and the established threshold. The significant differences existing between the thresholds can be explained by the fact that the thresholds are based on data sets from areas with different geological, geomorphological, and climatic settings.

Generally, empirical thresholds are presented as lower limit curves separating areas with specific combinations of values of plotted variables. Physically based thresholds attempt to link regional or local rainfall measurements to local soil or geological characteristics (e.g., slope gradient, soil type, lithology, etc.) through a hydrological model.

General Scheme of Hydrological Models

To model the relationships between rainfall and landslide occurrence, studies in literature generally follow two distinct approaches: *empirical* or *hydrological* and *complete* or *physically-based*.

The first ones is based on the identification of a mobility function, which depends on characteristics of the landslide and on antecedent rainfall, and is correlated to the probability of a movement.

The second ones try to reproduce the phenomena which occur in the slope by modelling the processes of rain infiltration, recharging and recession of the groundwater and surface runoff, so determining degrees of saturation, pore pressure and relative variations in soil strength.

The hydrological or empirical models attempt to identify the landslide-rainfall relationship on the basis of observed landslides and corresponding precipitations. In most cases, models identify a threshold value Y_{cr} of a mobility function *Y(t)* which separates the conditions *impossible mobilization* and *certain mobilization*. The mobility function is a generic function, based on rainfall observed over a fixed interval before the landslide.

The mobility function *Y(t)*, depending on antecedent rainfall, is related to probability *P[E(t)]* of landslide occurrence at the time *t*:

$$P[E(t)] = F[Y(t)] \tag{1}$$

Among the various admissible relationships beetween mobility function *Y(t)* and probability *P[E(t)]*, the simplest one is given by the threshold scheme:

$$\begin{aligned} P[E(t)] &= 0 \ if \ Y(t) \le Y_{cr} \\ P[E(t)] &= 1 \ if \ Y(t) \ge Y_{cr} \end{aligned} \tag{2}$$

in which Y_{cr} is the critical value of *Y(t)*.

Identification of *Y(t)*

The mobility function *Y(t)* is defined as:

$$Y(t) = f[X(\tau), \tau \le t] \tag{3}$$

Of course, the limitation of this kind of models is the identification of the mobility function *Y(t)* that should depend on a limited number of one or two parameters (Felice and Versace 1990). These parameters can be identified though the analysis of historical data.

In many cases, *Y(t)* coincides with the average intensity of rainfall (or with the cumulated rainfall), over time intervals, ranging from 1 to 24–48 h, while the critical value, $I_{lim} = Y_{lim}$ varies with the duration of rainfall. More complex models are available in literature, but the general theoretical framework is essentially the same.

In this case the mobility function is the cumulated rainfall in a time interval θ:

$$Y(t, \theta) = \int_{t-\theta}^{t} X(\tau) \cdot d\tau \tag{4}$$

Identification of Threshold Value Y_{lim}

For rainfall-induced slope failures a threshold may represent the minimum intensity or duration of rain, the minimum level of pore water pressure, the slope angle, the reduction of shear strength or the displacement required for a landslide to take place. Thresholds can also be defined for parameters controlling the occurrence of landslides, such as the antecedent hydrogeological conditions or the (minimum or maximum) soil depth required for failures to take place.

Threshold value Y_{lim} separates the conditions impossible mobilization and certain mobilization and it can be defined as:

$$Y_{lim} = \alpha \cdot \min_{i=1,n} \left[Y\left(t_i^*\right) \right] \tag{5}$$

where $\alpha < 1$ is a coefficient obtained trough the analysis of historical data and t_i^* represent the times of beginning movements that placed in the past (Sirangelo and Versace 2002).

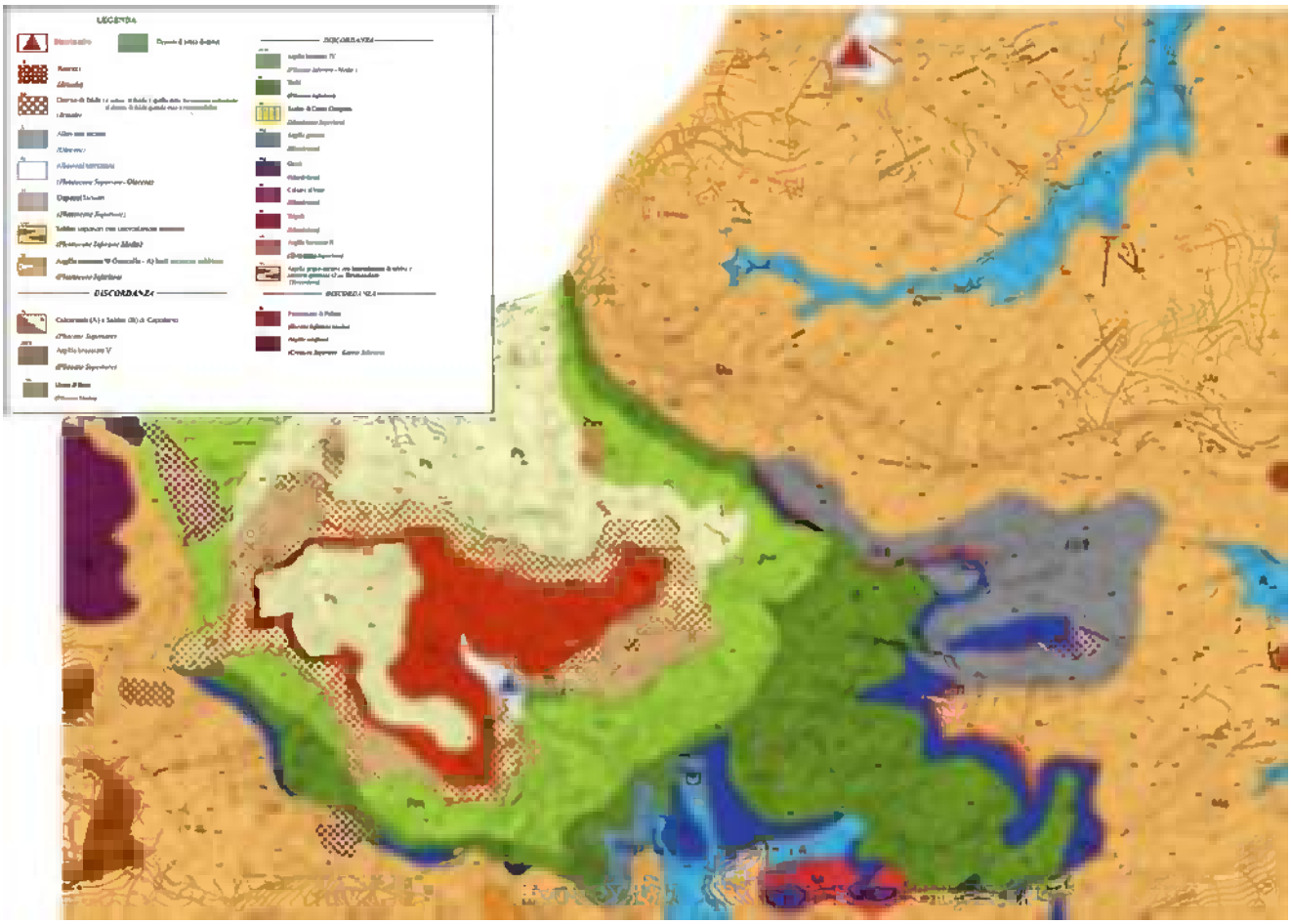


Fig. 3 Geological map of the Enna area

The times t_i^* in which the mobility function $Y(t)$ assumes the values $Y(t_i^*)$ are compared with the times of beginning movements that placed in the past.

Application to Enna Area (South Italy)

Lithological and Morphological Setting

The city of Enna is located in a hilly area, geologically made up of Numidian Flysch of Holigocene-lower age, marly and sandy brown clay of medium Miocene age, and river alluvium of Holocene age (Fig. 3).

The Enna area is characterized by the following lithostratigraphic main units: "trubi", Enna marls, calcarenites, grey-dark brown "brecciated" clays and grey-blue clays (Di Grande and Giandinoto 2002).

"Trubi": marly limestones and calcareous marls white, heavily fractured normal to the bedding. They often contain yellow-reddish ferruginous concretions, and grade upwards into an alternation of grey marls and white marly limestones.

"Argille Brecciate": grey-dark brown "brecciated" clays with diverse clasts including rare lenses a few meters thick of marly limestones or calcareous marls similar to Trubi, and white marls.

"Enna Marls": marls and grey-blue clayey marls, calcareous, white towards the base and yellow silt towards the top. They often lie unconformable above Trubi and sometimes on the older units.

"Centuripe Sandstones and Capodarso Calcarenites": they show stratigraphic continuity with the Enna Marls and quick heteropy, often within very small distances, among themselves.

Historical Rainfall Data

Climatic data on the Enna area are provided by the Sigonella Meteorological Station. The average daily temperature in the Enna area is about 14 °C and the temperature fluctuations caused by the day and night cycles are in the range between 15 °C/day.

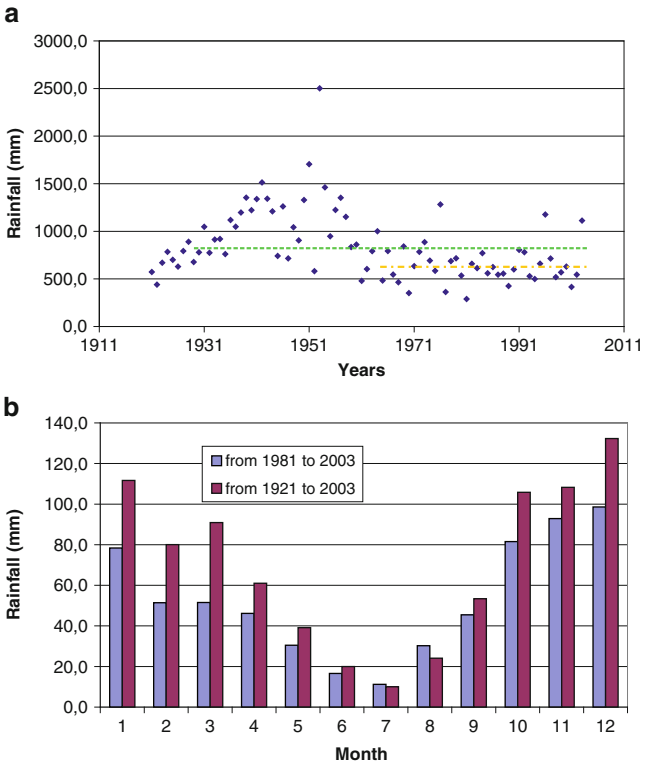


Fig. 4 Yearly (**a**) and monthly (**b**) rainfalls measured at Enna Meteorological Station

Usually, the heaviest precipitations in the area occur in November, December and January (Fig. 4). The precipitation percentage in the rainy season (October-March) accounts for 75 % of the total annual precipitation.

The rainfall is often in the form of a quick and hard torrential pouring rain, which stops suddenly. Normally it does not rain longer than 3 h. However, the precipitation amount can be very high. The highest calculated precipitation for 1 month (980 mm) occurred in December 1953.

Landslide Inventory

Landslide inventory map is the essential element of a landslide zonation and it involves the location, classification, volume, travel distance, state of activity and date of occurrence of landslides. It identifies the existing landslides and it represents a pre-requisite to perform analysis to define relationships between the distribution of landslides and the influence of parameters.

The landslide inventory map of the studied area is shown in Fig. 5. In the map with colours green, orange and yellow are indicated landslides due to mud flow, complex movement and slide respectively.

To verify the possibility to apply a hydrological method to this area (Enna-South Italy) a series of landslides events

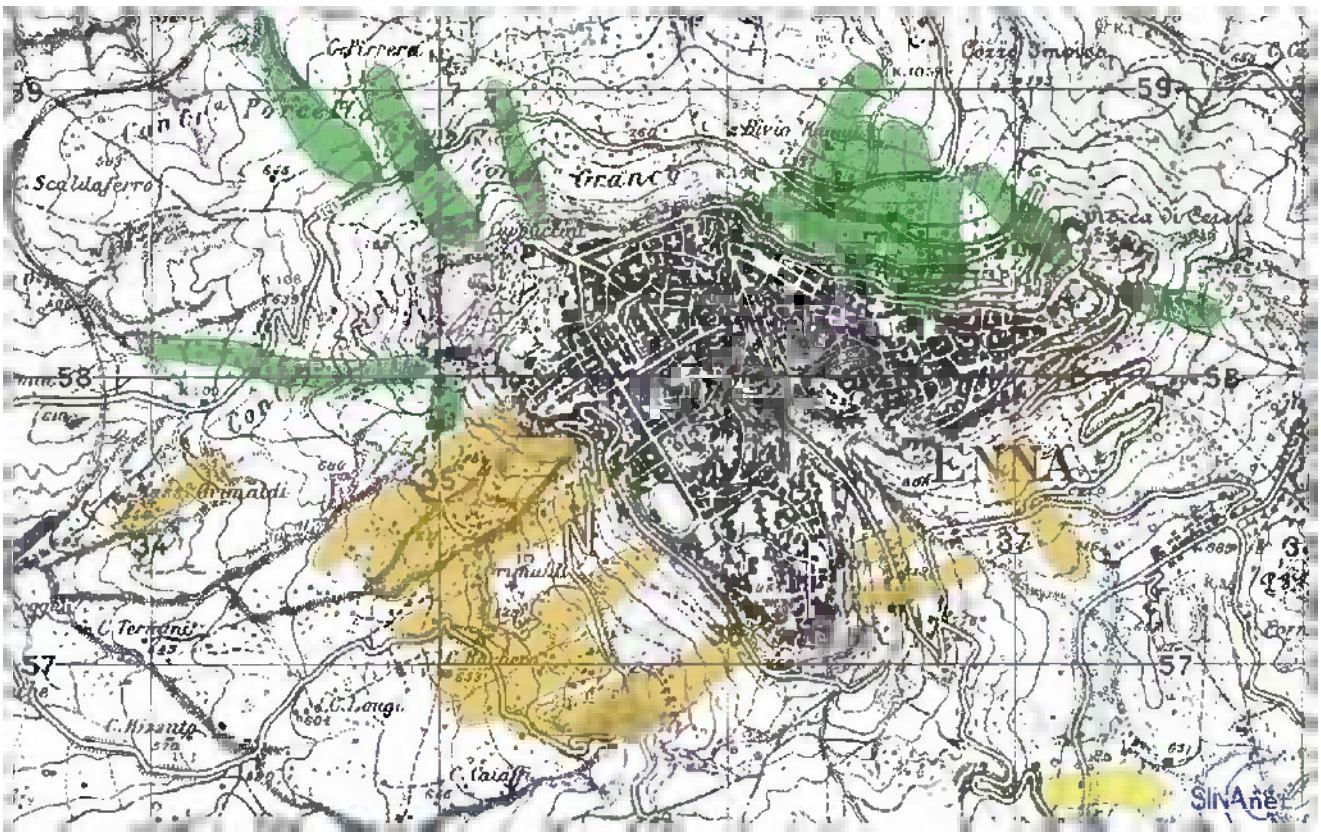


Fig. 5 Event landslide inventory map for the Enna area

Table 1 Cumulative rainfall, critical value and alert period for the landslides analysed and classified

Event *n* °	Date
1	13/10/1991
2	19/01/1996
3	02/04/1996
4–5–6–7	08/09/1999
8	30/11/1999
9–10	16/10/2003
11	30/11/2003
12–13	12/12/2003
14–15′–15″–15‴–16–17	06/03/2005
18–19	12/04/2005

triggered by rainfalls were analysed and classified with the date in which landslides occurred (Table 1).

For each of these landslides, apposite schedules were compiled. The schedules report number of event classified, the data in which movement occurred, type of movement and soil involved, slope angle and land cover. An example (10–11–15″–18) is reported in Fig. 6.

Rainfall Data

To investigate the rainfall conditions that resulted in landslides in the Enna area, rainfall measurements in the period form 1989 to 2005 obtained by Enna Meteorological Station were used (Fig. 7).

For example, the results obtained by the analysis of the event no. 1 occurred in 13 October 1991 are reported. Daily rain recorded from 13 April 1991 to 13 November 1991 is represented in Fig. 8: it can be observed that the peak of the registration coincides with the 13 October. The landslide began after intense rainfall and when the rain had exceeded 194.4 mm.

Cumulative rainfall for different values of θ is computed and five maximum values of cumulative rainfall are focused. Thus, the method consists in finding the correspondence between the data of landslide occurrence and the greatest of these values (*1 max*).

For the event no. 1 (13 October 1991) the correspondence has place for $\theta = 40$ days. Figure 9 shows cumulative rainfall for $\theta = 40$ days with $Y(t) = 255.4$ mm and a critical value $Y_{cr} = 229.9$ mm. The critical value $Y_{cr} = 229.9$ mm had exceeded for 7 days (alert period).

Table 2 summarized the result of this study in terms of cumulative rainfall, critical value and alert period for all landslides studied.

Conclusion

In the paper the application to Enna area (South Italy) of a hydrological model (Sirangelo and Versace 1992) correlating the rainfall amount and landslide occurrences is reported. A number of rainfall induced landslides occurred in the area are studied. The main objective is to perform a back-analysis in order to verify the reliability of the scheme.

The empirical thresholds described in this paper are a fundamental element of the implemented real-time warning systems, by verifying whether rainfall data permitted to reliably and promptly forecast the evolution of the considered landslide.

The main advantage of using hydrological models consists in readily allowing to identify the rainfall thresholds of slope movements whose historical movements are known, based on cheap and easy to collect data. Once calibrated, by suitably selecting a threshold for Y_{cr}, a promising tool to envisage the conditions of similar future activations in the same study area can be devised.

a

Event no.		*Movement*	*Material*	*Slop*	*Land cover*
10		Slide, Flow	Blue-gray clay with sand layers	25° - 30°	Sparsely vegetated
16/10/2003					

b

Event no.		*Movement*	*Material*	*Slop*	*Land cover*
11		Slide, Flow	Marls	45° - 50°	Sparsely vegetated
30/11/2003					

c

Event no.		*Movement*	*Material*	*Slop*	*Land cover*
15”		Slide, Flow	Blue-gray clay with sand layers	25° - 30°	Sparsely vegetated
06/03/2005					

d

Event no.		*Movement*	*Material*	*Slop*	*Land cover*
18		Slide, Flow	Blue-gray clay with sand layers	30° - 35°	Sparsely vegetated
12/04/2005					

Fig. 6 Rainfall-induced landslides in the Enna area

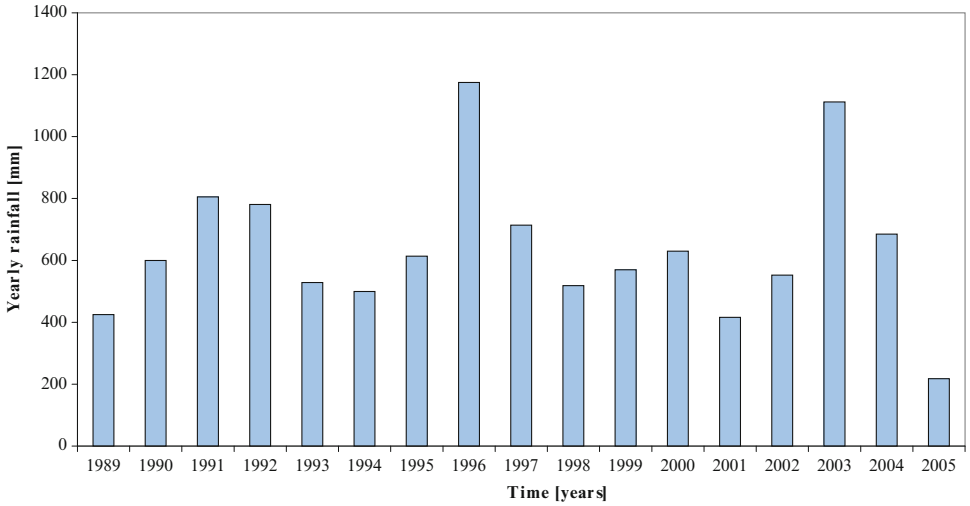


Fig. 7 Yearly rainfall recorded from 1989 to 2005

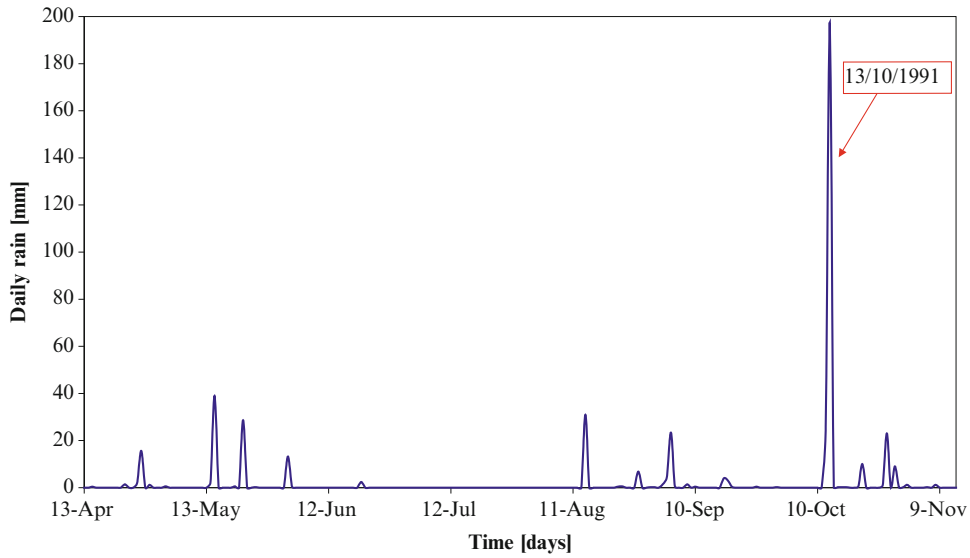


Fig. 8 Daily rain from 13 April 1991 to 13 November 1991

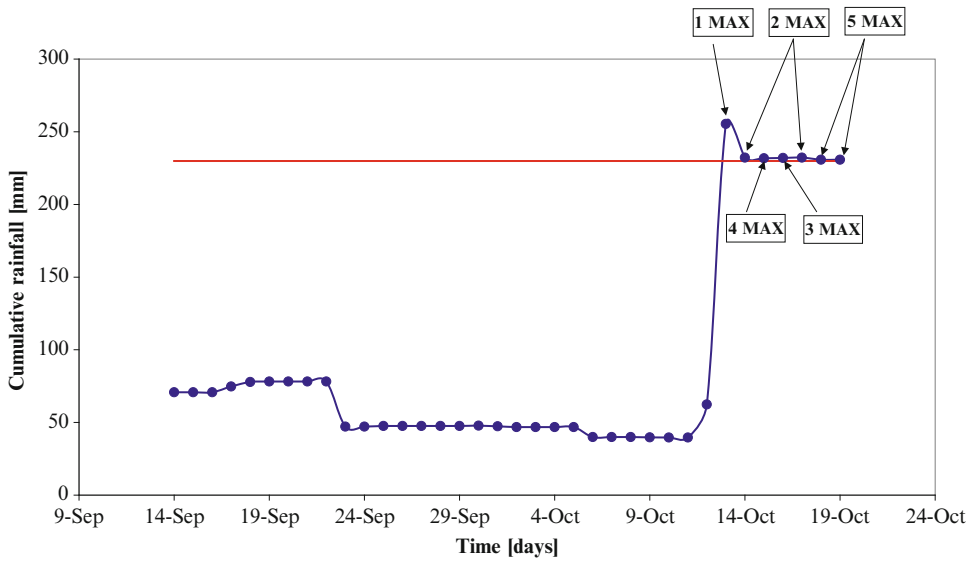


Fig. 9 Cumulative rainfall for 40 days

Table 2 Cumulative rainfall, critical value and alert period for all landslides classified

	Cumulative rainfall		Critical value	Alert period
Date	*d* (days)	*Y(t)* (mm)	Y_{cr} (mm)	W_P (days)
13/10/1991	40	255.4	229.9	7
19/01/1996	130	397.2	357.5	12
02/04/1996	120	582.4	524.2	29
08/09/1999	110	76.2	68.5	7
30/11/1999	84	270.0	243.0	7
16/10/2003	120	256.4	230.8	7
30/11/2003	47	347.2	312.5	7
12/12/2003	30	245.0	220.5	7
06/03/2005	8	41.6	37.4	7
12/04/2005	8	40.2	36.2	1

References

Aleotti P (2004) A warning system for rainfall-induced shallow failures. Eng Geol 73:247–265

D'Amato Avanzi G, Giannecchini R, Puccinelli A (2004) The influence of the geological and geomorphological settings on shallow landslides. An example in a temperate climate environment: the June 19, 1996 event in north-western Tuscany (Italy). Eng Geol 73(3–4):215–228

Di Grande A, Giandinoto V (2002) Plio-Pleistocene sedimentary facies and their evolution in centre-south-eastern Sicily: a working hypothesis. Eur Geosci Union Stephan Mueller Spec Publ Ser 1:211–221

Felice E, Versace P (1990) Identificazione delle piogge capaci di innescare movimenti franosi. In: Proceedings of the XXII Convegno Nazionale di Idraulica e Costruzioni Idrauliche, Cosenza Italy, 4–7 Ottobre, pp 343–369

Frattini P, Crosta GB, Fusi N, Dal Negro P (2004) Shallow landslides in pyroclastic soils: a distributed modelling approach for hazard assessment. Eng Geol 73:277–295

Guzzetti F, Cardinali M, Reichenbach P, Cipolla F, Sebastiani C, Galli M, Salvati P (2004) Landslides triggered by the 23 November 2000 rainfall event in the Imperia Province, Western Liguria, Italy. Eng Geol 73:229–245

Guzzetti F, Peruccacci S, Rossi M (2005) Definition of critical threshold for different scenarios. Action 1.16 Progetto Europeo Riskaware (INTERREG IIIB CADSES 3b064)

Maugeri M, Motta E (2011) Effects of heavy rainfalls on slope behaviour: the October 1, 2009 disaster of Messina (Italy). Geotechnics and earthquake geotechnics towards global sustainability. Susumu Iai Editor. ISBN/ISSN: 978-94-007

Sirangelo B, Braca G (2004) Identification of hazard conditions for mudflow occurrence by hydrological model. Application of FLaIR model to Sarno warning system. Eng Geol 73:267–276

Sirangelo B, Versace P (1992) Modelli stocastici di precipitazione e soglie pluviometriche di innesco dei movimenti franosi. In: Proceedings of XXIII Convegno Nazionale di Idraulica e Costruzioni Idrauliche, 31 Agosto–4 Settembre 1992, Florence, Italy, pp D361–D373

Sirangelo B, Versace P (2002) Un modello probabilistico per la predizione in tempo reale delle altezze di precipitazione a scala oraria. In: Proceedings of XXVIII Convegno Nazionale di Idraulica e Costruzioni Idrauliche, 16–19 Settembre 2002, Potenza, Italy, pp 395–414



Assessing Volume Earthwork by Using Unconventional Photogrammetry

Cheng-Yang Hsiao, Pao-Shan Hsieh, and Shu-Yeong Chi

Abstract

"Unconventional Photogrammetry" is a measurement methodology which does not require "Camera Calibration" and can use regular consumer camera. The calculation of its "internal and external parameters" is more complicated and less precise than "Traditional Photogrammetry". But when disaster occurs, Unconventional Photogrammetry can use readily available photos to reconstruct its 3D terrain data very quickly. By comparing this reconstructed terrain data with the terrain data before the disasters, we can quantify the changes in elevation during disasters.

In this paper, we chose a large-scale slope failure event which occurred on the Cidu section of Formosan Freeway on 2010/04/25 at 14:33 and used "Unconventional Photogrammetry" to reconstruct terrain data from two different periods. We estimated that the earthwork volume of the landslide was around 225,078.5 m^3; and this is close to the result published by Ministry of Transportation and Communications R.O.C. (2010a). It shows that this method is indeed feasible and is able to effectively, economically, rapidly, and quantitatively measure the terrain elevation variations before and after disasters.

Keywords

Unconventional photogrammetry • Computer vision • SIFT • SfM • Earthwork volume

Preface

Because of the many recent natural disasters, measurement methods and their protocols are being studied by the international experts (Ke Tao et al. 2010). They are usually referred to as "unconventional photogrammetry." It differs from the conventional photogrammetry in that it requires lower precision and has less limiting requirements. Its primary feature is its ability to utilize various image data that are easy to obtain such like post-disaster random aerial photos, UAV photography, photos provided by the locals or media and so on. Further, its data processing is semi-automatic, very convenient for post-disaster preliminary investigation. As digital camera becomes more popular, many disaster photos are taken at the site. However, due to these photos are often taken randomly in complications location and without coordinates, then this often look like convergent photography, not traditional parallel photography and not suitable for traditional photogrammetry (see Fig. 1). Because of the vast improvement in performances such as resolution and sampling rate and the development in measurement theories, digital photogrammetry begins to be used in the measurements and determination of different physical values as well as topographic maps and instant post-disaster data processing. Chen Chien-Chou et al. (2010) successfully replaced high-precision speedometer with consumer-style digital camera in determining the various modal parameters of stayed-cable. Sun Min (2007) and Zhao Xiao et al. (2004) also used digital camera to obtain industrial-grade precision

C.-Y. Hsiao (✉) • P.-S. Hsieh • S.-Y. Chi
Geo-technical Engineering Research Center, Sinotech Engineering Consults, Inc, Taipei, Basement, No. 7, Lane 26, Yat-Sen Road, Taipei 11071, Taiwan

C. Margottini et al. (eds.), *Landslide Science and Practice*, Vol. 2,
DOI 10.1007/978-3-642-31445-2_6, © Springer-Verlag Berlin Heidelberg 2013

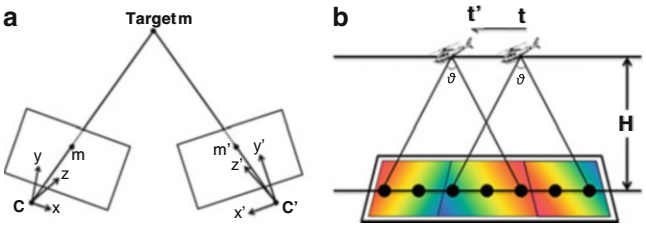


Fig. 1 Convergent and parallel photography: (**a**) convergent photography, (**b**) parallel photography

3-dimensional terrains through computer vision's multiple view geometry technology. In the 2010 Unconventional Photogrammetry Seminar hosted by Taiwan's Cheng Kung University, China's Wuhan University presented their protocols and results in data acquisition and processing during the 512 Sichuan earthquake through non-traditional photogrammetry (Ke Tao et al. 2010; Zhang Yong and Ke Tao 2010; Sun Ming-Chuan and Duan Yan 2010). Therefore, international experts classified Scale-Invariant Feature Transform (SIFT), Structure from Motion (SfM), and multi-view geometry as unconventional photogrammetry. Methods adopted by this study use either calibrated or uncalibrated camera to take a series of photos to calculate the motion parameters during the photographing and establish the related 3D geometric data (Lie Wen-Nung and Wei-Ji Chen 2010). This is an extremely popular 3-dimensional recreation in the field of Computer Vision (Pollefeys et al. 1996; Triggs 1997; Kraus 1997; Meng and Hu 2003; Zhao Xiao et al. 2004; Habed and Boufama 2004; Wang Liang fen 2010). SfM uses the Self-Calibration technology to acquire the relative camera position of each photo (Maybank and Faugeras 1992; Faugeras 1992; Pollefeys 1999; Lei et al. 2001; Zhang and Ou 2001) to obtain camera's rotation and translation parameters. From these two parameters and the axis that going through the point of origin, every photo is calibrated to the same criteria. In other words, 3-dimension recreation is conducted through multiple view geometry (Gordon and Lowe 2004; Sun Min 2007).

This study used the large slope failure at the 3.1 km mark of Freeway No. 3 on April 25, 2010 as a case study. Panasonic LX3 is consumer-style digital camera which was used to take images before and after the debris removal from different angles. 3-dimensional cloud point data were obtained from these images through unconventional photogrammetry. After some editing, the range of application was determined by using high-precision GPS measurements as the ground true data to verify the error in cloud point data. 3-dimensional graphics software Surfer was used to compare the digital terrains before and after debris removal to assess the volume of earth removed at this area in this particular event.

The Process of Unconventional Photogrammetry

Massive slope failure struck the right side of southbound Freeway No. 3 between Keelung and Hsichih on April 25, 2010 at 2:33 p.m. (Ministry of Transportation and Communications 2010b) The failure occurred on a windless, rainless, sunny day. Masses of debris destroyed the Dapu Bridge above Freeway No. 3 and buried six lines (including both northbound and southbound) of the freeway. The Jinshan-Keelung section was completely shutdown for both ways during the rescuing/repairing period. The estimated re-opening date was postponed from May 25, 2010 to June 1, 2010, with only conditional opening. Two-way traffic was then completely restored for all six lines, and the restrictions were lifted.

Because the collapsed earth volume cannot be easily estimated immediately after the disaster struck and safety procedures are complex and time-consuming, the re-opening data is prone to be delayed. Timely measurement/assessment of collapsed earth volume conducted after the disaster helps with the removal planning. Moreover, in a large disaster area, the distribution of hazards is often sporadic, and traffic is often disrupted, which makes manpower support difficult. This is further compounded by the fact that there are fewer equipments and operators that can perform quick measurement (i.e. LiDAR). Timely terrain measurement of all disaster areas is therefore difficult. Acquiring timely quantified data and, consequently, assessment of further earth removal measures are difficult.

The step of Assessing Volume Earthwork by Using Unconventional Photogrammetry are illustrated below:

1. Photographing Target in Multi-angle: 3-dimensional re-creation is similar to stereo vision. More than two photos taken from different angles are required for such a recreation. Longer the focal length from the target requires more photos taken from same distance and same angle (see Fig. 2). However, the resolution is better, which improves the accuracy and density of recreated 3-dimensional cloud point data, and as a result, the computer processing time is longer. Finally, these cloud point data undergo coordinate conversion by using reference control points. In order to identify these reference control points, the experiments performed in this study suggest they should contain at least 7×7 pixels.
2. Image Matching: Feature detection must be performed first, followed by feature matching. Feature must be robust and describable. This robustness requires the particular feature to maintain its invariance in rotation, scale, perspective, and brightness. By compiling statistics on feature points and through conversion or combination, they are transformed into descriptive formats that are

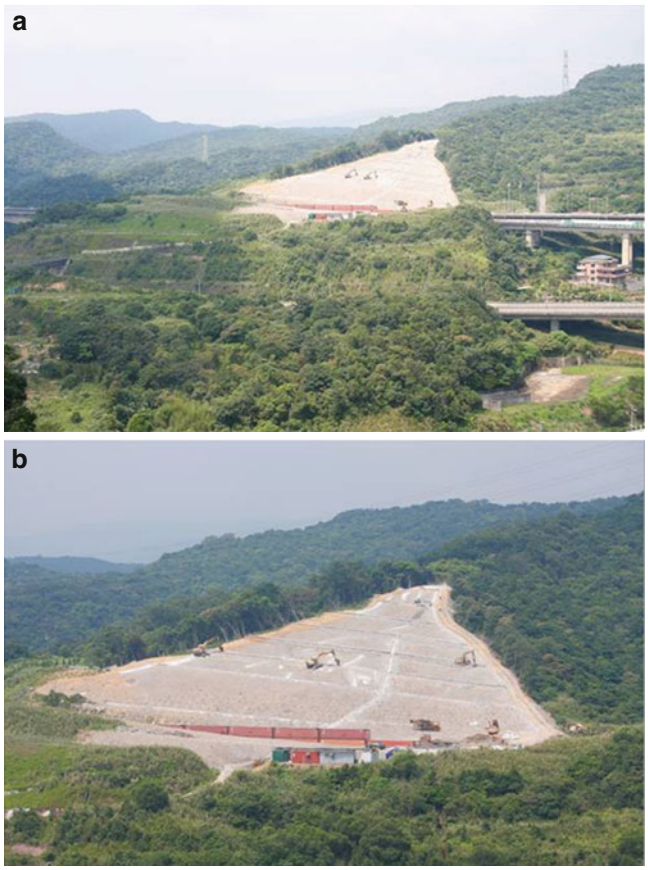


Fig. 2 Photos with different focal lengths at the same shooting place (Shorter focal length allows greater field of vision but has lower resolution): (**a**) short focal length (36 mm), (**b**) long focal length (70 mm)

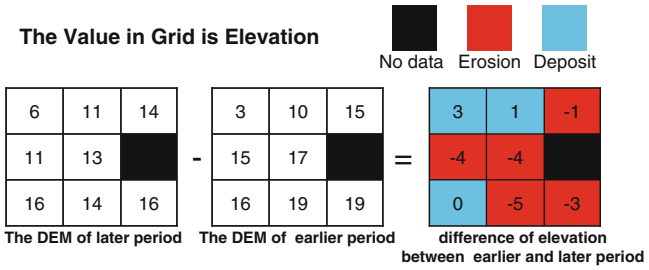


Fig. 3 Calculation of terrain change (Modified from Chen-Yang Hsiao 2009)

easily identifiable and matched. From there, robust match of two very different images can be performed. Therefore, this study used SIFT algorithm (Lowe 1999, 2004, 2006), which include "eigenvector creation" and "eigenvector matching" (Hu and Zhao Hui 2004). This allows acquisition of scale and rotation invariance as well as description operator to accomplish a good image match.

3. Acquisition of Camera Position and Parameter: Two images that have the most feature point matches are selected as the starting point. Sparse Bundle Adjustment Library (Lourakis and Argyros 2004) is used to reduce the target functions in each calculation cycle. Adjacent photos with sufficient feature point matches are then added in order. SfM cycle is repeated to calculate the camera position and parameters in each photo of the target until no photo is available for 3-dimensional recreation (Noah et al. 2010).
4. 3-dimensional Reconstruction: 3-dimensional reconstruction is based on the calculation of 3-dimensional cloud point data. This study used Multi-View Stereopsis (MVS) (Yasutaka and Jean 2010) and conducted calculation on the 3-dimensional cloud point data of specific images that already have camera parameters: MVS is accurate and efficient. Its calculation of the 3-dimensional cloud point data is also concentrated with the original RGB color codes.
5. Coordinate Transformation: 3-dimensional cloud point data of the target is converted from coordinates in the relative areas to those in the real world through reference control points. When conducting 3-dimensional recreation using non-metric camera, the distribution of the control-reference points need to satisfy calculation conditions. The entire area to be measured should be under control as much as possible. Too many reference control points, however, do not improve the precision. Six or more reference control points are recommended for coordinate conversion (Wang Lei 2002).
6. Camera is used as basis for data measurement, and the primary source of error is the camera and 3-dimensional recreation algorithm. Seitz et al. (2006) pointed out the accuracy of a 20 cm wide object in a 300,000 pixel (640 × 480) photo in most current 3-dimensional recreation algorithms can reach 0.1 cm. Recently, the accuracy of many photogrammetry by non-metric camera already can satisfy the requirement in creating topographic maps with scale between 1:100 and 1:200 (Wang Lei 2002). Measurement accuracy is very important to estimating terrain difference. Understanding the accuracy of terrain data is critical to determining the real difference from measurement error. Hsiao et al. (2009) used airborne LiDAR with accuracy of 50 cm as an example. If the terrain elevation difference between two periods is less than 50 cm, it is not recommended to be directly used in analysis and estimation. Therefore, this study used the reputable German brand Leica's high-precision GPS to measure and to recreate the 3-dimensional cloud point data to conduct measurement error comparison.
7. 3-dimensional cloud point data often include vegetation and other extraneous features (i.e. bulldozer or poles, etc.). Therefore, manual editing such as cloud point removal or elevation reduction should be conducted.

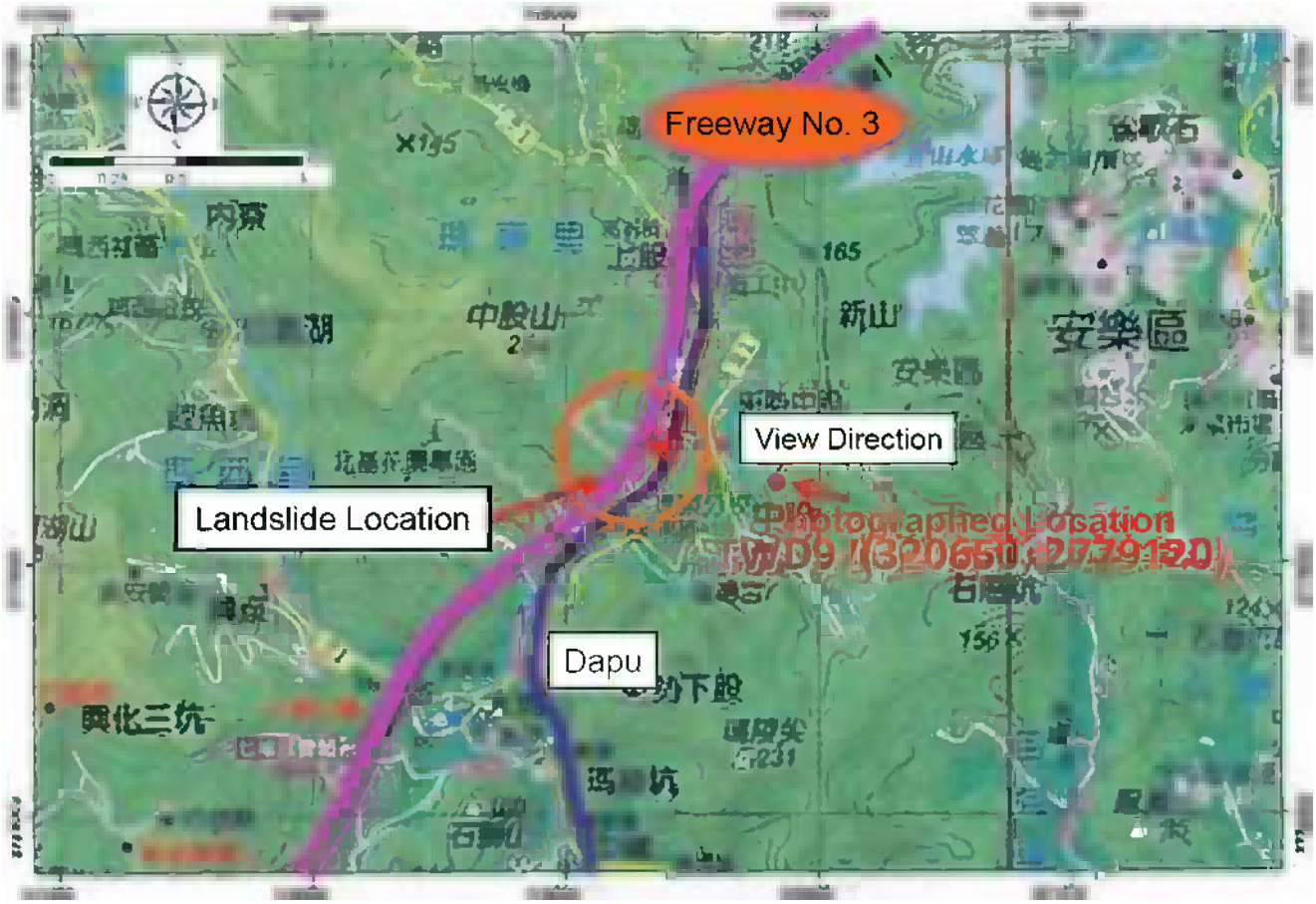


Fig. 4 Photographed location (From Ministry of Transportation and Communications 2010b)

3-dimensional scientific graphics software Surfer is then used to compare the digital terrains before and after the earth removal to estimate the collapsed earth volume. Figure 3 is a diagram that simulates the volume calculation of terrain changes. The high-precision digital terrain from the earlier period was subtracted from that of the later period. A negative grid value means outgoing earth volume, and a positive grid value indicates incoming earth volume. The result is multiplied by the area of the digital terrain grid, and that gives the terrain change within a single grid. Consequently, the earth volume removed/collapsed is the sum of the terrain change volumes.

Case Studies

This section uses the estimation of earth removal volume from the Dapu dip slope failure as a case study. 3-dimensional recreation, measurement error comparison, and collapsed earth volume estimation are described below.

3-Dimensional Recreation

After the collapse at the 3.1 km mark of Freeway No. 3, we arrived at the clearing on the Tzu-chiang Industrial Road (see Fig. 4) across from the disaster site to photograph the site (see Fig. 5) at 3:00 p.m. on April 25, 2010 (9 photos taken) and at 1:00 p.m. on September 16, 2010 (52 photos taken). Next, image matching and SfM calculation were performed on these photos. 5 photos from before the removal and 26 photos from after the removal were selected for 3-dimensional recreation, producing 964,021 and 1,590,206 cloud point data respectively. Finally, seven reference points measured by high-precision GPS coordinates were used for conversion to the real world and as reference control points (see Table 1). Figure 6 is the result of 3-dimensional recreation of the cloud point data

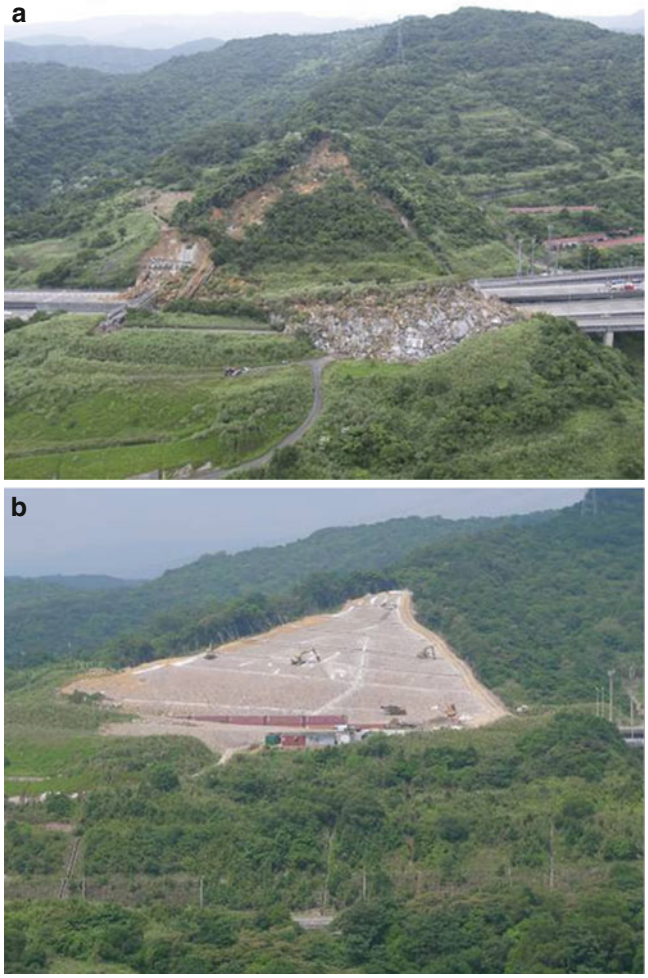


Fig. 5 Before and after the removal (**a**) April 25, 2010, (**b**) September 16, 2010

Table 1 Result of measurement by high-precision GPS coordinates

No.	TWD97_X	TWD97_Y	Elevation (M)	Purpose
1	320,092.16	2,779,282.87	111.25	Coordinate conversion
2	320,024.04	2,779,289.75	128.08	
3	319,998.46	2,779,288.23	134.63	
4	319,978.13	2,779,292.41	140.52	
5	319,958.26	2,779,299.91	146.63	
6	319,949.26	2,779,291.17	146.40	
7	319,962.33	2,779,276.91	142.65	
8	320,064.65	2,779,253.63	114.62	Error comparison
9	320,063.61	2,779,252.56	114.89	
10	320,027.11	2,779,266.49	125.31	
11	320,026.10	2,779,265.24	125.47	

(a) and (b) are cloud point data that contain 3-dimensional coordinates and RGB color codes (i.e. vegetations, poles, and bulldozers, etc.).

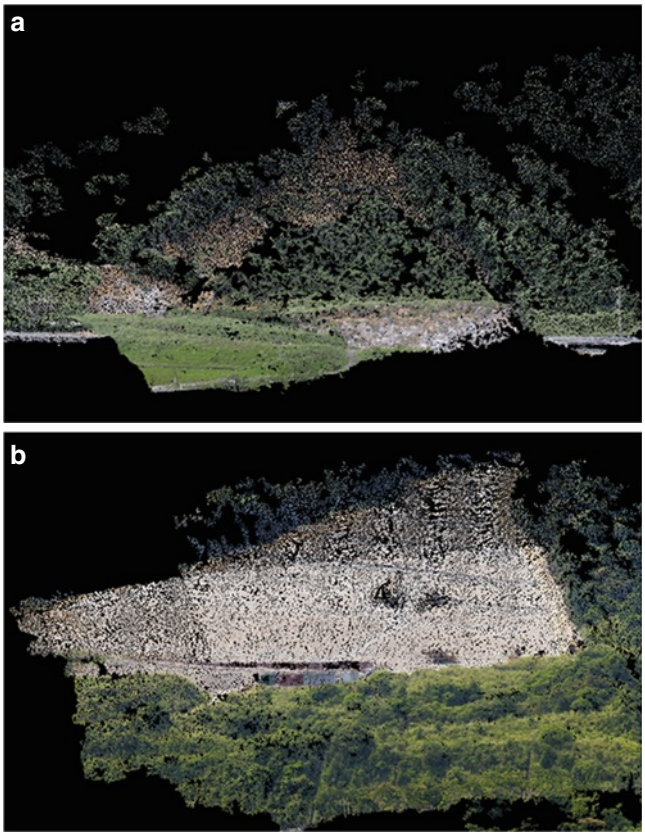


Fig. 6 3-dimensional cloud point recreation (**a**) April 25, 2010. (**b**) September 16, 2010

Measurement Error Comparison

Comparing the feature point coordinates from 3-dimensional recreation with the result of high-precision GPS site survey, the elevation error is between 11 and 16 cm (see Table 2) and meets the terrain measurement acceptance criteria by the Urban and Rural Development Branch of the Construction and Planning Agency (Wu et al. 2007). To increase its accuracy, cross-matching among different algorithms or upgrading camera equipments to increase resolution can reduce estimation error through comparison of standard indoor models.

Assessment of the Collapsed Earth Volume

After completing manually editing the cloud point data, Surfer was used to establish 5 × 5 m digital elevation models (DEM) before and after removal. Collapsed earth was visible on the slope before removal (see Fig. 7). After the removal, the slope was smooth and without any remaining earth (see Fig. 8). Figure 9 is illustrates the elevation changes before and after the earth removal.

Table 2 Error comparison

GPS measurement	TWD97_X	320,064.65	320,063.61	320,027.11	320,026.10
	TWD97_Y	2,779,253.63	2,779,252.56	2,779,266.49	2,779,265.24
	Elevation (m)	114.62	114.89	125.31	125.47
3-D recreation	TWD97_X	320,064.26	320,063.80	320,026.35	320,026.19
	TWD97_Y	2,779,250.99	2,779,250.83	2,77,9267.72	2,779,267.73
	Elevation (m)	114.78	114.76	125.42	125.31
Absolute elevation difference (m)[a]		0.16	0.13	0.11	0.16

[a]Absolute elevation difference = |GPS measured ellipsoid height – 3-D recreation measured ellipsoid height|

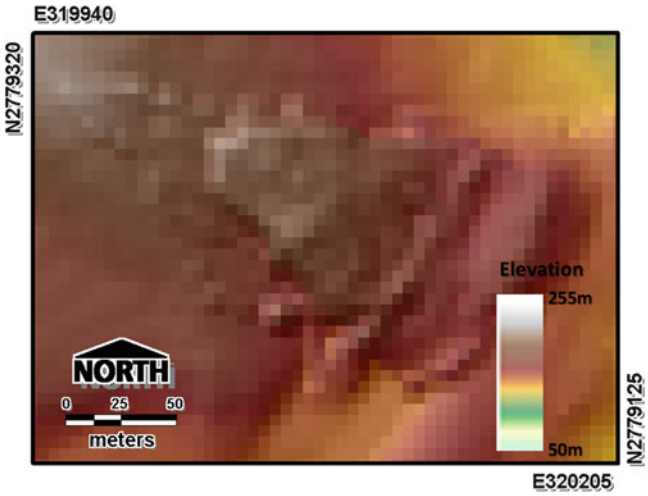


Fig. 7 Topographic shading map before removal

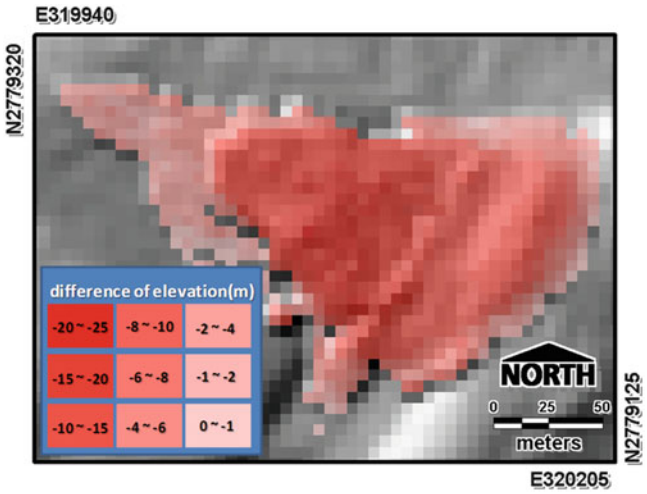


Fig. 9 Distribution of terrain elevation changes before and after the removal

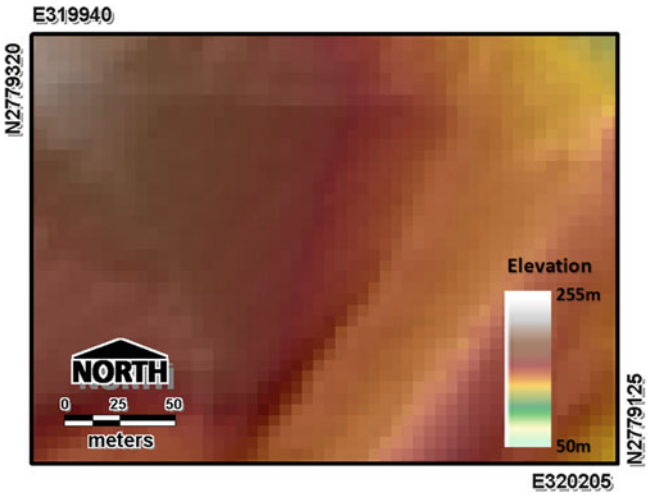


Fig. 8 Topographic shading map after removal

The estimated earth removed was approximately 225,078.5 m^3. Compared against the data posted by the Ministry of Transportation and Communications (2010a) of 219,527 m^3 removed, they were close with only 2.5 % of difference.

Conclusion and Recommendations

The unconventional photogrammetry described in this article uses self-calibration and does not require professional metric camera. Moreover, it is simple to operate, has few limitations, and can be applied to historical photos or photos taken by anyone after the disaster, drastically increasing its flexibility. Case studies suggest the measurement error was sufficient to assess the collapsed earth volume in this event, which was similar to the result of the final removal. Its effectiveness was thus confirmed. In addition to ground photography, we recommend combining UAV to overcome the limitation of photographing angles from the ground. Although self-calibration isn't yet stable, sometimes has lower accuracy, and has a high error rate which often results in failed 3-dimensional recreation, these can be compensated by collecting/taking more of target's photos to increase the 3-dimensional recreation success rate. If calibration before photographing is possible and the environment isn't excessively complex, we recommend using high-precision camera calibration (i.e. Tsai's Two-step Calibration (Tsai 1986), Weng's Calibration (Weng et al. 1992), Zhang's Calibration Square (Zhang 1999, 2000), Bouguet's Calibration (1999)

which is based on the Duality Principle, Heikkilä (2000) Calibration that uses circular symbol as the control point, and Ahn et al. (2001) Calibration, etc.) to replace the self-calibration raised by this article to reduce camera's calibration error rate.

Future Application

Unconventional photogrammetry can effectively, economically, and expediently perform terrain measurement. We recommend future application in the following areas:

1. Identifying the Disaster's Extent on the Surface and Scale: It can be used to establish quantified data for preliminary assessment of the disaster (i.e. failure, deposit, etc.) to effectively and timely reflect terrain changes as a reference for future policy making.
2. Geological Survey: For inaccessible locations (i.e. the other side of a canyon), it can be used to study the direction and angle of the formation.
3. Soil Erosion Investigation: Data obtained by erosion pins are merely points, but combining this method, sweeping data across the entire area can be acquired.
4. Quantifying Debris Flow and Failure Evolution: Long-term monitoring of the same debris-flow or failure region can establish its history.
5. Verifying 3-dimensional Digital Slope Simulation: Currently, 3-dimensional digital slope simulation is a hot topic. The development of rock slope's weak planes and expedient terrain measurement before/after the disaster are critical to proposing failure mechanism, setting model's boundaries, and correcting simulation parameters. The 3-dimensional digital rock slope simulations in Taiwan are mostly rockfall landslides (Ku et al. 1996, 2006; Ke Te-Chih and Chen 2006; Lo 2010), and the parameters often lack complete development of rock slope's weak planes and the digital elevation models before/after the disaster. This study provides a quick method to acquire relevant digital simulation data(including weak plane distribution such as tension fissures, joints, cleavages, schistosity). The accuracy of model's boundaries and the parameters entered are drastically improved, providing an important basis for an expedient determination of landslide's mechanism in the future.

Acknowledgments This study is indebted to Lecturer Chen-Teng Wu from the e-GPS Institute at Ching Yun University and Agent Yu-Cheng Hong from NexSurv for their assistance and suggestions.

References

Ahn SJ, Rauh W, Kim SI (2001) Circular coded target for automation of optical and 3D-measurement camera calibration. Int J Pattern Recogn Artif Intell 15:905–919

Bouguet J-Y (1999) Camera calibration from points and lines in dual-space geometry, 1999 technical note. URL: http://www.vision.caltech.edu/bouguetj/. Last accessed 3 Aug 2011

Chen CC, Cheng HZ, Wu WH, Lai GL, Xie YD (2010) The research of digital photography technology for measuring the vibration of the stayed cable parameter identification. 2010 Workshop on unconventional photogrammetry, Tainan (in Chinese)

Chen MM, Wei CY, Fei LY (2010b) The dip slope along geological analysis at National Highway No. 3. Geology 29(2):12–15 (in Chinese)

Faugeras O (1992) What can be seen in the three dimensions with an uncalibrated stereo rig? In: Proceedings of the 2nd European conference on computer vision, pp 563–578

Gordon I, Lowe DG (2004) Scene modeling, recognition and tracking with invariant image features. In: Proceedings of international symposium on mixed and augmented reality, ISMAR, pp 110–119

Habed A, Boufama B (2004) Camera self-calibration: a new approach for solving the modulus constraint, vol 4. ICPR, Washington, DC, pp 116–119

Heikkilä J (2000) Geometric camera calibration using circular control points. IEEE Trans Pattern Anal Mach Intell 22(10): 1066–1077

Hsiao CY, Lin BS, Cheng CT, Ku BH, Xu WC, Chi SY (2009) Application LiDAR technology monitoring sediment transport and evaluate sediment delivery ratio in watershed. Sinotech Eng J 105:17–25 (in Chinese)

Hu XF, Zhao H (2004) The practical case selection of image processing and recognition by using Visual C + +/MATLAB. Posts and Telecom Press, Beijing (in Chinese)

Ke Tao, Zhang ZX, Guo TH, Wang CC (2010) Aerial photogrammetry in the fast response. In: 2010 Workshop on unconventional photogrammetry, Tainan (in Chinese)

Kraus K (1997) Photogrammetry, vols I and II. Dümmler, Bonn

Ku CY, Chen JC, Wang MT (1996) The simulation of rockfall. In: 1996 Taiwan rock engineering symposium, Taipei, pp 243–252 (in Chinese)

Ku CY, Weng MJ, Kao XZ, Chen JZ, Li YX (2006) Application three-dimensional laser scanning technology to analysis of rockfall. In: 2006 Taiwan rock engineering symposium, Tainan, pp 387–396 (in Chinese)

Lei C, Wu FC, Hu ZY (2001) Kruppa equations and camera self-calibration. Acta Autom Sin 27(5):621–630 (in Chinese)

Lo CM (2010) Cliff recession and talus deposition pattern in rockfall area. Ph.D. thesis. Department of Civil Engineering, College of Engineering, National Taiwan University, Taipei (in Chinese)

Lourakis M, Argyros A (2004) The design and implementation of a generic sparse bundle adjustment software package based on the Levenberg-Marquardt algorithm. Technical report 340, Institute of Computer Science–FORTH, Heraklion, Crete, Greece, 2004. URL: http://www.ics.forth.gr/~lourakis/sba. Accessed 3 Aug 2011

Lowe DG (2004) Distinctive image features from scale-invariant key points. Int J Comput Vis 60:91–110

Lowe DG (2006) Distinctive image features from scale-invariant key points. Int J Comput Vis 74(1):59–73

Lowe DG (1999) Object recognition from local scale-invariant features. International conference on computer vision, Corfu, Greece, pp 1150–1157

Maybank S, Faugeras O (1992) A theory of self-calibration of a moving camera. Int J Comput Vis 8(2):123–151

Meng XQ, Hu ZY (2003) Recent progress in camera self-calibration. Acta Autom Sin 29(1):110–124 (in Chinese)

Ministry of Transportation and Communications (2010a) National Highway No. 3 3K +100 slope landslide events – the preliminary test assessment of slope (in Chinese)

Ministry of Transportation and Communications (2010b) Risk Management of National Highway – the powerpoint file of landslide event at National Highway No. 3 3.1 K (in Chinese)

Noah S, Ian S, Michael G, Richard S, Steven MS (2010) Scene reconstruction and visualization from community photo collections. Proc IEEE 98(8):1370–1390

Pollefeys M (1999) Self-calibration and metric 3D reconstruction from uncalibrated image sequences. Ph.D. thesis, Katholieke Universiteit Leuven

Pollefeys Marc, Gool Luc Van, Oosterlinck AndrÂe (1996) The modulus constraint: a new constraint for self-calibration. In: Proceedings of international conference of pattern recognition, pp 349–353

Seitz SM, Curless B, Diebel J, Scharstein D, Szeliski R (2006) A comparison and evaluation of multi-view stereo reconstruction algorithms. Proc IEEE 98(8)

Sun M (2007) Multiple view geometry and traditional photogrammetry theory. Acta Sci Nat Univ Pekin 43(4):453–459 (in Chinese)

Sun MC, Duan Yan (2010) Research Of tone balance method with least squares block adjustment. In: 2010 Workshop on unconventional photogrammetry, Tainan (in Chinese)

Triggs B (1997) Auto-calibration and the absolute quadric. In: Proceedings of computer vision and pattern recognition, pp 609–614

Tsai RY (1986) An efficient and accurate camera calibration technique for 3D machine vision. In: Proceedings of IEEE conference on computer vision and pattern recognition, pp 364–374

Wang Lei (2002) Military digital topographic map editing and output system based on MicroStation. Master thesis, The PLA Information Engineering University, Zhengzhou, China (in Chinese)

Wang LF (2010) Detection algorithm of moving objects based on sift features matching and dynamic updating background model. Comput Appl Softw 27(2):267–270 (in Chinese)

Weng J, Cohen P, Herniou M (1992) Camera calibration with distortion models and accuracy evaluation. IEEE Trans Pattern Anal Mach Intell (PAMI) 14(10):965–980

Wu TC, Feng ZY, Chen WF (2007) A study on precision of topography measurement for landslides and its influence on volume estimation. J Chin Soil Water Conserv 39(1):063–072 (in Chinese)

Xiao Z, Huang RI, Sui W (2004) Reconstruction on 3D topography based on computer vision. J Geol Hazard Environ Preserv 15 (2):74–77 (in Chinese)

Yasutaka F, Jean P (2010) Accurate, dense, and robust multiview stereopsis. IEEE Trans Pattern Anal Mach Intell 32(8):1362–1376

Zhang Z (1999) Flexible camera calibration by viewing a plane from unknown orientations. In: International conference on computer vision, pp 666–673

Zhang Z (2000) A flexible new technique for camera calibration. IEEE Trans Pattern Anal Mach Intell 22(11):1330–1334

Zhang Yong, Ke Tao (2010) Ortho updating by aerial triangulation based on the existing ortho-photos and DEM. In: 2010 Workshop on unconventional photogrammetry, Tainan (in Chinese)

Zhang YZ, Ou ZY (2001) A new linear method of camera calibration. Genamics JournalSeek 6(8):727–731 (in Chinese)



The Ancona Early Warning Centre, Instrumentation and Continuous Monitoring of the Landslides

Stefano Cardellini and Paolo Osimani

Abstract

The "Grande frana di Ancona" is a deep-seated landslide inside the city area, reactivated in 1982 after a long period of precipitation. In 2009 Ancona Administration, with a law specifically issued for the people living there, creates an Early Warning System and Emergency Plan; it was developed a surface monitoring system integrated by a subsurface in place geotechnical system

- Surface Monitoring System

  The combination of different instruments: GPS, Automatic Robotic Stations and tiltmeters sensors allows to monitor a great number of points previously identified.
- Geotechnical Monitoring System DMS

  In place Geotechnical Monitoring System DMS (patents and trademark CSG-Italy) was installed in February 2009 and is made by no. 3 Modular Dynamic System
- Early Warning Management

  In Ancona Early Warning Centre a staff controls the monitoring data and alerts the Coordinator in case of emergency.

Keywords

Complex composite landslide • Early warning system • Risk management

Introduction

On 13th December 1982 Ancona city, historical and capital region of Le Marche, Italy, located on the East coast of the Adriatic Sea, was involved in a large and deep landslide (Fig. 1).

An intense landslide, involving a volume of about 180 millions of cubic meters, affected the northern area of the city, the "Montagnolo" which started to slide towards the sea (Fig. 2).

Structures, infrastructures and some important public and strategic buildings, among them the Faculty of Medicine building, the Oncological Hospital, the Geriatric Hospital and the Tambroni retirement home were damaged. All the older people and the patients were moved to the nearest Hospitals for the first aid.

The National Railway MI-LE (Adriatica) and regional Highway Flaminia slid down 10 m towards the sea. The movements started from the lower border of the landslide and came up the slope. At the end of the event the surveyed displacements were: 8 m in horizontal at the base and 3 m on height, while on the top 5 m in horizontal and 2.5 m downwards.

On the 13th of December morning, after a night of uninterrupted movements and noises due to the opening fractures of buildings, the Residential Districts named "Posatora" and "Borghetto", were evacuated (Fig. 3).

The landslide damaged private houses and infrastructures and about 3,000 people were evacuated.

Municipality moved 1,582 people to hotels and other residences and they remained in that situation for a long time.

S. Cardellini (✉) • P. Osimani
Ancona monitoring Centre, Ancona Municipality, Largo XXIV Maggio 1, Ancona, Italy
e-mail: stefano.cardellini@comune.ancona.it

C. Margottini et al. (eds.), *Landslide Science and Practice*, Vol. 2,
DOI 10.1007/978-3-642-31445-2_7, © Springer-Verlag Berlin Heidelberg 2013

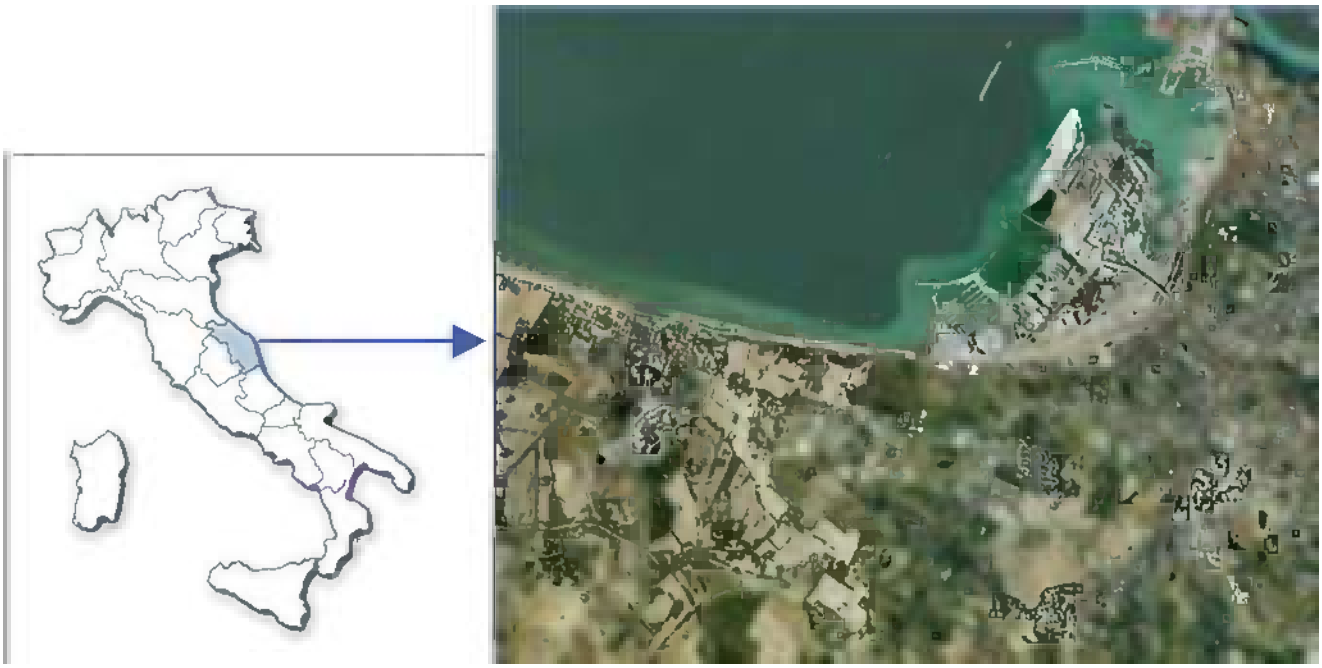


Fig. 1 Italy and Ancona city



Fig. 2 Area affected by the landslide in 1982



Fig. 3 The regional Highway Flaminia 1982

Gas and water supplies were interrupted too and the city remained for some days without the necessary services.

The more significant damages can be resumed as following:

- 220 ha extension (affecting 11 % urban area of Ancona)
- 3,661 people evacuated (1,071 families)
- 1,562 people moved to hotels and other residences by Municipality
- 280 buildings destroyed or damaged (a total of 865 residences)
- Faculty of Medicine Building, Oncological Hospital, Geriatric Hospital, Tambroni Retirement Home, were irreparably damaged
- 31 farms damaged
- 101 SME (small and medium enterprises)
- 3 industries
- 42 shops
- 500 people lost their jobs
- National Railway MI-LE (Adriatica) and regional Highway Flaminia blocked
- Gas and water supplies interrupted
- Luckily, no people died during the event!

The dynamic of the Landslide of Ancona can be explained in two steps:

1. A gravity settlement happened at high depth probably induced by some dislocations activated during the 1972 earthquake, then re-activated by the intense rain infiltration (some days before the event it rained for almost 6 days without any interruption).
2. After the first step we had an activation of superficial and medium landslides. These started to move after about 10 min, with consequent damages to buildings and infrastructures (this second step continued for some hours).

The superficial geomorphology of the Ancona landslide is influenced by many and complex movements. The colluvial soils, in some places of the flanks, where their thickness is about 10 m, have flown down as a mudslide. This dynamics was helped by the high rate of saturation.

Taking into account all the researches and both in-situ and laboratory investigations during the last 25 years, we can conclude that the Great Landslide of Ancona city is an Deep-seated landslide (complex, composite according to Cruden and Varnes 1996) reactivated after a long period of precipitation; new fractures were opened by a long period of earthquakes 10 years before (6 months duration) (Fig. 4).

The landslide involves clay and silty clay layers (Pliocene-Pleistocene) fractured with different OCR parameter, alternated with thin sand levels.

Overlapped sliding zones are active (maximum depth: 100–120 m, maximum depth 1982 event is 75 m bgl).

Across all the body of the landslide, in horizontal direction, parallel to the coast, there are two natural trenches that cross the slope. These trenches are upstream of old landslides slid down and now they are filled with heterogenic and plastic soils. These soils involve clay and silty clay, mud and thin sand level with some fragments of calcarenitic layers.

These trenches together with a complex structural system of fracture and discontinuity influenced the system of underground water.

All the geological and geotechnical analyses of the landslide mechanisms aimed at the preliminary consolidation design in the 2000; but the consolidation was unrealizable because of the high cost of the works and the environment effects; the works also would have changed the structure of the area with a deep socio-economical impact.

Ancona Administration decided then to live with the landslide reducing nevertheless the risk for the people living there.

Over the years, some partial interventions of the total preliminary design, for the consolidation stroke, have been made. Two drainage systems were done, one deep based on trenches and wells, and a more superficial one with canals. Reinforced bulkheads were built and in some part of the area reforestation was made.

Ancona Administration decided to continue the drainage systems both superficial and deep.

In 2002 the Regione Marche (one of the main administrative units in Italy) made a special law for the people that still live on the landslide area, in order to give Ancona Administration the responsibility of creating an Early Warning System and an Emergency Plan. The goal of the project is to control the safety of the population by a continuous monitoring plan of the landslide displacements.

The projected Early Warning System consists of an integrated and continuous monitoring system aimed at the control at both superficial and deep displacements over the whole area (Fig. 5).

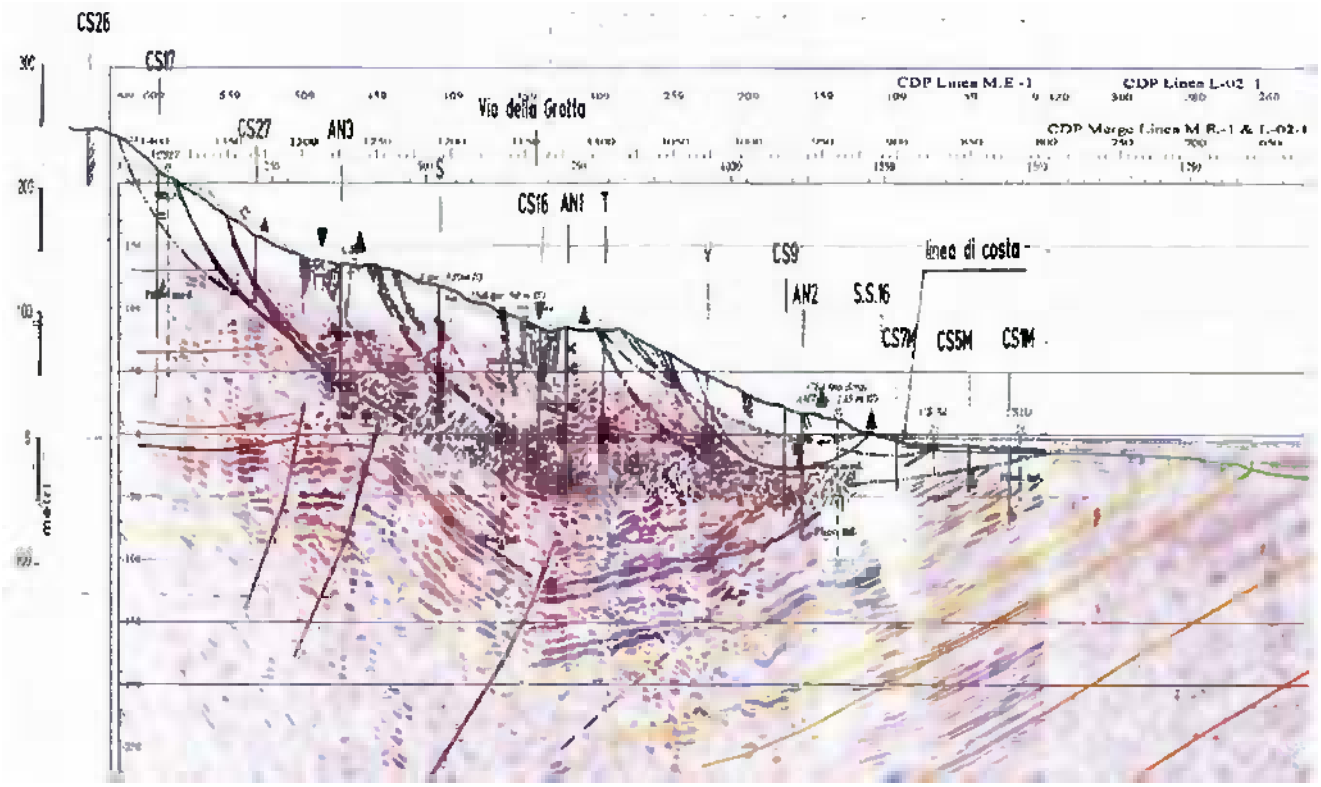


Fig. 4 Geomorphological and seismic section

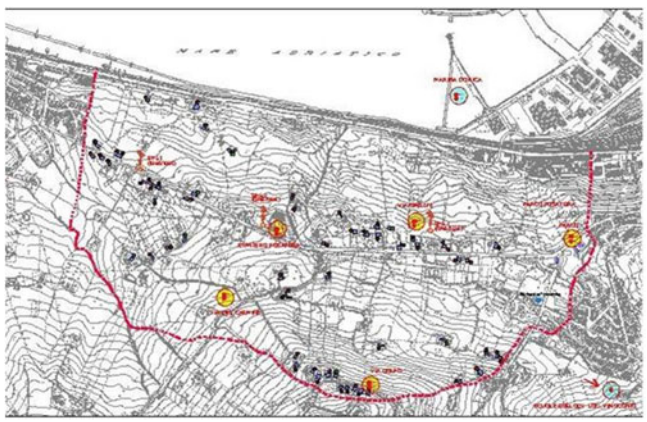


Fig. 5 Map of the instrumented sites

Surface Monitoring

The surface monitoring system is based on:

- Eight Automatic Robotic Stations (of high precision)
- Two hundred and thirty reflector points (installed partly on the 64 inhabited houses and on the structures and infrastructures)
- Twenty-six geodetic GPS (Global Position System) at single frequency L1 (installed on the 64 inhabited houses)
- Eight geodetic GPS at dual frequency L1 + L2 (reference)
- Eight high precision tiltmeters sensors for the stability control of the main stations of the I and II level of the net (automatic geodetic boxes).

The combination of the different instruments: GPS, Automatic Robotic Stations and the inclinometric sensors allows a 3D monitoring of a great number of points previously identified. The adoption of the geodetic GPS at dual frequency assures a high quality of the GPS measures, and a greater versatility at all the system.

The monitoring system was designed to detect every surface movement by sensors installed both in the area and on inhabited houses. A staff of technicians, in the 24 h Control Centre placed in the Town Hall, manages the system and evaluates the alarms to be forwarded to the Civil Protection.

The measuring cycle is set up on 30 min, but in emergency or after a long rainy period, the system can operate on every points of the dual frequency GPS net also in Real Time RTK, and with the 8 Automatic Robotic Stations (Fig. 6).

The surface monitoring is based on GPS system in three different active levels, on eight Automatic Robotic Stations and a later control with eight high precision inclinometric sensors for the stability control of the main stations of the I and II level of the net:



Fig. 6 The integrated monitoring station "Grotte"

A: GPS System

1. Main Network (I level active at the moment) formed by three main stations outside of the landslide area with three geodetic GPS at dual frequency L1 + L2 (reference) placed on two steady buildings (University and Collodi school), and a third one placed on a Geodetic box at Marina Dorica founded with a reinforced concrete pole (18 m).
2. Secondary Network (II level active at the moment), formed by five main stations inside the landslide area with five geodetic GPS at dual frequency L1 + L2 (reference) placed on one building and on four Geodetic boxes founded with reinforced concrete poles (12–18 m).

All these geodetic GPS (no. 3 + no. 5) form a high precision net working in the Early-warning system, on different control levels, to assure the GPS net (at single frequency L1), installed on 26 inhabited houses, a strong network; so that after an alarm it can work in real time RTK.

3. Third Network (III level active at the moment) formed by no. 26 geodetic GPS at single frequency L1 installed on 26 inhabited houses inside of the landslide area.

B: Automatic Robotic Stations

Eight high precision Automatic Robotic Stations are placed in the I and II level networks, in the same places of the geodetic GPS at dual frequency L1 + L2, except for the "Collodi school" building. They control (angles and distances) of 230 reflector spots placed on the inhabited buildings left and on the consolidation structures built inside the landslide.

Geotechnical Monitoring (DMS)

In February 2009 an in place Geotechnical Monitoring System DMS (patents and trademarks CSG-Italy) was installed. The system is composed of no. 3 Modular Dynamic System columns installed in three boreholes (100 m depth).

DMS columns are composed by modules containing the sensors, allowing in this way a continuous multiparametric measurement of the parameters for the whole length of the column. Modules are made of stainless steel, which makes DMS columns very robust and able to reach high depth, sensors are strictly tested to ensure a high level of accuracy. The modules are linked by special 2D/3D flexible joints that allow strong, continuous adaptability to bends and twists of the borehole, whilst maintaining rigorously the orientation with respect to a reference system defined during installation. Moreover DMS columns can be preassembled in lab and after installation in site can be repositioned extending or reducing the monitored depth; this activity can be done easily also on site.

Each column installed in Ancona is composed by 85 Biaxial Inclinometric modules (range ±20 °, resolution 0.01 °), 2 Piezometric Sensors (range 100 psi, resolution 0.01 m) and 85 Temperature Sensors (range 0–70 °C, resolution 0.1 °C). The total active length is 85 m (the first ten metres and the last five ones are without any instruments) with 173 transducers connected each other. Digital compasses are also on board.

DMS Early Warning Management

The control unit receives data from the DMS column by RS485 protocol; it compares them with threshold values (set by the user) and stores them in a circular buffer (Fig. 7).

In case of displacement values higher than the threshold values, the control unit sends a warning SMS/direct call to the staff on duty of the monitoring centre.

The same is for rapid changes of water-table level. Warning levels are counted from 1 to 4, in a growing order of danger.

In the monitoring centre, the management software GeoMaster takes care of downloading the data stored in the control unit memory buffer.

DMS Early Warning is the software that visualizes the subsurface data at the monitoring centre and wherever an Internet connection is possible. The software, in a compact check panel, allows the contextual control of displacement (E-W, N-S, Module diagrams, on Polar and Azimuthal plots) as well as the variations of the level of the water table and temperature; time history of each multiparametric module and displacement-velocity are also displayed at selected intervals.

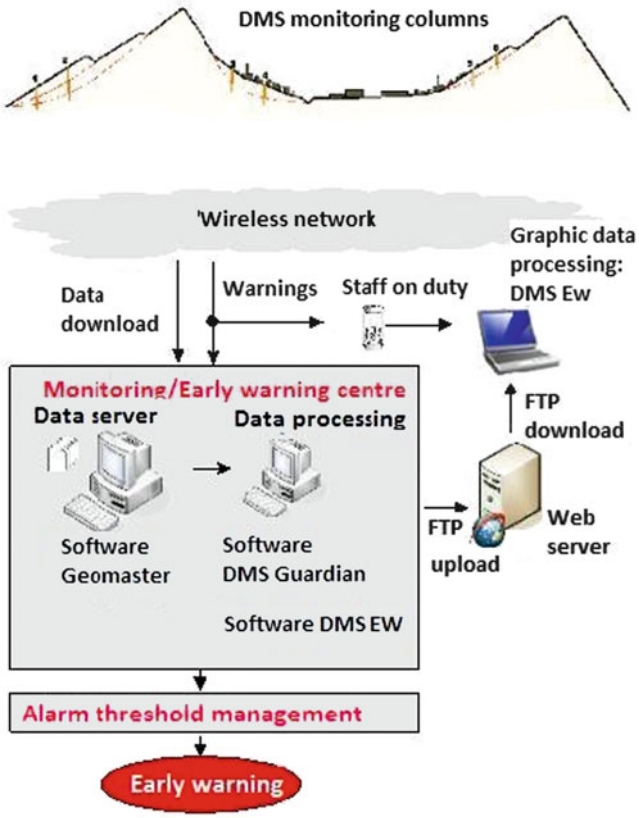


Fig. 7 DMS Early Warning system

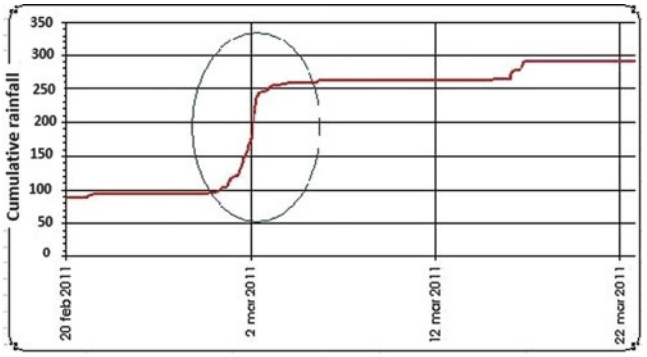


Fig. 8 Cumulative rainfall in March 2011

Transmission System

The transmitted data coming from the different sensors are collected according to the two following procedures:

I and II Level Net: data transmission in real time through a Wi-Fi Standard HyperLan to the Town Monitoring Centre. The system is based on a main radio line (spot to spot) between the Automatic Robotic Stations and the Ancona Municipality Monitoring Centre. Data transmission in real time works through some free frequencies radio links of 5.4 GHz (HyperLan).

III Level Net: data transmission through periodic GSM in "dialling" with a data acquisition every 6 h.

DMS data transmission is by GSM–GPRS.

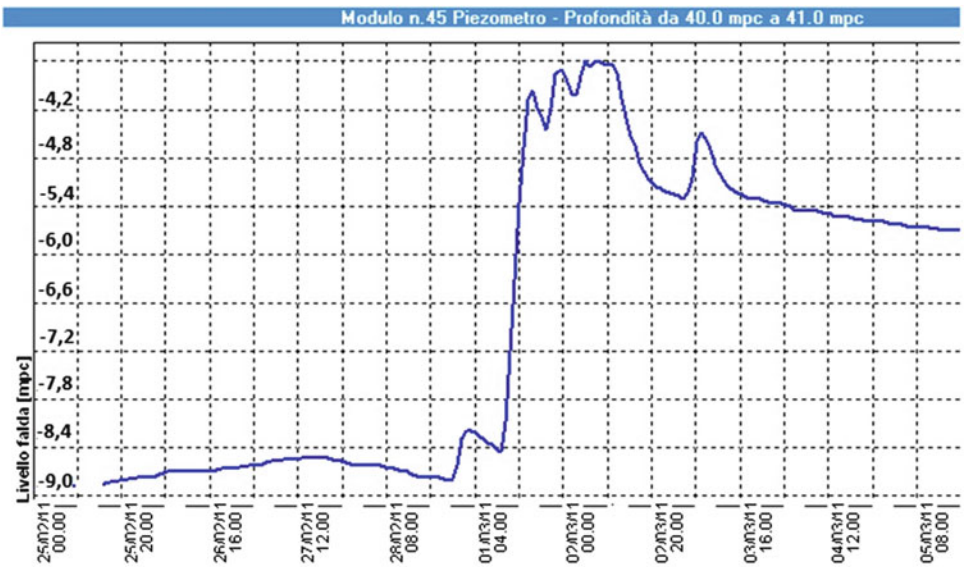


Fig. 9 Water table level on DMS_Ancona1 site

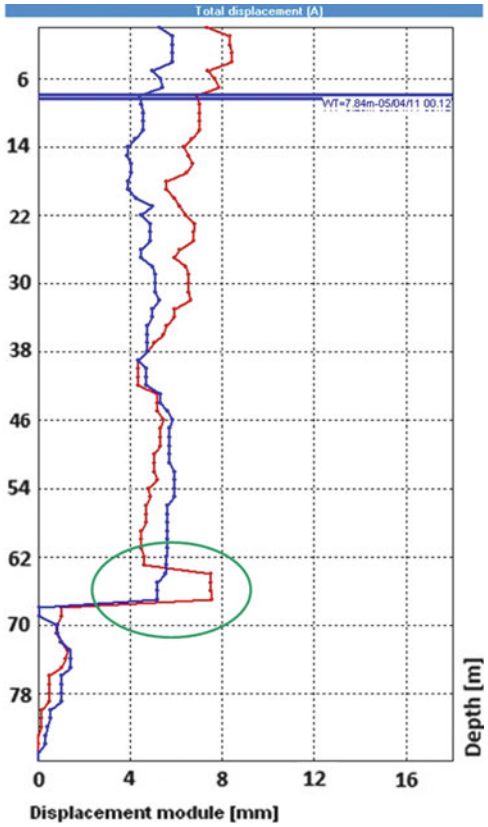


Fig. 10 Total displacements of DMS_Ancona1

Early Warning Evacuation Protocol

In order to increase the efficiency of the Civil Protection and guarantee the population safety an organization with the scope to follow and manage the evacuation protocol was developed.

The mayor of Ancona is the chief and has the responsibility of communicating both with the manager of Public works and the Civil Protection. The data collected by the monitoring systems are evaluated by two technical managers, one for the surface monitoring and one for the geotechnical monitoring, and by a representative for the civil protection.

With the aim of managing the situation of potential risk for the population an Evacuation Protocol was developed. In case of receiving an alarm the procedure must be followed step by step and, if the alarm is confirmed, must end with the activation of sirens. In case of activation of sirens the population must get out from their houses and follow the instruction of the Local Civil Protection Plan.

In the monitoring centre, technicians have the task to analyze data from instrumentations; the protocol includes a table of values used to evaluate the warning level in real time. The markers used are:

Signals (cracks or subsidence); Rain; GPS; TCA; NIVEL; DMS.

Once the alarms from the markers are validated, they are compared with the table which indicates the stages of activation warnings (attention, early alert, alert, early warning, and warning) and the resulting actions.

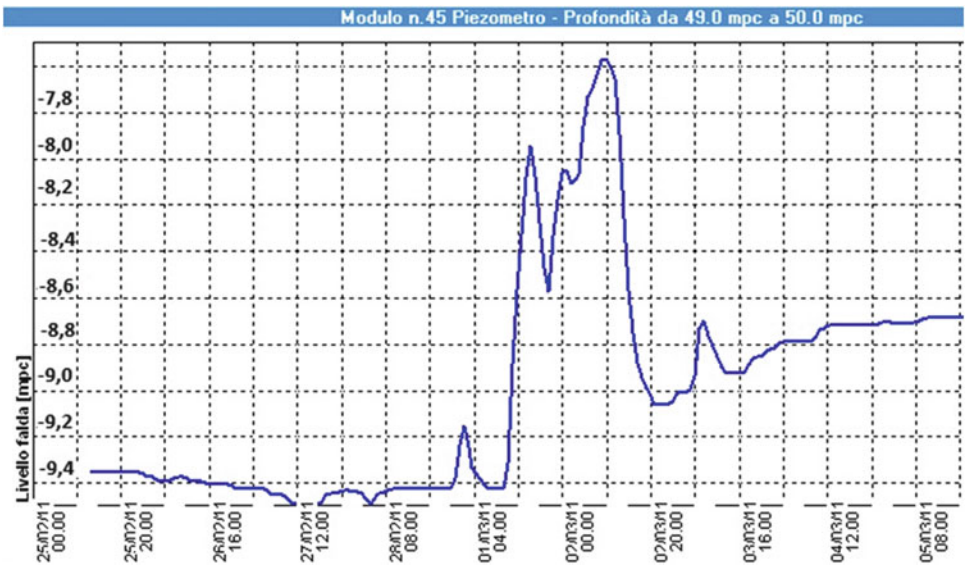


Fig. 11 Water table level on DMS_Ancona2 site

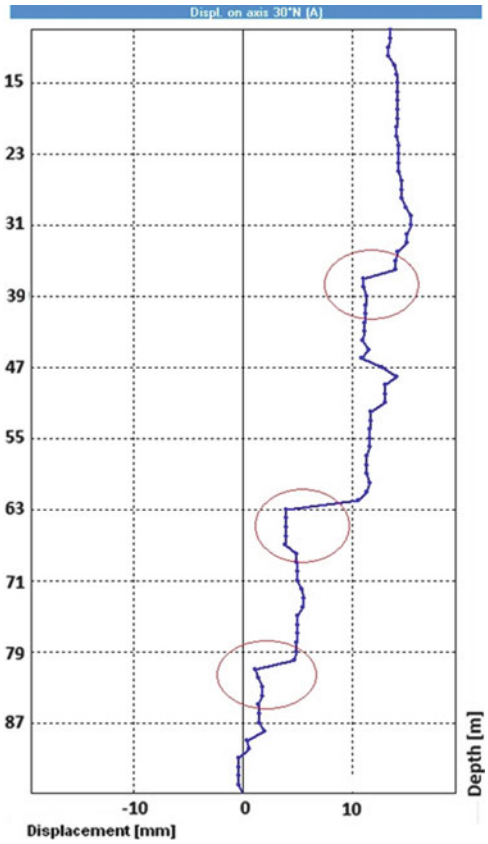


Fig. 12 Total displacements of DMS_Ancona2

Monitoring Data on Rainfall Event of March 2011

Being continuous monitoring instruments, DMS system are able to collect data in real time, thanks to this system it is possible to compare different data between them. In order to understand how rainfall, water table and displacements are linked, an analysis on the delay time between them was performed.

Analyzing rainfall events occurred in Ancona and data from DMS system the delay time between the rainfall events, the raising of water table level and the beginning of micromovements were calculated.

The 3 largest rainfall events occurred in Ancona since 2008:

1. From 27/02/2011 at 17:00 to 03/03/2011 at 6:00 with a cumulative rainfall of 161.8 mm
2. From 27/09/2010 at 15:00 to 01/10/2011 at 9:00 with a cumulative rainfall of 134.1 mm
3. From 03/03/2008 at 10:00 to 08/03/2008 at 16:00 with a cumulative rainfall of 109.2 mm

For the analysis the first event, happened in 2011 was chosen (Fig. 8).

On each of the three columns the delay time between the event and the raising of the water table was calculated, and it was evaluated if there were displacements soon after the events.

For the first column, called DMS Ancona1, the water level starts to rise on the 27th of February at 23:00, 30 h after the start of the pluviometric event (Fig. 9).

By aligning the column at the 27th of February, starting date of the event, it was possible to notice some micromovements (Fig. 10):

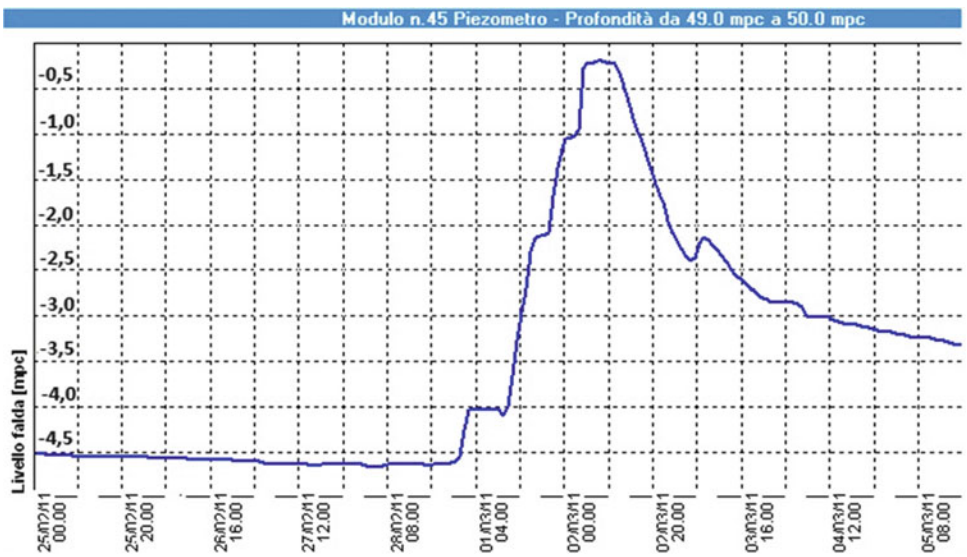


Fig. 13 Water table level on DMS_Ancona3 site

- On module 18, depth 67–68 m, from 29/03/11 to 05/04/11 (blue line)
- On module 22, depth 63–64 m, from 05/04/11 to 09/04/11 (red line)

So was possible to detect a triggering event, between 63 and 68 m bgl, shown a month after the beginning of the pluviometric event.

On the second column, Ancona2, the water table level raised on the 1st of March at 00:00, 31 h late (Fig. 11).

The column detects some micromovements occurring after that (Fig. 13):

- On module 14, depth 80–81 m, from 26/03/11 to 09/04/11
- On module 32 and 33, depth 61–63 m, from 26/03/11 to 09/04/11
- On module 58, depth 36–37 m, from 26/03/11 to 09/04/11

Figure 12 shows three triggering events developed with a delay, like the previous, of 1 month.

On the last column, Ancona3, the same procedure was implemented. The water table level raised the 29th of February at 23:00, 30 h late (Fig. 13).

In the analyzed period were not detected sensible indications, but a small events is shown by module 3, between 91 and 92 m bgl, from 19/05/11 to 21/05/11. This displacement could be very late than the rainfall event or caused by settlement.

The analysis shows a correlation of about 30 h between the beginning of the rains and their effect on water table level and a month of delay with the occurrence of displacement phenomena. This data allow the implementation of a forecasting model and the evaluation of the risk level in function of more parameters, unlike traditional instruments.

It is important to notice that this analysis could not be achievable with only surface systems because developed on micro-movements occurring at significative depths.

Conclusions

In this way, the Ancona administration has chosen the "LIVING WITH LANDSLIDE" policy: this new concept implies that the safety of the population is achieved through a high-quality and comprehensive early-warning system. This in contrast with the more static concept of standard engineering remedial works, which are clearly impracticable so far, in our case.

This project is the result of the best conjunction between human resources and a more reliable technology in the Early Warning monitoring field, put in use for a best safety and peacefulness for the people living on the Ancona landslide.

Reference

Cruden DM, Varnes DJ (1996) Landslides types and processes. In: Turner AK, Schuster RL (eds) Landslides: investigation and mitigation



Slope Stability Assessment and Monitoring of a Vulnerable Site on Rishikesh-Uttarkashi Highway, India

Shantanu Sarkar, Amitava Ghosh, Debi Prasanna Kanungo, and Zamir Ahmad

Abstract

Landslides are frequently occurring phenomenon in the Himalayas, in the Northern part of India. There were many landslide disasters in the recent past which have taken lives and caused extensive damage to property and public utility services. It is an imperative task to assess the slope instability and evaluate the risk where lives and property are at danger. A vulnerable slope on Rishikesh-Uttarkashi road having few houses, which are under distress, was studied for slope stability assessment. The slope instability was evident by road subsidence and development of cracks in few houses. A comprehensive geological and geotechnical investigation was carried out along with slope movement monitoring. The paper describes the findings of the study.

Keywords

Landslide • Himalaya • Movement • Monitoring

Introduction

In recent years, a number of major disasters have made the global community aware of the immense losses of human lives and property. Although an individual slope failure is, in general, not so spectacular or devastating as an earthquake, a volcanic eruption or a flood, yet, being much more frequent and wide spread over the years, landslides have caused considerable loss of property and life. In many countries, economic losses due to landslides are great and apparently are growing as development expands into unstable hill areas under the pressure of expanding populations. Hence assessment of landslide hazard and risk is an imperative task in the area of disaster management.

The occurrence of landslides is a common phenomenon in the Himalaya which is a conspicuous landscape in the northern part of the Indian subcontinent. The Himalaya presents rock types, tectonic zones, topographic reliefs and slopes of diverse nature. The structurally deformed rocks have been subjected to severe erosion by toe cutting action of rivers and streams. All these adverse characteristics contribute in making the terrain susceptible to landslide occurrence (Sarkar & Gupta, 2005). A large number of slope failures have affected the main highways in the Himalaya, which are important routes for pilgrims (Sarkar et al. 2005). Many landslides along these highways are triggered during the monsoon season. These landslides always threat human lives and properties, which include buildings, bridges, power transmission line etc. One such unstable slope on Rishikesh-Uttarkashi road near Agrakhal is causing road subsidence and affecting several houses situated on down hill slopes (Fig. 1). The present study was undertaken to assess the slope instability and monitor the slope movement. The paper presents the results of slope monitoring and the investigations carried out.

S. Sarkar (✉) • A. Ghosh • D.P. Kanungo • Z. Ahmad
CSIR-Central Building Research Institute, Roorkee, Uttarakhand, India
e-mail: shantanu_cbri@yahoo.co.in

C. Margottini et al. (eds.), *Landslide Science and Practice*, Vol. 2,
DOI 10.1007/978-3-642-31445-2_8, © Springer-Verlag Berlin Heidelberg 2013



Fig. 1 Study area



Fig. 2 Indications of slope instability manifested by cracks in houses, road subsidence and slope failure

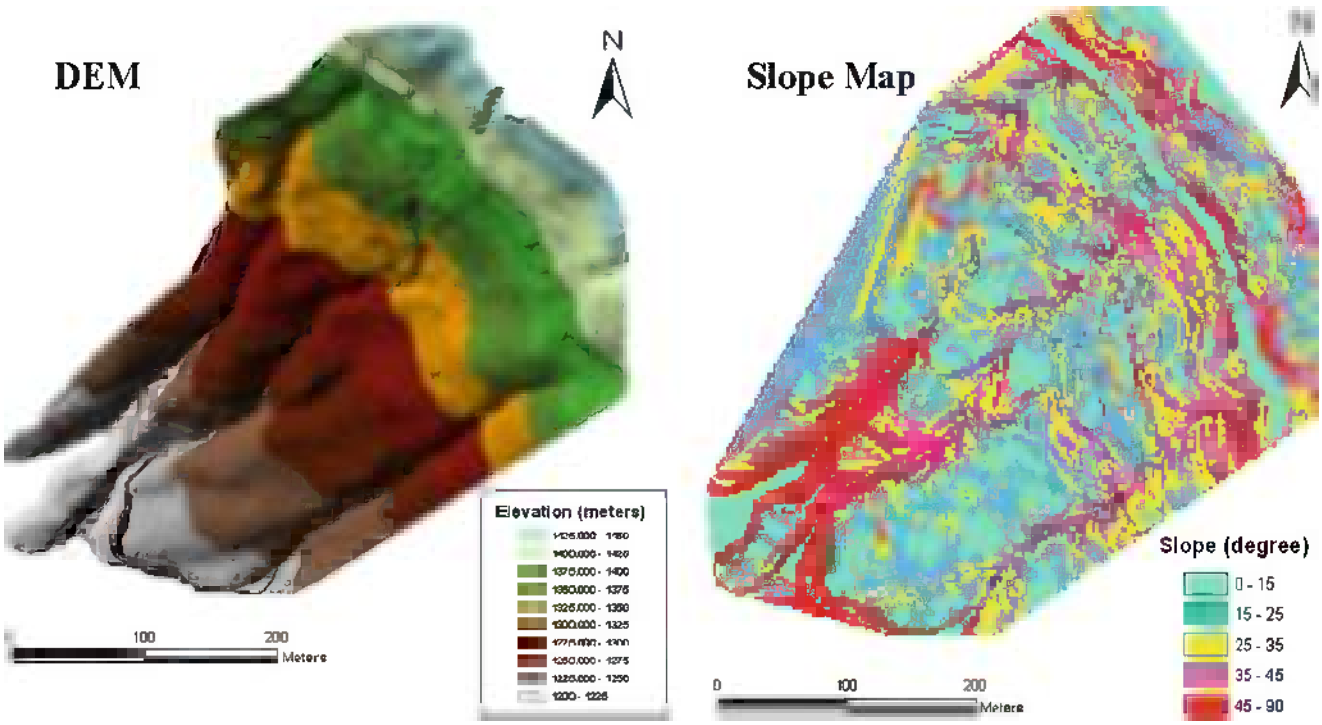


Fig. 3 DEM and slope map of the area

Geology and Slope Instability

Slope instability in the area is evident by road subsidence and development of cracks in the houses situated on the downhill slope (Fig. 2). Water seepage on the walls was noticed during the rains. There is a small slope failure along the discontinuity plane. It was told by the residents of the houses that cracks on the walls get widened every year. All these field observation have indicated that the slope is presently unstable.

Topographic analysis was carried out using a contour map (1:1,000 scale with 2 m contour interval) and DEM was generated in GIS (Fig. 3). A slope map showing the

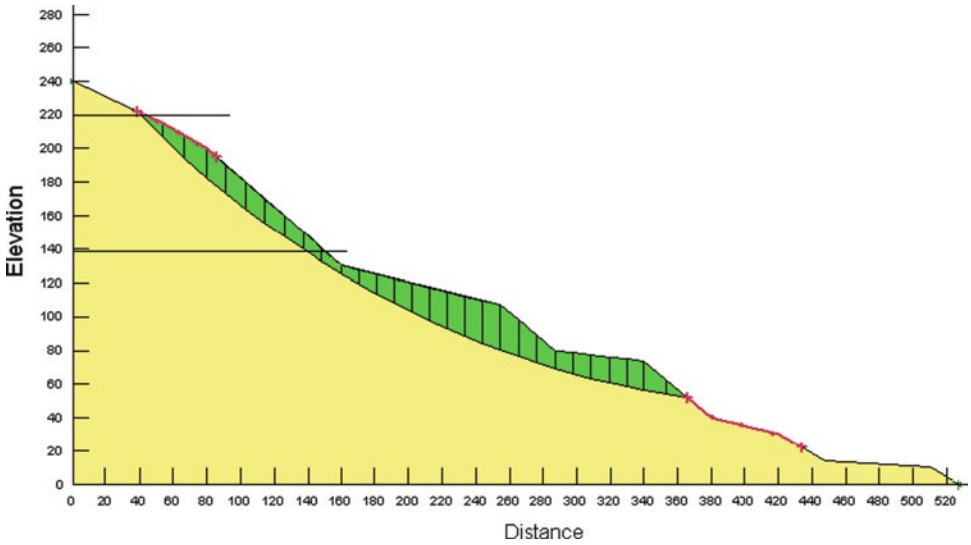


Fig. 4 Slope profile and probable slip surface

slope distribution of the area was derived from the DEM. Rocks present in the area are shale and Phyllites, which are highly weathered, fractured and thinly bedded. The rock beds dip 50 ° towards NW and there are two major joint sets, out of which one joint dipping towards NE is outward dipping favouring slope instability. The soil cover on the slope is varying from 5 to 10 m. There are three major drains on the slope. From the field investigation it is inferred that the unconsolidated overburden material lying above the soft geological strata is contributing slope instability in the area.

The topography of the slope and the slope material, which comprise mainly of gravels and sand, indicate that the area is probably a very old slide zone. Field investigation has shown that the sub-surface water flow during heavy rains is causing subsidence at various locations resulting into development of cracks in the houses. Resistivity survey has also indicated weathered and saturated soil at a depth of about 9 m. Hence the causes of slope instability can be listed as follows:

- Topography and soil cover indicates presence of an old slide.
- The geological investigation has indicated presence of fractured and weathered rocks, underlying loose overburden material allowing easy seepage of water.
- The structural data shows presence of unfavourable discontinuity.
- The rain water in the catchment area percolating underground and developing pore pressure.

Geotechnical Investigation

Laboratory investigation of soil samples was conducted. The soil comprises of gravel 34 %, sand 35 %, silt 29 % and clay 2 %. The cohesion varies between 0.02 and 0.11 kg/cm^2 and friction angle varies between 40 ° and 46 °. The slope geometry obtained from the DEM and the friction and cohesion values were used for carrying out the slope stability analysis. Factor of safety obtained from stability analysis using the Slope/W software (Fig. 4) under static condition shows that the slope is stable under dry condition (Factor of safety 1.4) which drops down to 1.19 under partially saturated condition. Dynamic slope stability analysis was also carried out considering the seismic effects and the displacement was found to be only 3–4 cm under dry condition but under saturated condition displacement was quite significant (Ghosh et al. 2010).

Monitoring Scheme

There are six houses on the slope which have shown distress manifested by development of cracks on the walls and floor subsidence. A monitoring scheme was planned to monitor the horizontal and vertical movements of these houses using Total station from a far distance outside the unstable zone. The Total station is an electronic theodolite integrated with an electronic distance meter (EDM) to obtain sloping, horizontal and vertical distances from the instrument to a particular point. Electronic Distance Measurement technology uses a ground-based, high-precision survey instrument that emits infra red wave to measure the time the wave travels from the instrument to a reflector prism installed on the moving object.

The accuracy of this type of surveying technique is high (mm accuracy), yielding much better basic surface movement data than the extensometers or inclinometers (Petley et al. 2004). However, movements associated with rotations of the objects upon which the targets are located may result into erroneous data. But even with these shortcomings, the datasets are excellent and allow a very high level of

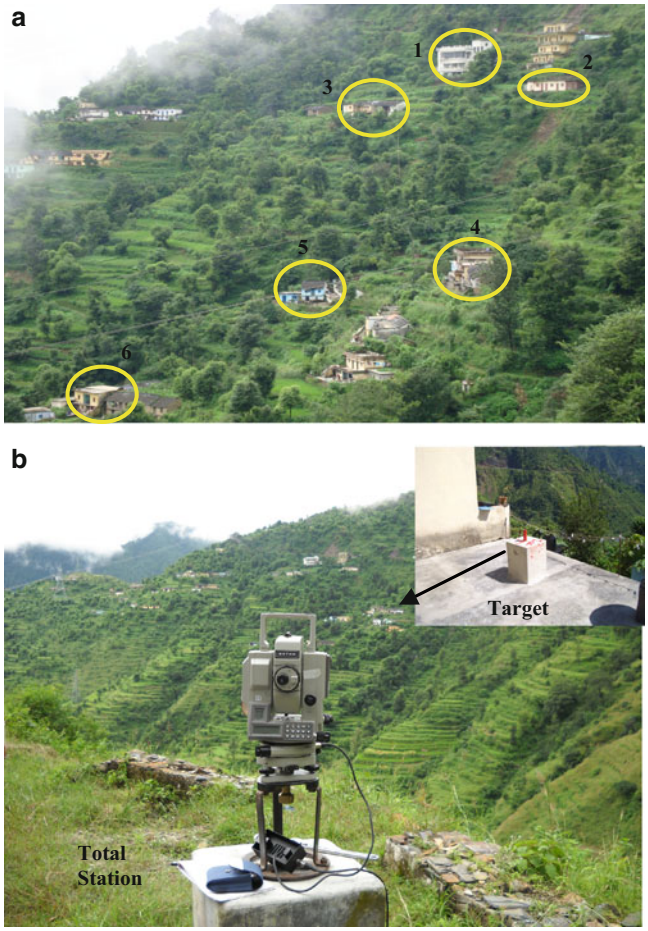


Fig. 5 Houses being monitored (**a**) and position of Total Station and target (**b**)

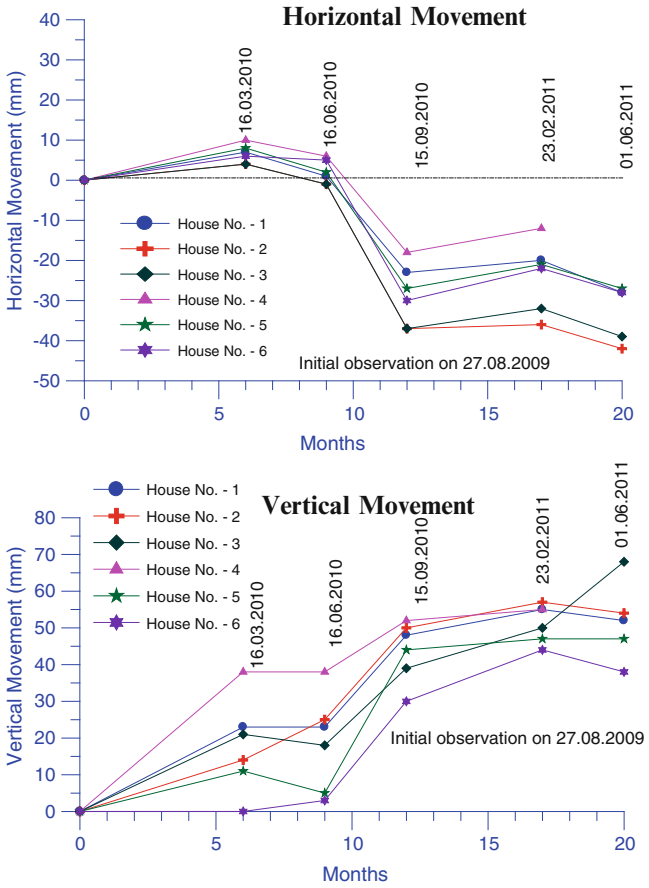


Fig. 6 Horizontal and vertical movements

understanding of surface movements as commented by Petley et al. (2004). The advantages and disadvantages associated with total station systems was commented by Savvaidis (2003). The main advantage of using total station instruments is that they provide three dimensional coordinate information of the points measured. The disadvantage is the requirement to have an unobstructed line-of-sight between the instrument and the targeting prism.

In the present study fixed points were installed as observation points on roof top of the six houses. A stable zone based on field observation was identified at a distance of 800 m from the unstable slope. The reference point was made at this location from where all the observation points could be seen without any hindrance (Fig. 5). At the time of taking observation the total station was fixed on this reference points and the data were collected from the six observation points located on the selected houses. The movement data were collected for the period August 2009 to June 2011. The horizontal and vertical movements of the observation points were calculated from the periodic monitoring data.

Monitoring of Movement

The movement data is shown in Fig. 6. An automatic rain gauge was installed at the site to collect rainfall data. The monthly rainfall data is shown in "Fig. 7". The rainfall data shows that in the monsoon period of 2009, the maximum rainfall was only 232 mm in the month of September. While in the year 2010 there was a heavy rainfall during July to September and rainfall of 950 mm was recorded for the month of July only.

The observation points of the six houses show varied vertical and horizontal movements. In case of vertical movement, the house no. 4 shows a vertical movement of 40 mm from August 2009 to March 2010 while the house no. 6 shows negligible vertical movement during that period. There is no considerable movement during March 2010 to June 2010. A considerable movement varying from 15 to 35 mm is shown by all the houses during June 2010 to September 2010. The movement data when compared with the rainfall data (Fig. 7), it was found that the sudden increase of vertical movement during June to September

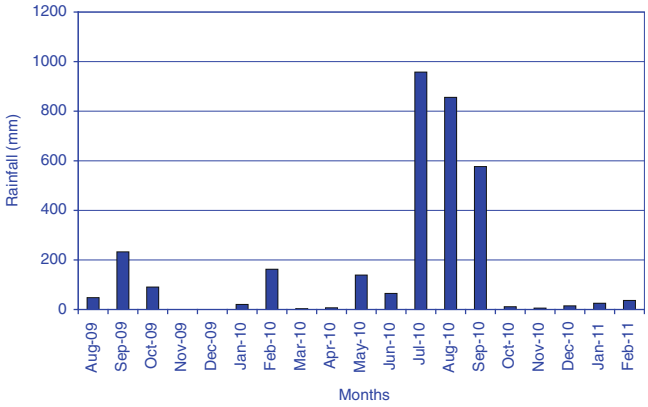


Fig. 7 Monthly rainfall data

2010 can be well explained by the heavy rainfall during that period. During September 2010 to February 2011 there is not much movement. However, it can be inferred from the figure that all the houses have shown movements of a similar trend.

When considering the horizontal movement the total maximum movement of 40 mm during the total monitoring period is shown by the house no. 2. The house no. 4 has shown the least horizontal movement of 18 mm. In this case also maximum movement was observed during the heavy rainfall period of June 2010 to September 2010. Hence, the movement monitoring data of the last two years has shown a cumulative vertical movement of 38–68 mm and cumulative horizontal movement of 20–40 mm. The monitoring study is being continued to assess the vulnerability of these houses against the slope instability.

Conclusions

A potential unstable slope was studied to determine the degree of instability in terms of factor of safety and the slope movement. Stability analysis has shown that the slope in dry condition is stable but under seismic and saturated condition this may suffer large displacement leading to landslide. There are few houses which have shown distress manifested by development of cracks and subsidence. Topography and soil cover indicates presence of an old slide zone and the geological discontinuity shows presence of unfavourable rock mass structure. However the prime cause for the distress in the houses is the sub-surface water seepage. The movement of the slope is being monitored by monitoring the vertical and horizontal movements of bench marks installed on the houses. This has shown vertical movement of 38–68 mm and horizontal movement of 27–39 mm for different houses for the period of about 2 years.

The risk elements in the area are few houses and the highway which are vulnerable to sliding activity. Few control measures such as surface drainage and retaining walls have been suggested to arrest the further damage to the houses. The area at present does not indicate a major landslide event to occur however, it cannot be ruled out in case of heavy precipitation accompanied by seismic shocks.

Acknowledgments Authors are grateful to the Director, CSIR-Central Building Research Institute, Roorkee for granting permission to publish this paper.

References

Ghosh A, Sarkar S, Kanungo, DP, Ahmad Z (2010) Stability assessment and suggestion for control measures of a potential landslide slope on NH 94, Uttarakhand Himalaya, India. In: Fifth international conference on recent advances in geotechnical earthquake engineering and soil dynamics, San Diego, California, 24–29 May 2010

Petley DN, Mantovani F, Bulmer, MH, Zannoni A (2004) The use of surface monitoring data for the interpretation of landslide movement patterns. Geomorphology, doi: 10.1016/j.geomorph.2004.09.011

Sarkar S, Gupta PK (2005) Techniques for landslide hazard zonation – application to Srinagar-Rudraprayag area, Garhwal Himalaya. Geol Soc India 65:217–230

Sarkar S, Kanung DP, Patra AK (2005) Landslides in the Alaknanda Valley of Garhwal Himalaya, India. Q J Eng Geol Hydrol 39:79–42

Savvaidis PD (2003) Existing landslide monitoring systems and techniques. From Stars to Earth and Culture. In honor of the memory of Professor Alexandros Tsioumis. The Aristotle University of Thessaloniki, Greece, pp 242–258



Landslide Displacement Monitoring from Multi-Temporal Terrestrial Digital Images: Case of the Valoria Landslide Site

Mirco Motta, Fabio Gabrieli, Alessandro Corsini, Vinicio Manzi, Francesco Ronchetti, and Simonetta Cola

Abstract

This work presents a low-cost method to measure the displacement of some points on the landslide surface. The method uses a sequence of terrestrial digital images. The Image Acquisition System (IAS) consists in a remote connected DSLR camera and controlled by software. The camera is fixed on a stable pillar, inside a transparent box and it periodically takes the pictures of the landslide. In order to rectify the image and to correct the little natural displacement of the image plane with respect to the landslide some fixed reference points are selected in the images. Moreover, some "well recognizable" optical targets are used in order to evaluate the displacement field. The image sequence is analyzed with a home-made digital image correlation code. The colour and size of the optical targets were evaluated in order to get the maximum accuracy of measurements and to improve the auto-matching function between the images. Taking pictures with bracketing function was proved to help the target searching phase for different weather conditions. The possibilities of the method are evaluated with reference to a sequence of images taken at the Valoria landslide site (Northern Apennines, Italy).

Keywords

Landslide monitoring • DIC • Digital images • Videometric

Introduction

In the last years computer vision and digital image processing have revolutionized traditional metrology sciences.

Also earth science took advantage of these challenges and capabilities in many tasks, from tomography at micro-scale to remote sensing for larger scales. Regardless of the scale of study, the spatial and temporal data inside any captured images (from microscopic X-ray photos to multi-band satellite images) provide a lot of useful information that can be used in many ways, such as for the 3D modelling of objects and environment, if the images are taken from different positions, or for the displacement detection, if the images are part of a temporal sequence.

The recent headway in technology and hardware introduced some new powerful equipments and contemporary, thanks to their large commercial diffusion, cut their costs. Particularly, in the field of digital photography, high technical development have been reached and now optical sensors with resolution greater than 18 MP are available at very low cost. At the same time, the researches in the image processing have been introduced a lot of interesting techniques that are now successfully employed in several applications, for example in the 3D object reconstruction, in surveying of surfaces and of joints orientation, or in measuring the displacement field.

M. Motta (✉) • A. Corsini • F. Ronchetti
Università di Modena e Reggio Emilia, Dip. di Scienze della Terra, Largo S. Eufemia 19, 41100 Modena, Italy
e-mail: mirco.climb@libero.it

F. Gabrieli • S. Cola
Università di Padova, Dip. Image, Via Ognissanti 39, 35129 Padova, Italy

V. Manzi
Università di Parma, Dip. Scienze della Terra, parco delle Scienze 157/a, 43100 Parma, Italy

C. Margottini et al. (eds.), *Landslide Science and Practice*, Vol. 2,
DOI 10.1007/978-3-642-31445-2_9, © Springer-Verlag Berlin Heidelberg 2013

Traditionally, the measurements of the landslide displacement are carried out using manual or automatic topographic surveys, like the so-called "Total Station". The usual accuracy and precision with these methods can be very high (from 1 to 1 mm), but in our opinion, especially for high deformable mass like mud-flows, too much high accuracy is not justified in relation to the expected displacement of the mass.

Nowadays, due to the need of having a larger number of points to be measured, the Total Station apparatus may be replaced by the Lidar or Laser Scanner surveys that permit a "diffuse" and accurate measure and a 3D reconstruction of a points cloud.

The photogrammetry survey actually represents a new interesting competitor of these methods. The advantages of the recent photogrammetric techniques are the quickness and simplicity to use it. Two or more photos can be used for 3D stereo reconstruction but also with a single photo is possible to obtain a lot of information from every pixel.

Moreover, it is possible to store the raw data (images) for further different analyses: this possibility is really interesting if we consider that many image processing algorithms are still in a development phase.

In this work a photogrammetric technique combining the image correlation and object detection algorithms will be introduced. It focuses on the processing of an images sequence of a landslide taken at different times from a fixed view by an Image Acquisition System (Delacourt et al. 2007; Travelletti et al. 2010).

In the following, the application of this method to the monitoring of a slow-moving landslide will be presented and some suggestions for the future developments will be reported at the end.

Boschi di Valoria Landslide

The Boschi di Valoria landslide was chosen for testing the technique of multi-temporal images processing. It is located near Frassinoro village in the Province of Modena (Italy-Northern Appennines). It extends close to the Dolo river over a distance of 3,500 m between an elevation of 1,350 m at the crown and 520 m at the toe. It has a surface of 1.4 km^2 and a mean slope of 24 ° (Fig. 1). The total volume of the sliding mass is approximately 16.1 mm^3.

The kinematics of the landslide is actually monitored by a Leica Total Station TCA2003 for automated precision measurements (0.15 mgon (0.5/1 mm + 1 ppm)), and GPS survey. The landslide has been reactivated several times in the last 10 years reaching a velocity of several metres in a day (Ronchetti et al. 2007).

The location falls into the IGM cartography sheet 86—Modena (1:100.000 scale) and sheet 235—Pievelago (1:50.000 scale). The Regional Technical Map number for the corresponding area is 235,070.

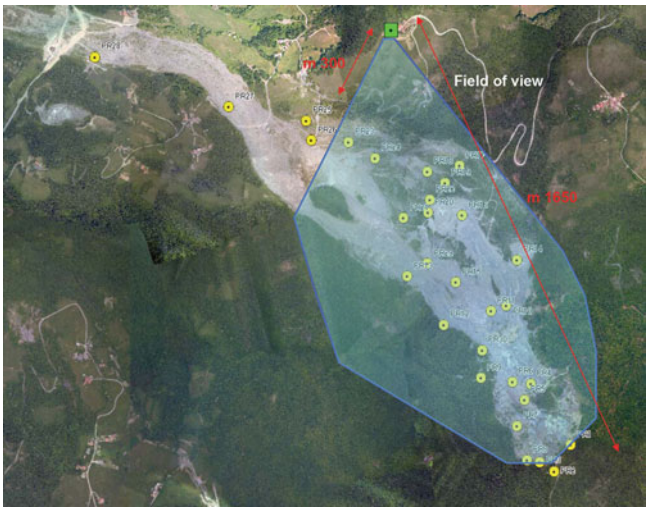


Fig. 1 Aerial map of the Boschi di Valoria landslide and location of the image acquisition system (*green square*)

Image Acquisition System

The actual position of the Total Station (Fig. 1) represents a good point of view for the upper part of the landslide and consequently it was considered as the better choice for the Image Acquisition System location. It is installed on a concrete pillar on a stable crest at a distance of 1,650 m from the crown and about 300 m from the main track of the landslide. We choose and set the apparatus to take pictures and measure the displacement of some points on the landslide in a range of distances 300–900 m.

The apparatus consists of a relatively low-cost reflex digital camera (Nikon D5000) that is PC-controlled; the power network from a near building provides the energy. The system is also connected with satellite data-network and/or GSM permitting remote control of the PC and camera.

The camera mounts a 38 mm lens with manual focus setting to prevent little displacement of the focal length that can produce radial artefacts. The default acquisition rate is one photo a day but it can be increased by means of remote control. A single acquisition step consists of three photographs in bracketing mode, registered 1–3 time in a day in order to get at least one image taken during good light conditions every day. All the photos have 12 Mpixels size (4,288 × 2,848) and are stored in the connected PC (Fig. 2).

In order to increase the visibility of the landslide surface we put some "well distinguishable" and simple Optical

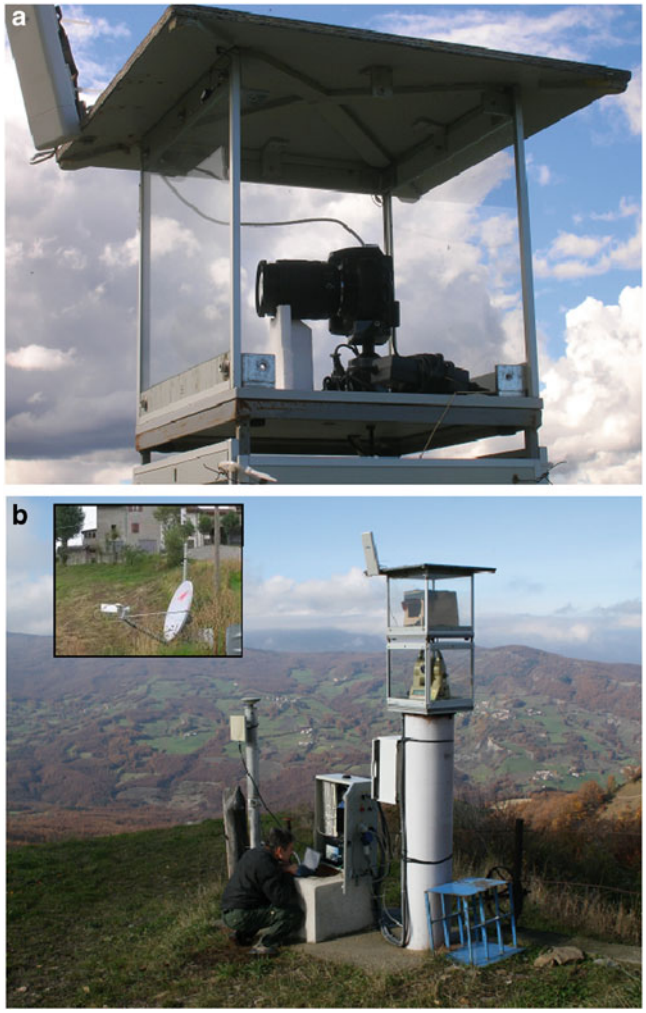


Fig. 2 View of the camera (**a**) and the whole image acquisition system mounted over the total station (**b**)

Targets (OT) for the digital camera in some area of the landslide. The optical targets are red plastic nets (1.5 m × 1 m) mounted on steel rods (Fig. 4).

Displacement Detection

The displacement of an object in the image plane could be simply obtained checking the same object in two photos captured from a fixed point of view, measuring the difference in image coordinates and then converting this value in a true metric value.

However, after the coming of digital photography, the automation of this process became possible and desirable in order to get higher accuracy and to process a larger number of objects and a long sequence of images.

The main steps at the base of displacement detection are the object detection process (or feature detection) and the matching process.

As the image is a 3D matrix of RGB intensity values for each pixel position, the information that can be used in the object detection algorithm are only image coordinates, colour values and the combination of this two information. These constitute the features of the single objects that facilitate the object detection: for example, one can use the location of red peaks to detect the position of red objects or, alternatively, the gradient of the red channel (colours value vs. position) can be used to recognize the border of these objects. These functions can also be mixed to detect specific reference point like corner or centre of objects in an image.

Other widely used algorithms, developed for the feature detection, employ the texture information (group of RGB values around a pixel) especially when the objects are not well defined or with lower pixel size (e.g. natural irregular surface, far objects, etc.). These examples and many other techniques are collected in the image-processing field and permits to enrich the quantity and quality of available information in a single image.

The second step of displacement detection is to match each detected object or feature in the first photo with the same object or feature in the second one. The approaches to obtain matching, and then 2D displacement from photos, are very numerous, but those attractive for our purposes essentially exploit two types of image processing algorithms. The first group estimates the displacement of a large number of undefined particles, by tracking the displacement of groups of them contained in some squared patch (matrix of pixels). This method, generally called the Particle Image Velocimetry (PIV), is well known in the fluid-dynamic research. In the last years it was also successfully adapted and applied for geotechnical application (see GeoPIV from White et al. 2003) and in the analysis of granular flows. The second group determines the displacement of each particle and is generally called Particle Tracking (PT); it is generally applied to a limited number of particles and with very well defined features (colour, shade, shape, size or boundaries) that permit an easy detection of every particle. It also requires a greater constancy (in shape, colour, etc.) in every frame of the image sequence and a better spatial and temporal resolution in comparison to PIV.

Landslide Displacement Detector

In order to measure the displacement field of a landslide we realized a special Landslide Displacement Detector (LDD) algorithm, compiled in Matlab language and using both PIV and PT algorithms (White et al. 2003). The advantage of this new method is to use both the algorithms at the same time in the image processing, but to permit to vary the parameters adopted in the methods in order to calibrate them in relation with the specific application and conditions.

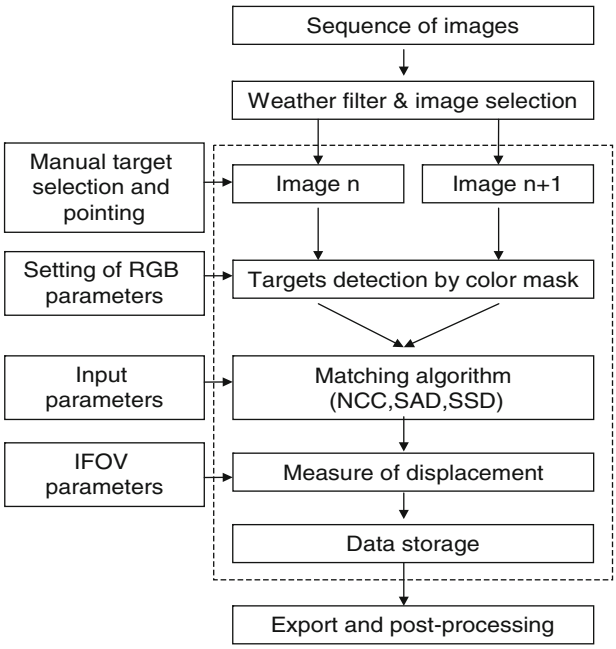


Fig. 3 Block diagram of the landslide displacement detector algorithm

A simple graphical interface helps the beginner users to start this activity without any deep knowledge about the image processing argument. The code block-scheme is depicted in Fig. 3. It is a semi-automatic method.

The code has some internal routines (or groups of routines) that can be resumed as follow:

1. A function that loads the sequence of images to be analyzed and helps to detect the initial targets points in the images (if they were specified). The initial position of the targets must be manually entered in the first photo and every time a new target is added on the landslide surface.
2. A semi- automatic colour masking technique that detects and points some significant objects in the image (group of pixel around the previous targets points) and highlights them with respect to the background.
3. Some routines that implement the matching algorithms based on techniques such as the normalized cross-correlation (NCC) or the sum of square differences (SSD) or the sum of absolute differences (SAD). They constitute the hearth of the code as they provide the displacement magnitude and direction of every selected target points.
4. A post-processing function that display the displacement field, export the results and helps the recognition of possible wrong displacement results.

It is important to note that in bad weather conditions (presence of rain, fog or snow) the images cannot be processed due to the lack of shade or simply because targets are completely hidden. The photos captured in these situations are firstly discarded by means of a pre-processed routine, also named "weather filter", that checks the quality of contrast in every photo.

Table 1 IFOVlin values for different cameras and distance

Camera	Nikon D70		Nikon D5000	
Focal length (mm)	38		38	
Sensor Size (px)	3,008 × 2,000		4,288 × 2,848	
Distance from the camera (m)	Pixel/m	IFOVlin (cm/px)	Pixel/m	IFOVlin (cm/px)
85	48	2	68.64	1.46
170	24	4	34.32	2.91
255	16	6.2	22.88	4.37
340	12	8.3	17.16	5.83
510	8	12.5	11.44	8.74
680	6	16.7	8.58	11.66
850	5	20	7.15	13.99
1020	4	25	5.72	17.48
1190	3.4	29.4	4.86	20.57
1700	2.4	41.7	3.43	29.14

A geometric un-distortion function prepares photographs before the analysis; it minimizes radial distortion and ensures that photos will be pure projection on the image plane.

Although the digital camera is steadily fixed above the Total Station, the local temperature variations cause micro-strains that lead to some little changes of orientation and, consequently, to very large errors in the subsequent displacement analysis, especially for very far objects. Some fixed points, external to the landslide zone, need to be detected in the photos and taken as "reference point" for a useful displacement differential correction.

A proper colour mask filter must be selected in the object detection phase in order to accurately detect the target points in every frame and to get the right matching algorithm results.

Then couples of photos are compared in sequence (the first one with the second, the second with the third and so on) using the selected processing algorithm.

Since the pixel to meter conversion factor depends on the distance of the object from the camera, the focal length and the sensor-camera resolution, some initial distance values were attributed to every point starting from a stereo-photogrammetric evaluation. Without any estimates of the distances, it is possible to obtain the IFOVlin (Brivio et al. 2006) and then the metric scale ratio directly from the knowledge of the real target size (Table 1).

Application of the LDD to the Boschi di Valoria Landslide

The LDD code was tested with a sequence of images taken at the Valoria Landslide site.



Fig. 4 View of the landslide with localization of the targets and detail of a *red* net (Optical Target 1)

The target points, or optical targets, consist on the four red plastic nets, 1 × 1.5 m large, fixed on the surface with steel rods (Fig. 4).

The nets were assumed normal to the image plane in all the images. The initial true position of nets and the distance between camera and nets were evaluated by means of a preliminary stereo-photogrammetric survey.

The optical targets were identified in the first photo and then their position in other frames was estimated using different algorithms with an auto-size of the patches that include a two to five pixels large border around the targets.

For the displacement computation, we preferred to analyse only the red channel (R) of the RGB images in order to take advantage of the colour contrast of the nets with respect to the background. At the same time, we observed that also the Red minus Blue (R-B) channel appeared to be an alternative channel assuring a good resolution. Moreover, we tested that the texture information combined with colour information provides the best choice in feature detection algorithm also for red nets.

Some preliminary tests were performed to check the goodness of the method, the best matching algorithm, the measurement accuracy and the effect of different weather and daylight condition.

At first, we analysed a four frame sequence obtained artificially translating the same single image of three preset pixel quantities. This test is trivial but it permits to evaluate the reliability of the available matching algorithms (NCC, SSD, SAD). All produced identical results that were equal to the fixed displacement values, as it was expected.

After then, we performed a second test with a group of photos taken in about 20 min manually moving the targets of about 1.5–3–4.5 m away for three times. Since the daylight conditions are approximately the same during the frame sequence, the aim of this test is to check the properly work and the performance of the object detection algorithms.

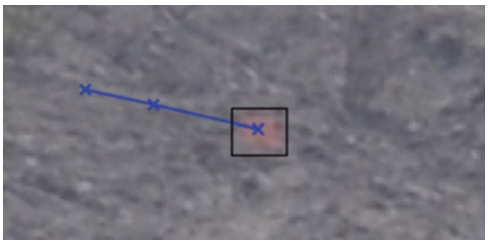


Fig. 5 Detail of the surface in which the OT1 target is *highlighted*. The displacements determined in a test with NCC algorithm are superimposed to the picture

Table 2 Measured velocities and error estimations for some optical targets

Target name	Distance[a] (m)	IFOV (m/pixel)	Observed max displacement rate (m/day)	Observed mean displacement rate (m/day)
OT 1	810	0.150	13.018 ± 0.600	1.320 ± 0.600
OT 2	733	0.107	5.700 ± 0.428	0.423 ± 0.428
OT 3	686	0.101	21.463 ± 0.404	1.660 ± 0.404
OT 4	548	0.071	0.261 ± 0.284	0.020 ± 0.284

[a]Evaluated by means of a stereo-photogrammetric survey

In this case, NCC algorithm provides the best results in terms of object recognition for all the target points.

In Fig. 5 was depicted the displacement of OT 1. (810 m far away from camera) (Table 2).

Finally, a sequence of 144 days from 26/6/2010 to 10/11/2010 was selected and taken as final test. Unfortunately, during this period the camera unexpectedly switched off several times without any reasonable reasons, causing the loss of many frames. Moreover, discarding with the weather filter the pictures captured in foggy and rainy conditions, only 33 × 3 photos were extracted from the list. The day-light conditions also affect the object detection particularly for our specific point of view of the camera that is south oriented, against sun. However, using only the R-B channel and the NCC algorithm we were able to follow the position of targets in 83 % of the images.

Results

Results of cumulative displacement of four optical targets during this period were resumed in Fig. 6.

As it could be noticed, observing Fig. 6, OT1, OT2 and OT4 fell down before the 10 November 2010 and they cannot be followed further.

It should be noted that all these steps introduce some errors in the displacement measures that cannot be easily estimated with accurateness. By the way, generally, these errors are lower than the expected displacement values.

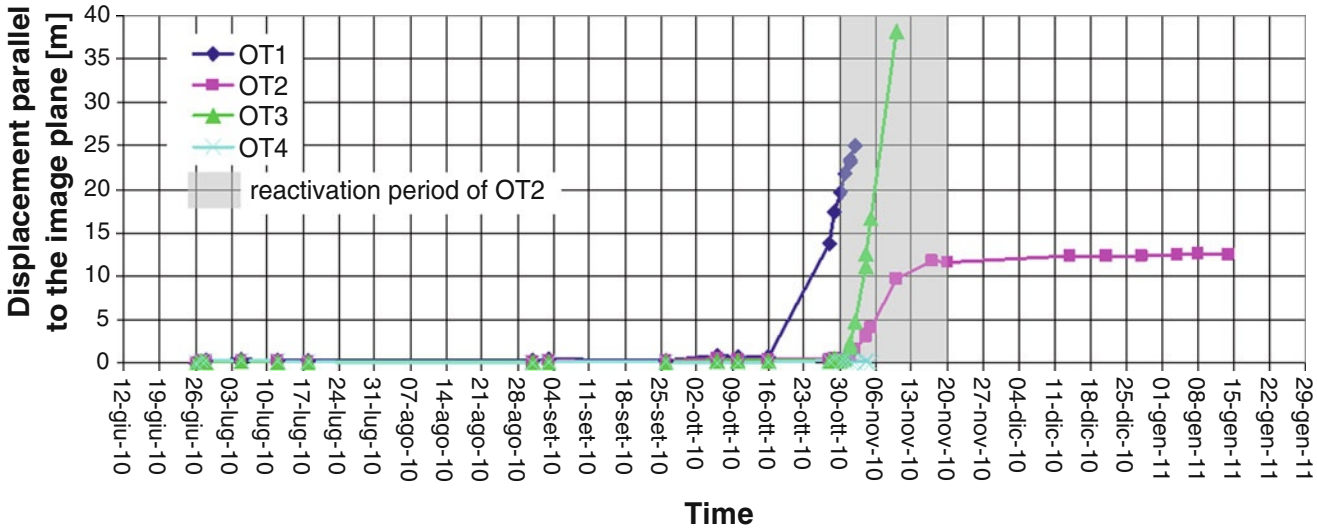


Fig. 6 Cumulative displacement for four optical targets

For example, considering a reasonable maximum error for the matching algorithm of two pixels (the theoretical minimum error is 1/10 pixel), a maximum error equal to two pixel for the geometrical distortion and a meter/pixel conversion dependent from the camera-distance, the absolute error of a sampled displacement are collected in Table 2.

Considering OT1, a maximum error of 60 cm for the true target position can be too much high for quasi-static target but satisfactory for large displacements (13 m/day). On the other hand, if the targets are close to the camera the error proportionally reduces; for example comparing OT1 and OT3 the relative error of the displacement rate reduces of about 30 %.

Conclusion

The Image Acquisition System combined with the Landslide Displacement Detector code provides a low-cost method for the surface displacement survey of landslides. It permits to simply analyse many points on a landslide with the condition that they are well distinguishable with respect to background.

In this work simple optical targets (red nets) were used, but in the future we are planning to test the use of natural objects like stones, little portions of greenery coverage and in general any kind of textured surfaces.

The obtained accuracy is not so high and then this method appears to be suitable for large deformable mass like mud-flows and not for quasi-static landslides or rock cliffs. However the error depends on the distance of objects from the camera, the type of targets, the focal length and the sensor-camera resolution. The existence of strategic points of view close to the surface to be monitored could improve results. Indeed, in the future, the commercial diffusion of cameras with higher resolution sensor could increase the quantitative goodness of this method.

The weather conditions strongly affect the possibility in measuring and probably this is the biggest fault of this technique. Photos with foggy condition need to be removed from the analysis and it does not permit an accurate measure of displacement in these periods. In addition, rainy condition avoided any kind of elaboration although it is a reasonable though that larger displacements probably occur just during rainy period.

Finally this method represents an interesting solution for displacement analysis of large portion of a landslide.

In the next future the possibility of a 3D displacement reconstruction will be explored by means of a stereo-photogrammetric evolution of this code.

References

Brivio PA, Lechi G, Zilioli E (2006) Principi e metodi di telerilevamento. Citta' Studi Ed, p 525 (in Italian)

Delacourt C, Allemand P, Berthier E, Raucoules D, Casson B, Grandjean P, Pambrun C, Varel E (2007) Remote-sensing techniques for analysing landslide kinematics: a review. Bul Soc Geol Fr 178(2):89–100

Ronchetti F, Borgatti L, Cervi F, Lucente CC, Veneziano M, Corsini A (2007) The Valoria landslide reactivation in 2005–2006 (Northern Apennines, Italy). Landslides 4(2):189–195

Travelletti J, Delacourt C, Allemand P, Malet J-P, Schmittbuhl J, Toussaint R, Bastard M (2010) Multi-temporal terrestrial photogrammetry for landslide monitoring. In: Proceedings of mountain risks international conference, Firenze, Italy, 24–26 Nov 2010, pp 183–191

White DJ, Take WA, Bolton MD (2003) Soil deformation measurement using particle image velocimetry (PIV) and photogrammetry. Geotechnique 53(7):619–631



A Geosensor Network Based Monitoring and Early Warning System for Landslides

Kurosch Thuro, John Singer, and Judith Festl

Abstract

In course of the alpEWAS (= alpine Early Warning System) research project a cost-effective landslide monitoring and early warning system has been developed during the last 3 years (2007–2010). The core of the project has been the development and testing of the three innovative, economically and continuously working measurement systems time domain reflectometry (TDR) for the detection of subsurface displacements in boreholes and reflectorless video tacheometry (VTPS) and a low cost GNSS sensor component for the determination of 3D surface movements. These measurements systems are combined together with other systems, monitoring trigger factors such as precipitation, in a geo sensor network which can be accessed remotely by a web interface, thus enabling to access all data in near real time. The Aggenalm Landslide (Bavarian Alps in the vicinity of Bayrischzell) was chosen as a field laboratory for the alpEWAS project. For 2 years now, the system has been working continuously except for minor disruptions, acquiring and recording all data.

Keywords

Landslides • Early warning system • Geo sensor network • Monitoring • TDR • GNSS • TPS

alpEWAS Project Details

The joint research project alpEWAS—development and testing of an integrative 3D early warning system for alpine instable slopes—aims to integrate innovative, efficient and cost-effective measurement techniques for landslide monitoring in a geo sensor network. The project has been funded by the geoscientific research and development program "Geotechnologien" of the German Federal Ministry of Education and Research (BMBF).

Events happening , also within the runtime of the research project, in the Alps as well as worldwide acknowledge the necessity to design efficient and cost-effective monitoring systems for instable slopes especially for areas that have yet not been monitored or only sporadically due to economic reasons. With the given option of a continuous remote access to the early warning system the stakeholder has the possibility to view and control all information of his scope centrally and to preserve the general survey given a situation in which for example due to heavy rainfall several landslides have to be evaluated simultaneously.

The subject of the joint research project is the testing and advancement of three measurement techniques (Fig. 1) time domain reflectometry (TDR), reflectorless video tacheometry (VTPS) and low-cost GNSS sensors as well as their coaction as an early warning system and their integrative data analysis.

The project alpEWAS (description in Thuro et al. (2009), Singer et al. (2009c), also see www.alpEWAS.de) can be outlined in five phases: (1) Selection and investigation of a project area. (2) Design and installation of the early warning system. (3) Learning phase of the early warning system.

K. Thuro (✉) • J. Singer • J. Festl
Technische Universität München, Engineering Geology, Arcisstr. 21, 80333 Munich, Germany
e-mail: thuro@tum.de

C. Margottini et al. (eds.), *Landslide Science and Practice*, Vol. 2,
DOI 10.1007/978-3-642-31445-2_10, © Springer-Verlag Berlin Heidelberg 2013

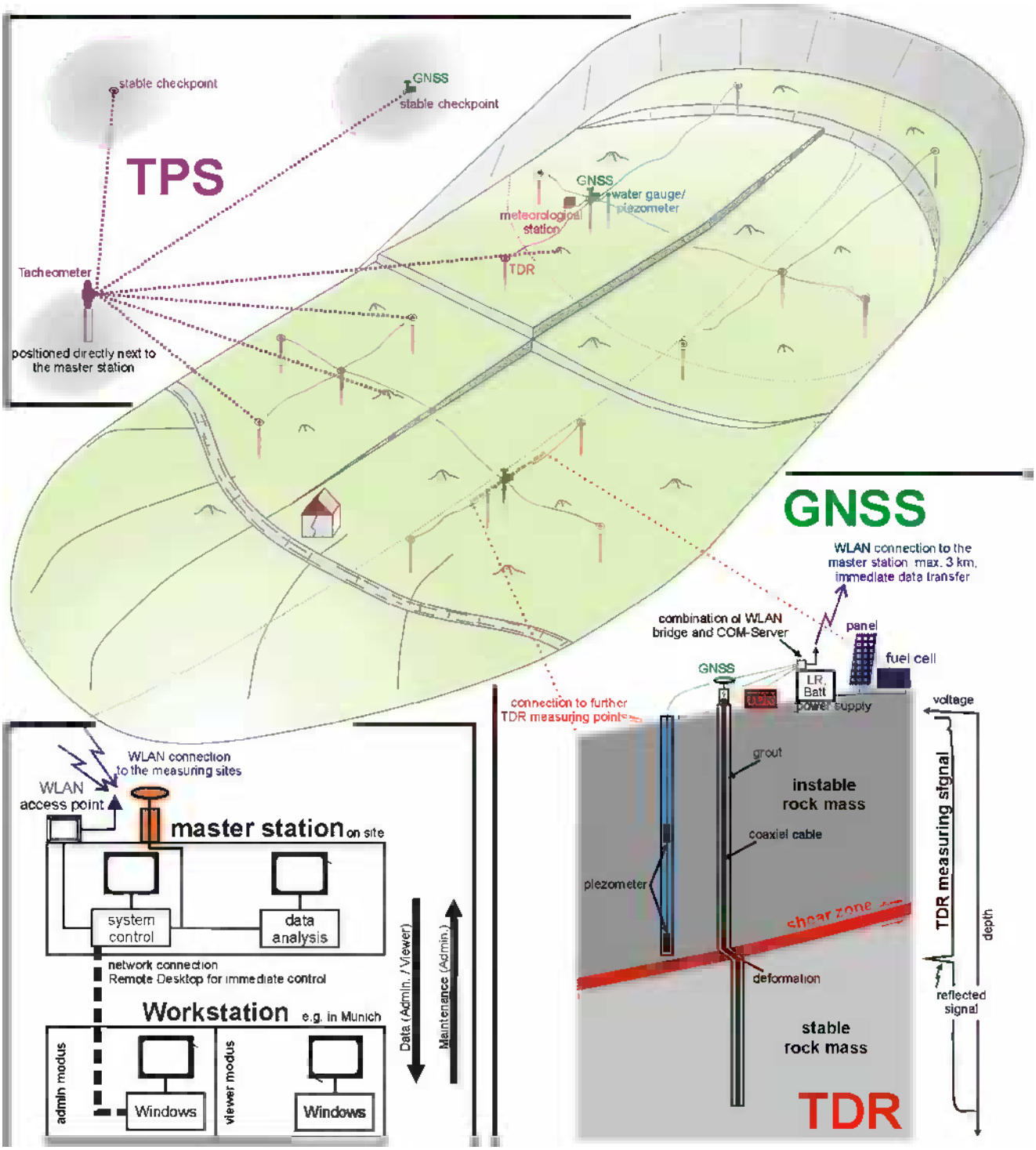


Fig. 1 Schematic depiction of the geo sensor network "alpEWAS" installed at the Aggenalm landslide

(4) Testing phase of the early warning system. (5) Automation and optimization of the early warning system.

In the Sudelfeld region—in close reconcilement with the Bavarian Environment Agency (Bayerisches Landesamt für Umwelt, BLfU)—the Aggenalm Landslide has been chosen as a test site since it features very good premises for the testing of new technologies in the field under alpine conditions. It became obvious that the present movement rates of 1 cm/a are smaller than expected at the initiation of the project. Therefore the assessment of threshold values may be affected or limited (project phase 2 and 3), eventually with the Aggenalm Landslide a project site for the

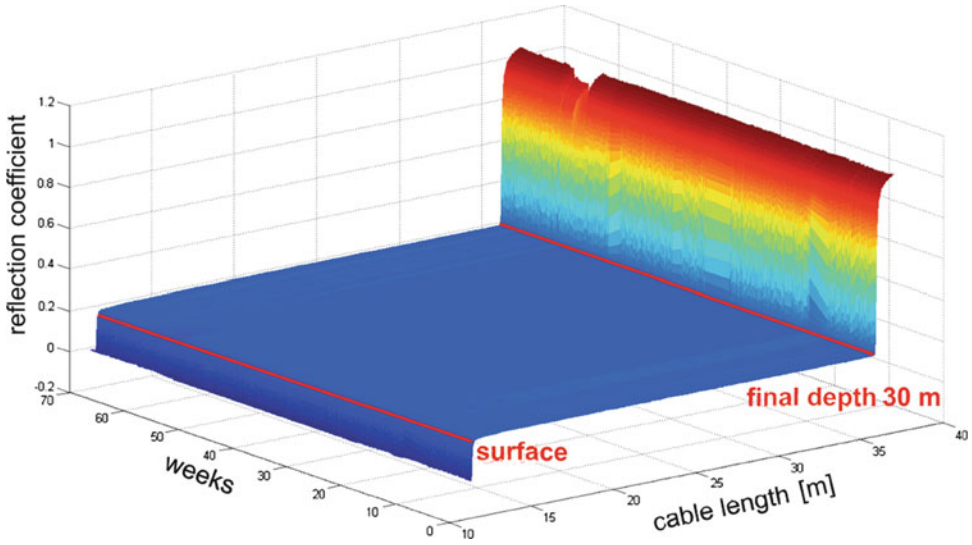


Fig. 2 Time series of the TDR measurements at the sensor node KB1 (Location: lower Lampl-Alm)

testing of the measurement systems with a low hazard potential exists. Within the scope of the project software applications for the sensor control, data management, complex data processing and integrative data analysis have been developed. After expiry of funding the monitoring of the Aggenalm Landslide will be continued by the involved institutes (Festl et al. 2011).

A geological overview is given by Singer et al. (2009c); the geo sensor network is described in Thuro et al. (2010). Consecutively in addition to the mentioned publications it will be reported on the three measurements techniques, the attained results as well as the combination and analysis of the data.

Researched Measurement Techniques

Time Domain Reflectometry (TDR)

Several different parameters—the type of cable used (lead and measurement cable) and the grout composition (cement, betonite, cement additives)—play an important role in the quantification of TDR deformation measurements below surface. These parameters have been tested by means of calibration tests in a comprehensive laboratory program (Singer et al. 2009b; Singer et al. 2010; Singer 2010).

The results of all the laboratory tests combined with experiences from field surveys of the TDR system were incorporated into an installation handbook, which gives standardized installation recommendations consisting of a combination of cable type and grout composition for different geological settings and typical mass movement mechanisms and velocities. Next to the preparation and completion of the installation handbook the TDR deformation analysis software was worked on and refined.

The TDR system, that has been installed at the Aggenalm Landslide, is continuously operating since November 2008 (begin of installation and operation September 2008) and acquires measurements hourly. The TDR system has proven a reliable measurement system at large. Over the total period since the beginning of operation (28 month), the data loss sums up to about 18 % of the planned measurements mostly because of power shortages and late data retrieval (full data storage before the start of the automatic data acquisition). For the time since the start of the fully automatic data retrieval the data loss adds up to 10 %. Here, a major annoyance in January 2010 accounts for the loss of data. It can be assumed that in future an even higher reliability can be achieved due to the automatic data retrieval and data storage as well as the developed Status Monitor Software as the time since February 2010 has already shown.

The field test at the Aggenalm has shown that most of the cables (lead and measuring cables, connectors; mostly installed subsurface) proved to be robust concerning the weather, also during winter. Up to date no significant deformations have been measured with the TDR system at the Aggenalm Landslide, therefore the signal and deformation analysis could only be used and tested for the evaluation of laboratory tests.

Figure 2 shows the results of the TDR measurements at the Lampl-Alm (KB1) node. Depicted are the reflection coefficient—depth curves as a time series in relation to the reference measurement in October 2008. The TDR time series shows no measureable deformations, the reflection coefficient doesn't change at all during the depicted time period, only the characteristic noise can be seen. This can be explained by the small amount of deformation which has not yet been able to fracture the grout surrounding the coaxial cable—a prerequisite for a deformation analysis with TDR.

Reflectorless Video Tacheometry (VTPS)

One of the goals of the alpEWAS project was to gain first practical experience in field using an innovative instrument type which is not commonly used for displacement monitoring, yet: a video tacheometer (VTPS—video tacheometric positioning system). At this stage the Topcon Imaging Station is the only instrument available on the market which in principle has a video functionality with the necessary precision (Topcon Positioning Systems, Inc. 2008). Other instruments—the Trimble Spatial Station VX and the Leica Viva TS15—could be used only with major cutbacks due to their image resolution and field of view (Trimble Navigation Limited 2010; Leica Geosystems 2007, 2010). All the instruments mentioned cannot be used scientifically, as the cameras cannot be read out by external devices. External camera control is only possible so far using a Leica Geosystems prototype, which has been coopered in a small batch of only five instruments. It consists of a TPS1200 tacheometer with access to all instrument subsystems, which has been modified with an internal camera (now called IATS2—Image Assisted Total Station second edition). Various limitations by design, especially regarding practical handling, need still to be accepted and have to be abolished by the manufacturer for later marketability. Among others, this includes the tentative cable guiding and the tarring of the modified telescope layout. The prototype is explained in Wasmeier (2009b) and, together with its extensive calibration, in Wasmeier (2009a). There also the possible accuracies were examined which in the field are approx. $\sigma < 1$ mgon on average, but under bad conditions up to $\sigma > 2$ mgon. Under laboratory conditions, a repeatable accuracy capability of < 0.15 mgon has been proofed.

At the Aggenalm project site the method was used to capture object points distributed on the slope from a central setup point by means of polar measurements and check for displacements. Beforehand, this is quite similar to the conventional setup of a permanent or temporarily tacheometric monitoring system without net measurement. But in contrary to that, in the alpEWAS approach only natural targets and no retroreflecting prisms were used. This goal, on the other hand, also implicates, that permanent measurements will not be possible due to slope exposition and the long-lasting snow coverage in the Sudelfeld area. If a real deformation detection is the goal, other methods can be used, which e.g. have been evaluated at the TU Wien using the same prototype instrument (Reiterer et al. 2010). Further application possibilities can be found in Thuro et al. (2010).

In Fig. 3 the measurement points in the Aggenalm test site are shown. The arrows mark the planar displacement vectors between fall 2008 and fall 2009 (red) and between fall 2009 and summer 2010 (orange). Tacheometric target points without vectors haven't been measured in all epochs due to single measurement failures in target detection or range measurement. The displacements are between 3 and 12 mm, which are not significant due to the necessary setup of the measurement pillar position using stable reference points in big distances, but regarding orientation and absolute value they are highly feasible, also compared to GNSS results.

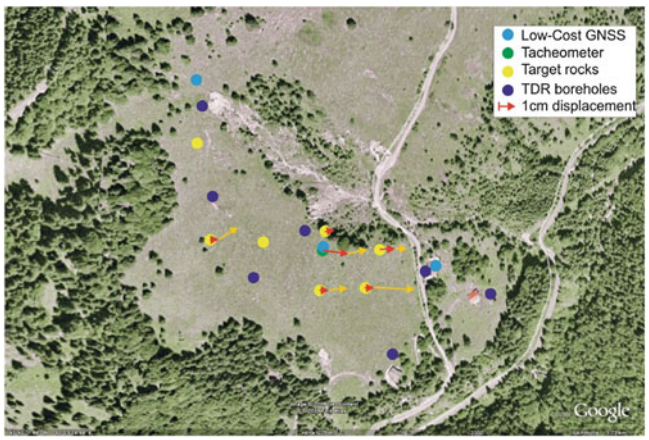


Fig. 3 Measurement points at the Aggenalm landslide. The *arrows mark* the displacement vectors of VTPS between fall 2008 and summer 2010. Target points without vector haven't been measured in all epochs due to some failures

The advantage of video tacheometry compared to conventional and approved methods lies in the variability of possible target structures which can be both artificial (target marks or reflectors) and natural.

Low-Cost Global Navigation Satellite System (LC GNSS)

The satellite supported monitoring component of the integrative monitoring system at the Aggenalm consists of an all-weather proof low cost GNSS measurement system based on simple robust navigation receivers produced for the mass market. The applied receivers allow a tracking of the American GPS as well as the Russian Glonass satellites. Such receivers are able to monitor discrete points at the surface of the sliding slope continuously with sub centimeter accuracy.

In order to achieve the aspired accuracy with low cost GNSS equipment, mainly 1-frequency code and carrier phase receivers are used in combination with a near real time post-processing analysis. This means that over a predefined period of time—usually 15 min—raw data is recorded continuously at the different receivers.

Using wireless communication techniques (WLAN) all raw data is transmitted "on the fly" to a central computing station. As soon as the raw data from the different locations—at least one station should be on stable ground

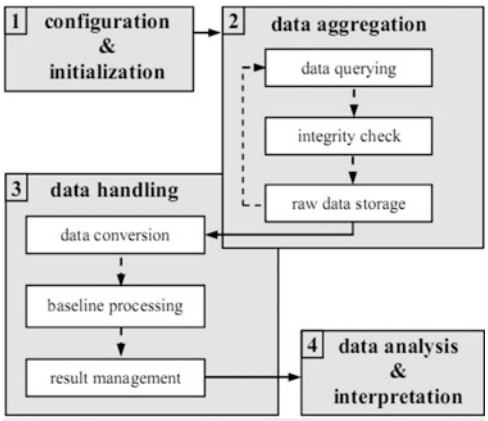


Fig. 4 Workflow of the central control application (Glabsch et al. 2010a)

(reference station) and the others are spread on the slope (there are three such stations at the Aggenalm)—is available the baseline processing can start immediately. If there are more reference stations disposable the possibility of a geodetic network adjustment based on least squares is given. In contrast to real time kinematic applications the whole evaluation with such a near real time approach can be designed and controlled by the operator. In the alpEWAS project it could be shown that with the near real time approach accuracies can be achieved which normally only can be obtained by geodetic high-end receivers. In context of a geo sensor network the GNSS stations are called sensor nodes in the following.

Beside the design and construction of the GNSS sensor nodes the core is the software component called Central Control Application (CCA). This software is developed by using the graphical programming language LabView®, National Instruments. All steps in the workflow (Fig. 4) from the configuration and initialization (1) to the continuous data recording (2) and the parallel operating near real time processing (3) to the transmission of results (4) is controlled and executed by the CCA. A modular, prospective design offers the option to integrate a great diversity of sensors. Only the corresponding program implementation has to be realized. Individual design of the evaluation is given by the steps 3 and 4. The information obtained from the GNSS nodes (coordinates, quality parameters, status information) is stored in a MySQL database and updated every 15 min. All data collected by the geo sensor network is promptly available in a central data sink for an integrated evaluation this way. For further technical details of the developed measuring system please see Glabsch et al. (2010b) and Glabsch et al. (2010a).

With the current state of the developed software and the designed GNSS sensor nodes a continuous and robust operation of the low cost GNSS monitoring component is realized. Currently, only very rare malfunctions occur which are mainly caused by energy shortages. Longer power outages in the 230 V electricity supply system lead to failures in particular at the central station and the multifunction node in the middle of the slope. Short power black outs can be bridged by an uninterrupted power supply (ups). Beside these energy shortages a secure GNSS system operation of the autonomous stations is a challenge especially in the alpine winter (partial complete snow cover of the antennas and solar panels for days or weeks). Only an appropriate choice of reliable equipment and the dimensioning of the devices lead to a reliable year-round operation.

Some results of the low cost GNSS monitoring component at the test side Aggenalm are presented in Fig. 5. In each case, the position components (easting Y, northing X, where Y is approximately slope direction) are depicted for the period March 2009—December 2010 by a moving average filtering based on the L1-norm estimator. The filter extends over 24 epochs (nodes 2 and 3) and 48 epochs (node 1). Using a time interval of 15 min to acquire the carrier phase measurements the filter length corresponds to 6 or 12 h. The choice of this filter type and length is the consequence of partial bad local obstructions at the sensor nodes that lead to temporarily incorrect processing results—even in some cases a successful solution cannot be computed at all. Despite some technical problems and the resulting data gaps longer-term trends of the movement of the three sensor nodes can be captured very well. As the time series at node 2 and 3 show an acceleration phase occurs during springtime (snow melt).

Presumably due to the low snow cover of the slope in spring 2010 (c) a comparable arise as in spring 2009 (a) cannot be seen. The effects of a heavy rainfall event in June 2009 (b) are also visible.

The all-weather proof low cost GNSS monitoring component based on standard components for sensors, power supply (batteries with solar panels) and WLAN communication developed in the project at a prototype stage is successfully tested at the Aggenalm. In the actual configuration a complete GNSS sensor node requires an investment of about 3,000 €. The developed Central Control Application allows a reliable system operation. Although the achieved accuracies with filter lengths of about 6 h already permits the possibility to evaluate long-term behaviour of the slope even with only small changes during the year, the full potential of using simple navigation receivers for surveillance tasks has not been tapped yet. For an improved early warning a (significant) shortening of the filter length is an essential challenge. Overall, it was possible to examine and to develop the use of low cost GNSS sensor technology so far that an introduction of this new measurement technique into practice can be started now. The gained results demonstrate that the low cost monitoring approach can successfully be used alternatively to precise tacheometric geodetic surveys or expensive high-end GNSS receivers (Glabsch et al. 2009).

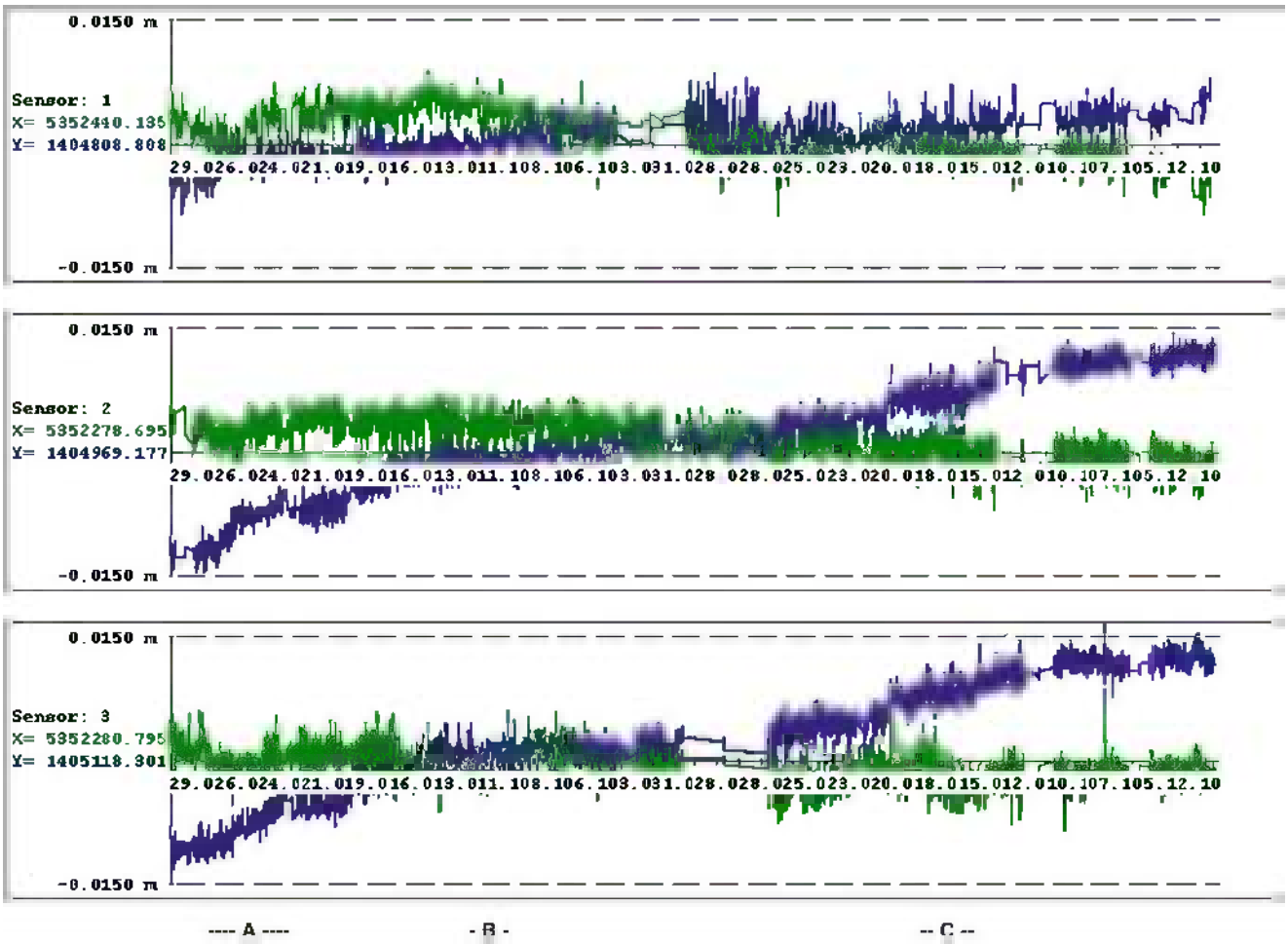


Fig. 5 Variations of the horizontal position of sensor nodes 1–3, time period March 2009 to December 2010, moving average (node 1: 12 h, nodes 2, and 3: 6 h)

Data Management and Integrative Data Analysis

Data Management

The alpEWAS Control software package (Fig. 6) was developed as a modular software package to control the entire data management within the project. The flexible layout offers an ideal adjustment of the software's sub-programs to the underlying measurement system.

A central component is the open source MySQL database. The link between the geo sensor network, respectively the sensors installed at the field site, and the database is established by the so called sensor plugins. Besides the sensor control, status monitoring and readout of raw data as well as the communication of information via a standardized communication protocol a first analysis is conducted to provide next to raw data also prompt usable information (first level results) in the database for further integrative analysis. Various monitoring tools permanently check the current status of the system in order to detect the exceedance of critical system parameters (such as thresholds) as well as failures of individual sensors or subprograms. If one of these is detected the system administrator is informed immediately, thus long-time data loss can be avoided.

An important interface is the link between the onsite computer center and the end user being interested in information about the current status. The data management concept is as follows: By reflecting the database constantly from the master computer to a second data server (slave) possessing a broadband connection at the project office high data integrity and an almost unlimited parallel data access from several users can be achieved. Complex and computationally intensive analysis can be split to several machines this way. For data exchange between heterogeneous systems (interoperability) it is possible to query all results by means of access authorizations via standardized interfaces. Standards such as the worldwide standard of handling space-orientated data for an interoperable benefit being developed by the Sensor Web Enablement (SWE) initiative of the Open Geospacial Consortium (OGC®) have been accounted for.

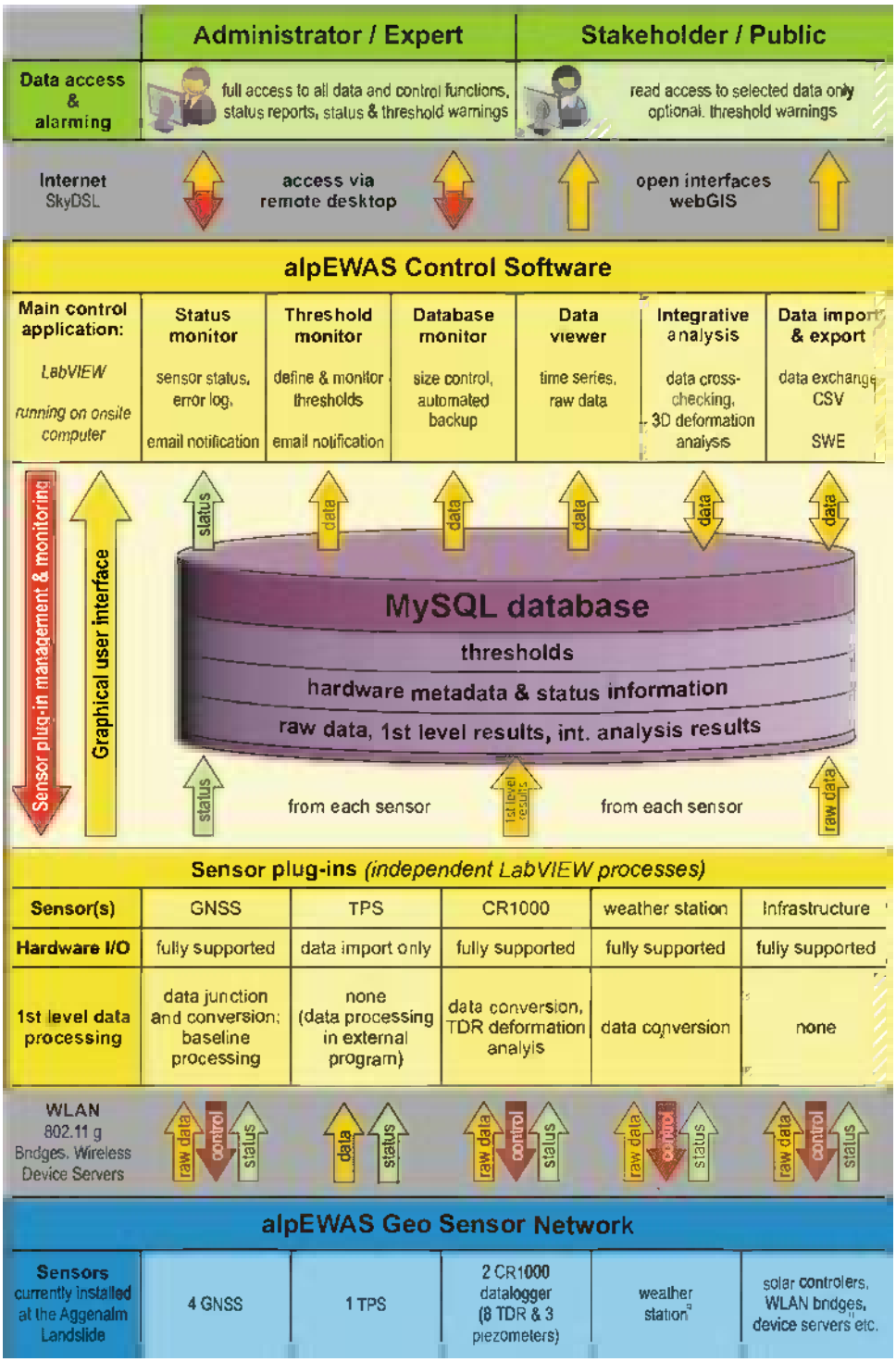


Fig. 6 alpEWAS Control, management and data analysis software

Conclusion and Perspective

The developed measurement techniques TDR and low cost GNSS are more or less based on already existing hardware components, while the video tacheometer hasn't been introduced to the market yet, and is available as a prototype from *Leica Geosystems* only. New developments in the video tacheometry were mostly accomplished in the fields of the adaption of the system layout for the measuring task "slope monitoring" and in signal analysis and sensor control. The efficiency of TDR and low cost GNSS for continuous monitoring could be proved. Decisive therefore are the developed software components for the data management

and complex data analysis. These two measurement techniques are now on the cusp of marketability, whereat the range of application isn't limited to mass movements, but can be extended to other monitoring tasks such as the monitoring of structural elements (Singer et al. 2009a).

References

Festl J, Singer J, Thuro K (2011) The Aggenalm landslide – first findings of the acquired monitoring data. In: International symposium on rock slope stability in open pit mining and civil engineering, Vancouver, Canada, 18–21 Sep 2011, p 7

Glabsch J, Heunecke O, Schuhbäck S (2009) Monitoring the Hornbergl landslide using a recently developed low cost GNSS sensor network. J Appl Geodesy 3:179–192

Glabsch J, Heunecke O, Schuhbäck S (2010a) Development and testing of a low cost sensor PDGNSS landslide monitoring system using the example of the Aggenalm Landslide in the Bavarian Alps. In: Altan O, Backhaus R, Boccardo P, Zlatanova S (eds) Geoinformation for disaster and risk management. JB GIS, Copenhagen, pp 63–70

Glabsch J, Heunecke O, Schuhbäck S (2010b) Überwachung von Rutschhängen mittels low-cost GNSS Empfängern im near real time processing. In: Wunderlich T (ed) Ingenieurvermessung 10. Wichmann, Berlin, pp 275–288

Leica Geosystems AG (2007) Leica TPS1200+ Series. XI.07 738600de, Herbrugg, 16pp

Leica Geosystems AG (2010) Leica Viva TS15. Data sheet, Herbrugg, 1pp

Reiterer A, Huber N, Bauer A (2010) Bildbasiertes Erfassen und Matching homologer Punkte mittels Feature-Vektoren – Funktionsweise und Evaluierung beim Einsatz in einem Deformationsmesssystem. In: Wunderlich T (ed) Ingenieurvermessung 10. Wichmann, Berlin, pp 241–254

Singer J (2010) Development of a continuous monitoring system for instable slopes using time domain reflectometry (TDR). PhD thesis, Technische Universität München, Munich, Germany, 189pp

Singer J, Grafinger H, Thuro K (2009a) Monitoring the deformation of a temporary top heading invert using time domain reflectometry. Geomech Tunnel 2:238–249

Singer J, Festl J, Thuro K (2009b) Computergestütze Auswertung von Time Domain Reflectometry Messdaten zur Überwachung von Hangbewegungen. In: Marschallinger R, Wanker W (eds) Geomonitoring, FE-Modellierung, Sturzprozesse und Massenbewegungen. Heidelberg, Wichmann, pp 19–34

Singer J, Schuhbäck S, Wasmeier P, Thuro K, Heunecke O, Wunderlich T, Glabsch J, Festl J (2009c) Monitoring the aggenalm landslide using economic deformation measurement techniques. Aust J Earth Sci 102:20–34

Singer J, Thuro K, Festl J (2010) Development and testing of a time domain reflectometry (TDR) monitoring system for subsurface deformations. In: Zhao J, Labiouse V, Dudt J-P, Mathier J-F (eds) Rock mechanics in civil and environmental engineering. Taylor & Francis Group, London, pp 613–616

Thuro K, Wunderlich T, Heunecke O, Singer J, Schuhbäck S, Wasmeier P, Glabsch J, Festl J (2009) Low cost 3D early warning system for alpine instable slopes – the Aggenalm landslide monitoring system. Geomech Tunnel 2:221–237

Thuro K, Singer J, Festl J, Wunderlich T, Wasmeier P, Reith C, Heunecke O, Glabsch J, Schuhbäck S (2010) New landslide monitoring techniques – developments and experiences of the alpEWAS project. J Appl Geodesy 4:69–90

Topcon Positioning Systems, Inc. (2008) Topcon imaging station – long-range scanning, imaging and robotic total station. Revision A 7010–0876, Livermore, 4pp

Trimble Navigation Limited (2010) Trimble VX spatial station – Datasheet, Singapore, 4pp

Wasmeier P (2009a) Grundlagen der Deformationsbestimmung mit Messdaten bildgebender Tachymeter. PhD thesis, Technische Universität München, Munich, Germany, 169pp

Wasmeier P (2009b) Videotachymetrie – Sensorfusion mit Potenzial. AVN, pp 261–267



Underground Landslide Displacement Monitoring: A New MMES Based Device

Andrea Segalini and Corrado Carini

Abstract

This paper describes the analysis of the effectiveness and reliability of a new type of inclinometric chain, which is still under development by the authors, and is intended to be applied in the underground slope monitoring field. In the first part, the paper describes the new instrumentation which should allow for a deeper and detailed understanding of the type, location and origin of slope movements that should, in turn, help in understanding the triggering causes and the evolution mechanisms of landslides, and provide an innovative and substantial contribution to their stability analysis and control. The second portion of the paper is dedicated to a comparison between the classic instruments and the new MUMS device, demonstrating the advantages of measurement automation and economy in the use of the proposed device, which could also be equipped with other electronic instruments that would allow the measurement of other interesting physical quantities (such as pore pressure, temperature, stresses, etc.) together with displacement components.

Keywords

Monitoring • MEMS • Inclinometers

Introduction

In the geological, geotechnical and geomechanical fields, automatic monitoring systems constitute a fundamental element in the comprehension and evaluation of both, the natural slope characteristics and dynamics and, the definition of the interactions between these slopes and the man-made structures that are related with them. In order to design and set up an efficient monitoring system, it is necessary to clearly define the main objectives (i.e., displacement control, variation of state of stress, variation of geometry, etc.) which precede the definition of the physical entities to be measured and recorded and, therefore, the choice of mechanical and/or electronic apparatus most suitable for those measures, in terms of precision, resolution, repeatability and reliability. The main issues regarding the choice of monitoring instrumentation is related to the environmental conditions to which these apparatuses will be exposed and to the commonly large extent of the monitored areas subjected to natural phenomena; moreover, these areas are often located at long distances from essentially urbanized lines such as electricity and telephone distribution networks that could be useful for the collection and distribution of data.

One of the most critical aspects, both for slope stability and settlement, relates to the automated monitoring of underground displacements. Until now, the underground monitoring of moving slopes has been carried out using inclinometers (Stark and Choi 2008) that require the presence of at least one operator to measure displacements along a vertical borehole; such measurements are carried out using a biaxial servo-accelerometer device that is repeatedly lowered and recovered from the borehole. This operation prevents the possibility of automated monitoring and, in response to this

A. Segalini (✉)
DICATeA, University of Parma, V.le G.P. Usberti 181/A, Parma, Italy
e-mail: andrea.segalini@unipr.it

C. Carini
GEIelettronica S.r.l., Via R. Koch 55/A, Pilastrello, PR, Italy

C. Margottini et al. (eds.), *Landslide Science and Practice*, Vol. 2,
DOI 10.1007/978-3-642-31445-2_11, © Springer-Verlag Berlin Heidelberg 2013

need, some authors (Lollino et al. 2002) have proposed the installation of automated mechanical systems which proved to be expensive and often unreliable due to mechanical problems related with casing deformation. Another proposed solution, which is still widely applied, is based on the installation of fixed inclinometer probes (an inclinometer chain) positioned around the predetermined sliding surface (or shear belt); however, this solution has its own drawbacks, mostly related to the large approximation of the measurements carried out at a restricted depth interval and to the high cost of the inclinometer probes, which are frequently lost in situ due to a large amount of displacement of the landslide body. Another solution is the application of Time Domain Reflectometry (TDR) to measure the position and amount of displacement along a vertical borehole (Pierce 1998; O'Connor and Murphy 1997): this system does not, however, resolve the problem of the automation of measurements unless a fixed readout unit is left in place for each vertical borehole, with an excessive increase of costs. Another drawback of the technique is related to the fact that it does not allow the recognition of the direction of movement.

In order to overcome these problems, a new Modular Underground Monitoring System (MUMS) has been studied and developed. The system is modular, having the possibility to accommodate various sensors such as pore pressure cells, extensimeter, load cell, etc., which can be installed in the same borehole and are connected and communicate along a single cable with a readout unit located at the borehole head; the readout unit interrogates these sensors alternately, recording their response. The main purpose of the MUMS, however, is the measurement of the underground displacements along the whole length of a borehole and its main apparatus is constituted of several devices spaced at known distances along the vertical borehole. The principle of the measurements is analogous to that of inclinometric probes but, instead of having a single probe to be inserted and moved along the borehole, this system has several units, each one containing a Micro Electro-Mechanical System (MEMS) that will remain in place underground; these are referred to as *nodes*. The spacing of these nodes is functional to the required precision, the presumed duration of monitoring and the estimated velocity of the landslide. The readout unit of the MUMS can be equipped with a data transmission system, either radio or GSM. Each MUMS apparatus has an on board memory (SD card) that backs up the measured data according to its memory capacity. The unit is powered up by a battery which can be associated, when the duration and frequency of measurements require it, with a photovoltaic panel for recharge.

Operating Principles

The measurement of underground deformation is normally carried out inside specifically drilled boreholes, using the inclinometric probe. With this instrumentation, the horizontal displacements are calculated from the measures of the inclination of the probe with respect to the vertical axis (gravity); the inclination is measured using biaxial acceleration sensors which resolve the components of the normalized gravity vector on the horizontal plane. Comparing the measurement at a given time with those made after the installation of the inclinometer casing (zero reading), one obtains the total horizontal displacement that has occurred in the time interval between the zero reading and the current measurement. This allows for the identification of the surface/shear band where there is a transition between the deep and stable portion of the ground and the upper unstable part of the monitored slope; furthermore, the calculated data enables the definition of the average speed and direction of the moving mass.

The measurement of these rotations is conditioned by the instrumental precision and by various types of errors which can be grouped in two main sets: bias errors and instrumental errors. Some of them can be compensated by appropriate measurement techniques, while others remain and are propagated in the calculations. The highest resolution of the instrumentation is 0.02 mm for 500 mm, while the repeatability of the measurements is ± 0.01 % FS (Durham Geo Slope Indicator 2009).

The MUMS instrumentation was born from the idea of replacing the above measurement procedure by locating appropriate nodes at a known distance from each other and positioned along a connecting pipe; these nodes will be originally aligned to each other and will have and maintain one of their axes coincident with that of the pipe. Each node is able to measure its local orientation from the vertical (gravitational acceleration) by means of a micromechanical 3D digital linear acceleration sensor (MEMS). This will allow us to determine the direction cosines of the pipe axis in each node and, by means of linear geometry and trigonometry, calculate its 3D shape and deformation along the whole borehole. The basic hypotheses of this procedure are: the lower node must be located in a stable portion of the soil/rock and must be accurately cemented to it; and the distance between two subsequent nodes along the pipe must not vary. From the static point of view, the system can be described as shown in Fig. 1. This configuration, although very practical and with a limited number of data to be recorded, requires particular attention during the installation procedure, since in order to achieve the required accuracy and a correct estimate of the displacement direction, it is mandatory that all of the nodes are originally aligned along a single diametral plane of the pipe. This mechanical condition can lead to errors, due to a possible spiralling of the pipe and to a possible incorrect assembly of the nodes, which could degrade the evaluation of the displacement heading and therefore compromise their final integration from the bottom up along the borehole. To avoid this inconvenience, it is possible to add to the node a 3D digital magnetic sensor which enables us to determine the heading (azimuth) of

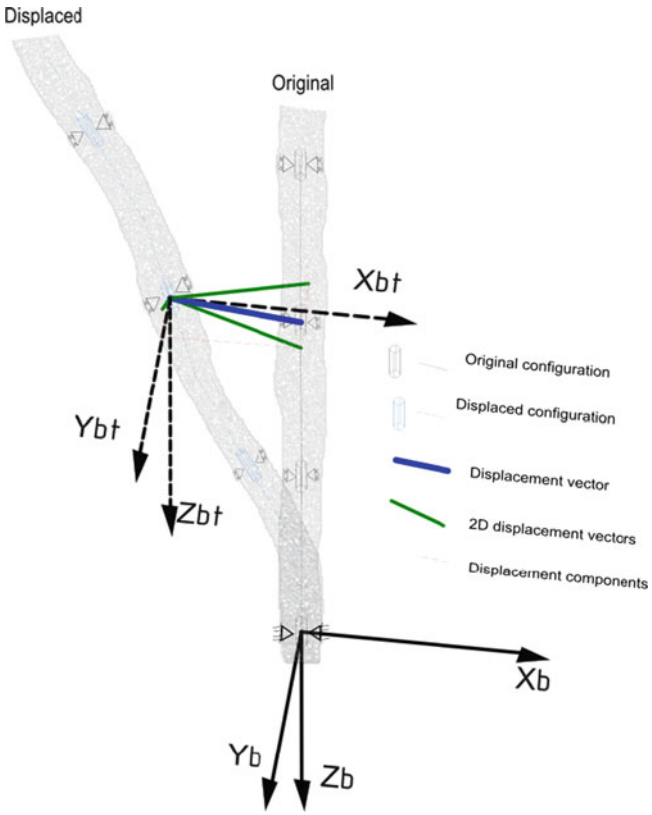


Fig. 1 Schematic representation of the original and displaced configuration. X_b, Y_b and Z_b are the global reference system axes (as further defined) while X_{bt}, Y_{bt} and Z_{bt} are the same axes translated in the node centre

each node related to magnetic north. This added element eliminates the uncertainties and any errors due to spiralling or to system assembly imprecisions. The accuracy of the measurements depends on the appropriate calibration of each node (carried out at the production laboratory) and on the site specific constants tied to the local orientation of the Earth's magnetic field. The Earth's magnetic field (Campbell 1997) is well known and accurately modelled by several geomagnetic models (EMM2010, HDGM, etc.) which are compiled from satellite, marine, aeromagnetic and ground magnetic surveys around the globe. These models are constantly updated and already in use by directional drillers as a natural reference frame to orient the drill. The calibration procedure reduces all the instrumental errors caused by the sensors and their assembly in each node, but it is not capable of correcting errors (although it does recognizes their presence) caused by local magnetic anomalies that may be present. However, this correction can be done once the vertical axis direction is known from accelerometer measurement, since the node is supposed to be still at the time of each reading and the only acceleration measured is that of gravity. With the increased complexity of each single node, the amount of data to be transferred along the MUMS system increases as well and, for this reason, an appropriate connecting system has been studied which allows for the use of a single cable (4 poles) for the serial querying of each node and data recording. The total number of data collected, when all the sensors described are installed, is a minimum of 7 for each node, considering also a temperature sensor that is deemed useful (for sensors compensation) especially on sites where severe variations are expected. Furthermore, the possibility is foreseen of adding, along the MUMS instrument, several other sensors for the measurement of more physical features (pore pressure, load cells, etc.) that might be needed.

Data Processing

Brief Description of the Standard Inclinometer Measurement

The standard inclinometer instrumentation normally used for the measurement of underground displacements requires the installation of an inclinometer casing inside a borehole appropriately drilled; the casing has two pairs of diametric grooves normal to each other, in which the inclinometric probe is inserted and lowered along the borehole. The casing normally has a diameter varying between 48 and 85 mm and is normally cemented inside boreholes of a diameter varying between 110 and 130 mm. The main requirement for measurement interpretation is the rigid connection of the lower part of the casing to a stable substratum (either soil or rock). The system operation requires a first reading usually called "zero reading", which is the reference measurement for all the subsequent surveys; the readings are carried out by an operator who lowers the probe to the end of the casing along the first couple of grooves, waits for the temperature stabilization of the sensors and then starts to retrieve the instrument at 50 cm intervals. At each interval the instrument is stopped and the measurement of the two axial accelerometers is recorded (after temperature stabilization) either manually or by means of a surface data logger. Once the first reading is completed, the probe is rotated through 90 ° and lowered again in the same set of grooves. The same procedure is done for the other set of grooves, recovering all the data needed for measurement analysis and displacement calculation. The entire procedure requires the operator on site for an average time of 1.5–3 min/m of casing (30/60 min for a 20 m long casing); to this operation time must be added the time to reach (and get back from) the location of the inclinometer hole. This is a time-consuming and costly task that doesn't allow for a frequent repetition of the surveys.

Description of the New MUMS Measurement

The new apparatus (Fig. 1) requires an installation procedure that is analogous to that of a standard inclinometer casing, except for the fact that the MUMS pipe has a diameter of only 5 cm, it is partially pre-assembled at the production laboratory for the requested length and can easily be introduced and installed in smaller boreholes and/or inside old inclinometer casings that are partially broken (and unusable) due to previous landslide movements. The average lifespan of a standard inclinometer ends up with a recorded horizontal displacement of 8–15 cm, depending upon the dimension of the shearing surface/band. During the laboratory pre-assembly, all the nodes are installed and fixed inside pipe portions of appropriate length, cabled between each other and tested for a correct response; their calibration files are recorded and stored on the data logger memory (SD card). Once the installation site is reached, the single pipe portions are aligned and permanently connected using a practical technique that provides compound glue and rivets. Note that the pipe does not need to be watertight, since each node is waterproofed independently; in fact, the connecting pipe has micro holes to allow the expected water to get into the pipe without any buoyancy effect during installation. Once the MUMS pipe is introduced all the way into the borehole (stabilized with a temporary casing if needed), cementing of the lower portion of it (1.5–3 m) is carried out by injecting a suitable fast-hardening grout from the bottom. The remaining portion of the borehole is then filled with clean gravel with a diameter of 3–8 mm, recovering the borehole stabilization casing in such a way to maintain 2–3 m difference between the level of the gravel inside the borehole and the bottom of the casing. The new conception MUMS instrumentation is based on principles that are analogous to those of the standard inclinometer, with a few substantial differences:

(a) It is formed by a series of nodes, which measure and record the absolute orientation of the MUMS pipe axis relative to the vertical (if the nodes are instrumented with a 3D digital axial accelerometer only), or the absolute orientation of the MUMS pipe axis relative to the vertical and the Earth's magnetic north (if the nodes have a 3D digital magnetic sensor as well); in this case the orientation of the nodes is determined using the flight convention attitude (Tait-Bryan angles), appropriately modified to treat our problem;
(b) The nodes remain inside the ground for the whole duration of the monitoring and will be lost at the end of it (unless they need to be recovered for environmental reasons using a coring technique); they are all connected by means of a single waterproof and durable cable with four poles which connects with a data logger that is installed at the top of the borehole;
(c) The distance between nodes can be chosen according to the precision required for the final output of displacement and, if deemed appropriate, can be varied along the MUMS axis (i.e., to monitor the expected shearing surface/band in greater detail);
(d) In addition to the determination of the 3D shape and configuration of the MUMS (and therefore of the underground soils/rock surrounding it), the system is also able to provide other measurements, such as pore pressure, temperature and other physical entities of interest;
(e) The instrument readings and their recordings are carried out automatically by means of an electronic control unit/data logger which is installed at the surface, preferably at the top of the borehole, and is powered by a battery or, if the local conditions permit, by mains electric power; the MUMS control unit is managed either locally, using a pre-programmed configuration transferred to the unit by insertion of an SD card, or remotely by GSM or radio signals.

The duration of a single complete readout of the MUMS depends on its length and the amount of sensors installed in it; the average readout time of each node varies between 0.2 and 0.6 s. Therefore, the readout time of a 20 m long MUMS with one node per meter varies between 4 and 12 s. The time interval between single readouts can be chosen by the operator based on the particular needs (expected velocity of the landslide, available memory, data recovery frequency, reason for the monitoring, etc.) and in a range starting from the single complete readout time of the MUMS and ending at 9,999 s.

Interpretation of the New MUMS Device

The data recorded by the MUMS control unit, at both the 3D digital linear accelerometer sensors and the 3D digital magnetometer sensors, associate each readout with the date and time of the reading and provide the three normalized components of the gravity vector along three axes of a coordinate system associated with the sensor's body (Fig. 2). In order to interpret the measurement and calculate the displacement, one needs to postulate that the lower portion of the MUMS (bottom node) is installed and fixed in a stable portion of the ground (i.e. stable portion of the slope) and the linear distance between two adjacent nodes remains the same. The data treatment is different depending upon the presence or absence of the 3D digital magnetic sensors.

MUMS Without 3D Digital Magnetic Sensors

For this case the procedure requires, for each reading, firstly the determination of the direction cosines of the MUMS pipe axis relative to a canonical orthonormal system, with the origin located in the center of the lower node, axis X

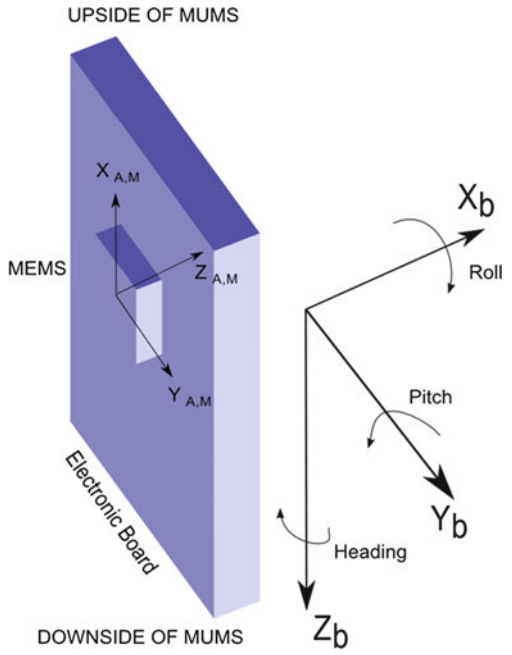


Fig. 2 Modified aircraft convention and relationship with MUMS orientation

directed toward the Earth's magnetic north and axis Z vertical (Diebel, 2006). The orientation of magnetic north is measured at the top of the borehole during installation and is the same for each node since they are hypothesized as aligned. Secondly, the absolute position of each node with respect to the same coordinate system must be determined. Using this technique, each system reading is independent from the previous one, and using a graphical function it is possible to plot the entire shape of the MUMS column in the 3D space. Then, in order to calculate the incremental deviation of each node from its previous position, it is easy to subtract from the coordinates of each node, calculated at a given time, those calculated at the beginning (or any other time) of monitoring. The MUMS system offers greater flexibility than the standard inclinometer, since the installation procedure allows for the deformation of the MUMS column and for it to precisely follow the underground deformation; in fact, the data analysis will give the displacement not only along the horizontal plane, but also along the vertical axis Z. The choice of the modulus of the vector (either on the horizontal or vertical plane) allows the calculation of the total displacement relative to a horizontal or vertical plane passing through the center of the node. In the first case, the displacements are directly comparable with those recorded by a standard inclinometer, while in the second case one obtains the total vertical displacement of each node. The charts that can be associated with the data analysis and interpretation could comprise, but not be limited to, the following:

- 3D graph of the shape and position of the MUMS system at time t;
- 2D graph of the total displacement of each node on the horizontal plane as a function of the depth (analogous to the chart of total displacement for the standard inclinometer);
- 2D graph of the total settlement of each node on the vertical plane as a function of depth;
- 2D polar representation of the direction of displacement of each node as a function of the azimuth (heading).

Obviously, due to the 3D nature of the acquired data, many other analyses are foreseen in order to highlight certain displacement components and features instead of others. In order to evaluate and double check the measurements obtained from the MUMS system, a linear measuring device at the top of the MUMS system is installed; this device will directly and independently measure the lowering of the upper node of the MUMS with respect to the surface and will be useful to check the operational functionality of the system for its entire duration.

MUMS Device with 3D Digital Magnetic Sensor

In this configuration, the aircraft convention, aptly modified, appears to be the most suitable for the indication of the nodes/tube axis orientation at each measured location along the MUMS. The aircraft convention defines a device body coordinate using three attitude angles (Gebre-Egziabher 2000): pitch, roll and heading as shown in Fig. 2. Three attitude angles are referenced to the local horizontal plane which is perpendicular to Earth's gravity. Heading is defined as the angle between the Xb axis and magnetic north on the horizontal plane, measured in a clockwise direction when viewed from the top of the device. Pitch is defined as the angle between the Xb axis and the horizontal plane. When rotating the device around the Yb axis with the Xb axis moving upwards, pitch is positive and increasing. Roll is defined as the angle between the Yb axis and the horizontal plane. When rotating the device around the Xb axis with the Yb axis moving downwards, roll is positive and increasing. For our application, however, the electronic board of each node is generally oriented as in Fig. 3 and therefore this convention needs to be modified accordingly. When the node is in the vertical position (Fig. 3) pitch and roll angles are 0 °. Then the heading angle can be determined as shown in Fig. 3, where the local magnetic field has a fixed component H_h on the horizontal plane pointing to the Earth's magnetic north. This component can be measured by the magnetic sensor sensing axes X_M and Y_M, which are named X_h and Y_h. In Fig. 3 when the device body X_b axis is parallel to H_h, which is pointing to the magnetic north, then $X_h = \max$ and $Y_h = 0$ so that heading = 0 °. Rotating the device clockwise on the horizontal plane,

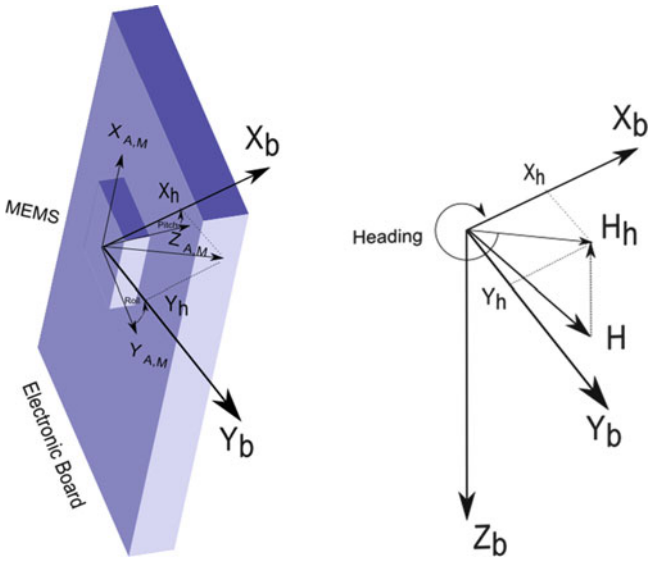


Fig. 3 Tilted node and components (*left*) and local earth magnetic field components (*right*)

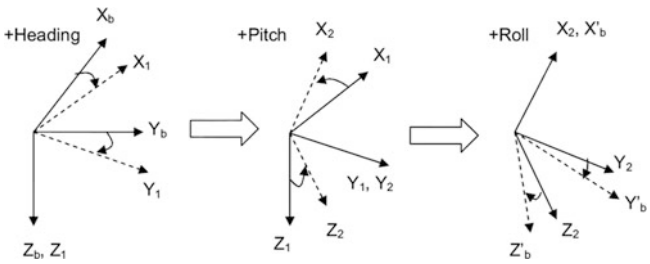


Fig. 4 Rotation procedures (From STMicroelectronics, 2010)

the heading increases. When $X_h = 0$ and $Y_h = \text{min}$, then heading = 90 °. When rotating until $X_h = \text{min}$ and $Y_h = 0$, then heading = 180 °. And so on. After a full 360 ° rotation, the user sees a centred circle if plotting X_h and Y_h values coming from the magnetic sensor measurements.

Pitch/roll/heading angles are referenced to the local horizontal plane which is perpendicular to the Earth's gravity:

- Heading (ψ) or azimuth is defined as the angle with respect to the magnetic north pole. It is always positive from 0 ° to +359 ° when rotating around the Zb axis clockwise, topview with the right-hand rule. If the heading with respect to geographic north is required, then the declination angle at the user's current geographic location should be added or subtracted from the magnetic heading;
- Pitch (ρ) is defined as the angle between the Xb axis and the horizontal plane. It goes from 0 ° to +90 ° when rotating around the Yb axis with the Xb axis moving upwards. When the Xb axis is moving downwards, the pitch angle goes from 0 ° to −90 °;
- Roll (γ) is defined as the angle between the Yb axis and the horizontal plane. It goes from 0 ° to +90 ° when rotating around the Xb axis with the Yb axis moving downwards. When the Yb axis is moving upwards, the roll angle goes from 0 ° to −90 °.

When the device node is at an arbitrary 3D position X'_b, Y'_b, and Z'_b, there are a few rotation procedures to rotate the device node from the local level frame X_b, Y_b, and Z_b, as shown in Fig. 2, to that 3D position. Different rotation procedures result in a different rotation matrix. The aircraft convention of angle rotation is used in this case. Firstly, rotate the device node around the Z_b axis clockwise at an angle (ψ) with the view from the origin to downwards. Then rotate the device around Y_b at an angle (ρ) with X_b moving upwards. Then rotate the device around X_b at an angle (γ) with Y_b moving downwards. The new node device body axes become X'_b, Y'_b, and Z'_b, as shown in Fig. 4.

Performance Analysis

Several prototypes of the MUMS system were constructed and tested in the laboratory in order to check their performance in a controlled environment. The first MUMS device was built using 10 nodes equally spaced at 50 mm. These nodes were equipped only with a 3D digital linear acceleration MEMS and connected with a double deformable wire solder in order to be able to keep the imposed geometrical configuration.

After the first series of experiments, the prototype MUMS size was increased to a distance between nodes of 500 mm for a total length of 5 m. This series of tests allowed us to evaluate the system's accuracy and the repeatability of measurements; in order to accomplish this task, several configurations of the prototype MUMS were deployed, performing various acquisitions for each configuration and comparing the results with those obtained by direct measuring of the device. In order to speed up the data analysis process, direct measuring was carried out using photogrammetry techniques; pictures were taken of each predetermined configuration of the MUMS prototype, using a Canon EOS 5D Mark II. The MUMS prototype configurations were rested against a wall in order to minimize errors induced by the photo restitution; however, image calibration techniques, as well as perspective corrections, were applied to the photographs in order to obtain a high precision photomap. Subsequently, the whole device was measured from these pictures, using colour and pattern matching techniques. At the same time several measurement samples were taken and analyzed with the MUMS obtaining the device configuration independently. Lastly, a comparison between the results of the measurements was carried out with satisfactory results. At a later stage, some other laboratory tests were carried out using a large scale tilt test

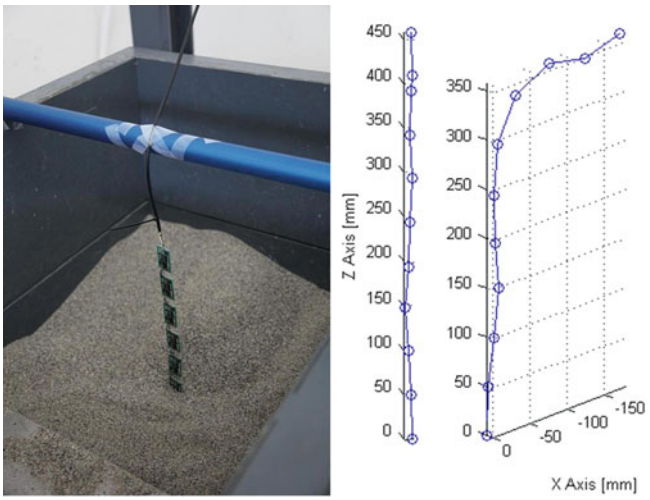


Fig. 5 MUMS prototype installation in the large scale tilt test box and output after 10 and 180 mm of horizontal displacement

machine (Fig. 5), that was built earlier by the one of the authors for different purposes (Migliazza et al. 2003). The tests were carried out by installing the MUMS prototype in the machine and fixing it to the bottom of the lower box, filling up the machine with dry sand and applying a shear displacement to the upper box while measuring the shearing displacement with an external linear potentiometric transducer. The results of the measurements were then compared with those calculated from the MUMS recordings.

Conclusion

This paper describes the functionality of a new apparatus that has been developed for the 3D measurement and monitoring of landslides and underground displacements. The new apparatus has been laboratory tested, examining its performance and reliability, and has subsequently been installed in a few landslides where its behaviour is compared with that of standard inclinometric probes. The paper presents the operating principles of the new device, and shows the basics for data manipulation and interpretation. It is believed that the new apparatus will generate a new and scientifically relevant approach to underground slope stability monitoring, comprehension and control. At this time, several further developments of the apparatus are foreseen, to improve its effectiveness as an innovative and modular underground monitoring tool.

References

Campbell WH (1997) Introduction to geomagnetic fields. Cambridge University Press, Cambridge. ISBN 571936

Diebel J (2006) Representing attitude: Euler angles, unit quaternions, and rotation vectors. Matrix. Citeseer. http://citeseerx.ist.psu.edu/viewdoc/download?doi=10.1.1.10.5134&rep=rep1&type=pdf

Durham Geo Slope Indicator (2009) Digitilt inclinometer probe datasheet. Mukilteo, Washington, DC

Gebre-Egziabher D (2000) A gyro-free quaternion-based attitude determination system suitable for implementation using low cost sensors. In: Proceedings of IEEE position location and navigations symposium (IEEE PLANS) San Diego, Aug. 2000. Electronic System Society. pp 185–192

Lollino G, Arattano M, Cuccureddu M (2002) The use of the automatic inclinometric system for landslide early warning: the case of Cabella Ligure (North-Western Italy). Phys Chem Earth 27(2002):1545–1550

Migliazza M, Segalini A, Tommasi P (2003) Experimental studies on the mechanical behaviour of vulcanoclastic materials. In: Soil rock America 2003 – 39th U.S. rock mechanics symposium, Cambridge, MA, 22–26 June, vol 1, pp 501–506. ISBN/ISSN: 3 7739 5985 0

O'Connor KM, Murphy EW (1997) TDR monitoring as a component of subsidence risk assessment over abandoned mines. Int J Rock Mech Min Sci 34(3–4):230e1–230e15

Pierce CE (1998) A compliant coaxial cable-grout composite for time domain reflectometry measurements of localized soil deformation. PhD dissertation, Department of Civil Engineering, Northwestern University, Evanston, IL

Stark TD, Choi H (2008) Slope inclinometers for landslides. Landslide 2008(5):339–350. doi:10.1007/s10346-008-0126-3



Groundwater Investigations Using Optical and Microwave Remote Sensing Data in Solani Watershed, India

Amed Bennia, S.K. Srivastav, and R.S. Chatterjee

Abstract

This article describes general hydrogeological set for the Solani watershed. Satellite imagery obtained from Landsat-7 ETM+ has been analysed to prepare the groundwater prospects map. By using SAR interferometry techniques, paleochannels, geomorphic units, lineaments, could be identified and delineated at a reasonable level of accuracy. In this study the following aspects have been covered: drainage map, geology, geomorphology, depth of water table map, water table contour map, EC (electric conductivity) distribution map etc. From these thematic maps ground water prospects map, has been prepared. As seen in these maps, the depth of water table in this area ranges from 2 m from ground level to more than 100 m; the EC of ground water varies from 284 to 2,000 μS/cm. Five different prospect zones: excellent, good, moderate, low, and runoff zone are identified according to the integration of thematic maps.

Keywords

SAR • In-SAR • Radar • Interferometry • DEM

Introduction

Groundwater is an important natural resource.

Worldwide, more than two billion people depend on groundwater for their daily supply. A large proportion of the world's agriculture and irrigation is dependent on groundwater, as are a large number of industries. Surface methods such as remote sensing and morphological analysis provide fast and relatively cheap information, complementary to classical field geology in order to study subsurface geology. Morphological analysis of topographic features, in particular lineaments, has long been applied in structural and tectonic studies and has become a fundamental tool in tectonic analyses using (stereo-) aerial photographs and other remotely sensed imagery.

Study Area

The study area is situated in the foothills of Siwalik; it is located between latitudes 29 ° 47′ 57″ and 30 ° 16′ 16″ N and longitudes 77 ° 44′ 05″ and 78 ° 04′ 26″ E. The area is covered by the rocks of Siwalik Group (upper Siwalik and Middle Siwalik), and Quaternary alluvial. Main Boundary Thrust (MBT) is the important tectonic discontinuity in the area.

Like the rest of the North India the study area is characterized by a sub-tropical rainy climate, essentially because of Himalayan chain and it also experiences four seasons in a year. According to the existing weather condition the study area has been divided into four different seasons: winter season is from December to February, summer season start from March to May, southwest monsoon season is from June to September, post monsoon season is from October to November.

A. Bennia (✉)
Centre for Space Techniques, Algerian Space Agency, 01 Avenue of Palestine Arzew, Oran 31200, Algeria
e-mail: redabennia@gmail.com

S. Srivastav • R. Chatterjee
Indian Institute of Remote Sensing IIRS, Dahradun, India

C. Margottini et al. (eds.), *Landslide Science and Practice*, Vol. 2,
DOI 10.1007/978-3-642-31445-2_12, © Springer-Verlag Berlin Heidelberg 2013

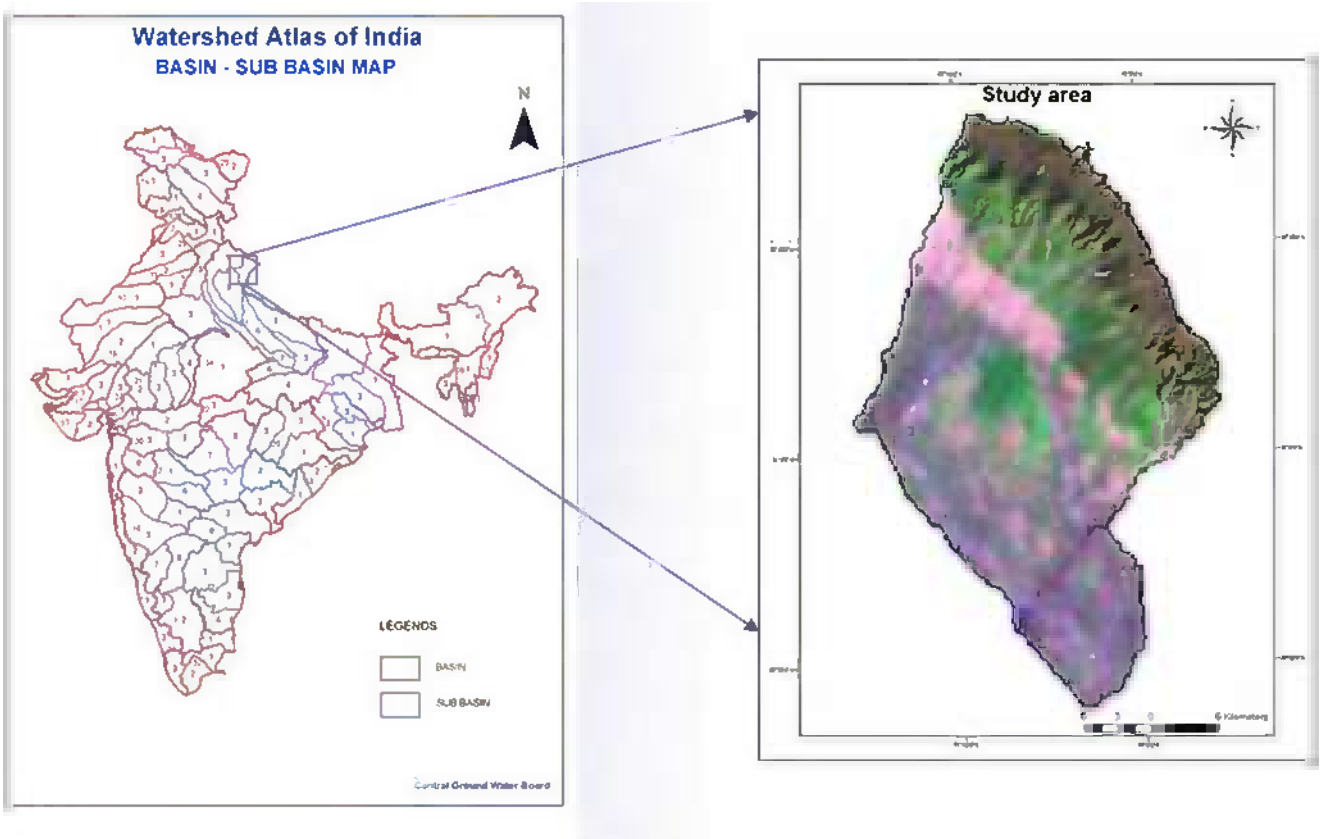


Fig. 1 Location map of study area

Its average maximum temperature is about 30 °C and the average minimum temperature is around 17 °C. It's also characterized by an average rainfall around 1,160 mm/annum. Westerly to North-Westerly are the surface wind in winter.

The forest types of study area are mostly moderate to open type and in the upper ridge of Siwalik it is degraded to great extent. The natural vegetation consists of trees, shrubs, and grasses. Taking into consideration the difference in the altitude and the climatic conditions the flora of the watershed may be divided in three main botanical divisions: the moist tropical forests, the tropical dry mixed deciduous forests, and the Siwalik chir forest.

Location map of study area is shown on "Fig. 1".

Methodology

The methodology adopted in the study consists of the following steps and flow diagram of the study is shown in "Fig. 2".

Fieldwork

Before fieldwork, satellite data were digitally processed and visually interpreted. Different photo image-elements like tone, texture, and geotechnical elements were taken into consideration for extraction of geological and geomorphological features. Based on landform analysis from satellite images, the pre-field geomorphological map was also prepared.

During the field study, a ground truth was carried out to check the geological and geomorphological interpretations made from satellite imagery. Collection of well inventory data and measuring water table observation of well yield well depth and type of aquifer were done.

Remote Sensing Data Processing and Analysis

Satellite, Radar images, DEM and each derived attribute map can be viewed as raster images and hence be processed using digital image processing procedures to increase the apparent distinction between features in the scenes.

The following image processing methods were used in this study are:

1. Georeferencing and subsequently enhancement of the satellite data such as contrast stretching, filtering, band rationing, color composite, etc., were accomplished with ERDAS IMAGINE software.
2. The reflectance/emittance of any object at different wavelength follows a pattern, which is characteristic of the than object known as "spectral signature". Proper interpretation

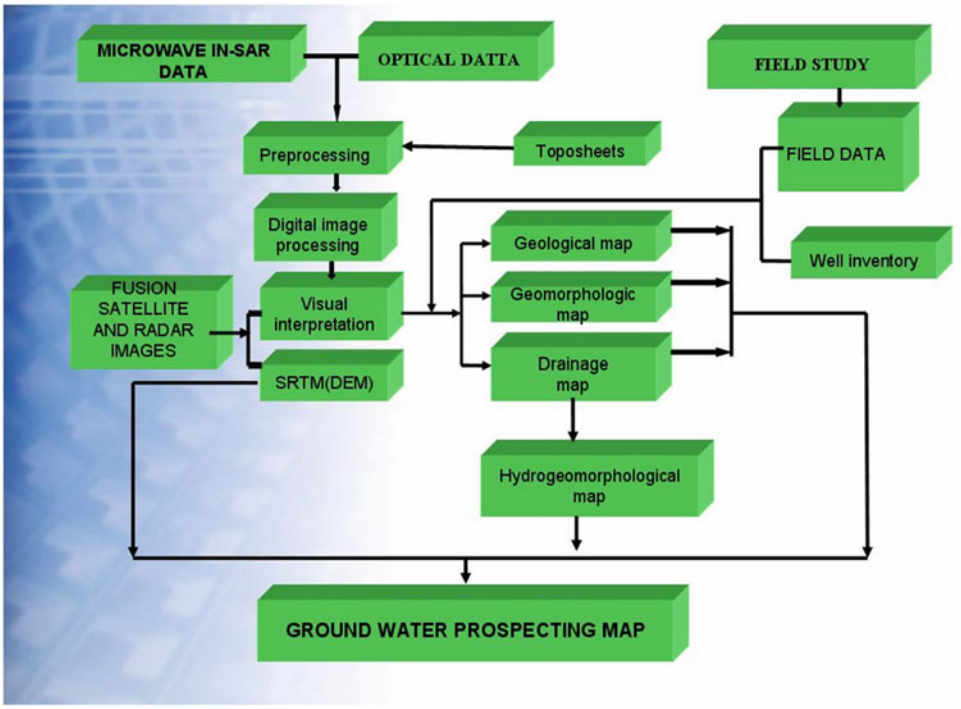


Fig. 2 Flow diagram of the study

of the spectral signature leads to the identification of the object. It is therefore very important to select the images taken in the proper spectral band so that optimum information can be extracted from the images. Landsat-7 ETM+, e.g. from 0.4 to 1.7 μm, in general 0.7–1.3 μm region exhibits high levels of reflectance because of high TR reflectivity of leaves due to their internal cellular structure. 1.3−2.5 μm is characterized by strong absorption by water present in the vegetation and reflectance by the soil.

In this study a DEM is generated by using ERS Fine 1 beam Interferometric SAR. After data fusion was done.

Fused product of ERS1 power and Landsat-7 ETM+ (542) and fused product of Landsat-7 ETM+ (542) and DEM are shown on Fig. 3. DEM can be used as supplement of Remote Sensing data to enhance some features for increasing interpretation accuracy.

The most widely examined and cited geomorphological feature extraction processes from DEM concerns the derivation of hydrological and fluvial features from surface models. The routing of water over the surface of a landscape represents a fundamental geomorphological process that is intimately tied to its form.

Results and Discussion

Analysis of Optical and SAR Data

A drainage map of a basin provides a reliable index of the permeability of the rocks and also gives an indication of the yield of the basin. The study area is sloping down towards southwest from the river from Mohand pass. The runoff water from the rivers, streams of the watershed area drain into the main rivers Solani. Due to moderate to very steep slope in Siwalik hill the drainage is excessive to well drain in piedmont area and well to poorly drain in alluvial plain.

Three lithologic units were mapped from the processed images which are Alluvium, upper Siwalik, and middle Siwalik. Geologically, the study area comprises the rocks of great antiquity (ranging from Neoproterozoic to Recent), belonging to Lesser Himalayan Range, Outer Himalayan Range and Indo-Gangetic Plain. A brief description is given below, and is mainly taken from A.K. Pachauri (1980), K.S. Valdiya (1988).

Delineation of Paleochannels and Some Perennial Rivers from In-SAR Data

Geological interpretation of radar image is based on the analysis of surface morphology, landforms and specific surface elements (dielectric property of materiel, surface roughness, and structures. . .).

The extraction of geomorphology, geological structure and lithology from radar imagery can be possible because of the higher sensitivity of radar to the surface geometry and surface roughness.

Drainage pattern can be delineated very clearly. The differentiated between perennial and paleochannels can be possible from simulated VV-polarized C-band SAR.

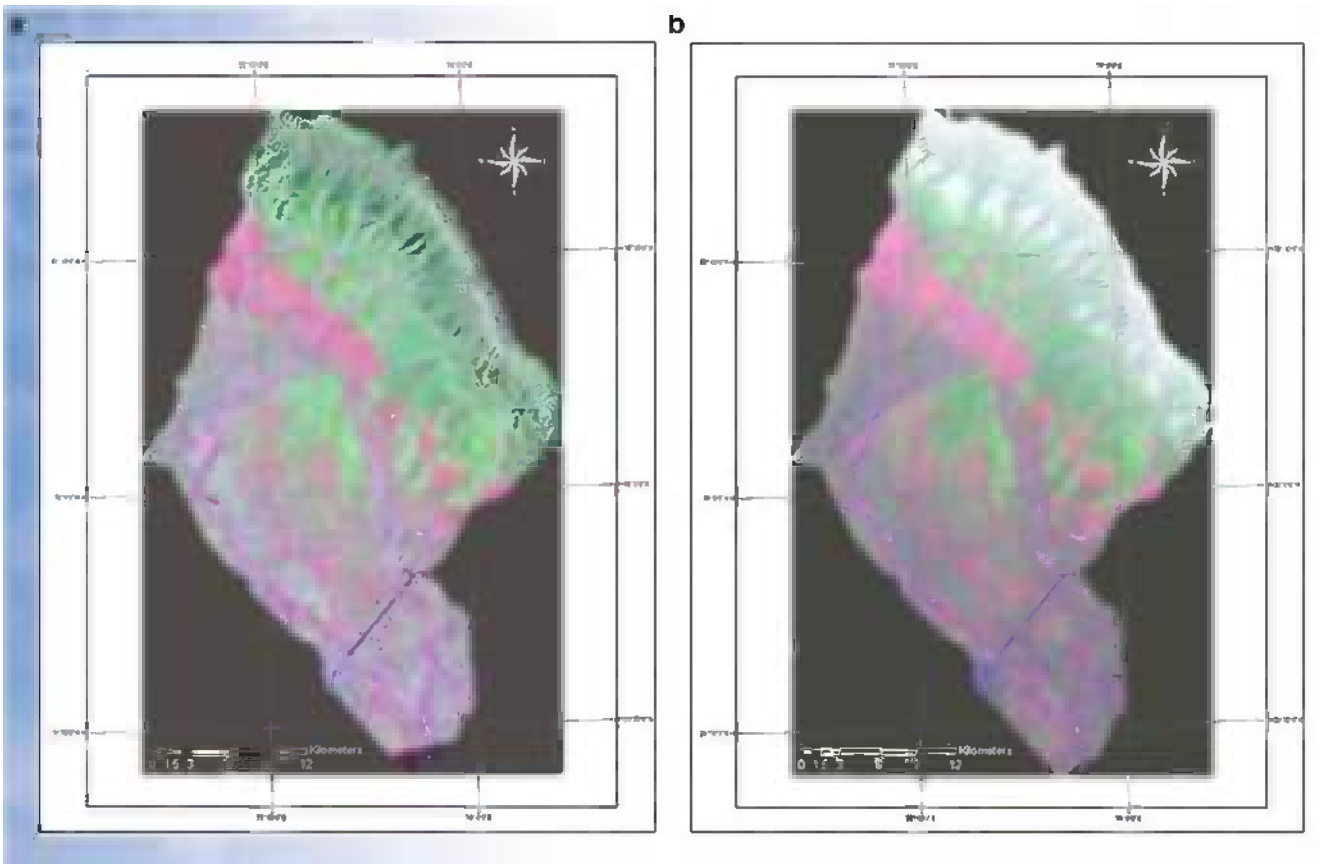


Fig. 3 (**a**) Fused product of ERS1 power and Landsat-7 ETM+ (542), (**b**) fused product of Landsat-7 ETM+ (542) and DEM

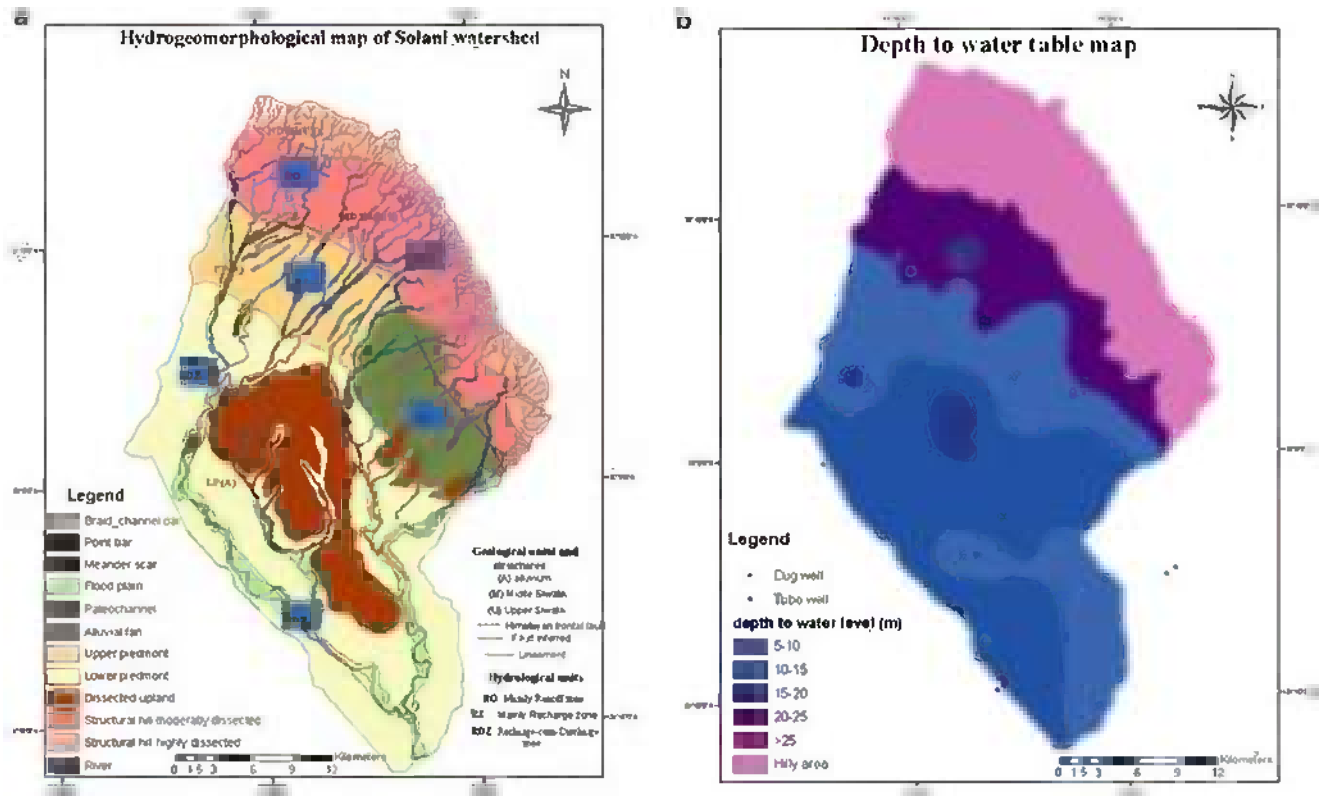


Fig. 4 (**a**) Hydrogeomorphological map, (**b**) depth of water table map

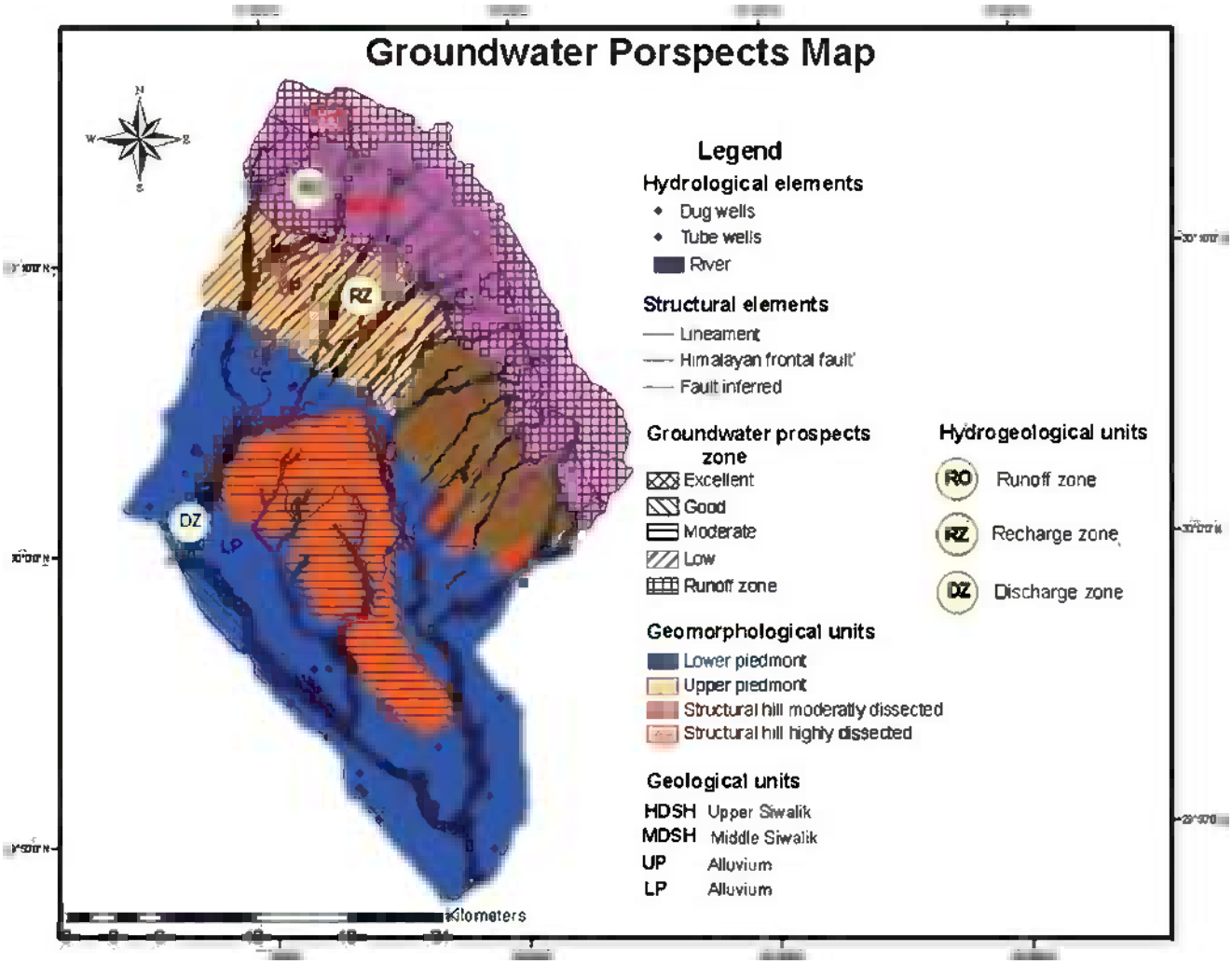


Fig. 5 Groundwater prospects map

The identification of linear features is possible from radar image which expressed that the most of these features are perpendicular to sub-perpendicular to the look direction (strong return backscattering).

Hydro-Geomorphology

Three different hydrogeomorphological units were identified according to the basic lithology, drainage geomorphology and aquifer characteristics which are: Runoff zone, Recharge zone, Discharge zone.

Runoff zone generally characterizes the areas which have a very high altitude, steep slope, and high drainage pattern. The dissected structural hill is considered as the main runoff zone of the study area. The main litho units which characterize this zone are Upper Siwalik and middle Siwalik rocks.

Recharge zone is the gentle slope, dry streams and the course materiel of boulder and gravels are the main characteristics of this recharge zone. The Upper Piedmont zone is considered as the mainly recharge zone in the study area.

Discharge zone is generally composed with a finer sediments as well as sand, silt, and clay layers. It is characterized by the shallow water level and flowing streams. The mainly discharge zone which characterize the study area is the lower piedmont zone.

Characteristic of Aquifer

The collected data during field work show that the most of these dug wells and tube wells are used for drinking and irrigation purpose; however some dug wells are unused and require cleaning.

The depth to water table map and water table contour map are prepared based on data collected from field work. As seen in these maps, the depth to water table in this area

ranges from 2 m from ground level to more than 100 m. On the basis of water table map and ground truth checking, it is observed that the water table is very deep from the ground level in the NE part of study area. In the entire area the groundwater flows towards south where the water table ranges from 240 to around 300 m.

The groundwater prospect map is prepared based on the hydrogeomorphology, lithology, and depth of water table. They are shown on "Fig. 4".

And final Ground Water Prospect Map is shown on Fig. 5.

Conclusions

The interpretation of Landsat-7 ETM+, radar data and analysis of digital models, together with field studies has made it possible to delineate and map geomorphic units, drainage pattern and tectonic features.

In-SAR data can be used for geological interpretation in terms of morphology, materials and structure recognition, in an acceptable level, particularly when some other data are not available.

Based on the present work, we can identify that the study area is formed by four geomorphic units: Highly dissected structural hill, moderately dissected structural hill, upper piedmont, and finally lower piedmont.

Based on hydrogeomorphological map, the study area is divided in three principal zones: runoff zone characterized structural hills units, recharge zone mainly occur in the upper piedmont and discharge zone mostly in lower piedmont of the area.

As seen in depth to water table map and water table contour map we can observe that the ground water level is deep around 100 m to shallow 3 m respectively from N to the S and the groundwater flow is from northeast to southeast.

The EC value collected from the field and the EC contribution map indicate that the most of ground water in the area is potable.

By integration of geomorphological, lithological, depth to water table map the groundwater map has been prepared which indicate five different prospect zones: excellent, good, moderate, low, and runoff zone.



Application of a Multiplet-Location Coupled Technique to Microseismic Data for Identification of Rock Slope Active Surfaces

Cristina Occhiena, Marina Pirulli, and Claudio Scavia

Abstract

In rock slope analysis, formation and growth of microcracks are usually coupled with the propagation of elastic waves that can be detected by a suitable microseismic monitoring system. The correct analysis and interpretation of the recorded activity can provide information on the size and the type of the rupture mechanisms. A combination of the coherency computation and the source location techniques, typically used in seismic signal processing, is here proposed to this aim. The application to a microseismic dataset recorded by the microseismic monitoring system installed on the Matterhorn Peak, has evidenced the effectiveness of this approach. In particular the coherency has allowed to identify a set of similar appearing events, while the location of the corresponding hypocenters has evidenced the alignment of the sources on a planar surface, whose orientation is closed to the orientation of a discontinuity system resulting from a morphostructural survey.

Keywords

Rock slope stability • Microseismicity • Source location • Coherency computation

Introduction

It is accepted today that most solids emit low level signals when stressed or deformed. This phenomenon is usually referred to as acoustic emission (AE) or microseismic activity (MS). These signals are due to the sudden release of stored elastic energy within the material.

In the rock material the instabilities usually involve the nucleation, growth and coalescence of microcracks due to a local stress concentration. This phenomenon causes the spatial localization of the damage and may lead to the creation of a macroscale discontinuity and to the failure of the material (Lockner 1993; Amitrano 2006). At the micro level when the rock material, which is polycrystalline, is subjected to a stress concentration, some movements along the grain boundaries may take place. At a macro scale the microcracks between the mineral grains may propagate till the fracturing of some portions of the rock material. When this happens a sudden strain release of stored elastic energy gives rise to elastic waves, which can be detected using an appropriate AE/MS monitoring system.

Once a suitable monitoring system is installed, the correct analysis and interpretation of the microseismic signals can provide information about the size and the location of the recorded sources and the deformation and rupture mechanisms of the medium crossed by the elastic waves. In the scientific literature different methods to analyse the microseismic data and to correlate them with the rock fracturing processes exist. The simple counting of the number of events prior to failure is the most direct method to correlate the AE/MS rate to the inelastic strain rate. Other areas of investigation involve the location of the hypocenters of source events and the whole waveform data analysis. In the frame of this third category, a way to proceed consists in the determination of fault plane solutions of microseismic source events from the first motion data. The aspect that will be discussed in the present paper concerns the

C. Occhiena (✉) • M. Pirulli • C. Scavia
Department of Structural and Geotechnical Engineering, Politecnico di Torino, Corso Duca degli Abruzzi, 24, Torino, Italy
e-mail: cristina.occhiena@polito.it

C. Margottini et al. (eds.), *Landslide Science and Practice*, Vol. 2,
DOI 10.1007/978-3-642-31445-2_13, © Springer-Verlag Berlin Heidelberg 2013

advantage of grouping microseismic events with high waveform similarity (referred to as multiplets of similar events).

The technique for the microseismic multiplet identification is based on the application of the correlation theory and of the coherency computation.

The relation between signals recorded in two different points of a net but caused by the same or by a very similar source mechanism is linear and stationary in time and frequency domain. On the contrary signals recorded at different time in the same point of a net are related between them with a linear and stationary relation only if the source mechanism is the same. Since the coherency is a measure of the linearity of the relation between two events, it can be considered as a measure of the similarity between both the waveforms and the source mechanism. To characterize the degree of similarity of a pair of events, the modulus of the coherency is used (Got et al. 1994).

In the present paper the above techniques are applied to a set of microseismic data recorded by the monitoring network installed on the Matterhorn Peak in the context of the "PERMAdataROC" project by the CNR-IRPI Torino (Italy).

Computing of the coherency for each recorded pair of events allowed grouping together similar appearing events. Then the effective presence of common rupture mechanism for the class of grouped events is investigated by the hypocenter location.

Multiplet Identification Technique

The microseismic activity that occurs in a given area rarely occur as spatially isolated; this is particularly true when considering long time periods. This information is lost when considering micro-earthquake as individual features and not their relations. A simple way to evidence this information is to study the existing correlations between events.

In fact, a part of this information may be recovered from the correlation of the signal waveforms.

The correlation between two signals may be defined starting from the concept of energy, E, of a signal $x(t)$ during a given time period T:

$$E = \int_0^T x^2(t)dt \tag{1}$$

and its mean power P:

$$P = \frac{1}{T}\int_0^T x^2(t)dt \tag{2}$$

From the above concepts the auto-correlation, Γ_{xx}, of a signal with itself delayed of a time interval τ, $x(t-\tau)$, can be defined as the mean power of interaction of the signal with itself, for a varying time delay τ:

$$\Gamma_{xx}(\tau) = \lim_{T\to\infty}\frac{1}{T}\int_0^T x(t)x(t-\tau)dt \tag{3}$$

Similarly the correlation between two different signals, $x(t)$ and $y(t)$, may be represented using the cross-correlation function, Γ_{xy}, representing the power of interaction between the two signals $x(t)$ and $y(t)$ delayed by τ:

$$\Gamma_{xy}(\tau) = \lim_{T\to\infty}\frac{1}{T}\int_0^T x(t)y(t-\tau)dt \tag{4}$$

The cross-correlation Γ_{xy} can be computed in the frequency and in the time domain. The operation to solve the (4) involves a convolution product; as a consequence, the slowness in computing cross-correlation in time domain have made the cross correlation in frequency domain (cross-spectral analysis) a more appealing method. Moreover using the cross-spectral analysis the measure of the time delay existing between two signals is easier.

Based on this, let $x(t)$ and $y(t)$ be two similar signals related by a linear relation:

$$x(t) = s(t) + n_1(t) \tag{5}$$

$$y(t) = as(t-\theta) + n_2(t) \tag{6}$$

where $n_1(t)$ and $n_2(t)$ are uncorrelated noises, also uncorrelated with the signal $s(t)$, which is a signal contained both in $x(t)$ and y(t); a is a constant and θ is a constant time.

Substituting (5) and (6) in (4) neglecting the noises term, is obtained:

$$\Gamma_{xy}(\tau) = \lim_{T\to\infty}\frac{a}{T}\int_0^T s(t-\theta)s(t-\tau)dt = a\Gamma_{ss}(\theta-\tau) \tag{7}$$

where $\Gamma_{ss}(t)$ is the auto-correlation function of the signal $s(t)$.

The cross correlation function in the frequency domain can be obtained through the Fourier Transform (FT) of (7):

$$FT\left[\Gamma_{xy}(\tau)\right] = FT[a\Gamma_{ss}(\theta-\tau)] \tag{8}$$

Assuming that the relation between $x(t)$ and $y(t)$, besides being linear is stationary in time and frequency domains, it can be defined as a linear and stationary filtering relation,

that is as a Wiener filter. Characterizing a Wiener relation between two signals consists in defining the transfer function ($\tilde{G}(f)$) of the Wiener filter, which, in the frequency domain, can be written as:

$$\tilde{G}(f) = \frac{\overline{\gamma_{xy}(f)}}{\overline{\gamma_{xx}(f)}} \tag{9}$$

where $\overline{\gamma_{xy}(f)}$ and $\overline{\gamma_{xx}(f)}$ are, respectively, the smoothed cross-spectrum of $x(t)$ and $y(t)$ and the auto-spectrum of $x(t)$. The transfer function $\tilde{G}(f)$ contains the module and the phase information concerning the filtering relation between the signals $x(t)$ and $y(t)$. The phase carries the information concerning the time delay between the two signals, while the module contains information in the amplitude ratio between the filter input/output signals $x(t)$ and $y(t)$. $\tilde{G}(f)$ is less biased, for similar signals, than the usual 'spectral ratio', which is defined as:

$$\left(\frac{\overline{\gamma_{yy}(f)}}{\overline{\gamma_{xx}(f)}}\right)^{\frac{1}{2}} \tag{10}$$

and is usually used in seismology to quantify the non necessarily linear relation existing between two non-necessarily similar signals.

Rewriting the (9) taking into account the (10) it is possible to express $\tilde{G}(f)$ as:

$$\tilde{G}(f) = \frac{\overline{\gamma_{xy}(f)}}{\overline{\gamma_{xx}(f)}^{\frac{1}{2}}\overline{\gamma_{yy}(f)}^{\frac{1}{2}}}\left(\frac{\overline{\gamma_{yy}(f)}}{\overline{\gamma_{xx}(f)}}\right)^{\frac{1}{2}} = \tilde{C}_{xy}(f)\left(\frac{\overline{\gamma_{yy}(f)}}{\overline{\gamma_{xx}(f)}}\right)^{\frac{1}{2}} \tag{11}$$

where $\tilde{C}_{xy}(f)$ is the coherency, which is given by the cross-spectrum normalized by the smoothed auto-spectra of the signal $x(t)$ and $y(t)$ respectively. Its value is minimal when the signals $x(t)$ and $y(t)$ are uncorrelated, while it increases up to unit in case of perfect correlation between the two signals. Furthermore it is a measure of the linearity and time and frequency stationariness of the mean transfer function.

Hypocenter Location Technique

The effective presence of common rupture mechanisms for the classes of grouped events can be verified through the hypocenter location. To this aim the open source NonLinLoc software (http://alomax.free.fr/nlloc/) has been here used.

NonLinLoc is a software package for locating earthquakes (Lomax & Curtis, 2001).

It supports a grid search method and two non-linear search methods: Metropolis-Gibbs sampling and Oct-Tree Importance algorithm. Furthermore it can operate with a spherical, longitude/latitude/depth coordinate system (GLOBAL mode) or with a 3D Grid structure, which defines a specific, gridded, rectangular-Cartesian volume (NON-GLOBAL mode).

The main advantages of NonLinLoc are (1) a complete mapping of the probability density function (PDF) of the earthquake location problem, (2) detection of multiple minima in the PDF, (3) 1D and pseudo-3D models for location, (4) solution quality assessment through non-linear error estimates (PDF), (5) Gaussian error estimates (confidence ellipsoid), and (6) additional software for evaluation (e.g. Seismicity Viewer).

Whitin the NonLinLoc package, the program Vel2Grid, which is a pre-processor to the velocity model computation. As usual in the seismic field, the velocity model can be defined as a horizontally layered model with constant or constant gradient velocity in each layer, or as a set of 2D polygonal model that can be converted in a pseudo 3D.

The possibility of using the software in a non-global mode and the existence of a pre-processor (Vel2Grid) that run independently from the location kernel (NLLoc) are among the main reasons that justified its selection for the application in the microseismic field.

Application to the Matterhorn Peak Case Study

The multiplet-location technique is here applied to the data recorded from the Matterhorn Peak microseismic monitoring system. The presence of multiplets (set of similar-appearing events) for the study site was investigated at first. Then the hypocenter location for the identified multiplets was used to verify the real presence of common rupture mechanisms.

The Matterhorn Peak Study Site

A microseismic monitoring system was installed on the S-W flank of the Matterhorn Peak, close to the J.A. Carrel hut, at 3,829 m a.s.l (Fig. 1), during the 2007 in the frame of the Interreg IIIA Alcotra "PERMAdataROC" project. The choice of this site was justified by the presence of the hut, which provides a unique logistic support, and because of the relevant number of rockfalls, which took place in recent years (Amitrano et al. 2010).

The microseismic monitoring system is made of an 18 channel acquisition system, which is placed inside the hut, five triaxial transducers for boreholes with a natural frequency of 100 Hz, a gps receiver, and a power supply group connected to solar panels. The data downloading can

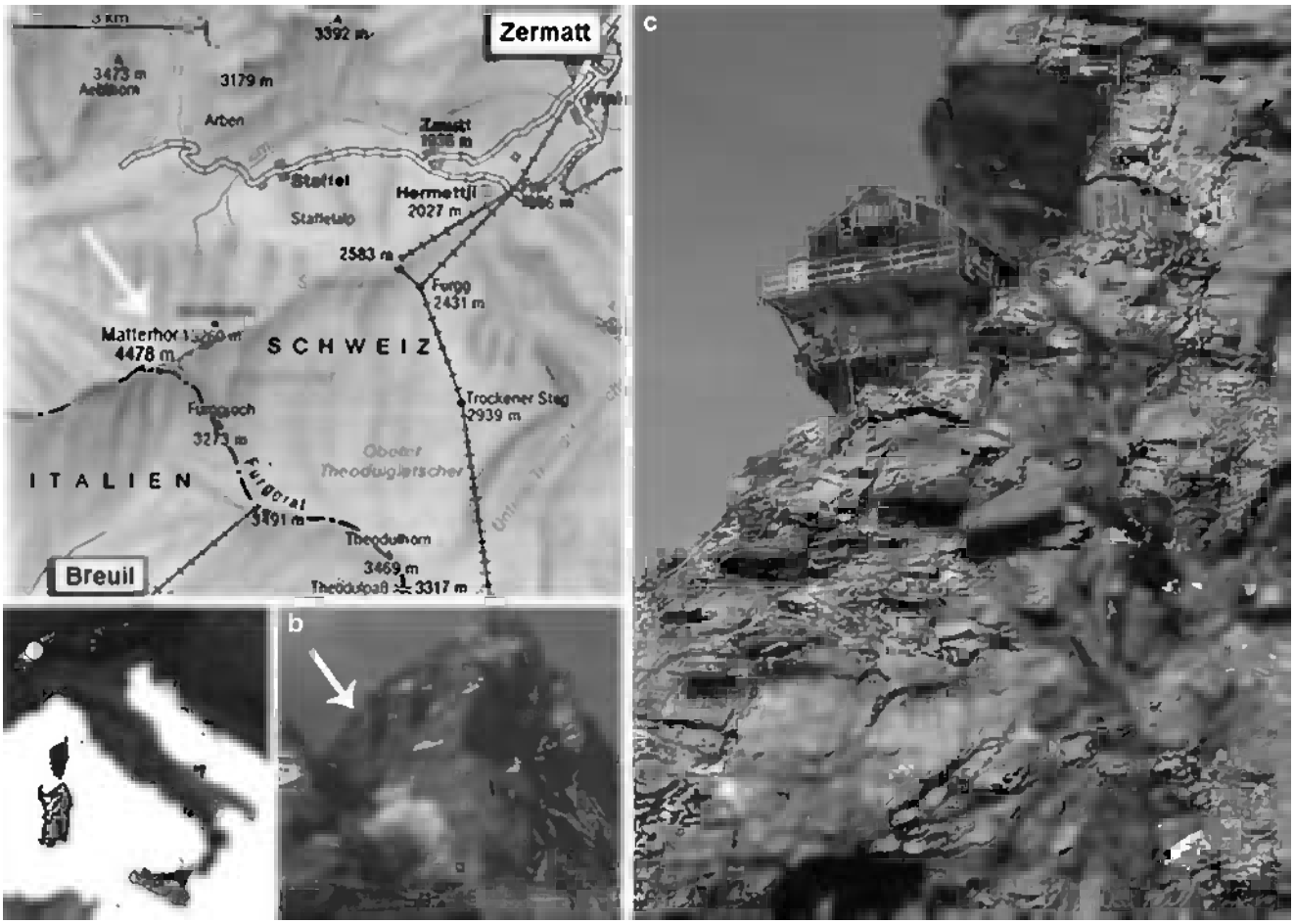


Fig. 1 (**a**) Location of the study site; (**b**) the Matterhorn Peak from the Italian side; (**c**) the J.A. Carrel hut (Image courtesy of Valle d'Aosta Region, Italy)

be made from the Italian village of Breuil-Cervinia, located in the valley floor, using the wireless data transmission system.

Two of the geophones were installed on surface (geophones 1 and 3 in Fig. 2) one was put at 5.2 m depth in borehole D (geophone 2 in Fig. 2) and the other two in the same borehole A, at a depth of 3 and 6.8 m, respectively (geophones 4 and 5 in Fig. 2). The type, number and position of the geophones were selected in consideration of the fracturation characterizing the rock mass in the Carrel hut surroundings.

The system is in stand-by until a triggering condition is exceeded. The threshold value was fixed, after a calibration period, equal to 0.01 mm/s to be exceeded simultaneously on at least six channels.

Once the installation was completed the system was tested by hammering some georeferenced points (Fig. 2). Furthermore the source time of each hammer stroke was recorded to allow the computation of the mean velocity values on the rays connecting each source point with each geophone.

Identification of Multiplets of Similar-Appearing Events

Calculation of the coherency between the signals recorded at each sensor was performed for the dataset of 627 events, recorded from November 1st, 2007 to April 7th, 2008.

The coherency has been computed for each pair of events as the mean of the values computed for each geophone. Since the sensors are triaxial, the coherency value assigned to each geophone has been computed as the mean of the three values obtained for each couple of channel of the two events.

The results have been stored in a symmetric matrix, which resume the coherency values for each pair of events. The plotting the coherency matrix (Fig. 3) has evidenced the presence of groups of events with similar coherency values. The events sharing high coherency values should also have similar waveforms and source mechanisms.

To select and identify the groups of similar events the Eardley's equivalence class algorithm (Press et al. 1996) has been applied to the coherency matrix: an event belongs to an

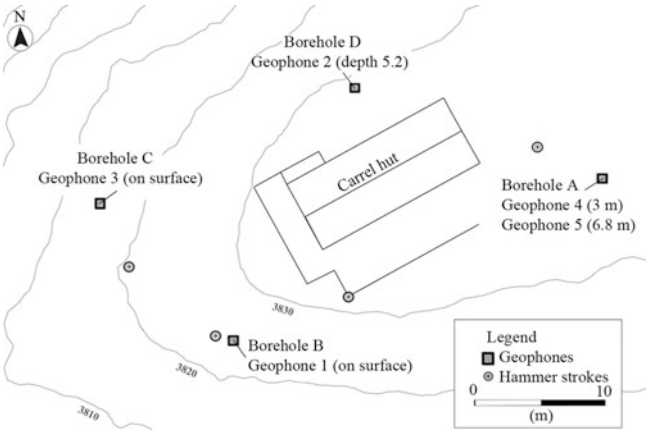


Fig. 2 The J.A. Carrel hut with indication of the position of the geophones and of the hammer strokes

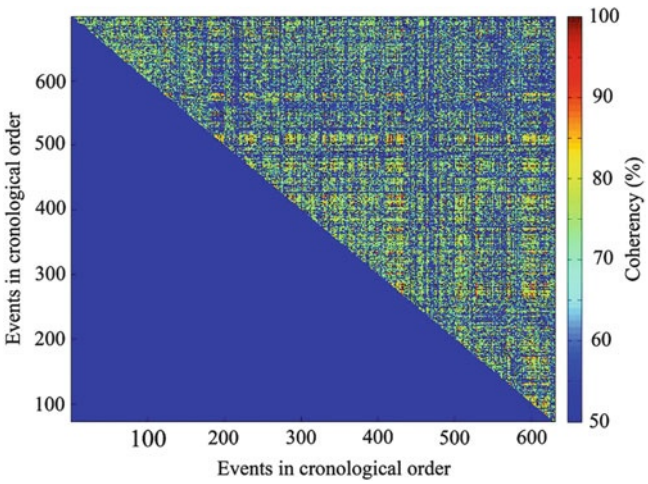


Fig. 3 Plot of the coherency value matrix

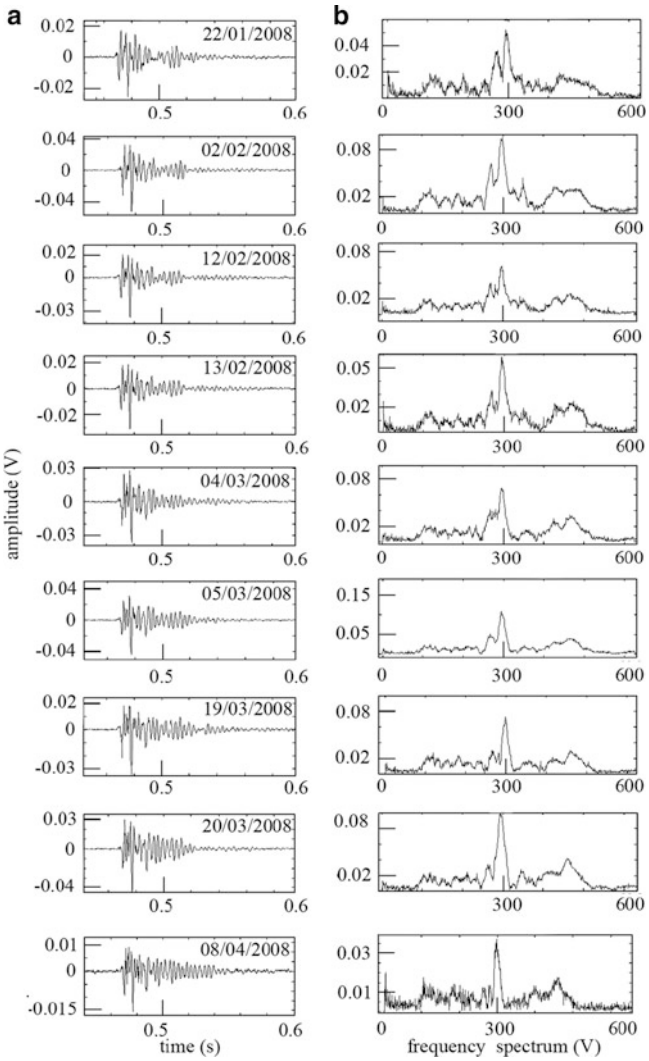


Fig. 4 Example of waveforms in time and frequency domains of the nine events collected in the same class as recorded on the x-axis of geophone 2

equivalent class if its coherency with each element of the class is higher than a given threshold. To perform a good selection it has been necessary to define the coherency threshold and the minimum number of events defining a class. It is desirable, in fact, collecting events as similar as possible (high threshold value) and, at the same time, as numerous as possible. An iterative process, changing the threshold value and verifying the effective waveform similarity, led to fix a final value equal to 95 %, allowing the identification of one class of nine very similar events, falling in different days of the investigated period.

As an example, in Fig. 4a the waveforms of the 9 events for the x-axis of the geophone 2 (that is installed at 5.2 m depth) are reported. It can be noticed a good correspondence between the main waveform characteristics (presence of significant peaks and wave polarization). The same correspondence can also be observed analyzing the frequency spectra corresponding to the nine signals (Fig. 4b): the nine events share common spectral features (as the dominant frequency and most of significant components).

Location of the Sources

In order to verify the effective presence of a common source mechanism the nine similar events have been located using the modified version of NonLinLoc.

To represent the complex topography of the Matterhorn Peak, it was necessary to introduce in the velocity model the possibility of distinguishing air sectors from rock sectors. As a consequence a heterogeneous velocity model was computed. The velocity model cube was discretized into $50 \times 50 \times 50$ cubic cell; the air sectors were identified computing the position of the centre of each cell and collecting together the centre coordinates identifying points located outside the limits of a portion of the Matterhorn Peak digital elevation model. The constant value of 325.2 m/s (velocity of sound in air at the average annual air temperature recorded on the Matterhorn Peak) was assigned

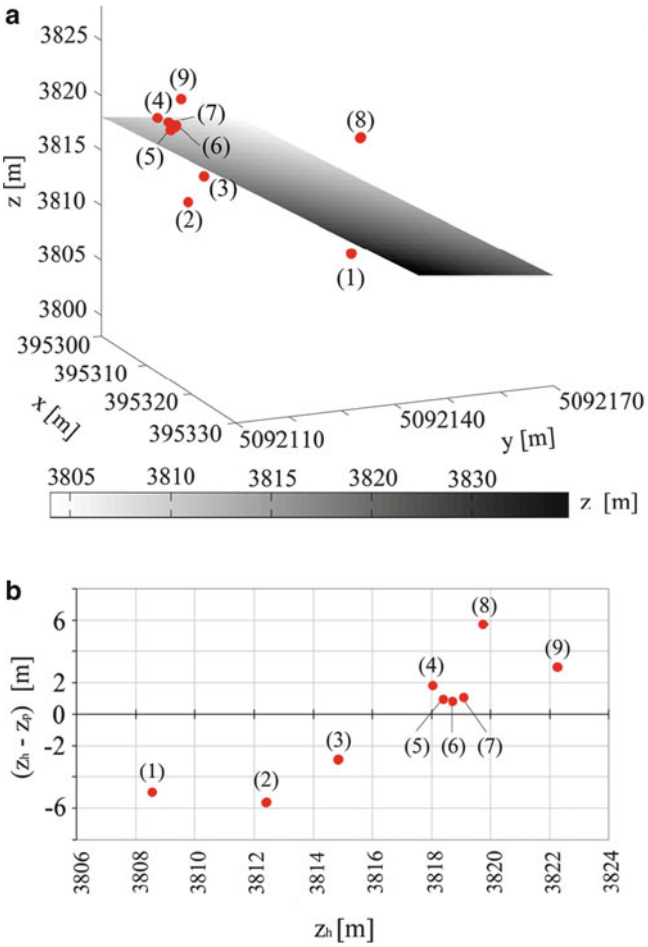


Fig. 5 Representation of (**a**) computed hypocenters and mean plane and (**b**) difference between event hypocenter elevation (z_h), as computed with NonLinLoc, and corresponding value on the mean plane (z_p) for the selected nine event class

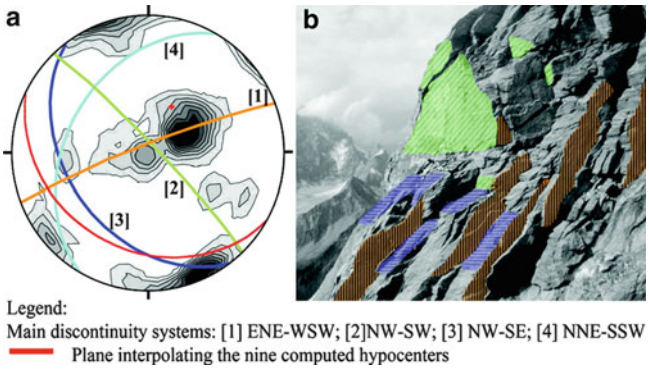


Fig. 6 (**a**) Stereographic projection plot of the 4 main discontinuity systems observed in site and of the mean plane interpolating the 9 hypocenters (*red line*); (**b**) identification of the main systems on a portion of the slope in the Carrel hut surroundings (Images modified after Pogliotti 2006)

to the air cells. In the rock sectors the velocity changes from point to point as a function of the mass local average characteristics.

Using the heterogeneous velocity model the nine events were located. The interpolation of the 9 obtained hypocenters has evidenced that the sources are by ± 6 m from the mean plane (Fig. 5).

The interpolating plane orientation was computed in terms of dip direction and dip angle and represented on a stereographic projection plot. A comparison with the results of a morphostructural survey, performed in 2006 in the Carrel hut surroundings (Pogliotti 2006) was then carried out.

The morphostructural survey allowed the identification of 16 main discontinuity systems along 5 scanlines around the Carrel hut. The observed systems were grouped into 4 main systems responsible of the main features of the ridge where the hut is placed (Fig. 6a). Plotting the plane interpolating the coordinates of the 9 hypocenters on the same stereographic projection of the surveyed system (red line in Fig. 6a), a good correspondence with one of the main discontinuity systems emerged (system (3) in Fig. 6a).

In Fig. 6b the 4 main discontinuity systems are identified on a portion of the slope just below the Carrel hut; the blue plane represents the system (3). Observing its orientation it emerges that a planar sliding can be hypothesized as a probable instability.

Conclusions

The coherency computation is a technique commonly used in signal processing and largely employed in many fields, since it is adaptable to different requirement, depending on the aims of the research under development.

In the frame of microseismic monitoring activity it has been here used to identify multiplets of similar appearing events, which could be therefore due to the same source mechanism. Once similar events are identified, their location can contribute in investigating the activity and fracturing process of a slope.

In particular, the coherency technique has been applied to a set of events recorded in the period November 1st, 2007–April 7th, 2008 by the microseismic monitoring system installed on the Matterhorn Peak, in the frame of the "PERMAdataROC" Project by the CNR-IRPI Torino (Italy).

A total of 627 events were analysed: computing the coherency for each recorded pair of events allowed the selection of similar events with identification of one multiplet of similar appearing events. Using a coherency threshold equal to 95 % (100 % means identical events) a class of nine very similar events was identified.

Afterwards the hypocenter location for the nine events classed as a multiplet, performed using the software

NonLinLoc (Lomax et al. 2000) evidenced the presence of a cloud of hypocenters aligned along a planar surface, whose attitude is very close to that of a discontinuity family surveyed on site. This family, combined with the others main discontinuity systems, identifies a possible planar sliding mechanism in the investigated area. Taking into account that signals recorded at different time in the same point of a net are similar only if they originated from the same source mechanism, or from similar sources, the obtained results have then evidenced the presence of a weakness zone in the Matterhorn fractured rock mass.

Acknowledgements The authors wish to thank Marta Chiarle, Giovanni Mortara and Massimo Arattano (CNR_IRPI Torino) for the involvement in the Interreg IIIA Alcotra Project n ° 196 "PERMAdataROC" and the MS data sharing.

References

Amitrano D (2006) Rupture by damage accumulation in rocks. Int J Fracturing 139:369–381

Amitrano D, Arattano M, Chiarle M, Mortara M, Occhiena C, Pirulli M, Scavia C (2010) Microseismic activity analysis for the study of the rupture mechanisms in unstable rock masses. Nat Hazards Earth Syst Sci 10:831–841

Got JL, Fréchet L, Klein FW (1994) Deep fault plane geometry inferred from multiplet relative relocation beheath the south flank of Kilauea. J Geophys Res 99(B8):15375–15386

Lockner DA (1993) The role of acoustic emission in the study of rock fracture. Int J Rock Mech Min Sci Geomech Abstr 30(7):883–899

Lomax A, Virieux J, Volant P, Thierry-Berge C (2000) Probabilistic earthquake location in 3D and layered models. In: Thurber CH, Rabinowitz N (eds) Advances in seismic location. Kluwer, Norwell, MA

Lomax A, Curtis A (2001) Fast probabilistic earthquake location in 3D models using Oct-Tree Importance Sampling. Geophys Res Abstr., 3

Pogliotti P (2006) Analisi morfostrutturale e caratterizzazione termica di ammassi rocciosi recentemente deglaciati. MS thesis, Università degli studi di Torino, Torino, Italy

Press W, Teukolsky SA, Vetterling WT, Flannery BP (1996) Numerical recipes in Fortran 90: the art of parallel scientific computing, vol 2, Secondth edn, Fortran numerical recipes. Cambridge University Press, New York



Slope Disaster Monitoring System Using Battery-Operated Wireless Sensor Network

Keigo Koizumi, Kenji Hirata, Kazuhiro Oda, Yukishige Fujita, and Sadayuki Kamide

Abstract

This paper develops a slope disaster monitoring system using distributed sensors. The sensor node has wireless communication and tilt detection capabilities. Each sensor node communicates to each other and sends the corrected data to a base station, which can send an alert message to administrators in case of emergency. The developed slope disaster monitoring system is installed on a slope along the Chugoku Expressway. This first experimental study showed a significant potential of the developed distributed sensor network for detecting slope failures, but it also clarify that the wireless communication capability is sensibly influenced by relative geometric alignments of each sensor nodes. The second experimental study has begun along the Maiduru-Wakasa expressway. Since the geometric alignments are modified, we are having an improved wireless communication correspondence.

Keywords

Monitoring • Slope disaster • Wireless sensor network

Introduction

Natural disasters such as unexpected heavy rainfalls and earthquakes cause severe damages to infrastructures, e.g., slope disasters along roads and railways. Health monitoring of civil structures which have been used for several decades becomes an important issue in order to provide adequate maintenances. It is necessary to develop a monitoring system that can be applied to a large scale man-made construction for detecting structural deformations to prevent severe damages (Schwab et al. 2007; Sako et al 2007).

This paper focuses on slope disasters along expressways that play an important role as a main lifeline for emergency basis. Enhancing surveillance for the expressway toward unexpected disasters is considerably important. To maintain safe and secure road networks, each structure's health has to be monitored by daily checks, and also a real-time monitoring to specific slopes in an emergency condition is necessary. This can prevent serious damages and reduce the time of closure of the expressways. However, except for a few slopes of which the priorities of maintenances and monitoring are the highest, it is difficult to take effective countermeasures from the standpoint of budget. Hence only a few slopes are monitored by expensive sensing devices, and the others are inspected at scheduled visual observation by technicians. Another difficulty for detecting slope deformations is that the best position to set up the sensors on the

K. Koizumi (✉) • K. Oda
Division of Global Architecture, Graduate School of Engineering, Osaka University, 2-1 Yamadaoka, Suita 565 0871, Osaka, Japan
e-mail: koizumi@civil.eng.osaka-u.ac.jp

K. Hirata
Department of Mechanical Engineering, Nagaoka University of Technology, Nagaoka 940 2188, Japan
e-mail: hirata@nagaokaut.ac.jp

Y. Fujita
EarthWatch Corporation, 1-10-206 Toyotsucho, Suita 564-0051, Japan
e-mail: fujita@earth-watch.jp

S. Kamide
West Nippon Expressway Kansai Engineering Co., Ltd, 5-26 Nishiekimae, Ibaraki 567 0032, Japan
e-mail: S_kamide@w-e-kansai.co.jp

C. Margottini et al. (eds.), *Landslide Science and Practice*, Vol. 2,
DOI 10.1007/978-3-642-31445-2_14, © Springer-Verlag Berlin Heidelberg 2013

slope cannot be effectively determined as yet. An advanced sensing technique with a relatively low-cost that can be applied to a large scale structure is required.

Sensor network technologies have been attracting significant interest from broad range of application areas (Gharavi and Kumar 2003). Wireless networked sensors are tried to use for a slope monitoring (Aoki et al. 2007; Kim and Han 2008). One is a wireless monitoring system that employs a star-type network was developed. Each sensor node need to communicate with the base station directly. Thus, a possible wireless communication distance depends on the feature of the wireless device and the field situation, and it is basically difficult to build robust network. A mesh-type network was also tried to develop a slope monitoring system, and the field test results were discussed in a previous study (Fukagawa et al. 2008). However the mesh-type network system does not use an intermittent mode and constantly apply electrical current, and it has a disadvantage from energy consumption point of view. Low power consumption functionality is quite essential to realize a long term monitoring in an outdoor environment.

We develop a distributed wireless sensor network system that can be applied to a large scale slope along the expressway and detect deformations due to heavy rainfalls or earthquakes in an early stage. The sensor node consists of a wireless communication device utilizing an intermittent mode, which is significantly effective to reduce energy consumption, and an acceleration sensor that is used as an inclination meter and developed by the MEMS (Micro Electro Mechanical Systems) technology. The low-cost sensor nodes with a mesh network function can be easily and densely set up on slopes. The accuracy of slope disaster detection will be improved by densely distributed sensor modules, and the total cost for monitoring can also be reduced. The sensor nodes connect to each other by wireless correspondence and autonomously organize a communication network, and the monitored data from each sensor node is sent to a base station which can connect to the Internet. If any deformation is found, a warning signal will be sent to the head office, and the administrators are also noticed by an Email through a cellular phone. The performance of wireless communications and accuracy of inclination meter of the developed sensor node are discussed.

The Developed Slope Disaster Detection System

Our focus is on the application of a wireless sensor network for the detection of slope failure. Wireless sensor networks are divided into several categories such as WAN (Wide Area Network), MAN (Metropolitan AN), LAN (Local AN) and PAN (Personal AN), depending on the communication distance (Sakata 2006). A wireless mesh network that is included in the wireless PAN is used in this paper. The sensor nodes communicate with each other without any relation to the access point. Even if some sensor nodes can no longer operate, the rest of the nodes still communicate with each other by automatically changing the communication pathway. On the other hand, some new sensor nodes are set up on the slope after the mesh network is constructed, these sensor nodes automatically connect to the network, and the new mesh network will be established.

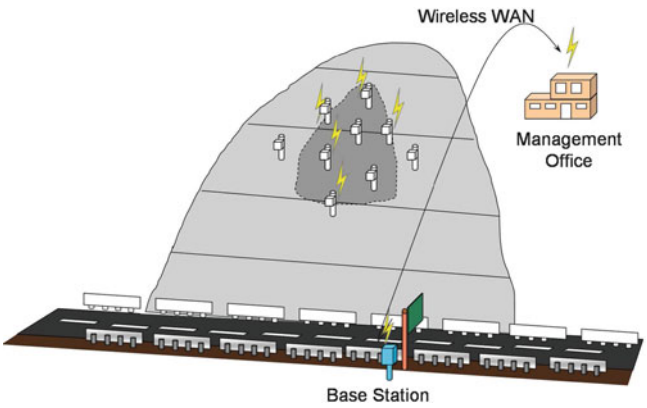


Fig. 1 Basic concept of the slope disaster detection system using mesh networked distributed sensors

Figure 1 shows overview of the developed slope disaster detection system. Each sensor node communicates with another, and the data are sent to a base station. The data can be monitored in the management office, and in the case of some deformations occurs on the slope, the alert signal and the detailed data will be transmitted to the management office through the base station.

The developed sensor node consists of a communication module, an acceleration sensor which is used as a tilt sensor and an interface board that connect the acceleration sensor and the communication module. We use MPR2600J or XM2210J as the communication module and MDA300 as the interface board, both are produced by Crossbow Technology. The acceleration sensor KXM52-1050 by Kionix, Inc. is connected to the communication board through the interface board MDA300, and the corrected data is transmitted through the mesh network communications of each sensor node.

Figure 2 shows a schematic diagram of the developed sensor node. The sensor node has a dust- and water-proof ability according to the IP65 standard for outdoor use. Dewfall is prevented with a filter that is resistant to water and is permeable.

An important issue of the distributed sensor network used in an outdoor field such as the system developed in this paper is the energy consumption. The developed sensor node is driven by two C-size batteries, and adopts the intermittent

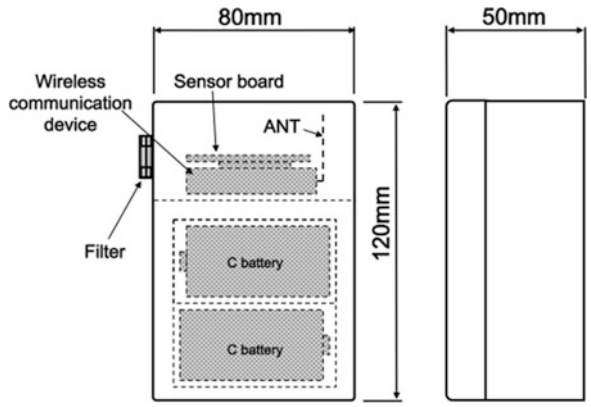


Fig. 2 A schematic diagram of the developed sensor node

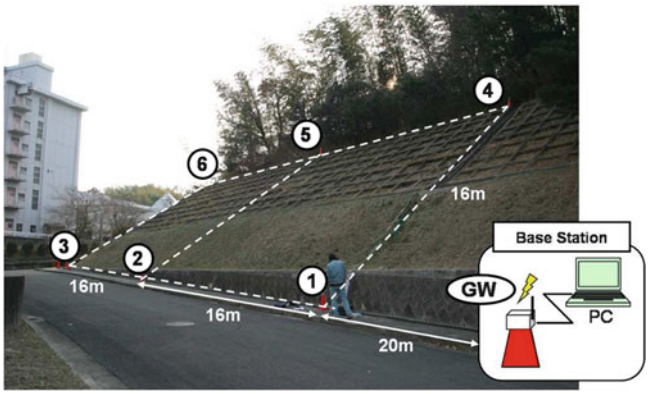


Fig. 3 Experimental overview

mode except for an emergency situation. This can reduce the required amounts of energy consumption, and a long-term monitoring becomes possible. The base station that needs AC 100 V power supply is set up at the call-box along the expressway where the power supply is possible.

Performance Evaluations of the Developed Sensor Node

This section describes experimental evaluations of the developed sensor node. Wireless communication ability was checked through a small filed test in the Osaka University campus. The accuracy of the acceleration sensor that will be used as a tilt sensor is also summarized.

Wireless Communications

Communication Distances

The performance of the communication device was evaluated through a filed measurement experiment. The decibel value is used as the evaluation index of the radio field intensity, and the decibel value Y (dBm) is calculated as follows.

$$Y = 10 \log_{10}(X/1\text{mW}) \quad (1)$$

X(mW) is the received power. The decibel value is typically referred as the RSSI (Received Signal Strength Indication), and we use the term RSSI as to denote the power of the received signal. The RSSI is influenced by the undulation of the ground surface and obstacles (typically metallic objects). Our preliminary experiments show that the RSSI stronger than −85 dBm is needed to establish a stable wireless communication. Thus, the RSSI −85 dBm is used as the threshold to evaluate the communication quality.

Our previous study indicates that the communication distances corresponding to −85 dBm are 22 m when the height of a sensor node from a ground is 0 to 47 m when the height is 0.5 m (Koizumi et al. 2010).

Mesh Networks

The communication environment in each sensor node at a height of 0.5 m on a slope in the Suita campus of Osaka University was observed. The experimental overview is shown in Fig. 3. The sensor nodes were installed on the slope at intervals of 16 m. The communication environment between the sensor nodes was confirmed by the RSSI at intervals of 10 s. The mean value of the RSSIs of around 60 sampled data at each node is shown in Table 1.

Some of the RSSI values in Table 1 fall below −85 dBm even if the communication distance is less than 47 m. Although the communication distance between the sensor nodes No. 1 and No. 4 is just 16 m (see Fig. 3 to find a geometric alignment), the RSSI indicates a value that is lower than usual. This is because the retaining wall in front of No. 1 probably becomes an obstacle. The same situations are found between the sensor nodes No. 1 and No. 5 or No. 2 and No. 6. On the other hand, compared between the sensor nodes No. 2 and No. 4 or No. 6, though the geometric alignments are almost the same, the RSSIs are different. This indicates that 2.4 GHz wireless communications that is used in our experimental setups has a feature of directivity. The RSSI may be affected by the communication distance and also the undulation due to the obstacles and weather conditions. To construct a robust network, it is necessary to build the layout in such a manner that two or more communication routes in each sensor node are ensured.

Accuracy of the MEMS Sensor

We used the acceleration sensor as an inclination meter and installed a low-pass filter to suppress the high frequency

Table 1 Result of the RSSI between sensor nodes

		Sending side					
		1	2	3	4	5	6
Receiving side	gw	−81.0	−89.1	88.4	−86.6	−89.4	−92.1
	1	–	−67.1	−80.0	−88.8	−83.4	−90.0
	2	−63.1	–	−68.2	−75.0	−84.7	−89.1
	3	−76.7	−65.9	–	−74.7	−74.7	−77.3
	4	−88.9	−81.4	−83.8	–	−74.3	−85.2
	5	−88.5	−81.2	−75.6	−74.1	–	−68.7
	6	−92.0	−89.1	−73.0	−83.2	−66.0	–

The data with the background color indicate the value that are lower than −85dBm

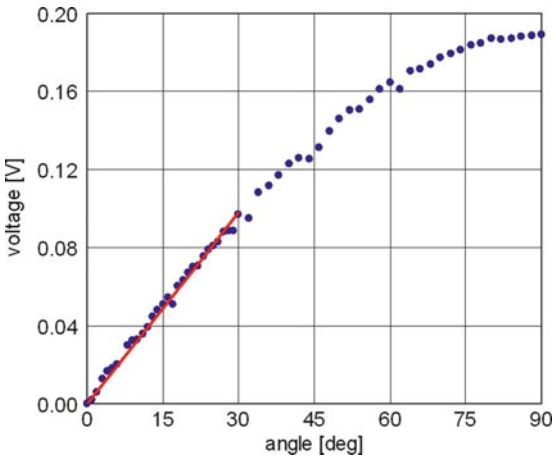


Fig. 4 Relation between tilt angles and voltage shifts

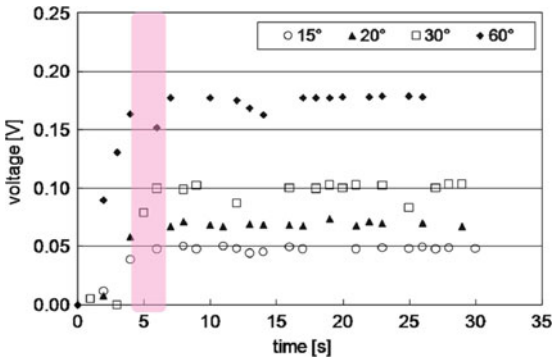


Fig. 5 Elapsed time to reach each angle

noises. The following sections concern the accuracy of the developed sensor nodes.

Resolutions

To transfer data from the acceleration sensor to the communication device, the interface board is used to connect them. Theoretical angle resolution is approximately 0.08 ° by the relation between the interface board MDA300 whose resolution is 0.6 mV and the acceleration sensor whose sensitivity is 660/9.8 mV/(m/s^2).

Linearity

The developed sensor node was set on an angle measurement device, and the output voltage of the acceleration sensor to the actual angle was measured. Figure 4 shows the resulting relation between the inclination angle and the sensor output voltage. The laboratory experiment was carried out under the constant temperature environment of 29 °C. When the angle is detected by using gravitational acceleration, the relation between the angle and the output value is expressed in the sine curve. However, it was showed that the data up to 30 ° can be approximated by a straight line with a relatively high accuracy. This means that the angle variation up to 30 °, which is a sufficient range to detect a slope deformation, can be detected accurately by using the regression line in Fig. 4.

Sensitivities

A second-order low-pass filter having a cutoff frequency at 1 Hz is used to suppress the high frequency noises. Since the installed low-pass filter may generate the time lag, we measure the required time to detect the inclinations. Figure 5 shows the elapsed time for reaching the actual values 15 °, 20 °, 30 °, and 60 °. The measurement interval is approximately every 1.5 s. The figure indicates that it takes 5–7 s for the output value to reach the actual value. However, it takes 3–5 s for the actual value to reach the specified angle because a hand operating angle measurement device is used. Therefore, it is understood that the output value reaches the actual value within approximately 2 s. To avoid misinterpretation and to judge accurately, the measurement duration time need to be set at least 2 s.

Tests of the Slope Disaster Detection System

This section discusses the advantage and the remaining problem of the wireless monitoring performed by the developed disaster monitoring system.

The field test site has horizontal length 100 m and height 40 m along the Chugoku Expressway. Fourteen nodes,

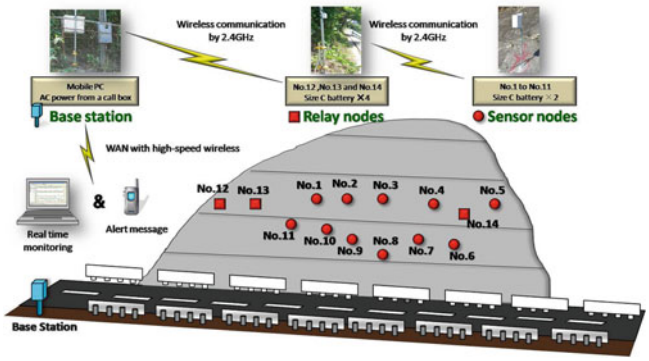


Fig. 6 Slope disaster detection system using the mesh network on a field test site

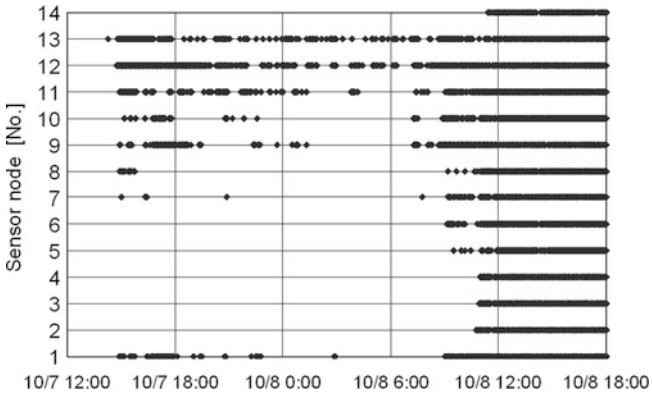


Fig. 7 Communication environment until network construction

including relay nodes, are installed on the slope as shown in Fig. 6.

The communication system is built by ad-hoc and multi-hop network, and each sensor node including relay node communicates with each other by its ad-hoc and multi-hop functionality. The relay node and the sensor node have the exactly same wireless communication feature, and the difference between them is that the relay node does not include acceleration meter.

The distance between two consecutive sensor nodes is less than 20 m, and the distance from the relay node No. 12 to the base station is approximately 450 m. To build wireless communication network between the base station and the relay node No. 12, a directive antenna is mounted on both the base station and the relay node No. 12. The relay node No. 12 is just a route to send data, and all the data from each sensor node relays No. 12 and is sent to the base station.

The base station comprises a receiver to collect the data from the sensor nodes and a wireless WAN that can communicate with the management office. The sampling rate of the data from each sensor node can be adjusted from any PC in a remote place that can connect to the base station through the Internet. The base station can send disaster alert messages to the specified PC and cellular phones by setting appropriate warning values.

The time required for each sensor node to establish the mesh network on the site is indicated in Fig. 7. The black dots in Fig. 7 show the communication record between the base station and each node. The communication from the sensor node No. 13 is confirmed as the first communication at time 14:14. In the communication conditions in Nos. 1, 7, 8, 9, 10, and 11, it can be seen that although the communications were confirmed once, they are intermittently interrupted.

Finally, at approximately 12 o'clock the next day, the communication of all the sensor nodes is confirmed. This result shows that it takes almost 22 h to confirm the mesh network by all the sensor nodes.

For establishing a stable mesh communication network, relatively long time period, i.e., almost 24 h, was required. Each sensor node should transmit data through two or more sensor or relay nodes as relay nodes because the distance between each sensor node and the relay node No. 12 that is the gateway to the base station is quite far. Each sensor node searches for the sensor and relay nodes for which the communication cost is the most reasonable, and this establishes the mesh communication network. In this field test, it was a shortage such that the relay node No. 12 is the only node that can communicate with the base station. A long distance between the base station and the relay node No. 12 reduces an arrival factor of packets from the base station to the sensor nodes through multi-hop between sensor and relay nodes. In addition, the intermittent mode, which is used in order to improve the battery consumption, also requires a time to synchronize each communication between the nodes. This is because it takes a long time to stabilize the communication network. In order to establish the mesh communication network with a much shorter stating up period. We may need to install other nodes that can communicate with the base station directly.

The wireless communication environment occasionally changes depending on the location and weather conditions of the filed site. It is a demerit of the proposed communication system as compared to a wired communication. To solve the problem and build a robust communication environment, at the early stage of this long term monitoring experiment, the software program of the sensor node has been improved as follows: When the wireless communication is interrupted because of some communication failure, a reset function on the software is executed; In addition, the software freezes due to some faulty condition, the reset function on the hardware is executed to recover from the non-responsive state into the normal operation. As a result, once the entire network is established, the network is not interrupted for 4 months that is the life period of the two C-size batteries in each sensor node. At each battery

Table 2 Measurement environment

Power-supply	C battery
Number of measurement days	129 days Oct. 8th to Nov. 17th and Nov. 26th to Feb. 22nd
Measurement interval	Every 5 min. for 40 days
	Every 30 min. for 89 days
Measurement entry	Acceleration (X and Y axis), Temperature, Relative Humidity, Voltage
Temp in the case (Min/Max)	−6°C/40°C
Humidity in the case (Min/Max)	34 %/98 % (RH)

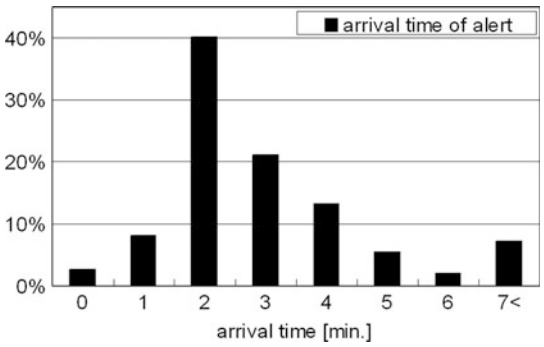


Fig. 8 Time required to receive alert Emails

maintenance period, although it takes a long time, i.e., almost 24 h, to establish a communication network, we can perform sustained monitoring over 4 months.

Table 2 briefly summarizes a slope monitoring experiment which can be performed by one pair of two C-size batteries. The sampling interval is 5 min for the first 40 days. The sampling interval of the last 89 days is changed from 5 to 30 min. The two C-size batteries used for each sensor node were needed to exchange after 129 days of observation, and the possible monitoring period is approximately 4 months. The sampling period can be enlarged depending on a required application, and a long sampling period can consume small amount of battery energy.

The total monitoring experiment has performed over 8 months. Although dew-fall due to rainfall is confirmed in a part of the sensor nodes, neither the sensor nor the communication device shorts out. The sensors might need to coated with silicon and be protected by a filter and silica gel to prevent short-circuit due to dewfall for prolonged use.

To detect the warning value purposely for the measurement period, an alert function is set. The time lag between the transmission time and the receipt time is measured by transmitting alert Emails regularly. Figure 8 shows the time required to receive the alert Emails from the base station. It can be seen that 51 % of all the Emails are received within

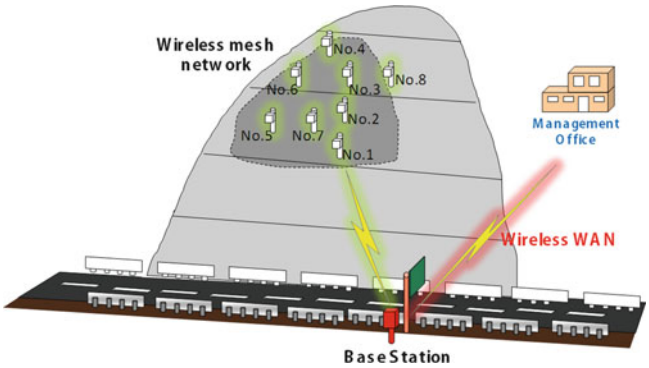


Fig. 9 Filed test of an improved battery-operated wireless sensor network

2 min and 71 % of all the Emails are received within 3 min. However, some Emails are received after more than 7 min. To minimize the damage of the slope disaster, the alert Emails should be received as soon as possible. It may be necessary to use a high-speed optical-fiber network for expressways administrators to play the role as the safety alarm of any emergencies, although wireless WAN is a reasonable communication device.

Filed Test of an Improved Battery-Operated Wireless Sensor Network

System Improvement

Based on the agenda of the Chap. 4, the wireless monitoring system is improved as following two points.

This mesh networked system did not work well in the first 22 h because of the positional relationship which was quite far from the base station to the sensor nodes. Therefore new base station should be installed near the slope as shown in Fig. 9. And MPR2600X which is an advanced communication module of MPR2600J and XM2210J is adopted. This figure shows a slope of 107.6 km from the starting point of the Maiduru-Wakasa expressway. Eight sensor nodes are installed on the slope. The distance between each sensor node is less than 30 m. And a distance between the base-station and each sensor node is around 100 m.

To operate this wireless sensor network system as an actual monitoring system, battery life must be improved.

According to a result of Chap. 4, 4 months is a rough indication of the battery life of alkaline size C battery. Therefore a new battery pack which works at least 3 years is designed.

In addition, the new senor node mounts not only the tilt sensor but also a soil-water sensor and a soil-water potential

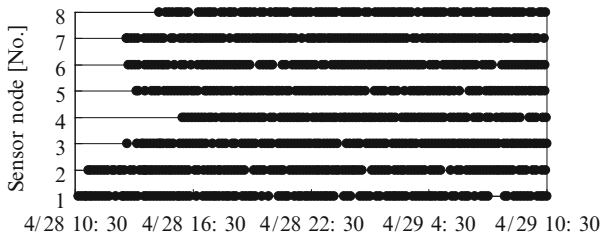


Fig. 10 Communication environment until network construction

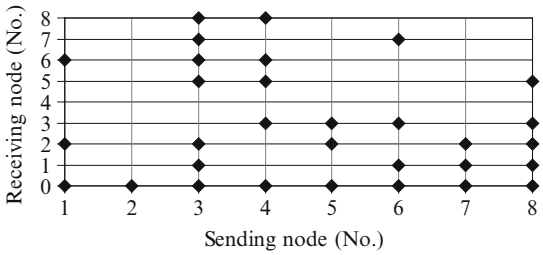


Fig. 11 Contact state between the senor nodes

sensor for a prediction of slope failure by heavy rains. Details will be reported at a later date.

Results

Figure 10 shows communication environment between the base station and each sensor node in the first 24 h. The sensor nodes were installed on the slope in order. It took 5 h including lunch break. Shortly after the power-on state of each sensor node, the wireless communications has started. The first contact to the base station is No. 1. The monitoring was started at 10:30 on April 28, 2011. There is no time lag such as Fig. 7. After the communication network was built there is no communication failure.

Figure 11 shows contact states between the sensor nodes. No. 0 of the receiving node in Fig. 11 indicates the base station. X-axis is sending node and Y-axis is receiving node. The results show that all the sensor nodes have communicated with the base station directly. In addition each sensor node has multi-communication pathways except for No. 2. It indicates that this communication state is well robust compared with the communication sate on the slope in Chap. 4.

The new battery pack consists of four lithium size D batteries which were built at parallel circuit. Theoretically the battery life is maintained for more than 3 years at interval of average 10 min.

Conclusions

This paper develops the slope disaster monitoring system using the distributed sensor nodes that consist of the communication device and the acceleration meter. The effectiveness of the developed disaster monitoring system is evaluated through the tests in a quite realistic situation along the Chugoku Expressway and the Maiduru Expressway. To build a disaster monitoring system using a wireless sensor network, it is necessary to take into account the stability of the communication connections, the power supply consumption, and the time required for receiving the alert messages. We have focused on disaster monitoring, understood the communication environment of a mesh network, and verified the accuracy of the MEMS sensor. The following conclusions can be formulated.

A robust network can be constructed by using a mesh network, although the communication environment at each point changes because of various obstacles when the wireless communication devices are used on the slope. In particular, multi-point monitoring on a slope is useful for not only building a robust network but also observing the slope accurately. To build mesh-network in a short time, a base station should be installed near multi-sensornodes. Around 100 m from a base station to sensor nodes is a reasonable distance to make robust mesh network. To maintain long term monitoring, compact battery pack which is mounted four lithium size D batteries is designed.

By using the MEMS sensor, we can accurately detect the angle variation over the meaningful angle range. The observed data is sent to the management office through the base station by the wireless WAN. It takes around 2 min for the message to arrive at the management office from the base station that is a required time to confirm the slope deformations at the management office.

Acknowledgment This research was partially supported by the Ministry of Land, Infrastructure, Transport and Tourism, Construction Technology Research and Development Subsidy Program.

References

Aoki H, Glaser S, Ikegawa Y, Bouda S, Miki H (2007) Development and application of a wireless sensor network for ground monitoring. J Soc Instr Contr Eng 46(2):1–5

Fukagawa R, Sako K, Yokota Y, Ookubo H, Shimakawa H, Harada F (2008) Research on a sensor network system for slope failure due to rainfall. In: Proceeding of the symposium of Jiban-no-Kankyou-Keisokugijutu, in Japanese, pp 21–26

Gharavi H, Kumar SP (2003) Special issue on sensor networks and applications. Proc IEEE 91(8):1151–1153

Kim K, Han J (2008) Design and implementation of a real-time slope monitoring system based of ubiquitous sensor network. In: The 25th international symposium on automation and robotics in construction, Canada 26–29 June 2008, pp 330–336

Koizumi K, Fujita Y, Kamide S, Watanabe T (2010) Application of ubiquitous network for slope disaster monitoring, 2010. In: International symposium on flexible automation, Japan, (CD-ROM), JPL-254

Sakata S (2006) Sensor network. Ohmusha, in Japanese, p 238

Sako K, Kitamura R, Fukagawa R, Yasukawa I (2007) Monitoring and warning system for slope failure due to heavy rainfall. In: Proceedings of the 3rd international conference on Structural Health Monitoring of Intelligent Infrastructure SHMII-3, paper no. 189 (CD), p 146

Schwab AK, Eschelbach K, Brower DJ (2007) Hazard mitigation and preparedness. Wiley, Hoboken



The Use of ERT for Investigation of Berzhita Landslide, Tirana Area, Albania

Hamza Reci, Ylber Muceku, and Idriz Jata

Abstract

In this paper we present an engineering geological-geophysical investigation of the Berzhita landslide, Tirana area, Albania. The work includes engineering-geological field investigation and geophysical measurements. A detailed field investigation was conducted to delineate the aerial extent and a general direction of movement of the landslide zone, assess lithological section, estimate the thickness of the sliding layer, and delineate water saturated zones. In order to study in detail this landslide, two perpendicular Electrical Resistance Tomography (ERT) profiles were carried out. A detailed engineering-geological study was conducted including, engineering mapping on scale 1:100, geotechnical investigations such as drilling and trial pits at 14 points with depths 3–4 m, soil sampling and laboratory tests for geotechnical parameter studies. The results of field investigations are presented as engineering geological map and several geological and resistivity images cross-sections which clarify the geometry and subsurface characteristics of the landslide.

Keywords

Landslide • Sliding surface • Electrical resistance tomography • Lithology • Geological-engineering • Resistivity images • Cross-section

Introduction

Engineering-geological and geophysical methods are widely used for studying and monitoring landslide zones. They consist in surface movement observations, such as direct measurements of sub-surface displacements, and other methods such as in-situ observations in holes and characteristics of geologic materials obtained from drill cores (Hutchinson 1983). However, even when drilled, when the maximum core recovery is recorded and geotechnical borehole logging has been successful, drill holes represent only single-point information in a lateral dimension. In contrast, geophysical methods are generally non-invasive and give highly resolved two dimensionally distributed data (Mauristsch et al. 2000). The feasibility of geophysical methods to resolve details of sliding masses, such as groundwater regime, the internal composition of sliding mass, geometry of the slide, and depth to bedrock, has been studied by Bogoslovsky and Ogilvy (1977), Muller (1977), Campagnoli and Santarato (1995), Mauristsch et al. (2000), and Lapenna et al. (2003). Geophysical methods do not replace drillings and sampling of test pits and trenches. Rather, they supplement these procedures and greatly reduce time and cost and environmental problems that often result from large-scale drilling operations. On the other hand, detailed engineering geological investigation can clarify many unknown aspects of a slide that helps to interpret the results of geophysical surveys. In recent years, engineering-geological and geophysical methods have been used for studying the landslide zones in Albania (Muceky and Reci 2006, 2008). In this research a combined engineering geological investigation and electrical resistivity tomography (ERT) method, has been used to investigate the Birzhita

H. Reci (✉) • Y. Muceku • I. Jata
Institute of Geosciences, Polytechnic University of Tirana,
str. Don Bosko nr. 60, Tirana, Albania
e-mail: jack@gmail.com

C. Margottini et al. (eds.), *Landslide Science and Practice*, Vol. 2,
DOI 10.1007/978-3-642-31445-2_15, © Springer-Verlag Berlin Heidelberg 2013

Landslide, at Tirana Area, its dimensions, causes of sliding, thickness and other physical-mechanical parameters.

The ERT method is used to study the thickness of sliding layer and sliding surface, water zones, and the depth of the bedrock through the true resistivity values distribution on 2D profiles.

Geomorphology and Geological Settings

The landslide of Berzhita, is of "Rock slide" type and an old one. It is located around 15 km southwest of Tirana, Albania (Fig. 1). It has the form of a wing chair with dimensions 350 m, along the sloping topography and 150–160 m on the other direction.

On the viewpoint of geomorphology, it constitutes on the hilly geomorphological unit and it is composed from Quaternary deluvional and eluvial deposits, overlaid on the Molassic rocks of Neogene (sequences of sandstone, claystone and silt). The relief of the zone is sloppy with dipping towards the east and heights from 230 m on the foot of the hill up to 316 m on the top of it. On the western part of studied area, the slope of the hill is greater than the eastern part. Thus, the western part slope has a dipping angle from 32–35 ° up to 40–45 °, while, on the eastern part the slope is more slight with variations from 7–10 ° up to 10–15 °.

The studied area constitutes from the following geological formations:

Quaternary formations (Q_4 al)

Molassic formation of Neogene (N_1^3t)

The Quaternary formations are represented from: alluvial facial deposits (Q_4 al), consisting on alluvial and delluvial facies. They have a spreading over all the studied area, overlaying to the molassic formation of Iba Suite. The thickness of them is from 1.5–2.0 m up to 3.5–5.5 m. The quaternary formations are compound from today delluviums hilly morphological unit and represented from unconsolidated light fine sands and fine clays, situated on the upper part of lithological section.

The molassic formations of Neogene (N_1^3t) are represented from Molassic formations of Tortonian age (N_1^3t). These formations are formed within the pre-oregonesis bending of post-geosynclinal epoch, overlain on the older formations of tectonic zones of Kruja, Krasta and Mirdita (Fig. 2).

The studied area on the aspect of the infiltration is characterized from two groups of rocks that are: (a) fine sands, (b) sandstone-claystone-silt of (N_1^3t). From the field observations of drillings it is seen that the level of underground waters is 2.0–2.5 m. The fine sand-clay layers that covers the bedrock formations has very low infiltration coefficient and practically they prevent the rainfall and surface waters as well to penetrate towards the bedrock formations.



Fig. 1 Location map and general view of Birzhita landslide. The two ERT profiles (longitudinal L1–L1 and transversal T1–T1) are shown with *black lines*. The interrupted *red line* shows the boundary of rock landslide body

Engineering-Geological and Geophysical Methodology

The works carried out in the studied area has been conducted in two phases. In the first phase were fixed the necessary field works to be conducted. In the second phase are carried out engineering geological field observations of 1:100 scales and two Electrical Resistance Profiles (ERT).

Engineering geological field works consisted to engineering-geological field observations. Works were conducted in oriented profiles of scale 1:100. There are included 14 works of trial pits, trenches and drilling with a depth 3.0–4.0 m, measurements with pocket penetrometer, sample taking to be analyzed in laboratory and the interpretation of the data taken from the field works, from which is done the correlation of geotechnical parameters of the studied area.

Geophysical techniques used consisted in the 2D ERT profiles. ERT is an active geoelectrical prospecting technique used to obtain 2D, 3D and 4D (with time) images of the subsurface electrical resistivity distribution. It has been applied for investigating areas of complex geology, such as volcanic and geothermal areas (Di Maio et al. 1998), seismotectonic structures (Caputo et al. 2003; Nguyen et al. 2005), archaeological sites (Tsokas et al. 2007; Reci et al. 2009) and areas of hydrogeologic phenomena and environmental problems (Ogilvy et al. 1999; Naudet et al. 2004). Recently, ERT has been used to delineate the geometry of complex landslides (Agnesi et al. 2005; Lapenna et al. 2005; Lebourg et al. 2005; Meric et al. 2005; Godio et al. 2006; Muceku and Reci 2006, 2008;

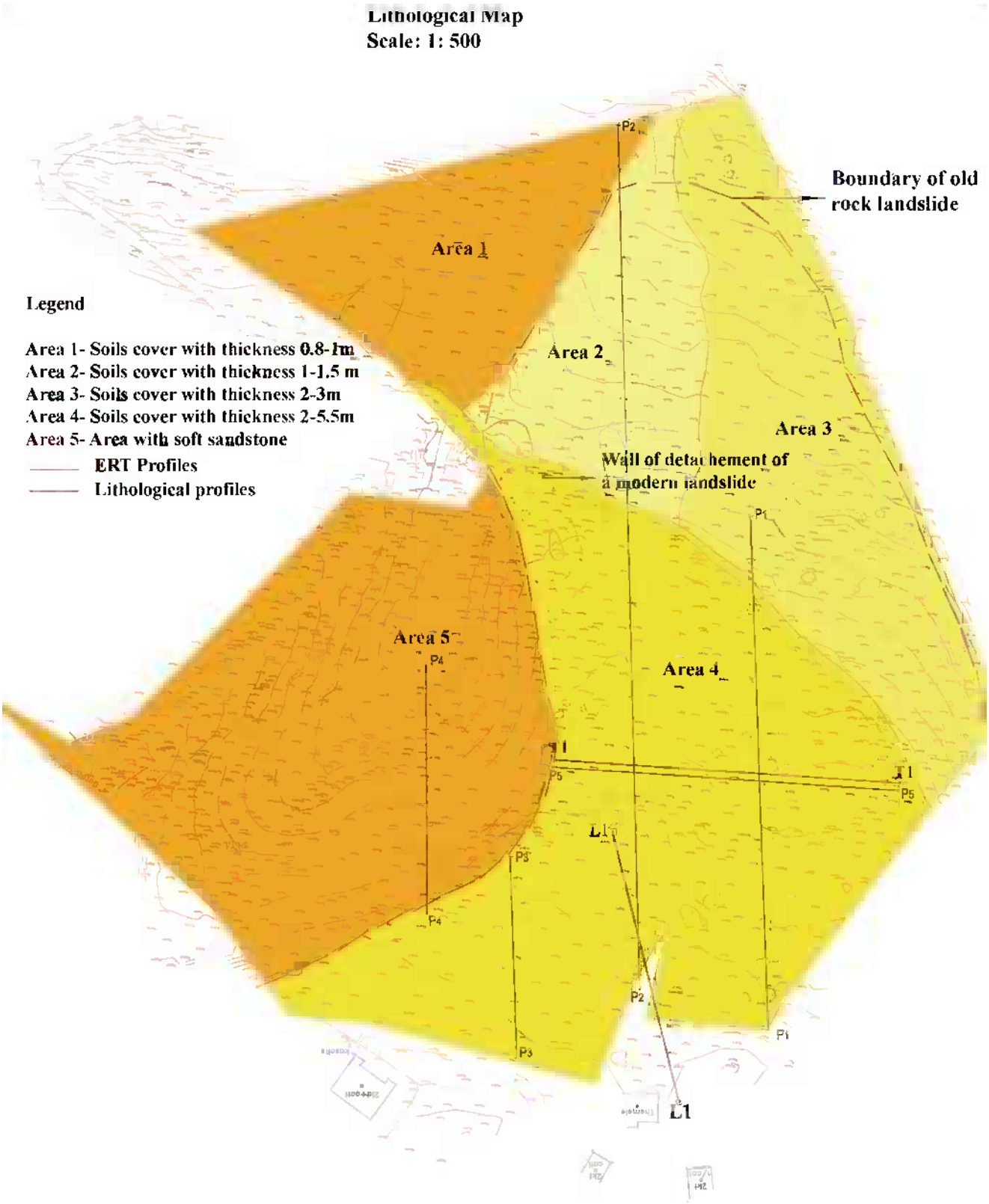


Fig. 2 Lithological map of the studied area. Location of lithological and ERT profiles is present

Sass et al. 2008). Technically the ERT is obtained by using different multielectrode arrays, such as the dipole-dipole, Wenner, Schlumberger, Wenner-Schlumberger, Gradient etc., the choice of which depends on the subsoil, the depth of investigation, the sensitivity to vertical and horizontal changes in the subsurface resistivity, the horizontal data coverage and the signal strength (Loke 1999). The current is injected into the ground through a couple of electrodes, and the resulting potential differences are measured between another couple of electrodes at the surface. The mathematical combination between electric currents (I) and voltage measurements (V) provides the apparent resistivity values.

$$\rho_a = k\frac{V}{I} \tag{1}$$

where k is the geometric factor which depends on the arrangement of the four electrodes. Using the algorithm RES2DINV proposed by Loke and Barker (1996) the apparent resistivity values are inverted in true resistivity values. The inversion routine is based on the smoothness constrained least-squares inversion implemented by using a quasi-Newton optimization technique. The subsurface is divided into rectangular blocks, the number of which corresponds to the number of measurement points. The optimization method adjusts the 2D resistivity model trying to iteratively reduce the difference between the calculated and measured apparent resistivity values. The root-mean-squared (RMS) error provides a measurement of this difference.

We applied this method in order to depict the geometric features of the landslide and to estimate the thickness of the sliding layer. We used three different electrode configurations (dipole-dipole, Wenner-Schlumberger and gradient) and a multielectrode system with 30 electrodes.

Two ERT profiles perpendicular to each-other has been carried out in order to see the depth of the sliding block and the sliding surface in two directions (Figs. 1 and 2). The resistivity measurements are carried out with the WDJD-3 Multi-Function Digital DC Resistivity/IP meter. The resistivity images consist on the true resistivity values of geological formations of the subsurface along the profile and toward depth. The length of the profiles is 90 m with 3 m distance between electrodes with maximum depth of investigation 17 m in gradient array. From the inversion of measured apparent resistivity values, the true resistivity values of the subsurface have been taken through an inversion interpretative methodology.

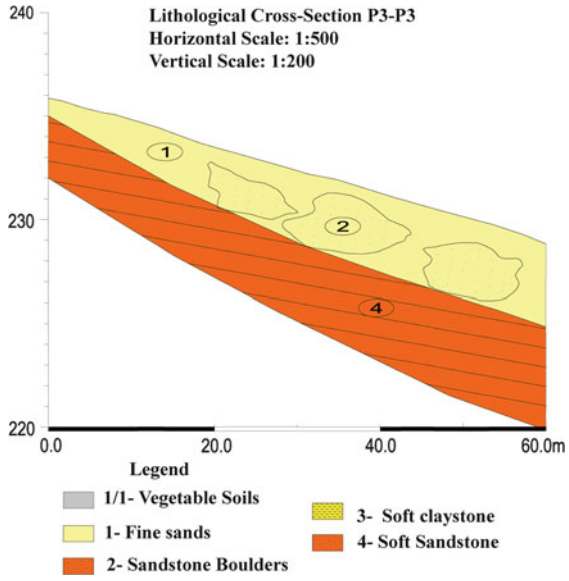


Fig. 3 Lithological cross-section P3–P3. *1*-Fine sands. *2*-Sandstone boulders. *4*-Soft sandstone

Results and Discussion

Engineering-Geological Conditions of the Studied Area

For the assessment of engineering-geological conditions of the area the main role is played by the physical-mechanical parameters of the layers. To determine the indicators of physical-mechanical properties, eight samples have taken in consolidated lithological formations and two others on unconsolidated ones.

According to lithological structure and the physical-mechanical properties of soils that builds this area, five layers have been distinguished (Figs. 3 and 4):

Layer nr-1/1

Is the upper part of the environment represented from unconsolidated vegetal soils, which have a thickness 0.5–0.7 m.

Layer nr-1

Layer nr. 1 is extended in the upper part of the lithological sections and is detected in all works done in the studied area. It is represented from: powdery soils of unconsolidated light fine sands until light fine clays, of beige color with brown spots; thin sandy interlayers; consistence of soft plasticity; low compressive with humidity. Within

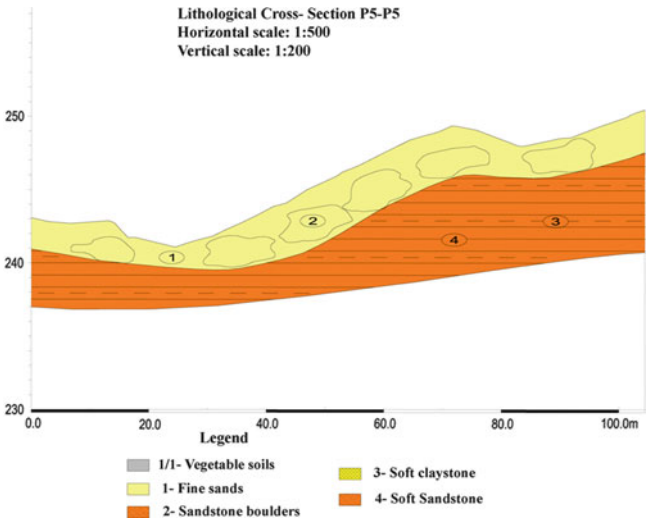


Fig. 4 Lithological cross-section P5–P5. *1*-Fine sands. *2*-Sandstone boulders. *3*-Soft claystone. *4*-Soft sandstone

those layers are seen sandstone boulders with dimensions 0.5–1 m^3 up to 2.5–3 m^3. The thickness of this layer is from 1.5–3 m up to 5.5 m.

Layer nr-2

It is represented by sandstone boulders, with dimensions 0.5–1 m^3 up to 2.5–3 m^3, which lay within the layer nr. 1. In engineering-geological aspect are soft sandstones with clayey cementation with beige color.

Layer nr-3

It is represented from interlayers of soft claystone and sandstone formations, with grey color.

Layer nr-4

It is represented from soft sandstone formations with beige color.

ERT Profiles

The true resistivity images of the subsurface, show a good agreement with other geotechnical methods used (Fig. 5). The resistivity values are depicted in logarithmic scale. For each profile are presented the resistivity values distribution for three electrode configurations used. From the interpretation of the ERT profiles, for each profile we see almost the same subsurface resistivity model on three geometrical array used. In longitudinal profile (L1–L1), which is along the topography of the slope the geological situation of the subsurface, is as follows; From the surface up to a depth 5–6 m, the geological formations with high resistivity values are present, which show the presence of the sliding layer composed from soils and sandstone blocks (Log $R > 1.8\ \Omega$). The lateral changes of the resistivity values are sandy content (Log $R < 1.8\ \Omega$), which is also the sliding surface of the landslide. Below this depth, we have the presence of a geological formation with high resistivity values which shows the presence of sandstone bedrock (Log $R > 1.8\ \Omega$). The extent of the layers along this profile is parallel to it and in accordance with the slope of topography. The transverse profile T1–T1, is perpendicular to the first one and the three geological layers mentioned above are present, with a dipping contact trend between their interfaces, toward the end of profile.

The sliding block thickness (Log $R > 1.8\ \Omega$) increases from the beginning of the profile 2–3 m, up to 5–6 m at the end of it. Below this depth still is present the geological formation with low resistivity values (log $R < 1.8\ \Omega$) related with water zone and clay and sandy layer content, which is the sliding surface. The bedrock which is sandstone is below the sliding plane and represented by very high resistivity values (Log $R > 1.8\ \Omega$). The ERT techniques used to study this landslide shows us the sliding block and sliding surface in both direction toward the slope of the topography and the same height, giving the dimensions of the sliding layer and the topography of the sliding surface.

Conclusions

In this research an engineering—geological and geophysical investigation of the Birzhita landslide, Tirana area, is presented. The work includes engineering geological investigation and 2D ERT profiles. The results indicated that:

The Birzhita landslide is an old one composed of eluvial materials, which build a heterogeneous body with sandstone boulders of different size, while its sliding surface (zone) develops along the contact plane between the eluvium and sandstone bedrock. ERT profiles indicate that high resistivity values correspond to the sliding block and bedrock, while low resistivity values correspond to the shale layers and water zones. The phenomenon of landsliding is developed and can be developed in all sectors taken for study. Formation of landslides is related to the morphology of the terrain, climatic conditions (rainfall) and human intervention. In this way, from the rainfall water, in central sector of studied area is formed a shallow landslide. It should also be mentioned that in the western part of the studied area, the cliff is in critical condition in relation to the phenomenon of landsliding. The phenomenon of landsliding has the greatest opportunity to be developed in rocks of the western side of the hilly slope, because the layering of geological structures coincides with that of the topographic slope. During rainfall seasons, surface waters will create serious problems

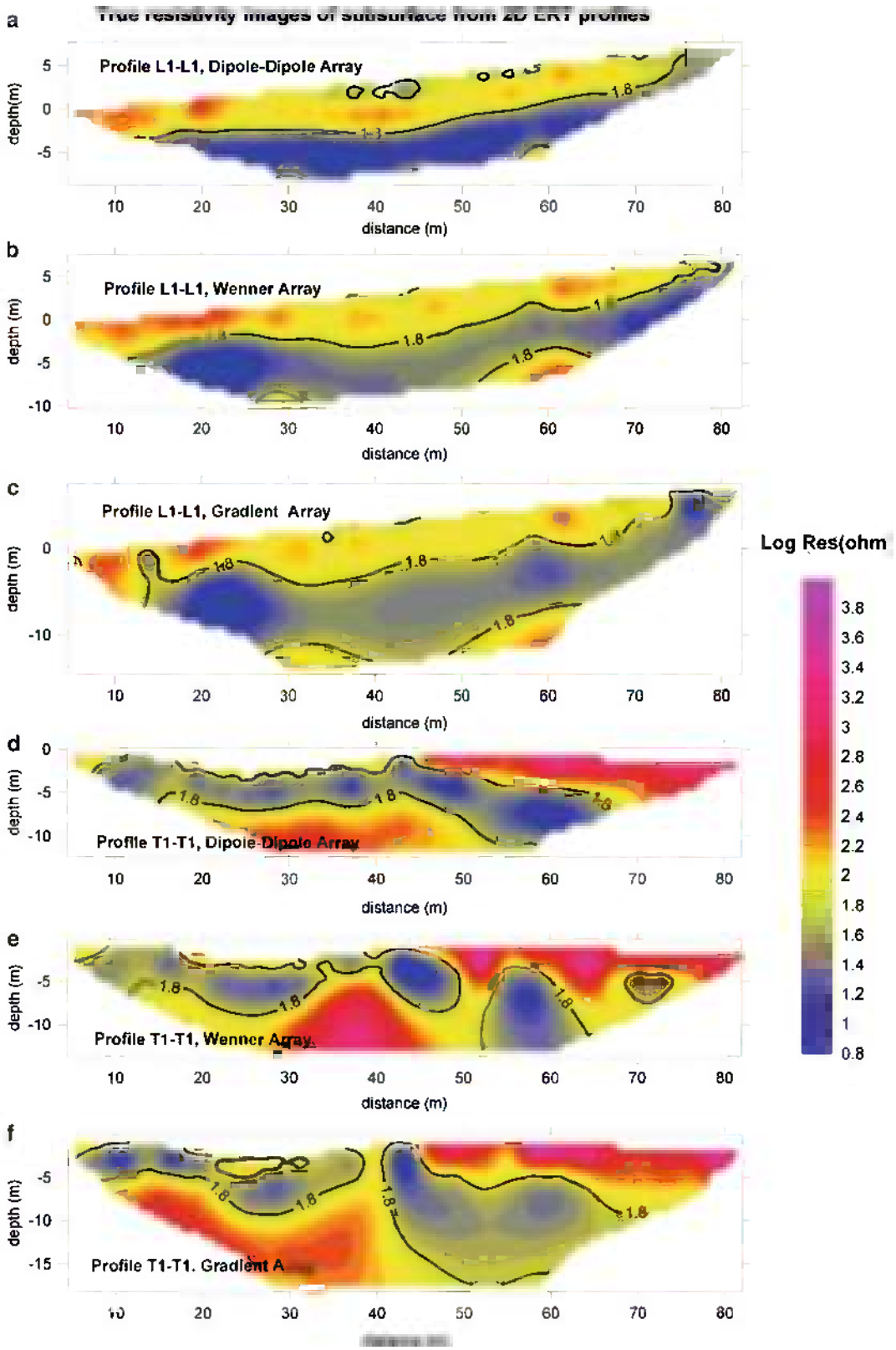


Fig. 5 Resistivity images of the subsurface from the ERT profiles. (L1–L1) Longitudinal ERT profile. (T1–T1) Transverse ERT profile

in the western slope of the hill-area and consequently the development of the landslide. Therefore it is necessary to manage the surface waters throughout a drainage system.

Acknowledgments This work was realized in the frame of a project undertaken from the commune of Birzhita, Tirana, where 35 buildings of 3 stories are planed to be constructed. We are very grateful to the financial support by the company "*LA-OR* shpk (selia rruga Tir-Elb km 14 Berzhite, Tirane-PALMANOVA)", which made possible the fieldwork measurements.

References

Agnesi V, Camarda M, Conoscenti C, Di Maggio C, Diliberto IS, Madonia P, Rotigliano E (2005) A multidisciplinary approach to the evaluation of the mechanism that triggered the Cerda landslide (Sicily, Italy). Geomorphology 65:101–116

Bogoslovsky VA, Ogilvy AA (1977) Geophysical methods for the investigation or landslides. Geophysics 42(3):562–571

Campagnoli I, Santarato G (1995) Monitoring creep movements by seismic refraction. In: 1st meeting, environmental and engineering geophysica, 25–27 Sep, Turin, Italy. Extended Abstracts: pp 6–9

Caputo R, Piscitelli S, Oliveto A, Rizzo E, Lapenna V (2003) High-resolution resistivity tomographies in active tectonic studies: examples from the Tyrnavos Basin, Greece. J Geodyn 36:19–35

Di Maio R, Mauriello P, Patella D, Petrillo Z, Piscitelli S, Siniscalchi A (1998) Electric and electromagnetic outline of the Mount Somma—Vesuvius structural setting. J Volcanol Geotherm Res 82:219–238

Godio A, Strobbia C, De Bacco G (2006) Geophysical characterisation of a rockslide in an alpine region. Eng Geol 83:273–286

Hutchinson JN (1983) Methods of locating slip surfaces in landslides. Bull Assoc Eng Geol 20(3):235–252

Lapenna V, Lorenzo P, Perrone A, Piscitelli S, Sado F, Rizzo E (2003) High resolution geo-electrical tomographies in the study of Giarrossa landslide (Southern Italy). Bull Eng Geol Environ 62:259–268

Lapenna V, Lorenzo P, Perrone A, Piscitelli S, Rizzo E, Sdao F (2005) Case history 2D electrical resistivity imaging of some complex landslides in the Lucanian Apennine chain, southern Italy. Geophysics 70(3):B11–B18

Lebourg T, Binet S, Tric E, Jomard H, El Bedoui S (2005) Geophysical survey to estimate the 3D sliding surface and the 4D evolution of the water pressure on part of a deep seated landslide. Terra Nova 5:399–406

Loke MH (1999) RES2DINV version 3.42. Geoelectrical Imaging 2D & 3D, User Manual, Geometrics, Inc. 2190 Fortune Drive San Jose, CA 95131, USA

Loke MH, Barker RD (1996) Rapid least-squares inversion of apparent resistivity pseudosections by a quasi-Newton method. Geophys Prospect 44:131–152

Mauristsch HT, Seiberl W, Arndt R, Romer A, Schneiderbauer K, Sendlhofer GP (2000) Geophysical investigations of large landslides in the Carnic region of southern Austria. Eng Geol 56:373–388

Meric O, Garambois S, Jongmans D, Wathelet M, Chatelain JL, Vengeon JM (2005) Application of geophysical methods for the investigation of the large gravitational mass movement of Sechilienne. Fr Can Geotech J 42:1105–1115

Muceku Y, Reci H (2008) Integrated geotechnical and geophysical approach to investigate Bovilla landslide at Tirana region, Albania. Albanian J Nat Tech Sci 2008(1):61–71, ISSN 2074-0867

Muceku Y, Reci H (2006) Mass movement and risk assessment in Komani hydropower area, Albania. In: Berga C et al (eds) Dams and reservoirs societies an environment in the 21st century. Taylor & Francis, London, pp 723–729. ISBN 0 415 40 423 1

Muller K (1977) Geophysical methods in investigation of slope failures. Bull Int Assoc Eng Geol 16:227–229

Naudet V, Revil A, Rizzo E, Bottero JY, Bassat P (2004) Groundwater redox conditions and conductivity in a contaminant plume from geoelectrical investigations. Hydrol Earth Syst Sci 8(1):8–22

Nguyen F, Garambois S, Jongmans D, Pirard E, Locke M (2005) Image processing of 2D resistivity data to locate precisely faults. J Appl Geophys 57:260–277

Ogilvy R, Meldrum P, Chambers J (1999) Imaging of industrial waste deposits and buried quarry geometry by 3-D resistivity tomography. Eur J Environ Eng Geophys 3:103–113

Reci H, Bushati S, Tsokas GN, Nenaj S, Kasapi S (2009) Use of 2-D resistivity images in search for buried objects at Rrogozhina Archaeological site (VIAEGNATIA). Albanian J Nat Tech Sci 2009(1):125–140, ISSN 2074-0867

Sass O, Bell R, Glade T (2008) Comparison of GPR, 2D-resistivity and traditional techniques for the subsurface exploration of the Oschingen landslide, Swabian Alb (Germany). Geomorphology 93:89–103

Tsokas GN, Stampolidis A, Mertzanidis I, Tsourlos P, Reci H, Chrisafis C, Ambonis D, Tavlakis I (2007) Geophysical exploration in the Church of Protaton at Karyes of Mount Athos (Holy Mountain) in Northern Greece. Archaeol Prospect 14:75–86



Conventional and Innovative Techniques for the Monitoring of Displacements in Landslide Affected Area

Loredana Antronico, Luigi Borrelli, Dario Peduto, Gianfranco Fornaro, Giovanni Gullà, Luca Paglia, and Giovanni Zeni

Abstract

This work shows a methodological approach for the joint use of geological and geomorphological studies and conventional/innovative monitoring data in densely urbanized areas at landslide risk. The methodology is applied to a test area in the Calabria region (southern Italy) extensively affected by several active landslides involving urban areas. These landslides have been studied and monitored via ground-based techniques for many years. In the study area the comparison and interpretation of DInSAR data with geomorphological studies and inclinometric monitoring has been carried out. The results obtained, thanks to the validation of remote sensed data via ground-truths, provide a further step towards the integrated use of DInSAR data within landslide risk mitigation strategies.

Keywords

Landslides • Multipass DInSAR • Natural hazards • Inclinometer monitoring

Introduction

Landslides are widespread all over the world with increasingly high societal and economic impact. Owing to the high risk for human life and/or structures and infrastructures associated with these phenomena, in the scientific literature several studies address landslide risk mitigation with the help of innovative monitoring systems.

In recent years, the multidisciplinary approach in the study of landslides has directed the scientific community towards the integrated use of conventional techniques and innovative satellite data. Among these, great attention deserves space-borne differential SAR interferometry which, although successfully tested with reference to different natural hazards, still needs detailed studies to fully exploit its applicability to landslide analyses.

In this work a test area representative of the typical geo-environmental contexts of Calabria and extensively affected by several active landslides involving urban areas has been selected. These landslides have been analysed via both geomorphological studies and field surveys and monitored via conventional geotechnical techniques for many years. Images acquired by Envisat satellite in the period from August 2003 to January 2010 have been firstly processed at both low- and full-resolution over the whole area and, then, interpreted on the basis of all the acquired knowledge.

The results obtained contribute to the development of procedures aiming at the detection and definition of kinematic features, which are typical of unstable areas within geologically homogeneous contexts.

L. Antronico (✉) • L. Borrelli • G. Gullà
CNR IRPI, UOS Cosenza, Via Cavour 4/6, Rende, CS 87030, Italy
e-mail: antronico@irpi.cnr.it

D. Peduto
Department of Civil Engineering, University of Salerno, Salerno, Italy

G. Fornaro • L. Paglia • G. Zeni
CNR IREA, Via Diocleziano 328, Naples 80124, Italy

C. Margottini et al. (eds.), *Landslide Science and Practice*, Vol. 2,
DOI 10.1007/978-3-642-31445-2_16, © Springer-Verlag Berlin Heidelberg 2013

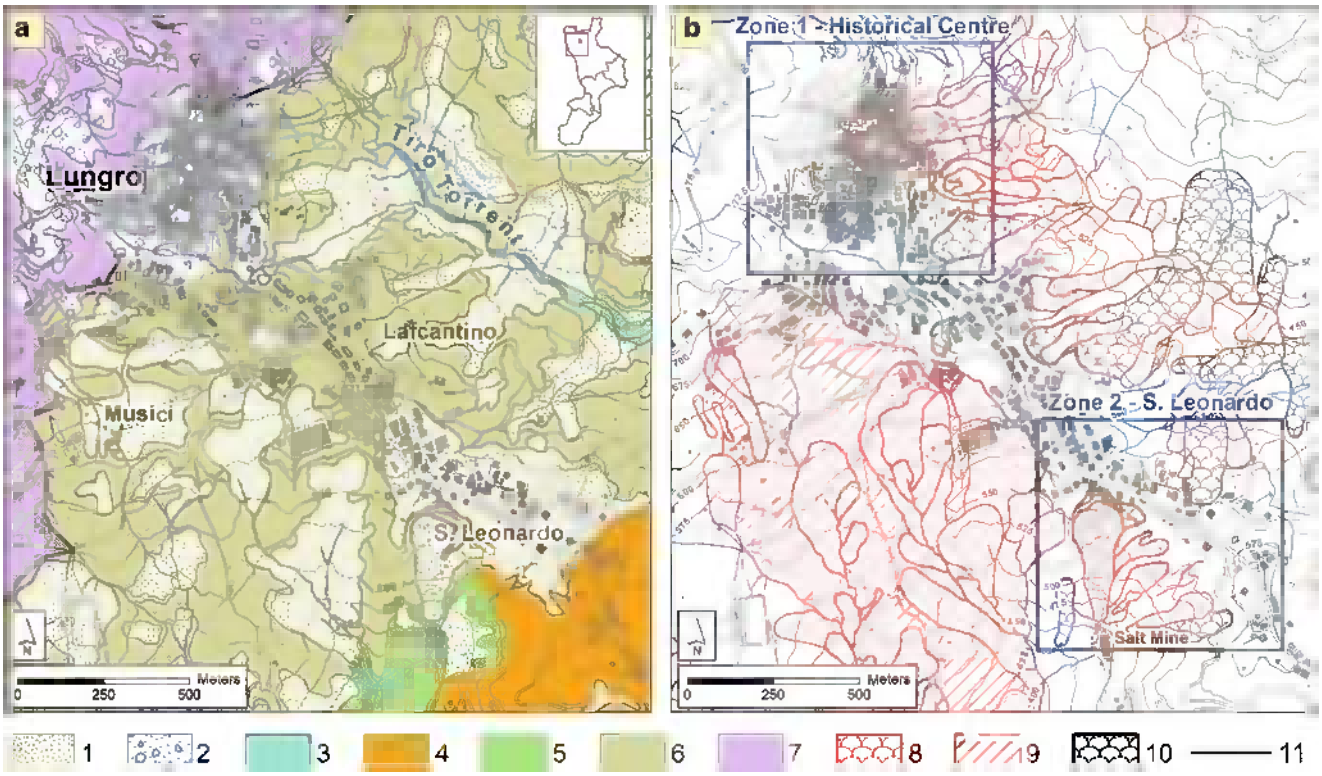


Fig. 1 (**a**) Geological map of the study area: (*1*) detritical-colluvial cover (Holocene); (*2*) detritical carbonate deposits (Holocene); (*3*) alluvial deposits (Holocene); (*4*) middle Pliocene-Pleistocene succession; (*5*) Middle Tortonian-Messinian succession; (*6*) Diamante-Terranova Unit (Lower Jurassic-Cretaceous); (*7*) Lungro-Verbicaro Unit (Anisian-Lower Burdigalian); (**b**) The landslide map of Lungro urban area: (*8*) active slide-flow; (*9*) uncertain boundary of active landslide zone; (*10*) dormant slide-flow; (*11*) tectonic contact

The Test Area

Geological and Geomorphological Sketches

The Lungro municipality (Fig. 1a, b), located in the north-west area of the Calabria region, is characterised by an extreme geological and structural complexity having direct impact on the instability of the town (both the historical centre and a newly developed urban area).

In this area Meso-Cenozoic sedimentary sequences of the Appennine domains are in tectonic contact with the Units of the Calabrian Arc (Amodio-Morelli et al. 1976) (Fig. 1a). In particular, in the north-western portion of the area, the Lungro-Verbicaro unit—whose base is made up of a thick sequence of green phyllites with carbonate intercalations potentially dating back to the medium Trias—crops out (Bousquet 1971; Bousquet et al. 1978; Ietto et al. 1992; Iannace et al. 2005). The basal portion of the sequence, gradually evolves into an interval of layers and banks of meta-limestones (Anisic-Carnic) which in turn evolves into clear dolomite rocks (Carnic). The Anisic-Carnic sequence is followed by an interval of saccharoid dolomite rocks (Norian–Rhaetian) with undistinguished layers, generally of cataclastic origin. Dark-grey and blackish calcareous rocks of Jurassic origin overlap the cataclastic dolostones in angular discordance and they are generally well stratified. The Lungro-Verbicaro Unit, lying next to the dwelled area of Lungro, moves towards the Ophiolitic Unit of Diamante-Terranova (Lower Jurassic-Cretaceous), with clear extensional tectonic contact (Fig. 1a). In particular, the cover of the Diamante-Terranova Unit crops out in the study area. The Diamante-Terranova Unit, being represented by phyllites and slate of prevalently dark grey colour is characterised by a good fissility. The foliation is commonly crinkled or wavy in appearance. Overall these lithotypes form a sort of "melange structure" made up of blocks and fragments of different nature (phyllites, clays and shales, calpionellids limestones and ophiolites) in a prevalently clayey matrix, derived from the degradation and claying of phyllites. An upper Tortonian-Messinian sequence lays, in angular discordance, on the metasediments of the Diamante-Terranova Unit (Di Nocera et al. 1974) and the sequence is made up of small outcrops of brown coarse sandstones, followed by grey-yellowish clays with gipsy sandstones, gypsum and some halite layers intercalations (Fig. 1a).

The early Miocenic succession then ends with sediments dating back to the middle Pliocenic-Pleistocenic period, represented by sandy-conglomeratic successions.

Some detritical deposits formed by stony elements of calcareous and/or dolomite origin dipped in a brown sandy and/or muddy matrix are present on the calcareous-dolomite slopes and at their base. A part of the inhabited area of Lungro, in the south western area of the village, has been built on such deposits. Moreover, some debris-colluvial covers and effective landslide debris, not clearly visible in the outcrops and with maximum thickness of about 10 m, are present prevalently on the phyllite unit of Diamante-Terranova.

The slopes in the area are affected by a large number of mainly active landslides (Fig. 1b) of different typologies, as testified in the scientific literature (Merenda 1990; Guerricchio et al. 1993, 2005; Gullà et al. 2006) and by aerial photo-interpretation carried out in different periods (1954, 1980, 1991, 2001).

The carbonate hillslopes above the historical centre are affected by topples and falls (Varnes 1978) due to many discontinuities and almost sub-vertical walls. In the same area (Fig. 1b), an arched scarp can be easily detected. This could be the outcome of an ancient rock block slide (Varnes 1978) as confirmed by the outcrop of carbonatic blocks (with volumes exceeding m^3 and thickness of over 10 m) within the area where the south-western sector of the historical centre develops.

Finally, the slopes with phyllites outcrops, characterized by a severe decrease of their physical and mechanical properties, are mainly affected by slope movements which can be classified as slides-flows (complex, according to Varnes 1978) and landslide zones. Landslide zone is not a real mass-movement type; it represents area affected by landslide phenomena of which it is impossible to distinguish the different bodies.

Landslides Activity

The instability of the area is well documented since long time (Almagià 1910). The analysis of historical data collected over the study area has highlighted that the historical centre of Lungro and the newly built up areas have been recurrently affected by landslide phenomena, usually slow ones, with a severe impact on both social development and business activities. Moreover, rainfalls seem to be the main cause of such slope instability in the area.

A building damage survey carried out in Lungro has highlighted that a number of the structures and infrastructures of the historical centre (see Zone 1 in Fig. 1b) displays many cracks which can be ascribed to slow ground displacements. In this regard, both geo-morphological analyses and field surveys suggest that the portion of the dwelled area affected by slow-moving phenomena corresponds to that mapped as "uncertain boundary of active landslide zone" in the Zone 1 of Fig. 1b; in this area diffuse and pervasive fractures were recorded to several buildings.

Moreover, as it can be noticed in Fig. 1b another portion of Zone 1 in the historical centre is affected by a slide evolving into flow towards Tiro torrent.

As for the stability of the structures/infrastructures, in the urban area, a key role seems to be played by their location along an extensional contact between tectonic units.

Around the second half of the last century an important urban development (Zone 2—San Leonardo in Fig. 1b) has taken place in the area southwards the historical centre. Despite the awareness of slope instability since past times, several houses, public buildings, facilities (such as council houses, health centres, a football ground, a new section of the graveyard, schools) as well as road network have been built up in the area. Recurring partial remobilisations and, therefore, the landslide activity are witnessed by some severe cracks and deformations in structures and infrastructures located inside the landslide bodies or in the vicinity of the main scarps. In particular, a 10-year observation activity shows that the buildings located in S. Leonardo Zone (two of which have lost their serviceability since 1998) have undergone a significant increase of the damage severity especially during the 2008–2011 period. This is testified by an increase in their tilt angles as well as by new cracks on previously undamaged buildings. Another problem of this area is caused by subsidence phenomena which may occur due to the presence of a salt mine disused since the 1980s and located at the slope foot.

DInSAR Data Analysis for the Test Area

Multipass DInSAR Algorithm and Image Dataset

Multipass DInSAR algorithms are widely used to retrieve information on displacement/velocity of the topographic surface. At present two classes of techniques are available for the analysis of phase signals in interferometric stacks: persistent scatterers interferometry (PSI) (Ferretti et al. 2000, 2001, etc.) and small baseline approaches (Berardino et al. 2002; Fornaro et al. 2009a, etc.). In the first class, the analysis is carried out at full resolution on stable scatterers in order to separate the atmospheric, topographic and deformation components. In the case of small baseline techniques, the scattering is supposed to be distributed within the resolution cell and spatial multilooking is implemented to enhance the phase stability. As a consequence of this operation, the spatial resolution is degraded with respect to the PSI approach. Nevertheless, a product of the small scale

analysis is the estimate of the atmospheric phase delay (APD), which allows the implementation of a subsequent large scale analysis carried out at full-resolution (Fornaro et al. 2009b).

The radar analysis carried out in this work is based on a two-step approach. In particular, the low-resolution analysis (with pixel spacing of almost 80 × 80 m) was performed via the original Small Baseline Subset (SBAS) algorithm (Berardino et al. 2002), then the full resolution analysis (with pixel spacing of 20 × 5 m) was carried out according to the tomographic analysis proposed by Fornaro et al. (2009b). This latter is a super-resolution analysis which was applied here in order to detect the dominant scatterer, as usually done for PSI.

The image dataset consists of a total of 64 ENVISAT images acquired on both ascending (no. 35, track 86 frame 783 from 27th August 2003 to 27th January 2010) and descending (no. 29 track 222 frame 2,817 from 4th May 2003 to 21st February 2010) orbit.

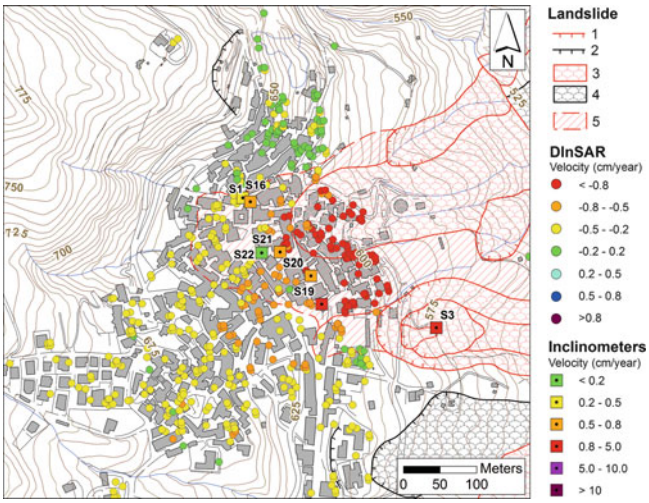


Fig. 2 The historical centre: distribution of full-resolution DInSAR data and benchmarks equipped with inclinometers: (*1*) active main scarp; (*2*) dormant main scarp; (*3*) active slide-flow; (*4*) dormant slide-flow; (*5*) uncertain body of active landslide zone

DInSAR Data Analysis

A preliminary product of DInSAR data processing is the low-resolution coherent pixel map. As described in Cascini et al. (2010) the analysis of low-resolution DInSAR data can be valuably used in analyses over large areas in order to get an overview of the features and kinematics in the area. Since the analysis in this work is carried out at large scale, low-resolution DInSAR data were only used to preliminarily test the remote sensing data coverage within the area of interest and to check evidence of general trends in velocity values as well. Then, the setting of the movement threshold of 0.2 cm/year (Cascini et al. 2009) allowed to preliminary highlight that all the covered landslides, independently from the state of activity reported on the landslide inventory map, contain at least one moving low-resolution DInSAR coherent pixel.

In order to further investigate this point the post-processed full-resolution (Fornaro et al. 2009b) DInSAR data were used (Figs. 2 and 3) over Zone 1 and Zone 2 of Lungro urban area as indicated in Fig. 1b. These data, indeed, can better suit analyses at large/detailed scale (i.e. 1:5,000; 1:2,000) aiming at the proper definition of both the boundaries and the state of activity of already mapped phenomena (Cascini et al. 2010). Moreover, DInSAR data can also be helpful in the detection of unmapped phenomena when geological/geomorphological information are available (Cascini et al. 2009).

Referring to the whole study area, DInSAR data highlight evidence of movements in different zones of Lungro town.

As for the historical centre (Fig. 2), full-resolution DInSAR data exhibit a good coverage also highlighting that different zones with varying ranges of DInSAR derived

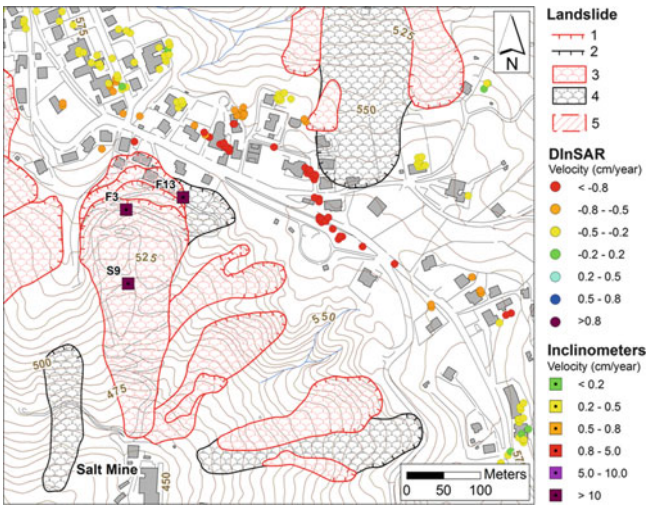


Fig. 3 The S. Leonardo area: distribution of full-resolution DInSAR data and benchmarks equipped with inclinometers: (*1*) active main scarp; (*2*) dormant main scarp; (*3*) active slide-flow; (*4*) dormant slide-flow; (*5*) uncertain body of active landslide zone

velocities (from 0 down to −1.33 mm/year) can be distinguished. Moreover, the map shows (Fig. 2) that the DInSAR coherent pixels with velocity values exceeding −0.8 cm/year (red dots) exhibit a spatial distribution which seems in agreement with the landslide inventory map. These data, indeed, overlay an active complex landslide involving Lungro old centre also involving portions of two other active complex landslides whose borders are not well defined on the basis of conventional methodologies. On the other hand, the DInSAR derived velocity values seem to decrease moving towards north and south-southwest directions.

With reference to S. Leonardo area (Fig. 3), the road heading to the centre stretches along the crest of the slope on whose right/left flanks groups of active/dormant complex phenomena are mapped. The analysis of DInSAR data reveals the presence of coherent pixels exhibiting velocity rates as high as 0.8 cm/year in proximity of both a group of complex landslides (whose widest portion is reported as dormant), on the north flank of the slope, and the head of an active complex phenomenon (on the south flank of the slope).

These data could be interpreted as due to a retrograding mechanism of the mapped landslides up to the road.

On the south-easternmost corner of Fig. 3—on the right side of the road—a group of moving full-resolution DInSAR coherent pixels, attaining velocity values as high as 1 cm/year, is located over a group of buildings. This area corresponds to that described in the previous section as located in proximity of the abandoned salt mine which could trigger subsidence-like displacements.

Validation and Integration of Kinematic Features

The study area has been analysed for long time via field surveys and geological/geomorphological studies in order to derive the geotechnical model of the most significant and representative landslide phenomena (Gullà et al. 2006). During the geotechnical investigations vertical inclinometers have been installed and measured; these data complemented other vertical lines derived from previous surveys started since 2006.

Monitoring results, which have provided useful indications on the kinematic features of the landslides affecting Lungro urban area, were then used for a preliminary validation and integration of DInSAR measurements.

To this end, first of all the displacement velocities derived from the vertical inclinometers located within the sectors under investigation have been computed referring to measures acquired at a depth of 1 m from ground level and across the whole reference period (February 2006 to May 2011).

The obtained velocity values range from 0.18 cm/year up to more than 50 cm/year. In Figs. 2 and 3 the selected vertical inclinometers have been labelled according to the DInSAR velocity classes in order to carry out a comparison with satellite data.

With reference to Fig. 2 inclinometric data seem to match the outcomes of geological and geomorphological analyses which outlined with difficulty the active state of the mass movements detected in the historical centre of Lungro. In particular, these phenomena are generally very slow according to Cruden and Varnes' (1996) classification since they exhibit velocity values not exceeding 5 cm/year. Moreover, Fig. 2 shows that the monitoring of deep seated

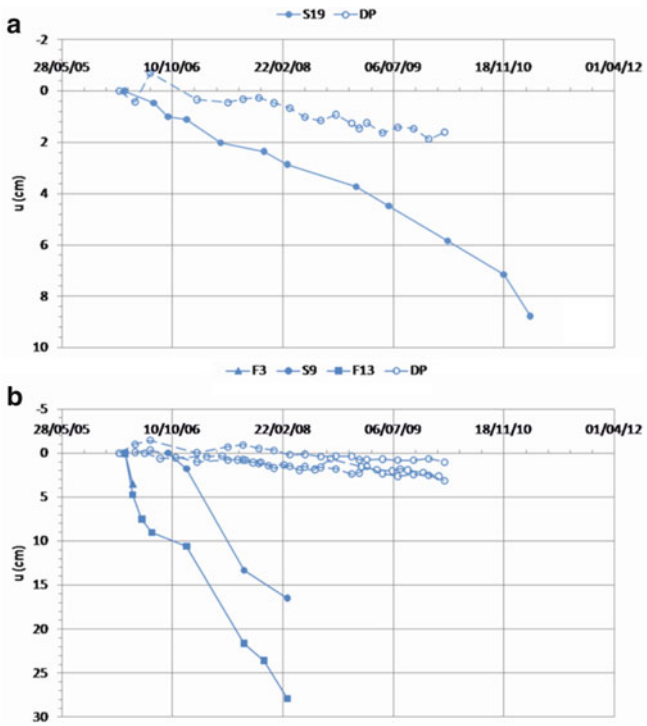


Fig. 4 Trend of displacements measured from inclinometer (S19, F3, S9, F13) and DP (full-resolution DInSAR coherent pixel) along the satellite Line Of Sight (L.O.S.): (**a**) historical centre, (**b**) S. Leonardo

displacement for the historical centre are consistent with the DInSAR—derived measurements.

As for the area of San Leonardo (Fig. 3), it can be noted that full-resolution DInSAR coherent pixel are scarcely present and the remote sensed velocity values do not match ground-based information. In this regard, it is worth stressing that velocity values relative to inclinometers on the southern slope of the ridge are always greater than 10 cm/year (with maximum values of over 50 cm/year), thus related to displacements too high to be detected via DInSAR data.

A preliminary quantitative comparison between the displacements measured by both each inclinometer and the nearest DInSAR coherent pixel is shown in Fig. 4a, b with reference to, respectively, the old town centre and S. Leonardo area. The discrepancy exhibited in the trends calls for further investigations concerning both considerations on the satellite acquisition geometry and the moving direction detected by each inclinometer.

Discussion

Geological and geomorphological studies carried out in the area under investigation provide a substantial reference framework of the complex condition of the instability affecting the structures and infrastructures of the urban area of Lungro.

In particular, such studies have outlined the most critical zones of the area: the historical centre and the newly developed urban area. In the first zone, the severe structural damages suffered from most of the buildings can be related to slow landslide phenomena that cannot be properly mapped from a geomorphological point of view; in the second zone, the deep cracks and deformations recorded to structures and infrastructures are the result of the several remobilizations of the landslides with a retrogressive evolution.

The analysis of full-resolution DInSAR data proved to be able to detect portions of the historical centre exhibiting different velocity values, thus helping in the definition of the state of activity of the related landslide phenomena. This could turn out to be extremely useful in further analyses aimed at forecasting related effects on the involved buildings.

With reference to S. Leonardo area, remote sensing data have provided information on the current boundary and kinematics of the covered phenomena also suggesting their likely evolution mechanisms (i.e. retrogression).

The outcomes of the displacement monitoring, carried out for a significant period of time, seem to confirm the kinematic characteristics of the sectors where velocities values fall within the intervals suitable for satellite analysis and—at the same time—they supplement such results in the sectors where velocities are faster.

Concluding Remarks

In the present work the potential of DInSAR data analyses carried out at both low- and full- resolution is highlighted with reference to the instability phenomena affecting the urban area of Lungro where previous detailed geological and geomorphological studies are available. In the area accurate displacement data obtained via inclinometer monitoring have also allowed the investigation of the kinematic features of the mapped very slow landslide phenomena.

The results obtained by means of this integrated approach show the great potential and complementarity of conventional and innovative techniques in analyses carried out at large scale and with reference to single phenomena occurring in complex geo-environmental contexts.

The comparison of the preliminary results obtained will be used for addressing further investigations in order to achieve an as much comprehensive view as possible of the kinematical features of the phenomena affecting the urban area of Lungro.

Acknowledgments Authors thank Luigi Aceto for his collaboration in the processing and interpretation of inclinometric data and Duilio D'Onofrio, Enzo Valente, Salvatore Guardia and Claudio Reali for their measurement of vertical inclinometers. Facilities have been implemented within the framework of the activities of the Civil Protection System of the Regione Calabria.

References

Almagià R (1910) Studi geografici sulle frane in Italia, vol 2, Memorie della Societa' Geografica Italiana. società geografica italiana, Roma, p 431

Amodio-Morelli L, Bonardi G, Colonna V, Dietrich D, Giunta G, Ippolito F, Liguori V, Lorenzoni S, Paglionico A, Perrone V, Piccarreta G, Russo M, Scandone P, Zanettin-Lorenzoni E, Zuppetta A (1976) L'arco Calabro-Peloritano nell'orogene appenninico-maghrebide. Mem Soc Geol It 17:1–60

Berardino P, Fornaro G, Lanari R, Sansosti E (2002) A new algorithm for surface deformation monitoring based on small baseline differential SAR interferograms. IEEE Trans Geosci Remote Sens 40(11):2375–2383

Bousquet JC (1971) La tectonique tangentielle des series calcareo-dolomitiques du Nord Est de l' Apennin calabro-lucanien (Italie meridionale). Geolog Romana 10:23–52

Bousquet JC, Megard-Galli J, Zoru H (1978) Quelques elements de datation du Trias Moyen et Superieur de l'Appennin calabro-lucanien (Italie Meridionale). Geolog Romana 17:41–103

Cascini L, Fornaro G, Peduto D (2009) Analysis at medium scale of low-resolution DInSAR data in slow-moving landslide-affected areas. ISPRS J Photogramm Remote Sens 64(6):598–611. doi:10.1016/j.isprsjprs.2009.05.003

Cascini L, Fornaro G, Peduto D (2010) Advanced low- and full-resolution DInSAR map generation for slow-moving landslide analysis at different scales. Eng Geol 112(1–4):29–42. doi:10.1016/j.enggeo.2010.01.003

Cruden DM, Varnes DJ (1996) Landslide type and processes. In: Turner AK, Schuster RL (eds) Landslides investigation and mitigation. Transportation Research Board Special Report no. 247, Washington DC, National Academy Press, pp 36–75

Di Nocera S, Ortolani F, Russo M, Torre M (1974) Successioni sedimentarie e limite Miocene-Pliocnella Calabria settentr. Boll Soc Geol It 98:559–587

Ferretti A, Prati C, Rocca F (2000) Nonlinear subsidence rate estimation using permanent scatterers in differential SAR interferometry. IEEE Trans Geosci Remote Sens 38(5):2202–2212

Ferretti A, Prati C, Rocca F (2001) Permanent scatterers in SAR interferometry. IEEE Trans Geosci Remote Sens 39(1):8–20

Fornaro G, Pauciullo A, Serafino F (2009a) Deformation monitoring over large areas with multipass differential SAR interferometry: a new approach based on the use of spatial differences. Int J Remote Sens 30(6):1455–1478

Fornaro G, Reale D, Serafino F (2009b) Four-dimensional SAR imaging for height estimation and monitoring of single and double scatterers. IEEE Trans Geosci Remote Sens 47(1):224–237

Guerricchio A, Bruno F, Mastromattei R (1993) Centri abitati instabili in Calabria: deformazioni gravitative profonde di versante e grandi frane nel territorio comunale di Lungro (Calabria settentrionale). Geolog Appl Idrogeolog 28:479–488

Guerricchio A, Biamonte V, Mastromattei R, Ponte M (2005) Land subsidence induced by slow gravitational deformations and by digging of rock-salt. In: Leonardo S (ed) (Lungro town, Calabria region, Southern Italy) Proceedings of the 7th symposium on land subsidence, Shanghai, China, 23–28 Oct 2005, pp 207–217

Gullà G, Antronico L, Borrelli L, Cilento M, Aceto L, Scionti V (2006) Esecuzione di un programma di studi ed indagini finalizzato all'individuazione delle cause che hanno determinato la gravissima condizione di dissesto idrogeologico nel territorio del Comune di Lungo della provincia di Cosenza. Ordinanza di prevenzione del Presidente del Consiglio dei Ministri (no. 3640 del 16 agosto 2005) Relazione Finale. Convenzione tra la Regione Calabria, Assessorato alla Protezione Civile e il Cnr-Irpi, UOS di Cosenza

Iannace A, Bonari G, D'Errico M, Mazzoli S, Perrone V, Vitale S (2005) Structural and tectonic evolution of the Apennine Units of northern Calabria. Tectonics. CR Geosci 337:1541–1550

Ietto A, Barilaro A, Calligaro G, Mancuso C (1992) Elementi per una revisione dei rapporti Appennino-Arco Calabro. Boll Soc Geol It 111:193–215

Merenda L (1990) Dati descrittivi della geologia, geomorfologia ed instabilità dei centri abitati, Lungro. In: il Dissesto Idrogeologico in Calabria, CNR-IRPI e Regione Calabria

Varnes DJ (1978) Slope movements: type and processes. In: Eckel EB (ed) Landslides analysis and control. Transportation Research Board Special Report no. 176, pp 11–33



Spatio-Temporal Evolution of Ground Displacement of the Tena Landslide (Spain)

Nguyen Anh Tuan, Saillard Marianne, Darrozes José, Oliver Marc, Herrera Garcia Gerardo, Garcia Lopez-Davalillo Joan Carlos, Gonzalez Nicieza Celestino, Álvarez Fernández Inmaculada, Monod Bernard, Mulas De Peña Joaquim, Soula Jean-Claude, Guerrero Nicole, and Courjaul-Radé Pierre

Abstract

The scope of the DO-SMS program is dedicated to the ground displacement observation. We present here our results for the Tena landslide (Spain). By combining geotechnical and remote sensing tools precise ground displacement maps were established. Using the multi-temporal photographs optical correlation was performed. Correlation is used for quantifying the north/east components of ground displacement of the area and the last component was calculated by using Permanent Scatterers. These results point out a new landslide history. An initial period (1994–2003) in which the upper part of the debris avalanches flowed westward. The second period commenced with the construction in 2004 of a car park and is marked by the deviation of the landslide downward to this car park. Geotechnical/geophysical data enable us to identify the principal rupture plane at ~40 m of depth. The analysis of the temporal series indicates non-linear displacement rates generally correlated with rainfall events and/or seasonal variations.

Keywords

Optical correlation • DinSAR • Landslide • TerraSAR-X • PS

Introduction

Landslide surveying is an important scientific deal in order to track the movement patterns of the landslide for mitigation purposes, and provide a warning system.

A wide variety of techniques and methodologies are used to investigate landslide displacement such as interferometry analysis using RADAR images (Luzi et al. 2004; Colesanti and Wasowski 2006; Herrera et al. 2010, among others), extensometers, inclinometers (Dunnicliff 1988; Dunnicliff and Green 1994; Aulakh et al. 2004; Keefer and Larsen 2007). Remote sensing is one of the most convenient tools for characterizing a landslide.

The scope of the European program DO-SMS (INTEREG IVB) is dedicated to the observation of the spatio-temporal evolution of ground displacement. Our study try to point out the efficiency of optical correlation in the survey and the prevention of landslide activity using the example of the Tena landslide (upper Tena valley, Spanish Pyrenees, Fig. 1). And we present a low cost methodology allowing identification of the oldest displacements and landslide evolution during the past 15 years. For this purpose, we used the optical correlation methodology as defined by Casson et al. (2003). The resulting 2D (X, Y) vector field of displacements point out to a new landslide history. Combining this analysis

N.A. Tuan (✉) • S. Marianne • D. José • S. Jean-Claude • G. Nicole • C.-R. Pierre
University Paul Sabatier (OMP, CNRS, IRD); GET, 14 av. E. Belin, Toulouse 31400, France
e-mail: natuanmdc@gmail.com

O. Marc • M. Bernard
Bureau de Recherches Géologiques et Minières, Ramonville Saint-Agne, France

H.G. Gerardo • G.L.-D.J. Carlos • M.D.P. Joaquim
Dirección de Recursos Minerales Y Geoambiente, Instituto Geológico y Minero de España; Unidad De Riesgos Geológicos, Madrid, Spain

G.N. Celestino • Á.F. Inmaculada
Universidad De Oviedo, Plaza De Riego, Oviedo, Spain

C. Margottini et al. (eds.), *Landslide Science and Practice*, Vol. 2,
DOI 10.1007/978-3-642-31445-2_17, © Springer-Verlag Berlin Heidelberg 2013

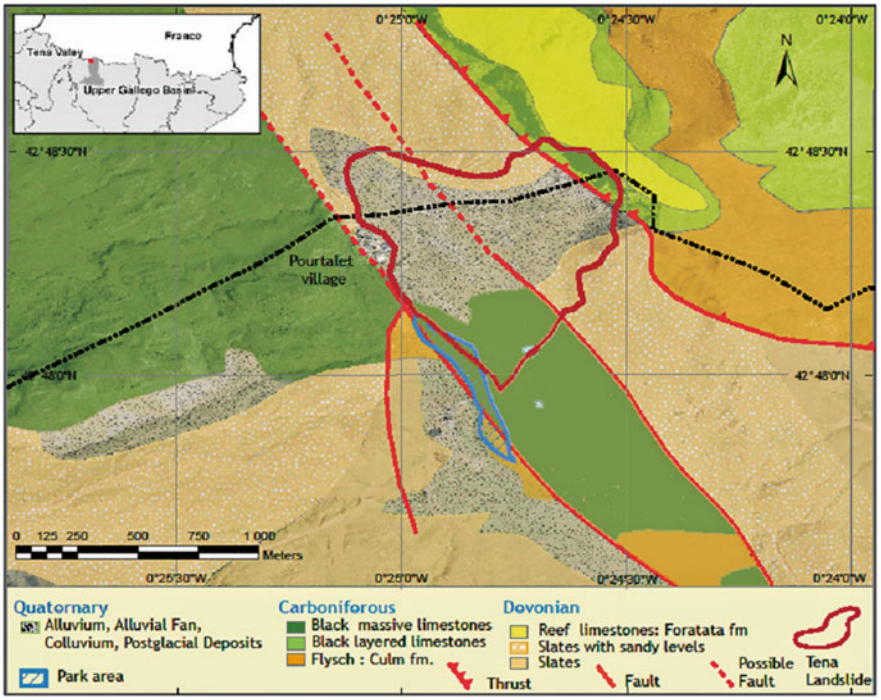


Fig. 1 Geological map of the valley of the Tena valley; the landslide is mainly located in schists and limestones. The north–western is covered with quaternary moraine. (Modified from BRGM@ geological map, scale: 1/50000)

with recent extensometer and DGPS data we show that the morphology of the landslide is more complex associating small superficial imbricate landslide and soil creeping.

Geological Setting: Experimental Site of Tena landslide

The Tena landslide is located in the upper watershed of the river Gállego in the upper Tena Valley (Central Pyrenees, Spain). It affects highly fractured Palaeozoic rocks (Fig. 1) of the Axial Zone of Pyrenees. The high relief of the Axial Zone is related to a large-scale antiformal stack structure (Muñoz 1992; Capote et al. 2002). The landslide area is located in gently-dipping (~15°) shales weathered in their upper part and affected by soil creeping. The morphology of the landslides of this area have been studied by Mulas and Fresno (1995). At the toe of the scarps are observed the accumulation of rock debris related to rock falls and/or rock avalanches (Notti et al. 2010). The landslide head is located on a thrust which transported Carboniferous schists and limestones over Devonian pelites. The main landslide scarp formed in the steep-dipping forelimb of the fault-related anticline (Fig. 1). This landslide appears to be due to the reactivation of an older landslide showing relatively deep rupture plane (≥40 m) and steep slope (25–35°). The reactivation has been ascribed to the constant erosive action of the river Gállego (Herrera et al. 2009). It exists several others active landslides in the Portalet area but with weaker displacements and a less economic interest.

The landslide (Lat: 42°48′00″N, long: 0°23′52″W, Z: 1802 m a.s.l.) is located on a southwest-facing hillside of Petrasis peak. The landslide area is characterized by a main scarp 500 m long and 700 m wide and an area of 0.35 km. The triggering factors capable of enhancing slipping include: (1) Mediterranean mountain climate influenced by Atlantic and continental currents (Creus and Gil 2001) inducing a strong seasonal variation; (2) moderate seismic activity of the Pyrenees (Mulas et al. 2010); (3) anthropic factors such as the car park of the ski station; (4) mica-rich composition of the rocks, dip of bedding/schistosity in the same direction as the topographic slope, and superficial weathering.

This landslide (Fig. 1) presents a strong risk for the local economy as it may at any time cut the unique road of the valley, thus interrupting the activity of the ski station, and cause huge damages to the car park.

Methodology of Remote Sensing Displacement Measurement

In addition to the classical methods of displacement measurements carried out by in situ analysis (DGPS, inclinometer, extensometer) which provide specific information on punctual displacements we used two methods of remote sensing measurements to spatialize the information. SPN method was used for the RADAR images and the optical correlation method was used for the aerial photographs.

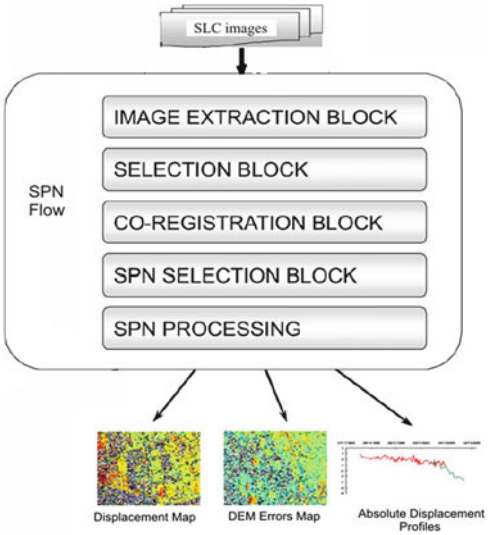


Fig. 2 SPN processing chain (Modified from Herrera 2010)

Stable Point Network (SPN)

SAR interferometry is well-suited for large-coverage surface displacement monitoring. This method was enhanced by the apparition of DinSAR technique (Gabriel et al. 1989; Arnaud 2003) but some limitations appeared with regards to temporal and geometric decorrelation. To overcome these limitations, the Persistent Scatterers method was developed by Ferretti and Rocca (2001), Arnaud et al. (2003), Crosetto et al. (2008) among others.

The SPN technique presented herein is the result of researches within the DInSAR data analysis field for the CNES (French Space Agency), ESA and Altamira Information SL. The chain developed by Altarima Information SL is presented in Fig. 2 and was the first "automatic" process able to use new ASAR data with classical ERS (1/2) data (Arnaud 2003).

It is a technique for the separation of the different components of the interferometric phase ϕ_{Interf}. These component are: the topography, ϕ_{Topo}, the movement, ϕ_{Mov}, the atmospheric contribution, ϕ_{APS} and the noise, ϕ_{Noise}. And PSN flow (Fig. 2) gives three results: a map of displacement rate, a map of DEM errors and a table of displacement time series which can lead to multi-temporal displacement profiles.

$$\phi_{interf} = \phi_{Topo} + \phi_{Mov} + \phi_{APS} + \phi_{Noise} \quad (1)$$

The measurement quality permits to obtain errors of 1 mm/y for the displacement rate and 2 m for height in the DEM error map (Herrera et al. 2010).

Optical Correlation

Optical correlation method. We used the optical correlation method as defined by Casson et al. (2003) upgraded by Ayoub et al. (2009) to obtain precise measurements of the displacements of the Tena landslide on the past 10–20 years.

Correlation information is used for quantifying ground displacement for each point of the image in the studied area. The correlation principle consists in recognizing identical intensity distribution patterns on a reference image and a second image after an event (here: landslide reactivation). The problem is solved in the frequency domain (Hild et al. 1999) by using Fast Fourier transform (FFT) and the Fourier shift theorem (2). We used the optical correlation method as defined by Casson et al. (2003) to measure, precisely, the displacements of the Tena landslide on the 10–20 last years. This methodology was upgraded by Ayoub et al. (2009) and it was performed in our data set.

Correlation information's is used for quantifying ground displacement for each point of the image in the studied area. The correlation principle is to recognize identical intensity distribution patterns on a reference image and a second image after an event in our case the landslide reactivation. The problem is solved in the frequency domain (Hild et al. 1999) by using Fast Fourier transform (FFT) and the Fourier shift theorem (2).

$$\begin{aligned} i_2(x,y) &= i_1(x-\Delta_x, y-\Delta_y) \quad \text{real space} \\ i_2(u,v) &= i_1(u,v)e^{-j\cdot(u\cdot\Delta_x+v\cdot\Delta_y)} \quad \text{frequency space} \end{aligned} \quad (2)$$

where i_2 *is* the post-event image and it has an EW offset Δ_x and a NS offset Δ_y; the representation of these offsets versus the reference image i_1 is given by (1) in the real (x,y) and the frequency (u,v) space.

The Cross-Correlation function (3) of a reference image and other post-displacement images is defined as:

$$CC_{(i,i_2)}(u,v) = \frac{I_1(u,v)\cdot I_2(u,v)}{|I_1(u,v)\cdot I_2(u,v)|} = e^{j\cdot(u\Delta x+v\Delta y)} \quad (3)$$

Where $I_1(u,v)$ is the reference image, $I_2(u,v)$ is one of the post event images and $CC(i_1i_2)(u,v)$ correspond to the cross correlation function, if it is close to 1, there is a relationship between the matching images and the Euclidean distance between the point coordinates of the reference image and the post-event image characterizes the relative displacement (4) in the horizontal plane (X,Y) of the image.

$$\phi(\Delta_x,\Delta_y) = \sum_{u=-x}^{x} W(u,v)\cdot\left|CC_{(i,i_2)}(u,v) - e^{j\cdot(u\Delta x+v\Delta y)}\right|^2 \quad (4)$$

where W is the weighting matrix and (Δ_x, Δ_y) is such that ϕ is minimum. By changing the position of the correlation filter we can quantify displacements for all pixels of the image. We also used a vector average calculation at different scales for identifying the global trend of landslide displacement (large scale) and the local displacement (small scale) due, for example to secondary displacement like soil creeping.

To quantify these displacements we used COSI-CORR (Leprince et al. 2007) add-on of the ENVI software which enabled us to obtain a good wedging of image from the selection of a large number of equivalent points. Figure 3 describes the complete work-flow.

With these images, it will be possible to monitor many periods in the landslide deformation. By means of the Fourier transform we fetch to find and refine the movement defined in the first phase by increasing the size of the research window for obtaining a ground displacement with a sub-pixel resolution of around 30 % of the pixel size. Leprince et al. (2006) indicate that the best results are obtained in theory for a correlation window size twice superior to the ground displacement. In practice, it is recommended to further enlarge the research windows. The displacement (Fig. 3) are decomposed in two components: the horizontal displacement along the East/West and North/South axes of the image. A third image is given which represents the normalized Signal Noise Ratio (SNR). This normalized value of SNR of a pixel represents the measure quality: the more this value tends towards 1, the more precise and reliable the measurement will be.

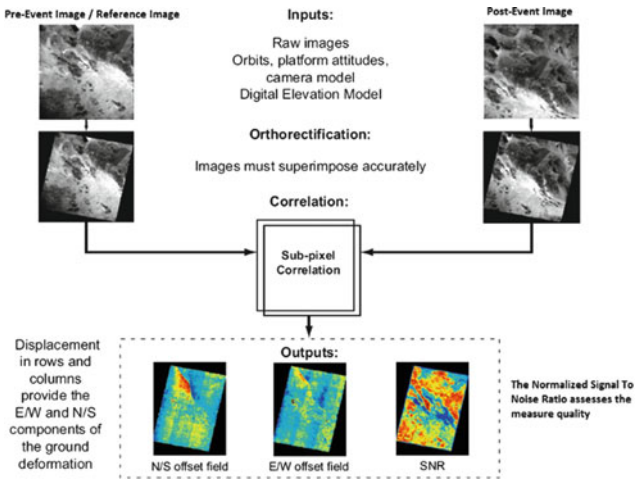


Fig. 3 Schematic flow of optical correlation for measuring horizontal ground displacement (Modified from Leprince 2008)

Database

DGPS Data

In order to monitor the Tena landslides, the Instituto Geologico y Minero de Espana (IGME) has performed Differential GPS (DGPS) investigations. The reference base for DGPS measurement is located in the opposite versant of the landslide and its coordinates are N 42° 47′ 53.12174″ of latitude, W 0° 25′ 5.93432″ of longitude and 1,872.84 m in height. This base was used to quantify the 3D distance between our base and 46 points in the active area of the landslide. The receivers used in the 2010 campaigns are two ZXTREM bi-frequency receivers with geodetic IV antenna. We measure displacements of ground and blocks between June and October 2010.

The DGPS methodology gives accurate measurements if the baseline (distance base/rover) is less than 40 km and in these cases one can expect errors ranging from 2 mm to 4 cm depending on the baseline distance and the satellite geometry (Bock and Doerflinger 2001; Doerflinger 1997). The difference measured in the coordinates of the 46 points obtained during the different campaigns gives the apparent 3D vector displacement of each point. This campaign gives a mean displacement of ~30 cm for a velocity of 90 cm/year. This velocity varies from 10 cm/year in areas of weak displacement (blocks move in the same way as the ground for 71.4 %) to more than 9 m/year for an isolated block.

Inclinometers and Extensometers Monitoring

Inclinometers are useful for detecting the onset of movement. They also reveal the precise depth of the slip plane and whether multiple slip planes are present. Between July and November 2010, inclinometer readings were performed and indicated that the first main slip surface was situated between 5 and 12 m in depth. It was found that the landslide cumulative displacements ranged from 19 to 215 mm in about 3 months. A deeper rupture plane is also identified at ~40 m, which corresponds to the main rupture plane.

A continuous monitoring of landslide displacements by extensometers is often required to better understand the complex relationship between the triggering factors and the displacement dynamics. In our case, these help to understand displacement obtain by means of optic correlation. Between July 2010 and February 2011, two extensometers located in the landslide foot have acquired displacement with a sampling frequency of 2 h, the extensometer lengths being close to 70 m. The displacement velocity measured ranged from 3.36 to 23 mm year^{-1} perpendicularly to the sliding direction (Ext 1, Fig. 4) and from 3.62 to 90 mm year^{-1} along the sliding direction.

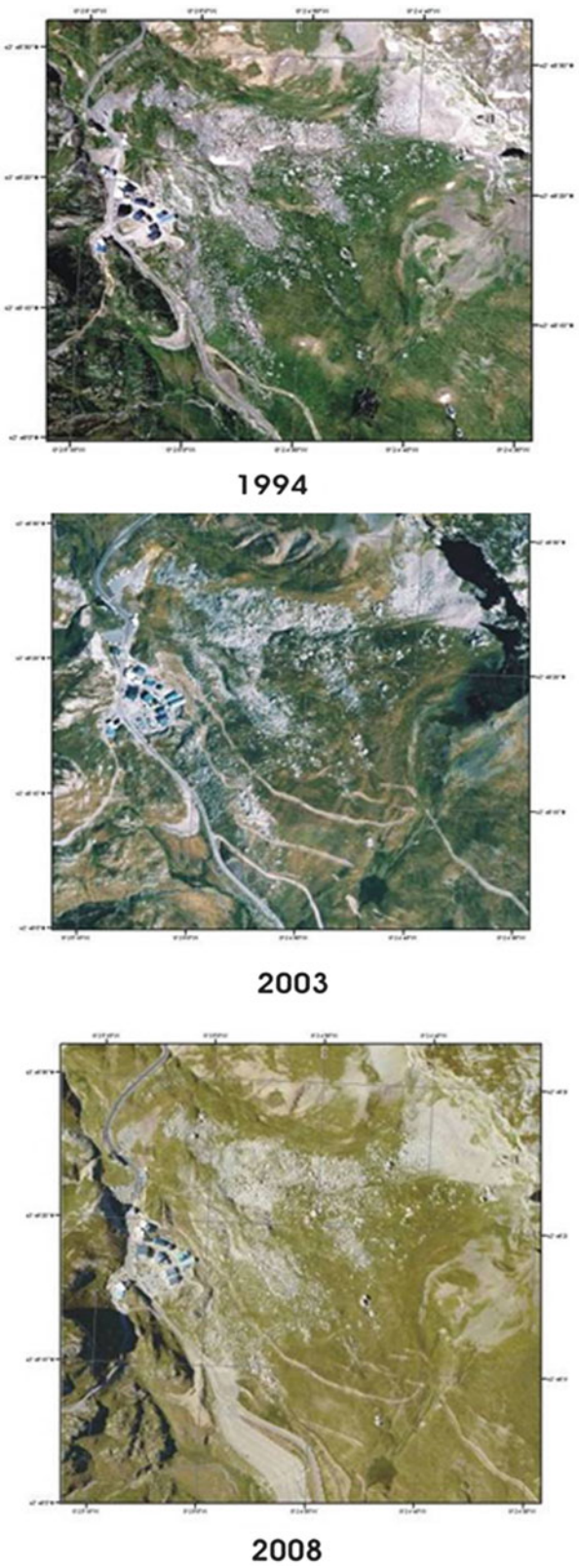


Fig. 4 Aerial photographs of the Tena Landslide. The 2008 image show the car park constructed in 2004

Radar Images

We used two sets of images. The temporal series used for surveying the Tena landslide ranged from May to October 2008. A set of 14 descending images was acquired from the TerraSAR-X satellite. This satellite presents the particularity of having a small revisiting time of few days which permits a good coherence between multi-date images. In our case time intervals between two subsequent images are 11 or 22 days. The temporal resolution obtained was impossible to achieve with other satellite (L or C band) due to a greater (>1 month) time intervals. The pixel length is close to 1 m which gives an excellent spatial accuracy to the TerraSAR-X images.

Aerial Photographs

The car park of our study area was built in 2004 at the foot of the landslide. In order to analyze the effects of its construction, we used the photographs taken in 1994 and 2003 before its construction and a photograph taken in 2008 after its construction.

The 1994 photography was acquired by Camera ZS 142830 at a height of 6219 m a.s.l. and camera focal of 153 mm with a pixel size of 0.8 m. The orthorectification was performed using 15 GCP and a high resolution DEM of the area with a pixel of ~1 m with a Mean Quadratic Errors (MQE) of 1 m in location and of ~2 m in elevation. The 2003 photography was acquired by Camera 25R, with a scale of about 1:68,000 at a height of 6,418 m a.s.l. with a pixel size of 0.5 m. The image orthorectification was performed by French National Geographic Institute (IGN) using GCP and a high resolution DEM with a pixel size of 5 m and a Mean Quadratic Errors (MQE) of ~1 m in location and of ~2 m in elevation. The 2008 orthorectified image was used as reference/master image.

Image Processing and Results

Radar Images

For the TerraSAR-X dataset (14 images) we used the orbit 4,967 as the master image, and 55 interferograms were calculated using a DEM (15 m of resolution) to remove the ϕ_{Topo} contribution. Due to the very narrow interferometric tube, the perpendicular baselines do not exceed 400 m in any of the interferometric combinations (Herrera et al. 2010). It is an important condition in SPN interferometry to avoid spatial and/or geometrical decorrelation (Gatelli et al. 1994). PS are selected taking into account the high interferometric coherence with a robust stability along time. 4,048 natural

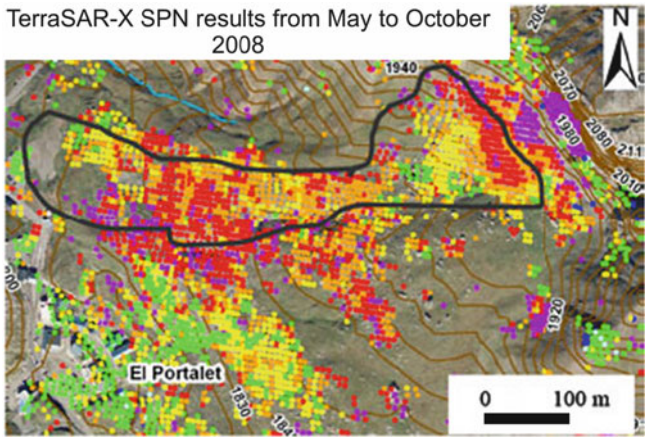


Fig. 5 Zoom of Tena SP map; the SP are mainly located on the EW oriented debris flow part of the landslide: *green dots* are displacements ranging from −3 to 3 mm/year and it represent the in stable areas, *yellow dot*: subsidence ranging from −3 to −5, *orange* from −5 to −7, *red*: from −7 to −10 and *purple upper* than −10 mm/year (Modified from Herrera et al. 2009)

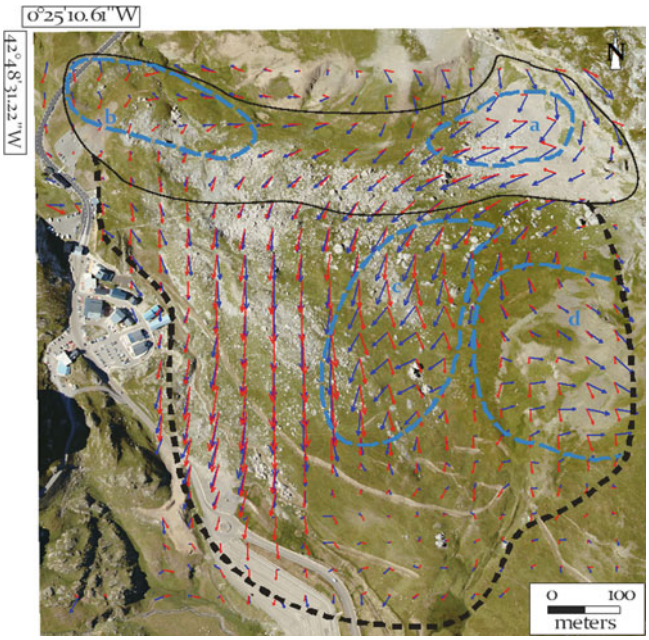


Fig. 6 Displacements map of the period 1994–2003 (*red*) and 1994–2008 (*blue*). Main landslide contoured by interupted thick line. Debris flow in the N-W contoured by thin line. Areas where appear marked changes in displacement direction contoured in blue

PS were selected, representing a high density of 8,261 PS/km^2. This high density of PS may be explained by (1) the very good spatial resolution of the calculated interferograms (~12 m), (2) the frequency sampling of 11–22 days which gives an excellent phase and a good coherence, and (3) the existence of numerous rock blocks (centimetric to metric) which constitute numerous candidates for natural PS. On the resulting map (Fig. 5) we can observe that the PS are located on the debris flow (black line on Fig. 6), which is an excellent candidate for PS selection. In the debris flow area, the PS have a subsidence rate ranging between −5 mm/year in the central part of the debris flow and more than 10 mm/year near the main scarps (red dots of the NE area in Fig. 6) and in the debris flow front (NW area). In the main landslide we can observe the same range of values but with lower subsidence rates (−3 to −7 mm).

The main limitation of PS detection is clearly highlighted in this landslide. The foot of the landslide is poorly defined in term of displacement due to a PS gap. This gap can be explained by the surface roughness of the area which is mainly constituted by grass with no metric block. Therefore, the surface can be regarded as stringer in term of roughness and in this case we have no candidate for natural PS.

The X band showed all their effectiveness in term of precision for subsidence and uplift measurements. The noise of measurement (RMSE ~ 3 mm) in glance with the quality of the results is finally rather weak and thus allows an excellent monitoring of landslides. The only restrictions are (1) the high cost of monitoring requiring a large radar database, (2) PS quality and quantity being clearly correlated to the surface roughness, and (3) displacements being in direction of the satellite i.e. according to the LOS and giving no information on the horizontal components. For a complete description of the XYZ components radar analyses were combined with aerial photographs correlation.

Aerial Photographs

The correlation method is less sensitive to noise if using relatively small correlation windows (Ayoub et al. 2009). In practice, the best window size is 64 × 64 pixels with a sliding step of 16 pixels in X (EW) and Y (NS) directions. The threshold value of the correlation factor was defined to be higher than 0.9, which indicates a strong correlation between the conjugated points.

Figure 6 synthesizes the results of the correlation analysis. The TerraSAR-X shows the vertical motion of blocks in the debris flow (contoured black, Fig. 5) which are in agreement with whose obtain by correlation (Fig. 6). The debris flow proceeded toward the west in its eastern part and flow direction changes progressively to southwest in the western part. Limited southward displacements are observed near the western boundary of the flow (Fig. 6). For the 1994–2008 period, the cumulative displacement is toward the southwest in the eastern part (Fig 6a) and changes progressively to northwest in the western part (Fig. 6b).

The main landslide, contoured in dot black, shows a main displacement toward the south for the too periods with local deviations toward the southeast near the eastern boundary

and toward the southwest near the western boundary for the period 1994–2003. For the 1994–2008 period, the displacement pattern is more complex. If the main mass the displacements are toward the south in the central/west and western part, we can observe too drastic change in the central/eastern and eastern part. The fist one (Fig. 6c) flow now toward the southeast in the central-western part where was built the car park. The second one (Fig. 6d) located East of the main mass another slide mass has formed where the displacements are toward the east. This eastern slide is now clearly separated from the main mass by a low displacement area whereas homogeneous displacements are observed for the 1994–2003 period. The central/east area move toward the south east which is quite orthogonal to the displacement observed during 1994–2003 period.

The geomorphological study shows that the debris flow has been constrained within a topographic corridor oriented east–west. The southward component of displacement evidenced for the 1994–2008 period (Fig. 6, north-east) indicates feeding from the north, likely due to another slide along a shallower slip surface. The main landslide mass appears to undergo a marked constriction in the south (with the partition of the initial slide mass into two independent slides).

A comparison of displacements for the 1994–2003 and 1994–2008 periods also shows that the displacements between 2003 and 2008 were deviated parallel to the car park and markedly increased, even though south-eastward displacements are observed in the south-west of the slide before the construction. The present study shows that the site chosen for the cark park was one of the worst to be selected in this area.

Discussion and Conclusion

The Tena landslide demonstrates the efficiency of optical correlation analyses for measuring horizontal displacements in areas where other methods are inoperative. Combined with DinSAR, these methods allow measurements of 3D ground displacements and may arrive at a clearer understanding of the landslide history.

In our case, a simple comparison of displacements having occurred before and after 2003 show how a rather homogeneous landslide may be partitioned into two unequal units with opposite displacement directions.

A large spectrum of satellite data and aerial photographs is now available and the number and accuracy of the data is to be increased in the next future. This and the probable improvement of analysis techniques may allow envisioning the development of this approach as a routine for landslide survey and risk mitigation. Drilling and geotechnical tools such as inclinometers and extensometers data, electrical profiles, terrestrial RADAR records or DGPS measurements will, however, be always necessary for identifying the rupture plane(s), which is inaccessible to pure remote sensing analyses. In fact, a comparison of both types of data may allow distinguishing what is a result of a large-scale motion or due to a more local cause or high frequency or rapid events such as high rainfalls or earthquakes.

Acknowledgements This research is supported by the INTEREG IVB European program and benefited from PhD grant from French and Vietnamese governments.

References

Arnaud A, Adam N, Hanssen R, Inglada J, Duro J, Closa J, Eineder M (2003) ASAR ERS interferometric phase continuity. In: IGARSS, Toulouse (France), CDROM, 21–25 July 2003. (for Arnaud 2003)

Aulakh NS, Singh N, Jain S (2004) Microbend resolution-enhancing technique for fiber optic based sensing and monitoring of landslides. Exp Tech 28(3):55

Ayoub F, Leprince S, Avouac JP (2009) Co-registration and correlation of aerial photographs for ground deformation measurements. ISPRS J Photogramm Remote Sens 64:551–560

Bock O, Doerflinger E (2001) Atmospheric modeling in GPS data analysis for high accuracy positioning. Phys Chem Earth 26(A6–8):373–383

Capote R, Muñoz JA, Simón JL, Liesa CL, Arlegui LE (2002) Alpine tectonics I: the Alpine system north of the Betic Cordillera. In: Moreno T, Gibbons W (eds) The geology of Spain. Geological Society, London, pp 367–400

Casson B, Delacourt C, Baratoux D, Allemand P (2003) Seventeen years of the "La Clapière" landslide evolution analysed from orthorectified aerial photographs. Eng Geol 68:123–139, for Casson et al. 2003

Colesanti C, Wasowski J (2006) Investigating landslides with spaceborne Synthetic Aperture Radar (SAR) interferometry. Eng Geol 88:173–199, for Colesanti and Wasowski 2006

Creus J, Gil M (2001) Clima in Estudio del Medio Fisico y de los Riesgos Naturales en los Pireneo Central, Ministerio de Ciencia y Tecnología (ed), IGME, Madrid, p 60

Crosetto M, Biescas E, Duro J, Closa J, Arnaud A (2008) Generation of advanced ERS and envisat interferometric SAR products using the stable point network technique. Photogramm Eng Remote Sens 74(4):443–451

Doerflinger E (1997) Utilisation de la méthode positionnement satellitaire GPS pour la détermination précise des altitudes relatives et absolues. In: Ph. D. thesis, Institut des Sciences de la Terre, de l'eau et de l'espace de Montpellier, France

Dunnicliff J (1988) Geotechical instrumentation for monitoring field performance. Wiley-Interscience, New York, p 577. ISBN 978-0471005469

Dunnicliff J, Green GE (1994) Geotechnical instrumentation for monitoring field performance. Wiley, New York, for Dunnicliff and J. Green 1994

Ferretti A, Rocca F (2001) Permanent scatterers in SAR interferometry. IEEE Trans Geosci Remote Sens 39(1):8–30

Gabriel AG, Goldstein RM, Zebker HA (1989) Mapping small elevation changes over large areas: differential radar interferometry. J Geophys Res V94(B7):9183–9191

Gatelli F, Guarnieri AM, Parizzi F, Pasquali P, Prati C, Rocca F (1994) The wavenumber shift in SAR interferometry. IEEE Tran Geosci Remote Sens 32(4):855–865

Herrera G, Fernández-Merodo JA, Mulas J, Pastor M, Luzi G, Monserrat O (2009) A landslide forecasting model using ground based SAR data: the portalet case study. Eng Geol 105:220–231

Herrera G, Garcia-Davalillo JC, Mora O, Cooksley G, Sanchez M, Arnaud A, Crosetto M (2010) Analysis with C and X band satellite SAR data of the Portalet landslide area. Landslides 49:161–170, for Herrera 2010

Hild F. Périé JN, Coret M (1999) Mesure de champs de déplacements 2D par intercorrélation d'images :CORRELI^{2D}, LMT-Cachan, rapport interne 230. (for Hild et al. 1999)

Keefer DK, Larsen MC (2007) Science perspectives: assessing landslide hazards. Science 316:1136–1138

Leprince S, Ayoub F, Klinger Y, Avouac JP (2007) Co-Registration of Optically Sensed Images and Correlation (COSI-Corr): an operational methodology for ground deformation measurements. In: IEEE international geoscience and remote sensing symposium (IGARSS 2007), Barcelona. (for Leprince et al. 2006)

Leprince S (2008) Monitoring earth surface dynamics with optical imagery. Ph.D. Thesis defense. (for Leprince 2008)

Luzi G, Pieraccini M, Mecatti D, Noferini L, Guidi G, Moia F, Atzeni C (2004) Ground-based radar interferometry for landslides monitoring: atmospheric and instrumental decorrelation sources on experimental data. IEEE Trans GeosciRemote Sens 42:11

Mulas de Peña J, Fresno-López F (1995) Estudio Geotechnico y Riesgo Naturales. Estudio del medio fisicoy de sus riegos naturales en un sector de los pyrenneos central, Ministerio de Ciencia y Tecnología (ed), IGME, Madrid, p 216

Mulas de la Peña J, Ponce de León Gil D, Pardo Sanjurjo JM, Bardasano L, Prieto Martín A, Lorenzo Carnicero C, Herrera García G (2010) Micronización sísmica de lasinestabilidades de ladera. Diseño de una metodología y su aplicación a una zona piloto en el Pirineo aragonés (Alto Tena, Huesca). IGME, Informes técnicos n° 2, Madrid. CD-ROM. + 12 pp. (for the Mulas et al. 2003)

Muñoz JA (1992) Evolution of a continental collision belt: ECORS-Pyrenees crustal balanced cross-section. In: McClay KR (ed) Thrust tectonics. Chapman and Hall, London, p 447

Notti D, Davalillo JC, Herrera G, Mora O (2010) Assessment of the performance of X-band satellite radar data for landslide mapping and monitoring: Upper Tena Valley case study. Nat Hazards Earth Syst Sci 10:1–11



Long-Term Analysis of Landslides Via SBAS-DInSAR Technique

Manuela Bonano, Fabiana Calò, Michele Manunta, Luca Paglia, and Giovanni Zeni

Abstract

Advanced techniques of multi-pass space-borne Differential Synthetic Aperture Radar (SAR) Interferometry (DInSAR) represent a valuable tool in landslide studies allowing to remotely investigate the behavior of mass movements on long time intervals by benefiting of large datasets of SAR images covering the same area and acquired at different epochs. Among these techniques, we apply the Small BAseline Subset (SBAS) approach for analyzing surface deformation at two spatial scales, i.e., regional and local scale.

In this work, developed within the framework of the DORIS FP7-EU project, we investigate mass movements occurred in the Umbria region (central Italy) during the last 20 years, by exploiting ERS-1/2 and ENVISAT SAR images spanning the 1992–2010 time interval. Our two-scale SBAS analysis allowed detecting active landslides over all the study area, and further giving more insights on the spatial and temporal pattern of localized phenomena.

Keywords

Differential SAR Interferometry (DInSAR) • SBAS technique • Umbria region • Italy

Introduction

Landslides threaten many regions in both developed and developing countries, often resulting in high socio-economic impacts on the affected communities. In such a context, the risk management plays a significant role, and focuses on defining appropriate prevention and mitigation strategies. To this aim, a deep understanding of the landslide kinematics is needed and can be effectively reached if long-term monitoring data are available.

M. Bonano (✉)
Istituto per il Rilevamento Elettromagnetico dell'Ambiente (IREA), CNR, Napoli, Italy

Dipartimento di Ingegneria Civile, Edile ed Ambientale (DICEA), Università degli Studi di Roma "La Sapienza", Roma, Italy
e-mail: bonano.m@irea.cnr.it

F. Calò • M. Manunta • L. Paglia • G. Zeni
Istituto per il Rilevamento Elettromagnetico dell'Ambiente (IREA), CNR, Napoli, Italy

Ground-monitoring networks require high management costs especially over large areas and their maintenance over time can result in a difficult task, often hampered by lack of economic resources as well as by technical problems. Space-borne radar sensors provide valuable data that, opportunely processed, can effectively integrate traditional methods of landslide investigation since their capability to "observe" wide areas with high spatial resolution.

In such context, Differential Synthetic Aperture Radar (SAR) Interferometry (DInSAR) is able to retrieve surface displacements with centimeter to millimeter accuracy, by exploiting the phase difference (i.e., the interferogram) between two SAR images acquired over the same area at different times. From the produced interferograms, DInSAR allows computing the projection of the displacements along the satellite Line of Sight (LOS).

More recently, multi-pass DInSAR techniques focusing on processing stacks of SAR data collected over the same scene during repeated passes of the satellite have been developed. They allow generating deformation maps and

C. Margottini et al. (eds.), *Landslide Science and Practice*, Vol. 2,
DOI 10.1007/978-3-642-31445-2_18, © Springer-Verlag Berlin Heidelberg 2013



Fig. 1 Location of the study area. *Red box* shows the footprint of descending ERS-1/2 and ENVISAT SAR data used in this study

furthermore associated time-series showing the temporal behavior of the investigated phenomena. Among these advanced DInSAR techniques, we apply the Small BAseline Subset (SBAS) approach for investigating landslide deformation at two spatial scales, i.e., regional and local scale (Berardino et al. 2002; Lanari et al. 2004a), in Umbria region, central Italy (Fig. 1). In particular, sets of ERS-1/2 and ENVISAT SAR data acquired from descending satellite orbits in the period 1992–2010 were exploited in order to map and monitor slope movements.

The Study Area

The study area, extending for more than 7,000 km^2 in Umbria, central Italy (Fig. 1), is geologically characterized by the presence of sedimentary rocks pertaining to the Umbria-Marche stratigraphic sequence, Lias to Eocene in age, overlaid by lake deposits, lower Pliocene to Quaternary in age, and by fluvial deposits of recent age (Cardinali et al. 2001).

The landscape shows a hilly or mountainous morphology, with open valleys and large intra mountain basins. The area is widely affected by slope instability phenomena, with relevant impacts on urban areas and infrastructures. Landslides are mainly triggered by meteoric events, including intense and prolonged rainfall and snow melt, and the main types are slides, earth-flows, complex and compound movements (Cruden and Varnes 1996; Guzzetti et al. 2008). As regards the state of activity, most of the landslides are dormant, while the active ones move with displacement rates ranging from slowly to very slowly (Cruden and Varnes 1996).

The SBAS-DInSAR Analysis

The SBAS-DInSAR approach (Berardino et al. 2002) has been successfully applied to the analysis of different geological hazards and human induced processes, such as volcanic activity (Tizzani et al. 2007), earthquakes (Lanari et al. 2010), subsidence caused by mining and water exploitation (Lanari et al. 2004b). As regards landslide applications, several published results (Berardino et al. 2003; Manzo et al. 2006; Lanari et al. 2007) pointed out the high potentiality of the SBAS technique in detecting and monitoring slow-moving phenomena.

The key point at the base of the SBAS technique is the selection of the SAR data pairs used for generating the interferograms. In order to mitigate the noise (i.e., the decorrelation phenomena) affecting interferograms, and to maximize the reliable measure points, only SAR data pairs characterized by small spatial and temporal separation (baseline) between the satellite orbits are considered for the processing (Berardino et al. 2002).

Originally designed for investigating deformation phenomena extending over very large areas, the SBAS algorithm has been subsequently modified in order to analyze also localized phenomena affecting individual man-made features. As result, the SBAS analysis can be currently carried out at two spatial scales, namely at regional and local scale (Lanari et al. 2004a).

At regional scale, the technique exploits average (multi-look) interferograms to produce deformation maps of wide areas (100 km × 100 km) at low spatial resolution (about 100 m × 100 m in the ERS and ENVISAT case); at local scale, single-look interferograms are exploited in order to generate maps at full spatial resolution (about 5 m × 20 m in the ERS and ENVISAT case), thus allowing to focus on local deformation affecting single elements at risk. At both scales, time-series showing the temporal evolution of surface displacements are generated.

Recent algorithm developments allowed to further extend the multi-scale SBAS analysis to the multi-sensor processing of SAR data collected by different radar systems acquiring with the same illumination geometry (ERS-1/2 and ENVISAT satellites), in order to fully exploit the large SAR data archive for the production of very long-term deformation time-series spanning a time period of almost 20 years (Bonano et al. 2012).

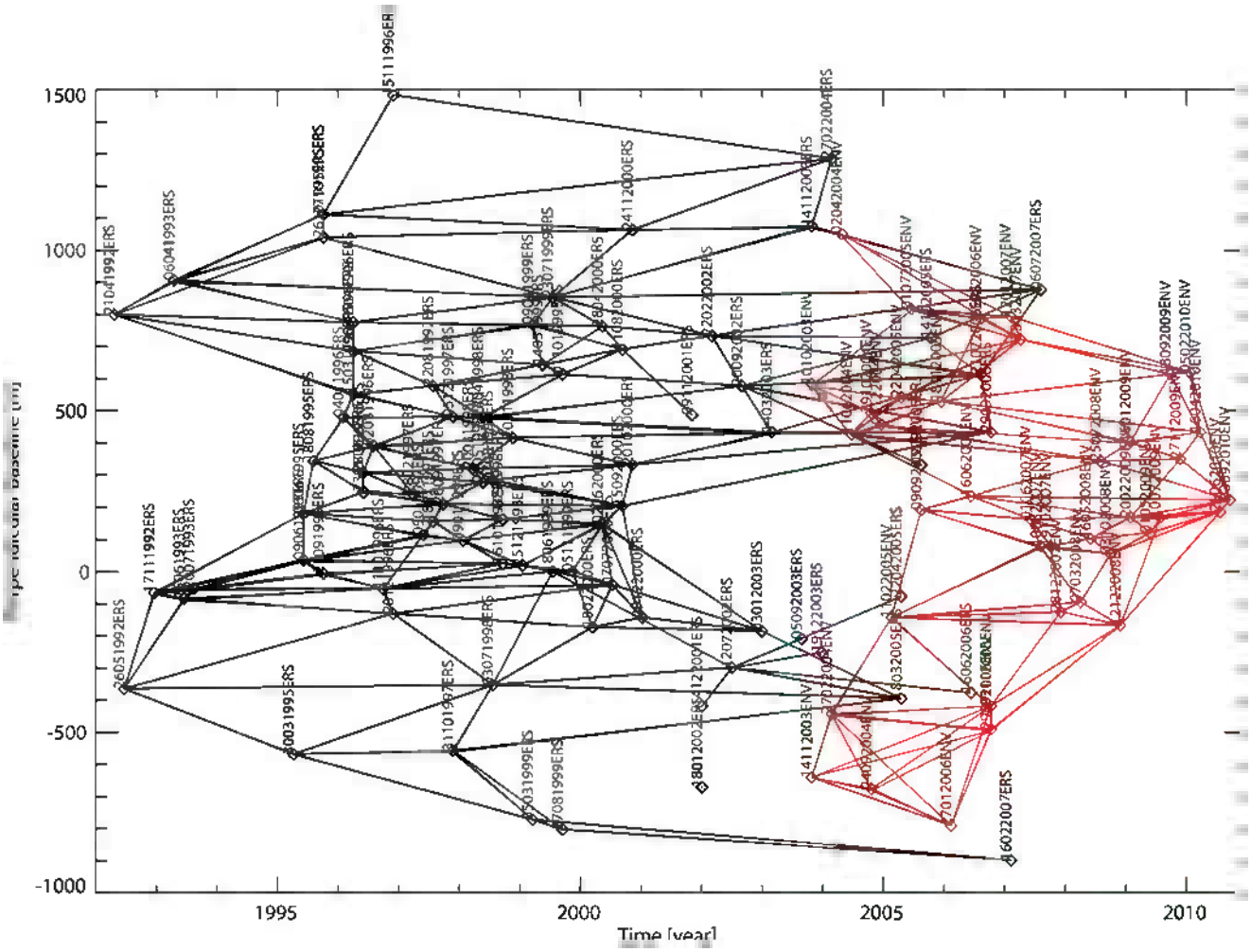


Fig. 2 Sketch of the SAR data distribution in the temporal/perpendicular baseline plane. The *black and red diamonds* represent the ERS and ENVISAT acquisitions, respectively; each arc of the graph corresponds to a generated interferogram

Results

Our two-scale SBAS-DInSAR analysis has been performed by processing a dataset of 116 SAR data acquired along descending satellite orbits (Fig. 2). In particular, the dataset is composed by 77 ERS-1/2 and 39 ENVISAT images, spanning the period between April 1992 and September 2010, from which 312 interferograms have been computed. The constraints imposed on the interferograms are 400 m and 1,500 days on the spatial and temporal baseline, respectively.

Figure 3 shows the low resolution deformation velocity map, obtained by processing the descending dataset, superimposed on an amplitude SAR image of the analyzed area. The deformation velocity map reveals an overall stability of the study area in the analyzed time interval. However, significant deformation patterns are present in the Valle Umbra, where a subsidence induced by water exploitation occurs, and in the area around Perugia. It is worth to point out that while the portion of Valle Umbra between Assisi and Foligno was affected by subsidence since 1992 (Fig. 3c), as already shown from the SBAS analysis conducted on the Umbria region by Guzzetti et al.

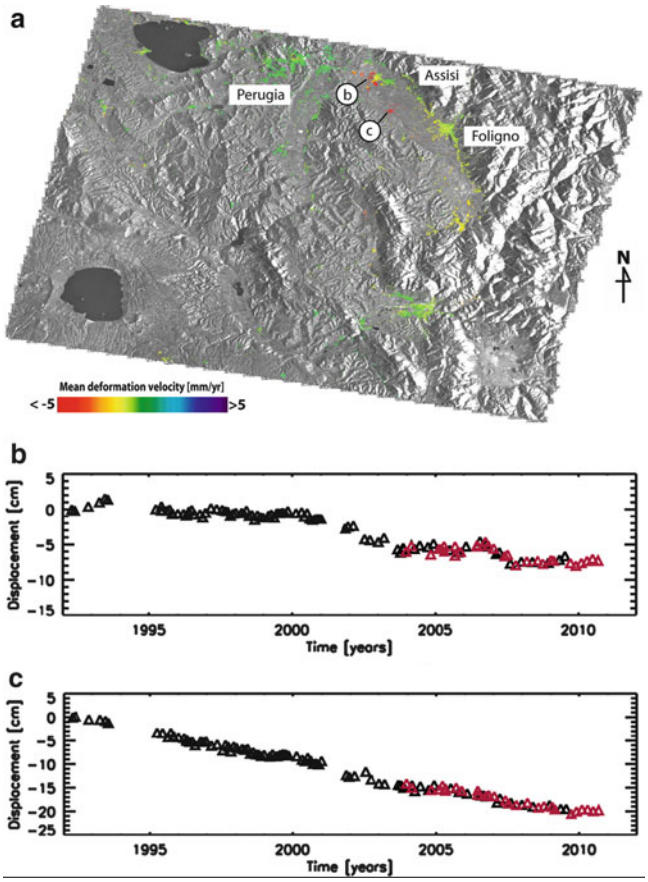


Fig. 3 (**a**) Geocoded mean deformation velocity map at low spatial resolution scale (pixel size ≈100 m × 100 m) of the whole study area, obtained from descending SAR data, and superimposed on the amplitude SAR image. Deformation values are measured along the satellite Line of Sight (LOS). (**b**) Deformation time-series relevant to the pixel labelled as (**b**) in Fig. 3a is shown. *Black and red triangles* represent ERS and ENVISAT acquisitions, respectively. (**c**) Same as (**b**) but referred to the pixel labelled as (**c**) in Fig. 3a

(2009), the Perugia area exhibits ground deformation since 2000, as clearly highlighted in the plot of Fig. 3b.

Subsequently, the full resolution SBAS processing allowed performing a detailed analysis of ground deformation and giving more insights on the behaviour of localized phenomena. Full resolution deformation velocity maps, and associated time-series, have been produced for selected hazardous areas. Figure 4 reports the results related to the active, slow-moving, deep-seated landslide affecting the Ivancich area, in the Assisi municipality, causing severe damage to buildings and urban roads. In particular, in Fig. 4a the full resolution velocity map superimposed on an optical image relevant to the city of Assisi is shown and a zoomed view of the area affected by the above mentioned landslide is pictured in Fig. 4b. The effectiveness of the two-scale SBAS approach to generate very long-term deformation time-series in order to analyze and monitor deformation phenomena affecting localized areas is clear.

This case study further confirms the relevance of such DInSAR analyses for the investigation of complex scenarios involving surface deformation, with the relevant impact on the definition of risk prevention and post-crisis management strategies.

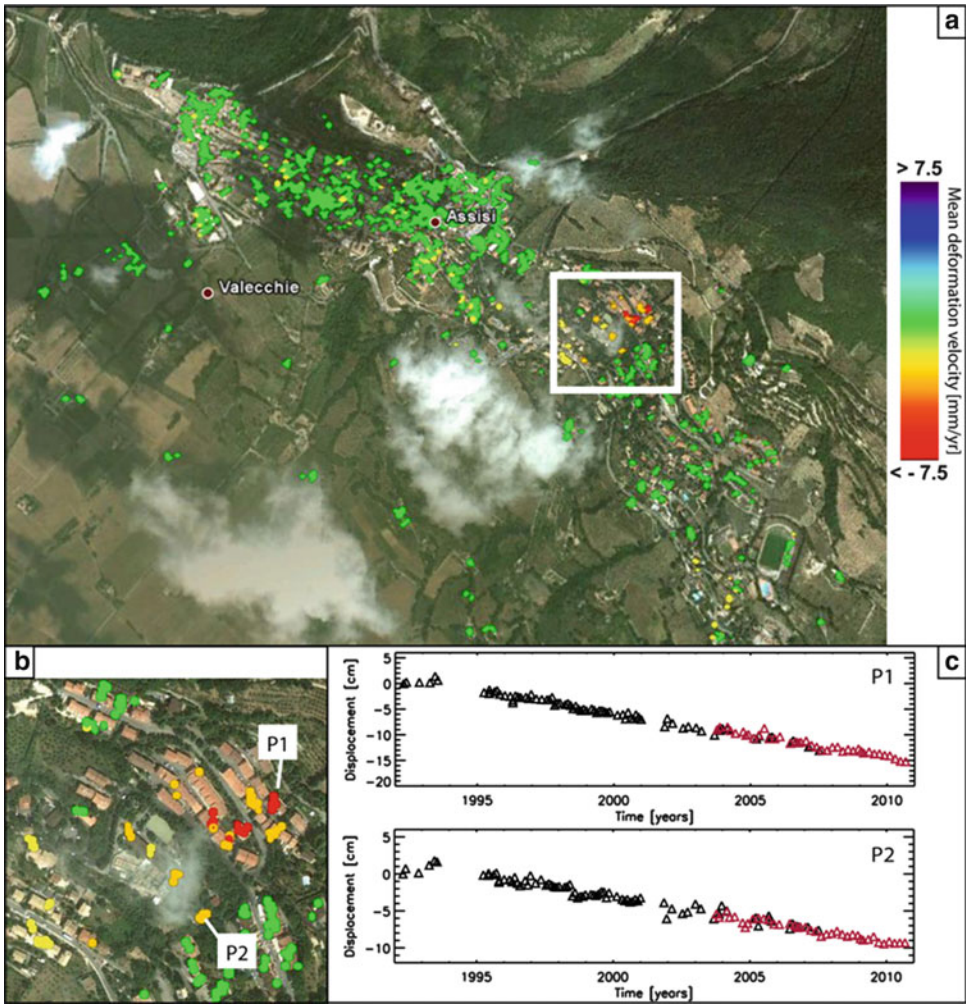


Fig. 4 (**a**) Geocoded mean deformation velocity map at full spatial resolution scale (pixel size ≈5 m × 20 m) relevant to the Assisi municipality and superimposed on an optical image of the analyzed area. Deformation values are measured along the satellite Line of Sight (LOS). (**b**) Zoomed view of the mean deformation velocity map of the area, highlighted by the *white box* in Fig. 4a, relevant to the Ivancich area affected by an active, slow-moving, deep-seated landslide. (**c**) Deformation time series relevant to the pixels labelled as *P1* and *P2* in Fig. 4b, respectively. *Black and red triangles* represent ERS and ENVISAT acquisitions, respectively

Conclusions

The SBAS-DInSAR technique can assume a key role in monitoring landslide-prone areas, thus preventing and mitigating the landslide risk, since the possibility to fully exploit very large archive of SAR data (over 20 years of SAR acquisitions). The results presented in this work show the effectiveness of such SBAS analyses in landslide applications, and suggest as the development of integrated monitoring systems, based on the joint use of ground measurements and DInSAR data, can significantly improve the landslide risk management; this latter can further benefit from the availability of improved temporal and spatial resolution SAR systems, as the Italian COSMO-SkyMed constellation.

References

Berardino P, Fornaro G, Lanari R, Sansosti E (2002) A new algorithm for surface deformation monitoring based on small baseline differential SAR interferograms. IEEE Trans Geosci Remote Sens 40(11):2375–2383

Berardino P, Costantini M, Franceschetti G, Iodice A, Pietranera L, Rizzo V (2003) Use of differential SAR interferometry in monitoring and modeling large slope instability at Maratea (Basilicata, Italy). Eng Geol 68:31–51

Bonano M, Manunta M, Marsella M, Lanari R (2012) Long-term ERS/ENVISAT deformation time-series generation at full spatial resolution via the extended SBAS technique. Int J Remote Sens 33 (15):4756–4783. doi:10.1080/01431161.2011.638340

Cardinali M, Antonini G, Reichenbach P, Guzzetti F (2001) Photogeological and landslide inventory map for the Upper Tiber River

basin. CNR, Gruppo Nazionale per la Difesa dalle Catastrofi Idrogeologiche, Publication no. 2154, scale 1:100,000

Cruden DM, Varnes DJ (1996) Landslide types and processes. In: Turner AK, Schuster RL (eds) Landslides, investigation and mitigation, vol 247, Transportation Research Board Special Report. National Academy Press, Washington, DC, pp 36–75

Guzzetti F, Ardizzone F, Cardinali M, Galli M, Reichenbach P, Rossi M (2008) Distribution of landslides in the upper Tiber River basin, central Italy. Geomorphology 46:105–122

Guzzetti F, Manunta M, Ardizzone F, Pepe A, Cardinali M, Zeni G, Reichenbach P, Lanari R (2009) Analysis of ground deformation detected using the SBAS-DInSAR technique in Umbria, Central Italy. Pure Appl Geophys. doi:10.1007/s00024-009-0491-4

Lanari R, Mora O, Manunta M, Mallorquí J, Berardino P, Sansosti E (2004a) A small baseline approach for investigating deformations on full resolution differential SAR interferograms. IEEE Trans Geosci Remote Sens 42:1377–1386

Lanari R, Lundgren P, Manzo M, Casu F (2004b) Satellite radar interferometry time series analysis of surface deformation for Los Angeles, California. Geophys Res Lett 31:L23613. doi:10.1029/2004GL021294

Lanari R, Casu F, Manzo M, Zeni G, Berardino P, Manunta M, Pepe A (2007) An overview of the small baseline subset algorithm: a DInSAR technique for surface deformation analysis. Pure Appl Geophys 164:637–661

Lanari R, Berardino P, Bonano M, Casu F, Manconi A, Manunta M, Manzo M, Pepe A, Pepe S, Sansosti E, Solaro G, Tizzani P, Zeni G (2010) Surface displacements associated with the L'Aquila 2009 Mw 6.3 earthquake (central Italy): new evidence from SBAS-DInSAR time series analysis. Geophys Res Lett 37:L20309. doi:10.1029/2010GL044780

Manzo M, Ricciardi GP, Casu F, Ventura G, Zeni G, Borgstrom S, Berardino P, Del Gaudio C, Lanari R (2006) Surface deformation analysis in the Ischia Island (Italy) based on spaceborne radar interferometry. J Volcanol Geotherm Res 151:399–416

Tizzani P, Berardino P, Casu F, Euillades P, Manzo M, Ricciardi GP, Zeni G, Lanari R (2007) Surface deformation of Long Valley Caldera and Mono Basin, California, investigated with the SBAS-InSAR approach. Remote Sens Environ 108(3):277–289



4D Monitoring of Active Landslides by Multi-Temporal Airborne LiDAR Data

Guido Ventura, Giuseppe Vilardo, Carlo Terranova, and Eliana Bellucci Sessa

Abstract

We present results of a multi-temporal analysis of airborne LiDAR data collected between 2006 and 2010 on the 3 km long active Montaguto landslide (Italy). Digital Terrain Models are constructed from data acquired on May 2006, July 2009, April 2010 and June 2010. The spatial distribution of selected morphometric parameters and the statistical analysis of the temporal variations of such parameters allow us to reconstruct the evolution of the landslide. We recognize zones of uplift and subsidence, estimate the volumes of removed or accumulated material, and determine the average rate of vertical and horizontal displacement. We also map the deformations structures and provide new insights on the sliding mechanisms. Zones in which the topographic features change due to handling/removal work are also analyzed. The approach proposed here provides new insight on the use of airborne LiDAR in the surveillance strategies of landslides and other gravity-controlled processes.

Keywords

LiDAR • Multi-temporal analysis • Gravity processes

Introduction

The use of airborne LiDAR in the remote sensing of gravity-controlled flows is undergoing a fast growth. The acquisition of high resolution 3D information on terrains affected by instability phenomena allows us to (a) identify weakness zones, (b) estimate the volumes of removed or accumulated material, and (c) monitor the evolution of sliding processes for hazard assessment purposes (Jaboyedoff et al. 2010). Recent studies based on LiDAR-derived DTMs or combined LiDAR and photogrammetric data on unstable terrains focus on the landslide boundary changes and on the estimate of the volume of accumulated or removed material (Burns et al. 2010). Here, we present the results of a multi-temporal airborne LiDAR survey (four aerial missions in the 2006–2010 period) of the active Montaguto landslide (Southern Apennines, Italy). This is one of larger and complex landslides in Europe and its activity compromises the functionality and safety of the Pan-European Rail Corridor infrastructures connecting the Tyrrhenian and Adriatic coasts of Italy (SS90 road and Benevento-Foggia railway line). The analysis of DTMs derived by the post-processing of LiDAR data allow us to (a) delimit the boundary of the landslide in different times, (b) recognize zones of uplift and subsidence, (c) estimate the volumes of removed and/or accumulated material, (d) determine average rates of vertical and horizontal movements, (e) detect zones characterized by different types of activity (e.g. fall, flow), (f) identify major and minor scarps, ridges, cracks and estimate the retreat rate of the crown, and (g) detect zones in which artificial modifications of the topography due to material handling occur. The results shed light on the natural and man-induced processes that affect the studied terrains.

G. Ventura (✉)
Istituto Nazionale di Geofisica e Vulcanologia, Via di Vigna Murata 605, Roma 00143, Italy
e-mail: guido.ventura@ingv.it

G. Vilardo • C. Terranova • E.B. Sessa
Istituto Nazionale di Geofisica e Vulcanologia, Osservatorio Vesuviano, Via Diocleziano 328, Napoli 80124, Italy

C. Margottini et al. (eds.), *Landslide Science and Practice*, Vol. 2,
DOI 10.1007/978-3-642-31445-2_19, © Springer-Verlag Berlin Heidelberg 2013

Geological Setting

The Montaguto landslide (ML; Fig. 1) is located along the axis of the Neogene Southern Apennine fold-and-thrust belt and emplaces on a south facing slope of a 870 m a.s.l. high, E-W elongated relief; ML mainly develops within a NNW-SSE striking synform with a nucleus constituted by Pliocene clays and sandy clays (Fig. 1b). These Pliocene deposits overlie Miocene calacarenitic and limestone breccias with alternated clays and marls. The main landslide body emplaces within a NNW-SSE striking valley. ML initiated in 2003. The water table in the slide body is at 2 m below the topographic surface in the central zone and 15–20 m in the toe zone (Commissariato di Governo della Regione Campania 2006). The thickness of the slide deposits also increases from 5 m in the central zone to 20 m at the toe. Sag ponds occur in the central and upper zone (Fig. 1a). The slide is artificially drained in the upper and middle-lower zones, while the sliding material is removed from the toe. On the basis of its morphological features, ML may be divided in four main sectors (Fig. 1b): Sector 1 (S1) includes the uppermost part of the slide, which includes the crown, main scarp and head. Sector 2 (S2) represents the displaced material within a ENE-WSW striking, 50–70 m wide valley. Sector 3 (S3) is 70 to about 200 m wide and it is characterized by material filling the above mentioned valley. Sector 4 (S4) represents the lowermost part of the landslide and incorporates to, which affected the Pan-European Rail Corridor infrastructures.

S1 involves Miocene calcarenites, whereas Pliocene clays outcrop in S2, S3 and S4.

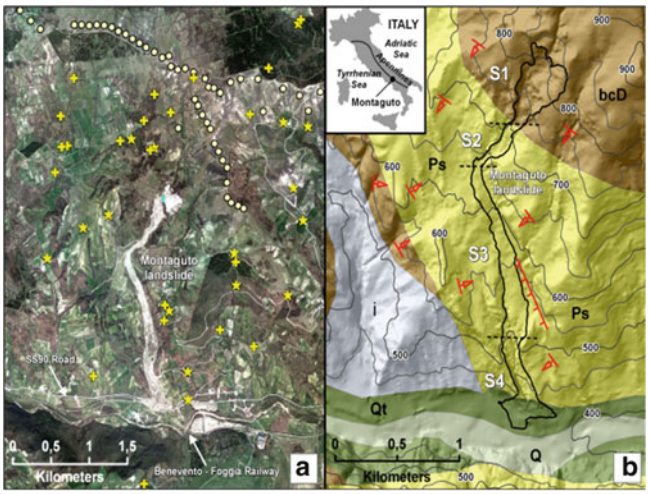


Fig. 1 (**a**) Digital colour orthophoto (March 29, 2010) showing the location of the Montaguto landslide, SS90 road and Benevento-Foggia railway. Symbols: *circle* = wind tower, *stars* = fountains, *cross* = springs. (**b**) Location and geological map of the Montaguto landslide area. Symbols: *bcd*: Miocene calcarenitic and limestone breccias with alternated clays and marls, Ps = Pliocene clays and sandy clays, i = clays and sandy clay with intercalated calcarenites, limestones, schists and jasper, Qt = Quaternary fluvial deposits, Q = Recent alluvial sediments, red line with arrow = strike and dip of strata, *red line* with barbs = fault. The different sectors of the landslide S1, S2, S3, and S4 are also reported

Data Acquisition and Pre-Processing

The ML analysis bases on multitemporal high-resolution LiDAR data sets collected using systems operating at frequencies from 50 to 135 kHz on board of a Partenavia P68. The LiDAR flight missions over the ML area were in May 2006, July 2009, April 2010 and June 2010. The survey consisted of flight lines side lapped of 20–25%, with additional crossing flight lines to provide a coverage on the steep topography and to ensure at least three points per square meter. The instrument calibration phases were performed in different times and in different ground calibration sites (Grumento Nova and Capodichino airports) using head runaway signs from intensity information and topographic control points. Differential corrections of the GPS trajectory of the aircraft were calculated for all the four flight missions from a same local base station. Laser rangefinder data have been computed in conjunction with recordings from the onboard differential Global Positioning System (DGPS) and inertial measurement unit (IMU), producing geocoded x, y, z coordinates of all the LiDAR points. The LiDAR data have a vertical accuracy of 12 cm and planimetric accuracy at 24 cm.

A regular 1 × 1 m grid DTM was created from LiDAR bare-earth points cloud by means of the inverse distance weighted interpolation method with a 3 m search radius. Hundreds of stable check points were selected over the ML surrounding area on buildings and roads; the elevation differences between the four LiDAR data sets have been computed and resulted to be between ±0.01 (2009–2006) and −0.475 m ± 0.15 (2010–June 2006). These values have been used to correct the offset between multitemporal LiDAR data.

Morphometric Parameters and Analytical Methods

Photo-interpretation of shaded relief maps and geomorphometric imagery (surface roughness, Fig. 2), and residual topographic surface (RTS; Fig. 3) allow the recognition and mapping of landslide phenomena. Surface roughness was estimated with a 3 × 3 m moving window as the ratio between the surface area (S = real) and the flat area (A = plan) of square cells. RTS (Grebby et al. 2010) was derived by separating the large scale topography from the fine scale

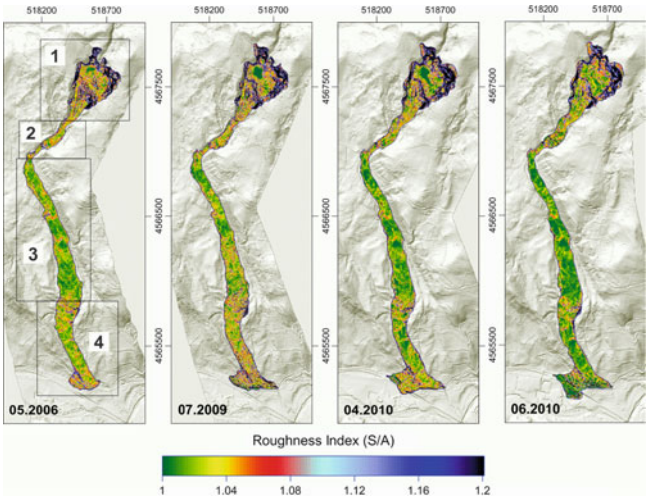


Fig. 2 Spatial distribution of surface roughness in different times

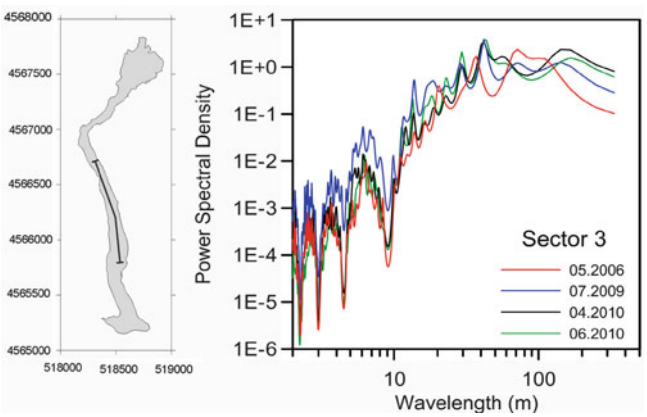


Fig. 4 Results of the one-dimensional spectral analysis of longitudinal residual topography profile in S3 at different time (see procedure in the text)

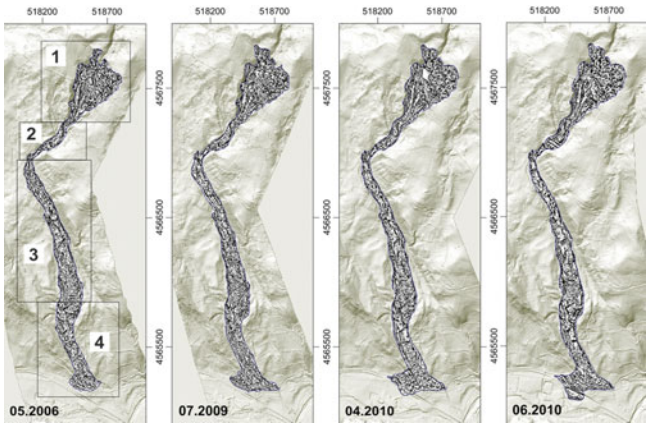


Fig. 3 Spatial distribution of RTS in different times

variability by considering a 9 × 9 pixel moving window. RTS of each DTM was calculated by subtracting the 9 m DTM from the 1 m DTM. One-dimensional spectral analysis has been applied in order to obtain information about the magnitude of the dominant surface periodicities in S3. Longitudinal cross-sections were extracted from the four RTS maps. Such one-dimensional residual elevation profiles, with mean elevation equal to zero, were low-pass filtered with a nine points moving-average filter and power spectra were calculated (Fig. 4). Statistical analysis of the surface roughness and RTS maps are summarized in Fig. 5 where box-plot diagrams representative of the pixel distribution in each sector of the landslide of the four DTMs are reported.

Results and Discussion

Results of the above analyses indicate a progressive increase of the ML area from May 2006 to June 2010 (i.e., from 36.7 to 42.7 ha). This increase of the ML surface is due the toe advancement and the progressive upslope migration of the ML crown in S1. S1 is mainly characterized by a disorganized distribution of the surface irregularities, which reflects the fall of dm- to m-sized calacarenitic fragments from the crown steep slope, and grain-flows. NW-SE striking scarps were also detected within the S1 zone at the base of the crown in 05.2006. These scarps were progressively covered by debris accumulated at the base of a new, major scar formed in the central part of S1 in 2009. In S2, the ML central body is bounded by NE-SW striking, parallel levees suggesting channelized flow processes in which ridges are related to the lateral pressure of the moving earthflow on the lateral walls of the channel. The S3 topography is smoother than that of S1 and S2. Longitudinal grooves delimit a central area characterized by the presence of lobes and folds. In the upper part of S3, the landslide width decreases from 2006 to 2010 so marking a narrowing of the transportation track. In the lower part, the fold bending and the local landslide width increase as the local slope decreases. Such morphological features suggest, according to Evans and De Graff (2005), a non-Newtonian behavior of the moving material. Spectral analysis evidences four stable peaks at wavelengths less than 30 m. At larger wavelengths, two major peaks occur at 40 and 70 m in May 2006, which, in the 2009.07–2010.06 period, shift to 45 and 180 m. The smaller-scale S3 periodicity remains stable over time, whereas the larger scale periodicity increases. Such an increase could be related to the basal sliding of the landslide in S3. The net effect of this process is a subsidence. In S4, fold-like structures prevail in 2006 and 2009, whereas longitudinal grooves form in the 2010.04–2010.06 period. This evolution indicates a withdrawal by flow processes along the main channel. The toe front advanced and expanded downslope from 2006.05 to 2010.04, and stopped when the artificial draining of the landslide and earth removal activities started. Terraces due to material handling were recognized in 2010.

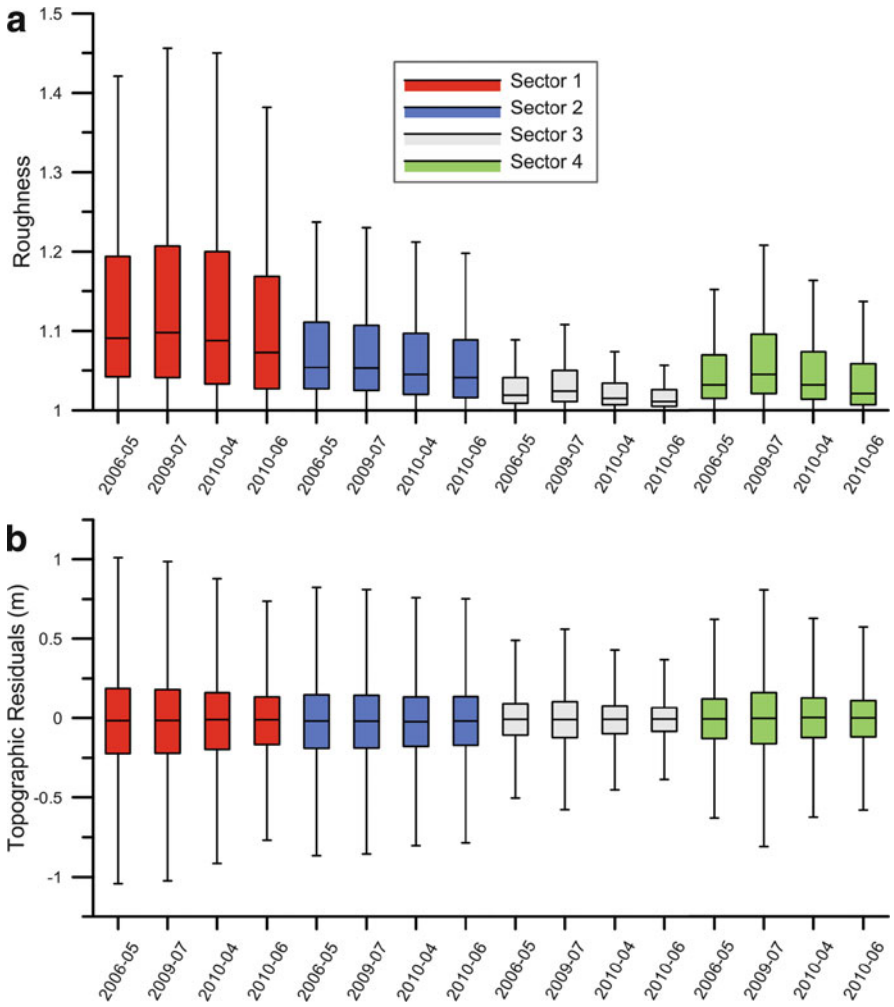


Fig. 5 *Box-plot* diagrams: (**a**) surface roughness; (**b**) RTS *horizontal bars* within *boxes* represent the median, the *tops* and *bottoms* of the *boxes* represent the 75th and 25th quantiles, and the whiskers represent the range excluding outliers

The larger variability of the surface roughness and RTS values (Fig. 6) occurs in the uppermost part of the slide (S1), where the crown surface and scarps transversely oriented to the sliding movement are located. The lower variability of these two parameters occurs in the central body of the landslide (S3), where the large scale surface shows a gentle slope and the landslide surface is characterized by small amplitude folds (Fig. 3). S2, which represents the zone of channelized flow, and S4, which incorporates the toe accumulation zone, exhibit intermediate surface roughness and RTS values. In addition to the spatial changes in the roughness and RTS values in the different ML sectors, the temporal pattern of these parameters also varies. The variation range of these two parameters decreases or maintain roughly constant in the different sectors between 2006.05 and 2010.06, even if a local increase is recognized in S3 and S4 between 2006.05 and 2009.07. The general decrease of surface roughness and RTS reflects basal sliding

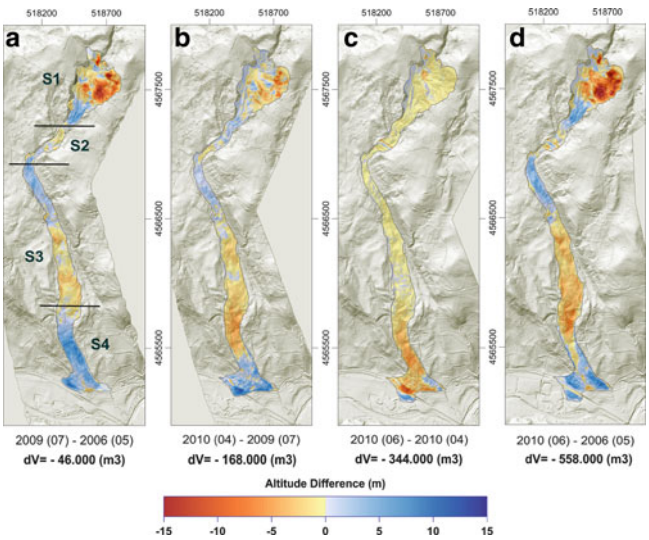


Fig. 6 Vertical displacement of ML in different time intervals

Table 1 Change in volume computed for different time intervals based on LiDAR-derived DEMs

Time interval	Erosion (m^3)	Deposition (m^3)	Volume balance (m^3)
2009 July–2006 May	494.000	448.000	−46.000
2010 April–2009 July	422.000	253.000	−169.000
2010 June–2010 April	391.000	47.000	−344.000
2010 June–2006 May	935.000	357.000	−578.000

processes, whereas the recognized increase of roughness and RTS values in S3 and S4 between 2006.05 and 2009.07 indicates a slowdown of flow. The recognized post-2009.07 decrease of the values of these parameters in S4 is mainly due to earth removal activity.

Elevation difference maps were produced by subtraction of DTMs with the aim to estimate the vertical displacement (Fig. 6). Table 1 summarizes the volumetric changes on the basis of the vertical displacement computations. In the 2006.05–2010.04 period, the crown area is mainly affected by subsidence, whereas uplift occurs in the lower zone of S1. Subsidence related to channel flows characterizes the upper zone of S2, whereas flow accumulation affects the lower zone. Between 2006.05 and 2009.07, the upper zone of S3 was characterized by prevailing accumulation from flows originated in S2, whereas the lower zone was affected by channel withdrawal. S4 was mainly affected by accumulation between 2006.05 and 2010.04 and by subsidence due to the artificial removal of material in 2010. The difference between the uplifted and subsided volumes is negative in all the considered time intervals (Table 1). Material removal explains the subsidence observed at the toe in S4, while basal sliding and runoff erosion processes justify the subsidence in S2 and S3. The analysis of DTMs allows us to estimate the average horizontal velocity along longitudinal cross sections in three ML sectors. The crown retreat rate was 53 m/year between 2009.07 and 2010.04. Between 2006.05 and 2010.04, the rate of downslope advancement of a major lobe in S1 was 11 m/year. The toe advancement rate between 2009.07 and 2010.04 was 60 m/year.

Conclusions

The multi-temporal analysis of LiDAR-derived DTMs allow us to (a) recognize different dynamic processes (rock-fall and flow) and (b) identify structures indicative of shallow or deep process (i.e., basal sliding vs. surface flow). Statistics of morphometric parameters and estimate of the volume changes shed light on the emplacement mechanism and its temporal evolution (e.g. channelized flow, ridge formation). In addition, horizontal velocities may be estimated from LiDAR data. The LiDAR multi-temporal analysis of mass movements has shown the potential to support monitoring strategies by identifying critical areas.

Acknowledgments We thank the Nuova Avioriprese Srl for the LiDAR data and V. Albanese (Dip. Prot. Civ.) for the access to the study area.

References

Burns WJ, Coe JA, Kaya BS, Lina MA (2010) Analysis of elevation changes detected from multi-temporal LiDAR surveys in forested landslide terrain in Western Oregon. Environ Eng Geosci 16:315–341

Evans SG, De Graff J (2005) Catastrophic landslides: effects, occurrence, and mechanisms. Geol Soc Am Rev Eng Geol 15:412

Grebby S, Cunningham D, Naden J, Tansey K (2010) Lithological mapping of the Troodos ophiolite, Cyprus, using airborne LiDAR topographic data. Remote Sens Environ 114:713–724. doi:10.1016/j.rse.2009.11.006

Jaboyedoff M, Oppikofer T, Abellán A, Derron MH, Loye A, Metzger R, Pedrazzini A (2010) Use of LIDAR in landslide investigations: a review. Nat Hazards. doi:10.1007/s11069-010-9634-2

Commissariato di Governo della Regione Campania (2006) Indagini geognostiche per la caratterizzazione del movimento franoso in atto nel territorio del comune di Montaguto–provincia di Avellino. Report 2006, p 42



Experiences of Debris-Flow Monitoring and Warning at Catchment Scale in the Pyrenees

Marcel Hürlimann, Claudia Abancó, and Jose Moya

Abstract

Debris-flow monitoring improves the understandings of debris flows and also provides fundamental information for an efficient early warning and alarm system (EWAS), which commonly focuses on ground vibration and flow depth. Preliminary results from the Senet station (Central Pyrenees, Spain) show that monitoring is a complex task, especially if different torrential processes should be distinguished using merely geophone data. Video images are not useful for an EWAS, but strongly improves the analysis, because they allow to identify the flow type and to characterise the ground vibrations corresponding to each type. In addition, an EWAS can also be based on triggering rainfall patterns, which have to be defined by a one-parameter o multi-parameter condition. Our first experiences on the possible implementation of an EWAS at Senet test site are promising, but indicate the complexity regarding the critical rainfall conditions, the definition of reliable thresholds to avoid false alarms and the difficulties related to technical shortcomings.

Keywords

Debris flow • Monitoring • Warning • Pyrenees

Introduction

Torrential processes like debris flows, debris floods or hyperconcentrated flows are one of the most hazardous processes in mountainous areas and provoke important economic losses and fatalities.

Data measured at debris-flow monitoring stations are of great importance to improve the understandings of triggering, flow behaviour and accumulation of these processes. There are several monitoring stations situated in the European Alps (Berti et al. 2000; Marchi et al. 2002; Hürlimann et al. 2003b; Huebl and Kaitna 2010), while other stations are located in Asia (Zhang 1993; Suwa et al. 2009) and other parts of the world (e.g. La Husen 2005).

The installation of an early warning and alarm system (EWAS) is an important topic in risk assessment and mitigation of hydrological and geological processes. Generally, an early warning system (EWS) is able to advice the stakeholders and affected people hours or even days in advance of an approaching event. Most of the recent investigations on EWS for shallow landslides and debris flows include rainfall thresholds (Aleotti 2004; Salameh et al. 2009; Baum and Godt 2010; Brunetti et al. 2010; Tiranti and Rabuffetti 2010). On the other side, an alarm system (AS) informs the stakeholders and affected persons immediately of the danger by optical or acoustic devices (e.g. light or siren). However, only very few alarm systems for torrential processes have been published in literature, and even fewer are operational (Bessason et al. 2007; Arattano and Marchi 2008; Kung et al. 2008; Badoux et al. 2009).

A total of three debris-flow monitoring stations are actually running in the Pyrenees (Hürlimann et al. 2011): the Senet and Erill sites and the Ensija site (Fig. 1).

M. Hürlimann (✉) • C. Abancó • J. Moya
Department of Geotechnical Engineering and Geosciences, Technical University of Catalonia, Barcelona, Spain
e-mail: marcel.hurlimann@upc.edu

C. Margottini et al. (eds.), *Landslide Science and Practice*, Vol. 2,
DOI 10.1007/978-3-642-31445-2_20, © Springer-Verlag Berlin Heidelberg 2013

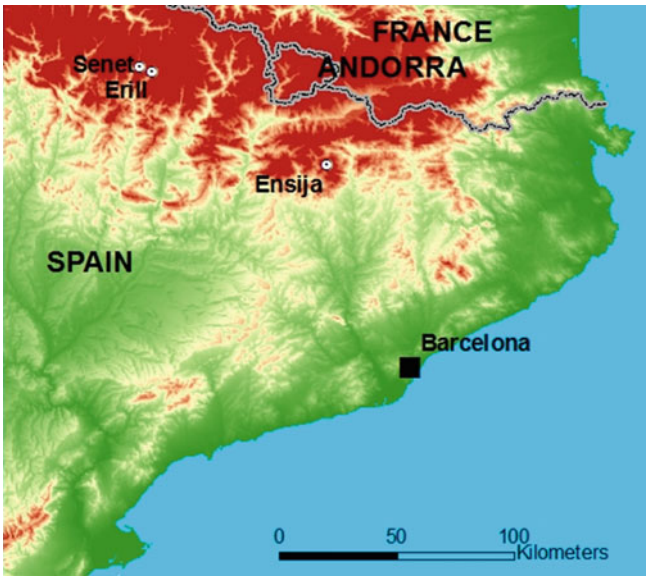


Fig. 1 Situation of the Senet test site and the other two debris-flow monitoring stations in the Central-Eastern Pyrenees

The purpose of this study is twofold. First, measurements recorded during the first 2 years of debris-flow monitoring in Senet are presented and experiences discussed. Second, implications for a future warning and alarm system are examined.

Settings

The Senet site is located in the Axial Pyrenees (Fig. 1). Bedrock consists of slates and the soil is a glacial (till) deposits.

The climate of the Central-Eastern Pyrenees is strongly influenced by two factors: the vicinity of the Mediterranean Sea and the orographic effects of the Pyrenean mountain range. The study of historic events showed that there are two typical rainfall conditions provoking debris flows in this area (Hürlimann et al. 2003a): (1) short duration, high intensity rainfalls related to convective summer storms, and (2) moderate intensity and long-lasting rainfall during autumn/winter.

Data from the first 2 years of record show that the Senet catchment is very active (the most active of the three sites monitored in the Pyrenees). Thus the majority of the results and experiences of this study concern this test site.

Description of the Monitoring

General Aspects

Two types of sensor clusters can generally be distinguished in the debris-flow monitoring. The first cluster includes meteorological sensors like a rain gauge and a thermometer,



Fig. 2 Overview of the Senet test site and the locations of the different sensors installed. *US* ultrasonic device, *VC* video camera

which can be used to analyse the initiation of the debris flows. The second cluster includes sensors related to the debris-flow detection and to the analysis of the dynamic behavior. Typical sensors for this task are geophones, devices measuring the flow depth (ultrasonic device, laser, radar etc.) and video cameras (Itakura et al. 2005; Arattano and Marchi 2008).

In conclusion, two types of sensors can be distinguished: (1) meteorological sensors, which can be used to analyze the initiation of the debris flows, and (2) sensors related to dynamic behaviour or the movement. In the following, these two types of sensor clusters will be distinguished and detailed information of the devices installed during summer 2009 in Senet is given.

Sensors Related to the Initiation

The meteorological station is located close to the upper part of the channel zone (between Geo2 and Geo3, Fig. 2). The station was originally situated near Geo1, but there it was damaged by rockfalls detached from the till.

The rain gauge is a standard tipping bucket device with a resolution of 0.1 mm. The recording interval of the meteorological sensors is defined constant as 5 min.

Because the rain gauge is unheated, the thermometer is necessary to distinguish if precipitation has been rain or snow. Nevertheless, the water equivalent of the snowfall

can only be approximated. This is an important drawback, because it has been observed that the initiation of some debris flows has been affected by snowmelt (Hürlimann et al. 2010). This is the reason why additional sensors measuring the snow height are planned to be installed.

Sensors Related to the Movement

Four geophones, one ultrasonic device and one video camera have been installed at the Senet test site in order to detect and record the movement of the flowing mass down the torrent (Fig. 2). The scan rate during an event is 1 Hz.

The geophones (GEOSPACE 20 DX-8Hz) measure the ground vibration generated by debris flows. An electronic signal conditioner, which is located next to the geophone, transforms the vibrations into a number of impulses per second (IMP/s). The geophone data can be used to estimate a mean front velocity between the different sensors. In addition, the geophones trigger the other measuring devices installed along the torrent. The initial condition for switching from the "no-event mode" into "event mode" was defined, if the ground vibration exceeded 20 IMP/s during 1 s.

The ultrasonic device measures the flow depth of a passing debris flow, but can also be used in combination with the geophone to estimate a mean flow velocity and finally a discharge. However, due to technical problems and the destruction of the sensor by a rockfall, this device was correctly running only during a few events.

Since spring 2011, a video camera (MOBOTIX M12D-Sec Dnight) is operational and provides visual information on the flow behaviour. This visual information is necessary, because geophone measurements are often not clear to distinguish between the different torrential processes like hyperconcentrated flows or debris flows.

Because of the uncertainty to determinate the exact torrential process, monitoring events were classified in four classes of likelihood (high, medium, low and null). These classes have been defined according to the ground vibration and morphologic changes in the channel (Hürlimann et al. 2011). The classes null and low may represent episodes without debris-flow behaviour, while the classes medium and high possibly correspond to debris flows or hyperconcentrated flows with a high solid concentration. These uncertainties have been eliminated by the installation of the video camera and the subsequent visual information on the flow behaviour of the processes.

Data Storage and Transmission

As mentioned above, two different clusters are installed: the "meteo-cluster" including the meteorological sensors, and the "flow-cluster" including the sensors related to the flow behaviour. Both clusters are independent and incorporate a datalogger and a GSM modem for data transmission. Each cluster is powered by a battery, which is recharged by a solar panel.

Results of the Monitoring

In the following, two types of monitoring data will be presented focussing on a future implementation into an early warning and alarm system. First, the ground vibrations recorded from the passing debris flows are discussed. This information can be used for an alarm system. Second, the critical rainfall conditions for debris-flow initiation are analysed. This information, once coupled with rainfall forecasting, can be used for an early warning system.

Analysis of Ground Vibration

During the first 2 years of monitoring (from August 2009 until May 2011), 74 different events have been recorded. Figure 3 shows that most of these events occurred during summer.

One of the major challenges in monitoring and alarm systems of debris flows is the differentiation between true events and false alarms. This task is of particular difficulty, if only ground vibration measurements by geophone are used.

In Senet, between July 2009 and July 2010, the monitoring system triggered 296 events, from which 237 were clearly false events. False events have been provoked by technical problems or other phenomena not related to torrential processes (Fig. 4). In August 2010, an important improvement has been introduced in the system and the amount of false events has strongly been reduced. The threshold of ground vibration was enlarged from 1 to 3 s, which means that during 3 s a minimum vibration of 20 IMP/s must be recorded to switch the system to "event-mode".

The ground vibration at the four geophones have been analysed for more than 100 events and some general conclusions could be obtained. Important differences of the ground response could be observed for each geophone even during the same event. These differences can be associated with different morphological and geological situations and also the different distances between geophone and active channel. An example of these differences could be observed during the debris flow occurred on July 11, 2010 (Fig. 5).

In spite of all these drawbacks, general preliminary correlations of ground vibrations could be established. An example of such a relation is shown in Fig. 6, where the duration of the registered ground vibration is compared with the maximum value of impulses per second.

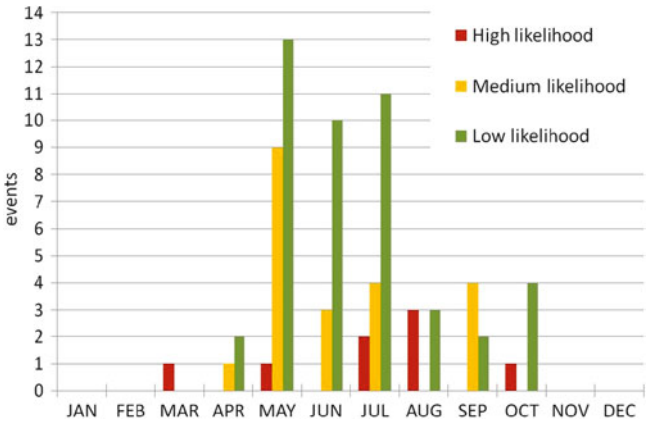


Fig. 3 Monthly distribution of the events recorded in the Senet monitoring site

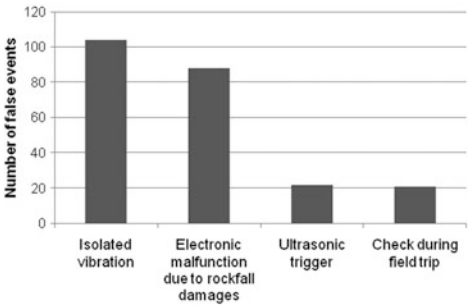


Fig. 4 Causes of false events during the first-year test period

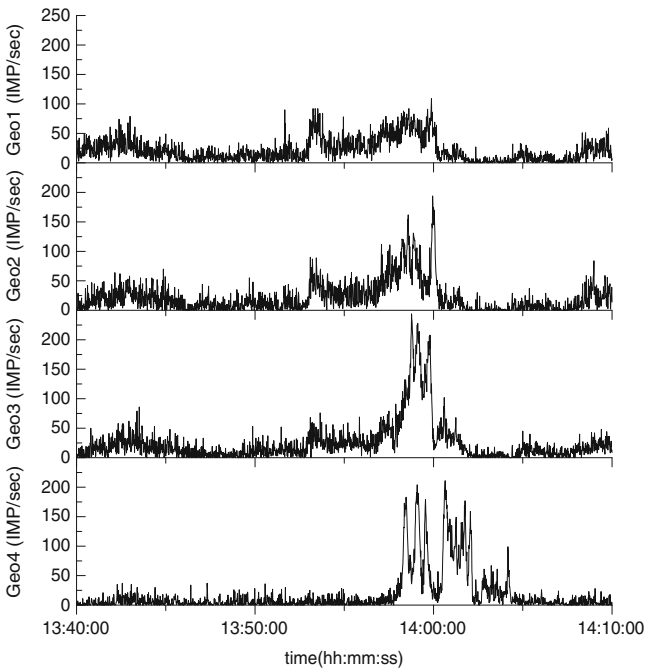


Fig. 5 Geophone data recorded during event on July 11, 2010

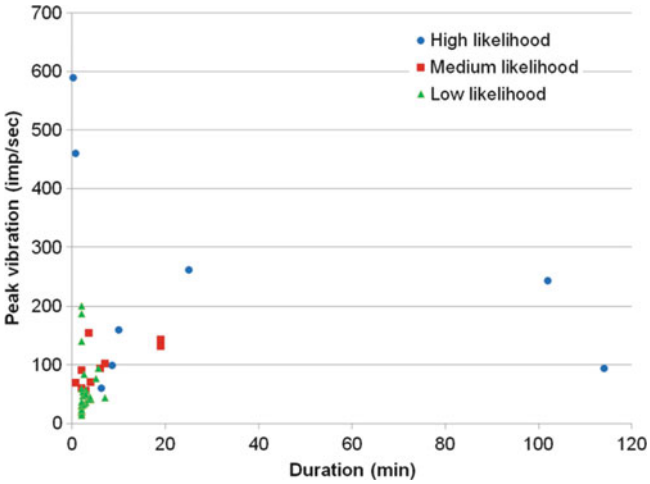


Fig. 6 Duration of ground vibration versus maximum value of impulse per second measured at the four geophones distinguishing between different likelihood classes

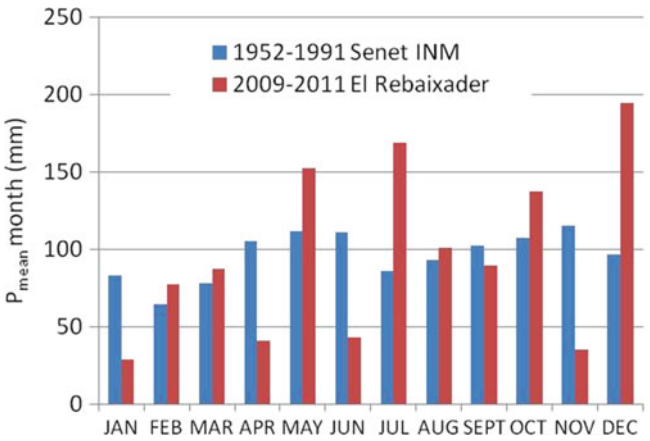


Fig. 7 Mean monthly rainfall. Comparison between historic values measured at Senet station by the National Agency of Meteorology (INM) and the recent values recorded in our catchment (Rebaixader)

Analysis of Critical Rainfall

As indicated in Fig. 3, most of the triggering events occurred during summer and they cannot be related to the monthly rainfall distribution of the area (Fig. 7).

In order to establish the critical or limiting rainfall conditions, the rainfall characteristics that provoked a torrential process (herein called "event") have been compared with other rainfalls that did not trigger an event (herein called "no-events"). Finally, a total of 15 "no-event" and 22 "events" have been compared.

The analysis of all these rainfall episodes shows several general trends. Total rainfall amounts for debris-flow triggering are very variable and range from less than 10 mm up to almost 100 mm (Fig. 8). The surprising small total rainfall of about 10 mm can mostly be explained by

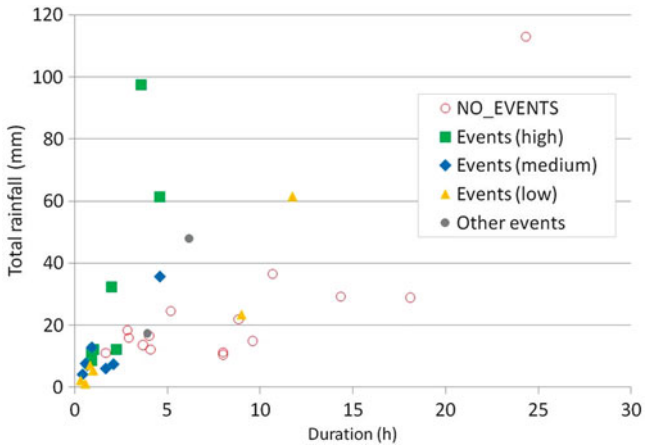


Fig. 8 Rainfall duration versus total rainfall distinguishing events with different likelihood

antecedent rainfall (see below) or additional water input due to snowmelt (Hürlimann et al. 2010).

The results also indicate that the rainfalls, that triggered debris flows in the Senet catchment, lasted generally only a few hours and had mostly a high hourly intensity, between ~5 and ~50 mm/h (Fig. 9a). However, the data indicate that a smaller recording interval (e.g. 5 min) better reveals the characteristics of the short duration and high-intensity triggering rainfalls (Fig. 9b).

In addition, the antecedent rainfall has been analysed, because there are several studies proposing the influence of this factor on landslide initiation (e.g. Guzzetti et al. 2008). Here, the antecedent intervals of 1, 3, and 10 days have been analysed. These intervals have been selected after a simple hydrological calculation including the concentration time and the subsurface flow in the till deposit, which revealed that the maximum time of 10 days should be a realistic duration for the water reaching the main scarp of the debris-flow source zone.

The results of Senet show that the effect of antecedent rainfall on debris-flow triggering is not clearly visible (Fig. 10). However, a general trend of smaller intensity of the triggering rainfall can be observed for larger amounts of antecedent rainfalls. This trend is better visible for an antecedent rainfall interval of 10 days.

Implications for a Warning and Alarm System

As previously mentioned, two types of data must be analysed previously to the design of the early warning and alarm system. On one side the critical rainfall conditions must be defined for the EWS, which could advise the stakeholder person hours before a possible event. On the other side, critical ground vibration and/or flow depth have to be delimited for the alarm system (AS), which should emit an

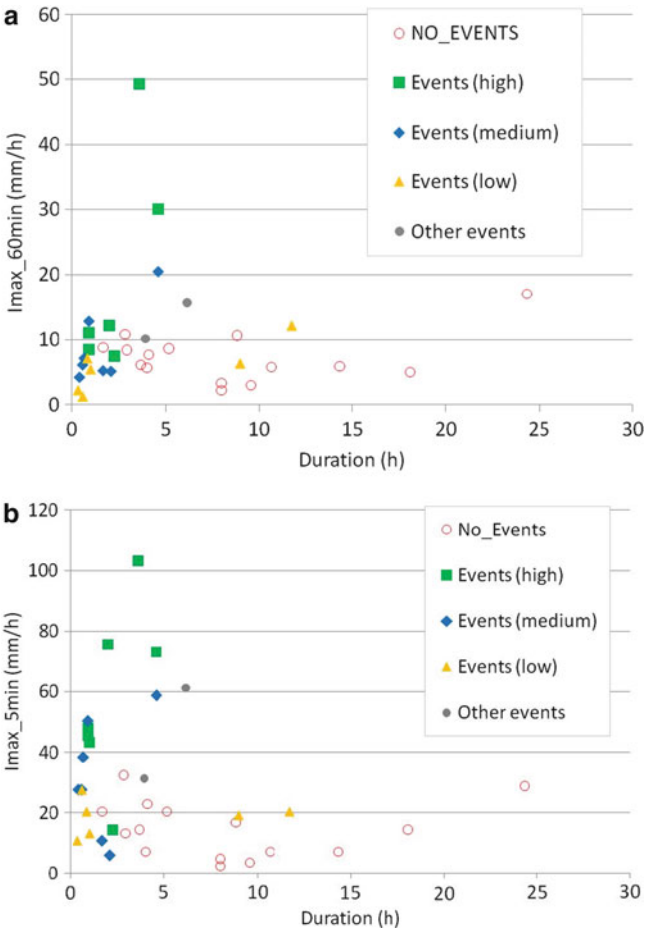


Fig. 9 Rainfall duration versus maximum hourly rainfall (**a**) and maximum 5-min rainfall (**b**) distinguishing events with different likelihood

alarm by optical or acoustic devices (e.g. lights or siren). In the following, first, the critical rainfall conditions for and EWS in Senet will be discussed. Then, the critical ground vibration will be analysed. Finally, some other conclusions and experiences from the Senet test site will be described.

Critical Rainfall for Warning

As demonstrated in the previous section and also published by other authors (e.g. Aleotti 2004), two types of rainfall information should be distinguished for an early warning system: (1) the antecedent rainfall; and (2) the triggering or event rainfall.

The effect of antecedent rainfall, however, is very site specific and strongly depends on the lithological, morphological and hydrological characteristics of a catchment. Alternatively, there are studies that indicate the irrelevance of antecedent rainfall on debris-flow triggering. In the case of Senet, a slight trend could be observed and the effect of antecedent rainfall may be included into a warning system.

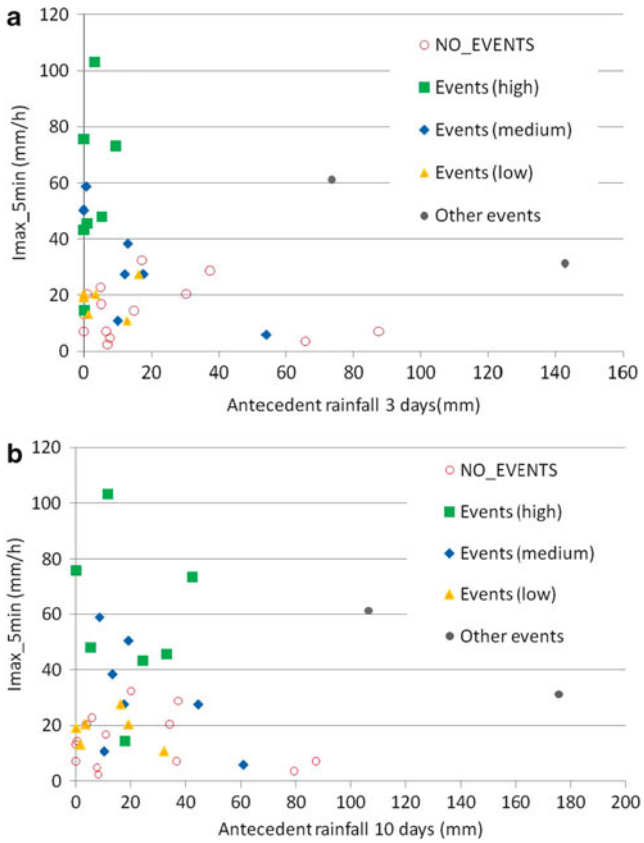


Fig. 10 Effect of antecedent rainfall for the initiation of debris flows in the Senet catchment. (**a**) 3-day antecedent rainfall and the maximum 5-min triggering rainfall, (**b**) 10-day antecedent rainfall and the maximum 5-min triggering rainfall

In contrast, the triggering rainfall related to short-duration and high intensity rainstorms are easier to incorporate into an EWS. The most common implementation is the use of an empirical rainfall threshold combining duration and mean intensity (e.g. Guzzetti et al. 2008; Brunetti et al. 2010). The data gathered in Senet during the first 2 years provide first important information on the rainfall conditions, which can trigger debris flows. The Senet data are coinciding with other published data (Deganutti et al. 2000; Badoux et al. 2009), but do not yet allow the determination of a reliable threshold (Fig. 11).

Critical Ground Vibration for Alarm

The Senet data indicate that the definition of a threshold for critical ground vibration is a very complex task. In particular, the short time available between the initiation of ground vibration and the decision between "true event" or "false event" complicates the correct functioning of an alarm system.

The experiences gathered in Senet indicate that a ground vibration of a duration of at least 3 s may be adequate in order to avoid false alarms.

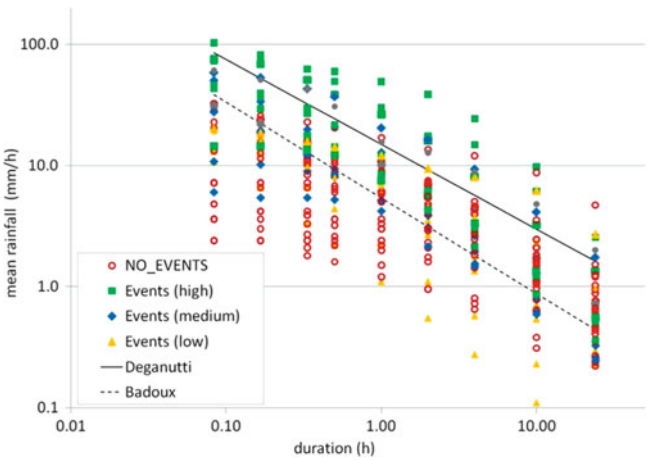


Fig. 11 Duration-intensity plot of the critical rainfalls observed at Senet and comparison with thresholds published (Deganutti et al. 2000; Badoux et al. 2009)

A similar condition is actually applied in the Illgraben alarm system, where a predefined number of impulses per second during 5 s must be exceeded to trigger the alarm (Badoux et al. 2009). A more sophisticated system is used in the West Fjords region in Iceland (Bessason et al. 2007), which distinguishes processes (rockfall, debris flows etc.) by analysing the ground vibration.

In addition, other sensors measuring the flow depth may complete and improve the alarm system, but also increase installation efforts and costs.

Application of Wireless Technique

Our experiences show that wireless technique would strongly improve the trouble-free function of an EWAS. There are two principal advantages of a wireless sensor network to traditional sensor networks. First, they have generally a safer data transmission, because there is no possible cable breakdown due to landslides, vandalism etc. Second, a wireless network can generally be installed easier and faster, because no cable connections between devices are necessary.

The application of wireless technique in the monitoring of natural hazards is nowadays a major and novel research task at international level (Nittel et al. 2008). Nevertheless, there are only very few studies related to wireless techniques and the mitigation of torrential processes (e.g. Cho et al. 2008; Lee et al. 2010).

Conclusions

The installation of early warning and alarm systems is an important topic in risk assessment and the mitigation of geological processes.

The data and experiences collected at the Senet monitoring site show that a sophisticated EWAS should consist of two parts: (1) an early warning module focussing on the critical rainfall, and (2) an alarm module focussing on ground vibration.

There are several regions where empirical rainfall thresholds have been incorporated into a debris-flow or landslide warning system (e.g. Wilson 2004), but all of these systems include important uncertainties. New technologies and sensors may improve these systems crosschecking rainfall measurements at a rain gauge with the data from weather radars (e.g. Cheung et al. 2006) or sensors related to soil moisture (e.g. Baum and Godt 2010).

The geophone measurements seems to be very site specific, but the preliminary results show that most of the false alarms can be avoided by an selection of an adequate vibration intensity and duration. However, more investigation is necessary in order to establish clear thresholds (not only for the duration, but also for the vibration intensity) in order to achieve a reliable alarm system.

Acknowledgments The Senet monitoring site was funded by the Spanish Ministry of Science and Innovation, contract CGL2008-00299/BTE (project DEBRISCATCH). Support from the EC FP7 projects IMPRINTS and SafeLand, is also acknowledged.

References

Aleotti P (2004) A warning system for rainfall-induced shallow failures. Eng Geol 73(3–4):247–265

Arattano M, Marchi L (2008) Systems and sensors for debris-flow monitoring and warning. Sensors 8(4):2436–2452

Badoux A, Graf C, Rhyner J, Kuntner R, McArdell B (2009) A debris-flow alarm system for the Alpine Illgraben catchment: design and performance. Nat Hazards 49:517–539

Baum RL, Godt JW (2010) Early warning of rainfall-induced shallow landslides and debris flows in the USA. Landslides 7(3):259–272

Berti M, Genevois R, La Husen R, Simoni A, Tecca PR (2000) Debris flow monitoring in the Acquabona watershed on the Dolomites (Italian Alps). Phys Chem Earth 25(9):707–715

Bessason B, Eiriksson G, Thorarinsson O, Thorarinsson A, Einarsson S (2007) Automatic detection of avalanches and debris flows by seismic methods. J Glaciol 53(182):461

Brunetti MT, Peruccacci S, Rossi M, Luciani S, Valigi D, Guzzetti F (2010) Rainfall thresholds for the possible occurrence of landslides in Italy. Nat Hazards Earth Syst Sci 10(3):447–458

Cheung SPY, Wong MC, Yeung LHY (2006) Application of rainstorm nowcast to real-time warning of landslide hazards in Hong Kong. WMO PWS workshop on warnings of real-time hazards by using nowcasting technology, Sydney, Australia, p 21

Cho CY, Chou PH, Chung YC, King CT, Tsai MJ, Lee BJ, Chou TY (2008) Wireless sensor networks for debris flow observation, 2008. In: 5th annual IEEE communications society conference on Sensor, Mesh and Ad Hoc communications and networks, SECON, San Francisco, CA, pp 615–617

Deganutti AM, Marchi L, Arattano M (2000) Rainfall and debris-flow occurrence in the Moscardo basin (Italian Alps). In: Wieczorek GF, Naeser ND (eds) Debris-flow hazards mitigation, Balkema, Rotterdam, pp 67–72

Guzzetti F, Peruccacci S, Rossi M, Stark CP (2008) The rainfall intensity-duration control of shallow landslides and debris flows: an update. Landslides 5:3–17

Huebl J, Kaitna R (2010) Sediment delivery from the Lattenbach catchment by debris floods and debris flows. EGU General Assembly, 2–7 May 2010, Vienna, Austria, p 10585

Hürlimann M, Corominas J, Moya J, Copons R (2003a) Debris-flow events in the Eastern Pyrenees. Preliminary study on initiation and propagation. In: Rickenmann D, Chen C (eds) 3rd international conference on debris-flow hazards mitigation, Davos, pp 115–126

Hürlimann M, Rickenmann D, Graf C (2003b) Field and monitoring data of debris-flow events in the Swiss Alps. Can Geotech J 40 (1):161–175

Hürlimann M, Abancó C, Moya J (2010) Debris-flow initiation affected by snowmelt: case study of the Senet monitoring site, Eastern Pyrenees. A. Mountain risks: bringing science to society. In: Proceedings of the mountain risks international conference, Florence, Italy, 24–26 Nov 2010, pp 81–86

Hürlimann M, Abancó C, Moya J, Raïmat C, Luis-Fonseca R (2011) Debris-flow monitoring stations in the Eastern Pyrenees. Description of instrumentation, first experiences and preliminary results. In: 4th international conference on debris-flow hazards mitigation, Padua (in press)

Itakura Y, Inaba H, Sawada T (2005) A debris-flow monitoring devices and methods bibliography. Nat Hazards Earth Syst Sci 5(6):971–977

Kung HY, Ku HH, Wu CI, Lin CY (2008) Intelligent and situation-aware pervasive system to support debris-flow disaster prediction and alerting in Taiwan. J Netw Comput Appl 31(1):1–18

La Husen R (2005) Debris-flow instrumentation. In: Jakob M, Hungr O (eds) Debris-flow hazards and related phenomena. Springer, Berlin, pp 291–304

Lee HC, Banerjee A, Fang YM, Lee BJ, King CT (2010) Design of a multifunctional wireless sensor for in-situ monitoring of debris flows. IEEE Trans Instrum Meas 59(11):2958–2967

Marchi L, Arattano M, Deganutti AM (2002) Ten years of debris-flow monitoring in the Moscardo Torrent (Italian Alps). Geomorphology 46(1–2):1–17

Nittel S, Labrinidis A, Stefanidis A (2008) GeoSensor Networks. In: Second international conference, lecture notes in computer science, vol 4505. Springer, Berlin, Boston, MA, USA, p 271

Salameh T, Zêzere J, Trigo R (2009) Development of an early warning system for precipitation triggered landslides in Portugal, EGU General Assembly 2009. Geophys Res Abstr, Vienna, p 2458

Suwa H, Okano K, Kanno T (2009) Behavior of debris flows monitored on test slopes of Kamikamihorizawa Creek, Mount Yakedake. Jpn Int J Erosion Control Eng 2:33–45

Tiranti D, Rabuffetti D (2010) Estimation of rainfall thresholds triggering shallow landslides for an operational warning system implementation. Landslides 7(4):471–481

Wilson RC (2004) The rise and fall of a debris-flow warning system for the San Francisco Bay Region, California. In: Glade T, Anderson MG, Crozier MJ (eds) Landslide hazard and risk. Wiley, Chichester, pp 493–516

Zhang S (1993) A comprehensive approach to the observation and prevention of debris flows in China. Nat Hazards 7:1–23



Setup of a Landslide Monitoring System on the Philippine Island of Leyte Near the Village of Malinao (Municipality of St. Bernard)

Christian Arnhardt and Olaf Neussner

Abstract

This article describes the setup and first results of a landslide monitoring system near the village of Malinao, municipality of St. Bernard on the Philippine Island of Leyte. The monitoring system combines wireless sensor network (WSN) technology with low-cost but precise micro sensors (MEMS). The system was developed in the framework of the joint project "SLEWS—A Sensor-based Landslide Early Warning System" that deals with the development of a prototype Alarm- and Early Warning System (EWS) for different types of landslides. The sensors integrated in the WSN are acceleration sensors, tilt sensors and barometric pressure sensors. The system was installed in November 2010 in a landslide prone area near the village of Malinao. For longer data transmission of about 15 km the SLEWS-System was combined with the already existing WLAN-based monitoring system for Flood Early Warning (FEWS) from the *Deutsche Gesellschaft für Internationale Zusammenarbeit* (GIZ).

Keywords

Landslide • Landslide monitoring • Wireless sensor networks (WSN) • Micro sensors (MEMS)

Introduction

Natural hazards are part of everyday life in the Philippines. With the occurrence of volcanic eruptions, earthquakes, floods, storms, typhoons and landslides, the bandwidth of natural hazards is manifold. Landslides are frequent in the Philippines and are triggered especially by rainfall and to some extent by earthquakes.

One of the biggest landsides occurred in February 2006. In Southern Leyte a huge rock avalanche destroyed the village Guinsaugon (municipality of St. Bernard) (Fig. 1). The disaster happened after 10 days of heavy rainfall and a minor earthquake of magnitude 4.3 on the Richter Scale (Evans et al. 2007). Over 1,100 people perished when the village of Guinsaugon was overwhelmed directly in the path of the landslide (Fig. 1).

In 2010 new cracks were observed at a slope about 850 away from the small village of Malinao. This village lies about 5.0 km in the north of the Guinsaugon landslide with similar topographic and geological settings. Furthermore, a new open crack of about 7.0 m in length, a width of about 1.0 m and a depth of about 1.5 m was detected in November on the left flank of the potential sliding area. Thus, clear hints existed for a slope movement in this area

Due to the new cracks and deformations the analysis of the potential landslide risk and the threat for the village Malinao became of main interest.

In cooperation with the ***Deutsche Gesellschaft für Internationale Zusammenarbeit (GIZ)*** and the ***Department***

C. Arnhardt (✉)
Department of Engineering Geology and Hydrogeology (LIH), University of Aachen, Aachen, Germany
e-mail: carnhardt@arcor.de

O. Neussner
Deutsche Gesellschaft für Internationale Zusammenarbeit GmbH (GIZ), Disaster Risk Management in the Eastern Visayas, Tacloban City, Leyte, Philippines

C. Margottini et al. (eds.), *Landslide Science and Practice*, Vol. 2,
DOI 10.1007/978-3-642-31445-2_21, © Springer-Verlag Berlin Heidelberg 2013



Fig. 1 Guinsaugon landslide (Evans et al. 2007)

of Engineering Geology and Hydrogeology (LIH) of the RWTH Aachen University, a landslide monitoring system was installed in this area in November 2010.

The Landslide Monitoring System SLEWS

In the framework of the joint project "SLEWS—A Sensor-based Landslide Early Warning System", a prototype monitoring system for the detection of movement processes and deformations in landslide areas was developed at the LIH. It combines the modern technology of wireless sensor networks with low cost but precise micro sensors (MEMS). The developed wireless sensor network for landslide monitoring is characterized by a self-organizing (ad-hoc), energy-saving structure, with bi-directional wireless communication in real-time. The main components of the system are described in the following sub-sections.

The Used Wireless Sensor Network

Modern, so called ad-hoc wireless sensor networks (WSN) are characterized by a self organization and self-healing capacity of the system (autonomous systems), without predefined infrastructures (Arnhardt et al. 2008). The use of a wireless system eliminates the need of extensive cabling outside in the monitored area and so reduces material costs and increases system reliability. The sensor network used in this project uses the licence free 868 MHz frequency band for sending radio signals (ISM band). The frequency band is divided in further 30 sub-bands to avoid noisy channels. Data rates range from 4.8 to 115 kbits/s at transmission distances from 10 m to 1.2 km.

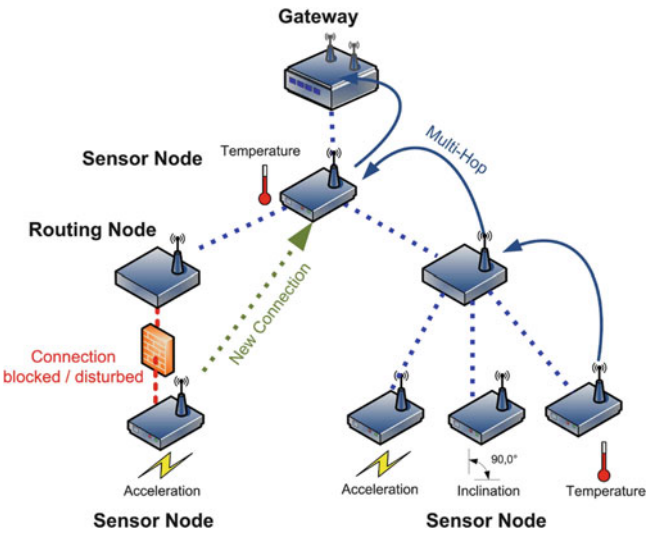


Fig. 2 The-SLEWS wireless sensor network with many sensor nodes and routing nodes and a data collection point (gateway)

The network consists of numerous sensor nodes (or motes) that can interact with neighbour nodes (Fig. 2) and perform simple data processing.

Data packages from each node are sent via radio directly or over other nodes (Multi-Hop) to a collection point (gateway). Data transfer is performed by time-synchronized communication and depending on connection and connection strength each sensor node is able to search individually the best link to other points of the network. This helps also to avoid the failure of the system even if some of the nodes break down. The bidirectional structure of the system enables data transfer from each node over the gateway-interfaces to the main computer unit (PC, Laptop, Server), but also allows to transmit commands like data requests as well as software-updates and add-ons to individual nodes or a group of nodes. The modular setup of the hardware used allows an easy adaption or integration in existing solutions. The main components of the system are:

- Sensor nodes (with sensor board) for data transfer with integrated sensor for detecting different movement processes in the landslide area
- Gateway for data collection and data transmission to the data processing unit (i.e. gateway control server) outside of the landslide area
- Gateway control server for data processing, analyzing and information forwarding to different end-users and applications.

Sensor Nodes and Integrated Measuring Sensors

For the detection and direct monitoring of different kinds of landslide processes and deformations, a new sensor board

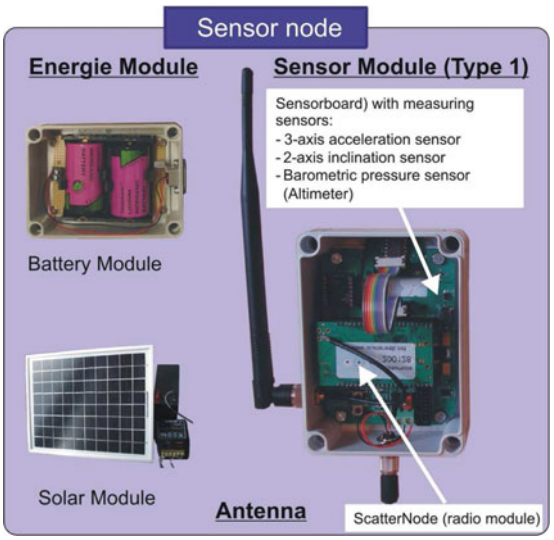


Fig. 3 The SLEWS sensor node, consisting of the sensor module, antenna and energy module

was developed, that includes the measuring sensors and the radio module for data and command transfer in the WSN (Fig. 3).

Antenna, sensor board and energy supply represent one sensor node and are own units of the system. Each is protected against weather influence by a robust box (protection class: IP 66). For the energy supply a battery pack (3 × 3.6 V batteries), a single battery with 12 V power supply or a solar panel with rechargeable battery (12 V) can be used.

To fulfill the requirements of low energy consumption, small size, low-cost but also high precision, accuracy and data stability, micro sensors, so called ***Micro-Electro-Mechanical Systems (MEMS)*** were selected. Technical progress allows to increasingly manufacture sensors on a microscopic scale as micro sensors that are using the MEMS technology (Fraden 2004).

The chosen 3 axis acceleration sensor has an digital SPI interface, with a sensitivity of 1,333 counts/g, acceleration range of ±2 g, Operating temperature from −40 ° to 125 °C, bandwidth of 45 Hz and a low current consumption of 480 μA by 2.5 V. Main task of this sensor is the detection of speed changes and vibration (dynamic processes), but also static accelerations (tilting) in landslide areas.

The inclination sensor or tilt sensor (inclinometer or tiltmeter) is a 2-axis measuring sensors and has a digital SPI interface, with a bandwidth of 8–28 Hz, an operating temperature of also −40° to +125 °C and a current consumption of about 4 mA by 5 V. As nearly all ground movement exhibits some degree of rotation and tilting (Applied Geomechanics 2008), this sensor is used to detect inclination and toppling processes.

The digital absolute barometric pressure sensor has a resolution of 1.5 Pa with a low <10 μA current consumption

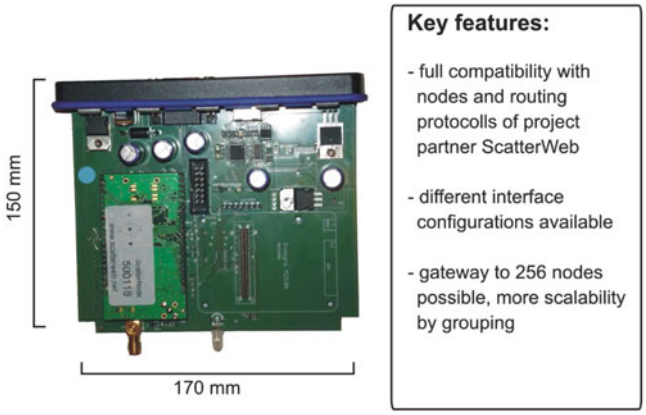


Fig. 4 Circuit board of the SLEWS-gateway

and is used for measuring sub-meter height changes (altimeter). The measuring range goes from 30 to 120 kPa, with a operating temperature from −20 °C to +70 °C. The relative pressure accuracy is specified with ±50 Pa. It also has a standard SPI digital interface and an internal temperature device. Typical applications of this sensor are barometric pressure measurement and altimeter applications, usage for home weather stations, medical applications and level gauging.

Data Collection Point (Gateway)

A gateway, also called protocol converter, is a network point that acts as an entrance to another network, which uses different protocols (Castillo-Effer et al. 2004). In a wireless sensor network the gateway has a key role, as all the data from the sensor nodes congregate in this point. In contrast to the single sensor nodes, a failure of the gateway can lead to the collapse of the whole system. Thus, the functionality of the gateway must be guaranteed. To reach this, stable gateway technology and protocols but also a sufficient energy supply are necessary. Another possibility is the usage of a reserve-gateway that can take over the functionality, if the other gateway is not working anymore.

The SLEWS gateway allows data gathering from the SLEWS sensor network, as well as sending configuration commands to single nodes or to larger groups (bi-directional communication). The used SLEWS-gateway can handle up to 256 nodes. To build larger networks, gateways can be clustered. The hardware of the SLEWS-gateway consists of a radio module on a circuit board with electronic components and different interfaces like RS232, USB, Ethernet, WLAN or GSM (Fig. 4).

One possibility for data-transfer from the gateway to computer, laptop or other processing unit, is the direct cable plug-in via USB-connection or RS232 interface. Another option is the data transfer by using radio

communication. A GSM-modem can be installed on the gateway board. Via commercial SIM-card plugged in the GSM-modem, data from the WSN in the field can be send with mobile radio communication (GSM) to the gateway control server (see next section) for further data processing.

Energy supply via solar panel and battery or direct connection via main adapter (12 V) to the normal power socket for example in a building are possible.

Gateway Control Server

The components of the WSN do not possess an extended structure for network and internet communications or differentiated mechanisms for data processing. Nodes and gateway itself allow only fundamental functions for network processing in order to ensure high energy efficiency for the sensor network. Therefore, the development of a more sophisticated controlling level was necessary.

The development of a modular gateway- or control-server allows the communication of different client applications with the gateway of the WSN and thus also the integration in other databases. The Multi Client Module enables the communication between client and gateway with TCP/IP socket, while the Data Logger Module in a SQLdatabase. The TCP/IP sockets and the database provide an interface for various project partners. Bidirectional communication with the network was implemented. Furthermore, local software allows access to the network and database environment for sensor tests and calibration of sensor nodes.

Installation of the SLEWS Monitoring System Near the Village of Malinao

Site of the Location

This village of Malinao is located in the South of the Philippine Island of Leyte (Fig. 5). It lies about 5.0 km in the north of the Guinsaugon landslide with similar topographic and geological settings.

Due to the new appeared structures and deformations along a slope about 850 m away from this village, the analysis of the potential landslide risk and the threat for the village Malinao was of main interest.

System Setup

From 18.11.2010 until 23.11.2010 the SLEWS System was setup at the potential landslide area near Malinao (Fig. 6) together with the Philippine engineering company GTek.

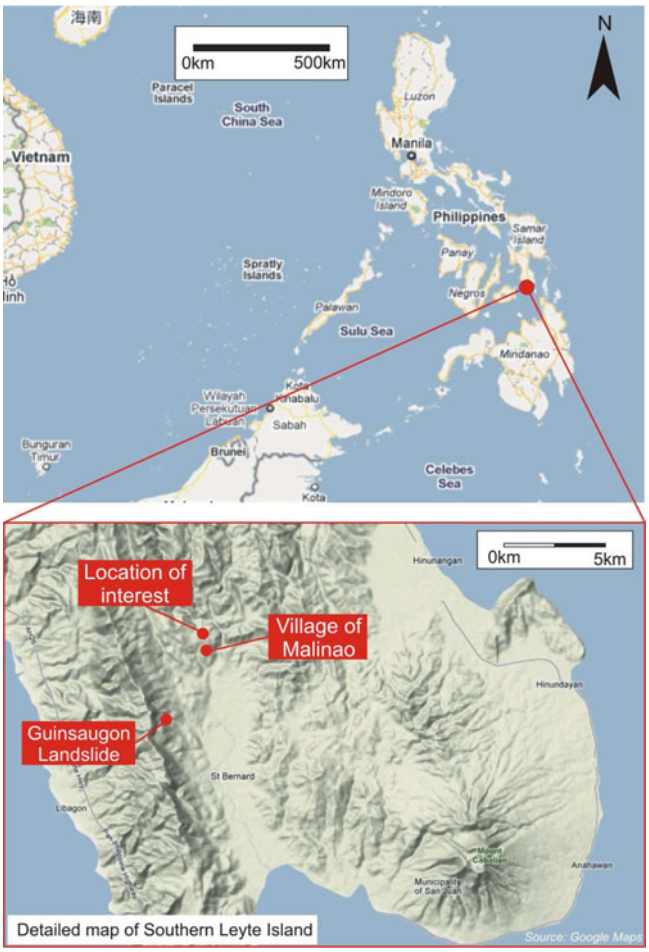


Fig. 5 Overview map, showing the Guinsaugon landslide, village of Malinao and the location, where the system was installed

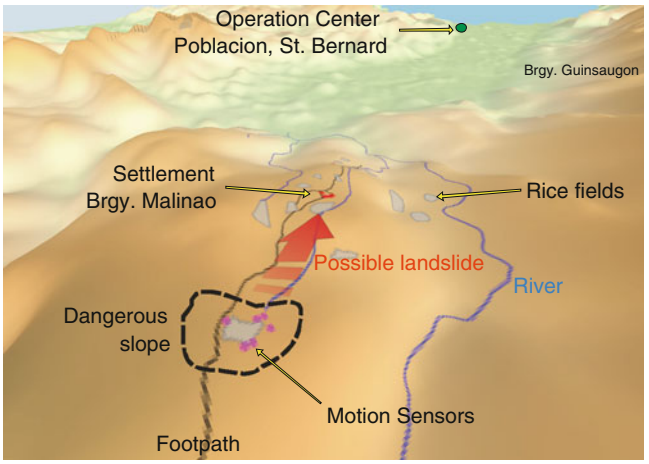


Fig. 6 Location of the dangerous slope, the endangered settlement of Malinao and the operation centre in St. Bernard

All sensor nodes were placed near bigger cracks and fissures in the field. In total five sensor nodes were installed in the region (Fig. 7).

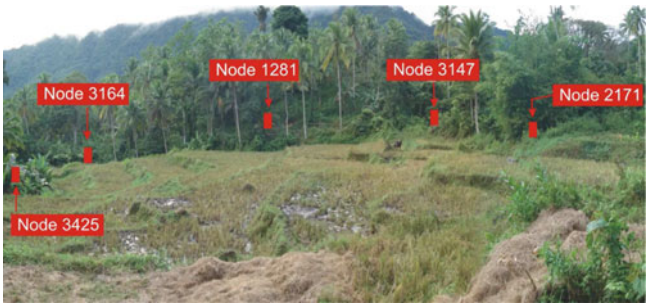


Fig. 7 Positioning of the sensor nodes in the potential landslide area in the north of Malinao. Picture is taken from the position of the gateway. Setup of the sensor nodes in the field

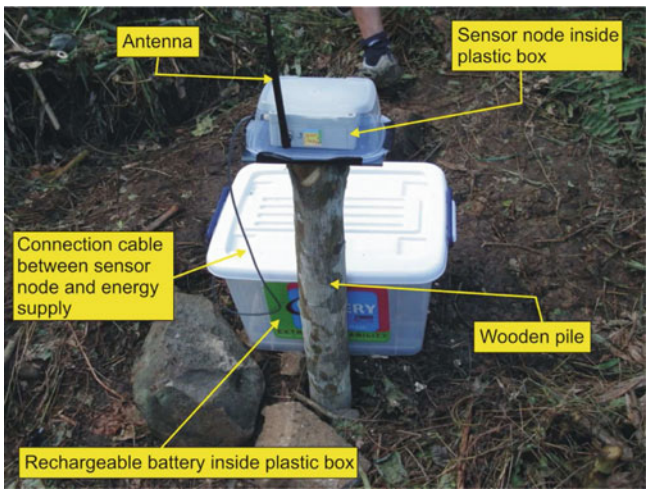


Fig. 8 Setup of the sensor nodes in the field

Each measuring point consists of the node itself and antenna (Fig. 8). For two nodes an antenna extension cable was used to mount the antenna higher and thus allow a better connection and communication with the network. Each sensor node was fixed on a small plastic plate that was again mounted with nails on a wooden pile. Every wooden pile has a length of about 1.5 m and was rammed up to 1.0 m to the ground (Fig. 8). Due to this construction, displacements and tilting of the piles resulting from the ground movement can be detected and thus give direct information about the activity in the region. When the whole area starts moving, all the installed devices should show changes in there measured data from the different sensors. Thus the sum of data changes from many nodes gives spatial information about the moving sites in this area.

Furthermore this easy setup also allows the relocation of the sensor nodes to other places, if more activity is observed there. Thus a very flexible and adaptable monitoring is possible. For the energy supply a 12 V, 20 Ah rechargeable battery was used for each sensor node. The batteries were connected via a small cable with the sensor node (Fig. 8).

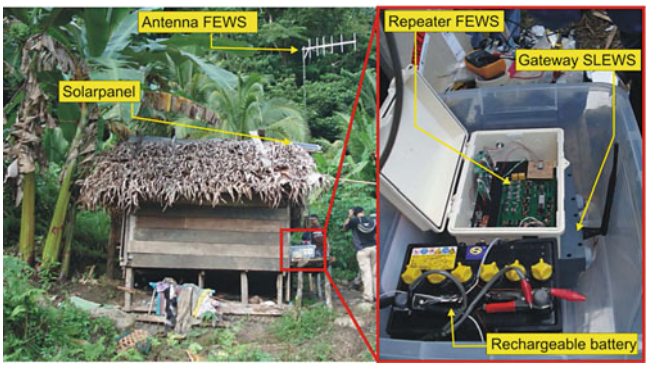


Fig. 9 Setup of the gateway in the potential landslide area and connection with the FEWS repeater of the GIZ

For further protection against strong rainfall, battery and node were placed each in a small plastic box.

Because the maximum data transmission range from node to node or rather from node to data collection point (gateway) is <1 km (under natural outer conditions <500 m is more realistic), it was not possible to send the data directly from the potential Malinao landslide area to the about 15 km away control centre in the St. Bernard Municipal Hall. Therefore the SLEWS-gateway was placed in the field near the sensor nodes and was connected directly with a repeater from the already working ***Flood Early Warning System (FEWS)*** of the GIZ. For a stable linkage between these two devices different adaptations were necessary. For better protection against heavy rainfall, both SLEWS-gateway and FEWS-repeater were positioned in one plastic box together with a rechargeable battery for energy supply (Fig. 9).

Via the repeater of the GIZ Flood Early Warning System, data from the SLEWS sensor network were sent to the appropriate transceiver of the flood early warnings system that was sited at the operation centre (OC) in the municipal hall of St. Bernard.

In St. Bernard at the OC a laptop using Linux was installed. On this system the Gateway-Control-Server for receiving, preparation, storage and visualization of SLEWS data was established. Furthermore, date from the OC in St. Bernard was forwarded via internet-connection to the MySQL-database in Aachen. In Aachen a second date storage, but also data transformations from raw-data to measuring data with unit-values (degree, acceleration and pressure) and data analyses took place. This rather circuitous way was chosen, as a specific database management system did not exist on the laptop at the OC and could not be implemented during this short stay. However, this required on the other side a stable internet-connection to enable a synchronisation of the databases in St. Bernard and Aachen.

The connection between sensor network at the site and operation centre was established by GIZ via the directional radio setup (i.e. repeater FEWS and receiver FEWS).

All functionalities of the SLEWS-server had to be adjusted specifically in situ for the system. Thus different adaptations and changes were done during the installation to allow the running of the gateway server also under the conditions of the St. Bernard network structure.

First data from the sensors at the potential landslide area in Malinao were received at the Municipal Hall in St. Bernard on November 23rd. The data-transmission to Aachen worked, too.

Experiences and Difficulties

One of the biggest challenges during this installation was the combination of the two systems SLEWS and FEWS in a very short time of less than 10 days. Apart from field observation, and installation of the sensor nodes in the potential landslide area, adaptation and calibration between SLEWS-gateway and FEWS-repeater on one side and configuration between FEWS-receiver and SLEWS-gateway control server had to be done. Only the close collaboration between GIZ, LIH and local experts and authorities made this possible. Even though it was possible to receive measuring data from the sensors in the field at the Operation Centre in St. Bernard, various difficulties occurred, that could not be solved during this short time period. As the devices of the FEWS only enable one-way communication, bi-directional communication of the SLEWS system was not possible any more. Thus, remote control and steering of the system was not possible after setup. In addition, a precise adaptation of transmission rate and package size was not possible. Trough this the missing of single data streams occurred and led to gaps in the data values. Also the local network and special network services (DHCP) were not working properly. Thus, the communication between Gateway Server and local network were interrupted. As no stable internet-connection could be setup during that time, no stable data synchronization with the database in Germany was possible.

Due to these difficulties, but also the time delay in process of establishing directional radio setup, the testing phase and configuration of data preparation and visualization was very short and could not be analyzed for longer time periods.

Measuring Results

The following Figs. 10 and 11 are two examples of measuring data that arrived from the potential landslide area in Malinao (Philippines) in the database in Aachen (Germany). As it can be seen, bigger gaps between the measuring values exist, that result from different problems described above. In total, no changes in the data values could be observed during the measuring period until December The already

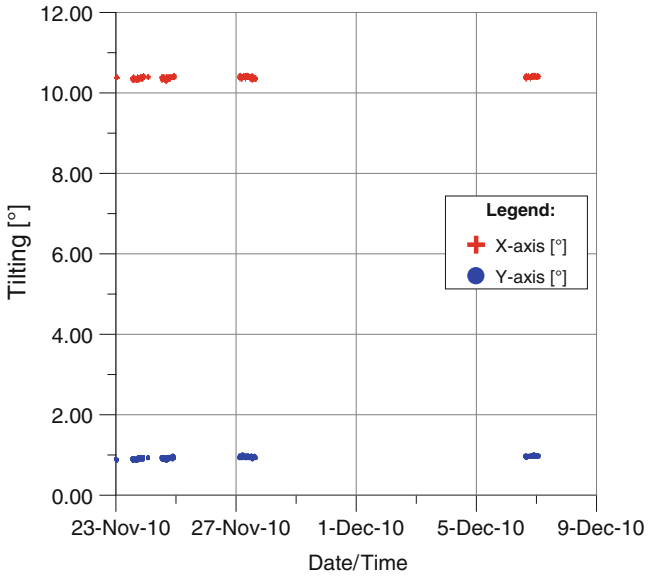


Fig. 10 Tilt-values of one sensor node (node 2171)

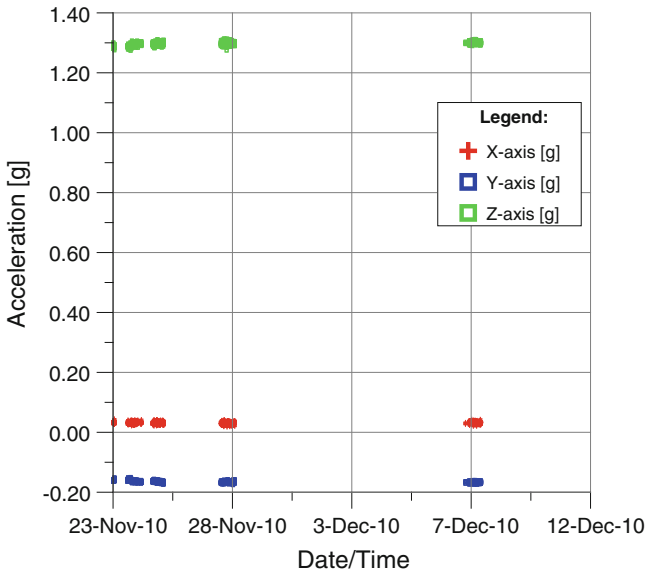


Fig. 11 Acceleration data of one node (node)

existing data sets illustrate quite stable conditions and did not show any information about ground moving during this time span.

The first data sets were used to define a first technical threshold value, resulting from the data spreading of the sensors itself. As every sensor has a natural data fluctuation, resulting from the sensor construction itself, ambient noise and a certain inaccuracies, movements can only be detected and monitored if they are outside of this fluctuation range of the sensor. Thus the analyze of these first values was used to define a first tolerance- or threshold value, that results from the normal sensor-spreading itself.

Summary and Conclusion

From November 18th until November 23rd the SLEWS sensor based monitoring system for movement detections in landslide regions was setup together with devices of the Flood Early Warning System of the GIZ near the small village of Malinao at the Philippines Island of Leyte. In order to get information about slope activity in this area, that might endanger the village of Malinao, the installed system should help to deliver suitable information.

The field work showed that the developed SLEWS monitoring system could be installed very fast in the landslide area and could be integrated in the existing network structures in the Philippines. A further positive aspect was the combination of the SLEWS landslide system with the FEWS-system supported by GIZ. Problems at the beginning could be solved as far as possible and a data transfer from the landslide area to the database at the University of Aachen was possible.

Anyhow, the installation also demonstrated that the combination of the two systems is a difficult and time consuming task with adjustemnets of different configurations and also hardware adaptations. All this could not be completely solved during this fieldwork. Furthermore the diffrent infrastsrutures on the Philippines complicated the implementation of the developed server structure.

In summary it can be said that the first approach allowed a first setup of the SLEWS system on the Philippine Island of Leyte with a data transfer to the database in Aachen. The first incomming data did not show stronger data changes that could be traced back any landlside acivity. Longer data series are currently collected. Due to the small amount of data available, interpretations or definitions of threshold values were not possible yet. Refinements are possible in the future if more data are gathered and analyzed. Once this is done the SLEWS will be used to warn the inhabitants of suspicious movements uphill from their settlement.

Remark

On January 2, 2011, several landslides happened in St. Bernard after heavy rains pounded the area. There was no landslide near Malinao but the municipal mayor decided to relocate the residents of Malinao permanently. With this development the sensors were moved to another village within St. Bernard, named Tambis 2. The sensors are producing and transmit data since February 2011 from the new location.

References

Applied Geomechanics (2008) Tiltmeters for slope monitoring. http://www.carboceramics.com/agi/tiltmeters-for-slope-monitoring/.

Arnhardt C, Nakaten B, Fernandez-Steeger TM, Azzam R (2008) Data-fusion of MEMS-sensors in a wireless ad-hoc multi-hop sensor network for landslide monitoring and real-time early warning, In: Schriftenreihe der Deutschen Gesellschaft für Geowissenschaften, International Conference and 160th annual meeting of the Deutsche Geologische Gesellschaft für Geowissenschaften e.V. and 98 annual meeting of the Geologische Vereiningung e.V., Geo 2008 Aachen, 176

Castillo-Effer M, Quintela DH, Moreno W, Jordan R, Westhoff W (2004) Wireless sensor networks for flash-flood alerting. In: Proceedings of the fifth IEEE international Caracas conference on devices, circuits and systems, (IEEE Cat. No. 04TH8783) 2004, vol 1, 3–5 Nov 2004, Conference Publications, pp 142–146

Evans SG, Guthrie RH, Roberts NJ, Bishop NF (2007) The disastrous 17 February 2006 rockslide-debris avalanche on Leyte Island, Philippines: a catastrophic landslide in tropical mountain terrain. Nat Hazards Earth Syst Sci 7:89–101

Fraden J (2004) Handbook of modern sensors: physics, design and application, 3rd edn. Springer, New York



Application of the Newly Frequency Domain Electromagnetic Method Survey in a Landslide Area

Gen Furuya, Tatsuo Katayama, Akira Suemine, Takayuki Kozato, Takahiro Watanabe, and Hideaki Marui

Abstract

Geophysical survey in a Landslide area is mainly perfomred by measuring the elastic wave velocity or electric resistivity. The electrical resistivity is well known to reflect the information in a slope, which can be obtained by the seismic prospecting or electrical resistivity survey. The commonly used electrical resistivity survey has disadvantage sometimes due to local ground conditions during the installation of electrodes and layout of electric cables on the hard material. On the other hand, the frequency domain electromagnetic method (FDEM), one of the electromagnetic methods, has advantages due to its nondestructive measurement nature and also its simple operation. In this study, we used a newly developed FDEM survey apparatus to examine its applicability in the exploration of landslide. The results showed good consistency with the structure of the landslide mass, which had been indentified by many other apporaches during the passing decades. Therefore, we concluded that FDEM is an effective method in exploring the area and also the inner structure of landsliding mass.

Keywords

Multi-frequency measurement • Electrical resistivity • Induction balance • Depth of sliding surface • Crystalline schist

Introduction

Identifying the area of landslide mass, especially the location of sliding surface, is of great importance to clarifying the mechanism of landslide movement and then giving appropriate plans of countermeasure. Generally, estimating the location of sliding surface is carried out by means of drilling and subsequent deformation/displacement monitoring. Many drillings and monitoring points are normally required to give reliable evidences for determining the location of sliding surface and volume of the landslide mass. Drilling is a workable method, but it has the problem in cost.

In recent years, it has become possible to grasp information of landslide mass with the progress of geophysical survey technology. Seismic prospecting and electrical resistivity survey, especially, are useful methods and have been widely used in obtaining the overview of the structure

G. Furuya (✉)
Department of Environmental Engineering, Faculty of Engineering, Toyama Prefectural University, 5180 Kurokawa, Imizu-shi, Toyama 939-0398, Japan
e-mail: gfuruya@pu-toyama.ac.jp

T. Katayama • T. Kozato • T. Watanabe
The General Environmental Technos Co., Ltd., Osaka, 1-3-5 Azuchimachi, Cyuo-ku, Osaka 541-0052, Japan

A. Suemine
Disaster Prevention Research Institute, Tokushima Landslide Observatory, Kyoto University, Ikeda-cho shuzu, Miyoshi, Tokushima 778-0020, Japan

H. Marui
Research Institute for Natural Hazards and Disaster Recovery, Niigata University, Ikarashi Ninocho 8050, Nishi-ku, Niiigata 950-2181, Japan

C. Margottini et al. (eds.), *Landslide Science and Practice*, Vol. 2,
DOI 10.1007/978-3-642-31445-2_22, © Springer-Verlag Berlin Heidelberg 2013

of soil layers. However, these methods sometimes have disadvantages resulting from the possible changes in local ground conditions during the installation of electrodes, and also from the difficulties in the layout of electric cables on hard material. On the other hand, the frequency domain electromagnetic method (FDEM), one of the electromagnetic method, has advantage to measure many survey points in short time, because it is not necessary to install electrodes.

In this study, we applied a newly FDEM survey instrument in a landslide field to examine the applicability of this approach in the landslide survey. This landslide field had been investigated in very details before by a lot of drilling and long term monitoring.

Overview of the Newly FDEM Survey Instrument

FDEM

The FDEM, in which the loop-loop technique (Slingram method) is normally employed, was developed some decades ago. Two coils (transmitting coil and receiving coil) are used in FDEM. During survey, these two coils are moved along the survey line while the distance between them is kept the same, and the in-phase component and in-shift component of the secondary magnetic field are measured (Fig. 1).

The principle of FDEM is measuring the apparent resistivity that is presented by the parameter of frequency obtained by the receiving coil, while arbitrary signals of alternating current are applied from the transmitting coil. It is well known that when the electromagnetic fields with a wide range of frequencies were transmitted into the ground, the electromagnetic field with lower frequency will be transmitted deeper. Thus, the information of ground (slope) from shallow layer to deep layer can be obtained by sequentially transmitting operation from high frequency to low one. Then, anomaly materials or faults in the ground can be identified by a profile of resistivity based on measurement results.

Figure 1 also shows a schematic diagram of electromagnetic intensity in the case of loop-loop (Slingram) method. In the case of homogeneous slope, the distribution of magnetic field intensity will have the shape of normal distribution curve with the peak value being in the center of two coils, and the peak value of the intensity will become smaller when the soil layer becomes deeper. If there were an anomalous material in the slope, the magnetic field will be changed. Especially, when this material is smaller than the distance between the coils, the measurement will be in low resolution, because the vaules are averaged by the distance between the coils. On the other hand, if the magnetic field intensity could be made to be of higher directivity, higher resolution could be expected.

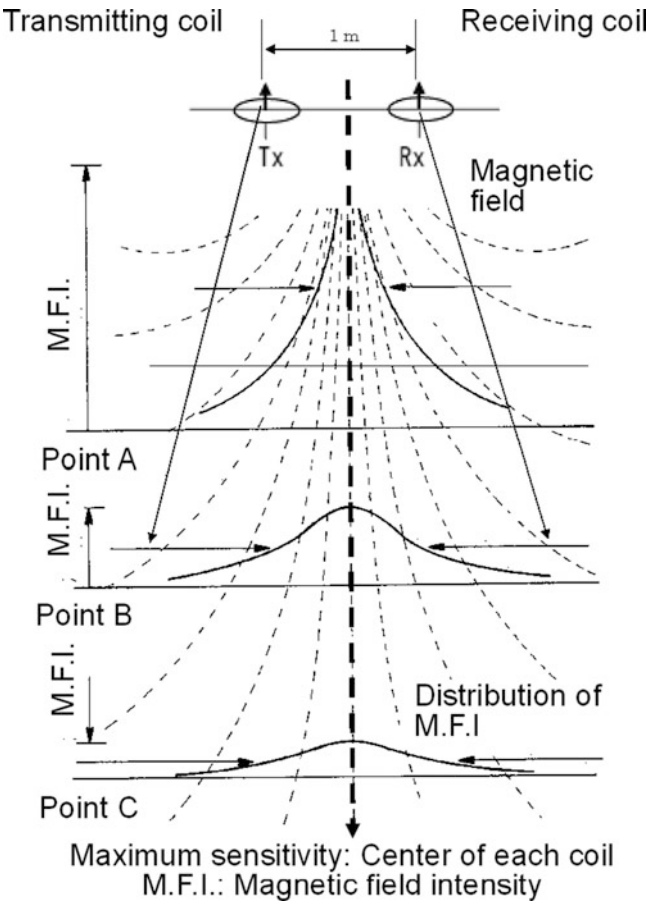


Fig. 1 Schematic diagram for distribution of magnetic field intensity in the loop-loop (Slingram) method

Principle of the Induction Balance Method

To make higher directivity of the magnetic field intensity we used the induction balance method in the survey. Figure 2 shows a schematic diagram of the induction balance method. Two receiving coils, whose winding directions oppsite each other (coaxial coil), are set above and below the transmitting coil, respectively. And the locations of these coils are adjusted such that the initial output voltage reaches zero when the measuring system is not inside of the surveying area. In this condition, when there is an electric conductor, the output voltage will be changed due to the disturbance in the magnetic balance. The phase difference between the transmitting current and the output current will be changed proportinal to the value of output voltage. The output voltage will become higher, when the conductivity value (reciprocal of electrical resistivity) becomes higher, or the the electrical conductor is closer to the coils. As a new survey instrument of FDEM can then be developed by measuring the phase difference or the output voltage at different frequencies (Katayama et al. 2011).

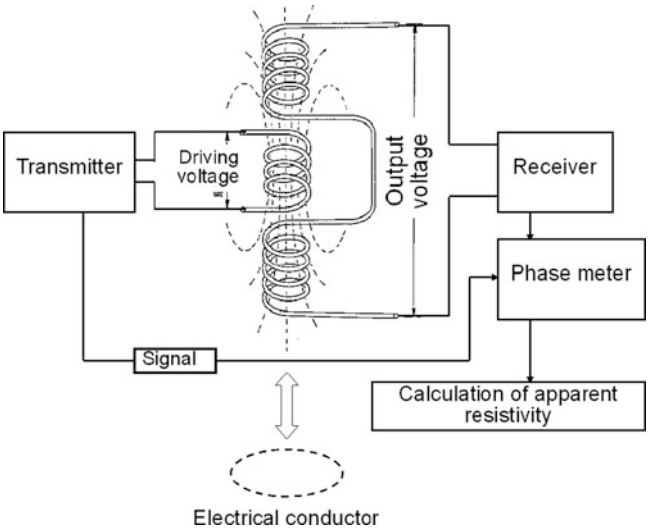


Fig. 2 Principle of the induction balance method

Specification of the Newly FDEM Survey Instrument

Photo 1 shows a view of a newly developed FDEM survey instrument. Some features of this instrument are shown in Table 1. The coaxial coil consists of (1) a transmitting coil that is winded in the middle of a bobbin (diameter is 25 cm), and (2) two receiving coils that are winded oppositing each other and placed above and below the transmitting coil in this bobbin, respectly. Around each coil is conductor-free space. Zero adjustment is performed by adjusting the positons of the transmitting coil and receving coil such that the output voltage of the receiving coil (monitored by an osillograph) becomes zero. This instrument enables the monitoring of 16 differenent frequencies with high efficiency (1 min per point). The weight of the FDEM survey instrument is about 15 kg. The maximum measurement depth is approximately 40 m.

Calculation of the Resistivity

The apparent resistivity measured by the FDEM instrument in this study is the reciprocal electrical conductivity calculated by the Maxwell's equations of the electromagnetism. The detailed calculation method is described in (Katayama et al. 2011). Here we outline the calculation in the following.

Magnetic field on the central axis of loop in the cylindrical coordinate system writes as in (1).

$$H_{0z} = \frac{aI}{2}\int_0^{\infty} \frac{2\lambda}{\lambda + \sqrt{\lambda^2 - k^2}} J(a\lambda)\, d\lambda \tag{1}$$

Where H_{0z} is the magnetic field at the central axis of loop, α is the coil radius, I is the amplitude of vibration, λ is the



Photo 1 Coaxial type of the FDEM survey instrument

Table 1 Specification of the instrument

Measurement frequency (16ch)	364, 256, 216, 182, 128, 108, 91, 64, 54, 45.5, 32, 27, 22.8, 16, 13.5, 11.4 (kHz)
Coil	Transmitting: Diameter = 25cm, Coil turns = 10 Receiving: Diameter = 25cm, Coil turns = 40
Transmitter	High-frequency linear amplifier (Sinusoidal current: 2-6 A)
Receiver	Phase difference detection circuit by Direct digital synthesizer: Phase drift < 0.02 degree
Dimension, Weight	1100 (L) X 400 (W) X 250 (H) mm, Approx. 15 kg
Serial cable	RS232C (Maximum length = 50 m)
Measurement control	PC controlled
	Fastest measurement time: 1 min/point
Power	AC 100 V (Portable generator)

constant of variable separation, J is the imaginary unit, k is the wave number, σ is the electric conductivity (inverse of the resistivity), μ_0 is the vacuum permeability, ω is the angular rate of frequency f (= 2πf).

In addition, k^2 writes as

$$k^2 = j\omega\mu_0\sigma \tag{2}$$

The integration of (1) is used for the constant of variable separation (γ) that can be expressed as

$$\gamma^2 = \omega\mu_0\sigma a^2/2 \tag{3}$$

The integral value of (1) results in (4).

$$H_{0z} = \frac{I}{2a}\cdot\frac{j}{\gamma^2}\left[3 + e^{-\gamma}(\cos\gamma + j\sin\gamma)\left\{j2\gamma^2 - 3(1-j) - 3\right\}\right] \tag{4}$$

This equation can be divided into two parts, i.e., real part and imaginary part, as follows

$$H^R{}_{0z} = \frac{-e^{-\gamma}}{\gamma^2}\left[\left(2\gamma^2 + 3\gamma\right)\cos\gamma - (3\gamma + 3)\sin\gamma\right] \tag{5}$$

$$H^{I}{}_{0z} = \frac{1}{\gamma^2}\left[3 - e^{-\gamma}\left\{(3\gamma + 3)\cos\gamma + \left(2\gamma^2 + 3\gamma\right)\sin\gamma\right\}\right] \tag{6}$$

Equation 5 means in-phase component with the primary magnetic field, and (6) means in-shift component with a certain phase separation. The phase angle φ is given in (7).

$$\varphi = \tan^{-1}\left(\frac{H^{I}{}_{0z}}{H^{R}{}_{0z}}\right) \tag{7}$$

The relationship between φ and γ can be examined in advance. After measuring φ through field survey, we can then calculate γ, and finally obtain the electric conductivity through (3).

The measured data through the FDEM survey is the apparent resistivity for each frequency. The frequency is regarded as the parameter of soil depth in this case. The resistivity of the soil is calculated through following steps based on the measured apparent resistivity (Katayama et al. 2009).

1. Setting the initial resistivity structure and the thickness of each layer for a given measurement point by using a multilayer model
2. Calculating the theoretical magnetic field response for the above mentioned model. Here the magnetic field response means the ratio of primary magnetic field intensity and the secondary one
3. Calculating the square sum of the errors between the theoretical value and measurement value of the magnetic field response
4. Modifying the resistivity and thickness in each layer until the square sum of the errors is less than the acceptable error (Iteration)
5. Using the best fit result as the resistivity structure of the given point
6. Repeating steps 1–5 for the next survey point.

In addition, it is also possible to make a cross section profile of resistivity distributions by the two dimensional smoothing process.

Interpretation of the relationship between electrical resistivity and geotechnical character is normally performed semi-empirically through the results of former case studies. Figure 3 and Table 2 present the results of some former case studies.

Overview of the Test Site

Figure 4 shows the location of test site, Nishi-ikawa landslide, in this study. This landslide has been triggered by cutting of lower slope in old landslide mass. The Nishi-ikawa landslide consists mainly of green schist and partially

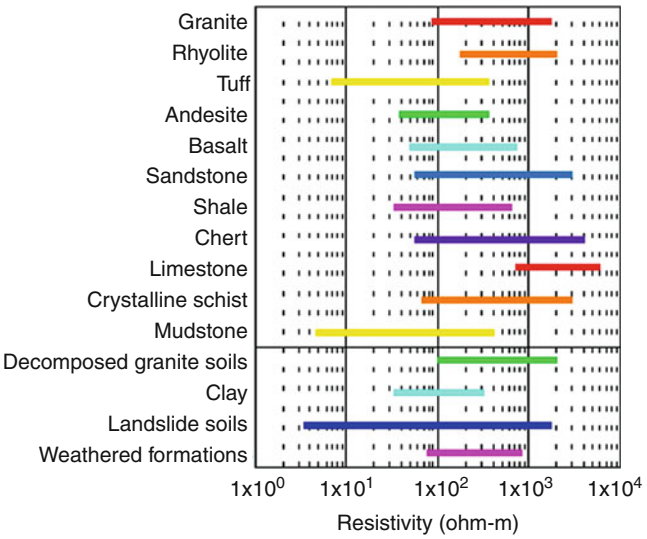


Fig. 3 Distribution of electrical resistivity for rock and soil formations (Matui et al. 2000)

Table 2 Influential factors for electrical resistivity

Factor		Resistivity of material		Geotechnical condition
		Low	High	
Porosity	Saturate	High	Low	Weathered, Fracture zone
	Dry	Low	High	
Degreee of saturation		High	Low	Groundwater
Volume water content		Large	Small	Weathered, Fracture zone
Clay content		Rich	Poor	Weathered, Altered
Resistivity of groundwater		Low	High	Na-Cl water etc.
Temperature		High	Low	Geothermal, Hot water

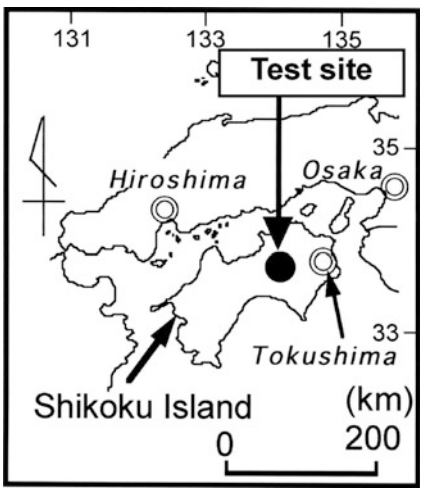


Fig. 4 Location of the test site (Nishi-ikawa landslide)

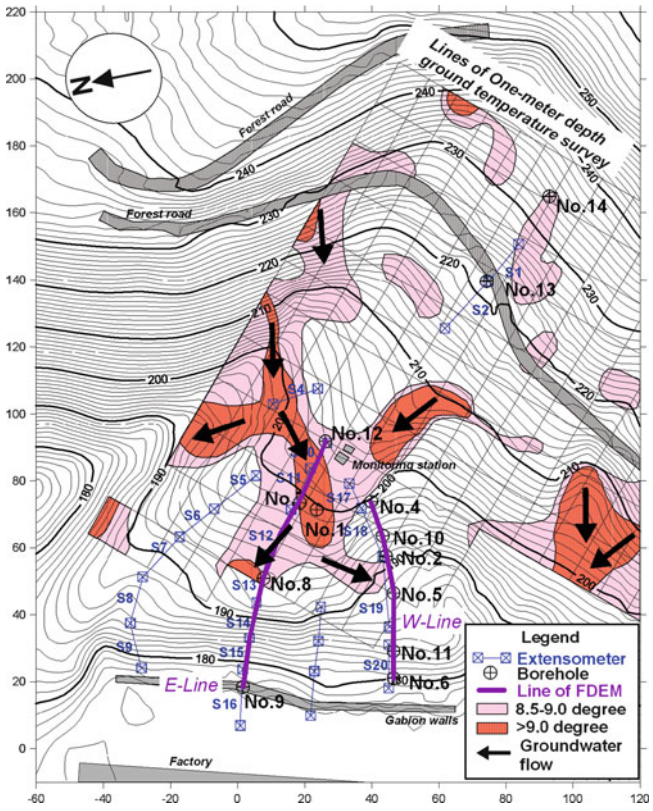


Fig. 5 Plan of the Nishi-ikawa landslide

of politic schist. This landslide has been well studied through drillings and various monitoring since 1973 (Suemine et al. 1980; Suemine 2004). 1-m-depth ground temperature survey had also been carried out to examine the possible distribution of ground water flow. Details on the principle and the way of 1-m-depth ground temperature survey can be referred by Takeuchi (1980) and Furuya et al. (2006).

Figure 5 shows plan of the Nishi-ikawa landslide. The FDEM survey is carried out along E-Line and W-Line tracing the boreholes and extensometers. In this figure, the veins of groundwater flow estimated by the results of 1-m-depth ground temperature survey on January 2000 are also shown. Because it was in the winter, the area affected by vein of groundwater flow was 8.5 ° higher than their sorrounding areas in temperature. Schematically, groundwater flows directions shown by arrows are mainly of northeast to southwest and partially southeast to northwest. Both lines are recognized to be concentrated by groundwater flows, subsequently, also to be more active in sliding than other area.

Measurement points of the FDEM survey were No. 2, No. 4, No. 5, No. 6, No. 10, and No. 11 in the W line, and No. 7, No. 8, No. 9, No. 12, Midpoint of 8–9, Midpoint of 7–8, and Midpoint of 7–12 in the E line (totally, 13 points were surveyed). At point No. 9, the measured data was apparentaly affected by the greenhouse with metal fram, and then was excluded in the estimation.

Results and Discussions

In this study, we compared the results obtained by the FDEM survey and other different investigation methods to examine the applicability of FDEM survey as a landslide investigation tool. Selected data for previous investigations are obtained from drilling record, standard penetration test, core investigation, monitoring of pipe strain gauge, and 1-m-depth ground temperature survey. The results obtained through these methods along E-line and W-line are incorporated in Figs. 6 and 7, respectively. In addition, Table 3 shows the list of estimated sliding surface by drilling (core) investigations, monitoring of the pipe strain gauges, and resistivity of the FDEM survey.

The sliding surface estimated by the FDEM survey is assumed to be located on the bottom of a zone with smallest resistivity, while the estimated sliding surface by the drilling is assumed to be located on those places with clay layer, spring (seepage), and smaller N values.

As shown in Fig. 6 and Table 3, with exception of survey point No. 6, the FDEM survey showed good agreement with the results obtained by other investigation. Namely, those places consisting of clayey soils with sudden changes in N value have smallest resistivity. The sliding surface obtained by the FDEM also showed good agreement with those inferred from the densliy monitored deformation/displacement by means of vertical extensometers and pipe strain gauge. The resistivity of the No. 5 is smaller than other points, probably due to: (1) it locates on a small catchment, (2) groundwater may flow into this area, which had been identified by the 1-m-depth ground temperature survey, and also artesian flow after heavy rain had been witted often. For No. 6, at the depth of 6 m are measured the lowest resistivity in spite of the fact that N value is significantly large. However, the sliding surface revealed by the monitoring of pipe strain gauge is about 2 m. Concerning this big difference, further study is needed and is on the plan at present.

As revealed by the Fig. 7 and Table 3, the lowest resistivity zones in E line are locating at the depth of 6–8 m. Comparing the resistivity and the N value in No. 7 and 8, we can find that the lowest resistivity locates on the lower part of the soil layer where N value changed sharply in No. 7, and locates on the soil layer where N value increased slightly in No. 8. Comparing the resistivity to the results monitored by pipe strain gauge, we can find that the lowest resistivity in No. 7 locates roughly on the same location as the sliding surface estimated by the pipe strain gauge. However, there is a difference in the approximately 7 m for the results of between FDEM survey and monitoring of pipe strain gauge in No. 8. This result means that the lowest resistivity obtained by the FDEM survey in this study may be not necessarily representative of the sliding surface in a certain case. It is probably

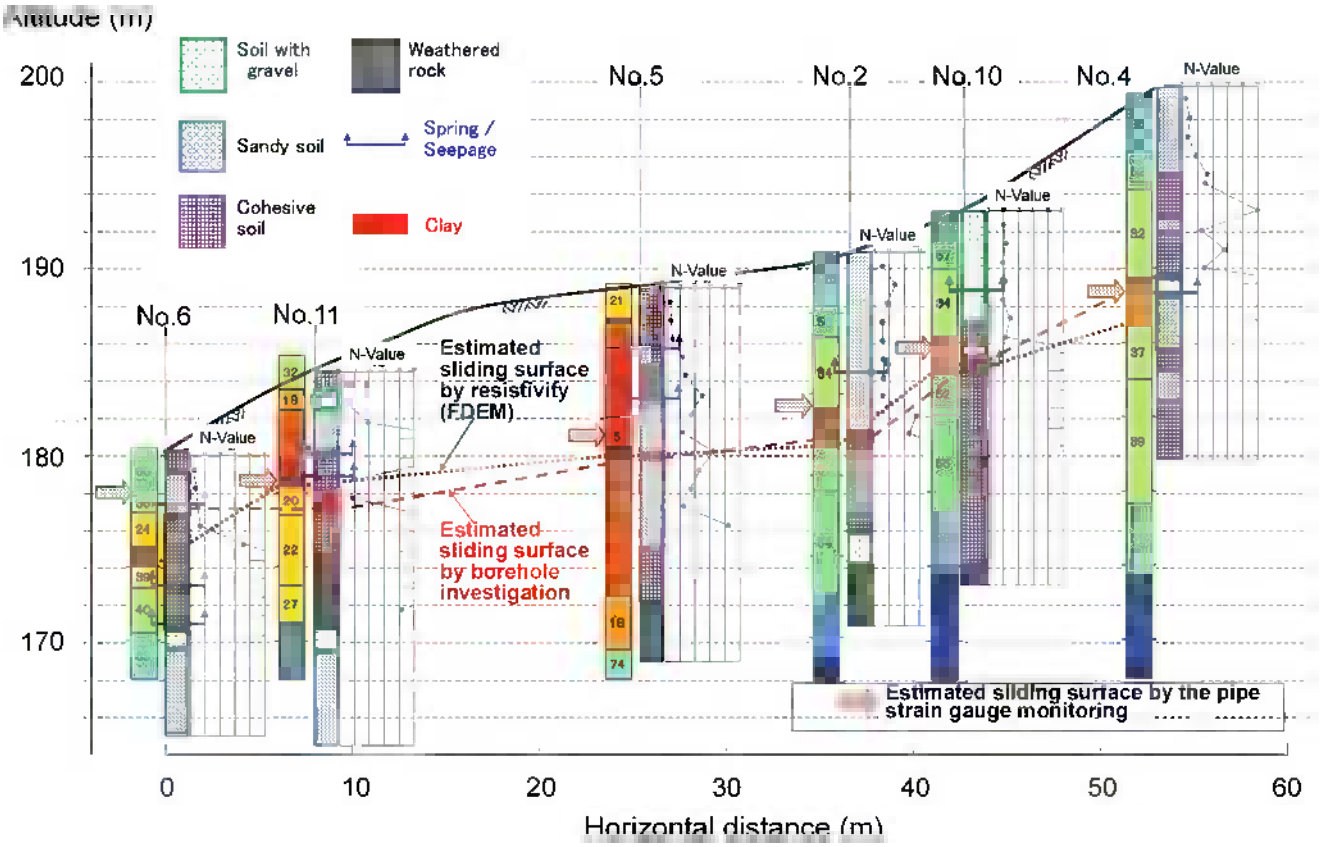


Fig. 6 Results from the FDEM survey, the borehole investigation, and pipe strain gauge monitoring in the W line

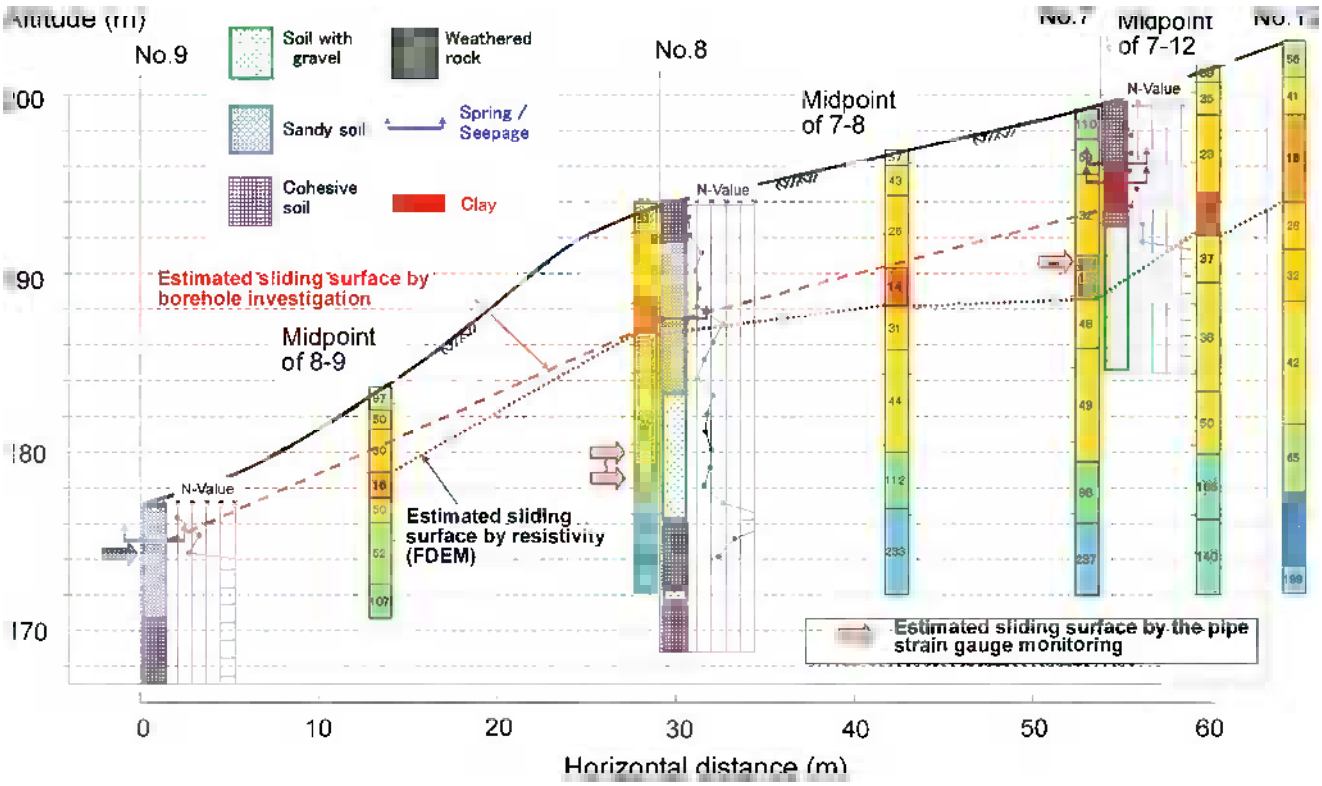


Fig. 7 Results from the FDEM survey, borehole investigation, and pipe strain gauge monitoring in the W line

Table 3 Estimated sliding surfaces by borehole investigations, pipe strain gauge monitoring, and resistivity distribution

Bor. No.	No.2	No.4	No.5	No.6	No.7	No.8	No.9	No.10	No.11	No.12
Borehole investigation (Spring/Seepage)	9.2–10.0	10.1–10.2	8.7–9.1	(2.9)	3.6–6.0	(6.4–6.5)	(2.2)	7.6–7.7	7.0–7.5	N.D.
Pipe strain gauge	7.5	11.0	8.3	2.0	8.6	14.0-15.5	2.8	7.5	6.9	8.5
Resistivity distribution (FDEM)	10.5	12.5	9.2	6.4	10.7	7.5	M.D.	8.7	7.0	9.0

mainly due to the fact that some times the minimum thickness detectable by the electromagnetic method, such as the FDEM survey, may be deeper than the sliding surface. To elevate the accuracy of FDEM survey, it is necessary to examine the detailed reasons for this kind of big difference in a certain case or a special environment through the accumulation of case studies. Nevertheless, from the results presented in Figs. 6 and 7, we conclude that FDEM survey instrument is a workable tool for landslide investigation.

Conclusions

In this paper, we developed a new FDEM survey instrument by using the induction balance method through introduciton of coaxial coil. We also examined the applicability of this instrument for landslide investigation at the Nishi-ikawa landslide consisting of mainly crystalline schist, in Japan. The examination is carried out by comparing the results obtained by this instrument to those obtained by borehole investigation, and monitoring of pipe strain gauge. The sliding surfaces revealed by the new FDEM suevery showed good consistancy with those obtained by borehole investigaton and monitoring of pipe strain gauge. Although there are some aspects needing further examination, we concluded that this instrument is of high applicability for landslide investigation. Furhter study is needed and planed to elevate the precision in identifying the soil structure of landsliding mass through the accumulation of case studies.

Acknowledgments We wish to thank Prof. M. Kaibori (Hiroshima University) for providing topographical survey data, Dr. K. Araiba (Ministry of Internal Affairs and Communications) and Dr. A. Takeuchi (formerly of the Disaster Prevention Research Institute, Kyoto University) for their help in the 1-m-depth ground temperature survey, and Dr. G. Wang (Disaster Prevention Research Institute, Kyoto University) for discussion.

References

Furuya G, Suemine A, Sassa K, Komatsubara T, Watanabe N, Marui H (2006) Relationship between groundwater flow estimated by soil temperature and slope failures caused by heavy rainfall, Shikoku Island, southwestern Japan. Eng Geol 85:332–346

Katayama T, Kozato T, Kato H, Kusumi H, Matuoka T (2009) Development of FDEM and applicability to river embankment survey. Jpn Geotech J 4(4):331–340 (in Japanese with English abstract)

Katayama T, Kozato T, Watanabe T, Furuya G, Suemine A, Kusumi H, Nishigaki M (2011) Study of resistivity prospecting by induction balance method with coaxial coil. Jpn Geotech J (submitted to). (in Japanese with English abstract)

Matui T, Park S, Park M, Matsuura S (2000) Relationship between electrical resistivity and physical properties of rocks. In: Proceedings of an international conference on geotechnical & geological engineering, "GeoEng2000", Melbourne, Australia (CD-ROM), G0987, p 6

Suemine A (2004) Observational result of groundwater table at landslide occurrence. J Jpn Landslide Soc 41(1):43–48 (in Japanese)

Suemine A, Shima M, Konishi T (1980) Some remarks on landslide mechanism (an example of fractured zone landslide). Disaster Prev Res Inst Annuals 23(B-1):345–355 (in Japanese with English synopsis)

Takeuchi A (1980) Method of investigating groundwater-vein-streams by measuring one-meter-depth in landslide areas (I). J Jpn Assoc Groundwater Hydrol 22(2):11–39



Characterization and Study of a Complex Landslide Site in Northern Italy

Roberto Passalacqua and Rossella Bovolenta

Abstract

The present paper deals with a diffused and continuous kinematic phenomenon in Liguria (Italy). In order to study this complex and wide landslide many data have been collected in a unique platform in GIS (Geographic Information System) obtaining a 3D model of a large area, whose morphology and features are variable. The platform integrates hydrological and geotechnical data and allows stability analyses.

Keywords

Landslide • Geotechnics • GIS

Introduction

A quite large area (~5 km^2) in the north-east sector of the Genoa Province (see Fig. 1), which is part of the Liguria Region (Northern Italy), is subjected to a diffused and continuous kinematic phenomenon. A small town and six of its surrounding hamlets are there located. Normally almost 1,250 inhabitants reside but, being this locality a well renown resort for both the winter and summer vacations, during a whole quarter of the year the residents' number rises up to four times.

The area of interest is sited on a top-valley gentle slope (mean angle 11 °), which downgrades directly from the south-side faces of the Northern Apennines summits, locally arriving at 1,800 m a.s.l.

The entire area is a large relict landslide, formed by a pliocenic glacial till and characterized by widely assorted sediments.

The main trigger actions on the soil body's behaviour are the seasonal rain/snow falls on the watershed.

The soil heterogeneity and the complicated hydrologic conditions of the zone induce significant displacements. Many buildings and generic structures (retaining walls, small bridges etc.) exhibit damages, imputable to the widespread and locally differential movements at ground level. The State Institutions, Land Authorities, as well as some of the private Citizens, are applying their economical efforts in the rehabilitations and the assessment/control of the active phenomena.

Considering the extension and complexity of the site, a GIS-based platform was created. It integrates the digital terrain model (DTM), the water table and the bedrock layers. *GRASS* (***G**eographic **R**esources **A**nalysis **S**upport **S**ystem*) has been chosen. It is a free and open source GIS (Westervelt et al. 1987), whose main characteristic is to allow the usage of existing algorithms and procedures, as well as the integration of additional features that can be shared within the GRASS community as freeware utilities.

The Loose Soils' Thickness

From the geological and morphological points of view, the entire area was formed by a pliocenic glacial till and its body of widely assorted sediments had been reckoned as a large relict landslide. The loose-soils' thickness spans from few meters up to 90, before of reaching the bedrock formations (argillites, sandstones, mudstones, ophiolites and diabases in pillows).

R. Passalacqua (✉) • R. Bovolenta
DICAT: Department of Civil, Environmental and Architectural Engineering, University of Genoa, Via Montallegro 1, Genoa 16145, Italy
e-mail: Passalacqua@dicat.unige.it

C. Margottini et al. (eds.), *Landslide Science and Practice*, Vol. 2,
DOI 10.1007/978-3-642-31445-2_23, © Springer-Verlag Berlin Heidelberg 2013



Fig. 1 The Santo Stefano d'Aveto site (Liguria-Italy)

Information about the subsoil have been deduced from:

- Soil tests,
- Data from inclinometers and piezometers,
- Seismic prospecting and MASW 2D,
- Topographical surveying and monitoring,
- GPS surveying and monitoring,
- Synthetic Aperture Radar (SAR) interferometry.

The typical characterization techniques appear generally improper on such a wide scale and extremely variable loose-soils deposit. Consequently, the authors have in this instance employed some non-conventional methods of deep-soundings and criteria of interpretation, in order to assess affordable but reliable site recognition over all its extension. Dealing with a rather large territorial dimension, one of the relevant issues is to find the proper techniques to distribute spatially the loose-soils' depths information and the pertinent geotechnical parameters which, usually, are all gathered at spot locations but, as it is obvious, are needed on the whole area in order to allow a widespread slope stability analysis approach.

Since the buried bedrock spatial morphology, depth and steepness have a key role on these particular types of landslides, for a further characterization of the site, geophysical tests have been performed.

Simplified seismological experimental methodologies, focused on the ambient noise recordings, may be very effective for site investigation. These methods are based on the analysis of the dispersion of Rayleigh and Love waves components induced by the ambient noise, in order to define the amplification function of a site in terms of its fundamental frequency F_O.

These methodologies are used to evaluate the shear wave velocity V_S and, by the following relationship (1), the thickness H of a sediment layer:

$$H = \frac{V_S}{4 \cdot F_O} \tag{1}$$

Both the Nakamura (1989) and *Seismic Array* techniques were here used, to investigate the micro-tremor characteristics of the site and to correlate the emerging data to the properties of the shallow geotechnical and geophysical structures.

The noise measurements were made at more than 70 points, placed on different parts of the loose-soil body and of the surrounding exposed rock formations (see Fig. 2).

Some of the recordings were carried out in proximity of those boreholes which had reached the bedrock depth, with the aim of assessing the V_S values of the glacial till materials. By using the spectral-ratio techniques, a good image of the resonance frequencies of the loose-soils was obtained.

Moreover, an array set-up of six seismic stations allowed the study of the Rayleigh and Love wave dispersion.

Finally, the whole set of both the existing and the obtained data have been spatially distributed, by using the standard interpolators available within the Geographical Information System (GIS) platform.

The Water Table

Since the subsurface water influence on the phenomenon is very important, the site was studied and tested from the hydrological point of view. The local watershed of Santo Stefano d'Aveto shows some particular features (see Fig. 3):

- The presence of two almost-parallel rivers (*Fossato Grosso* and *Rio Freddo*), flanking the glacial till;
- A sudden deviation of *Rio Freddo* toward NE, due to a relict landslide toe and called *bretella* in Fig. 3, crosses the small town of Santo Stefano and then pours into Fossato Grosso;
- The presence of little and sparse streams, whose bed is not very deep or higher than the neighbouring terrain;
- The presence of a unique lower outflow (denoted by *P* in Fig. 3).

The study of the superficial water flow is based on a linear reservoir model. For the sake of brevity, the pertinent study is not described here.

In the sequel, greater attention is devoted to the water flow inside of the glacial till, because the kinematic phenomenon is particularly influenced by the pore pressures build-up.

The analysis is based on the assumption that the glacial till can be schematized as an irregular parallelepiped (length ≈3,000 m; width ≈450 m; slope ≈15 %). Only the rain fall is considered as input and only one out flowing mouth is introduced. Consequently, the single watercourses are neglected in this analysis.

The study is based on the kinematic wave model.

The glacial till is considered as a porous, homogeneous and isotropic medium, being the Darcy law applied.

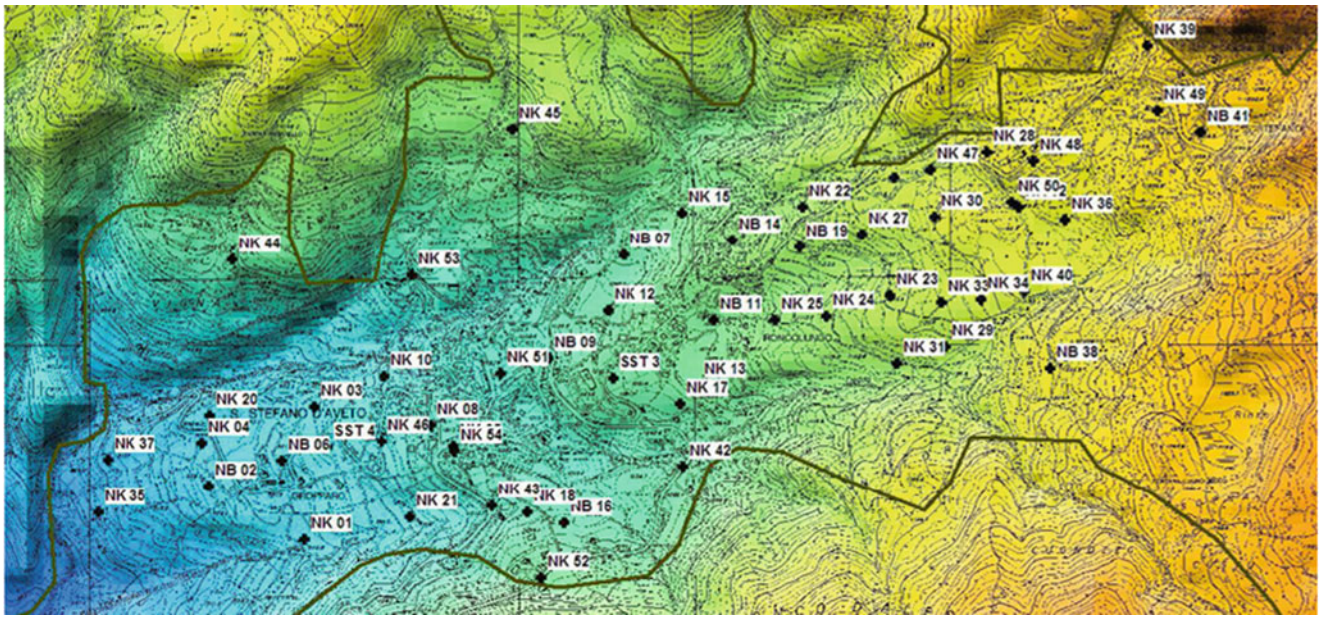


Fig. 2 Noise measurement points

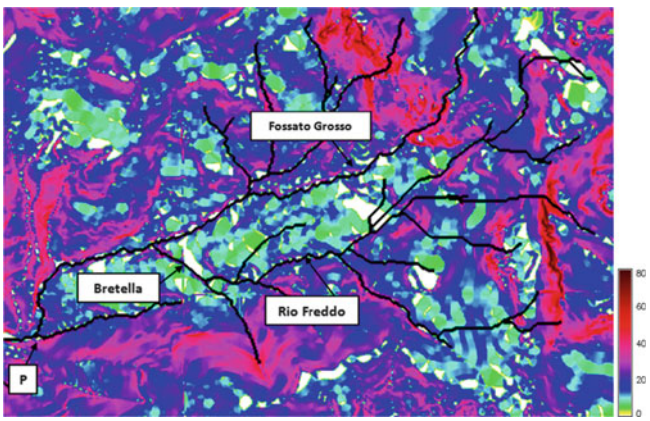


Fig. 3 The ground surface's Steepness (color dithered, in degrees) and the streambeds' layout (*black p-lines*) maps

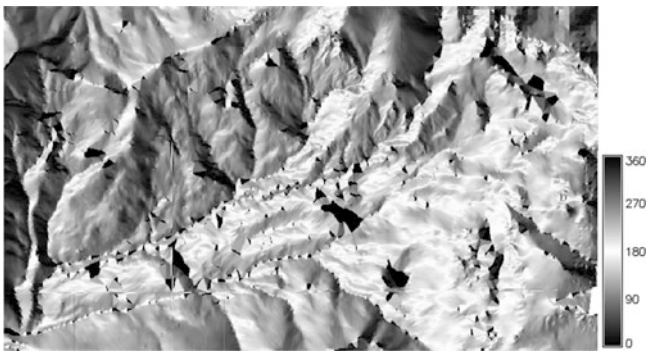


Fig. 4 The gray-dithered cardinal exposition map, in degrees from East

The input is represented by a long sequence of the same year rainfalls (i.e. the year 2010), as registered by an on-site rain-gauge, being the soil considered dry at the beginning of the wetting simulation process.

Suitable values of the soil permeability have been chosen, in order to keep the resulting water table in reasonable agreement with the available evidences collected from the on-site monitoring.

The GIS Platform

GIS is a useful tool for the integration and analysis of georeferenced information for the territory monitoring, management and planning, also in support of risk analyses.

In this research, the available and measured data were georeferenced into the GIS platform database by *GRASS* ver. 6.4, in order to allow the study of the site.

The spatial data had been thoroughly scrutinized, verified, assessed and assigned to different thematic layers. Then, the datasets had been analyzed by specific procedures to present in output the resulting charts.

The location was setup in a Gauss-Boaga cylindrical projection (datum Rome 40), to which the available and official Regional Technical Cartography conforms.

The whole surface was discretized by adopting a terrain tessellation into squares, having a 5×5 m resolution. Additional and relevant information were also added to the GIS database, in the form of both raster and numerical layers such as the local sweep of the regional *DTM* (***D**igital **T**errain **M**odel*) grid, the soil usage, the geo-lithological survey, the reckoned landslides and the results of a Permanent Scatterers' Interferometry analysis

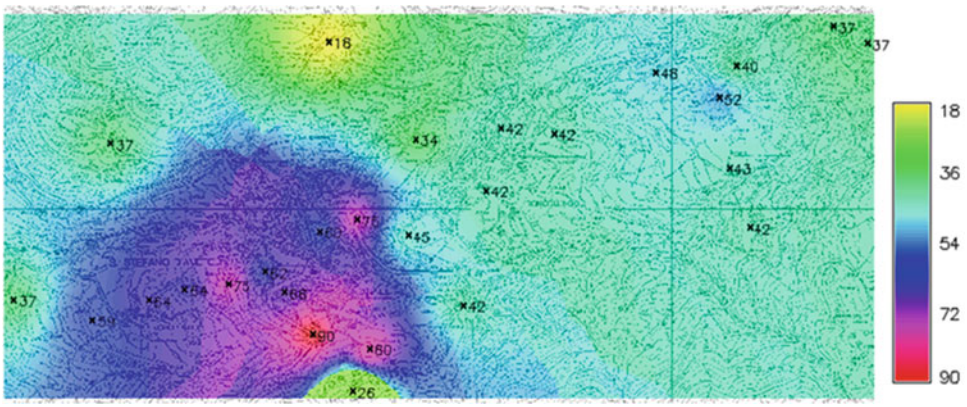


Fig. 5 The bedrock surface, in a plan view color rendering (depths from G.L. in meters)

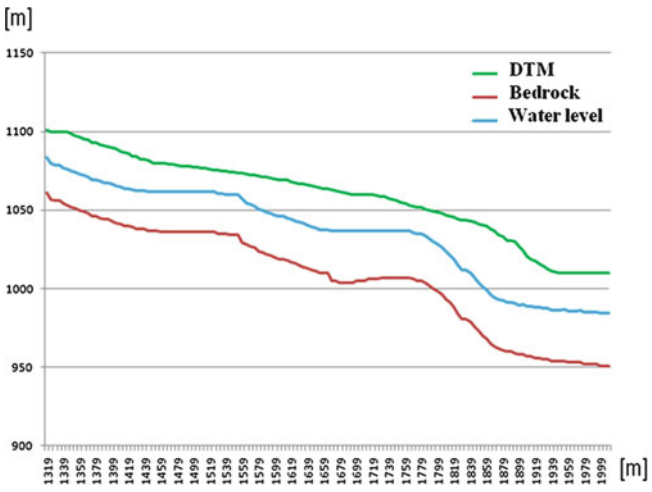


Fig. 6 Sample of a cross section, automatically extracted from the 3D model

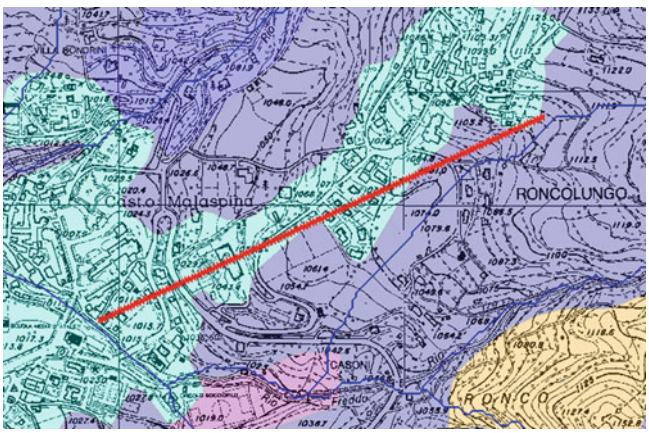


Fig. 7 The DTM and Land Use maps at the GIS interface, with the alignment to be investigated draw as a *red line*

on *SAR* images (PSInSAR), this as was yet performed by others (Gorziglia et al. 2008).

The analyses made on the DTM grid allowed to obtain both the cardinal exposition (see Fig. 4) and the steepness maps (Fig. 3).

The overall watershed study was based on the downward cells' seepage capacity; as a final result, the steady and spatial distribution of the phreatic surface was obtained by taking into full account of both the exposed surface and the buried bedrock morphologies, the stream beds' layout and, of utmost importance, the flowing quantities directly measured at many sections along their courses.

The loose soils' thickness was computed by the shear wave velocities (V_S) and the frequencies (F_0) measured at the spots marked in Fig. 2, as yet said above, using the relationship (1). Then, a 3D model of the loose soils' thickness spatial distribution was obtained, after having selected the most appropriate technique.

This very process is determinant to obtain a reliable continuous description from locally available data and it needs to:

- Interpolate within of the investigated area;
- Extrapolate outwards of it.

These aspects have great relevance to assess a proper model, thus we devoted them particular attentions.

As far as the modelling of the interface between loose soil and bedrock, many surface interpolation methods have been tested.

After many tests, switching the available interpolation methods and their pertinent parameters, the *Inverse Distance Weighted* one (choosing a number of interpolation points, $npoint = 6$) has been recognised as the best one. In fact, the

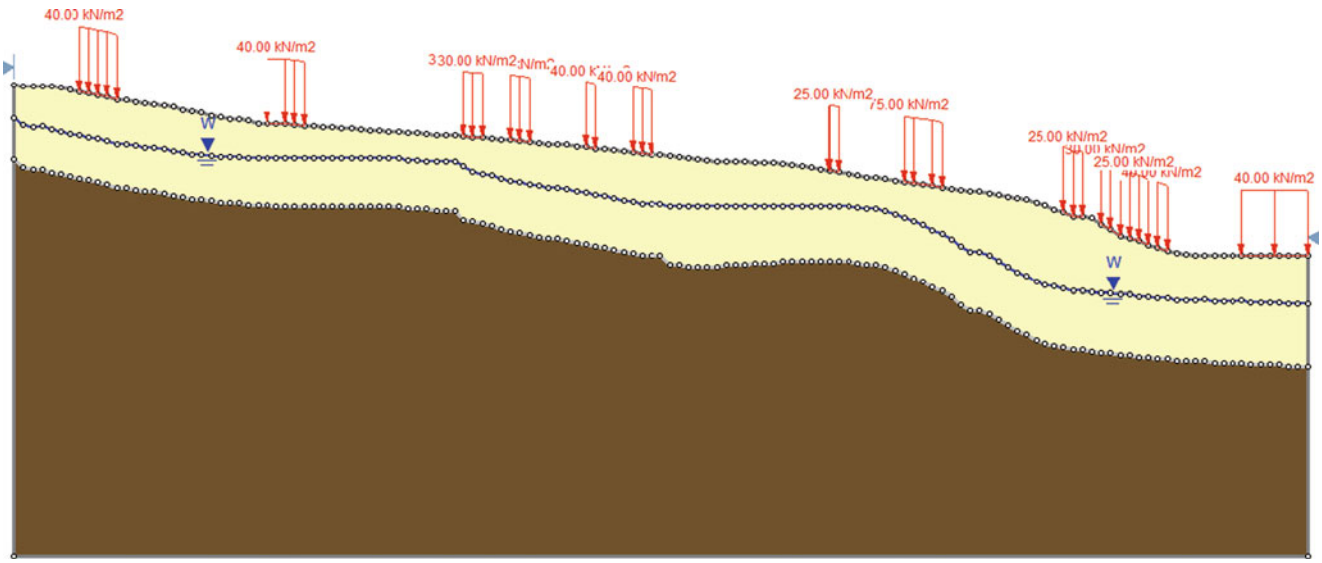


Fig. 8 The GIS-obtained cross section of the alignment in Fig. 7, imported in *Slide*©

obtained surface (see Fig. 5) is realistic and, more than that, in good agreement with the experimental data gathered at boreholes.

As far as the water table is concerned, the surface has been obtained by adopting the routine available in GRASS called *v.surf.idw*, with *npoints* = 1, and it is based on the values deduced by the above exposed hydrological analysis.

Consequently, the 3D model realised in GRASS contains three surfaces, corresponding to the digital terrain model (DTM), the water table and the bedrock. Cross sections of the three-dimensional model can be extracted in a very easy and quick way (see an example in Fig. 6). Thus, long and complex cross sections can be rapidly extracted to perform stability analyses.

First Application of the Model to Slope Stability Analyses

The above described model, which is still in progress, has been adopted in order to carry out 2D stability analyses by means of the code *Slide*© (Rocscience 2010). This, among the many others commercially available, allows one to evaluate the stability of a slope, using some of the *Global Limit Equilibrium* methods. Thus, a potential or real sliding phenomenon can be studied.

The use of this program is quite simple but, particular care has to be devoted to the description of the problem. Obviously, the definition of the geometry is rather demanding when a cross section is long and complex. This difficulty can be get over by the use of a 3D-model such as the one illustrated above.

In fact, a cross section can be quickly defined and the pertinent information deduced (i.e. the topography, the water table, the stratification, etc.). Figure 7 shows a red line in plan view, to which the cross section in Fig. 8 corresponds. All the relevant information for stability analyses can be easy determined and imported in *Slide*©. Potential sliding surfaces and the corresponding safety factors can be obtained. In Fig. 9 all of the examined surfaces and their safety factors are reported for this cross section, consequently the most critical zones can be recognized. In order to verify the significance of the obtained results, the available PSInSAR data have been carefully considered (see Fig. 10).

Up to this point, even if still preliminary, the following considerations may be however stated:

- The Limit Equilibrium Methods seem not to be the correct approach, in this case, because the kinematic phenomenon in Santo Stefano d'Aveto is not a *typical shear-band landslide*;
- The examined volume is a small portion (even if this cross section is 700 m long), being "extracted" from the entire mass;
- The soil information are poor, largely sparse and indicative, from the geotechnical point of view, of the lone upper strata;
- A direct comparison with the SAR results is not properly correct, because they offer the ground level displacements (it is worth recalling that all the *Global Limit Equilibrium Methods* neglect any strain balance), even because the very SAR methodology is often debated for its scatterings and local inconsistencies.

The present study and comparison is anyhow encouraging. In fact, the more dangerous zones have been easily recognized.

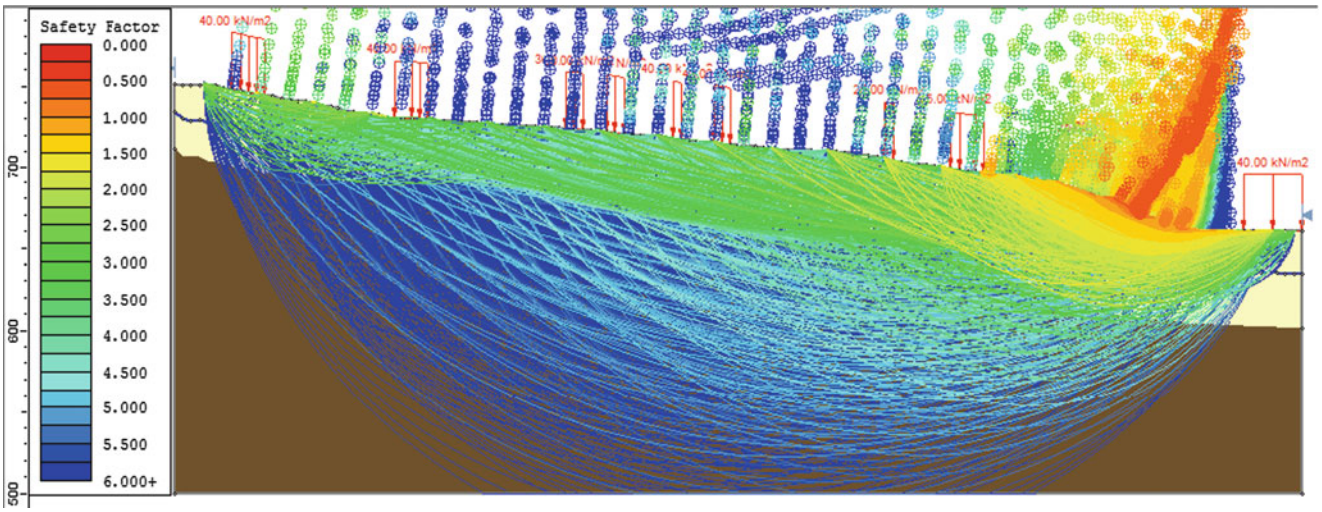


Fig. 9 Graphical render of the stability analysis results

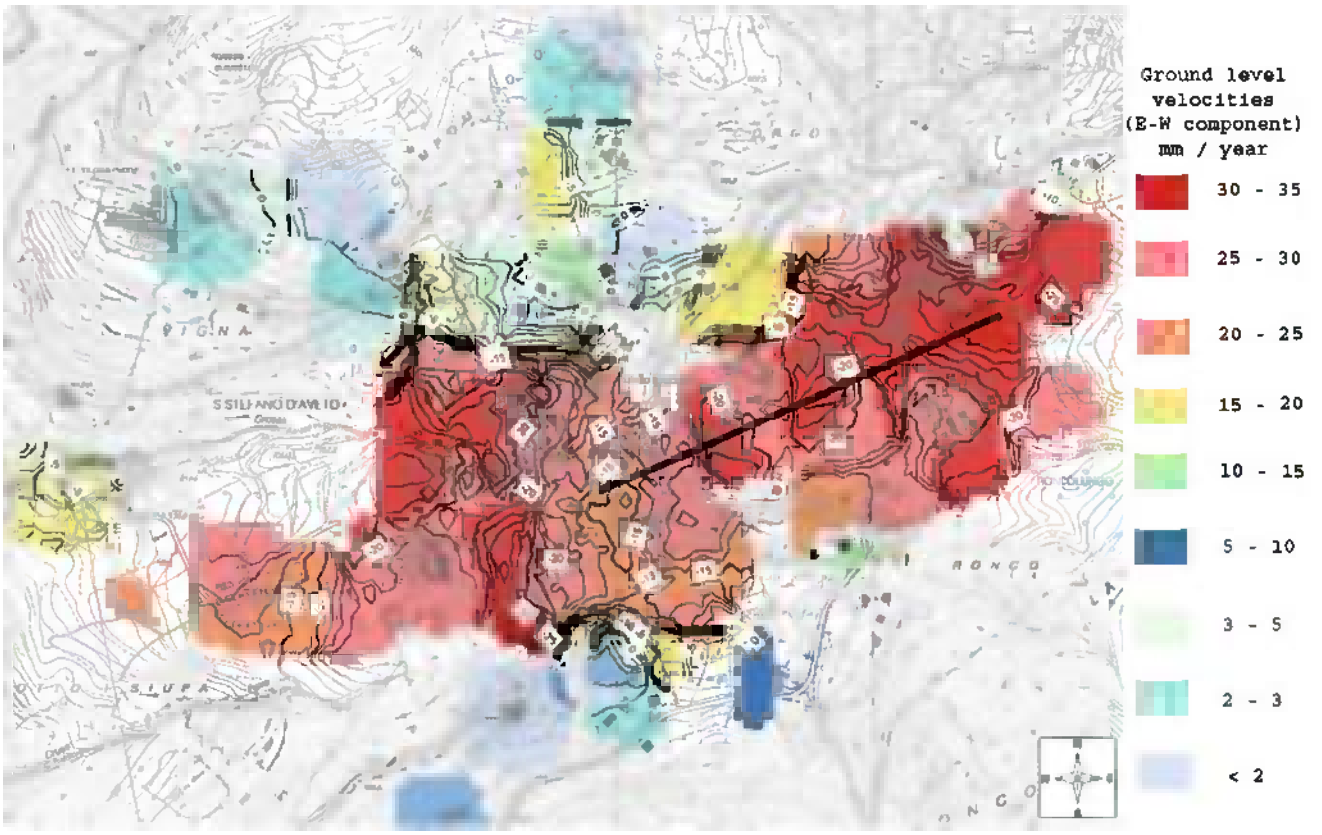


Fig. 10 The ground level velocities (E-W comp. in mm/year), contoured and color-dithered as from the *PSInSAR's* data interpolations: the examined cross section line is set in *black*

Conclusions

In the work herein referred all the relevant data, yet available for the site under study, had been collected and examined. They are represented by the geotechnical—geophysical characterizations and monitoring, the topographical—GPS surveys and the results of a PSInSAR analysis.

By using a common GIS platform, a fully georeferenced integration of the raster, vector and spot information had been obtained, making possible the study of their eventual inter-correlations.

More than that, this first phase of implementation was of great help into choosing the on-site positions where additional investigations had to be carried out, in order to obtain a proper dataset cover on the whole area.

The results attained up to now in this work, which is still in progress, are represented by the 3D modeling of the phreatic surface and of the loose soils' thickness for the overall area. These were obtained by rather simple correlation techniques and interpolation procedures, applied on specific geophysical and hydrological measures collected on-site for these very purposes.

Great advantages are established by such an integrated working platform. In fact, our final objective lies into make possible to easily conduct classical, but widespread, 2D slope stability analyses (*Global Limit Equilibrium* methods), or better, apply non-standard 3D simulations (viscous-creep behaviour by FDM) on this micro-territorial complexity.

Since the pore pressures build-up is the main trigger factor, a yet planned further development consists in the simulation of the evolutions of the phreatic level by modeling the whole sediments' body as a charging-discharging subsurface reservoir, fed from selected rainfall histories.

To carry out this capacity, yet implemented in similar instances (Passalacqua and Baretto 2003), a proper description of the site rainfall-runoff response capacity is needed, and this may be attained using an overall Curve Numbers' grid (Soil Conservation Service – U.S. Department of Agriculture 1972, 1975) whose values may be scored, mostly, from the observation of the site's georeferenced aerial images on the GIS interface.

Thus, this work is just the basic part of a more sophisticated model, which has the ambition to simulate and predict the kinematic behaviour of an ample territorial surface.

Notwithstanding this, the above described 3D model is already a valid support. In fact, it allows a more proper land use planning and a better placement/design of accurate rehabilitation measures.

References

Gorziglia G, Bottero D, Poggi F, Castello R, Minervini G (2008) Final report on the Santo Stefano d'Aveto site surveys (in Italian). By Regione Liguria, Dipartimento Ambiente, Settore Assetto del Territorio, referenced as fasc. 2008/G13.2.1/13, landslide I.F.F.I. code nr. 010.056.001, Genoa, Italy

Nakamura Y (1989) A method for dynamic characteristics estimation of subsurface using microtremor on the ground surface. Report of the Railway Technical Research Institute (RTRI), vol 30(1), Tokyo, Japan

Passalacqua R, Baretto A (2003) Landslides and rockfalls predictions by G.I.S. in Western Liguria. In: Picarelli L (ed) Proceedings of the international conference on fast slope movements prediction and prevention for risk mitigation (FSM2003) held on 11–13 May 2003 at Naples (I), (Pàtron). ISBN 8855526995, pp 421–429

Rocscience Inc. (2010) Slide©: 2D limit equilibrium slope stability for soil and rock slopes, version 6.0, Toronto, ON, Canada

Soil Conservation Service (1972) Hydrology. In: National engineering handbook, section 4, U.S. Department of Agriculture (available from the U.S. Government Printing Office), Washington DC

Soil Conservation Service (1975) Urban hydrology for small watersheds. Technical release no. 55, U.S. Department of Agriculture, Washington DC

Westervelt JD, Shapiro M, Goran WD, Gerdes DP (1987) Geographic resources analysis support system (*GRASS*), User's reference manual, U.S. Army Construction Engineering Research Laboratory (USA-CERL) report no. 87/22, Champaign, IL



HR Satellite Imaging and Borehole Monitoring of Landslides in Daunia, Italy

Janusz Wasowski, Caterina Lamanna, Giuseppe Gigante, Domenico Casarano, and Pier Paolo Limoni

Abstract

We examine the instability of slopes in a catchment traversed by a 11 km long mid-slope road, characterized by the widespread presence of clay materials with poor geotechnical properties. High Resolution (HR) multispectral satellite imagery is used to provide focus on the landslides affecting the road and on their close association with poorly drained sites (wet areas, concentration of roadway runoff). The origin of many wet areas mapped from the satellite imagery is linked to the seasonally persistent high groundwater levels revealed through the piezometer monitoring. The remotely sensed data integrated with the in situ controls and subsurface monitoring show that the slopes traversed by the road are poorly drained and marginally stable. Thus even relatively moderate rainfall events (e.g. several tens of mm of rain in few days) can lead to landslide re-activations, which typically occur in the second half of fall and winter periods characterized by higher groundwater levels.

Keywords

Landslide • Satellite remote sensing • Piezometer • Inclinometer • Monitoring

Introduction

This work considers the instability of slopes in a 16 km^2 catchment area traversed by a 11 km long mid-slope road SP99bis, in the municipal territory of Rocchetta Sant'Antonio (Daunia Apennines, southern Italy). Although the local setting is that of moderate relief mountains with elevations not exceeding 800 m above sea level and low slope inclinations (10° in average), and the area receives modest amount of precipitation (total annual rainfall varies from 600 to 750 mm), landsliding is common (Wasowski et al. 2007; Lamanna et al. 2009); slope failures are linked to the widespread presence of clay materials (Miocene age and older flysch units) with poor geotechnical properties (Φ'_r varying from 6.9° to 16.5°, Wasowski et al. 2010a). In recent years the road SP99bis has been repeatedly damaged by landslides and is currently closed to traffic.

Here we build upon an earlier study (Wasowski et al. 2010b) which, using one meter (panchromatic) resolution satellite imagery (IKONOS) acquired on-demand in early spring 2006 following a particularly wet winter period, resulted in the recognition of numerous landslides and sites with features indicative of drainage conditions deleterious for the local slope stability (ponded water, wet areas, concentration of roadway runoff). Importantly, the remotely sensed data provided focus on the landslides affecting the road and on their close association with poorly drained sites. This information helped to plan the subsequent subsurface investigation and borehole monitoring aimed at detailed landslide assessment that was necessary to identify adequate slope stabilization measures.

In particular, during 2007–2008 period several tens of boreholes were drilled and instrumented with piezometers and inclinometers. The borehole monitoring, which began in

J. Wasowski (✉) • C. Lamanna • D. Casarano • P.P. Limoni
CNR-IRPI (Consiglio Nazionale delle Ricerche, Istituto di Ricerca per la Protezione Idrogeologica), Bari, Italy
e-mail: j.wasowski@ba.irpi.cnr.it

G. Gigante
Chartered Geologist, Alberobello, Italy

C. Margottini et al. (eds.), *Landslide Science and Practice*, Vol. 2,
DOI 10.1007/978-3-642-31445-2_24, © Springer-Verlag Berlin Heidelberg 2013

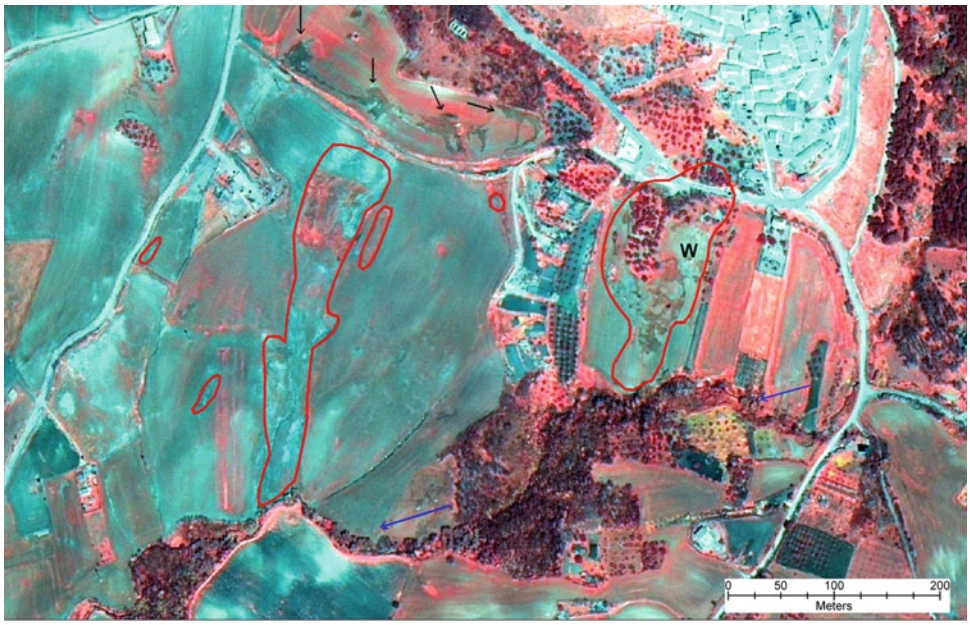


Fig. 1 Pan-sharpened IKONOS image acquired in 2006 (two visible plus near IR band) showing water flow and ponding, respectively indicated by *black arrows* and "W"; landslides are marked in *red* and the flow direction of a local stream is indicated by *blue arrows*

2009 and is still ongoing, revealed significant seasonal and shorter term variations of piezometric levels.

Using the daily rainfall records it is shown here how these variations are related to the local precipitation pattern. It is also demonstrated that the origin of many wet areas mapped from the IKONOS imagery is linked to the seasonally persistent high groundwater levels revealed through the piezometer monitoring. Furthermore, by combining the piezometer and inclinometer monitoring data we indicate a temporal relation between the high groundwater levels and periods of increased landslide activity.

Finally, we emphasize that the outcomes of this investigation, and in particular the data from piezometer borehole monitoring combined with satellite-derived map of poorly drained areas, have already been used to guide the design of more adequate slope and road SP99bis drainage systems. This demonstrates the practical applicability of high resolution multispectral satellite imagery in detailed engineering geology landslide investigations.

Landsliding in the Study Area

The study area belongs to the Daunia Apennines, which are known for recurrent landslide problems (e.g. Zezza et al. 1994; Iovine et al. 1996; Magliulo et al. 2008; Wasowski et al. 2008; Cotecchia et al. 2010). Mossa et al. (2005) presented a GIS-based assessment of landsliding regarding the area neighbouring to the north-west the territory of Rocchetta Sant'Antonio. They reported frequency of landslides exceeding 20 % for the overall area (132 km^2), indicative of high susceptibility of slopes to failure. It was also shown that the landslide frequency is the highest in 10–15° slope class, followed by 5–10 and 15–20 slope classes.

With reference to agricultural hillslopes, Wasowski et al. (2007) provided the first, preliminary assessment of the landslide activity in a 27 km^2 test area within the municipality of Rocchetta Sant'Antonio. They indicated significant impact of land use change on the susceptibility of rural slopes to landsliding and showed that widespread shallow landsliding can occur on slopes with cereal cultivation following wet winter periods. Lamanna et al. (2009) and Wasowski et al. (2010a) investigated the entire territory of Rocchetta Sant'Antonio (72 km^2), and showed that the pronounced land use changes that made the local slopes more susceptible to landsliding (in particular, deep ploughing of steeper marginal land for cultivation), followed the European Union economic incentives for durum wheat production introduced in mid-late seventies in southern Italy.

Mapping of Instability Factors

The study area considered in this paper has already been investigated by Wasowski et al. (2010b), who thanks to the high resolution of both panchromatic and multi-spectral satellite imagery were able to map numerous active landslides (many less than 10 m in width) and obtain detailed information on water runoff in the slope areas along the

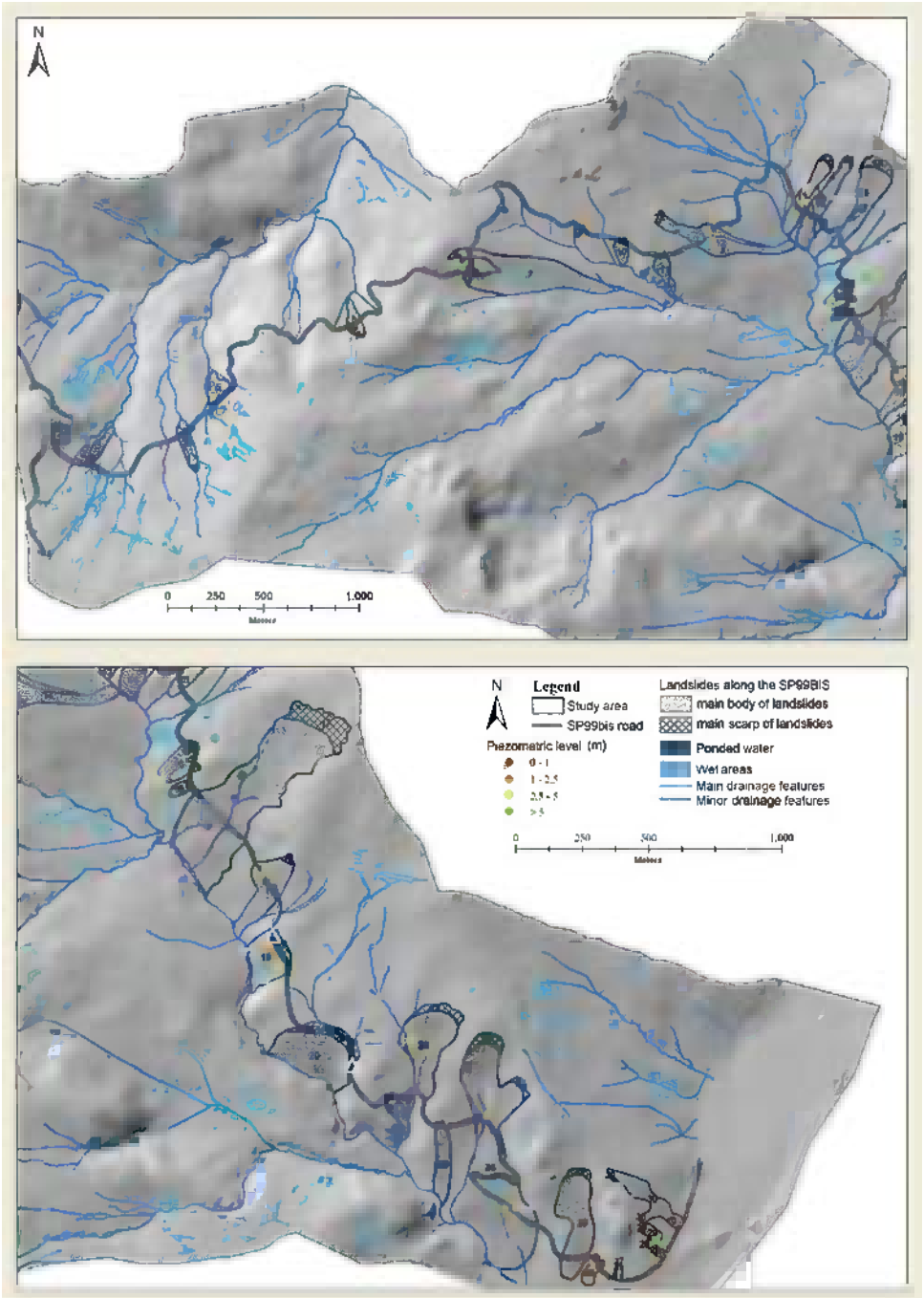


Fig. 2 DEM of the study area showing the distribution of the investigated landslides (numbered from 1 to 30), wet areas, drainage network and piezometer boreholes marked by different *color circles* according to the observed depths (below ground surface) of groundwater level fluctuations: *red* = between 0 and 1 m; *orange* = 1–2.5 m; *yellow* = 2.5–5 m; *green* = > 5 m. *White arrows and triangles* indicate, respectively, eight borehole piezometers and two inclinometers, whose monitoring records are shown in Figs. 3 and 4

damaged road Sp99bis. Particular attention was paid to features indicative of the drainage conditions deleterious for the local slope (and the road) stability; these included ponded water, wet areas, concentration of roadway runoff. Furthermore, the satellite image was used to map the natural surface drainage network in the entire study area. Figure 1 shows an example of landslides and wet zones detected in Rocchetta Sant'Antonio using the satellite data.

These data, confronted with the distribution of landslides, revealed that many failures are closely associated with wet areas and poorly drained hillslope sites (Fig. 2), as well as with discharge points of disordered road runoff onto the lower slopes. The reconstruction of the natural surface drainage network from IKONOS imagery added extra detail with respect to the information available on 1:5000 scale topographic maps.

Table 1 Landslides and borehole piezometers discussed in the text

Landslide-piezometer	Cell depth (m)	Wet zone distance (m)	Shear surface depth (m)
F3-2P	10.2	0	8
F6-1P	7.4	5	4
F14-1P	5.0	2	9
F20-1P	8.3	3	9; 17
F13-1P	8.0	44	11
F19-4P	6.5	45	14
F24-1P	4.0	153	14
F24-6P	4.0	47	14

Note: Casagrande cell depths, minimum distances from wet zones and depths of landsliding based on inclinometer measurements (landslide 20 has two shear surfaces). Variation of piezometric levels is shown in Fig. 3

Subsurface Investigation

The satellite-based results integrated with in situ controls assisted in planning the subsurface investigation of the slopes and landslides traversed by the Sp99bis road. During 2007–2008 period several tens of continuously cored boreholes were drilled and instrumented with piezometers (Casagrande type) and inclinometers. Since the initial geomorphological assessment of the slopes indicated that most of the landslides were shallow (i.e. <15 m in thickness), the depth of the boreholes was generally limited to 20–25 m.

The location of the investigated landslides (numbered from 1 to 30), wet areas, drainage network, piezometer boreholes, as well as the two inclinometer boreholes discussed further in the text, is shown on a digital elevation model (DEM) of the study area (Fig. 2). Most of the boreholes were positioned in the vicinity of the Sp99bis road. Nevertheless, in locating many piezometer boreholes we took into account also the distribution of wet areas and poorly drained sites mapped from the satellite imagery. Thus several piezometers were sited at a close distance from wet areas (generally variable from a few to several tens of meters).

Finally, the piezometer cells were positioned at variable depths (from 2 to 24 m from ground surface, although typically not exceeding 10 m). The information on the positioning of the piezometers with respect to the minimum distance from the wet zones and the depth of landslides is summarized in Table 1.

Results of Borehole Monitoring

Piezometer Data

The borehole monitoring began in early 2009 and revealed significant seasonal and shorter term variations of piezometric levels. This is illustrated in Fig. 3, which includes the data from the selected eight borehole piezometers grouped according to the minimum distance from the closest wet zone.

To show the relation between the groundwater level fluctuations and precipitation, the piezometric records are plotted together with 5-day cumulative rainfall data (Fig. 3) obtained from the pluviometric station located at Rocchetta Sant'Antonio (within less than 10 km distance from the study area). Five-day cumulative precipitation data are used here, because the predominantly shallow landslides that occur in the Rocchetta Sant'Antonio territory are often triggered by short-term rainfall events (Wasowski et al. 2010a).

The selected piezometers exhibit groundwater level variations that do not exceed 2–3 m, with maxima and minima, respectively in typically dry (summer/early fall) and in (or following) rainy (late fall/winter/early spring) seasons (Fig. 3). Significantly, during the rainy seasons the four borehole piezometers sited within a few meter minimum distance from the wet zones have regularly recorded persistent periods of very high groundwater levels, i.e. at or within less than 1 m from ground surface (Fig. 3a). The other four borehole piezometers, sited within a few tens of meter distance from the wet zones (Fig. 3b), have also recorded relatively high groundwater levels, which however, have never reached the ground surface (with the maxima generally 1.5 m below the ground).

Considering that the depths of Casagrande cells in both groups of piezometers are closely comparable (Table 1), the above results suggest that the wet areas initially identified via the satellite imagery are indicative of local, seasonally persistent groundwater levels within several investigated landslides (cf. Figs. 2 and 3).

Inclinometer Data

The inclinometer borehole monitoring began in early 2009. The results showed that most of the landslides are shallow, i.e. not exceeding 15 m depth (cf. Table 1). The measurements revealed the presence of very slow movements, on the order of few cm or less per year (Fig. 4). As expected, the greater displacements were detected during rainy seasons (late fall, winter, early spring).

Furthermore, despite the short observation period, the inclinometer data indicated the presence of small but significant variability of landslide movements. The greatest displacements were registered by the end of fall 2010 (Fig. 4). Indeed, the 2010 fall season was characterized by the well above average precipitation in the months of September, October and November (respectively, 105, 166 and 140 mm), as well as the occurrence of few day long periods of relatively intense rainfall (Fig. 3).

Importantly, following a 4-day mid-October 2010 event with nearly 100 mm of rainfall, there has been a significant rise of groundwater, which reached ground surface in

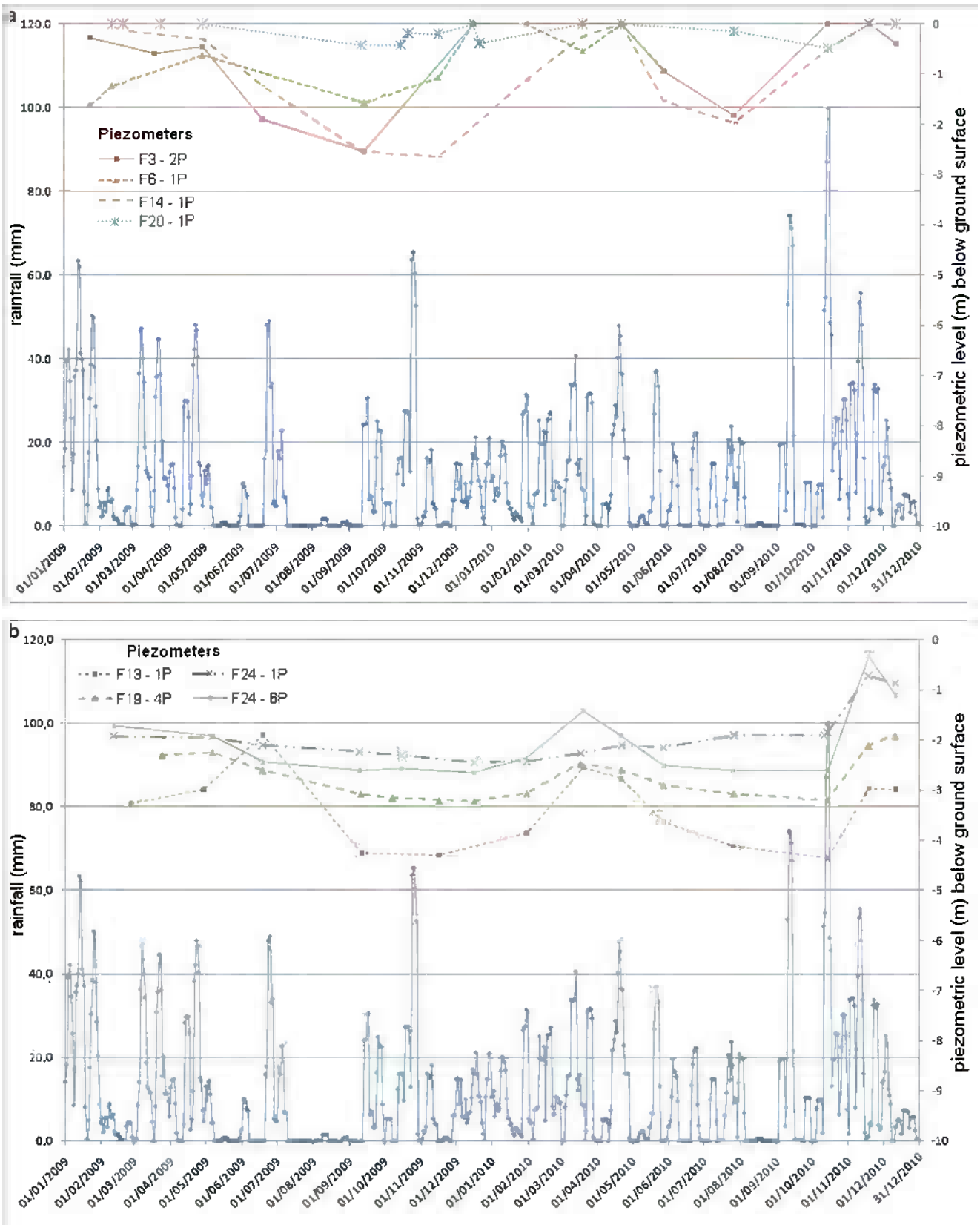


Fig. 3 Groundwater level variations in selected landslides and 5 day cumulative rainfall at Rocchetta Sant'Antonio; the data from the Casagrande piezometers for boreholes sited at a few meter distance and at tens of meter minimum distance from wet zones are shown, respectively, in Fig. 3a, b. See Fig. 2 for location of boreholes and Table 1 for additional details

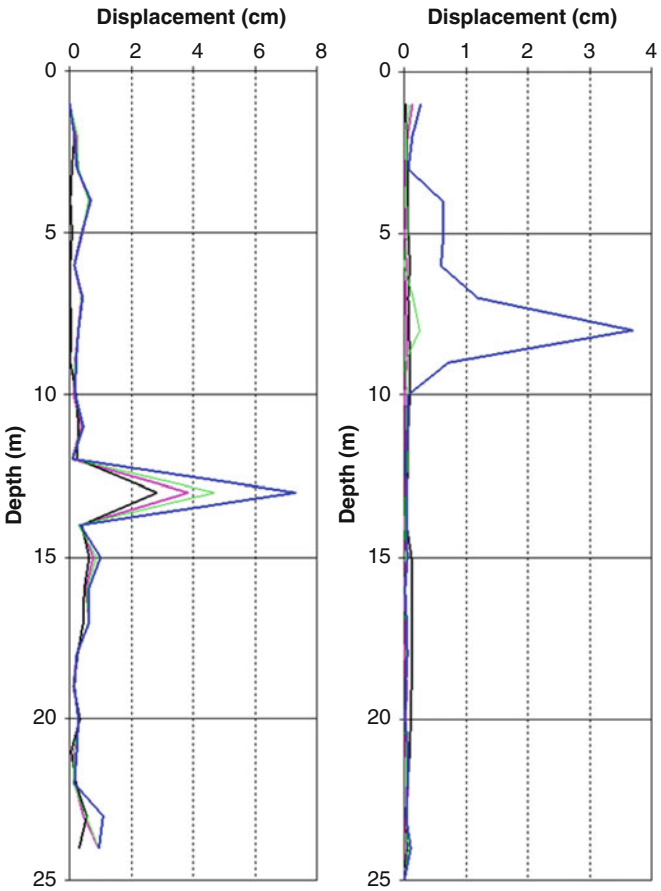


Fig. 4 Results of inclinometer measurements: *left diagram*—landslide 19, borehole 2I (initial reading on 24.03.2009); *right diagram*—landslide 20, borehole 8I (initial reading on 21.10.2009). See Fig. 2 for location

boreholes positioned within a few meters of the wet zones, as well as very high levels in sites distant few tens of meters from the wet zones (Fig. 3). The persistence of such high groundwater levels was documented in the second half of December, which was also the time of the inclinometer measurements (cf. Figs. 3 and 4).

Discussion and Conclusions

The results of this work demonstrate some of the benefits of the combined use of satellite remote sensing and in situ engineering geology investigation for detailed scale assessment and monitoring of the landslides that damaged a mid-slope road in the Apennine Mountains. In particular, we show that high resolution multispectral satellite imagery can be profitably exploited not only for mapping the landslides, but also for pinpointing their association with poorly drained sites. This information, which is difficult to retrieved from standard (panchromatic) aerial photos, assisted in planning the subsequent subsurface investigation and monitoring.

Significantly, the origin of many wet areas mapped from the satellite imagery can be linked to the seasonally persistent high groundwater levels revealed through the piezometer borehole monitoring. The remotely sensed data integrated with the in situ controls and piezometer and inclinometer monitoring showed that the slopes traversed by the road are poorly drained and marginally stable. Therefore, even relatively moderate rainfall events (e.g. several tens of mm of rain in few days) can lead to landslide re-activations, which typically occur in winter periods characterized by higher groundwater levels.

The outcomes of this investigation, and in particular the satellite-based map of poorly drained areas associated with the road landslides, combined with the results from piezometer (and inclinometer) monitoring have already been used to produce a preliminary design of new, more adequate slope and road drainage systems. This example, the growing availability and improving resolution (and decreasing costs) of space-borne optical imagery hold the premise for more frequent integrated use of satellite remote sensing and ground/subsurface exploration in engineering geology investigations of landslides.

Acknowledgments This work was conducted within the agreement between CNR-IRPI and Prefettura di Foggia. We thank the municipal administration of Rocchetta Sant'Antonio and in particular A. Magnotta, as well as G. Amoruso and G. Tedeschi of Regione Puglia for their support.

References

Cotecchia F, Santaloia F, Lollino P, Vitone C, Mitaritonna G (2010) Deterministic landslide hazard assessment at regional scale. In: Proceedings of Geo-Florida 2010, 20–24 Feb 2010, West Palm Beach, FL, pp 3155–3164

Iovine G, Parise M, Crescenzi E (1996) Analisi della franosità nel settore centrale dell'Appennino Dauno. Mem Soc Geol Ital 51:633–641

Lamanna C, Casarano D, Wasowski J (2009) Cambiamenti dell'uso del suolo e aumento dell'attività franosa nel territorio di Rocchetta Sant'Antonio (Appennino dauno). Il quaternario-Ital J Q Sci 22(2):139–156

Magliulo P, Di Lisio A, Russo F, Zelano A (2008) Geomorphology and landslide susceptibility assessment using GIS and bivariate statistics: a case study in southern Italy. Nat Hazards 47(3):411–435

Mossa S, Capolongo D, Pennetta L, Wasowski J (2005) A GIS-based assessment of landsliding in the Daunia Apennines, southern Italy. In: Proceedings of the international conference mass movement hazard in various environments, 20–21 Oct 2005, Cracow, Poland, pp 86–91

Wasowski J, Casarano D, Lamanna C (2007) Is the current landslide activity in the Daunia region (Italy) controlled by climate or land use change? In: Proceedings of the international conference on landslides and climate change, Ventor, Isle of Wight, 21–24 May 2007, pp 41–49

Wasowski J, Casarano D, Bovenga F, Refice A, Conte D, Nutricato R, Nitti DO (2008) Landslide-prone towns in Daunia (Italy): PS-interferometry based investigation. In: Chen et al. (eds) Proceedings of the 10th international symposium on landslides and engineered slopes, Xi'an, China, pp 513–518

Wasowski J, Lamanna C, Casarano D (2010a) Influence of land-use change and precipitation patterns on landslide activity in the Daunia Apennines, Italy. Q J Eng Geol Hydrogeol 43:1–17

Wasowski J, Lamanna C, Casarano D (2010b) Mapping mid-slope road landslides and instability factors with high resolution satellite imagery. In: Proceedings of 11th congress of the IAEG, Auckland, New Zealand, 5–10 Sep 2010, pp 2563–2570

Zezza F, Merenda L, Bruno G, Crescenzi E, Iovine G (1994) Condizioni di instabilità e rischio da frana nei comuni dell'Appennino Dauno Pugliese. Geol Appl Idrogeol 29:77–141



Monitoring Concepts and Requirements for Large Rockslides in Norway

Las Harald Blikra and Lene Kristensen

Abstract

The risk due to large rockslides in Norway is due to large run-out, the possibilities for river damming and the generation of disastrous tsunamis in fjords. The investigations, monitoring and early-warning that have been designed and implemented for the Norwegian rockslides follows requirements guided in national codes and international standards for geotechnical design. The investigation program is composed of the following main parts: (1) Surface investigations; (2) Ground (subsurface) investigations; (3) Analysis and modeling; (4) Evaluation of physical mitigation; and (5) Documentation. The design and implementation of monitoring systems follows the following main concepts: (1) Sensors on the surface and in boreholes that gives sufficiently knowledge about movements; (2) Sensors giving information about controlling mechanisms for movements (Meteorological station and water pressure); and (3) Backup systems for all critical sectors by establishing different types of monitoring systems. The infrastructure including power-supply system and data communication from the site is designed to fulfill the demand of redundancy. Based on the historical data and information from historical rockslide events elsewhere, early-warning levels have been implemented in the operational system.

Keywords

Rockslide • Early warning • Monitoring • Instrumentation • Displacements

Introduction

In general we seek to reduce landslide risk by avoiding building in hazard areas by doing hazard mapping and proper planning. For existing buildings and infrastructure with unacceptable hazard we normally try to perform physical mitigation. In some occasions, physical mitigation is impossible, difficult, or economically too costly due to the size and complexity of the landslide. For some of the large rockslides in Norway, which can lead to large catastrophes and major consequences for life and property, the government has therefore opened for establishing monitoring and early warning to reduce the risk.

The Norwegian building code has strong requirements to the monitoring and the permanent handling of the early-warning system. However, there exist no guidelines or handbooks that define specific requirements for the type and level of investigations and the monitoring systems needed in order to perform reliable early-warning of large landslides. On the basis of the high-risk related to large rockslides and tsunamis, our requirements have been relatively extensive. Examples are given from large rockslides situated in different climatic conditions in Norway (Fig. 1).

Investigations: Methods and Design

The principles of the investigation program and data from some selected key investigations in Norway are shown.

L.H. Blikra (✉) • L. Kristensen
Åknes/TafjordEarly-Warning Centre, Ødegårdsvegen 176, Stranda N-6200, Norway
e-mail: lhb@aknes.no

C. Margottini et al. (eds.), *Landslide Science and Practice*, Vol. 2,
DOI 10.1007/978-3-642-31445-2_25, © Springer-Verlag Berlin Heidelberg 2013



Fig. 1 Locations of rock-slope failures in Norway with implemented monitoring and early-warning

Principles

The design of the investigation program is important for several critical issues. Firstly, the rockslide scenarios need to be defined as the base for rockslide and tsunami modeling. Realistic volume and scenarios has vital impacts on the risk management in the hazard areas. Secondly, the distribution of the unstable area and the displacement pattern is the most important knowledge for the design and implementation of a proper and qualitatively acceptable monitoring system. Thirdly, an extensive knowledge platform is needed in order to be able to perform reliable and real-time operative monitoring and early warning. The understanding of the deformation dynamics is especially important during critical events, when decisions regarding alarm levels and evacuation have to be taken on relatively short notice.

There exist no guidelines or handbooks that define specific requirements for the type and level of investigations needed in order to perform reliable monitoring and early-warning of large landslides. However, the European Standard EN 1997–2:2007 (Eurocode 7) describes principles and requirements related to geotechnical design and ground investigations. The requirements are based on these standards and the national technical building codes. It had to be stressed however, that the final design of the investigations needs to be based on the local conditions.

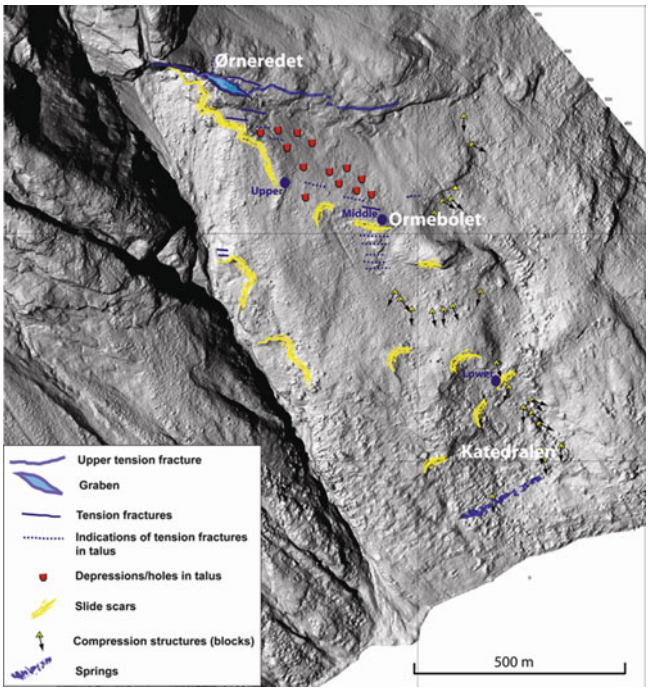


Fig. 2 Shaded-relief map with morphological features of the Åknes rockslide. The borehole locations are shown with *blue circles*

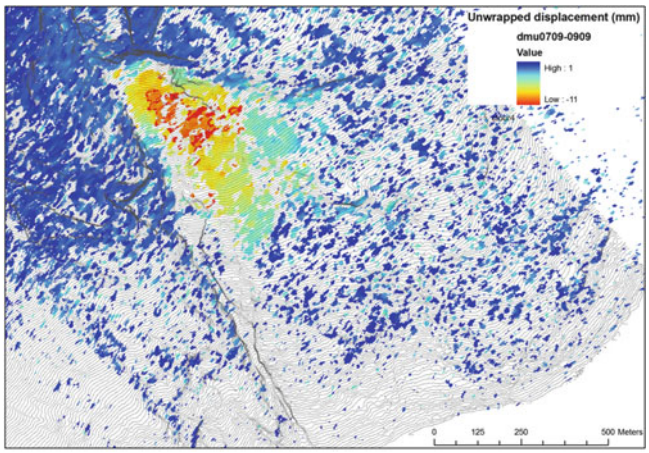


Fig. 3 Displacements measured by the LiSALab ground-based radar campaign. These are unwrapped data from the period 9th of July to 9th of September 2009. The moving area is clearly defined (*yellow and red areas*), and shows large movements in the upper southwestern corner (*upper left*)

Surface Investigations

Different types of surface investigations needs to be performed, including collection of high-resolution topographic data (e.g. air-based or ground-based LIDAR), detailed geological mapping (structural geology, geomorphology, hydrology) and mapping of surface displacements (satellite or ground-based radar, ground-based LIDAR, periodic GPS or total station). Figure 2 show an example of a simplified geomorphologic map of the Åknes rockslide, and the results from the ground-based radar campaign in 2009 is shown in Fig. 3. The surface investigations need to define the distribution of the unstable area and an overview of the deformation in different sectors of the landslide.

Ground (Subsurface) Investigations

In order to be able to have a good understanding of the landslide it is of vital importance to achieve subsurface geological data, including the depth of the instability and the related deformation. The investigations need to give a realistic 3D geometric model of the instability. There will thus be need for some selected borehole drillings combined with geophysical measurements.

At Åknes, there were performed relatively extensive 2D resistivity measurements, supplemented with some refraction and reflection seismic (Rønning et al. 2006, 2007). Deep core drillings down to 200 m depth was performed at three localities (Fig. 2), with geophysical logging and core logging (Ganerød et al. 2007). The rock cores give essential overview of the rock quality and the locations of sliding planes. Alternatively destructive drillings combined with televiewer logging can be used to characterize the rock and the structures (fractures, foliation and breccias). In addition to the geophysical logging (e.g. temperature, conductivity, resistivity, velocity), several methods were used for identification and characterizing the groundwater flow in the boreholes (Rønning et al. 2006; Thöny 2008).

The instrumentation in boreholes is essential for both the investigations of subsurface characteristics (sliding planes, volumes etc.) and for real-time operative early-warning. At Åknes and Mannen, four boreholes have been instrumented by the DMS system (Differential Monitoring of Stability) (Lovisolo et al. 2003). The DMS column is like a sensorized spiral cord or "snake" composed of a sequence of hard tabular modules connected to each other by special joints. The present systems used are 100–120 m long columns measuring the movement in 2D. The 120 m long columns consists of totally 245 sensors. The sensors include biaxial inclinometers, temperature sensors as well as piezometers and digital compasses in selected modules. Figure 4 shows an example of recent data from the upper borehole at Åknes measured in the period November 2010 until March 2011. It clearly documents the sliding zone at 50 m depth, in accordance with core and borehole data.

Analysis and Modeling

In order to perform stability modeling, there is a need for samples to be taken in the field or from drill cores for analyzing shear strength and other input parameters. Although a stability model cannot give us any conclusive answer about the stability, it should be done in order to understand the critical parameters for an event (sensitivity

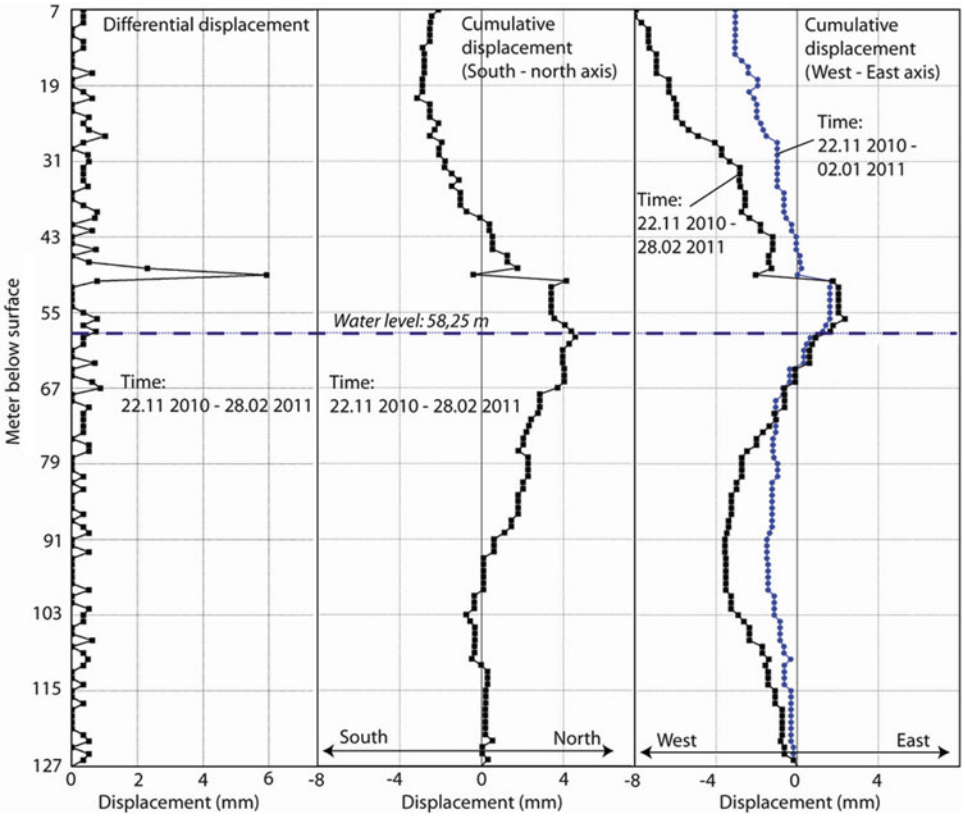


Fig. 4 Data from the DMS column in upper borehole from 22nd of November 2010 until 28th of February 2011. The 120 m long column covers the depths from 7 to 127 m, and shows the differential displacements to the *left*, south-north axis in the *middle*, and the total displacements for two different time periods to the *right*

analysis). Several models were used at the Åknes rockslide, including UDEC 2D (Kveldsvik 2008) and 3D FLAC (Grøneng et al. 2010). The modeling of the landslide run-out needs to be performed as an integrated part of the investigation program, including slide modeling and tsunami modeling (Glimsdal and Harbitz 2011).

Evaluation of Physical Mitigation

The Norwegian regulations require an evaluation of the possibilities for physical mitigation as alternative methods for reducing the risk. For large rockslides, this will normally be an evaluation for large-scale drainage of water to reduce the water pressure in fractures.

Documentation and Quality Control

The investigations need to be fully documented and reviewed. The Åknes/Tafjord Early warning centre has established an international group of experts giving advice to the centre regarding the design of investigations.

Monitoring: Methods and Design

Large and complex rockslides need extensive monitoring system in order to handle the early warning issues. The concepts and design is described briefly below.

Principles

The Norwegian monitoring systems has been designed in order to achieve a high level of robustness and redundancy, and at the same time giving different type of data which is the basis for analysis and decisions during a future event. The main principles for the design are based on the following main criteria:

1. Sensors on the surface and in boreholes that gives sufficiently knowledge about movements. The sensors needed to cover all important sectors or parts of the unstable area, and need to cover both local deformations across different fractures and the total displacements on the surface and in the subsurface.
2. Sensors giving information about controlling mechanisms for movements (meteorological station and water pressure).
3. Backup systems for all critical sectors by establishing different types of monitoring systems. The infrastructure including power-supply system and data communication from the site is designed to fulfill the demand of redundancy (backup systems).

Design

In order to establish a robust, reliable and redundant continuous monitoring network, a series of methods are used, both



Fig. 5 Examples of monitoring systems. (**a**) GPS antenna at Åknes; (**b**) location of total station at Åknes; (**c**) single lasers measuring across deep upper fracture at Åknes; (**d**) the borehole DMS instrumentation at Mannen, GPS antenna to the *left*

on the surface and in boreholes (Fig. 5). The array of sensors is chosen to provide the most complete information as possible in order to cover the entire unstable slopes, including all important sectors, see example of the final established monitoring system at Åknes (Fig. 6). However, there are a series of practical limitations in terms of distance from measured points to the monitoring instrument, local slope conditions, rockfall and snow-avalanche hazard and problematic atmospheric conditions. The changing atmospheric conditions along fjords and especially measurements across the fjord are especially demanding.

Surface Monitoring

Monitoring of the total displacements has in the Norwegian examples at Åknes, Mannen and Nordnes included a permanent GPS network (Figs. 5a and 6), and at Åknes also supplemented with total station measuring the distance to a large number of prisms. At Mannen, Hegguraksla and Åknes a permanent ground-based radar is emplaced to cover a larger area, but has some challenges during winter time with large amounts of snow. The GPS systems has been operating in an excellent way, and is one of the most important sensors (Nordvik and Nyrnes 2009), see example from Nordnes in Fig. 7. Although the resolution is not the best, it has been very stable. The data from the total station has been problematic due to large atmospheric changes and relatively large distances, and especially during the winter time it has been difficult to get reliable measurements. The data from the ground-based radar has some of the same problems, but gives important overview and data in inaccessible areas.

Local measurements include normally different types of extensometers and crackmeters, or single lasers when the distance across fractures is large (Fig. 5c). The extensometers and crackmeters give excellent data with limited noise (Fig. 8). The single lasers are relatively stable, but get large noise in bad weather, especially during periods of snow and fog.

At Åknes it has also been installed microsesimic network of eight 3-component geophones. The microseismic sensors are very stable and give reliable data. Also a series of surface 2D tiltmeters are placed at different sectors on all of the monitored rockslides.

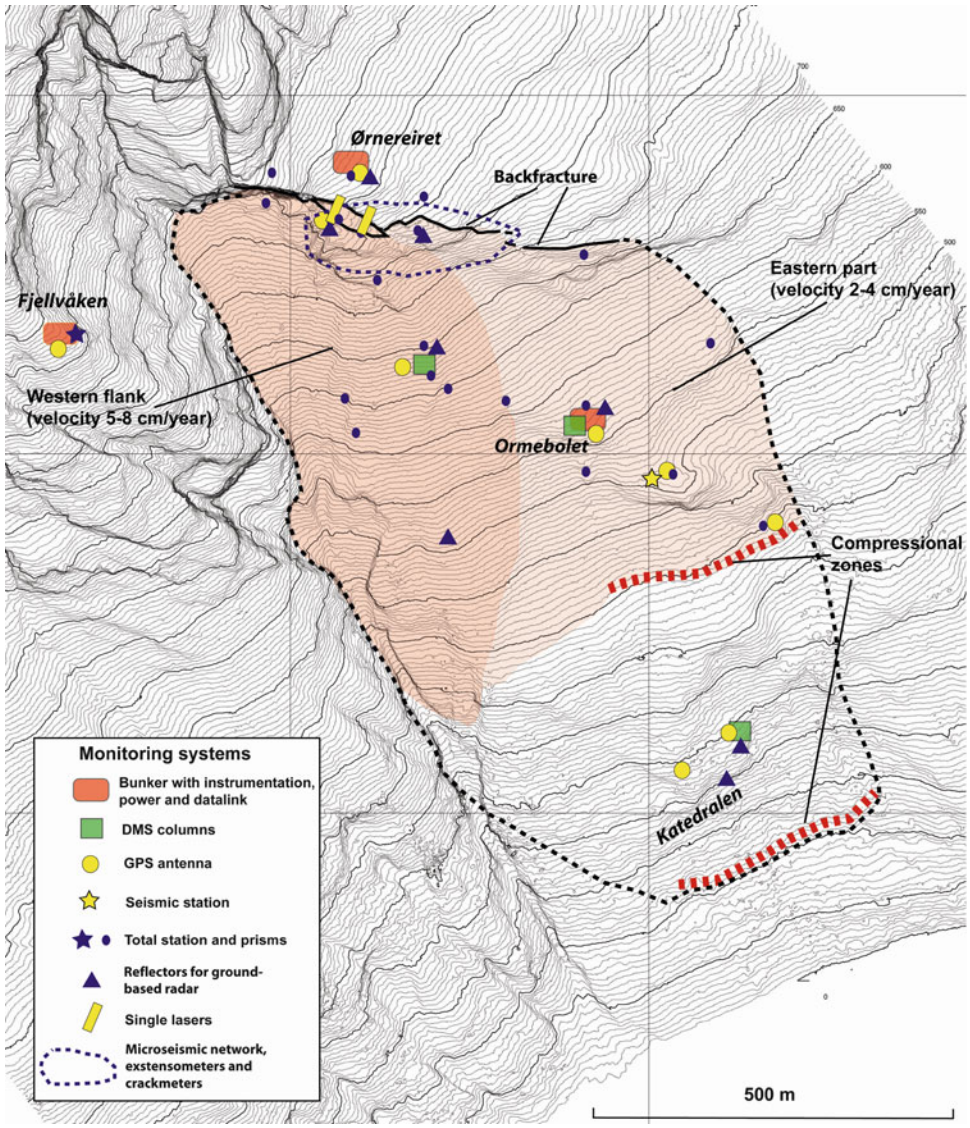


Fig. 6 The Åknes rockslide with the tree different sectors and an overview of the final established monitoring systems

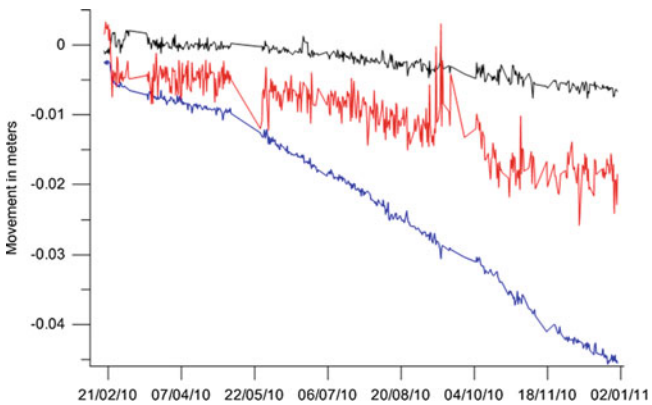


Fig. 7 One year of displacements from one of the GPS antennas at the most active sector at Nordnes, showing all three directions. *Blue* is movements towards west, *black* towards south and *red* is vertical

Subsurface Sensors

The Åknes and Mannen rockslides have established a permanent subsurface instrumentation composed of 100–120 m long DMS columns (Fig. 5d), which are linked to a fully real-time operational early-warning system. The system is very stable and gives continuous data with high resolution, see example of data in Fig. 4. These instruments are to be seen as laboratories inside the moving rocks and gives detailed knowledge about the deformation mechanisms.

Early Warning

The established monitoring and early-warning system at Åknes, Mannen and Hegguraksla are today fully operated by the permanent organization Åknes/Tafjord Early

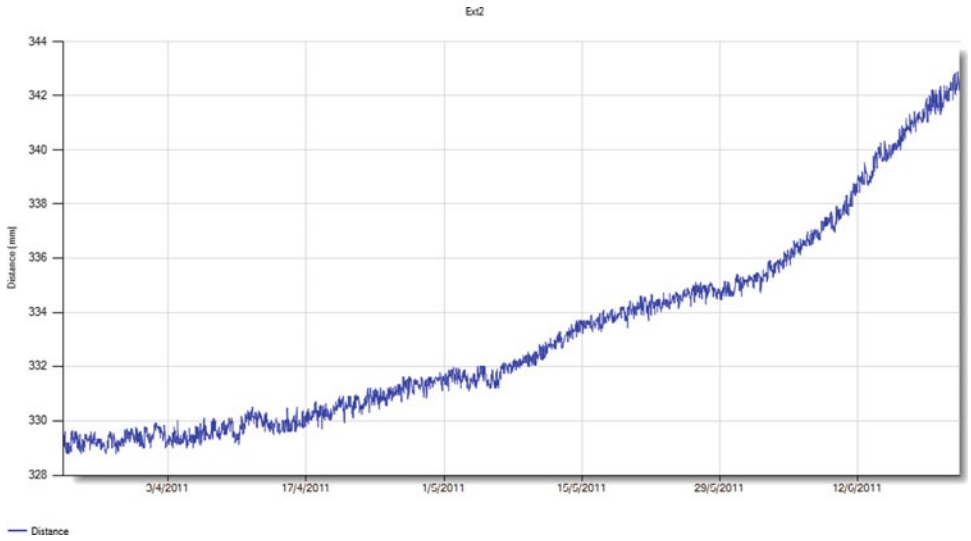


Fig. 8 Extensometer data from Mannen covering 3 months in 2011

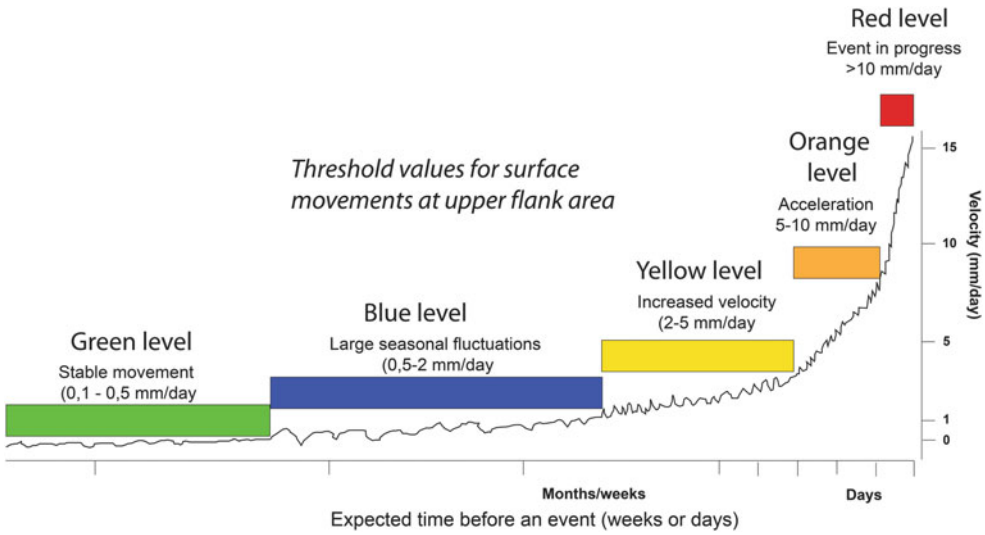


Fig. 9 Schematic diagram showing early-warning levels together with a possible development of the Åknes rockslide (Revised from Blikra, 2008)

Warning Centre, which have established a real-time operational handling on both the technical and geological part. The centre has also the operational responsibility for the geological part at the Nordnes rockslides. All the monitoring data achieved from the unstable areas are processed and analysed in order to find movement behaviour and velocity trends. This is also the basis for establishing threshold values for definition of warning levels. So far we use velocity and acceleration as the criteria for the different levels, see example for Åknes in Fig. 9 (Blikra 2008). The implementation of the thresholds has been based on the historical data from Åknes and the experience from other international studies (Crosta and Agliardi 2003). This concept has also been used for the early-warning system at Turtle Mountain in Canada (Froese and Moreno 2011).

The operational system today is based on the following routines: (1) Daily check of all sensors by the person on duty; (2) Daily data check by geologist on duty; (3) SMS messages on selected sensors; and (4) Contracts with monitoring companies with different types of operational level (SMS messages, daily check, availability etc.).

SMS messages and/or e-mail warning are difficult to implement and one main issue is to find the different types of noise in the data and finally to define thresholds that does not give to many false alarms, but still catching real events. One of the challenges is that sensors with large noise levels create a large amount of messages (e.g. the single lasers). SMS messages will never be used alone to change alarm levels, but is an important support and help for the persons on duty. The DMS system in the boreholes and the GPS sensors is very stable and SMS messages have been implemented for a long time.

The early-warning system also includes the implementation of warning methods that for the Åknes rockslide focus on two lines. Firstly a system of phone messages based on a

continuous updated database in addition to automatic SMS messages based on regional coverage from the mobile network companies. For the Åknes case, electronic typhoons are established in all the villages situated in the tsunami hazard zones. In addition, there has been a large effort in planning and establishing evacuation routes for all the inhabitants in the tsunami hazard zones. The hazard zones have been established on the basis of the slide scenarios and the results from the tsunami modelling (Glimsdal and Harbitz 2011).

Conclusions

The investigations, monitoring and early-warning that have been designed and implemented for the Norwegian rockslides follows requirements guided in national building codes and international standards for geotechnical design. The high risk due to a rockslide that has large run-out distances and can dam rivers and generate disastrous tsunamis has been the fundamental basis for the requirements and the design. The main aim has been to achieve a reliable knowledge base of the geology and the deformation model, in addition to a robust and redundant monitoring systems and related infrastructure for the early warning. The work has shown the importance of including both surface and subsurface investigations and monitoring. The established real-time monitoring systems and related infrastructure have reduced the risk to an acceptable level.

Acknowledgments The investigations and implemented monitoring systems are based on investigations and research corporation with a series of national and international partners. These include the Geological Survey of Norway, Norwegian Geotechnical Institute, NORSAR, Norwegian University for Science and Technology, University Centre of Svalbard, University of Bergen, University of Oslo, University of Milano-Bicoccca, University of Lausanne, ETH, and the companies Ellegi srl, CSG, Cautus Geo and Fugro. We will also thank the Norwegian Water and Energy Directorate (NVE) for financing the governmental part of the early-warning centre and for discussions regarding requirements.

References

Blikra LH (2008) The Åknes rockslide: monitoring, threshold values and early-warning. In: Zuyu Chen, Jian-Min Zhang, Ken Ho, Fa-Quan Wu, Zhong-Kui Li (eds) Landslides and engineered slopes. From the past to the future. Proceedings of the 10th international symposium on landslides and engineered slopes, 30 June–4 July 2008, Xi'an, China, Taylor & Francis. ISBN: 978-0-415-41196-7

Crosta GC, Agliardi F (2003) Failure forecast for large rock slides by surface displacement measurements. Can Goetech J 40:176–191

Froese CR, Moreno F (2011) Structure and components for the emergency response and warning system on Turtle Mountain, Alberta, Canada. Nat Hazards. doi:10.1007/s11069-011-9714-y

Ganerød GV, Grøneng G, Aardal IB, Kveldsvik V (2007) Core logging of seven boreholes from Åknes, Stranda municipality, Møre and Romsdal County. Geological Survey of Norway report no. 2007.020, p 222

Glimsdal S, Harbitz CB (2011) Numerical simulations of tsunamis from potential and historical rock slides in Storfjorden: hazard zoning and comparison with 3D laboratory experiments. Norwegian Geotechnical Institute Report 20051018-00-1-R, pp 250

Grøneng G, Lu M, Nilsen B, Jenssen AK (2010) Modelling of time-dependent behaviour of the basal sliding surface of the Åknes rock slide area in western Norway. Eng Geol 114:414–422

Kveldsvik V (2008) Static and dynamic stability analyses of the 800 m high Åknes rock slope, western Norway. Ph.D. thesis, Norwegian University of Science and Technology (NTNU), Department of Geology and Mineral Resources Engineering, p 128

Lovisolo M, Ghirotto S, Scardia G, Battaglio M (2003) The use of differential monitoring stability (D.M.S.) for remote monitoring of excavation and landslide movements. In: Myrvoll (ed) Proceedings of the sixth international symposium on field measurements in geomechanics, Oslo, Balkema, pp 519–524

Nordvik T, Nyrnes E (2009) Statistical analysis of surface displacements – an example from the Åknes rockslide, western Norway. Nat Hazards Earth Syst Sci 9(3):713–724

Rønning JS, Dalsegg E, Elvebakk H, Ganerød G, Tønnesen JF (2006) Geofysiske målinger Åknes og Tafjord, Stranda og Nordal kommuner, Møre og Romsdal (in Norwegain). Geological Survey of Norway report 2006.002, pp 1–66

Rønning JS, Dalsegg E, Heincke BH, Tønnesen JF (2007) Geofysiske målinger på bakken og ved Hegguraksla, Stranda og Norddal kommuner, Møre og Romsdal (in Norwegian). Geological Survey of Norway report 2007.023

Thöny R (2008) Dynamic fluid electric conductivity logging for identification and characterization of preferential groundwater flow in the Åknes rockslide (Norway). M.Sc. thesis, Department of Earth Sciences, ETH Zurich, p 105



Continuous Monitoring and Near-Real Time Processing of GPS Observations for Landslide Analysis: A Methodological Framework

Jean-Philippe Malet, Patrice Ulrich, Aline Déprez, Frédéric Masson, Candide Lissak, and Olivier Maquaire

Abstract

The objective of this work is to present a methodology for the near-real time characterization of displacements using permanent GPS stations on landslides. In France, several GPS receivers have been installed on active landslides since a few years. These landslides show very different displacement rates and kinematic regimes. For the monitoring of landslides where the required degree of accuracy is millimetric, GPS has been mainly used for repeated measurements, as a complement to conventional geodetic methods. Permanent monitoring is still not usually performed operationally.

Keywords

GPS • Geodesy • Kinematics • Permanent monitoring

Introduction

A large variety of techniques is available for the monitoring of landslide displacements, ranging from classical geodetic methods providing a local measurement of the deformation to advanced laser and radar methods providing a global image of the deformation (LCPC 1994; Angeli et al. 2000). Distancemeters, total stations and *Global Positioning Systems* (GPS) receivers allow to precisely locate the position of targets installed within a landslide over time (Duranthon 2000). Terrestrial or airborne stereo-photogrammetry, laser scanning or radar interferometry provide images of the unstable slope at very high spatial resolution and accuracy and allow to generate detailed DEMs, geomorphological maps and velocity maps (Weber and Herrmann 2000; Mora et al. 2003; Peyret et al. 2008; Baldi et al. 2008).

Among these techniques, the conventional geodetic methods (total station, GPS) remain the most commonly used because it is possible to reach an accuracy of a few millimetres on short baselines of a few kilometres and to access to a precise 3D absolute coordinates. These techniques are also commonly used for the precise co-registration of images acquired with high-resolution cameras, LiDAR and radar systems.

The objective of this work is to present a methodology developed for the near-real time characterization of displacements using permanent GPS stations. By tracking the electromagnetic waves that the GPS satellites are sending continuously, the system can obtain the antenna position (Longitude, Latitude, and Height, or X, Y, Z coordinates). The use of the phase measurements allows determining the relative positions of points located as far as several hundred kilometres apart with an accuracy of 2–5 mm in planimetry and 5–10 mm in altimetry. This accuracy allows the fast detection of weak displacements and, thus the survey of the temporal evolution of crustal deformation (Dixon 1991) and natural hazards. A review of the monitoring applications is given in Malet et al. (2002).

J.-P. Malet (✉) • P. Ulrich • A. Déprez • F. Masson
Institut de Physique du Globe de Strasbourg, CNRS UMR 7516, Université de Strasbourg, Ecole et Observatoire des Sciences de la Terre, 5 rue Descartes, Strasbourg F-67084, France
e-mail: jeanphilippe.malet@unistra.fr

C. Lissak • O. Maquaire
Géographie Physique et Environnement, CNRS UMR 6554, Université de Caen-Basse-Normandie, Esplanade de la Paix, Caen Cedex F-14032, France

C. Margottini et al. (eds.), *Landslide Science and Practice*, Vol. 2,
DOI 10.1007/978-3-642-31445-2_26, © Springer-Verlag Berlin Heidelberg 2013

The objectives of this manuscript are (1) to present the permanent GPS monitoring system and data transfer system installed on several landslides in France, (2) to present the automatic processing of the data, and (3) to define quantitatively the contribution of permanent GPS observations for the fast detection of small displacements.

The GPS Survey Network of the OMIV Observatory

A Network of Permanent GPS Receivers on Landslides

In France, several GPS receivers have been installed on active landslides (e.g. *La Clapière* rockslide, *Avignonet* and *Villerville* rotational slides, *Super-Sauze* and *La Valette* mudslides) since a few years. These landslides show very different displacement rates (ranging from a few centimetres to several meters per year) and different kinematic regimes (e.g. continuous displacement of nearly constant rate or succession of periods of acceleration/deceleration). All these landslides are part of the French *Observatory of Landslides* (e.g. OMIV), a collaborative structure of the French Research Council (CNRS) aiming at collecting the same type of kinematic, hydrologic and seismic observations on landslides and at disseminating the data to the scientific community (e.g. http://eost.u-strasbg.fr/omiv).

For the monitoring of landslides where the required degree of accuracy is millimetric, GPS has been mainly used for repeated measurements (Gili et al. 2000; Coe et al. 2003; Squarzoni et al. 2005; Brückl et al. 2006), as a complement to conventional geodetic methods. Permanent monitoring is still not usually performed operationally, mostly because of the cost of the GPS system compared to conventional deformation monitoring techniques. In addition, if GPS measurements can reach a millimetre-level of accuracy for long observation sessions (typically 12 h), their accuracy decreases with the duration of the observation sessions, because of errors introduced by variations of the satellite constellation and multi-path effects at the sites (Genrich and Bock 1992). Moreover, one millimetre-level accuracy requires sophisticated *a posteriori* data processing techniques. However, to acquire a very precise 3D coordinate that can be used as a reference for other monitoring techniques and to develop early-warning systems based on real-time displacement analysis, permanent GPS with automatic transmission of the data is certainly the only solution that can be used on very constraining sites with difficult accessibility, absence of long-term stability of the slopes around the landslide, or absence of direct visibility.

The few permanent applications of GPS applications on landslides are by Malet et al. (2002) at the *Super-Sauze* landslide (France) using single-frequency (L1) GPS receivers, Chen et al. (2005) at the *Xiaowan* landslide (China) using multi-antenna systems, and Reid et al. (2008) at the *Fremont* landslide (California, USA).

Equipment, Field Installation and Data Transfer

On the landslides monitored by OMIV, a similar monitoring strategy has been set up and consists in the installation of 2 or 3 GPS receivers within the landslide (e.g. 'moving GPS'), and 1 GPS receiver outside the landslide boundaries in stable areas (e.g. 'base GPS'). The GPS data are acquired with TRIMBLE NetRS or TRIMBLE R9 geodetic dual-frequency receivers equipped with TRM41249.00 antenna and a TZGD radome.

Every day, one 30-s daily file (i.e. 2880 sessions) and 24 1-s hourly files (i.e. 3,600 sessions) are produced. The data are stored locally and, within 1 day, a wireless access point allows the data transmission to a local database server (located at EOST) and the processing. A communication problem does not cause any data loss, as the GPS receivers have an on-board memory of several weeks. Figure 1 presents, as an example, the installation of the GPS receivers at the *La Valette* landslide (south French Alps) and the designed geodetic monuments. Figure 2 presents the location of the GPS stations at the *La Valette* landslide and at the *Villerville* landslide which is a rotational landslide located in Normandy in the North-East of France.

GPS Data Processing and Automated Scripting

The processing of the data has been performed following two main ideas: (1) the processing has to be as simple as possible to avoid large computation time, and (2) the precision of the results (e.g. the accuracy on the baseline determination from the GPS stations located on the landslides to the GPS stations outside of the landslides) has to attain a millimetric range.

The processing is performed with the GAMIT/GLOBK package (Herring et al. 2003a, b), dedicated to the estimation of three-dimensional relative positions of ground stations and satellite orbits. A loosely constrained daily solution (H-) file of parameter estimates and covariances is the output of GAMIT. The GLOBK package combines the daily solutions to estimate station positions and velocities. Orbital and Earth-rotation parameters can also be estimated.

A script (Fig. 3) has been developed to obtain the positions of each station. The script is activated daily and integrates automatically the most recent available GPS data

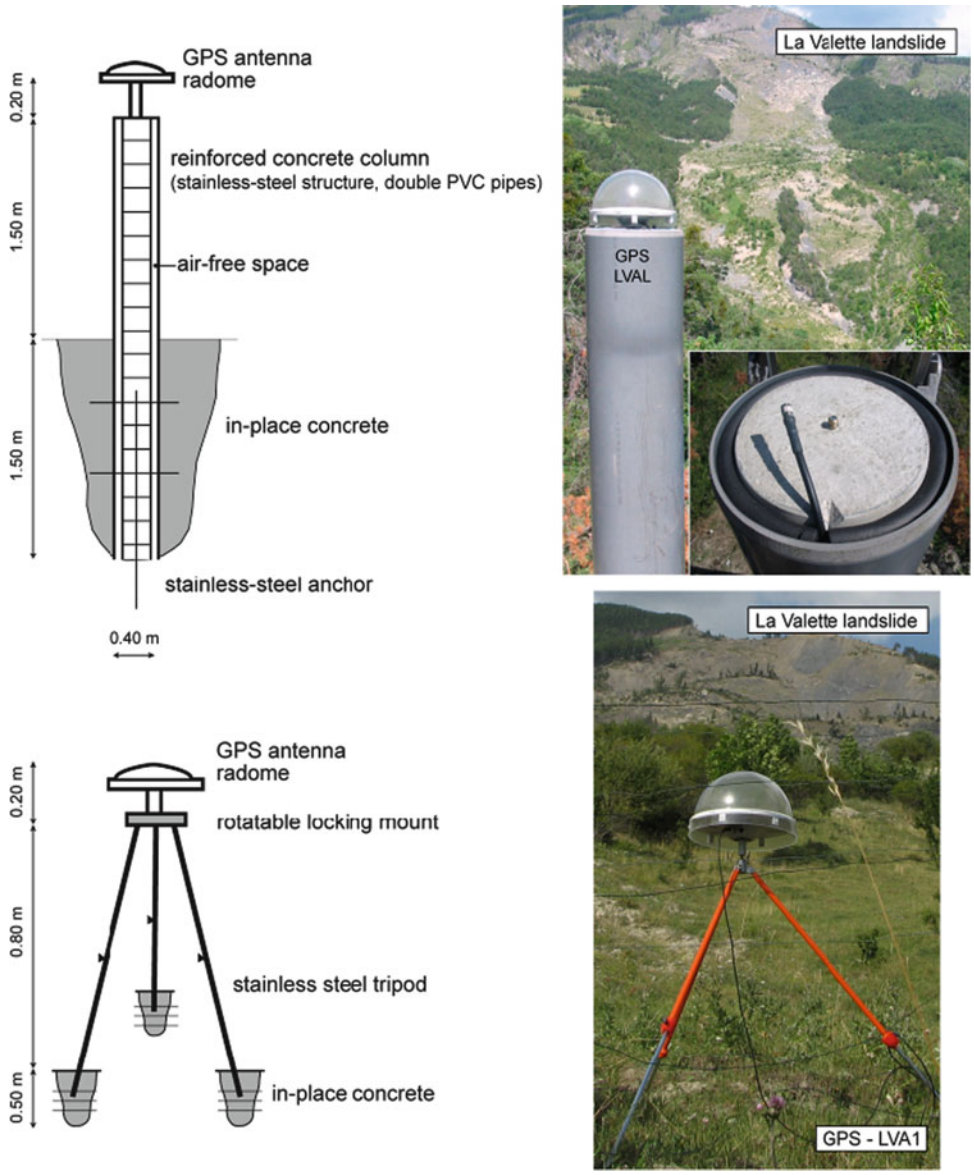


Fig. 1 Example of the installation of the GPS receivers at the *La Valette* landslide (South French Alps). *Top*: Installation of the base station LVAL, and geometry of the geodetic monument. *Bottom*: Installation of the moving station lva1, and geodetic monument

to calculate the baseline and position time series. The geodetic coordinates (latitude, longitude and ellipsoid height) and the baseline lengths are extracted from the output file of GLOBK. The geodetic coordinates are then converted to local geographical coordinate systems (Lambert zone; North, East and altitude) with the Circé, software developed by the French Topographic Survey IGN (Institut Géographique National).

Two processing modes have been set up: a first calculation is carried out within 2 days of the data transmission by using the rapid orbits of International GNSS Service (IGS), and a second calculation is carried out within 30 days of the data transmission in order to integrate the final precise orbits of the satellites. A test over a 100 days data sample indicated that differences on the baseline lengths calculated with the rapid orbits in comparison to the final precise orbits were negligible, in the order of hundredth of millimetres. The 30 days delay type of processing is nevertheless useful because it allows updating the GPS database with all RINEX files recorded. This two-step methodology allows also to overcome occasional broadcasting problems.

Performance of the GPS Processing Strategy

The best processing protocol has been defined according to some constraints mainly on the accuracy of the baseline determination; e.g. the evaluation of baselines of a few hundreds of meters with a very high accuracy of a few millimetres.

The geometry of the GPS network and the processing parameters has been chosen by performing numerous tests. For the implementation of the processing strategy, the GPS



Fig. 2 Installation of the GPS stations at the La Valette landslide (**a**, **b**) with the location of the base receivers LVAL on a stable crest and the two moving GPS lva1 (toe) and lva2 (crown), and at the Villerville landslide (**c**, **d**) with the location of the base receiver VLRV uphill of the main scarp and the two moving GPS vlrh and vlrb at the toe nearby the shoreline

data acquired at the *Villerville* landslide over a continuous period of 175 days (slightly less than 6 months) and several configurations of GPS networks (Fig. 4) have been used.

GAMIT allows estimating position and satellite orbit parameters. The estimation of the orbit parameters necessitates the introduction of GPS data from stations far from the studied area; in practice, a European scale network is needed. This can make the processing cumbersome without providing any better accuracy (Fig. 5). According to these results, a strategy without a re-assessment of the orbits has been chosen and the calculation mode 'ONLY POSITION' has been selected as it requires only the introduction of a few regional GPS stations (Fig. 4). Because of the distances between the regional stations and the GPS on the landslides, a linear combination of the two frequencies L1 and L2 is used in order to filter ionospheric delays.

The differences in the determination of the baseline lengths with the global and the regional networks (Fig. 6, top) are close to zero and without bias for the short baseline on the landslide (VLRV-vlrb), slightly larger and with a small bias for the longer baseline outside the landslide (CAEN-VLRV). Even if the differences are slightly higher, the same result is globally observed for the global and local networks (Fig. 6, bottom). Within the local network, the evaluations were made with each station successively omitted. The differences observed on local baseline values were a few tenths of millimetres. These results are confirmed by the analysis of the baseline time series. The time series of the VLRV-Vlrb computed using a global, a regional and a local

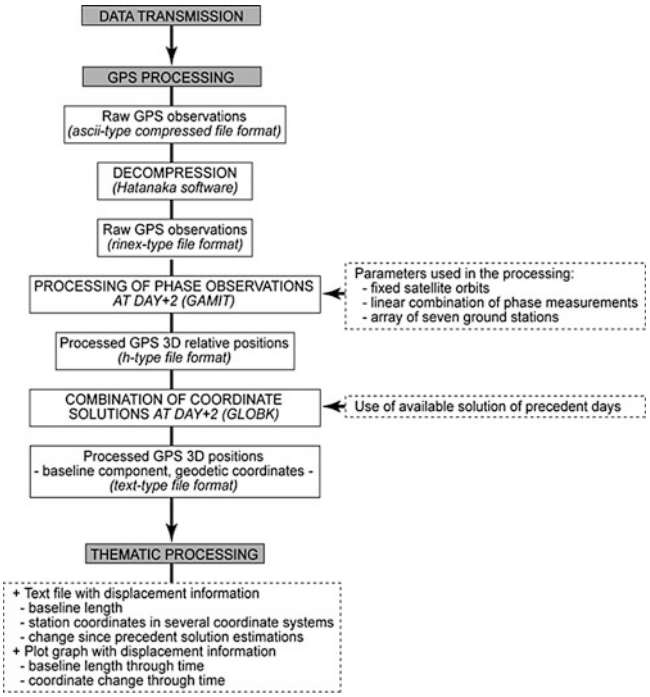


Fig. 3 Flowchart of GPS data automatic processing

network are detailed on Fig. 7. Differences are always smaller than 1 mm, and generally smaller than 0.5 mm.

The influence of the session duration on the baseline evaluation has been tested by computing a solution for respective records of 3, 6 and 12 h. As expected, comparisons with the daily solution (considered as the reference) indicate that the precision is decreased when the duration of the session decreases (Fig. 8). This result is consistent with previous observations obtained by Malet et al. (2002) for the *Super-Sauze* landslide.

From these results, the processing strategy consisted in the use of a local network and of 24-h sessions. The local network (Fig. 4) is composed of seven stations to avoid a lack of result in case of technical problem on some stations (antenna breakdown, broadcasting problem).

Analysis and Interpretation of the Results: Example of the *Villerville* Landslide

The variations in baseline lengths at the *Villerville* landslide are used to illustrate the potentials of the processing strategy. The *Villerville* landslide (e.g. 'Cirque des Graves') is located on the cliffs of the Pays d'Auge plateau (up to 140 m)

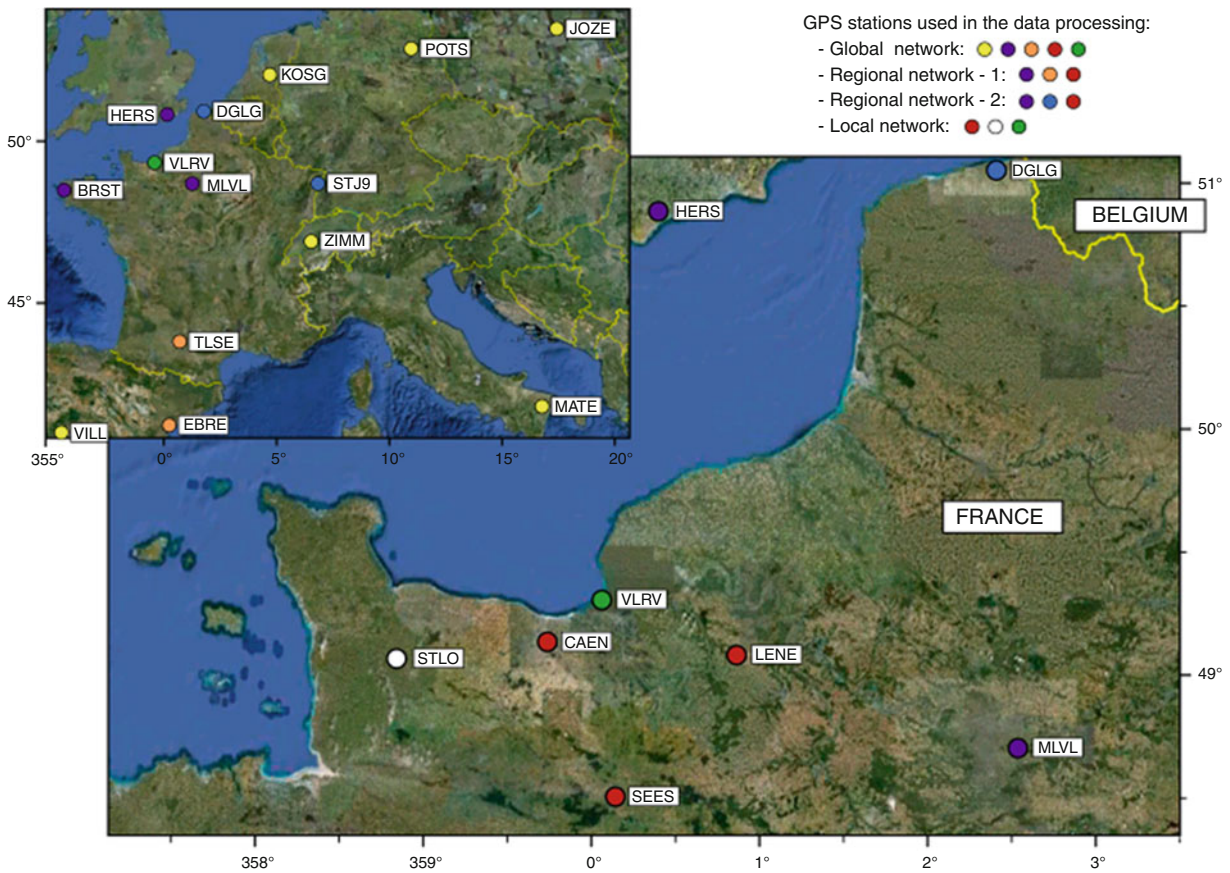


Fig. 4 Map of the different GPS networks (global, region-1, region-2, local) used for the tests at the *Villerville* landslide

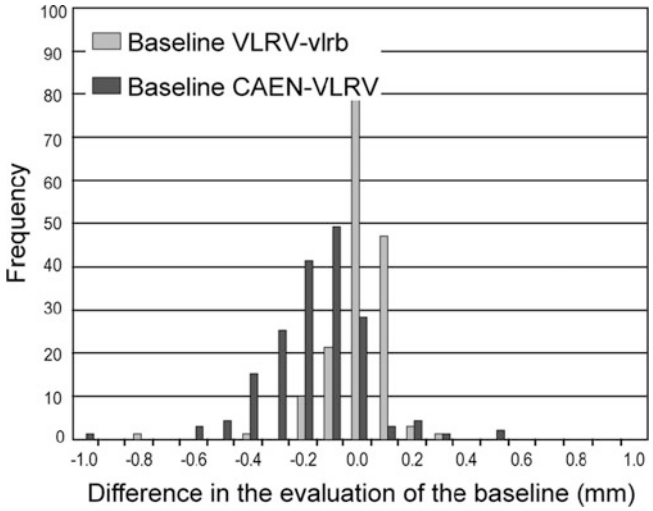


Fig. 5 Comparison of the baseline evaluations with the use of fixed or not fixed satellite orbit parameters. The processing using the orbit parameters requires the download of additional data. The CAEN-VLRV baseline is about 50 km in length and the VLRV-vlrb baseline (the longest baseline on the landslide) is about 500 m in length. Standard deviations of 0.18 mm for the CAEN-VLRV baseline and of 0.11 mm for the VLRV-vlrb baseline are observed

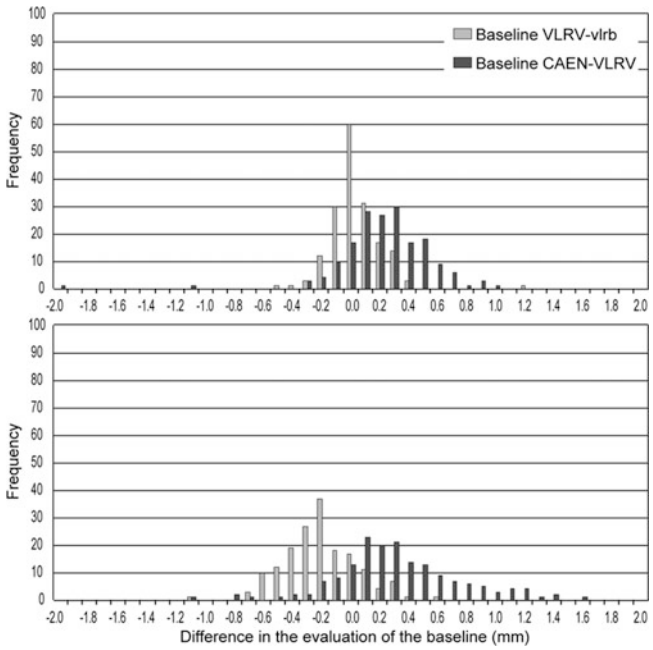


Fig. 6 Comparison of the baseline length evaluations for different GPS networks. *Top*: Differences among the determination with the global and the regional network. *Bottom*: Differences among the determination with the global and the local network (see Fig. 4 for the definition of the GPS networks)

between Trouville and Honfleur (Fig. 4), and is mainly developed in marls (Flageollet and Helluin 1987). The landslide covers approximately 8 ha surrounding the village of Villerville, and is defined as an active, slow-moving,

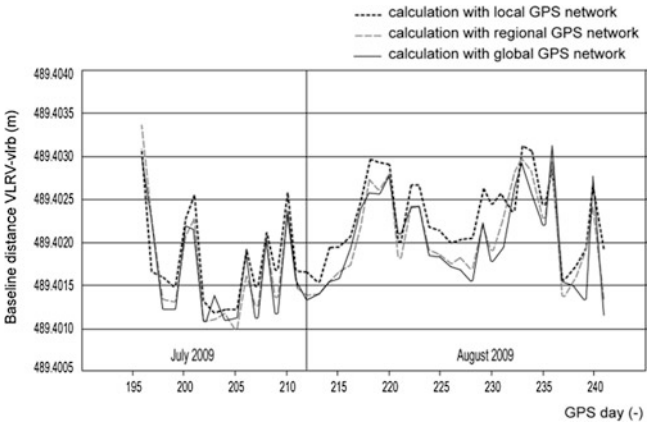


Fig. 7 Temporal variations of VLRV-vlrb baseline computed with different GPS networks

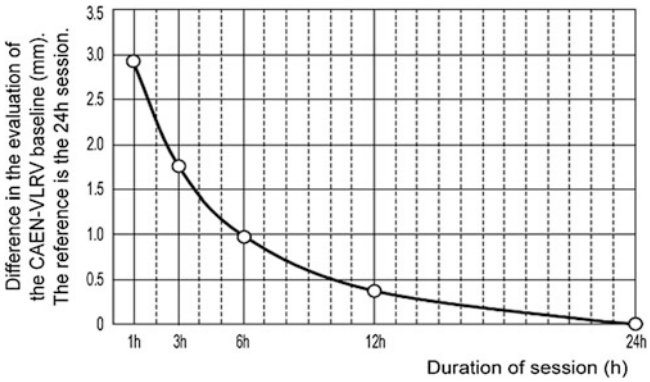


Fig. 8 Changes in accuracy of the baseline length as a function of the session duration

rotational landslide according to the Cruden and Varnes (1996) classification.

Since the first reactivation in 1982, the slope is affected by slow movement (0.05–0.10 m year^{-1}). Three other reactivations (February 1988, January 1995 and March 2001) have been observed (Lissak et al. 2010). Since 1984, the landslide is investigated for a better understanding of the processes. The actual monitoring network is composed of 24 benchmarks implanted according to accessibility, vegetation constraints and to specific geomorphological features. The three permanent GPS receivers are installed since July 2009 to provide continuous observations and to implement an early-warning system (Fig. 9).

Analysis of repeated GPS data on the topographic benchmarks allows identifying the direction and amplitude of displacements. Sectors with differences in rates and magnitudes of displacement are identified. Results of the permanent GPS monitoring allow interpreting the temporal pattern of the kinematics. For example, the cumulated displacements between January and July 2010 are respectively of 0.06 and 0.02 m for the vlrb and vlrh stations.

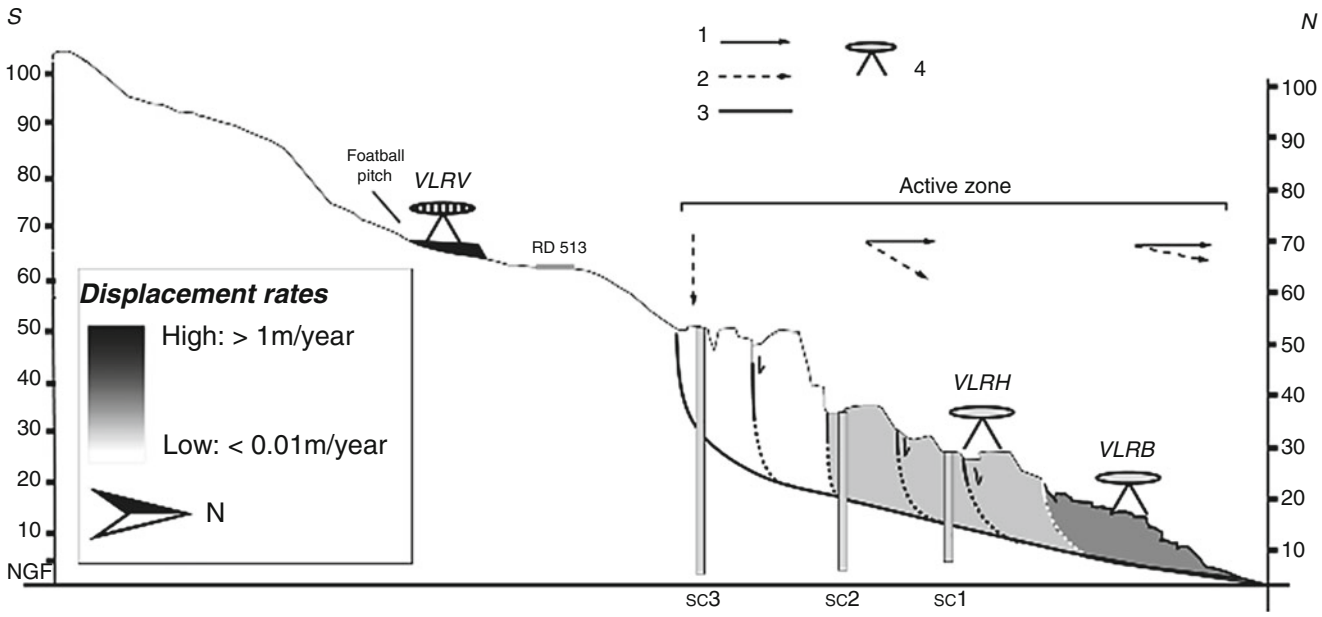


Fig. 9 Geometry of the *Villerville* landslide (Cirque des Graves), with indication of the main sliding surfaces and the displacement vectors at the surface: (*1*) horizontal displacement, (*2*) vertical displacement, (*3*) sliding surface, (*4*) GPS receivers

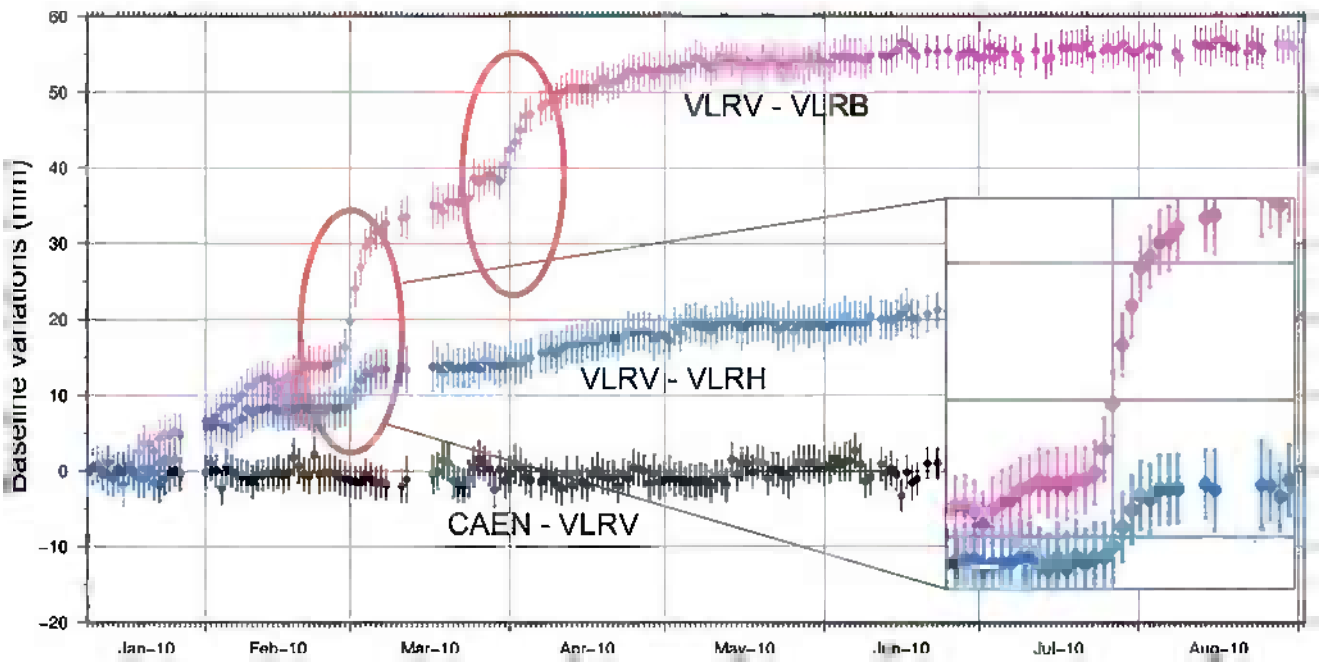


Fig. 10 Changes in baseline lengths between VLRV (local reference station) – CAEN (regional reference station, and VLRV-vlrh; VLRV-vlrb) for the period January 2010–August 2010. The baseline VRLV – CAEN allows to determine the accuracy on the GPS solutions, which is estimated at ca. 5 mm in all directions

Two acceleration periods are observed at both stations (Fig. 10), in January and February 2010, with a time lag of about 5 days in the peak in velocity among the stations. The acceleration of early March 2010 is controlled by changes in the pore water pressure regime within the landslide body, while the acceleration of April 2010 is caused by high wind velocities and sea waves which have eroded the toe of the landslide. During April and May 2010, a decrease of the groundwater level is monitored and no movement is observed on the landslide.

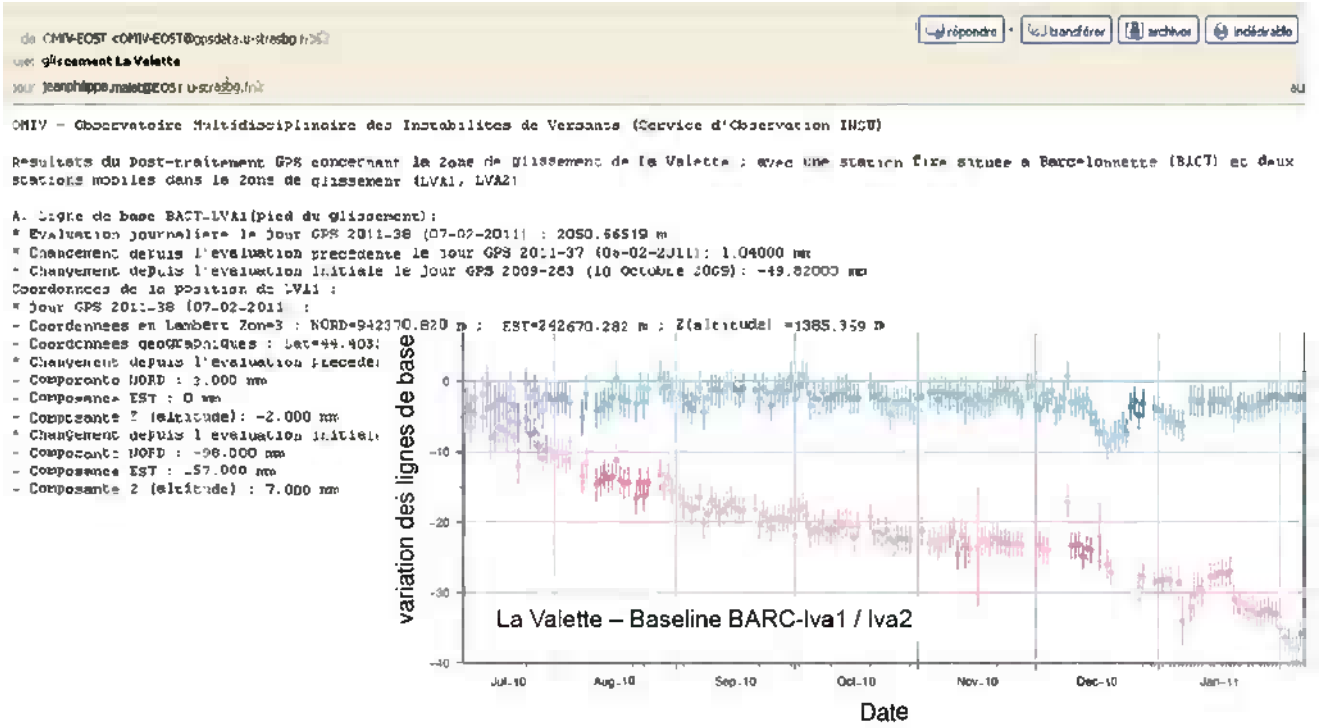


Fig. 11 Example of daily text-message send to stakeholder with a synthesis of the calculations and associated graphs: 'Moving' GPS lva1–lva2 for the period July 2010–January 2011

A Graphical Interface for an Automatic Recognition of the Displacement

As part of the implementation of a warning system, the automated script allows processing of the data, collecting the results and updating a text-files database with the solution easily readable in different coordinate systems (station coordinates, value of baseline lengths, components of the baseline). Daily, the figures and the text-files generated by the script are sent by e-mail to stakeholders. An example of automated email is presented in Fig. 11.

Conclusion

A methodology and a processing flowchart have been developed for the near-real time characterization of displacements using permanent GPS stations. The processing is fully automated, from the data acquisition on site, to the data transmission and storage on local servers, and to the processing and the diffusion of the information through relevant graphs and emails.

The work demonstrates that in order to acquire a very precise 3D coordinate (that can be used as a reference for other monitoring techniques and/or to develop early-warning systems based on real-time displacement analysis), permanent GPS with automatic transmission of the data is certainly the only solution that can be used on very constraining sites. All aspects of the setup of the system on site (location of the stations, skyplot visibility, energy consumption) and on the processing (selection of appropriate GPS networks to constrain the calculation, duration and sampling rate of the observation session) have been carefully evaluated before further development of additional GPS stations on other landslides. Actually, 12 GPS stations are part of the calculation on five different landslides in France.

Acknowledgments This research was funded through the ANR Risk-Nat project *SISCA: Système intégré de Surveillance de Crises de glissements de terrain* (2009–2011), the Project CPER *GR2TC: Gestion des Ressources, Risques et Technologies du domaine Côtier* (2007–2013), and the European Project FP7 *SafeLand: Living with landslide risk in Europe* (2009–2012). The GPS systems and the automated processing have been set up by the OMIV-EOST team at Strasbourg.

References

Angeli MC, Pasuto A, Silvano S (2000) A critical review of landslide monitoring experiences. Eng Geol 55:133–147

Baldi P, Cenni N, Fabris M, Zanutta A (2008) Kinematics of a landslide derived from archival photogrammetry and GPS data. Geomorphology 102:435–444

Brückl E, Brunner FK, Kraus K (2006) Kinematics of a deep-seated landslide derived from photogrammetric, GPS and geophysical data. Eng Geol 88:149–159

Chen Y, He X, Ding X, Sang W (2005) Steep-slope monitoring: GPS multiple-antenna system at Xiaowan Dam. GPS World, November 1, pp 93–98

Coe JA, Ellis WL, Godt JW, Savage WZ, Savage JE, Michael JA, Kibler JD, Powers PS, Lidke DJ, Debray S (2003) Seasonal movement of the Slumgullion landslide determined from Global Positioning System surveys and field instrumentation, July 1998–March 2002. Eng Geol 68(1–2):67–101

Cruden DM, Varnes DJ (1996) Landslide types and processes. Landslides, investigation and mitigation, pp 36–75

Dixon TH (1991) The global positioning system. Rev Geophys 29:249–276

Duranthon J-P (2000) Application de la méthode GPS de localisation par satellite à la surveillance de sites naturels instables. Bull Liaison Lab Ponts Chaussées 228:47–53

Flageollet J-C, Helluin E (1987) Morphological investigations of the sliding areas along the coast of Pays d'Auge, near Villerville, Normandy, France. In: Proceedings of the 1st international conference on geomorphology, vol 1, pp 477–486

Genrich JF, Bock Y (1992) Rapid resolution of crustal motion at short ranges with Global Positioning System. J Geophys Res 96:3261–3269

Gili JA, Corominas J, Rius J (2000) Using Global Positioning System techniques in landslide monitoring. Eng Geol 55:167–192

Herring TA, King RW, McClusky SC (2003a) GLOBK: Global Kalman filter VLBI and GPS analysis program. Version 10.1: Internal Memorandum. Massachusetts Institute of Technology, Cambridge, p 87

Herring TA, King, RW, McClusky SC (2003b) GAMIT, GPS analysis at MIT. Release 10.3: Internal Memorandum. Massachusetts Institute of Technology, Cambridge, p 182

Laboratoire Central des Ponts et Chaussées (LCPC) (1994) Surveillance des pentes instables. Guide Technique, Publication LCPC, Paris, p 125

Lissak C, Maquaire O, Malet J.-P, Déprez A, Masson F, Ulrich P, Peters ET (2010) Multi-technique permanent monitoring of a slow-moving coastal landslide in Normandy. In: Malet J-P, Glade T, Casagli N (eds) Proceedings of the international conference mountain risks: bringing science to society, CERG Editions, Strasbourg, pp 267–272

Malet J-P, Maquaire O, Calais E (2002) The use of GPS for the continuous monitoring of landslides application to the Super Sauze earthflow (Alpes-de-Haute-Provence, France). Geomorphology 43:33–54

Mora P, Baldi P, Casula G, Fabris M, Ghirotti M, Mazzini E, Pesci A (2003) Global Positioning Systems and digital photogrammetry for the monitoring of mass movements: application to the Ca' di Malta landslide (Northern Apennines, Italy). Eng Geol 68(1–2):103–121

Peyret M, Djamour Y, Rizza M, Ritz J-F, Hurtrez J-E, Goudarzi MA, Nankali H, Chéry J, Le Dortz K, Uri F (2008) Monitoring of the large slow Kahrod landslide in Alborz mountain range (Iran) by GPS and SAR interferometry. Eng Geol 100(3–4):131–141

Reid ME, Baum RL, LaHusen RG, Ellis WL (2008) Capturing landslide dynamics and hydrologic triggers using near-real-time monitoring. In: Chen Z-Y, Zhang J-M, Ho K, Wu F-Q, Li Z-K (eds) Landslides and engineered slopes, from the past to the future. Proceedings of the tenth international symposium on landslides and engineered slopes. Taylor & Francis Group, London, pp 179–191

Squarzoni C, Delacourt C, Allemand P (2005) Differential single-frequency GPS monitoring of the La Valette landslide (French Alps). Eng Geol 79(3–4):215–229

Weber D, Herrmann A (2000) Reconstitution de l'évolution géomorphologique de versants instables par photogrammétrie numérique: l'exemple du glissement de terrain de Super-Sauze (Alpes-de-Haute-Provence, France). Bull Soc Géolog France 171:637–648



Retrogressive Slope Failures in Natural Slope: A Case Study

Che Hassandi Abdullah and Ghazali Hussin

Abstract

A study has been carried out to investigate a slope in a granitic formation, that has been slowly but constantly moving since a small part near the toe of the natural slope was regraded in 1986 to make way for a road construction. Many scars on the slope surface suggest retrogressive failures have taken place. Investigation has been carried out to identify the causes and the extent of the failures so that an effective solution can be found. Site investigation with the geophysical procedures data shows the relatively shallow water table. Correlation between the pore pressure build up in the slope with the slope movements indicates that initiation of movement occurs quite consistently at a certain ground water level. The data gathered will be used to provide effective solutions to the slope movements and predict the quantum of the movements.

Keywords

Retrogressive failure • Investigation • Water table

Introduction

A study has been carried out to investigate a slope in a granitic formation that has been slowly but constantly moving since a small part of the slope was cut approximately to make way for a road construction some 20 m above the toe of the natural slope. The site is located towards the north-east of Kuala Lumpur at Km 8.25, on Jelawang – Gua Musang Road. The gradient of the slope averages approximately 15 ° and the length extend more than 1 km from the road to the peak of the hill where the slope is located. The slope is gentler nearer to the location where the slope is cut and steeper in the upper part of the slope. The slope is well vegetated small to medium size trees. Another feature of the slope is the high ground water level, especially at the toe of the cut slope where it meets the road and particularly so during rainy seasons. A gabion wall measuring 2 m high that was constructed to prevent the movements has moved onto the road, hence the road has to be realigned slightly to prevent encroachment of the landslide mass. Many landslide scars and large tension cracks on the slope surface suggest retrogressive failures have taken place. The purpose of this study is to investigate the causes of these movements, the depth of the slip surface near the road, the extent of the failures for the purpose assessing the risk to the road users and also to mitigate further movements if necessary.

Site Characteristics

The slope is made up of granitic residual soils hills with gradient between 10 ° and 25 ° (Jamaludin et al. 2011). The slope is steeper in the upper slope and less steep near the road. Like all natural and relatively undisturbed slopes in Malaysia the slope is well vegetated sometimes relic scars are difficult to identify since they are covered with vegetation. Figure 1

C.H. Abdullah (✉)
Slope Engineering Branch, Public Works Department Malaysia, Jalan Sultan Salahuddin, Kuala Lumpur 50582, Malaysia
e-mail: hassandi@jkr.gov.my

G. Hussin
Kumpulan Ikram Sdn. Bhd, Unipark Suria, Kajang, Selangor 43000, Malaysia

C. Margottini et al. (eds.), *Landslide Science and Practice*, Vol. 2,
DOI 10.1007/978-3-642-31445-2_27, © Springer-Verlag Berlin Heidelberg 2013



Fig. 1 A relatively recent scar seen partly covered with under growth

shows one of the scars that is partly covered with vegetation. Seasonal water channels can be seen during rainy seasons, the channel would dry up during long dry spells.

Conventional site investigation, seismic and resistivity surveys were carried out to understand the characteristics of the site. A total of eight boreholes were sunk at various locations on the slope. These boreholes were later used for installation of instruments such as inclinometers and piezometers. The boreholes were purposely sunk in pairs near each other so that correlation between movement and water level and pore water pressure can be directly compared. Survey of the area was carried out with locations of scars, tension cracks and other relevant features were mapped. Figure 2 shows the layout plan of the area with locations of all the boreholes.

As mentioned previously the slope has shown persistant movements since it was cut to make way for the road. The slope movements could have happened even earlier before the natural slope was cut. The height of the cut measures no more than 3 m high. To halt the movement, a 2-m gabion wall was constructed at the toe of the cut (Fig. 3). The work was done more as temporary measures to prevent encroachment of the landslide mass onto the road. Due to lack of fund, there was no study carried out to ascertain the depth of the slip surface and the cause of the movements. The gabion wall was pushed outward and upward as shown in Fig. 3. Prior to the construction of the gabion wall, the debris was intermittently removed as it encroached onto the road by the district engineer's office.

The slope has several seasonal streams that traverse across the length of the slope. During rainy seasons water were seen ponding near the top of the cut slope as shown in Fig. 2. The slope is made up of clay, silt and sand. Boulders are sometimes exposed at the surface and were also encountered during the boring process. Figure 4 shows the subsoil profile obtained from the borelogs of BH 1 to BH 7. Based on the SPT, the subsoil profile shows that the top 2–6 m consists of soft clay and silt or loose sand. Hard layer is encountered at 9–14 m below the ground surface.

The seismic survey data shows three distinct layers of soft or loose soil with thicknesses varying from 2 to 5 m followed by a denser layer measuring 5–15 m thick and finally followed by a very dense layer below it. Figure 5 shows typical p-wave velocity obtained from the seismic survey.

Instruments Installed

Instruments were installed at the locations of the boreholes to establish the location of the slip plane, to correlate the relationship between rainfall or ground water level and slope movement. Several types of instruments were installed to monitor the ground water level, the movements of some parts of the slope, soil moisture content and rain gage at the site. Most of the instruments were installed inside the boreholes sunk during the site investigation. Figure 6 shows the locations of these instruments. Vibrating wire piezometers were installed in boreholes BH 2, BH 4, BH 6 and BH 8. In-place Inclinometers (IPI) were located at boreholes BH 3 and BH 7 at three different depths; 4, 7 and 9 m below the ground surface, and the conventional inclinometers at boreholes BH 1 and BH 5. The piezometers and inclinometers were purposely placed near each other so that correlations can be easily drawn. Soil moisture probes were installed near boreholes BH 1 and BH 7. Standpipe piezometers were placed in boreholes BH 2 and BH 4 together with the vibrating wire piezometers. Except for standpipe piezometers and conventional inclinometers the rest of the instruments data was automatically transmitted to the data logger which was housed near the rain gauge located by the side of the road. Since there is no telephone signal available in the area, the data was then downloaded to a laptop at every 2 or 3 month's interval.

Results and Observations

Reliable data was obtained from the instruments from July 2009 to December 2010. The geomorphological mapping carried out for the site shows successive cascading scars on the slope indicating retrogressive failures have taken. The slope angle near the cut leading to the roadway is also gentler than the upper part of the slope signifying the movements have resulted in more stable mass. However, the movements have not ceased completely. The movement of the slope is believed to be in tandem with the rise in the water table.

The manually read inclinometer was one of the first instruments to be installed. The reason this is so because the use of in-place inclinometer requires approximate location of the slip plane to be identified so that slide can be monitored. Once the slip plane has been identified, the

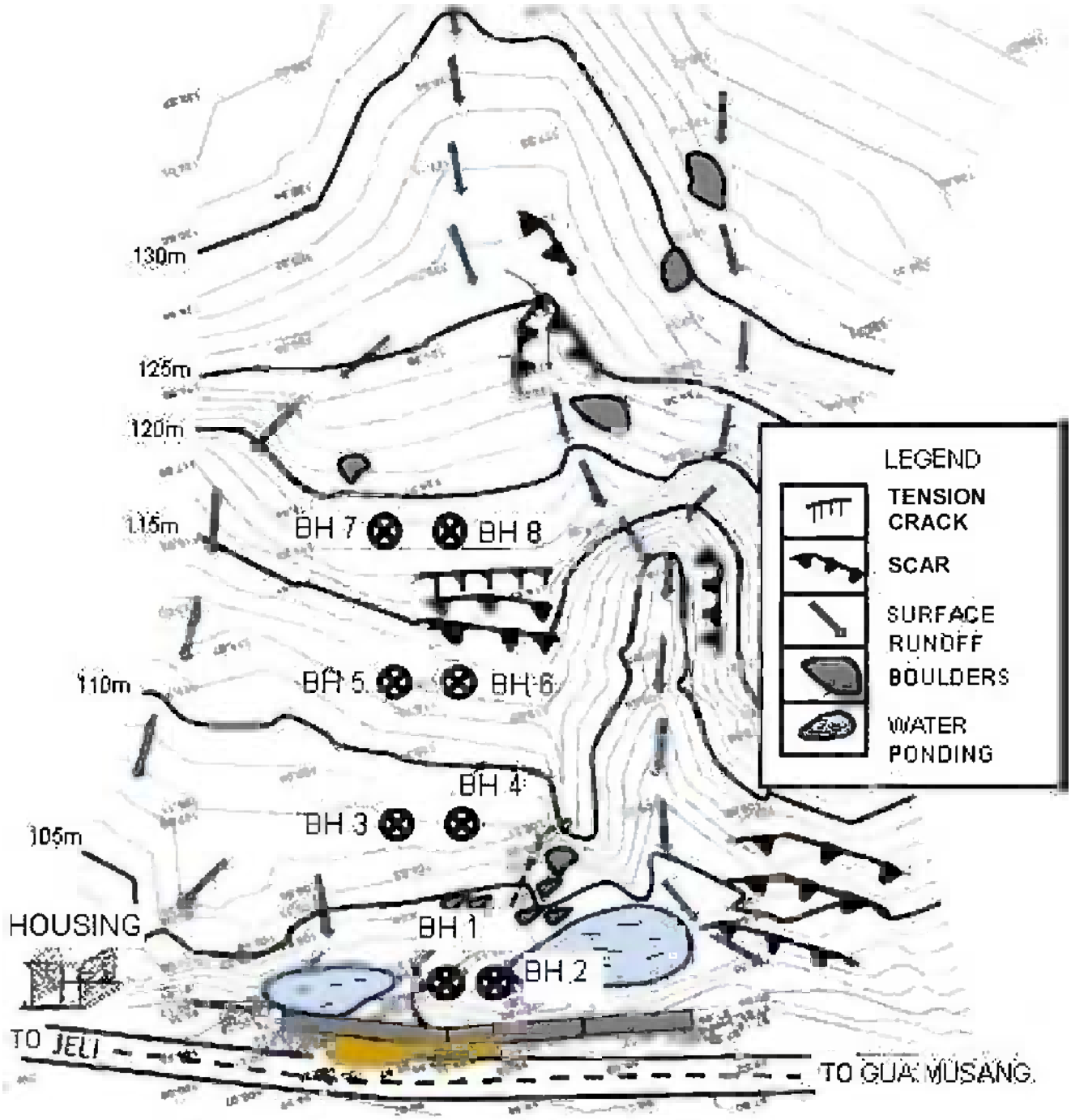


Fig. 2 Layout plan of the area showing the boreholes and slope features

in-place inclinometers were installed with one of the sensors located at the depth where the slip plane is located. Figure 7 shows the lateral shear movement of the inclinometer placed in borehole BH 1 near the cut slope. The shear displacement



Fig. 3 The gabion wall was pushed outward and upward as a result of the slope movement

was too large for manual measurement to be performed in November 2009 – 13 months after the inclinometer was installed, however, the in-place inclinometer was still providing tangible results.

The slope movement is due to changes in water table as a result of continuous and high intensity rainfall as can be seen in Fig. 8, where rainfall chart, water level and movements at different depths are plotted. The movements were recorded from IPI 1 placed in borehole BH 3. The sensors were located at 4, 7 and 9 m below the ground level. As expected, active movements were detected at the 9 m level. Little relative lateral movement of the ground at 4 and 7 m sensors placed from the ground surface indicating that at these locations the soil mass is sliding vertically and consistently along the slip plane.

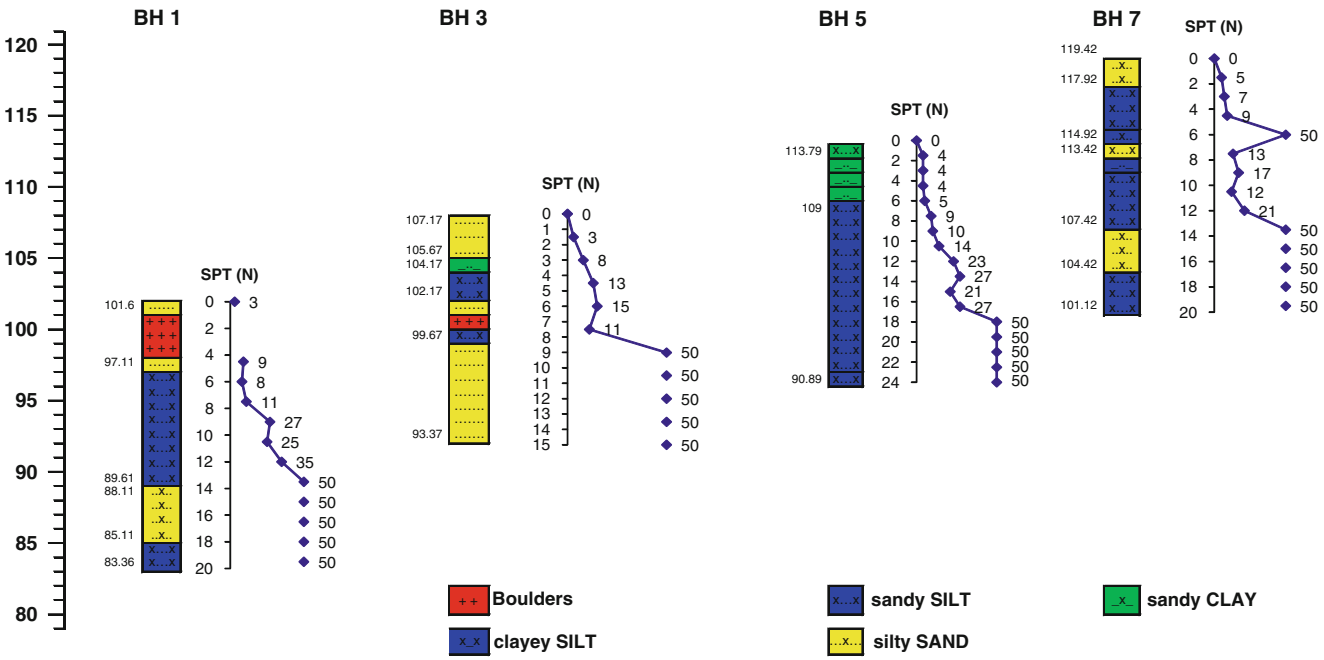


Fig. 4 Subsoil profile along part of the slope under scrutiny

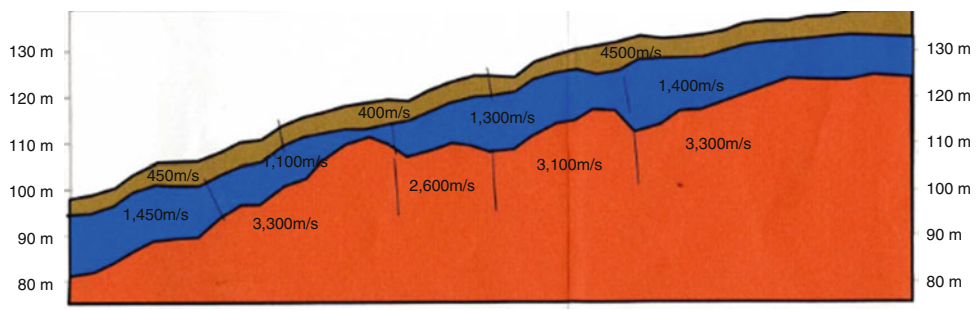


Fig. 5 Various subsoil layers identified by distinct p-wave velocities

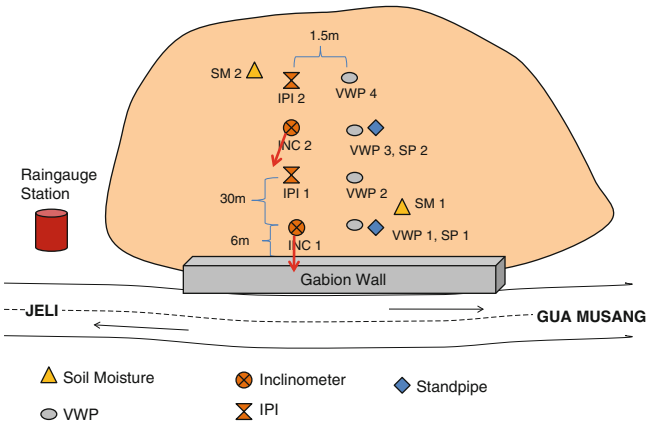


Fig. 6 Diagram showing the instruments installed on the slope

The figure also shows that the slope will only slide if the ground water level exceeds the threshold as indicated by the horizontal dotted line drawn in Fig. 8. Another observation that can be drawn from the figure that if water level rises higher than the threshold the lateral movement will also be higher almost proportionate in value.

The moisture probes installed were found to be defective, therefore the data is of little use. Even if they works, it will not provide any additional information pertaining to slope movement since the movement has little to do with the lost of suction but more as a result of the rise in the ground water level.

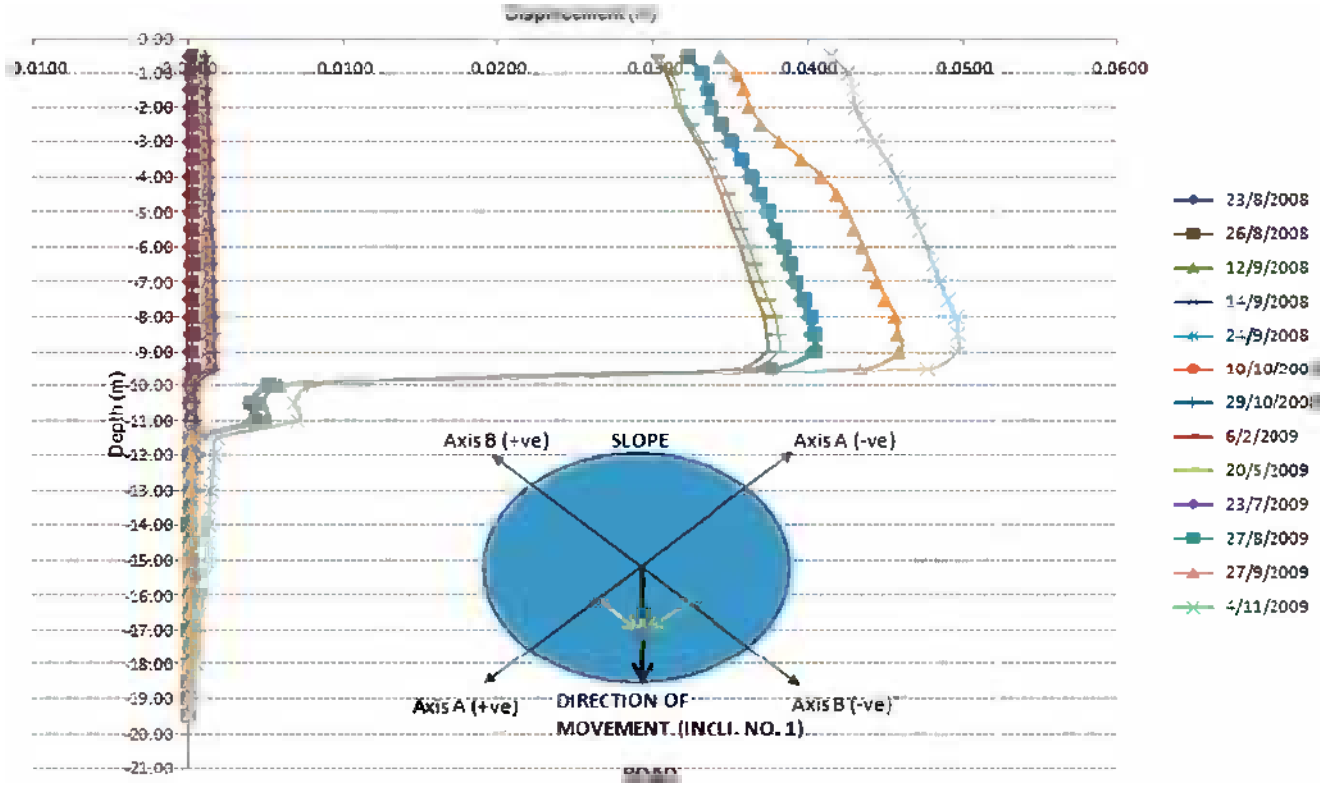


Fig. 7 Lateral shear movement is most prominent at approximately 10 m below the ground

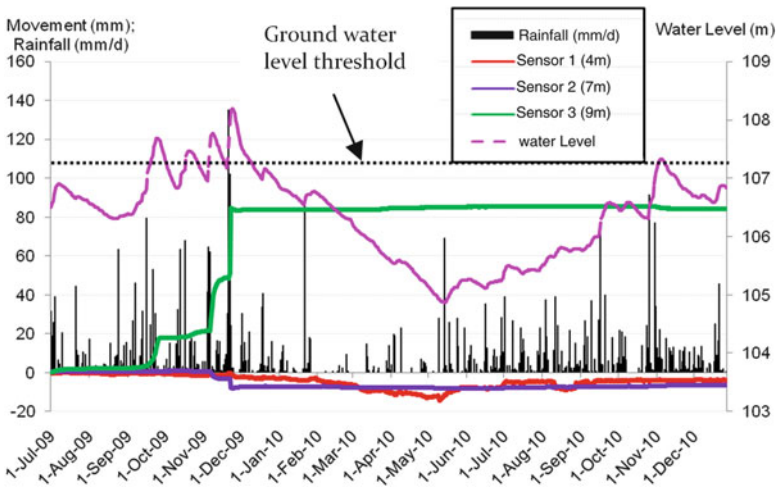


Fig. 8 The diagram shows relationship between rainfall, ground water level and lateral movement of the slope when threshold ground water level is exceeded

Conclusions

The results and observation of data obtained from monitoring of the instruments through two rainy seasons indicate that the slope has moved slightly more than 80 mm. According to Cruden and Varnes (1996) the slope movement can be categorised as slow moving landslide which, in this case carry a low risk but requires constant maintenance and repair of the slope.

The results also shows that slope movement will only take place once the threshold ground water level in the slope is breached. Instruments placed at the right locations were able to identify the location of the slip plane and can provide the necessary data to properly design or mitigates against the creep movement.

The slow movement of the slope has been going on for more than 25 years since the construction of the road or may be even earlier. Cascading scars on the slope indicate retrogressive failures have been going on these numbers of years or more. From the observations, a simple solution to stop the slope movement would be to provide subsoil drainage to prevent the water level from exceeding the threshold value.

References

Cruden DM, Varnes DJ (1996) Landside types and processes. In: Turner AK, Schuster RL (eds) Landslide investigation and mitigation, vol 247, Transportation Research Board, Special Report. National Academy Press, Washington, DC, pp 36–75

Jamaludin S, Zainuddin NE, Abdullah CH, Jaafar KB (2011) Monitoring of slow moving landslide at Km 8.25, Jelawang – Gua Musang road in the state of Kelantan. In: Proceedings of 3rd international conference on geotechnical engineering for disaster mitigation and rehabilitation 2011 (GEDMAR 2011), Semarang, Indonesia, pp 6–11



Performance of Image Correlation Techniques for Landslide Displacement Monitoring

Julien Travelletti, Christophe Delacourt, Jean-Philippe Malet, Pascal Allemand, Jean Schmittbuhl, and Renaud Toussaint

Abstract

The objective of this work is to present the applicability of image correlation techniques (applied to very-high resolution terrestrial optical photographs and to very dense Terrestrial Laser Scanning (TLS) point clouds) to monitor the displacement of continuously active landslides. The method has been developed to characterize the kinematics of very active landslides with cumulated displacement of several decimeters per year. The data are processed with a cross-correlation algorithm applied on the full resolution images (photographs and DEMs produced from the TLS data) in the acquisition geometry. Then, the calculated 2D displacement field is ortho-rectified with a back projection technique. The method allows to characterize the heterogeneous displacement field of the landslide in time and space, and to produce displacement maps. The performance of the technique is assessed using as reference differential GPS surveys of a series of benchmarks.

The sources of error affecting the results are discussed. Because the proposed methodology can be routinely and automatically applied, it offers promising perspectives for operational applications like, for instance, in early warning systems.

Keywords

Image cross-correlation • Image matching • Time-lapse acquisition • Displacement monitoring • LiDAR, landslide

Introduction

Remote-sensing techniques are interesting tools to obtain spatially-distributed information on landslide kinematics (Delacourt et al. 2007). They give the possibility to discriminate stable and unstable areas and to map sectors within the landslide with different kinematics from a regional to a local scale (Casson et al. 2005; Teza et al. 2008; Oppikofer et al. 2008). Three main categories of remote sensing techniques, either operated from terrestrial or airborne platforms, are used in landslide monitoring: Synthetic Aperture Radar Interferometry (InSAR), Laser Scanning (LiDAR) and Optical Photogrammetry (OP).

The objective of this work is to highlight the possible applications and limitations of cross-correlation techniques applied both on airborne and terrestrial LiDAR point clouds and on very-high resolution optical images. Several datasets

J. Travelletti • J.-P. Malet (✉) • J. Schmittbuhl • R. Toussaint
Institut de Physique du Globe de Strasbourg, CNRS UMR 7516, Université de Strasbourg, Ecole et Observatoire des Sciences de la Terre, 5 rue Descartes, Strasbourg F-67084, France
e-mail: jeanphilippe.malet@unistra.fr

C. Delacourt
Laboratoire Domaines Océaniques, CNRS UMR 6538, Institut Universitaire Européen de la Mer, Université de Bretagne Occidentale, Rue Dumont d'Urville, Plouzané F-29280, France

P. Allemand
Laboratoire de Géologie de Lyon – Terre, Planète, Environnement, CNRS UMR 5276, Université de Lyon 1 et Ecole Normale Supérieure de Lyon, 2 rue Raphaël Dubois, Villeurbanne Cedex F-69622, France

C. Margottini et al. (eds.), *Landslide Science and Practice*, Vol. 2,
DOI 10.1007/978-3-642-31445-2_28, © Springer-Verlag Berlin Heidelberg 2013

of multi-source images acquired on the La Valette and Super-Sauze landslides (South French Alps) over the period 2007–2010 from different platforms are analysed. The influence of external factors on the precision and the accuracy of the results are discussed.

Principle of the Image Correlation Technique

Using matching techniques, two-dimensional displacement fields can be derived by tracking objects in two images acquired at different time. The technique is based on the automatic identification of identical texture patterns within an image by maximizing a correlation function (Lewis 1995). So far, Image Correlation techniques have been applied only on aerial and satellite images (e.g. SPOT, QuickBird, OrbView, EROS) for the creation of landslide displacement maps (Delacourt et al. 2004). Its principle adapted for landslide kinematics analysis is described in Delacourt et al. (2007).

In this work, a sub-pixel hierarchical correlation technique is used (Hild 2003). The original images are first converted in gray-scale images on which a 3 × 3 pixel Sobel convolution matrix is applied to highlight the ground surface texture. The gradient values are then correlated. Four successive degradations of the image resolution are applied following a pyramidal approach for changing the physical size of the correlation window and of the explored area by down-sampling the gradient values of the full resolution image (Kumar and Banerjee 1998) (Fig. 1).

The correlation starts with the lowest resolution image in order to determine the largest displacements. Then the location of the pixel with the maximum cross-correlation value is used as the centre of the zone of interest for the next correlation step at a higher resolution. The spatial location of the maximum correlation value in the highest resolution image is thus progressively better estimated (Fig. 1). Ignoring high resolution information at the first computational step decreases the probability to reach a local minimum of the correlation function and, consequently, to obtain a wrong matching in the correspondence solution (Alaoui and Ibn-Elhaj 2009). In addition, this approach ensures very often a higher probability of detecting a reliable correlation peak. The sub-pixel displacement is computed after the correlation at the highest resolution image. An iterative procedure is used to find the maxima of the correlation function interpolated with a bi-parabolic formula and with a maximization procedure based on the simplex method (Press et al. 1997).

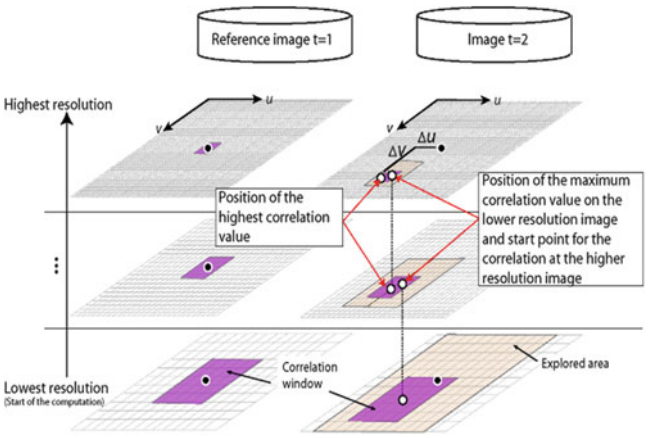


Fig. 1 Principle of the normalized hierarchical image correlation technique

The correlation results consist in matrices of displacement Δu and Δv along the u- and v-axes in the image plane with their associated correlation index (Fig. 1). In case of orthorectified airborne images, the pixel size is constant, only the effective pixel size at the ground has to be calculated to estimate metric displacements. In case of terrestrial images, the pixel size is not constant in the image due to the oblique acquisition; the displacements field correlated in the image plane cannot be directly interpreted in terms of metric displacements and an orthorectification procedure is compulsory for a quantitative analysis.

Application 1: Image Correlation of Terrestrial Photographs

A set of images acquired at the Super-Sauze landslide over the period May–July 2008 is used to illustrate the potential of the technique for the characterization of the kinematics during an acceleration period (Travelletti et al. in press).

Figure 2 presents the monitoring system installed in front of the landslide. The instrumentation consists in a low-cost D70 Nikon reflex digital camera installed on a concrete pillar located at a distance of 300 m from the lower part and 900 m from the main scarp (Fig. 2a, b). The acquisition system is controlled by a datalogger and the power is provided by a 40 W solar panel. Every four days, a series of images is acquired at 11:00, 12:00, 13:00 and 14:00 GMT.

Figure 3 shows an example of displacement rates (in pixel day^{-1}) of the ground surface in the image plane derived from image pairs of 20–28 May 2008, 1–4 June 2008 and 9 June–13 June 2008. The reference is the image

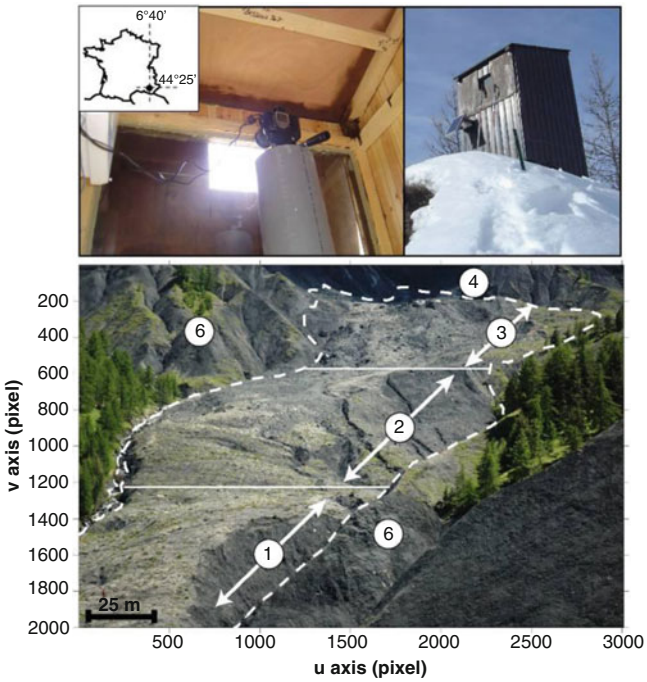


Fig. 2 Monitoring system with a very-high resolution camera installed in front of the Super-Sauze landslide on a stable crest. *Top*: monitoring system. *Bottom*: image acquired by the monitoring system presenting the different parts of the landslide from the camera location. The numbers refer to: (*1*) Lower part (toe) of the landslide, (*2*) Middle part (transition zone), (*3*) Upper part (abalation zone), (*4*) Main scarp (1,980 m), (*5*) Front (1,734 m), (*6*) Stable crests

of 20 May 2008. The contrast in displacement rates between the landslide area and the stable area gives confidence on the calculated velocity field. One can notice that the pattern of displacement rate is heterogeneous spatially and temporally.

The upper part of the landslide displays the highest velocity ranging from 1 to 7 pixels day^{-1} while the lower part displays velocity of less than 4 pixels day^{-1}. From the 20 May to the 13 June, cumulated displacements up to 110 pixels are observed in the upper part. The maximum of displacement rate is observed around the 1st June. Then the landslide decelerates to displacement rate of about 1 pixel day^{-1}. No quantitative comparisons can be carried out at this stage because the pixel sizes vary strongly in the image.

The displacement fields computed in the image plane are then orthorectified in a local geographic coordinate system using the collinearity equations (Kraus and Waldhäusl 1994). The details of the methodology are explained in Travelletti et al. (in press). Figure 4 presents the amplitude of the 3D orthorectified displacement rates for the period 1–4 June. The difference of kinematics between the upper (until 3 m day^{-1}) and the lower (until 1 m day^{-1}) parts is important. The geometrical effect induced by the presence of the stable *in-situ* crest on the landslide kinematics is also clearly pointed out.

The precision of the computed displacements is assessed by performing a null hypothesis on the stable areas. Only the points with a correlation coefficient $r > 0.8$ are taken into account. In the image plane coordinate system, the average error μ ranges from 0.5 to 0.9 pixels with standard deviation σ of 0.3 to 1.2 pixels for the image pairs between the 20 May and the 25 June 2008. In the local coordinate system, the average error μ ranges from 0.03 to 0.11 m with standard deviation σ of 0.10–0.31 m for the image pairs between the 20 May and the 25 June 2008.

The performance of the method has been evaluated by comparing the displacements derived from the image correlation, and the displacement monitored by dGPS on several benchmarks distributed in the stable parts and on the landslide. A correlation coefficient of $r = 0.95$ is found on 219 measurements and an average relative accuracy of 20 % is determined (Travelletti et al. in press).

Application 2: Image Correlation of Terrestrial LiDAR Point Clouds (TLS)

The potential of terrestrial LiDAR (TLS) for the monitoring of geomorphologic processes has been demonstrated in the last years, mainly for defining the structure of rocky slopes susceptible to rockfalls and rockslides (Abellán et al. 2009; Oppikofer et al. 2008) or characterizing the dynamics of ice glaciers (Avian et al. 2009) and landslides (Teza et al. 2008). Automatic matching algorithms applicable to TLS data have started to be developed because of their capability to fully exploit all the geometric information available in the point clouds. The approach is to find correspondences among typical features located in multi-temporal point clouds assuming that the tracked object has a constant geometry in time and/or a perfectly rigid behaviour.

Correlation techniques can be applied on repeated TLS acquisitions in order to characterize the 3D displacement field. The hypothesis is that for objects scanned from a unique view point, simple 2D correlation functions can be applied on multi-temporal point clouds and yield the same range of accuracy than complex and time-consuming 3D surface matching algorithms (Teza et al. 2008). The performance of the cross-correlation algorithm is tested on datasets acquired at the toe of the Super-Sauze landslide. A long-range terrestrial laser scanner Optech ILRIS-3D has been used for the monitoring (Travelletti et al. submitted).

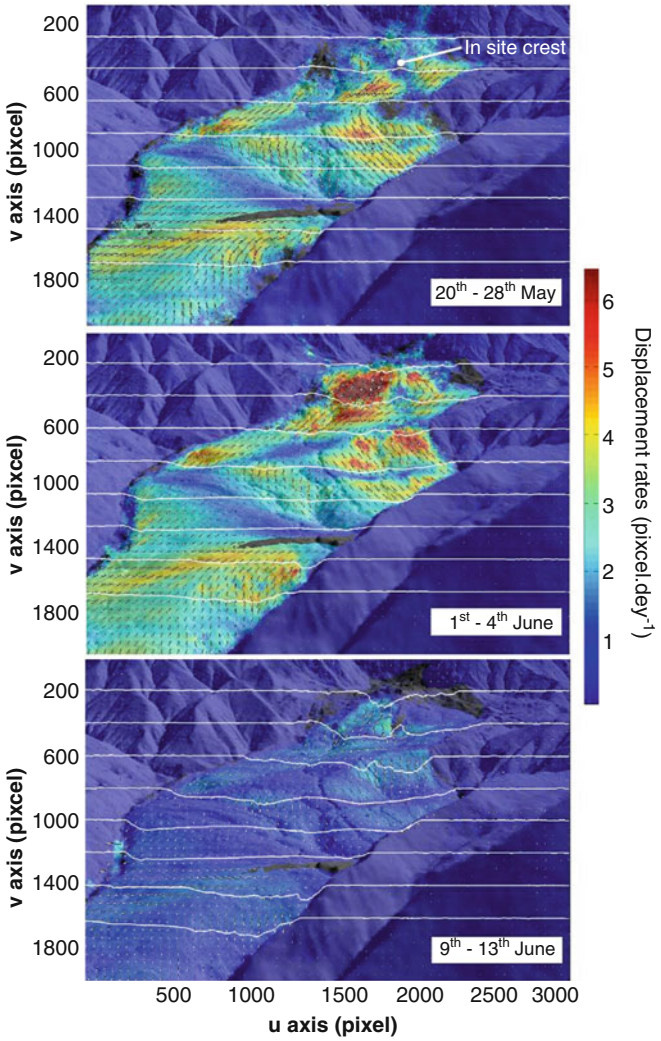


Fig. 3 Displacement rates amplitude (*color*) and direction (*arrows*) in the image plane and cumulated displacements along eight profiles crossing the landslide over the period 20 May–25 June 2008. In order to highlight the displacement direction, the *arrow* length is normalized for each image

Ten acquisitions were acquired between October 2007 and May 2010 for the same base station at an average distance of 100 m from the landslide toe (Fig. 5). At this distance, the laser diameter on the ground surface is estimated between 3 and 5 cm. Only the last return pulse is registered to maximize the number of points reflected on the ground surface. The average point density at the ground surface varies from 153.0 to 234.9 pts m^{-2} with a standard deviation up to 351.7 pts m^{-2} and a maximal density of 1,148.3 pts m^{-2}.

Filtering of vegetation and co-registration of the point clouds have been carried out with the software Polyworks 11 (Innovmetric 2009). A projective transformation is used to represent the entire geometrical information in a plan perpendicular to the viewing direction of the laser scan using the collinearity equations Kraus and Waldhäusl (1994).

The point density varies from 0.78 to 0.94 pt $pixels^{-1}$ with a relatively low standard deviation of 0.18 pt $pixel^{-1}$. The distance between the point clouds to the position of the laser scanner is then determined and linearly interpolated in a regular grid.

Because the correlation function gives better results where the input data contains regions of rapidly varying pixel information, the norm of the 2D gradient in u and v directions of the distance between the point clouds and the TLS station is calculated for emphasizing the morphology of the landslide. The generated images are then converted in grey-scale values (16 bits) and are used as inputs for the image correlation algorithm (Fig. 6).

The computed displacements are generally well reproduced for all periods of acquisition. Two acquisition periods (July–October 2008, July–October 2009) are

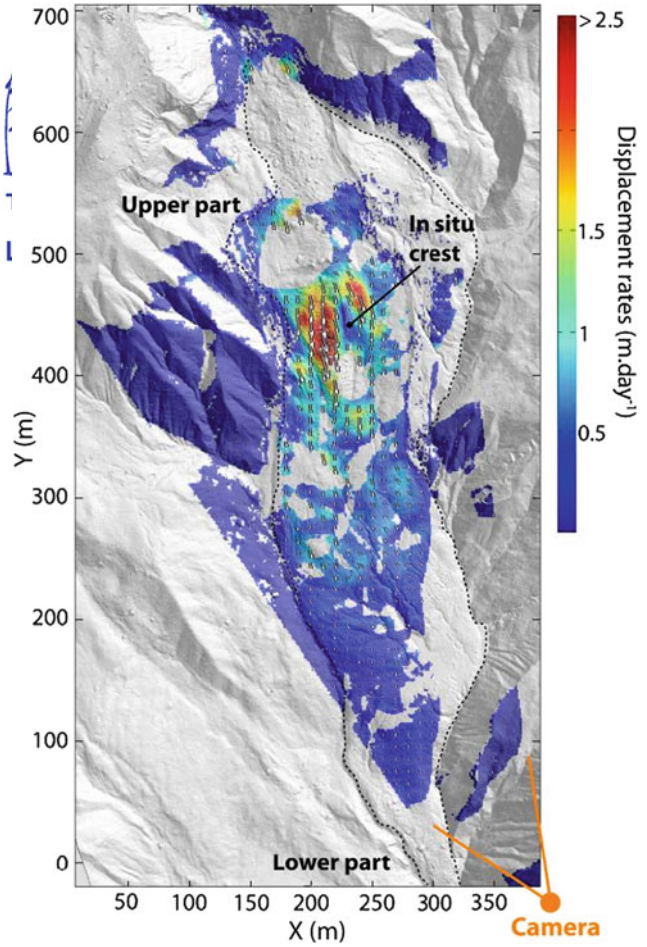


Fig. 4 Displacement rates map for the period 1–4 June 2008 in the local geographic coordinate system

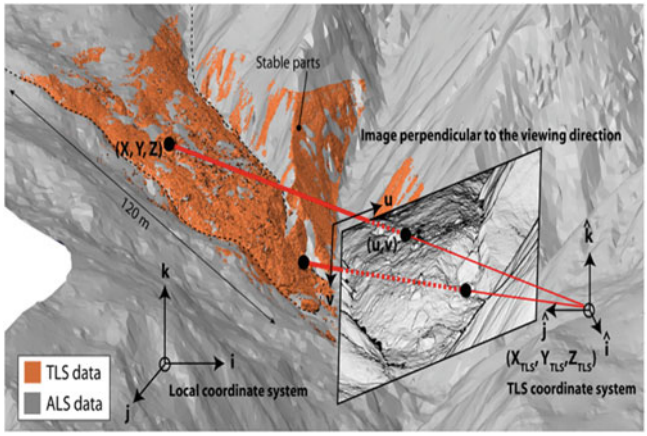


Fig. 5 View of the scanned area at the Super-Sauze landslide from the TLS base station, and schematic presentation of the projective projection applied on the TLS point clouds with the different coordinate systems involved in the procedure. The alignment of the stable parts of TLS point clouds on the ALS (airborne laser scanner) point cloud is indicated

presented to illustrate the performance of the approach and the behaviour of the landslide (Fig. 7). For the period July–October 2008, displacements between 0.5 and 1.5 m are observed, corresponding to an average displacement rate of 0.6 to 1.7 cm day^{-1}. The displacement field displays significant spatial heterogeneities. The largest displacements are detected in the front of the toe where the slope gradient increases. The detachment of a toe compartment is also highlighted in the front.

During the period July–October 2009, the landslide displays a very different kinematics both in terms of magnitude and spatial distribution. Displacements are shorter and range from 0.1 m at the front to 0.6 m in the upper part, corresponding to an average displacement rate of 0.1–0.8 cm day^{-1}.

The computed displacements are validated by comparing the displacement values to dGPS observations of a series of blocks easily recognizable in the TLS point clouds. This comparison allows evaluating the accuracy of the approach by taking into account the noise in the data with the co-registering errors between two acquisitions. The displacements perfectly correlate ($r^2 = 0.99$), and a mean error and a standard deviation of 0.04 m and 0.03 m are determined (Fig. 8). This results show that the error due to the co-registering is about 3 cm.

Application 3: Image Correlation of Airborne LiDAR Point Clouds (ALS)

A similar approach can be used for the creation of displacements maps from repeated airborne LiDAR point clouds (ALS). In this case, the landslide of La Valette is taken as example to illustrate the potential of the technique. Two DEMs with 1 m mesh size are interpolated from airborne LiDAR data acquired in October 2007 and July 2009. The average point density at the ground surface varies from 0.7 to 7.2 pts m^{-2} with a standard deviation up to 12.1 pts m^{-2}. Two complementary pieces of information are directly derived from the DEMs (Fig. 9):

+ the elevation differences (Z component) indicating an accumulation of mass in the transit zone;
+ the horizontal displacement field (E-N components) obtained by correlating the 2D gradient of the topography with a size of the correlation window of 20 m; the results indicate a decrease of the displacement magnitudes from

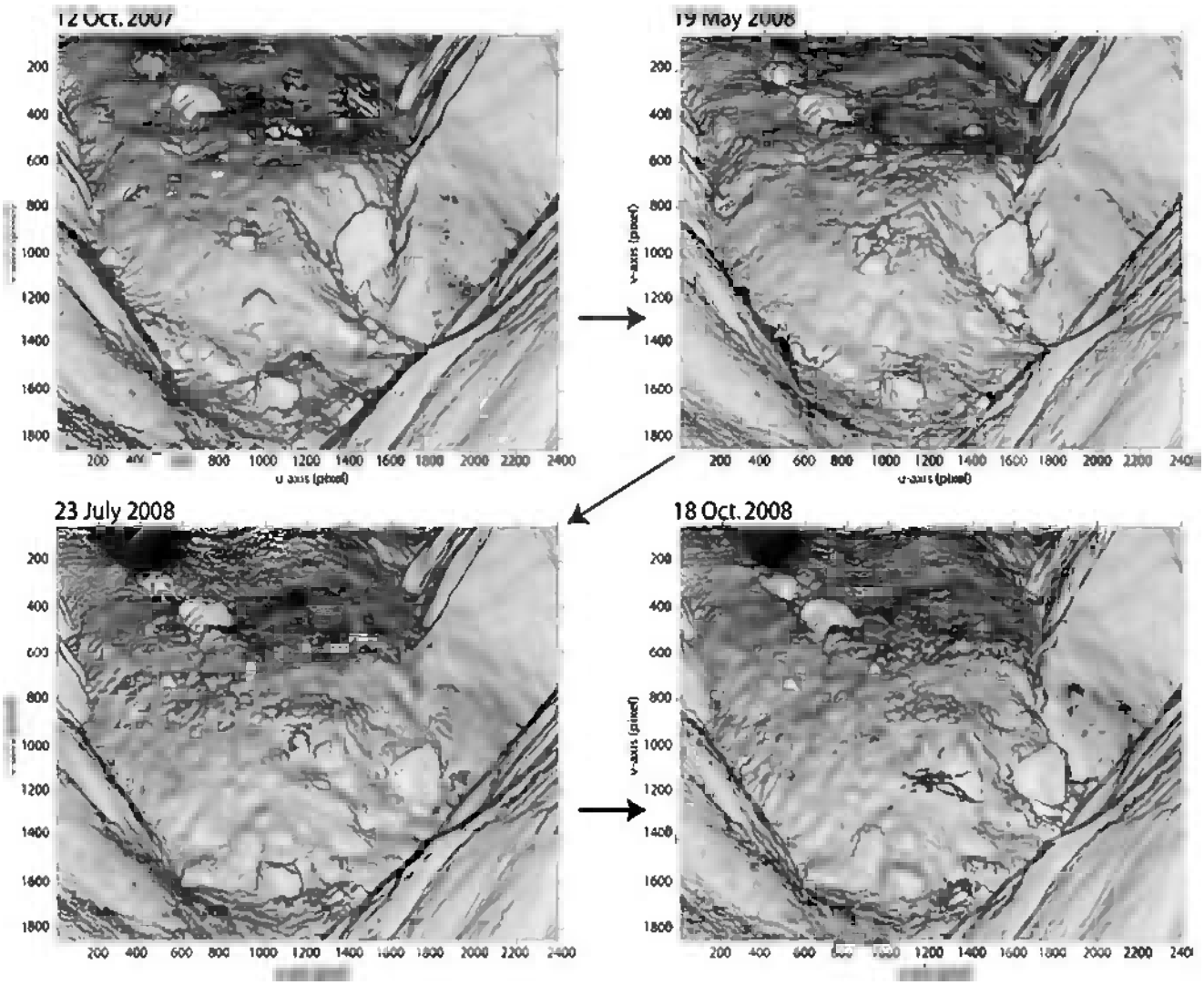


Fig. 6 Images derived from the gradient calculation on the TLS point clouds for the period October 2007–October 2008 at Super-Sauze. The morphology of the landslide toe is very well represented and the progression of the landslide toe is highlighted

the transit zone to the accumulation zone where nearly null displacements are observed.

The landslide behavior is controlled by a drainage system installed to stabilize the accumulation zone. Consequently, an increase of strain and an accumulation of mass occur near the Serre road demonstrating that the drainage system might not be the best solution to control the long term behavior of the slope.

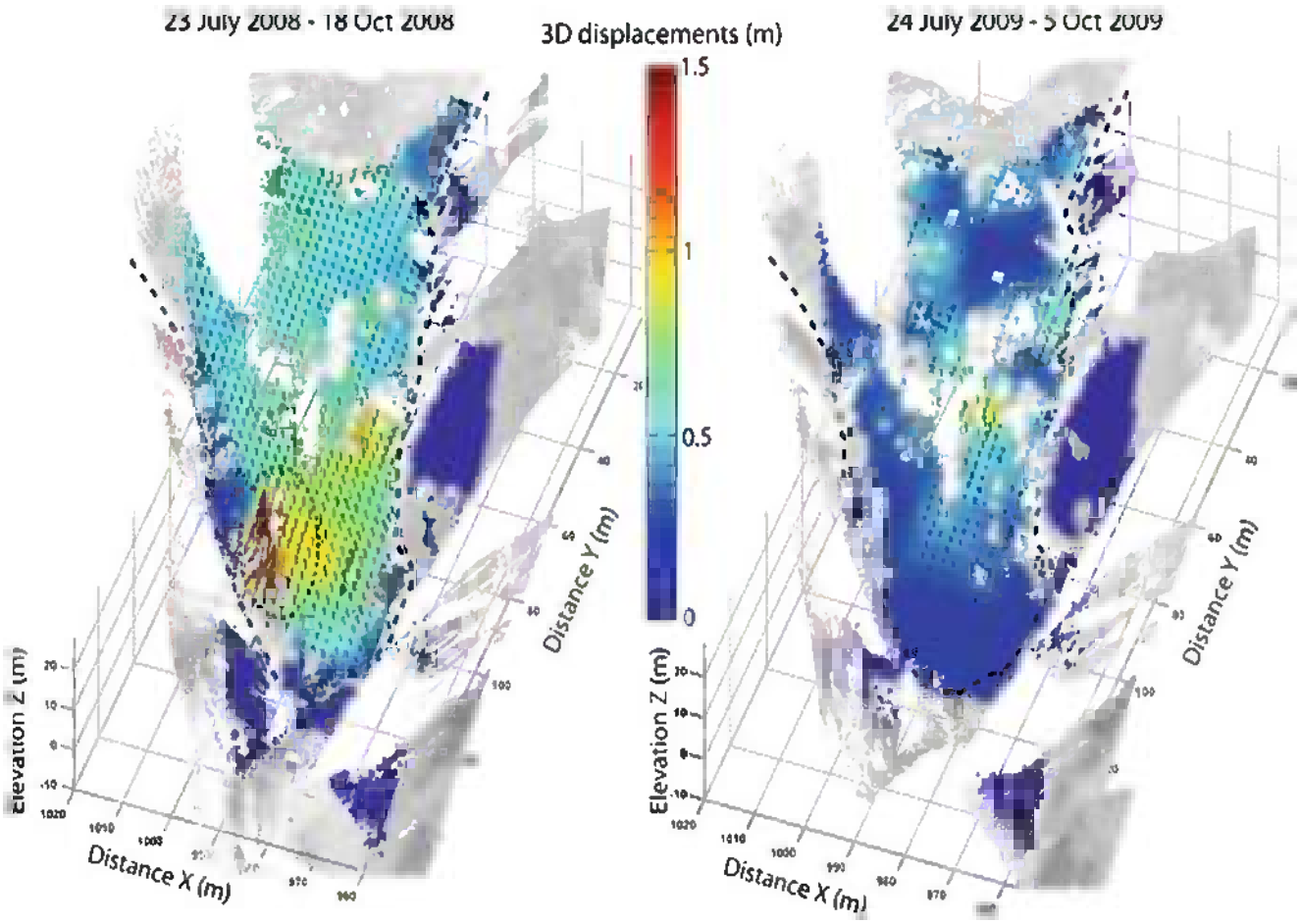


Fig. 7 3D displacements field obtained by TLS measurements related to the acquisition periods of July–October of the years 2008 and 2009. The *dashed circle* indicates the detachment of compartment at the front of the toe

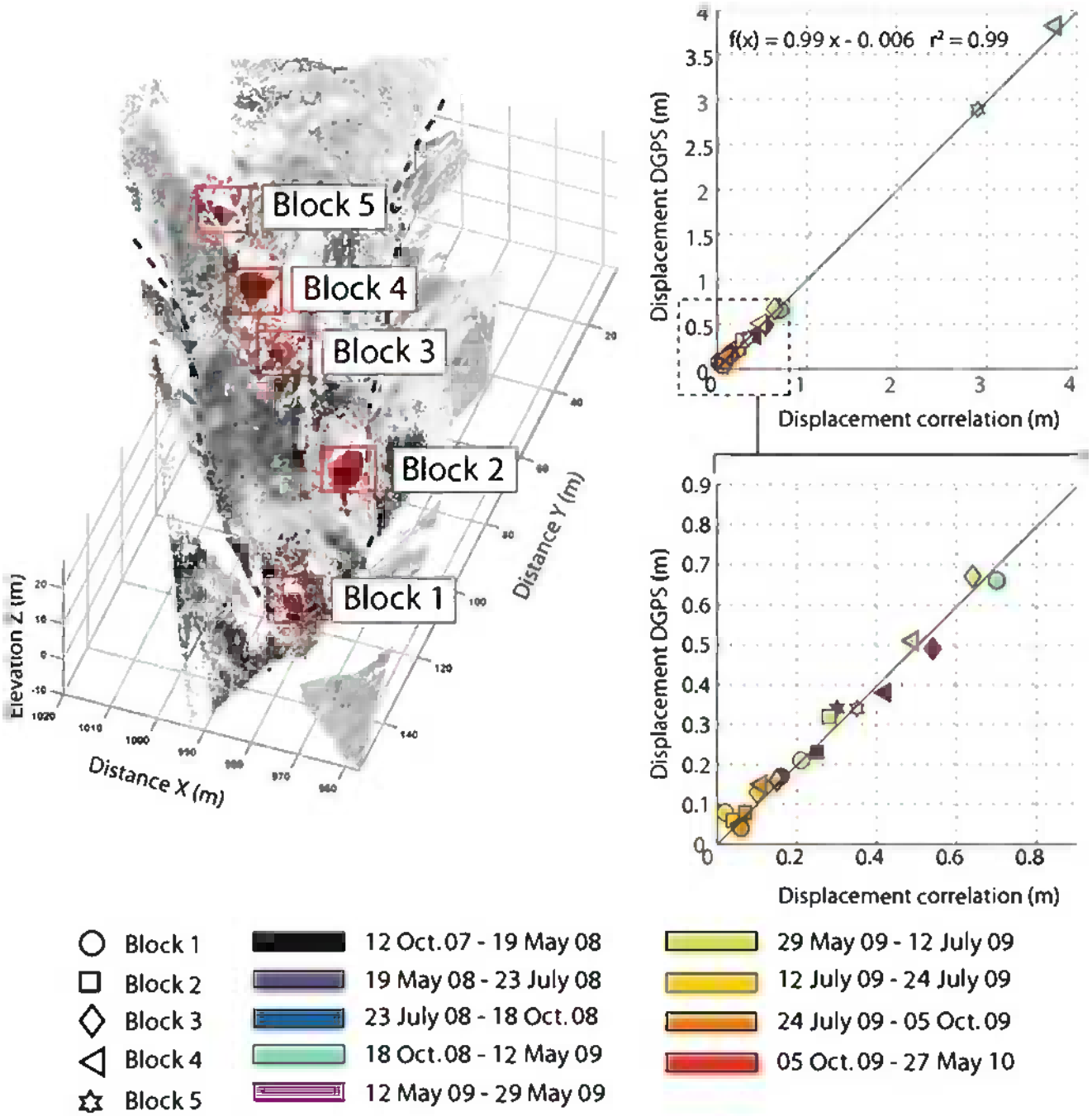


Fig. 8 Comparison and validation of the displacements obtained by correlation with dDGPS observations on a series of blocks

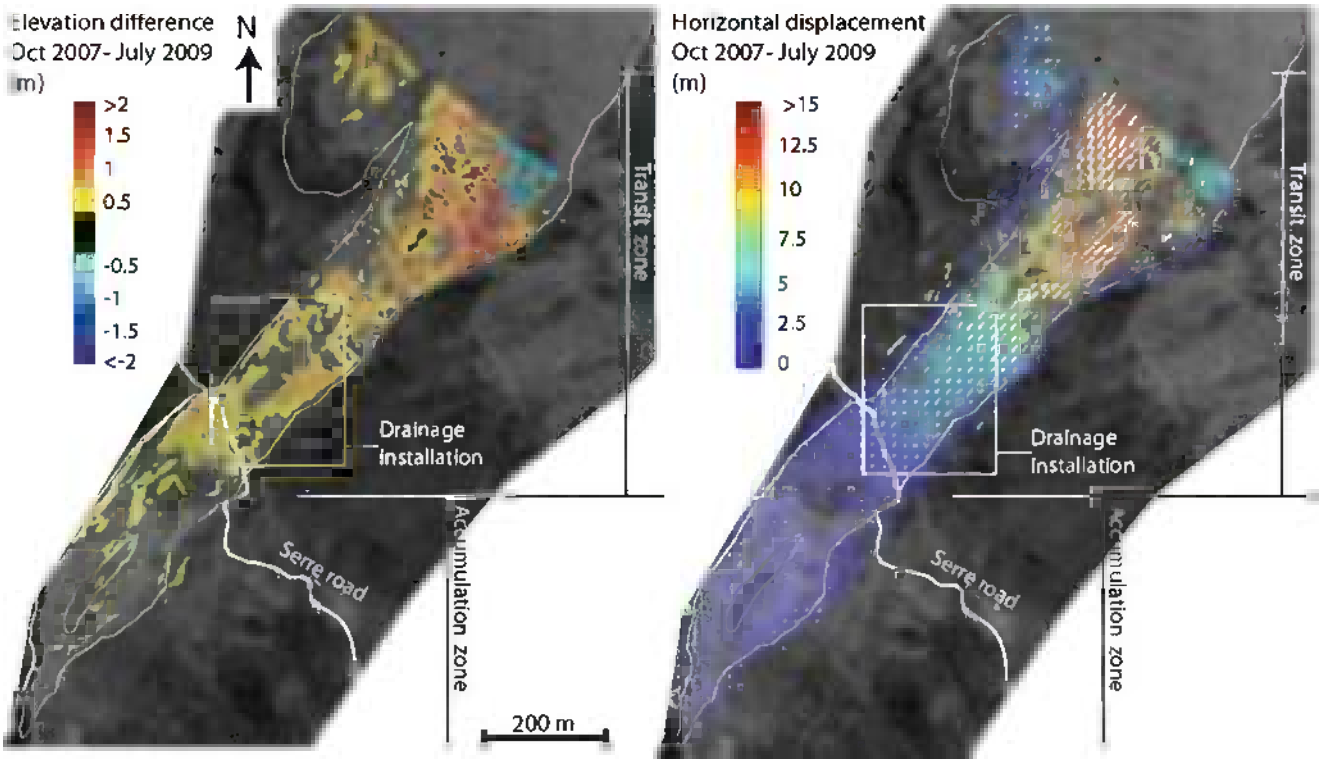


Fig. 9 Displacement field calculated at the La Valette landslide from two airborne LiDAR acquisitions in October 2007 and July 2009. *Left*: Displacement field in the Z direction indicating changes in elevation, and possible zones of material accumulation or erosion. *Right*: Displacement field in planimetry indicating changes in distribution of mass

Conclusion

The potential of Image Correlation technique applied to multi-temporal terrestrial photographs or airborne or terrestrial LiDAR point clouds has been evaluated using datasets available on the Super-Sauze and La Valette landslides (South French Alps). Operational methodologies are available to compute displacement rates both in the image plane coordinate system and in local geographic coordinate systems. The technique allows one to clearly characterize heterogeneous displacement field of landslides in space and in time, with a high detection thresholds (cm day^{-1}). The displacements maps computed from the images are in good agreement with local information on the displacement rates observed with classical geodetic techniques such a dGPS.

Using terrestrial images, the effect of pixel size at the ground (according to the distance to the target), the incidence of the line of sight to the ground and the resolution of the image are limiting factors to detect low displacement rates. Moreover, areas of low incidence angles (<5 °) are very sensitive to small movements of the acquisition platform, that can partly be corrected. Other limiting factors for optical images are related to the meteorological and illumination conditions and the ground surface changes inducing partial or complete loss of coherence between image pairs.

The results demonstrate that Image Correlation techniques implemented in permanent monitoring system are particularly interesting for monitoring landslides characterized by annual pluri-decimetric displacements.

This work offers very promising perspectives for operational applications which can be potentially integrated in early warning systems by considering additional efforts in direct data transmission. Finally, inversion of the displacement field could be developed to characterize the macroscopic rheological properties of the landslide material.

Acknowledgments This work was partly supported by the European Commission under the Marie Curie Contract *Mountain Risks: from prediction to management and governance* (FP6, MCRTN-035798; 2007–2010), and the European Project FP7 *SafeLand: Living with landslide risk in Europe* (2009–2012). The authors are grateful to Mr. G. Skupinski (University of Strasbourg) for his support in the acquisition of the Terrestrial Laser Scanning data.

References

Abellán A, Jaboyedoff M, Oppikoffer T, Vilaplana JM (2009) Detection of millimetric deformation using a terrestrial laser scanner: experiment and application to a rockfall event. Nat Hazards Earth Syst Sci 9:365–372

Avian M, Kellerer-Pirklbauer A, Bauer A (2009) LiDAR for monitoring mass movements in permafrost environments at the cirque Hinteres Langtal, Austria, between 2000 and 2008. Nat Hazards Earth Syst Sci 9:1087–1094

Casson B, Delacourt C, Allemand P (2005) Contribution of multi-temporal sensing images to characterize landslide slip surface – application to the La Clapière Landslide (France). Nat Hazards Earth Syst Sci 5:425–437

Delacourt C, Allemand P, Casson B, Vadon H (2004) Velocity field of the "La Clapiere" landslide measured by the correlation of aerial and quick-bird satellite images. Geophys Res Lett 31:1–5

Delacourt C, Allemand P, Berthier E, Raucoules D, Casson B, Grandjean P, Pambrun C, Varel E (2007) Remote-sensing techniques for analysing landslide kinematics: a review. Bull Soc Géolog 178:89–100

El Alaoui MI, Ibn-Elhaj E (2009) A robust hierarchical motion estimation algorithm in noisy image sequences in the bispectrum domain. Sign Image Video Process 3:291–302

Hild F (2003) Mesure de champs de déplacement par corrélation d'images et applications en mécanique des solides. Notes de cours IPSI. Laboratoire de Mécanique et Technologie, CNRS-UMR 8535, Université Paris 6, France

InnovMetric (2009) PolyWorks User's Manual – 3-D scanner and 3-D digitizer software from InnovMetric Software Inc., http://www.innovmetric.com/

Kraus K, Waldhäusl P (1994) Photogrammetry, fundamentals and standard processes. In: Hermès (ed), vol 1, Paris

Kumar S, Banerjee S (1998) Development and application of a hierarchical system for digital particle image velocimetry to free-surface turbulence. Phys Fluids 10:160–177

Lewis JP (1995) Fast normalized cross-correlation. Vision Interface, pp 120–123

Oppikofer T, Jaboyedoff M, Kreusen H-R (2008) Collapse at the eastern Eiger flank in the Swiss Alps. Nat Geosci 8:531–535

Press WH, Flannery BP, Teukolsky SA, Vetterling WT (1997) Numerical recipes. Cambridge University Press, New York

Teza G, Pesci A, Genevois R, Galgaro A (2008) Characterization of landslide ground surface kinematics from terrestrial laser scanning and strain field computation. Geomorphology 97:424–437

Travelletti J, Delacourt C, Allemand P, Malet J-P, Schmittbuhl J, Toussaint R, Bastard M (2011) Correlation of multi-temporal ground-based images for landslide monitoring: application, potential and limitations. Int J Photogram Remote Sens 25 (in press)

Travelletti J, Malet J-P, Delacourt C (submitted, in review) Multi-date correlation of terrestrial laser scanning data for the characterization of landslide kinematics. Geomorphology 15 (in review)



A Novel Fiber Optic Sensing System for Monitoring Debris Flows

Chung-Ray Chu, Ching-Jer Huang, and Tsung-Mo Tien

Abstract

This study presents a novel fiber optic sensing system for monitoring debris flows. Thanks to their light weight, immunity to electromagnetic interference, high sensitivity, and very low optical loss, fiber optic sensors can be potentially utilized to monitor debris flows, which usually occur in mountainous regions far from available electricity. The ground vibrations caused by debris flows can be sensed by a Fiber Bragg Grating (FBG) Accelerometer (Gavea Sensor GS 6500) and the associated light source, and data logger are provided by a Braggscope (Fiber Sensing FS 5500). Four FBG Accelerometers were deployed along the Ai-Yu-Zi Creek and the Chu-Shui Creek in Nan-Tou County, Taiwan, respectively; and the Braggscope was located at the front data-receiving center. The calibration experiment was carried out to compare the performance of FBG accelerometer with other sensors used for detecting debris flows, such as geophone and microphone. The signal-to-noise ratio (SNR) of FBG accelerometer was higher than that of geophone, while the two instruments sensed the same vibration source. The results showed that fiber optic sensing technique could be used as an alternative for monitoring debris flows.

Keywords

FBG accelerometer • Fiber optic sensing system • Debris flow monitoring

Introduction

Debris flow is a rapid, gravity-induced flow of mixture of rocks, mud, and water (Johnson and Rodine 1984; Iverson et al. 1997). It is among the most hazardous nature process in mountainous region of Taiwan, because of the steep topographical feature, young and weak geological formation, heavy rain, and frequent earthquakes on this island. Debris flow has the following characteristics: (1) The forefront looks like a bore and accumulates the largest rocks; (2) the flow following the forefront appears as a mudflow with a gradually decreasing discharge; (3) the flow is accompanied by loud noise and ground vibration (Takahashi 1991).

Development of sensors for debris flow monitoring and warning is crucial to prevent the fatalities and financial losses. The debris flow warning systems can be divided into two categories: advance warning system and event warning system. Advance warning systems are based on monitoring the hydro-meteorological processes, typically rainfall, to predict the possibility of debris flows occurrences. Event warning systems are based on detecting the debris flows when they are in progress, such as ground vibration sensing (Arattano and Marchi 2008). Compared with the advance warning system, the event warning systems provide very short evacuating time but precise alarm signals.

Ground vibrations caused by debris flows have been investigated by many authors (Okuda et al. 1980; Itakura et al. 1997; Berti et al. 2000; Lavigne et al. 2000; Massimo 2000; Arattano 2003; Itakura et al. 2005; Huang et al. 2007;

C.-R. Chu (✉) • C.-J. Huang • T.-M. Tien
Department of Hydraulic and Ocean Engineering, National Cheng Kung University, No.1, University Road, Tainan City 701, Taiwan
e-mail: n8896106@mail.ncku.edu.tw; n8896106@mail.ncku.edu.tw; n8896106@mail.ncku.edu.tw

C. Margottini et al. (eds.), *Landslide Science and Practice*, Vol. 2,
DOI 10.1007/978-3-642-31445-2_29, © Springer-Verlag Berlin Heidelberg 2013

Burtin et al. 2009; Lin et al. 2010). Usually, geophones or seismometers are utilized to detect the ground vibrations produced by debris flows. The detected data can also be used to identify the main characteristics of ground vibrations due to debris flows. Nevertheless, the prone areas of debris flows are usually far from available electricity. The sensors established as a sensing network are dispersed on a wide region. The electrical power supply and the signal attenuation make a long range monitoring of debris flows difficult.

Over the past decade, fiber optic sensors and sensing systems play an important role on measuring strain, temperature, and pressure. Because of their light weight, immunity to electromagnetic interference, high sensitivity, and very low optical loss, this technique is appropriate for remote sensing purpose. In this study, fiber optic sensing technique was applied to develop a sensing system for monitoring debris flows in mountainous area in Taiwan. The comparison of measurements from fiber optic sensors and geophones was implemented and described in the following sections.

Fiber-Optic Sensor

In recent years, application of fiber optic sensors and sensing systems for sensing various physical signals has been increasing due to their inherent optical advantages and multiplexibility. The physical signals include strain, temperature, pressure, and acceleration. In this study, the Fiber Bragg Grating (FBG) sensor was used as an accelerometer to measure the ground vibrations generated by debris flows.

The basic principle of a FBG sensor is to utilize the variation of periodic refraction index in fiber section to reflect a unique wavelength light from a broadband light source, which is based on the effective refractive index and the pitch of the grating. By the photosensitive effect in optical fiber (Hill et al. 1978), intense UV light can cause a permanent change in refractive index of optical fiber. To create a periodic change in the refractive index, an interference pattern of UV radiation is generated to focus onto the core of the fiber. The period of the grating structure is called the grating pitch, Λ, as shown in Fig. 1. With broadband light incident in the grating, a narrowband component, or spectral slice is reflected back at the Bragg resonance wavelength (Kersey 1997), which is determined by,

$$\lambda_B = 2n\Lambda \tag{1}$$

where n is the effective index of the core. When the effective index and the grating period vary with the strain and temperature changes, the Bragg resonance wavelength would shift to different wavelengths in response to applied mechanical field. For most applications, the shift of the wavelengths is considered as a linear combination with the thermal-mechanical

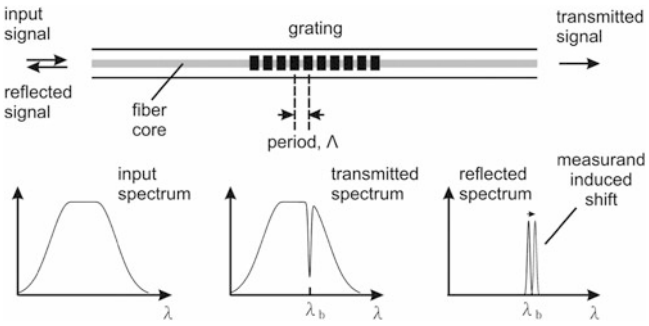


Fig. 1 Basic Bragg grating-sensing mechanism

loading. The shift of Bragg wavelength due to strain and temperature changes is given by (Kersey et al. 1997),

$$\Delta\lambda_B = 2n\Lambda\left(\left\{1 - \left(\frac{n^2}{2}\right)[P_{12} - v(P_{11} + P_{12})]\right\}\varepsilon + \left[\alpha + \frac{\left(\frac{dn}{dT}\right)}{n}\right]\Delta T\right) \tag{2}$$

where ε is the applied strain, P_{ij} are the Pickel's (piezo) coefficients of the stress-optic tensor, v is Poisson's ratio, α is the coefficient of thermal expansion (CTE) of the fiber material (e.g. silica), and ΔT is the temperature change. However, in sensing applications where only one phenomenon is of interest, the separation of temperature and strain becomes necessary. In respect to measurand of ground vibrations generated by debris flows, thermal effects are relative to very-low frequency operation. Therefore, thermal term can be ignored and (2) is simplified as

$$\frac{\Delta\lambda_B}{\lambda_B} = P_e\varepsilon \tag{3}$$

where P_e is the elasto-optic coefficient, which is a constant calculated by the strain term of (2).

In order to measure the ground vibration generated by debris flows, this study utilized an FBG sensor as an accelerometer. Over the past decade, there were multiple schemes to construct such a device, and multiple commercial products were offered. For understanding the concept of FBG accelerometer, a simple linear spring model is examined with the FBG accelerometer acting as the spring system, as shown in Fig. 2. In the following analysis, the accelerometer is modeled by a single-degree-of-freedom system with no damping. In this case, it can be shown that an acceleration carried by external force causes a mass displacement, said Δy, and the strain experienced by the FBG sensor can be defined as,

$$\epsilon = \frac{\Delta L}{L} = \frac{\Delta\Lambda}{\Lambda} = \frac{1}{P_e}\frac{\Delta\lambda_B}{\lambda_B} \tag{4}$$

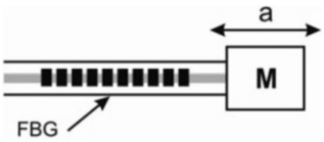


Fig. 2 Diagram of simple FBG accelerometer design

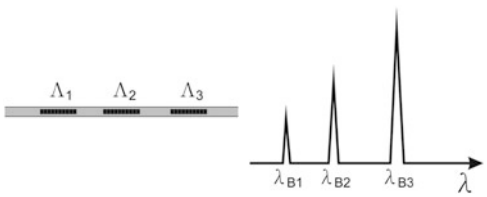


Fig. 3 FBG sensor serial multiplexing

where L is the effective fiber length. According to the simple dynamic model of such a system, the simple relationship between fiber length change and acceleration can be shown as,

$$\Delta L = \frac{M}{K}a \tag{5}$$

with the first resonant frequency of device occurring at K/M, where M is the mass load, K is the spring constant of fiber. In this case, the spring constant is described as,

$$K = \frac{EA}{L} \tag{6}$$

where E is the elastic modulus of the fiber, A is the cross-sectional area of the fiber. From (4), (5), and (6), the relationship of strain, resonant frequency shift, and acceleration are combined as,

$$\frac{\Delta\lambda_B}{\lambda_B} = \frac{P_e M}{EA}a \tag{7}$$

Multiplexing is one of the most critical advantages offered by FBG sensors. Because the sensed information is directly bound up with wavelength, which is an absolute parameter, the output is independent with total light levels, loss in the propagation fiber path and couplers, or source power. This is widely acknowledged as the benefit to facilitate multiplexing by allowing each sensor to be assigned to a different slice of the available source spectrum. As shown in Fig. 3, serial multiplexing is carried out by connecting a sequence of separated FBG sensors in one optical fiber, each with different grating periods, Λ_i, $i = 1, 2, 3, \ldots, n$. The reflected spectrum contains a series of peaks, each associated with a different wavelength given by $\lambda_{Bi} = 2n\Lambda_i$, where λ_{Bi} and Λ_i are the Bragg wavelength and the ith grating period. The limit to the number of gratings addressed in this way depends on the source spectrum width and the operational wavelength bandwidth required for each grating element (Kersey et al. 1997).

Fiber Optic Sensing System for Debris Flow

This study set up a fiber optical sensing system for monitoring debris flows in mountainous region far from available electricity. Two sensing systems were deployed along the Ai-Yu-Zi Creek and the Chu-Shui Creek in Nantou County, Taiwan. In each sensing system four accelerometers were installed in line array at the bank of the creeks. Line array construction is suitable for advance detection of debris flows and spatial analysis of the moving process. The associated broadband light source and data logger were incorporated into the Braggscope, which locates in the front data receiving center built near the monitored creeks. The topographical map of study area and setup of fiber optical monitoring systems are presented in Fig. 4. The geometrical distances between each sensor and the data receiving center were listed in Table 1. One of the advantages of using fiber sensing system is that the attenuation of optical signal transmitted in fiber path is low. The decay rate was 0.383 dB/km, that is, 0.328 dB (7 %) of maximum attenuation in our sensing system.

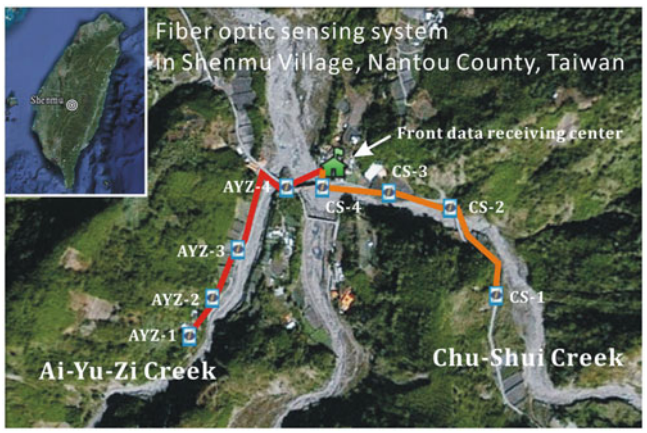


Fig. 4 Topographic map and the fiber optical sensing systems deployed along the Ai-Yu-Zi creek and the Chu-Shui creek. In each system four accelerometers were installed along the bank of the creek. Data were stored in a data logger incorporated in the Braggscope located in the front data receiving center. (*Top left*) Location of study area in Central Taiwan

The sensor used in this study is the single-axis accelerometer GS6500 with a sensitivity of 10 pm/g. This instrument has a flat response up to 300 Hz, which cover the frequency range of ground vibration generated by debris flows. The measurement range of this instrument is ±40 g, with accuracy of 20 mg. The operation temperature and humidity are −20 to 80 °C and <90 % at 40 °C, which is an appropriate condition operated in the typhoon or rainy season. The Braggscope FS5500 made by FiberSensing

Table 1 Distances between the sensors and the data receiving center

Name of creek	Sensor 1 (m)	Sensor 2 (m)	Sensor 3 (m)	Sensor 4 (m)
Ai-Yu-Zi	625	520	340	144
Chu-Shui	595	368	195	50

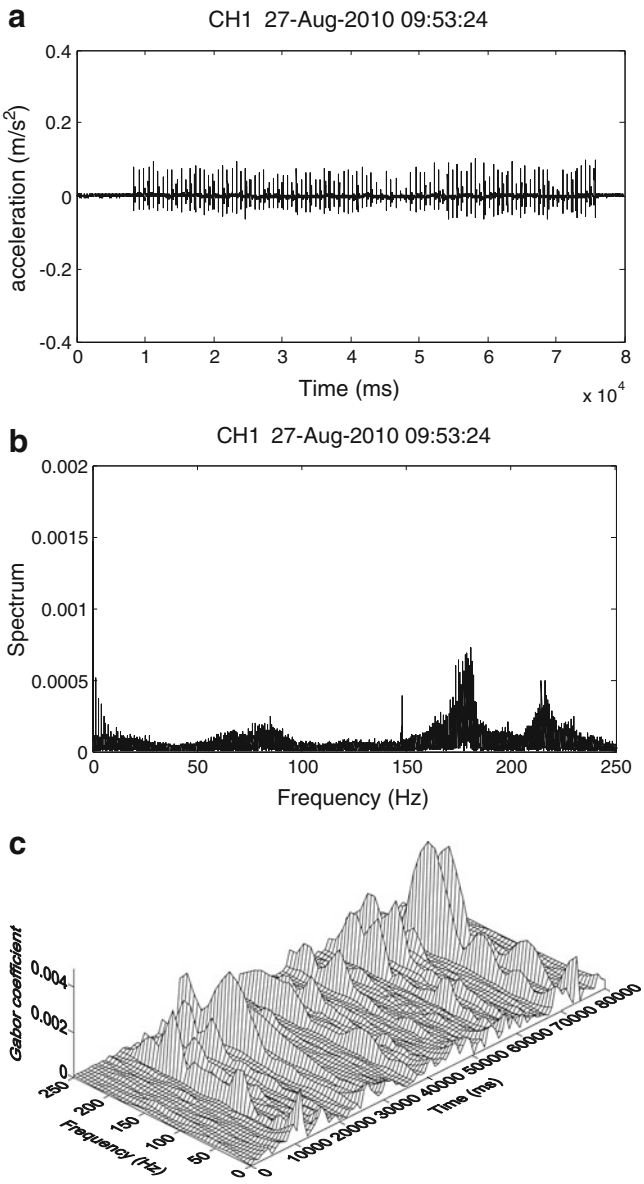


Fig. 5 Testing signal measured by AYZ-4 sensor: (**a**) time domain, (**b**) frequency domain, and (**c**) time-frequency domain by Gabor transformation

Company was located in the data receiving center to provide the broadband light source and to store the recorded data in sampling rate of 500 Hz.

The channel beds of Chu-Shui creek and Ai-Yu-Zi creek are almost dry except during the rainy season or typhoon events. The geological conditions are similar between two creeks. Because of the debris flow occurred in August, 2008, the rock, boulder, and soil in the channel bed of Chu-Shui and Ai-Yu-Zi creek are loosely packed, presenting a rugged bed with randomly spread, different size rocks. The bedrock of these two creeks primarily consists of sandstone and a shale interlayer. The soil is mainly loam, sandy loam and sand.

The accelerometers, mounted separately in a plastic box, were installed on the bank of the creek. To test the sensitivity of the installed sensors, artificial vibration signals were generated by knocking the neighboring bank of the sensors with a stone. The testing signals were measured and shown in Fig. 5. Figure 5a presents the time-series data of the vibrations detected by Sensor 4 of the Ai-Yu-Zi creek. The signals produced by each hit of the rock against the bank can be identified. Figure 5b shows the signals in the frequency domain obtained by FFT, while Fig. 5c shows the time-frequency domain of the signals obtained by Gabor transform, which is equivalent to the short-time Fourier transform. The low-level ambient noise is mainly caused by few farming activities and traveling cars. During the typhoon period, the thunders and heavy rain may produce significant ambient noises. It will take a long time to understand the effect of ambient noise on the data quality.

Calibration Experiment

This study carried out a calibration experiment to examine the performance of fiber optical monitoring system for detecting debris flows. Geophones and seismometers have been often used to detect the ground vibration generated by debris flows. As mentioned in the introduction due to the limitation of power supply and the attenuation of the signals in the cable, they cannot be installed too far away from the base station where power is available. However, for an early detection of debris flows, the fiber optic sensors can be installed close to the sources where debris flows originate. Hence, in the real application the fiber optic sensing system may provide an alternative way to monitor the slope-related disasters, such as debris flows. In order to recognize the performance of such an innovative sensing system compared to the conventional ones, such as that involves geophones or microphones, we carried out a field experiment to measure the ground vibrations and airborne sounds generated by an artificial debris flow using three different sensing systems. The three sensing systems are the following. The first one is the fiber optic sensing system presented in this paper. The second one is the conventional sensing system involving a three-dimensional geophone (GS-20DX), which detects frequencies in the range of 8–1,500 Hz. The third one is a system which detects the airborne sounds generated by

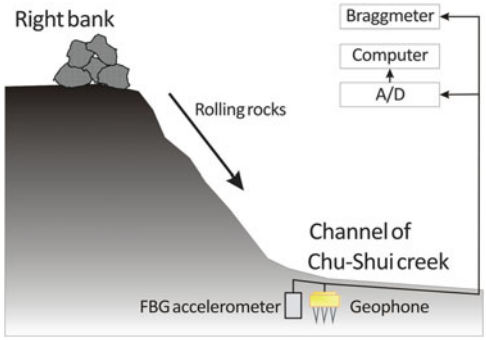


Fig. 6 Sketch of calibration experiment setup



Fig. 7 Picture of experimental site

debris flows using a microphone (B&K 4190). The microphone detects frequencies from 3 to 20 kHz.

The artificial debris flow was simulated by putting rocks and boulders of different sizes to roll down a steep and rugged bank of Chu-Shui creek, see Figs. 6 and 7. A fiber optic sensor and a geophone were buried in the creek bed to detect the ground vibrations caused by this artificial debris flow. A microphone was also installed nearby on a big boulder to detect the airborne sounds due to the artificial debris flow. The frequency response of geo-sound generated by debris flow depends on the rock size, geological conditions, and type of debris flow, etc. Based on the study of Huang et al. (2007) the frequency range of the ground vibrations produced by debris flows is coincident with that produced by a single boulder hitting against the ground. Hence, we may safely assume that the ground vibrations produced by the artificial debris flow are representative of the real ones. Figure 6 shows the sketch of calibration experiment setup, and Fig. 7 is the picture of experimental site.

The signals measured by the Z-axis component of geophone and by the fiber optic accelerometer are presented in Fig. 8. Both the time-series data and the signals in the frequency domain obtained using FFT were presented. The sampling rate was 500 Hz. For synchronizing the signals obtained by these two instruments, cross-correlation was used to align the two signals by the first impact pulse. The signals last 30 s from beginning were used to compute the power spectral density (PSD). Notably from the PSD results that the frequency range of the ground vibrations generated by rocks hitting against the ground was 20–250 Hz. The frequency range of ground vibrations sensed by FBG accelerometer is consistent with that measured by geophone except that in the latter signals frequencies higher than 170 Hz have comparable acceleration magnitude with those at lower frequencies. This may suggest that the FBG accelerometer is more sensitive to sense tremors of higher frequencies.

Signal-to-noise ratio (SNR) can be used to evaluate the performance of different sensors for various physical signals (Itakura et al. 2000). According to time-series data in Fig. 8, the signal base of SNR was defined as the duration containing the pulses generated by rocks hitting against the ground. During the experiment, the drizzle generated some ambient noises. The short pulses with tiny amplitude produced by rain drops may raise the energy of ambient noise. Therefore, the data received for 20 s before the beginning of experiment was representative of the noise base of SNR. The definition of SNR is shown as follows.

$$\mathrm{SNR} = 10\log\left(\frac{\mathrm{S_E}}{\mathrm{N_{mean}}}\right) \tag{8}$$

$$S_{\mathrm{E}} = \int_0^T S^2(t)dt/T$$

$$N_{\mathrm{mean}} = \frac{1}{M}\sum_{j=1}^{M}\left(\int_0^T N_j^2(t)dt/T\right)$$

where S_{E} represents a cumulated signal energy received in T interval, N_{mean} is the mean of cumulated noise energy received in T interval. In this study, we took $T = 1$ s as the computing interval, and $M = 20$ s for taking mean. The SNR plot is shown in Fig. 9. Obviously, from Fig. 9, the SNR of FBG accelerometer is higher than which of geophone we used. Thus, it demonstrates that the fiber optic sensing system is more sensitive than the conventional sensing system involving moving-coil sensors. However, the fiber optic sensor is also sensitive to the variation of the ambient temperature. The effect of the temperature change on the recorded physical signals should be clarified in the future to avoid misunderstanding of the detected signals. Besides, although the airborne sound measured by the microphone was taken as additional information, this experiment showed

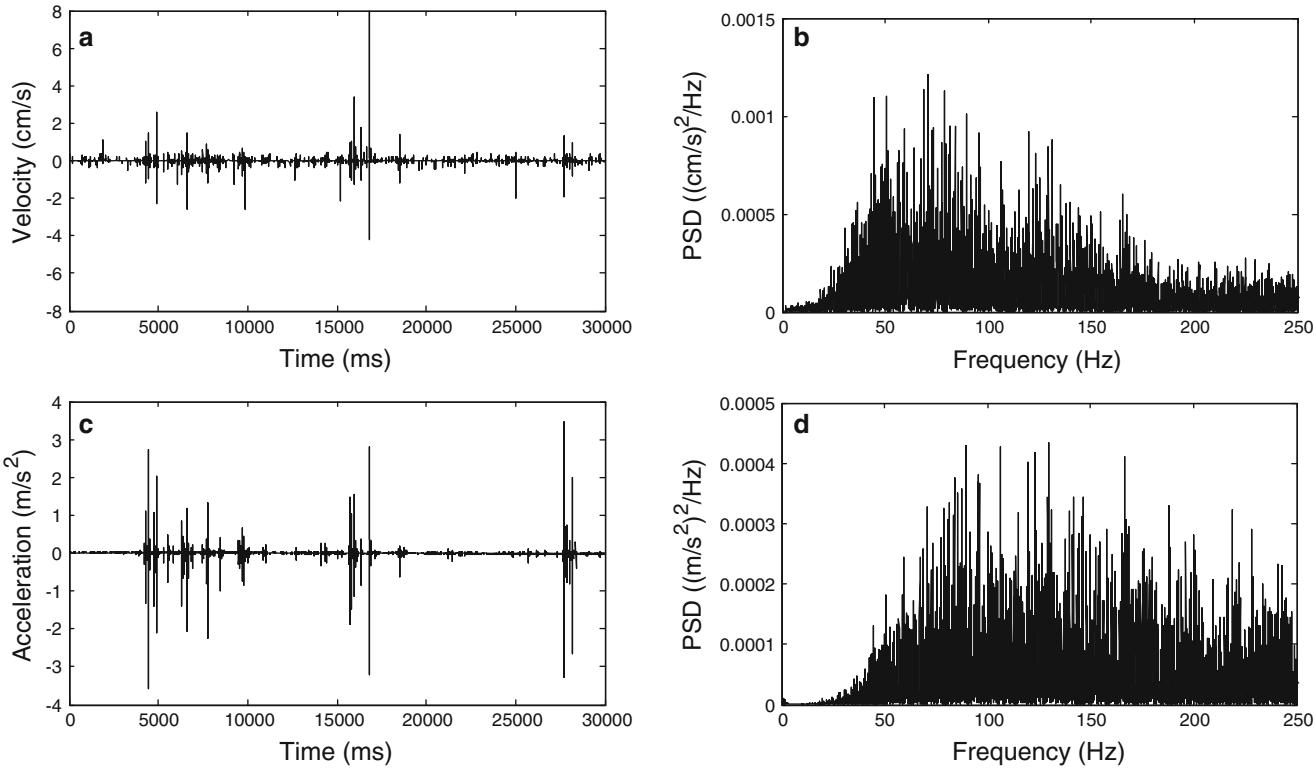


Fig. 8 Vertical ground vibration measured by the Z-axis component of geophone versus vertical acceleration of ground vibration measured by the FBG accelerometer. The signals were recorded for 30 s, and well aligned to the first impact pulse. (**a**) Vertical velocity of ground vibration in time domain, and (**b**) in frequency domain. (**c**) Vertical acceleration of ground vibration in time domain, and (**d**) in frequency domain

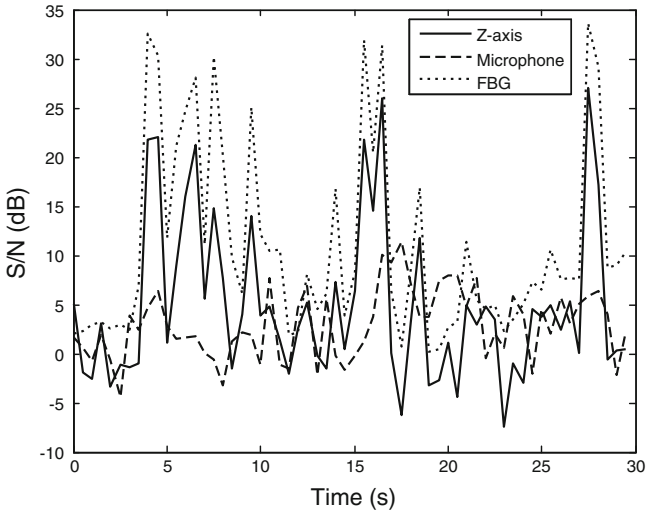


Fig. 9 Signal-to-noise ratio (SNR) calculated through the time axis. SNR from Z-axis of geophone (*solid line*), FBG accelerometer (*dotted line*), and microphone (*dashed line*)

that the SNR of microphone was the worst among the three instruments because the detected signals were weak and the ambient noises caused by air turbulent were loud.

Conclusions

This study presents a novel fiber optic sensing system for monitoring debris flows. The Fiber Bragg Grating (FBG) sensor was used as an accelerometer to measure the ground vibrations generated by debris flows. Two sensing systems were deployed along the Ai-Yu-Zi Creek and the Chu-Shui Creek in Nantou County, Taiwan for monitoring debris flows. In each system four accelerometers were installed in the bank of the creek as line arrays.

A calibration experiment was carried out to compare the performance of FBG accelerometer with other sensors used for detecting debris flows, such as geophone and microphone. The artificial debris flow was simulated by putting rocks and boulders to roll down a steep and rugged bank. The geo-sound as the source due to rocks and boulders hitting against the ground was received near-simultaneously by FBG accelerometer and geophone at the same place. The result showed that the SNR of FBG accelerometer was higher than geophone; moreover, was much higher than microphone measuring airborne sound which is induced by the same ground

vibrations. The different performance was born of the sensitivities of the used sensors.

Even though the sensing capability of FBG accelerometer seems better than geophone, the temperature effect and other ambient noise should be considerable, because these phenomena are probably sensed by FBG sensor. Low frequency contribution would be involved from the temperature changes. Ambient noises would be sensed from traffic, water flow, or other tremors. These effects will cause the false alarm of detecting and warning system. The proper filter can be used to eliminate the low frequency effects. Dynamic threshold setting will be the discussion of this topic in the future.

Acknowledgments The authors would like to thank the Soil and Water Conservation Bureau of the Council of Agriculture, Taiwan, for financially supporting this research.

References

Arattano M (2003) Monitoring the presence of the debris-flow front and its velocity through ground vibration detectors. In: Debris-flow hazards mitigation: mechanics, prediction, and assessment. Proceedings of the third international conference on debris-flow hazards mitigation, Davos/Rotterdam, 10–12 Sep 2003, Millpress, pp 719–730

Arattano M, Marchi L (2008) Systems and sensors for debris-flow monitoring and warning. Sensors 8(4):2436–2452

Berti M, Genevois R, LaHusen R, Simoni A, Tecca PR (2000) Debris flow monitoring in the Acquabona watershed on the Dolomites (Italian Alps). Phys Chem Earth B: Hydrol Oceans Atmos 25 (9):707–715

Burtin A, Bollinger L, Cattin R, Vergne J, Nabelek JL (2009) Spatio-temporal sequence of Himalayan debris flow from analysis of high-frequency seismic noise. J Geophys Res Earth Surf 114. doi:F04009 10.1029/2008jf001198

Hill KO, Fujii Y, Johnson DC, Kawasaki BS (1978) Photosensitivity in optical fiber waveguides – application to reflection filter fabrication. Appl Phys Lett 32(10):647–649

Huang C-J, Yin H-Y, Chen C-Y, Yeh C-H, Wang C-L (2007) Ground vibrations produced by rock motions and debris flows. J Geophys Res 112:F02014

Itakura Y, Fujii N, Sawada T (2000) Basic characteristics of ground vibration sensors for the detection of debris flow. Phys Chem Earth (B) 25(9):717–720

Itakura Y, Inaba H, Sawada T (2005) A debris-flow monitoring devices and methods bibliography. Nat Hazards Earth Syst Sci 5(6):971–977

Itakura Y, Koga Y, Takahama JI, Nowa Y (1997) Acoustic detection sensor for debris flow. In: Debris-flow hazards mitigation: mechanics, prediction, and assessment. Proceedings of the first international conference, New York. American Society of Civil Engineers, pp 747–756

Iverson RM, Reid ME, LaHusen RG (1997) Debris-flow mobilization from landslides. Annu Rev Earth Planet Sci 25:85–138

Johnson AM, Rodine JR (1984) Debris flows. In: Brunsden D, Prior DB (eds) Slope instability. Wiley, Chichester, pp 257–361

Kersey AD (1997) Multiplexing techniques for fiber-optic sensors. In: Dakin J, Culshaw B (eds) Optical fiber sensors: applications, analysis, and future trends, vol IV. Artech House, Boston, pp 369–407

Kersey AD, Davis MA, Patrick HJ, LeBlanc M, Koo KP, Askins CG, Putnam MA, Friebele EJ (1997) Fiber grating sensors. J Lightwave Technol 15(8):1442–1463

Lavigne F, Thouret JC, Voight B, Young K, LaHusen R, Marso J, Suwa H, Sumaryono A, Sayudi DS, Dejean M (2000) Instrumental lahar monitoring at Merapi Volcano, Central Java, Indonesia. J Volcanol Geotherm Res 100(1–4):457–478

Lin CH, Kumagai H, Ando M, Shin TC (2010) Detection of landslides and submarine slumps using broadband seismic networks. Geophys Res Lett 37. doi:10.1029/2010GL044685

Massimo A (2000) On debris flow front evolution along a rorrent. Phys Chem Earth (B) 25(9):733–740

Okuda S, Okunishi K, Suwa H (1980) Observation of debris flow at Kamikamihori Valley of Mt. Yakedade. In: The 3rd meeting of IGU commission on field experiment in geomorphology, Disaster Prevention Research Institute, Kyoto University, Japan, 1980, pp 127–130

Takahashi T (1991) Debris flow. A A Balkema, Rotterdam



Integrated Monitoring of Lateral Spreading Phenomena Along the North-West Coast of the Island of Malta

Stefano Devoto, Emanuele Forte, Matteo Mantovani, Arianna Mocnik, Alessandro Pasuto, Daniela Piacentini, and Mauro Soldati

Abstract

Landslides, and especially lateral spreading, are responsible for the main landforms observable along the north-western coast of the Island of Malta. A series of rock spreading phenomena, and associated mass movements, have been recognised in this area and the most significant cases have been investigated by means of a multi-technical approach which envisaged geomorphological survey and mapping, geophysical analyses and monitoring of displacements. The aim of the study was to define whether rock spreading phenomena are active along the investigated coastal stretch and, possibly, to determine the rate of movement of the most relevant cases. In this framework, a multidisciplinary approach was used and different techniques were tested and applied on a specific site, which was selected for the presence of an extensive rock spread phenomenon which may induce hazard conditions. The site is located at Il-Prajjet (Anchor Bay), a narrow inlet where a tourist attraction is located. Research activities have been carried out at Il-Prajjet since 2006 when a GPS network of eight benchmarks was installed. This technique was chosen because it proved to be a powerful tool in the study of similar ground deformation in coastal and mountain areas, showing high accuracy and reliability. Once GPS monitoring had showed that rock spreading was active, further techniques were applied in order to achieve an in-depth knowledge of the instability processes occurring at Il-Prajjet. The paper illustrates the results so far achieved thanks to GPS monitoring, tape extensometer measurements, SAR interferometric analyses and GPR investigations.

Keywords

Coastal instability • Rock spreading • GPS • SAR interferometry • GPR • Malta

Introduction

The investigation of landslides is sometimes limited to a purely descriptive approach without quantitative assessments and continuous monitoring. This is especially the case of very slow mass movements, such as rock spreading (cf. Pasuto and Soldati 1996). These phenomena are rarely monitored over long periods, though this is, in most cases, the only way to achieve enough data to properly understand their kinematics and triggering mechanisms (e.g., Guerricchio et al. 1988; Vlcko 2004; Prokop and Panholzer 2009; Lissak et al. 2010).

In these situations, monitoring techniques have become a powerful tool in landslide analyses due to the high accuracy

S. Devoto (✉) • D. Piacentini • M. Soldati
Dipartimento di Scienze della Terra, Università di Modena e Reggio Emilia, Largo S. Eufemia 19, Modena 41121, Italy
e-mail: stefano.devoto@unimore.it

E. Forte • A. Mocnik
Dipartimento di Geoscienze, Università di Trieste, Via Weiss 2, Trieste 34127, Italy

M. Mantovani • A. Pasuto
Istituto di Ricerca per la Protezione Idrogeologica (IRPI), Consiglio Nazionale delle Ricerche, Corso Stati Uniti 4, Padova 35127, Italy

C. Margottini et al. (eds.), *Landslide Science and Practice*, Vol. 2,
DOI 10.1007/978-3-642-31445-2_30, © Springer-Verlag Berlin Heidelberg 2013



Fig. 1 Panoramic view of the north side of Anchor Bay (north-west coast of Malta)

and reliability that recent instrumentation provides (Dunnicliff 1995; Angeli et al. 2000; Corominas et al. 2000; Malet et al. 2002; Corsini et al. 2005; Petley et al. 2005; Lissak et al. 2010).

Nevertheless, long-term monitoring of rock spreading phenomena is still quite rare due to the fact that this type of mass movement normally is not considered as hazardous, due to the slow rate of movement. Nevertheless, it should be emphasized that rock spreading, can be highly hazardous for engineering structures or buildings, since it may act over wide areas, during long periods of time and involving large volumes of rock masses. Moreover, these phenomena can evolve into faster movements, which can determine catastrophic failures (i.e. block slides) or they can favour and trigger a series of collateral landslides (i.e. block slides, rock falls and topples, rotational slides, earth slides and flows) occurring at the edges of the areas affected by spreading (Pasuto and Soldati 1996; Pasuto et al. 1997).

In this context, the coupling of conventional monitoring techniques (e.g., topographic and extensometric measurements) with innovative ones (e.g., ground-based GPS or satellite SAR interferometric analysis) make up a reliable solution to detect and survey active deformation due to rock spreading, with promising perspectives in terms of hazard assessment and possible mitigation actions.

Research activities have been carried out in the frame of a co-operation programme between the University of Modena and Reggio Emilia (Italy), the Italian National Research Council (CNR), the University of Malta, the University of Trieste (Italy) and the University of Cantabria (Spain) which also included the mobility of young researchers. The objectives of the research, which is still in progress, are pursued through multidisciplinary investigations which foresee an integrated geomorphological and engineering-geological approach.

The attention has been focused along the north-western coast of the Island of Malta (central Mediterranean Sea) where exemplary cases of lateral spreading phenomena are found (Magri et al. 2007, 2008; Magri 2009). The latter develop because of the superimposition of rock types having very different mechanical behaviour (limestones over clayey terrains).

In particular, extensive rock spreading phenomena have been recognized, mapped and monitored at Il-Prajjet (Anchor Bay), with the aim of assessing the hazard conditions of one of the main tourist attractions of the Maltese Islands, an amusement park which was developed in the early 1980s (Fig. 1).

Physical Setting of the Study Area

The study site is located at Il-Prajjet (Anchor Bay) which is a narrow inlet along the north-western coast of the Island of Malta (Fig. 2), and in particular along its north side (Said and Schembri 2010). This sector of the bay is characterised in its upper portion by a 20–30 m high escarpment, which runs in an E-W direction (Fig. 3).

The origin of the bay is clearly linked to the presence of two faults (WSW-ENE oriented) which follow the general tectonic trend of the area (Pedley et al. 2002) (Fig. 3).

From a geological point of view, the northern part of the bay is characterised by the outcrop of terrains belonging to the Blue Clay Formation (at the base) and to the Upper Coralline Limestone Formation (at the top), the latter making up the younger rock units of the Maltese stratigraphic sequence (Pedley et al. 1978, 2002). The limestones give rise to a wide karst plateau bounded toward the sea by steep cliffs, whereas the Blue Clays outcrop near the sea level, often covered by limestone blocks and debris accumulations (Fig. 4).

The *Upper Coralline Limestone Formation* (Upper Miocene) covers the above mentioned stratigraphic unit giving rise to vertical cliffs of varying heights along the coastline, up to over 30 m. It is mainly composed by shallow marine sediments, making up hard limestones affected by a dense

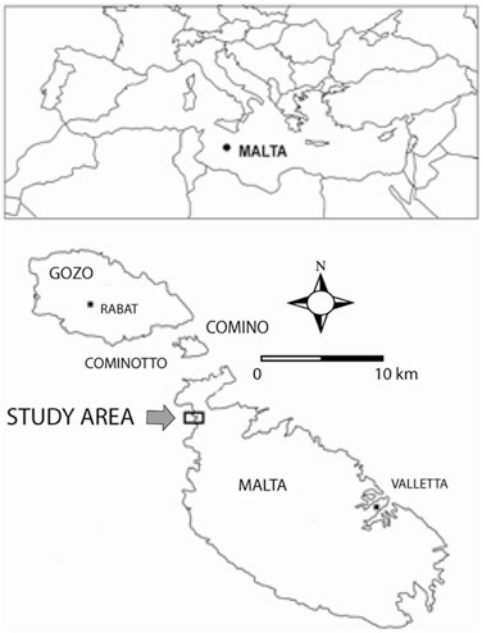


Fig. 2 The location of Il-Prajjet (Anchor Bay) within the Maltese archipelago

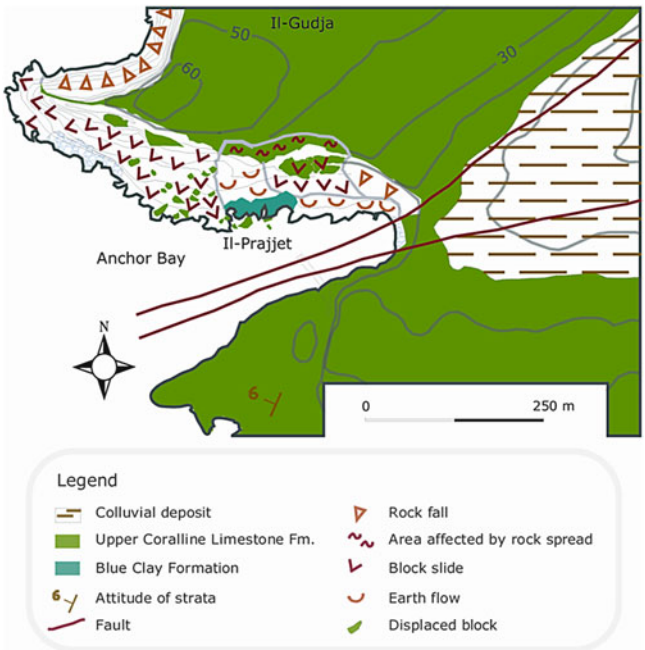


Fig. 3 Geomorphological sketch map of the study area. The map clearly shows the extensive landslide accumulations, which characterise the northern part of the bay

network of joints which provides the rock masses with a brittle behaviour.

The *Blue Clay Formation* (Middle Miocene) can reach a thickness of 65 m in the Maltese archipelago and is composed by silty sands, marls and clays showing poor



Fig. 4 The northern sector of Anchor Bay, where the Upper Coralline Limestone Formation is characterised by steep cliffs and the Blue Clay Formation outcrops near the sea level



Fig. 5 The rock blocks detached from the limestone plateau, as a result of block sliding, determine a hazard conditions for the tourist infrastructure located beneath

geotechnical properties which favour the onest of slope movements including the spreading of the overlying limestones.

The different mechanical behaviour of the Blue Clay and the Upper Coralline Limestone formations favours the development of a peculiar rock spreading phenomenon at Il-Prajjet which has evolved into a large block slide (Magri et al. 2008; Magri 2009) (Fig. 5). Also the different hydrogeological properties of the two formations mentioned above have to be considered, since a karst aquifer may be formed just above their contact surface (Mangion 1991). The evolution of this complex coastal instability phenomenon may induce hazard conditions to the tourist infrastructure located between the coastline and the foot of the block

slide, for the assessment of which the understanding of the movement rates of the overall area is crucial.

The southern part of Anchor Bay is instead characterised by vertical Upper Coralline Limestone cliffs which directly reach the sea. The absence of outcrops of the Blue Clay Formation prevents the occurrence of lateral spreading phenomena on this side of the bay.

The climate is typically Mediterranean, with hot, dry and long summers, warm and short winters. In the last 50 years the average annual precipitation is of about 550 mm, hardly exceeding 800 mm, with an average of about 70 rainy days per year.

Methods and Results

The investigations have been developed through a multidisciplinary approach which has envisaged the following methods and techniques:

- GPS monitoring
- Tape extensometer measurements
- SAR interferometric analyses
- GPR survey.

GPS Monitoring

GPS techniques have been already proved to be a powerful tool in ground deformation analysis. Several papers dealing with landslide monitoring demonstrated the capability of GPS to measure deformations with high accuracy and reliability (Gili et al. 2000; Malet et al. 2002; Coe et al. 2003; Lissak et al. 2010). For this reason, a GPS monitoring network has been installed since October 2006 and is still operating. The first aim of the installation of the network was to define whether rock spreading and block sliding phenomena were active at Il-Prajjet and, if so, to determine the rates of movement within the unstable area.

GPS measurements have been taking place with reference to eight benchmarks spread all over the unstable area. Within the upper sector, corresponding to the edge limestone plateau, three benchmarks were installed, whereas five more benchmarks were positioned on the large blocks overhanging the buildings of the tourist infrastructure (Fig. 6). In order to guarantee the uniformity of the surveys, avoiding positioning errors, a forced centring device for the antenna was performed for each benchmark.

Considering the extremely slow rate of deformation, GPS surveys have been conducted using at least two dual frequencies receivers, using a static relative positioning technique, which achieve more accurate results. It was chosen a period of acquisition of 20 min and a 2 s sampling rate. Field monitoring activities have been planned using broadcasting almanacs to exploit the temporal windows with the best possible satellite configuration within a reliable value of the GDOP parameter.

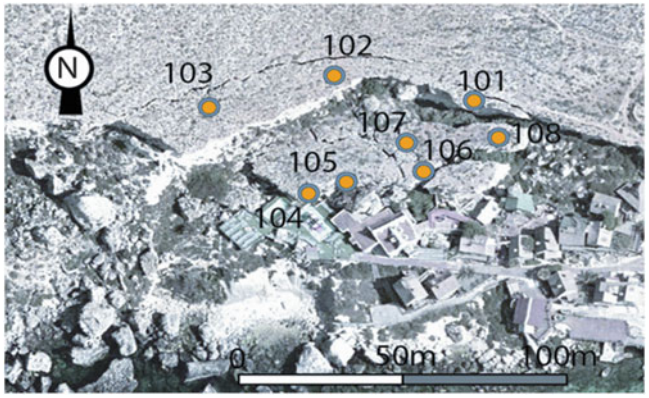


Fig. 6 The aerial photograph shows the benchmarks installed in the areas affected by rock spreading (101–103) and block sliding (104–108)

Table 1 Cumulative planar and vertical displacements measured by means of the GPS technique at Il-Prajjet during the period October 2006–November 2010

Benchmark	Planar displacement (cm)	Vertical displacement (cm)
101	2.9	Negligible
102	2.7	5.8
103	3.2	10.2
104	5.8	4.0
105	5.2	4.0
106	3.4	Negligible
107	5.0	Negligible
108	2.8	Negligible

Surveys have been carried out twice per year, in March and November, corresponding to the end of the wet season and the end of the dry one, respectively, in order to investigate the relationship between landslide activity and rainfall.

Since the first GPS measurements it was clear that both the rock spreading and block sliding sectors were active, affecting a large area of Il-Prajjet. The series of readings carried out over a 49 months period (October 2006–November 2010) showed significant displacements of all the eight benchmarks, with cumulative displacements ranging from 2.7 to 10.2 cm. In particular, vertical displacements appeared to be higher in the area affected by rock spreading (benchmark 103 was lowered of 10.2 cm and benchmark 102 of 5.8 cm) while planar movements prevail in the block sliding sector (benchmark 104 was lowered of 5.8 cm and benchmark 105 of 5.2 cm) (Fig. 6, Table 1).

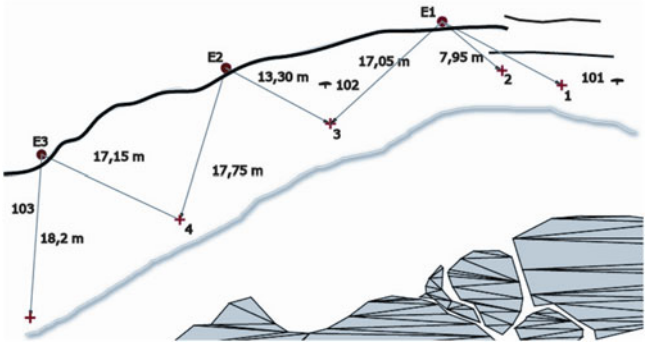


Fig. 7 Tape extensometers measure the relative distances between couple of reference points, located on the rock spreading scarp and on the rock mass beneath

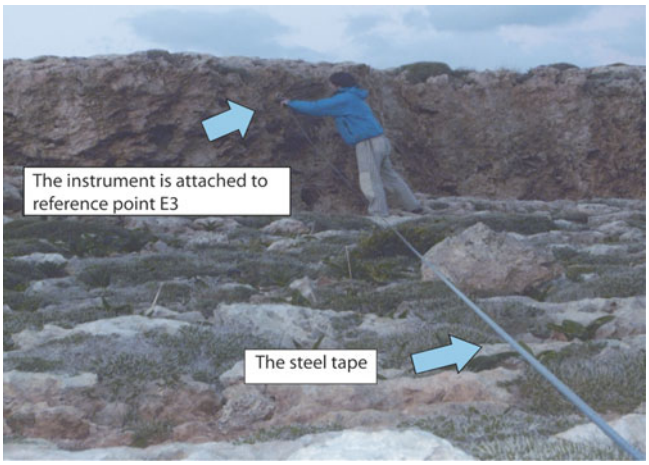


Fig. 8 The extensometer is anchored by the operator to a reference ring on the main scarp and to another ring located on the rock mass beneath

Tape Extensometer Measurements

A tape extensometer network has been installed in the area affected by rock spreading at the end of December 2009. Tape extensometer is a mobile instrument, equipped with a micrometer which can measure distances reaching 20 m, with a sub-millimetre precision. An invar steel tape has been used to monitor relative changes in the distance between couple of reference points (Figs. 7 and 8).

Reference points have been placed in the area where rock spreading is more active. In particular, reference points E1, E2 and E3 have been anchored to the main scarp within the rock spreading sector (Fig. 8). The surveys have been carried out approximately every 3 months, corresponding to the end of each season.

Table 2 shows relative ground deformations recorded along seven scanlines, connecting couples of reference points, during three field surveys performed in 2010. The two higher cumulative displacements have been measured between the couples E2-4 and E3-5 (Fig. 8), reaching a total annual rate of deformation respectively of 5.6 and 4.0 mm. The displacements recorded in the eastern sector are lower and do not exceed 3.0 mm, confirming that the western sector is the most active area affected by rock spreading phenomena.

Table 2 Deformations recorded during 2010

Scanline	Displacement March (mm)	Displacement July (mm)	Displacement November (mm)
E1-1	+3.2	−6.5	+3.45
E1-2	+3.9	−4.1	+3.25
E1-3	+12.9	−7.5	−2.80
E2-3	+0.1	−2.45	−0,25
E2-4	+0.90	−1.60	+6.30
E3-4	+2.05	−4.35	+0.80
E3-5	+0.20	−1.90	+5.70

Positive rates correspond to cumulative widening of fractures (sliding movement towards the plateau), whereas negative values display narrowing of fractures

Tape extensometer results have been correlated with GPS displacements, recorded by benchmarks 101, 102, and 103 (cf. Fig. 6), Finally, the outputs of these techniques showed comparable movement rates.

Interferometric Analyses

To support the monitoring results, interferometric analyses (satellite SAR) have been carried out along all the north-western coast of the Island of Malta. The analyses of radar images consisted in two phases. In a first phase, the database of ERS 1 and ERS 2 images, collected since 1992, has been exploited to evaluate the deformation eventually occurred before the realization of the GPS network. In a second phase, images acquired from ENVISAT satellites have been processed in order to define the state of deformation in the last decade.

In particular, the interferometric analysis of the latter satellite images were aiming at the integration and validation of the results achieved with the GPS technique. To detect and monitor ground movements classical DInSAR (advanced Differential Sar Interferometry) and PSI (Persistent Scatterers Interferometry) have been applied, which can reach a subcentimetric precision. Table 3 shows the number of images processed and the time period covered by satellites data.

PSI conducted over the entire stretch of the north-western coast highlighted the presence of deformation induced by lateral spreading phenomena. Tens of limestone boulders with a scatterer point-wise behaviour recorded rates of displacement along the sensor line of sight (23 ° with respect to the vertical) ranging from 1.5 to 4 mm/year. Unfortunately,

Table 3 Satellite images used for interferometric analyses

Platform	Images	First image	Last image
ERS 1	14	05/06/1992	14/01/1996
ERS 2	41	15/01/1995	04/12/2000
ENVISAT	33	28/04/2003	20/07/2009



Fig. 9 GPR data acquisition (profile spacing 1 m; trace interval 5 cm)

no natural persistent scatterers were so far detected over the site of Il-Prajjet where the GPS network has been installed and therefore a validation of the results is at present unfeasible.

GPR Survey

Geophysical surveys have been carried out to investigate the geometry of the limestone blocks which are located beneath the rock spreading area and to identify the underground contact with the Blue Clays. Data were acquired using a Ground Penetrating Radar (GPR) equipped with 300 and 500 MHz bistatic shielded antennas. Profiles were recorded along a dense grid (22 m by 7 m wide) (Fig. 9). 2D processed GPR data were combined in order to obtain a 3D data volume. The GPR technique allowed us to recognise (1) a high-reflective zone interpreted as layered limestones; (2) a semi-transparent portion interpreted as non-stratified, massive limestone (probably the Mtarfa Member of the Upper Coralline Formation) and (3) a high-attenuating area having its top at a depth of about 13 m. The latter level corresponds to the contact between the limestone blocks and the Blue Clay Formation. In addition, several evident vertical or sub-vertical discontinuities have been outlined, showing high persistencies (Fig. 10).

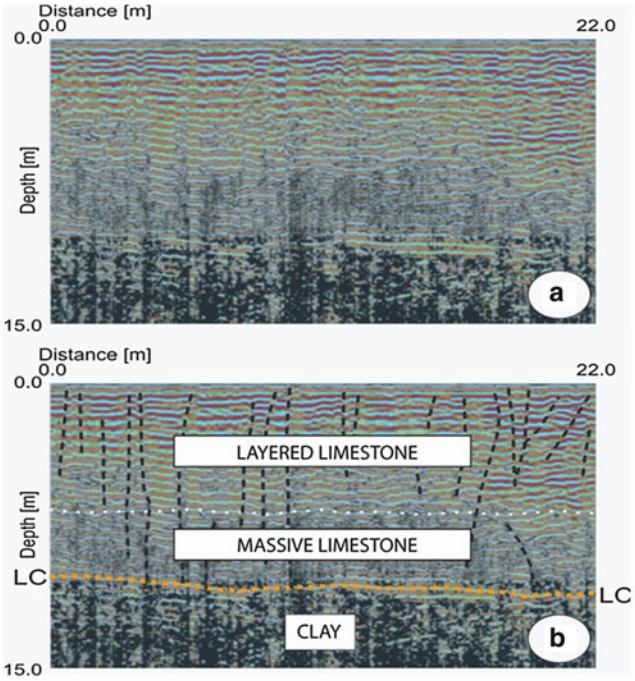


Fig. 10 Example of processed and depth-converted 300 MHz GPR profile (cosine of instantaneous phase superimposed on reflection amplitude) acquired on the widest limestone block within the block slide area (**a**) and the same profile with interpretation superimposed (**b**). LC corresponds to the contact between the limestone blocks and the Blue Clay Formation. Several vertical or sub-vertical discontinuities are outlined. The deepest portion of the limestone blocks shows low amplitude reflections and can be interpreted as a massive material, while the shallowest part is clearly layered. The profile is plotted without vertical exaggeration

Conclusions

A spectacular case of rock spreading evolving into block sliding has been investigated at Il-Prajjet, a small inlet located along the north-western coast of the Island of Malta. Slope instability processes in the area are strictly linked to the geological and structural settings of the bay, which foresees the superimposition of deeply jointed limestones on clayey materials.

The multidisciplinary and integrated approach applied within the study has allowed the understanding of the present evolution of the instability phenomena affecting Il-Prajjet and has provided the basis for defining future scenarios of evolution, which are essential for the assessment of hazard to which the tourist attraction located in the area is exposed.

In particular, the integration of results obtained from different monitoring systems, such as GPS and tape extensometer, has proved to be fundamental to define the state of activity and the rate of movement of both rock spread and block slide. In addition, the outputs of GPR surveys have provided detailed information on the geometry and volumes involved in the block slide as well as the location of the limestone-clay contact and discontinuity persistence values, which are essential to implement a proper subsurface geological model of the unstable area. Finally, the preliminary results of interferometric analyses, which actually refer to the entire north-western coast of Malta, show ongoing deformation which

has however to be further analysed with respect to the study area of Il-Prajjet.

Acknowledgments The research activities were funded by (i) the EUR-OPA Major Hazards Agreement of the Council of Europe through the European Centre of Geomorphological Hazards (CERG) in the frame of the project "*Coastline at risk: methods for multi-hazard assessment*" (Co-ordinator M. Soldati) and (ii) the Fondazione Cassa di Risparmio di Modena and Reggio Emilia within the project *Multidisciplinary research in the open-air laboratory of the island of Malta: an international network for landslide hazard assessment in coastal areas* (Co-ordinator M. Soldati).
Interferometric analyses have been carried out under an ESA Category-1 project (C1P.7044). The authors acknowledge the European Space Agency for providing ERS and ENVISAT data.
The authors are also thankful to Darren Saliba for his precious collaboration during field work and Julie Anne Mizzi for her helpful suggestions about Maltese geology.

References

Angeli MG, Pasuto A, Silvano S (2000) A critical review of landslide monitoring experiences. Eng Geol 55:133–147

Coe JA, Ellis WL, Godt JW, Savage WE, Savage JE, Michael JA, Kibler JD, Powers PS, Lidke DJ, Debray S (2003) Seasonal movements of the Slumgullion landslide determined from Global Positioning System surveys and field instrumentation, July 1998–March 2002. Eng Geol 68:67–101

Corominas J, Moya A, Lloret J, Gili JA, Angeli MG, Pasuto A, Silvano S (2000) Measurement of landslide displacements using a wire extensometer. Eng Geol 55(3):149–166

Corsini A, Pasuto A, Soldati M, Zannoni A (2005) Field monitoring of the Corvara landslide (Dolomites, Italy) and its relevance for hazard assessment. Geomorphology 66(1–4):149–165

Dunnicliff J (1995) Keynote paper: monitoring and instrumentation of landslides. In: Bell DH (ed) Landslides. Proceedings of 6th ISL, Christchurch (NZ). Balkema, Rotterdam, vol 3, pp 1881–1895

Gili JA, Corominas J, Rius J (2000) Using global positioning system techniques in landslide monitoring. Eng Geol 55:167–192

Guerricchio A, Melidoro G, Rizzo V (1988) Instrumental observations of the slope deformations and deep phenomena in Maratea Valley (Italy). In: Bonnard C (ed) Landslides. Proceedings of 5th ISL, Lausanne, Switzerland. Balkema, Rotterdam, vol 2, pp 415–422

Lissak C, Maquaire O, Malet J-P, Déprez A, Masson F, Ulrich Peters E (2010) Multi-technique permanent monitoring of a slow-moving coastal landslide in Normandy. In: Malet J-P, Glade T, Casagli N (eds) Mountain risks: bringing science to society. CERG Editions, Strasbourg, France, pp 267–274

Magri O (2009) Investigation of landslides along the North-West coast of Malta and related hazard issues. Ph.D. thesis, University of Modena and Reggio Emilia, Modena, Italy

Magri O, Mantovani M, Pasuto A, Soldati M (2007) Monitoring the state of activity of lateral spreading phenomena along the north-west coast of Malta using the GPS technique. Ana Univ Din Oradea 17:5–10

Magri O, Mantovani M, Pasuto A, Soldati M (2008) Geomorphological investigation and monitoring of lateral spreading phenomena along the north-west coast of Malta. Geogr Fis Dinam Q 31(2):171–180

Malet JP, Maquaire O, Calais E (2002) The use of Global Positioning System techniques for the continuous monitoring of landslides: application to the Super-Sauze earthflow (Alpes-de-Haute-Provence, France). Geomorphology 43(1–2):33–54

Mangion M (1991) Impact of geological structural features on the hydrology and hydrogeology of Malta. Bachelor thesis, University of Malta, Msida, Malta

Pasuto A, Soldati M (1996) Rock spreading. In: Dikau R, Brunsden D, Schrott L, Ibsen M-L (eds) Landslide recognition: identification, movement and causes. Wiley, Chichester, pp 122–136

Pasuto A, Silvano S, Soldati M (1997) Deformazioni gravitative profonde di versante e frane: casi di studio nella Valle del Boite (Dolomiti, Italia). Geogr Fis Dinam Q 20:107–111

Pedley HM, House MR, Waugh B (1978) The geology of the Pelagian Block: the Maltese Islands. In: Nairn AEM, Kanes WH, Steheli FG (eds) The ocean basins and margins, vol 4B, The Western Mediterranean. Plenum Press, London, pp 417–433

Pedley M, Hughes Clarke M, Galea P (2002) Limestone isles in a crystal sea: the geology of the Maltese Islands. PEG Ltd, Malta, 109

Petley DN, Mantovani F, Bulmer MH, Zannoni A (2005) The use of surface monitoring data for the interpretation of landslide movement patterns. Geomorphology 66(1–4):133–147

Prokop A, Panholzer H (2009) Assessing the capability of terrestrial laser scanning for monitoring slow moving landslides. Nat Hazard Earth Syst Sci 9(6):1921–1928

Said G, Schembri J (2010) Malta. In: Bird ECF (ed) Encyclopedia of the world's coastal landforms – vol 1. Springer Science + Business Media B.V, Dordrecht, pp 751–759

Vlcko J (2004) Extremely slow slope movements influencing the stability of Spis Castle, UNESCO site. Landslides 1(1):67–71

InSAR Data for Mapping and Monitoring Landslides in Tena Valley

Juan-Carlos García-Davalillo, Gerardo Herrera, Davide Notti, Mario Hernández-Ruiz, Jose-Antonio Fernández-Merodo, Inmaculada Álvarez-Fernández, Celestino González-Nicieza, Tazio Strozzi, and Oscar Mora

Abstract

In the last 20 years the exploitation of satellite SAR interferometry has shown a considerable improvement due to the development of new InSAR PSI techniques and the availability of the new satellite sensors with higher spatial and temporal resolution. One of the most interesting applications is the possibility of mapping slow landslides processes. In this paper we present an analysis of the advantages and disadvantages of using L-, C- and X-band sensors for mapping and monitoring landslides in the Rio Gállego upper basin (Central Pyrenees, Spain) techniques.

Keywords

InSAR • Landslides • Mapping • Monitoring • Tena • Pyrenees • Radar

Introduction

The Tena Valley is located in the Upper Gállego River basin (Central Pyrenees, Spain). The river descends through the valley following a WNW-ESE direction from 2,000 to 1,200 m a.s.l. in Lanuza reservoir (Fig. 1). In this valley the anthropic print is significant: apart from the settlements of Portalet, Formigal and Sallent de Gállego, two dams, and the connection road to France, there is a wide ski-area.

J.-C. García-Davalillo (✉)
Instituto Geológico y Minero de España (IGME) in Valencia, Cirilo Amorós 42, Valencia 46004, Spain

G. Herrera • M. Hernández-Ruiz • J.-A. Fernández-Merodo
IGME, Geological Hazard and Risk Investigation Area, Madrid, Spain

D. Notti
Earth Sciences Department, University of Pavia, Pavia, Italy

I. Álvarez-Fernández • C. González-Nicieza
Department of Mining Engineering, University of Oviedo, Asturias, Spain

T. Strozzi
Gamma Remote Sensing, Worbstrasse 225, 3073 Gümligen, Switzerland

O. Mora
Altamira Information, c/Còrsega, 381-387, Barcelona 08037, Spain

Due to its geological setting this is a landslide prone area that has been studied by several authors (Mulas and Fresno 1995; García-Ruiz et al. 2004). The type and distribution of landslides is controlled by the structural and geological setting, as well as by the glacial, the fluvial action and erosion. In a recent work by Notti et al. (2010) a landslide inventory was updated through the combination of available orthophotos, radar data and field work (Fig. 1).

The updated landslides inventory of the Upper Tena Valley consists of 103 landslides that cover about 28 % of the total area. From the total amount 53 % are relict landslides that affect the shale formations. Shale formations are characterized by gentle slopes (15–20), and present a considerable thickness of weathered rocks and colluvial deposits. These landslides were triggered by the glacial retire and, nowadays, they are in a relict state of activity. Nevertheless, local reactivation is frequently observing flow/slide movements triggered by the erosive action of River Gállego and the great seasonal variation of soil humidity in old landslide deposits. These reactivations locally trigger slow flows, roto-translational slides and soil/ice creep processes. The mechanisms that control these landslides are complex and involve roto-translation with flow. In some cases, these landslides transport rock fall and rock avalanche deposits derived from the upper massive rock scarps. The areas affected by rock fall or rock avalanche processes represent

C. Margottini et al. (eds.), *Landslide Science and Practice*, Vol. 2,
DOI 10.1007/978-3-642-31445-2_31, © Springer-Verlag Berlin Heidelberg 2013

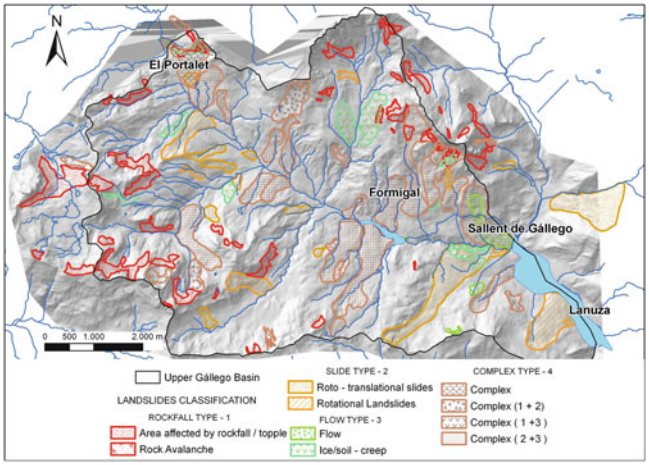


Fig. 1 Upper Tena Valley Landslides Inventory (Notti et al. 2010)

Table 1 Data specifications for each C-, X- and L-band analysis made in Tena Valley

Satellite	Time period	No. of images	No. of interferograms	Data processing
ERS1 and ERS2	1995–2001	30	115	SPN
ERS2 and Envisat	2001–2007	43	163	SPN
TerraSAR-X	May–Oct 2008	11	55	SPN
ALOS	June 2007–June 2009	6	4	DInSAR

47 % of the total but the accumulation of rock deposits at the toe of the scarps are usually of smaller size. These types of landslides are concentrated in the Southwest and Northern part of the study area where the steepest slopes (>35 °) and massive formations (limestone, sandstone, conglomerate, and intrusive rocks) coincide. The presence of badlands and rill erosion can also be noticed in the area.

To acquire an updated landslides database is fundamental to support the territorial planning and infrastructure development. Recently landslide mapping and monitoring has been improved through the use of ground base radar (Herrera et al. 2009a), C-band satellite data (Herrera et al. 2009b), and X-band satellite data (Herrera et al. 2010; Notti et al. 2010). Based on the results obtained in this works we present the following analysis of the advantages and disadvantages of InSAR techniques for mapping, and monitoring landslides.

The SAR Data Available and Processing

In the interpherometric study of Tena Valley we have SAR datasets available from 1995 to 2009 in 90 images of five different satellites with sensors in L, C and X bands (Table 1).

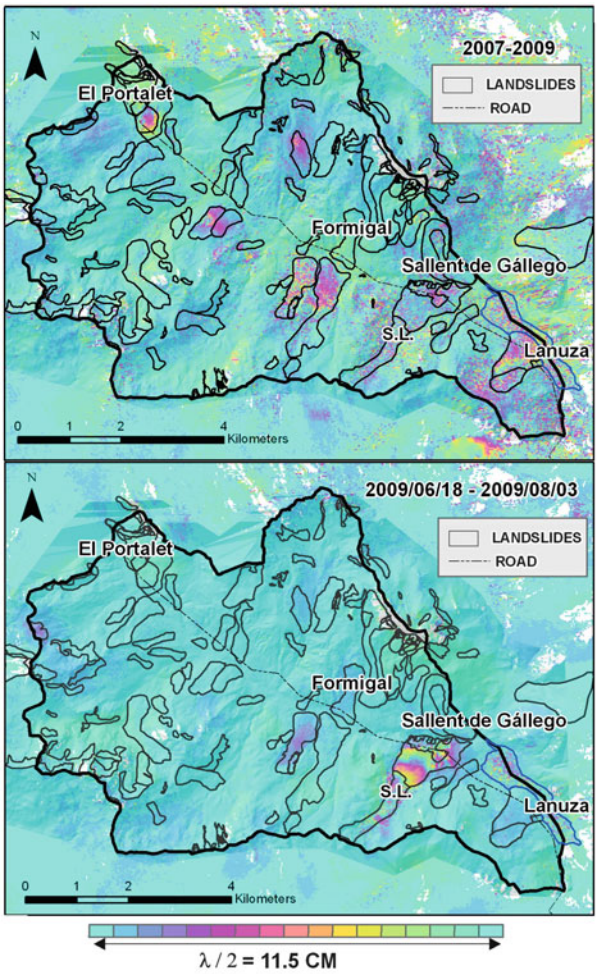


Fig. 2 Tena landslides inventory compared with ALOS PALSAR differential interferograms: from 13 June 2007 to 03 August 2009 (*upper*) and from 18 June 2009 to 03 August 2009 (*bottom*). S.L. is the *La Selva* landslide

DInSAR processing has been used for L band data and the PSI SPN technique for X and C bands.

DInSAR Processing

The standard differential interferometry (DInSAR) compares two SAR images acquired at different moments in time over the same area, detecting ground surface deformations that have occurred between the acquisition dates of both images. Several authors have applied standard DInSAR to landslide investigations (Carnec et al. 1996; Catani et al. 2005; Strozzi et al. 2005; Corsini et al. 2006), being a good method to detect landslides with a significant displacement during the acquisition of the two images that form the interferogram.

An example of the good results obtained by calculating interferograms in Tena Valley is the 2009 summer ALOS PALSAR interferogram (Fig. 2 bottom) that shows a clear

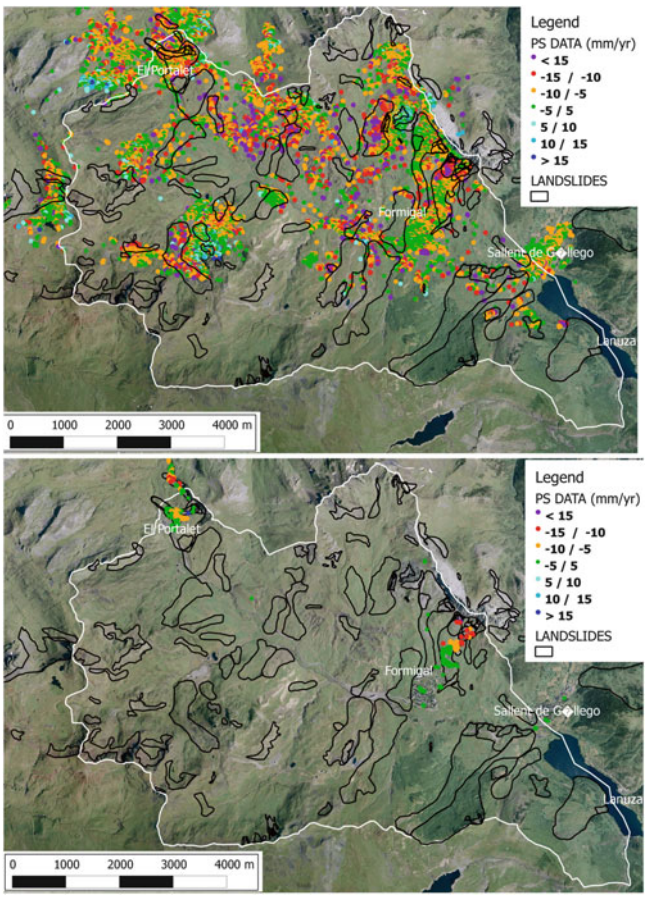


Fig. 3 SPN displacement velocity maps retrieved over Tena Valley using TerraSAR-X (X), Envisat (C)

deformation signal (19 cm in 46 days) in *La Selva* landslide. This post-glacial paleo-landslide is developed from 1,920 m to 1,300 m a.s.l. over a 1.25 km^2 area. The clear signal observed in the bottom part show how in the summer 2009, after a humid period, *La Selva* landslide was re-activated producing damages to the A-136 road located in his foot. On the other hand in the highest part of the landslide decorrelation is observed. This is due to the forest located in this area that prevents the L-band signal to provide adequate deformation measurements.

PSI Processing

Standard DInSAR limitations have been partially resolved by the so-called Persistent Scatterers Interferometry techniques. They make use of large sets of SAR images acquired at different moments in time over the same area, permitting the observation of the temporal evolution of the displacement of every detected ground target with high precision and spatial resolution. To date, most of the PSI applications have focused on subsidence analysis and only a few landslide applications are available, e.g. see Farina et al. (2006), Colesanti and Wasowski (2006), Meisina et al. (2006, 2008, 2010), Pancioli et al. (2008), Wasowski et al. (2008), Notti et al. (2008), Herrera et al. (2009b, 2010), Cascini et al. (2009), Fernández et al. (2009), Righini et al. (2010).

Table 2 Principal available SAR data acquisition satellites and evaluation of our maximum displacement detectable

Satellite	Date mission	Band/ wavelength (cm)	Revisit time (days)	60 % of max. displacement (cm/year)
ERS 1, ERS 2 and Envisat	1991–2012	C	35	8.8
		5.6		
TerraSAR-X	2008–2012	X	11	14.9
		3		
ALOS	2006–2012	L	46	27.4
		23		

One of these advanced processing techniques, the SPN technique (Arnaud et al. 2003; Duro et al. 2005), has been used to process SAR data in the Tena Valley (Fig. 3). Figure 3 shows the annual movement rate (mm/year) of the detected measurement points (PS). In red are those items with significant negative vertical movements, green colours represent stable points and the blue points upward motion. Note that the majority of the landslides with PS data are located in SW-facing slopes.

Landslide Analysis by Means of SAR Applications

To analyze and understand the results for each satellite band it is necessary to know first the main limitations of PSI techniques when we study landslide dynamics.

Maximum Observable Velocity

With a standard elaboration and without any a priori information, the maximum rate of measurable displacement is ¼ of the radar wavelength between two consecutive acquisitions. Considering this aspect and the revisiting time of the satellite we may calculate the theoretical maximum measurable annual displacement (Table 2).

However these are the maximum theoretical movements considering a perfect linear movement and with all temporal series of the images available for the processing. In the practical experience the real maximum real movements are no more than the 60 % of theoretical movements.

Time Series Limitations

The PSI techniques present the possibility to monitor the evolution of the displacement in time. This kind of analysis

enables to study the accelerations and decelerations of the moving mass with respect to conditioning or triggering factors. The main problem of this kind of analysis is the number of images available the PSI processing techniques requires at least 20 SAR images to be reliable. Note that the time lapse between two acquisitions depends on the satellite revisiting time (Table 2). Nevertheless even if all the SAR images are available a successful landslide time series analysis depends on the velocity of the displacement with respect to the temporal separation of the image acquisitions. As a consequence of a limited number of SAR images available for the PSI processing noise will affect the TS preventing to identify different trends of the landslide dynamics. This has occurred in the study area with ALOS and ERS and ENVISAT data. In the case of TerraSAR-X due to higher resolution and shorter revisiting time period time series landslide analysis has been possible as it will be discussed in the following sections.

Measurement Point Detection

One of the main limitations of PSI techniques (Colesanti and Wasowski 2006) is the absence of data over the area of interest. Some authors like Cascini et al. (2009) proposed an a priori visibility map of SAR data. Recently Notti et al. (2010) presented a model (RC index) that predicts the distribution of radar targets based on the slope, the radar geometry (R-index), and the land use information (LU index). This model has been tested in our study area calculating the R-index considering three different satellites with different LOS orientation: (D 23°) descending orbit with 23° incidence angle (like ERS and Envisat satellite); (A 34°) ascending orbit with 34° of incidence angle (like ALOS PALSAR sensors); (D 45°) descending orbit with 45° incidence angle (like TerraSAR-X sensor). The results of this model (Fig. 4) explain the great differences observed on the results obtained in our study area with TerraSAR-X and ERS-Envisat sensors (Fig. 4). The TerraSAR-X analysis yielded a very dense PS dataset, which allows one to obtain a very good spatial sampling of the area of interest.

Regional Analysis

The update of landslides inventories in Valle de Tena was made with the sum of different methodologies: aerial photo interpretation, field survey and interpretation of SAR data. For this purpose we mainly used TerraSAR-X data that provided the greatest PS density, ALOS data processed with DInSAR showed good results for several landslides, and ERS and Envisat data covered only few landsides, but confirmed the observations made with TerraSAR-X data.

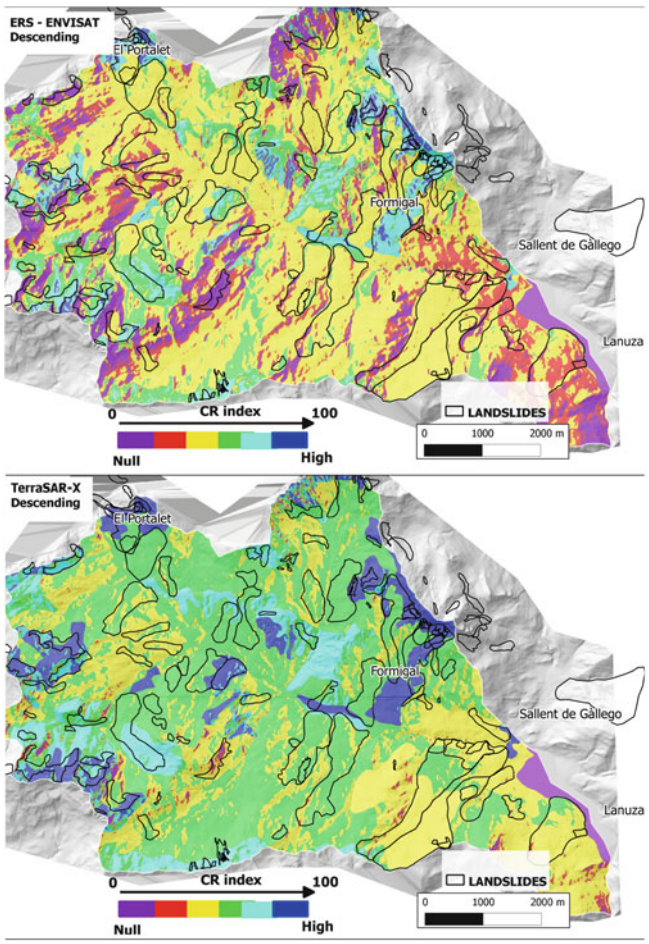


Fig. 4 CR index for TerraSAR-X and ENVISAT

In Tena Valley in order to detect possible new landslides we used the concept of the "anomalous areas" (Meisina et al. 2008). When a cluster of PS is observed, we can evaluate his average movement rate and his density. These parameters are indicative of possible active geological process. To create the anomalous areas we have performed an "Inverse Distance Weighted" interpolation of the displacement velocity values of those areas with more than 1,000 PSI/km^2 and then we have selected those areas greater than 1,000 m^2 with an average displacement rate greater than 5 mm/year. Moreover, this approach has permitted us to identify six new landslides and to redefine the boundaries of eight other landslides. It is important to remind that all the observations made with SAR are always compared with geomorphological observations in order to confirm the first interpretation.

Another important issue is that PS techniques can only provide an update of slow landslides (Colesanti and Wasowski 2006). From the total amount of landslides (103) inventoried by Notti et al. (2010), only 49 are considered slow type landslides. From this amount, if we consider only those that contain at least 100 PS/km^2 in a SPN analysis, only 4 of

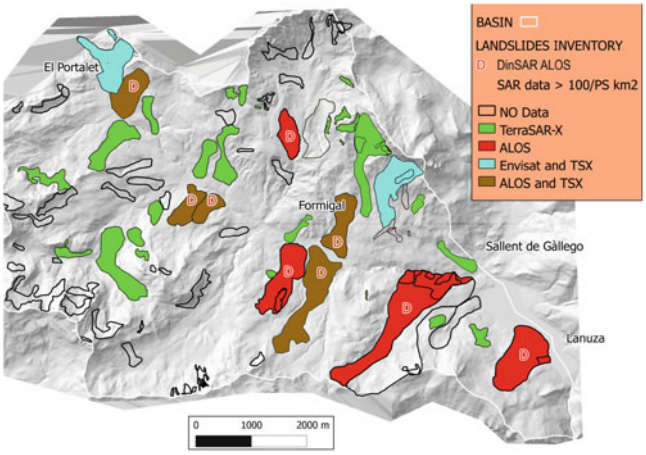


Fig. 5 Upper Tena Valley Landslides Inventory in function of SAR data availability

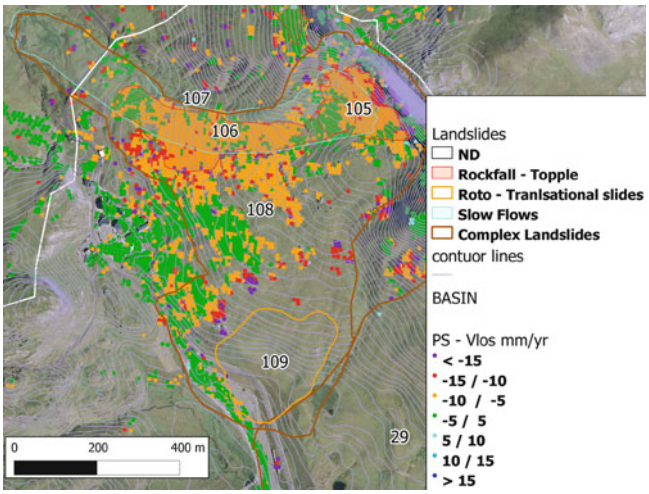


Fig. 6 TSX displacement rate measured in Portalet landslide

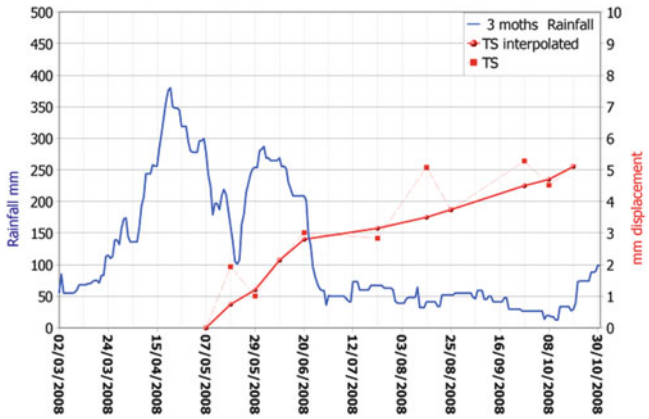


Fig. 7 Displacement TerraSAR-X time series of parking lot landslide compared with 6-m rainfall (Herrera et al. 2010)

them were detected from C-band data (Herrera et al. 2009b) and 27 from X-band data (Notti et al. 2010). Additionally with L-band DInSAR analysis we have been detected nine landslides (red D in Fig. 5), from which four of them were not previously detected by the SPN analysis. Overall through the combination of the three bands, 70 % of the slow landslides have been detected and monitored successfully. L-band has complemented C- and X-band results because of the ascending orbit acquisition mode that has permitted to monitor E, and NNE oriented slopes, against the W and SSW oriented slopes that could be monitored from the C and X band orbit descending modes. Another reason is that the L-band wavelength performance permits to detect faster movements even if moderate vegetation is present and rock deposits or urban areas are absent. In addition it is interesting to note that ALOS data processed with traditional DInSAR techniques allowed to detect too fast movements for the PS techniques to be detected (15 cm in 2 months).

Local Analysis

The interpretation of SPN data enables to improve the understanding of a landslide processes. In detailed landslide studies, PS are one of the post-monitoring systems (Colesanti and Wasowski 2006; Calò 2009) that can help in the development and validation of numerical models (Herrera et al. 2009a). The results of SAR processing can be validated with the information coming from in situ monitoring data. This is the typical case of the well known landsides with many information. The PS data can be considered as one of the many tools that, with an integration, can improve the understanding of a landslide. The PS data can suggest the areas where to carry out more accurate investigations.

An example of time series analysis was made by Herrera et al. (2010) in "El Portalet" landslide, which is located in the North-Western sector of the Upper Tena Valley (Fig. 6). In this area it is possible to identify three main landslides developed from 1,850 and 1,600 m a.s.l. along the southwest-facing hillside of Petrusos Peak, which slightly deviates the route of the Gállego River channel to the South. These are complex types of landslides, probably triggered by the retirement of glaciers. The dynamics of the movement seem to be controlled by the slow flow of the upper part of the Quaternary sediments, the colluvial deposits and the weathered shale bedrock. The excavation at the foot of the slope, carried out to build a parking area in the summer of 2004, generated new sliding surfaces (probably a roto-translational slide) with a faster movement affecting the connection road to France and evidence of tension cracks in the slope.

With TerraSAR-X data obtained from May to October 2008, it was possible to analyse the average TS displacement of all the PS close to the crown of the parking lot landslide. These results were compared with the rainfall data (from March to October 2008) available from the nearest rain-gauge. In Fig. 7 the average TS displacement of the selected PS is represented by the red dashed line, whereas the red line

represents the interpolated average TS displacement, and the blue line represents the accumulated rainfall every 30 days.

In the parking lot landslide, the PSs selected surrounding the crown of the deposit show two different trends (Fig. 7):

1. The highest displacement rate is measured from May to June (25 mm/year), coinciding with the greatest concentration of rainfall events and the snow melting period.
2. The displacement rate is decelerated from June to October (6 mm/year), coinciding with a period when the concentration of rainfall events is significantly reduced.

Conclusions

In this work we have analysed the results obtained from the standard DInSAR and PSI processing of L-C- and X-band satellite data to study landslides in Tena Valley. The following final considerations should be outlined:

1. InSAR results depend highly on the number of images available, the satellite revisiting time, and the geometry of the acquisition.
2. The use of a predictive model of radar targets before the InSAR processing maybe a cost effective tool to achieve the best results with the lowest cost.
3. TerraSAR-X show a high PS density due to the high resolution and the 45 ° incidence angle. These results were useful to update the landslide inventory. From a local scale point of view the 11 day revisiting time allowed to correlate well Portalet landslide displacement time series with rainfall.
4. ERS and ENVISAT dataset showed the lowest PS density due to the low resolution of SAR images and the 23 °incidence angle. The advantage of these satellites ios that they provide data since 1995 permitting to perform historical analysis.
5. ALOS data were processed with traditional DInSAR due to the low number of available SAR images. This analysis was specially useful to map too rapid landslides and E, and NNE oriented landslides that could not be detected with the PSI processing of C- and X-band descending datasets.
6. Overall through the combination of the three bands, 70 % of the slow landslides have been detected and monitored successfully.

Acknowledgments This work has been partially funded by the SPAINSLIDES element of the Terrafirma project of the GMES programme from ESA, by the GALAHAD project of the EU 6FP (Global Change and Ecosystems, Contract No. 018409), by the project DO-SMS (SUDOE INTERREG IV B) and by the Spanish Geological and Mining Institute (IGME) within project 2004051. The DEM and aerial photographs used in this work have been provided by the Cartographical Service of the Government of Aragón (Spain). The TerraSAR-X data used were provided as part of the DLR science service (proposal MTH0263). ALOS PALSAR data courtesy AOALO-3550, JAXA.

References

Arnaud A, Adam N, Hanssen R, Inglada J, Duro J, Closa J, Eineder M (2003) ASAR ERS interferometric phase continuity, IGARSS, 21–25 July 2003, Toulouse (France), CDROM

Calò F (2009) Analysis of slow-moving landslides in Southern Apennines by integrating groundmonitoring and remote sensing techniques. Ph.D. thesis, University of Naples Federico II, Italy

Carnec C, Massonnet D, King C (1996) Two examples of the application of SAR interferometry to sites of small extent. Geophys Res Lett 23:3579–3582

Cascini L, Fornaro G, Peduto D (2009) Analysis at medium scale of low-resolution DInSAR data in slow-moving landslide-affected areas, 2009. ISPRS J Photogramm Remote Sens 64 (6):598–611

Catani F, Farina P, Moretti S, Nico G, Strozzi T (2005) On the application of SAR interferometry to geomorphological studies: estimation of landform attributes and mass movements. Geomorphology 66:119–131

Colesanti C, Wasowski J (2006) Investigating landslides with space-borne synthetic aperture radar (SAR) interferometry. Eng Geol 88 (3–4):173–199

Corsini A, Farina P, Antonello G, Barbieri M, Casagli N, Coren F, Guerri L, Ronchetti F, Sterzai P, Tarchi D (2006) Spaceborne and ground-based SAR interferometry as tools for landslide hazard management in civil protection. Int J Remote Sens 27(12):2351–2369

Mulas de la Peña J, Fresno-López F (1995) Estudio Geotécnico y de Riesgos Naturales. Estudio, del Medio Físico y de sus Riesgos Naturales en un Sector del Pirineo Central. Instituto Geológico y Minero de España, Madrid. Report, p 216

Duro J, Closa J, Biescas E, Crosetto M, Arnaud A (2005) High resolution differential interferometry using time series of ERS and ENVISAT SAR data. In: Proceedings of 6th geomatic week conference, 8–11 February, Barcelona (on CDROM)

Farina P, Colombo D, Fumagalli A, Marks F, Moretti S (2006) Permanent scatterers for landslide investigations: outcomes from ESA-SLAM project. Eng Geol 88:200–217

Fernández P, Irigaray C, Jiménez J, El Hamdouni R, Crosetto M, Montserrat O, Chacón J (2009) First delimitation of areas affected by ground deformations in the Guadalfeo River Valley and Granada metropolitan area (Spain) using the DInSAR technique. Eng Geol 105:84–101

García-Ruiz JM, Chueca J, Julián A (2004) Los movimientos en masa del Alto Gállego. In: Peña JL, Longares LA, Sánchez M (eds) Geografía Física de Aragón: aspectos generales y temáticos. Universidad de Zaragoza e Institución Fernando el Católico, Zaragoza, pp 142–152

Herrera G, Fernández-Merodo JA, Mulas J, Pastor M, Luzi G, Monserrat O (2009a) Use of ground based SAR data in landslide forecasting models: the Portalet case study. Eng Geol 105 (3–4):220–230

Herrera G, Davalillo JC, Mulas J, Cooksley JG, Monserrat O, Pancioli V (2009b) Mapping and monitoring geomorphological processes in mountainous areas using PSI data: Central Pyrenees case study. NHEES 9(5):1587–1598

Herrera G, Notti D, García-Davalillo JC, Mora O, Cooksley G, Sánchez M, Arnaud A, Crosetto M (2010) Analysis with C- and X-band satellite SAR data of the Portalet landslide area, Landslides. Online First™, 7 Sep 2010, doi:10.1007/s10346-010-0239-3

Meisina C, Zucca F, Fossati D, Ceriani M, Allievi J (2006) Ground deformation monitoring by using the permanent scatterers technique: the example of the Oltrepo Pavese (Lombardia, Italy). Eng Geol 88:240–259

Meisina C, Zucca F, Notti D, Colombo A, Cucchi A, Savio G, Giannico C, Bianchi M (2008) Geological interpretation of PSInSAR data at regional scale. Sensors 11:7469–7492

Meisina C, Zucca F, Notti D (2010) Regional interpretation of PSInSAR(TM) data for landslide investigations. In: Proceedings of EGU 2010 general assembly, 03–07 May 2010, Vienna

Notti D, Meisina C, Zucca F, Colombo A, Cucchi SG, Giannico C, Bianchi M (2008) PS interferometry-based studies of landslides at regional scale. In: Proceedings of the first World landslide forum United Nations University, Tokyo, pp 439–442

Notti D, Davalillo JC, Herrera G, Mora O (2010) Assessment of the performance of X-band satellite radar data for landslide mapping and monitoring: Upper Tena valley case study. Nat Hazards Earth Syst Sci 10:1865–1875

Pancioli V, Raetzo H, Campolmi T, Casagli N (2008) Terrafirma landslide services for Europe based on space-borne InSAR data. In: Proceedings of the first world landslide forum United Nations University, Tokyo, pp 81–84

Righini G, Pancioli V, Casagli N (2010) Updating landslide inventory maps using persistent scatterers interferometry (PSI) in the Biferno River Basin (Central Italy). In: Proceedings of EGU 2010 General Assembly, 03–07 May 2010, Vienna

Strozzi T, Farina P, Corsini A, Ambrosi C, Thüring M, Zilger J, Wiesmann A, Wegmüller U, Werner C (2005) Survey and monitoring of landslide displacements by means of L-band satellite SAR interferometry. Landslides 2(3):193–201

Wasowski J, Bovenga F, Florio N, Gigante G (2008) PSInSAR for the investigating of unstable slopes and landslides. In: Proceedings of the 1st world landslide forum, Tokyo, pp 653–655



Monitoring Displacement on the Mannen Rockslide in Western Norway

Lene Kristensen and Lars Harald Blikra

Abstract

In Norway, four large rock slides are considered high-risk objects and equipped with real time early warning system. The mountain Mannen is the most recently instrumented of those. Construction and instrumentation was started in 2009 and was almost completed in 2010. To ensure redundancy, several types of instruments are used, such as lasers, realtime DGPS, extensometers, ground based InSAR system, borehole instrumentation and a meteorological station. The surface displacement is about 3 cm/year, with the largest velocity in the upper part, where the annual probability of failure estimated to 1/100. Strong subsurface deformation is measured in a 120 m borehole, suggesting a complex movement in a graben structure at the back-crack.

Keywords

Rockslide • Monitoring • Displacement

Introduction and Site Description

In Norway large rock slides are rare, but have historically cost many lives – in particular tsunamis created from rockslides have been deadly (Fylkesmannen i Møre og Romsdal 2011). Large rockslides are usually being pre-warned by accelerated movement, seen as opening and widening of cracks and increased rockfall activity. Monitoring these parameters allows for "forecasting" a rockslide event (Blikra 2008; Crosta and Agliardi 2003). The Geological Survey of Norway (NGU) has identified four high-risk objects in Norway, where both the probability and consequence of a failure is large, and an early warning system thus necessary.

The mountain Mannen, Møre and Romsdal, western Norway (Fig. 1) is the most recently identified and instrumented of the four high risk objects, and Åknes/Tafjord Early Warning Centre is responsible for the instrumentation and monitoring.

Mannen is a 1,295 m high mountain which is a part of a plateau above the steep, glacial eroded valley Romsdalen. A part of the plateau (100 mill. m^3) towards the valley is bounded by deep clefts indicating past movement, but most of this appear inactive today. A block of possibly 15–20 mill. m^3 has been lowered 15–20 m from the plateau, and a block in the upper part of this (2–3 mill. m^3) has been measured periodically with DGPS, showing an yearly movement of 5–6 cm dipping 45–50 against ENE. These blocks are the basis of the scenarios (A and B) drawn in Fig. 1. NGU and the County Governor have estimated that the yearly probability of A; a 2–3 mill. m^3 rock slide is about 1/100.

Modelling work shows that a rockslide of such magnitude would destroy the road and railroad at the valley bottom as well as several houses. Furthermore, the rock debris may dam the river Rauma, with a subsequent risk of dam collapse and flooding downstream of the river.

L. Kristensen (✉)
Åknes/Tafjord Early Warning Centre, Stranda, Ødegårdsvegen 176 N-6200, Norway
e-mail: Lene.Kristensen@aknes.no

L.H. Blikra
Åknes/Tafjord Early Warning Centre, Stranda, Ødegårdsvegen 176 N-6200, Norway

Sogn og Fjordane University Collage, P.O. Box 133, Sogndal, N-6851, Norway

C. Margottini et al. (eds.), *Landslide Science and Practice*, Vol. 2,
DOI 10.1007/978-3-642-31445-2_32, © Springer-Verlag Berlin Heidelberg 2013

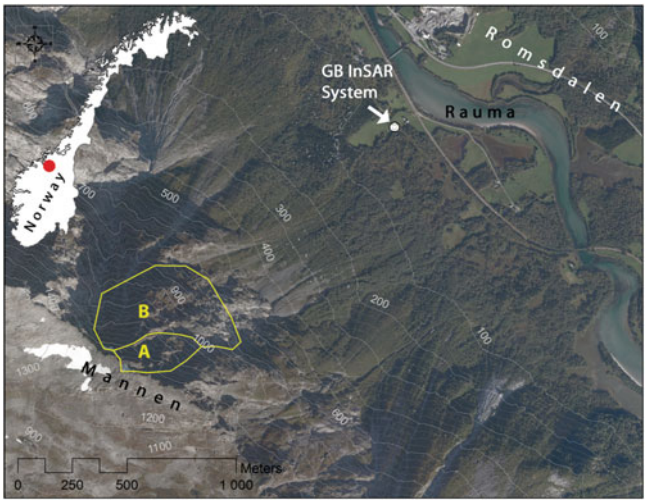


Fig. 1 The mountain of Mannen and the valley Romsdalen. The two scenarios, A and B are indicated in *yellow* as well as the position of the GB InSAR system in the valley

This paper presents the first results of the displacement measurements, which is the basis of the monitoring work at the Early Warning Centre. The displacement measurements are also important input to the understanding of the geological evolution of the rockslide.

Measurements of Displacement

The instrumentation and monitoring of Mannen is focused on identifying surface and subsurface deformation using state of the art technology. Several types of instruments are used, such as lasers, realtime DGPS, extensometers, a DMS borehole column that in real time measures detailed displacement for every meter between 0 and 120 m depth. At the valley bottom, a Ground Based Interferometric Radar system (GB INSar) measures spatially distributed displacement of the mountain side, and also ensure redundancy in case of loss of power or communication on the mountain. A meteorological station record controlling factors for the landslide such as heavy precipitation, snow melt etc.

The lasers have measured since October 2009, the GB InSAR system since February 2010, the climate station since June 2010, the extensometers since August 2010, the DMS column and the GPS's since November 2010. The different start time of the data series is evident in the plots.

The data is send to the Åknes Early Warning Centre using radiolink and stored. For the daily work we have web-based solutions for display of all data collected in the mountain, meaning that it is possible to access the data from everywhere. For selected sensors automatic alarms are sent, if the displacement is greater than pre-defined thresholds.

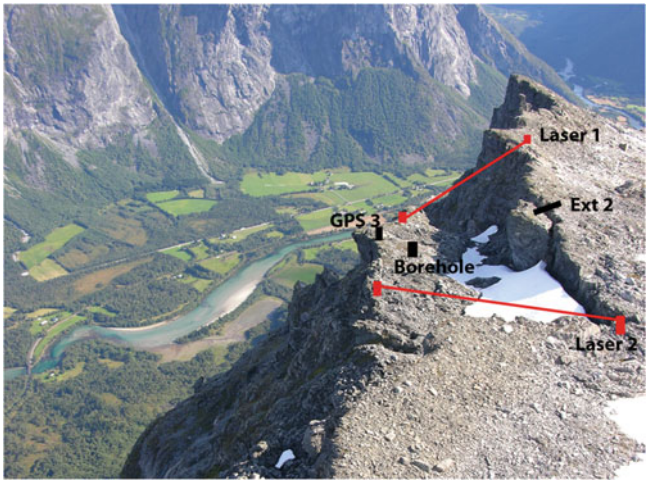


Fig. 2 Photo of the upper back-crack area and the plateau which has sunk 15–20 m. The position of some instruments is drawn

Extensometers and Lasers

Seven extensometers are located inside various cracks in the upper part of the landslide. They are steel rods fixed to the bedrock on either side of the cracks, and they measure extension as increased electric resistance. The extensometers are reliable instruments which provide data with little noise. A challenge at Mannen is to find unfractured bedrock to attach the instrument.

The largest movement of the extensometers is found in extensometer 2. It is located in a large crack behind a tilting block, as clearly seen in Fig. 2. Extensometer 2 has measured 25 mm of displacement in 10 months, corresponding to 30 mm/year (Fig. 3). The movement is clearly dependent on season, with a velocity of 6 mm/month in August and September 2010, a slowdown in mid October to about 0.5 mm/month in January to March 2011. As the snow started to melt again in spring 2011 the velocity increased again to 9 mm/month in May and June. Figure 3 shows the close coupling between the movement recorded by this extensometer and air temperature. The controlling factor of the variation of velocity is probably snow melt in the spring and wet conditions throughout the summer, rather than temperature itself.

Five other extensometers have recorded less than 2 mm total displacement.

Two lasers measure distance across the main back crack and down to the depressed plateau (Fig. 2). They send a laser beam to a passive reflector and record the two way travel time to measure the distance. In 19 months they have recorded a displacement of 30 and 36 mm for laser 1 and 2 respectively (Fig. 3) corresponding to 19 and 23 mm/year.

There seem to be periods of higher and lower velocity of both lasers, but they do not coincide. The measured displacement is smaller than previously seen by periodic GPS measurements. This may be explained by the fact that the

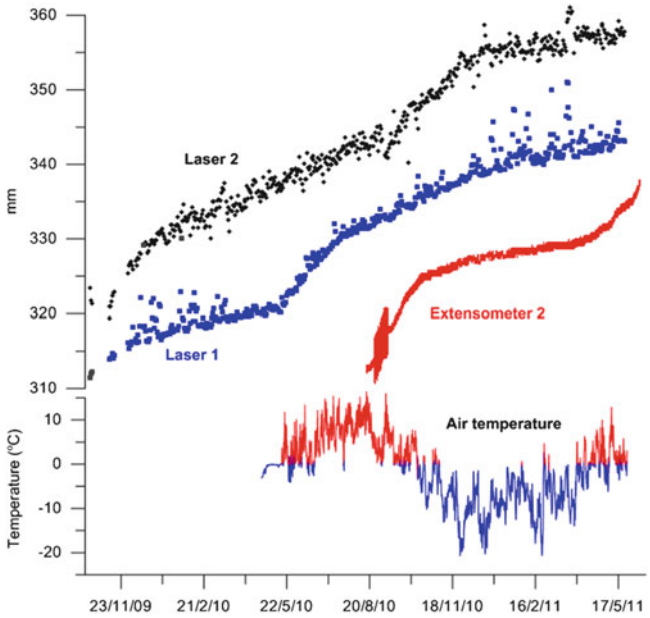


Fig. 3 Measurement of displacement of the two lasers and extensometer 2. Also shown is the air temperature, *red* are positive and *blue* are negative temperatures

direction of the laser beam is different than the direction of displacement. Their velocities are also smaller than that of extensometer 2, but this extensometer is placed at a block which was identified as the fastest in the rock slide (Fig. 2).

Differential GPS

Eight GPS antennas are placed at Mannen to record absolute displacement in 3D. Two of those are placed at assumed stable location and works as reference stations. The analyzed period covers the stable time from November 2010 to the end of May 2011, which judging from extensometer 2 is a quiet period. GPS 3 on the sunken plateau (position Figs. 2 and 5) is the fastest of the GPS antennas, with a movement of 9 mm down and 3 mm east, corresponding to a velocity of 17 mm/year. From November to January it appeared to move 4 mm north (as expected), but after that it moved somewhat towards south (Fig. 4).

GPS 4, 5, 6 and 7 moved north, with velocities between 3 and 8 mm/year. The movement is statistically significant, but quite small compared to the level of uncertainty of the method. GPS 8 was stable in the time interval. The locations, velocities and horizontal direction of the GPS antennas are summarized in Fig. 5.

Ground Based InSAR Measurements

A Ground Based Interferometric Synthetic Aperture Radar (GB InSAR) is located at the bottom of Romsdalen,

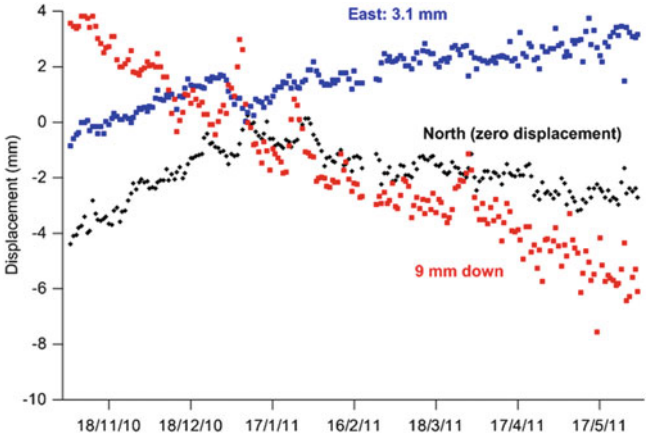


Fig. 4 The displacement of GPS 3 in three directions

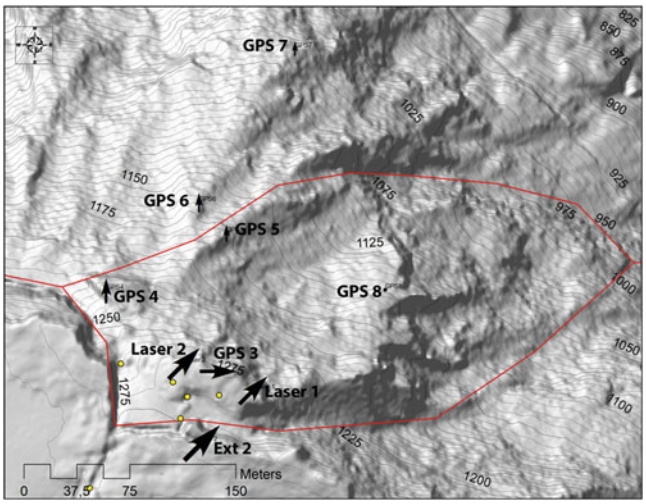


Fig. 5 The velocity measured by the GPS antennas, the lasers and extensometer 2. The direction of movement of the GPS antennas is reflected by the *arrows*, while the direction of the two lasers and extensometer 2 is set to NE, as this is expected

measuring displacement of the large parts of the mountain side (Fig. 6). For the principle of radar interferometry, see Ferretti et al. (2007). The system used is a LiSALab radar from Ellegi Srl.

Figures 6 and 7 show radar measurements of displacement from February to early November 2010 projected on a DEM. Positive numbers mean movement away from the system and negative numbers towards the system. This mean that red and orange is movement downhill and green/yellow are stable areas.

The areas without data-coverage are in topographic shade and not seen by the radar. The measured displacement is in the line of sight to the radar, which may be shorter than the real displacement.

Large parts of block A is seen to move about 20 mm towards the radar in 9 months, corresponding to 27 mm/year.

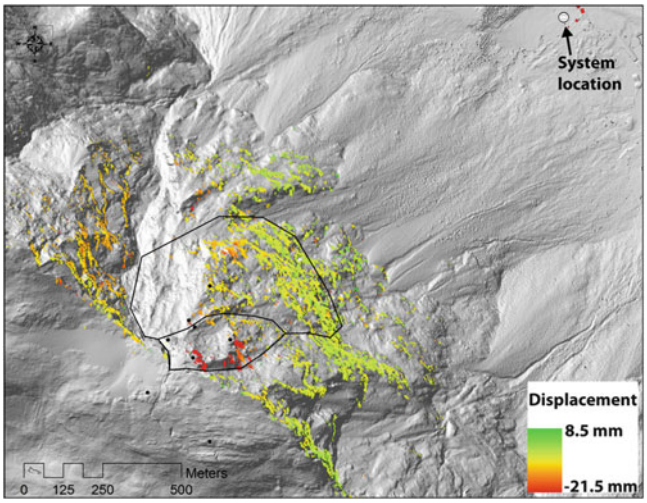


Fig. 6 The distribution of the GB InSAR measurements on Mannen. The system location and the scenations are drawn

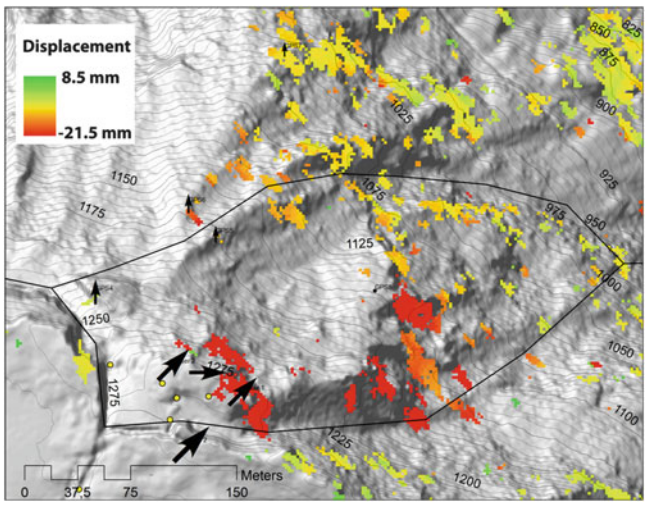


Fig. 7 Close up of the upper part of Mannen, with the radar measurements and the *velocity arrows* from Fig. 5

Measurements of Surface Displacement

With about a year of data from most sensors of surface displacement the data seem to correspond well with typical rates of displacement of 2–3 cm/year. This is a little less movement than previously found by periodic GPS measurements of about 5 cm/year. Some of this may be because the direction of measurement does not completely correspond to the direction of movement. Probably longer time series are important to evaluate the pattern of displacement as for instance the GPS's have only been working since November 2010.



Fig. 8 Crushed bedrock at 28 m depth

In general the GB InSAR measurements seem to fit well with the measurements. However, it measured quite high velocity last summer at the location of GPS 8, which in turn was stable this winter. We need coinciding time interval in order to evaluate such discrepancies better. The GB InSAR measurements also support the suggested scenarios with the highest rates of displacement within scenario A (2–3 mill. m^3). Some displacement is also seen further down the slope, in areas where it is very difficult to place other instruments.

Mechanisms of Displacement

Evidence from a Borehole

Measurements within the ground are necessary to understand the processes in a rockslide. A 137 m deep borehole was drilled at the sunken plateau in the Autumn 2011. Logging of the core proved that the bed-rock is highly fractured to a depth of 113 m, with several levels of breccia as well as bedrock crushed to silt fraction (Fig. 8).

A 120 m DMS column from C.S.G. S.r.l. was installed in the borehole. The column consists of 120 modules with flexible joints, and each module records displacement in two directions and temperature. A few modules record the water pressure.

In the borehole, no water was found. Two modules showed movement of more than 2 mm; they are in 24 and 28 m depth (Fig. 9). At these depths crushed bedrock were logged and they are important sliding zones. The cummulated northward displacement in the time interval is almost 50 mm. This is an order of magnitude more than recorded by the nearby GPS in the same time interval. A possible explanation for this is discussed at the end of the paper.

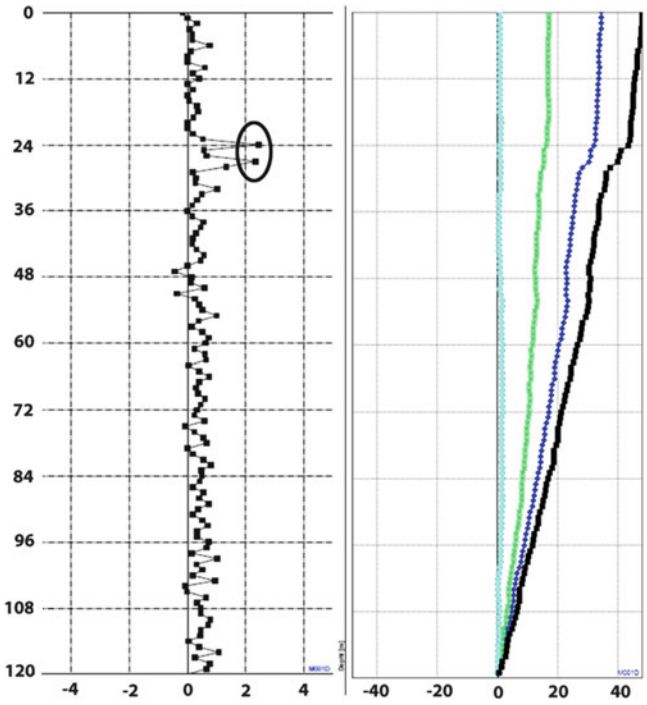


Fig. 9 Displacement of the DMS column in the period 24 February 2011 to 2 June 2011. The x-axis is in millimeters and positive is movement towards north. *Left*: Differential plot showing displacement in each module *Right*: Cumulative displacement at four time intervals

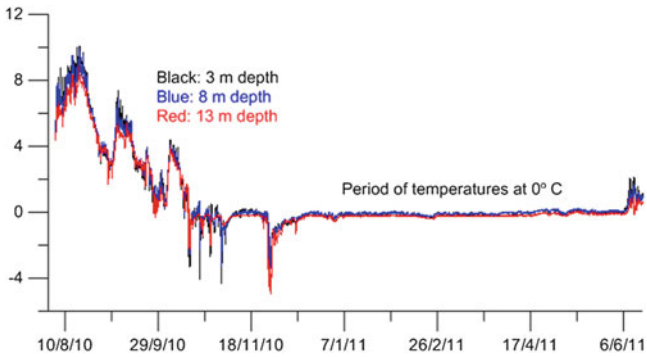


Fig. 10 Temperature in a deep open crack at the plateau at Mannen. Temperatures at three different depth intervals are shown

Possibility for Permafrost

It has been suggested that permafrost at the north facing 1,295 m high Mannen might be a factor to consider. Little is known of alpine permafrost in western Norway. Frost and ice segregation within bedrock can be a powerful mechanism for weathering rock (Murton et al. 2006) and perhaps for further crack opening.

The measurements collected so far, however, suggest that permafrost is not present at Mannen. In the borehole, temperatures down to 120 m are around +1 °C. Measurements from August 2010 to June 2011 in a deep open crack at the top of the plateau with sensors from 3 to 13 m below the surface, show that by early January the crack is isothermal at 0 °C (Fig. 10). If permafrost is present the temperature would be lower than 0 °C.

It is possible that isolated "cold pockets" of permafrost are found in the upper parts of the north facing Mannen. However, as seen in Fig. 3 most of the crack opening takes place in the snow melt season and summer. It is not likely that refreezing in the cracks is responsible for the crack development during this season, as the temperature is not cold enough to facilitate substantial refreezing.

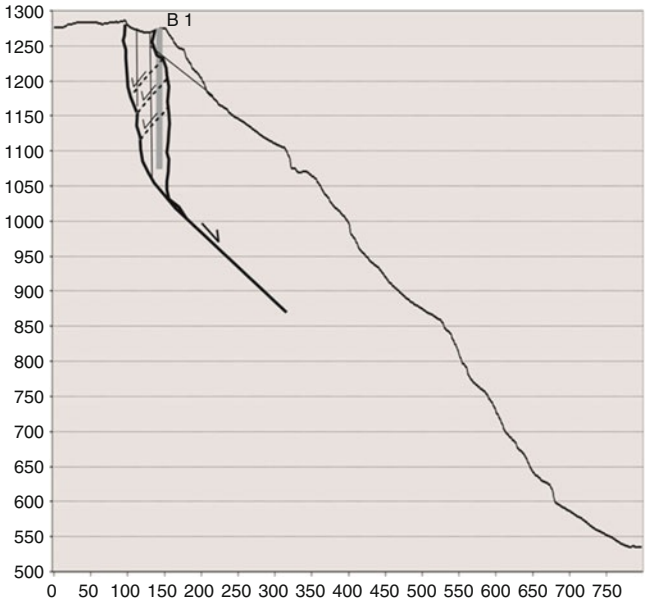


Fig. 11 The borehole at the sunken plateau. Some of the northward movement is suggested to take place as backward sliding into a graben structure at the back crack

Sliding Planes and Backward Tilt into a Graben Structure

The DMS measurements and the core logging show clearly active sliding zones in 24 and 28 m depth. However, a northward displacement is seen in most modules and cumulative the displacement is much larger than what is recorded by the surface instruments.

The mechanism we propose is responsible for the movement is a periodic backward sliding into open space in a graben structure in the back-crack area (Fig. 11).

It also fit well with the sudden "southward" shift in direction of GPS 3, seen in early January (Fig. 4). We need

to make more investigations to understand this hypothesised process better. First steps to be carried out in the summer 2011 are drilling of a second borehole further down the slope as well as geophysical investigations.

Conclusions

Displacement has been measured using various instruments at the active rock slide Mannen, western Norway for about a year. In general the surface displacement is in agreement with earlier periodic GPS measurements. Local measurements on the mountain fit well with GB InSAR measurements from the valley bottom, and also support the failure scenarios proposed before the detailed monitoring was initiated. Measurements in a 120 m borehole instrument show two clear sliding planes in 24 and 28 m depth. At both these depths, core logging show that bands of the bedrock was crushed to silt fraction. However, the entire core was highly fractured to 113 m depth, and the borehole instrument has measured a cumulated northward displacement 10 times higher than what was measured on the surface by a GPS antenna. We suggest that backward sliding into a graben structure at the back-crack may be responsible for this displacement. Another borehole and geophysical investigations are planned for this summer, to better understand the processes in the subsurface.

References

Blikra LH (2008) The Åknes rockslide; monitoring, threshold values and early-warning. In: Proceedings of the 10th international symposium on landslides and engineered slopes, 30 June–04 July 2008, Xi'an, China, Taylor & Francis

Crosta GC, Agliardi F (2003) Failure forecast for large rock slides by 306 surface displacement measurements. Can Goetech J 40: 176–191

Ferretti A, Monti-Guarnieri A, Prati C, Rocca F (2007) InSAR principles: guidelines for SAR interferometry processing and interpretation. ESA Publications, Noordwijk, The Netherlands. ISBN: 92-9092-233-8

Fylkesmannen I Møre og Romsdal, Møre og Romsdal fylkeskommune, NGU (2011) Risiko-og sårbarheitsanalyse for fjellskred i Møre og Romsdal. Molde, p 106

Murton JB, Peterson R, Ozout JC (2006) Bedrock fracture by ice segregation in cold regions. Science 314(5802):1127–1129



Multitemporal Study of the San Martino Sulla Marrucina Landslide (Central Italy)

Elisa Damiano, Daniele Giordan, Paolo Allasia, Marco Baldo, Nicola Sciarra, and Giorgio Lollino

Abstract

In this study, we aim at achieving details on the San Martino Sulla Marrucina (SM) landslide failure mechanisms. The SM landslide represents one of the most complex and large-scale mass movements recently occurred in the Chieti province (Central Italy). We present the preliminary results of an integrated study based on a multidisciplinary approach. The investigated phenomenon represents a local reactivation of a wider quiescent landslide and that its morphological evolution is doubtless characterized by a retrogressive trend. Furthermore, we propose a geodynamic model based on deep kinematic conditioning. The data collected, integrated with those already existent, will permit further investigations of the landslide susceptibility in the municipality territory and in the surrounding areas.

Keywords

Landslide • Multitemporal analysis • Geographic Information Systems

Introduction

During the spring 2001, a huge slope instability event occurred in San Martino Sulla Marrucina (SM), involving an area of about 2.5 km^2 and approximately 100 mm^3 of soil in the vicinity of to the town and its road network. SM landslide presented a paroxysm phase from 2001 to 2004, when scarps of over 20 m high were formed. Nowadays, the mass movement is almost quiescent and the displacements that have been measured since the peak of activity have been interpreted as the result of a residual activity.

Some peculiarities of the SM landslide, such as its past evolution, the amount of the soil involved and the characteristics of the movement, along with a high territorial vulnerability, make this phenomenon a particularly complex case of study.

This paper describes the main results of an integrated study of the SM landslide, aiming at indicating the mechanism of instability, a preliminary evolutionary model of the landslide and its implications for the risk assessment and mitigation. To better understand the kinematic factors that rule the current evolution of the phenomenon, we have focused on reconstructing the main geomorphologic and topographical changes that have occurred on the slope over the last 80 years.

E. Damiano (✉)
Dipartimento di Geotecnologie per l'Ambiente ed il Territorio, DiGAT, Università G. d'Annunzio di Chieti-Pescara, Via dei Vestini 31, Chieti Scalo 66013, Italy

Istituto di Ricerca per la Protezione Idrogeologica, CNR IRPI, Consiglio Nazionale delle Ricerche, Strada delle Cacce 73, Torino 10135, Italy
e-mail: elisa.damiano@irpi.cnr.it

D. Giordan • P. Allasia • M. Baldo • G. Lollino
Istituto di Ricerca per la Protezione Idrogeologica, CNR IRPI, Consiglio Nazionale delle Ricerche, Strada delle Cacce 73, Torino 10135, Italy

N. Sciarra
Dipartimento di Geotecnologie per l'Ambiente ed il Territorio, DiGAT, Università G. d'Annunzio di Chieti-Pescara, Via dei Vestini 31, Chieti Scalo 66013, Italy

C. Margottini et al. (eds.), *Landslide Science and Practice*, Vol. 2,
DOI 10.1007/978-3-642-31445-2_33, © Springer-Verlag Berlin Heidelberg 2013

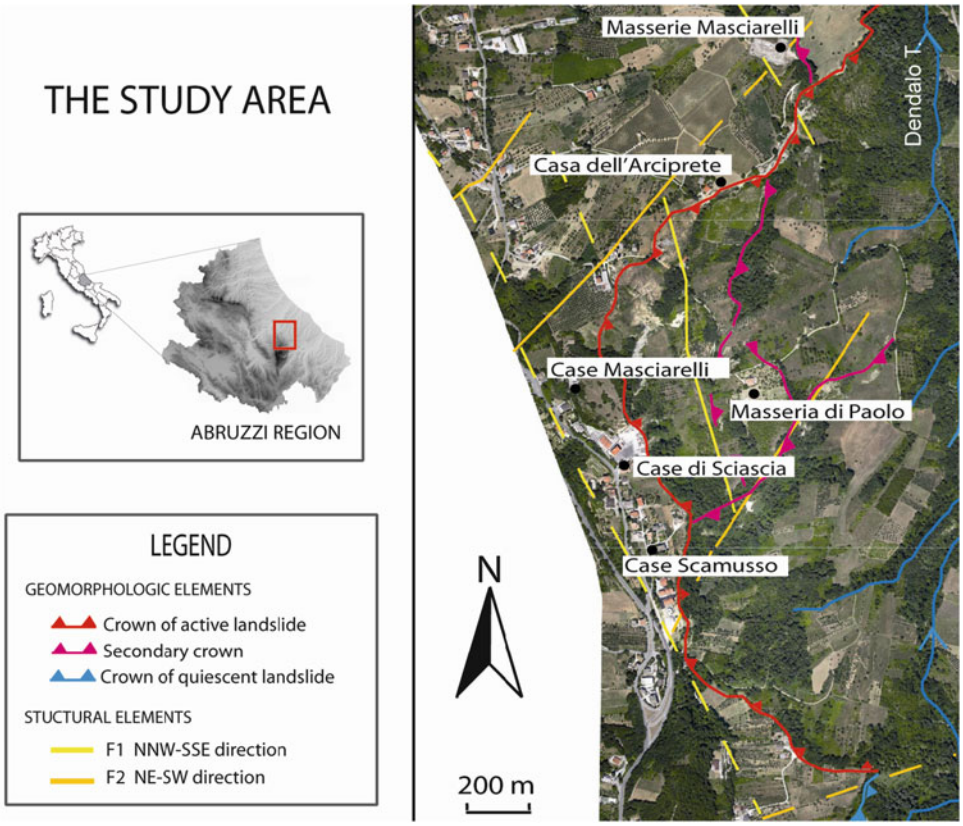


Fig. 1 Geographic localisation and main geomorphological traits of San Martino landslide. Cartographical base: orthophoto elaborated by LiDAR 2006

The Study Area

Geographical Localisation

The area of study (Fig. 1) is located in the central-eastern Abruzzi region and lies within the Periadriatic hill belt. It is situated between the Majella Massif of the Apennine chain towards the West, and the Adriatic coast towards the East.

The landslide affects the Eastern side of the slope of a small ridge NNW-SSE oriented, which hosts the San Martino Sulla Marrucina village in the Chieti Province. The latter ridge is bordered on the West by the Vasole Ditch and on the East by the Dendalo Torrent.

A geomorphologic detailed field study has been carried out focusing on an area of about 6 km^2 surrounding the landslide. Its Northern part belongs to the San Martino Sulla Marrucina and its Southern to the Guardiagrele municipality.

Geologic Setting

Stratigraphy

The studied area is located near the contact point between the Meso-Cenozoic carbonate lithotypes relating to the Majella massif and the Plio-Pleistocene terrigenous deposits relating to the Abruzzi Periadriatic Basin (Alberti et al. 1962; Catenacci 1974; Crescenti et al. 1980).

It is characterised by the presence of terrigenous elements of the Upper Pliocene and Lower Pleistocene. The outcropped Upper Pliocene terms are members of the Mutignano Formation, mainly constituted by clay, grey-azure marny-clay and, at the top, by levels of sands and conglomerates. This succession is partly masked by more recent continental formations.

The Quaternary continental deposits of Lower Pleistocene (made by alluvial deposits, terraced soils, grounds and cover detritus), lie in stratigraphic discordance over the Mutignano succession.

The Mutignano Formation lithotypes lies within a transgressive contact, over the chalky-sulphurous Cellino Formation of the Lower Pliocene.

Structural Aspects

The examined area has a complex structural history. Its tectonic evolution is a thrust belt built up during the Neogene period, related to the evolution of an orogenic system according to a chain – foredeep – foreland model (Patacca and Scandone 1989; Cipollari et al. 1997; Calamita et al. 1999).

The Periadriatic belt sequences are affected by overthrusts and faults linked to the Mio- Pliocene compression tectonic phases, and by mainly straight faults due to the distensive Quaternary phases (Alberti et al. 1962).

The temporal and spatial tectonic stress distribution has generally migrated from the more western towards the more eastern sector (Crescenti et al. 1980; Del Monte et al. 1996; Currado and Fredi 2000; Currado and D'Ambrogi 2002; D'Alessandro et al. 2003a, b).

As detailed field observations highlighted, a very complex tectonic system (Fig. 1) characterizes the SM territory. The existence in the area of two main systems of normal faults NNW-SSE and NE-SW oriented (Aucelli et al. 1996, Buccolini et al. 2004) is confirmed, at high scale, by an intense state of fracturing, mainly developed in the clayey lithotypes.

Geomorphologic Setting

The phenomenon occurs in an area of about 2.5 km^2 extending between 425 and 308 m, it presents a medium length of about 750 m and a width of the rupture surface of about 1,900 m. The landslide presents a main crown of about 2.5 km long, which is more than 20 m high in some traits.

A trait of a secondary crown has developed near its middle part close to Casa dell'Arciprete (Fig. 1).

The geometrical development of the main and the subordinate crowns are clearly influenced by the spatial disposition of the fault systems. The planimetric development of the scarps (Fig. 1), corresponding in part to the disposition of the families of faults, shows how the geomorphologic processes have been conditioned by the structural setting (Buccolini et al. 2004).

The area that surrounds the currently active landslide also presents an old and generalized familiarity with the slope instability processes. Relict shapes and quiescent minor instability phenomena have been observed thanks to detailed field surveys and stereoscopic observations.

Description of the Historical Background

In general, the characterization of the historical background for landslides represents a valid support for the identification of the main kinematic mechanisms that rule the current slope activity.

In the SM case, the oldest historical data collected for the multitemporal analysis are represented by the oral accounts. According to them, the upper part, close to Masserie Masciarelli, of SM landslide, began moving in 1930 (Fig. 2) and, during the following years, it affected different parts of the slope.

Only during the second part of the 60s, its activities caused the definition of scarps, causing damages to the cultivations and road network.

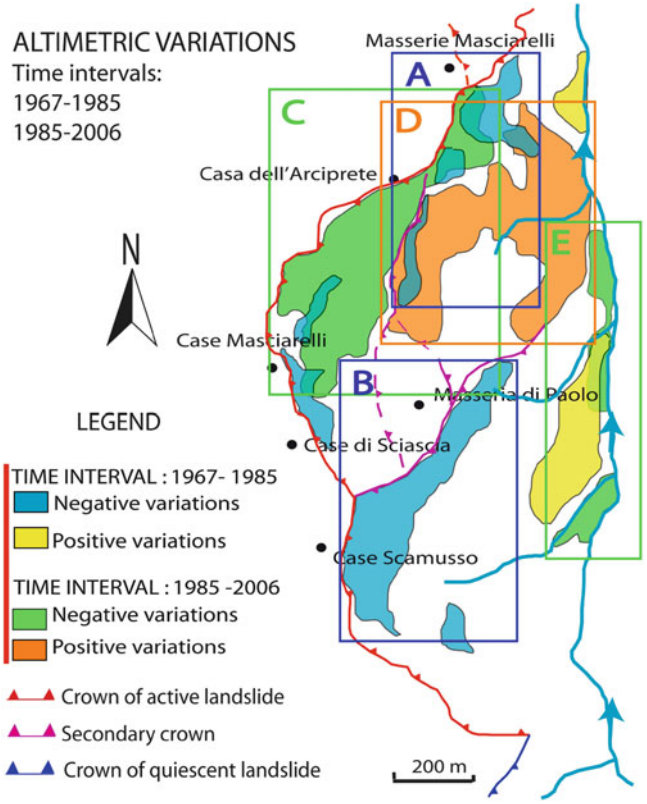


Fig. 2 Geographic distribution of the altimetric variations during the time intervals 1967–1985 and 1985–2006

The dataset used for the multitemporal analysis of SM landslide are constituted by maps (technical surveys of 1967 and technical cartography of 1985), aerial photos (1975 and 2002), DTM and an orthophoto derived from LiDAR – Light Detection and Ranging – survey (2006), detailed geomorphologic field surveys (2010) and instrumental measures and investigations (from 2006 to 2009).

Despite their different origin and the fact that they are not very continuous in time, these data offer the possibility of inferring some descriptive and quantitative remarks about the evolutive trend of the studied landslide. All the information derived from the dataset have been organized in a GIS – *Geographic Information System* – in order to describe the slope evolution from the geomorphological point of view analyzing in particular the periods before and after the main event of 2001.

Spatial Distribution of Main Vertical Variations

Three-dimensional ground surface reconstruction using Digital Terrain Model (DTM) constitutes a helpful support in performing morphological analyses of the earth's surface and afterwards its temporal changes (Dewitte et al. 2008).

A DTM subtraction yields a direct estimate of the vertical displacement of each landslide pixel during the considered time interval (Van Westen and Getahun 2003; Baldi et al. 2005; Casson et al. 2005; Hapke 2005; Brückl et al. 2006; Schiefer and Gilbert 2007). A direct comparison between 3D models becomes possible realising operation of subtraction. It is necessary choose the same cell size for both DTMs, this parameter depends from the accuracy of the cartographical original data.

To characterize the spatial distribution of the instability processes during the last 40 years, we considered the DTMs related to 1967, 1985 and 2006. The first two DTMs have been extracted from the related cartographical data and the third one is derived by the Lidar datum; the operations have been performed using the GIS facilities.

Their direct comparisons led to a description of the distribution of the areas that were subjected to the main altimetric variations during the two intervals of time 1967–1985 and 1985–2006.

In Fig. 2, different colours mark the zones affected by instability processes in the two considered intervals. For each interval of time, both the positive and negative vertical variations have been identified.

These distinctions allowed us individuating which sectors of the slope have been subjected to detachment or accumulation related to the landslide activity.

The sector D is characterized by a complex history because during the period 1967–1985 was subjected to a negative altimetric variation, and in the period 1985–2006 was subjected to a positive one.

In the early stages of study of SM landslide, the secondary crown was generally interpreted as a result of differential movements occurred into the displaced mass during the paroxysm phase (2001–2004).

Figure 2 offers some helpful remarks for the interpretation of this element's evolution suggesting that it could be a relict structure derived by previous activity.

After the activation in the 1967–1985 period, the crown answered passively and rigidly to the subsequent movement induced. The recent phase, started in 2001, involved in particular the sectors C and D, where the main landslide activity effects are recorded (Fig. 3).

The sector E is characterized by a vertical negative variation related to the Dendalo torrent erosion processes.

Evaluation of Volume Variation

We realised in GIS a direct measure of the volume variation in the area affected by the landslide for the period 1985–2006 (Fig. 3). It has been performed thanks to the procedure of subtraction between the DTM (Lollino et al. 2007; Baldo et al. 2009) of the respective years.

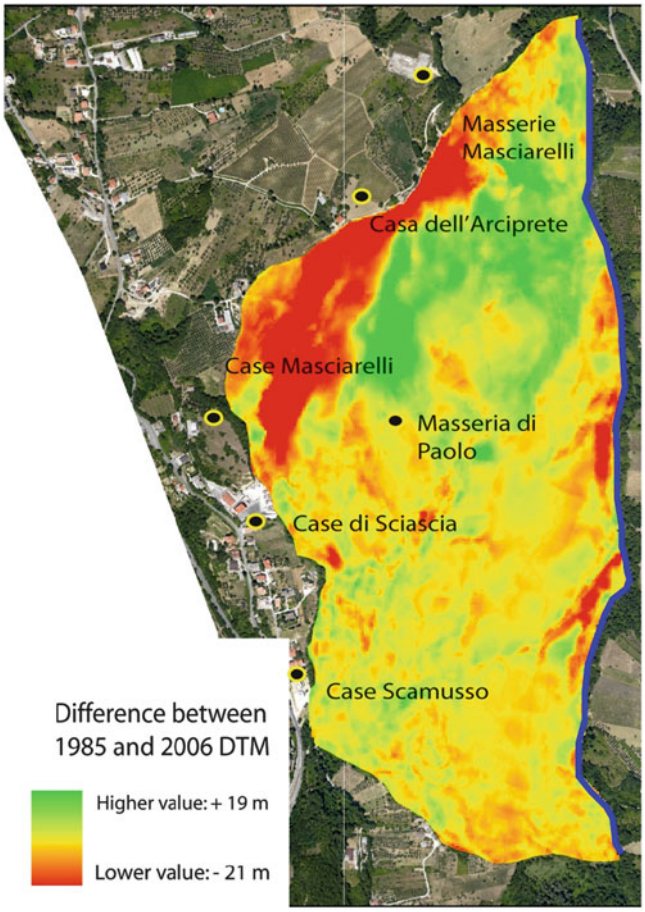


Fig. 3 Difference between 1987 and 2006 DTM

The mass balance gives a negative value of about –83,000 m^3 ±5,000 m^3.

This is a very unusual result for a case of landslide and represented for us, the preliminary remarks for considering the studied phenomenon as characterised by a mass reduction.

Spatial Description of Recent Movement Vectors

For the analysis of SM landslide recent evolution it has been realized a monitoring network controlling both the superficial and the deep movement of the slope and of the water table (Lollino et al. 2003).

The network interests the area where the main activation of 2001 caused the major damage to the buildings and the cultivations and the one where the future evolution could cause further damage.

The latter consists of a system for inclinometric, piezometric and GPS RTK – *real time kinematic* – measurements (Fig. 4).

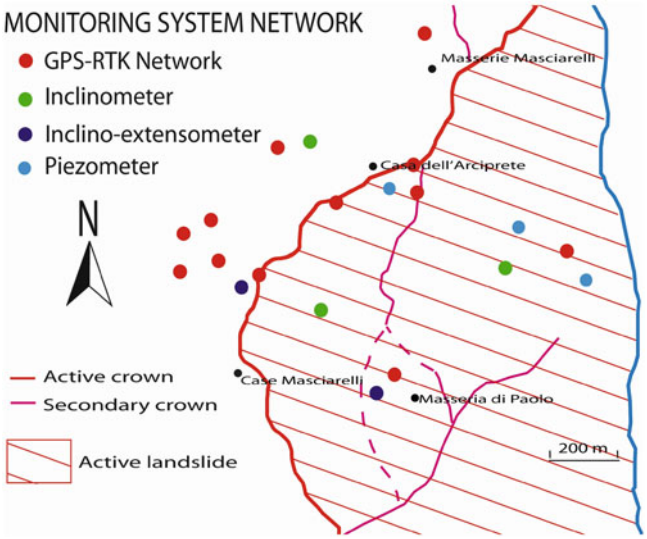


Fig. 4 Location of the monitoring networks

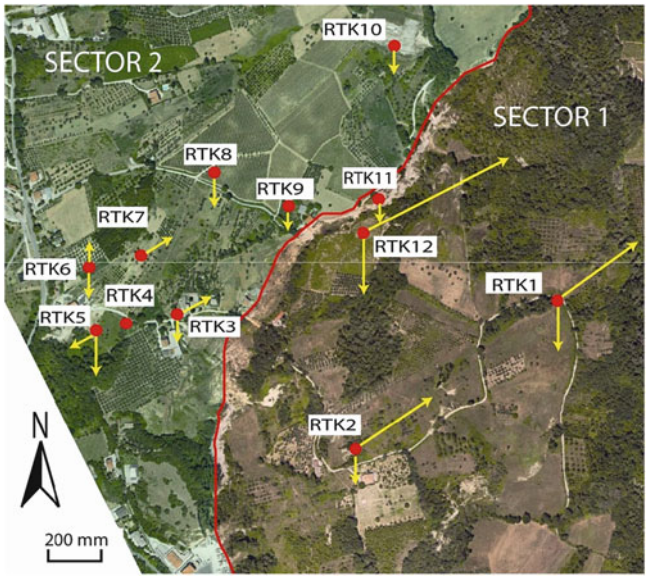


Fig. 5 GPS monitoring network: cumulative values for the period 2006–2009

The GPS monitoring network (Gili et al. 2000) is made up of 12 points of measure, and its dataset consists of 4 measures carried out during the period 2006–2009.

The inclinometric monitoring system is composed by eight inclinometers and two of these are equipped for extensometric measurements.

The inclinometric measurements have been lead during the period 2006–2007 and demonstrated the existence, in the middle part of the landslide, of several movement surfaces located between few meters and over 40 m of depth and entirely developed in the clayey formation.

The vertical component of the displacements has been mainly evaluated via GPS data, and with the analysis of few extensometric measures. The cumulative values of superficial displacement relative to GPS network is summarized in Fig. 5.

The higher values of negative vertical variation (about 30 cm in the period 2006–2009) have been recorded close to the Casa dell'Arciprete (point RTK12) and confirm the negative trend of this area recorded by the DTM comparison.

Kinematic heterogeneities in the landslide body are recognised by the GPS data analysis, identifying zones affected by different superficial activity. The main planimetric displacements are localized in the sector 1, (Fig. 5) and they are directly connected to the displacement of the mass involved in the landslide. The distribution of the vertical negative values is more generalised and also regards the sector 2 where cumulative values between few mm and 20 cm have been recorded by the instrumental network.

In the sector 2, the geomorphologic field surveys point to the existence of a system of aligned trenches of recent formation. These trenches are connected to an extensive trend and are related to lowering movements of the slope. We suppose that these structures represent the answer of the slope to the presence of a scarp more than 20 m high that create a local instability. Therefore, we can affirm that the evolution of the sector 2 is the result of an underway retrogressive process.

Finally, relatively to the GPS and inclinometrical measures, the data analysis shows that superficial and deep displacements follow the same preferential direction of movement SW-NE.

Discussion

The analysis of the data collected led us to define a preliminary kinematic model of the SM landslide.

The proposed model has been based on the characterisation of the movement vectors (both the recent and the previous), on the evaluation of the volume variation and on the detailed description of the current geomorphologic setting.

As mentioned before, the studied area has been subjected to the most important geomorphologic transformation after the landslide activation of the spring 2001.

During this paroxysmal phase, which continued until 2004, the sector between Casa dell'Arciprete and Case Masciarelli (sector I, Fig. 6) underwent important vertical movements. They led to the development of a the main scarp between the sector I and the sector II, and to the formation of a well defined landslide terrace in the head zone of the landslide between the main and the secondary crowns.

As confirmed by instrumental data, the presence of the high main crown in this area triggers the current retrogressive trend of the sector II. The comparison between DTM led

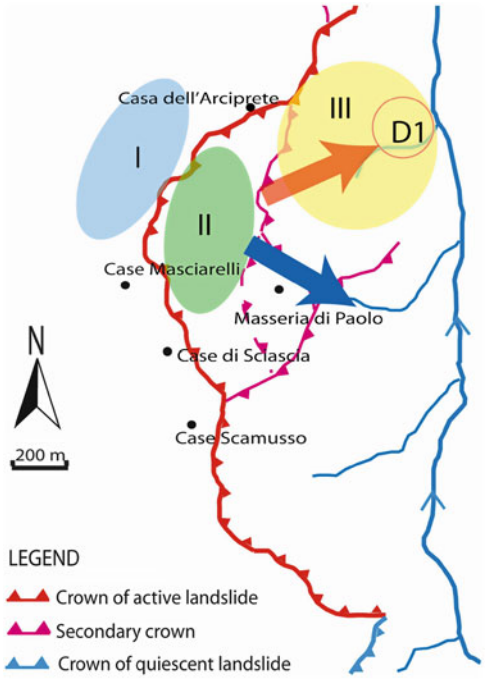


Fig. 6 Preliminary kinematic model suggested for the San Martino Sulla Marrucina landslide

to recognize an important negative volume variation in the sector I that is due to the morphological evolution of the landslide.

By the comparison between the pre-event topography and the current slope geometry, it is possible to underline some important elements. First, the recorded landslide movement direction is SW-NE (red arrow, Fig. 6) and not the NNW-SSE, that is the main slope dip related to the pre-event scenario (blue arrow in Fig. 6).

Then, the paroxysm event started in 2001 generating the main accumulation element in the sector III (Fig. 6); the displaced mass affected a portion of the slope that extends as far as the Dendalo Torrent. Nevertheless, it has been possible to demonstrate that does not exist any interaction between the slope and fluvial dynamic. The field data underlined that the accumulation sector does not reach the torrent and the area of the landslide toe is not affected by erosion by the Dendalo torrent. The DTM comparison confirms filed data as does not recognize important variation in this sector.

In addition, the multitemporal analysis of cartographic data reveals that this torrent has not been affected by planimetric variation during the last 50 years.

Moreover, the negative balance registered by the DTM comparison need an explanation; as is excluded an interaction between landslide and torrent, the only possibility is related to the presence of a depocentral zone that triggered the landslide and allow the mass reduction.

If this hypothesis will be confirmed the SM landslide could be considered as the superficial evidence of a deep seated activity. Considering the distribution of the movement vector and the aspect regarding the evolution of the sector III, the position of this depocentral zone (D1) could be located under the landslide toe.

In this kinematic setting the current slope morphology is the result of the interaction of deep activity, structural conditioning and gravitational evolution.

The presence in this area of the Cellino formation (chalky-sulphurous formation of the Lower Pliocene) led us to suppose that the morphological evolution of the SM slope could be conditioned by the deep lithological setting.

Conclusion

The municipality territory of San Martino Sulla Marrucina is characterized by natural instability processes. In the past, many buildings and cultivations, and a large portion of its the road network have been subjected to damage caused by the paroxysmal event of 2001. Nowadays, the movements recorded by the monitoring network are due to a residual activity, but the areas surrounding the central portion of the main scarp are currently affected by a significant local instability due to the retrogressive evolution of the phenomenon.

According to these remarks, we recognised that the susceptibility of the SM territory depends, above all, on the future evolution of the retrogressive trend.

Further studies are necessary, and they should be focused even on the definition of the deep trigger factor than on a better definition of the risk assessment of this area. Nevertheless, the risk evaluation could be difficult because of the complexity of the kinematic conditions.

Up to now, the studies of the SM landslide have only covered a limited area, and they have only focused on the zone directly influenced by the complex movement. Nowadays, we do not get enough elements to define the geologic cause of the depocentral area and its future evolution. Only locating the phenomenon in a more complex geological system, involving deeper slope instability will be probably possible to identify its triggering cause and to understand the future evolution of the slope.

Acknowledgements This work is carried out during a PhD work of DiGAT Department of Chieti University in collaboration with CNR IRPI Institute of Turin.

References

Alberti A, Lipparini T, Stamponi G (1962) Note illustrative della carta geologica d'Italia alla scala 1:100000, foglio 141 Pescara. Servizio Geolologico d'Italia, Roma

Aucelli PPC, Cavinato GP, Cinque A (1996) Indizi geomorfologici di tettonica plio-quaternaria sul piedimonte adriatico dell'Appennino abruzzese. Il Quater 9(1):299–302, Verona

Baldi P, Fabris M, Marsella M, Monticelli R (2005) Monitoring the morphological evolution of the Sciara del Fuoco during the

2002–2003 Stromboli eruption using multi-temporal photogrammetry. ISPRS J Photogramm Remote Sens 59(4):199–211

Baldo M, Bicocchi C, Chiocchini U, Giordan D, Lollino G (2009) LIDAR monitoring of mass wasting processes: the Radicofani landslide, province of Siena, Central Italy. Gemorphology 105(3–4):193–201

Brückl E, Brunner FK, Krausì K (2006) Kinematics of a deep-seated landslide derived from photogrammetric, GPS and geophysical data. Eng Geol 88(3–4):149–159

Buccolini M, D'Alessandro L, Miccadei E, Sciarra N (2004) Susceptibility assessment of an area subject to a large landslide: the case of San Martino Sulla Marrucina (Chieti province – central Italy). In: Proceedings of IV international conference on computer simulation in risk analysis and hazard mitigation. WIT Press, Rodhes (ISBN 1-85312-736-1), pp 245–255

Calamita F, Coltorti M, Pierantoni PP, Pizzi A, Turco E, Scisciani V (1999) Relazioni tra le faglie quaternarie e la sismicità nella Dorsale appenninica umbromarchigiana: l'area di Colfiorito. Studi Geol Camerti XIV(1996/7):177–191

Casson B, Delacourt C, Allemand P (2005) Contribution of multitemporal remote sensing images to characterize landslide slip surface – application to the La Clapiere landslide France. Nat Hazards Earth Syst Sci 5(3):425–437

Catenacci V (1974) Foglio 147 Lanciano. Note ill. Carta Geol. d'Italia, Scala 1:100.000, p 87

Cipollari P, Cosentino P, Parotto M (1997) Modello kinematico-strutturale dell'Italia centrale. Studi Geol Camerti Spec 1995 (2):135–143

Crescenti U, D'Amato C, Balduzzi A, Tonna M (1980) Il Plio-Pleistocene del sottosuolo abruzzese-marchigiano tra Ascoli Piceno e Pescara. Geol Romana 19:63–84, Roma

Currado C, D'Ambrogi C (2002) Plio-Pleistocene morphostructural evolution of Chieti sector in the Periadriatic Basin: an example of integrated analysis. Mem Soc Geol It 57:501–508

Currado C, Fredi P (2000) Morphometric parameters of drainage basin and morphotectonic setting of eastern Abruzzo. Mem Soc Geol It 55:411–419, Roma

D'Alessandro L, Berti D, Buccolini M, Miccadei E, Piacentini T, Urbani A (2003a) Relationships between the geological-structural framework and landslide types in Abruzzi (Central Apennine). In: Atti 1° Congresso Nazionale AIGA, Chieti, 19–20 Febbraio 2003, Rendina Editori, Roma, pp 255–275

D'Alessandro L, Miccadei E, Piacentini T (2003b) Morphostructural elements of central eastern Abruzzi: contributions to the study of the role of tectonics on the morphogenesis of the Apennine chain. In: Uplift and erosion: driving processes and resulting landforms, Quaternary International, 101-102C. Elsevier Science Ltd and INQUA, Oxford, UK, pp 115–124

Del Monte M, Di Bucci D, Trigari A (1996) Assetto morfotettonico della regione compresa tra la Maiella e il mare Adriatico (Appennino Abruzzese). Mem Soc Geol It, 51, Roma, pp 419–430

Dewitte O, Jasselette JC, Cornet Y, Van Den Eeckhaut M, Collignon A, Poesen J, Demoulin A (2008) Tracking landslide displacements by multi-temporal DTMs: a combined aerial stereophotogrammetric and LIDAR approach in western Belgium. Eng Geol 99:11–22

Gili J, Corominas J, Rius J (2000) Using global position system techniques in landslide monitoring. Eng Geol 55:167–192

Hapke CJ (2005) Estimation of regional material yield from coastal landslides based on historical digital terrain modelling. Earth Surf Proc Land 30(6):679–697

Lollino G, Lollino P, Bertolini G (2003) Analysis of the behaviour of a landslide in structurally complex soils by means of monitoring field data. In: International conference on fast slope movements – FSM2003, Napoli, vol 1, Patron Editore (Bologna), pp 317–324

Lollino G, Pasculli A, Sciarra N, Baldo M, Giordan D (2007) An integrated methodology based on LIDAR, GPS and photogrammetric surveys applied to a large landslide in San Martino Sulla Marruccina (Central Italy). In: Proceedings of the 1st North American Landslide conference, Vail, Colorado

Patacca E, Scandone P (1989) Post-Tortonian mountain building in the Apennines. The role of the passive sinking of a relic lithospheric slab. In: The lithosphere in Italy. Accademia Nazionale dei Lincei 80, Accademia Nazionale dei Lincei, Roma, pp 157–176

Schiefer E, Gilbert R (2007) Reconstructing morphometric change in a proglacial landscape using historical aerial photography and automated DEM generation. Geomorphology 88:167–178

Servizio Geologico Nazionale: Carta Geologica d'Italia a scala 1:100.000, Fogli 147 Lanciano

Van Westen CJ, Getahun FL (2003) Analyzing the evolution of the Tessina landslide using aerial photographs and digital elevation models. Geomorphology 54(1–2):77–89



Surface and Deep Displacements Evaluated by GPS and Inclinometers in a Clayey Slope

Caterina Di Maio, Roberto Vassallo, Margherita Vallario, Stefano Calcaterra, and Piera Gambino

Abstract

The continuous deformations of two landslides of a clayey slope of the Italian Southern Apennines cause damage to buildings and infrastructures. In 2004, 11 inclinometer casings were installed to monitor them. In 2006, fixed-in-place probes with continuous data acquisition were installed in two of those casings, in correspondence to the detected slip surfaces. In 2010, such probes went out of use, thus were removed and periodical measurements restarted. The validity of the interpretation of previous localized measurements could thus be ascertained.

In 2006, GPS permanent and non-permanent stations had also been installed. By taking into account a possible mechanism of interaction soil-GPS station, displacements very close to those obtained by nearby inclinometers with fixed casing tip are obtained.

Depending on its particular properties, one of the landslides undergoes uniform displacements in each transversal section of the channel. So, GPS data can also give useful information on the movement of the whole section.

Keywords

Landslide • Clay • Displacements • GPS • Inclinometer

Introduction

The landslides under examination develop in a slope facing the valley of the Basento river, in a site called Costa della Gaveta, east of Potenza, Southern Italy (Fig. 1). They are ancient and complex landslides and develop in the geological formation of the Varicoloured Clays (extensively described by Pescatore et al. 1999), constituted by tectonized, fissured and heterogeneous clay shales. The main characteristics of landslide B are described by Di Maio et al. (2010) who show that displacements can be considered uniform in each transversal section of the earth slide channel. The displacement rate decreases from upslope to downslope because of the increase in the areas of transversal sections, the "soil discharge" being practically constant. Landslide A (Fig. 1) is much more complex. It has been analyzed by various research groups who traced different boundaries. Our current studies seem to show that the zone delimited in Fig. 1 is only a small portion of a large and complex landslide system much more extended towards the eastern side (boundary close to the line with question marks in Fig. 1) than previously evaluated.

For both landslides, the average rate of displacement is in the order of about 1 cm/year, however, some sites are characterized by much higher rates, about 10 cm/year. In these sites, the highway and the railway, whose tunnel crosses one of the accumulation zones, need frequent maintenance and strengthening, besides continuous monitoring by extensometers, inclinometers and topographic measurements. Actually,

C. Di Maio (✉) • R. Vassallo • M. Vallario
School of Engineering, University of Basilicata, v. dell'Ateneo Lucano 10, Potenza, Italy
e-mail: caterina.dimaio@unibas.it

S. Calcaterra • P. Gambino
Geological Survey of Italy, Land Protection and Georesources Department, Institute for Environmental Protection and Research – ISPRA, v. Brancati 48, Rome, Italy

C. Margottini et al. (eds.), *Landslide Science and Practice*, Vol. 2,
DOI 10.1007/978-3-642-31445-2_34, © Springer-Verlag Berlin Heidelberg 2013

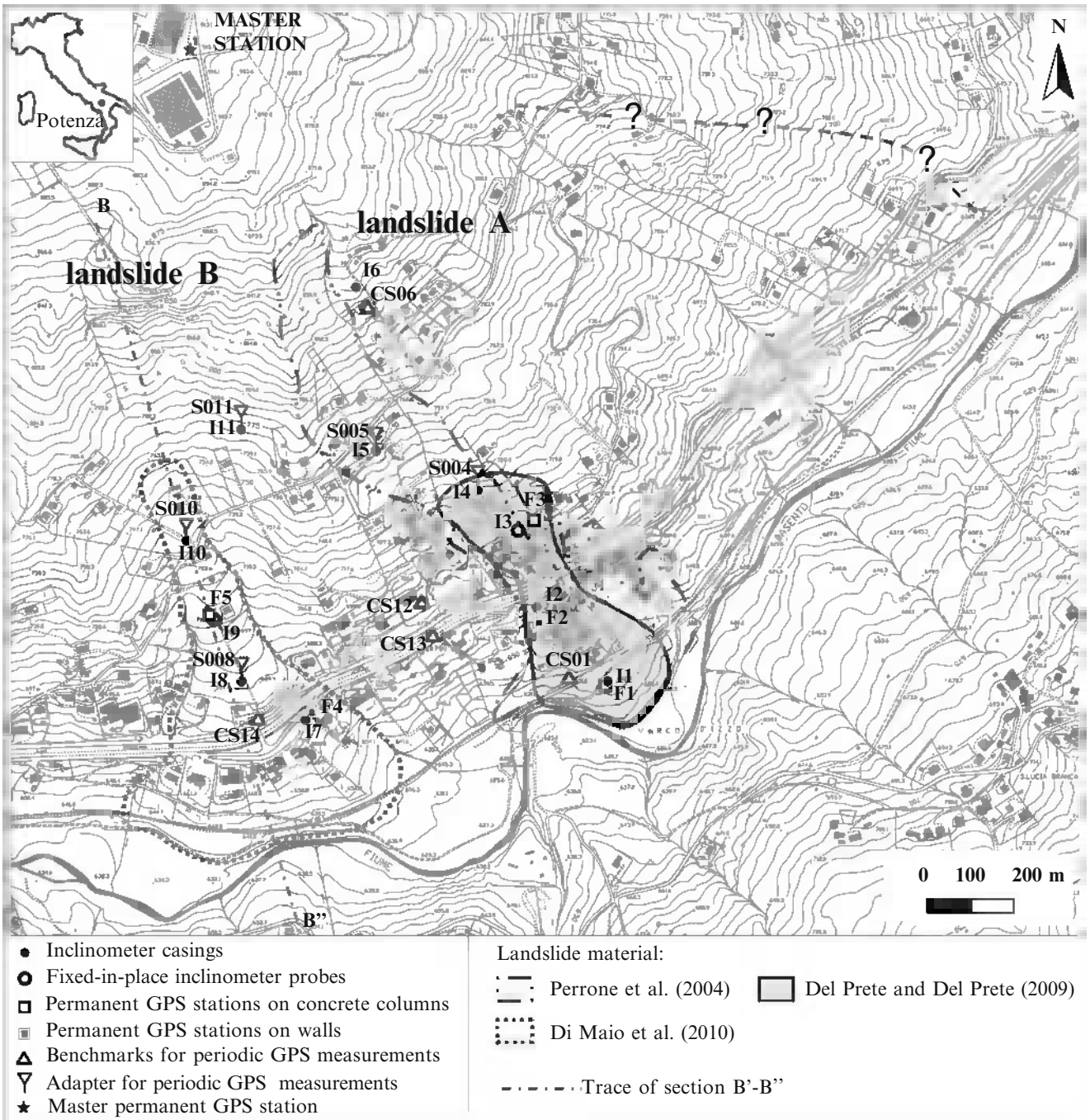


Fig. 1 Boundaries of the landslides and location of inclinometer boreholes and GPS stations

the displacements have caused some buildings evacuation and the removal of an overpass at risk of collapse (Fig. 2).

In 2004, the local public administration (Basilicata Region) provided funds for a geotechnical investigation. Eleven continuous coring boreholes were equipped with piezometers, and eleven core-destruction boreholes were equipped with inclinometer casings (Fig. 1). Standard inclinometer measurements started at the beginning of 2005. In 2006, fixed-in-place inclinometer probes, with continuous data acquisition, were installed in two of those casings (in one of which they went soon out of use), in correspondence to the slip surfaces detected by previous periodical inclinometer measurements. In the same period, six GPS permanent stations and ten non-permanent ones were installed, in collaboration with the Geological Survey of Italy – Geophysical Service (Calcaterra et al. 2008).

Calcaterra et al. (2012) compared the displacements obtained by using different instruments. Firstly, they showed



Fig. 2 Building severely damaged (**a**); removal of a pedestrian overpass of the highway (**b**)

the advantage of the integrated system constituted by mobile and fixed-in-place inclinometer probes. In the case under examination, the first periodical measurements showed that most deformations were concentrated in a thin zone around the slip surface. So, a few fixed-in-place probes installed around it were considered sufficient for a satisfactory monitoring of the landslide. Experimental data collected in the meanwhile confirm the validity of the hypothesis. In fact, in July 2010, the fixed-in place-probes were removed from I9 and standard inclinometer measurements by mobile probe along the whole casing height were carried out again. This paper shows that the results are consistent with previous predictions based on the few fixed probes, and allows to ascertain the strong correlation, hypothesized by Di Maio et al. (2010), with the displacements of the other sections of the landslide channel.

Calcaterra et al. (2012) also showed that the surface displacements evaluated by the GPS stations are consistent with the surface displacements evaluated by the inclinometer profiles. This paper reports further data and shows that by taking into account the mechanical interaction soil-GPS station, GPS displacements are very close to those obtained by nearby inclinometers with fixed casing tip.

The paper reports some evidence of the usefulness of the integrated instrument system and of its limits. In the case of landslide A, GPS data give a warning on the possibility of a deeper slip surface not clearly detected by inclinometer measurements. In the case of landslide B, because of the displacement uniformity in each transversal section, GPS data can also give qualitative information on deep displacements in the time period between two consecutive periodical inclinometer measurements. However, acceleration or deceleration registered by GPS was found to be due to the superficial soil layer and not relevant for civil protection purposes.

Inclinometer Measurements

Eleven core-destruction boreholes, up to 50 m deep, were equipped with inclinometer casings in the two landslides under examination (Fig. 1). First profiles, as in the case of I9 in the landslide B (Fig. 3c), were almost uniform from the ground to the slip surface, with the localization of shear displacements in a thin zone around the slip surface. So, to carry out a continuous and not expensive monitoring, in July 2006, only three fixed-in-place probes (85 cm long) were installed in the casing I9, one across the slip surface and the other two above and below it, in the landslide body and in the stable soil respectively. In particular, the central probe was installed with its barycentre at a depth of 25 m from the ground level and the other two probes at 20 and 30 m respectively (Fig. 3a). As expected, the upper and lower probes did not register any inclination increment in about 3 years, whereas the central probe registered increasing inclination (Fig. 3b). The shear displacement on the slip surface was obtained by attributing such inclination to a 1 m thick soil layer. This interpretation made the results of the continuous measurements consistent with those of periodic ones. Under the hypothesis that above and below the slip surface no deformations have occurred, similarly to the zones around the upper and lower probes, displacement profiles were obtained like that reported in Fig. 3c by a dotted line. It is worth noting that the corresponding azimuth profile (Fig. 3d) is consistent with those obtained by standard periodical measurements and constant with time.

In January 2009, the fixed-in-place probes went out of use. Di Maio et al. (2010) observed that, in the contemporaneous period of monitoring, the displacements of I9 at 25 m depth were about twofold those evaluated in I8 at about 37 m depth (Fig. 4) even during displacement accelerations. On the basis of the evaluation of the areas of transversal sections, they hypothesized that one of the possible causes of this strong correlation is the constancy of soil discharge in the landslide channel. So, after January 2009, in the lack of other data, the Authors extrapolated the displacements in I9 from those in I8. In July 2010, the fixed-in-place probes were removed and inclinometer measurements were carried out by mobile probe again. Figure 4 shows that the displacements in I9 at 25 m depth thus evaluated on the slip surface are equal to those inferred from I8 and consistent

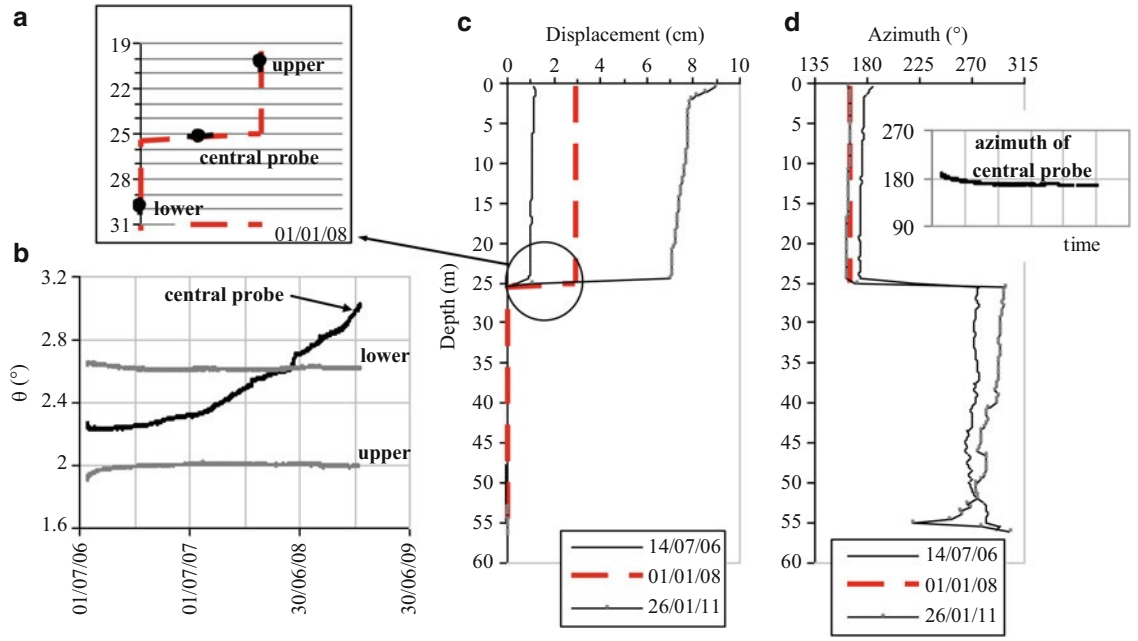


Fig. 3 Installation scheme of the fixed-in-place probes in I9 (**a**); angle increment with respect to the vertical for the three fixed-in-place probes (**b**); displacement profiles obtained by standard mobile probe, and by the three fixed-in-place probes (**c**); azimuth profiles and azimuth against time of the central probe (**d**)

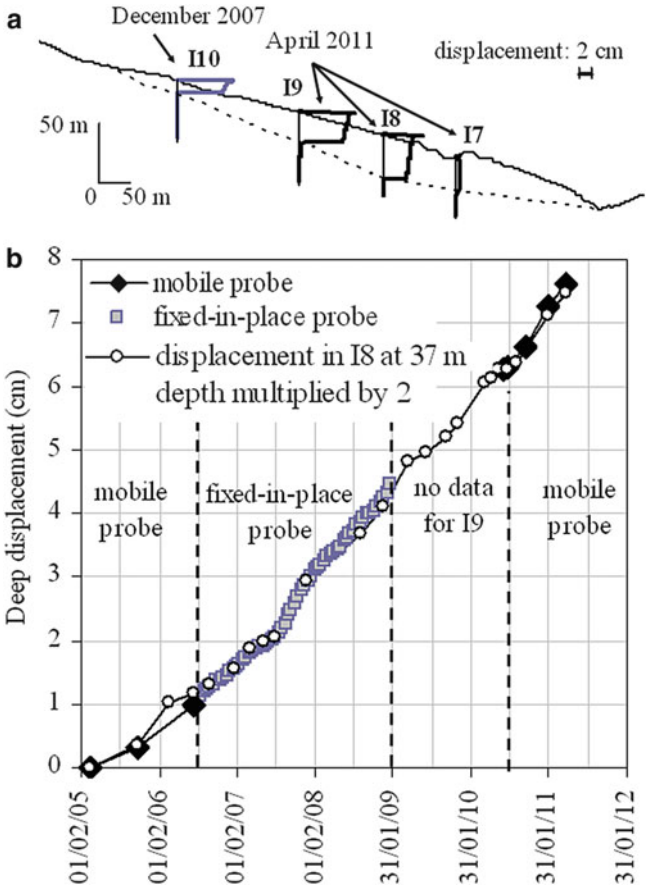


Fig. 4 Longitudinal section B′B″ of landslide B with inclinometer profiles (**a**); displacements in I9 at 25 m depth obtained by different instruments and displacements in I8 at 37 m depth multiplied by 2 (**b**)

with the displacements previously determined by the fixed-in-place probes. A strong correlation has been found also with the displacement in I10. In the case of the channel of landslide B, a little information on a part can thus give information on the other parts.

GPS Measurements

The GPS network consists of six permanent stations and ten non-permanent ones (Fig. 1). Measurements started in July 2007 for the former and in July 2006 for the latter. The master permanent station was installed in a stable area, upslope from the landslides. The other five permanent stations (F1–F5), all located in the two landslides, were equipped with a dual frequency geodetic antenna (Calcaterra et al. 2012). Three permanent stations (F1, F3 and F5) were installed on concrete columns, with a foundation 1.5 m deep (Fig. 7b). The other two were placed on a low concrete wall (F2) and on a building (F4) with shallow foundations (about 1.5 m depth). The results are reported in Figs. 5 and 6. The permanent station F3 registered the highest horizontal displacement and a noticeable vertical one. The other stations underwent lower horizontal displacements and consequently their vertical displacements are very low or still in the error order of magnitude.

Five GPS non-permanent stations are situated on the top of inclinometer casings by means of apposite mobile adapters. The other five are positioned mainly on walls of

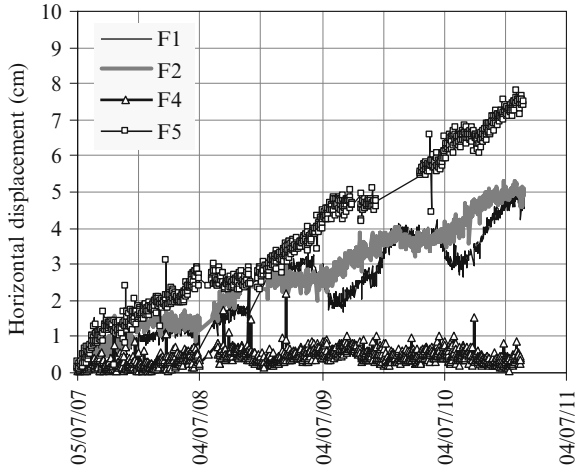


Fig. 5 Horizontal displacements of permanent GPS stations

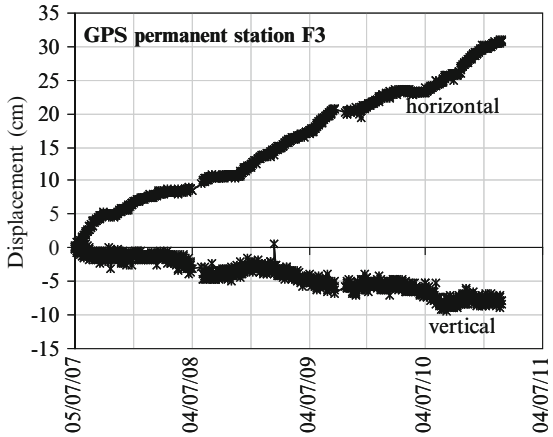


Fig. 6 Horizontal and vertical displacements of permanent F3 station

various types. The few available results (Figs. 8, 9, and 10) are significant if compared to those of the other instruments.

Comparison Between Different Measurements

It is possible to compare the displacements of the GPS antennas to the cumulative displacement obtained by inclinometers at 0.25 m depth from the ground surface. Figure 7 schematizes the cases of non-permanent station on the top of the inclinometer casing (Fig. 7a) and that of permanent antenna on the top of concrete column (Fig. 7b). Most of inclinometer casings underwent increasing inclination with time. So, the displacement of point P in Fig. 7a can be obtained from that of P′ by subtracting the component Δs. The same procedure was used in the case of Fig. 7b under the hypothesis that the column with its foundation tilted rigidly with an inclination equal to the average inclination of the upper 1.5 m of the nearby casing. Figure 8 shows that the

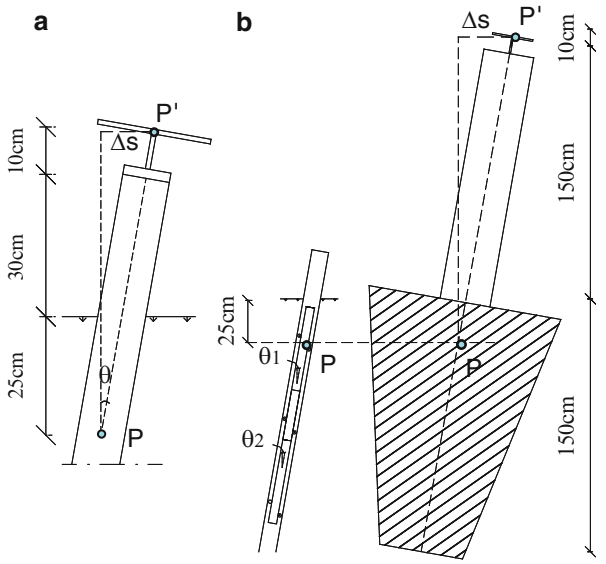


Fig. 7 Schemes used to compare GPS displacement (*point P′*) and cumulative inclinometer superficial displacement (*point P*)

displacements of point P thus evaluated are very close to those evaluated by means of inclinometers.

Also the other GPS antennas located on rigid structures provided data practically coincident with those of inclinometers. Figure 9 reports for the landslides A and B other superficial displacements evaluated with the different instruments. The figure shows that, almost in any position, measurements relative to different instruments are close to each other. One exception is constituted by GPS CS06, positioned on a wall close to inclinometer I6. As shown by Fig. 10, in this case the GPS station registers displacements higher than those, negligible, of the inclinometer.

The displacements of CS06 result almost parallel to the wall, so the influence of possible wall tilting can be excluded. As a matter of fact, superficial displacement of inclinometer I6 reported in the figure is cumulated from a depth of 40 m up to the ground surface, whereas the casing is 50 m long. This because a few months after the installation, the casing became not accessible beneath 40 m depth. At that time, it was not clear why. On the basis of current results, it seems reasonable to hypothesize the cause was the existence of a slip surface at that depth.

The difference between the superficial and the deep displacements is small (Figs. 9 and 11). So, GPS data can also give information on deep displacements in the time period between two consecutive periodical inclinometer measurements, or when the inclinometer casings go out of use.

However, GPS data cannot be used to evaluate the landslide acceleration on the slip surface. In fact, while the superficial displacement rates seem to be interested by seasonal variation, above all in the accumulation zone, the rate

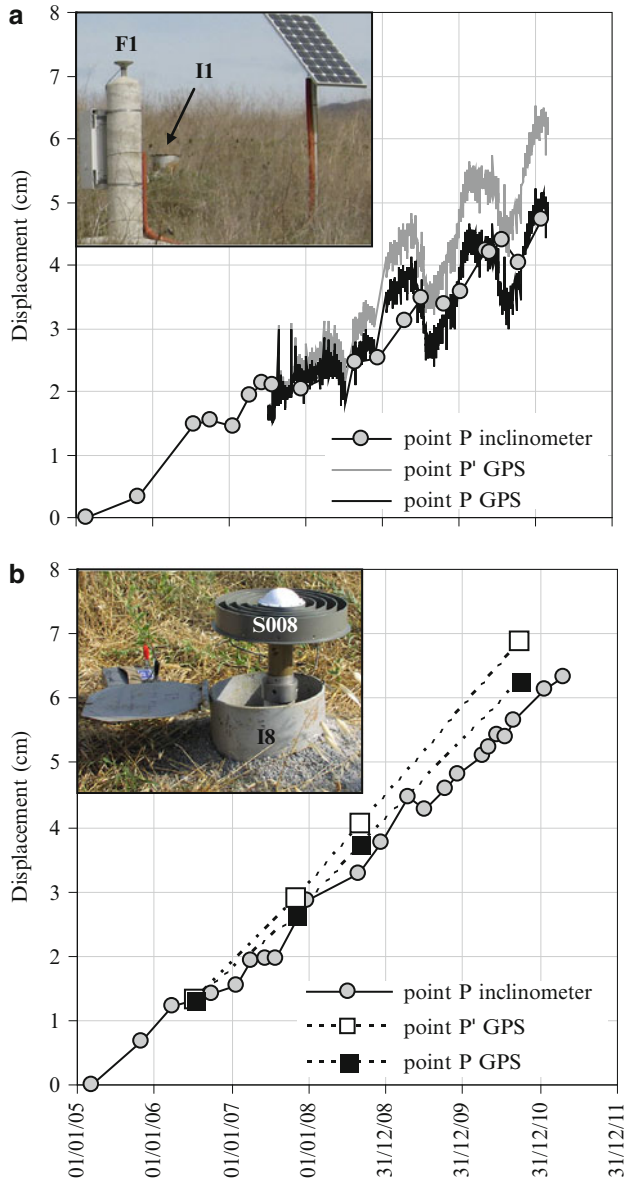


Fig. 8 Comparison between displacements evaluated by inclinometers and GPS in points P and P′ defined in Fig. 7

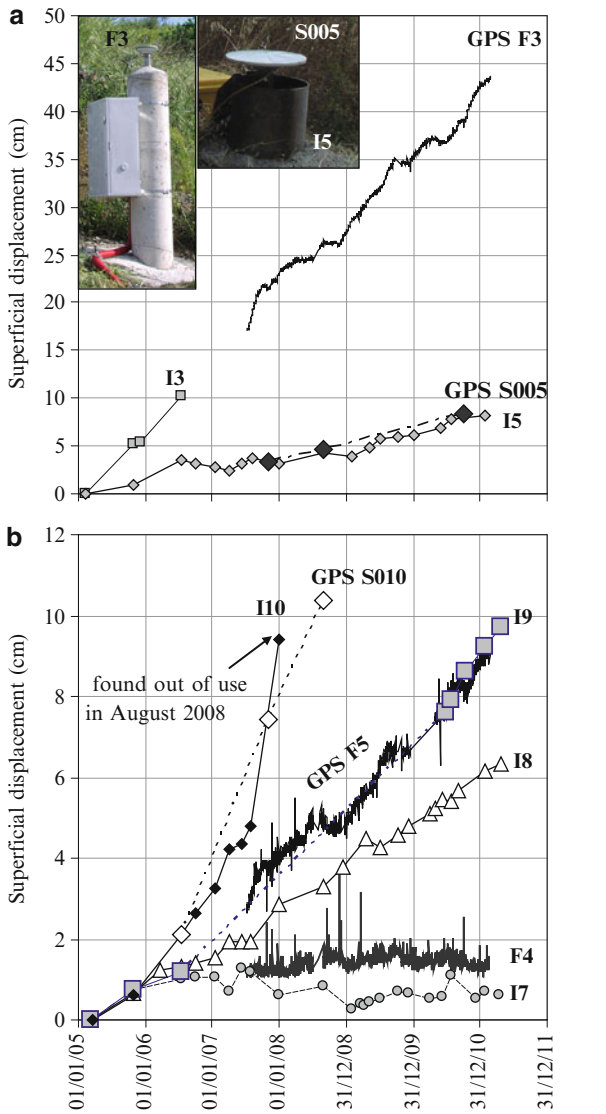


Fig. 9 Displacements at 0.25 m depth evaluated by the different instruments: landslide A (**a**), landslide B (**b**)

of deep displacement is almost constant (Fig. 11). In particular, the comparison between the deep displacements evaluated by fixed-in-place probes in I9 (Fig. 4) and superficial displacements in the nearby GPS station F5 (Fig. 5) shows that to the acceleration of this latter does not correspond acceleration on the slip surface. The mechanics of deep displacements is currently under examination and is analyzed in a companion paper presented at this same conference (Vassallo et al. 2013).

Conclusions

This paper reports the results of inclinometer and of GPS measurements in two slow, deep and ancient clayey landslides. Mobile and fixed-in-place inclinometer probes, permanent and non-permanent GPS stations on various supports were used. Installation was performed, and data interpretation was carried out, so as to make results of the different instruments consistent with each other. This allows to take advantage from the integrated monitoring system. In fact, a satisfactory monitoring can be obtained by a few fixed-in-place probes with continuous data acquisition, installed around the deep slip surfaces previously detected by standard measurements along the whole casing height. Furthermore, if the kinematics of the landslide is sufficiently studied, and if the difference between superficial and deep displacement is clearly understood, GPS continuous data can give significant information in the time period between periodical inclinometer measurements or when the inclinometer casings go out of use. GPS data can also be used to understand the landslide

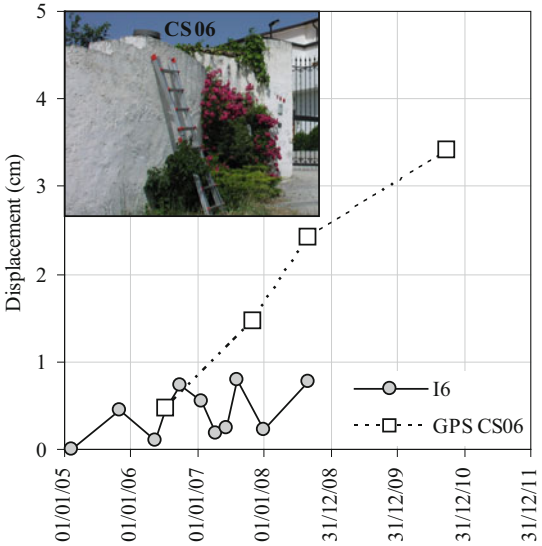


Fig. 10 Comparison between non-permanent GPS station CS06 and surface I6 inclinometer displacements cumulated from 40 m depth. At the end of 2008 the casing was no more accessible

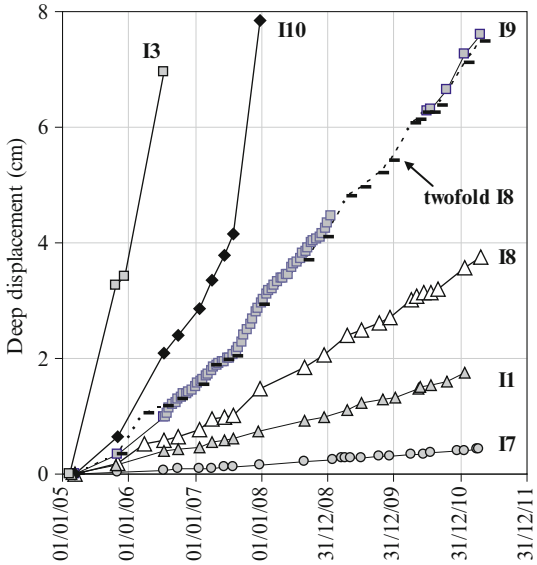


Fig. 11 Displacements on the slip surfaces against time for both landslides

mechanisms but, alone, in this type of landslide, cannot be used to give alarm to population. On the other hand, GPS data can indicate the possibility of the existence of slip surfaces deeper than the inclinometer.

Acknowledgments Part of this work has been conducted under the financial support of Regione Basilicata and of the National Civil Protection. The authors would like to thank Mr. M. Belvedere who carried out some *in situ* measurements and Dr. N. D'Agostino (INGV) for useful discussion on GPS data elaboration.

References

Calcaterra S, Cesi C, Gambino P (2008) Reti di monitoraggio integrato GPS-geotecnico delle frane di Lago (CS) e Costa della Gaveta (PZ). In: Proceedings of XII national conference ASITA, 21–24 Oct 2008, vol 1. L'Aquila, Italy, pp 581–586

Calcaterra S, Cesi C, Di Maio C, Gambino P, Merli K, Vallario M, Vassallo R (2012) Surface displacements of two landslides evaluated by GPS and inclinometer systems: a case study in Southern Apennines, Italy. Nat Hazards 61: 257–266. doi:10.1007/s11069-010-9633-3

Del Prete M, Del Prete R (2009) Classification, hazard and occurrence of flow-like mass movements in relation to the geology of a large area of Southern Italy. J Tech Environ Geol 1-2-3-4:6–96

Di Maio C, Vassallo R, Vallario M, Pascale S, Sdao F (2010) Structure and kinematics of a landslide in a complex clayey formation of the Italian Southern Apennines. Eng Geol 116:311–322. doi:10.1016/j.enggeo.2010.09.012

Perrone A, Iannuzzi A, Lapenna V, Lorenzo P, Piscitelli S, Rizzo E, Sdao F (2004) High-resolution electrical imaging of the Varco d'Izzo earthflow (Southern Italy). J Appl Geophys 56:17–29. doi:10.1016/j.jappgeo.2004.03.004

Pescatore T, Renda P, Schiattarella M, Tramutoli M (1999) Stratigraphic and structural relationships between Meso-cenozoic Lagonegro basin and coeval carbonate platforms in southern Italy. Tectonophysics 315:286–295

Vassallo R, Di Maio C, Vallario M (2013) A possible mechanism of movement of an ancient clayey landslide. Proceedings of II World Landslide Forum, 3–9 October 2011. Rome, Italy. vol.2, pp. 273–282



A Possible Mechanism of Movement of an Ancient Clayey Landslide

Roberto Vassallo, Caterina Di Maio, and Margherita Vallario

Abstract

The displacement rate of the considered ancient clayey earth slide varies noticeably along its longitudinal axis, however it is practically constant from the slip surface to the ground along four inclinometer profiles. In this paper, the displacement uniformity and the absence of viscous deformation are discussed and justified. The comparison among the theoretical shear stress distribution—within the landslide body and on the slip surface—the experimental peak shear strength and the residual shear strength shows that shear stresses are lower than or equal to residual strength. This latter, in turn, is much lower than the peak strength. Furthermore, long term shear tests carried out under controlled shear forces suggest that only primary creep occurs at shear stresses lower than residual strength. So, the landslide displacements can be hypothesized uniform in each entire transversal section of the channel.

Keywords

Landslide • Clay • Displacements • Stress distribution • Creep

Introduction

The main characteristics of the landslide system of Costa della Gaveta (Potenza, Southern Italy) are reported in a companion paper presented at this conference (Di Maio et al. 2012). This paper is focused on one landslide of the system, whose structure and kinematics are described by Di Maio et al. (2010). Figure 1 reports the Digital Terrain Model (DTM) with the earth slide, the positions of the inclinometer boreholes and those of other boreholes equipped with either Casagrande piezometers or pore pressure transducers. Monitoring started in 2005 and is still going on. The main results of the field experimentation are that the slip surface is very deep (up to about 40 m), the rate of displacement is very low (about 1 cm/year) and the displacement profiles are almost uniform from the slip surface to the ground surface. The aim of this study is to justify the aspect of displacement uniformity.

Figure 1 shows the channel of the earth slide and its fan shaped accumulation zone which has been interested, in the past, by intense river erosion. The figure also shows, on the right hand side, the slip surface. This latter has been reconstructed on the basis of inclinometer profiles and of the elaboration of the ground surface geometry, following Di Maio et al. (2010). The 3D representation puts in evidence the regularity of the slip surface. Furthermore, Fig. 1 reports the boundary of the depletion area which is supposed to coincide with that of the area interested by the landslide in the past. Based on simplified hypotheses, Di Maio et al. (2010) evaluated that the volume between the assumed ancient ground surface and the current one is about 6 million m^3, much higher than that of the current landslide body which is about 2.5–3 million m^3. So, this landslide has probably undergone very large displacements in its history. The large displacements and the regularity of the slip surface suggest that post-peak shear strength very close to the residual strength should be available on the slip

R. Vassallo (✉) • C. Di Maio • M. Vallario
School of Engineering, University of Basilicata, V. Ateneo Lucano, 10, Potenza, Italy
e-mail: roberto.vassallo@unibas.it

C. Margottini et al. (eds.), *Landslide Science and Practice*, Vol. 2,
DOI 10.1007/978-3-642-31445-2_35, © Springer-Verlag Berlin Heidelberg 2013

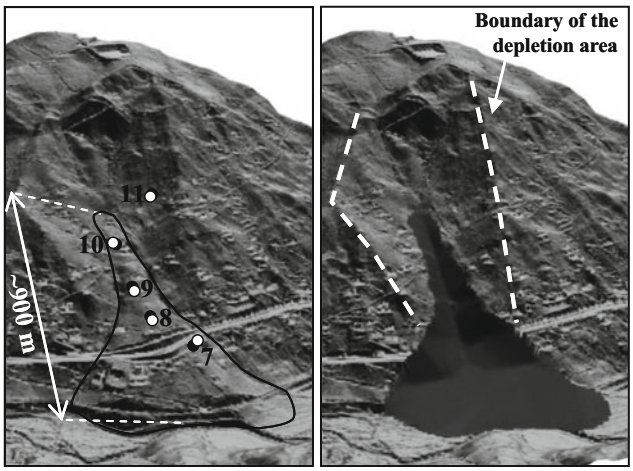


Fig. 1 DTM of the landslide with location of continuous coring boreholes equipped with piezometers (o) and core destruction boreholes equipped with inclinometer casings (•). The image on the *right hand side* shows the hypothesized slip surface

surface. Accordingly, the results of first stability analyses show that the available strength on the slip surface is close to the residual strength determined by laboratory tests on the material extracted from the landslide body. Furthermore, this strength is much lower than the experimental peak strength of the material of the landslide body. In order to use such information for the study of the landslide kinematics, it is necessary to evaluate the stress distribution within the landslide. It is reasonable to hypothesize that shear stresses close to the residual strength, and thus much lower than the peak strength, act within the landslide body. To investigate this hypothesis, theoretical analyses of the stress distribution within the landslide have been carried out.

According to studies on the rheological behaviour of soils (e.g. Suklje 1969), a shear stress distribution like that described above should not induce significant creep deformation. This was verified on the material of the landslide body by carrying out long term direct shear tests under controlled shear stresses. The results of our theoretical and experimental study seem thus to justify the shape of the inclinometer profiles evaluated by in situ measurements.

Laboratory Test Results

The considered subsoil is very heterogeneous, both in composition and in fabric. In the finer material, the clay fraction, c.f., can be as high as 50 %. Consistently, the liquid limit w_L can reach 80 %. In the Casagrande chart, the investigated soil is classified as inorganic clay with medium to high plasticity. The activity index A is close to that of illite. Table 1 reports the ranges of some physical characteristics.

Table 1 Ranges of variation of some physical characteristics and index properties: specific gravity G, dry specific gravity Gd, porosity n, degree of saturation S, plasticity index PI

G	Gd	n (%)	S (%)	PI (%)
2.05–2.15	1.60–1.80	33–42	95–100	20–55

Because of the diffuse presence of rock fragments, only a few undisturbed samples could be extracted to evaluate the mechanical properties.

On these samples, the peak shear strength of the landslide material was evaluated by triaxial tests. Isotropically consolidated—undrained (CIU) tests were carried out (Fig. 2a). The specimens, 33 mm in diameter and 72 mm in height, were isotropically consolidated and sheared at a rate of 0.03 mm/min. The experimental points at failure are well fitted by a straight line with an intercept $\mu = 102$ kPa on the deviatoric stress axis and a slope $M = 0.53$, corresponding to cohesion $c' = 50$ kPa and to a friction angle $\varphi' = 14\,^{\circ}$. Such noticeable cohesion and relatively low friction angle could be partly due to over consolidation and partly to bonding ($CaCO_3$ content up to 12 %).

The residual strength was evaluated by direct shear tests on both the undisturbed and the reconstituted material. The results (Fig. 2b) show that experimental points are well interpolated by a straight line through the origin giving a residual friction angle φ'_r of about 10 °. The comparison with the peak strength line of the landslide material shows a noticeable drop of strength from peak to residual.

In order to analyse the role of creep in the displacements of the studied landslide, direct shear tests were carried out under constant shear forces. For a given value of normal stress, different shear forces were applied, each held constant over a long time, investigating the shear stress range indicated in Fig. 2b.

Figure 3a reports the results relative to a specimen reconstituted with distilled water, which was first sheared by standard procedure, under constant shearing rate (5 μm/min), at various normal stresses. Once the residual shear strength at $\sigma'_n = 202$ kPa was reached (Fig. 3a), the specimen was submitted to creep tests and sheared under constant shear forces. Figure 3b reports the results in terms of shear displacements against time for values of average shear stress on the shear surface increasing from 0 to 32 kPa. Each symbol corresponds to one of the 22 different average shear stresses τ which were applied. For the figure clarity, the legend reports only four τ values. Creep always resulted of the primary type, i.e., the rate of observed shear displacements induced by constant shear stress decreased with time down to 0. This trend was verified for long time periods. In particular, under $\tau = 28$ kPa, close to the highest applied shear stress, primary creep was observed for about one year. The absence of intense creep confirms the hypothesis formulated by Suklje (1969).

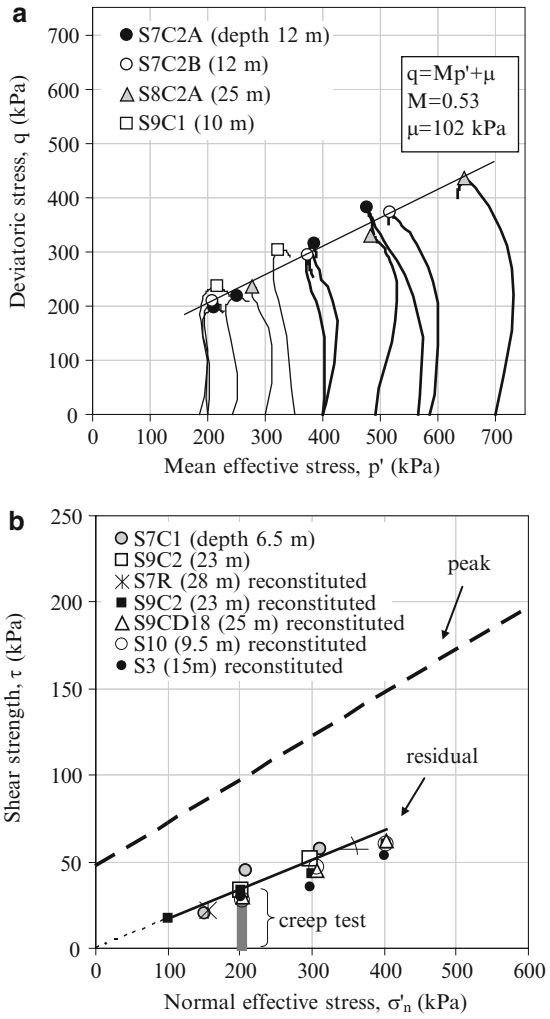


Fig. 2 Results of triaxial CU tests: effective stress paths and peak shear strength of undisturbed samples (**a**); residual shear strength against effective normal stress from direct shear tests and comparison with the *straight line* interpolating peak strength values (**b**)

Further direct shear creep tests, whose first results seem in agreement with those mentioned above, are being carried out on other reconstituted specimens, either with or without a preliminary stage of shearing to residual conditions.

Displacement Profiles

The landslide studied in this paper is an earth slide, it has a regular slip surface, over which large displacements took place in the past, so that the residual strength is now available. One of its main kinematic characteristics is that the displacement rate decreases in the downslope direction. This is shown by Fig. 4 which reports some cumulative profiles obtained by inclinometer measurements in the casings located as reported in Fig. 1. Di Maio et al. (2010) explained such decrease with the increase in the areas of transversal sections, the "soil discharge" being practically constant. It is worth noting that, because of the high displacement rate, the I10 casing went out of use at the beginning of 2008, whereas the displacements obtained in I7 on the slip surface are still quite small. It is mainly for their regularity in time that such displacements are not considered the result of a measurement error.

Displacement profiles resulted practically uniform above the slip surface in the 6-years monitoring period, as shown by the same Fig. 4. It is by hypothesizing that the displacement uniformity could be extended to each entire transversal section that the mentioned soil discharge was found constant.

To justify the particular shape of displacement profiles, which indicates the absence of creep for almost the whole height of the earth slide, the theoretical analysis of the stress distribution reported in the next section was carried out.

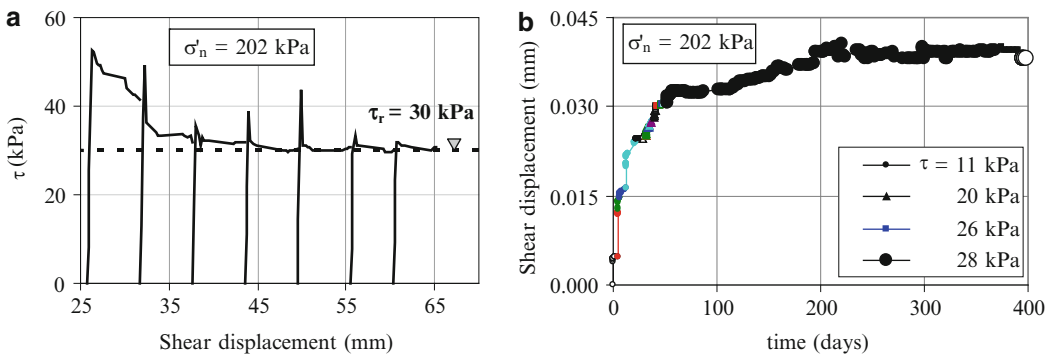


Fig. 3 Shear strength against shear displacement for a reconstituted specimen consolidated at $\sigma'_n = 202$ kPa and sheared under constant displacement rate of 5 μm/min (**a**). Shear displacement against time of the same specimen under constant average shear stresses (**b**)

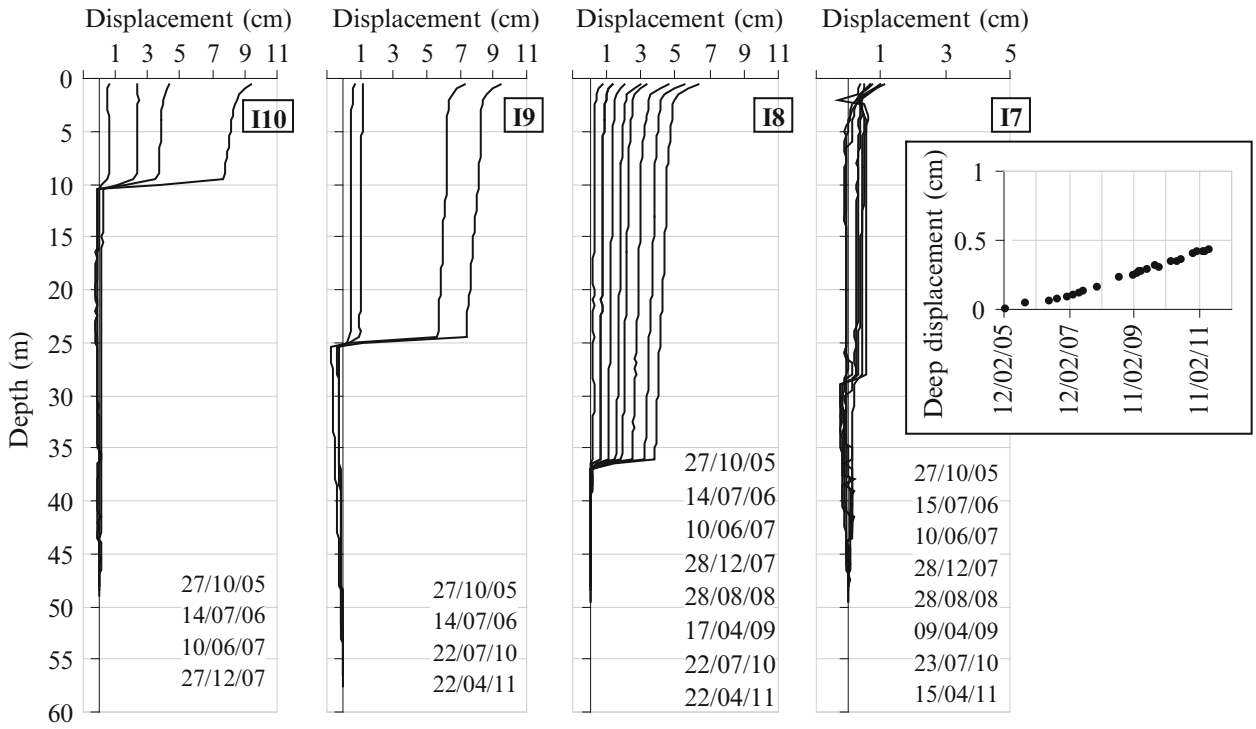


Fig. 4 Inclinometer cumulative displacement profiles (zero measurements: March 2005)

Stress Distribution

According to literature theoretical analyses and experimental results (Ter Stepanian 1963; Suklje 1969; Yen 1969), when the subsoil is characterized by very different values of peak and residual shear strengths, intense creep can only occur for stress conditions close to the peak shear envelope. D'Elia (1979, 1975) verified that the absence of creep deformations in the case of a mudslide with uniform displacement profiles could be explained with the above theories. Van Asch and Van Genuchten (1990) used the same concepts as Suklje (1969) to describe the creep contribution—limited to a maximum of 15 % of the total—to the displacements of a landslide in varved clays.

Stress distribution, within the landslide body and on the slip surface, will be estimated in this section by using different approaches. Preliminarily, it is useful to show the results of a simple back-analysis based on the limit-equilibrium method.

The considered slip surface is the one detected by the inclinometers. The safety factor on such slip surface was evaluated by assuming three different pore pressure distributions (Di Maio et al. 2010), obtained for (a) zero normal flux on the ground surface ($q_n = 0$, corresponding to dry weather); (b) zero pore pressure on the ground surface ($u = 0$, corresponding to rainfall intensity higher than the soil permeability, so as to generate surface runoff); (c) fixed phreatic surface, based on the minimum water level found in the piezometers, with constant hydraulic head in each vertical (Fig. 5). It is worth noting that, as shown by Di Maio et al. (2010), distribution (a) overestimates pore pressures with respect to those measured by piezometers in most of the monitoring period. Moreover, due to the effect of the 3D landslide geometry, distribution (b) provides pressure values

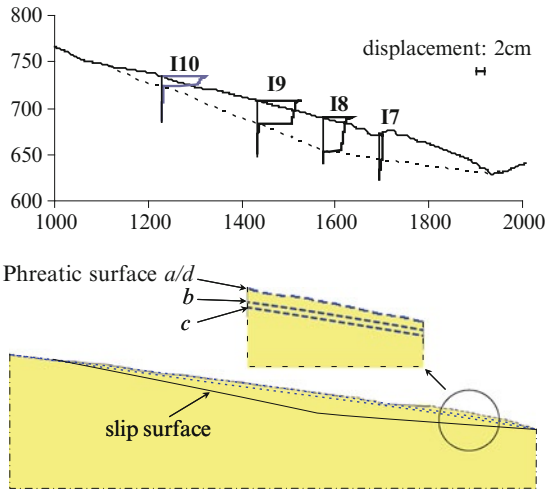


Fig. 5 Stability analyses: slip surface evaluated by the inclinometer profiles; positions of the phreatic surface for the considered pore pressure distributions: zero pore pressure at the ground level (*a*/*d*), zero normal flux at the ground level (*b*); phreatic surface deriving from piezometric measurements (*c*)

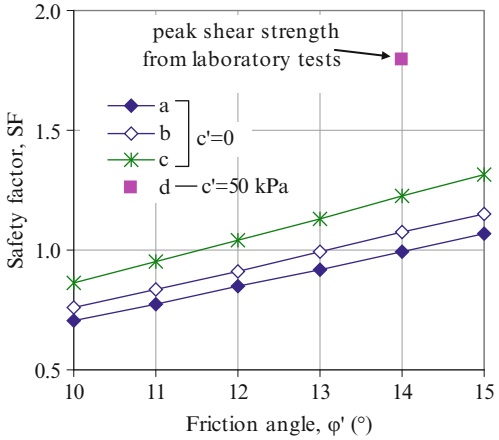


Fig. 6 Safety factor against friction angle, for unit weight $\varphi = 21$ kN/m^3, cohesion $c' = 0$ and $c' = 50$ kPa and for pore pressure distributions relative to: zero pore pressure at the ground level (*a*/*d*), zero normal flux at the ground level (*b*); phreatic surface deriving from piezometric measurements (*c*)

higher than the minimums observed in the piezometers. Distribution (c) has been considered the most representative one. Since the landslide has undergone large displacements, zero cohesion c' was assumed on the slip surface. Figure 6 reports safety factor SF, obtained by the Morgenstern-Price method, against effective friction angle φ'. The mobilized friction angle is about 13 ° for the pore pressure distribution (a) and increases to 14 ° for case (b). Distribution (c)—fixed phreatic surface—yields the minimum value of mobilized friction angle, between 11 ° and 12 °. These values are close to the residual friction angle range obtained experimentally and shown in the previous sections. This is consistent with the fact that the studied ancient landslide has undergone large displacements on a regular slip surface. Much higher SF is obtained by considering the peak shear strength parameters (Fig. 6).

The results of such analyses, based on the method of slices, could also be used to estimate stresses at the base of each slice, i.e. to obtain the stress distribution on the slip surface. To obtain the stress distribution in the landslide body, a different procedure is necessary.

Stresses were first estimated in I10, I9 and I8 by using in each vertical the equations of an infinite slope with ground inclination equal to the average inclination of the ground surface in correspondence to that vertical. Total normal stresses and shear stresses on surfaces parallel to the ground of such infinite slopes were computed as a function of depth. Of course, just equilibrium equations were sufficient to carry out such calculation. Shear stresses so obtained are plotted in Fig. 7.

The figure also compares shear stresses to shear strength. This latter was estimated on the basis of effective stresses, i.e. of the difference between the calculated total normal stresses and the pore pressures. We used the pore pressure

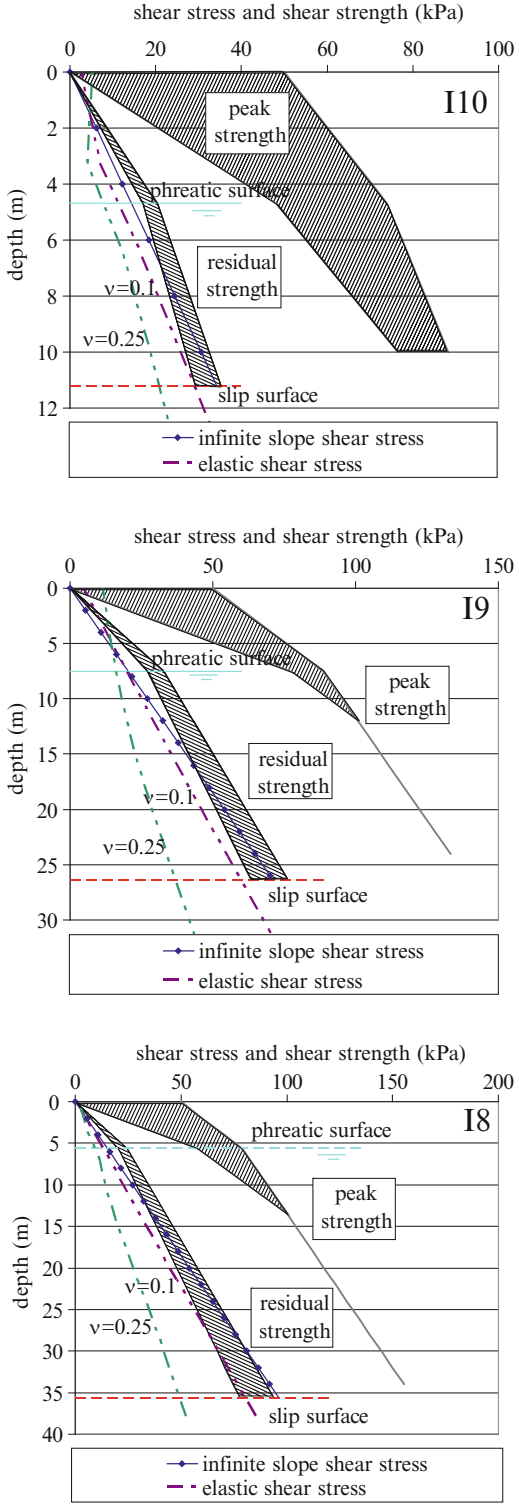


Fig. 7 Shear stress and shear strength distribution within the landslide body and on the slip surface for verticals I10, I9, I8

distribution relative to phreatic surface (c) of Fig. 5; zero pore pressure was assumed above the phreatic surface.

As for peak shear strength, a range of possible values, corresponding to the hatched region of Fig. 7, was considered

for $\sigma' \leq 200$ kPa. In fact, it is worth recalling that strength parameters $\varphi' = 14°$ and $c' = 50$ kPa resulted from laboratory tests in the range $p' \geq 200$ kPa. Thus, a maximum possible value of strength was estimated by assuming that the same strength parameters apply for lower confining stresses (i.e., in situ, up to the ground surface). A minimum value was obtained under the hypothesis that the strength is null for $\sigma' = 0$ and varies linearly with σ' in the range $0 \leq \sigma' \leq 200$ kPa. For $\sigma' \geq 200$ kPa, a single value of peak shear strength was considered for each depth, corresponding to $\varphi' = 14°$ and $c' = 50$ kPa.

As for residual shear strength, the considered range, which is represented by another hatched region in Fig. 7, corresponds to friction angles between 10° and 12°.

Figure 7 highlights that shear stresses are close to the residual strength along each vertical. So in the landslide body, above the slip surface, they are significantly lower than the peak shear strength.

To further investigate this aspect, other analyses, whose results are also reported in Fig. 7, were carried out by considering the 2D geometry of the slope as it is in Fig. 5. The soil was assumed to be linearly elastic and the total stresses induced by its own weight were calculated by a finite element code (Geoslope SIGMA/W). The obtained stress distribution is independent of the Young modulus E. The computed distributions of shear stresses for two values of the Poisson ratio (0.1 and 0.25) are plotted as shear stresses acting on surfaces parallel to the ground surface against depth.

Such elastic analyses also provided total normal stress distributions, from which effective stresses and then shear strength were estimated, by using the same procedure as the infinite slope analysis. The obtained distributions of peak and residual shear strength is practically coincident with that of the infinite slope analysis. So, the shear strength ranges reported in Fig. 7 can be considered common to both kind of analyses. It is worth noting that, on the slip surface, the obtained normal stresses—and thus the computed available strength—are also very similar to those which resulted from limit equilibrium, being evidently dominated by equilibrium conditions.

From the comparison of shear stresses and shear strength estimated from the elastic analyses one can draw conclusions quite similar to those relative to the infinite slope analysis.

All the above seems to confirm the hypothesis that stresses in the landslide body are quite lower than the peak strength and thus sliding on the slip surface, with negligible deformation of the landslide mass, is the main expected type of movement, consistently with the evaluated inclinometer profiles of Fig. 4.

It is intuitive that also in the transversal direction, within the landslide body, delimited by the slip surface on which the residual strength is available, shear stresses on vertical planes are lower than the peak shear strength. This makes displacements uniform in the entire transversal section. As a matter of fact, the hypothesis of such uniformity leads to the result of constant soil discharge in the landslide channel. This result, in turn, is consistent with the negligible lateral alimentation. Furthermore, it is consistent with the displacement time trend which shows that, in the observation period, displacements have always been simultaneous along the landslide (Di Maio et al. 2012).

Conclusions

The regularity of the slip surface of the considered ancient landslide, that has probably undergone large displacements in its history, suggests that the residual shear strength is the available strength upon it. Back-analysis confirms that the mobilized strength is close to the residual one determined in laboratory. Within the landslide body, shear stresses lower than or equal to the residual strength were estimated. This latter, in turn, is much lower than the peak strength of the landslide body. The results of laboratory long term direct shear tests carried out under controlled shear forces show that shear stresses lower than the residual strength produce only primary creep.

All the above results seem to justify the displacement uniformity determined by inclinometer measurements. Furthermore they suggest that such uniformity probably interests the entire transversal section.

The different sections are characterized by different displacement rates. However, Di Maio et al. (2010) and Di Maio et al. (2012) showed that strong correlations apply among the kinematic characteristics of the different sections. So, displacement measurements in a few stations can give useful information on the displacements of the other sites of the landslide, at least in the period of some months.

The absence of creep, the constancy with time of displacement rate and the contemporary displacements of the earth slide lead to the hypothesis that river erosion at the toe is the major cause of movement. This aspect is currently under examination.

Acknowledgments Part of this work has been conducted under the financial support of Regione Basilicata. The authors would like to thank Mr. M. Belvedere who carried out some in situ measurements. Special thanks to engineering company GEOCART for providing the digital terrain model used in this study.

References

Di Maio C, Vassallo R, Vallario M, Pascale S, Sdao F (2010) Structure and kinematics of a landslide in a complex clayey formation of the Italian Southern Apennines. Eng Geol 116: 311–322

Di Maio C, Vassallo R, Vallario M, Calcaterra S, Gambino P (2012) Comparison among displacements evaluated by GPS, mobile and fixed in place inclinometer probes in two deep clayey landslides. In: Proceedings of II World Landslide Forum, vol. 2, Rome, 3–9 Oct 2011, pp 265–271

D'Elia B (1975) Aspetti meccanici delle frane tipo "colata". Ital Geotech J 9:32–425

D'Elia B (1979) Caratteri cinematici delle colate: interventi di stabilizzazione. Ital Geotech J 2:122–136

Suklje L (1969) Rheological aspects of soil mechanics. Wiley-Interscience, London

Ter Stepanian MG (1963) On the long-term stability of slopes. Norwegian Geotechnical Institute, Publication no 52:1–13

Van Asch TJW, Van Genuchten PMB (1990) A comparison between theoretical and measured creep profiles of landslides. Geomorphology 3:45–55

Yen BC (1969) Stability of slopes undergoing creep deformation. J Soil Mech Found Eng ASCE 95(SM 4):1075–1096



Results of Geoelectrical Monitoring of Landslides Collected by the SafeLand/TEMPEL Network

Robert Supper, Birgit Jochum, Ivo Baroň, Alexander Römer, Mario Lovisolo, David Ottowitz, and Stefano Cardellini

Abstract

Based on the promising results from a pilot monitoring project the GEOMON4D geoelectrical monitoring system was applied to several landslide monitoring tests sites, where also permanent monitoring data of displacement and hydrology are available to investigate the correlation of electrical parameters with other data. This monitoring network was set up in frame of the FP7 project SafeLand and the project TEMPEL (Austrian Science Fund) starting from October 2009 on. Analysis of the first monitoring results confirmed the potential of geoelectrical parameters as additional indicators to be applied within future early warning systems of landslides.

Keywords

Geoelectric monitoring • Displacement • Early warning

Introduction

Landslides are one of the major natural threats to human lives, settlements and infrastructure, causing enormous human suffering and property losses. The best way to restrain such high losses on property and lives is through effective land-use planning, based especially on a good knowledge of the landslide susceptibility, hazard and risk within specific areas as a part of mitigation. However, this ideal approach is, due to several natural, historical or political reasons in many places impossible. E.g., many human settlements and infrastructure lines have already existed in landslide-prone areas or on dormant landslide bodies decades before the establishment of detailed hazard zone maps. In most cases it is not possible to resettle people living in such areas. Consequently it is the goal of stakeholders to guarantee a safe daily life of the people concerned.

A good knowledge about structure, dynamics, triggers, history and possible magnitude of such high-risk landslides is an important task to be able to evaluate actual hazard and, eventually, to alert people before a catastrophic event in advance. This knowledge is obtainable only through a complex approach consisting of investigations by many different interdisciplinary methods and techniques, long-time continuous monitoring of deformation and triggering factors and by establishing early warning systems/centres. The most commonly used early warning parameters are pore water pressure and displacement. However recent research has shown that other parameters exist, which might give indications on impending triggering even a longer time before an actual displacement is measureable.

Aspects of Geoelectrical Monitoring of Landslides

With geoelectric investigations it is possible to determine the distribution of the specific electrical resistivity of the subsurface, which mainly depends on porosity, water

R. Supper (✉) • B. Jochum • I. Baroň • A. Römer • D. Ottowitz
Geological Survey of Austria, Neulinggasse 38, Vienna 1030, Austria
e-mail: robert.supper@geologie.ac.at

M. Lovisolo
Centro Servizzi di Geoingegneria, Ricaldone, Italy

S. Cardellini
Ancona Monitoring Centre, Municipality of Ancona, Ancona, Italy

C. Margottini et al. (eds.), *Landslide Science and Practice*, Vol. 2,
DOI 10.1007/978-3-642-31445-2_36, © Springer-Verlag Berlin Heidelberg 2013

saturation, conductivity of pore fluid and clay content. Since most of the European landslide events are intimately related to precipitation and to influence of underground water on slope stability (pore-water pressure, change of water flow regime, saturation), registering temporal changes of the geoelectric parameters seems to be a promising method for monitoring of landslides. Therefore research was started to evaluate temporal changes of geoelectrical properties of the subsurface as possible indicators of future failure of high risk landslides; such additional indicators would be beneficial to any effective early warning system.

The geoelectric parameters, promising progress in landslide monitoring, and which are investigated in our project, are direct current resistivity (DC), self potential (SP) and induced polarisation (IP) measurements.

The Development of the GEOMON4D System

In 2000, after the successful application of the geoelectric method to investigate the structure of the large landslide of Rindberg near Sibratsgfäll (Jaritz et al. 2004; Supper et al. 2008) following the mass wasting event in 1999, the Geophysical Department of the Geological Survey was contracted by the Torrent and Avalanche Control Vorarlberg to develop a permanent geoelectrical monitoring system for landslides. It was found that most of the commercially available systems were optimised to perform conventional investigation surveys. On the contrary, at that time they were not suitable for the requirements of permanent monitoring (high speed of data acquisition, recording of full signal samples for noise detection, remote controlled maintenance and automatic data transfer - for more details see Supper et al. 2009). Therefore in late 2000 the design of an innovative system was decided and started (Supper and Römer 2003). The first 29-electrode prototype was installed to observe the mudflow of Rindberg near Sibratsgfäll in the spring 2002, where it was continuously measuring until the end of 2007 with a few unforeseen interruptions due to lightning strokes. Based on the results gathered during operation of the prototype, the system was redesigned and optimised for monitoring purpose as well as for "conventional" field surveys within the following years and finally reached its maturity state in 2006. The GEOMON4D instrument, as it is today, is based on technically mature components and offers a completely open architecture, allowing installation of any number of current or potential electrodes by adding parallel or serial cards. The principal characteristics are the high speed of data acquisition (approx. 3,000 measurements/h in single channel mode) and recording of the full signal (usually 1,000 samples per single configuration) for noise analysis and filtering. Moreover GPRS (General Packet Radio Service) data transfer was implemented. Therefore maintenance can be performed fully remote-controlled. Data (measurement results, test sequences and log files, containing information about system and GPRS connection status) are sent automatically via email to the data processing centre. Consequently, immediate availability of information for local stakeholders can be guaranteed. Additionally the optimum way of installing the arrays (surface, trenches, different kinds of cables and connectors) was tested over years and a lightning protection device for multi-core cables had to be developed.

At the end of 2007 after 5 years of operation, the maintenance of the system at Rindberg/Sibratsgfäll was determined since a significant part of the cables had been cut due to large displacements. The geoelectrical data showed interesting anomalies, suggesting correlations with the displacement pattern; however detailed interpretation was hindered by the fact that no permanent (at least hourly) displacement data was available at that time.

Monitoring Network of the SafeLand and TEMPEL Projects

The results from Rindberg clearly showed that in depth interpretation of time series of permanent geoelectric measurements is only possible if coupled also with permanent displacement and hydrological monitoring data. Consequently starting from 2009 on, several long-periodic monitoring experiments were started within the projects SafeLand (FP7) and TEMPEL (Austrian Science Found) at several landslides of different types around Europe (Fig. 1). At the test sites of Gschliefgraben (A), Bagnaschino (I), Ampflwang (A) and Ancona (I) innovative permanent geoelectric monitoring (using the GEOMON4D tool) and high resolution displacement monitoring using the DMS device (differential monitoring of stability), a high resolution automatic inclinometer (Foglino et al. 2006), were applied together with other traditional parameter in frame of actual monitoring or early warning projects. Additionally complex structural investigation (remote sensing, airborne and ground geophysics) were performed to investigate the underlying triggering processes. Moreover close to the glacier of Mölltal (A) a specifically adopted GEOMON system was installed to monitor permafrost thawing in the subsurface at an altitude of 2,800 m. Finally in May 2011 another system was installed at the landslide of Super Sauze in France, a quickly moving mudflow. For autumn 2011 two more installations, most probably in Rosano (I) and Recica (CZ) are planned. A preliminary comparative evaluation of the results coming from these test sites will be presented. The outcome clearly highlights the potential capabilities of geoelectrics as a pre-alarm

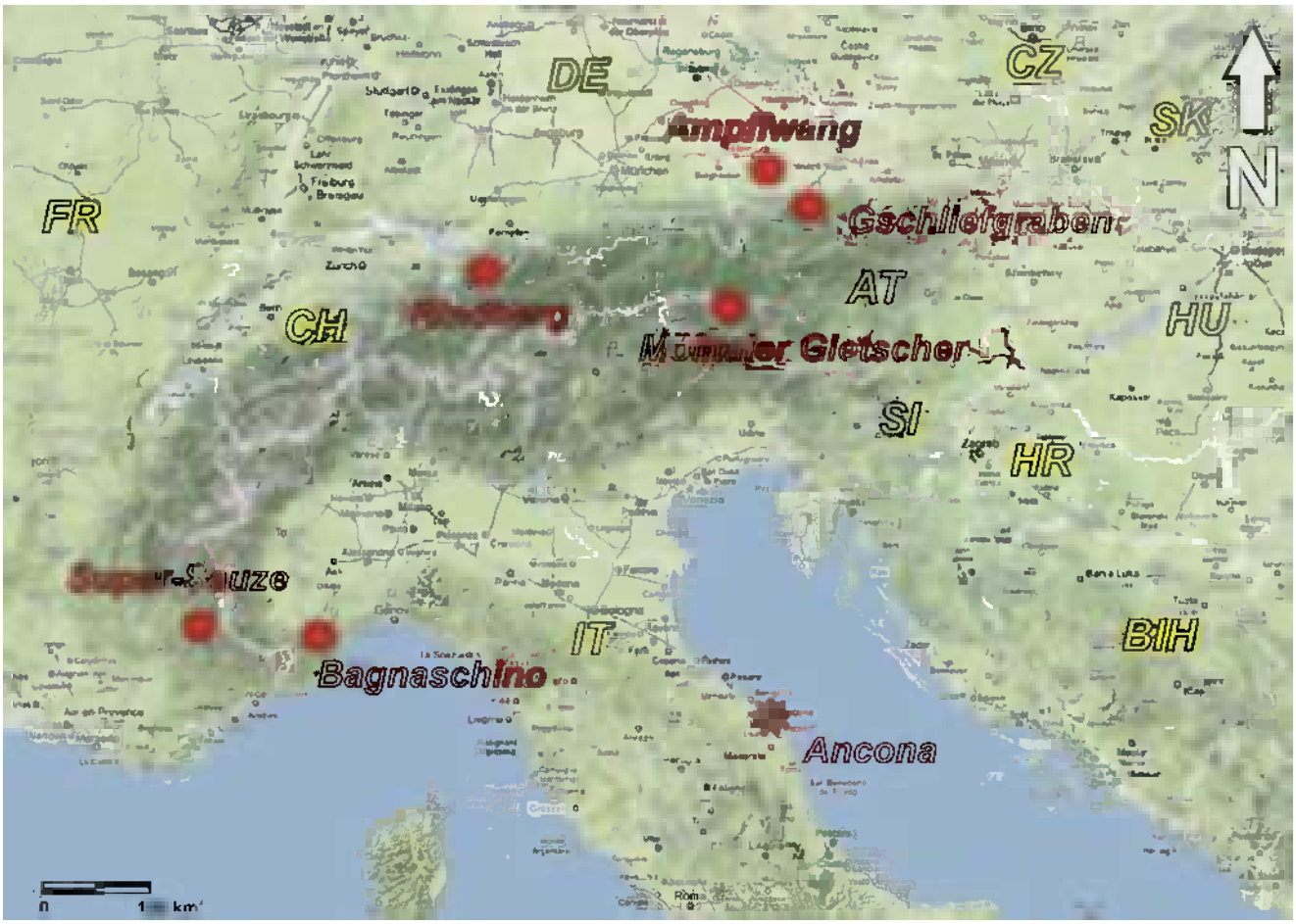


Fig. 1 Location of the GEOMON4D permanent monitoring installations

parameter, which, in combination with DMS and precipitation monitoring, could result in an effective sensor platform for early warning systems for landslides.

Site Settings and First Results

Gschliefgraben

The Gschliefgraben site is one of the most prominent and recently studied slope failures in Central Europe. It comprises a large complex of geologically controlled landslides, earth flows, topples, rockfalls and deep-seated gravitational deformations in the Gschliefgraben valley and along the slopes of the Northern Calcareous Alps. The area of Gschliefgraben is a 2.85 km long and 0.85 km wide valley along the foot of the Northern Calcareous Alps (Fig. 1) south of the town of Gmunden. The valley is divided into small sub-parallel catchments; its topography is strongly controlled by complicated tectonic structure and a very complex lithology, as well as by mass wasting that has been active here since the end of the last glacial period. In late November 2007, a landslide of about 3.8 million m^3 of colluvial mass was reactivated in the central and western parts of the valley within old earthflow and other deposits. Displacement velocity was up to 4.7 m/day at the beginning and 55 buildings had to be evacuated. Recently, the Gschliefgraben landslide is a test site of the European FP7 project SafeLand where the new techniques have been tested for an effective early warning, consisting of, e.g., a complex of airborne and ground-based geophysical surveys, the GEOMON system and the D.M.S. monitoring systems. Figure 3 shows the monitoring results at the site of Gschliefgraben. The case study so far proved the reliability of the method for long term monitoring. It clearly shows the long term stability of geoelectrical parameters and their response to changes in the hydrological system of the subsurface. The results showed that intense rainfalls had a direct and immediate impact without any delay on the displacement and resistivity pattern causing very small, but clearly identifiable changes in both parameters.

However, since during the observation period no significant changes in the displacement pattern took place in that area, a direct evaluation of the ability of geoelectrics as an

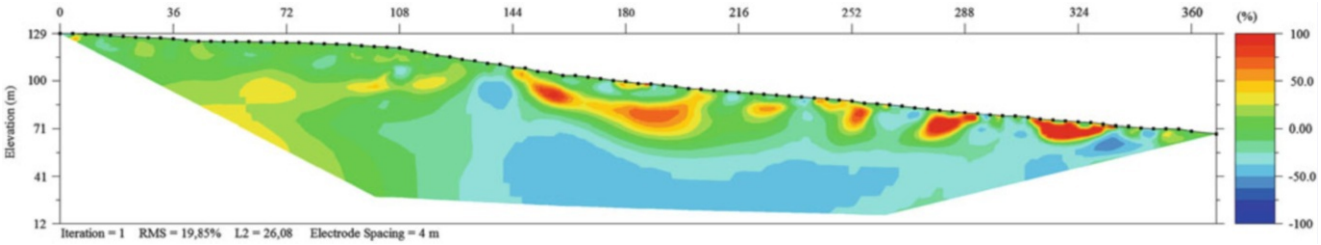


Fig. 2 Results of the time-lapse inversion of 2 data sets from April and June 2011: *red areas*: resistivity increase, *blue areas*: resistivity decrease

early warning parameter could not be performed. For this purpose, longer observation periods are necessary. However observation after the period shown in Fig. 3 did not determine any changes in the displacement pattern but a smooth and permanent decay.

The Ancona Test Site

The Ancona site represents a large and deep landslide, which affected the Ancona city located on the East coast of the Adriatic Sea on 13th December, 1982 (Cardellini and Osimani 2010). The event involved about 180 million m of Lower and Middle Pliocene homogenous and well-stratified marly clays and clayey marls with high silt content and rarely with the presence of thin sandy beds, and covered an estimated area of 2.2×10^4 m (Cotecchia 2006). The 1982 landslide caused extensive damage to structures and infrastructure, such as the University Medical Faculty and the local hospital (Anon, Cotecchia; both in Cotecchia 2006) and about 3,000 people were evacuated. Gas and water supplies were interrupted too and the city remained for some days without the necessary services (Cardellini and Osimani 2010).

In 2002, the Regione Marche decided to establish an Early Warning System and an Emergency Plan. The core of the monitoring system consists of 7 Automatic Robotic Stations, 230 reflector points (installed partly on the 64 inhabited houses and on the structures and infrastructures), 26 geodetic GPS, 8 geodetic GPS (dual frequency), 7 high precision clinometric sensors, complemented with the automated inclinometers, thermometers and piezometers of D.M.S. (Differential Monitoring of Stability—patent and trade mark CSG-Italy), which have been installed inside 3 boreholes up to 100 m deep (Cardellini and Osimani 2010). The GEOMON system was installed in April 2011 in the lower central portion of the landslide. The main purpose of the geoelectrical monitoring system at this site, since no major movements are expected in near future, is focused on investigating seasonal changes of the groundwater pattern and its correlation with sea-water intrusions and the effectiveness of the drainage system. Although data from a period of only 2 months is currently available for interpretation, clear changes in the resistivity pattern (Fig. 2) could already be detected. In the first 25 m, which mainly consist of clay and sand layers, a increase of resistivity due to drying of the structures is visible whereas in the deeper part of the section a decrease of resistivity, most probably due to infiltration of sea water and retreat of fresh water due to less surface infiltration by precipitation, can be determined (Fig. 2).

The Ampflwang Test Site

The Ampflwang monitoring site represents a new landslide formed after a house construction within the area of an old deep-seated landslide. The deep-seated rockslide developed in Upper Tertiary rocks, i.e.: fluvial gravels of Hausruck Formation (HF) at the top, limnic to fluvial coal-rich clay with brown coal beds of Ampflwang formation (AF) in the middle, and in marine silty-sandy marl to silty sand of Ottnang Formation (OF) at the base. The dimensions of the reactivated part, based on topographic changes and inclinometric data, are about 40 m (length), 40 m width and about 4 m thickness. A newly constructed family house was partly damaged. The monitoring of the reactivated landslide comprises fully remotely controlled continuous D.M.S. and GEOMON systems. Figure 4 shows the results collected at this site. Within the observation period, four main displacement events could be detected. Event 1, which showed the by far largest acceleration at this site, was correlated with several days of snow melting before the event and an intense rainfall some hours before, event 2 with snow melting, event 3 with snow melting and rainfall and event 4 just with rainfall. All events showed a clearly pronounced decrease of resistivity, which already could be observed some hours before the start of the movement. Later rain events, although of similar or larger intensity and also correlated with a (however smaller) resistivity anomaly did not trigger any acceleration. Therefore we conclude that for this test site pre-filling of the subsurface due to water from snow melt was the pre-condition for an acceleration of the landslide in case of additional rainfalls. Within the next months the effect of intense rain in connection with summer thunder storms will be investigated.

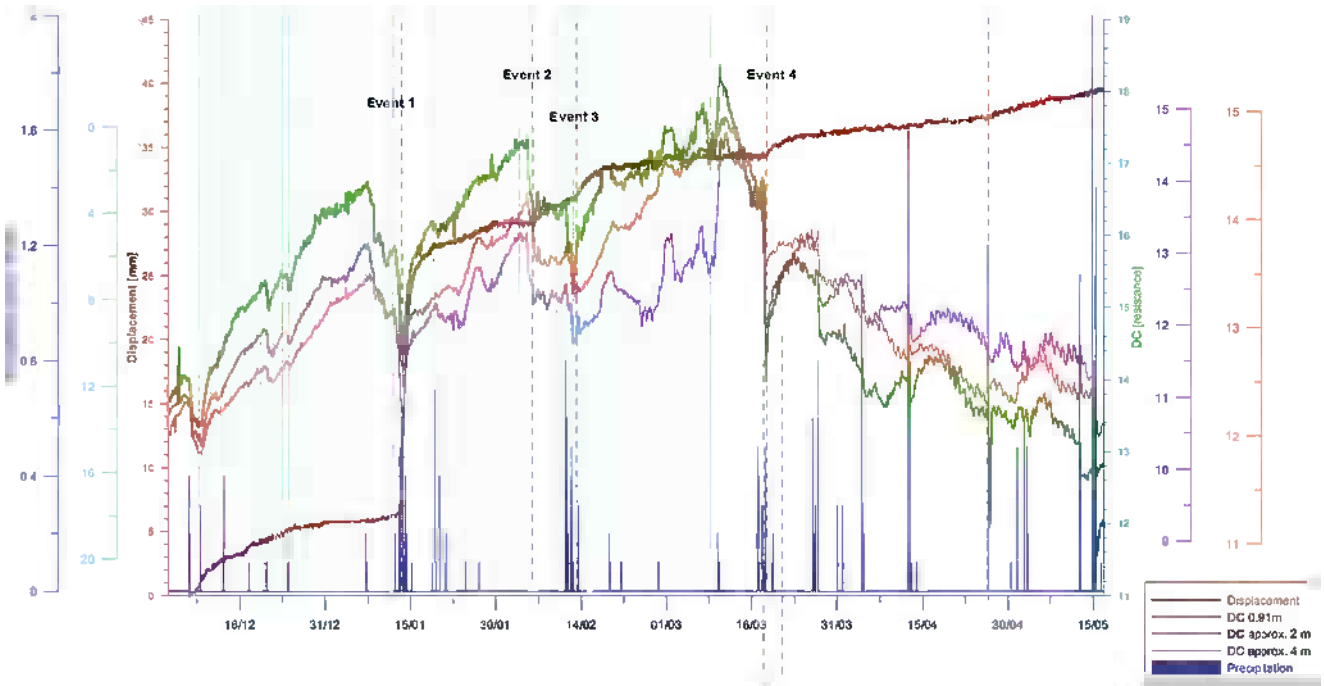


Fig. 3 Results of monitoring data from the site of Ampflwang (*green, orange and purple*: apparent resistance time series at different apparent penetration depths, *red*: displacement, *blue*: precipitation, *light blue* areas: freezing periods)

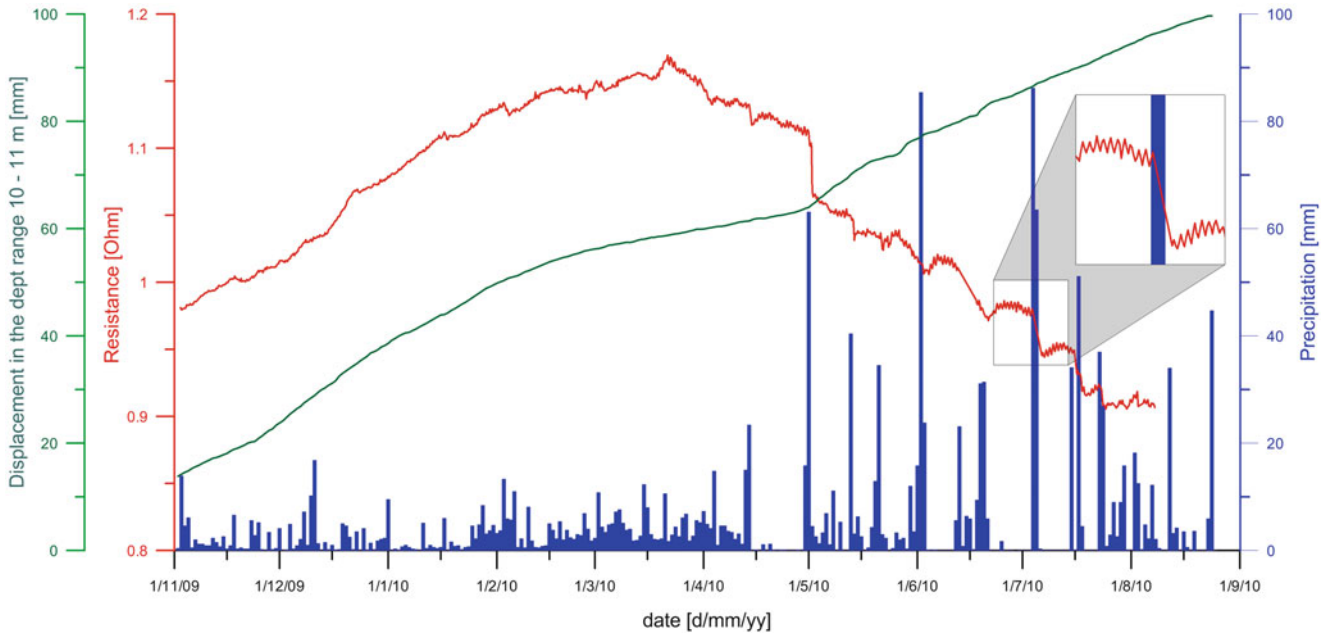


Fig. 4 Results of monitoring data from the site of Gschliefgraben (*red*: apparent resistance, *green*: displacement, *blue*: precipitation)

The Bagnaschino Test Site

The Bagnaschino site represents a landslide/earthflow reactivated within an old landslide mass. The old landslide is situated on the E slopes of the Val Casotto about 4 km SE of Torre Mondovì (NW Italy) and developed in tectonically densely jointed calcareous-mica schist and diamictic colluvium superimposed on altered amphibolite and prasinite. Evident indications of deep-seated gravitational deformation (crowns and scarps, zone of accumulation of large paleoslides, etc.) suggest that the current slopes are in a condition of limit-equilibrium and are predisposed to slow

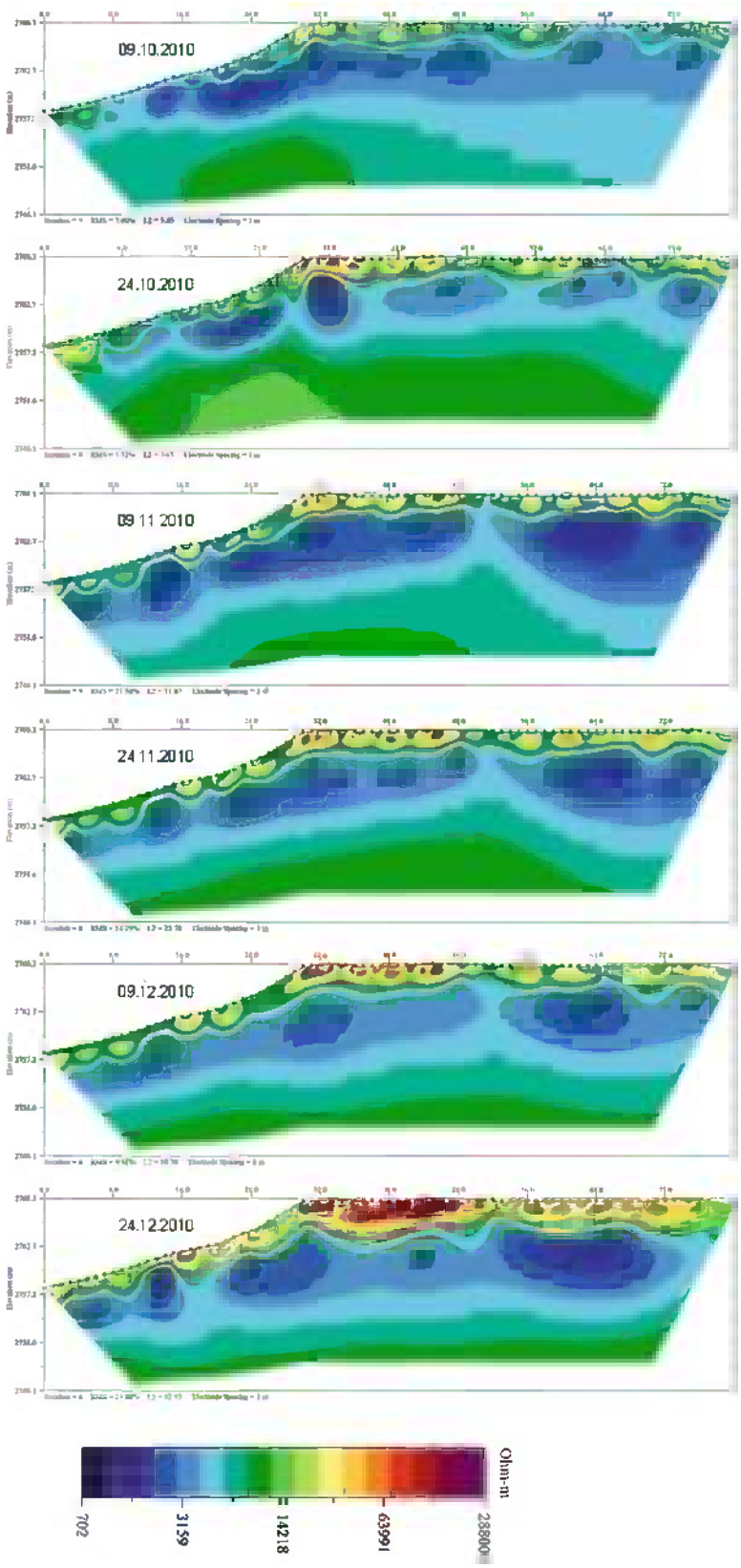


Fig. 5 Inversion results of permafrost monitoring between October 2010 and December 2010 at 15 days intervals

instability, triggered most probably by rain and/or snow melting and river erosion at the foot (Lovisolo 2010). The recent landslide was activated during 1994 rainfall event. It covers an estimated area of 150,000 m and comprises a displaced material of 1.2 million m (only the flow part). It endangers a regional highway and potential formation of a

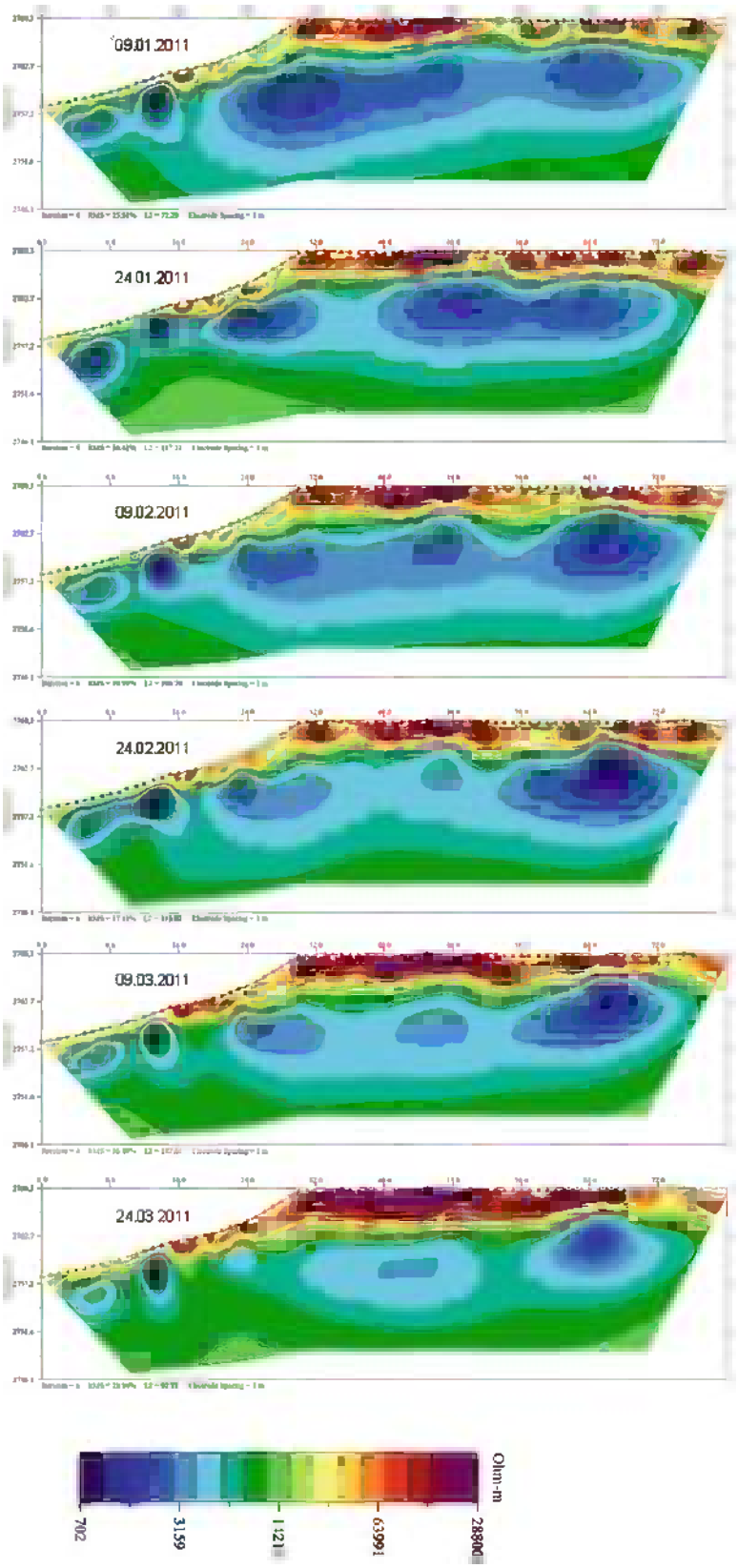


Fig. 6 Inversion results of permafrost monitoring between January 2011 and March 2011 at 15 days intervals

dam. DMS monitoring column 60 m long was installed in October 2008 and it allowed investigating several displacement events, based at a depth of 8 m b.g.l. A perched ground water level was registered at a depth of about 6.5 m b.g.l., which is probably the main triggering factor of the active sliding zone. The displacement has performed distinct relation to rainfall events or snow melting. Except that rather shallow movement, deep creep of the old landslide has been recognized about 30–44 m b.g.l. Total displacement recorded by DMS during the events between 2008 and 2010 was 600 mm. Subsequently, the GEOMON technique was installed there in 2010. The main aim of the monitoring is early warning for Civil Protection. The data of this site is currently being processed and will be shown at the conference.

The Mölltal Test Site

Changes of climate parameters due to global warming generate increased permafrost "warming" in Alpine regions, thus involving severe environmental and engineering problems. Underlying processes are still not completely understood.

The geoelectrical method could be the method of choice to monitor these processes. To test the GEOMON4D system for permanent monitoring in permafrost areas, a test profile was set up close to the Mölltal Glacier at an altitude of 2,770 m. Based on prior results several adoptions had to be made to the geoelectrical monitoring device (e.g. constant current injection, high sensitivity current sensor. . .) to make it suitable for measuring very high resistivities. The results of the monitoring period between October 2010 and March 2011 show a good correlation of resistivity variations with temperature changes and freezing processes. Especially within the first 3 m of the sub-surface, major changes due to freezing were recorded. In the area below, hardly any changes took place (see Figs. 5 and 6). Consequently we conclude that although the profile was located at 2,770 m, permafrost might not be present at medium depth due to the relatively low resistivities measured for the whole period.

Discussion and Conclusions

The preliminary results obtained within the first period of monitoring clearly highlight the possible potential of the geoelectric method to act as an additional indicator for developing subsurface processes. At the site of Gschliefgraben acceleration of movements were directly correlated with rainfall events and also with distinct resistivity and SP anomalies. However since the cause of the acceleration acted immediate, no prewarning intervals could be determined. On the contrary at the site of Ampflwang, a decrease of resistivity could be recognised several hours before an event. At the Ancona test site, variations of the hydraulic system could be monitored, although no significant movements were triggered. It can be concluded, that the first results obtained by the TEMPEL monitoring network are quite promising, however longer observation intervals and the occurrence of major events at some sites are necessary for investigating the correlation of parameters in detail.

Acknowledgments The authors would like to acknowledge the excellent cooperation with Torrent and Avalanche Control (WLV), Section Upper Austria, ZT Büro Moser/Jaritz, Gmunden (Austria), the Ancona Monitoring Center, KELAG and Jean-Philippe Malet from CNRS France. The study was supported by the 7th FP project "SafeLand—Living with the landslide risk in Europe" and the project "TEMPEL—Temporal changes of geoelectrical properties as possible indicator of future failure of high risk landslides", funded by the Austrian Science Fund (FWF)-TRP 175-N21.

References

Cardellini S, Osimani P (2010) Living with landslides: the Ancona case history and early warning system. In: Supper R, Baron I (eds) Landslide monitoring technologies & early warning systems, Berichte der Geologischen Bundesanstalt vol 82, pp 61–66, published by the Geological Survey of Austria

Cotecchia V (2006) The second Hans Cloos lecture, experience drawn from the great Ancona landslide of 1982. Bull Eng Geol Environ 65:1–41

Foglino L, Lovisolo M, Della Giusta A (2006) Contribution of DMS monitoring systems in the analysis of slide micro-movements for early warning management, risk assessment and evaluation of mitigating actions. Geophys Res Abstr 8:06122

Jaritz W, Reiterer A, Supper R (2004) Landslide Rindberg (Vorarlberg): multidiscipline research. In: Proceedings of the 10th interpraevent congress, Riva del Garda

Lovisolo M (2010) Bagnaschino landslide: from early warning to site-specific kinematic analysis. In: Supper R, Baron I (eds) Landslide monitoring technologies & early warning systems, Berichte der Geologischen Bundesanstalt, vol 82, pp 61–66, published by the Geological Survey of Austria

Supper R, Römer A (2003) New achievements in developing a high speed geoelectrical monitoring system for landslide monitoring. In: Proceedings of the environmental and engineering geophysical society. In: 9th meeting Prag, ISBN 8023913328 9788023913323

Supper R, Ahl A, Römer A, Jochum B, Bieber G (2008) A complex geo-scientific strategy for landslide hazard mitigation – from airborne mapping to ground monitoring. Adv Geosci 14:1–6

Supper R, Römer A, Jochum B (2009) Geoelectrical measurements for natural hazard monitoring. In: SEGJ 9th international symposium, Extended abstracts, Sapporo



Geophysical-Geotechnical Sensor Networks for Landslide Monitoring

Jonathan Chambers, Philip Meldrum, David Gunn, Paul Wilkinson, Andrew Merritt, William Murphy, Jared West, Oliver Kuras, Edward Haslam, Peter Hobbs, Catherine Pennington, and Chris Munro

Abstract

In this study we describe the development of an integrated geophysical/geotechnical sensor network for monitoring an active inland landslide near Malton, North Yorkshire, UK. The network is based around an automated time-lapse electrical resistivity tomography (ALERT) monitoring system, which has been expanded to incorporate geotechnical sensor arrays. The system can be interrogated remotely using wireless telemetry to enable the near-real-time measurement of geoelectric, geotechnical and hydrologic properties.

The overarching objective of the research is to develop a 4D landslide monitoring system that can characterise the subsurface structure of the landslide, detect changes in the slope, and reveal the hydraulic precursors to movement. Results to-date have shown that ALERT can characterise 3D landslide features, and detect changes associated seasonal temperature and subsurface moisture content changes, and crucially, the displacement of geophysical sensor arrays that allows the motion of the landslide to be monitored in near-real-time.

Keywords

Electrical resistivity tomography (ERT) • Sensor-network • Wireless • Telemetry • Monitoring

Introduction

Geoelectrical ground imaging techniques, such as electrical resistivity tomography (ERT) and self-potential are being increasingly applied to study landslide structure and the processes associated with slope failure (Jongmans and Garambois 2007). The great strengths of these techniques are that they provide spatial or volumetric subsurface information at the site scale, which, when calibrated with appropriate geotechnical and hydrogeological data, have the potential to characterise lithological variability and monitor hydraulic changes associated with failure events (Lebourg et al. 2005). Here we describe the development and application of an integrated geoelectrical and geotechnical monitoring network on an active landslide in the UK, with the aim of developing new investigative and predictive tools for slope assessment.

J. Chambers (✉) • P. Meldrum • D. Gunn • P. Wilkinson • O. Kuras • E. Haslam • P. Hobbs • C. Pennington • C. Munro
British Geological Survey, Geophysical Tomography, Nottingham NG12 5GG, UK
e-mail: Jonathan.Chambers@bgs.ac.uk

A. Merritt
British Geological Survey, Geophysical Tomography, Nottingham NG12 5GG, UK

School of Earth and Environment, University of Leeds, Leeds LS2 9JT, UK

W. Murphy • J. West
School of Earth and Environment, University of Leeds, Leeds LS2 9JT, UK

C. Margottini et al. (eds.), *Landslide Science and Practice*, Vol. 2,
DOI 10.1007/978-3-642-31445-2_37, © Springer-Verlag Berlin Heidelberg 2013

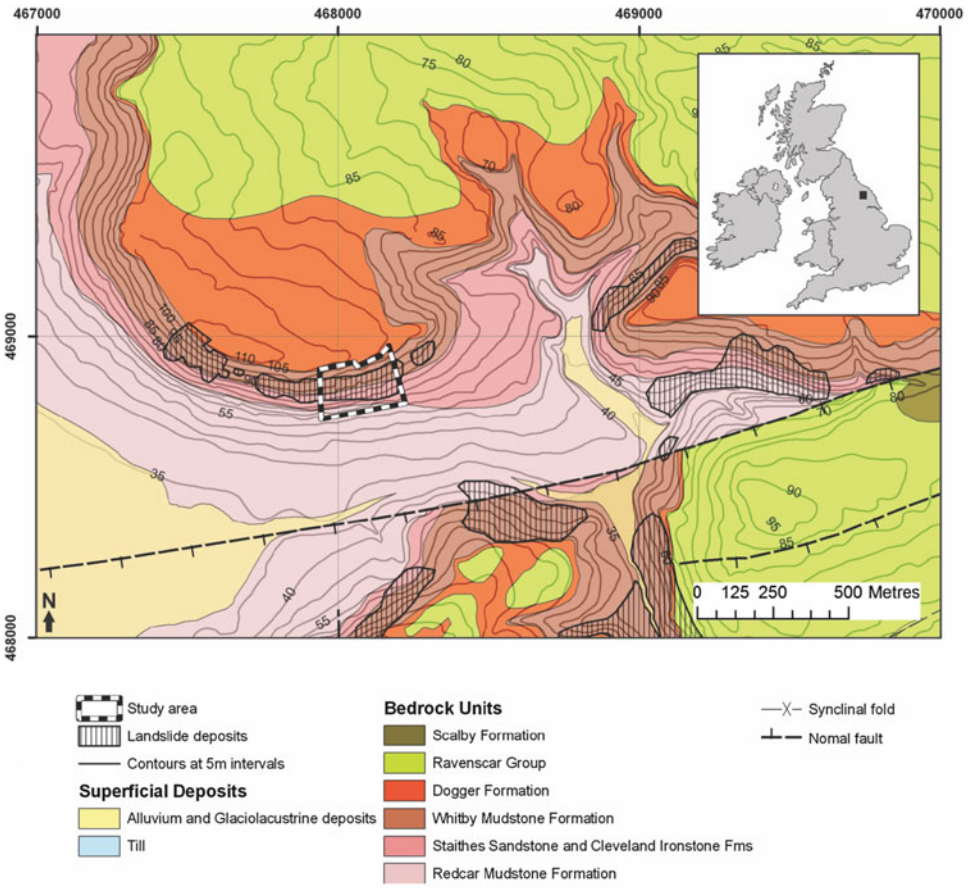


Fig. 1 Geological map based on the geological resurvey of the area, showing the location of the study site and the distribution of landslide deposits. Coordinate systems are given as British National Grid (*bold*) and latitude and longitude (*normal*). Inset map (*top right*) shows the location of the study site within the UK

Site Description

The research site is located near Malton, North Yorkshire, UK, on a south facing valley side with a slope of approximately 12 ° (Fig. 1). The bedrock geology (Ford in press), from the base to top of slope, comprises the Lias Group Redcar Mudstone Formation (RMF), Staithes Sandstone and Cleveland Ironstone Formation (SSF), and Whitby Mudstone Formation (WMF), which are overlain at the top of the hill by the Dogger Formation (DF). The bedrock is relatively flat lying with a gentle dip to the north. Slope failure at the site is occurring in the weathered WMF, which is highly prone to landsliding.

The landslide is characterized by shallow rotational failures at the top of the slope that feed into larger-scale slowly moving lobes of slumped material; the rotational features and active lobes extend approximately 150 m down the slope from the top of the hill, and extend laterally more than 1 km along the valley side. In recent years, movement of the lobes has been in the order of tens of centimetres per annum. Movement typically occurs in the winter months (i.e. January and February) when the slope is at its wettest. During this period water can be observed accumulating in the sag ponds caused by rotational slips towards the top of the slope, and can be seen emerging from the front of the lobes. Drainage from the site also occurs along a spring line at the base of the SSF, where groundwater runs off the surface of the less permeable underlying RMF. Piezometers installed at the site have revealed elevated pore pressures at the failure planes within the slipped WMF and at the interface between the slipped WMF material and the underlying SSF.

Methodology

Monitoring Instrumentation (ALERT)

Monitoring at the site is based around the ALERT (Automated time-Lapse Electrical Resistivity Tomography) survey concept (Kuras et al. 2009; Ogilvy et al. 2009; Wilkinson et al. 2010a). The ALERT system provides the full capability for remote measurement, storage and transmission of geoelectrical data. It has been designed as a single case unit that can be deployed at a remote location. Once set up at a monitoring site, the system is designed to operate autonomously (Fig. 2). It comprises several intelligent sub-systems that co-ordinate and control all the major functions: data collection, data storage, data transmission

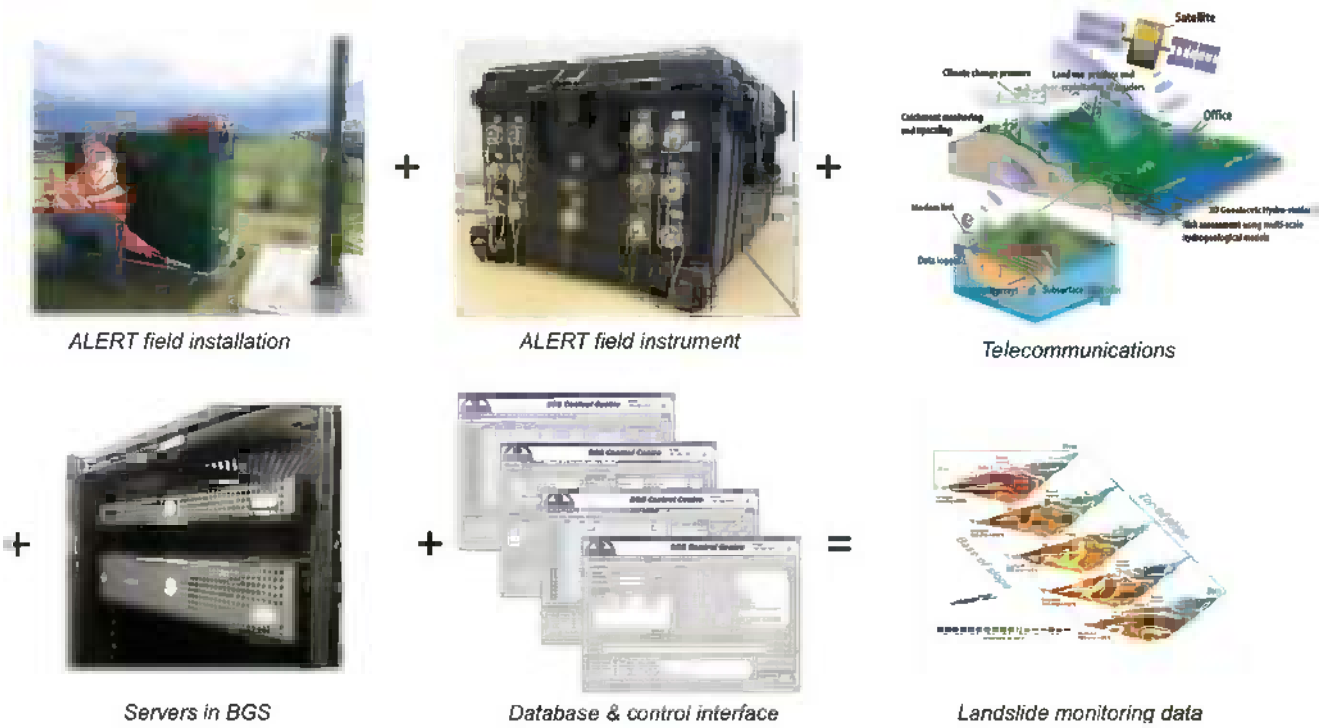


Fig. 2 ALERT (Automated time-lapse electrical resistivity tomography) concept overview

(to a remote host PC) and handling of data and control scheduling issues. The system is remotely configurable, with measurement commands and timings updated and changed by the user through Command Centre software run on a standard PC. The Command Centre software allows data to be automatically downloaded at given intervals from the measurement system. A data management scheme has been implemented that allows data to be automatically stored and catalogued in a database making it easily accessible for retrieval, processing and interpretation. Data transmission is via the TCP/IP protocol allowing the use of several existing types of remote telecommunications including GSM, PSTN, GPRS and 3G. Enhancements to the ALERT system at this site have included additional logging capability to address additional sensor types, including environmental and geotechnical sensors. The system is housed in a weatherproof enclosure and is powered by batteries charged by a wind turbine and solar panels, with back-up power supplied by a fuel cell.

Sensor Network

ERT electrode arrays were permanently installed within a grid with dimensions $x = 38$ m and $y = 147.25$ m (Fig. 3). Electrodes were separated by 4.75 m in the y-direction and by 9.5 m in the x-direction, and were installed in segments, each comprising 16 electrodes. This segmented design was used so that individual sections of the array are relatively easy to replace when breakage occurs due to ground movement. Each of the 16-way array segments and additional geotechnical and environmental sensors has been connected to the ALERT instrument located in the centre of the imaging area. A weather station, tilt meters, pressure transducers for pore pressure measurement, and multilevel temperature sensor arrays have been installed at the site.

Geoelectrical Data Collection and Inversion

The 3D ERT data sets are collected using a dipole-dipole array with dipole sizes (a) of 4.75, 9.5, 14.25, and 19 m and dipole separations (n) of 1a to 8a, and include a full set of reciprocal measurements. The data were inverted using l1-norm implementations of the regularized least-squares optimization method (Loke and Barker 1996). The forward problem was solved using the finite-element method, in which node positions were adjusted to allow topography to be taken into account in the inversion process (Loke 2000).

Property Interrelationships

Field observations are being supported by laboratory testingof site materials to establish geophysical-geotechnical property interrelationships for the calibration of the

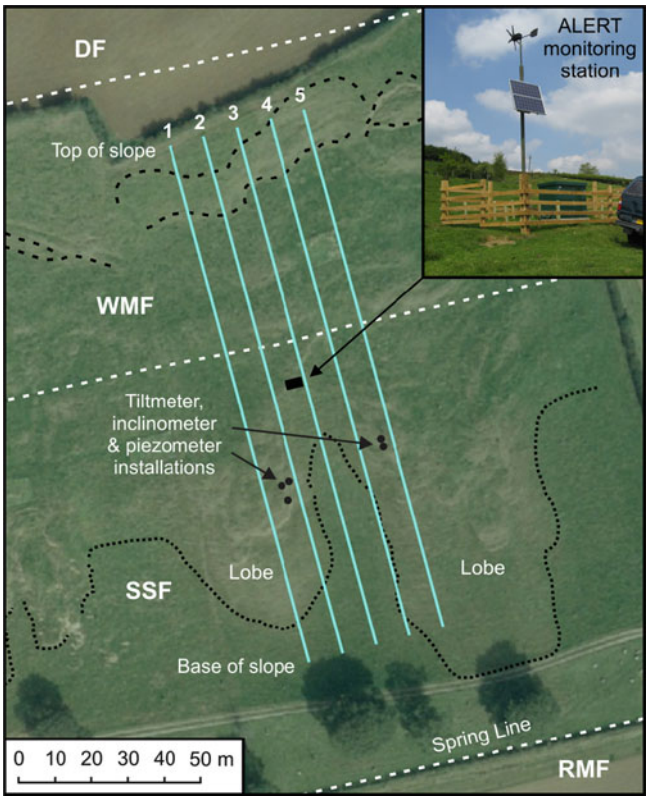


Fig. 3 Site plan showing the location of the ALERT station, ERT monitoring arrays (*blue lines*, numbered), major geomorphologic features (*top and base* of the main scarp—*black dashed lines*; toe of the earth flows—*dotted black lines*) and bedrock geological boundaries (*white dashed lines*) between the DF, WMF, SSF, & RMF (Aerial Photo © UKP/Getmapping Licence No. UKP2006/01)

time-lapse geophysical images (e.g. Cassiani et al. 2009). The aim of this testing is to establish resistivity-moisture content, and moisture content-pore pressure relationships for WMF and SSF.

Results

3D Characterisation

A 3D ERT model generated from data collected shortly after ALERT system installation is shown in Fig. 4. This model serves to both reveal the 3D structure of the landslide and provide a reference model for subsequent ERT monitoring events.

The succession from low resistivity RMF, to more resistive SSF, to low resistivity WMF is clearly displayed, and is consistent with borehole results for the site (Chambers et al 2011). The interface between the SSF and the WMF indicates a dip of ~5° to the north. The low surface resistivities (blue-green) of the 3D ERT model show the distribution and thickness of slipped WMF of the eastern and western lobes. Calibration using the intrusive data has allowed an improved interpretation of the extent of the landslide within the 3D ERT survey area. In this case, imaging of the buried interface between the SSF and the WMF has allowed the extent of the zones of depletion and zones of accumulation to be accurately determined.

Time-Lapse Monitoring

Preliminary time-lapse images generated from the electrodes on the western boundary of the imaging area are presented in Fig. 5, and include resistivity sections from August 2008 (t_1) and February 2009 (t_2), along with a difference plot showing the change during this period. These two times were chosen as they represent a dry period (t_1) and a wet period during which movement was occurring (t_2). A broad resistivity increase of ~20 % occurred in the top few metres (Fig. 5c) between t_1 and t_2. It is likely that this is due to seasonal temperature variations, which are masking the effects of increased moisture (which would normally decrease the resistivity) during the winter. Air temperatures in the 2 months leading up to t_1 and t_2 were on average 16 °C and 3.5 °C respectively. The magnitude and extent of these apparent temperature effects are broadly consistent with those observed by Hayley et al. (2007), assuming their empirical linear approximation of ~2 % change in resistivity per degree C, with seasonal air temperature influences extending to between 5 and 10 m below ground level. Monitoring using multi-level sensors is currently being undertaken within the imaging area to determine seasonal temperature changes in the subsurface; these data will be used to correct the time-lapse ERT image for temperature effects using the methodology described by Hayley et al. (2007).

Model resistivities decreased between t_1 and t_2, below depths of 5 m, with the most pronounced decrease having occurred in the region of the model where SSF was overlain by slipped WMF. This was at a depth where temperature should be constant, and so the decrease was probably due to increased moisture content resulting from drainage of water through the disturbed WMF into the SSF during the winter months. Laboratory testing of borehole core recovered from the site is being undertaken to determine the resistivity-moisture content relationships for the WMF and SSF, which will then be used to calibrate the resistivity model.

Significant variability in model resistivity changes were seen across the top of the model between $y = 35$ and 75 m. Walkover surveys revealed very significant fissuring and movement in this area during the monitoring period. Very substantial increases in moisture content were also observed in this region at t_2. Variability in the both the resistivity (Fig. 5b) and differential models (Fig. 5c) is likely to be a

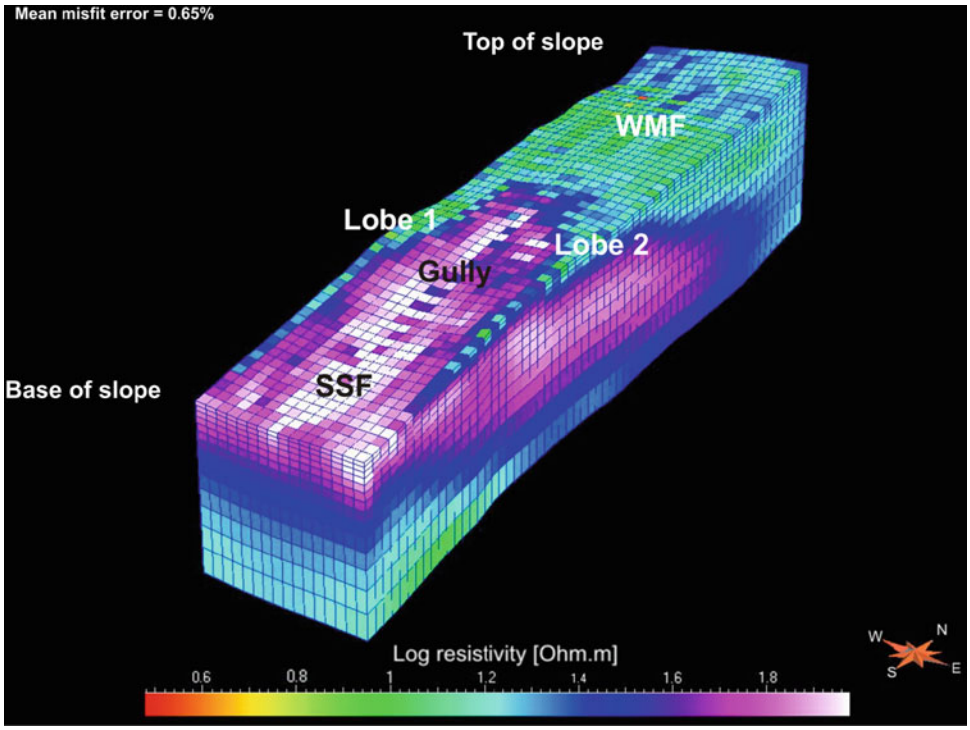


Fig. 4 Baseline 3D ERT model of the landslide generated from ALERT data

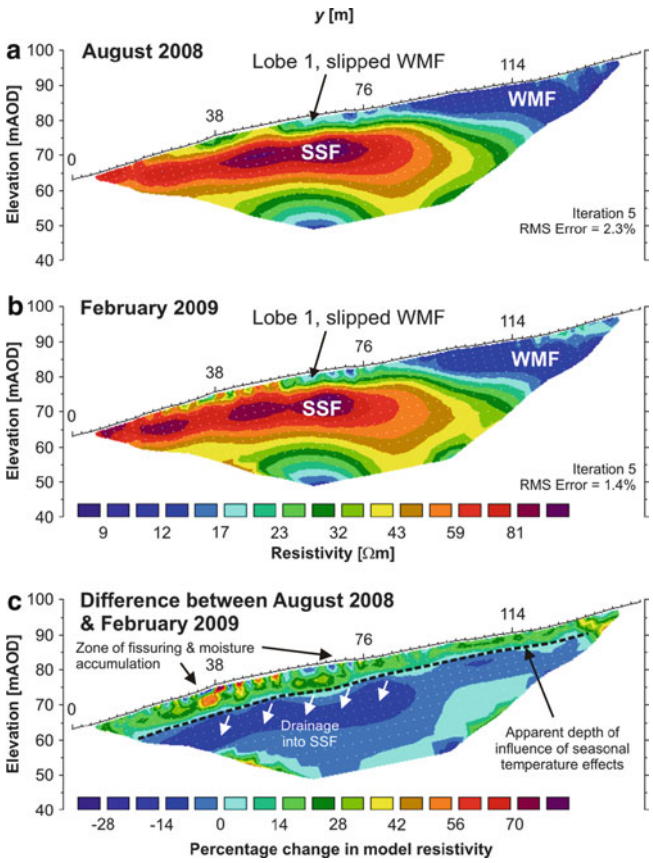


Fig. 5 Time-lapse resistivity results from dipole-dipole data (a = 4.75, 9.5, 14.25, and 19 m, and n = 1–8) shown as 2D resistivity sections through Lobe 1. (**a**) August 2008 and (**b**) February 2009 ERT models, and (**c**) resulting differential resistivity image

function of the changed subsurface structure and moisture distribution. It is also the case that the movement of electrodes, which has not yet been accounted for in the modelling, has also caused distortions in the resistivity image. Geometric corrections to account for electrode movement will be applied to future datasets using the methodology described in the following section.

Electrode Movement Monitoring

ERT monitoring is particularly well suited to studying landslide processes since resistivity is sensitive to changes in saturation. However, the measured potentials depend not only on the subsurface resistivity, but also on the positions of the electrodes. These are usually assumed to be known and fixed, but on an active landslide the electrodes will move over time, typically in the order of tens of cm/year in this case. If incorrect positions are used in the inversion (e.g. if the electrodes are not resurveyed after a period of movement) then artefacts will occur in the resulting image that can obscure genuine resistivity changes in the subsurface.

We have developed a method to estimate the displacements of the electrodes solely from time-lapse resistivity data (Wilkinson et al. 2010b). This has enabled us to track their movements over a complete seasonal cycle without repeated manual resurveying of their positions. Briefly the method calculates the ratio of the resistivity data at the present time to the data at a baseline time when the electrode positions were known. The ratio data are fitted to a simple

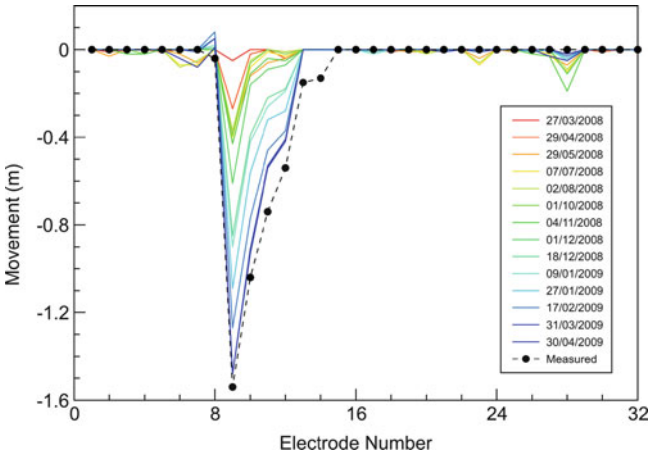


Fig. 6 Predicted downslope electrode movements between March 2008 and May 2009. The measured positions in August 2009 are shown by *filled circles*. The electrode number increases to the north (i.e. up the slope)

model which incorporates electrode movement and layered resistivity changes consistent with those caused by seasonal temperature variations. This model is inverted to yield the estimated electrode movements from their baseline positions. The algorithm currently only works in the longitudinal direction, and does not account for small-scale resistivity changes, but we have found that the predicted movements are accurate to within 4 % of the unit electrode spacing. This is sufficient to track the electrodes over time and to correct any artefacts in the resistivity images caused by using the wrong positions. An example of the predicted movements as a function of time is shown in Fig. 5. The data were measured on line 1, which crosses one of the active earth flows, for just over 1 year and the results match the expected seasonal behaviour (no movement during the spring and summer months, but significant activity during late autumn and winter). Our research is ongoing into combining resistivity and position inversion in a single model and incorporating lateral movement, both of which should improve the accuracy of the results (Fig. 6).

Summary

A fully operational geophysical/geotechnical monitoring system has been installed on an active landslide in the UK. Initial results have demonstrated that the system can reveal 3D structure of the landslide and monitor temporal changes in the slope, including changes in moisture content and the movement of the landslide. The long-term goal is to produce calibrated 3D models of the subsurface moisture content variations from the time-lapse resistivity data. This will require petrophysical resistivity-saturation and resistivity-temperature relationships, derived from in-situ monitoring and laboratory studies.

Acknowledgments We would like extend our sincerest gratitude to Mr. and Mrs. Gibson (the landowners) for their involvement and cooperation in this research. This paper is published with permission of the Executive Director of the British Geological Survey (NERC).

References

Cassiani G, Godio A, Stocco S, Villa A, Deiana R, Frattini P, Rossi M (2009) Monitoring the hydrologic behaviour of a mountain slope via time-lapse electrical resistivity tomography. Near Surf Geophy 7(5–6):475–486

Chambers JE, Wilkinson PB, Kuras O, Ford JR, Gunn DA, Meldrum PI, Pennington CVL, Weller AL, Hobbs PRN, Ogilvy RD (2011) Three-dimensional geophysical anatomy of an active landslide in Lias group mudrocks, Cleveland Basin, UK. Geomorphology 125:472–484

Ford JR Geological map of the high Stittenham Area (Sheet SE66NE). British Geological Survey, Nottingham, UK (in press)

Hayley K, Bentley LR, Gharibi M, Nightingale M (2007) Low temperature dependence of electrical resistivity: implications for near surface geophysical monitoring. Geophys Res Lett 34:L18402

Jongmans D, Garambois S (2007) Geophysical investigation of landslides: a review. Bull Soc Geolog France 178(2):101–112

Kuras O, Pritchard JD, Meldrum PI, Chambers JE, Wilkinson PB, Ogilvy RD, Wealthall GP (2009) Monitoring hydraulic processes with automated time-lapse electrical resistivity tomography (ALERT). CR Geosci 341(10–11):868–885

Lebourg T, Binet S, Tric E, Jomard H, El Bedoui S (2005) Geophysical survey to estimate the 3D sliding surface and the 4D evolution of the water pressure on part of a deep seated landslide. Terra Nova 17(5):399–406

Loke MH (2000) Topographic modelling in electrical imaging inversion EAGE. In: 62nd conference and technical exhibition, Glasgow, Scotland

Loke MH, Barker RD (1996) Practical techniques for 3D resistivity surveys and data inversion. Geophys Prospect 44(3):499–523

Ogilvy RD, Meldrum PI, Kuras O, Wilkinson PB, Chambers JE, Sen M, Pulido-Bosch A, Gisbert J, Jorreto S, Frances I, Tsourlos P (2009) Automated monitoring of coastal aquifers with electrical resistivity tomography. Near Surf Geophys 7(5–6):367–375

Wilkinson PB, Meldrum PI, Kuras O, Chambers JE, Holyoake SJ, Ogilvy RD (2010a) High-resolution electrical resistivity tomography monitoring of a tracer test in a confined aquifer. J Appl Geophys 70(4):268–276

Wilkinson PB, Chambers JE, Meldrum PI, Gunn DA, Ogilvy RD, Kuras O (2010b) Predicting the movements of permanently installed electrodes on an active landslide using time-lapse geoelectrical resistivity data only. Geophys J Int 183(2):543–556



Remedial Works on the Smrečje Landslide, Croatia

Željko Arbanas, Vedrana Galijašević, Petra Đomlija, and Martina Vivoda

Abstract

The Smrečje Landslide was occurred on the county road near the Gerovo village in Gorski Kotar region, Croatia, before more than 10 years. The landslide location is forming in clastic formations of shale, sandstone and marl rock masses from Triassic age. The landslide was overtaken 100 m long part of the road construction. The instability was evidenced in long term creep process with deformation increments associated with the seasonal water content variations in the clayey superficial deposit. Deformations on the pavement construction were reaching unacceptable values during 2008 that caused necessity of complete landslide remediation. Field investigations were executed and the remediation measures were designed. Field investigations were included investigation drilling, soil and rock mass samples taken, geophysical measurements using seismic refraction and geoelectrical tomography techniques so as engineering geological surface mapping. In the paper we will present description of the Smrečje landslide, results of the conducted field investigations, so as designed remediation measures. Based on the remediation design, the remediation works were constructed in the spring 2009.

Keywords

Field investigation • Remediation • Retaining wall • Drainage • Monitoring

Introduction

The Smrečje Landslide was occurred on the county road near the Gerovo village in Gorski Kotar region before more than 10 years. The instability was evidenced in long term creep process with deformation increments associated with the seasonal water content variations in the clayey superficial deposit. Movements were overtaken 100 m long part of the road construction and caused cracks and subsidence on the pavement construction. Integral remedial works weren't executed during long time period of creep deformation, excluding emergency measures of pavement reparation with new asphalt layers adding. Increasing of deformations on the pavement construction was reaching unacceptable values in the spring 2008 that caused necessity of the complete landslide remediation. To determine the geological setting, dimension and mechanism of the instability occurrence, as a base for remediation, the field investigations were conducted. Field investigations were included investigation drilling, soil and rock mass samples taken, geophysical measurements using seismic refraction and electric resistivity techniques so as engineering geological surface mapping. Inclinometers and piesometers were installed in boreholes immediately after drilling, and monitoring of the landslide was started.

Using results of conducted field investigations, the geotechnical model was established and soil and rock properties were determined. Back analysis to determine the strength

Ž. Arbanas (✉) • P. Đomlija • M. Vivoda
Faculty of Civil Engineering, Rijeka, University of Rijeka,
Viktora Cara Emina St. 5, Rijeka 51000, Croatia
e-mail: zeljko.arbanas@gradri.hr

V. Galijašević
Department of Geotechnics, Civil Engineering Institute IGH,
Slavka Tomašića St. 5, Rijeka 51000, Croatia

C. Margottini et al. (eds.), *Landslide Science and Practice*, Vol. 2,
DOI 10.1007/978-3-642-31445-2_38, © Springer-Verlag Berlin Heidelberg 2013

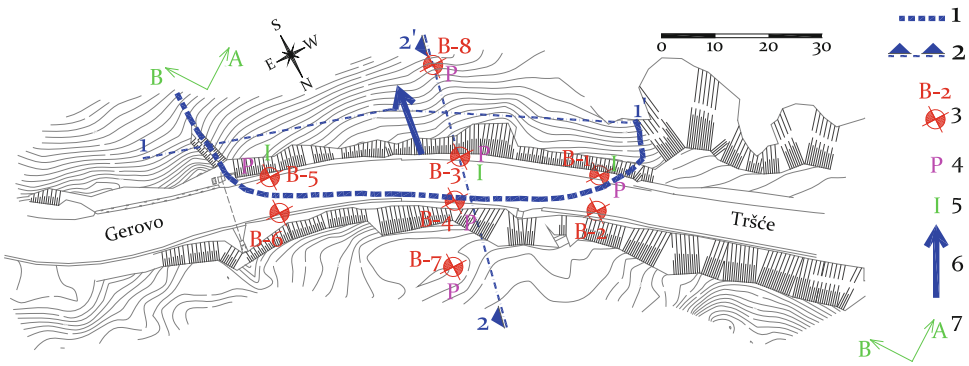


Fig. 1 Map of the Smrečje Landslide witht: (*1*) tension crack, (*2*) engineering geological cross section position, (*3*) borehole position, (*4*) piezometer position, (*5*) inclinometer position, (*6*) sliding direction, (*7*) directions of inclinometer measuring

parameters of the soil on slip surface, and stability analysis for the remediation measures were carried out using GEO Slope, Slope/W software. Remedial works were designed and conducted to stop further sliding and to increase general stability of the slope. Cantilever retaining wall in the toe of the landslide and boring drain system above the road were constructed.

Field Investigation and Geological Properties of the Landslide

The tectonical base of geological unit Gorski Kotar is composed of Jurassic limestones, covered by Palaeozoic and Triassic clastic sediments and all the deposits are of allochthonuous position (Velić and Vlahović 2009). The bedrock consists of ritmical deposited sandstones, shales and siltstones with occasional interbedded of conglomerate layers. Sandstones and siltstones are the main lithological components and are strongly tectonized. The clastic rock masses are intensively subjected to mechanical and chemical weathering, and therefore the slopes are covered with thick layer of colluvial deposits. During the morphological evolution of the slope accumulated material was formed by the processes of erosion, physical and chemical weathering and gravitational transport from hypsometrically higher parts of the slope (Aljinović et al. 2003).

Field Investigations

To determine the geological setting, dimension and mechanism of the instability occurrence, as a base for remediation, the field investigations were conducted. Field investigations were included investigation drilling, soil and rock mass samples taken, geophysical measurements using seismic refraction and electric tomography techniques so as engineering geological surface mapping. The ability of engineering geological mapping was reduced since the slope is being covered with thick layer of superficial deposits.

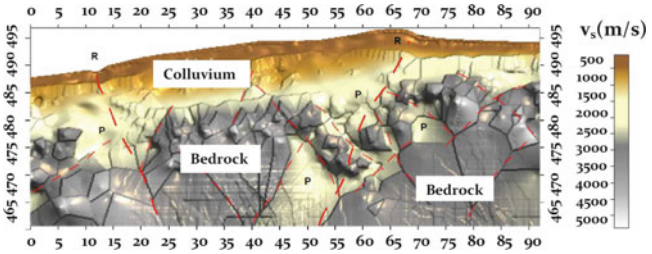


Fig. 2 Seismic refraction cross-section 1-1′. Embankment fill and colluvial deposits 0–1,000 m/s; bedrock 1,000–5,000 m/s

Eight investigation boreholes of depth from 10 to 12 m were drilled (Fig. 1) and representative soil and rock samples were chosen and tested in the laboratory. The geophysical methods of investigation, surface seismic refraction and geoelectrical tomography, were combined. The geoelectrical tomography survey was used to determine the litological characteristics of deposits, while the seismic refraction method is being used to obtain the information about distribution of soil and rock mass layers so as a degree of rock mass weathering.

Inclinometers and piesometers were installed in boreholes immediately after drilling (Fig. 1), and monitoring of the landslide was started.

Engineering-Geological Properties of the Slope

The investigated landslide is being situated on the slope generally inclined toward southwest with an average dip of 15 °. Since the location is being covered with slope deposits the geological fabric could be established from the borehole core so as results of geophysical surveying. Because of complex geological setting, the main source to geological cross-section establish were results of the surface seismic refraction and electric tomography (Figs. 2 and 3). It was determined that the geological cross-section consists of embankment fill, colluvial deposits and clastic rock mass in the bedrock (Fig. 4).

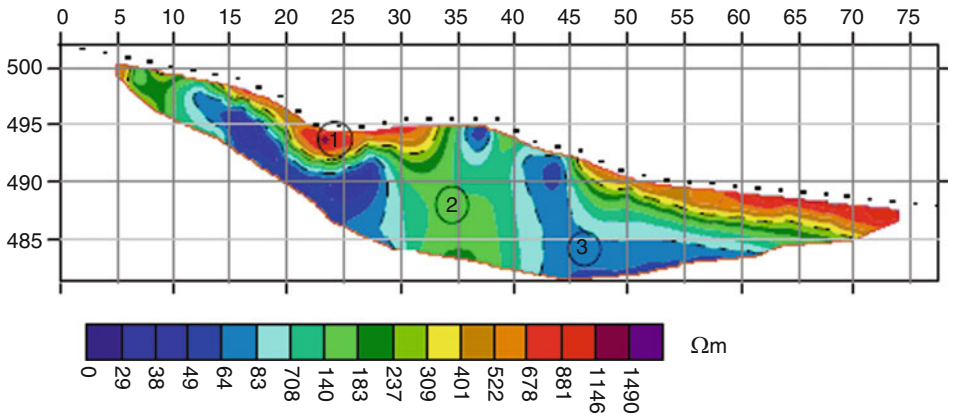


Fig. 3 Geoelectric tomography cross-section 2-2′: (*1*) embankment fill, (*2*) shales and siltsones in alternation with thin layers of weathered sandstone, (*3*) colluvial deposits

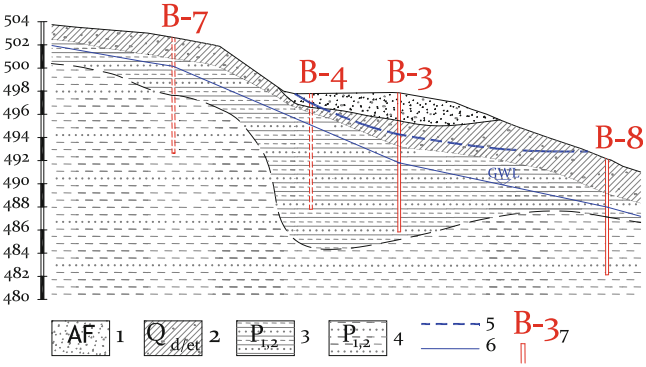


Fig. 4 Engineering geological cross-section 2-2′: (*1*) AF—embankment fill, (*2*) Q—colluvial deposits, (*3*) $P_{1,2}$—shales in alternation with thin layers of weathered sandstone, (*4*) $P_{1,2}$—siltstone with thin layers of weathered sandstone, (*5*) slip surface, (*6*) groundwater level, (*7*) borehole mark

The embankment fill consists of the mixture of the stone blocks and fragments originally from the bedrock and different content of brownish to grayish silty clay. The thickness of the fill varies from 0.80 to 2.40 m, and is present only at the area of the road embankment.

Slope deposits consists of colluvial material, composed of brown gray to yellow high plasticity clayey silt (MH), with high content of stone fragments. This material is the product of intensive weathering process of the clastic rock mass. The thickness varies from 0.20 m in the upper part of the slope to 3.00 m determined in the boreholes in the lower part of the landslide body.

The clastic bedrock consists of very heterogeneous composition of dark gray to black shales and dark gray siltstones from the Palaeosoic age, from the lower to the middle Permian period ($P_{1,2}$) (Aljinović et al. 2003). The rock mass is thinly stratified and laminated with the bed thickness from few millimeters to few centimeters. Shales are highly weathered than the siltstones; in the zones close to the bedrock surface the rock mass is medium to highly weathered (MW/HW) (ISRM 1978). In deeper parts the shale's rock mass is predominantly slightly weathered (SW). Siltstones are most slightly to medium weathered (SW/MW). The shales and siltstones contain the blocks and thin layers of highly weathered sandstones. Relating to different weathering grades, the thickness of the weathering zone differs, and it is difficult to define the boundary between the bedrock and colluvial deposits with high content of rock mass fragments (Arbanas et al. 2004).

Geotechnical Properties of Landslide

During the morphological evolution of the slope accumulated material was formed by the processes of erosion, physical and chemical weathering and gravitational transport from hypsometrically higher parts of the slope. The position of the slip surface, on the contact between superficial deposit and the bedrock, is the direct result of the geological fabric of deposits.

The instability was evidenced in long term creep process with deformation increments associated with the seasonal water content variations in the clayey superficial deposit during 10 years period before investigation. The most of deformations were occurred during the spring seasons after snow melting and the rate of deformation decreased during the summer seasons with smaller amounts of precipitations. Deformations were overtaken 150 m long part of the road construction and caused cracks and subsidence on the pavement construction but without visible continuous open tensile crack that could define position of landslide crown. It was also very hard to determine mechanism and position of slip surface and predict possible development of the phenomena. The road maintenance office was decided for pavement construction reparation with new asphalt layers adding

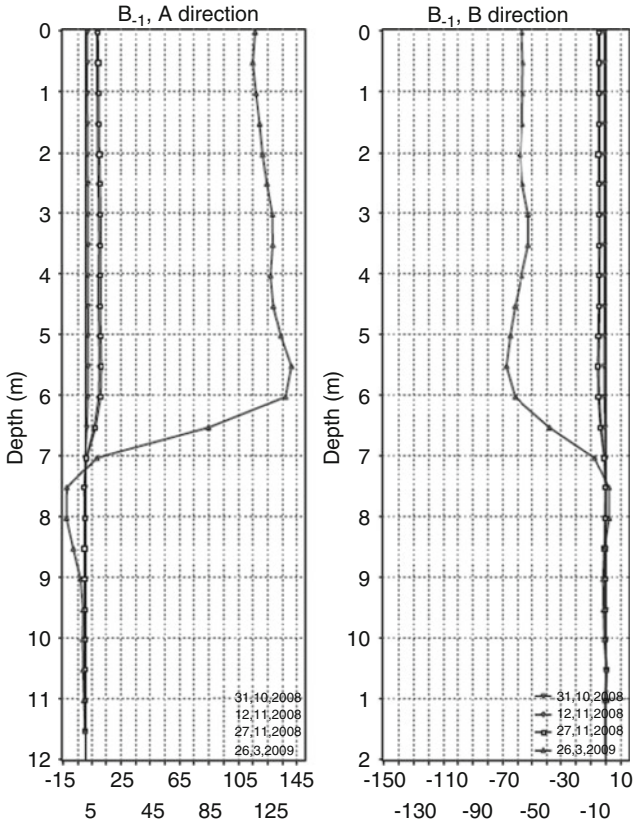


Fig. 5 Measured displacements (in mm) on inclinometer in borehole B-1 in A and B direction

without field investigations and systematic landslide remediation. Finally, in the autumn 2008, deformations on the pavement construction were reaching unacceptable values and progressive damages of the road. The traffic was stopped, and it was necessary to start field investigations and complete landslide remediation works.

Field investigations were executed but some of existing vagueness weren't solved. It wasn't clear mechanism of the movement: lack of visible continuous open tensile crack that could define position of landslide crown and undeterminable position of slip surface from borehole cores pointed on long term creep mechanism in the slope. The problem was solved using monitoring results from installed inclinometers (Fig. 1). The measured displacements after inclinometer installation were relatively small until the first more significant snow melting in spring 2009; measured displacements clearly indicate position of slip surface (Fig. 5).

Using results of conducted stability back analyzes and adopted position of slip surface on the inclinometers position, it was possible to determine probable position of landslide body. The proposed position of the landslide body was confirmed during the road reconstruction. Since the landslide body was not clearly expressed, it was hard to precisely define all elements of the landslide, and some elements were assumed (IAEG 1990):

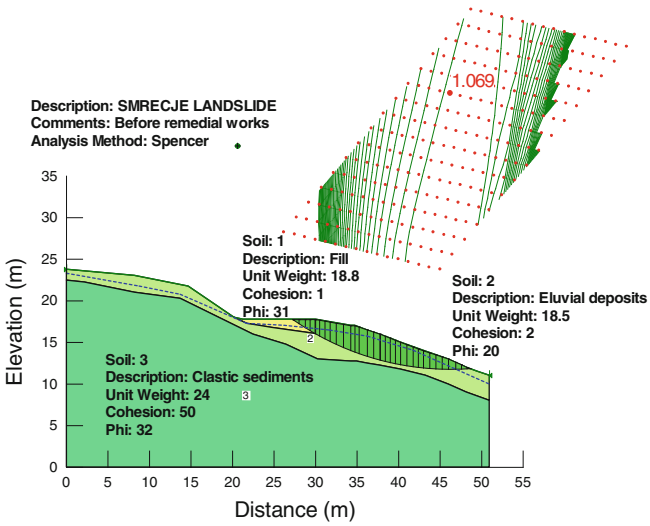


Fig. 6 Slope stability back analyzes for the postion of the assumed slip surface

- Total landslide length L = 20 m;
- Length of the displaced mass L_d = 20 m;
- Length of the slip surface L_r = 24 m;
- Width of the displaced mass W_d = 60 m;
- Width of the slip surface W_r = 60 m;
- Thickness of the displaces mass D_d = 6.0 m;
- Depth of the slope surface D_r = 6.0 m;
- Total height ΔH = 6 m;
- The average incline of the slope α = 15 °.

Considering the properties of material and slope morphogenesis, landslides in such environments are usually of retrogressive type (Cruden and Varnes 1996). The sliding process is developing from the bottom of the slope towards its top, and this presumption was taken into account during remediation designing.

Slope Stability Analyses

After geotechnical field and laboratory investigation works and determination of the engineering geological cross-section and geotechnical model of the landslide, slope stability analyses were done in order to confirm satisfying stability for predicted remedial measures. Back stability analysis to determine the strength parameters of the soil on slip surface, and stability analysis for the remediation measures were carried out using GEO Slope, Slope/W software (GEO-Slope 2002).

Back stability analyses for the present slope conditions were made. Groundwater level was assumed from the measurements in installed piezometers. Strength parameters for soil layers were confirmed for critical slip surface corresponds to the position of assumed instability (Fig. 6).

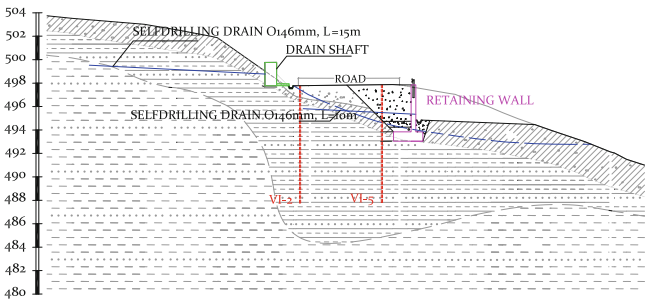


Fig. 7 Cross section 2-2′ with designed retaining wall and boring drains

Remedial works were designed to stop further sliding and to increase general stability of the slope. The remedial works design was predicted cantilever retaining wall in the toe of the landslide and boring drain system above the road. For average strength parameters determined in back analyzes, slope stability analyzes including remediation measures were carried out resulting with satisfying factors of safety with value greater than 1.5.

Remedial Works on the Smrečje Landslide

Design of landslide remediation was proposed two main measures: (1) increasing shears resistance on the slip surface; and (2) reduce the pore pressures on the slip surface by lowering groundwater level in the slope.

To increasing shears resistance on the slip surface, the construction of the retaining wall at the edge of the road was chosen. Proposed reinforced concrete retaining wall was designed and constructed as cantilever wall founded in the bedrock. The cantilever foot of the wall was positioned below the road embankment and the mass of this part of embankment significantly increase overall stability of construction (Fig. 7). The wall is predicted in the total length of 80.00 m and it is from 4.00 to 6.60 m high.

Reducing of pore pressure on the slip surface consequently induce increasing of effective normal stresses and shear strength of the soil. To lower groundwater level, two rows of boring drains were designed: the upper line of 15 m long drains bored in the slope above the road; and second line of 10 m long drains bored trough retaining wall (Fig. 7). Distance between drains is 6 m.

Remedial works construction was started in the spring 2009. The remediation measure were performed in accordance with proposed construction plan: (1) groundwater level decreasing by boring drains installation in upper part of the slope; (2) retaining wall construction and replacing existing fill behind the retaining wall with crushed stone material; (3) boring drains installation trough retaining wall;



Fig. 8 Retaining wall construction on the Smrečje landslide, summer 2009

(4) construction of surface water drainage system using drainage trenches and open channels; and (5) remediation of the pavement construction. The most important part of remediation was the stage of retaining wall construction. By excavation for retaining wall construction, the significant part of material in the landslide toe was removing, that could be important in state of overall landslide stability. This part of remediation was performed with precautions: the retaining wall was constructed in very short sections and in very short construction time (Fig. 8).

The remedial works were finished in the summer 2009, before the rainy period. The sliding was successfully stopped without significant changes in proposed design.

Conclusions

The Smrečje Landslide was occurred on the county road near the Gerovo village in Gorski Kotar region before more than 10 years. The instability was evidenced in long term creep process with deformation increments associated with the seasonal water content variations in the clayey superficial deposit. Movements were overtaken 100 m long part of the road construction and caused cracks and subsidence on the pavement construction. Integral remedial works weren't executed during long time period of creep deformation, excluding emergency measures of pavement reparation with new asphalt layers adding. Increasing of deformations on the pavement construction was reaching unacceptable values in spring 2008 that caused necessity of the complete landslide remediation. To determine the geological setting, dimension and mechanism of the instability occurrence, as a base for remediation, the field investigations were conducted. Performed field investigations included investigation drilling, soil and rock mass samples taken,

geophysical measurements using seismic refraction and electric resistivity techniques so as engineering geological surface mapping. Field investigations were executed but some of existing vagueness weren't solved. It wasn't clear mechanism of the movement: lack of visible continuous open tensile crack that could define position of landslide crown and undeterminable position of slip surface from borehole cores pointed on long term creep mechanism in the slope. The problem was solved using monitoring results from installed inclinometers, based on measured displacements.

Design of landslide remediation was proposed two main measures: (1) increasing shear resistance on the slip surface; and (2) reduce the pore pressures on the slip surface by lowering groundwater level in the slope. To increasing shears resistance on the slip surface, the construction of the retaining wall at the edge of the road was chosen. To decrease groundwater level, two rows of boring drains were designed: the upper line drains bored in the slope above the road; and second line drains bored trough retaining wall.

The remedial works were finished in the summer 2009, and the further sliding was successfully stopped without significant changes in proposed design.

References

Aljinović D, Sremac J, Ibrahimpašić H (2003) Permian and lower triassic facies of velebit Mt. and the Gorski Kotar region (NW part of external Dinarides). In: Proceedings of 22nd IAS meeting of sedimentology, Opatija 2003. Field trip guidebook, Institute of Geology, Zagreb, pp 185–206

Arbanas Ž, Benac Č, Jardas B (2004) Landslides in the Čabranka river valley, Croatia. landslides: evaluation and stabilization. In: Lacerda WA, Erlich M, Fontoura SAB, Sayao ASF (eds) Proceedings of 9th international symposium on landslides, Rio de Janeiro, Brazil. Taylor & Francis Group, London, pp 909–911

Cruden DM, Varnes DJ (1996) Landslide type and processes. In: Turner AK, Schuster RL (eds) Landslides: investigation and mitigation, vol 247, Special report. National Academy Press, Washington, DC, pp 36–75

GEO-Slope (2002) User's guide GEO-slope analysis, slope/W, version 5.13. GEO-Slope, Calgary, Alberta, Canada

IAEG (1990) Suggested nomenclature for landslides. Bull Eng Geol Environ 41:13–16

ISRM, Commission on Standardization of Laboratory and Field Test (1978) Suggested methods for the quantitative description of discontinuities in rock masses. Int Jour Rock Mech Min Sci & Geomech Abstr 15: 319–368

Velić I, Vlahović I (2009) Basic geological map of Croatia M 1:300.000. Croatian Geological Survey, Zagreb



Monitoring Slow-Moving Landslides Using Spatially Adaptive Least Squares Image Matching

Misganu Debella-Gilo and Andreas Kääb

Abstract

This study presents and evaluates an algorithm which uses the least squares image matching (LSM) with spatially adaptive and high-order geometric models to estimate horizontal surface displacements of slow-moving landslides from repeat optical images. Pairs of high resolution optical images over a rockglacier creep and a slow-moving landslide are orthorectified and co-registered. Image matching is applied first using the conventional normalised cross-correlation (NCC), then using the LSM algorithm with image-wide single geometric models, and finally using the LSM with spatially adaptive geometric models. The spatially adaptive algorithm operates in such a way that for each template the model that produces the lowest sum of square of intensity difference is considered the best fitting model. Affine, projective and second-degree polynomial geometric models are included. The algorithms are evaluated in reference to the NCC algorithm based on the signal-to-noise ratio of reconstructing the reference image from the search image.

Keywords

Image matching • Least squares • Spatially adaptive • Landslide • Rockglacier

Introduction

One of the techniques with which slope stability is monitored is remote sensing. Most commonly, repeat images are matched and the displacement and deformation of the masses are computed from the change in position and geometry (e.g. Delacourt et al. 2004; Kaufmann and Ladstädter 2003; Kääb et al. 1997). The most widely used image matching method is the area-based method in which image patches, usually of square shape and certain size, are matched using a given similarity measure such as the normalized cross-correlation (NCC). The patch that maximizes similarity or minimizes dissimilarity (depending on the statistic used) is considered as the most likely match. Displacement is then computed as the Euclidean distance between the template's position in the reference and the matching images.

Often used of the similarity measures is the NCC due to the normalization that makes it insensitive to differences in illumination and brightness. However, the NCC is subject to a number of shortcomings. It is only reliable in cases where there is no significant deformation within the template as it does not account for such deformations. It does not account for radiometric differences as well except normalizing it. Besides, the precision with which the matching position is located is limited to the pixel size unless some sub-pixel-precision algorithms (Debella-Gilo and Kääb 2011) are applied.

In response to these shortcomings of the NCC and the other area-based similarity measures, the Least Squares Matching (LSM) was developed (Förstner 1982). The basis for its development is that the geometric distortion of the image patches being matched is not always represented best by rigid body motion but by other geometric transformation models. The LSM adjusts the shape, size and orientation of

M. Debella-Gilo (✉) • A. Kääb
Institute of Geosciences, University of Oslo, Oslo, PO Box 1047, Norway
e-mail: m.d.gilo@geo.uio.no

C. Margottini et al. (eds.), *Landslide Science and Practice*, Vol. 2,
DOI 10.1007/978-3-642-31445-2_39, © Springer-Verlag Berlin Heidelberg 2013

the matching template using spatial transformation parameters until a template that has the least sum of square difference (SSD) with the reference is found. The matching template can therefore be located at sub-pixel positions leading to higher precision of the estimated displacement.

There is little application of this powerful image matching approach in mass movement analysis as image matching itself is young in this area. The limited applications so far (Kaufmann and Ladstädter 2003; Maas et al. 2010; Whillans and Tseng 1995) use only one geometric model, namely the affine model. The affine model incorporates movements that involve change in position, linear and constant changes in size in each direction (i.e. scaling), and shearing. However, Earth surface masses can also be tilted, bent and deformed non-linearly depending on the form, process and material of the slope. The problem gets more complicated as in reality the pattern of deformation can vary spatially on a slope. One geometric model may thus not fit to all deformation types on a slope.

This study aims at applying LSM with spatially adaptive geometric models to the displacement measurement of slow-moving landslide and rockglacier creep. The geometric models are extended from affine to the projective and second degree polynomial models. The algorithms are evaluated based on their performance in reconstructing the reference image from the search image.

The LSM in Mass Movement Analysis

The application of the least squares solution to image matching was first introduced by (Förstner 1982) in one dimension out of concern for geometric precision of the then existing image matching methods. The method was later extended to 2D with further modifications (Ackermann 1984; Gruen and Baltsavias 1987) and then 3D (Gruen and Akca 2005). The procedures for more advanced geometric models, i.e. projective and second degree polynomials are also worked out (Bethmann and Luhmann 2010). The following outline is adapted from these earlier works.

Let's assume that a discrete two-dimensional function F(x, y) represents intensity data of a subset of an image taken over a certain area at a time t_1 and G(x′, y′) is that of a subset of another image taken over the same area at some other time t_2. In principle, if the two subsets (hereafter referred to as reference and search templates respectively) match, the two functions will be equal. However, due to the likely presence of noises in both images, random noise (e) is added (1). In an ideal situation e or its expectation equals zero. In the displacement measurement of Earth surface mass movements such as slow-moving landslide, the two images are often taken with wide temporal baselines. Consequently, there exist other sources of radiometric differences that can even create some systematic radiometric changes due to various factors such as changes in surface conditions, illumination, noise, imaging conditions, and geometric distortions. It is often assumed that the systematic radiometric differences can satisfactorily be accounted for by gain (λ) and offset (η) parameters as in (2).

$$F(x,y) = G\left(x^{'},y^{'}\right) + e \tag{1}$$

$$F(x,y) = G\left(x^{'},y^{'}\right)\lambda + \eta + e \tag{2}$$

When the reference template has moved to a new location, it might have changed geometrically. Some kind of geometric transformation function, characterized by a set of parameters (p_i), relates the pixels of the reference template to that of the search template for each dimension ((3) and (4) and writen in matrix for as in (5)). The relationship between the two intensity data will now accommodate this spatial transformation (6). The transformation models considered here are presented in Fig. 1. A section of the aerial photographic images over the Muragl rockglacier (400 m × 600 m) taken on 7 September 1981 (left), and QuickBird panchromatic satellite image over the La Clapiére landslide (1,600 m × 2,430 m) taken on 06 September 2003 (right)

Table 1 together with their parameters whose values are unknown a priori.

$$x = f_x(x^{'},y^{'}) \tag{3}$$

$$y = f_y(x^{'},y^{'}) \tag{4}$$

$$[P1\ldots Pn]\begin{bmatrix}x'\\y'\end{bmatrix} = \begin{bmatrix}x\\y\end{bmatrix} \tag{5}$$

$$F(x,y) = G\left(f_x\left(p_1,\ldots,p_n,x^{'},y^{'}\right),f_y\left(p_1,\ldots,p_n,x^{'},y^{'}\right)\right) \lambda+\eta+\mathrm{e} \tag{6}$$

Once a model is chosen, the parameter values of the model can be estimated from the gray-level values using the least squares adjustment. LSM is a non-linear adjustment problem which requires a higher number of equations than the unknowns to solve its unknowns. The solution is found by minimizing the SSD of the gray-values between the reference and search templates. In this case (x′, y′) are determined indirectly by determining the parameters $p_{1\ldots n}$. Since it is a non-linear problem, (2) is linearized in Taylor series expansion as in (7) which (with (8) incorporated) is assumed to hold for every pixel of the template. The linearization helps to make the unknown matching positions to be sought as adjustments

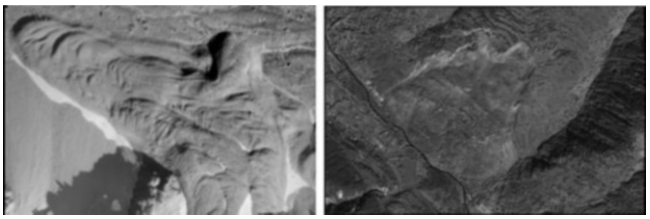


Fig. 1 A section of the aerial photographic images over the Muragl rockglacier (400 m × 600 m) taken on 7 September 1981 (*left*), and QuickBird panchromatic satellite image over the La Clapiére landslide (1,600 m × 2,430 m) taken on 06 September 2003 (*right*)

Table 1 The spatial transformation models and their parameters

Name	Spatial transformation model	Number of parameters
Affine	$x' = p_1 + p_2x + p_3y$	6
	$y' = p_4 + p_5x + p_6y$	
Projective	$X' = (p_1 + p_2x + p_3y)$ $/(1 + p_7x + p_8y)$	8
	$y' = (p_4 + p_5x + p_6y)$ $/(1 + p_7x + p_8y)$	
Polynomial (second degree)	$x' = p_1 + p_2x + p_3y + p_7xy$ $+ p_9x^2 + p_{10}y^2$	12
	$y' = p_4 + p_5x + p_6y + p_8xy$ $+ p_{11}x^2 + p_{12}y^2$	

(dx, dy) to the initial positions (x_0, y_0). Linearization then makes the unknowns converted to the adjustments to the initial parameters (dp_i) as in (8). The initial values of the parameters are obtained by finding the initial estimate of the matching by other simpler and faster methods such as the NCC. LSM searches only within a couple of pixels distance (Gruen 1996).

The vector of the unknown parameters (i.e. corrections to the initial transformation parameters), dp, are related linearly to the design matrix containing the differentl quotations (A) and the gray-values differences (l) to produce the estimate of the residuals as written in matrix form in (9). The l's are computed from the reference template and the search template and the A's are computed from the gray-values gradients of the search template in which case it needs to be recomputed at each iteration step or from the reference template in which case it is constant throughout the iteration steps. If the first option is chosen, the gray-valuess are interpolated for the newly computed sub-pixel positions and the gradient is computed from these gray-valuess at each iteration step. The solution for the dp's is sought according to L2-norm iteratively until the SSD of the gray-valuess is minimized using (10), i.e. the adjustments converge to zero or close to zero. Here π is a weight matrix which is often an identity matrix but can be determined based on the significance of each pixel basically downplaying the role of outlying pixels. The dp's stand for the adjustments of the geometric and the two radiometric parameters (11).

$$F(x,y) - \varepsilon = (G^0(x_0,y_0) + \frac{\partial G^0(x_0,y_0)}{\partial x}dx + \frac{\partial G^0(x_0,y_0)}{\partial y}dy)\lambda + \eta \quad (7)$$

$$dx = \frac{\partial x}{\partial p_i}dp_i, dy = \frac{\partial y}{\partial p_i}dp_i \quad (8)$$

$$v = A^*dp - l \quad (9)$$

$$dp = (A'\pi A)^{-1}A'\pi l \quad (10)$$

$$dp = \{dp_1, \ldots, dp_n, d\lambda, d\eta\} \quad (11)$$

Once the parameter values of the spatial transformation model are known, the model can be used to compute the new location of each pixel of the template. The horizontal surface displacement for each pixel is then computed as the Euclidean distance between the old and the new locations and the horizontal surface velocity is computed as the displacement divided by the temporal baseline of the image acquistions.

Methods

Image Datasets

Two pairs of bi-temporal images of two different types of mass movements are used in the study. The first bi-temporal image pair (Fig. 1 right) was taken over the rockglacier in the Muragl valley of the Upper Engadine area of the Swiss Alps (approx. 9 °55′30″E, 46 °30′15″N). Rockglaciers consist of permanently frozen debris that slowly deforms down-slope under gravity. The rockglacier has been under investigation for decades using technologies such as photogrammetry, geodesy and geophysics to understand its mechanics (Kääb and Vollmer 2000). The orthoimages used in the present study are based on aerial images taken on 7 September 1981 and 23 August 1994 with 13 years of temporal baseline and 0.2 m of spatial resolution.

The second set of bi-temporal images (Fig. 1 middle) are panchromatic images from the high spatial resolution QuickBird satellite over the La Clapiére landslide (approx. lat 44 °15′08″N, lon 6 °56′30″E) in the French Alps around the town of Saint-Etienne-de-Tinee. The images were taken on 06 September 2003 and 27 September 2010 respectively. The ground pixel size of the images is 0.6 m. The images were orthorectified using the SRTM DEM and the French

3D Geoportail web service. As the orthorectification based on this base-map does not result in accurate co-registration, a mean co-registration error of about 1.2 m (2 pixels) is recorded. Detailed description of the landslide is found in many publications (Casson et al. 2003; Gaffet et al. 2010).

Image Matching

Estimation of Initial Parameters

Considering the older images as reference and the newer images as search images, the images are first matched using the NCC. Template sizes of 51 × 51 pixels are used for the matching. Smaller template sizes are avoided to fully suppress noises and avoid ambiguity. As the LSM is applied in a next step, the presence of displacement gradients in such large templates is not of a concern. The search distance is decided based on the expected maximum displacement in each of the image pairs. This relatively coarse matching is used to estimate the initial parameters for the least squares adjustment. The initial parameters we refer to here are the pixel-precision matching position and the accompanying spatial transformation parameters. Initially the matching templates are assumed to have the same geometry (except position) with the reference template. Therefore, for each dimension a unit geometric and radiometric scaling factor is used keeping the other parameters at zero. The least squares iteration starts using these initial values.

Least Squares Iteration

Once the pixel-precision matching position and the initial parameters of the template are known, the LSM is implemented as follows. First, the gradients and the residuals are computed from the matching template. The adjustments to the initial parameters are then computed from the gradients and the residuals. New parameter values are recomputed from the initial values by adding their respective adjustments. The new parameter values are used to compute the new location of the matching template. The new location might be at sub-pixel-precision. Therefore, intensity values at those sub-pixel positions need to be interpolated. Cubic convolution is used to interpolate the intensity values at the sub-pixel positions as it is the closest to the *sinc* interpolation which is believed to be the most accurate in image interpolation (Dodgson 1992). The gradients and the residuals are recomputed using the newly interpolated intensity data. The process is then repeated until the adjustments are very close to zero, i.e. converge. The limit for the convergence is set to 10^{-4} for the rockglacier but 10^{-3} for the landslide due the expected high noise level from the presence of vegetation. Maximum number of iterations is set to 30 for cases where the parameters do not converge faster.

The above procedure is applied for each of the spatial transformation models image-wide turn by turn. The adaptive algorithm is then applied as follows. For each template the affine, projective and the polynomial models are applied turn by turn. When each of them has converged their resulting SSD are registered and compared. The model that produces the smallest SSD is considered to be the best fitting model for the template as the LSM is based on minimising the SSD between the two templates.

Computation of Displacment

After the parameters have converged, the horizontal surface displacement of each pixel is computed separately as Euclidian distance between the pixels' position in the reference and the matching images. The horizontal surface velocity is then computed as the displacement divided by the temporal baseline of the image pair. Therefore, pixels of the same template have different velocities unless the template moves rigidly. The slide direction is computed as the arctangent of the ratio of the displacements of the easting and northing directions, i.e. in angles from the north.

Evaluation

The relative advantage of using the LSM over the conventional NCC is evaluated using the signal-to-noise ratio (SNR) of the matching as detailed in Debella-Gilo and Kääb (in review). Here, the algorithms are evaluated based on how well they reconstruct the reference image from the search image as the reliability of the estimated displacement is directly related to the reliability of the image matching (reconstruction). The relative gains in SNR of the methods were compared. Visual evaluation was also performed prior to the quantitative evaluation. The different spatial transformation models are used turn by turn for the evaluation.

Result

To give an overview of the velocity of the mass movements the velocity statistics are presented in Table 2. The table shows that the velocities of the two mass movements are in the order of tens of cma^{-1}. The rest of the results will be presented in two subsections.

Rockglacier Creep

The velocity vectors of the muragl rockglacier are presented in Fig. 2a. The velocity maps are given for both the conventional NCC algorithm (B) and the LSM algorithm with spatially adaptive geometric models (C). One can already observe the

Table 2 Velocity statistics for the two mass movement types

Mass movement	Mean velocity (ma^{-1})	Maximum velocity (ma^{-1})	Standard deviation (ma^{-1})
Muragl Rockglacier creep	0.18	0.5	0.10
La Clapiére Landslide	0.62	2.28	0.35

realistic picture of the velocity map produced using the LSM algorithm. The gaps in the velocity maps are outliers removed based on the correlation coefficient thresholding of the NCC and the convergence criteria of the LSM.

Table 3 presents the SNR and the relative gain in SNR of each algorithm in reconstructing the reference image from the search image. The LSM in general improves the SNR of the reconstruction by over 25 % in all cases. Up to 33 % improvement in the gain of the SNR can be obtained by using the adaptive algorithm. This value is close to the one obtained by the second degree polynomial model (31 %). In fact, 65 % of the adaptive algorithm resulted in the polynomial registering the lowest SSD, followed by projective (20 %) and affine (15 %) models. It indicates that the 2D surface deformation of the Muragl rockglacier is best modeled by the second degree polynomial although locally adaptive approach produces a little better result.

Landslide

Figure 3 presents the velocity vectors (A) and the velocity maps computed using the NCC algorithm (B) and the LSM algorithm (C) for the La Clapiére landslide. The figure shows that the upper part of the landslide is moving with relatively higher speed. Quantitiative comparison (Table 4) shows that the spatially adaptive LSM matches the images with 35 % better SNR compared to the NCC. This value is not much higher than those produced using the polynomial model. 60 % of the adaptive algorithm resulted in the second degree polynomial registering the lowest SSD, followed by projective (21 %) and affine (19 %). Again it indicates how robust the polynomial algorithm is. Both in this and in the rockglacier case the difference between the performances of the affine and the projective models is not impressive. The overall performance grade in decreasing order is as follows: spatially adaptive, polynomial, projective/affine and NCC (rigid-body translation).

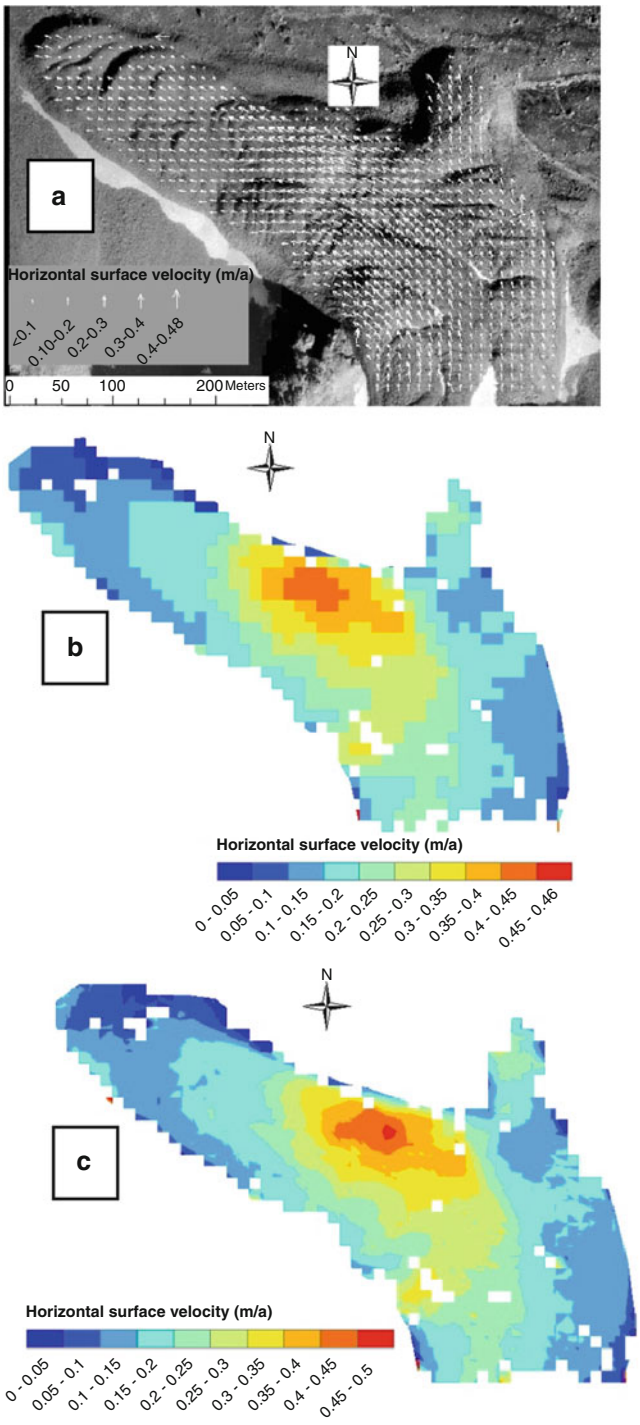


Fig. 2 Velocity vectors (**a**), velocity map computed using the NCC alone (**b**) and velocity map computed using the LSM with the spatially adaptive LSM algorithm (**c**) for the Muragl rockglacier creep

Discussion

As the results show, the LSM can successfully be used to compute the velocity of slow-moving landslides despite the long temporal baselines needed and sometimes inevitable surface changes due to for example vegetation cover. The overall higher performance of the LSM in comparison with NCC is attributed to its capability to model both geometric and radiometric distortions and to find the best matching template.

Table 3 The relative improvements in the SNR of image reconstruction for the different image matching algorithms for the Muragl rockglacier creep

Reconstructed by	SNR	SNR gain by reconstruction	SNR gain in reference to the conventional NCC
Original search image (no reconstruction)	0.41	0.00	
NCC	0.69	0.28	0
Affine	0.76	0.36	27
Projective	0.765	0.356	26
Polynomial	0.778	0.369	31
Adaptive	0.782	0.374	33

Besides, the position of the matching template is more precisie as it is fixed at sub-pixel resolution. This better performance in matching translates to better accuracy of the estimated displacements and velocities. This is actually the basis for the evaluation technique used in the study as reference velocity data do not exist.

As theoretically hypothesised, one type of geometric model could not optimally fit the deformations of the mass movements of the entire scene. The variations in the results of the different transformation models and the higher performance registered by the adaptive algorithm are testimonies to this. At least for these two particular mass movement cases, spatially adapting the transformation models optimises the matching. The adaptive algortihm is computationally expensive. Compromise between accuracy improvement and computational cost is of course case dependent. In cases where the slide looks non-uniform in its mode of movement, it might be worthwhile to use the adaptive algorithm.

Monitoring of such slow-moving landslides from repeat images is not a realtime process. Therfore, it is still beneficial to use the adaptive algorithm if one is interested in higher accuracies despite its computational cost. In cases where one geometric model is to be used for the whole image, the polynomial model is preferable. The affine model is actually a polynomial model with zero values for the non-linear parameters. Its difference from the second degree polynomial in linear deformation is only that the quadratic may overparametrise the model. The performances of projective and affine are expectedly similar as the only difference between them is the addition of the perspective parameters (related to tilting and slumping) which are not very common in real mass movements. The projective model might be more important when matching raw, i.e. not orthorectified, images to model the projective distortion of the camera.

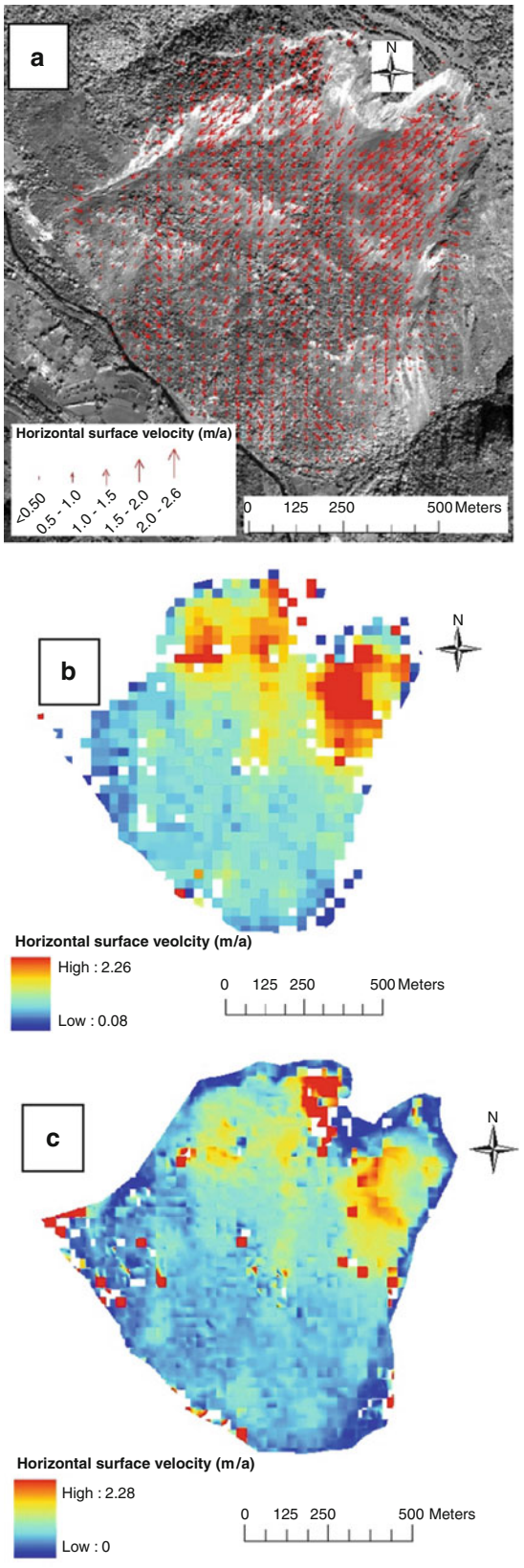


Fig. 3 Velocity vectors (**a**), velocity map computed using NCC alone (**b**) and velocity map computed using LSM with spatially adaptive geometric model (**c**) for the La Clapiére landslide

Table 4 The relative improvements in the SNR of image reconstruction for the different image matching algorithms for the La Clapiére landslide

Reconstructed by	SNR	SNR gain by reconstruction	SNR gain in reference to the conventional NCC
original	0.519	0.000	
NCC	0.918	0.399	0
Affine	1.048	0.529	26
Projective	0.992	0.473	28
Polynomial	1.027	0.508	32
Adaptive	1.059	0.540	35

Conclusion

This study has implemented and evaluated the LSM with spatially adapative and advanced spatial transformation models in matching bi-temporal image pairs of two mass movement types. The results show that over 25 % improvements in the reliability of the matching can be obtained by shifting from the NCC to the LSM algorithm. If the LSM is applied with spatially adaptive geometric models, up to 35 % gain in SNR can be obtained. This in principle translates to equivalent improvements in the reliability of the estimated displacements and velocities.

Although the spatially adaptive algorithm performs best, it is computationally expensive. The polynomial model is robust enough to cover the major part of both the affine and the projective distortions. Therefore, the use of the polynomial model is encouraged in cases where a single image-wide transformation model is to be used.

Since the NCC is used in estimating the initial matching position it remains crucial in estimating the displacement of Earth surface masses from repeat images.

Further resarch is needed to verify the findings under different environments, mass movement types and imagery.

Acknowledgements This study was supported by The Research Council of Norway (NFR) through the CORRIA project (no. 185906/V30), the International Centre for Geohazards (SFF-ICG 146035/420), and the ESA GlobGlacier and Climate Change Initiative "glaciers and ice caps" project. The orthoimages of the Muragl rockglacier are based on airphotos acquired by the Swisstopo/flight service (BA057212, BA081844).

References

Ackermann F (1984) Digital image correlation: performance and potential application in photogrammetry. Photogramm Rec 11(64):429–439

Bethmann F, Luhmann T (2010) Least-squares matching with advanced geometric transformation models. In: International archives of photogrammetry, remote sensing and spatial information sciences commission V symposium, Commission V, WG V/4, Newcastle upon Tyne, UK, pp 86–91

Casson B, Delacourt C, Baratoux D, Allemand P (2003) Seventeen years of the "La Clapière" landslide evolution analysed from orthorectified aerial photographs. Eng Geol 68(1–2):123–139

Debella-Gilo M, Kääb A (2011) Sub-pixel-precision image matching for measuring surface displacements on mass movements using normalized cross-correlation. Remote Sens Environ 115(1):130–142

Debella-Gilo M, Kääb A (2012) Locally adaptive template sizes for matching repeat images of Earth surface mass movements. ISPRS J Photogramm Remote Sens 69(1):10–28

Delacourt C, Allemand P, Casson B, Vadon H (2004) Velocity field of the "La Clapière" landslide measured by the correlation of aerial and QuickBird satellite images. Geophys Res Lett 31(15):15–19

Dodgson NA (1992) Image resampling. University of Cambridge Computer Laboratory, London, p 264

Förstner W (1982) On the geometric precision of digital image correlation. In: Proceedings of the ISPRS symposium mathematical models, accuracy aspects and quality control. International Archives of Photogrammetry, Finland, pp 176–189

Gaffet S, Guglielmi Y, Cappa F, Pambrun C, Monfret T, Amitrano D (2010) Use of the simultaneous seismic, GPS and meteorological monitoring for the characterization of a large unstable mountain slope in the southern French Alps. Geophys J Int 182(3):1395–1410

Gruen A (1996) Least squares matching: a fundamental measurement algorithm. In: Atkinson KB (ed) Close range photogrammetry and machine vision. Whittles, Caithness, pp 217–255

Gruen A, Akca D (2005) Least squares 3D surface and curve matching. ISPRS J Photogramm Remote Sens 59(3):151–174

Gruen AW, Baltsavias EP (1987) High-precision image matching for digital terrain model generation. Photogrammetria 42(3):97–112

Kääb A, Vollmer M (2000) Surface geometry, thickness changes and flow fields on creeping mountain permafrost: automatic extraction by digital image analysis. Permafrost Periglac Proc 11(4):315–326

Kääb A, Haeberli W, Gudmundsson GH (1997) Analysing the creep of mountain permafrost using high precision aerial photogrammetry: 25 years of monitoring Gruben Rock Glacier, Swiss Alps. Permafrost Periglac Proc 8(4):409–426

Kaufmann V, Ladstädter R (2003) Quantitative analysis of rock glacier creep by means of digital photogrammetry using multi-temporal aerial photographs: two case studies in the Austrian Alps. In: Phillips M, Springman SM, Arenson LU (eds) Eighth international conference on permafrost. Taylor & Francis, Zurich, pp 525–530

Maas HG, Casassa G, Schneider D, Schwalbe E, Wendt A (2010) Photogrammetric determination of spatio-temporal velocity fields at Glaciar San Rafael in the Northern Patagonian Icefield. Cryosphere Discuss 4(4):2415–2432

Whillans IM, Tseng YH (1995) Automatic tracking of crevasses on satellite images. Cold Reg Sci Technol 23(2):201–214



Seismometric Monitoring of Hypogeous Failures Due to Slope Deformations

Luca Lenti, Salvatore Martino, Antonella Paciello, Alberto Prestininzi, and Stefano Rivellino

Abstract

Results from a seismometric monitoring of rock mass failures affecting a karstified slope are here presented. The slope, located in Central Apennines (Italy), hosts a drainage plant and is involved in gravity-induced deformations.

Starting from September 4, 2008 four accelerometric stations were installed within the tunnels of the drainage plant.

More than 1,000 events, referred to both earthquakes and hypogeous rock mass failures, were recorded.

The frequencies of occurrence of earthquakes and rock mass failures result to be generally well correlated; nevertheless, many hypogeous instabilities can be directly associated to the continuous slope deformations.

The trend of the cumulative Arias intensity derived for the hypogeous instabilities shows a time variable rate which was used as a tool for monitoring the deformational process of the slope as well as for managing the associated geological risk by the use of alert or alarm plans.

Keywords

Seismometric monitoring • Rock mass spreading • Hypogeous failures

L. Lenti
Institut Français des Sciences et Technologies des Transports, de l'Aménagement et des Réseaux (IFSTTAR-Paris) – 14-20 Boulevard Newton Cité Descartes, Champs sur Marne F-77447, Marne la Vallée Cedex 2, France

S. Martino (✉) • A. Prestininzi
CE.RI., Research Centre on Prevention, Prediction and Control of Geological Risks, "Sapienza" Università di Roma, Piazza U. Pilozzi 9, Valmontone (RM) 00038, Italy

Department of Earth Sciences, "Sapienza" Università di Roma, P.le Aldo Moro 5, Rome 00185, Italy
e-mail: salvatore.martino@uniroma1.it

A. Paciello
Agenzia Nazionale per le Nuove Tecnologie, l'Energia e lo Sviluppo Economico Sostenibile ENEA – C.R. Casaccia – Via Anguillarese 301, 00123 S. Maria di Galeria Rome, Italy

S. Rivellino
CE.RI., Research Centre on Prevention, Prediction and Control of Geological Risks, "Sapienza" Università di Roma, Piazza U. Pilozzi 9, Valmontone (RM) 00038, Italy

Introduction

Pre-failure behaviour of rock masses represents a complex geomechanical topic, since the existing stress conditions, the jointing conditions and the joint setting can strongly constrain pre-failure effects such as generation of new cracks, opening or closing of pre-existing joints and readjustment of the stress field within the rock mass. Recognizing pre-failure events by geological surveys as well as monitoring natural and anthropogenic systems is a major goal for the mitigation of risks due to the above mentioned "unexpected" and "rapid" events (Szwedzicki 2003). All the mentioned "failure precursors" can be monitored by use of specific devices.

In particular, the above mentioned transitional phase toward ultimate equilibrium conditions represents a useful chance to focus the process which is occurring, if a monitoring of the related events is performed.

C. Margottini et al. (eds.), *Landslide Science and Practice*, Vol. 2,
DOI 10.1007/978-3-642-31445-2_40, © Springer-Verlag Berlin Heidelberg 2013

More complex scenarios of failure involving rock masses can be associated with impulsive triggers (i.e. explosions, collapses) or earthquakes. In these cases precursors do not necessarily occur, while the events representing possible triggers can be monitored.

Some experiments have been performed in mines or in landslide areas that were aimed at monitoring failure precursors by use of acoustic as well as seismometric devices (Lei et al. 2004, 2006; Deparis et al. 2008). On the other hand hypogeous instabilities triggered by impulsive events were recorded during experiments of controlled explosions and collapses of caves in mine areas (Miller et al. 1989; Phillips et al. 1997). Moreover, laboratory tests were performed on brittle materials to analyze possible correlations between acoustic emissions and observed microfracturing (Ganne et al. 2007).

Characteristic waveforms and frequency spectral features of microseismic emissions due to rock falls, collapses and explosions, both natural and artificially induced, were collected and analysed by many authors (Phillips et al. 1997; Heng 2009). On the whole, these studies proved that only a specific comparison among signals generated by different events (i.e. among natural events or among natural and artificial ones) allows a reliable discrimination.

The analysis of sequences of precursors as well as of post-failure events (i.e. hypogeous instabilities induced by impulsive triggers) can be considered a very useful tool for managing early warning, since monitoring the phases of failure propagation provides information on the changes which are involving the rock mass, but also on possible occurrence of more critical conditions (i.e. generalized collapse).

This study used a seismometric monitoring system to record precursors, post-failure events and triggering impulsive events within a karstified rock mass which hosts the major drainage system of Rome's aqueduct. The recorded sequences of the earthquakes as well as of the induced failures within the rock mass were analysed with the aim of evaluating possible trigger thresholds and recognising different levels of attention, based on the observed trends of events.

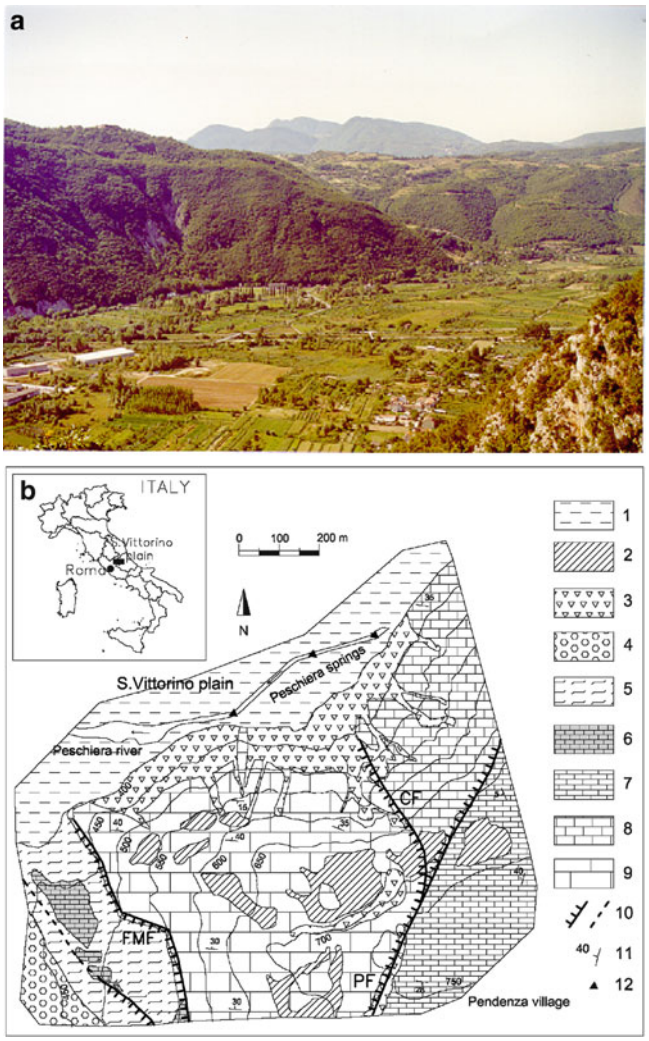


Fig. 1 Panoramic view from NE (**a**) and Geological sketch (**b**) of the Peschiera Springs slope: (*1*) Recent alluvial deposits of the Velino River; (*2*) Reddish soils; (*3*) Slope debris; (*4*) Gravel and conglomerate (upper Pliocene part–lower Pleistocene part); (*5*) Sandy-clayey flysch (upperMiocene); (*6*) Marly limestone (upper Cretaceous–lower Miocene); (*7*) Birdeyes micritic Limestone (lower Cretaceous); (*8*) Coral limestone (upper Malm); (*9*) Coral and echinids limestone (Malm part); (*10*) Fault (dashed if supposed): FMF Fiamignano-Micciani Fault, CF – Canalone Fault, PF – Pendenza Fault; (*11*) Strike and dip of strata; (*12*) Spring

Geological Setting of the Peschiera Spring Slope

The Peschiera Springs slope corresponds to the south-western flank of Mt. Nuria (Central Apennines, Italy) (Fig. 1) and is composed of limestones which belong to the Mt. Nuria unit (Ciotoli et al. 2001) and are ascrivable to the Malm part-Lower Cretaceous part interval.

The structural setting of the slope is monoclinic, with EW-trending and N-dipping (30–40 °) strata; many faults cross the slope with roughly NS and N35E trends (Fig. 1).

The slope also hosts a major karst aquifer which represents the drainage system of the Nuria-Velino-western Fucino and western Marsica (Velino-Sirente) mountains (total surface area: 1,016 km^2), whose main springs are the Peschiera-Canetra ones (measured total discharge: roughly 18–21 m^3/s; Boni et al. 1995).

Through geomorphological surveys as well as a recent digital, high-resolution (2 m), elevation model of the slope derived by a LIDAR (Light Detection And Ranging) remote survey, numerous gravity-induced morphological elements (e.g. scarps, trenches, sinkholes and tension cracks) were identified (Figs. 2 and 3). These landforms are indicative of

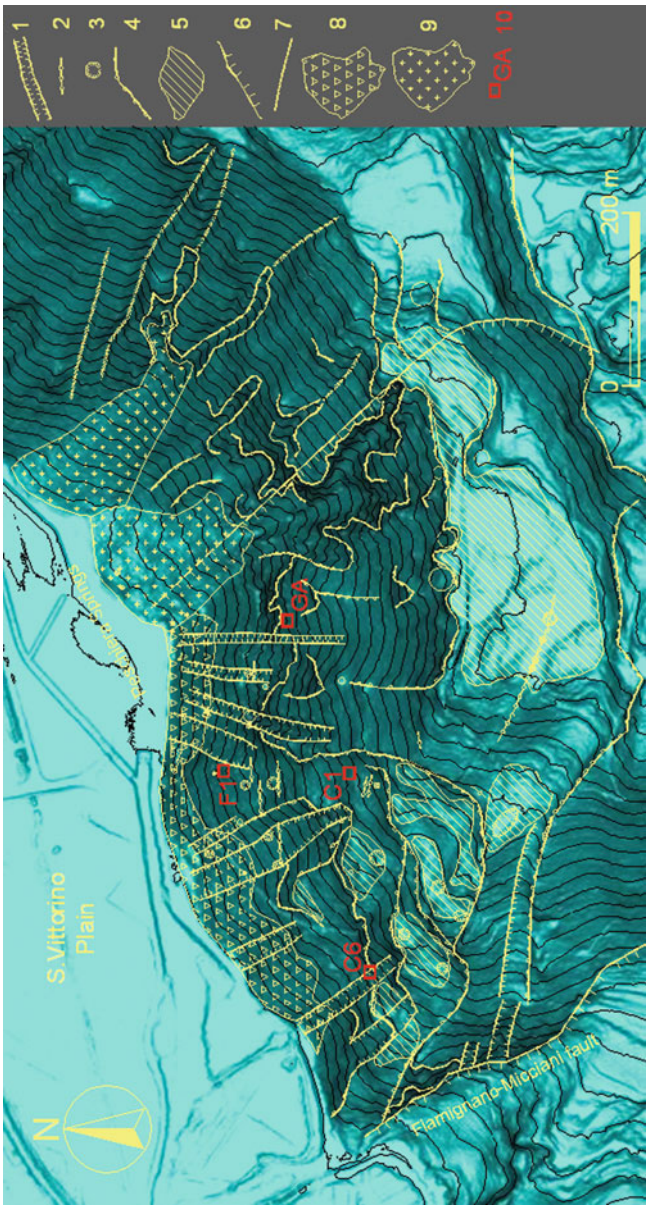


Fig. 2 Digital elevation model (DEM) from the LIDAR flight with geomorphological features. (*1*) Trench; (*2*) Tension crack; (*3*) Sinkhole; (*4*) Scarp; (*5*) Karstified flat; (*6*) Fault; (*7*) Gully; (*8*) Slope debris; (*9*) Debris fan deposit; (*10*) Accelerometric station within the drainage plant

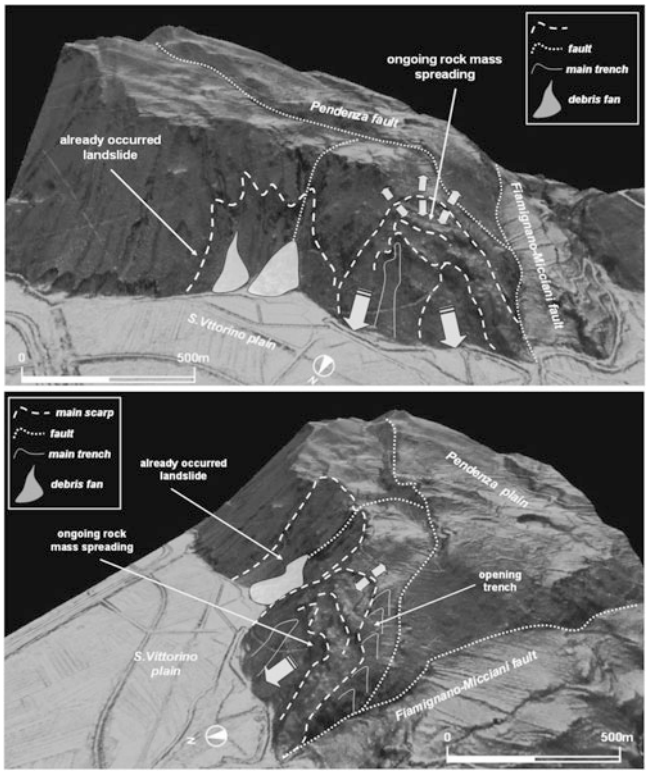


Fig. 3 3D views from the DEM of Fig. 2 showing the already occurred landslide and the ongoing rock mass spreading which involves the Peschiera Springs slope

slow, intense and pervasive slope deformations, which affect the entire slope and which correspond to various evolutionary stages ascribable to different portions of the slope, as proved by already published outputs of a stress–strain monitoring system installed within the drainage plant (Martino et al. 2004; Maffei et al. 2005).

Tens of sinkholes and depressions of variable size (diameter: 5 m to about 15 m; depth: 0.5 m to about 9 m) can be observed all along the slope; sometimes aligned along opened tension cracks.

Many scarps (with a height varying from 5 up to 15 m) are arranged both longitudinally and transversely to the slope.

All the collected geomorphological evidences enabled the recognition of three slope sectors with ongoing gravity-induced processes at different evolutionary stages (Martino et al. 2004; Casini et al. 2006): (1) a sector, including the southern portion of the slope and its top, with evidence of incipient, but limited deformation, in their early evolutionary stages; (2) a western sector, with evidence of mature, but not yet advanced evolution of gravity-induced deformations, where the major deformations are concentrated near the most marked gravity-induced elements and (3) an eastern sector, with evidence of advanced evolution characterised by pervasive deformation and pronounced gravity-induced elements, such as scarps, trenches and sinkholes.

The geological-evolutionary model of the slope reflects a complex deep-seated gravitational deformation, which initiates as a rock mass creep (Chigira 1992) and continuously evolves from a rock mass spreading to a rock-block mass deformation (Martino et al. 2004). In particular, the rock mass spreading can be clearly observed in the western portion of the slope (Fig. 3).

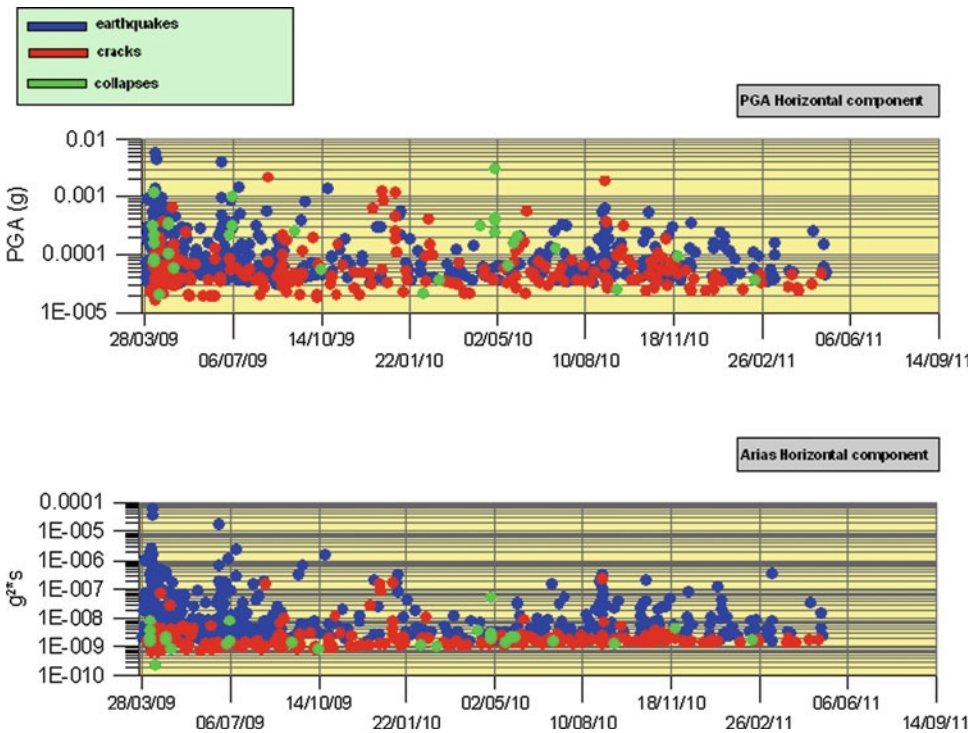


Fig. 4 PGA and Arias intensity (horizontal component – station C1) of all the events (earthquakes, cracks and collapses) recorded form March 2009 until May 2011

Seismometric Monitoring

Accelerometric Network

Starting from September 4, 2008 four accelerometric stations (GA, C1, F1 and C6 of Fig. 2) were installed by ACEA-ATO2 S.p.A. within the drainage plant of the Peschiera Springs in order to record both seismic events and hypogeous collapses. Each station was instrumented by a triaxial accelerometer (EPISENSOR KINEMETRICS) directly installed on bedrock. The four accelerometers were connected via cable to a digital data-logger (K2 KINEMETRICS) set to the absolute local time by a GPS device.

The monitoring system was managed by the Research Centre for Geological Risks (CERI) of the University of Rome "Sapienza" in order to properly set the recording device, analyze the collected data and suggest possible plans of management in case of a seismic crisis or a sequence of hypogeous events.

Two pass-band filters of the KINEMETRICS library ("classic strong motion" with a pass-band about 1–10 Hz and "IIRC" with a band-pass about 1–20 Hz) were alternatively applied to the channels of each station.

Moreover, some channels were set with a threshold trigger fixed according to their noise level, while others were set in STA/LTA (short time amplitude/long time amplitude) trigger mode, which is particularly devoted to the detection of low-magnitude earthquakes.

Recorded Data

Until the end of March 2009 only 7 events were recorded within the slope, but from April 2009, until May 2011 more than 1,000 events (about 800 earthquakes and 300 hypogeous instabilities) were recorded on the whole (Fig. 4).

To distinguish among different kinds of recorded events, a specific software was implemented through SAC (Seismic Analysis Code) and Fortran codes on Unix platform, taking into account the records obtained from the accelerometric network as well as the data collected by use of a temporary velocimetric array, which operated within the plant for about 5 months. The software allows to classify the events on the basis of their physical properties (i.e. energy, time duration, kinetic parameters and frequency content) and, in particular, to recognise among earthquakes, cracks and hypogeous collapses.

Magnitude and location of the recorded earthquakes were attributed according to the on-line data published by INGV (www.ingv.it).

The up to now recorded seismic sequences include the L'Aquila sequence, which started on March 28, 2009 and reached Mw 6.3 on April 6th and some seismic sequences from the M.nts Reatini seismogenetic area, which is about 30 km far from the Peschiera Spring plant and is characterized by intermediate-low magnitudes (i.e. up to 4.0).

Moreover, some far-field intermediate-high magnitudes earthquakes (i.e. higher than 5.0) were recorded, such as the Balcanic Peninsula, Southern Thyrrenian Sea, Japan (Lenti

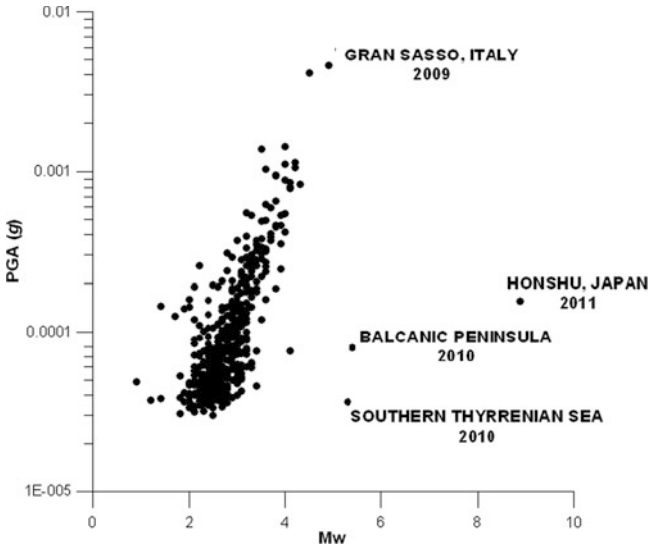


Fig. 5 PGA versus Mw for the earthquakes recorded from March 2009 until April 2011 by the Peschiera Spring accelerometric network

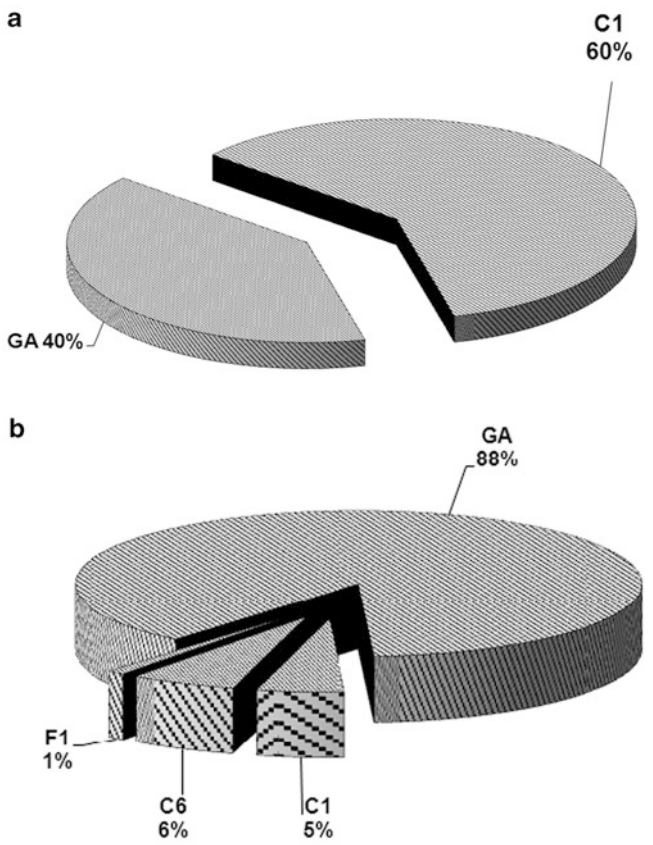


Fig. 6 (**a**) Distribution of the maximum PGA (horizontal component) at the recordings station referred to 30 recorded collapses; (**b**) distribution of the maximum PGA (horizontal component) at the recordings station referred to 270 recorded cracks

et al. 2011). The PGA and the Arias intensity values of the recorded earthquakes reach 0.1 m/s^2 and 10^{-4} g^{2}s respectively.

Taking into account the not seismic events the maximum average PGA related to the collapses (about 5.8×10^{-4} g) was obtained on the vertical component of C1 station, while for the cracks the maximum average PGA (about 2.6×10^{-4} g) was obtained on the horizontal components of GA station (Fig. 5), while the average Arias intensity obtained from the hypogeous events (i.e. both collapses and cracks) does not exceed 5.5×10^{-9} g^{2}s (horizontal component of GA station).

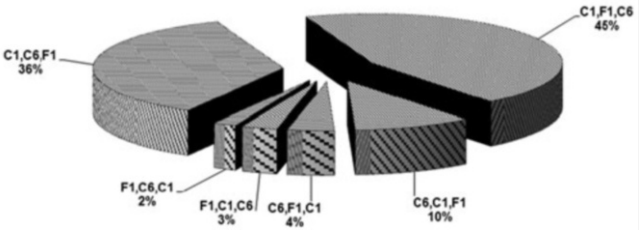


Fig. 7 Distribution of PGA attenuation respect to stations C1, F1 and C6, referred to the recorded crack events which were characterised by a maximum PGA at station GA (horizontal component)

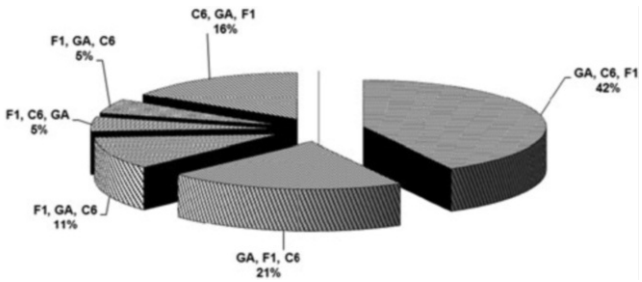


Fig. 8 Distribution of PGA attenuation respect to stations GA, F1 and C6, referred to the 30 recorded collapses which were characterised by a maximum PGA at station C1 (vertical component)

About 60 % of the recorded collapses show the maximum PGA at C1 station, on the vertical component of the motion, while the remnant 40 % at station GA (Fig. 6a). On the other hand, about 90 % of the recorded cracks show the maximum PGA at GA station and these maximum values are not associated to a specific component of the motion (Fig. 6b).

The time duration of the earthquakes is significantly greater (some tens of seconds) with respect to the not seismic events, since the cracks last some seconds and the collapses not exceed 1 s. Moreover, while the main frequency content of the earthquakes is limited to about 10 Hz, the cracks show a relevant frequency content up to 60 Hz and the collapses reach higher frequencies.

Based on the PGA spatial attenuation resulting from the network, the cracks are mainly located in the eastern portion of the slope and are mainly felt at stations GA and C1, while they are felt with a significantly reduced magnitude by the other stations, particularly by F1 station which is located very close to the external slope (Fig. 7). On the other hand, the collapses mainly occurred close to C1 station, which is located about 250 m far from the adjacent alluvial plain, and were mainly felt by GA station (Fig. 8).

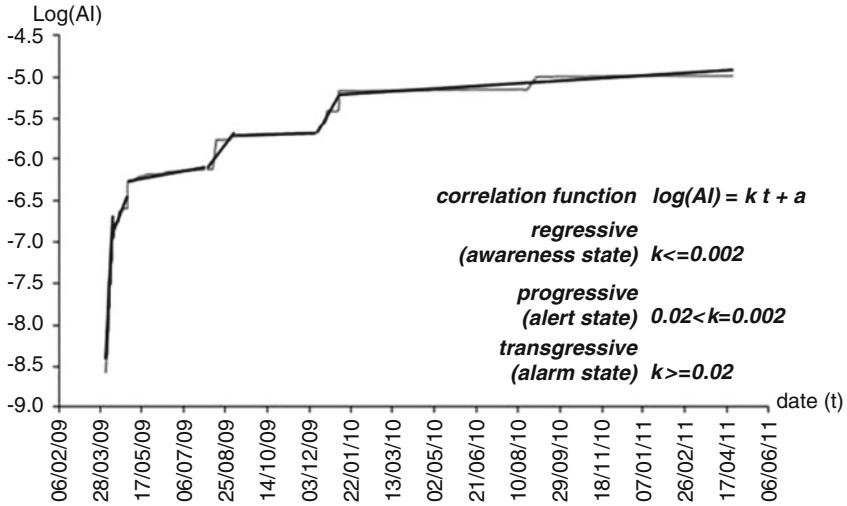


Fig. 9 Sequential analysis of the events recorded within the Peschiera Springs slope in the time interval 28 March 2009–25 April 2011. The time intervals are characterised by different trends of cumulative of Arias intensity (AI) and correspond to different attention levels for the management of the plant

Discussion

All the recorded collapses show maximum PGAs at station C1 or GA, while about 90 % of the crack events show maximum PGAs at station GA; these results are in good agreement with the evolutionary model of the deformational processes affecting the slope, which differentiates an eastern sector (station GA), characterised by an intensely jointed rock mass, and a western sector (station C1), where the highest deformations occur close to the main released rock mass bands, which correspond to a concentration of hypogeous caves (Maffei et al. 2005).

In general, the frequencies of occurrence of the seismic sequences and of the hypogeous instabilities are strongly correlated, even though many hypogeous instabilities can be associated to the continuous slope deformations since their frequency increasing cannot be directly related to seismic events. In this regard the hypogeous instabilities recorded during the April–May 2010 time interval are not related to any seismic event/sequence but they occurred some week before the Reatini M.nts sequence of September 2010.

In order to synthesise some features of the recorded dataset, the cumulative Arias intensity of the earthquakes and of the hypogeous instabilities was plotted versus time (Fig. 9).

This evidence suggests that different trends of increment of the cumulative Arias intensity can be derived from the above described plot. As an example, an increasing-rate trend was observed during the first 5 days after L'Aquila mainshock (i.e. until April 10, 2009); a constant-rate trend was observed during the following 3 weeks (i.e. until April 30, 2009); a decreasing-rate trend was observed in the following period (i.e. until the end of August 2009). Linear correlations were obtained for the logarithm of the cumulative Arias intensity vs. time in the before mentioned time intervals; these correlations correspond to angular coefficients (k in Fig. 9) which decrease of one order of magnitude per time interval down to 2×10^{-3}. These results are in good agreement with the monitoring of some indicators such as displacements, stresses, frequency of acoustic or microseismic emissions and magnitude of the emitted signals (Szwedzicki 2001, 2003), which can help to distinguish different trends associated to a decreasing, a stationary and an increasing hazard of failure and could be named as "regressive", "progressive" or "transgressive" respectively (Fig. 9).

The transgressive, progressive and regressive sequences of hypogeous instabilities referred to the hypogeous failures, which can be derived from the trend of cumulative Arias intensity, suggest different proceedings to manage the geological risk of the Peschiera Springs drainage plant; these proceedings have been referred to "alarm", "alert" and "awareness" levels of attention, which can be detected by transgressive, progressive and regressive sequences of hypogeous events respectively. In this regard, a more extended discussion and an upgrade of the recorded data was recently published by the Authors (Lenti et al. 2012).

Conclusion

The gravity-induced deformations involving the Peschiera Springs slope (Central Italy) are responsible for hypogeous instabilities within the rock mass. An accelerometric array, installed within the drainage plant of the Peschiera Springs (i.e. inside the slope), recorded about 800 earthquakes and about 300 not seismic events, including cracks and collapses, in about 30 months (September 2009–May 2011). The highest frequency of occurrence of the not seismic events was recorded immediately after the 6 April 2009 L'Aquila mainshock (Mw 6.3) (INGV, 2009).

On the other hand, many hypogeous instabilities can be associated to the continuous slope deformations since

their frequency increasing cannot be directly related to seismic events/sequences.

Since the derived trend of cumulative Arias intensity referred to the hypogeous failures correspond to "transgressive", "progressive" and "regressive" sequences of such events, this detection drives to management proceedings, consisting in "alarm", "alert" and "awareness" levels of attention, which aims at mitigating the geological risk associated to the Peschiera Springs drainage plant.

Acknowledgments Authors wish to thank ACEA-ATO2 S.p.A. for the provided data; Ing. G. Martino for the authorisation to data publishing; Dott. C. Romagnoli for the revision of the data and for the useful technical discussions.

References

Boni CF, Capelli G, Petitta M (1995) Carta idrogeologica dell'alta e media Valle del F. Velino. Elaborazione cartografica e stampa System Cart, Rome

Casini S, Martino S, Petitta M, Prestininzi A (2006) A physical analogue model to analyse interactions between tensile stresses and dissolution in carbonate slopes. Hydrogeol J 14:1387–1402

Chigira M (1992) Long-term gravitational deformation of rocks by mass rock creep. Eng Geol 32:157–184

Ciotoli G, Di Filippo M, Nisio S, Romagnoli C (2001) La Piana di S. Vittorino: dati preliminari sugli studi geologici, strutturali, geomorfologici, geofisici e geochimici. Mem Soc Geol It 56:297–308

Deparis J, Jongmans J, Cotton F, Bailler L, Thouvenot F, Hantz D (2008) Analysis of rock-fall and rock-fall avalanche seismograms in the French Alps. Bull Seism Soc Am 98(2):1781–1796

Ganne P, Vervoort A, Wevers M (2007) Quantification of pre-peak brittle damage: correlation between acoustic emission and observed micro-fracturing. Int J Rock Mech Min Sci 44:720–729

Heng IS (2009) Rotating stellar core-collapse waveform decomposition: a principal component analysis approach. Class Quantum Grav 26:105005

INGV (2009) La sequenza sismica dell'Aquilano, Aprile 2009. Web site: http://portale.ingv.it/primo-piano/archivio-primo-piano/notizie-2009/terremoto-6-aprile/copy_of_la-sequenza-sismica-dell-aquilano-aprile-2009/

Lai XP, Cai MF, Xie MW (2006) In situ monitoring and analysis of rock mass behavior prior to collapse of the main transport roadway in Linglong Gold Mine, China. Int J Rock Mech Min Sci 43:640–646

Lei X, Masuda K, Nishizawa O, Jouniaux L, Liu L, Ma W, Satoh T, Kusunose K (2004) Detailed analysis of acoustic emission activity during catastrophic fracture of faults in rock. J Struct Geol 26:247–258

Lenti L, Martino S, Paciello A, Prestininzi A, Romeo R (2011) Insights into the ground motion records of the Honshu (Japan) earthquake of 11 March 2011. Ital J Eng Geol Environ 1:5–16

Lenti L, Martino S, Paciello A, Prestininzi A, Rivellino S (2012) Microseismicity within a karstified rock mass due to cracks and collapses as a tool for risk management. Natural Hazards 64:359–379

Maffei A, Martino S, Prestininzi A (2005) From the geological to the numerical model in the analysis of the gravity-induced slope deformations: an example from the Central Apennines (Italy). Eng Geol 78:215–236

Martino S, Prestininzi A, Scarascia Mugnozza G (2004) Geological evolutionary model of a gravity-induced slope deformation in the carbonate central Apennines (Italy). Quart J Eng Geol Hydrogeol 37(1):31–47

Miller A, Richards JA, McCann DM, Browitt CWA, Jackson PD (1989) Microseismic techniques for monitoring incipient hazardous collapse conditions above abandoned limestone mines. Quart J Eng Geol London 22:1–18

Phillips WS, Pearson DC, Edwards CL, Stump BW (1997) Microseismicity induced by a controlled, mine collapse at white pine, Michigan. Int J Rock Mech Min Sci 34(314):246

Szwedzicki T (2001) Geotechnical precursors to large-scale ground collapse in mines. Int J Rock Mech Min Sci 38:957–965

Szwedzicki T (2003) Rock mass behaviour prior to failure. Int J Rock Mech Min Sci 40:573–584



Use of Persistent Scatterer InSAR within Terrafirma Landslide Services

Sandro Moretti, Francesca Cigna, Federico Raspini, Geraint Cooksley, Marie-Josée Banwell, Hugo Raetzo, Gerardo Herrera, Davide Notti, and Juan Carlos García Davalillo

Abstract

Landslide Services of the pan-European project Terrafirma are presented. LandSlide Inventory (LSI) and LandSlide Monitoring (LSM) exploit satellite Persistent Scatterer InSAR (Synthetic Aperture Radar Interferometry) to monitor extremely to very slow moving landslides at both regional and local scale. Validated case studies of LSI in the Upper Tena Valley (Central Pyrenees, Spain) and LSM in Val Lumnez (Switzerland) are described. 14 TerraSAR-X descending images acquired in May–October 2008 are processed with the Stable Point Network (SPN) technique, and used to update the landslide inventory of the Upper Tena Valley, significantly improving the pre-existing landslide mapping. 68 ERS1/2 and ENVISAT ascending scenes, acquired in May 1992–October 2005 and processed with the Interferometric Point Target Analysis (IPTA) technique, are combined with topographic levelling measurements performed in 1887–1992, and exploited to monitor the Val Lumnez landslide and to improve the geomorphologic zonation.

Keywords

Landslide inventory • Landslide monitoring • Persistent scatterer interferometry • Synthetic aperture radar • IPTA • SPN • Terrafirma

Introduction

Persistent Scatterer InSAR (Synthetic Aperture Radar Interferometry) is demonstrating its suitability for detection and monitoring of extremely to very slow moving landslides (Cruden and Varnes 1996), ranging from regional to local scale. This technique provides measurements of ground deformation, analyzing long temporal stacks of satellite radar images and identifying on the ground reflective targets, for which the history of deformation can be reconstructed with millimetre precision (e.g., Arnaud et al. 2003; Werner et al. 2003; Duro et al. 2003).

Integrating conventional instrumentation for the analysis of landslide-induced deformation, this advanced technique allows both spatial and temporal characterization of landslide phenomena, improving the quality of landslide maps, resolving the temporal variability of slope movements, and also assessing their state of activity and intensity (e.g., Farina et al. 2004, 2006; Cigna et al. 2010; Righini et al. in press).

The exploitation of Persistent Scatterer (PS) techniques within landslide analysis has been recently promoted by several European initiatives, such as the Terrafirma project

S. Moretti (✉) • F. Cigna • F. Raspini
Department of Earth Sciences, University of Firenze, Firenze, Italy
e-mail: sandro.moretti@unifi.it

G. Cooksley • Marie-Josée Banwell
Altamira Information, Barcelona, Spain

H. Raetzo
Federal Office for the Environment, Ittigen, Switzerland

G. Herrera • J.C.G. Davalillo
Instituto Geológico y Minero de España, Departamento de Investigación y Prospectiva Geocientífica, Área de Peligrosidad y Riesgos Geológicos, Madrid, Spain

D. Notti
Department of Earth Sciences, University of Pavia, Pavia, Italy

C. Margottini et al. (eds.), *Landslide Science and Practice*, Vol. 2,
DOI 10.1007/978-3-642-31445-2_41, © Springer-Verlag Berlin Heidelberg 2013

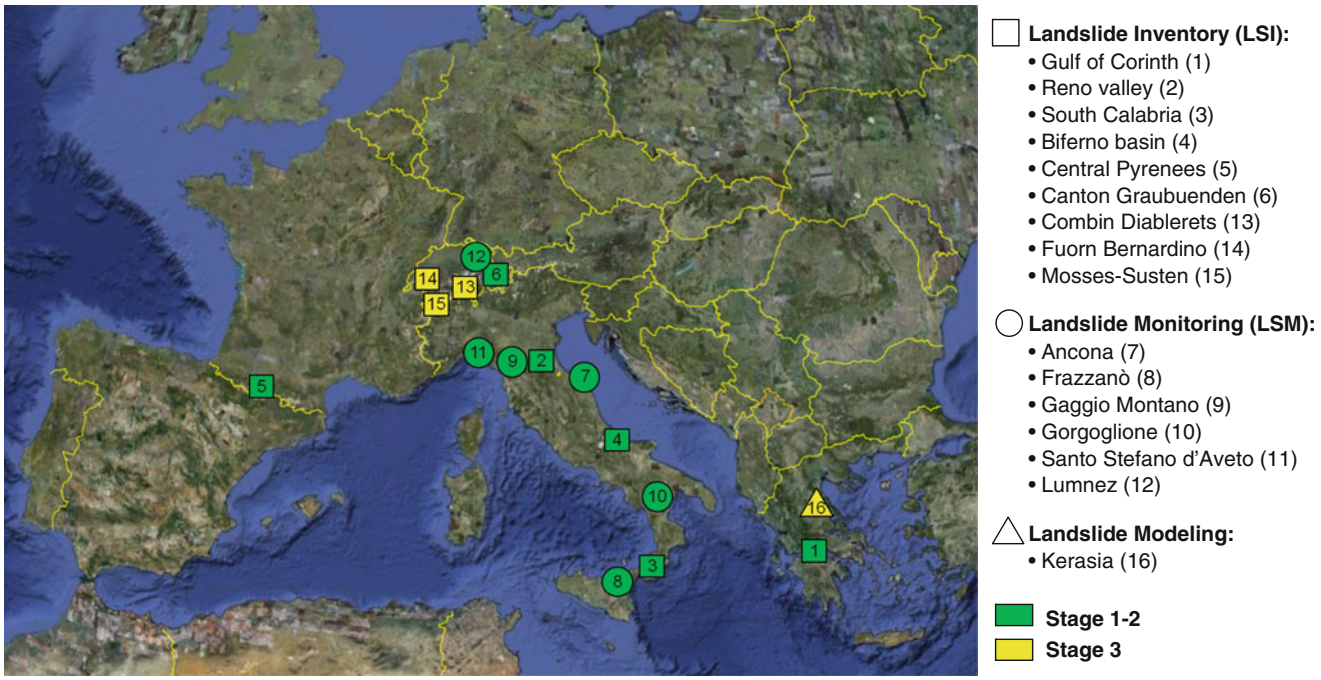


Fig. 1 Coverage of Terrafirma Landslide Services in Europe

(http://www.terrafirma.eu.com/), a pan-European ground motion hazard information service supported by the European Space Agency's GMES (Global Monitoring for Environment and Security) programme.

Terrafirma Stage 3 was launched in December 2009 and has as its aim the sustainability of the terrain motion service. This stage features a new focus on several thematic lines for terrain motion analysis: Tectonics, Flooding, Hydrogeology (ground water, landslides and inactive mines) and the innovative Wide Area service, aimed at measuring land deformation at pan-European scale. Terrafirma Stage 3 consortium is lead by Altamira Information, with the Dutch Geological Survey leading the Flood Theme, the Italian National Institute of Geophysics and Volcanology leading the Tectonics Theme, the University of Firenze leading the Hydrogeology Theme, and the German Space Agency leading the Wide Area Mapping task.

As in previous stages, Terrafirma services are based on advanced interferometry products, mainly PS methodologies; however they exploit additional data sources, including non-EO, coupled with site-specific expert interpretation. These services are delivered to civil protection agencies, disaster management organisms, and coastal, rail and motorway authorities to support risk assessment and mitigation.

Part of the Hydrogeology theme, Landslide services cover mountainous areas affected by slope instability, providing LandSlide Inventory (LSI), LandSlide Monitoring (LSM) and Landslide Modeling products (Fig. 1). Validated case studies of LSI in Central Pyrenees (Spain) and LSM in Lumnez (Switzerland) are presented, showing the essential contribution of PS and InSAR data for the detection and analysis of landslide-induced movements at both regional and local scale, and demonstrating their fundamental role for the improvement of hazard and risk management strategies.

LandSlide Inventory (LSI)

Methodology

LSI provides information on the spatial distribution of mass movements. This approach is based on the possibility of assigning a spatial meaning to the ground displacement measurements provided by scattered points (the Persistent Scatterers).

LSI generally operates at regional scale and integrates pre-existing landslide inventories, produced with conventional geomorphologic tools, with multi-temporal aerial and/or satellite optical imagery, thematic, geological and topographic data (Digital Elevation Model and its derived maps) and field surveys. This analysis is aimed at identifying terrain features and landforms related to slope instability (Farina et al. 2006, 2008; Cigna et al. 2010; Righini et al. in press) and assessing similarities and differences in landslide spatial distribution and activity with respect to PS data; qualitative and quantitative information of each mapped phenomenon may be improved, and those phenomena not previously identified through conventional in situ investigations may be detected.

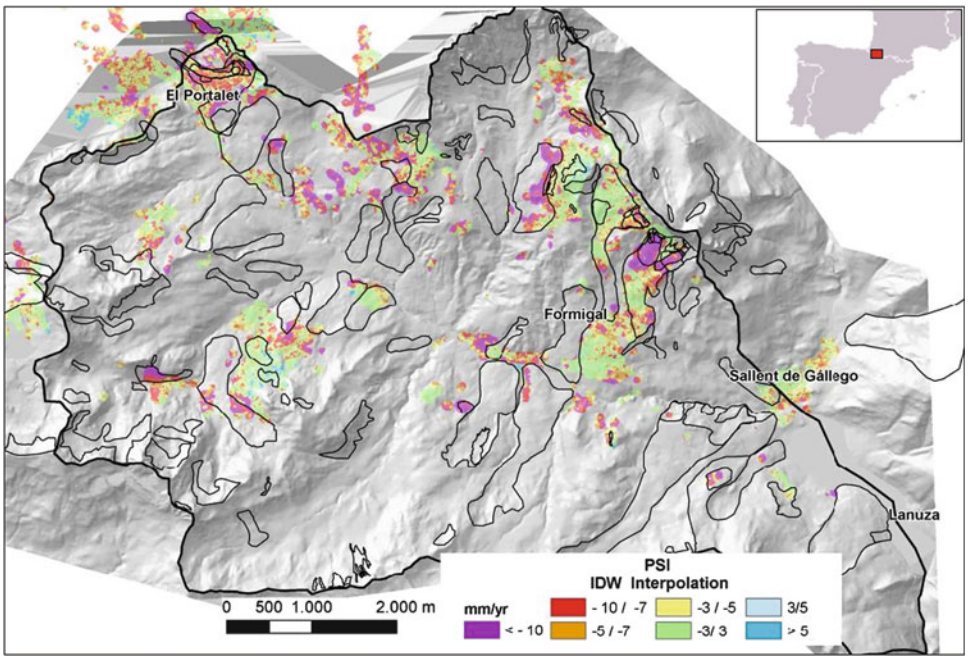


Fig. 2 LOS deformation rates of TerraSAR-X PS data (interpolated with IDW) and landslide distribution in the area of Upper Tena Valley, Central Pyrenees (Spain)

Central Pyrenees Case Study

The Upper Tena Valley (Central Pyrenees, Spain) is occupied by the magmatic and Paleozoic complex of the axial Pyrenees that is affected by the Hercinian folding phase. The centre of the valley is characterised by the outcrop of the Devonian Shale, whereas in the northern part this formation is overthrusted by the Carboniferous Limestone formation (Rios-Argues et al. 1987). Permian sandstone, conglomerate and Carboniferous greywacke crop out in the SW. These materials are usually covered by Quaternary sediments: alluvial or alluvial fan deposits in the valley, and colluvial deposits on the slopes that present significant thickness favoured by weathering process of shale formations. The scarp toes are usually covered by talus or rock fall deposits. In the past, glacial action was very relevant especially in the upper part of the basin (SW area) with many glacial cirques and morenic deposits.

The type and distribution of landslides in this area is controlled by its structural and geological setting, as well as by glacial, fluvial action and erosion. Massive rock outcrops (limestone, sandstone, conglomerate, and intrusive rocks) present an abrupt morphology with steep slopes and structural scarps. These lithologies are affected by rock fall or rock avalanche processes that favour accumulation of rock deposits at the scarp toes. Shale formations occupy gentle slopes and present considerable thickness of weathered rocks and colluvial deposits. These formations are usually affected by slow flow landslides, and soil/ice creep processes. Frequently these are shallow and active landslides, but deep seated landslides can also be found. In some cases, these landslides transport rock fall and rock avalanche deposits derived from the upper massive rock scarps. These landslides were triggered by glacial melting and, nowadays, the whole body is in a relict state of activity. Nevertheless, local reactivations affecting the infrastructure (mainly roads and ski facilities) are frequent. Several flow/slide movements occur, triggered by erosive action of River Gallego and great seasonal variation of soil humidity in old landslide deposits.

A set of 14 TerraSAR-X StripMap images of the Tena Valley was processed using the Stable Point Network (SPN) technique, a PSI approach developed by Arnaud et al. (2003) and Duro et al. (2003). These data cover the period from May to October 2008, with time intervals between subsequent images of 11 or 22 days, and were acquired along descending orbits. The processing of X-band SAR images with the SPN technique allowed the detection of more than 35,000 PS (1,000 PS/km^2) in the study area. In some areas a density greater than 10,000 PS/km^2 was detected where rock fall and rock avalanche deposits are found (Fig. 2).

The analysis of the PS velocities showed that, using a threshold of ±3 mm/year, the stable PS were 34 % of total. The high percentage of PS (66 %) with greater velocities was due to the short monitoring period (only 6 months) that allowed the detection of high target densities in areas affected by active superficial processes (e.g., debris flow, soil flux, erosion). Probably, using longer monitoring periods, PS would not have been detected in correspondence of this kind of processes or, at least, would have been detected in a lower amount. Comparison of the PS dataset with the landslide

inventory highlighted that 54 landslides (53 % of total) showed 1 or more PS within their boundaries. Detected PS were considered indicative of landslide displacement when at least 3 PS and a density up to 100 PSI/km^2 were identified within the landslide boundary. According to that, in the study area the landslides suitable for PS analysis were 22, which correspond to 21 % of total inventory, and 54 % of the slow moving landslides (Notti et al. 2010). Exploitation of X-band data provided a great density of PS. Inverse Distance Weighted (IDW) interpolation of the displacement velocity values was performed for the areas with more than 1,000 PSI/km^2; those areas larger than 1,000 m^2 and showing average displacement rates greater than 5 mm/year were then selected to perform further interpretation. In Fig. 2, a good correlation between the selected areas and mapped landslides can be observed.

The LSI analysis allowed identification of four new landslides and redefinition of boundaries of eight other phenomena. Not all the areas showing significant deformation corresponded to landslides: in some cases the movement was explained with settlement of new buildings or other processes, while in other cases it was not easy to understand and further investigations were required.

The Formigal landslide area is a very good example of a landslide where the PSI technique provided a great PS density and turned out to be very useful for landslide mapping (Fig. 3). The geological setting of this area is defined on the top by the limestone formation (Foratata Peak) where rock fall and rock avalanche processes are found. The associated rock deposits are widespread from the upper to the lower part of the slope where highly weathered and altered shale formations are found. The area close to Formigal village is affected by three large deep seated paleo-landslides (landslides 1, 2, and 3 in Fig. 3a) of the complex type. As it has been previously described, these landslides were triggered by glacial melting. Today the whole body of these landslides can be considered inactive, even though within their area of influence slow flows of the weathering shale formations are present.

As shown in Fig. 3, dynamics of these processes were detected and monitored with great detail with the SPN analysis of X-band SAR data. Very high PS density was detected especially on the rock deposits located at the scarp toes (15,000 PS/km^2), as well as in Formigal urban area (7,000 PS/km^2). In the upper part at the limestone cliff toe, two areas (1A and 1B in Fig. 3) with strong movement separated by a stable area (1S in Fig. 3) were identified. From the PS data analysis different processes that are confirmed by the evidence of aerial photo and field survey were

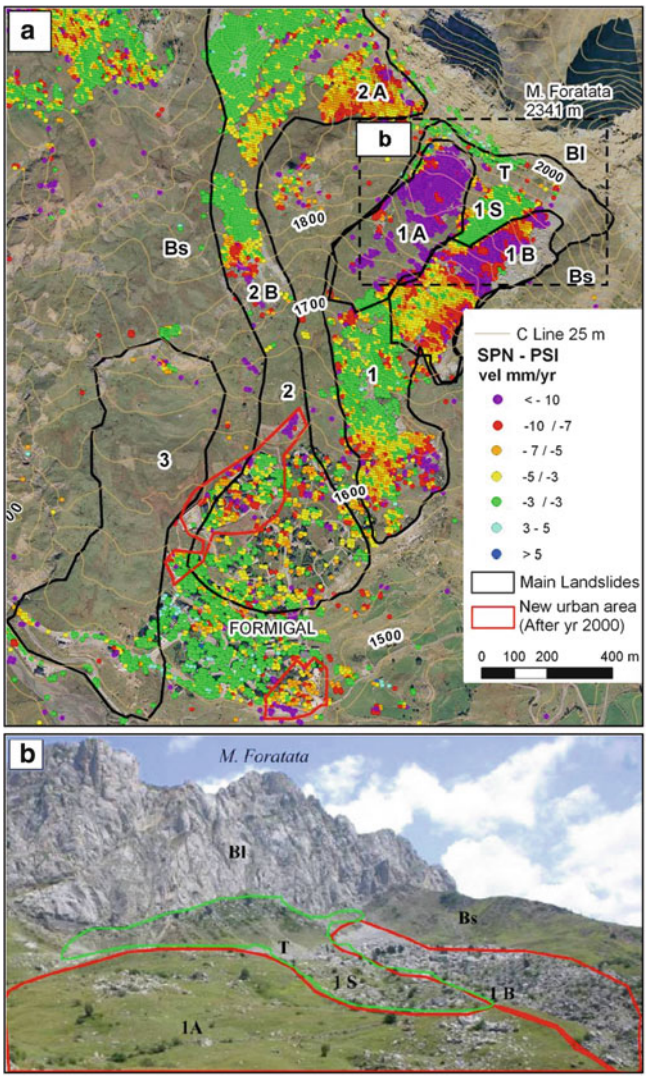


Fig. 3 Displacement rates measured with TerraSAR-X PSI data for the Formigal landslide (**a**) and complex landslides with rock fall blocks (**b**). *1A*, slow flow; *1S*, stable area covered by talus (*T*) and rock fall deposit; *1B*, rock avalanche deposit over a slow flow; *Bl*, Bedrock Limestone; *Bs*, bedrock shale

detected. The landslide 2 affects the slope north of Formigal and in the upper part it is separated by a small ridge from landslide 1. For this landslide, PS data did not show strong movements except for the upper eastern part (2A in Fig. 3) and the scarps located at 1,800 m a.s.l. (2B in Fig. 3). The toe of landslide 2 affects the upper part of Formigal village where slow to moderate displacements were detected. These displacements correspond to settlement of new buildings and infrastructure that were identified through comparison of two aerial photos of 2000 and 2006 (red polygons in Fig. 3a).

LandSlide Monitoring (LSM)

Methodology

LSM operates at local scale and relies on long term monitoring of displacements induced by specific slope movements, using both PS data and conventional in situ networks (e.g. topographic levelling, inclinometers, extensometers, GPS). Within LSM analyses, PS data are well suited for assessing the temporal evolution of landslides affecting built-up areas, by providing precise measures of ground motions without necessity of positioning any targets on the ground or any physical contact with the slope.

Besides the use of PS data, single-interferograms (conventional InSAR) could also be exploited to analyze the temporal variability of landslide-induced motions with a step-wise approach; use of single-interferograms allows analyzing not only motion velocities exceeding the limitation of the PS approaches (i.e. few tens of cm/year), but also deformation trends significantly differing from the deformation model (e.g. linear) used during the multi-temporal PS processing (e.g. non-linear and/or accelerated motion).

Lumnez Case Study

The Val Lumnez is one of the most active landslide zones in built-up areas of the Swiss territory. Located in the Canton of Grisons/Graubünden in the SE part of Switzerland, the Lumnez valley is NE-SW oriented with a ground instability affecting the SE-facing slope which is characterised by deep-seated roto-translational sliding process (*sackung*), with shallower phenomena.

The depth of the main shear surface of the sagging was estimated by Ziegler (1982) using the friction circle method. According to this method the shear surface is located at about 130 m. The landslide affects an area of 32 km^2 (length, 4 km; width, 8 km). The toe of the landslide is eroded by the river Glenner/Glogn. Many debris flows were initiated by this landslide activity and the damage downstream is considerable. Inside the unstable area 8 settlements are affected by ground movements. For this reason several projects of remedial works were realised during the last decades. In the 1940s drainage system took place. As a consequence of these works, the displacement rate indicates a clear decrease of movements of the Lumnez landslide (Noverraz et al. 1998).

The Val Lumnez in the Canton of Grisons/Graubünden is part of the Swiss Alps and, therefore, from a geological point of view has to be seen in the complex context of the tectonic evolution of the Alps. The NW flank of the Lumnez valley is made up of Mesozoic sediments of the Gotthard massif (clayey and sandy limestones, quartzites), with layers of schists showing bedding parallel to the slope which promotes sliding processes. The SE flank is composed by subpennic *Bündner slate*.

From aerial images, land coverage is recognizable, consisting of predominantly meadows, some forests and a few built-up areas, with agricultural areas located around the villages. The geomorphologic characteristics of the Val Lumnez differ on both sides of the Glenner river due to different geological settings and the presence of the landslide: while the NW flank of the valley is deeply modified by instability processes and characterised by a disturbed and hummocky morphology, the SE flank shows a smooth slope with incisions caused by fluvial erosion.

The satellite analysis for the Lumnez landslide was performed using the IPTA (Interferometric Point Target Analysis) technique (Werner et al. 2003; Strozzi et al. 2005), which belongs to the multi-interferometric approaches, and integrating 68 ascending SAR scenes from ERS-1/-2 and ENVISAT missions spanning the time interval May 1992–Oct 2005. Figure 4 gives an overview of the IPTA results for the Lumnez landslide as measured along the satellite line of sight and expressed in mm/year. The spatial distribution of the total number of 1,256 IPTA points yields to a density of 39 PS/km^2, varying with the presence of backscattering structures at the surface, and therefore prevailing in the urban areas.

The village of Lumbrein remains stable in the monitored period. The highest movements of up to 62 mm/year have been measured in Peiden in the NE zone of the landslide close to the Glenner river. Moreover, further high displacement rates of up to 50 mm/year are present in the middle part of the slope (Vignogn and Degen). In the N-NE part of the slope the movements decrease from 30 mm/year to less than 5 mm/year.

The geomorphologic zonation, which was carried out using DTM, its derivates (shaded relief and slope map) and aerial images, was improved through IPTA results (Fig. 4); different areas characterized by homogenous geomorphologic feature were identified.

Apart from the spatial distribution of movements, the IPTA analysis provided information on the temporal evolution of displacement rates from a backscattering structure on the ground. The temporal evolution of displacements indicates for all IPTA points a linear movement without any accelerations or decelerations. The linear behaviour of the IPTA results in the interval 1992–2005 corresponds to the deep-seated movement of the Lumnez landslide. As a consequence it has to be stated that the IPTA analysis has not detected superficial movements, or superficial movements also show a linear trend: a further explanation for the linear trend could arise from the IPTA processing.

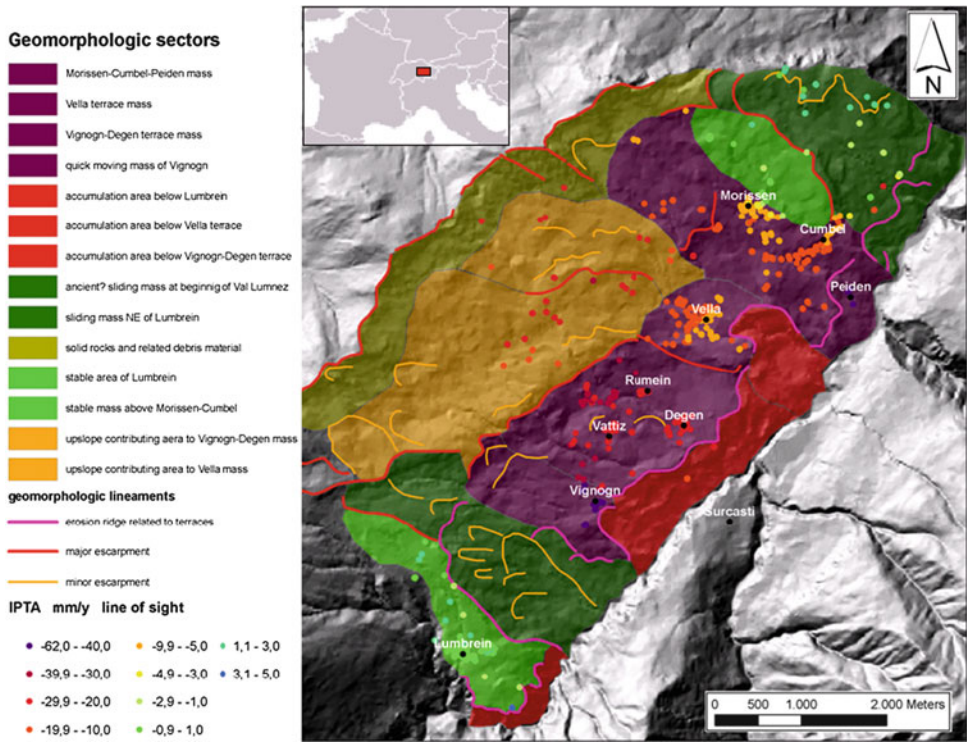


Fig. 4 Lumnez landslide geomorphologic zonation using IPTA results

In addition to a field campaign, for the validation of the IPTA analysis a joint analysis of ground displacements as measured by the available in situ instrumentation and by the PSI analysis was performed. In Noverraz et al. (1998) the measurements acquired by a topographic network from the EPFL institute (*École Polytechnique Fédérale de Lausanne*) for the period 1887–1992 is described. Even if the measurement period ends at the beginning of the IPTA analysis, the topographic network measurements were useful indicators of the spatial distribution of the velocity rates for the Lumnez landslide and showed the general trend of displacements. The overall orientation of the displacements measured during geodetic campaign is 120–140 °, which corresponds to the orientation of the Lumnez slope. For each topographic station, a representative PS was selected as the closest target to the analyzed station; PS rates were then converted into slope-parallel movements and compared with the topographic data (Fig. 5), highlighting an evident correlation between the two datasets.

The fitting line shows a strong agreement between the measurements (black line), even if they were not recorded in the same time period. The orange line indicates the location of the best fitting (correlation equals to 1; $x = y$). The discrepancy in terms of magnitude of velocities may be explained with the degradation of the slope movements occurred in the last decades, as a consequence of the remedial works (e.g., drainage system) implemented in 1940s.

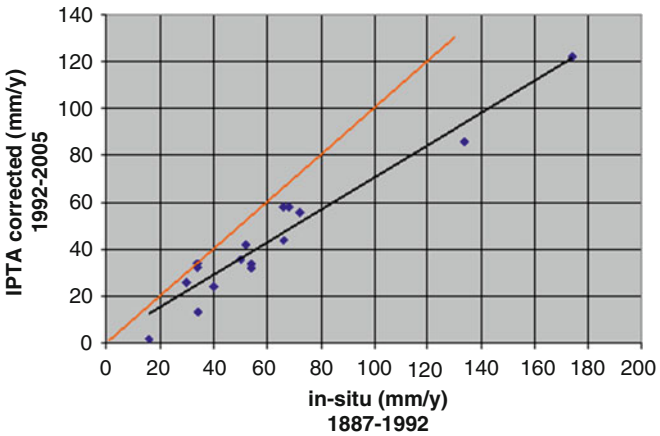


Fig. 5 Comparison of IPTA (1992–2005) results and in situ measurements (1887–1992) for 16 topographic stations

Conclusion

Two validated Landslide Services of the pan-European project Terrafirma were presented. LandSlide Inventory (LSI) in the Upper Tena Valley (Central Pyrenees, Spain) was carried out exploiting 14 TerraSAR-X descending images acquired in May–October 2008 and processed with the SPN technique. The landslide inventory of the valley was successfully updated, significantly improving

the pre-existing landslide mapping. LandSlide Monitoring (LSM) in Val Lumnez (Switzerland) was performed using 68 ERS1/2 and ENVISAT ascending scenes acquired in May 1992–October 2005 and processed with the IPTA technique. Satellite data were combined with topographic levelling measurements performed in 1887–1992, and exploited to monitor the Val Lumnez landslide and to improve its geomorphologic zonation. These case studies demonstrated the suitability of Persistent Scatterer InSAR data for detection and monitoring of extremely to very slow moving landslides (Cruden and Varnes 1996), ranging from regional to local scale.

Acknowledgments This work was funded by the project Terrafirma (http://www.terrafirma.eu.com/) and its Spainslide element, supported by the European Space Agency's GMES (Global Monitoring for Environment and Security) programme. The authors acknowledge also the project DO-SMS–SUDOE INTERREG IV B, for partially funding the Central Pyrenees LSI, Spain.

References

Arnaud A, Adam N, Hanssen R, Inglada J, Duro J, Closa J, Eineder M (2003) ASAR ERS interferometric phase continuity. IGARSS 2003, Toulouse, CDROM, 21–25 July 2003

Cigna F, Bianchini S, Righini G, Proietti C, Casagli N (2010) Updating landslide inventory maps in mountain areas by means of Persistent Scatterer Interferometry (PSI) and photo-interpretation: Central Calabria (Italy) case study. In: Malet JP, Glade T, Casagli N (eds) Mountain risks: bringing science to society, Florence, pp 3–9, 24–26 Nov 2010

Cruden DM, Varnes DJ (1996) Landslide types and processes. In: Turner AK, Schuster RL (eds) Landslides: investigation and mitigation, vol 247, Special Report. Transportation Research Board, National research Council. National Academy Press, Washington DC, pp 36–75

Duro J, Inglada J, Closa J, Adam N, Arnaud A (2003) High resolution differential interferometry using time series of ERS and ENVISAT SAR data. Fringe 2003, Frascati, 1–5 Dec 2003

Farina P, Moretti S, Colombo D, Fumagalli A, Manunta P (2004) Landslide risk analysis by means of remote sensing techniques: results from the ESA/SLAM project. IGARSS 2004, Anchorage, Alaska, pp 62–65, 20 Sep 2004

Farina P, Colombo D, Fumagalli A, Marks F, Moretti S (2006) Permanent scatterers for landslide investigations: outcomes from the ESA-SLAM project. Eng Geol 88:200–217

Farina P, Casagli N, Ferretti A (2008) Radar-interpretation of InSAR measurements for landslide investigations in civil protection practices. In: 1st North American landslide conference, Vail, Colorado, 3–7 June 2007, pp 2720–3283

Notti D, Davalillo JC, Herrera G, Mora O (2010) Assessment of the performance of X-band satellite radar data for landslide mapping and monitoring: Upper Tena Valley case study. Nat Hazards Earth Syst Sci 10:1865–1875

Noverraz F, Bonnard C, Dupraz H, Huguenin L (1998) Grands glissements de versants et climat. Hochschluverlag AG, Zurich, 341 p

Righini G, Pancioli V, Casagli N Updating landslide inventory maps using persistent scatterer interferometry (PSI). Int J Remote Sens (in press)

Rios-Argues LM, Galera-Fernandez JM, Barettino-Fraile D (1987) Mapa Geologica de Espana escala 1:50.000F. 145. Sallent de Gallego, Instituto Geologico Y Minero de Espana

Strozzi T, Farina P, Corsini A, Ambrosi C, Thüring M, Zilger J, Wiesmann A, Wegmüller U, Werner C (2005) Survey and monitoring of landslide displacements by means of L-band satellite SAR interferometry. Landslides 2(3):193–201

Werner C, Wegmuller U, Strozzi T, Wiesmann A (2003) Interferometric point target analysis for deformation mapping. IGARSS 2003, Toulouse, pp 4362–4364, 21–25 July 2003

Ziegler HJ (1982) Die Hangbewegungen in Lugnez, am Heinzenberg und bei Schunders (Graubünden). Ph.D. thesis, Geologie und Geomechanik, University of Berne, Switzerland



Detection and Characterization of Rock Slope Instabilities Using a Portable Radar Interferometer (GPRI)

Andrew Kos, Tazio Strozzi, Reto Stockmann, Andreas Wiesmann, and Charles Werner

Abstract

A portable radar interferomter was used to periodically monitor a rock wall, where millimeter-scale displacements (0.5–0.6 mm/month) on an unstable rock slab were detected. Preliminary interpretation of a radar images acquired over a 5 month period revealed evidence for combined toppling and buckling failure mechanisms on the rock slab. The rock wall of interest has a history of block fall activity, which directly endangers a roadway in Canton Graubünden, Switzerland.

Keywords

Portable radar interferometer • Ground based radar interferometry • Rock fall

Introduction

The detection of discrete instabilities on rock slopes are often problematic because failure may only be noted when it reaches an easily detectable state, for example when surface morphological features develop, or in the worst case failure occurs unexpectedly with apparently little warning. Traditional methods such as those utilizing laser distance metering (e.g. total stations etc.) or in situ methods such as tilt meters, extensometers etc., are limited by their capability to measure single points only. Therefore, to attain large area coverage, and to reduce the uncertainties related to the 'geological extrapolation' between measured points, a great deal of instrumentation is required.

Ground-based remote sensing is an increasingly attractive alternative to traditional methods due to its high precision and sensitivity to measuring displacements in a spatial and temporal context. In particular, radar interferometry has been established in recent years as a reliable method for spatial displacement monitoring of rock slopes (e.g. Leva et al. 2003; Tarchi et al. 2003a, b). Preliminary results from a monitoring campaign on a rock wall are presentedin this study, where a portable radar interferometer (GPRI-I) was used to detect and monitor mm-scale displacments taking place on a large rock slab.

A. Kos (✉)
Institute for Geotechnical Engineering, ETH Zurich, Switzerland

Terrarsense Switzerland AG, Werdenberg, Switzerland
e-mail: kos@erdw.ethz.ch

T. Strozzi • A. Wiesmann • C. Werner
Gamma Remote Sensing AG, Gümlingen, Switzerland

R. Stockmann
Institute for Geotechnical Engineering, ETH Zurich, Switzerland

Methods and Results

The Portable Radar Interferometer (GPRI-I)

GPRI-I (Gamma portable radar interferometer, version 1) is a new development in ground-based radar technology for measuring deformation. The GPRI-I is an FMCW radar with a fan-beam antenna array that rotates around a central axis. The system combines great portability, high precision and a rapid sampling rate of up to 10 °/s (Werner et al. 2008; Wiesmann et al. 2008). The system allows for a flexible set-up, which includes a standard geodetic tripod and/or survey monuments that are designed for traditional geodetic survey instruments such as tachymeters and GPS systems etc.

C. Margottini et al. (eds.), *Landslide Science and Practice*, Vol. 2,
DOI 10.1007/978-3-642-31445-2_42, © Springer-Verlag Berlin Heidelberg 2013

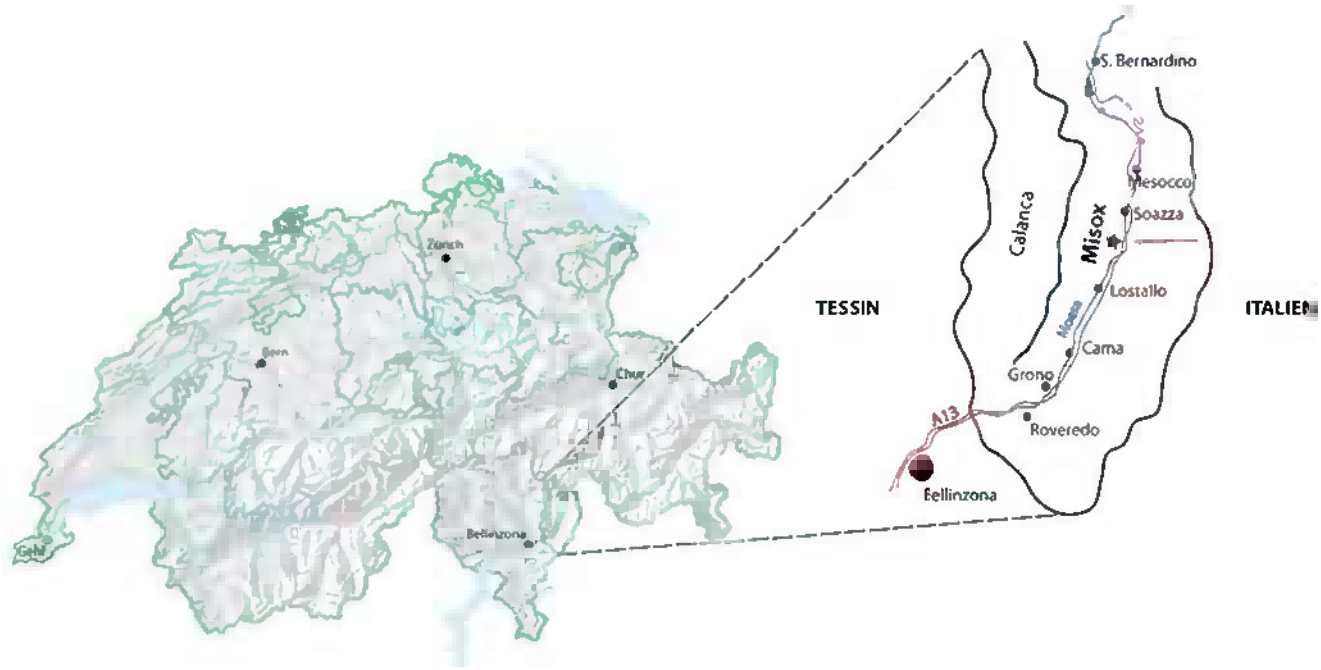


Fig. 1 Location of the case study area, Soazza in Switzerland



Fig. 2 The rockwall at Soazza showing sites of previous block failure

Case Study: Block Failure at Soazza

Soazza is located in the southern part of Canton Graubünden, Switzerland, adjacent to a state roadway (Fig. 1).

The locality consists of a rock wall approx. 600 m in length and 300 m in height that has been the scene of several block failures, the largest of which occurred in 2007 (~3,000 m^3), followed by two smaller failures in 2008 and 2009 (Fig. 2). The rock fall activity directly endangers a roadway running parallel near the foot of the slope in Canton Graubünden, Switzerland.

In collaboration with the state road authority of Graubünden, radar interferometric measurements were undertaken as part of research project into rock fall release mechanisms in March 2010. Repeat measurements took place in May and August of the same year. Measurements where undertaken with the GPRI-I using a standard geodetic set-up, where



Fig. 3 Set-up of the GPRI-I at Soazza using a survey tripod, levelled and centred with respect to a fixed point

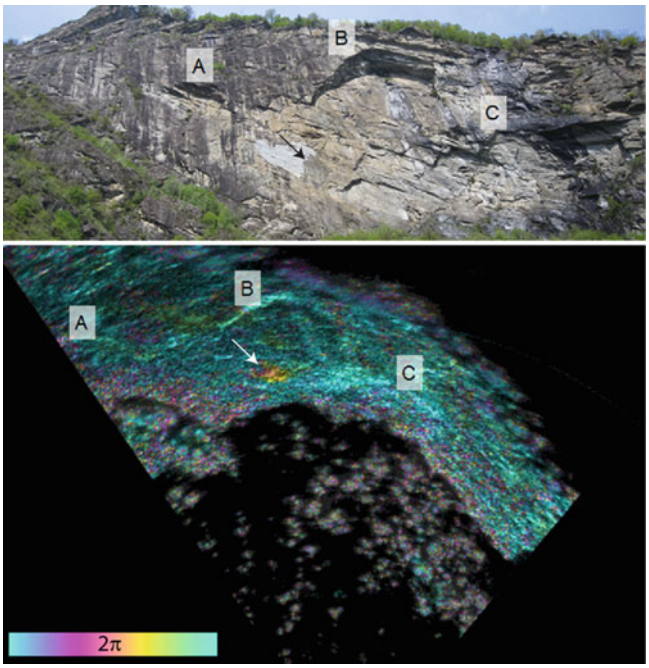


Fig. 4 Interferogram showing total displacements for the period March–August 2010

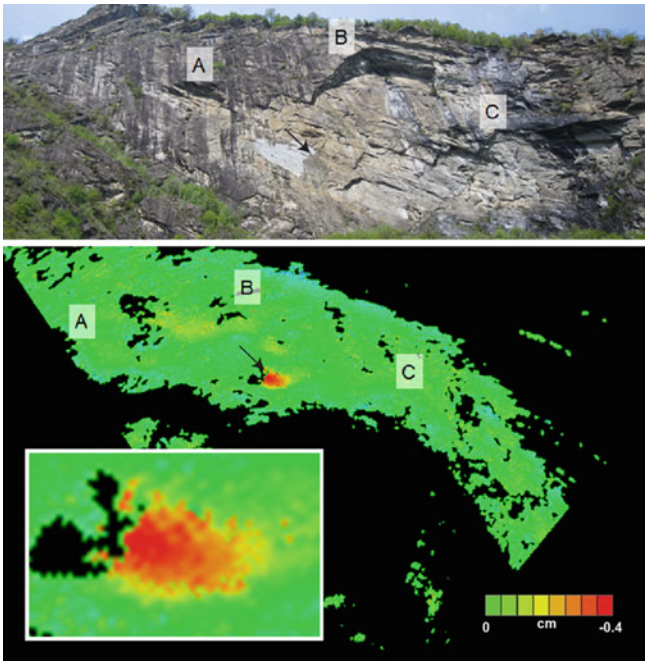


Fig. 6 Displacement map (i.e. phase unwrapped) for the period March–August 2010

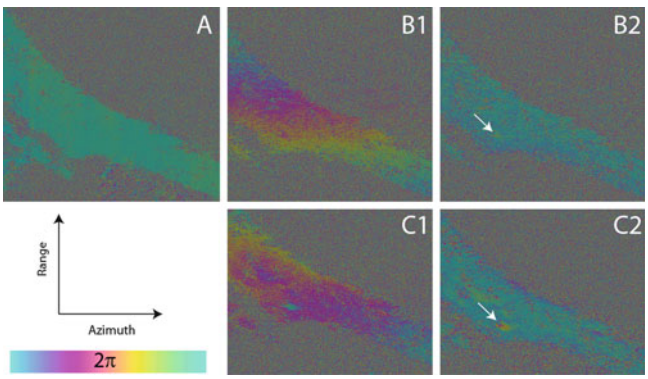


Fig. 5 Interferograms for three measurement intervals undertaken at Soazza (see text for details). *A*: March 2010 reference measurement, *B1* and *B2*: March–May 2010, *C1* and *C2*: May–August 2010

the radar was levelled and centred with reference to a fixed survey point (Fig. 3). During each campaign, 3–4 h of continuous data was acquired with the antennae programmed to rotate through a sector of about 70 °.

Results of the March–August 2010 campaigns are shown in Fig. 4 as a 5 month interferogram depicting cumulative displacements for the three measurement campaigns undertaken.

In Fig. 4, a reflectivity image (e.g. intensity of back-scattered energy) is overlain by a filtered interferogram where atmospheric phase noise has been removed. Points, A, B and C have been included to aid the reader's orientation with respect to the rock wall. Clearly visible is the slightly defocused top edge of the rock wall (which is lined with vegetation), areas of backscattering consisting of both strong

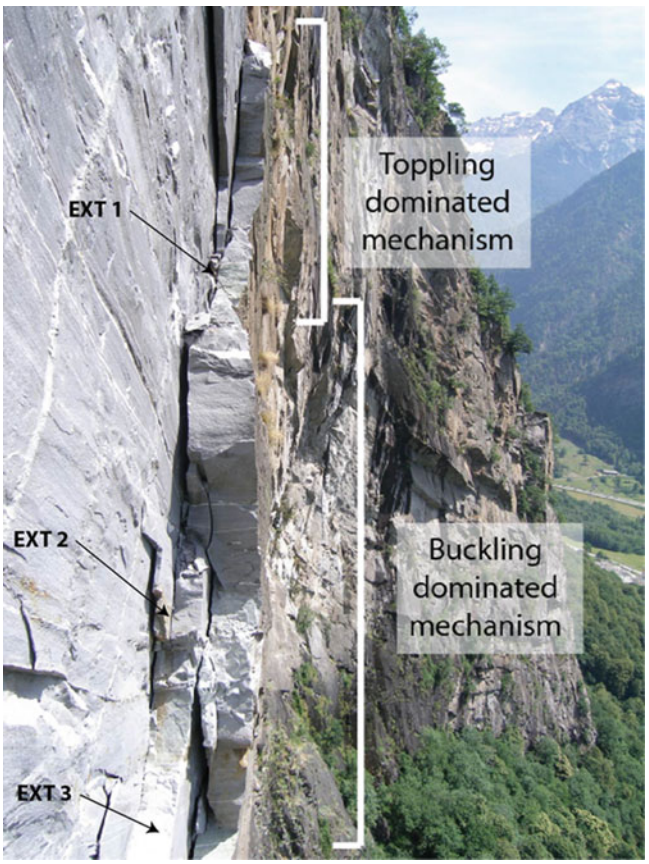


Fig. 7 View across the rock slab showing zones of toppling and buckling. The approximate position of in situ crack meters labelled EXT 1–3 are shown

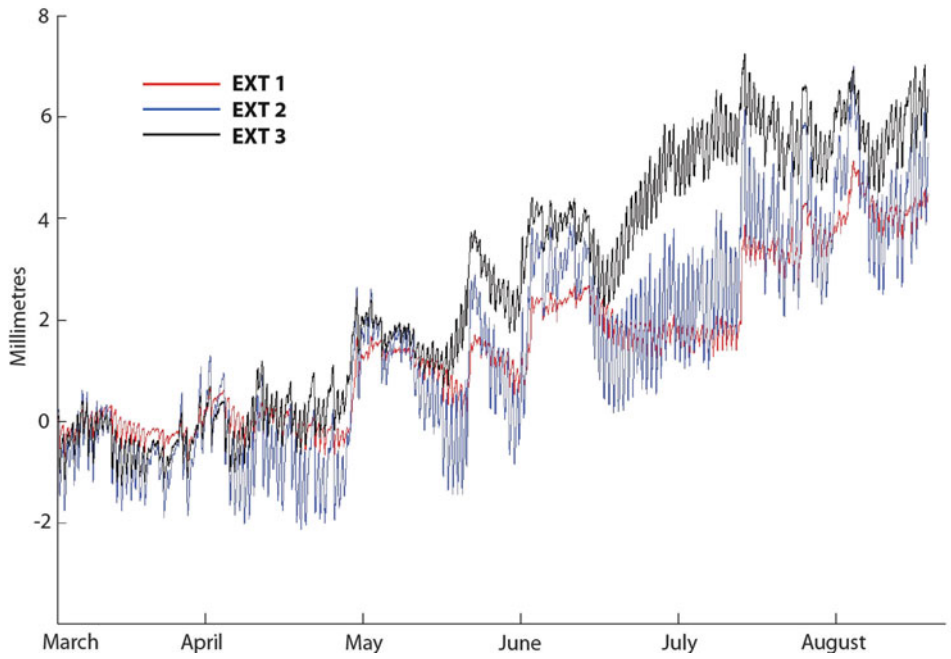


Fig. 8 Displacement trends for *3* in situ crack meters located on the *left-hand side* of the rock slab (see Fig. 7 for location of crack meters)

and weak natural reflectors, and forested areas directly at the foot of the rock wall. Coherent signals are evident on the rock wall, whilst decorrelation is notable in the vegetated areas.

Details of the March to August radar acquisitions are shown as a series of interferograms in Fig. 5. Interferograms in Fig. 4 are displayed in radar coordinates (e.g. range and azimuth). "A" demonstrates the relatively good phase stability for the reference measurement taken in March 2010, "B1" is an unfiltered interferogram for the period March–May 2010 showing a linear atmospheric effects on phase, whilst "B2" has atmosphere removed using a low-pass filtering method. A notable feature in "B2" is the emergence of a weak signal corresponding to the rock block adjacent to the failure from 2007 (deformation signal indicated with arrow). "C2" shows the interferogram for the interval May-August 2010, where the previous "weak" signal is stronger and more evident (deformation signal indicated with arrow).

Discussion

Spatially distributed displacements measured at Soazza show a discrete area of movement corresponding to a large rock slab similar in dimension to the block failure of 2007 (~3,000 m^3).

Qualitatively, the displacement field shows a relatively rapid change in the displacement gradient (i.e. velocity changes over a short distance) towards the lower boundary, whilst toward the right-hand boundary the gradient is apparently more gradual. The upper boundary of the block is also characterized by a relatively gradual displacement gradient.

Coherent signals show measured average displacements on the order of 0.5–0.6 mm/month (total displacement 3.5–4.0 mm). Phase unwrapping revealed a deformation map (Fig. 6) that clearly delineates the displacements associated with the large rock slab. Although the displacements are relatively small the radar signature depicted in Fig. 6 shows a greater degree of movement in the middle-left part of the block.

The radar signature appears consistent with a toppling mechanism taking place across the upper portion of the block, whilst in the mid-region, particularly toward the left margin, an outward buckling mechanism is observed. The toppling/buckling mechanism is consistent with field observation (Fig. 7).

In addition, preliminary analysis of three in situ crack meters located on the left margin of the rock slab; (EXT 1–3 in Fig. 7) show a greater degree of displacement occurring on the middle section (EXT 2 and 3) of the block compared to the upper part (Fig. 8).

Conclusions and Outlook

A rock slab approximately 3,000 m^3 characterized by average displacements of 0.5–0.6 mm/month was measured over a 5 month period (e.g. 3 measurement campaigns) using

a portable radar interferometer. The radar signature indicates a combined toppling and bucking failure mechanism.

The goal of ongoing research seeks to elucidate further details of the failure mechanism(s), through the application of periodic high resolution laser scanning, monitoring using in situ crack meters and a micro seismic network. Additionally, various environmental parameters are being monitored to understand possible external forcing factors relevant for driving failure processes.

Acknowledgments This project is supported through an initiative of the Swiss Government to foster and promote scientific and technological competences related to space activities. Financial supprt is coordinated by the Swiss Space Office of the Swiss State Secretariat for Education and Research. We further acknowledge the ongoing support provided by the State road authority (Tiefbauamt) in Canton Graubünden, namely, Mr. Christoph Nänni.

References

Leva D, Nico G, Tarchi D, Fortuny-Guasch J, Sieber A (2003) Temporal analysis of a landslide by means of a ground-based SAR interferometer. IEEE Trans Geosci Remote Sens 41(4):745–752

Tarchi D, Casagli N, Fanti R, Leva D, Luzi G, Pasuto A, Pieraccini M, Silvano S (2003a) Landslide monitoring by using ground-based SAR interferometry: an example of application to the Tessina landslide in Italy. Eng Geol 68:15–30

Tarchi D, Casagli N, Moretti S, Leva D, Sieber AJ (2003b) Monitoring landslide displacements by using ground-based synthetic aperture radar interferometry: application to the Ruinon landslide in the Italian Alps. J Geophys Res 108(B8):2387. doi:10.1029/2002JB002204, 2003b

Werner C, Strozzi T, Wiesmann A, Wegmüller U (2008) GAMMA's portable radar interferometer. In: Proceedings of 13th FIG/4th IAG, Lisbon, Portugal

Wiesmann A, Werner C, Strozzi T, Wegmüller U (2008) Measuring deformation and topography with a portable radar interferometer. In: Proceedings of 13th FIG/4th IAG, Lisbon, Portugal



Landslides and Hydro-Climatic Conditions in the Hutná Catchment Area (Central Slovakia)

Roberta Prokešová, Alžbeta Medveďová, and Zora Snopková

Abstract

This contribution presents preliminary results obtained by hydro-climatic analysis of the Hutná catchment area in Central Slovakia, where several landslide reactivations were recorded in last decades as a consequence of weather anomalies. The majority of these landslides reach the inhabited areas, thus continuously threatening individuals who live there. We have been focused on evaluation of hydro-climatic conditions that preceded the reactivation events to better understand relationships between precipitation, antecedent hydrological conditions of the catchment and initiation (or reactivation) of movements. Our analysis confirms that antecedent hydrological conditions can be crucial for failure initiation in slopes with thick colluvial deposits. While the rainy seasons following a long-lasting wet periods were responsible for failure initiations and/or landslide reactivations, only slight acceleration of creep movements were recorded after the rainy seasons (although exceptional and several moths long) following dry period.

Keywords

Slovakia • Hutná catchment • Hydro-climatic conditions • Slope failure

Introduction

Landslides and other slope deformations are important landforms as well as serious endangers in the Western Carpathians. According to the most recent data (Kopecký et al. 2008) about 21,200 slope deformations have been registered until 2006 covering almost 5.25 % of the total area of Slovakia. The most disturbed areas in Slovak part of the Western Carpathians are those build up of Palaeogene and Mesozoic rocks of the Pieniny Klippen Belt (14.8 %), Palaeogene rocks of the Flysch Belt (12.7 %) and Neogene Volcanic areas (9.3 %).

Landslides in Neogene Volcanic areas are evolved in low-gradient slopes with thick accumulation of quarternary slope deposits on the foothill of extinct and highly degraded stratovolcanoes (Nemčok 1982). Some of the most-known landslides in Slovakia are located in this region including the greatest disaster in Slovak part of the Western Carpathians that originated in December 1960 in the town of Handlová (more than 150 residences destroyed besides infrastructure damage; e.g. Záruba and Mencl 1969; Nemčok 1982; Ondrášik 2002). Other well-known events in this area are the Lubietova landslide (e.g. Nemčok 1982; Prokešová et al. 2010; Greif and Vlčko 2012) reactivated at the end of February 1977 or the Velka Čausa landslide periodically active since 1969 (e.g. Jelinek and Wagner 2007).

All the above-mentioned landslides, along with many others in the Western Carpathians, were triggered by an increase of pore-water pressure after prolonged period of rainfall (frequently associated with snowmelt) although their

R. Prokešová (✉)
Matej Bel University, Cesta na amfiteáter 1, Banská Bystrica 974 01, Slovakia
e-mail: roberta.prokesova@gmail.com

A. Medveďová
Matej Bel University, Banská Bystrica, Slovakia

Z. Snopková
Slovak Hydrometeorological Institute, Banská Bystrica, Slovakia

C. Margottini et al. (eds.), *Landslide Science and Practice*, Vol. 2,
DOI 10.1007/978-3-642-31445-2_43, © Springer-Verlag Berlin Heidelberg 2013

response to precipitation is rather delayed and unclear. Therefore, the increase of their displacement rates and future behaviour are difficult to predict (Greif and Vlčko 2012).

Year 2010 can be considered as record-breaking with respect to long-term precipitation records in majority of regions of Slovakia. Numerous regions in Slovakia have been injured by heavy and extensive rainfalls mainly in May and in early June of 2010. The humid weather conditions continued until the end of the year. Consequently, hundreds of landslides (reactivations as well as new failures) were recorded in landslide prone areas in Slovakia (Liščák et al. 2010). The similar situations were reported also from neighbouring Central European regions (e.g. Baroň et al. 2011).

This paper presents results of hydro-climatic analysis carried out in the Hutná catchment in Central Slovakia. The area is known by several landslide events in the recent history that were linked to extreme precipitation. However, neither new slope failures nor reactivations were recorded in the area after the extremely rainy year of 2010 with the highest annual precipitation since 1950. We analyse hydro-climatic conditions of 2010 with respect to those preceding reactivation events in the 1960s and 1970s to assess whether the rainfalls (an associated snowmelts) were the main triggers of previous slope failures or some other concurring factors could have played a favourable role.

Materials and Methods

Study Area

The Hutná catchment is located at the northern slopes of the Poľana stratovolcano, which is a part of the Central Slovakia Neogene Volcanic Field (Fig. 1). It is rather small catchment (45,169 km^2) with predominantly natural character. Its elongated area consists of five sub-basins (marked as I–V in Fig. 1a) that extend from about 390 to about 1,270 m a.s.l. (Fig. 1b). The climate in the catchment area should be characterised as moderately warm, very humid to moderately cool with average annual rainfall ranging from 749 mm (computed from measurements of rain gauge "R1" located at altitude 477 m a.s.l.) to about 848 mm (computed from measurements of rain gauge "R2" located at altitude 1,080 m a.s.l., about 300 m eastward from the watershed). In terms of annual course of precipitation, the highest monthly totals are occurring in June, while the lowest ones in February and March (Fig. 3a).

Slope deformations are widespread at the left side of the Hutná River where they are conditioned by superposition of two rock complexes with different strength and permeability.

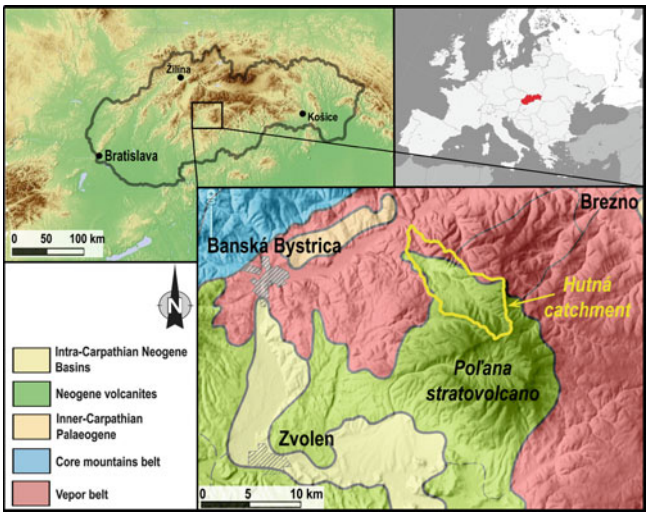


Fig. 1 Location of the study area

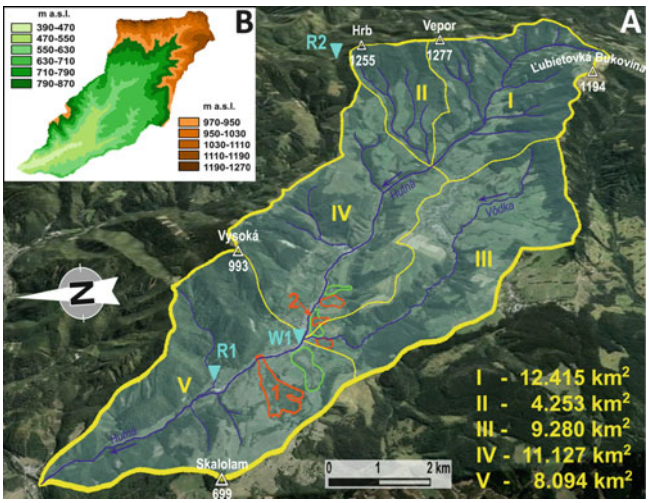


Fig. 2 The Hutná catchment area. (**a**) The catchment area with location of active (*red*) and potential (*green*) landslide bodies, position of rain gauge and flow gauge stations, and sub-basin areas. (**b**) Hypsometry of the area

Hard, rigid and permeable andesitic epiclastic breccias to conglomerates together with polymict gravels to conglomerates outcropping at the higher altitudes superimpose soft and impermeable Palaeogene and Neogene argillaceous formations. Landslides are evolved in gently-inclined (average slope gradient 6–7 °) lower parts of slopes that are covered by thick (up to 30 m) quaternary colluvial deposits. Several landslide events were recorded in this area in the second half of the twentieth century. The most devastating of them was so called "catastrophic landslide" (Landslide-1 in Fig. 2) that started at the end of February 1977 after prolonged period of rainfall and snowmelt. Before this event, several reactivations happened in the area of old

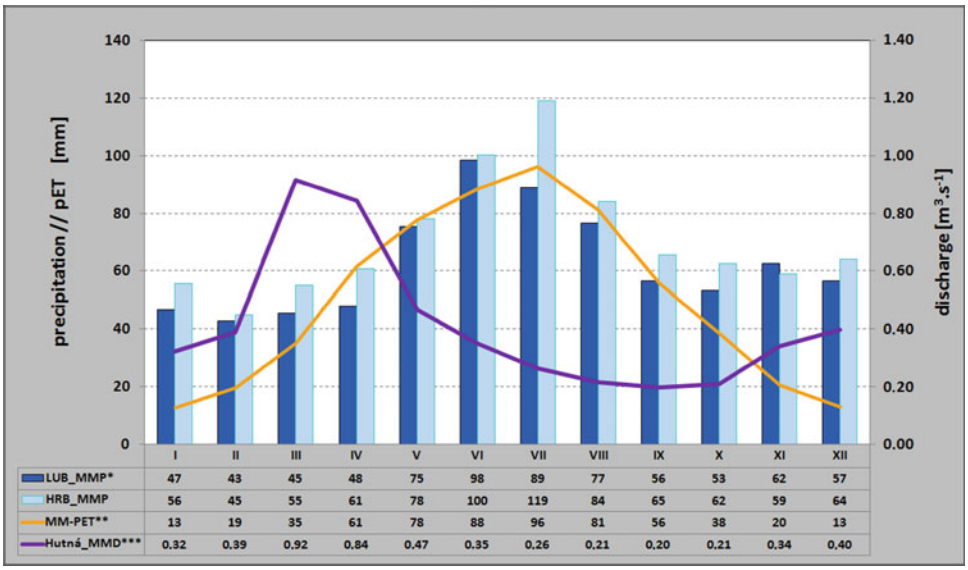


Fig. 3 Graphical illustrations of main meteorological and hydrological characteristics of the Hutná catchment. Abbreviations: MMP – mean monthly precipitation totals computed from R1 and R2 rain gauges (1951–2009), MM_pET – mean monthly potential evapotranspiration (1984–2009), MMD – mean monthly discharge (1976–2009)

dormant landslide (Landslide-2 in Fig. 2) near the football field, mainly in the 1960s.

Data

Hydro-climatic conditions in the Hutná catchment area have been analysed using data of rain gauge and flow gauge stations that are situated in the catchment area (Fig. 2). Monthly precipitation totals since 1951, and daily precipitation totals since 1981 from the Ľubietová rain gauge station (R1 in Fig. 2) and average daily discharge of Hutná since November 1975 from the flow gauge station (W1) are the basic data stored by Slovak Hydrometeorological Institute in digital form.

Since a weak correlation between "normal" precipitation (P) and moderately to deep-seated landslide initiation and/or movement acceleration has been usually reported, effective precipitation (EP) can be evaluated with higher success. According to definitions, the "effective precipitation" is a fraction of the total precipitation that reaches the groundwater table (Kruhl and Liefrinck 1946; Dakshinamurti et al. 1961). Therefore, this is the portion of precipitation that should be responsible for groundwater table increase and landslide initiation. In fact, real effective precipitation is influenced by many factors, such as antecedent soil moisture and soil storage, intra-annual variability in soil-infiltration capacity, evapotranspiration, and surface runoff and is rather hardly quantified precisely. Consequently, we use term "potential effective precipitation" (*pEP*) as rough indicator of those fraction of precipitation that is available for infiltration. Potential effective precipitation was computed as excess of precipitation over potential evapotranspiration (*pET*):

$$pEP_i = P_i - pET_i \quad (1)$$

Therefore, the pEP can be understood as analogue of the climate moisture index – CMI (Hogg 1997). Thus, positive values of pEP lead to recharge of soil moisture reserves until saturation, while negative ones should indicate release of moisture from the soil reserves.

With respect to available data, monthly values of pET were calculated using simple empiric formula by Novák (1995):

$$pET_i = 0,0018(25 + Tm_i)^2(100 - r_i)[mm] \quad (2)$$

where Tm_i is average air temperature in the month "*i*" and [°C] and r_i is average air relative humidity [%] in the month "*i*". Because temperature and relative humidity are not available for Lubietova rain gauge station, data were taken from the meteorological station Brezno, situated at the same elevation as the Lubietova rain gauge. Average values characterizing mean monthly precipitation totals and mean monthly potential evapotranspirations in the investigated area are illustrated in Fig. 3.

To better understand the relationships between precipitation (snowmelt), antecedent moisture conditions, and failure initiation, the mean daily discharge of the Hutná River (available since October 1975 thus including the date of catastrophic failure in February 1977) have been evaluated and used as indicator of temporal and spatial response of the catchment to rainfalls that is conditioned primarily by antecedent hydrological conditions (Reichenbach et al. 1998) of the area. Daily and monthly precipitation volumes in the area of sub-catchments II–V (37,075 km^2) and daily and monthly discharge amounts have been calculated as input

data for computation of monthly precipitation/discharge ratio (P/D-R_{month}).

Results

Accepting the idea that moderately to deep-seated landslides (defined here as landslide with slip plane below 3 m, affecting area above 0.1 km^2, with volume above 10^5 m^3), are characterised by slow and complex precipitation-failure relationships (e.g. van Asch et al. 1999; Lindenmaier et al. 2008), meteorological data ranging from daily to monthly precipitation and evapotranspiration values should be sufficient for analysis.

Analysis of "normal" precipitation showed that correlations between precipitation totals and time of failures initiation are rather questionable. The most indicative graphical solution seems to be seasonal precipitation totals plotted against seasonal long-term averages (Fig. 3a), where April to September as warm season and October to March as cool season are considered in accordance to standard climatic analysis in Slovakia. However, although several important wet seasons (>150 % of seasonal mean precipitation values) are detectable in Fig. 4a, only two of them were connected with the important slope failure events in the area.

Consequently, it was examined how important the evapotranspiration as factor influencing groundwater regime in the deeper parts of the slopes is. For this goal the pET as indicator of antecedent moisture condition have been computed using (1) and (2). The most informative graphical expression is the summation curve of pEP, in which the rising and downward sloping sections indicate periods of moisture infiltration and releasing, respectively, while the horizontal ones represent equilibrium between precipitation and evapotranspiration (Fig. 4b).

The summation curve can be successfully used as indicator of suitable condition for failure initiation, especially if its course is assessed with respect to its mean trend. As critical appear the steep sections of summation curve that cross-up the trend line or lie above it, which represent long-lasting rainy periods (i.e. several seasons) leading to surplus of moisture and consequent oversaturation of the area or shorter rainy seasons during the long-lasting periods of high moisture condition in the area, respectively. On the other hand, also several dry periods when the moisture was rather releasing from the soils and subsoils, are indicated. The most important are 1985–1993 and 2006–2009 periods (Fig. 4b). It is clear, that one rainy season following those long-lasting dry periods does not have to lead to the landsliding even though the precipitations are exceptionally high. Instead, only slight acceleration of creep movements can be registered. This can be confirmed by geodetic monitoring in the Landslide-1 that is carried out by SGIDS since 1988. Although geodetic measurements have been realised irregularly and rather rarely, some acceleration phases can be correlated with rainy-seasons (indicated small green arrows in Fig. 4b, see also Table 1).

We have also studied whether the Hutná discharge can be used as indicator of critical hydrological conditions leading to slope failure events. According to Reichenbach et al. (1998), runoff intensity can roughly measure the temporal and spatial response of a catchment to the meteorological events as well as catchment hydrological conditions, despite the fact that it is the result of complex interactions.

To better assess antecedent hydrological conditions in the catchment at the time of slope failure, we calculated monthly "precipitation/discharge ratio" (PDR_M) as a ratio of monthly volumes of precipitation fallen in the catchment area (up to the flow gauge W1) and monthly volume discharge of Hutná. Low PDR_M values (i.e. <1) indicate snowmelt periods, PDR_M about 1 indicate roughly equal values of monthly volume discharge and monthly precipitation volume (either high or low), whereas high PDR_M values (>4) indicate occurrence of high rainfall event during rather under-saturated (dry) long-term conditions. Plotting PDR_M curve against monthly Hutná discharge (Fig. 5) critical periods can be identified. We can emphasise a considerably different hydrological conditions in the late 1970s (Fig. 5a) with respect to those in the 2002–2010 period (Fig. 5b) when only short-lasting (although intense) summer storm rainfalls and/or spring snowmelts occurred during generally under-saturated conditions of the area caused above all by drier cool seasons and warmer summers (with higher pET) during 2002–2009. Thus exceptionally rainy-season of 2010 follows after several years long dry period.

Discussion and Conclusions

Moderately to deep-seated landslides are usually initiated after long-lasting wet periods rather than single, even exceptionally intensive, rainfall event (e.g. van Asch et al. 1999; Lindenmaier et al. 2008). Therefore, they are characterised by slow and complex precipitation-failure relationships, when evapotranspiration and antecedent hydrological conditions of the slope are also important. As a result, it can be difficult to forecast slope failure initiation for any one specific landslide body, let alone for wider area.

Presented analysis of hydro-climatic conditions that preceded slope failure events in the Hutná catchment area confirms that antecedent hydrological conditions can be crucial for failure initiation in slopes with thick colluvial deposits. This can be proved mainly by analysis of potential effective precipitation. All the important landslide events occurred during long-lasting wet periods that led to persistent moisture excess. These periods are expressed as the

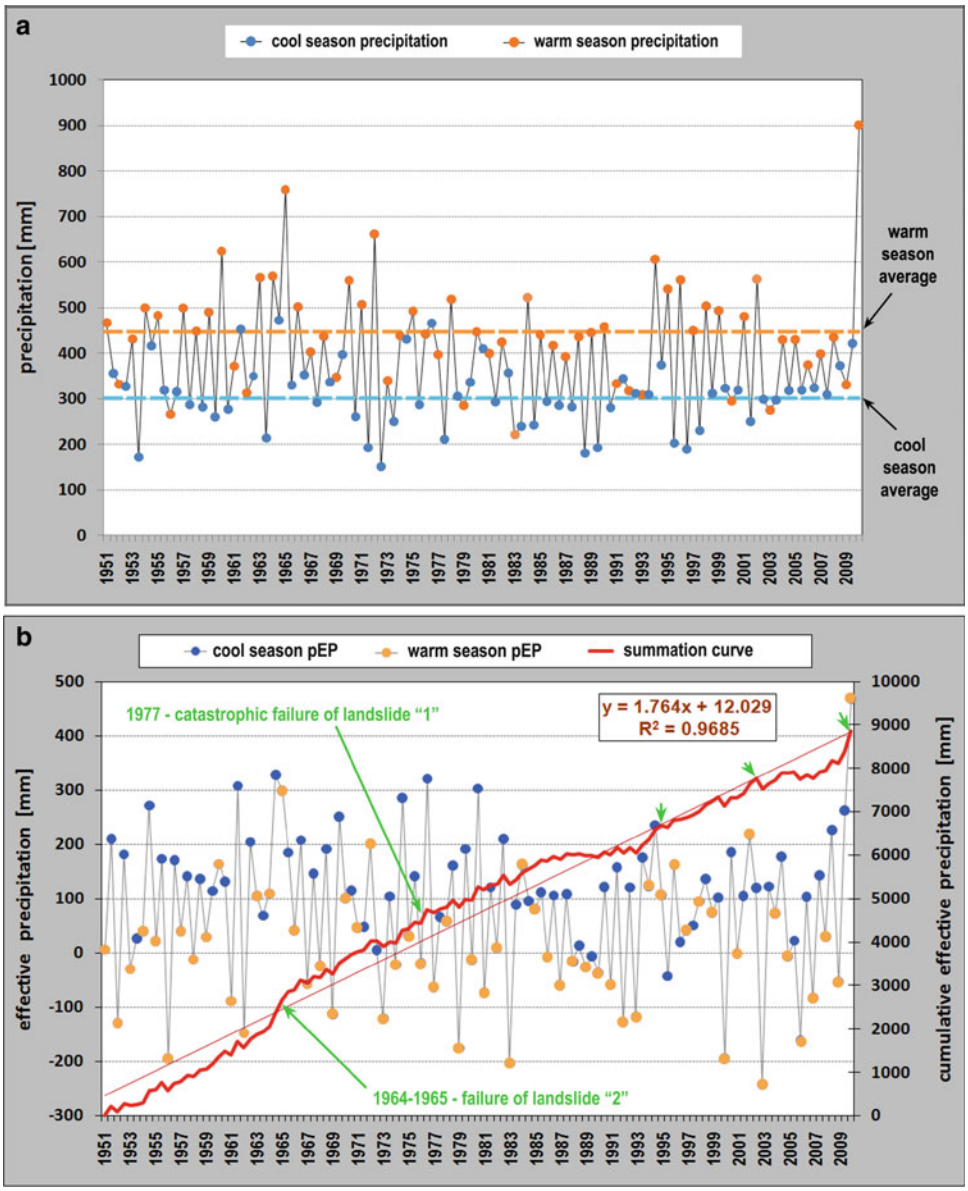


Fig. 4 Graphic expressions of "normal" and "effective" seasonal precipitation totals since 1951. (**a**) Seasonal precipitation totals plotted against long-term seasonal averages. (**b**) Seasonal pEP totals, summation curve of pEP (*thick red line*) and trend line of cumulative pEP (*thin red line*). Small green arrows – accelerations of creep movements recorded in the Landslide-1

Table 1 Average annual displacements of monitoring points in the Landslide-1

Period	Average annual displacements (m)	Average annual displacements of the most active points (m)
1988–1993	0.015	0.052 (2/25)[b]
1993–1994	**0.016**	**0.041 (4/25)**
1994–1996	0.013	0.039 (3/25)
1996–1999	0.011	0.026 (3/25)
1999–2001	0.026	0.056 (2/25)
2001–2002	**0.024**	**0.078 (3/25)**
2002–2004	0.007	0.022 (2/25)
2004–2006	0.007	0.016 (2/25)
2007–2008	0.015	————
2008–2009	0.005	0.019 (4/24)
2009–2010	0.013	0.033 (2/29)
2010–2010[a]	**0.016**	**0.042 (9/33)**

Data from 1988 to 2006 were taken from SGIDS (2011)
[a]Measured interval: April 2010 to October 2010.
[b]Number of points in calculation/number of all monitored points.

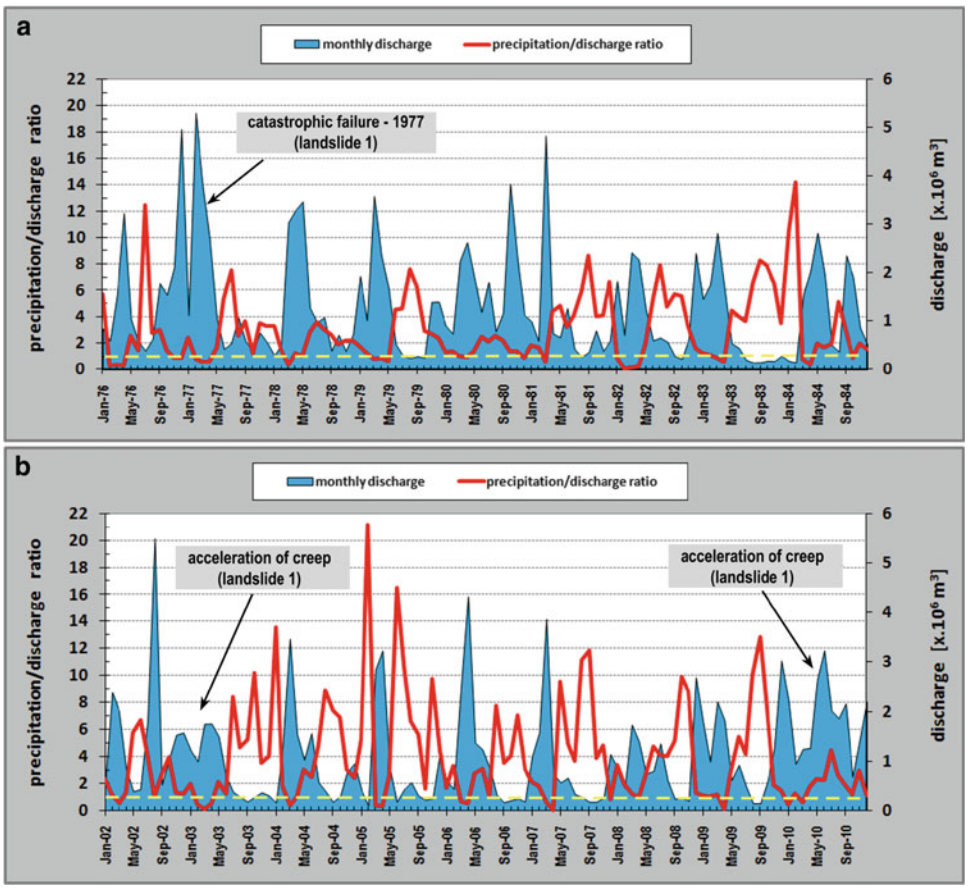


Fig. 5 Monthly "precipitation/discharge ratio" (PDR_M) plotted against monthly Hutná discharge

steep sections of pEP-summation curve, which either climb-up across the long-term trend-line or lie above it (Fig. 4b). Analogous results were obtained by analysis of the Hutná discharge. Monthly values of PDR plotted against monthly Hutná discharge have been used as rough indicator of hydrological conditions of the area. The catchment response to rainfall surely depends on a variety of factors affecting the shape of hydrograph, but most of them, such as topography, geological conditions, soil types or shape of the drainage basin, remain unchanged over time for specific catchment. Therefore soil saturation along with rainfall rates and intensity, vegetation, and evapotranspiration can be taken as main factor influencing this response.

Our analysis can help to explain, why the extreme precipitation of 2010 did not cause any landslide reactivations in the area, despite their exceptionality (the highest annual precipitation totals at least since 1951). We believe that some (possibly all) of the following factors were active simultaneously.

1. Several foregoing seasons of low pEP led to continual releasing of moisture from the slopes. This led to high degree of under-saturation of deeper parts of slopes that require longer period of precipitation leading to moisture surplus.
2. Lateral river erosion at the toe of Landslide-1 is now prevented by remedial works.
3. Partial functionality of the drainage system on Landslide-1 (created after the disastrous failure in 1977) still can be considered despite that its effectiveness is gradually decreasing.
4. Rank vegetation in the Landslide-1 helps to increase real evapotranspiration in the area thus lowering both the overall landslide risk in precipitation-rich warm seasons and reactivation of shallower partial slides.

Given that the influence of factors 2–4 can be considered only for the Landslide-1, the importance of the factor "1" is thus emphasized. On the other hand, the impact of some man-induced factors such as inappropriate slope reclamations at the area of Landslide-1 in the early 1970s and/or slope undercutting due to football field widening at the area of the Landslide-2 should be considered in the previous slope-failure events.

Our preliminary results confirm that antecedent hydrological conditions can be one of the most important factors influencing moderately to deep-seated landslides behaviour in the low gradient slopes. Long (e.g. several years) dry period can increase the stability of the slope to such an extent that one isolated rainy season, even though exceptionally

intensive, will not initiate the slope failure. The following research will be focused on more detailed analysis of the Landslide-1 to better understand the relationships between meteorological conditions, ground-water level fluctuations, and movement patterns whereby obtain more specific and generally applicable results.

Acknowledgments This contribution was supported by the Scientific Grant Agency of SR – VEGA project 1/0157/10.

References

Baroň I, Řehánek T, Vošmik I, Musel V, Kondrová L (2011) Report on a recent deep-seated landslide at Gírová Mt., Czech Republic, triggered by a heavy rainfall: the Gírová Mt., Outer West Carpathians, Czech Republic. Landslide 8:355–361

Dakshinamurti C, Saxena PN, Rao KG (1961) Evaluation of effective rainfall and irrigation from ground-water measurements. Nature 190:1100–1101

Greif V, Vlčko J (2012) Monitoring of post-failure landslide deformation by the PS-InSAR technique at Lubietova in Central Slovakia. Environ Earth Sci 66:1585–1595

Hogg EH (1997) Temporal scaling of moisture and the forest–grassland boundary in western Canada. Agric Forest Meteorol 84:115–122

Jelinek R, Wagner P (2007) Landslide hazard zonation by deterministic analysis (Veľká Čausa landslide area, Slovakia). Landslides 4:339–350

Kopecký M, Ondrášik M, Martinčeková T, Šimeková J (2008) Atlas of slope failures. Enviromagazín 5:8–9

Kruhl WFJM, Liefrinck FA (1946) Recent groundwater investigations in the Netherlands. Elsevier Pub. Co. Inc., Amsterdam, 78pp

Lindenmaier F, Zehe E, Wienhöfer J, Ihringer J (2008) Hydrological patterns and processes of a deep seated creeping slope at Ebnit, Vorarlberg. In: INTERPRAEVENT 2008 – conference proceedings, vol. 2, pp 183–194

Liščák P, Pauditš P, Petro Ľ, Iglárová Ľ, Ondrejka P, Dananaj I, Brček M, Baráth I, Vlačiky M, Németh Z, Záhorová Ľ, Antalík M, Repčiak M, Drotár D (2010) Registration and evaluation of newly evolved slope failures in 2010 in Prešov and Košice regions. Miner Slovaca 42(2):393–406

Nemčok A (1982) Zosuvy v Slovenských Karpatoch. Veda, Bratislava, 319pp

Novák v (1995) vyparovanie vody v prírode a metódy jeho určovania. Veda, Bratislava (ISBN: 80-224-0409-8), 260pp

Prokešová R, Kardoš M, Medveďová A (2010) Landslide dynamics from high-resolution aerial photographs: a case study from the Western Carpathians, Slovakia. Geomorphology 115(1–2): 90–101

Reichenbach P, Cardinali V, DeVita P, Guzzetti F (1998) Regional hydrological thresholds for landslides and floods in the Tiber River Basin (central Italy). Environ Geol 35(2–3):146–159

SGIDS (2011) Centre of partial monitoring system. http://dionysos.gssr.sk/cmsgf/result/db_result_zosuvanie.php Accessed 10 Mar 2011

Van Asch TWJ, Buma J, Van Beek LPH (1999) A view on some hydrological triggering systems in landslides. Geomorphology 30:25–32

Záruba Q, Mencl V (1969) Landslides and their control. Elsevier, Amsterdam, 340pp



Landslide Umka: The First Automated Monitoring Project in Serbia

Biljana Abolmasov, Svetozar Milenković, Branko Jelisavac, and Vladeta Vujanić

Abstract

In the past decade, there has been a gradual introduction of systematic monitoring on the largest landslides in Serbia by establishing a network of monitoring facilities. The first manual monitoring system was installed near Belgrade on Umka landslide including survey points, inclinometers, piezometers, triaxial deformeters etc. As the rapid adoption of new technologies continues – the natural evolution of equipment for landslide monitoring has started. The technological evolution of GPS based systems creates the potential for automated remote collection of accurate, high resolution data and represents step forward that will increase speed, precision, cost effectiveness and overall quality of landslide investigations. This paper presents first results, features and benefits of introducing automated approach in order to provide high quality data as a base for detailed landslide investigations.

Keywords

Landslide • GPS • Monitoring • Real time

Introduction

Various professions deal with research and investigation of the landslide processes and landslides as occurrences, but basically the main aim of the greatest part of the research is to design appropriate remedial measures which would enable permanent stability of the slopes or cuts. For that reason, the greatest number of researches is directed to establishing the geometry of the landslides and physical-mechanical characteristics of sliding mass affected by the sliding process and parameters of shear strength in the zone of the sliding surface itself. Monitoring of the landslides is an integral part and very important element of the research process. However, in practice, it most often results in non-continual or observation intervals that are too short, inappropriate or incomplete equipment, which globally leads to insufficient amount of reliable data on parameters that are followed during the monitoring. Apart from traditional survey methods of monitoring (i.e. landmarks, reference points) monitoring systems also imply the use of geotechnical instruments, such as piezometers, inclinometers, or various types of sensors (in rainfall measuring stations, for measuring the moisture content in the soil etc.). In all active landslides they represent the minimum of equipment which enables obtaining various types of data necessary to understand the dynamics and mechanisms of landslide movement, actually being the basic prerequisite in designing successful remedial measures.

The technological evolution of Global Position System (GPS) technology and sensors for monitoring of landslide activity in real time started not so many years ago. Gili et al. (2000) give a general overview of the GPS principles and discuss its applicability to landslide monitoring on landslide Vallcebre (Spain). Using GPS technology to provide differential position information with subcentimeter level accuracy in structural and land monitoring applications was

B. Abolmasov (✉)
University of Belgrade, Djušina 7, Belgrade, Serbia
e-mail: biljana@rgf.bg.ac.rs

S. Milenković • B. Jelisavac • V. Vujanić
Geotechnical Department, The Highway Institute, Kumodraška 257, Belgrade, Serbia

C. Margottini et al. (eds.), *Landslide Science and Practice*, Vol. 2,
DOI 10.1007/978-3-642-31445-2_44, © Springer-Verlag Berlin Heidelberg 2013

investigated by Manetti et al. (2002a, b). The motion of the Super-Sauze earthflow (France) is clearly detected by the GPS measurements and the results have been compared with those obtained with conventional geodetic methods (Malet et al. 2002). Seasonal movement of the Slumgullion landslide (USA) determined from GPS surveys and field instrumentation from July 1998–March 2002 was presented in Coe et al. (2003). GPS monitoring experiment results from the Ya'an-Xiakou landslide (China) have demonstrated that GPS can provide sufficient accuracy to meet landslide displacement monitoring requirements, leading to the replacement of the conventional geodetic surveying methods (Zhou et al. 2005). Combination of GPS and photogrammetry methods can significantly improve the efficiency of landslide monitoring (Mora et al. 2003; Baldi et al. 2008). Brückl et al. (2006) describe a long experience of monitoring a deep seated mass movement in Gradenbach (Austria) with RGPS. It was concluded that is suitable for measuring relatively large displacements (slow and the upper range of very slow movements), which cannot be captured by inclinometers or extensometers. Bertacchini et al. (2009) established integrated surveying system for landslide monitoring of the Valoria landslide (Italy). The research deals with the integration of surface displacement measurements obtained using geodetic and topographic instruments such as satellite GPS and traditional one, like automatic total station, in a large-scale active earth-slide. Monitoring data have been collected inside and outside the landslide with sensors and loggers recording on a semi-continuous basis: rainfall, air temperature, groundwater flow and displacement rates (with wire extensometers, inclinometers). Barla et al. (2010) describe monitoring of the Beauregard landslide (Italy) using advanced and conventional techniques.

GPS measuring has proved to be an effective and reliable tool especially for measuring surface deformations on large and slow-moving landslides (Mansour et al. 2011). This paper presents first results, features and benefits of introducing automated GPS monitoring system on landslide Umka, Serbia.

Materials and Methods

Case Study

Serbia is known for numerous landslide phenomena. This is particularly stressed in the valley banks of rivers Sava and Danube and their respective tributaries. By both General and Preliminary designs of motorway from Belgrade to South Adriatic, i.e. E-763, at the exit from Belgrade, road facility corridor is located at the right bank of Sava river, on the meandering apex, crossing the landslide Umka–Duboko in the length of 3 km. Large active landslide in the depth of 10–26 m, created in marly clays, takes up the area of 1.8 km^2 (Fig. 1).

Pannonian sediments i.e. silty–clayey massive soft rocks have the dominant role in geologic composition of terrain, and these are: marls (M_3^2L), more than 200 m thick, and marly clays (M_3^2GL), 10–25 m thick. Stable landslide underlying stratum is made of grey marls. Under the triaxial test conditions, the shearing strength parameters within the natural moisture amount to $\varphi = 18–28\ ^\circ$ and $c = 30–200$ kPa.

Colluvial deposits (ko) emerged from the gravitational motion of rock masses down the slopes. Material set in motion in the course of time changed its primary structure, water content, and physical-mechanical properties. As a rule, colluvium thickness is predisposed by border between more plastic weathered marly clays and hard marls. Physical-mechanical properties of the colluvium vary in a wide range due to the complexity of its composition and susceptibility to external impacts. Shearing strength parameters along active sliding surfaces are $\varphi_r = 7–13\ ^\circ$, $c_r = 0$ kPa, $w = 30–45$ %.

This landslide is fan-shaped, with the length along the slope of 900 m, toe width of 1,450 m, area of 100 ha, average depth of 14 m, volume 14,000,000 m^3 and average gradient of 9 °. Upstream landslide part is surrounding the steep frontal scar with the height from 5 to 25 m, whereas downstream landslide part doesn't have a pronounced leap.

The last observations have been made on installed 29 inclinometers, 20 piezometers and 2 exploratory shafts during 2004–2005 years. According to morphology and sliding mechanism three blocks have been singled out: A, B, and C (Fig. 2). The length of blocks along the river is 850, 350 and 250 m. During 2005–2006 years, due to extensive displacements, majority of inclinometers were discontinued. The deepest displacements were recorded in block A – 26 m (Fig. 3), while in blocks B and C they amounted 5–15 m. Displacements as a rule have translational pattern along slightly inclined parting planes. Displacement speed is increasing during the diminution of Sava river level.

After 2005, research and monitoring were not performed, nor were there any remedial measures undertaken. Landslide Umka is still an active landslide with visible deformations on the M-19 road and local residential buildings.

System Architecture

In March 2010, a completely automated monitoring system was installed at the Umka landslide in the body of the landslide in bloc B (Fig. 2). Monitoring station was installed on the roof of the building which was estimated to enable the equipment to operate uninterruptedly (Fig. 5). Two reference points, Belgrade and Lazarevac were established as stable points. A double-frequency GPS receiver Leica SR530 and AT502 with monitoring and recording the satellite

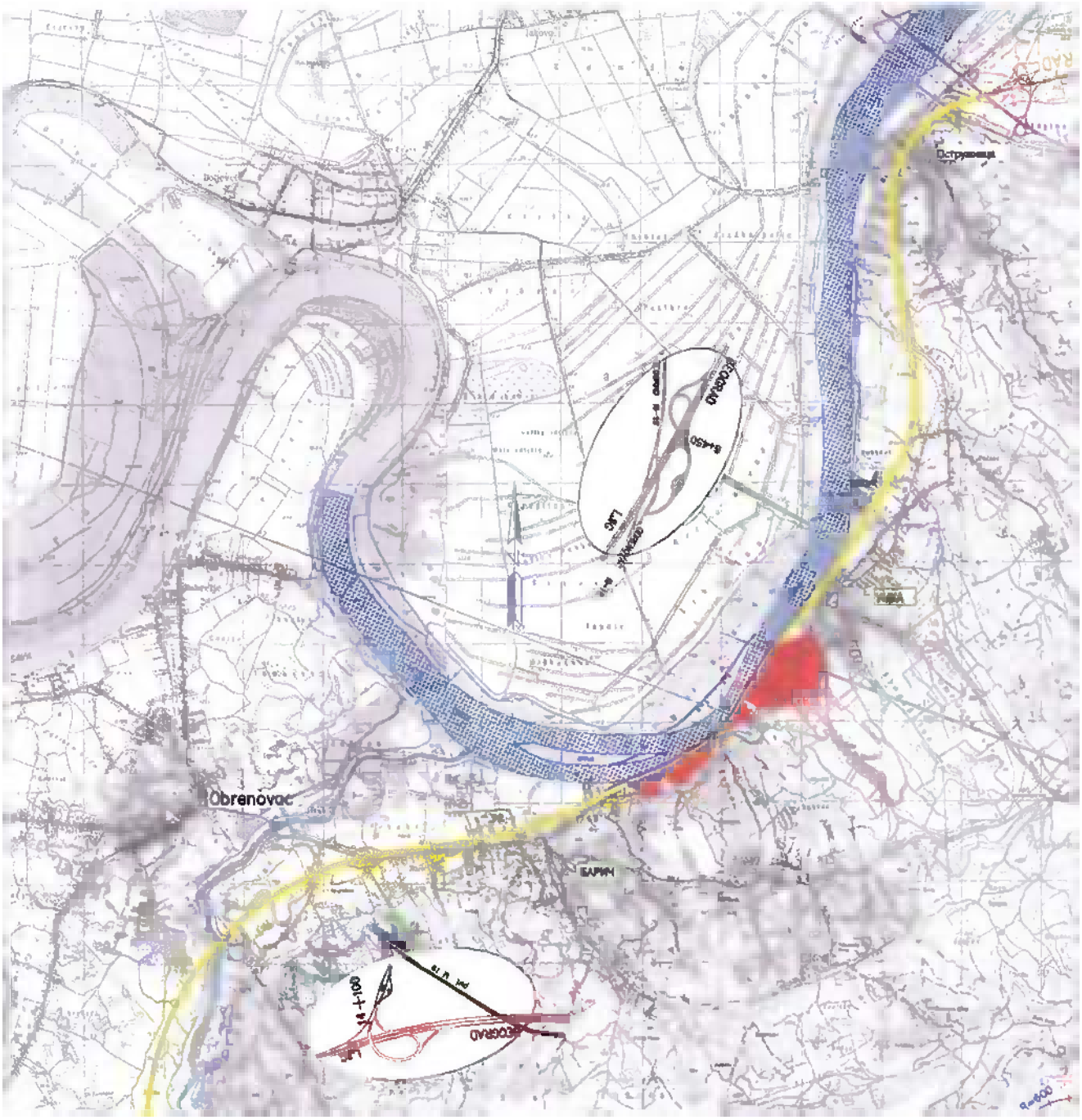


Fig. 1 Geographical position of Umka landslide

observations every 30 s (Fig. 4a, b) was installed. Automatic upload/download of files of recorded data has been pre-set at every 12 h (Fig. 7), while GSM modem for communication was used for the remote control and download of data, considering that the internet connection was of poor quality. Calculations of 2D and 3D coordinates of the monitoring station every 12 and 24 h was programmed from both reference stations of Belgrade and Lazarevac, as well as the control monitoring of both stations. Leica GNSS Spider software was used for real time and post processing analysis (Fig. 5).

Results and Discussion

The aim of establishing the GPS monitoring system was to monitor movements in the bloc B of the Umka landslide at low cost. These movements were already possible

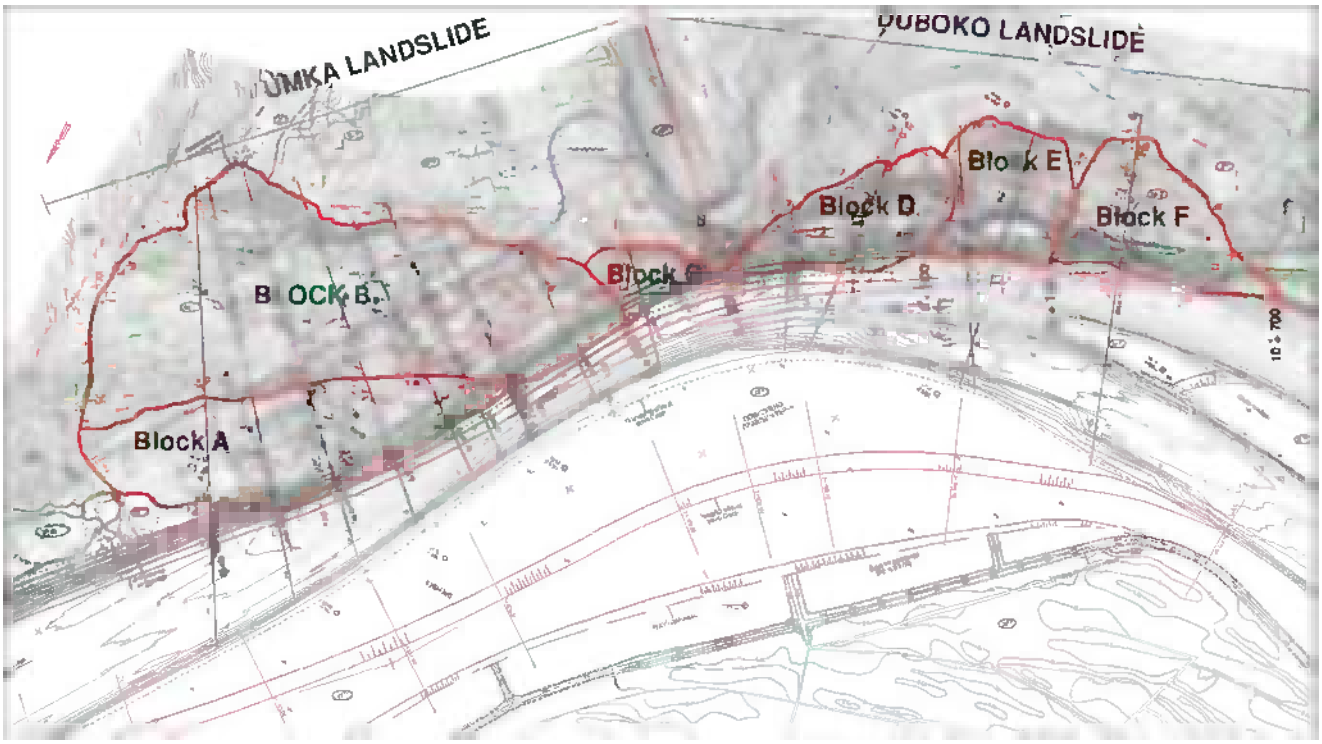


Fig. 2 Zoning of Umka–Duboko landslide as per sliding mechanism and dynamics; GPS station *black triangle*

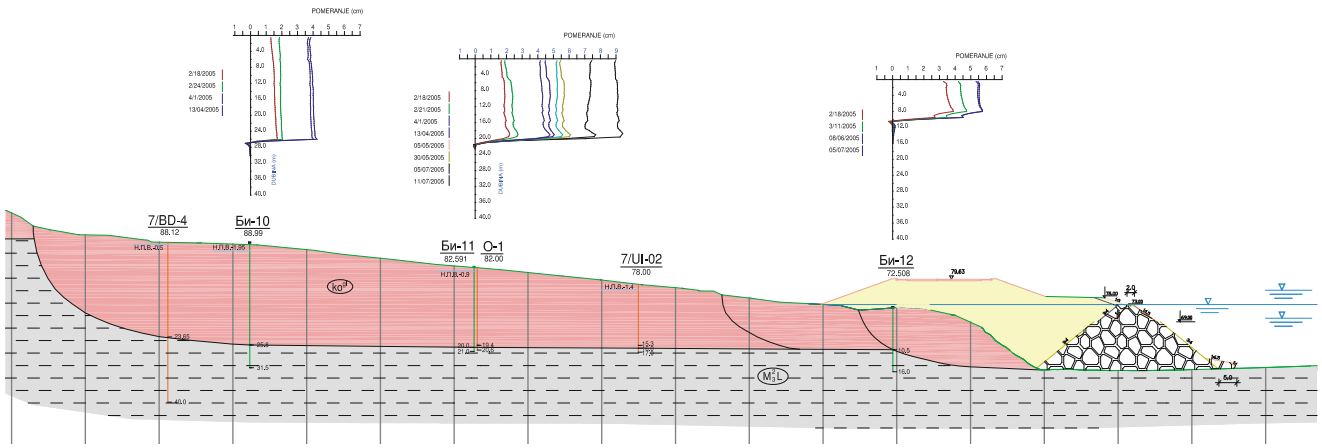


Fig. 3 Engineering geological cross-section km 8 + 151, Block A

to assess visually on the M-19 road and surrounding residential buildings the permanent deformations. There were no possibilities to install more GPS sensors, or to link in additional equipment (inclinometers, extensometers, piezometers or rainfall measuring stations) in the whole monitoring system.

Analysis of the results obtained by automatic monitoring of the landslide movement during the period from 28 March 2010 until 17 June 2011 showed that the movements were continuous and that they cumulatively amounted to 54 cm (2D and 3D movement diagram). There are two significant interruptions in measurements from 25-Jul-2010 until 20-Sep-2010 and from 30-Jan-2011 to 20-May-2011. Both times the system was restarted and the measuring equipment was calibrated. First interruption in measurements occurred due to a breakdown of the equipment, and the GSM modem was replaced. Second interruption occurred due to the equipment being turned off because of the internal decorating of the building. Fully automated GPS monitoring system in real time was re-established after 20 May 2011.

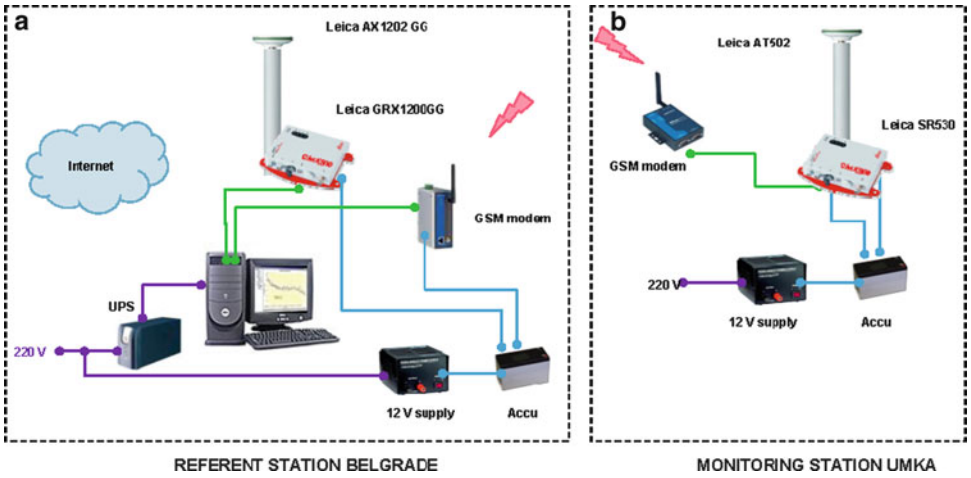


Fig. 4 (**a**) Architecture of monitoring system-left equipment of referent stations Belgrade and Lazarevac, (**b**) equipment of Umka station



Fig. 5 (**a**) Secondary landslide scarp in front of the house, (**b**) GNSS equipment in the box and (**c**) antenna on the roof of the house

During the monitoring, only one leap was recorded when there was a movement of around 2 cm in a single day (21-Jul-2010) (Fig. 6a, b). A crack in the staircase in the yard of the building was also recorded then. Calculations of 2D and 3D movements imply that in the period between 30-Jan-2011 and 20-May-2011, during which there was no monitoring or measuring, the movement amounted to more than 20 cm (Figs. 6a and 7). Movement coincided with springtime, during which the amount of movement is usually greater than during the other seasons because of the precipitations and the increase in the water level of the river Sava. For the same period during which the GPS monitoring was being done, the analysis of the effects of precipitations and the level of Sava was not performed, considering the significant distance of the closest measuring stations.

Conclusion

Establishing the automatic GPS monitoring system for the first time in Serbia on the landslide of Umka close to Belgrade had a goal to monitor the movements of the landslide during the period when there were no financial possibilities of establishing an integrated monitoring system. Single point GPS unit is not sufficient to track movements of this large bloc landslide. Furthermore, inexperience in operating the GPS real time monitoring systems and sensitivity of the equipment were the cause of some of the interruptions in measurements, which will be avoided in the upcoming period. It is planned to install additional equipment at the landslide – further two GPS receivers, automatic rainfall gauge, and one more inclinometer, i.e. TDR equipment after this first year during which the equipment testing was also performed.

Establishing a fully integrated and equipped system which would be suitable for Umka landslide is still very expensive. However, the experience gained during the first year of monitoring and measuring clearly indicate the advantages of this type of monitoring system as well as the need to also install standard geotechnical equipment apart from the GPS sensors in extra-large and deep seated slow moving landslides. That is the only way to perform complete monitoring and obtain results that will help us in better understanding of the mechanism and dynamics of landslides.

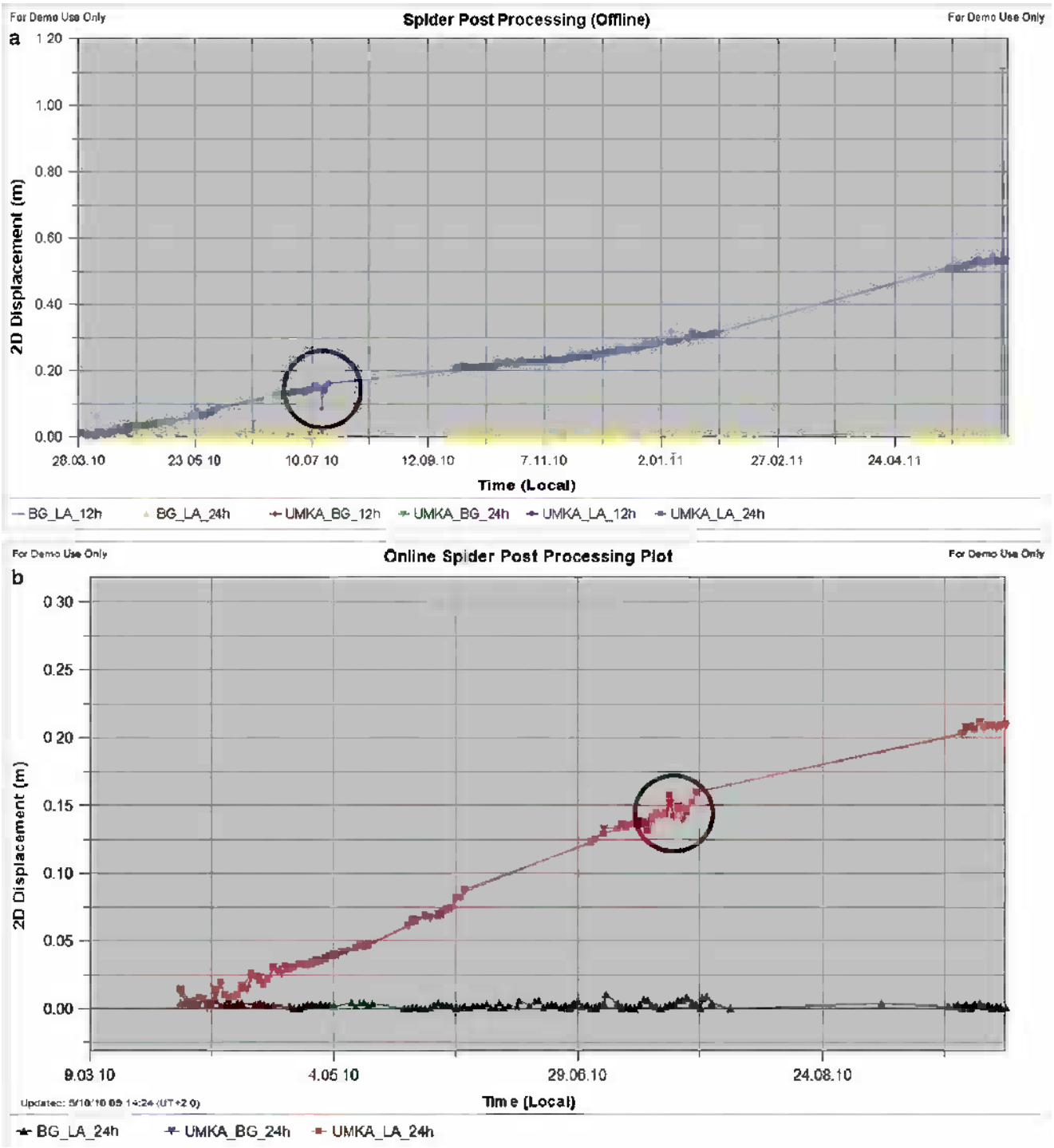


Fig. 6 (**a**) 2D displacement plot from 28 March 2010 to 17 June 2011; *Blue line*-displacement of GPS point; *Circle mark* shows detail of 21 July moving; *Yellow line*-stability of referent stations. (**b**) 2D displacement detail plot with marked displacement on 21 July 2010

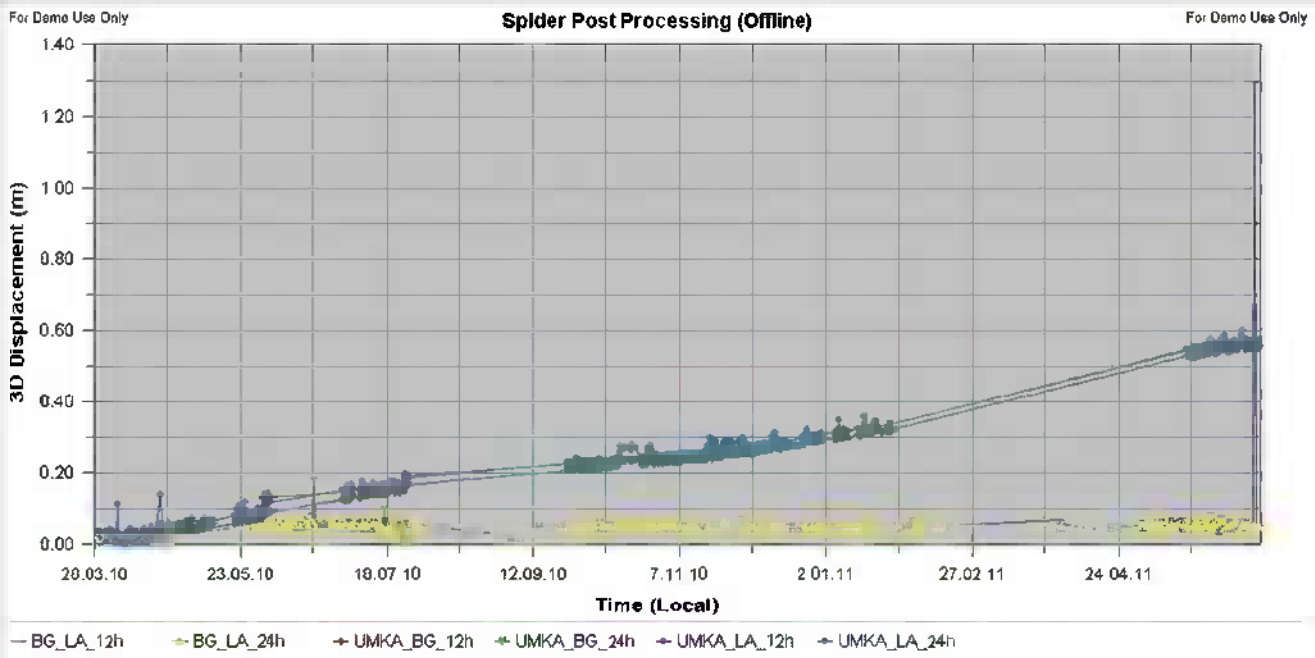


Fig. 7 3D displacement plot from 28 March 2010 to 17 June 2011

Acknowledgments The authors wish to acnowledge Goran Stepanović and Marko Pantić for their support in the GPS data acquisition and processing. The study would have not been possible without Vekom Geo. d.o.o., Beograd, Serbia. The research was supported by the Ministry of Science and Technology of the Republic of Serbia Project No. TR 36009.

References

Baldi P, Cenni N, Fabris M, Zanutta A (2008) Kinematics of a landslide derived from archival photogrammetry and GPS data. Geomorphology 102(3–4):435–444

Barla G, Antolini F, Barla M, Mensi E, Piovano G (2010) Monitoring of the Beauregard landslide (Aosta Valley, Italy) using advanced and conventional techniques. Eng Geol 116(3–4):218–235

Bertacchini E, Capitani A, Capra A, Castagnetti C, Corsini A, Dubbini M, Ronchetti F (2009) Integrated surveying system for landslide monitoring, Valoria landslide (Appennines of Modena, Italy). FIG working week 2009. Surveyors key role in accelerated development, Eilat, 3–8 May 2009. TS 3 F – Tectonic Processes, Landslides and Deformation Analysis. URL: www.fig.net/pub/fig2009/ppt/ts03f/ts03f_bertachini_capra_etal_3343.pdf

Brückl E, Brunner FK, Kraus K (2006) Kinematics of a deep-seated landslide derived from photogrammetric, GPS and geophysical data. Eng Geol 88(3–4):149–159

Coe JA, Ellis WL, Godt JW, Savage WZ, Savage JE, Michael JA, Kibler JD, Powers PS, Lidke DJ, Debray S (2003) Seasonal movement of the Slumgullion landslide determined from Global Positioning System surveys and field instrumentation, July 1998–March 2002. Eng Geol 68(1–2):67–101

Gili JA, Corominas J, Rius J (2000) Using Global Positioning System techniques in landslide monitoring. Eng Geol 55(3):167–192

Malet JP, Maquaire O, Calais E (2002) The use of Global Positioning System techniques for the continuous monitoring of landslides: application to the Super-Sauze earthflow (Alpes-de-Haute-Provence, France). Geomorphology 43(1–2):33–54

Manetti L, Terribilini A, Knecht A (2002a) Autonomous remote monitoring system for landslides. In: SPIE 9th annual international symposium on smart structures and materials. Smart sensor technology and measurement systems (ss03), vol 4694, San Diego, 17–21 Mar 2002, pp 230–235

Manetti L, Frapolli M, Knecht A (2002b) Permanent, autonomous monitoring of landslide movements with GPS. In: 1st European conference on landslides, Prague, 24–26 June 2002, pp 245–249

Mansour MF, Morgenstern NR, Martin CD (2011) Expected damage from displacement of slow-moving slides. Landslides 8(1):117–131

Mora P, Baldi P, Casula G, Fabris M, Ghirottia M, Mazzini M, Pesci A (2003) Global Positioning Systems and digital photogrammetry for the monitoring of mass movements: application to the Ca' di Malta landslide (northern Apennines, Italy). Eng Geol 68(1–2):103–121

Zhou P, Zhou B, Guo J, Li D, Ding Z, Feng Y (2005) A demonstrative GPS-aided automatic landslide monitoring system in Sichuan Province. J Global Position Syst 4(1–2):184–191

Landslide-Related PS Data Interpretation by Means of Different Techniques

Diego Di Martire, Gabriele De Luca, Massimo Ramondini, and Domenico Calcaterra

Abstract

Two different techniques aimed at assessing deformation data related to slow-moving landslides are here discussed, both being based upon Persistent Scatterer Interferometry. To this scope, a case-study from Calitri, Campania region, Italy is dealt with, represented by a large complex landslide re-activated by the 23 November 1980 M = 6.9 earthquake. Through the first technique, ascending and descending geometry dataset have been used, creating synthetic PS and vertical and easting displacement maps. The second procedure consisted in a morphometric decomposition of the velocity vector for each PS with respect to the maximum downhill slope angle and slope aspect. The results from both techniques were finally compared and discussed.

Keywords

Landslides • SAR interferometry • Persistent scatterers • Calitri • Italy

Introduction

A regular and continuous monitoring is an essential key to prevent and hopefully avoid adverse consequences of instability phenomena such as landslides, subsidence, sinkholes, etc.. In relatively recent years, natural hazard management has greatly benefited from the capabilities of the Remote Sensing techniques, among which the Differential Interferometry Synthetic Aperture Radar (DInSAR) proved to be an effective tool to detect ground deformations, especially by means of advanced interferometry methods, the so called Persistent Scatterers Interferometry (PSI), patented in 1999 by the Politecnico of Milan, Italy.

Direct interpretation of a given PS dataset in ascending and descending orbits acquisition is difficult and often causes real motion perception problems to the user. Many times data acquired under a different Line Of Sight (LOS) produce ambiguity in the definition of the real movement of the terrain.

This ambiguity in the PS data display represents one of major constraint in the spreading and in the use of this kind of data. The present work describes two different procedures proposed by TeleRilevamento Europa (T.R.E. 2008) and PODIS Project Campania (2008) respectively, that allow an easier interpretation of the PS data as confirmed by Italian Ministry for the Environment, Territory and Sea – MATTM (2009). Thanks to a cooperation protocol with MATTM, ERS 1-2 and ENVISAT PS interferometric data related to the 1992–2008 time span were made available to the present research, thus allowing to apply the above approaches to the case-study of Calitri (De Luca 2011), Italy, where a large, complex landslide involves the urban area since historical times.

Geological Setting and Landslides

Calitri is a small town in the Avellino province, Campania region, Italy, lying on the left side of the Ofanto River (Fig. 1). In the Calitri area, the oldest outcropping deposits belong to the Varicoloured Clay Group (Lower Cretaceous – Lower

D. Di Martire (✉) • G. De Luca • M. Ramondini • D. Calcaterra
Department of Hydraulic, Geotechnical and Environmental Engineering, Federico II University of Naples, Naples, Italy
e-mail: diego.dimartire@unina.it

C. Margottini et al. (eds.), *Landslide Science and Practice*, Vol. 2,
DOI 10.1007/978-3-642-31445-2_45, © Springer-Verlag Berlin Heidelberg 2013

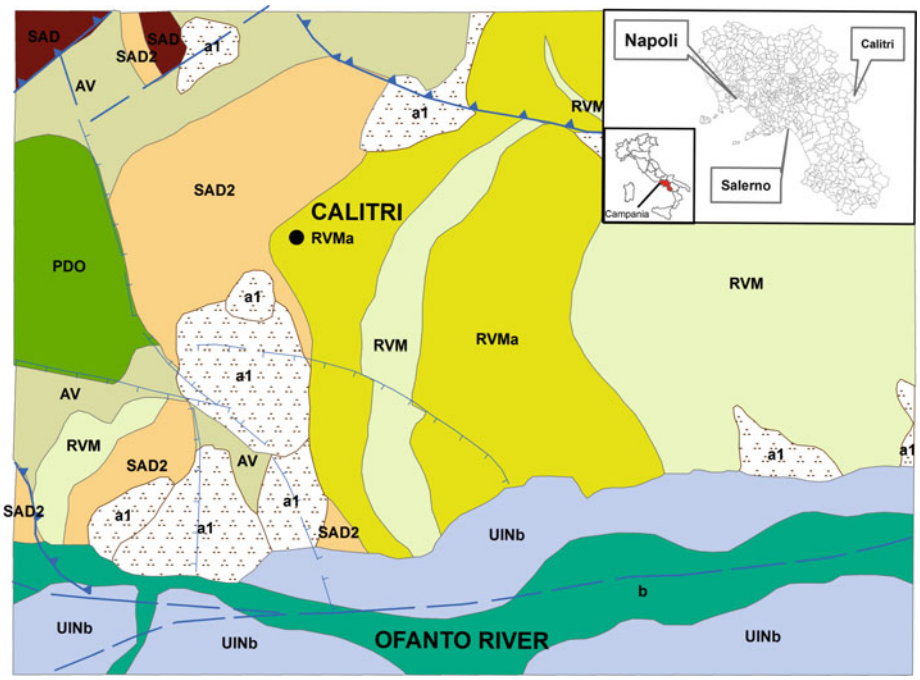


Fig. 1 Geological scheme of the Calitri area (APAT 2006 – redrawn). Legend: *UINb* alluvial deposits, *a1* old and recent landslides, *RVM, RVMa* Ruvo del Monte Synthem, *SAD, SAD2* Andretta Synthem, *PDO* Paola Doce Formation, *AV* Varicoloured Clay Group

Miocene), made up of chaotic scaly clays (Fig. 1). The latter are interposed as olistostromic lenses within the Pliocene deposits of the Ariano Irpino Super Synthem, in the area represented by the Ruvo del Monte and Andretta synthems (clayey to arenaceous-conglomeratic sediments).

The southern slope of the Calitri hill is affected, since historical times, by a large complex landslide (roto-translational evolved into earthflow), which prevailingly involves the pelitic terms (silty and marly clays, sands) of the Ariano Irpino Super Synthem. The last reactivation of the Calitri landslide, studied by several authors (e.g. Del Prete and Trisorio Liuzzi 1981; Hutchinson and Del Prete 1985; Budetta et al. 1990; Parise and Wasowski 1998, 1999; Martino and Scarascia Mugnozza 2005), occurred about 3½ h after the main shock of the Campania-Basilicata 23 November 1980 M = 6.9 earthquake (Martino and Scarascia Mugnozza 2005). Del Prete and Trisorio Liuzzi (1981) assessed the volume of the 1980 reactivation in the order of about 23 Mm^3, while, on the basis of some inclinometer readings, Hutchinson and Del Prete (1985) placed the maximum depth of the rototranslational body's rupture surface at about 100 m from ground surface. Boreholes drilled in the toe zone revealed the shallower depth of the earthflow, which sealed about 4 m of alluvial terrace deposits (Hutchinson and Del Prete 1985; Budetta et al. 1990). Several historical records of landslide activity at Calitri were found (Parise and Wasowski 1999; Martino and Scarascia Mugnozza 2005), the oldest of which dates back to 1694. The present-day state of activity of the landsides at Calitri has been briefly reported by Calò (2009) who, in the time span 1995–2009, recognized several small active landslides, mainly interesting the erosion areas in the eastern part of the main landslide (Fig. 2).

Methodology

Synthetic PS Procedure

The synthetic PS algorithm, developed by the SAR team at the Politecnico of Milan and Tele-Rilevamento Europa (T.R.E. 2008), is able to combine PS data sets of mean velocity along the LOS in both ascending and descending acquisition geometries. Thus the components of the velocity vector in the horizontal direction East-West and in vertical direction (Zenith – Nadir) can be assessed. However, any displacement in the North-South direction cannot be detected due to specific reasons of the acquisition system geometry (semi-polar orbit).

In order to obtain the decomposition of the velocity vector, a resampling of the PS data on a geographical grid with a regular mesh is necessary. The methodology for the



Fig. 2 Landslide-inventory map of the southern side of the Calitri hill (Calò 2009, redrawn). Legend: Blue = active landslide; Black = dormant landslide; Violet = active erosion area; Green = dormant erosion area

combination of PS ascending and descending data is outlined in Fig. 3.

The mean velocity value of PS points inside each mesh is calculated in order to obtain synthetic PS values for each cell. Such value is assigned to the center of gravity of the mesh.

For each cell the coefficient of variation is then calculated, allowing for comparison between different types of data. The coefficient of variation is defined as the ratio of standard deviation (σ_x) and the arithmetic means of speed value ($\bar{x}$). As such, it may be influenced by the contemporary presence of positive and negative values and thus, it becomes critical in presence of non-linear distortions:

$$RSD = \sigma_r = \frac{\sigma_x}{\bar{x}}; \tag{1}$$

also, meshes with a coefficient of variation greater than 0.5 and lower than −0.5 are discarded.

This procedure is applied to both ascending and descending data sets, as to assess the component of velocity vector on a common grid of 'pseudo-PS'.

The decomposition of the velocity vector can be better understood by considering a x, y, z Cartesian coordinate system, in which the three directions coincide with the horizontal E-W and N-S and vertical, respectively.

In such reference system the velocity vector V can be calculated as:

$$\bar{V} = V_x \cdot \bar{s}_x + V_y \cdot \bar{s}_y + V_z \cdot \bar{s}_z \tag{2}$$

where V_x, V_y and V_z are the velocity vector components along the horizontal (E-W and N-S) and vertical directions, and s_x, s_y, s_z the unit vectors of the three coordinate axes of the Cartesian system. Thus, using mean velocity values V_a and V_d, obtained from the PS database, the following system is obtained:

$$\begin{cases} V_a = Vx \cdot s_{xasce} + Vy \cdot s_{yasce} + Vz \cdot s_{zasce} \\ V_d = Vx \cdot s_{xdesce} + Vy \cdot s_{ydesce} + Vz \cdot s_{zdesce} \end{cases} \tag{3}$$

where s_{xasce}, s_{yasce}, s_{zasce}, s_{xdesce}, s_{ydesce}, and s_{zdesce} represent the direction cosines of the respective velocity vectors V_a and V_d.

In this reference system the number of unknown variables (V_x, V_y and V_z) is higher than that of the equations and therefore it cannot be solved. However, due to the geometrical characteristics of the acquisition, the component on N-S direction appears to be negligible.

Velocity in this direction is acceptably approximated to zero, thus allowing to solve the previous system and to assess motion components in E-W and vertical directions (corresponding to x and z directions):

$$\begin{cases} V_a = V_V \cos\ \theta_{asce} + V_E \sin\ \theta_{asce} \\ V_d = V_V \cos\ \theta_{desce} + V_E \sin\ \theta_{desce} \end{cases} \tag{4}$$

where V_a and V_d are respectively the velocity values in ascending and descending geometry and θ_{asce} and θ_{desce} are the incidence angles in the two geometries. In the present paper, based on the data acquired by ERS and ENVISAT

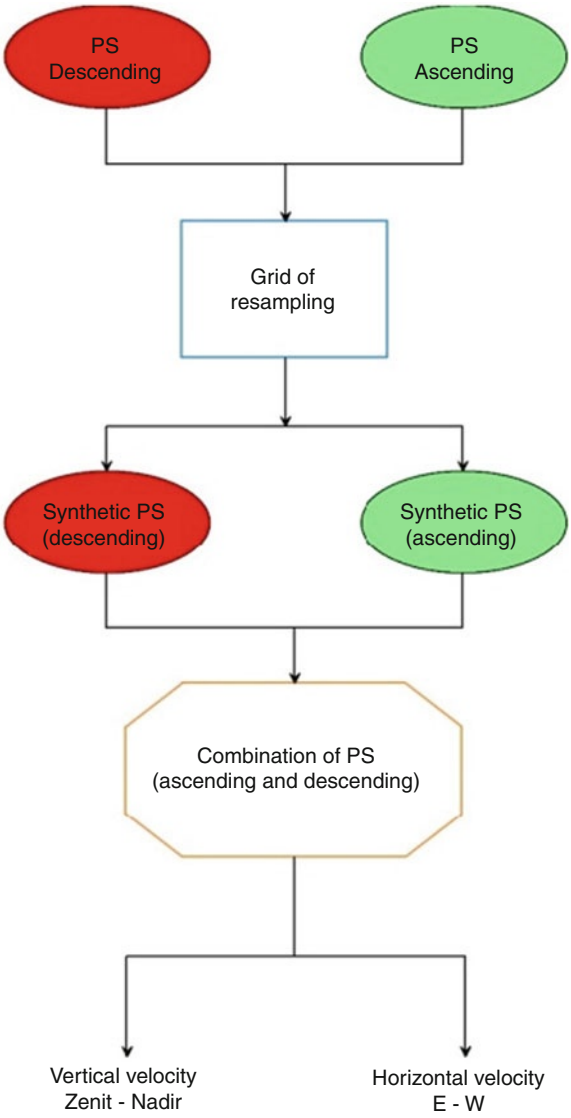


Fig. 3 Synthetic PS procedure flow-chart

satellites, the incident angles in ascending and descending geometry are the same and correspond to 23°.

TELLUS Procedure

This approach has been tested by the Campania Region in the TELLUS project (PODIS Project Campania 2008).

A 'pre-processing' statistical analysis based on frequency distributions of PS mean velocities in all the available datasets was carried out. Q1 (25 %), Q2 (50 %) and Q3 (75 %) quartiles were calculated. The range (Q3–Q1) is defined as the "interquartile range" (IQR). Mean velocity falling outside this interval (outliers) were discarded. More precisely, the values in the range [Q1–(1.5 × IQR)] and [Q3 + (1.5 × IQR)], which are also characterized by a low

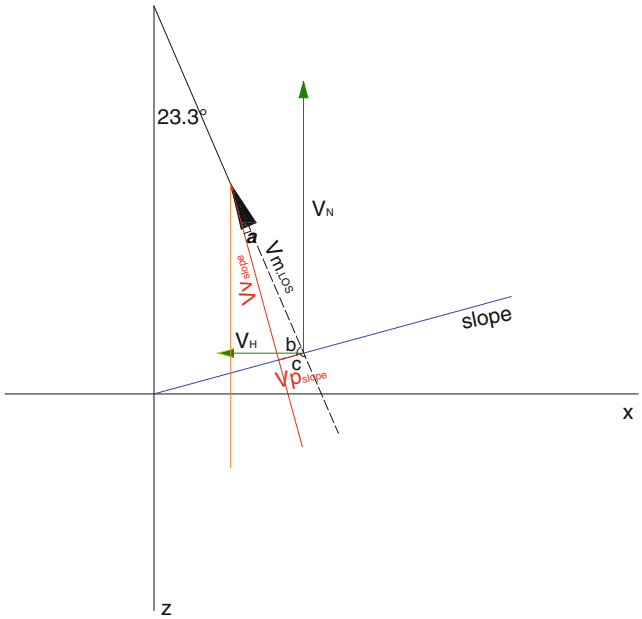


Fig. 4 Projection of the velocity vector along the direction of the maximum slope angle ("Morphometric correction" after PODIS Project Campania 2008, modified)

average velocity, are considered to be the most reliable and therefore are defined as "normal".

The procedure provides a morphometric approach, represented by the "correction" of the PS data, achieved by its projection on the slope considering both the slope angle and aspect information obtained from a Digital Terrain Model with a 10 × 10 m cell resolution. Such "correction" is not applied to PS with slope angle value close to 3° and, consequently, provided with flat aspect. For this reason, prior to PS values statistical analysis, a database "cleaning" (elimination of PS with slope angle value lower than 3°) is necessary.

For the ERS and ENVISAT datasets, the incidence angle of the sensor is equal to 23.3° and for the latitudes of interest a deviation of the orbit azimuth of 12.3° is calculated.

The mean velocity vector V_{mLOS} is projected along the direction of the maximum slope angle (Fig. 4) where:

$a = 90° - b = 8.3° = 23.3° - \text{slope}$

$b = 180° - c = 180° - 98.3° = 90° - a = 66.7° + \text{slope}$

$c = 180° - 66.7° - \text{slope} = 180° - 66.7° - \text{slope} = 180° - 81.7° = 98.3°$

The value of the projected velocity vector (V_{pslope}) is:

$$V_{pslope} = V_{mLOS} \cos\ b = V_{mLOS} \cos\ (66,7° + \text{slope}) \quad (5)$$

or

$$= V_{mLOS} \sin\ a = V_{mLOS} \sin(23,3° - \text{slope}) \quad (6)$$

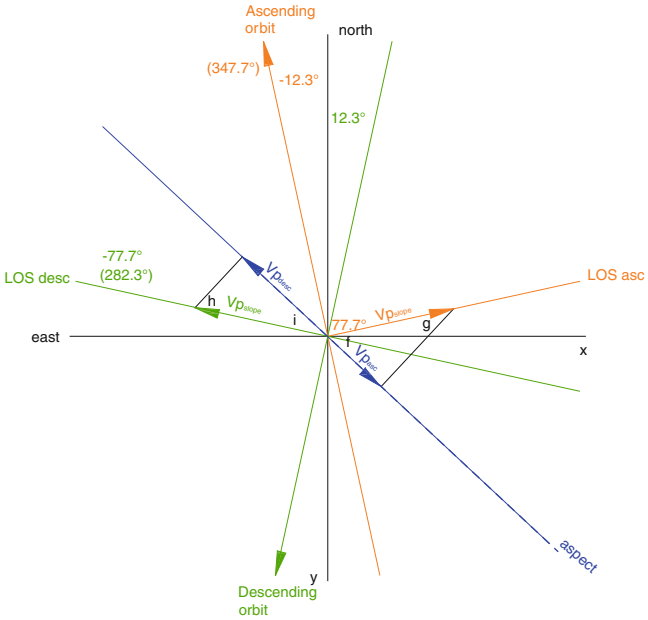


Fig. 5 Projection of the velocity vector along the slope aspect ("Morphometric correction" after PODIS Project Campania 2008, modified)

and in orthogonal direction (V_{vslope}) is:

$$V_{vslope} = V_{mLOS} \cos\ a = V_{mLOS} \cos\ (23,3° - slope) \quad (7)$$

or

$$= V_{mLOS} \sin\ b = V_{mLOS} \sin\ (66,7° + slope). \quad (8)$$

The obtained V_{pslope} is decomposed and projected along the slope aspect (Fig. 5) in ascending and descending orbit of acquisition, where:

f = aspect – 77.7°

g = 90° – f = 167.7° – aspect

h = 90° – i = 90° – 102.3° – aspect = – (12.3° + aspect)

i = 282.3° – (180° – aspect) = 102.3° + aspect.

The V_{pslope} projected along the slope aspect is equal to:

$$\begin{aligned} V_{pasc} &= V_{pslope} \cos f = V_{pslope} \cos\ (aspect - 77,7°) \\ &= V_{pslope} \sin g = V_{pslope} \sin\ (167,7° - 77,7°) \end{aligned} \quad (9)$$

and

$$\begin{aligned} V_{pdesc} &= V_{pslope} \cos i = V_{pslope} \cos\ (aspect + 102,3°) \\ &= V_{pslope} \sin h = V_{pslope} \sin\ (-12,3° - aspect). \end{aligned} \quad (10)$$

	FID	Shape *	CODE	VEL	V_STDEV	COHERENCE
▶	0	Point	0F1Wr000WCn	0	0	0.87
	1	Point	0F1Wr000IRy	-2	0.8	0.67
	2	Point	0F1Wr000ITQ	-1.4	0.7	0.67
	3	Point	0F1Wr000IUK	-0.4	0.7	0.68
	4	Point	0F1Wr000IUW	0.6	0.6	0.77
	5	Point	0F1Wr000IUY	2.6	0.6	0.76
	6	Point	0F1Wr000IUc	-1.8	0.6	0.76
	7	Point	0F1Wr000IUg	-0.2	0.8	0.66
	8	Point	0F1Wr000IUz	-3.1	0.7	0.72
	9	Point	0F1Wr000IV5	-0.4	0.7	
	10	Point	0F1Wr000IV6	-0.7	0.8	
	11	Point	0F1Wr000IV7	-0.3	0.6	

a

V_2002	VSTD_2002	V_2003	VSTD_2003	V_2004	VSTD_2004
-9999	-9999	0	0	0	0
-9999	-9999	2.1	9.6	-1.6	8.2
-9999	-9999	5.8	8.3	-0.4	5.6
-9999	-9999	9.8	6.9	-3.5	5.7
-9999	-9999	-0.2	7.2	5.4	6.4
-9999	-9999	5.1	6.9	5.7	6.1
-9999	-9999	-0.1	7.9	0	
-9999	-9999	8.5	8.4	-2.9	
-9999	-9999	-0.4	6.7	-1.7	

b

D20021129	D20030103	D20030418	D20030627	D20030801	D20031010
0	0	0	0	0	0
0	-0.2	-7.9	-3.2	8.7	-6.9
0	1.1	8.9	4.5	15	-1.5
0	-0.5	3.8	5.4	9.3	1.3
0	-1.1	-3.1	2.6	2.6	
0	0.6	3.1	9.7	8.5	
0	6	2.9	0.8	4.1	
0	3.2	-8.8	0.8	3.4	

c

Fig. 6 PS database: (**a**) Mean velocity, standard deviation of the velocity and coherence value; (**b**) Mean velocity value for each year of acquisition; (**c**) Rate of displacement for each acquisition date

The result of this correction cannot replace the original PS, but it can resolve the reading ambiguities with respect to the slope instability morphodynamics.

PS Dataset

The data consist of the PS shapefile obtained by ERS 1-2 and ENVISAT image processing acquired between 1992 and 2008 by means of PSInSAR technique developed and patented by Politecnico of Milan and licensed to TeleRilevamento-Europa Ltd in 2000 (Ferretti et al. 2000, 2001; Colesanti et al. 2003).

The dataset has 5002 PS measurement points identified in the town of Calitri, divided as follows: 887 ERS ascending, 1364 ERS descending, 1968 ENVISAT ascending, and 783 ENVISAT descending.

PS database reports the coherence value, standard deviation and average velocity related to the time of acquisition (Fig. 6a), the average velocity and standard deviation for each year (Fig. 6b) and, finally, the rate of displacement for each acquisition date expressed in mm (Fig. 6c). This paper

Table 1 Synthetic PS obtained by the processing

Satellite (m × m)	Synthetic PS
ERS 50 × 50	17
ENVISAT 50 × 50	18
ERS 70 × 70	11
ENVISAT 70 × 70	14
ERS 100 × 100	6
ENVISAT 100 × 100	7

refers to the values obtained over the entire interval of acquisition.

Results

Both the above procedures were applied to the entire available dataset. In order to provide clearer results, we focus here on a limited area near the scar of the Calitri main landslide re-activated by the November 23rd, 1980 earthquake.

For the first procedure, and in particular during the data resampling, three different regular mesh sides have been used (50, 70 and 100 m). For each mesh the number of PS, the average velocity and standard deviation were calculated, in order to establish which mesh provided the best results. The results highlight a significant difference in synthetic PS obtained for different size of the mesh, as shown in Table 1.

Most of the synthetic PS are located at the upper-middle part of the landslide because this zone coincides with the most urbanized area. The decomposition of the mean velocity vector of synthetic PS calculated according to the vertical (V_V) and horizontal direction E-W(V_E), gave the results shown in Fig. 7.

For both ERS and ENVISAT satellite missions, the synthetic PS show that the horizontal components of displacement are always in agreement with the morphology of the territory. In particular, in this area ERS shows the dominance of the horizontal component, while the ENVISAT synthetic PS offers a prevalence of the vertical component.

Following the second procedure, after the phase of preprocessing, i.e. elimination of PS with slope values lower than 3° and PS outliers, the results reported in Table 2 have been obtained. Accordingly, about 20 % of PS data acquired in both satellite missions were discarded.

The results show that mean velocity values of all PS are very low, varying between −1 and 1 mm/year for PS ascending and descending ERS and ascending ENVISAT.

On the contrary, higher values (about 3 mm/year) have been found for the PS descending ENVISAT in the northwest of the landslide.

Figure 8 reports the components of the ascending and descending PS, along with the average velocity vectors obtained from this procedure.

Discussion and Conclusions

The PSInSAR technique is recognized as a valuable and useful tool which elaborates SAR images series acquired by SAR sensors on a satellite instrumented platform. This method allows for terrain surface deformation assessment and monitoring with millimetric precision over wide areas.

Using the PS Synthetic procedure, most of the synthetic PS resulted to fall in the middle-upper part of the analyzed landslide and both ERS and ENVISAT PS horizontal displacement components follow the slope attitude. ERS showed dominance of the horizontal component, while for the ENVISAT synthetic PS the vertical component prevails. Since the ERS and ENVISAT dataset cover two different time periods, we presume that this difference could be related to a different behavior of the landslide over time. This is also confirmed by the inclinometer readings measured for the period 1992–1994 which show a dominance of horizontal component. In our experience displacement components values (V_E and V_V) always proved to be rather low and often negligible.

The results deriving from the application of the TELLUS procedure show that also in this case very low values of the mean velocity components are obtained. A possible explanation lies in the fact that, owing to very low vector values in the original PS data set, the subsequent vector decomposition produced negligible slope direction components, which proved to be strongly correlated to the slope angle values, as also reported by Cascini et al. (2009, 2010).

Therefore, both procedures provide similar results and they suggest that the studied landslide is apparently stable.

The PS technique is a recently acquired operative tool; a preliminary definition of the PS nature identified by SAR sensors appears to be necessary in order to verify the PS reliability. Indeed, this study shows that movement measured by PS not always corresponds to real ground displacement; on the contrary, such evidence could be referred to different causal factors, such as a thermal expansion of metallic structures.

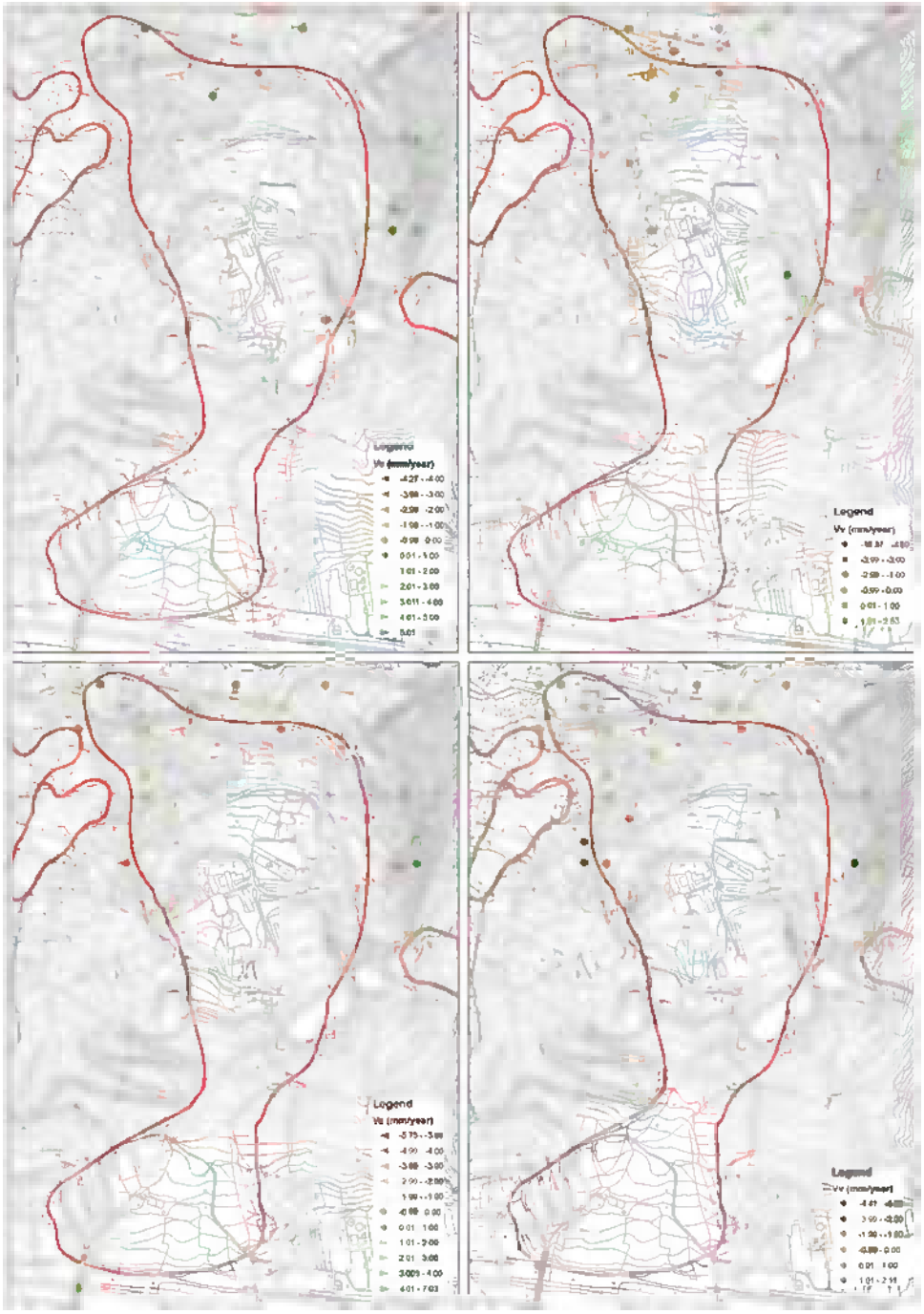


Fig. 7 Horizontal and vertical component for synthetic PS: ERS (*above*), ENVISAT (*below*)

Table 2 PS obtained from pre-processing

Satellite	Total PS	PS pre-processing
ERS asc	67	51
ERS desc	116	93
ENVISAT asc	148	122
ENVISAT desc	82	65

As reported by other Authors (e.g. Meisina et al. 2006, 2008) the lack of reliable PS inside the landslide area, and in particular in its middle-lower part, was the main difficulty met, since this area is covered by vegetation which generates low coherence values during images' processing.

In order to overcome this constraint thriedral corner reflectors were installed. Moreover, a mobile GPS network has been set up in order to complete and compare movements identified by means of PS techniques. Furthermore, our research is focused on the development of an algorithm which can allow to infer a three dimensional surface displacement field by combining SAR images of ascending and descending orbits acquired by new satellite

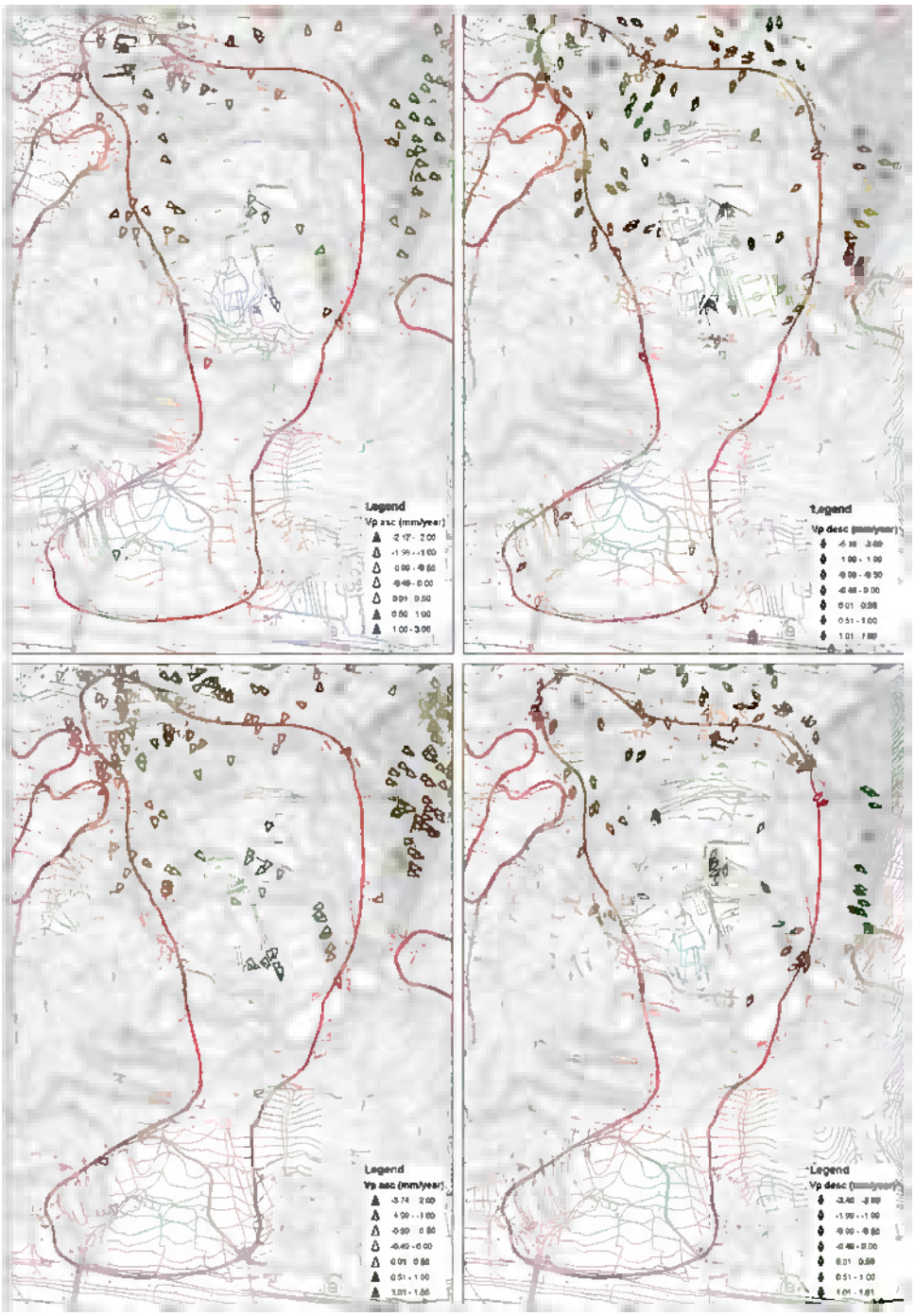


Fig. 8 Component of velocity for ERS (*above*) and ENVISAT (*below*) PS by means of TELLUS procedure

generation (Cosmo-SkyMed) and repeated GPS measurements (Fialko et al. 2001; Wright et al. 2004; Ferretti et al. 2007).

Acknowledgments Dr. Salvatore Costabile (MATTM) is gratefully acknowledged for having promoted the cooperation protocol between MATTM and Federico II University of Naples.

References

APAT (2006) Geological Map of Italy – Sheet n. 451 Melfi. http://www.isprambiente.gov.it/MEDIA/carg/451_MELFI/Foglio.html. Last accessed 10 June 2011

Budetta P, Calcaterra D, de Riso R, Santo A (1990) Geology and landslides of the Upper valley of the Ofanto River southern

Apennines. Memorie Società Geologica Italiana 45:309–324 (in Italian)
Calò F (2009) Analysis of slow-moving landslides in Southern Apennines by integrating ground monitoring and Remote Sensing techniques. Ph.D. thesis, Federico II University of Naples, Italy
Cascini L, Fornaro G, Peduto D (2009) Analysis at medium scale of low-resolution DInSAR data in slow-moving landslide-affected areas. ISPRS J Photogramm Rem Sens 64(6):598–611
Cascini L, Fornaro G, Peduto D (2010) Advanced low- and full-resolution DInSAR map generation for slow-moving landslide analysis at different scales. Eng Geol 112:29–42
Colesanti C, Ferretti A, Novali F, Prati C, Rocca F (2003) SAR monitoring of progressive and seasonal ground deformation using the Permanent Scatterers Technique. IEEE Trans Geosci Rem Sens 41(7):1685–1701
De Luca G (2011) Application of the PSInSAR technique to the monitoring of slow-moving landslides. MS thesis, Federico II University of Naples, Italy, (in Italian)
Del Prete M, Trisorio Liuzzi G (1981) Results of the preliminary study of the Calitri landslide (AV) mobilized by the 23/11/1980 earthquake. Geologia Applicata ed Idrogeologia 16:153–65 (in Italian)
Ferretti A, Prati C, Rocca F (2000) Non-linear subsidence rate estimation using Permanent Scatterers in Differential SAR Interferometry. IEEE Trans Geosci Rem Sens 38(5):2202–2212
Ferretti A, Prati C, Rocca F (2001) Permanent scatterers in SAR interferometry. IEEE Trans Geosci Rem Sens 39(1):8–20
Ferretti A, Savio G, Barzaghi R, Borghi A, Musazzi S, Novali F, Prati C, Rocca F (2007) Submillimeter accuracy of InSAR time series: experimental validation. IEEE Trans Geosci Rem Sens 45(5):1142–1153
Fialko Y, Simons M, Agnew D (2001) The complete (3-D) surface displacement field in the epicentral area of the 1999 Mw 7.1 Hector Mine earthquake, California, from space geodetic observations. Geophys Res Lett 28(16):3063–3066
Hutchinson JN, Del Prete M (1985) Landslides at Calitri, southern Apennines, reactivated by the earthquake of 23rd November 1980. Geologia Applicata ed Idrogeologia 20(1):9–38
Italian Ministry for Environment, Territory and Sea (2009) Guidelines to the analysis of satellite interferometric data in areas exposed to instability phenomena. Version 1.0, 108 p, (in Italian)
Martino S, Scarascia Mugnozza G (2005) The role of the seismic trigger in the Calitri landslide (Italy): historical reconstruction and dynamic analysis. Soil Dyn Earthq Eng 25:933–950
Meisina C, Zucca F, Fossati D, Ceriani M, Allievi J (2006) Ground deformation monitoring by using the Permanent Scatterers Technique: the example of the Oltrepo Pavese (Lombardia, Italy). Eng Geol 88:240–259
Meisina C, Zucca F, Notti D, Colombo A, Cucchi A, Savio G, Giannico C, Bianchi M (2008) Geological interpretation of PSInSAR data at regional scale. Sensors 8(11):7469–7492
Parise M, Wasowski J (1998) Evolutive aspects and landslide activity in the surroundings of Calitri. In: Proceedings of international conference on "La prevenzione delle catastrofi idrogeologiche: il contributo della ricerca scientifica", Alba, vol 1, 5–7 Nov 1996, pp 135–144, (in Italian)
Parise M, Wasowski J (1999) Landslide activity maps for landslide hazard evaluation: three case studies from Southern Italy. Nat Hazards 20:159–183
PODIS Project Campania (2008) Technical descriptive notes of the elaboration made by the PODIS TELLUS Project (PON ATAS 2000–2006) on the PSinSAR data of Campania region. http://www.difesa.suolo.regione.campania.it. Last accessed 10 June 2011, (in Italian)
T.R.E. (2008) PSInSAR™ user's manual. TeleRilevamento Europa, Milan, 84 p, (in Italian)
Wright TJ, Parsons BE, Lu Z (2004) Toward mapping surface deformation in three dimensions using InSAR. Geophys Res Lett 31:L01607. doi:10.1029/2003GL018827



Advanced Image Analysis for Automated Mapping of Landslide Surface Fissures

A. Stumpf, U. Niethhammer, S. Rothmund, A. Mathieu, J.P. Malet, N. Kerle, and M. Joswig

Abstract

Surface fissures are potential indicators of slope instabilities and considerably influence infiltration characteristics of the soil. The increasing availability of unmanned aerial vehicles (UAVs) enables the observation of surface features at unprecedented detail and this study develops an image processing method combining Gaussian filters and object-oriented image analysis to map such features in very-high resolution (VHR) aerial images largely automatically. At three different time steps the results of the technique are compared with expert elaborated maps.

Keywords

Line detection • Gaussian filter • Object-oriented image analysis • Landslide surface fissures • Unmanned aerial vehicle

Introduction

Surface features of slopes and rock cliffs reveal important information about the past and present patterns of deformation; their observation and interpretation can contribute to a better understanding of the controlling physical processes and help for the assessment of the related hazards (Fleming and Johnson 1989; McCalpin 1984; Parise 2003). Detailed mapping and analysis of structural discontinuities is a powerful tool to identify and characterize potentially unstable areas in hard rocks (Günther et al. 2004; Hoek and Bray 1981; Jaboyedoff et al. 2004; Matheson 1983; Priest 1993; Selby 1993), and surface fissures may serve as a geo-indicator for initial failure states in soft sediments (Abramson et al. 2001; Chowdhury and Zhang 1991; Petley et al. 2006; Krauskopf et al. 1939; Shreve 1966).

The surface characteristics also influence hydrological processes, such as infiltration and drainage patterns, which in turn effect the ground-water system and the kinematic response of slopes to hydrological events (Malet et al. 2003, 2005; van Asch et al. 2009). Especially tension cracks and fissures modify the infiltration and pore-water response considerably, and their integration into physically-based models may yield more reliable kinematic forecasts and estimates of the hazard level (Baum and Fleming 1991; Corominas et al. 2002; Iverson 2000; Lindenmaier et al. 2005; Malet et al. 2005; van Beek and van Asch 1999).

Detailed maps of surface deformation features can be obtained by extensive field surveys either through the direct

A. Stumpf (✉)
Faculty of Geo-Information Science and Earth Observation, ITC, University of Twente, Enschede, The Netherlands

Laboratoire Image, Ville, Environnement, CNRS ERL7230, University of Strasbourg, Strasbourg, France
e-mail: stumpf24883@itc.nl

U. Niethhammer • M. Joswig
Institut für Geophysik, University of Stuttgart, Stuttgart, Germany

S. Rothmund
Institut für Geophysik, University of Stuttgart, Stuttgart, Germany

Institut de Physique du Globe de Strasbourg, CNRS UMR 7516, University of Strasbourg, Strasbourg, France

A. Mathieu • J.P. Malet
Institut de Physique du Globe de Strasbourg, CNRS UMR 7516, University of Strasbourg, Strasbourg, France

N. Kerle
Faculty of Geo-Information Science and Earth Observation, ITC, University of Twente, Enschede, The Netherlands

C. Margottini et al. (eds.), *Landslide Science and Practice*, Vol. 2,
DOI 10.1007/978-3-642-31445-2_46, © Springer-Verlag Berlin Heidelberg 2013

observation of the topography (cf. Fleming et al. 1999; Meisina 2006) or indirectly through the analysis of seismic waves acquired in tomography set-ups (Grandjean et al. 2011; Bièvre et al. 2011). The surface deformation pattern can also be obtained over larger areas from the analysis of VHR aerial images (especially those acquired from low-cost Unmanned Aerial Vehicles UAVs); (Niethammer et al. 2011). In this study, we targeted the development of a largely automatized image analysis technique to detect, map and characterize surface fissures from VHR aerial images. The developed method is based on a combination of Gaussian directional filters and object-oriented image analysis (OOA) and was tested on a set of multi-temporal VHR images acquired at the Super Sauze mudslide in Southeast French Alps. The obtained results were compared to manual mappings carried out by experts combining image interpretation and field surveys.

Study Site and Data

The Super Sauze mudslide is an active landslide located in the Barcelonnette Basin in the Southern French Alps (Fig. 1). It is a complex style movement that developed in clay-rich black marls since the 1970s and features highly variable displacement rates controlled by the local hydrological conditions (Malet et al. 2005). For this study we used subsets (≈14,000 m^2) of three aerial images acquired with a UAV (Fig. 1) by Niethammer et al. (2011) in 2008/09 and a fourth image taken in July 2009 with a H4D-50 digital camera mounted on a helicopter. At the time of the helicopter survey an aerial LiDAR scan was also conducted and the resulting point cloud was rendered to a 0.5 m resolution raster to derive the general hydrological drainage pattern.

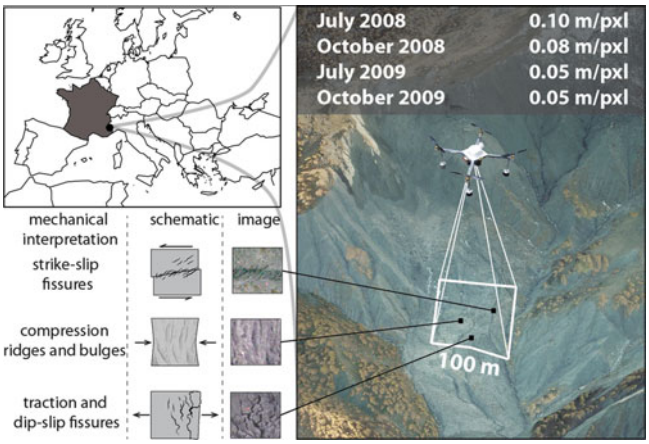


Fig. 1 Location of the Super Sauze mudslide and details of typical surface features

Methods

Fissure Characteristics and Special Challenges

The surface fissures observed at the landslide surface are essentially openings of the topsoil layer induced by lateral and/or basal shear, and the development of compression and extension features. In the field, fissure widths of 1–50 cm and lengths of typically above 100 cm are observed (e.g. Fig. 2a). In the images they can be recognized as dark curve-linear or angled lines as soon as their width approaches one pixel in size, whereas the highly textured landslide surface poses a noisy background that makes the visual and automatic mapping of the fine linear structures a challenging task. Further difficulties arise from variable illumination conditions and image resolutions among the different acquisitions.

Since most classical image processing techniques for the extraction of linear features return signals on both lines and edges (e.g. Sobel filter, Canny edge detector) and/or specifically target straight linear elements (e.g. Hough transform) they are not well-suited for the detection of the fissures.

Similar issues have motivated numerous studies in the field of medical image processing and a well-studied problem is the detection of dark blood vessels in photographs of the human retina. Based on the observation that the cross-profiles of the vessels approximate well a Gaussian distribution, Chaudhuri et al. (1989) proposed the use of a matched filter (MF) that is essentially a Gaussian convolution kernel subtracted by its own mean value. As Fig. 2 illustrates, the cross-sections of surface fissures can be approximated well with a Gaussian distribution. Since the fissures can take any possible orientation and the MF will only give a peak response when crossing the dark line at an angle close to 90°, in practice the filter must be rotated in all possible directions and only the maximum response is retained.

Combining Gaussian Filters

Since MF not only capture thin lines but still provide spurious responses at image features such as step edges (Fig. 3c), numerous extensions (Hoover et al. 2000; Sofka and Stewart 2006) and complex alternative approaches (Mendonca and Campilho 2006; Soares et al. 2006) have been proposed. Their enhanced results, however, incur considerable computational costs (which constitute a problem when the methods are to be applied on VHR remote sensing imagery easily containing 20 times more pixels then retinal images), and are based on assumptions applicable to vascular networks but not necessarily for the investigated fissure patterns. Recently Zhang et al. (2010) proposed a computationally efficient modification of the original MF filtering approach,

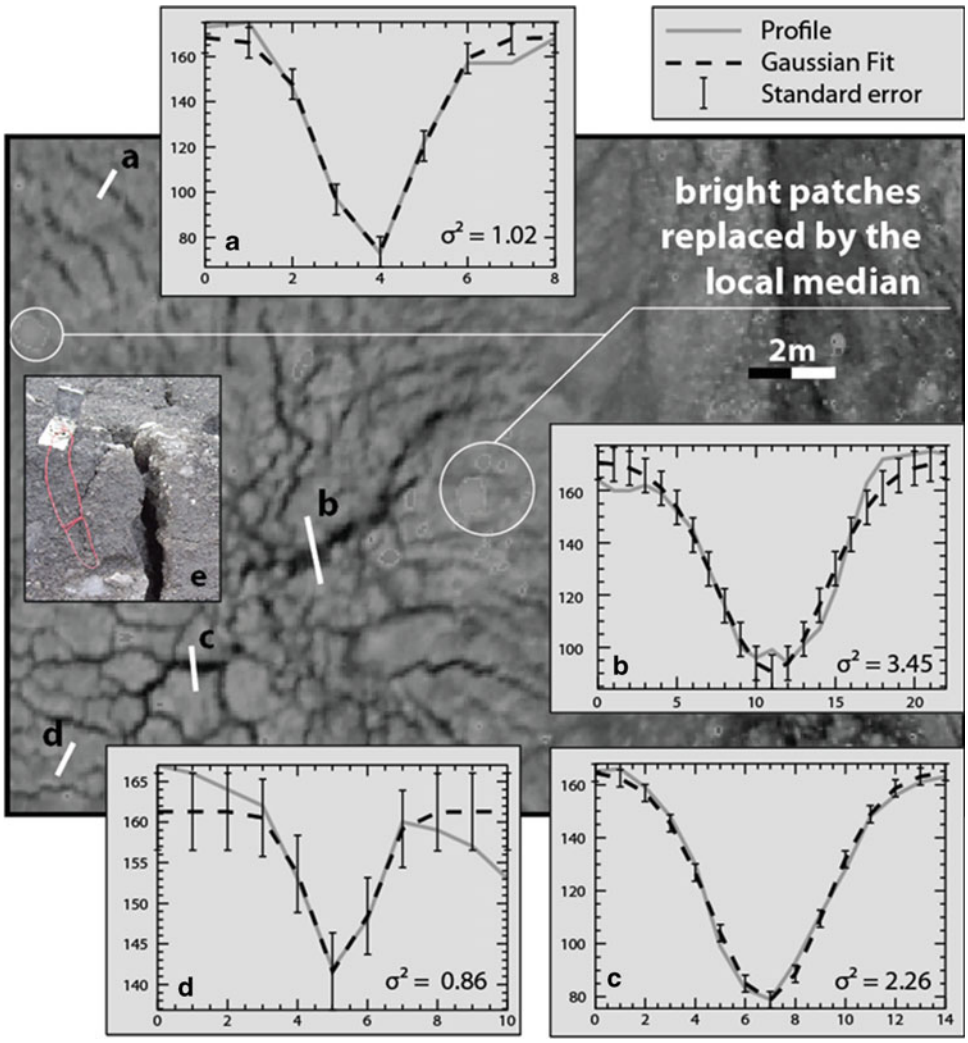


Fig. 2 Subset of the UAV image from October 2008 showing typical fissure patterns and grey-value profiles (green channel) approximated with Gaussian curve (**a**–**d**). Field terrestrial photograph taken in October 2009(**e**)

using additionally a first order derivative of a Gaussian function (FDOG) to locally adapt the thresholds separating dark line from non-target features. Inspired by their proposed method, a similar approach has been implemented in ENVI-IDL 4.8 (ITT Visual Information Solutions); the steps in the processing chain are described in the following.

The MF is a two dimensional kernel defined in the x-direction by an inverted Gaussian profile (Fig. 3b), and in the y-direction by replicates of the same profile. It may be denoted as:

$$MF = g(x, y; \sigma) = -\frac{1}{\sqrt{2\pi}\sigma} e^{\left(-\frac{x^2}{2\sigma^2}\right)} - m, \qquad (1)$$

for $|x| \leq 3\sigma$, $|y| \leq L/2$.

where σ denotes the standard deviation of the Gaussian functions and relates to the width of the targeted feature, whereas L defines the extent of the kernel in the y-direction and can be related to the length of the fissures. As illustrated in Fig. 3c–d the matched filter still responds to dark and bright step edges. The spurious detection resulting from bright step edges can be addressed with a simple pre-filtering where every pixel value that is 2σ above the mean grey level intensity of the image is replaced with the local median (Fig. 2).

Another more general strategy is to adopt the response of the FDOG to locally adjust the thresholds applied on the MF response to classify fissure and non-fissure structures. In analogy to 1, the first order derivative filter kernel may be denoted as:

$$FDOG = g'(x, y; \sigma) = -\frac{1}{\sqrt{2\pi}\sigma^3} e^{\left(-\frac{x^2}{2\sigma^2}\right)} \qquad (2)$$

for $|x| \leq 3\sigma$, $|y| \leq L/2$.

Figure 3e shows that unlike the response to edges the FDOG signal yields a zero crossing in the middle of the idealized fissure structure. Convolving the FDOG response with a simple mean filter it is further possible to broaden the zero crossing to a plateau covering the whole width of the

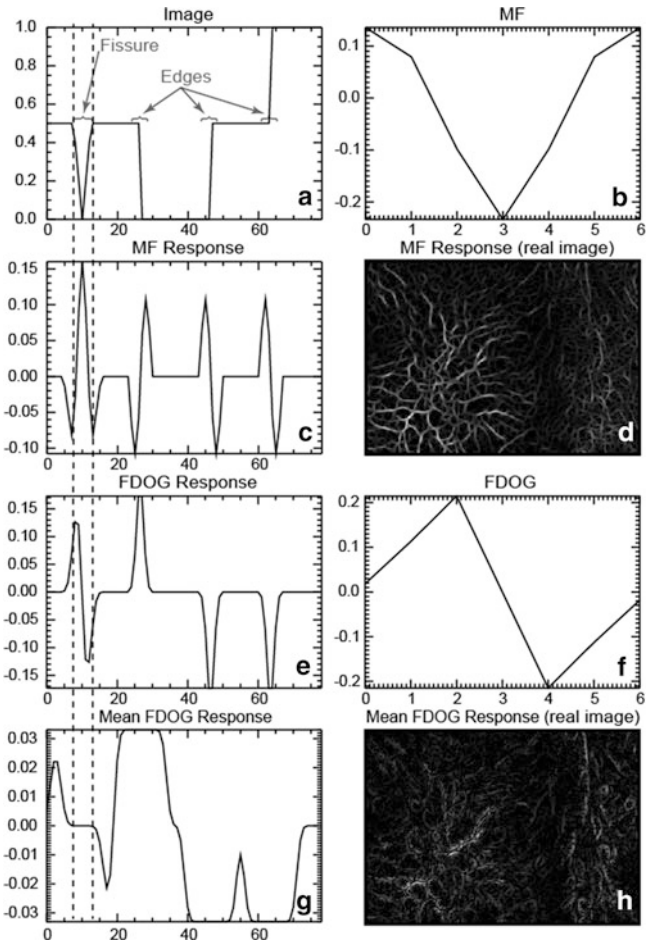


Fig. 3 Illustration of the principles of the Gaussian filtering for a simplified one dimensional case (**a**–c, **e**–**g**) and the filter response on the image subset in Fig. 2 (**d**, **h**)

fissure, whereas the high absolute values at the step edge are retained to later increase the thresholds locally at step edges.

As noted above, a fissure may be aligned at any orientation and in practice matched filters at multiple directions are evaluated and for each pixel only the maximum response value is retained. This can also be considered as finding the angle $\theta_{max(x,y)}$ which maximizes the filter response at a given position (x,y) and can be denoted as:

$$\theta_{\max(x,y)} = \arg\max\left(I_{(x,y)} \otimes MF_{\theta_i}\right) \tag{3}$$

for $0<\theta_i \leq \pi$

where I denotes the image, $\otimes$ the convolution operator and θ_i the orientation of the MF. The calculation of the maximum value at each pixel in the MF response image R can be expressed by:

$$R_{(x,y)} = I_{(x,y)} \otimes MF_{\theta_{max}} \tag{4}$$

Table 1 Parameter set of the Gaussian filters for the processed images

Image date	July 2008	July 2009	October 2009
Pixel size	0.1 m	0.05 m	0.05 m
σ [pixel]	0.67	1.34	1.34
L [pixel]	10	20	20
θ_n	36	36	36
c	3.0	3.0	3.0

and the response of the FDOG filter D can be denoted accordingly by:

$$D_{(x,y)} = I_{(x,y)} \otimes FDOG_{\theta_{max}} \otimes M \tag{5}$$

In the latter expression, M denotes the mean filter used to convolve the response of FDOG filter oriented at the same direction where the MF provided the maximum response. While Zhang et al. (2010) suggested a fixed and very broad mean filter we suggest to use a kernel size that matches the width of the Gaussian kernel (6σ) and is consequently close to the width of the fissures.

The response of the FDOG filtering is used to locally adjust the threshold T that is applied on R according to the following formula:

$$T = \left(1 + \overline{D}\right) * \mu_R * c$$

where $\overline{D}$ denotes D after a normalization to a value range between 0 and 1, μ_R is the mean of the response image R and c is a user defined parameter that typically range from 2 to 3 and influences the sensitivity of the detection.

In summary, the user needs to specify four simple parameters, namely (1) the scale of the filter kernels in terms of σ, (2) the length L of the kernel, (3) a constant c to adjust the thresholding, and (4) the number of orientations (θ_n) at which the filters are calculated. An adjustment of the latter, however, is only relevant with very large kernels and/or images where the computational time may become an issue. In our experience 12 angular steps are already sufficient to capture linear features at all orientations.

The smallest visible fissures at the coarsest resolution are approximately 10 cm wide, and extracting several cross profiles on the smallest elements, standard deviations σ between 0.6 and 0.7 are observed for the best fitting Gaussian function. In our experience, σ establishes the lower bound for the width of the targeted features, whereas the filters still remain sensitive to features which are up to five times larger. For L, the minimum length of the fissures is chosen, which is typically at least 1 m. σ and L were kept the same for all experiments and only scaled according to the pixel size of each image (Table 1). In all experiments the green channel was used because it provided the best contrast between the surface fissures and the background.

Object-Oriented Post-Processing

The filtering process generally performed well in detecting the dark linear structures, whereas several visually similar surface features such as erosion features (rills, small thalwegs) and elongated shadows induced by the microtopography and vegetation still yield numerous false positive detections. Their removal requires a higher level understanding of the scene context. In order to put spatial reasoning into an explicit form and to automatize the post-processing we propose an object-oriented approach implemented in eCognition 8.64 (Trimble 2011).

First, the ratio of shadow around each detected element is evaluated and the element is removed as false positive if the area ratio is larger than 0.33. Vegetation generally shows a higher reflectance in the green and red compared to the blue channel, whose contribution to the sum of all channels is generally less than one third. The exact threshold may, however, depend on illumination conditions and the season, and Otsu's method (Otsu 1979) was adopted to automatically determine the threshold constraining the search space to ratio blue values below 0.33. Fissure candidates covered by the resulting vegetation class, or having a relative border length larger than 0.15, were subsequently removed.

False detections may originate from small elongated elements nested in larger features such as gullies, whereas fissures can be distinguished from false positives as soon as their orientation significantly deviates from the main orientation of the larger linear feature. To exploit this relationship the Gaussian filtering was repeated with the settings indicated in Table 1, but with a two times increased scale σ and on a five times coarser image representation. Resampling was performed with a bilinear interpolation scheme. The resulting large linear features were overlaid with the map containing the fissure candidates, and the difference of their main angles was calculated. An intermediate result is illustrated Fig. 4. We tested angular thresholds of 10–45° and selected a rather conservative cut-off value of 13°. All candidates overlapping a larger feature and differing in their main direction less than 13° were consequently removed (Fig. 4).

The same operation was performed once more using the main drainage lines extracted from a LiDAR surface model (0.5 m raster resolution) instead of the coarse scale linear features.

A final clean-up step was implemented removing all candidates not longer than 0.4 m, an area smaller than 0.1 m^2, and a fissure class density lower than 1 % in a surrounding neighbourhood of 10 m^2. Table 2 displays that most adopted thresholds were kept the same among all scenes, whereas the classification rule for shade areas had to be adopted to compensate for the different illumination conditions (direct sunlight in July vs. diffuse light in October).

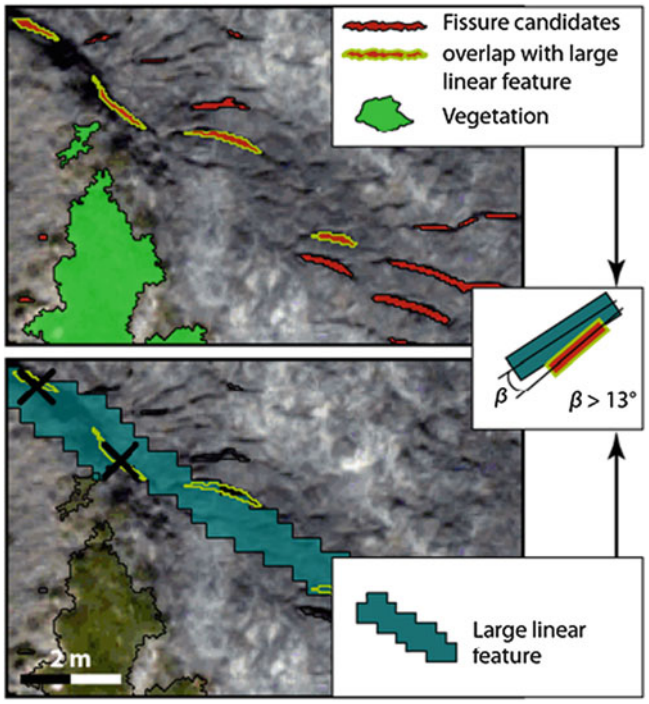


Fig. 4 Illustration of an intermediate processing step in the object-oriented post-processing routine. Fissure candidates that are overlapped by larger linear features and aligned with them (±13°) are excluded

Table 2 Summary of the thresholds adopted in the object-oriented post-processing routine

	July 2008	July 2009	October 2009
Shadows	Red < 100	Red < 100	Red < 40
Shadow ratio	≤0.33	≤0.33	≤0.33
Rel. border to vegetation	≤0.15	≤0.15	≤0.15
Min. angular difference	>13°	>13°	>13°
Min. length (clean up)	≥0.4 m	≥0.4 m	≥0.4 m
Min. length (clean up)	>0.1 m^2	>0.1 m^2	>0.1 m^2
Min. fissure class density	>1 %/10 m^2	>1 %/10 m^2	>1 %/10 m^2

Results and Discussion

The imagery acquired in July 2008, July 2009 and October 2009 was processed with the parameter setting described above where at the highest spatial resolution (≈ 5 Megapixel) the routine required less than 5 min to complete (Intel Core Duo 2.8 GHz, 4 GB RAM). Relative good agreement of the general fissure patterns was found by comparing the results obtained with expert maps based on field surveys and those obtained from visual image interpretation (Fig. 5).

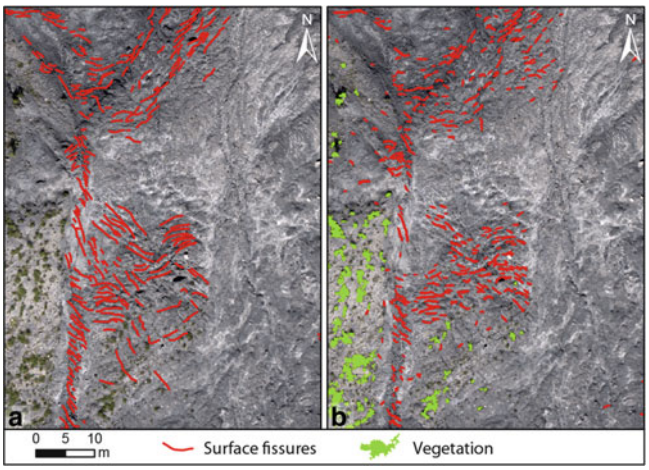


Fig. 5 Comparison between manual expert mapping (**a**) and the automatically extracted fissures (**b**) for a subset of the scene acquired in July 2009

Especially in areas with an abundant occurrence of fissures the visual appearance of expert and automatic mappings is similar, whereas most remaining mismatches originate from features detected by the proposed technique but not registered in the expert maps.

In order to obtain a quantitative estimate of the match between both mapping, line densities were calculated from the original maps varying the kernel size and the resolution of the output raster between 2 and 6 m. Figure 6f shows that for all time steps the agreement between expert and automatic maps is higher at coarser spatial scales. This is in agreement with the observed similar spatial patterns in both mappings, whereas there are still significant differences at the scale of individual fissures.

While it is important to note that also the manual mappings comprise a yet not quantified degree of uncertainties, a significant number of false detection can still be clearly attributed to cast shadows that resemble the elongated shape of fissures. Somewhat counter intuitive this leads to a more robust performance of the proposed mapping technique on low contrast images acquired under cloudy conditions because cloudy sky yields a diffuse and more uniform illumination of the surface. Indeed the best match was achieved with the UAV images acquired in October 2009 (Fig. 6a–e).

Besides quantitative differences it should also be noted that the original expert map comprises information about the type of the fissure which at present cannot be resolved with the proposed technique, whereas the automated mapping yields information about the vegetation cover as by product.

Acknowledgments The work described in this paper was supported by the project SafeLand "*Living with landslide risk in Europe: Assessment, effects of global change, and risk management strategies*" under Grant Agreement No. 226479 in the 7th Framework Programme of the European Commission, the project SISCA '*Système Intégré de Surveillance de Crises de Glissements de Terrain*' funded by the French Research Agency (ANR), and the project Grosshang "Coupling of Flow and Deformation Processes for Modeling the Movement of Natural Slopes" funded by the Deutsche Forschungsgemeinschaft (DFG). These supports are gratefully acknowledged.

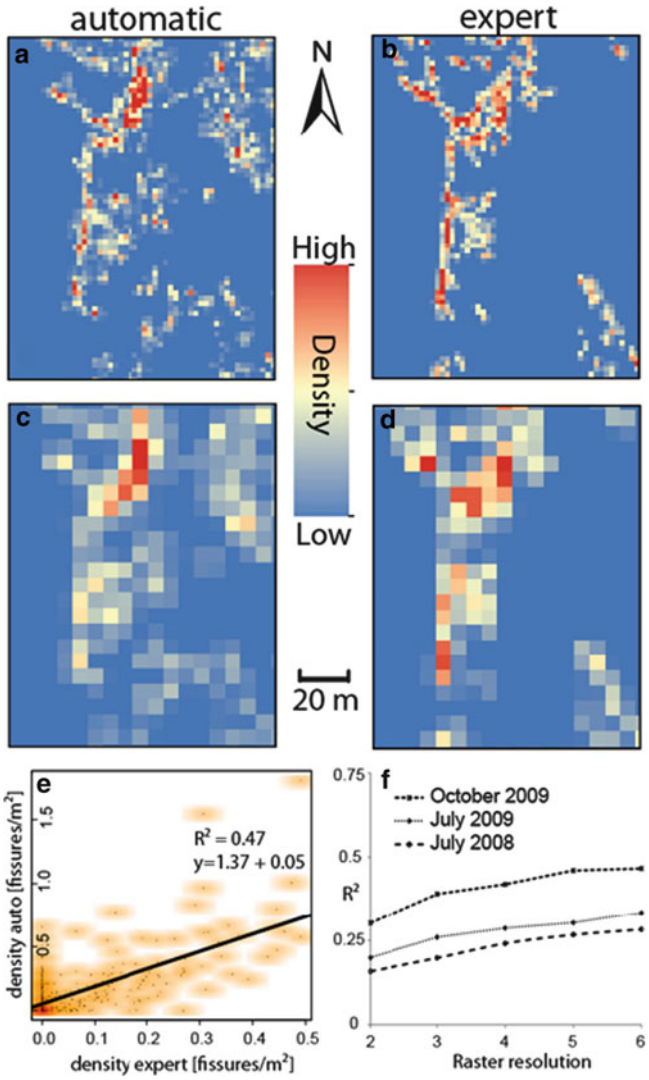


Fig. 6 Comparison of fissure density maps derived from the proposed automated approach and the corresponding expert maps (October 2009). Density raster with resolutions of 2 m (**a**, **b**) and 6 m (**c**, **d**) are displayed. The regression (**e**) shows the relation between the maps c and d. The agreement between the maps depends on the resolution of the density is calculation (**f**)

References

Abramson LW, Lee TS, Sharma S, Boyce GM (2001) Slope stability and stabilization methods. In: vol 2nd edn. Wiley, p 736

Baum RL, Fleming RW (1991) Use of longitudinal strain in identifying driving and resisting elements of landslides. Geol Soc Am Bull 103:1121–1132

Bièvre G, Jongmans D, Winiarski T, Zumbo V (2011) Application of geophysical measurements for assessing the role of fissures in water infiltration within a clay landslide (Trièves area, French Alps). Hydrol Process. doi:n/a-n/a. doi:10.1002/hyp. 7986

Chaudhuri S, Chatterjee S, Katz N, Nelson M, Goldbaum M (1989) Detection of blood vessels in retinal images using two-dimensional matched filters. IEEE Trans Med Imag 8(3):263–269

Chowdhury RN, Zhang S (1991) Tension cracks and slope failure. In: Paper presented at the international conference in slope stability engineering: developments and applications. Proceedings of an international conference, Isle of Wight

Corominas J, Moya J, Hürlimann M (2002) Landslide rainfall triggers in the Spanish eastern Pyrenees. In: Paper presented at the 4th EGS Plinius conference on Mediterranean storms, Mallorca, 4 Oct

Fleming RW, Baum RL, Giardino M (1999) Map and description of the active part of the slumgullion landslide, Hinsdale County. Geologic invstigations Series Map I-2672. U.S. Geologcial Survey, p 36

Fleming RW, Johnson AM (1989) Structures associated with strike-slip faults that bound landslide elements. Eng Geol 27(1–4):39–114. doi:10.1016/0013-7952(89)90031-8

Grandjean G, Bitri A, Krzeminska DM (2011) Characterisation of a landslide fissure pattern by integrating seismic azimuth tomography and geotechnical testing. Hydrol Process. doi:n/a-n/a. doi:10.1002/hyp.7993

Günther A, Carstensen A, Pohl W (2004) Automated sliding susceptibility mapping of rock slopes. Nat Hazards Ear Syst Sci 4:95–102

Hoek E, Bray JW (1981) Rock slope engineering. The Institution of Mining and Metallurgy, London

Hoover AD, Kouznetsova V, Goldbaum M (2000) Locating blood vessels in retinal images by piecewise threshold probing of a matched filter response. IEEE Trans Med Imag 19(3):203–210

Iverson RM (2000) Landslide triggering by rain infiltration. Water Resour Res 36(7):1897–1910

Jaboyedoff M, Baillifard F, Couture R, Locat J, Locat P (2004) Toward preliminary hazard assessment using DEM topographic analysis and simple mechanical modeling by means of sloping local base level. In: Lacerda WA, Ehrlich M, Fontoura AB, Sayão A (eds) Landslides: evaluation and stabilization. Taylor & Francis Group, London, pp 199–205

Krauskopf KB, Feitler S, Griggs AB et al (1939) Structural features of a landslide near Gilroy, California. J Geol 47(6):630–648

Lindenmaier F, Zehe E, Dittfurth A, Ihringer J (2005) Process identification at a slow-moving landslide in the Vorarlberg Alps. Hydrol Process 19(8):1635–1651. doi:10.1002/hyp. 5592

Malet J-P, Auzet A-V, Maquaire O, Ambroise B, Descroix L, Esteves M, Vandervaere J-P, Truchet E (2003) Soil surface characteristics influence on infiltration in black marls: application to the Super-Sauze earth flow (southern Alps, France). Earth Surf Process Land 28(5):547–564

Malet JP, van Asch TWJ, van Beek R, Maquaire O (2005) Forecasting the behaviour of complex landslides with a spatially distributed hydrological model. Nat Hazards Ear Syst Sci 5(1):71–85. doi:10.5194/nhess-5-71-2005

Matheson GD (1983) Rock stability assessment in preliminary site investigations – graphical methods. vol Report 1039. Transport and Road Research Laboratory, Crownthorne

McCalpin J (1984) Preliminary age classification of landslides for inventory mapping. In: Paper presented at the 21st Annual engineering geology and soils engineering symposium, Moscow, 5–6 April

Meisina C (2006) Characterisation of weathered clayey soils responsible for shallow landslides. Nat Hazards Ear Syst Sci 6(5):825–838. doi:10.5194/nhess-6-825-2006

Mendonca AM, Campilho A (2006) Segmentation of retinal blood vessels by combining the detection of centerlines and morphological reconstruction. IEEE Trans Med Imag 25(9):1200–1213

Niethammer U, James MR, Rothmund S, Travelletti J, Joswig M (2011) UAV-based remote sensing of the Super-Sauze landslide: evaluation and results. Engineering geology, Accepted Manuscript. doi:10.1016/j.enggeo.2011.03.012 (in press)

Otsu N (1979) A threshold selection method from gray-level histograms. IEEE Trans Systs Man Cybernetics 9(1):62–66

Parise M (2003) Observation of surface features on an active landslide, and implications for understanding its history of movement. Nat Hazards Ear Syst Sci 3(6):569–580. doi:10.5194/nhess-3-569-2003

Petley D, Dunning S, Rosser N, Kausar AB (2006) Incipient landslides in the Jhelum Valley, Pakistan following the 8th October 2005 earthquake. In: Paper presented at the disaster mitigation of debris flows, slope failures and landslides, Tokyo

Priest SD (1993) Discontinuity analysis for rock engineering. Chapman & Hall, London, UK

Selby MJ (1993) Hillslope materials and processes, vol Second. Oxford University Press, Oxford, UK

Shreve RL (1966) Sherman Landslide, Alaska. Science 154(3757):1639–1643. doi:10.1126/science.154.3757.1639

Soares JVB, Leandro JJG, Cesar RM, Jelinek HF, Cree MJ (2006) Retinal vessel segmentation using the 2-D Gabor wavelet and supervised classification. IEEE Trans Med Imag 25(9):1214–1222

Sofka M, Stewart CV (2006) Retinal vessel centerline extraction using multiscale matched filters, confidence and edge measures. IEEE Trans Med Imag 25(12):1531–1546

Trimble (2011) Trimble eCognition® 8.64.0 Release Notes

van Asch TWJ, van Beek LPH, Bogaard TA (2009) The diversity in hydrological triggering systems of landslides. In: The First Italian workshop on landslide, Napoli, 8–10 June 2009, pp 151–156

van Beek L, van Asch T (1999) A combined conceptual model for the effects of fissure-induced infiltration on slope stability. In: Hergarten S, Neugebauer H (eds) Process modelling and landform evolution, vol 78. Lecture notes in Earth sciences. Springer, Berlin/Heidelberg, pp 147–167. doi:10.1007/BFb0009724

Zhang B, Zhang L, Zhang L, Karray F (2010) Retinal vessel extraction by matched filter with first-order derivative of Gaussian. Comput Biol Med 40(4):438–445. doi:10.1016/j.compbiomed.2010.02.008



Portable Ring Shear Apparatus and Its Application

Maja Ostric, Kyoji Sassa, Bin He, Kaoru Takara, and Yosuke Yamashiki

Abstract

The paper presents the concept, design and construction of new ring shear apparatus, ICL-1. The new apparatus is, compared to previous ones (DPRI-5, 6, 7), much smaller in dimensions and has higher performances. It can keep undrained condition up to 1 MPa of pore water pressure (up to two times more than in previous versions of apparatus) and load normal stress up to 1 MPa. This makes it suitable for investigation of large- scale and deep seated landslides. Speed control test and undrained cyclic loading tests were performed to show experimental procedures in details. Typical test results are presented to show the efficiency of this ring shear apparatus.

Keywords

Ring-shear test • Undrained loading • Landslide

Introduction

The ring-shear apparatus was designed initially to investigate the residual shear resistance under the drained condition along the sliding surface at large shear displacements in landslides because it allows unlimited deformation of the specimen. It has been widely used in the analysis of slope stability due to its ability to attain much greater shear displacement than other testing devices (Bishop et al. 1971; Sassa et al. 1996; Tika and Hutchinson 1999). Sassa et al. have developed undrained high speed ring shear apparatus (DPRI-5, 6, 7) to reproduce a rapid landslide motion after failure and to measure the generated pore pressure and the shear resistance mobilized on the sliding surface during motion.

A new Croatia-Japan Joint Project "Risk identification and land-use planning for disaster mitigation of landslides and floods in Croatia" was initiated in 2009. The group planned to develop much inexpensive and transportable undrained ring shear apparatus to be used in different counterpart organizations with a standard electricity available anywhere. This paper presents the outline and initial test results of the developed portable ring shear apparatus.

The initial series of tests are implemented to examine the precision and performance of drained and undrained speed control tests and shear stress control tests including cyclic loading tests using the silicilclastic sands. Thereafter, this apparatus was applied to examine the dyamic shear behaviour of siliciclastic and volcanoclastic sand layer samples and will be used in further studies in Croatia- Japan Joint

M. Ostric (✉)
Department of Environmental Engineering, Graduate School of Engineering, Kyoto University, Gokasho, Uji City, Kyoto 611-0011, Japan
e-mail: ostric.maja@gmail.com

K. Sassa
International Consortium on Landslides, UNITWIN Headquarters Building, Kyoto University, Gokasho, Uji City, Kyoto 611-0011, Japan

B. He
Center for Promotion of Interdisciplinary Education and Research, Educational Unit for Adaptation and Resilience for a Sustainable Society, Kyoto University, Gokasho, Uji, Kyoto 611-0011, Japan

Disaster Prevention Research Institute (DPRI), Kyoto University, Gokasho, Uji, Kyoto 611-0011, Japan

K. Takara • Y. Yamashiki
Disaster Prevention Research Institute (DPRI), Kyoto University, Gokasho, Uji, Kyoto 611-0011, Japan

C. Margottini et al. (eds.), *Landslide Science and Practice*, Vol. 2,
DOI 10.1007/978-3-642-31445-2_47, © Springer-Verlag Berlin Heidelberg 2013

Table 1 Features of new Ring Shear Apparatus, ICL-1, compared with the previous versions of DPRI- 6 and 7

Author	Sassa (1997) DPRI-6	Sassa (2004) DPRI-7	Sassa (2011) ICL-1
Inner diameter (cm)	25.0	27.0	10.0
Outer diameter (cm)	35.0	35.0	14.0
Max. height of sample (cm)	15.0	11.5	5.2
Ratio max. height/width	3.0	2.88	2.6
Shear area (cm^2)	471.24	389.56	75.36
Max. normal stress (kPa)	3,000	500	1,000
Max. shear speed (cm/s)	224.0	300.0	5.4
Cyclic torque control testing (max. frequency)	5 Hz	5 Hz	1.0 Hz
Undrained testing and pore pressure monitoring	Yes	Yes	Yes
Max. data acquisition rate (readings/s)	200	1,000	1,000
Max pore water pressure	400–600	400–600	1,000

Project for the investigation of large-scale and deep seated landslides in Croatia and Japan.

The shear box is smaller than DPRI-5, 6, 7 and the necessary volume of sample for one test is app. 300 cm^3 which is suitable for limited amount of samples that are taken from drilled cores and used for investigation of large-scale and deep seated landslides.

Table 1 presents the major characteristics of new ring-shear apparatus in comparison to the previous versions of apparatus (DPRI-6 and 7) that were developed by Sassa and colleagues at the DPRI (Disaster Prevention Research Institute), Kyoto University.

Concept of the Ring Shear Apparatus

The current undrained ring-shear apparatus geotechnically simulates the formation of the landslide shear surface and the following post-failure motion and observes the consequence of mobilized shear resistance, as well as the post-failure shear displacement and generated pore-water pressure.

The concept is illustrated in Fig. 1. Samples are taken from the layer in which a previous landslide occurred, or the layer in which a sliding surface can be formed in the future. The sample is set in the ring shear box which is divided by a static upper half and a rotary lower half (Fig. 2). All stresses acting on the potential sliding surface; normal and shear stresses due to gravity and seismic stress due to seismic shaking as well as pore pressures in excess,can be reproduced in the shear box. When stresses are high enough to trigger sample failure, a shear surface will develop within the shear box, and the rotary lower half of the shear box will start to turn. During the process of shear failure development and subsequent post-failure motion, resulting excess pore pressure build up, mobilized shear resistance, and shear displacement during and after seismic or cyclic loading are monitored by load cells and displacement sensor (Fig. 2).

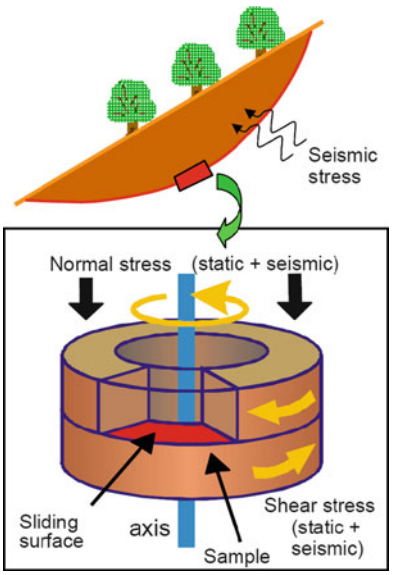


Fig. 1 Concept of the Ring Shear Apparatus

Structure and Control System of the Apparatus

The structure of undrained dynamic loading ring shear apparatus used in this study is shown in Fig. 2, while Fig. 3 presents an illustration of the electrical control system of the apparatus.

This apparatus was developed as a part of project of SATREPS (Science and Technology Research Partnership for Sustainable Development) project "Risk identification and land-use planning for disaster mitigation of landslides and floods in Croatia" (IPL-161).

Vertical load is given by pulling the central axis instead of large and tall loading frame used in the previous apparatus. This enabled to make the apparatus more compact, decreasing the size of the apparatus and increasing the upper limit of undrained capability.

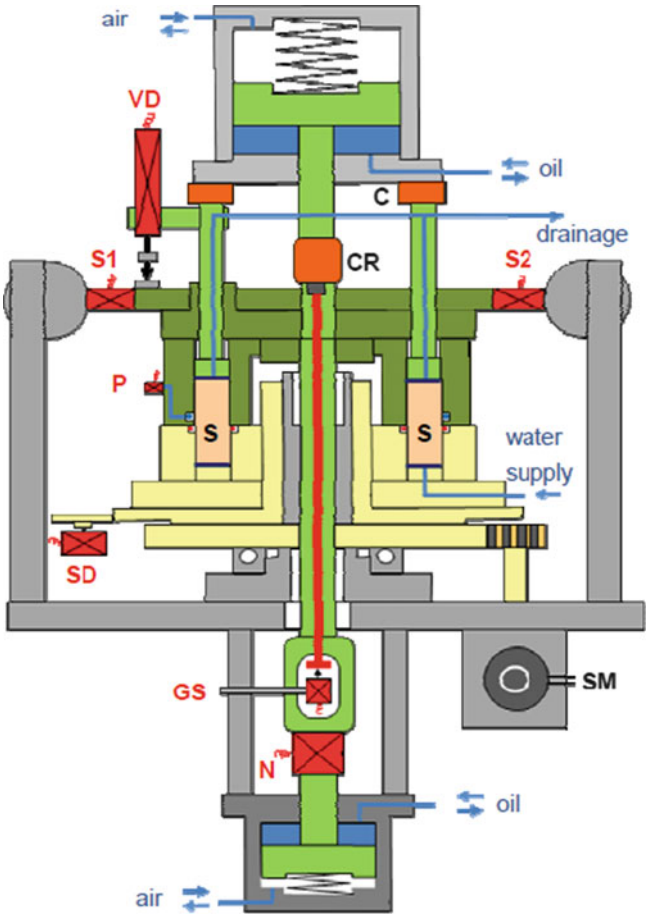


Fig. 2 Mechanical structure of the apparatus

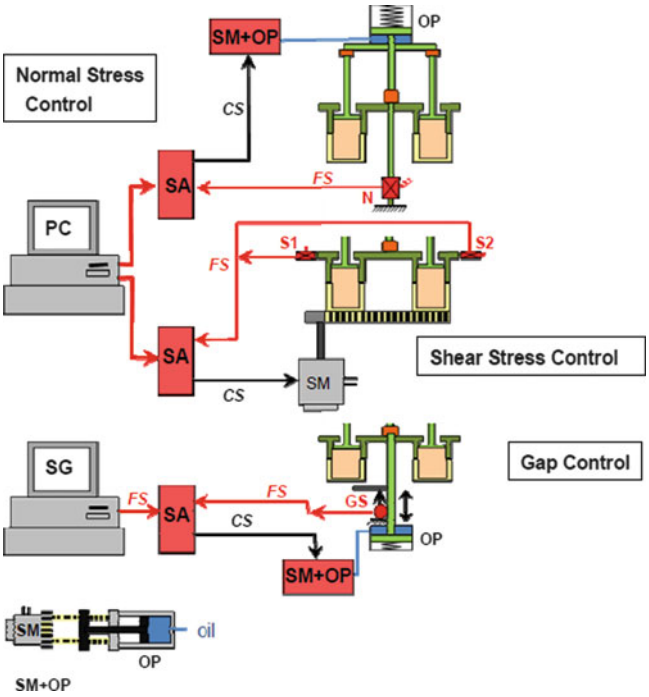


Fig. 3 Electronic Control System

The shear stress is given by a servo-control motor either by shear stress control or speed control. Normal stress is given by another servo-control motor through oil piston. The gap of the upper shear box and the lower shear box is automatically controlled by the third servo-motor through an oil piston to keep the contact pressure of rubber edge to the edge of shear box always greater than generated pore pressure within the shear box. Gap control system (oil piston and gap sensor, GS), enable prevention of leakage of water and sample during high-speed shearing.

Pore pressure generated in the shear zone is monitored by a pore pressure transducer P (Fig. 2) connected to a gutter extending around the whole circumference of the inner wall of the outer and upper ring. The gutter is covered by two metal filters and a felt cloth filter. The normal stress acting on the shear surface is monitored by the load cell N through retaining the upper shear box vertically (Fig. 2). The shear stress acting on the shear surface is monitored by a pair of shear load cells (S1 and S2 on Fig. 2) through retaining the upper shear box horizontally.

The developed portable ring-shear apparatus (ICL-1) has smaller dimensions and it can produce higher normal stress and pore pressure (Table 1). It has weight of app 100 kg, maximum height of 95 cm, and dimensions 50 × 50 cm and is set on a handcart. The sample box is 100 mm inner diameter and 140 mm outer diameter. The significant reduction in dimensions of the latest apparatus was possible because of smaller shear velocity and new loading system in which the normal stress is applied by pulling of the central axis. The previous apparatuses (DPRI-6 and DPRI-7) needed high electricity and the great capacity of servo-motor of 37 kW to shear soils at a high velocity up to 2–3 m/s in the centre of sample. High velocity required big motor and consequently much bigger size of apparatus. However, the series of test results presented that the generated pore pressure and the mobilized shear resistance at the steady state motion is hardly affected by the velocity, but they depend on the shear displacement. According to those findings, the shear velocity of ICL-1 is only 5.4 cm/s. 200 W servo-motor is enough for normal stress loading and 400 W servo-motor is used for shear stress loading. Electricity is single phase 100 or 200 V.

Beside the smaller dimensions, ICL-1 can succeed to maintain undrained condition up to 1 MPa of pore water pressure. While the undrained condition was possible up to 400–600 kPa of pore water pressure in DPRI 6 and 7 (Table 1) (Sassa 2004a). This became possible because of new loading system with a short loading axis and higher precision of upper and lower ring height and the smoothing of inner and outer rubber edge height.

Testing Procedure

For the experiments to be successfully performed, it is necessary to set the testing procedure. The procedure consists of the following: sample saturation, sample consolidation and loading (by shear speed control; stress control – either cyclic or seismic loading).

First, the gap value should be adjusted to avoid leakage of water and sample, by applying vertical load of 1 kN. When the gap of the upper and the lower shear box is adjusted, it should be kept constant during the test.

Shear box without sample is filled with CO_2 and de-aired water. Then, sample that was saturated by de- aired water during night could be slowly placed in shear box. After that, the water circulation could start to enable full water saturation of the sample. De-aired water was slowly supplied through the lower drainage line, and discharged from the upper drainage line until all air bubbles were expelled.

The saturation of sample was then checked by measuring B_D value that for fully saturated samples should be greater than 0.95. B_D is a pore pressure parameter in direct shear state, related to the degree of saturation that was proposed by Sassa (1988), and is formulated as:

$$B_D = \Delta u/\Delta\sigma \quad (1)$$

Where Δu and $\Delta\sigma$ are increments of pore pressure and normal stress, respectively.

After sample was fully saturated, the initial stress state of soils only due to gravity should be created. So, the sample was normally consolidated under pre-decided normal and shear stress, depending on the sample depth and slope angle. For samples used in Figs. 4 and 5, we used normal stress of 1,000 kPa and shear stress of 140 kPa. After the consolidation, shearing is applied by stress control mode (cyclic test) or speed control test.

Ring Shear Apparatus Application on samples

In this study, we made two types of tests: cycling loading in undrained condition and speed control test. Siliciclastic and vulcanoclastic sand layer samples were used in testing.

Cyclic Loading Test

Undrained cyclic loading test was performed on a saturated sililiciclastic sand layer sample ($B_D = 0.99$ was obtained). After consolidation of the sample (by applying normal stress of 1,000 kPa and shear stress of 140 kPa, in drained condition), dynamic, cyclic loading was applied. 15 cycles of sine wave shear stress was loaded at 0.1 Hz and stepping up shear stress by 40 kPa/cycle.

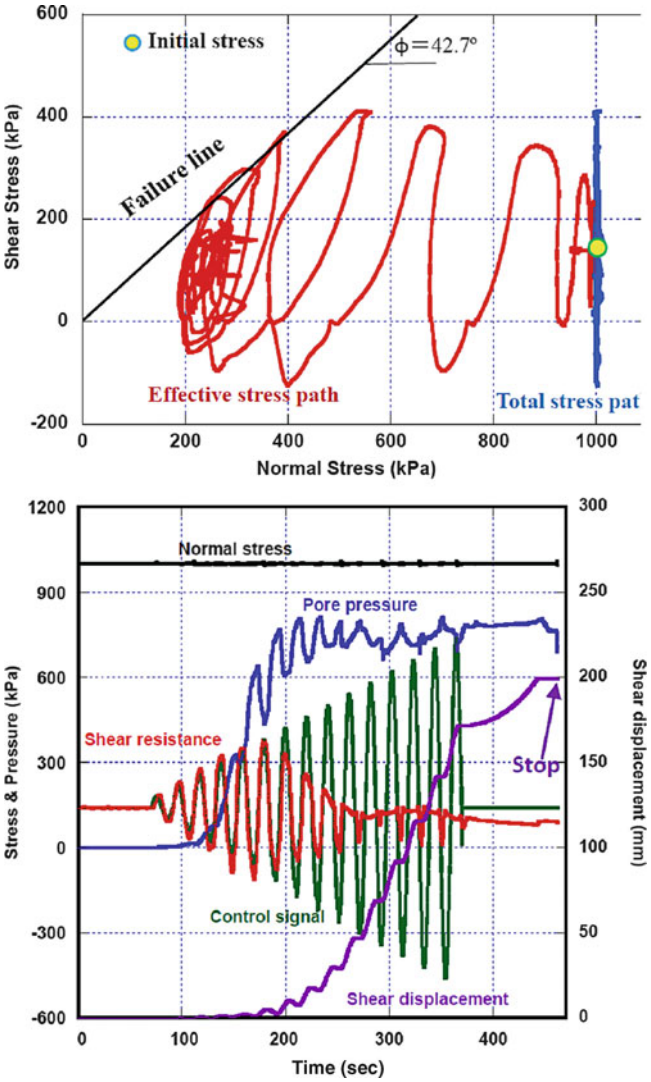


Fig. 4 Undrained cyclic loading test on saturated siliciclastic sand layer ($B_D = 0.99$; initial dry density: 1.56 g/cm^3, specific gravity, Gs = 2.88). (**a**) stress path; (**b**) time series data for stress, pressure and shear displacement

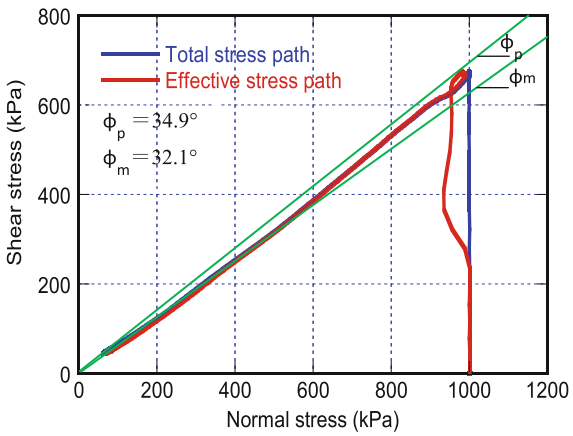


Fig. 5 Stress Path of Speed Control Test on saturated vulcanoclastic sand layer ($B_D = 0.98$; initial dry density: 1.27 g/cm^3, specific gravity, Gs = 2.55)

The results of a test are presented in Fig. 4. Figure 4a shows stress path of this test and it successfully created the failure. The blue line is total stress path (TSP) and the red line is the effective stress path (ESP). The mobilized friction angle at failure was $\varphi_p = 42.7^\circ$.

Figure 4b shows the time series data of the test. The green line shows the control signal for shear stress which was given to the servo-stress control motor. The red line shows the shear resistance mobilized on the sliding surface, the blue line shows pore pressure and the purple line shows the shear displacement. Figure 4b visualized pore pressure generation during cyclic loading, failure of soils, and further increase of pore water pressure with progress of shear displacement, and resulting reduction of shear resistance until a certain steady state shear strength. This phenomenon is termed as "sliding surface liquefaction" (Sassa 1996).

The accelerated motion was produced after failure. Initially both lines of the control signal for shear stress and the mobilized shear resistance are the same. However, after failure, both lines differ. Shear resistance will decrease down to the steady state of shear resistance though greater control signal is continued to be given. The difference of stress is used for acceleration of shear motion. Motion is decelerated and stopped after the stop of cyclic loading.

Speed Control Test

Speed control test was performed on a saturated vulcanoclastic sand sample ($B_D = 0.98$ was obtained). After consolidation of the sample (by applying normal stress up to 1,000 kPa in drained condition), speed control test was conducted under constant shear speed of 0.1 cm/s.

The results of a test are presented in Fig. 5, showing the effective stress path (ESP) and total stress path (TSP) as well as peak friction angle ($\varphi_p = 34.9^\circ$) and mobilized friction angle ($\varphi_m = 32.1^\circ$). The reason why peak value of the sample is lower than usual for this type of material is that this test was performed immediately after the undrained cyclic loading test without changing sample.

Summary and Conclusions

The paper has presented the design and construction of newly developed ring shear apparatus, ICL-1. Initial plan was to develop inexpensive and transportable undrained ring shear apparatus. Compared to previous ring shear apparatus (DPRI-6,7), the latest one has much smaller dimensions and higher performances: it can keep the undrained condition of shear box up to 1 MPa and produce normal stress up to 1 MPa. This makes it suitable for investigation of large-scale and deep seated landslides.

By performing tests (speed control test and undrained cyclic test) on siliciclastic and vulcanoclastic sand layer samples, related experimental procedures are presented in details. Typical test results are presented to show the efficiency of this ring shear apparatus.

Acknowledgments The design and construction of the ring shear apparatus ICL-1, was conducted under the support of SATREPS (Science and Technology Research Partnership for Sustainable Development) programme of the Government of Japan. This research is a part of the International Programme on Landslides (IPL-161Risk identification and land-use planning for disaster mitigation of landslides and floods in Croatia).

References

Bishop AW, Green GE, Garge VK, Andersen A, Brown JD (1971) A new ring shear apparatus and its application to the measurement of residual strength. Géotechique 21:273–328

Sassa K (1996) Prediction of earthquake induced landslides. In: Proceedings of 7th international symposium on landslides, A.A. Balkema, Rotterdam, vol 1, pp 115–132

Sassa K, Fukuoka H, Wang G, Ishikawa N (2004a) Undrained dynamic-loading ring-shear apparatus and its application to landslide dynamics. Landslides 1(1):7–19

Sassa K, Wang G, Fukuoka H, Wang FW, Ochiai T, Sugiyama M, Sekiguchi T (2004b) Landslide risk evaluation and hazard mapping for rapid and long-travel landslides in urban development areas. Landslides 1(3):221–235

Sassa K, Fukuoka H, Wang FW, Wang GH (2007) Landslides induced by a combined effects of earthquake and rainfall. In: Sassa K, Fukuoka H, Wang FW, Wang GH (eds) Progress in landslide science. Springer, Berlin, pp 311–325

Tika THE, Hutchinson JN (1999) Ring shear tests on soil from the Vaiont landslide slip surface. Géotechnique 49:59–74



Assessing of Spatio-Temporal Factors Influencing Landslides Using PSInSAR

Mateja Jemec Auflič, Magda Čarman, and Marko Komac

Abstract

The need of living together with landslides in a sustainable way requires a strong effort in terms of landslide analysis. Traditional methods used for mapping and monitoring mass movements can benefit from the application of remote sensing techniques coupled with GIS analysis. The use of remote sensing technologies, whether air, satellite or ground based allows a rapid acquisition of quantitative data over wide areas, reducing the field work and, as a consequence, the costs. A modern satellite radar interferometry method of Permanent scatters (PSInSAR) is very useful. At Geological Survey of Slovenia, the PSInSAR™ data were used to assess spatio-temporal factors which influence on slope mass movements and small, long lasting ground deformations were defined in the Škofjeloško Cerkljansko area during the years 1992–2000.

Keywords

Landslides • Radar interferometry • PSInSAR • Monitoring • Slovenia

Introduction

The PSInSAR™ (Permanent Scatterers Interferometry Synthetic Aperture Radar) was evolved by scientific from the Politecnico di Milano (POLIMI) in 1999 (Ferretti et al. 1999) and it is based on a multi-interferogram approach. In particular, this technique involves the interferometric phase comparison of several radar images of the same scene (a portion of the earth surface, wide 100 × 100 km) taken at different times along the same orbit by the satellite radar sensors. ERS1 and ERS2 satellites orbit are at an elevation 780 km and take on the same image every 35 days. The critical deformation rate is 2.8 cm in 35 days or 0.8 mm in a day. Accuracy of PSInSAR technique depends on the number of radar images used in processing. In order to obtain good results about 20 images are required as a minimum. Not all the acquired images are suitable for interferometric analysis, so that the time interval between two consecutive images can be longer.

The processing technique is based on the identification of the radar benchmarks, named Permanent Scatterers, which are stable natural reflectors (Fig. 1) (rock outcrops, buildings and urban structures), characterized by stable individual radar bright and radar phase over long temporal series of interferometroc SAR images. This technique has proved useful at exploring slow movements of the earth surface, induced by natural and man-induced phenomena such as land subsidence, landslides, seismic faults, tectonic deformations, with very high spatial resolution, both at a local and at a regional scale (Colesanti et al. 2003; Farina et al. 2006). The final results are:

- A map of the PS identified in the image and their coordinates: latitude and precise elevation (accuracy on elevation better than 1 m); each PS is labelled by a code;

M.J. Auflič (✉)
Geological Survey of Slovenia, Geological Information Centre, Dimičeva ulica 14, Ljubljana 1000, Slovenia
e-mail: mateja.jemec@geo-zs.si.

M. Čarman
Geological Survey of Slovenia, Mineral Resources, Ljubljana, Slovenia

M. Komac
Geological Survey of Slovenia, Geological Information Centre, Ljubljana, Slovenia

C. Margottini et al. (eds.), *Landslide Science and Practice*, Vol. 2,
DOI 10.1007/978-3-642-31445-2_48, © Springer-Verlag Berlin Heidelberg 2013



Fig. 1 Examples of natural target of PS points in Škofjeloško Cerkljansko area

- Average LOS deformation rate of every PS (expressed as average velocity with accuracy usually between 0.1 and 1 mm year^{-1}), depending on the number of available interferograms and on the phase stability of each single PS (Milone and Scepi 2011);
- Displacement time series showing the relative (i.e. with respect to a unique reference image) LOS position of PS in correspondence of each SAR acquisition. The time series represent, therefore the motion component of the PS in the direction of the Line of Sight (LOS) as a function of the time (accuracy on single measurements usually ranging from 1 to 3 mm).

As in all differential interferometry applications, the results are not absolute both in time and space, but the deformation data are referred to the master image (in time) and the results are computed with respect to a reference point of known elevation and motion (in space). The traditional radar interferometry can be affected by atmospheric noise, but the PSInSAR^{TM} technique is capable to highly reduce the effect of time decorrelation and atmospheric phase (Ferretti et al. 2001).

In this article we focused on PSInSAR measurements which were used to assess spatio-temporal factors that influence slope mass movements. Based on classes of susceptibility the relation between PSInSAR data and lithology were examined.

Study Area

The study area is located in the western central part of Slovenia, northwest of Ljubljana, and it occupies approximately 640 km^2 (Fig. 2). Škofjeloško Cerkljansko area has a complex geological structure from Carboniferous and Permian (shales and quartz sandstones), Permian (quartz conglomerates, sandstones and shales), Triassic (dolomite and limestones, pseudozilian formation –dark grey claystones with green tuff and tuffite and sandstones intercalations), Jurassic and Cretaceous (shaly calystones and marlstones) and fluvial sediments in valleys dating from the Quaternary period.

Also the tectonic setting of the area is very complex. This area is border place between geotectonic units of External Dinarides and Southern Alps (Placer 1999). Nortwestern part of the External Dinarides is composed of large nappes thrusted from the NE towards the SW. The uppermost part belongs to the Trnovo nappe which comprises Idrija – Žiri and Škofja Loka – Polhov Gradec region. Trnovo nappe is composed of Palaeozoic clastic rocks (Placer et al. 2000). It is overthrusted from NE to SW on the Hrušica nappe, whereas from north soutwards the Southern Alps are overthrusted on it along Southalpine front. Hrušica nappe consist of Pseudozilian formation.

It is characterized by a number of settlements, very diverse morphology that reflects several geodynamic processes, active tectonics with numerous faults and thrusts, which produce a complex ground deformation pattern. These factors make the studied region particularly threatened with landslide risk.

Methodology

In total, 67 ERS scenes acquired between 1992 and 2000 by the ERS1 and ERS2 sensors along descending orbits were used for the interferometric and statistical analyses of the Škofja Loka and Cerkljansko hils (Fig. 2). About 2787 PS were identified, with a coherence value between 0.58 and 0.96. The distance is centred, for each point, with respect to the distance that the same point has with the satellite in the image termed as master. The geocoding accuracy of the PS locations was around +15 m easting and +4 m in the north-south direction, while the estimated accuracy of the elevation values was usually better than 2 m. The line of sight direction (LOS) displacement rates vary from +7.26 to −18.75 mm/year and are relative to a reference point located in the town Železniki and assumed motionless. The time series of the measured displacement allows us to identify areas in which there is a significant time dependent component to the deformation field and enables the analysis of the deformation evolution of the PS over time.

Two types of PS analyses were performed: Standard Permanent Scatterers Analysis (SPSA) and Advanced Analysis (APSA). The SPSA is suitable for mapping the territory at a regional scale, in order to identify unstable areas that deserve further detailed studies. The APSA is suitable for small areas where a full exploitation of the information content of the satellite data is required. With APSA it is possible to search for nonlinear motions and for PS with variable characteristics in time, significantly increasing the PS density. Based on the terrain properties and displacement of permanent scatterers in line of sight basic statistical properties (*mean, min, max, standard deviation, variance*) were calculated in radius 10 m around each PS points for

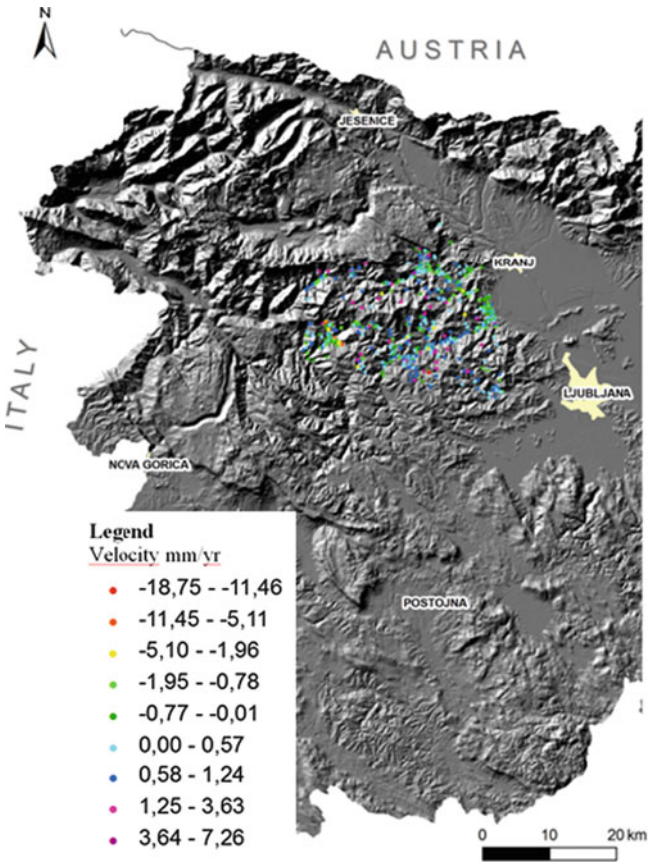


Fig. 2 Distribution of PSInSAR points through the research area Škofjeloško Cerkljansko. Negative values represent points which are "subsiding" and positive "uplifting"

main preparatory factors (lithology, land use, slope, aspect) that often govern mass movements. To interpret preparatory factors the "*mean*" values were used.

Results

Evaluation of Preparatory Spatio-Temporal Factors

Landuse

Distribution of PS points according land use map was based on Corine Landcover 2000. In order to obtain the most relevant landuse clasess we homogenized 11 landuse classes into three main classes (Table 1), base on their characteristic of keeping constant the scattering properties in time (Cascini et al. 2009). Classes were grouped according to the PS density and coherence. Thus, class I represents urbanized areas and areas where prevailing infrastructure; in class II, non irrigated and irrigated arable land, agricultural land and predominantly agricultural land with significant areas of natural vegetated are combined; class III include different

Table 1 The three main homogenized landuse classes

Class	Typology
Class I	Urban area
	Infrastructures
Class II	Non irrigated arable land
	Irrigated arable land
	Agricultural land
	Predominantly agricultural land with significant areas of natural vegetation
Class III	Deciduous forest
	Coniferous forest
	Mixed forest
	Natural pastures
	Scrubs

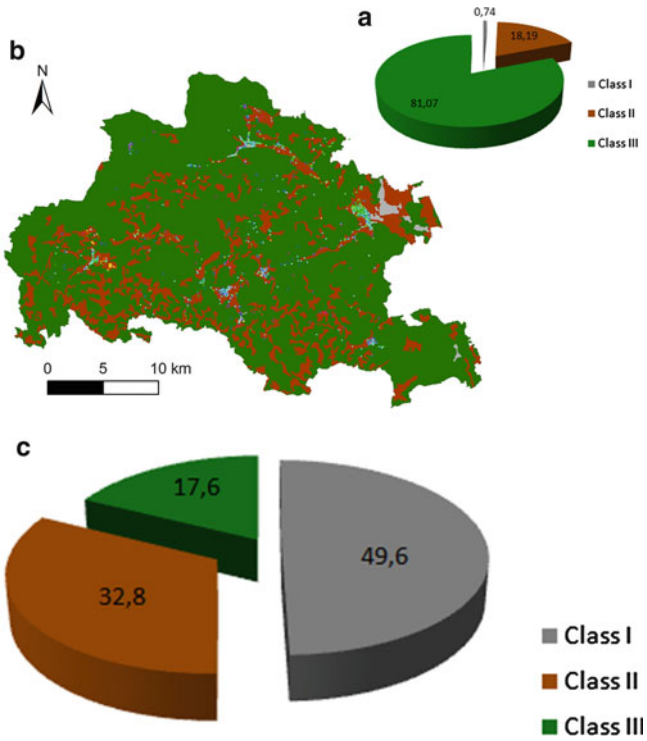


Fig. 3 Distribution of PS points regarding landuse map: (**a**) areal distribution of land use classes; (**b**) PSInSAR distribution over the homogenized landuse map; (**c**) distribution of PSInSAR points regarding the three different landuse classes

type of forest and natural pastures. According to the very hilly vegetated terrain with individual settlements the landuse Class III covers more than 80 % of the whole area whereas Class II 18.2 % and Class I less than 1 % (Fig. 3a, b). But in case of PS records, we noticed different situation. Almost 50 % of all PS records coincide with Class I of urban areas (Fig. 3c), where the density of buildings or natural reflectors is very high. About 30 % of PS data belong to Class II (agricultural land) and about 17 % of PS points cover Class III (Fig. 3c).

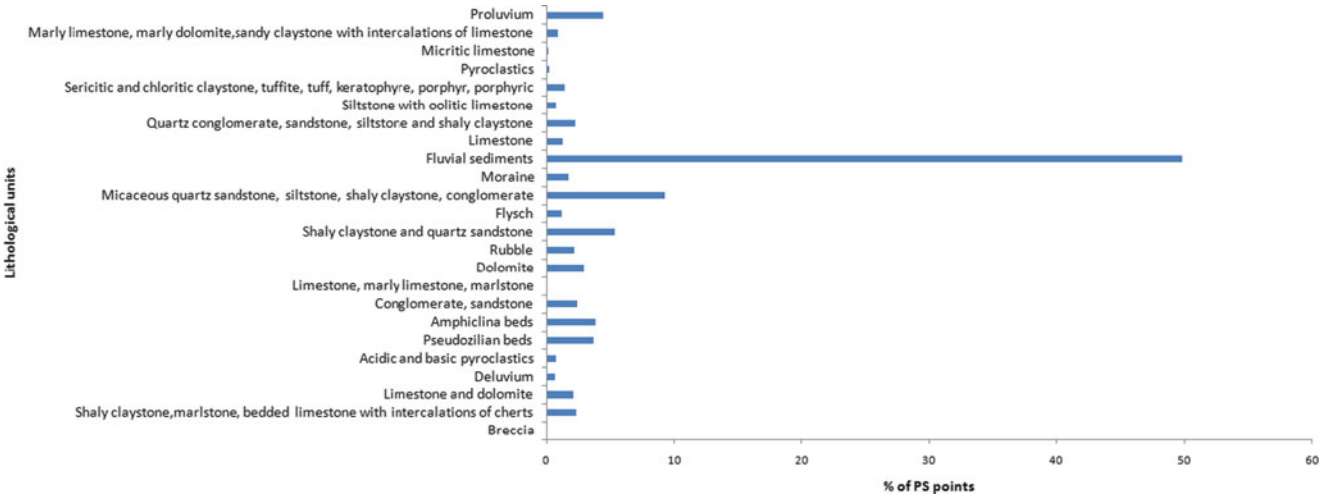


Fig. 4 Distribution of PS points regarding the homogenized lithological units

Lithology

The Basic Geological Map of Yugoslavia (Buser 1987; Grad and Ferjančič 1974) at the scale of 1:100,000 served as a source for the geological data. Figure 4 shows the distribution of PS points regarding the lithological units. 50 % of PS points coincide with fluvial and quaternary sediments that often cover the flat terrain. On flat ground are buildings which represent stable radar points. In terms of mass movements, more interesting are soft rocks. In the research area, the beds of shaly claystone, pseudozilian beds, marlstone and the mixed rock are the most exposed to landslides occurrences that represent around 30 % of all measurements.

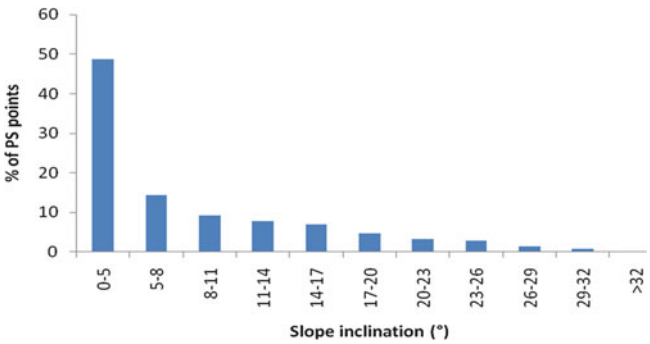


Fig. 5 Distribution of PS points regarding the slope inclination

Slope and Aspect

Slope and aspect were derived from DEM. About 50 % of all PS points are placed on slope with inclination between 0 and 5°. These results are strongly linked with landuse and lithology, where prevail flat terrain with high density of PSInSAR points. With raising slopes inclination the % of PS points decrease and mean that on steep slopes density of stable radar target is lower than on flat terrain (Fig. 5). These differences are reflected in the coherence. PS data with higher coherence are mostly in flat terrain, where density of buildings, infrastructures and other natural reflectors is high. In contrary, on steep slopes density of natural benchmarks are relatively low and PS data with lower coherence sometimes not represent sufficient certainty.

In the research area, mountain slopes facing the west are visible from the satellite, while those facing the east will be more affected from perspective deformations and consequently, the general aspect of PS points located there is toward south and south-west (Fig. 6).

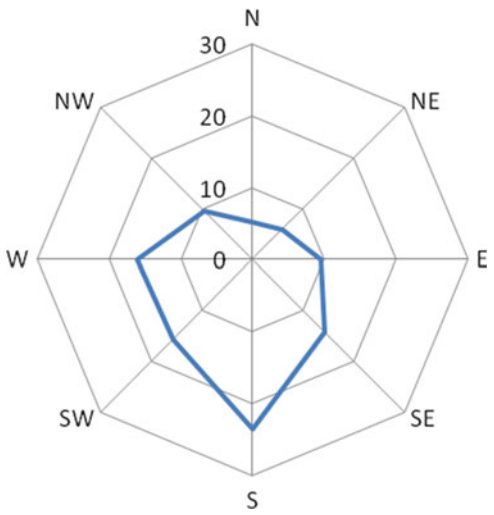


Fig. 6 Distribution of PS points regarding the aspect inclination

Table 2 Landslide susceptibility classes define on expert decision

Landslide susceptibility class	Lithological units
6	Pseudozilian beds and Amphiclina beds
	Shaly claystone and quartz sandstone
	Flysch, Proluvium, Deluvium
	Micaceous quartz sandstone, siltstone, shaly claystone
	Quartz conglomerate, sandstone, siltstone, shaly claystone
5	Shaly claystone, marlstone, bedded limestone
	Limestone, marly limestone, marlstone
	Siltstone with oolitic limestone, Pyroclastics
	Sericitic and chloritic claystone, tuffite, tuff
	Marly limestone, marly dolomite, sandy claystone
4	Rubble, Moraine, Fluvial sediments
3	Acidic and basic pyroclastics
	Conglomerate, sandstone, Limestone, Breccia
2	Limestone and dolomite

Relation Between PSInSAR and Lithology

Lithology plays one of the most important preparatory factors to trigger slope failure. Due to mechanical properties of rock mass, especially soft rocks (shaly claystone, claystone, and marlstone) that prevail in the research area, soils are very unstable and fail rapidly under rainy conditions. Based on expert decision of susceptibility of lithological units to the landslide occurrence PS points were classified according to lithological units in six landslide susceptibility classes where value 1 represents areas with negligible landslide occurrence potential and value 6 areas with very high landslide occurrence potential (Table 2). More than half PS points were classified into the third class with low susceptibility and 30 % of points to sixth class with very high susceptibility to landslide occurrence. The remaining 20 % of permanent scatterers were classified in the class with very low and medium landslide occurrence potential.

In order to calculate statistical properties and identify relation or differences between PSInSAR records and landslide susceptibility classes we filtered all PS data that have negative sign or indicate subsiding The PS data are filtered after three determined criterion: (1) The coherence is greater than 0.60; (2) Slope inclination is greater than 5°; (3) Choice among six determined landslide susceptibility classes.

From Fig. 7 it can be seen temporal behaviour of descriptive statistical parameters (Mean, Standard deviation, Minimum and Maximum) from June 1992 to December 2000 that determine general displacement line. Calculated statistical parameters *Mean, Standard Deviation, Minimum and* Maximum and their distribution showing that PS point which lay on soils ranged to landslide susceptibility class with very high landslide occurrence moving faster than other PS points. Figure 7 also shows that among all lines that characterized relative movements of PS points on a given day in each landslide susceptibility class the highest values prevailing in the sixth class followed by fifth, fourth, third and second.

Regarding preparatory factors, field investigation and correlations of temporal displacement series of permanent scatteters several clusters of PS points at several locations throughout research area have been detected (Fig. 8). The clustered PS are spatially defined by coordinates and PSInSAR displacements, so that the interpretation of their deformation trend can be referred to a map showing the spatial distribution of the different ground deformation trend. For these groups of points it can be said that are spatially related and that their displacements can indicate slow slope movements, namely creeping.

Conclusion

A PSInSAR method is proposed and applied to study area taking into account the large amount of ERS SAR data, the extension of the study area and the great variability of geological processes. The results show that the described technique is suitable to complement and integrate information derived from conventional methods for landslides mapping in a significant, although limited, number of cases. In present study descriptive statistics and filtering are appropriate procedure to show relation between PSInSAR records and lithology. Furthermore, the analysis shows that lithological units contribute to creeping even though the authors not include other important triggering factors to landslide occurrences e.g. rainfall, tectonics or earthquakes.

Nevertheless, the success of the technique depends also on the typology of landslides and their related kinematics. The PSInSAR method is best suited for assessing the temporal evolution of slow and extremely slow landslides with constant velocity deformations. Thanks to the high PS density it was possible to identify some areas with constant subsiding. Landslides with intermittent behaviour, such as that triggered by rainfall, are difficult to detect due to rapid slope failure.

The PS density depends mainly on the presence of targets (rocks, buildings, antenna), on the topographic effects (layovering, shadowing, etc.), on the vegetation and snow cover and also on the numbers of scenes elaborated.

Detailed geomorphological, geological studies and field checks in the anomalous areas allow accurate

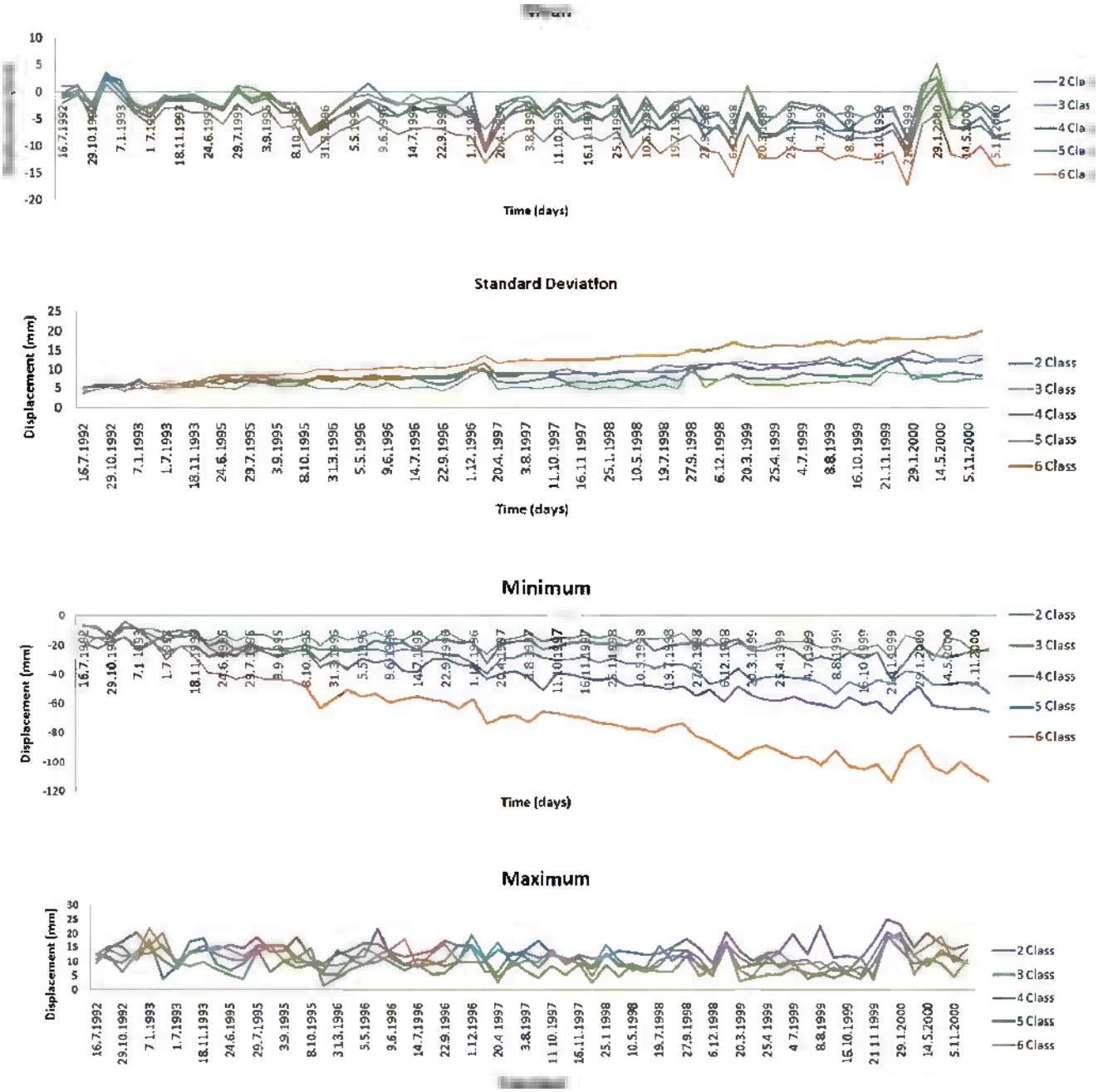


Fig. 7 Temporal displacement of PS points for main statistical parameters (Mean, Standard deviation, Minimum, Maximum). All displacements are given in mm and are projected to the vertical axis. The figure shows the displacement time span from June 1992 to December 2000. Names of temporal displacements that combine lithological units from very high to very low landslide susceptibility: *Orange*-very high landslide susceptibility (6), *Light blue*-high landslide susceptibility (5), *Violet*-medium landslide susceptibility (4), *Green*- low landslide susceptibility (3), *Dark blue*- very low landslide susceptibility (2)

interpretation of the displacements identified in the PSInSAR analysis. Among all observed spatio-temporal factors, lithological units and slope have played one of the important roles at triggering landslides. Slopes covered with Carboniferous and Permian claystone, shale and quartz sandstone and also Triassic Pseudozillian beds with claystone, marlstone and sandstone are the most exposed to landslides.

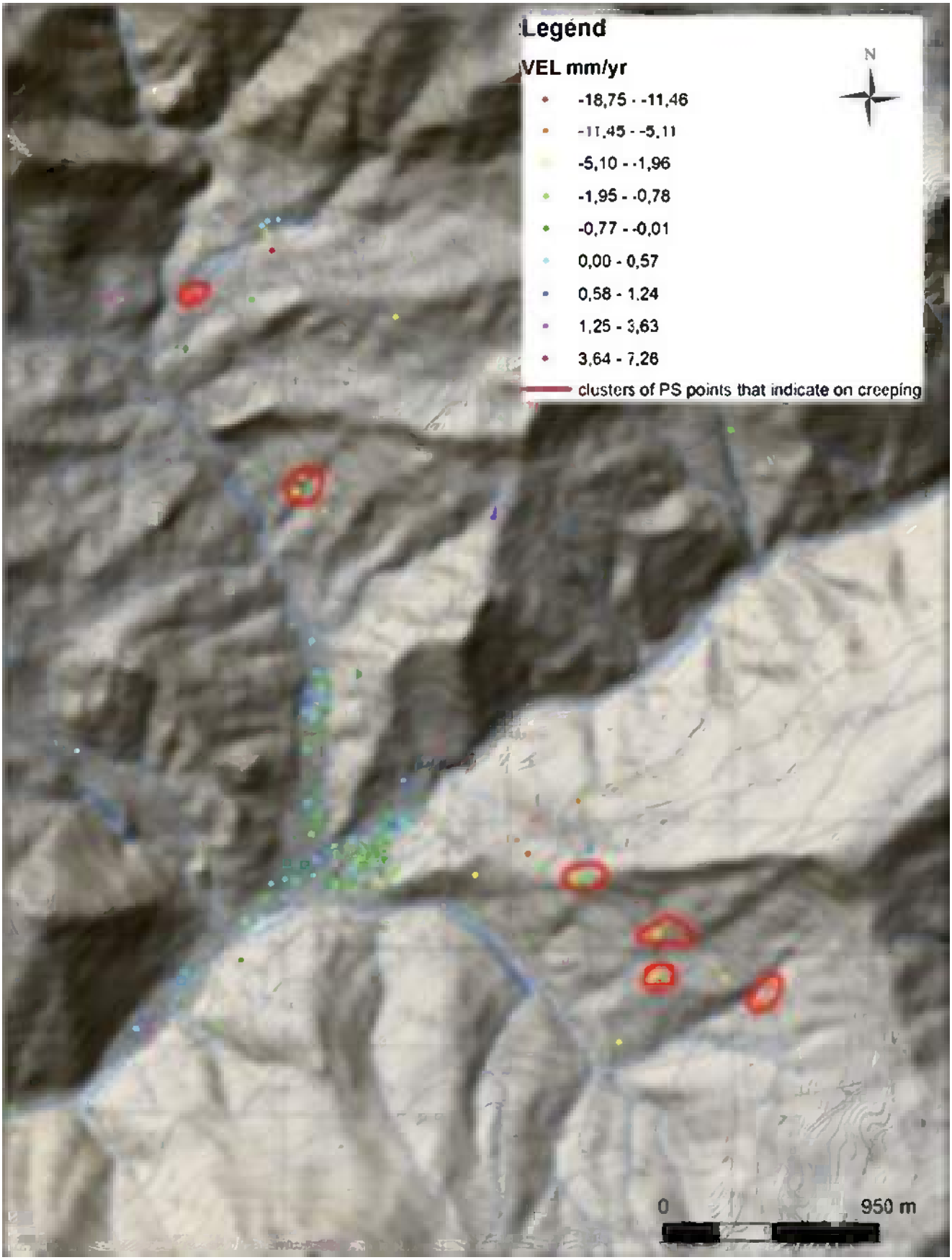


Fig. 8 Part of investigated area (Planina pri Cerknem, Čeplez) where PSInSAR technique measured stable target with velocity between −1 and −5 mm per year in line of sight. Red lines combine PS points with similar spatio-temporal displacement through the observed period between 1992 and 2000 and indicate on soil creeping

Acknowledgments The authors would like to thank the Research Agency of the Republic of Slovenia (ARRS) for funding the research (J1-0913) and JTS of Alpine Space-European Territorial cooperation programme for co-funding the research through the AdaptAlp project.

References

Buser S (1987) Osnovna geološka karta SFRJ, list Tolmin in Videm, 1: 100,000 = basic geological map of Yugoslavia, Tolmin and Udine, scale 1: 100,000. Zvezni geološki zavod, Belgrade

Cascini C, Fornaro G, Peduto D (2009) Analysis at medium scale of low resolution DInSAR data in slow moving landslide affected areas. ISPRS J Photogramm Rem Sens 64(6):598–611

Colesanti C, Ferretti A, Novali F, Prati C, Rocca F (2003) SAR monitoring of progressive and seasonal ground deformation using the Permanent Scatterers Techniques. IEEE Trans Geosci Rem Sens 41(7):1685–1701

Farina SD, Colombo A, Fumagalli F, Marks S, Moretti S (2006) Permanent Scatterers for landslide investigations: outcomes from the ESA-SLAM project. Eng Geol 88:200–217

Ferretti A, Prati C, Rocca F (1999) Non-uniform motion monitoring using the permanent scatterers technique. In: Second international workshop on ERS SAR interferometry

Ferretti A, Prati C, Rocca F (2001) Permanent scatterers in SAR interferometry. IEEE Trans Geosci Rem Sens 39(1):8–20

Grad K, Ferjančič L (1974) Osnovna geološka karta SFRJ, list Kranj, 1: 100,000 = basic geological map of Yugoslavia, Map Kranj, scale 1: 100,000. Zvezni geološki zavod, Belgrade

Milone G, Scepi G (2011) A clustering approach for studying ground deformation trends in Campania region through PS-InSAR^{TM} time series analysis. J Appl Sci 11:610–620

Placer L (1999) Contribution to the macrotectonic subdivision of the border region between Southern Alps and External Dinarides. Geologija 41:223–255, Ljubljana

Placer L, Rajver D, Trajanova M, Ogorelec B, Skabarne D, Mlakar I (2000) Borehole Ce-2795 at Cerkno at the boundary between the Southeren Alps and the External Dinarides (Slovenia). Geologija 43 (2):251–266, Ljubljana



Methodological and Technological Advances in the Application of Spaceborne DInSAR for Landslide Monitoring

G. Fornaro, D.O. Nitti, R. Nutricato, F. Bovenga, D. Peduto, and L. Cascini

Abstract

Differential Interferometry Synthetic Aperture Radar is a mature remote sensing technique broadly used for the measurement of slow deformations with major application in several fields. In the last years, the application to slow moving landslides has grown quickly and several examples of the monitoring capability can be found in the literature. Main goal of this work is the description of the advances in terms of products that can be achieved from both an innovative methodological approach to DInSAR data analysis and the technological improvements related to the last generation of sensors.

Keywords

Differential SAR Interferometry • Persistent Scatterers Interferometry • Landslide monitoring

Introduction

Multipass Differential Interferometry Synthetic Aperture Radar (DInSAR) is today a well established technique for the monitoring of ground deformation related to several natural hazards. Compared to classical geodetic techniques, such as leveling and GPS, it provides advantages in terms of costs, coverage, data accessibility and availability of data archives. The application to monitoring of volcanoes, tectonic movements, urban areas, infrastructures and slope movements has been already successfully demonstrated.

G. Fornaro (✉)
CNR-IREA, Via Diocleziano 328, Naples I-80124, Italy
e-mail: fornaro.g@irea.cnr.it

D.O. Nitti • R. Nutricato
GAP srl, Dip. Interateneo di Fisica, Politecnico di Bari,
Via Amendola 173, Bari 70126, Italy

F. Bovenga
CNR-ISSIA, Via Amendola 122/D, Bari 70126, Italy

D. Peduto • L. Cascini
Department of Civil Engineering, University of Salerno,
via Ponte don Melillo, Fisciano (Salerno) 84084, Italy

As far as the landslide phenomena are concerned, the monitoring of surface deformation via the DInSAR technique may provide useful information regarding the spatial and the temporal distribution of slow-moving landslides and their kinematics. However, landslides monitoring is particularly critical when dealing with vegetated and steep slopes. Accordingly, the interpretation of the measurements can be extremely difficult due to the 3D direction of the surface movements as well as the geometric distortions induced by the topography variations.

Most of the DInSAR applications have been carried out in the past on medium resolution data acquired by the ERS, Envisat and Radarsat sensors.

The new generation of high-resolution X-Band SAR sensors, such as TerraSAR-X and the COSMO-SkyMed constellation, allows acquiring data with finer spatial resolution (i.e metric/submetric values) with respect to C-band data. As a result, X-band InSAR applications appear very promising for the monitoring of single man-made structures, even isolated, also in areas where C-band data show low density of coherent scatterers.

This work aims, firstly, to discuss the advances in terms of methodological development for DInSAR data interpretation in landslide analyses and, secondly, to provide a "view"

C. Margottini et al. (eds.), *Landslide Science and Practice*, Vol. 2,
DOI 10.1007/978-3-642-31445-2_49, © Springer-Verlag Berlin Heidelberg 2013

on the improvements associated with the new generation high resolution SAR sensors. In particular, a DInSAR data interpretation approach based on the joint use of remote sensed data and simplified geomorphological models is presented. This procedure (Cascini et al. 2009, 2010), tested via the application of a two-scale analysis with ESD (Fornaro et al. 2009a) at lowresolution and an amplitude and phase based algorithm (4D imaging) at full-resolution algorithm (Fornaro et al. 2009b) to data acquired by the medium resolution ERS-1 and ERS-2 satellites, allows the estimation of the ground displacement vector, thus improving the result interpretation.

Furthermore, the results of the application of a Persistent Scatterers Interferometry (PSI) technique, namely the SPINUA (Stable Point INterferometry over Unurbanized Areas) algorithm, to data acquired by the high resolution X-band SAR sensor onboard of the COSMO-satellite constellation are shown with reference to a test area affected by well-known landslides.

Integration of SAR Measurements and Geomorphological Models

The framework developed for DInSAR data analysis at different scales is sketched in Fig. 1. The first step consists of the generation of the a priori DInSAR landslide visibility map (Peduto 2008; Cascini et al. 2009), which can be used to distinguish in advance whether an area is expected to be visible from space-borne SAR sensors, thus driving data-users through the image dataset selection. Once SAR images have been processed, if an adequate knowledge of landslide phenomena is available, a procedure for 1D-LOS DInSAR data projection can be implemented to generate the advanced DInSAR landslide velocity map.

As for the scale of the study, low-resolution DInSAR data can be used for landslide analyses at 1:25,000 scale whereas full-resolution DInSAR data allow studies at more detailed scale (i.e.1:5,000) according to the almost point-wise information.

The procedures were tested within a sample area belonging to the northern portion of the territory of the National Basin Authority of Liri-Garigliano and Volturno rivers (NBA LGV) in Central-Southern Italy, extending for around 489 km^2 and including 11 municipalities, belonging to 2 Regions (Lazio and Abruzzo). This territory was selected due to the availability of both base and thematic maps at 1:25,000 scale. These maps were produced in 2001 as results of the activities of the PSAI (Piano Stralcio per l'Assetto Idrogeologico) project in accordance with the Act of Italian Parliament (L. 365/2000), aimed to develop emergency plans at national scale (Cascini 2008).

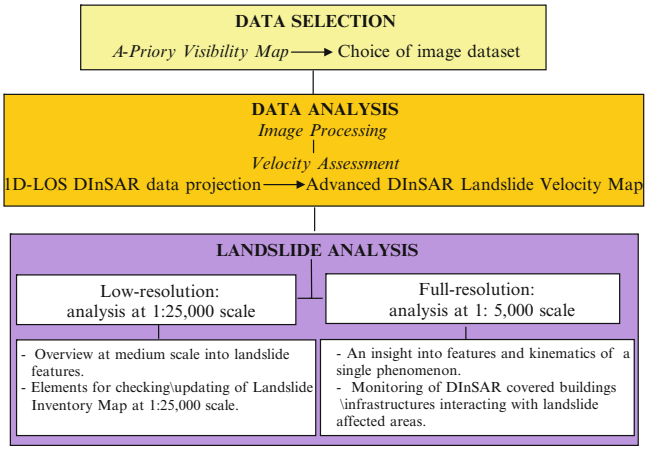


Fig. 1 The framework of DInSAR data analyses for landslide studies (Cascini et al. 2010)

The A Priori Visibility Map

The choice of the most suitable SAR image dataset represents a key step for DInSAR data exploitation in landslide studies, since the visibility of a certain portion of a slope depends on several factors such as slope aspect and inclination, vegetation cover, presence of buildings/infrastructures.

An example of the a-priori DInSAR landslide visibility map over a portion of the study area is presented at 1:25,000 scale (Fig. 2). As described in details in Cascini et al. (2009), the input data consist of the following available maps: landslide inventory map; aspect map; slope angle map; land-use map; urbanised area map. The described procedure can be easily applied at 1:5,000 scale if base and derived maps are available at this scale.

The Advanced DInSAR Landslide Velocity Map

A further step in the analysis of DInSAR data is represented by the generation of the advanced DInSAR landslide velocity map (Cascini et al. 2010). The flow-chart for the generation of this map is shown in Fig. 3. Key-points can be summarized as follows:

- Conditions of movement/no-movement depend on whether the mean velocity of the DInSAR coherent pixel exceeds the fixed velocity threshold (Cascini et al. 2010);
- The direction of movement is assumed consistent with the geomorphological scheme of the landslide (see Cascini et al. 2010) on which each DInSAR coherent pixel is located;
- The projected velocity value is assumed as a reliable value if the condition number (see the Appendix in Cascini et al. 2010) does not exceed the fixed threshold.

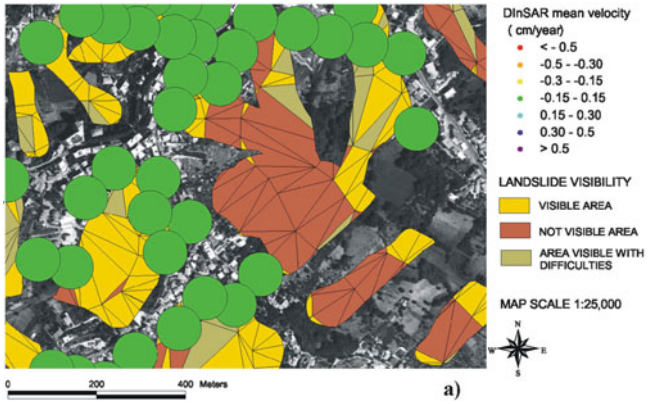


Fig. 2 The "a priori DInSAR landslide visibility map" on descending orbits with low-resolution ESD DInSAR coherent pixel distribution (Cascini et al. 2009)

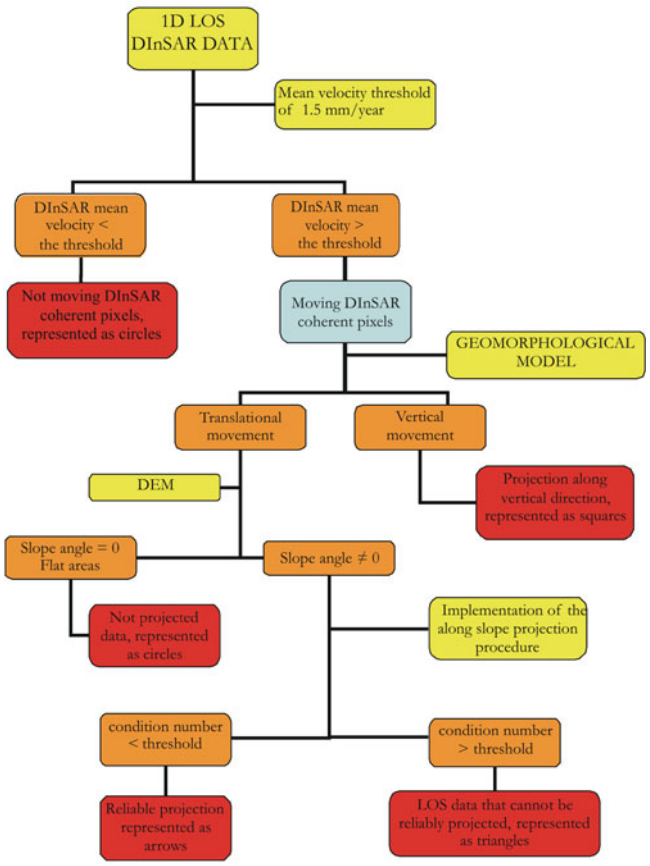


Fig. 3 Flow-chart for the generation of the advanced DInSAR landslide velocity map (Cascini et al. 2010)

Landslide Analysis Via Low-Resolution DInSAR Data

The advanced low-resolution DInSAR landslide velocity map was developed at 1:25,000 scale for all the test area in ADB-LGV according to the schemes in Fig. 3 so as to analyse rotational slides, earth flows and rotational slides-earth flows, whose total amount is 553; 185 (around 33 %) of those resulted covered by DInSAR data. An example is reported with reference to the municipalities of Frosinone and Torrice (Lazio Region) in Fig. 4 where very few moving low-resolution DInSAR pixels are detected over an area of about 3 × 6 km where dormant phenomena prevail.

Within this area, the directions of movement (see the four red arrows), derived by modelling the available 1D LOS DInSAR data, seem congruent with the assumption of the geomorphological schemes (downward direction along slope).

Moreover, by extending the analysis of moving/not moving coherent pixels on those portions of the territory mapped as hollows (i.e. areas characterized by geomorphological settings quite similar to landslide-affected areas, also exhibiting the same landslide predisposing factors) it was possible to detect a clear evidence of movement for 63 hollows. This can certainly provide elements for a check/update of the landslide inventory map that represents the starting point for the landslide risk analysis as described in Fell et al. (2008).

Landslide Analysis Via Full-Resolution DInSAR Data

Analyses of landslide phenomena at more detailed scale (i.e. 1:5,000) can exploit full-resolution DInSAR data following the flow-chart in Fig. 3. Two main goals can be pursued: the preliminary analysis of landslide features (i.e. check of mapped boundaries; detection of ground displacement out of mapped areas); an insight into different kinematic behaviour characterizing different portions of the same phenomenon.

Several examples are reported in Cascini et al. (2010); here, a portion of the municipality of Frosinone (Fig. 5) highlighting evidences of movements both inside and outside the landslide boundaries is shown. In particular, full-resolution DInSAR coherent pixels exhibit mean velocity values exceeding 0.3 cm/year within two dormant earth flows (labelled with letters A and D) and creep zones (labelled with letters B and C) as well as the areas framed with the circle and the square, respectively. As for the zone framed with the circle, a cross check via the geomorphological map showed that the buildings in the area were built on an hollow.

The area framed by a rectangle highlights the presence of moving full-resolution DInSAR coherent pixels in proximity of a landslide classified as active earth flow in the landslide inventory map at 1:25,000 scale. In this case a more detailed analysis was possible thanks to the availability of a map of the phenomenon, drawn at 1:5,000 scale by the NBA-LGV technicians.

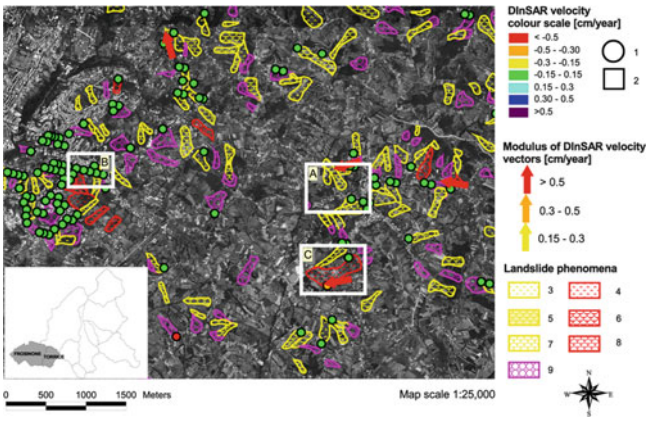


Fig. 4 An example of advanced low-resolution DInSAR landslide velocity map for the municipality of Frosinone and Torrice (Lazio Region, Italy). *1* Not moving DInSAR coherent pixel or on flat areas, *2* DInSAR coherent pixel moving on vertical direction, *3* dormant rotational slide, *4* active rotational slide, *5* dormant earth flow, *6* active earth flow, *7* dormant rotational slide – earth flow, *8* active rotational slide – earth flow, *9* creep phenomenon (Cascini et al. 2010)

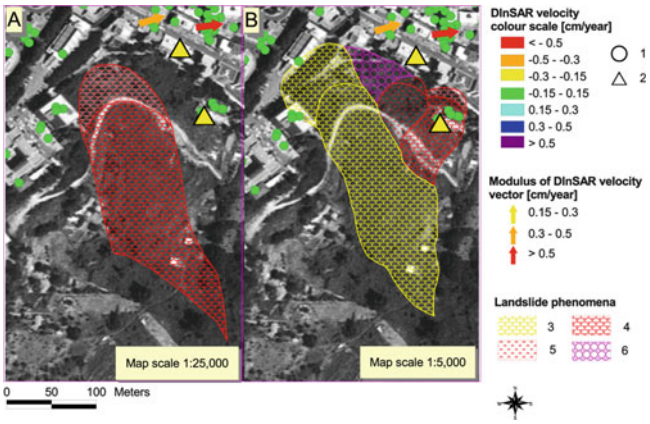


Fig. 6 Frosinone urban area: advanced full-resolution DInSAR landslide velocity map overlaid to an orthophoto and a map of one landslide mapped at 1:25,000 scale (**a**) and 1:5,000 scale (**b**). *1* Not moving DInSAR coherent pixel or on flat areas, *2* not projected translational displacement owing to high condition number, *3* dormant rotational slide–earth flow, *4* active rotational slide–earth flow, *5* active rotational slide, *6* creep phenomenon (Cascini et al. 2010)

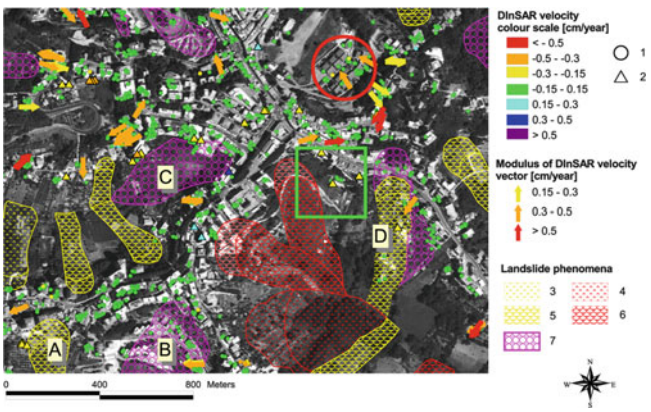


Fig. 5 Advanced full-resolution DInSAR landslide velocity map for a portion of the municipality of Frosinone (Lazio Region, Italy). *1* Not moving DInSAR coherent pixel or on flat areas, *2* not projected translational displacement owing to high condition number, *3* dormant rotational slide, *4* active rotational slide, *5* dormant earth flow, *6* active earth flow, *7* creep phenomenon (Cascini et al. 2010)

Figure 6a, b shows the landslide mapped at both 1:25,000 and 1:5,000 scale. In the former, full-resolution DInSAR data seem not to match the results of landslide inventory, on the contrary in Fig. 6b the landslide can be divided into four small different phenomena: a dormant rotational slide–earth flow; a creeping zone; an active rotational slide–earth flow and an active rotational slide. The superimposition of full-resolution DInSAR data on this enhanced inventory map points out that the moving coherent pixel (labelled with the yellow triangle) falls within the small active rotational slide–earth flow; on the contrary, the stable coherent pixels (labelled with green circles) are located within the head of the dormant rotational slide–earth flow. Moreover, the two yellow triangles located on buildings just up the heads of the mapped phenomena suggest a retrogression of the movement towards the top of the hill; accordingly in situ surveys could turn out to be necessary in order to analyse the current slope evolution.

Perspectives Associated with the New Generation, High Resolution SAR Sensors

X-band data provided by the COSMO-SkyMed (CSK) constellation represent a great opportunity with reference to previous experiments that use C-band data for DInSAR applications to landslide phenomena. The CSK constellation is acquiring data from its four SAR satellites in several imaging modes, to be processed into standard and higher level end products. In particular, these new sensors provide spatial resolution one order of magnitude better than the previous available satellite SAR data, as well as short revisit time (up to 4 days for repeat pass interferometry with the full constellation).

In spite of a shorter wavelength ($\lambda \approx 3$ cm in X-band, 5.6 cm in C-band), the tenfold improved spatial resolution along ground range direction ensures critical baseline values 5÷6 times higher than in C-band, thus strongly limiting, in theory, the effects of the geometrical decorrelation. Furthermore, the faster revisit of the same Area of Interest (AOI) of the actual X-band missions somehow counter-balances the possible negative effect of the shorter wavelength on the temporal analysis in presence of high rate displacements.

In this work the potentialities of monitoring landslide induced deformation pattern with CSK X-band SAR are investigated. In particular the SPINUA algorithm, which is a PS-like technique developed with the aim of detection and

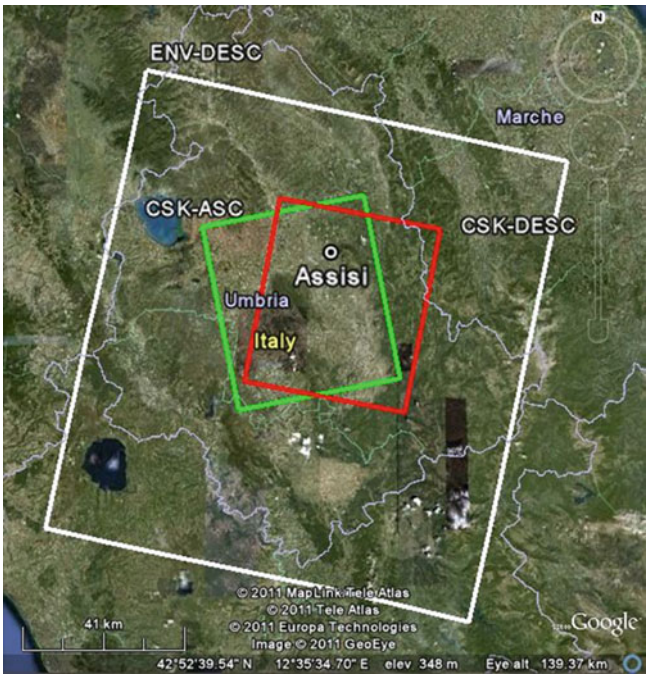


Fig. 7 Ground coverage of CSK ascending dataset (*green frame*), CSK descending dataset (*red frame*), and ENVISAT descending dataset (*white frame*)

monitoring of coherent PS targets in scarcely-urbanized areas (Bovenga et al. 2004, 2006) has been used. The processing chain has been further updated in order to deal properly with X-band data from both CSK and TerraSAR-X. Thanks to the higher resolution of new generation of X-band SAR as well as to ad-hoc solutions adopted by the SPINUA algorithm (as patch-wise processing for atmospheric estimation), it is possible to infer reliable estimates of the displacements by using a number of SAR scenes lower than in C-band. A first experiment carried out with TerraSAR-X data on highly urbanized small areas (Bovenga et al. 2010) confirmed that by using even about 15 SAR acquisitions it is still possible to reliably infer displacement rates.

The results concerning the investigation of a landslide phenomenon located in Umbrian Apennine (Central Italy), namely the Ivancich landslide, involving the urban area of the Assisi Municipality. It is a slow moving, deep-seated landslide of the slide type which caused repeated damage to roads, buildings, and retaining structures (Guzzetti et al. 2009). This work was carried out in the framework of MORFEO (MOnitoraggio e Rischio da Frana mediante dati EO) project, which has been funded by the Italian Space Agency (ASI) with the aim to develop and demonstrate a system for landslide risk assessment based on the joint use of Earth Observation (EO) multi-mission satellite data, together with traditional in situ methodologies.

Both C-band and X-band SAR data were made available within the MORFEO project on the Ivancich test case. The X-band CSK dataset consists of 17 HIMAGE SLCs acquired between March 2009 and October 2010 along descending passes, with mean incident angle of around 29° (Beam HI-03; POL: HH, red frame in Fig. 7), and 20 HIMAGE SLCs acquired between May 2009 and September 2010 along ascending passes, with mean incident angle of around 26° (Beam HI-01; POL: HH, green frame in Fig. 7).

Despite the limited X-band dataset (17 images) the capability in deformation measurement of CSK X-band SAR data was tested. A possible approach to provide a useful support to the landslide monitoring, could be based on products generated by using limited resources in terms of SAR images as well as processing time. In particular, we adopted a processing strategy aimed at providing deformation maps able to identify stable and unstable areas on the ground. This product can be of help in the monitoring of unstable areas, searching for ground instabilities, for instance, after triggering events.

It was designed a strategy to decrease the probability of selecting false PS by adding a constraint on the correlation of the deformation signal in the spatial domain: a pixel which shows a displacement rate different with reference to the mean behaviour of the neighbouring pixels are considered as a potential outlier and discharged. This masked out displacements occurring on a pixel basis, thus ensuring a spatial homogeneity in the final displacement field.

Figure 8 shows the displacement rate maps obtained by processing the CSK images acquired along ascending passes (A) and descending passes (B). The background consists of an optical image from Google EarthTM, on which the landslide polygons derived from the Italian landslide inventory of the IFFI Project (APAT 2007) are superimposed. The coherence thresholds adopted for the PS selection is 0.93. In both maps a cluster of moving PS is visible, resulting located on the well known active sliding area of Ivancich. Moreover, the different values of the displacement rate between ascending (A) and descending (B) passes could suggest the presence of an horizontal component of the movement as confirmed by displacement vectors derived through a GPS network (Fastellini et al. 2010).

In order to cross-validate the X-band results, a C-band dataset was also processed consisting of 39 ENVISAT ASAR SLCs acquired between October 2003 and May 2010 along descending passes (Track 351, Frame 2741, white frame in Fig. 7). Figure 8c shows the displacement map derived by using a threshold on the temporal coherence of 0.75. The displacement maps at X-Band and C-Band over descending passes sketched in Fig. 8 (subplots B and C) are fully comparable. In particular the moving pixels lie on one of the landslide bodies defined by the IFFI polygons. In the present case the DInSAR based displacements allows to discriminate between stable and unstable areas or between active and dormant/inactive landslides where previous knowledge on landslide events is available. Finally it is interesting to note that, despite the fact that the number of

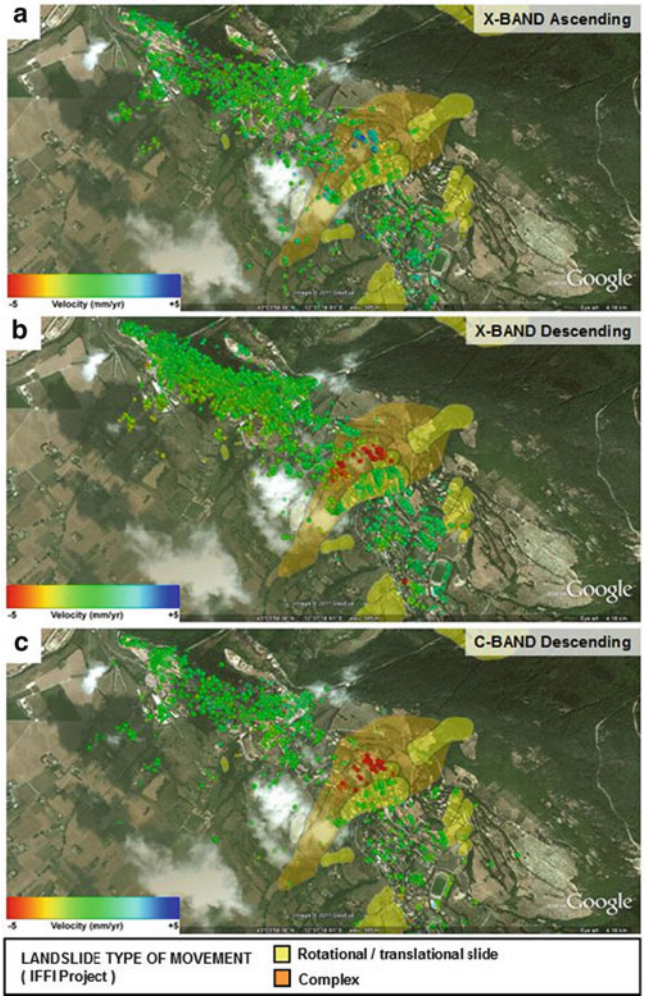


Fig. 8 Distribution of the average line of sight (LOS) velocity of PS detected through SPINUA algorithm over Assisi town (Umbria, Italy) by processing X-band CSK data acquired along ascending passes (**a**) and descending passes (**b**), as well as C-band ENVISAT descending data (**c**). On the background, an optical image from Google EarthTM, and the landslide polygons derived from the Italian landslide inventory of the IFFI Project (APAT 2007)

acquisition of CSK is much lower (almost a half in the best case) of the ASAR images, the spatial density of the monitored pixels (over typically persistent ground structures) of the X-Band system is much higher than the C-Band one as a result of the effect of mitigation of both the temporal decorrelation and the spatial decorrelation due to the increase in the resolution capabilities.

Conclusions

In few years remote sensing techniques such as DInSAR data will be applied on a routine basis to slow-moving landslide analysis. To this end, the scientific research needs to pursue both the development of suitable procedures for a confident use of DInSAR data and the exploitation of data provided by the sensors of the ultimate generation. These two key points have been addressed in the present work with reference to well—known case studies, highlighting that valuable contributions can be furnished to slow-moving landslide analyses at different scales to be integrated within the landslide risk management framework.

Acknowledgments ENVISAT and COSMO-SkyMED images on Ivancich test case were provided respectively by ESA and ASI in the framework of the MORFEO project (ASI Contract n. I/045/07/0).

References

APAT (2007) Rapporto sulle frane in Italia. Il Progetto IFFI – Metodologia, risultati e rapporti regionali. APAT Report 78/2007, Roma

Bovenga F, Refice A, Nutricato R, Guerriero L, Chiaradia MT (2004) SPINUA: a flexible processing chain for ERS/ENVISAT long term Interferometry. In: Proceedings of ESA-ENVISAT symposium, Salzburg, 6–10 Sept 2004

Bovenga F, Nutricato R, Refice A, Wasowski J (2006) Application of multi-temporal differential interferometry to slope instability detection in urban/peri-urban areas. Eng Geol. Special issue on remote sensing and ground-based geophysical techniques for recognition, characterization and monitoring of unstable slopes, 88(3–4):218–239

Bovenga F, Nitti DO, Refice A, Nutricato R, Chiaradia MT (2010) Multi-temporal DInSAR analysis with X-band high-resolution SAR data: examples and potential. In: Proceedings of SPIE remote sensing, Centre de Congrès Pierre Baudis, Toulouse, 20–23 Sept 2010

Cascini L (2008) Applicability of landslide susceptibility and hazard zoning at different scales. Eng Geol 102(3–4):164–177

Cascini L, Fornaro G, Peduto D (2009) Analysis at medium scale of low-resolution DInSAR data in slow-moving landslide-affected areas. ISPRS J Photogramm Rem Sens 64(6):598–611. doi:10.1016/j.isprsjprs.2009.05.003

Cascini L, Fornaro G, Peduto D (2010) Advanced low- and full-resolution DInSAR map generation for slow-moving landslide analysis at different scales. Eng Geol 112(1–4):29–42. doi:10.1016/j.enggeo.2010.01.003

Fastellini G, Radicioni F, Stoppini A (2010) The Assisi landslide monitoring: a multi-year activity based on geomatic techniques. Appl Geomatics 3(2):91–100

Fornaro G, Pauciullo A, Serafino F (2009a) Deformation monitoring over large areas with multipass differential SAR interferometry: a new approach based on the use of spatial differences. Int J Rem Sens 30(6):1455–1478

Fornaro G, Reale D, Serafino F (2009b) Four-dimensional SAR imaging for height estimation and monitoring of single and double Scatterers. IEEE Trans Geosci Rem Sens 47(1):224–237

Fell R, Corominas J, Bonnard C, Cascini L, Leroi E, Savage WZ (2008) Guidelines for landslide susceptibility, hazard and risk zoning for land-use planning. Eng Geol 102(3–4):99–111

Guzzetti F, Manunta M, Ardizzone F, Pepe A, Cardinali M, Zeni G, Reichenbach P, Lanari R (2009) Analysis of ground deformation detected using the SBAS-DInSAR technique in Umbria, Central Italy. Pure Appl Geophys 166:1425–1459

Peduto D (2008) Analysis of ground deformations related to subsidence and landslide phenomena via DInSAR techniques. Ph.D. thesis, University of Salerno, Italy, May 2008. Tutor: Prof. Cascini L.; co-tutor: Dr. G. Fornaro



Freeze-Thaw Cycle and Rockfall Monitoring

Diego Arosio, Laura Longoni, Fabrizio Mazza, Monica Papini, and Luigi Zanzi

Abstract

Among several weathering processes that may contribute to rock fall generation, a particular issue is related to freeze-thaw cycles. Several studies claim that many rock falls originate from thawing of the fractured bedrock during seasonal freezing (Matsuoka and Marton Permafrost Periglac Process 19(2):195–210, 2008; Matsuoka Cold Reg Scid Technol 17(3):253–270, 1990). Other authors have recently suggested that ice segregation is the real cause behind bedrock fracturing (Hallet Science 314(5802):1092–1093, 2006; Murton et al. Permafrost Periglac Process 12(3):255–266, 2001, Science 314(5802):1127–1129, 2006). Consequently, freeze and thaw processes will be deeply investigated in order to discover possible relationships between triggering mechanisms concerning rockfalls and monitoring datasets.

Laboratory tests have been carried out to investigate the rupture process caused by the abovementioned cycles. Preliminary analyses were performed both in lab and on the field with the aim of testing the capability of different transducers to register micro seismic signals.

Keywords

Freeze-thaw • Rockfall • Acoustic emissions • Monitoring

Introduction

Rock falls and rock avalanches represent a diffused problem in Alpine areas featuring sudden occurrence, subtle preliminary signs and great destructive power. Progressive expansion of human settlements and climate changes that have been taking place since the last decades are probably the two main factors increasing the impact of rock falls on human settlements. The low effectiveness/cost ratio of structural measures together with great economic consequences of rock falls are driving research efforts towards the development of non-structural mitigation approaches, like rock fall forecasting systems.

One of the physical factors promoting rock falls is freeze-thaw attack, a physical mechanism causing rock mass degradation in those zones where, because of latitude and altitude, atmospheric conditions are such that 0 °C temperature is crossed several times during a year. In such situation the presence of water, which might be due to precipitations or water circulation inside the rock mass, produces cycles during which ice is consecutively formed and melt. In the traditional interpretation of the phenomenon this produces stress cycles that repeatedly load and release the rock mass, because of the 9 % volumetric expansion of water becoming ice. According to this model freeze-thaw should be able to break rock masses along pre-existent fractures. Recent investigations highlighted the existence of another freeze-thaw mechanism, namely ice segregation (Murton et al. 2001, 2006). For the example of a porous medium, this process can be schematically resumed as

D. Arosio (✉) • L. Zanzi
Dipartimento di Ingegneria strutturale, Politecnico di Milano, Piazza L. da Vinci 32, Milano, Italy
e-mail: diego.arosio@polimi.it

L. Longoni • F. Mazza • M. Papini
Dipartimento di Ingegneria Idraulica, Ambientale, Infrastrutture Viarie, Rilevamento, Politecnico di Milano, Piazza L. da Vinci 32, Milano, Italy

C. Margottini et al. (eds.), *Landslide Science and Practice*, Vol. 2,
DOI 10.1007/978-3-642-31445-2_50, © Springer-Verlag Berlin Heidelberg 2013

follows: low temperatures lead to the formation of ice lenses inside pores, covered by a film of water. This water film is able to attract water from surrounding rock through capillary cavities. This contributes to the growth of the ice lens that expands putting water in pressure; this in turn put in pressure the surrounding rock.

For these grounds, freeze-thaw can act both as a preparing cause and as a triggering factor for rock falls.

Materials and Methods

In the last decades considerable efforts have been addressed to the increasing number of rock fall events affecting human activities. Factors contributing to rock mass instabilities in the pre-Alpine foothills are: (a) the frequency and intensity of freeze-thaw cycles (60 cycles/year in average), (b) tectonization of lythotipes, (c) high dips of the slopes and (d) karsts phenomena. It has been argued (Amitrano et al. 2010) that even global climate changes could have a significant role in increasing the number of rockfalls.

Structural mitigation interventions like rock bolting, rock fall fences, rock fall nets and ditches are effective only for events involving small to medium rock volumes and low kinetic energies. For other cases non-structural measures, like monitoring systems and hazard assessment, seem to be the most effective solution for risk reduction. While hazard assessment is more suitable for land use planning stages, monitoring systems constitute an appropriate choice to reduce the risk for human settlements in built areas susceptible to rock fall events. Several kinds of instruments seem to be adequate for rock slope monitoring applications.

Conventional instruments, like extensometers and crack meters, have been extensively used in the past for rock mass monitoring, but they are able to provide only local information, giving no clue about the evolution of the global rupture process. Modern remote sensing instruments, like laser scanners and interferometric radars, feature high accuracy and scanning frequency, but yield only measures of surface movements. Because of the sudden nature of rock mass collapses, the bearing capacity of the rock mass is almost lost and failure is imminent when it is possible to detect a displacement on the surface (Arosio et al 2009). Consequently this kind of instruments is not suitable for rock mass monitoring. Conversely, previous studies pointed out that passive micro-seismic technique allows detecting stress waves released by breaking rock, providing real-time information about fracture formation, propagation and coalescence (Amitrano et al. 2010; Backers 2004; Eberhardt et al. 1998; Cai et al. 2004; Senfaute et al. 2009). Pioneer applications of acoustic and micro-seismic emission monitoring were focused on rough prediction of sudden failures in mining and tunnel construction, like rock burst and roof fall. The advent of digital technologies along with the growth of nuclear and petroleum industries fostered the development of more complex applications implying source localization and source mechanism identification. Such kind of systems have been used to optimize excavation methods to reduce the additional degree of fracturing caused by excavation in nuclear waste disposals (Cai et al 2004). Despite these progresses, applications to rock slopes are still rare at the time, because of additional complications like arduous installation conditions, huge involved volumes and presence of damaged rock mass that interferes with wave propagation resulting in signal attenuation and difficult data interpretation.

The Monitoring Network of Mount S. Martino

Mount San Martino, one of the first reliefs facing at the north side of the Po Valley, towers above the north side of the town of Lecco, 40 Km north of Milan, Italy. This mountain, characterized by vertical walls, has been historically interested by rock fall events involving material ranging from single decimetric blocks to thousands of cubic meters. Its walls are constituted by limestone belonging to the Esino Formation (middle Triassic) and represent the front of Coltignone tectonic thrust, the southernmost among the ones belonging to the Grigne group. Rock stratification is almost indistinct and is characterized by weak inclination opposing the dip-direction of the 300 m high slopes, which ranges from 70° to 90° (Agostoni et al. 2000). Fractures with N-S and E-W trends pass through the rock mass isolating dihedrals prone to toppling and wedge sliding. At the base of the cliffs debris accumulations with a maximum thickness of some tenth of meters partially hide the contact with the underlying Angolo Limestone, a calcareous formation featuring a greater degree of erodibility and thinner strata with respect to Esino limestone. This debris constitutes a slope with an inclination almost corresponding to their angle of repose, jointing the town of Lecco and Mount San Martino. This slope acts as a natural defence against rock falls on which bouncing blocks loose part of their kinetic energy.

The most catastrophic event took place in the night between 22 and 23 February 1969, when 10,000–15,000 m^3 of rock detached from the rock cliff, causing the partially destruction of a building, seven fatalities and three wounded. After the 1969 calamity a series of mitigation measures have been adopted: unstable blocks have been removed from the cliff or secured with rock bolts and concrete injections. Below the cliff rock fall fences and ditches have been realized to stop bouncing blocks.

The cliff is still active: in the last 20 years a series of rock fall events involving volumes below 100 m^3 have been taking place in coincidence with intense precipitations and freeze-thaw cycles.

Description of the Monitoring Network

A monitoring network has been installed in the zone of the cliff enclosing the unstable dihedral of rock adjacent to the source zone of the 1969 event where persistent fractures with centimetric aperture are present. The monitoring network is composed of eight triaxial MEMS accelerometers, three triaxial geophones and two extensometers. The average distance between sensors is about 5 m. In particular, distance between high-quality geophones is higher, while cheaper accelerometers are denser. All the microseismic monitoring instruments have been placed in cylindrical aluminium vessels solidly fixed to the rock mass ensuring a good acoustic coupling. Temperature sensors have been also placed in the boxes together with buffers that keep in memory recorded data between two following data polling performed by the acquisition system deployed at the top of the rock face.

Data saved locally are sent to the control room placed in Lecco through a radio link operating at 5.4 GHz and stored in a database.

Laboratory Tests

Freeze-thaw is a poorly understood phenomenon that is known to play an important role in creating favorable conditions for rock falls to happen and that can even act as a triggering factor. Laboratory analysis allows the simulation of particular phenomena decoupling them from others factors that are present on site. Acoustic emission monitoring can be both an instrument to investigate freeze-thaw mechanism and a tool to control the degree of evolution of rupture.

Studies published on this argument during the years have mostly focused on defining the number of freeze-thaw cycles causing rock fracture. Other studies (Matsuoka 1990, 1995; Davidson and Nye 1985; Tharp 1987) had the scope of understanding the mechanism of the phenomena, by analyzing water pressures acting on rock specimens. This second group of works is the most interesting for the target of our research.

Design and Preliminary Results of Freeze-Thaw Tests

To start analyzing the freeze-thaw process in Esino Limestone we decided to make new laboratory tests in which temperature of both air and rock, opening deformation of the slot (COD), ice pressure on rock and acoustic emissions are monitored.

One important task that has to be assured before it will be possible to monitor damage evolution in freezing conditions is to distinguish acoustic emission signals due to ice formation and slip on rock surfaces from those caused by crack propagation and coalescence. To avoid useless complications in this stage of the study we decided to work with the same material we have in the field, that is Esino limestone.

Standardized procedures for freeze-thaw testing of rocks are designed to test their suitability to be used as building materials in locations where freeze-thaw phenomenon is quite severe (UNI-087 2010). Unfortunately these tests are not suitable to investigate the mechanism of freeze-thaw attack as we wanted to do. For this reason we chose to design our first tests on the base of previous studies (Matsuoka 1990).

Esino limestone blocks (Table 1) gathered in the talus zone under S. Martino relief have been cut into cubic specimens with edges length equal to 10 cm. Slots with different sizes have been cut into these blocks as outlined in Fig. 1 and Table 2.

Sample slots have been filled with water before the samples undergone temperature cycles in a climatic cell in our laboratory. During the temperature tests we have monitored: (1) temperature on the surface and inside the samples; (2) pressure in 2–3 points along symmetry axes of the slots;

Table 1 Main characteristics of Esino Limestone

P-waves velocity (in intact rock) [m/s]	5,300
Young modulus [GPa]	38
Compressive strength [MPa]	150–200
Density [kN/m^3]	26

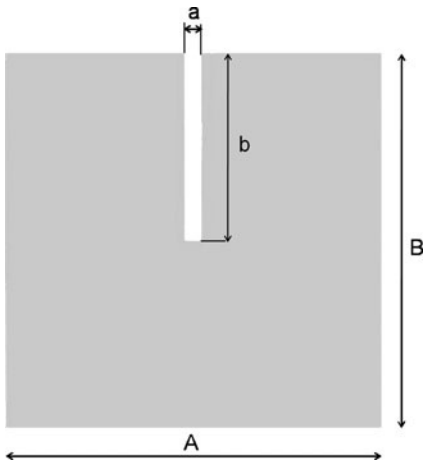


Fig. 1 Rock specimen employed in the laboratory tests

Table 2 Dimensions of the samples used in freeze-thaw tests

Sample	1	2	3	4
A (= B) [mm]	100	100	100	100
a [mm]	50	50	80	20
b [mm]	4	8	4	4
Shape factor	0.08	0.16	0.05	0.20

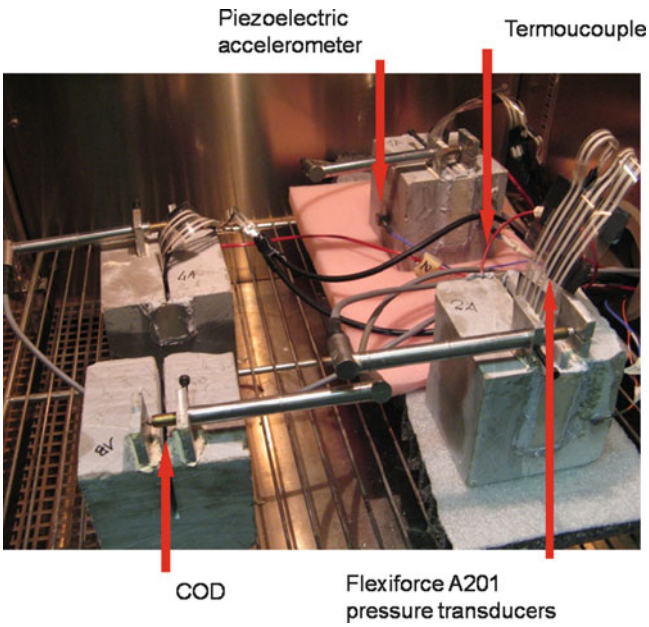


Fig. 2 Specimens and transducers layout in the climatic cell

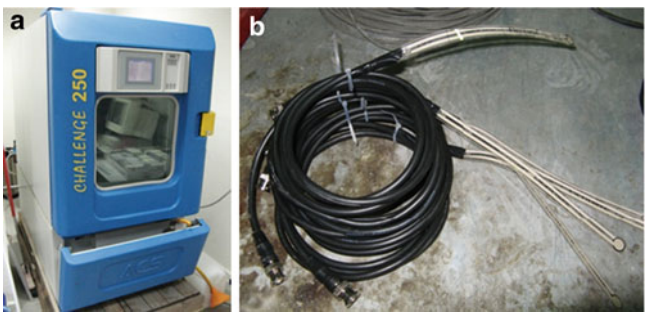


Fig. 3 Equipment used for freeze-thaw test: (**a**) climatic cell and (**b**) Flexiforce film pressure sensors

(3) acoustic emissions sensed by broadband accelerometers (Figs 2 and 3).

The first test has been performed without filling the slot to check the equipment functionality and to collect acoustic emissions generated by the climatic cell itself. Data gathered at this stage have been used to filter signals collected in the following tests.

The following three tests have been conducted with: (1) one temperature cycle; (2) two temperature cycles; (3) seven temperature cycles. Cycle duration is a key parameter influencing drastically the action of ice, probably more than the lowest temperature reached. In fact, ice expansion reaches its maximum at −4 °C. On the contrary, the duration of the cycle acts on the chance of water to freeze completely as well as of the ice to melt completely. Extreme temperatures used in these cycles have been defined with reference to conditions acting averagely in zones of the province of Lecco more prone to rock falls. In these experiments we simulate the effect of freeze-thaw on open superficial fractures. According to these considerations we performed cycles in which temperatures spanned from −4 °C to 4 °C. Cycle duration was fixed to 8 h to speed up the tests. During all tests with water/ice a COD sensor installed on an unfilled sample inside the cell, has been used to measure reference values of crack opening, in order to take into account thermal deformation of the specimens.

Figure 4 illustrates an example of parameters recorded during a 7-cycle test on a dry specimen whose cut has been filled with water. Temperatures of both the cell chamber and the specimen surface have been monitored (Fig. 4 top) while pressure of the ice on the cut sides have been recorded placing sensors at the bottom and at the middle height of the fracture (Fig. 4 middle). Pressure trend during the test is well in agreement with temperature oscillations. Higher pressures are registered by the bottom transducer while both sensors display an increase of the recorded pressures as the cycles proceed.

As far as acoustic emissions are concerned (Fig. 4 bottom), we can observe the occurrence of several events in the freezing phase and of fewer events in the melting phase. Surely, part of the recorded emissions are due to the ice formation and melting processes. On the other hand, the fact that cumulative curves of collected acoustic emissions can be very different even when testing identical specimens suggests that part of the events are, with a certain degree of confidence, related to the breaking of the rock structure. Besides the influence of different slots, different behaviors of the specimens in generating acoustic emissions may be related to initial degree of fracturation and to the presence of heterogeneities that may act as preferential paths for fracture formation propagation.

Conclusions

The use of microseismic monitoring systems for rockfalls investigation and forecasting is an open problem. In order to face this issue it is necessary to analyze each triggering factor that may cause acoustic emissions.

Our work is oriented to understand one of the most significant triggering factors in the pre-alpine area, i.e., the freeze-thaw phenomenon. Our preliminary researches have addressed simple laboratory tests in which non-porous limestone specimens with a single water-filled artificial fracture have been subjected to temperature oscillations. Pressure displacements and acoustic emissions have been recorded with suitable sensors and a complete interpretation of collected parameters is still underway. Preliminary results are promising and during future investigations we aim to discriminate microseismic signals related to rock structure degradation from other events. In the future we plan to employ laboratory results to improve

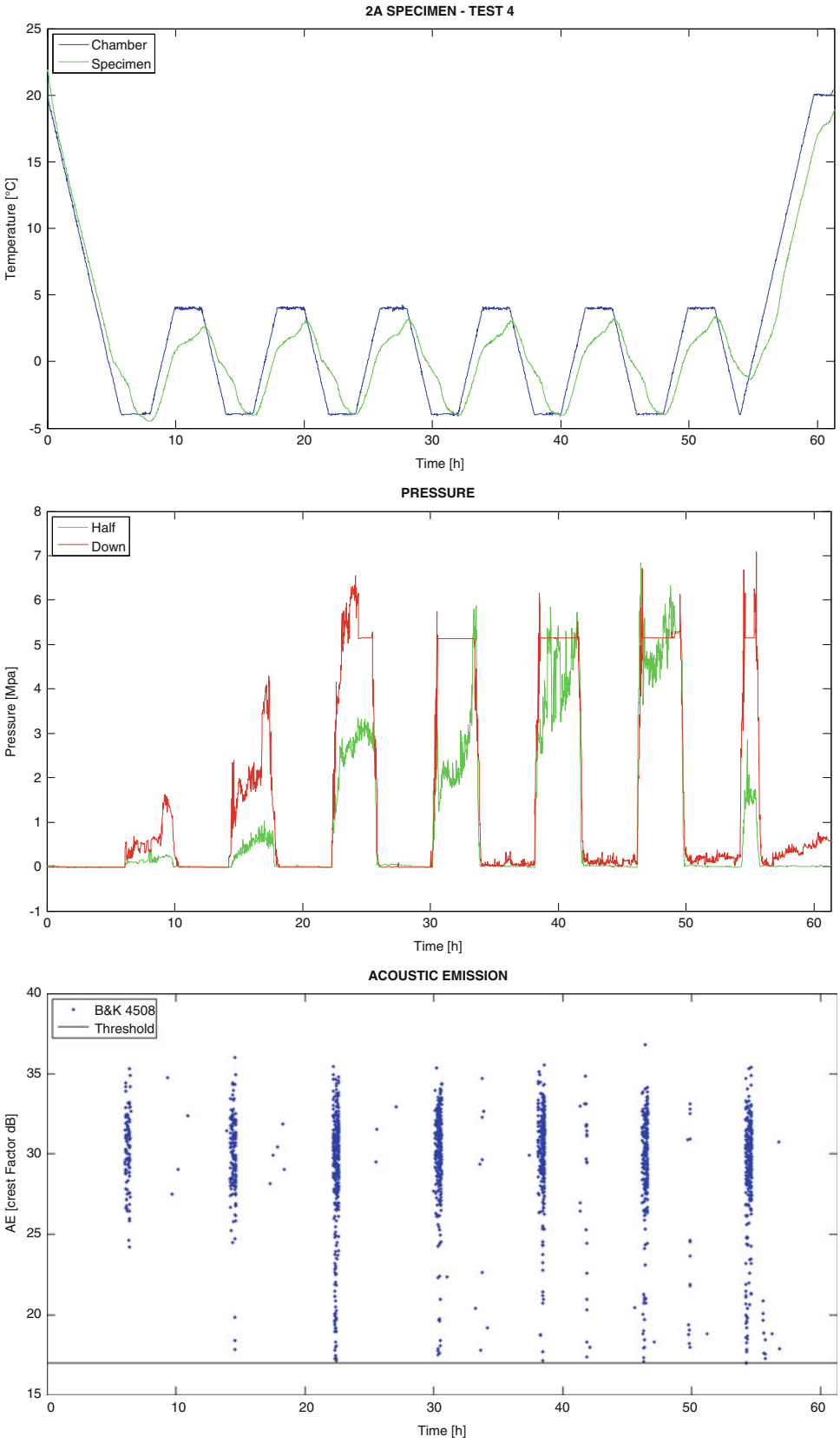


Fig. 4 Example of freeze-thaw test on a limestone specimen with recorded temperature (*top*), pressure (*middle*) and acoustic emissions (*bottom*)

the interpretation of the signals collected with the monitoring network deployed on Mount San Martino.

References

Agostoni S, Cantone G, Laffi R, Ratti R, Sciunnach D (2000) Centri abitati instabili della provincia di Lecco. Pubblicazione CNR-GNDCI n. 2066

Amitrano D, Arattano M, Chiarle M, Mortora G, Occhiena C, Pirulli M, Scavia C (2010) Microseismic activity analysis for the study of the rupture mechanisms in unstable rock masses. Nat Hazards Ear Syst Sci 10:831–41

Arosio D, Longoni L, Papini M, Scaioni M, Zanzi L, Alba M (2009) Towards rockfall forecasting through observing deformations and listening to microseismic emissions. Nat Hazards Ear Syst Sci 9:1119–31

Backers T (2004) Fracture toughness determination and micromechanics of rock under mode I and mode II loading, Institut für Geowissenschaften Sektion 3.2 Deformation und Rheologie des GFZ Potsdam

Cai M, Kaiser PK, Tasaka Y, Maejima T, Morioka H, Minami M (2004) Generalized crack initiation and crack damage stress thresholds of brittle rock masses near underground excavations. Int J Rock Mech Mining Sci 41(5):833–847

Davidson GP, Nye JF (1985) A photoelastic study of ice pressure in rock cracks. Cold Reg Sci Technol 11(2):141–153

Eberhardt E, Stead D, Stimpson B, Read RS (1998) Identifying crack initiation and propagation thresholds in brittle rock. Can Geotech J 35(2):222–233

Matsuoka N (1990) Mechanisms of rock breakdown by frost action: an experimental approach. Cold Reg Scid Technol 17(3):253–270

Matsuoka N (1995) A laboratory simulation on freezing expansion of a fractured rock: preliminary data. Annu Rep Univ Tsukuba Inst Geosci 21:5–8

Murton JB, Coutard J, Lautridou J, Ozouf J, Robinson DA, Williams RBG (2001) Physical modelling of bedrock brecciation by ice segregation in permafrost. Permafrost Periglac Process 12 (3):255–266

Murton JB, Peterson R, Ozouf J (2006) Bedrock fracture by ice segregation in cold regions. Science 314(5802):1127–1129

Senfaute G, Duperret A, Lawrence JA (2009) Micro-seismic precursory cracks prior to rock-fall on coastal chalk cliffs: a case study at Mesnil-Val, Normandie, NW France. Nat Hazards Ear Syst Sci 9(5):1625–1641

Tharp TM (1987) Conditions for crack propagation by frost wedging. Geol Soc Am Bull 99(1):94–102

UNI-087 – UNI: PRODOTTI, PROCESSI E SISTEMI PER L'ORGANISMO EDILIZIO (2010) Natural stone test methods – determination of frost resistance



Rapid Assessment of Landslide Activity in Emilia Romagna Using GB-InSAR Short Surveys

Alessandro Corsini, Matteo Berti, Antonio Monni, Marco Pizziolo, Francesco Bonacini, Federico Cervi, Giuseppe Ciccarese, Francesco Ronchetti, Eleonora Bertacchini, Alessandro Capra, Angela Gallucci, Mauro Generali, Giampiero Gozza, Valeria Pancioli, Sara Pignone, and Giovanni Truffelli

Abstract

Rapid assessment of landslide activity is important in case of adverse climatic conditions leading to civil protection's alerts that require increased surveillance of risk areas. GB-InSAR is nowadays becoming a consolidated near-sensing monitoring technique for slope movements. It can be installed rapidly and it can rapidly provide results in the form of displacement maps. However, it has never been thoroughly tested in radar-hostile conditions such as these posed by large-scale earth slides – earth flows covered by a canopy of trees bushes and meadows, that are the typical landslides in Emilia Romagna Apennine. As sparse small villages, buildings, roads and other lifelines are often built on these landslide bodies, they are of particular concern for civil protection, especially during prolonged rainfall periods that determine attention/alerting conditions. To test the possibility to achieve improved surveillance capability in case of attention needed, a series of GB-InSAR spot campaigns lasting from a week to a month, was carried out in 2010–11 in several landslides of Emilia Romagna Apennine using a commercial interferometric radar. The aim was to evaluate the performance of the technique for rapid assessment of landslide activity, even in case of partly vegetated soil coverage conditions. The paper deals with the results obtained in 3 out of the 11 monitored sites.

Keywords

Landslides • Ground-Based InSAR • Monitoring • Northern Apennines

Introduction

Ground-based interferometric SAR (GB-InSAR) was applied to landslide monitoring since the early-mid 90s (Antonello et al. 2004; Nico et al. 2004). Being applicable in several risk management conditions (Corsini et al. 2006) it is nowadays becoming a consolidated near-sensing monitoring technique for slope movements (Noferini et al. 2007; Barla et al. 2010).

GB-InSAR performance is optimal in non vegetated slopes, where maximum coherence of the backscattered radar signal is obtained. In these conditions displacement maps can be calculate for slopes located in a range up to 4 km from the radar device, with accuracies in the order of millimetres and with an almost continuous spatial coverage. On the other hand, slopes covered by vegetation are typically

A. Corsini (✉) • F. Bonacini • F. Cervi • G. Ciccarese • F. Ronchetti • E. Bertacchini • A. Capra
Earth Sciences Department and Mechanical and Civil Engineering Department, University of Modena and Reggio Emilia,
Largo S. Eufemia 19, Modena 41121, Italy
e-mail: alessandro.corsini@unimore.it

M. Berti
Earth Sciences Department, University of Bologna, Bologna, Italy

A. Monni • M. Pizziolo • A. Gallucci • M. Generali • G. Gozza • V. Pancioli • S. Pignone • G. Truffelli
Civil Protection Agency, Geological Survey, Technical Basin Service of Po river affluent, Emilia Romagna Region, Bologna and Parma, Italy

C. Margottini et al. (eds.), *Landslide Science and Practice*, Vol. 2,
DOI 10.1007/978-3-642-31445-2_51, © Springer-Verlag Berlin Heidelberg 2013

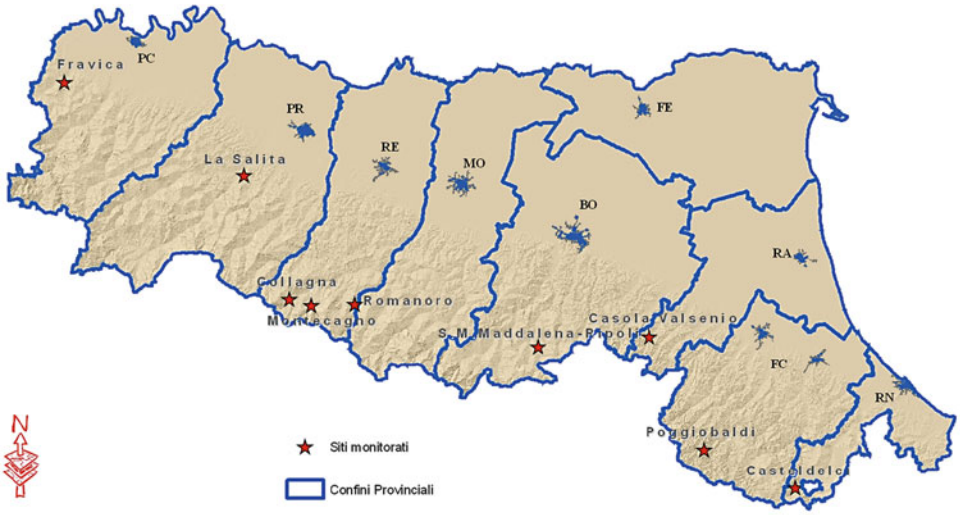


Fig. 1 Location of monitored landslides

considered radar-hostile. Canopy decreases the coherence between subsequent radar acquisitions, coherent points decrease in number and, as a consequence, the computation of the atmospheric component becomes also problematic.

Such radar hostile conditions are often found in earth slides – earth flows of the northern Apennines. However, the continuous improvement of hardware and software tools in the last years, has increased the possibility to successfully apply the technique even in slopes that are covered by sparse trees, bushes, meadows and, occasionally, some buildings agglomerates.

The Agency for Civil Protection of Emilia Romagna Region (Italy) promoted a collaboration between universities and other operative offices, to evaluate the performance of commercially available radar devices for rapid assessment of the state of activity of typical landslides in Emilia Romagna Apennines by using short monitoring campaigns lasting from a week to a month.

Priority was given to: (1) recently reactivated landslides, with the aim to assess the capacity of the system to rapidly and cost-effectively detect possible residual movements; (2) dormant landslides, with the aim to detect slow moving areas within the landslide body that can endanger villages and other infrastructures located on their surface. A total of 11 landslides were monitored using spot campaigns spanning from 10 to more than 30 days each. The paper deals with the results obtained in three of the monitored sites.

Operative Setting

The IBIS-L synthetic aperture radar (SAR) was used. It consists of a Stepped Frequency Continuous Wave (SF-CW) SAR unit equipped with a 2 m Linear rail. Its maximum operational range distance is 4 km, max range resolution is 0.5 m and max cross-range resolution is 4.38 mrad. The Ku frequency band was used (17.1–17.3 GHz), so that the maximum displacement between two subsequent radar acquisitions computable without solving phase ambiguity is 4.4 mm ($\lambda/4$).

Field installation was carried out by fixing the radar rail to permanent structures or to specifically positioned concrete cubes that were partially buried in the ground for 30–50 cm. Power supply was generally available. No shelters of the radar device from rain or snow were used, so to test the robustness of the system to adverse meteorological conditions. Data were acquired in practically all possible weathers, from rainy to snowy autumn-winter days, to hot and dry spring days.

Monitoring campaigns were carried out in 11 landslide areas located at elevation ranges from few hundreds to more than a thousand metres above sea level (Fig. 1).

Each single campaign in a specific site lasted from a minimum of 10 days to a maximum of more than 1 month. However, some sites have been revisited for subsequent campaigns, by re-fixing the radar to the rigs previously left on site. The distance between the radar and the monitored unstable slopes ranged from about 0.5 to 3 km, while the maximum range distance was generally set between 1.5 and 3.5 km. Depending on the maximum range distance selected, the single acquisition time ranged from about 5 to 10 min. Inter-acquisition delay of few seconds was used, hence hundreds of radar acquisitions were collected in each test site.

Data Processing

Data processing has been carried out using the commercially available IDS proprietary software suite. This software suite experienced several improvements during the monitoring

project. The processing chain adopted using the software configuration of early 2010 has been presented by Corsini et al. (2010). The latest releases make it possible to perform the following operations in an integrated way: (1) analyze from two to an unlimited number of raw scenes (.GBD files) to identify radar benchmarks at various level of coherence and power; (2) adopt a selection mask that allows to trim the radar image – using irregular polygonal shapes – and retain the most coherent zones; (3) create a calibration dataset (CalSet) on the basis of a certain number of raw scenes, i.e. identify pixels that remain above defined coherence and signal/noise thresholds; (4) application of step ii, and iii to all images (i.e. transforming .GBD into .PSV datasets on the basis of the CalSet); (5) perform a multi-image interferometric analysis, using atmospheric correction algorithms based on the statistical identification of stable points and filtering methods for spatial and temporal computation; (6) display movement rates and displacements draped over an hillshaded DEM; (7) derive and export displacement time series for points or areas.

In this processing chain, there are milestones that affect the quantity and the quality of results: (a) the raw scenes used to create the CalSet; (b) the threshold value of the accepted coherence; (c) the shape/extent of the masked area; (d) the total number and the temporal sampling of processed scenes.

(a) The number and timing of scenes used to create the CalSet is of crucial importance, as it influences the number of pixels that are considered sufficiently coherent and which are consequently retained to calculate displacements. In canopy covered slopes, a given pixel might result above a specific coherence threshold for a limited time span (i.e. a limited number of scenes), as coherence might be influenced by changes of ground and atmospheric conditions. It is practically feasible to obtain a CalSet based on a very limited number of scenes. However, a CalSet based on a limited number of scenes, might retain pixels that are not sufficiently representative of the trends in space and time of coherence over the survey. The risk is that displacement will be calculated in too many poorly coherent pixels in subsequent acquisitions, determining "noisy" computed displacement maps (i.e. maps in which displacement values vary significantly and randomly between adjacent pixels). This issue has an impact on practical operational usage if the aim is to reach an almost real-time monitoring capability, as once the CalSet is defined by the operator – and – the remaining processing steps can be routinely and automatically carried out by the software for each newly acquired scene. While a noisy displacement map is certainly not a inhibiting factor when there is a clear predominant movement component in certain portions of the radar scenes, a noisy displacement map can actually be a problem if it ends up masking slow movements and makes displacement estimates unreliable. In order to

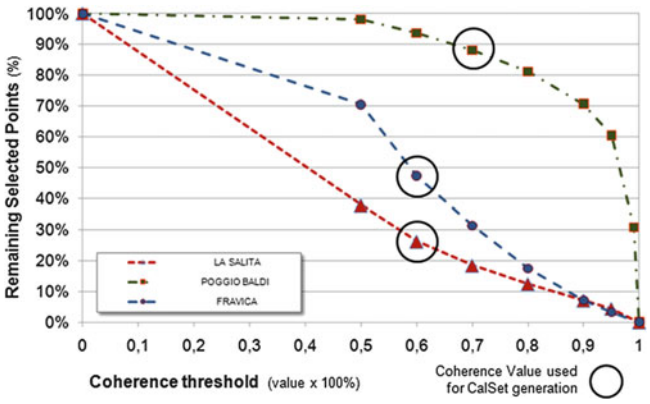


Fig. 2 Plot of coherence vs. % of remaining selected points, using the first 30 scenes of the spot survey

balance between the necessary rapidity of assessment and the confidence on results, we've opted for creating CalSets by selecting at least 30 scenes. They were either the first 30 scenes (i.e. allowing for a quite reliable CalSet being created a few hours after installation) or 30 scene selected from subsequent nights (so to retain only pixels that were coherent over the whole survey time).

(b) The "coherence threshold" used for CalSet generation affects the number – and the "quality" – of pixels that will be used to compute displacement and to estimate atmospheric influence. In canopy covered slopes, an high threshold reduces significantly the percentage of remaining selected points. This behaviour is less prominent in slopes with limited vegetation coverage. The three results examples presented in the following paragraphs are quite representative of this situation, with Poggio Baldi landslides (prevalently bare ground) retaining 90 % of available points at coherence 65 %, the Fravica landslide (mix of bare ground and meadows) retaining a bit less than 50/ of available points at coherence 60 %, and La Salita landslide (meadows and woods) about 50/ of available points at coherence 60 % (Fig. 2). Setting high threshold coherence values provides an advantage in terms of robustness of the processing but it has a couple of significant drawbacks: (1) it generates maps with a limited number of displacement points, eroding one of the major advantages of this technique, that is the ability to provide spatially distributed displacement fields; (2) if only too few coherent points are in the CalSet, atmospheric correction algorithm has problems running efficiently, as it requires, by default, at least 80 % of pixels being stable and distributed in the scene in order to run efficiently. In order to balance between these factors, a coherence threshold value between 60 % and 70 % was adopted in all the test sites.

(c) The extent of the "mask area" also plays a similar role of coherence thresholds in determining the quality of results. A general rule is that the extent f the mask area should be sufficiently large to include a large number of pixels that are actually stable, so to improve the robustness of the statistical

computation of the atmospheric phase component. As mentioned beforehand, the processing software runs by considering by default that at least 80 % of pixels are stable. So a problem might arise if most of the pixels remaining in the "mask area" are actually moving pixels that the software erroneously considers stable to reach 80 %. In the monitored test sites, to avoid as much as possible this problem, we've always extended the selection masks significantly to areas outside the landslide body.

(d) The total number of scenes processed affects significantly the "noisiness" of displacement maps. This is because in vegetated slopes the balance between the above mentioned factors causes, almost inevitably, that each displacement estimation step is affected by a small amount of atmospheric residual. Therefore, the larger is the number of scenes processed, the larger is effectively the amount of atmospheric bias that we're adding with each processes scene. This bias might even end up masking the real movement trend during spot campaign in case of very slow movements. In most of the monitored test sites, given the quite slow movement rates, the general approach for processing data in an optimized manner was to actually compute displacement by processing 1 GBD per hour, i.e. by significantly under sampling the collected dataset. In some sites, with longer duration of the campaign, it was necessary to under-sample to 1 GBD every 6 h.

Results: "Fravica" Landslide

The Fravica landslide (Municipality of Pianello Val Tidone, Province of Piacenza) is a pre-historic earth slide – earth flow reactivated on 27th April 2009. The reactivated landslide was approx. 1,5 km long, up to 500 m wide and had sliding surfaces at depth of more than 20 m (Fig. 3).

The reactivation caused the destruction of: about 500 m of National Road n. 60; about 300 m of Municipality Road, two houses. Moreover, the retrogression of the main scarp damaged 2 more houses. In 15th May 2009 the Emergency Status was declared.

Specific objectives of the GB-InSAR spot monitoring campaign (26/04/2010–06/05/2010) were: (1) to evaluate the response of the reactivated landslide –1 year after the main event – to the large cumulated rainfalls of winter 2009–2010 and to single rainfall events; (2) to assess – in absence of other monitoring systems – which parts of the landslide were still mostly active, also in the perspective of a slope consolidation project.

The GB-SAR monitoring campaign was carried out from a frontal panoramic position (Fig. 4a) with the following settings: max range distance 2,000 m; max cross-range distance +/−1,000 m; range resolution 0,5 m; cross-Range resolution 4.4 mrad; antenna type 20 Db. Each radar scene took about 7 min to complete.



Fig. 3 Fravica landslide from radar position (Photo A. Corsini)

Slope coverage at time of survey includes prevalently meadows with patches of bare ground. The radar scene covered also wine-yards in stable areas (that due to metal wires produced high power – coherence signals, Fig. 4b, c). By limiting the coherence threshold to 60 %, we were able to retain almost 50 % of available points, covering the toe and source area of the landslide, as well as stable wine yard areas.

Cumulated displacement at the end of the survey (Fig. 4d) showed a general stability of the toe zone (with some movements only in limited areas) and a general instability in the source zone. In the track zone, the radar was not able to provide any coherent point so no displacement computation was possible.

The time series of displacement in the source zone show almost no delay between increased displacement and onset of rainfall (Fig. 4e, f). On such basis, it was possible to speculate that part of the landslide was, 1 year after the main event, still active and particularly sensitive to rainfall, and therefore was a priority for slope consolidation and drainage.

Results: "Poggio Baldi" Landslide

The "Poggio Baldi" landslide (Municipality of Santa Sofia, Province of Forlì-Cesena) is rotational rock slide evolving into an earth slide – earth flow. The landslide underwent several reactivations in historic times. On the 18th March 2010, following a large rock failure in the source zone, a major reactivation of the entire landslide occurred (Fig. 5). The landslide was approx. 1 km long, up to 300 m wide and mobilized about two million cubic meters. This caused Emergency for the destruction of a 200 m long stretch of a Province Road and of a gas pipeline, the destruction of a couple of house, the evacuation of other houses

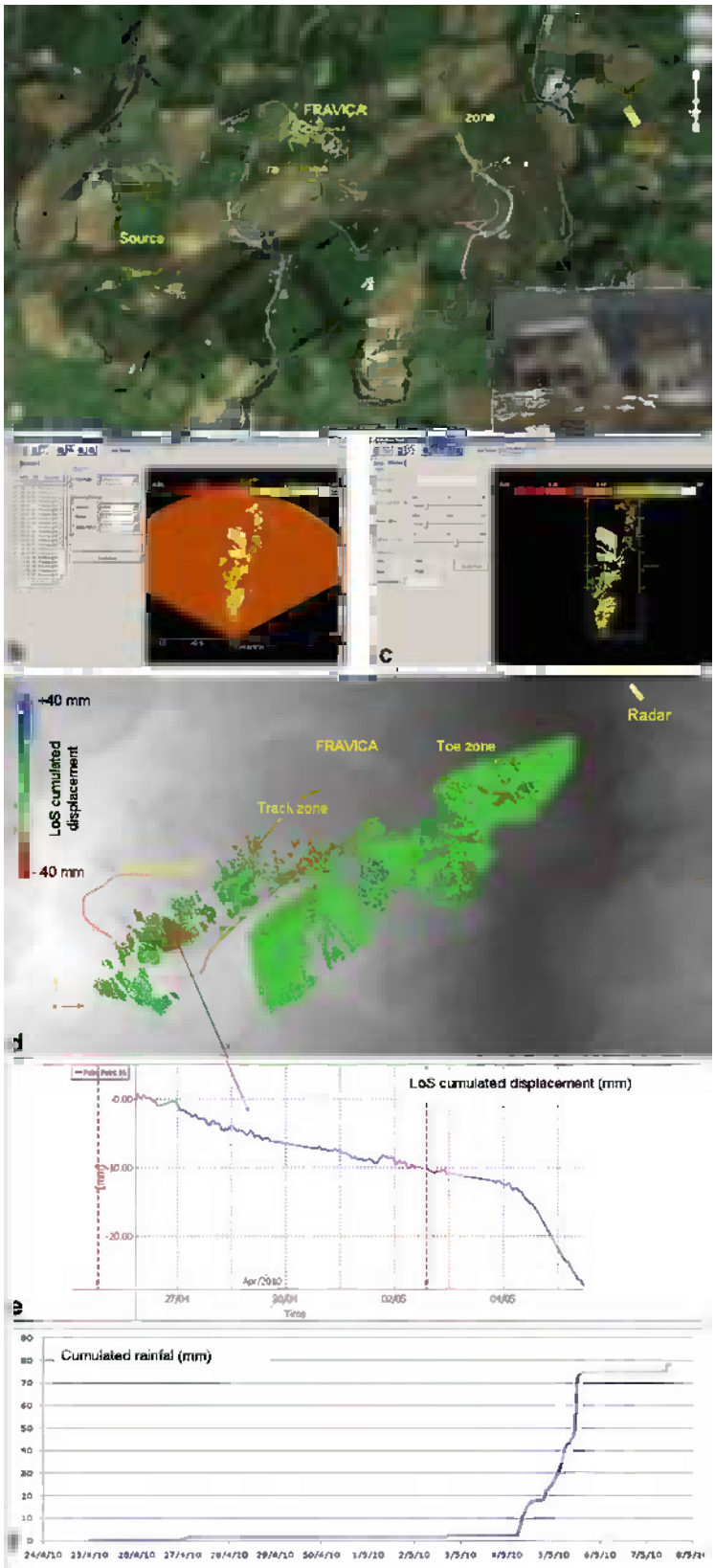


Fig. 4 Fravica landslide (survey from 26/04/2010 to 06/05/2010). (**a**) Aerial photographs after the 2009 event (the inserted picture is of one of the destroyed houses). (**b**) Selection mask for the CalSet creation based on the first 30 radar scenes. (**c**) Selected points in the CalSet based on the first 30 radar scenes and coherence threshold of 60 %. (**d**) Displacement map visualized in stretched values over a shaded DEM in the Guardian software. (**e**) Time history of displacement for one point in the source zone. (**f**) Cumulated rainfall



Fig. 5 Poggio Baldi landslide 6 April 2010 (Photo M. Generali)

(Fig. 6a) and the damming of the Bidente torrent at the toe of the landslide, that caused the formation of a dam lake of several hundred thousand cubic meters. During summer and autumn 2010 slope re-profiling, drainage works and GPS periodic monitoring were carried out on the earth slide body. However, concern among geologists derived by the uncertain stability conditions in fractured rock ridge located on the right side of the source zone, since cracks opened upslope, close to the main scarp area.

Specific objectives of the GB-InSAR spot campaign (14/12/2010–07/01/2011) were: (1) to evaluate the stability conditions of the source zone, and in particular; (2) to assess stability conditions of the rock ridge located on the right side of the source zone.

The GB-SAR monitoring campaign was carried out from a frontal panoramic position of the source zone (Fig. 6a) with the following settings: max range distance 1,000 m; max cross-range distance +/−1,000 m; range resolution 0.5 m; cross-Range resolution 4.4 mrad; antenna type 20 Db. Each radar scene acquisition took about 5 min to complete. Slope coverage at time of survey included bare debris and exposed rocks. Trees coverage was only present in the upper part of the potentially unstable rock ridge, close to the cracks. Thank to the favorable conditions, we were able to retain almost 90 % of the survey points using a coherence threshold of 65 % (with almost 80 % points with coherence values exceeding 90 %) (Fig. 6b, c).

Results showed no generalized movement in the rock ridge zone, supporting the interpretation of cracks opening in the upper part being ascribable to movements affecting only the debris coverage (Fig. 6d). On the other hand, results showed that in several steep sectors of the source area the landslide was still moving significantly in response to rainfall inputs.

A maximum cumulated displacement of more than 90 mm was obtained in the about 20 days of survey. This estimate is affected by uncertainties related to phase cycle slips in the fast moving zones occurred during radar stops. The effects of phase ambiguity generated by movements exceeding the λ/4 limit, is quite evident in the time series of points selected among the active zones (Fig. 6e).

Results: "La Salita" Landslide

The La Salita landslide (Municipality of Borgo Taro Province of Parma) is an earth slide partially reactivated in 2004. The reactivated area was approx. 300 m long and 300 m wide, and almost involved houses located at the bottom of the slope (Fig. 5a). The specific objective of the GB-InSAR spot campaign (19/04/2010–26/04/2010) was to: (1) evaluate the stability of the slope, in absence of other monitoring systems; (2) assess the response to rainfall.

The GB-SAR monitoring campaign was carried out from a frontal panoramic position (Fig. 7a). Device settings were: max range distance 1,000 m; max cross-range distance +/−1,000 m; range resolution 0.5 m; cross-range resolution 4.4 mrad; antenna type 20 Db. Each radar scene acquisition took about 5 min to complete. Slope coverage at time of survey included buildings, a landslide area covered by meadows, bushes and sparse trees, and a background of wooden areas. On a radar application perspective, the challenge was to evaluate the system performance in a small vegetated slope, having in the foreground highly reflective buildings. The presence of buildings resulted in high power and high coherence signals in the foreground of the radar scene, dominating the power and coherence map (Fig. 7b, c), actually producing a strong scattering effect that is causing the semicircular lineaments visible in maps (Fig. 7b). By limiting the coherence threshold to 60 %, we were able to retain about 25 % of available points, a good number of which located in the landslide area. Cumulated displacement at the end of the survey campaign (Fig. 7d) showed movements up to about 40 mm in the upper landslide portion, an area that was also visibly unstable, but also at the landslides toe. Up to about 20 mm of displacement were obtained in the adjacent retrogression area, partially covered by sparse trees.

Conclusions

Results showed that spot monitoring campaigns of few days to few weeks with GB-InSAR allow the rapid assessment of landslide activity even in radar-hostile, partially vegetated slopes. The research made also evident that at very low displacement rates, i.e. few mm during the survey period, and in presence of predominantly vegetated grounds, data processing can affect movement quantification significantly, as a robust atmospheric correction is made difficult by the lack of coherence continuity in the scene and by the difficulties in discerning stable and moving points unambiguously.

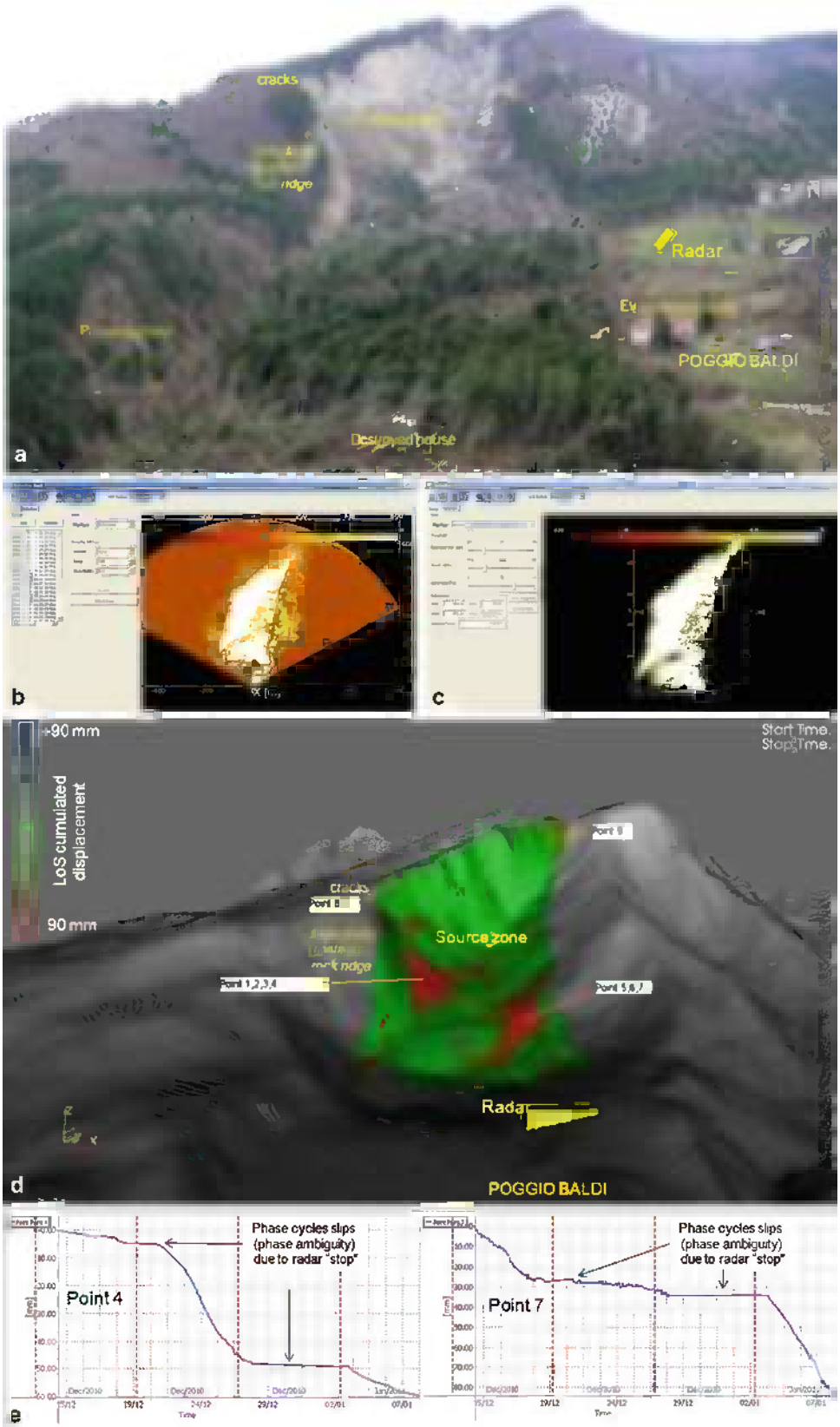


Fig. 6 Poggio Baldi landslide (survey from 14/12/2010 to 07/01/2011). (**a**) Panoramic picture in March 2010 after reactivation in 2010. (**b**) Selection mask for the CalSet based on the first 30 radar scenes. (**c**) Selected points in the CalSet based on the first 30 radar scenes and 60 % threshold coherence. (**d**) Displacement map over a 3D shaded DEM in Guardian software. (**e**) Time history of displacement for two points

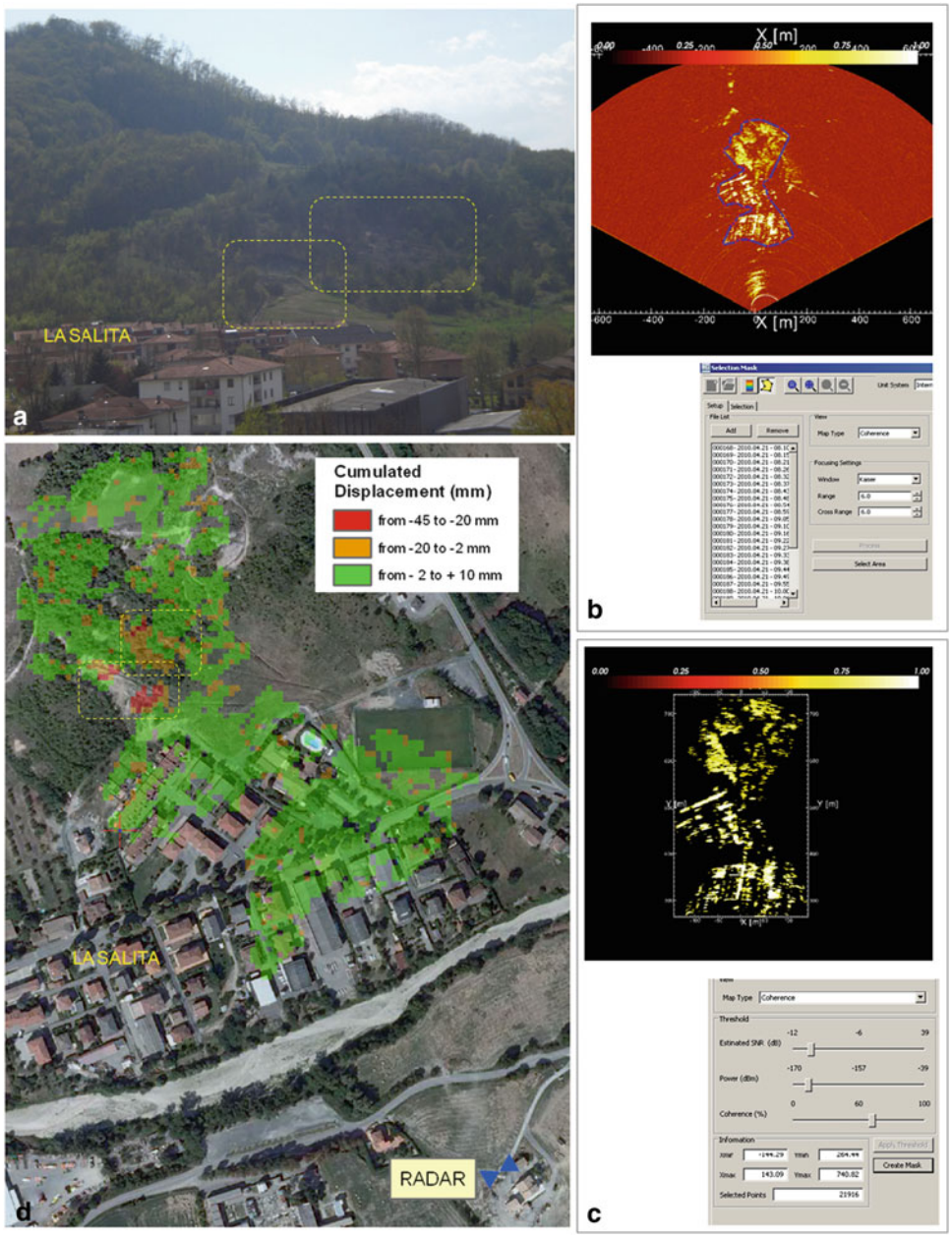


Fig. 7 La Salita landslide (survey from 19/04/2010 to 26/04/2010). (**a**) Picture from radar position. (**b**) Selection mask for the creation of the CalSet based on the first 30 radar scenes. (**c**) Selected points in the CalSet based on the first 30 radar scenes and coherence threshold of 60 %. (**d**) Displacement map visualized over an orthophoto 2008

On a final user perspective the application campaign was certainly positive. A first positive point was the rapid installation and operability of the systems, and the possibility to obtain displacement maps in basically real time just after a few hours from installation. Also, the possibility to operate in several different slope coverage conditions, at distances of up to few km, in relatively slow moving landslides was certainly a plus. Another plus, was the possibility to immediately visualize the resulting maps on shaded DEMs directly in the processing software (see Figs. 4d and 6d for a three dimensional visualization) or very easily import georeferenced results in GIS (see Fig. 7d).

Acknowledgments Research carried out in the frame of the collaborative project "Special activities on support to the forecast and emergency planning of Civil Protection with respect to hydrogeological risk" (Agenzia Protezione Civile Regione Emilia Romagna, Università di Modena e Reggio Emilia, Università di Bologna. Reference persons: A. Monni, S. Pignone, A. Corsini, M. Berti). Authors wish to acknowledge the operative support during field installation of several officials of Regione Emilia Romagna.

References

Antonello G, Casagli N, Farina P, Leva D, Nico G, Sieber AJ, Tarchi D (2004) Ground-based SAR interferometry for monitoring mass movements. Landslides 1(1):21–28

Barla G, Antolini F, Barla M, Mensi E, Piovano G (2010) Monitoring of the Beauregard landslide (Aosta Valley, Italy) using advanced and conventional techniques. Eng Geol 116:218–235

Corsini A, Farina P, Antonello G, Barbieri M, Casagli N, Coren F, Guerri L, Ronchetti F, Sterzai P, Tarchi D (2006) Space-borne and ground-based SAR interferometry as tools for landslide hazard management in civil protection. Int J Rem Sens 27(12): 2351–2369

Corsini A, Cervi F, Ciccarese G, Iannacone JP, Ronchetti F, Bertacchini E, Capra A, Berti M, Brancaleoni E, Mora P, Pancioli V, Gallucci A, Gozza G, Monni A, Generali M, Pizziolo M, Caputo G, Truffelli G, Manzi V, Ghiselli F, Guida M, Minardi G, Lucente CC, Bernardi A, Benini A (2010) Surveillance of landslide risk areas with ground-based interferometric SAR for Civil Protection in Emilia Romagna (Italy). In: Malet JP, Glade T, Casagli N (eds) Mountain risks: bringing science to society. CERG Editions, Strasbourg, ISBN 2-95183317-1-5., pp 283–290

Nico G, Leva D, Antonello G, Tarchi D (2004) Ground-based SAR interferometry for terrain mapping: theory and sen-sitivity analysis. IEEE Trans Geosci Rem Sens 42(6):1344–1350

Noferini L, Pieraccini M, Mecatti D, Macaluso G, Atzeni C, Mantovani M, Marcato G, Pasuto A, Silvano S, Tagliavini F (2007) Using GB-SAR technique to monitor slow moving landslide. Eng Geol 95:88–98



Resolving Landslide-Bedrock Interaction by Nanoseismic Monitoring

Marco Walter and Manfred Joswig

Abstract

Applying high-resolution Nanoseismic Monitoring to different slope instabilities in the Alps, we were able to observe the existence of fracture processes that resolve the creeping of slope material into sequences of discrete 'slide quake' events. At Heumoes slope, Austria, the locations of slide quakes are clustered in the mid-part of the slope exhibiting lower displacement rates than the remaining slope. In contrast, at the mudslide in Super-Sauze, France, the epicenters of located slide quakes correlates well with areas of highest displacement rates. These different behaviors are caused by the completely different layout of bedrock topography which directly influences dilatation and stress relief within the slope material.

Keywords

Landslide monitoring • Seismic monitoring • Slope dynamics • Fractures • Slide quakes • Landslide-bedrock interaction

Introduction

Seismic Monitoring of Slope Dynamics

The interaction of hydrological, hydraulic and soil-mechanical mechanisms influencing landslide dynamics is still not comprehensively investigated due to their spatio-temporal complexity and non-linearity. In this context, passive seismic monitoring offers the opportunity to determine both in high temporal and spatial resolution, soil-mechanical dynamics and possible trigger mechanisms. Our investigations are focused on the determination of slope dynamics (fracture processes, i.e. slide quakes) caused by initial stress relief of the respective slope material.

A pilot study at the Heumoes slope in the Austrian Alps was carried out in 2005, where we were able to demonstrate the existence of measurable fracture processes during the movement of soft rock landslides by the use of Nanoseismic Monitoring (Walter and Joswig 2008). The existence of such signals was not expected due to the lack of brittle material deformation that would generate impulsive fracture release within such weak sediments.

Fracture processes on landslides consisting of hard rock (fragments) were monitored by e.g. Brückl and Mertl (2006) in the Austrian Alps, Spillmann et al. (2007) in the Swiss Alps, Helmstetter and Garambois (2010) at a rockslide in the French Alps and Roth et al. (2005) at the Aknes fjord in Norway. The detected fractures in these studies are probably caused by brittle deformation of the respective slope material. Compared to these studies, our work is focused on the characterization of seismic signals caused by fracturing of soft rock landslide material. Due to the assumed analogues of landslide failure processes and stress relief along tectonic fault systems, Gomberg et al. (1995) suggested to establish the term of 'slide quakes' describing the fracturing or initial stress relief of slope material by means of brittle failure.

M. Walter (✉) • M. Joswig
Universität Stuttgart, Institute of Geophysics, Azenbergstrasse 16, Stuttgart 70174, Germany
e-mail: Marco.Walter@geophys.uni-stuttgart.de

C. Margottini et al. (eds.), *Landslide Science and Practice*, Vol. 2,
DOI 10.1007/978-3-642-31445-2_52, © Springer-Verlag Berlin Heidelberg 2013

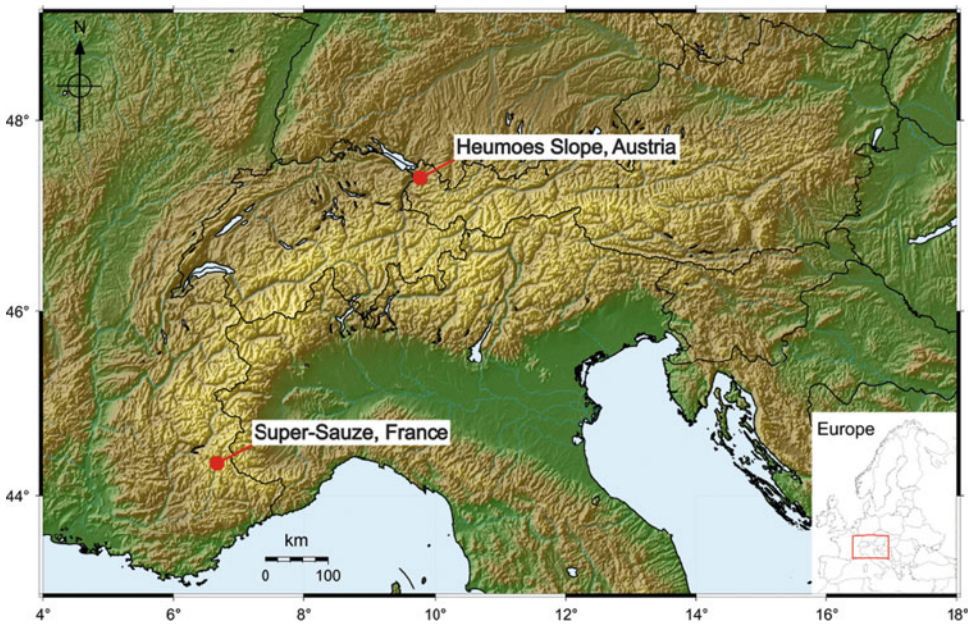


Fig. 1 Geography of the Alps and locations of the Heumoes slope in the northern alpine upland, Austria, and the mudslide at Super-Sauze in the French Maritime Alps

Nanoseismic Monitoring

Nanoseismic Monitoring (Joswig 2008) must be seen in a line of several approaches to extend the capabilities of seismic event location down to the level of ambient noise. Reference for these improvements is the classical concept of microseismic networks (e.g. Lee and Stewart 1981). Seismicity is recorded by individual stations, reliable phase picking demands clear onsets and location utilizes the iterative Geiger approach. The quality control of location results is based on residual analysis of onset times. The complete opposite of microseismic networks properties is an approach recently adapted from exploration seismics, named Passive Seismic (e.g. Artman 2006; Kochnev et al. 2007). The region of interest is covered by a large number of sensors, seismograms are stacked automatically in a grid-search method and potential events are identified by accumulation of radiated energy. No individual phase onsets can be identified, no single events can be separated out of a sequence of activity, nor can seismicity be distinguished from collocated noise sources.

Between these two methods, Nanoseismic Monitoring offers a kind of third approach to improve the sensitivity of seismic monitoring down to background noise but to maintain the aspect of single event identification. The improvement is based on the increase in instrumental efforts by upgrading selected microseismic network sites to small arrays. Any small array (Seismic Navigating System – SNS) is comprised of a centre, 3c sensor, and a minimum of three outer instruments, 1c seismometers in about 25–30 m distance. An even greater rate of success is due to an innovative concept for seismogram processing and event location, realized by the software HypoLine (Joswig 2008): Any phase picking immediately results in displaying the related solution constraints, e.g. a circle for any t_S-t_P, a hyperbolae for any t_P-t_P permutation from different stations, or an array beam for related SNS phases. The quality of location is judged in a map by maximum concentration of information (circles, hyperbolae, beams or "hypolines"). The visual access to all aspects of location constraints supports a scheme of event processing where the analyst tests options, rates plausibility, and identifies forensic noise bursts.

Beside landslide monitoring, Nanoseismic Monitoring has been successively applied to pre-collapse identification of sinkholes in Israel (Wust-Bloch and Joswig 2006), to investigate small aftershocks after strong earthquakes (Häge and Joswig 2009a), and to determine the microseismicity in different tectonic regimes (e.g. Häge and Joswig 2009b).

Study Areas

Nanoseismic Monitoring was applied at two slope instabilities in the Alps which both consist of soft rock sediments, mostly silty and clayey material (Lindenmaier et al. 2005; Amitrano et al. 2007), but whose dynamic processes differ significantly from each other: at the slow-moving (creeping) Heumoes slope in the Vorarlberg Alps, Austria (Fig. 1), with movement velocities of a few centimetres per year and at the fast-moving mudslide in Super-Sauze, French Alps, with displacements of up to 40 cm per day.

The Heumoes slope is located in the Vorarlberg Alps, Austria, around 25 km south of Bregenz. The slope can be divided in three areas showing different movement velocities at the surface: the eastern part moves with >10 cm/year, the mid-part between 0 and 5 cm/year and the western part with up to 10 cm/year (Depenthal and Schmitt 2003, Fig. 2). Compared to the Heumoes slope, the

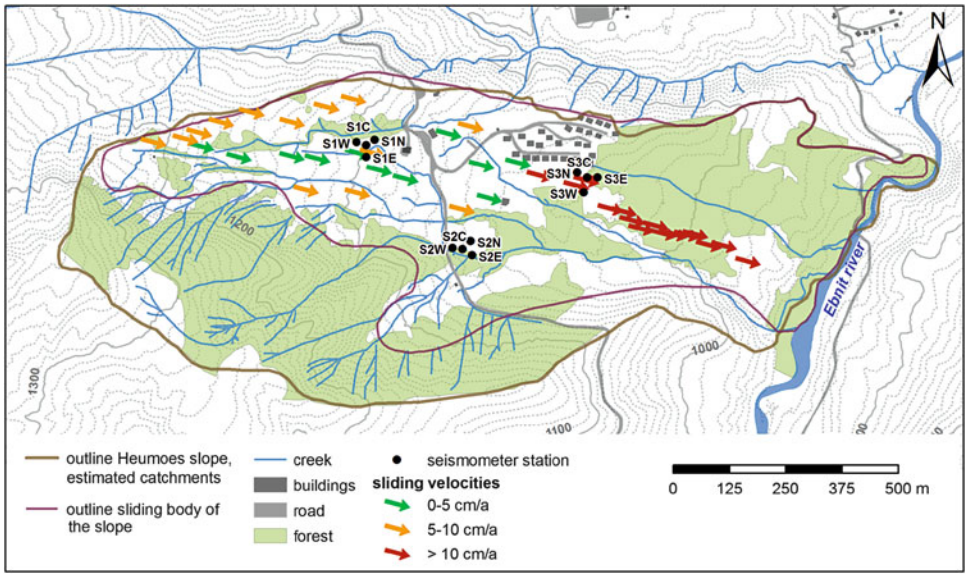


Fig. 2 General set-up of the Heumoes slope, average sliding velocities and seismometer stations of the permanent seismic network (modified after Depenthal and Schmitt 2003, Lindenmaier et al. 2005)

mudslide in Super-Sauze moves averaged between 0.2 and more than 3 cm per day (Amitrano et al. 2007, Fig. 3). By contrast to the Heumoes slope, the highest displacements in Super-Sauze were observed in the mid-part of the slope.

Seismic Monitoring of Slide Quakes

Applying Nanoseismic Monitoring to the landslides in Austria and France, we were able to resolve their creeping behaviour in discrete fracture episodes, i.e. slide quakes. Based on field campaigns between 2005 and 2008, where we discovered the generation of slide quakes at the Heumoes slope for the first time (Walter and Joswig 2008, Walter et al. 2011), a permanent seismic network consisting of three SNS was installed in July 2009 at Heumoes slope (Fig. 2). The presented results are based on data processing until November 2010. In Super-Sauze, a field-campaign was carried out between 14th and 24th July 2008, where four SNS were installed (Fig. 3).

In the time-period between 10th July 2009 and 15th November 2010, we detected and located 76 slide quakes with magnitudes between $-2.5 \leq M_L \leq -0.5$ caused by initial stress relief of the unstable material at Heumoes slope. The epicentres are mainly clustered in the mid-part of the slope (Fig. 4). At Super-Sauze, we detected and located 34 events with magnitudes between $-3.2 \leq M_L \leq -1.3$, again clustered in the mid-part of the slope (Walter and Joswig 2009, Fig. 5).

Compared to the Heumoes slope, the ambient noise level at Super-Sauze is ~20 dB lower what results in a lower detection threshold causing varying magnitude ranges of the observed slide quakes in both study areas. Additionally to the differing detection thresholds, the varying movement velocities of the landslides cause an unequal amount of

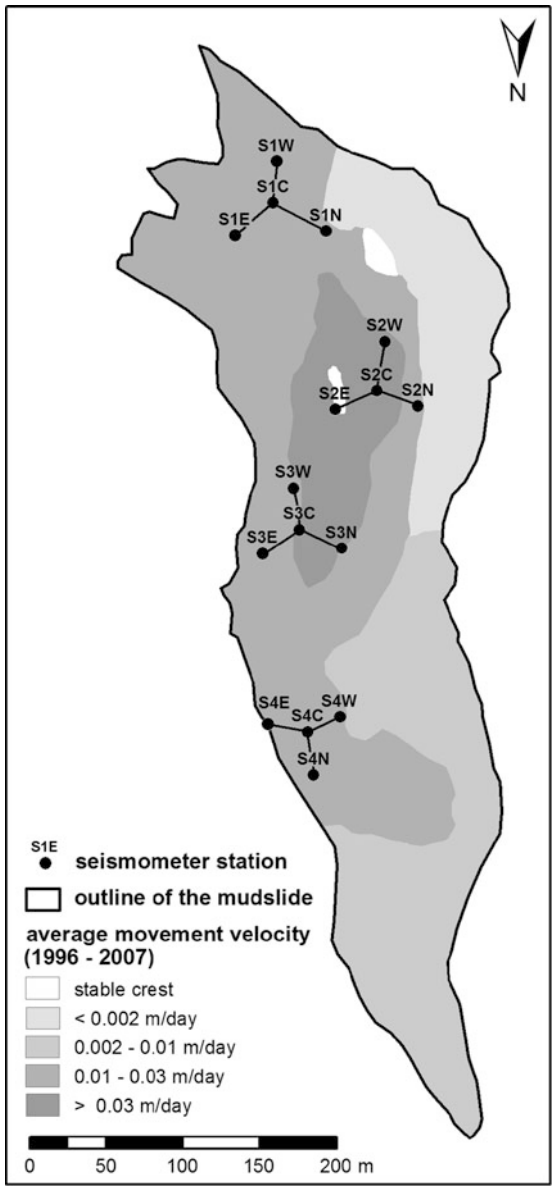


Fig. 3 Location of the installed seismometer stations at the mudslide in Super-Sauze in July 2008

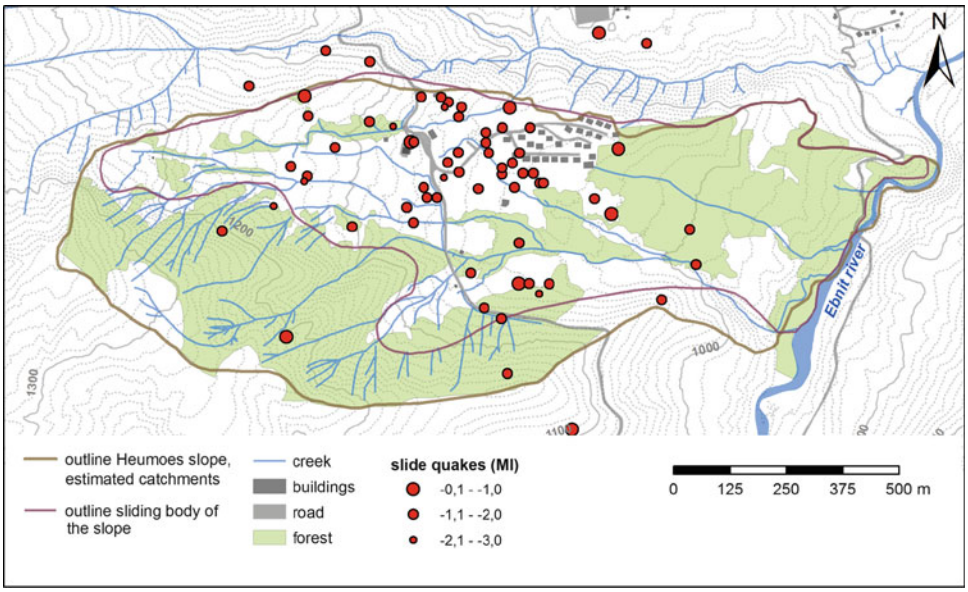


Fig. 4 Epicenters of located slide quakes at Heumoes slope recorded by the permanent network (Fig. 2)

observed slide quakes: 76 events in ~16 months at Heumoes slope compared to 34 events in 10 days at Super-Sauze.

At Heumoes slope, the spatial distribution of located slide quakes correlates with parts of the slope showing lower displacement rates at the surface (compare Figs. 2 and 4), while at Super-Sauze the cluster of located slide quakes correlates with the part of the slope showing the highest superficial displacement rates (compare Figs. 3 and 5). What seems to be a form of contradiction on the first sight, can be explained by the comprehension of the respective bedrock topography. At the Heumoes slope, a significant raise of the bedrock was observed by refraction seismic measurements in the mid-part of the slope. This bedrock elevation is perpendicularly orientated to the movement direction of the entire slope, and defines obviously a form of barrier for the slope dynamics. We hypothesize, that this barrier causes a stress accumulation within the slope material in that specific area and causes initial stress relief while showing lower displacement rates at the surface. Compared to that, e.g. the most eastern part of the Heumoes slope is defined by a successive increase of the sediment layer's thickness where the material deformation is mainly effected by a 'barrier-free' flow of the material. In that slope area, no slide quakes were observed (Fig. 4).

By contrast to the Heumoes slope, the bedrock topography of the mudslide in Super-Sauze is dominated by hidden in-situ crests which are orientated in the direction of movement. These crests canalize the unstable material and directly affect the dynamics of the entire mudslide (Amitrano et al. 2007, Fig. 5). Compared to the Heumoes slope, the orientation of these crests does not mark a barrier for the sliding material and therefore, the locations of observed slide quakes correlate with parts of the mudslide showing higher movement rates at the surface.

Conclusions and Discussion

Applying Nanoseismic Monitoring to different slope instabilities, we were able to resolve the creeping of the respective sliding material in sequences of discrete slide quake events. At Heumoes slope the locations of slide quakes are clustered in the mid-part of the slope, which is defined by lower displacement rates at the surface. Compared to that, at the mudslide in Super-Sauze the epicenters of located slide quakes correlates well with the part showing highest displacement rates. This observation is caused by the bedrock topography which directly influences initial stress relief within the slope material.

As both landslides consist of weak sediments, further crucial properties of the material relating to the generation of deformation processes have to be considered. Intitial stress relief in a brittle manner is generally needed to generate the observed slide quakes. But, the deformation of weak sediments occurs in dependence of the water saturation of the material Maquaire et al. (2003) carried out ring shear tests with the slope material of the Super-Sauze mudslide in order to obtain information on the strength and the effects of moisture content on the effective cohesion and effective angle of friction. They determined the deformations of the slope material in dependence of its water content. With up to 27–28 % water content, the material deforms in a brittle manner, while a higher water content leads to flow deformations. These material properties can be observed in the field when the material dries out in summertime. Then, the surface of the slope shows lots of fissures which reach a maximum depth of around 1 m, the material below is completely water saturated. We can therefore assume that these observed slide quakes are caused by initial stress relief,

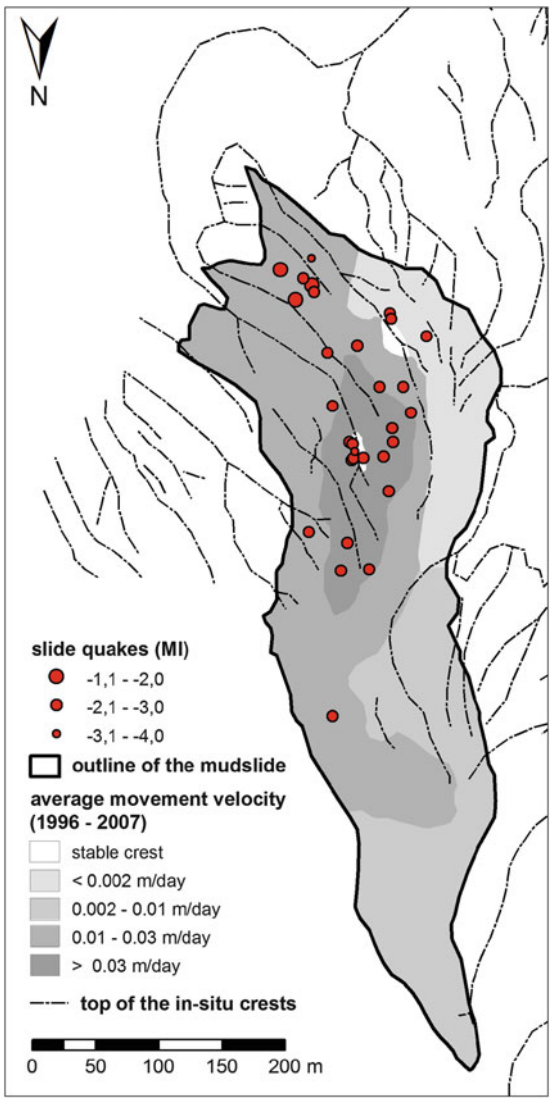


Fig. 5 Epicenters of the located slide quakes at Super-Sauze located in July 2008 (Fig. 3) mapped on the average movement velocities of the mudslide and the bedrock's topography

or brittle failure processes, within the first meter of the slope material. Brittle material deformation is actually needed for both: initial stress relief, fracture processes respectively, and fissure development at the mudslide's surface (Walter et al. 2009).

At Heumoes slope, the geological structure of the unstable material is much more complex. The material consists of very heterogeneous, partly layered, sediments which cause up to three different groundwater levels (Lindenmaier et al. 2005). As therefore the material properties change not only laterally but also in depth, the depth of slide quake generation can not be estimated.

The investigation of source mechanisms which could generate the observed slide quakes marks the main task of future work.

Acknowledgments The authors are especially grateful to Jean-Philippe Malet (school and observatory of earth sciences, University of Strasbourg, France) for both providing several datasets and for the very helpful discussions and improvements. We are thankful to all the colleagues who joined and supported us in the field. This research was performed within the research unit 'Natural Slopes – Coupling of Flow and Deformation Processes for Modeling the Movement of Natural Slopes' which is funded by the DFG (German Research Foundation).

References

Amitrano D, Gaffet S, Malet J-P, Maquaire O (2007) Understanding mudslides through micro-seismic monitoring: the Super-Sauze (South-East French Alps) case study. Bulletin de la Société Géologique de France 178(2):149–157

Artman B (2006) Imaging passive seismic data. Geophysics 71:177–187

Brückl E, Mertl S (2006) Seismic monitoring of deep-seated mass movements. In: Proceedings of INTERPRAEVENT international symposium "Disaster mitigation of debris flows, slope failures and landslides." Universal Academy Press, Tokyo, pp 571–580

Depenthal C, Schmitt, G (2003) Monitoring of a landslide in Vorarlberg / Austria. in: Stiros S, Pytharouli S. (Eds.), Proceedings 11th International FIG Symposium on Deformation Measurements, Santorini (Thera) Island, Greece, pp. 289–295.

Gomberg J, Bodin P, Savage W, Jackson ME (1995) Landslide faults and tectonic faults, analogs? The Slumgullion earthflow, Colorado. Geology 23(1):41–44

Häge M, Joswig M (2009a) Spatiotemporal distribution of aftershocks of the 2004 December 5 $M_L = 5.4$ Waldkirch (Germany) earthquake. Geophys J Int 178:1523–1532

Häge M, Joswig M (2009b) Spatiotemporal characterization of interswarm period seismicity in the focal area Nový Kostel (West Bohemia/Vogtland) by a short-term microseismic study. Geophys J Int 179:1071–1079

Helmstetter A, Garambois S (2010) Seismic monitoring of Séchilienne rockslide (French Alps): analysis of seismic signals and their correlation with rainfalls. J Geophys Res. 115. F03016. doi:10.1029/2009JF001532

Joswig M (2008) Nanoseismic Monitoring fills the gap between microseismic networks and passive seismic. First Break 26:121–128

Kochnev VA, Goz IV, Polyakov VS, Murtayev IS, Savin VG, Zommer BK, Bryksin IV (2007) Imaging hydraulic fracture zones from surface passive seismic data. First Break 25:77–80

Lee WHK, Stewart SW (1981) Principles and applications of microseismic networks. Adv Geophys. Suppl. 2. Academic Press, London, 293p

Lindenmaier F, Zehe E, Dittfurth A, Ihringer J (2005) Process identification at a slow-moving landslide in the Vorarlberg Alps. Hydrol Process 19:1635–1651

Maquaire O, Malet J-P, Remaître A, Locat J, Klotz S, Guillon J (2003) Instability conditions of marly hillslopes: towards landsliding or gullying? The case of the Barcelonnette Basin, South East France. Eng Geol 70:109–130

Roth M, Dietrich M, Blikra LH, Lecomte I (2005) Seismic monitoring of the unsTable rock slope at Åknes, Norway. NORSAR, Report for the International Centre for Geohazards

Spillmann T, Maurer H, Green AG, Heincke B, Willenberg H, Husen S (2007) Microseismic investigations of an unstable mountain slope in the Swiss Alps. J Geophys Res 112:B07301

Walter M, Joswig M (2008) Seismic monitoring of fracture processes generated by a creeping landslide in the Vorarlberg Alps. First Break 26:131–135

Walter M, Joswig M (2009) Seismic characterization of slope dynamics caused by softrock-landslides: the Super-Sauze case study. In: Malet JP, Remaître A, Boogard T (eds) Proceedings of the international conference on landslide processes: from geomorphologic mapping to dynamic modelling, Strasbourg. CERG Editions. pp 215–220

Walter M, Niethammer U, Rothmund S, Joswig M (2009) Joint analysis of the Super-Sauze (French Alps) mudslide by nano-seismic monitoring and UAV-based remote sensing. First Break 27(8):75–82

Walter M, Walser M, Joswig M (2011) Mapping rainfall-triggered slidequakes and seismic landslide-volume estimation at heumoes slope. Vadose Zone J 10(2):487–495. doi:10.2136/vzj2009.0147

Wust-Bloch H, Joswig M (2006) Pre-collapse identification of sinkholes in unconsolidated media at Dead Sea area by "nanoseismic monitoring" (graphical jackknife location of weak sources by few, low-SNR records). Geophys J Int 167:1220–1232



SAR Interferometry for Landslides Risk Assessment at Local Scale: The Case Study of Castagnola (Northern Apennines, Italy)

Francesco Antolini, Veronica Tofani, Chiara Del Ventisette, Guido Luzi, Nicola Casagli, and Sandro Moretti

Abstract

In this work we describe the application of remote monitoring techniques based on radar interferometry (PSI and GB-InSAR) to assess the state of activity and the associated risks of the Castagnola landslide located in Northern Apennines (Liguria, Italy). The ongoing slope instability affecting the Castagnola area is a complex and still poorly understood phenomenon which in the last few decades has undergone numerous reactivations leading to damage to buildings and civil infrastructures. Following a geomorphological field characterization and an aerial photo interpretation of the site, we have analyzed and compared the past long term evolution of the ground movements using Persistent Scatterers Interferometry technique (PSI) from a set of ERS 1/ERS2 space-borne data acquired between 1992 and 2001 and the recent landslide displacements obtained from Ground-Based Interferometric Synthetic Aperture Radar (GB-InSAR) surveys. The results of the space-borne inteferometric data analysis have been compared both with the deformation measured at the head of 10 inclinometric tubes and with the openings of some cracks on buildings. The GB-InSAR monitoring has been carried out in three distinct campaigns from October 2008 to March 2009. The interpretation of the results has allowed to derive a multi-temporal deformation maps of the landslide, showing the up-to-date displacement field and the mean landslide velocity. On the basis of the outcomes of GB-InSAR monitoring, the pre-existent boundaries of the Castagnola landslide have been modified.

Keywords

Landslide • Monitoring • SAR • Risk assessment • Northern Apennines

Introduction

Landslide risk assessment at local scale implies the full knowledge of landslide behaviour and its state of activity. This is particularly important in large-size landslides or complex slope movements, which are characterized by different displacement patterns. Apart from the relative dimension of the phenomena, in the earth sciences landslide occurrence and the associated hazard are generally evaluated on the basis of geomorphologic investigations carried out through field survey and aerial photographs interpretation (Carrara et al. 2003). Hence the behaviour of a mass movement, the overall area affected by displacements and the forecast of its short-term evolution which directly contribute to define the landslide hazard, can be assessed by detecting the superficial morphological changes of the detachment and the accumulation areas. Generally the conventional monitoring techniques – both geotechnical (extensometers, inclinometers, distometers, piezometers, etc.) and topographic (manual triangulation, total station and GPS measurements) – only provide accurate information on a determined number of points on the slopes affected by the

F. Antolini (✉) • V. Tofani • C. Del Ventisette • G. Luzi • N. Casagli • S. Moretti
Dipartimento Di Scienze Della Terra, Università Degli Studi Di Firenze, Via La Pira 4, Florence 50121, Italy
e-mail: francesco.antolini@polito.it

C. Margottini et al. (eds.), *Landslide Science and Practice*, Vol. 2,
DOI 10.1007/978-3-642-31445-2_53, © Springer-Verlag Berlin Heidelberg 2013

instability phenomena. Single-point data very often cannot be considered representative of the behaviour of the whole landslide mass. Extensive conventional monitoring networks are usually installed on landslides to fix this spatial limitation but however cannot be employed on landslide sectors which are at high risk or not accessible.

Remote sensing monitoring systems based on radar techniques (PSI and GB-InSAR) can overcome most of these limitations. Radar sensors can operate over wide areas in almost any weather conditions, continuously over a long time, providing real-time widespread information with millimetric accuracy without the need of accessing to the study area.

In this paper, following a general overview of both geologic, geomorphologic and tectonic settings of the area and the conventional monitoring data available, we describe the application of both satellite and ground-based radar interferometry techniques to monitor the Castagnola landslide. The PSI analysis performed on ERS1/ERS2 images acquired from 1992 to 2001 has allowed to confirm the area affected by the instability and to define the past velocities of movement. The PSI terrain displacement have been subsequently compared with a set of in-situ measurements obtained by traditional geotechnical systems (inclinometers). The results of the GBInSAR survey campaigns carried out discontinuously from October 2008 to March 2009 has allowed to modify the boundaries and the state of activity of the landslide, distinguishing two sectors characterized by different displacement rates and extending the area affected by movements. The integration of advanced monitoring techniques (GB-InSAR and PSI) with the in situ geotechnical instrumentation has provided a new tool for risk assessment and risk management at the local scale.

Site Description

The Castagnola landslide is a large composite landslide (Cruden and Varnes 1996) with an estimated volume of about 3 Mm^3 located in the Northern Apennines, about 25 km to the N of La Spezia city and 2.5 km to the N-NE from the Eastern Ligurian coast.

The Ligurian Apennines and their coastal area are characterized by the extensive outcrops of rocks belonging to the Internal Ligurian Domain. These successions consist of a Jurassic-Paleocene oceanic sequence ("Supergruppo della Val di Vara", Abbate et al. 1980), with ophiolites. The ophiolites include a gabbro and serpentinite basement and a portion of a volcano-sedimentary complex (ophiolitic breccias and basaltic lavas) followed upward by a marine sedimentary cover (Monte Alpe Cherts, Calpionelle Limestone and Palombini Shales) of Callovian – Santonian age (Principi et al. 2004).

The geological model of the landslide was developed by integrating a new detailed geomorphological investigation with sub-surface data acquired from 10 boreholes drilled between February and March 2001 (Vannini et al. 2004). The boreholes were subsequently equipped with inclinometric tubes on which also piezometric levels were monitored. The inclinometric and piezometric survey lasted 1 year (from April 2001 to April 2002), being the instrumentation monitored monthly.

The instability affects the right flank of the Castagnola river valley, stretching from an altitude of about 350 m a.s.l. to the river bed (100 m a.s.l.) on a surface of 0.5 km^2 (1.3 km in length and 0.4 km wide). The right side of the valley constitutes the reversed flank of an anticline verging towards NE where the overturned sequence Palombini Shales – Monte Alpe Cherts –Ophiolites crops out (Figs. 1 and 2). The sequence slightly dips to SW (10°–20°) and the anticline core is limited by two major normal faults trending NW-SE.

The landslide mass is bounded to the NE by an articulated major scarp, while on the SE it is limited by the deep incision of the Rovereto creek. The landslide mass extends to SW, reaching at the toe the right bank of the Castagnola river which has been diverted by the progressive landslide accumulation (Fig. 1).

The aerial photo interpretation, the morphological characteristics and the geological arrangement of the area highlight the presence of several rotational slips on which are superimposed minor shallow planar and – to a lesser extent – flow-like instability phenomena (Fig. 1). The different landslide portions are characterized by a different state of activity and have undergone distinct reactivation phases. On surface the landslide structure is therefore partially masked by the presence of discontinuous terraced alluvial deposits, colluvial and talus debris. The landslide mass lithology is heterogeneous and predominantly consists of altered argillite with limestone and ophiolitic blocks interbedded with clays and silty-clays layers with cobbles and gravels. The bedrock along the slope is constituted predominantly by Palombini Shales and by Ophiolitic rocks (Serpentinites and Gabbro). The thickness of the altered and loose materials varies across the different slope sectors and progressively increases from the head scarp (7–10 m) toward the toe of the landslide (Fig. 2), reaching a thickness of 25 m on the borehole S7.

The landslide activity has disrupted the vegetation cover which now consists of sparse olive trees, rows of vines and bushes, delineating a noticeably different pattern with respect to the surrounding stable area.

The landslide interaction with the civil infrastructures is extensively documented: many buildings in Castagnola

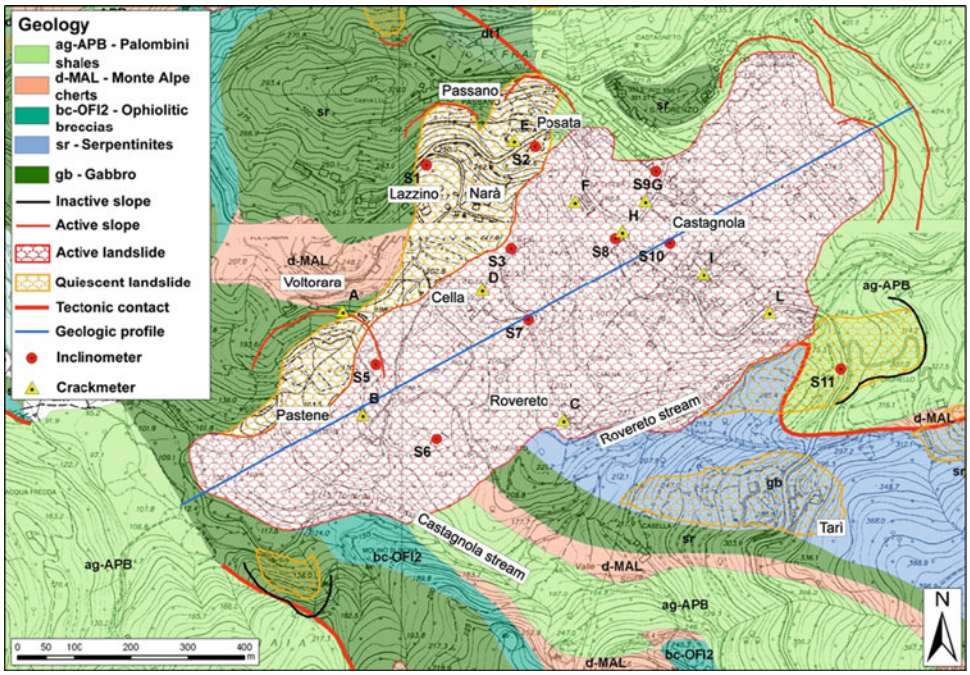


Fig. 1 Geologic and geomorphologic map of Castagnola area

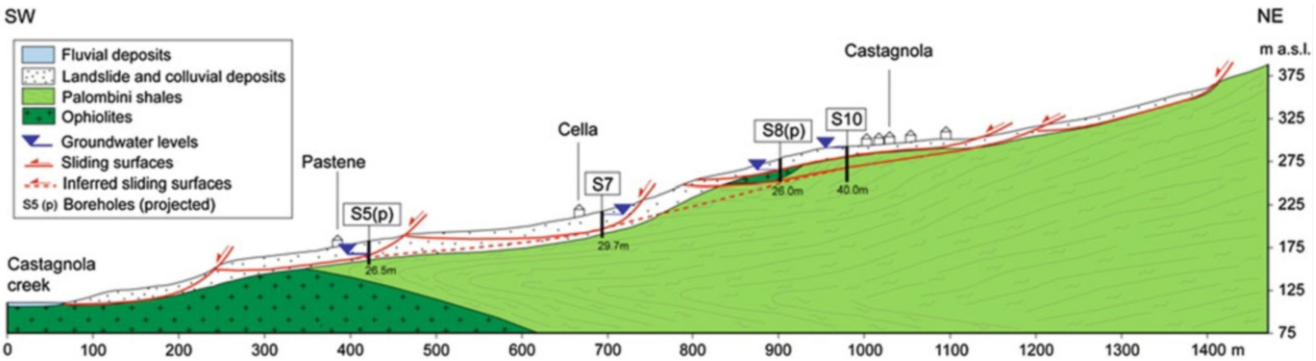


Fig. 2 Geologic section across the landslide

village and the surroundings show structural damages due to the landslide activity.

Landslide Monitoring

Conventional Techniques

From April 2001 to April 2002, the deformational pattern of the Castagnola slope has been monitored by 10 inclinometric tubes (S1–S11) and 10 crackmeters (A-L) installed on damaged buildings, retaining walls and roads.

The analysis of the inclinometric data highlights the presence of well developed sliding surfaces at depths variable from 8 to 25 m on S5, S7, S8, S9, S10 and S11 inclinometers located on the SE sector of the landslide. The maximum annual displacements, respectively of 175 and 163 mm, have been measured at the head of the S7 and S11 inclinometers, although these instruments were sheared off at a depth of 20 m shortly after the installation, probably not capturing the total amount of the movement. Also the inclinometers S8 and S10 which have recorded a total displacement of 33 and 82 mm, were sheared off respectively at a depth of 11 and 25 m.

The other inclinometric tubes installed in the N landslide sector (S1, S2 and S3) have showed slower deformation rates (40–60 mm year^{-1}) not localized along well-defined levels (S1 and S2). Only on the inclinometric tube S3, a very superficial shear surface at a depth of 3 m is evident. Regarding the crackmeters, the larger absolute displacements equal to 12 mm year^{-1}, have been recorded by F crackmeter, installed on a damaged wall of the Castagnola

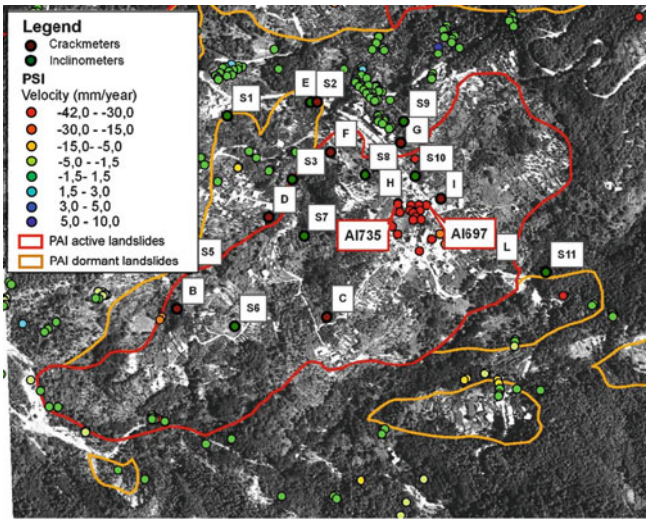


Fig. 3 Persistent scatterers distribution and in-situ monitoring systems within the perimeter of the Castagnola landslide as mapped in PAI

cemetery. The other instruments (in particular A, C, and H crackmeters) have showed cumulated absolute displacements ranging from 5 to 10 mm year^{-1}.

PSI Analysis

The landslide has been monitored with PSI technique using a set of ERS1-ERS2 satellite images, in descending orbits, covering a period between 1992 and 2001.

The distribution of persistent scatterers inside the active landslide, as mapped in the PAI (Piano di Assetto Idrogeologico – Provincia di La Spezia), is shown in Fig. 3. The colour scale displays the values of superficial movements measured along the satellite line of sight (l.o.s.) expressed in mm year^{-1}. The negative sign indicates a movement away from the SAR sensor, while positive values represent a movement towards the sensor.

A total of 39 persistent scatterers are present over the landslide body, mainly distributed in the central part of the landslide. The displacement velocities registered by the satellite during the acquiring period are not homogeneous, ranging between 0.9 and 42.2 mm year^{-1} as absolute value, with a mean velocity equal to 24.6 mm year^{-1}. The highest velocities values (25–42 mm year^{-1}) are recorded in the central part of the slope, while the lowest are measured near the NW and SW landslide boundaries. The field surveys have confirmed the ground movements identified by the space-borne radar interferometry since the buildings and the roads are extensively interested by damages and cracks.

The displacement field measured by the PSI technique matches the landslide's boundary in the PAI. In particular it's worth noticing that the radar benchmarks located just outside NW portion of the landslide show velocity values



Fig. 4 Close-up view of the GB-InSAR system installed in front of the monitored area

less than 1 mm year^{-1}., Despite the error of the technique, these PS can be considered as stable points.

GB-InSAR Analysis

The GB-InSAR system installed in Castagnola belongs to the interferometer series called LISA (LInear Synthetic Aperture high-resolution radar) designed by JRC – Joint Research Centre of the European Commission (Rudolf et al. 1999) and manufactured by Ellegi-LISALab Company.

GB-InSAR system is a coherent microwave transreceiver unit based on a precision network analyzer (PNA) working at Ku band. The signal, which consists of a sweep of electromagnetic waves of proper duration at different frequencies, is then amplified and transmitted to the antennas. The synthetic aperture is realized by moving, via a linear positioner, a motorized sled hosting the radar head along a straight rail 2.7 m long (Fig. 4).

The ground resolution in the range direction, which is a function of the employed bandwidth, was about 1.5 m while the cross-range resolution (perpendicular to the range direction) was variable from 0.3 to 2.6 m.

GB-InSAR system was installed on the roof of a municipal warehouse, at a mean distance of about 700 m from the landslide area (Fig. 4). The first survey campaign was carried out over 7 days, between 23rd and 29th of October 2008. Image acquisition were repeated at time intervals of about 10 min, acquiring a total of 907 radar images. During the second periodical check survey (from 10th to the 18th of February 2009) the GB-InSAR system was installed again in the same position (zero baseline) acquiring a total of 1,231 images.

The daily analysis of the interferograms acquired in the second periodical check campaign has revealed conspicuous slope deformations.

To follow the evolution of the landslide and to avoid possible phase wrapping effect in the long-term interferograms, it has been decided to rapidly resume the radar

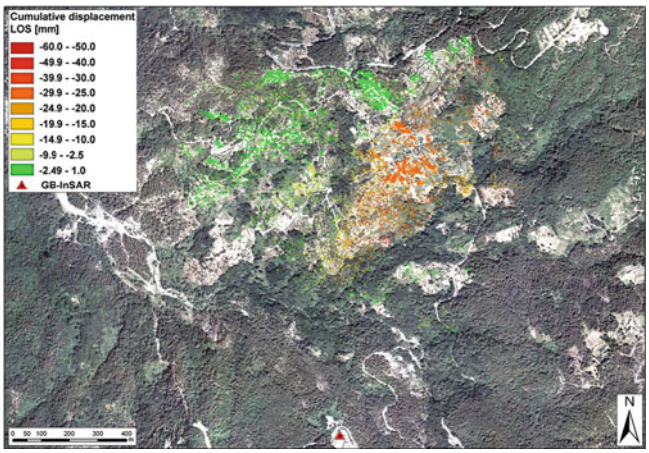


Fig. 5 Cumulated displacement map of the Castagnola landslide (11/02/2009–13/03/2009)

survey in order to provide the local authorities with a near real-time monitoring service. The last survey campaign was performed from 23rd of February to 13th of March 2009, acquiring 2,727 images. During each campaign, radar data were daily transferred via ftp to the processing unit for the generations of both the interferograms and the cumulative displacement maps.

The analysis of the interferograms sequence related to the first campaign (October 2008) did not show any significant slope movements. The total displacements recorded during the second (February 2009) and third (February–March 2009) campaigns are represented by the cumulated displacements map of Fig. 5.

The displacement map analysis highlights a huge sector affected by movements which extends approximately between 500 and 1,300 m away from the radar sensor and corresponds to the SE sector of the landslide. The cumulative displacement map shows a maximum displacement rate of about 60 mm month^{-1} in the head scarp area, in the Rovereto area and on the left side of the Rovereto stream valley. The area where the Castagnola village is located, is instead characterized by a lower deformation rate, equal to 20–25 mm month^{-1}. Moving towards the NW, ground deformation decreases dramatically, reaching a value of 4–5 mm/month^{-1} in the vicinity of Passano, Posata, Lazzino, Narà and Voltorara villages. Regarding the state of activity of the landslide toe (SW landslide sector close to Castagnola stream), the area was not covered by the radar signal and therefore the displacement information are missing.

The long-term interferogram spanning 122 days (from October 2008 to February 2009) reveals a paucity of coherent pixels in the radar image due to the application of a coherence mask with an high threshold value which has discarded the low coherence areas from the images (Fig. 6). On the basis of the long-term analysis results, the Castagnola landslide can be subdivided into three distinct sectors (Fig. 6):

- "A" sector characterized by a substantial stability;
- "B" sector where a marked loss of coherence of the signal backscattered from the scene, has prevented a long-term satisfactory analysis;
- "C" sector characterized by displacements close to instrument precision.

The loss of coherence in B sector can be related both to the geometric changes of the monitored scene due to the displacements occurred since the end of October 2008 and partially to the growth of the vegetation cover.

Discussion

The analysis of the Castagnola slope by means of the PSI technique has allowed to confirm the landslide boundaries and to define the past mean velocity of movements. Inclinometric monitoring of the landslide was carried out for 1 year, from May 2001 to April 2002 in ten boreholes. A detailed quantitative comparison of PSI and the in-situ geotechnical instrumentation was carried out.

The inclinometers have detected the main slip surface of the landslide at a depth between 15 20 m. Along the slip surface a total displacement up to 20 mm year^{-1} has been recorded. In the same period (April 2001–April 2002) 10 crackmeters installed on some damaged buildings have measured cracks openings up to 7 mm.

A comparison between the PSI and inclinometer results, has showed a good agreement in terms of direction and deformation rates, even though the two datasets were acquired during different periods (1992–2001 vs. 2001–2002). Taking into account the acquisition geometry of the satellite descending orbits, the radar measurements are compatible with the SW direction of movement recorded by the inclinometers.

Figure 7 shows a comparison between the time series of PSI, inclinometers and crackmeters. Even though there is no perfect overlap between the different datasets since they were acquired in different periods (1992–2001 vs. 2001–2002), the magnitude of displacement measured both by satellite, inclinometers and crackmeters is the same. In particular, in Fig. 7a it can be observed that the velocity of the radar benchmark AI735 between 1999 and 2001, is comparable with the mean annual velocity of the crackmeter F and the inclinometer 8 located nearby. In Fig. 7b it can be observed a good agreement, in terms of velocity, between the crackmeter H and the persistent scatterer AI697, while the inclinometer 10 measures higher deformations and detects a phase of acceleration not inferable by the other instruments.

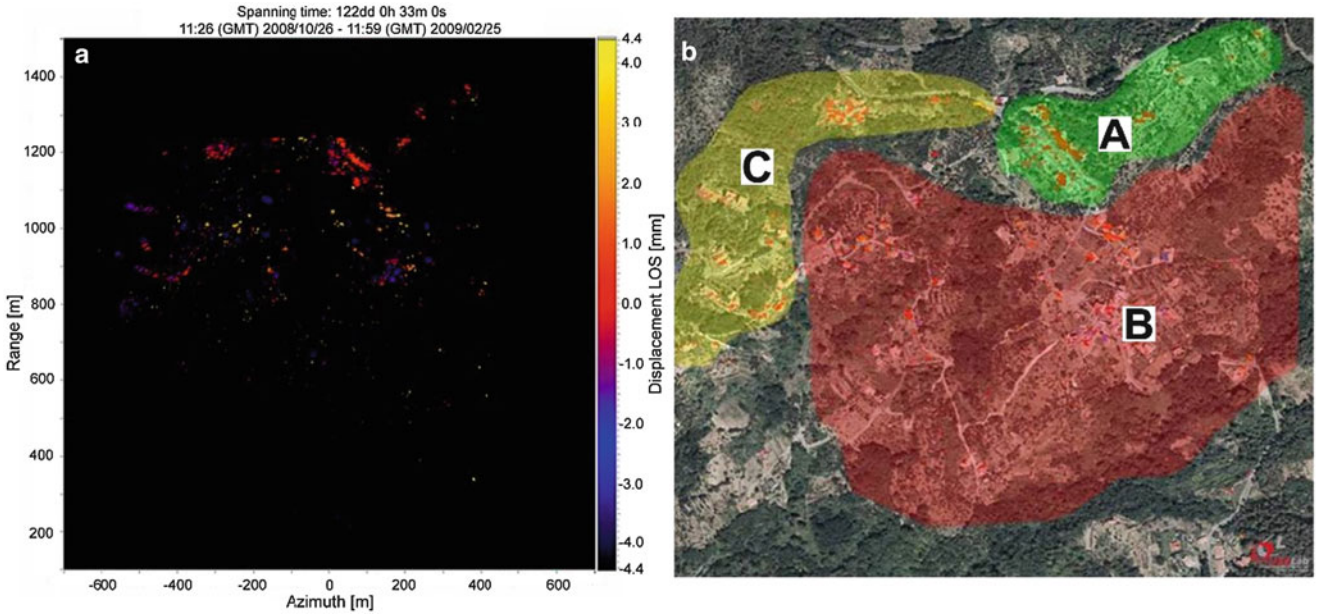


Fig. 6 (**a**) Interferogram spanning 122 days obtained through a sequence of radar images acquired during the first (October 2008) and the second (February 2009) periodical check campaigns; (**b**) Subdivision of the monitored area on the basis of the results of GBInSAR data long-term analysis (see text for explanations)

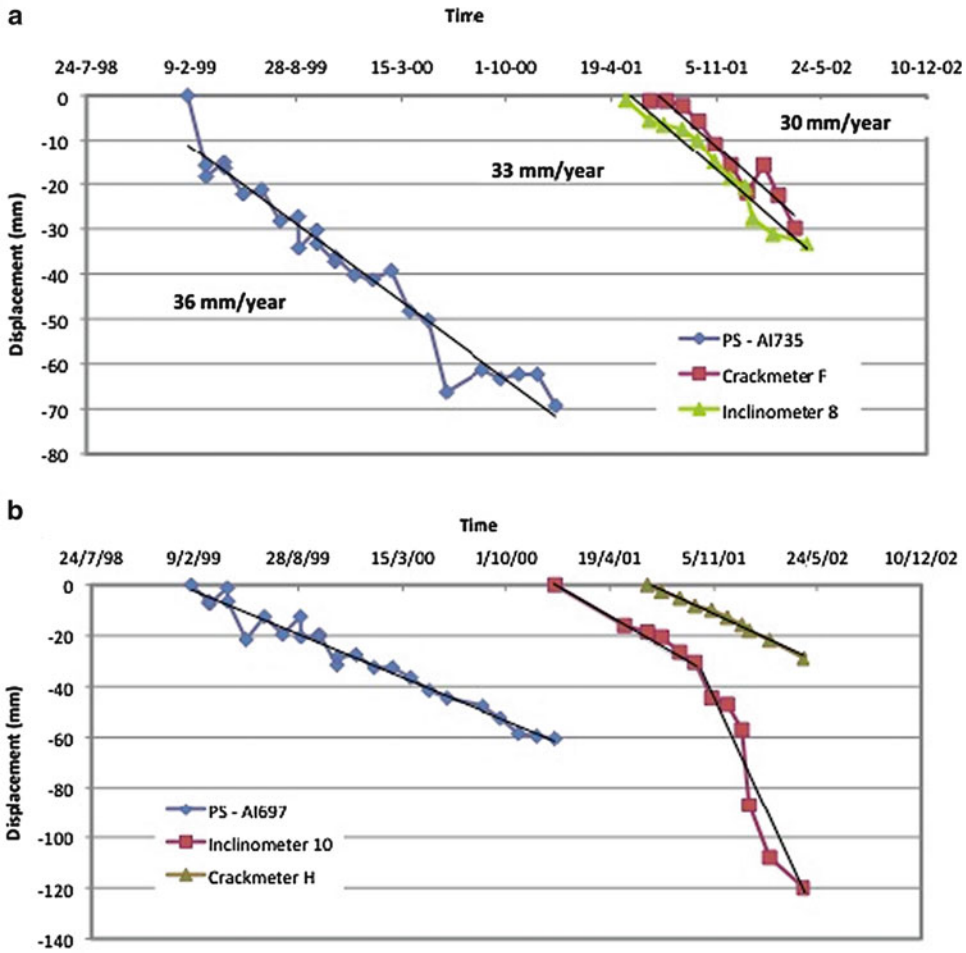


Fig. 7 Quantitative comparison between Persistent Scatterers, Inclinometers and Crackmeters. The location of the instruments in reported in Fig. 1. The location of the PS is reported in Fig. 3

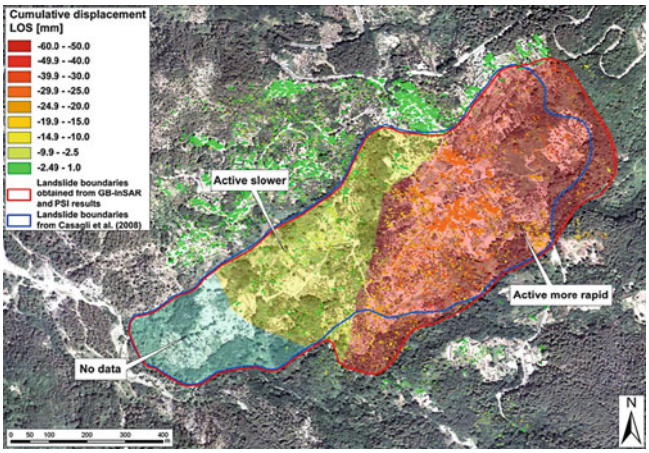


Fig. 8 Results of GBInSAR monitoring: updated landslide boundaries and assessment of the state of activity

The results of the GB-InSAR surveys, have shown that the E and the SE landslide sectors during February and March 2009, have been characterized by a maximum deformation rates one order of magnitude higher (up to 50 mm month^{-1}) than the mean deformation rates recorded with the PSI technique during the period 1992–2001. The spatial distribution of displacements detected by the two techniques is similar, with a huge sector affected by major movements extending approximately on the SE portion of the slope.

Based on the results of the GB-InSAR campaign, the boundaries of the Castagnola landslide (Casagli et al. 2008) have been updated and extended (Fig. 8) towards NE (main scarp area) and towards S (Rovereto – Pallareto area). Moreover it has been possible to differentiate an E sector (red in Fig. 8) characterized by an average rate of deformation of about 0.055 mm h^{-1} and a W sector (yellow in Fig. 8) characterized by a lower average deformation rate (0.025 mm h^{-1}). Any consideration about the state of activity of the landslide toe (light blue area in Fig. 8) cannot be drawn since the area was not covered by the radar signal.

The differences between PSI and GB-InSAR deformation rates have to be ascribed both to the different acquisition period (1992–2001 vs. 2009) and to the intrinsic difference of the techniques. The PS analysis is carried out only on stable scatterers distributed over the landslide surface whose phase response is enough coherent over time. Due to the temporal baseline of the space-borne radar sensor (35 days for ERS 1-ERS 2), areas characterized by rapid geometric changes (i.e. rapid deformations) are discarded from the PSI analysis.

Conclusion

The paper deals with the application of satellite and ground-based radar interferometry integrated with conventional monitoring systems, for the analysis of the risk associated to the Castagnola landslide.

In particular the satellite SAR interferometry (PSI technique) has provided to:

- Reconstruct past long time series (1992–2001) of landslide deformations;
- Confirm the landslide boundaries mapped in the PAI;
- Define the landslide intensity in terms of velocity.

A qualitative comparison of PSI results and inclinometric measurements has showed a good agreement between the two techniques in terms of direction and deformation rates of the movement.

This example of "back-monitoring" demonstrates that the integration of PSI data, which provide long deformation time series, and in-situ investigations, which provide information on the slip surface and materials, has to be always envisaged.

The results of the monitoring campaign by means of ground-based radar interferometry (GB-InSAR) has shown in general higher deformation rates than the PSI technique. This type of analysis gives information on the actual spatial and temporal landside deformation pattern and is fundamental for evaluating the possible landslide evolution, defining deformation thresholds for early warning purpose. Based on the outcomes of GB-InSAR monitoring, the boundaries of the Castagnola landslide defined by Casagli et al. (2008) have been updated.

Finally, while the PSI analysis can be considered as a "back monitoring" tool for landslide risk assessment purposes, the GB-InSAR system is an effective early warning tool for risk management, able to provide near real time information which can be employed in civil protection actions and plans.

Acknowledgements The work described in this paper was performed in the framework of two research projects "Monitoraggio dei fenomeni franosi in località Castagnola (La Spezia) mediante interferometria con sensori basati a terra" and "Monitoraggio dei fenomeni franosi in località Castagnola (La Spezia) mediante interferometria SAR satellitare" between Earth Sciences Department of Università degli Studi di Firenze (DST-UNIFI) and Provincia di La Spezia. The authors would like to acknowledge Provincia di La Spezia for providing the in-situ monitoring data, Ellegi LiSALab for the elaboration of the GB-InSAR data and Tele-Rilevamento Europa for the analysis of the PSInSAR data.

References

Abbate E, Bortolotti V, Principi G (1980) Apennine ophiolites: a peculiar oceanic crust. Ofioliti 1:59–96

Carrara A, Crosta G, Frattini P (2003) Geomorphological and historical data in assessing the landslide hazard. Earth Surf Process Land 28:1125–1142

Casagli N, Moretti S, Catani F, Tofani V (2008) Metodologia per la riperimetrazione e declassazione dei movimenti franosi: Applicazione alla frana di Castagnola (Rapporto preliminare). Convenzione di ricerca con la Regione Liguria – Servizio Politiche dell'Assetto del Territorio (SPAT-RL). Internal Report

Cruden DM, Varnes DJ (1996) Landslide types and processes. – Chapter 3 In: Turner AK, Schuster RL (eds) Landslides-investigation and mitigation, Transportation Research Board, Special Report 247, National Research Council, USA, pp 36–75

Principi G, Bortolotti V, Chiari M, Cortesogno L, Gaggero L, Marcucci M, Saccani E, Treves B (2004) The pre-orogenic volcano-sedimentary covers of the Western Tethys oceanic basin: a review. Ofioliti 29(2):177–211

Rudolf H, Leva D, Tarchi D, Sieber AJ (1999) A mobile and versatile SAR system. Proc IGARSS 99:592–594

Vannini E, Vannucci S, Zanicchi M, Mastorci G, con la consulenza di Puccinelli A (2004) Progetto preliminare finalizzato al consolidamento del versante di Castagnola in comune di Framura – Relazione geologica preliminare con allegati. Committente: Comunità Montana Riviera Spezzina. EPTA Consult p.s.c.r.l., 47 pp



In Situ and Remote Long Term Real-Time Monitoring of a Large Alpine Rock Slide

Federico Agliardi, Giovanni B. Crosta, Rosanna Sosio, Carlo Rivolta, and Gregorio Mannucci

Abstract

We analyze a long term monitoring dataset collected for a deep-seated rockslide (Ruinon, Lombardy, Italy), which activity is documented by ground-based and remote sensing data since 1997. The monitoring data allowed to set-up and update the geological model, to identify rockslide complexities (e.g. uncertain geometry, composite failure mechanisms, seasonal behavior) and their impact on the reliability and early warning potential of monitoring data. GB-InSAR data allowed to identify different behaviors for sectors characterized by outcropping bedrock, thick debris cover, or close to major structures, and to set-up a "virtual monitoring network" by a posteriori selection of critical locations. Displacement time series extracted from GB-InSAR provide a large amount of data even in debris-covered areas, when ground-based instrumentation fails. Such spatially-distributed, improved information, validated by selected ground-based measurements, allowed to establish new velocity and displacement thresholds for early warning purposes.

Keywords

Rockslide • Monitoring • GB-InSAR • Warning thresholds

Introduction

Large rockslides in alpine valleys can evolve into rock avalanches and pose extraordinary risks where morphological conditions and valuable elements occur. The evolution of these phenomena is controlled by lithological, structural, hydrological and meteo-climatic factors. As a consequence, their activity can be highly variable in time, with acceleration and deceleration periods depending on external factors. Snow melting and heavy rainfall are the main triggers of most annually recorded displacements in alpine environments.

Forecasting the failure of these landslides is difficult, due to non linear displacement trends and the superposition of seasonal effects. Large rockslides can exhibit creep-type deformation patterns possibly characterized by continuous acceleration until catastrophic failure (Crosta and Agliardi 2003).

Nevertheless, the temporal pattern of displacements (slow vs. catastrophic, continuous vs. episodic) usually depends on the evolutionary stage, reference time interval, and whether the landslide actually reaches a critical acceleration stage (Broadbent and Zavodni 1982). Several empirical and physics based models account for the creep-type behaviour of landslides (Saito and Uezawa 1961; Fukuzono 1985; Voight 1988; Amitrano and Helmstetter 2006) in order to estimate their time to failure. Although these methods perform quite well in simple cases with continuous acceleration, they fail to provide reliable failure time estimates for large rockslides with complex response to external actions

F. Agliardi (✉) • G.B. Crosta • R. Sosio
Dipartimento di Scienze Geologiche e Geotecnologie, Università degli Studi di Milano-Bicocca, Piazza delle Scienza, 4, Milan 20126, Italy
e-mail: federico.agliardi@unimib.it

C. Rivolta
Ellegi s.r.l, Corso Magenta, 12, Milan 20123, Italy

G. Mannucci
ARPA Lombardia, Settore Suolo, Risorse Idriche e Meteoclimatologia, Viale Francesco Restelli, 3/1, Milan 20124, Italy

C. Margottini et al. (eds.), *Landslide Science and Practice*, Vol. 2,
DOI 10.1007/978-3-642-31445-2_54, © Springer-Verlag Berlin Heidelberg 2013

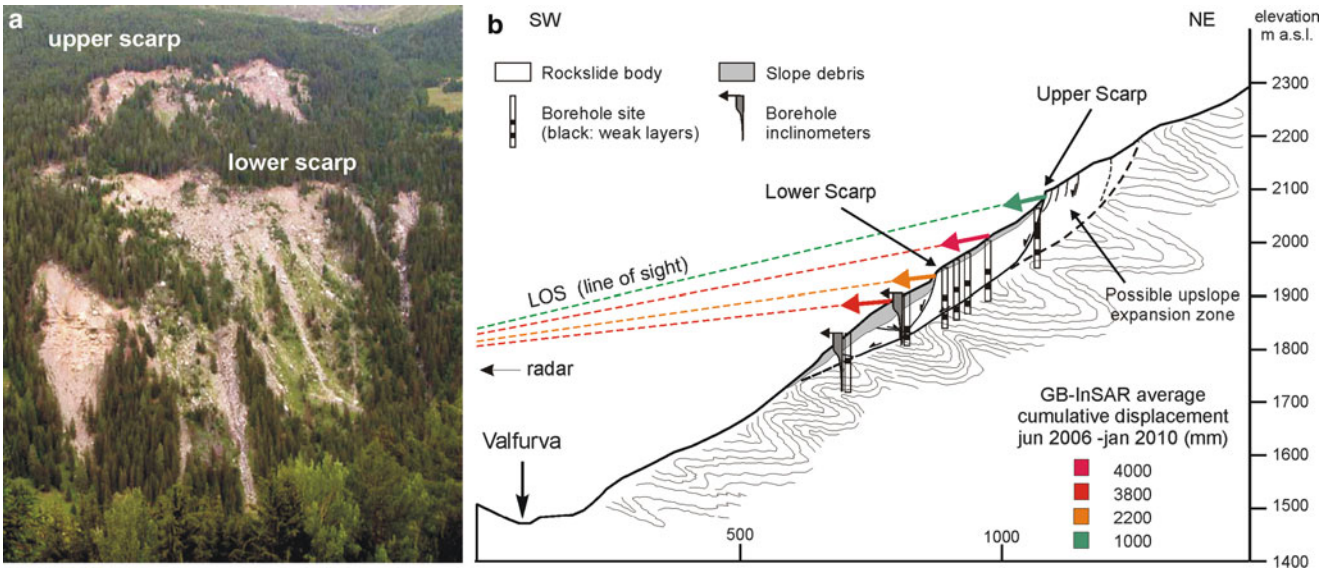


Fig. 1 (**a**) Front view and (**b**) geological cross section (updated after Crosta and Agliardi 2003) of the Ruinon rockslide, showing the main morphological features, rockslide shear surfaces, site investigations, and general distribution of measured displacements

(e.g. seasonal pattern of displacements controlled by rainfall and snowmelt) or complex failure mechanisms. In these cases, suitable monitoring data and technologies are required to constrain rockslide kinematics, establish correlations with triggering factors, and predict future displacements or possible failure.

Traditional monitoring activities exploit topographic and ground-based, point-like measurement techniques. Although very useful to understand landslide behavior, these offer limited capabilities of: spatially-distributed description of rockslide kinematics, network implementation/maintenance, and suitability for early warning. On the other hand, significant recent advances in remote sensing have provided largely unexplored opportunities to overcome these limitations.

We propose an innovative approach to the quantitative analysis of GB-InSAR data for Early Warning. We present the case study of the Ruinon rockslide, a large, deep-seated rockslide in the Central Italian Alps. This approach overcomes the limitations of traditional ground-based monitoring data by setting up a posteriori monitoring networks based on refined geological models, constrained by the interpretation of GB-InSAR displacement fields. Based on the spatially-distributed, improved information provided by GB-InSAR, we exploited different approaches to establish displacement rate and rainfall thresholds for Early Warning purposes. We also discuss the advantages and limitation of adopted data and approaches, and the suitability of different descriptors to predict landslide evolution to failure.

The Ruinon Rock Slide

The Ruinon rock slide is located in the Upper Valtellina (Italian Central Alps), which is characterized by typical continental-alpine rainfall regime (i.e. rainy summer and autumn) with annual average, maximum, and minimum rainfall of 750, 1,300, and 300 mm, respectively. Slope instability involves pre-Permian phyllites of the Austroalpine Campo Nappe, as well as glacial and talus deposits.

The rockslide occurs in the lower sector of a deep-seated gravitational slope deformation affecting the slope up to 3,000 m a.s.l., and is characterised by the Upper Scarp (US, 2,100 m a.s.l.), mainly exposing disturbed rock masses, and the Lower Scarp (LS, 1,950 m a.s.l.), involving disintegrated rock and a thick debris cover (Fig. 1). Scarps and trenches located upslope from the US suggest possible expansion up to 2,200 m a.s.l..

Geotechnical site investigations carried out in the period 1988–2004, including eight borehole logs, inclinometers and piezometers, allowed to constrain the complex geometry, kinematics, and hydrology of the rockslide. It consists of a compound sliding of about 13 Mm^3 of phyllite along surfaces 30–70 m deep, both in debris and rock (Crosta and Agliardi 2003; Casagli et al. 2010). The inferred slide toe (1,700 m a.s.l.) is suspended above the valley floor (1,450 m a.s.l.), suggesting possible evolution into a rock avalanche in case of catastrophic failure (Fig. 1).

The rockslide is active since 1960 and it entered a significant accelerating stage since 1997.

Rockslide Monitoring

Rockslide displacement measurements have been carried out since 1997 through a ground-based monitoring network (including wire extensometer, GPS, and distometer baselines), and in recent years by remote sensing techniques (i.e. satellite, PS-InSAR, and ground-based, GB-InSAR, radar interferometry). Ground-based instrumentation is spread over the rockslide, and clustered along the US and the LS. It provides the longer and more continuous displacement time series (11-year time period). DInSAR data collected using the Permanent Scatterers technique cover about 18 years by exploiting different imagery (ERS1-2, Radarsat) and provide spatially-distributed information widespread over the entire slope, including slower sectors located upslope and outside the rockslide area. GB-InSAR measurements span over 5 years, and cover about 50 % of the rockslide area and larger upslope sectors, thus allowing a comparison/integration with PS-InSAR data.

A LiSALab GBInSAR sensor (by Ellegi s.r.l. for ARPA Lombardia) has been installed on June 2006. The system is placed on the opposite valley side, at a distance from the rockslide area ranging between 800 m (rockslide toe) and 1,700 m (US). The system was initially installed as a research experiment, and later incorporated in the real-time monitoring network operated by ARPA Lombardia for civil protection purposes. In order to fit operational needs, the entire system (i.e. sensor, related hardware and software tools), has been specifically designed and implemented through the years to ensure the requested level of reliability, availability and robustness.

In the present configuration, the LiSALab system synthesizes an aperture of 3 m, covering a visible area of approximately 1 Km^2. The permanent monitoring settings of the system allow to acquire radar images and displacement maps with a range resolution of 1.5 m, an azimuthal resolution between 2.6 and 5.2 m, providing approximately 5 displacement maps per hour. The system has been equipped with rugged hi-speed data transmission connections, redundant power supply system, near real time connection with a weather station, and high resolution webcams. The system now provides the most comprehensive and integrated information about the rockslide behavior and evolution, in order to undertake the risk mitigation actions requested by the civil protection plan. In this perspective, LiSALAb GBInSAR is able to provide to remote users near- and real-time results in term of geo-referenced displacement maps and time series at pre-defined points of interest (POI).

Monitoring data provided by the ground based instrumentation allowed the identification of rockslide sectors characterised by different styles of activity and different responses to external triggers. Crosta and Agliardi (2003) identified three different patterns of displacement trend,

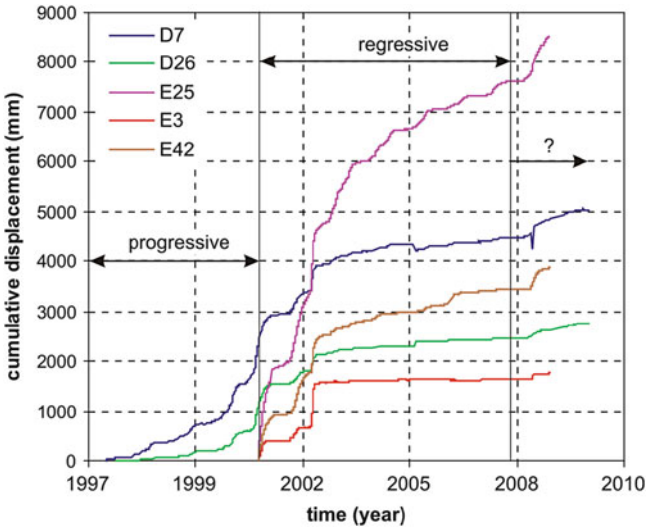


Fig. 2 Long term evolution of the Ruinon, from ground-based displacement measurements. The rock slide is known to be active from decades, reactivates seasonally, and entered a significant accelerating stage since 1997

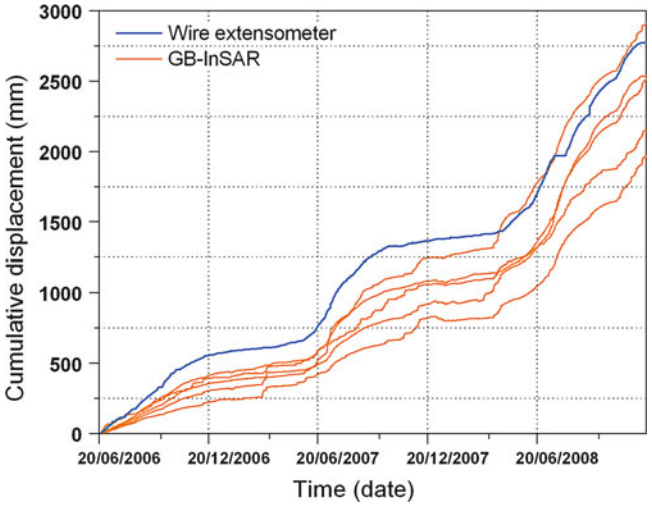


Fig. 3 Comparison among GB-InSAR and extensometer data

namely: "brittle", with stick-slip movement of limited rock mass volumes; "chaotic", observed in areas of debris/disrupted rock and lacking a well-defined trend; and "seasonal creep" (Fig. 2), with non-linear acceleration phases during wet seasons and resting periods during winter and early spring. Seasonal reactivations, associated to rainfall and snowmelt, have been superimposed over a general progressive trend from 1997 to 2002, whereas the rockslide experiences a stage of long-term stabilisation between 2003 and 2007. From 2008, the rockslide started accelerating again, suggesting that "seasonal" behavior occurs at different timescales due to complex deformation and failure mechanisms.

Data from ground-based instrumentation also allowed to validate/correct the spatially-distributed displacement data provided by the GB-InSAR system since 22/06/2006. Since

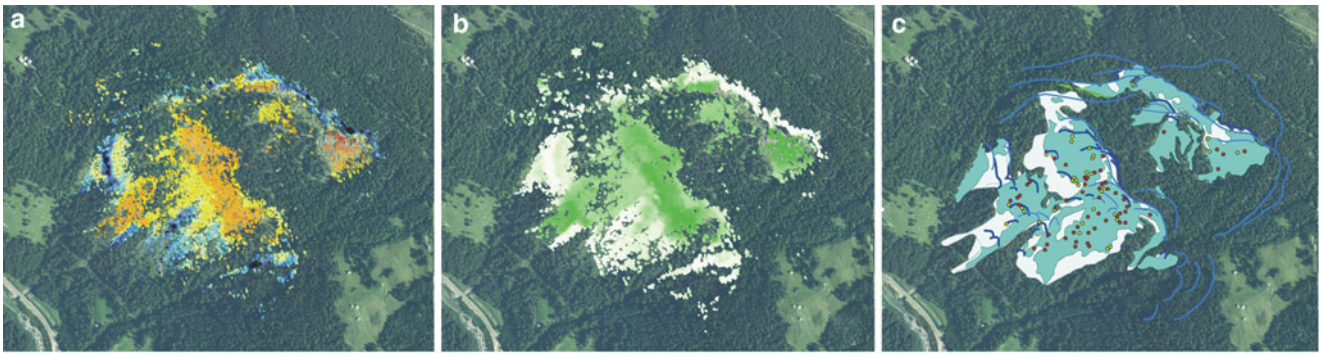


Fig. 4 Steps for the rockslide zonation into homogeneous sub-domains. Cumulative displacement map (**a**) were obtained from the analyses of the GBinSAR data. The rockslide subareas were derived by applying the neighborhood statistics to the cumulative displacement map (**b**) and by geomorphological mapping (**c**)

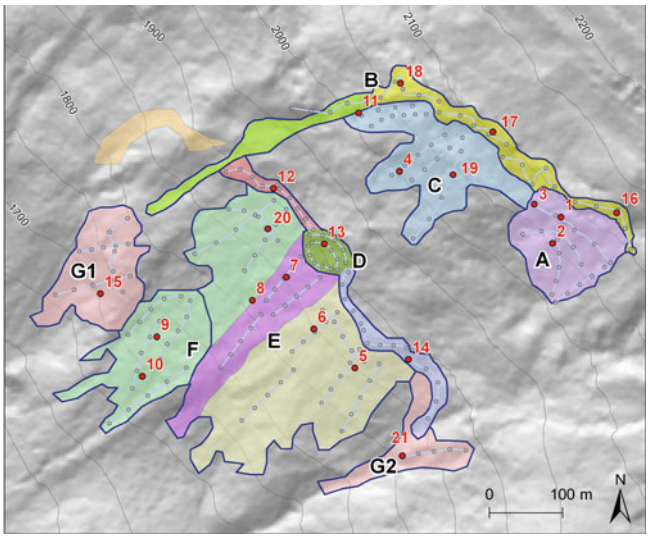


Fig. 5 Rockslide homogeneous sub-areas (13), indicated by *colours* and identified with respect to: style of activity, displacement trend, and inferred instability mechanisms. Letters A to F indicate rockslide "Early Warning domains"

displacements are measured along the radar Line of Sight (LOS), the recorded component of the local displacement vector varies at each slope location, requiring ground-truthing. The comparison between GB-InSAR and wire extensometer data (Fig. 2) revealed a good match among the recorded displacements, with extensometer data providing upper bounds (i.e. estimates of total displacement) (Fig. 3).

Advanced Analysis of GB-InSAR Displacement Data

Data Processing

The spatially-distributed character of GB-InSAR measurements provided the opportunity to refine the existing geological model of the rockslide in order to better understand its kinematics for Early Warning purposes. In this perspective, we analyzed the remote sensing displacement data up to 10/02/2010 (Fig. 4), and identified homogenous sub-areas characterized by similar behavior (Fig. 5).

GB-InSAR displacement maps have been automatically extracted as 5483 geo-referenced GridAscii files (one every 6 h; grid size: 1500 × 1500 pixels; average cell size: 1 m) for further processing in ArcGIS™. As a first step, displacements have been cumulated over 30-day periods to obtain multi-temporal Cumulative Displacement (CD) maps. Incremental Displacement (ID) maps were also derived from CD.

Preliminary analysis of monthly CD maps allowed to identify the magnitude and spatial pattern of rockslide displacement fields, whereas ID maps provided insights in the temporal pattern of displacements (i.e. seasonality, major displacement events).

Definition of Rockslide Sub-Areas

The analysis of CD and ID maps (either raw or smoothed by neighbourhood statistical techniques) allowed the initial definition of sub-areas with homogeneous displacement pattern and rate. This was refined through multi-temporal geomorphological mapping based on photo-interpretation and field observations, aimed at identifying debris-covered areas, rock outcrops, major structures, and kinematic evidence.

This allowed to identify 13 sub-areas (Fig. 5) with homogeneous landslide behaviour and style of activity, depending on the involved material (bedrock, fine or coarse debris cover) or to local structural controls (e.g. distance to major fractures and lineaments).

These sub-areas have been further grouped into seven larger domains (A to G, Fig. 5), which provide consistent information about the evolution of different rockslide sectors in a practical Early Warning perspective. In particular, domain "A" includes a fast moving area involving disrupted rock masses at the eastern tip of the Upper Scarp (US),

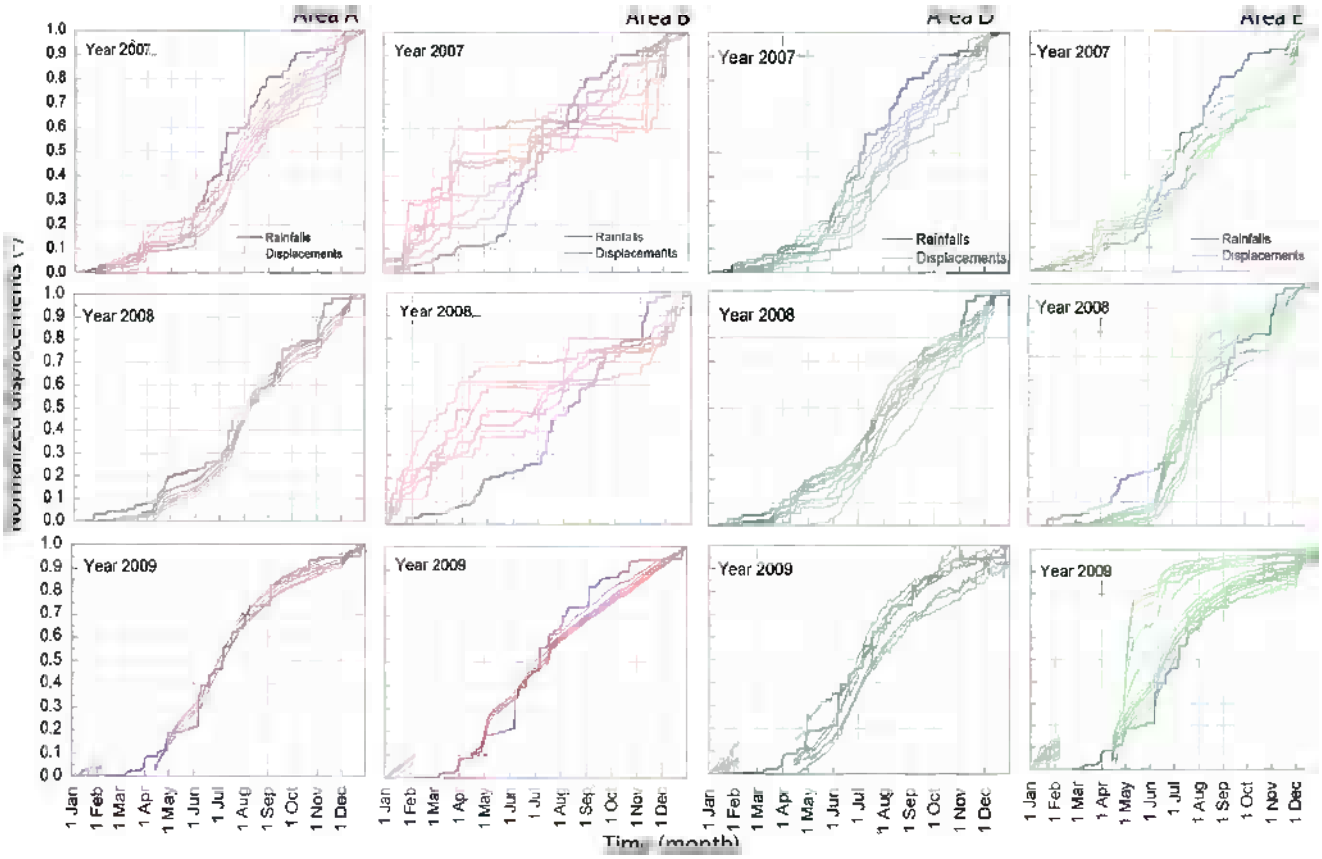


Fig. 6 Normalized displacements, cumulated over 1 year, for monitoring domains: "A" (*left Upper Scarp*), "B" (*Upper Scarp*), "D" (*Lower Scarp*), and "E" (Fig. 5). Displacement trends are compared to normalized rainfall cumulated over the same periods

inferred to reflect the evolution of a quite large portion of the rockslide; domain "B" includes the US crown, characterised by small displacements and providing a passive feedback of rockslide global movement; domain "C" includes the rockslide displaced head, with a thin debris cover mantling the bedrock, reflecting large-scale rockslide movement, as well as domain "D", which includes the Lower Scarp (LS); domain "E" includes the thick rockslide debris and reworked glacial deposits downslope of the LS, undergoing large displacements and responding to rainfall events through debris flows and debris slide activity; domain "F": area involved in a large individual debris slide; and domains "G", including relatively stable areas, possibly providing passive feedbacks for catastrophic failure.

Extraction of Displacement Time Series

We set up a virtual monitoring network made of 205 slope locations considered representative of specific kinematic features of the related sub-domains (Fig. 5). For each location, we extracted displacement time series from the stack of 5483 Cumulative Displacement Maps (one every 6 h). One hundred and thirty two continuous time histories (i.e. covering the entire 5 monitoring years) were validated against ground truth and processed in order to remove the effects of "phase wrapping". Corrected time series allowed a final refinement of rockslide sub-area zoning depending on: cumulative displacement and rate of displacement, sensitivity to and acceleration in consequence of specific triggering events (Fig. 6).

Early Warning Threshold Definition

Establishing physically-based threshold values of suitable descriptors for Early Warning for large rockslides is still difficult, due to their complex geometry, kinematics and hydrology, and to the complex interactions among triggering agents and rockslide mechanism. For these landslides, it is very difficult to identify individual displacement "events" and to correlate them with possible triggers (e.g. rainfall and snowmelt). Furthermore, rockslides often give different feedbacks to similar triggering events depending on the season or year.

In addition, remote monitoring techniques as GB-InSAR have usually been used to describe and follow slope instability, but not for quantitative predictions of slope deformation and failure.

Different approaches have been attempted here to exploit GB-InSAR data for Early Warning, in order to provide threshold values in terms of either displacement rate and rainfall to be used as civil protection management tools.

Rock Slide Collapse: Velocity Thresholds

Modelling the failure of large, complex rockslides as the Ruinon would require a detailed knowledge of rockslide geometry and structure, the constitutive behavior of the involved materials, as well as the boundary conditions and related variations in space and time. This approach is usually unfeasible for Early Warning purposes, because of the large underlying uncertainties and the required modelling effort, generally incompatible with real-time monitoring and decision making.

Several empirical/phenomenological approaches based on the "slope creep" theory (Saito and Uezawa 1961; Fukuzono 1985; Voight 1988) allow to overcome the above-mentioned difficulties when attempting to forecast rockslide failure by the analysis of time series of monitoring data. For large landslides with complex kinematics and response to external triggers, Crosta and Agliardi (2003) proposed a methodology to obtain physically-based alert velocity thresholds. The method is based on the Fukuzono-Voight equation (Voight 1988), which establishes a non-linear relationship between acceleration and displacement rate. Since seasonal behaviour usually hampers a reliable estimation of the time to failure of complex rockslides, the authors used the equation, integrated to a power law of displacements vs. time, to fit time series of measured cumulative displacements (Fig. 7). Non-linear fitting procedures allow to derive model parameters (A, α, and t_f) typical of the current state of the physical system evolving towards failure. Synthetic velocity-time curves are then derived from these parameters (Fig. 7), providing a quantitative basis to establish alert velocity threshold values. These correspond to different time intervals before expected failure conditions and are useful for Early Warning.

Although the method had been developed with ground-based data (e.g. distometer baselines, wire extensometers), GB-InSAR data proved to be the most flexible technique to apply this forecasting approach. In fact, GB-InSAR: (a) provides spatially-distributed data from which the most suitable time series can be selected; (b) provide real-time measurements to keep the analysis updated; (c) provide high-frequency measurements resulting in nearly instantaneous velocity estimates for practical applications.

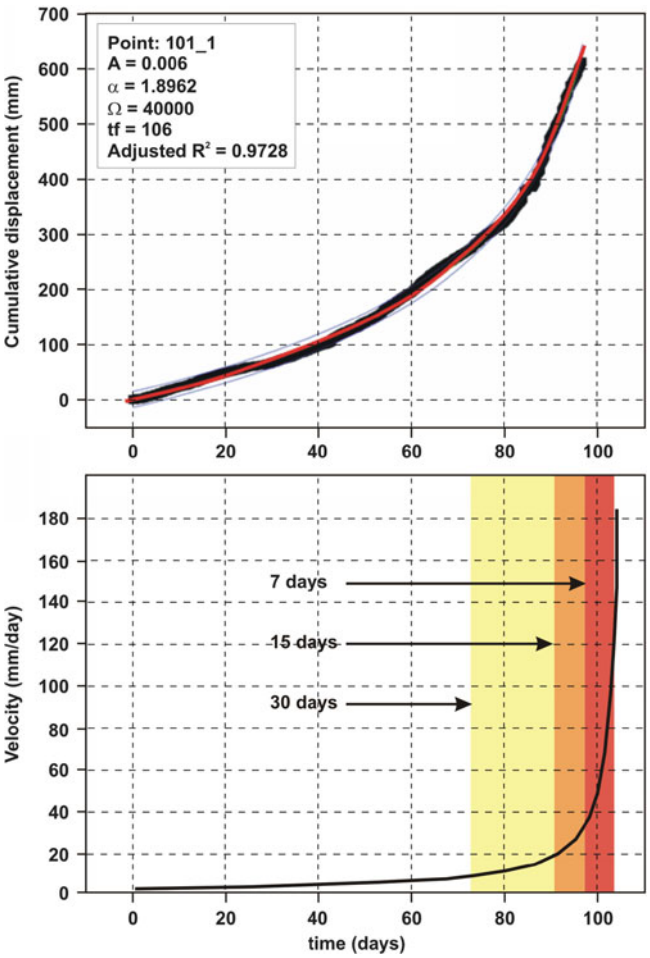


Fig. 7 Alert velocity threshold definition by non-linear fit of cumulative displacement series (example: year 2008)

For the Ruinon rockslide, time series of cumulated displacements for the period april-july 2008 (i.e. the most critical period in the time window covered by GB-InSAR) have been fitted at 22 representative locations spread over the 7 above mentioned domains (Fig. 5). Resulting threshold values are being used by the regional authority in charge of Early Warning.

Rock Slide Reactivation: Towards Rainfall Threshold

The qualitative comparison between displacement trends and rainfall time series (Fig. 6) suggests a complex interplay between rainfall inputs and the Ruinon rockslide response. Time series of antecedent rainfall, cumulated over 1, 7, 15, 30, 45, 60, and 90 days were derived from available rain gauge datasets, and used to explore their controls on the overall rockslide response. The best correlation was found for 60-day cumulative rainfall, which

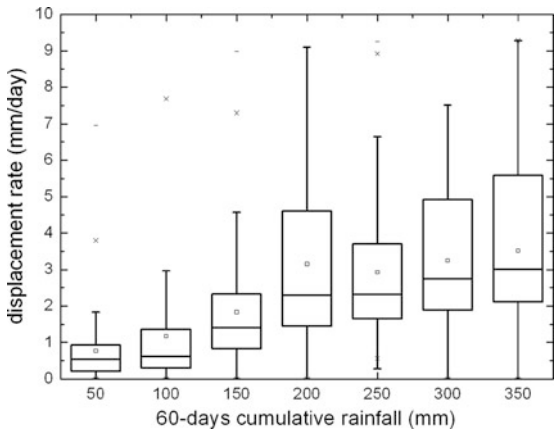


Fig. 8 Relationship between displacement rates and antecedent 60-day rainfall (maximum class values are showed). All available displacement and rainfall data were used

results in increased displacement rates over values of 150–200 mm. Nevertheless, the results obtained for the whole rockslide lack statistical significance and cannot be used as predictive tools, except for a preliminary evaluation of lower bounds of rockslide responses (e.g. associated to a quantile of observed displacements) to pre-defined rainfall input (Fig. 8).

The expected response of the rockslide to rainfall inputs, outlined in this way, requires to be evaluated against the behavior of different rockslide sectors (Fig. 6). For example, displacements of the disrupted rock masses in the domain "A" and along the LS ("C" in Fig. 5) follow quite closely the rainfall patterns at the seasonal timescale, but show complex responses to individual rainfall periods. Along the US ("B" in Fig. 5) most of the annual displacements occur until early spring, suggesting the role of snowmelt to overcome that of rainfall inputs. In the debris-covered area below the LS ("E" in Fig. 5), most annual displacements usually follow well-defined, short periods of intense rainfall. In this area, the maximum response in terms of displacements and displacement rates should be expected.

Conclusions

We proposed a novel approach to the quantitative analysis of GB-InSAR data for Early Warning purposes. This allows to overcome the limitations of traditional ground-based instrumentation, by setting up a posteriori monitoring networks, based on radar displacement fields and constrained by refined geological models. GB-InSAR provides a large amount of data even in debris-covered areas, when ground-based instrumentation fails. These data, validated by selected ground-based measurements, allows to establish specific warning thresholds for homogeneous rockslide sub-areas.

Acknowledgments We thank ARPA Lombardia for collaboration. Ellegi s.r.l. staff, and especially Ing. Davide Leva, is thanked for continuous supporting in the development of GB_InSAR software and equipment. The research was partly supported by EU FP7 project SAFELAND – (GA 226479).

References

Crosta GB, Agliardi F (2003) Failure forecast for large rock slides by surface displacement measurements. Can Geotech J 40(1):176–191

Casagli N, Catani F, Del Ventisette C, Luzi G (2010) Monitoring, prediction, and early warning using ground-based radar interferometry. Landslides 7:291–301

Amitrano D, Helmstetter A (2006) Brittle creep, damage, and time to failure in rocks. J Geophys Res 111:B11201

Broadbent CD, Zavodni ZM (1982) Influence of rock structure on stability. Stability in Surface Mining, 3, Soc of Mining Engineers

Fukuzono T (1985) A new method for predicting the failure time of a slope. In: Proceedings of 4th international conference and field workshop on landslides, Tokyo University Press, Tokyo, pp 145–150

Saito M, Uezawa H (1961) Failure of soil due to creep. In: Proceedings of the 5th international conference on soil mechanics and foundation engineering, Paris, vol 1, pp 315–318

Voight B (1988) A method for prediction of volcanic eruption. Nature 332:125–130



C/X-Band SAR Interferometry Used to Monitor Slope Instability in Daunia, Italy

Raffaele Nutricato, Janusz Wasowski, Fabio Bovenga, Alberto Refice, Guido Pasquariello, Davide Oscar Nitti, and Maria Teresa Chiaradia

Abstract

We apply multi-temporal Persistent Scatterer Interferometry (PSI) analysis to investigate slope instability in the Daunia region in the Southern Apennine Mountains. Daunia includes many small hill-top towns affected by landslides and is of particular interest for the Civil Protection – Regione Puglia Authority, one of the end users of the PSI deformation maps. The SPINUA algorithm is used to perform interferometric analysis and detect, with mm precision, the presence of ground surface movements. Consistent results on very slow displacements are obtained using the radar imagery acquired between 2002 and 2010 by the ENVISAT ESA satellite (C-band, medium spatial resolution sensor) and the images acquired between 2010 and 2011 by the X-band high resolution sensor onboard the TerraSAR-X satellite. Thanks to the finer spatial resolution the X-band PSI applications are very promising for monitoring single man-made structures and slope/ground instability in areas where C-band PS density is low.

Keywords

Slope instability • Daunia • SAR interferometry • C/X-band radar data

Introduction

The space-borne Synthetic Aperture Radar (SAR) Differential Interferometry (DInSAR) techniques are attractive for landslide investigations because of their capability to provide regional scale coverage and, under favourable conditions, spatially dense information on small ground surface deformations (e.g. Colesanti and Wasowski 2006). In particular, advanced multi-temporal InSAR techniques such as Persistent Scatterer Interferometry (PSI) (Ferretti et al. 2001) allow detecting and monitoring with millimetre precision displacements occurring on selected radar targets (PS) exhibiting coherent radar backscattering properties (mainly man-made structures, and secondarily rock outcrops).

In the present work, we apply a PSI multi-temporal processing technique denominated SPINUA (Stable Point INterferometry over Un-urbanised Areas) (Bovenga et al. 2004) to the Daunia region located in Southern Apennines, Italy. This region includes many small hill-top towns with slope instability problems (e.g. Zezza et al. 1994; Wasowski

R. Nutricato (✉)
GAP srl, c/o Dipartimento Interateneo di Fisica, Politecnico di Bari, Via Amendola 173, Bari, Italy
e-mail: raffaele.nutricato@gapsrl.eu

J. Wasowski
IRPI, Research National Council of Italy, Via Amendola 122/D, Bari 70126, Italy

F. Bovenga • A. Refice • G. Pasquariello
ISSIA, Research National Council of Italy, Via Amendola 122/D, Bari 70126, Italy

D.O. Nitti
GAP srl, c/o Dipartimento Interateneo di Fisica, Politecnico di Bari, Via Amendola 173, Bari, Italy

DIF, Politecnico di Bari, Via Amendola 173, Bari 70126, Italy

M.T. Chiaradia
DIF, Politecnico di Bari, Via Amendola 173, Bari 70126, Italy

C. Margottini et al. (eds.), *Landslide Science and Practice*, Vol. 2,
DOI 10.1007/978-3-642-31445-2_55, © Springer-Verlag Berlin Heidelberg 2013

et al. 2010b) and is of particular interest for the Civil Protection – Regione Puglia Authority, one of the end users of the PSI-derived deformation maps.

In particular, we present results obtained by processing SAR data acquired by the ESA's radar satellite ENVISAT (C-band, medium spatial resolution) in the period 2002–2010, as well as by the German Space Agency (DLR) satellite TerraSAR-X (X-band, high resolution) in the period 2010–2011. The displacements maps obtained by processing both C- and X-band SAR data are shown for the selected four towns affected by slope instability problems: Bovino, Casalvecchio di Puglia, Pietra Montecorvino, Volturino (Fig. 1). The results are interpreted and discussed paying attention to the advantages provided by the new generation of high resolution X-band space-borne SAR sensors.

Landsliding and Earlier PSI Investigations in Daunia

The investigated area belongs to the Daunia Apennines, which are moderate relief mountains only locally exceeding 1,000 m above sea level. The region, located only few tens of kilometres from the Adriatic Sea, is characterised by a Mediterranean sub-humid (sub-Apennine) climate with total annual rainfall typically varying from 600 to 800 mm.

Clay-rich flysch formations with poor geotechnical properties are widespread in Daunia and make slopes susceptible to landsliding. The presence of highly deformed geological units is another factor favouring instability. Indeed slope failures are common throughout the Daunia Apennines (e.g. Magliulo et al. 2008; Wasowski et al. 2010a) and many urban areas, as well as road network have experienced landslide problems in the past (Zezza et al. 1994) and in recent years (e.g. Wasowski et al. 2008b, 2010b).

Daunia counts over 20 hilltop towns and in the 1990s there has been an apparent increase in landslide occurrence in several urban and peri-urban areas. It is likely that the stability of slopes bordering the hilltop towns has gradually worsened because of the residential development over the recent decades. This has resulted in reactivations of pre-existing old landslides as well as first-time failures of marginally stable slopes.

The Daunia region has already been investigated via interferometric analysis using the European Space Agency (ESA) C-band ERS-1/2 SAR data covering the period 1995–1999 (Bovenga et al. 2006; Wasowski et al. 2008a, b). With reference to the PSI results from four urban areas (Casalnuovo Monterotaro, Pietra Montecorvino, Motta Montecorvino and Volturino), it was concluded that displacements apparently related to slope failure processes or simply to ground instability occur mainly in the peripheries of the Daunia hilltop towns, where the urban expansion is more recent and the man-made structures acting as PS are situated close to the marginally stable slopes.

Furthermore, Wasowski et al. (2008b) emphasized that the interpretation of the PSI results from urbanized slopes can be difficult, because the detected movements (typically very slow) can arise from a variety of processes: (1) natural or anthropogenic subsidence, (2) settlements of engineering structures, (3) volumetric strains within soils, (4) deterioration of man-made structures, (5) extremely slow slope deformations that may or may not lead to failure. It was also argued that where true landslide movements are detected by PSI, they likely reflect long-term post-failure displacements (and local settlements).

SAR Data Processing

The SAR data processed for the present experiment consist of two datasets. The C-band dataset includes 47 SAR images acquired between November 2002 and January 2010 by ENVISAT ASAR sensor in stripmap mode along ascending orbits (Track 358, Frame 824). The spatial resolution is about 20 and 5 m, respectively along range and azimuth directions. The X-band dataset consists of 13 SAR images acquired between January 2010 and March 2011 by the TerraSAR-X (TSX) SAR sensor in stripmap mode along ascending orbits. These are spaceborne SAR data of last generation with high spatial resolution: about 3 m in both azimuth and range directions for this specific acquisition mode.

Data were processed by the SPINUA algorithm, a PSI-like technique developed through a joint effort of the Remote Sensing Group of the Department of Physics at Politecnico di Bari and the ISSIA-CNR institute. The algorithm was originally developed with the aim of detection and monitoring of coherent PS targets in scarcely-urbanized areas (Bovenga et al. 2004, 2006) and recently has been updated in order to properly process high-resolution X-band data from both COSMO/SkyMed and TSX sensors. It adopts a patch-wise processing scheme consisting in processing small image patches (usually a few km^2) selected according to the density and the distribution of potential PS. This solution enables to obtain fast results on small areas by processing even scarcely populated stacks of SAR images (for more details see Bovenga et al. 2010).

This was the case of the Daunia TSX dataset that consists of only 13 images. Although the displacement maps derived from this dataset can be locally affected by some residual noise, they seem to be in good agreement with those obtained by processing the more populated C-band dataset.

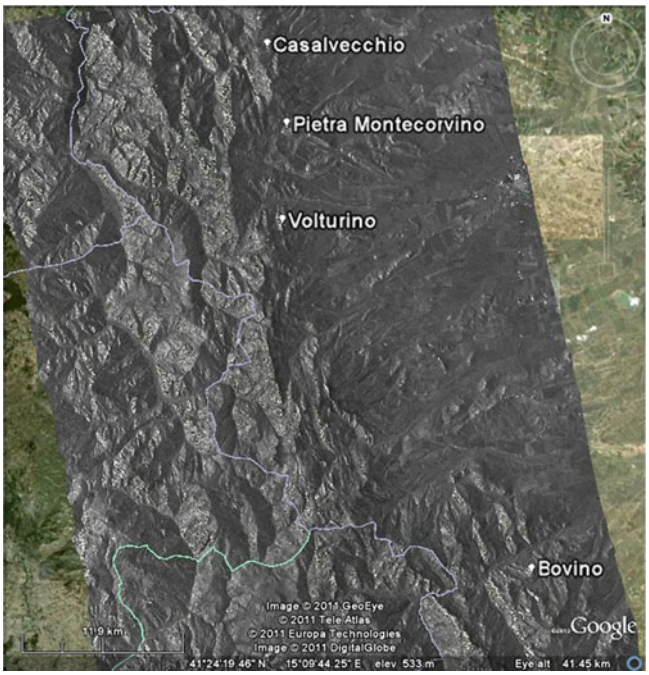


Fig. 1 Geocoded SAR amplitude image of the Daunia region illustrating the moderate relief hillslope topography rarely exceeding 800 m above the sea level. The urban areas (enclosed by *white rectangles*) of Bovino, Volturino Pietra Montecorvino and Casalvecchio di Puglia, are the focus of this work

Results of PSI Analysis for Selected Town Areas

To highlight the PSI results obtained from the ENVISAT and TSX datasets, we selected four urban/peri-urban areas that can be regarded as representative of the geomorphologic and geologic conditions in the Daunia region (Fig. 1). The first two cases concern the areas of Bovino and Volturino, for which only ENVISAT data are presented. The other two cases regard the towns of Pietra Montecorvino and Casalvecchio di Puglia, with both ENVISAT and TSX results.

Town of Bovino

At first glance (Fig. 2) the interpretation of the PSI results at Bovino appears quite straightforward. Most of the PS are not moving, indicating general stability; however, a southern portion of the town includes a cluster of PS characterized by average velocity of around 6–7 mm/year. These PS occur on a gently inclined (approx. 5°) part of a south-east facing slope, which is a site of an old, deep earth-slide (Mossa et al. 2005). The failed slope has been subject to stabilization works in the last decade and now the area shows no obvious signs of instability. However, the results of inclinometer borehole monitoring of the central portion of the slide, conducted by CNR-IRPI since 2008, indicate the presence of extremely slow displacements (up to 1.5 cm/year) occurring at a depth of a few tens of meters (F. Santaloia – personal communication).

To compare the PSI and inclinometer results one needs to consider the geometry of the satellite Line Of Sight (LOS) and of the slope. Considering these and assuming the shear displacement parallel to the ground surface at the mid-portion of the landslides (which includes the moving PS), the radar sensor sensitivity to detect the horizontal component of the landslide movement is between 20 % and 25 %. This explains only in part the discrepancy between the inclinometer results, which indicate approximately two times larger displacements with respect to the PSI results.

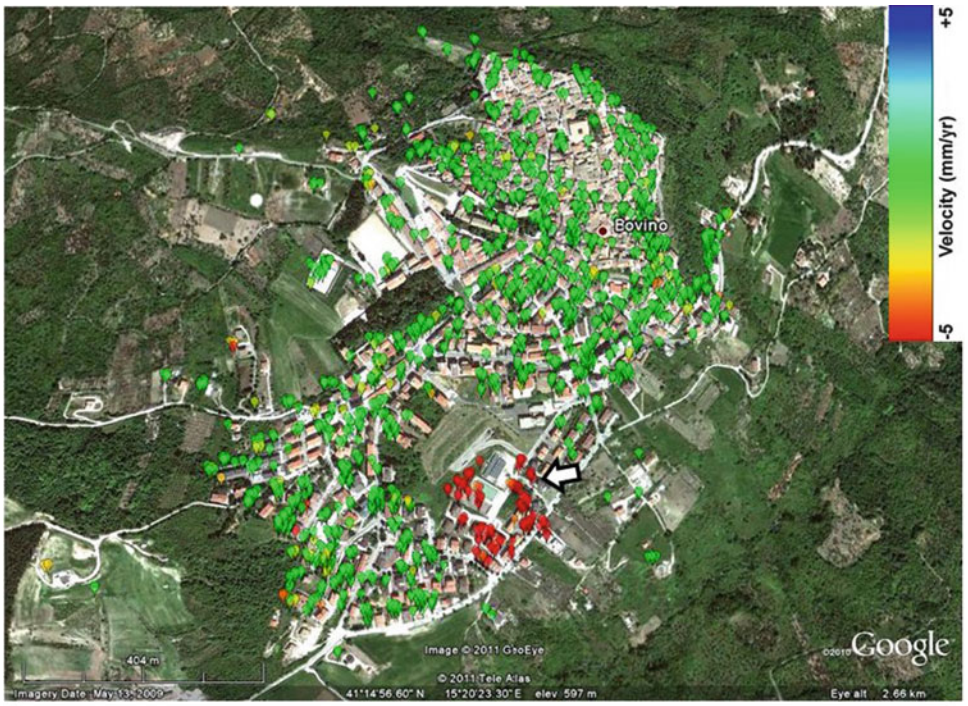
Thus a significant portion of the deformations detected by PSI is likely linked to other processes. In particular, local ground settlements in response to loading by houses and other engineering structures appear plausible, taking into account the presence of clay-rich (compressible) landslide materials and the recent urbanization history of the mid-part of the slide (which started in late 1970s, G. Rampino – personal communication).

Town of Volturino

The ENVISAT results indicate the persistence of slope/ground instabilities in the southern peripheries of the town (e.g. the Fontana di Monte area, Fig. 3), which have already been detected using the 1995–1999 ERS radar images (Bovenga et al. 2006). Furthermore, the rate of the deformations (within 5 mm/year) is very similar.

As at Bovino, also in this case the data available from borehole inclinometer monitoring, conducted since late 2008 in the SW part of Volturino (Lollino et al. 2010), registered displacements averaging to about 1.5 cm/year. Again, the much slower movements resulting from the PSI analysis can be linked to the low sensitivity of the satellite sensor to detect horizontal displacements (with reference to LOS and slope geometry).

Some additional information has been obtained thanks to the presence of PS along the road network north of Volturino (Fig. 3). Although the majority of radar targets are stable, there are some isolated moving PS indicating the presence of very slow (few mm/year) deformations locally affecting the road infrastructure. In one case the moving PS coincides with the site of a landslide that damaged the road in winter 2003 (unpublished CNR-IRPI report to the Department of Civil Protection, Rome); even though the background optical image (from GoogleEarth™) in Fig. 3 is from late 2003, the area affected by this slide can still be easily recognized. One should be very cautious when using isolated PS to infer infrastructure instability. However, as illustrated by the above example, useful inferences can be made when specific ground information is available.



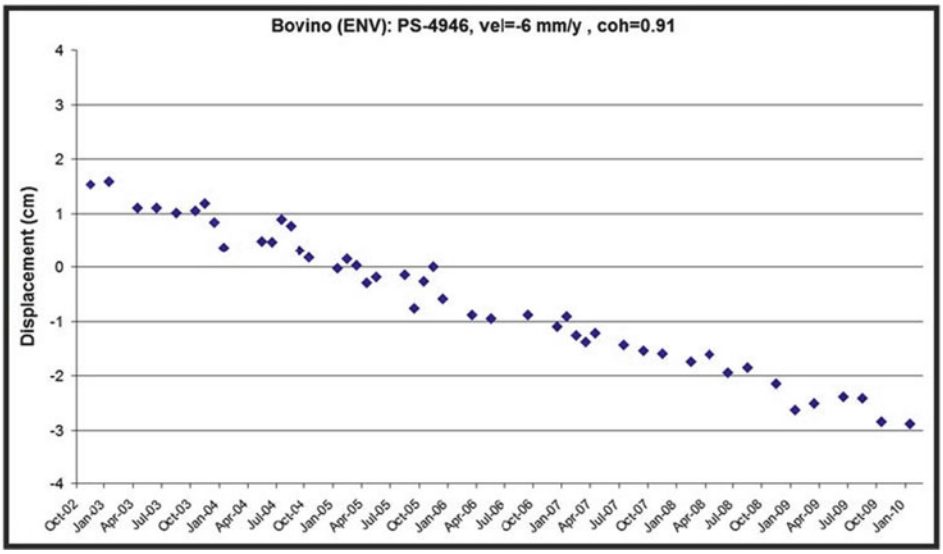


Fig. 2 (*Upper figure*) Distribution and average LOS velocity of PS (marked by *colour dots*) in the Bovino area (ENVISAT ascending data). Note group of several tens of moving PS that coincide with a middle portion of an old, deep landslide. (*Lower figure*) Time series of a representative PS (indicated by *arrow*)

Town of Pietra Montecorvino

The PS displacement maps based on ENVISAT and TerraSAR-X data are shown in Fig. 4. The results are comparable, and indicate the presence of very slow movements in the eastern and south-southern parts of the town. This outcome is also comparable with the results based on ERS C-band data from the period 1995 to 1999 (Wasowski et al. 2008a, b).

Importantly, the PSI map based on X-band data offers more complete information thanks to the higher density of PS (Fig. 4). Also valuable is the presence of X-band PS in areas for which no usable C-band PS were identified. This situation is well visible especially in the peripheral parts of the town.

The presence of numerous very slowly moving PS (typically around 5 mm/year) at Pietra Montecorvino is not surprising considering that a good portion of the town is built on an old large landslide (Zezza et al. 1994) and that surrounding slopes have been affected by active landsliding in recent years (Wasowski et al. 2008a, b). Furthermore, the presence of many damaged buildings indicates the persistence of conditions of ground and/or structural instability. However, we stress that the radar satellite 1-D LOS displacement data alone are insufficient to ascertain the origin of the detected deformations, i.e. whether they represent predominantly downslope(landslide or creep) movements or vertical movements (settlements) or a combination of both.

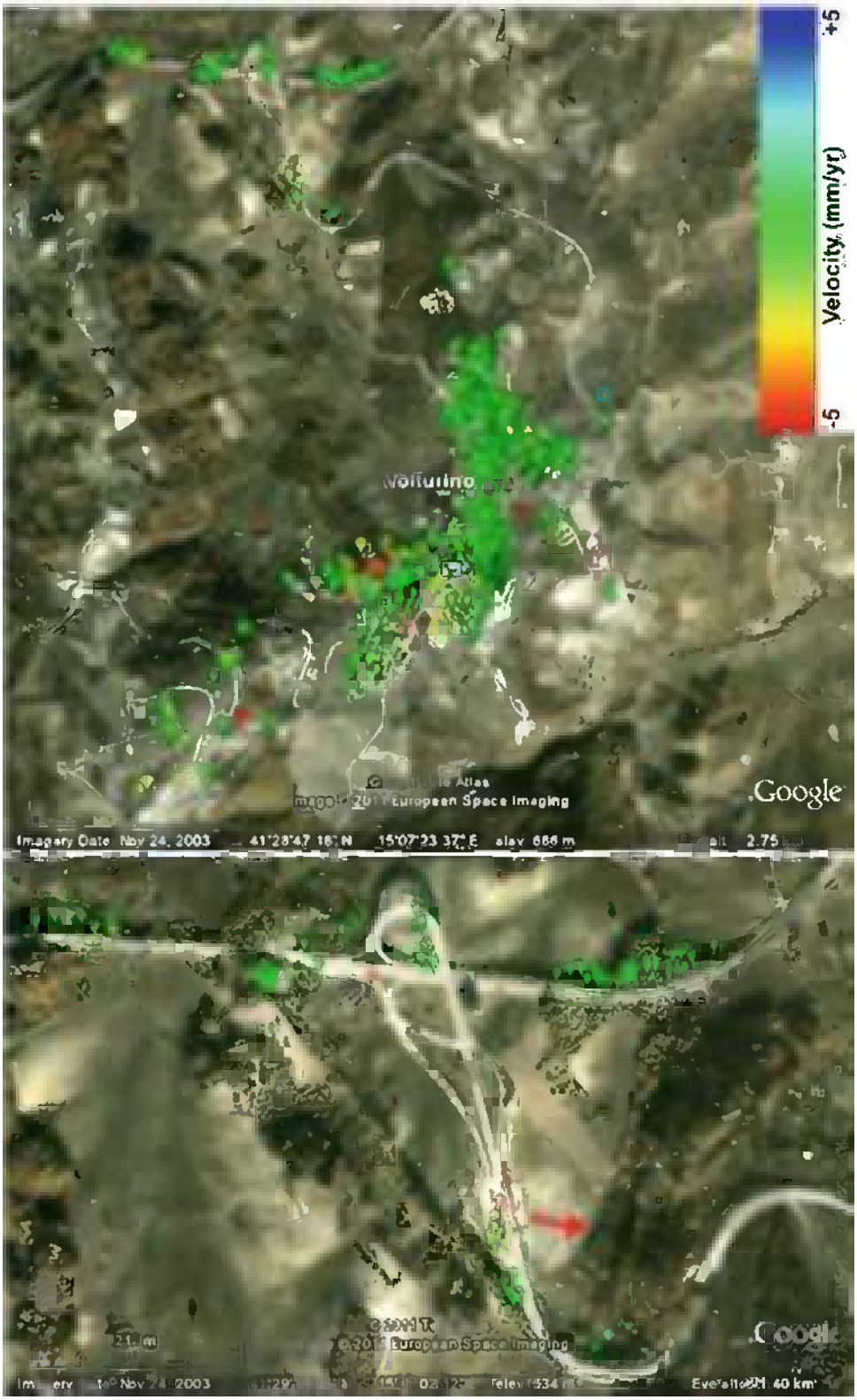


Fig. 3 Distribution and average LOS velocity of PS (marked by *colour dots*) in the Volturino area (ENVISAT ascending data). LOS velocity is saturated at ±5 mm/year for visualization purposes. Background optical image is from GoogleEarth™. (*Upper figure*) Overview of the urban and peri-urban area; (*Lower figure*) Close-up of the road network north of Volturino showing isolated moving PS indicative of the presence of very slow (few mm/year) deformations locally affecting the road infrastructure. One moving PS coincides with the site of a slope failure that damaged the road in 2003 (mass movement direction is indicated by a *red arrow*)

Town of Casalvecchio di Puglia

Also in this case both ENVISAT and TSX PSI results were obtained. A comparison of the C-band and X-band displacement maps (Fig. 5) shows very good agreement. In particular, the same sites of instability are identified in the north-eastern periphery of the town. Significantly, Zezza et al. (1994) recognized that this same peri-urban area has been involved in an old, large slope movement. Hence its current susceptibility to ground instability is not surprising.

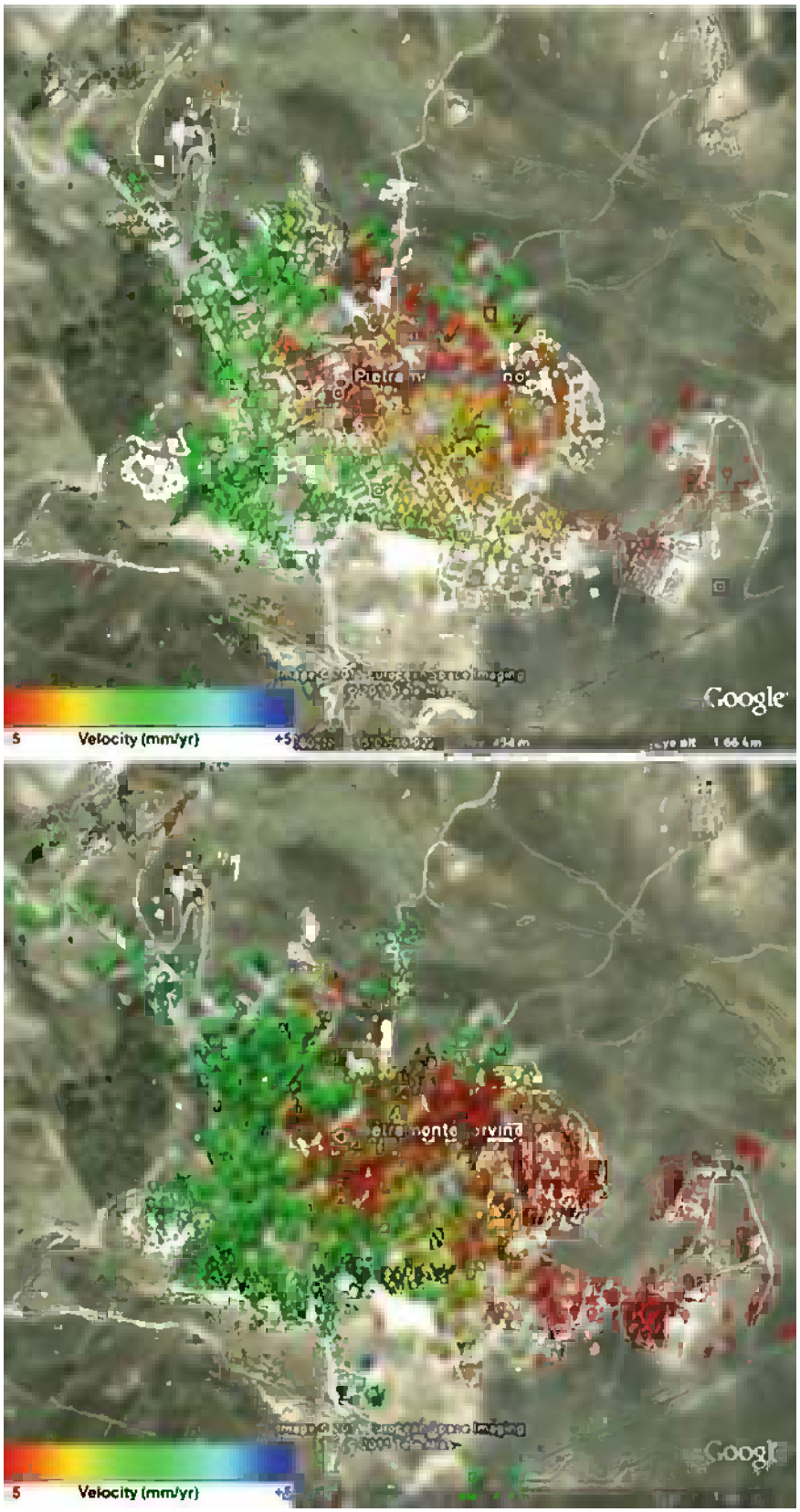


Fig. 4 Distribution and average LOS velocity of PS (marked by *color dots*) in Pietra Montecorvino. (*Upper figure*) ENVISAT ascending data; (*Lower figure*) TSX ascending data. LOS velocity is saturated at ±5 mm/year for visualization purposes. Background optical image is from GoogleEarth™. Note that results based on C-band and X-band data appear very similar, although the displacement map based on TSX data provides more information thanks to the higher density of PS; this well visible especially along the town peripheries

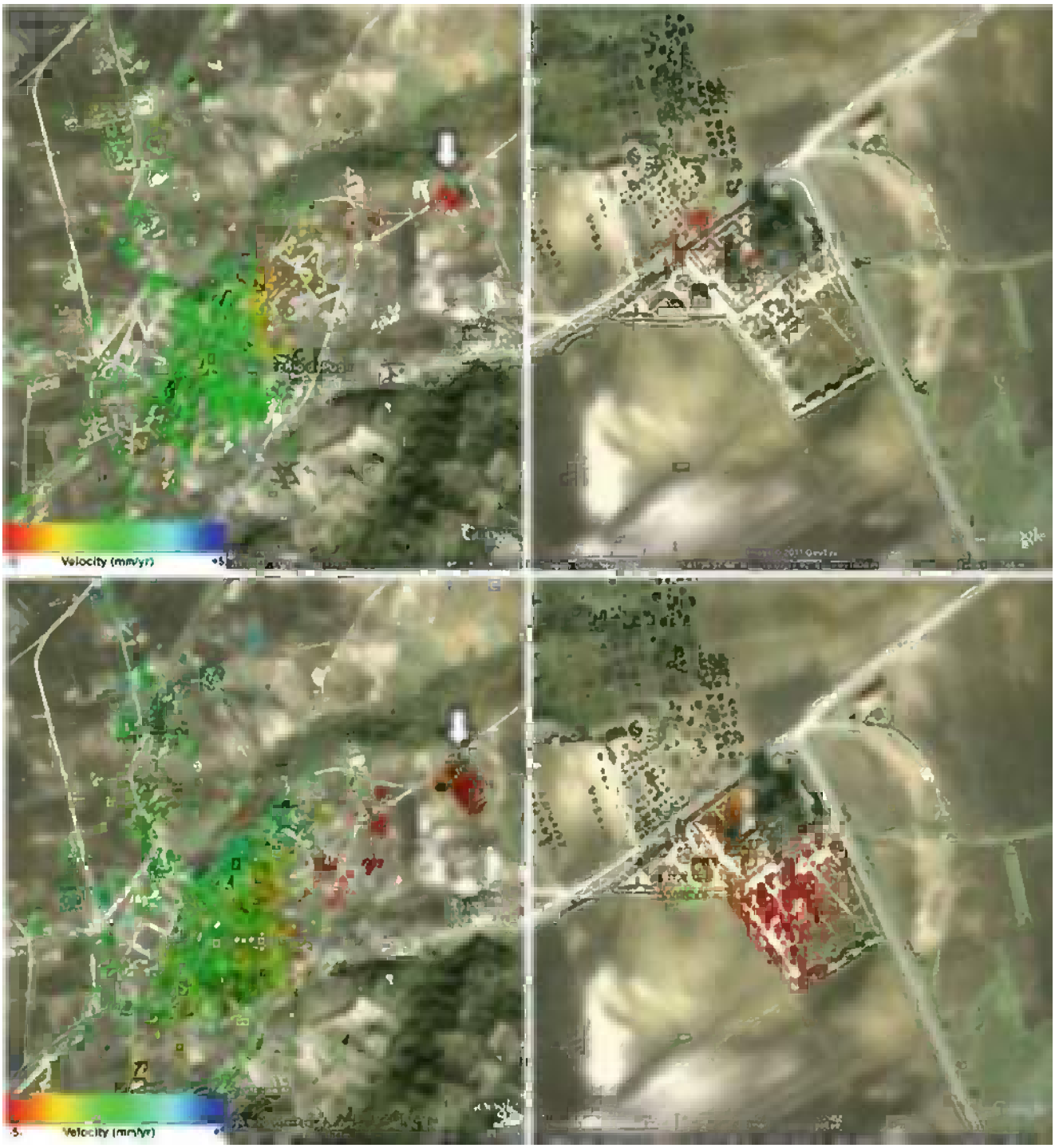


Fig. 5 Distribution and average line of sight (LOS) velocity of radar targets (PS marked by *color dots*) in Casalvecchio di Puglia. (*Upper figures*) ENVISAT ascending data; (*Lower figures*) TSX ascending data. *White arrows* indicate the cemetery area, whose close-ups are shown in the right figures. LOS velocity is saturated at ±5 mm/year for visualization purposes. Background optical image is from GoogleEarth™. Note that, in terms of the distinction between stable and deforming areas, the displacement maps based on ENVISAT and TSX data are closely comparable. However, the density of X-band PS is considerably higher – this is better visible in the peri-urban area and on the close-up figures

The case of Casalvecchio di Puglia is also of interest, because it demonstrates that the density of the PS obtained from X-band data is much higher with respect to that of C-band PS (Fig. 5). Again, this situation can be better appreciated in the peripheries of the town.

In particular, a quick visual examination of the cemetery area, located to the ENE of the town (Fig. 5), shows that the density of X-band PS is approximately four times greater with respect to that of C-band PS.

Discussion and Conclusions

The results of this work show that PSI can be profitably used to investigate the urban and peri-urban areas in the Apennine mountains affected by slope instability problems. Thanks to the finer spatial resolution, X-band PSI applications are very promising for monitoring single man-made structures, as well as areas where C-band PS density is low. This is the case of the scarcely urbanised Daunia region, where the results obtained indicate that more man-made and natural targets behave as PS in X-band than in C-band.

Moreover, thanks to the higher resolution in X-band, it is possible to infer reliable estimates of the displacement rates with a number of SAR scenes lower than in the C-band case within the same time span, or by using more images acquired in a shorter period. Also, with shorter wavelengths in X-band, the sensitivity to LOS displacements is increased (Bovenga et al. 2010) together with the capability of detecting very slow movements (as often seems to be the case of pre- and post-failure movements related to landslides occurring in clay-rich materials).

Finally, as stressed in earlier studies (e.g. Bovenga et al. 2006; Colesanti and Wasowski 2006), the interpretation of the exact origin of very slow displacements detected on urbanized slopes by radar interferometry is not straightforward. A detailed field-based evaluation of PSI results will usually be needed before attempting to use them for landslide hazard zonation and warning purposes.

Acknowledgments Work supported by Puglia Region in the framework of the project "FRANE PUGLIA – Rilevamento di deformazioni al suolo con tecniche satellitari avanzate". ENVISAT data are provided by ESA under CAT-1 project ID 2653. TerraSAR-X data are provided by DLR under TerraSAR-X General AO Project ID MTH0432.

References

Bovenga F, Refice A, Nutricato R, Guerriero L, Chiaradia MT (2004) SPINUA: a flexible processing chain for ERS/ENVISAT long term Interferometry. In: Proceedings of ESA-ENVISAT symposium, Salzburg, 6–10 Sept 2004

Bovenga F, Nutricato R, Refice A, Wasowski J (2006) Application of multi-temporal differential interferometry to slope instability detection in urban/peri-urban areas. Eng Geol. Special issue on remote sensing and ground-based geophysical techniques for recognition, characterisation and monitoring of unstable slopes, 88(3–4):218–239

Bovenga F, Nitti D O, Refice A, Nutricato R, Chiaradia MT (2010) Multi-temporal DInSAR analysis with X-band high-resolution SAR data: examples and potential. In: Proceedings of SPIE remote sensing, Centre de Congrès Pierre Baudis, Toulouse, 20–23 Sept 2010

Colesanti C, Wasowski J (2006) Investigating landslides with space-borne Synthetic Aperture Radar (SAR) interferometry. Eng Geol 88:173–199

Ferretti A, Prati C, Rocca F (2001) Permanent scatterers in SAR interferometry. IEEE Transactions on Geoscience and Remote Sensing, vol. 39(1):8–20

Mossa S, Capolongo D, Pennetta L, Wasowski J (2005) A GIS-based assessment of landsliding in the Daunia Apennines, southern Italy. In: Proceedings of the international conference "Mass movement hazard in various environments", Cracow, 20–21 Oct 2005, pp 86–91

Lollino P, Elia G, Cotecchia F, Mitaritonna G (2010) Analysis of landslide reactivation in Daunia clay slopes by means of limit equilibrium and FEM methods. In: Proceedings of Geo-Florida 2010, West Palm Beach, 20–24 Feb 2010, pp 3155–3164

Magliulo P, Di Lisio A, Russo F, Zelano A (2008) Geomorphology and landslide susceptibility assessment using GIS and bivariate statistics: a case study in southern Italy. Nat Hazards 47(3):411–435

Wasowski J, Bovenga F, Florio N, Gigante G (2008a) PSInSAR for the investigating of unstable slopes and landslides. In: Proceedings of the first World landslide forum, Tokyo, 18–21 Nov 2008, pp 653–655

Wasowski J, Casarano D, Bovenga F, Refice A, Conte D, Nutricato R, Nitti DO (2008b) Landslide-prone towns in Daunia (Italy): PS-interferometry based investigation. In: Chen et al. (eds) Proceedings of the 10th international symposium on landslides and engineered slopes, Xi'an, pp 513–518

Wasowski J, Lamanna C, Casarano D (2010a) Influence of land-use change and precipitation patterns on landslide activity in the Daunia Apennines, Italy. Q J Eng Geol Hydrogeol 43:1–17

Wasowski J, Lamanna C, Casarano D (2010b) Mapping mid-slope road landslides and instability factors with high resolution satellite imagery. In: Proceedings of 11th Congress of the IAEG, Auckland, 5–10 Sept 2010, pp 2563–2570

Zezza F, Merenda L, Bruno G, Crescenzi E, Iovine G (1994) Condizioni di instabilità e rischio da frana nei comuni dell'Appennino Dauno Pugliese. Geologia Applicata e Idrogeologia 29:77–141



Landslide 3D Surface Deformation Model Obtained Via RTS Measurements

Andrea Manconi, Paolo Allasia, Daniele Giordan, Marco Baldo, Giorgio Lollino, Angelo Corazza, and Vincenzo Albanese

Abstract

We present a new procedure that allows retrieving in near-real-time 3D surface deformation models starting from data acquired via Robotized Total Stations (RTS). The RTS measurements are first pre-processed and then implemented on 3D maps that include vector arrows representative of the intensities and of the real directions of motion in a given system of coordinates. The 3D surface deformation models are finally overlain on a DTM and/or on an updated picture of the monitored area. We discuss an example of application to an active large-scale landslide located in the area of Montaguto (southern Italy, ca. 100 km northeast from Naples). In this complex landslide scenario, the use of 3D representations of the surface deformation simplified the understanding of the evolution of the landslide phenomenon and received positive feedbacks from operators of the Italian Civil Protection Department.

Keywords

Near-real-time landslide monitoring • Surface deformation • Robotized Total Stations

Introduction

The identification and interpretation of surface displacements plays an important role in many landslide scenarios (Liu et al. 2004; Rizzo and Leggeri 2004). In these contexts, the use of Robotized Total Stations (RTS) is frequently preferred due to its relatively simple installation, its straightforward operational use and data processing modalities, as well as its limited costs compared with new-generation instruments employed for topographic surveys. By using RTS is possible to retrieve changes of the x, y and z coordinates of a set of targets (usually optical prisms) with sub-centimetre accuracies. Moreover, depending on the number of prisms installed and on the availability of power supply, RTS may allow following the temporal evolution of the surface displacements of a landslide in near-real-time.

In RTS surveys, measurements occur at the point targets only, thus the spatial representation of surface displacements is intrinsically limited. In order to overcome this limitation, especially when the landslide phenomenon presents complex spatial heterogeneities (e.g. areas with different directions and velocities of motion), it is envisaged an accurate planning of the network and an increase of the prisms number installed in the monitored area. Depending on the complexity of the phenomenon, the understanding of its kinematic with the classical visualization of RTS displacement time series might be very difficult (see example in Fig. 2b–c). In addition, since the surface displacement monitoring is frequently aimed also at guaranteeing safety conditions of people and/or infrastructures, many operators of different scientific and technical backgrounds collaborate. Therefore, a straightforward and clear representation of the surface displacement evolution in near-real-time is necessary in order to support authorities and decision makers.

A. Manconi • P. Allasia • D. Giordan (✉) • M. Baldo • G. Lollino
CNR-IRPI, Gruppo di Geo-Monitoraggio, Strada delle Cacce 73, Torino 10135, Italy
e-mail: daniele.giordan@irpi.cnr.it

A. Corazza • V. Albanese
Dipartimento della Protezione Civile, Rischi Idrogeologici e Antropici, Rome, Italy

C. Margottini et al. (eds.), *Landslide Science and Practice*, Vol. 2,
DOI 10.1007/978-3-642-31445-2_56, © Springer-Verlag Berlin Heidelberg 2013

In this work, we present a procedure that allows retrieving in near-real-time three-dimensional models of the surface displacements by using RTS measurements. After the acquisition step, the measurements are opportunely pre-processed and then implemented in 3D surface deformation maps, including also vector arrows representative of their intensity and direction of motion. The procedure may consider different interpolation algorithms and includes also the possibility to take into account as input a set of constraints, which may involve geological and/or structural discontinuities. In the following, we first describe the procedure and then we present the results of a real application to a large-scale landslide located in the area of Montaguto (southern Italy, ca. 100 km northeast from Naples).

Methods

RTS are modern theodolites coupled with precise distance meters that can measure automatically the position of a set of artificial targets, usually optical prisms. RTS measure three parameters: a vertical angle (Vz), a horizontal angle (Hz) and the distance (D) to the prism. By measuring Vz, Hz and D, the prism's three-dimensional coordinates x, y and z can be derived by straightforward trigonometric equations. In Fig. 1, we outline the main steps considered for a standard RTS survey after a proper installation of the station, of the relative reference points (at locations hypothesized relatively stable with respect to the targets) and of the prisms at the observation targets. Every measurement cycle is characterized by the acquisition of the Vz, Hz and D at a certain date and time. The acquisitions are sent to a computer (that might be directly connected to the RTS or located remotely) where specific software facilities treat the raw data and calculate the actual x, y, and z coordinates of the target. In addition, by checking the relative positions of reference targets the RTS measurements are validated. The results of repeated acquisitions can be considered to build-up time series that, depending on the monitoring scenario, can be either the displacements in the three directions or their resultants in a two or three dimensional context and/or eventually the associated velocities in a specific period of time. Usually, the results are presented in the form of 2D graphs that are updated at every new measurement cycle (see Fig. 2b–c).

As explained in the introduction, in certain cases these plots might be of difficult reading and interpretation, especially when the number of prisms increases and people of different backgrounds are involved in the monitored area (e.g. scientists, authorities, civil protection operators, decision makers, etc.) Thus, we propose an alternative visualization for a correct interpretation and a subsequent divulgation of the surface displacement evolution. We introduce an

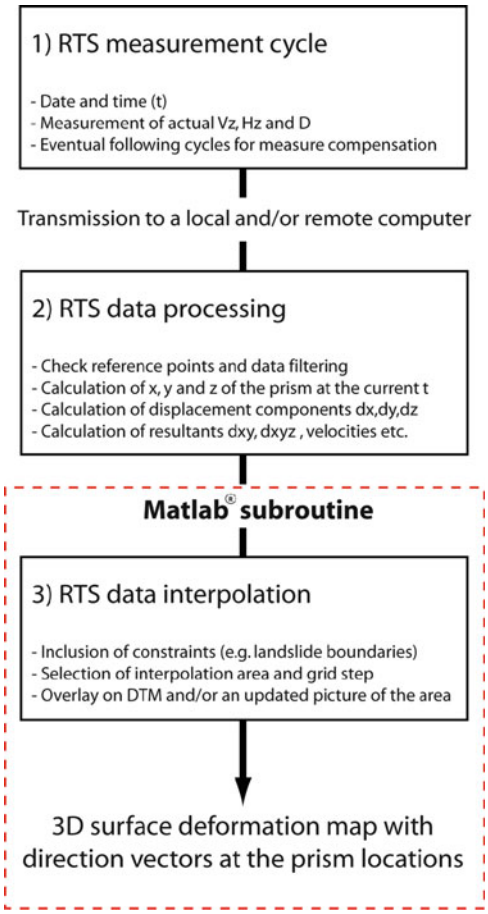


Fig. 1 Flow-chart of the procedure implemented for obtaining 3D surface deformation models starting from RTS point measurements

additional step that allows to complete the standard representation of the results with a three dimensional representation of the surface deformation. We implemented a subroutine in Matlab®, a high-level programming language. The software allows for using a number of interpolation algorithms and (e.g. nearest neighbour, bilinear, triangular, see D'Errico 2006) and has several built-in features that facilitate the RTS data import as well as the final graphical representation output. The selection of the spatial extension of the interpolation field as well as the interpolation grid step can be modified depending on the peculiarities of the monitored area. Moreover, information on the boundary and/or structural discontinuities present in the monitored area can be included as input and then passed to the interpolation subroutine as point coordinates with an associated known displacement (e.g. zero). The resulting deformation map consists in a representation of a 3D surface, where the colour scale can be either relevant to the displacements with respect to the previous measurement cycle, the deformation rate or the acceleration in an arbitrary time interval depending on the available data (e.g. day, month or year). Moreover, by considering that the RTS measure displacements in the three

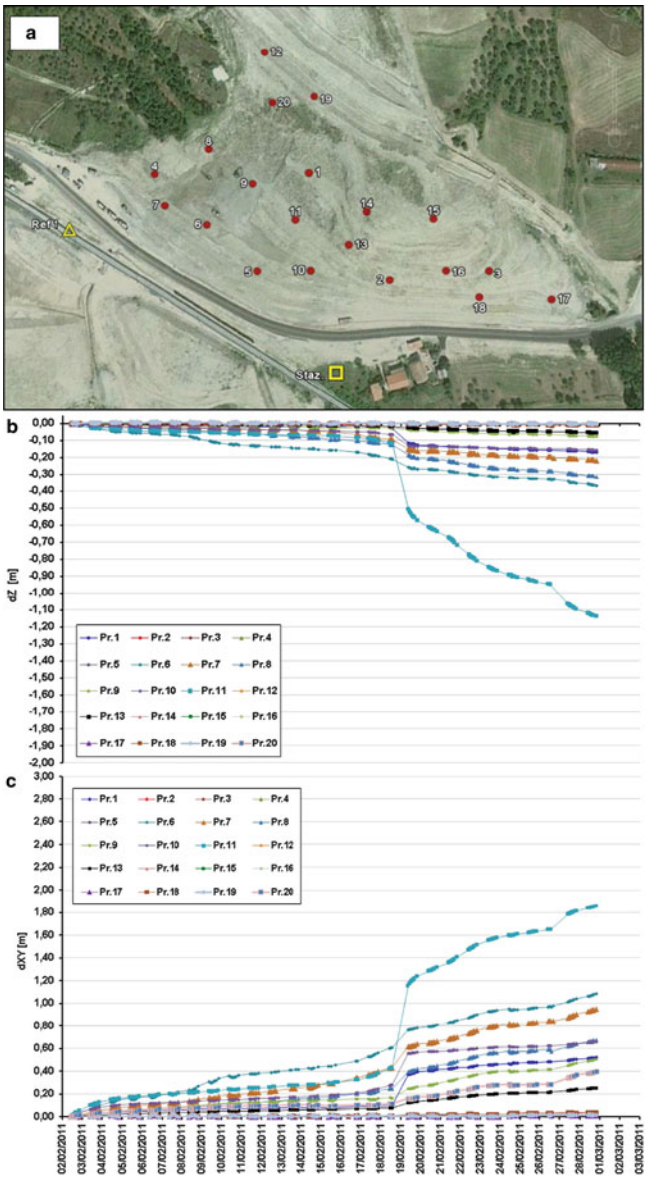


Fig. 2 Monitoring displacements at the Montaguto landslide's toe. (**a**) Setup of the RTS network overlain on a Google Earth map of the area (GeoEye Image, August 20, 2010); STAZ is the location of the RTS. Red dots are the locations of the prisms monitored *White arrows* indicate the two preferential direction of motion revealed in the field; (**b**) and (**c**) show a standard representation of the displacement time series for the vertical (dz) and the planar (dxy) components, respectively

directions at a certain time, we associate to the prisms also vector arrows representative of the real direction of motion in the considered system of coordinates. In addition, the dimension of the arrows, opportunely scaled, can represent also the real intensity of the displacement vectors.

In landslide hazard assessment, the understanding of the evolution of the surface displacements with respect to the actual situation of the topographic relief is crucial. Thus, in many cases the association of the RTS monitoring data to a relatively updated Digital Terrain Model (DTM) of the area represents a convenient approach. For this reason, our procedure allows also the inclusion of 3D surface deformation model (resulting from the interpolation) over an available DTM of the monitored area. This step is performed by referencing the RTS network in a convenient geographic system of coordinates (e.g. UTM-WGS84). Moreover, we also implemented the possibility to overlay the 3D surface deformation maps on a picture of the monitored area. This procedure is possible by knowing the coordinates of the camera in the considered system of coordinates (either local or geographic) and some additional camera parameters (e.g., tilting during the shot, viewing angle, zoom, etc.). The advantage of this second visualization is mainly that a new picture can be easily taken from the same position and

updated with higher frequencies with respect to a DTM of the area. In addition, this visualization is particularly convenient in cases of landslides that present rapid surface modifications of the monitored area.

The procedure described above can be applied in near-real-time after the conclusion of a RTS measurement cycle and data processing/filtering (steps 1 and 2 in Fig. 1). The subroutine has been compiled (by considering the Matlab® Compiler facilities) and treated as a stand-alone executable (e.g. a.exe file under a Windows operative system). This means that the local and/or remote computer used for the RTS survey does not need to have installed the Matlab® software on board and that all settings for the interpolation and for the visualization can be easily changed and/or adjusted via an external input file in text format.

Application: The Montaguto Landslide

In the area of Montaguto (Southern Italy, ca. 100 km north-east from Naples) a large-scale earthflow is active since 2006. In the spring of 2010 the landslide's toe reached the bottom of the valley with a velocity of several meters/day, damaging the Naples – Bari railway and the main road linking all the towns of the valley. During such an emergency phase, the Italian Civil Protection Department (DPC) started work to mitigate the effects of the landslide and restore the traffic and train circulation (Italian Civil Protection Department 2011). In this scenario, we provided support to the DPC for the monitoring activities mainly building a RTS network aimed at ensuring the safety conditions for the workers involved in the risk mitigation (Giordan et al. manuscript submitted). One of the peculiarities evidenced in our first observations at the Montaguto landslide's toe was that the surface displacements presented severe spatial heterogeneities, in terms of both velocities and of directions of motion. The two arrows in Fig. 2a indicate the preferential directions of the landslide material evidenced during the first observation period, when the landslide surface displacements reached velocities that were in the order of several meters/day. The western sector of the landslide's toe was characterized by very high surface displacement rates especially in its central portions. The dominating directions of motion were south-southwest. On the other hand, the eastern sector presented surface displacement rates that were also moderately high (ca. 1 m/day), but after the April 2010 paroxysm phase velocities decreased substantially. In this sector, the direction of motion was mostly southeast. In addition, the monitoring scenario was locally affected by the DPC activities aimed at the restoration of the viability of the road.

In Fig. 2a, we show the setup of the RTS network installed at the Montaguto landslide's toe. The RTS is a Leica TCA 2003 and monitors 20 prisms (+1 reference point), providing a good coverage of the overall landslide's toe. The RTS is powered via solar panels and is controlled via a GSM system to switch on/off the acquisition. The RTS measurements are transferred to a computer located about 1 km distance via radio modem. At this location, the data is processed and subsequently the results are sent to a remote server (located in Turin at CNR IRPI), where the displacement time series are analysed, eventually corrected by checking the relative position of reference points and/or filtered. The measurement revisit time is of 1 h and the duration of every measurement cycle is less than 10 min. The results of this continuous monitoring are sent daily to the DPC and authorities involved in the mitigation management. In Fig. 2b, c we show respectively the vertical (dz) and planar (dxy) components of displacement as time series, both relevant to February 2011. With an accurate inspection of Fig. 2, an expert RTS user might identify clusters of prisms that share homogeneous behaviour and also infer the principal directions of motion. However, the landslide kinematic is not unambiguously clear just looking at the displacement time series. In addition, the scenario resulting from these time series plots is certainly not clear to non-specialists and to people with different backgrounds, not used to handle RTS displacement results.

In Fig. 3 we show the results of the application of our procedure described in the previous sections and relevant to the same dataset presented in Fig. 2. Figure 3a shows the application of the interpolation subroutine by overlain on a DTM (1×1 m resolution) of the Montaguto landslide. The latter has been generated with data acquired via an airborne LiDAR survey performed in June 2010 (courtesy of DPC). On the other hand, Fig. 3b depicts the surface displacements overlain on a picture of the Montaguto landslide taken in November 2010.

In both maps, the yellow-red colour scale indicates the intensity of the deformation (dxyz) relative to the month of February 2011, interpolated over a selected area with a grid of 1×1 m.

The landslide boundaries, as well as the areas outside from the network (e.g. the road) have been set as discontinuities with zero displacement over time. The dxyz intensity is also evidenced at the prisms location by vector arrows (see scale in Fig. 3b). The arrows also indicate the real direction of motion in the system of coordinates (UTM-WGS84). Visual inspection of Fig. 3 provides an immediately clear scenario: the portion of the western sector close to prism 11 presents the largest displacements (>2 m) with a strong vertical component. Moreover, the landslide front (monitored by prisms 5, 6, 7 and 10) is interested by

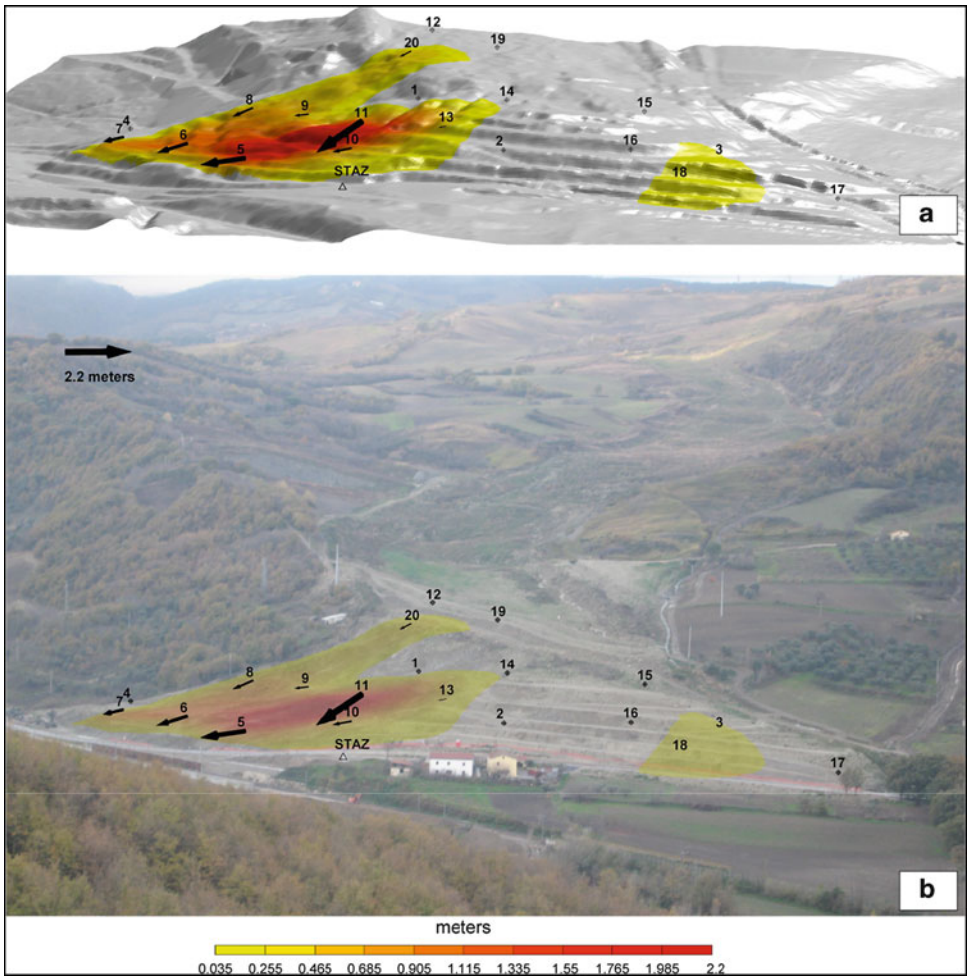


Fig. 3 3D representation of the surface displacements measured at the Montaguto landslide relevant to February 2011. STAZ is the location of the RTS. *Arrows* represent the intensity (note scale in Fig. 2b *top left*) and direction of the displacements prism in the corresponding time interval; (**a**) 3D deformation overlain on a DTM (airborne LiDAR survey June, 2010) of the monitored area; (**b**) 3D deformation overlain on a picture of the monitored area taken in November 2011

displacements in the order of 0.6–1 m with a dominant south-southwest component. In addition, a retrogressive mechanism interested the areas monitored by the prism 20, which present displacements up to 0.5 m.

Furthermore, with the surface displacement representation shown in Fig. 3 the sharp gradient towards the eastern sector is directly clear. In fact, the displacement values are below a pre-selected minimum threshold; however, there is a small area, monitored by prisms 3 and 18, where local displacements between 3.5 and 25.5 cm are evidenced. These displacements were likely triggered by the anthropic remedial activities, since during the herein analysed period of observation the DPC restoration works were mostly concentrated in this zone. For brevity, in this paper we presented only one map relative to the total deformation measured in the month of February 2011. However, we remind that similar maps can be produced in near-real-time after every RTS measurement cycle. In the case of the monitoring network described above, the time required from the beginning of the RTS measurement cycle up to the availability of a new 3D surface deformation map is about 10 min.

Conclusions

In this paper, we presented a new procedure that allows passing from the classical representation of displacements measured via RTS to a 3D visualization of the surface deformation. We described the main characteristics of the subroutine that interpolates the values measured at point targets over a selected region of interest and with a predefined grid step. Moreover, the procedure allows for the implementation of discontinuities/constraints and the 3D surface deformation map can be directly overlain on a DTM and/or an

updated picture of the monitored area, enhancing the possibilities of exploitation of the information contained in the RTS measurement.

We have shown an application to a landslide scenario: the Montaguto landslide. In this particular case, we exploited the data measured via a Leica TCA 2003 that monitors the evolution of the surface displacements at 20-point targets installed at the landslide's toe. The application of our procedure allows gaining at every measurement cycle (1 h) a straightforward 3D representation of the surface deformation in near-real-time (ca. 10 min). Thus, the use of our tool simplified not only the understanding of the evolution of the landslide phenomenon, but also the communication of the actual situation of the surface motions to DPC operators involved in the remedial activities.

We remark that the number of prisms, their location over the monitored area as well as the selection of the boundary constraints and/or the presence of discontinuities in the deformation field are very important parameters for a correct representation of a realistic 3D surface deformation map starting from point measurements. These factors have to be accurately evaluated while planning the RTS network and require a good a priori knowledge of the monitored phenomenon in order to avoid misleading results.

We conclude pointing out that the herein presented procedure has several potential applications not only in landslide scenarios but also in all contexts where the use of RTS for monitoring extended areas is considered (e.g. open pit mines, monitoring of infrastructures, etc.).

Acknowledgments This project was partially fund by Italian DPC. AM is partially fund by the Piedmont Regional Government (L.R. n. 4/2006 art. 2A, 3-4). Matlab® is available at www.mathworks.com.

References

D'Errico J (2006) Surface fitting using gridfit (http://www.mathworks.com/matlabcentral/fileexchange/8998), MATLAB® Central File Exchange. Retrieved May 18 2006

Italian Civil Protection Department (2011) Hydrogeological risk current emergencies, The Montaguto Landslide, http://www.protezionecivile.gov.it/jcms/en/montaguto_idrogeologico.wp?request_locale=en

Giordan D, Allasia P, Manconi A, Baldo M, Lollino G, Santangelo M, Cardinali M, Guzzetti F. Morphological evolution of a large earthflow: the Montaguto landslide, southern Italy, manuscript submitted

Liu DA, Yang ZF, Tang CH, Wang J, Liu Y (2004) An automatic monitoring system for the shiplock slope of Wuqiangxi Hydropower Station. Eng Geol 76:79–91

Rizzo V, Leggeri M (2004) Slope instability and sagging reactivation at Maratea (Potenza, Basilicata, Italy). Eng Geol 71:181–198



Application of SqueeSAR™ to the Characterization of Deep Seated Gravitational Slope Deformations: The Berceto Case Study (Parma, Italy)

Andrea Tamburini, Sara Del Conte, Gianfranco Larini, Luigi Lopardo, Claudio Malaguti, and Paolo Vescovi

Abstract

SqueeSAR™ SAR interferometry is today one of the most advanced technologies for surface deformation monitoring capable of overcoming most of the limitations of conventional differential radar interferometry. It exploits long temporal series of satellite radar data, acquired over the same area of interest at different times, to identify "natural radar targets" where very precise displacement information can be retrieved.

Thanks to its capability to detect millimetre level displacements over long periods and large areas, SqueeSAR™ analysis can be considered complementary to conventional geological and geomorphological studies in landslide detection and monitoring, supporting the performance of landslide inventories at regional scale. The availability of surface displacement time series for all the radar benchmarks identified makes it also possible to change the scale of the analysis from regional to local, allowing an in depth study of the evolution of single instability phenomena, supporting the design of traditional monitoring networks, and even verifying the efficiency of remedial works.

The above approach was applied to study the Berceto deep seated gravitational slope deformation (DSGSD) (Parma, Italy) by processing satellite SAR data relevant to the 1992–2000 time span. By combining results obtained in both ascending and descending acquisition geometries, it was possible to retrieve both vertical and E-W components of surface displacements.

A correlation with the results of the geophysical investigations will be proposed, with a preliminary interpretation of the surface displacement trends in the upper part of the slope.

Keywords

InSAR • Permanent scatterers • DGSD • Berceto

Introduction

The Berceto village is located near the top of an unstable slope, characterized by periodical reactivations often following intense meteorological events. These reactivations have been responsible for damages to buildings and infrastructures since a long time. The Berceto unstable slope is reported in the Italian Landslide Inventory (IFFI) Project, partly funded by ISPRA (Italian Institute for Environmental Protection and Research).

Geophysical surveys and borehole investigations have been recently carried out in order to obtain subsurface data

A. Tamburini (✉) • S. Del Conte
Tele-Rilevamento Europa – T.R.E. S.r.l., Ripa di Porta Ticinese 79, Milan 20149, Italy
e-mail: andrea.tamburini@treuropa.com

G. Larini • L. Lopardo • C. Malaguti
Regione Emilia Romagna, Servizio Tecnico Bacini degli Affluenti del Po (STBPO). via Garibaldi 75, Parma 43121, Italy

P. Vescovi
Dipartimento Scienze della Terra, Università di Parma. Campus Universitario, Viale G.P. Usberti 157/A, Parma 43124, Italy

C. Margottini et al. (eds.), *Landslide Science and Practice*, Vol. 2,
DOI 10.1007/978-3-642-31445-2_57, © Springer-Verlag Berlin Heidelberg 2013

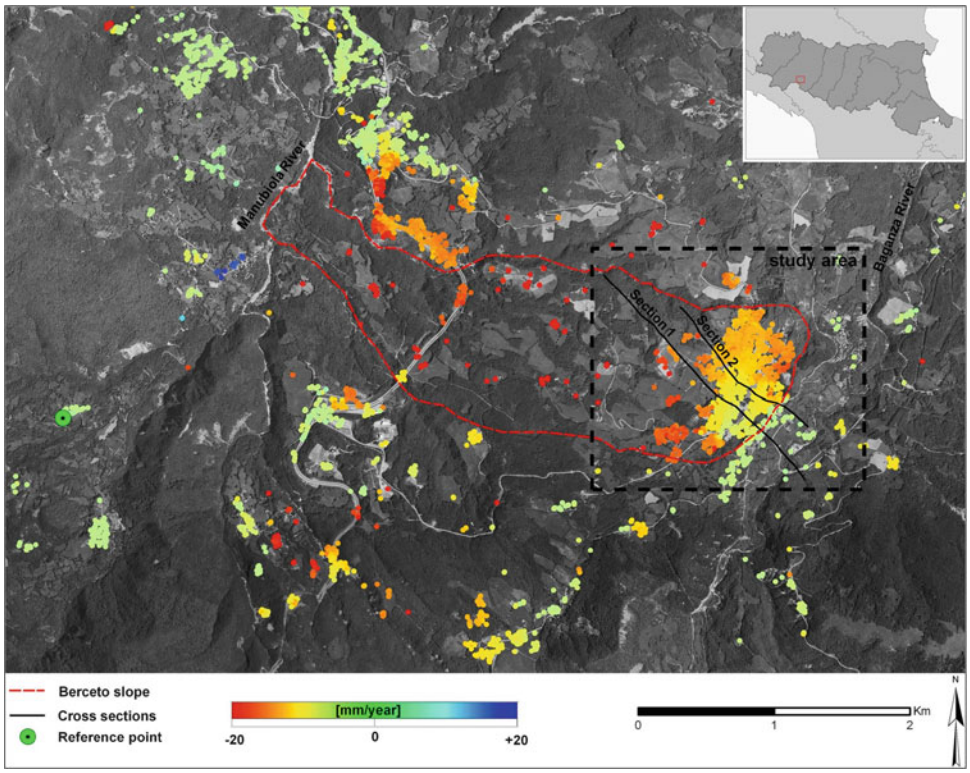


Fig. 1 Location map of the study area, with the average yearly surface displacement velocity measured along the satellite LOS

enabling a better understanding of the slope behaviour. Eight DC resistivity tomography profiles were recorded in the upper part of the slope and continuous-core boreholes were drilled.

At the end of last year, satellite radar data have been processed with SqueeSAR™ technique, based on an algorithm developed by Politecnico di Milano (POLIMI) and licensed exclusively to TRE, which enables to overcome the errors introduced into signal phase values by atmospheric artefacts, which typically affect the traditional interferometric approach. By exploiting the ESA (European Space Agency) ERS1-2 archives, surface displacement data relevant to 1992–2000 period were obtained.

An integrated approach based on the correlation among the above data, aimed at assessing the risk related to the landslide evolution, is still in progress; some preliminary results will be presented in this paper.

Geological Setting

The Berceto area is located along a regional SW-NE tectonic discontinuity, separating two different sectors of the Apennine chain: the Ligurian-Emilian to the NW and the Tuscan-Emilian to the SE. In the NW Apennine segment thick External Ligurian Units are preserved; in the SE segment, more exhumated by tectonic uplift, the underlying foredeep units are exposed (Bernini et al. 1997). This tectonic uplift took place during Pleistocene (Argnani et al. 2003), accompanied by extensional NW-SE faults on the Tyrrhenian side of the Apennines (Bernini and Papani 2002).

In the Berceto area, close to the divide between the Manubiola and Baganza rivers (Fig. 1), the transversal deformation band produced SW-NE sinistral strike-slip faults, NNE-SSW extensional faults, and superimposed NW-SE normal faults (Bertoldi et al. 2004). The stack of Ligurian Units largely outcrops (Vescovi 2002). The overturned M.Caio Flysch, affected by SW-NE high-angle transpressive faults is tectonically overlain by Shaly Chaotic Complex, consisting of black and grey shale, with pervasive development of scaly fabric (Pini 1999), often associated with ophiolitic bodies. The Shaly Chaotic Complex is overthrust by the Scabiazza Sandstone, about 100 m thick, stratigraphically overlying the Mt. Rizzone Shale and Limestone, outcropping in excavations located near the village (Bertoldi et al. 2004). The Scabiazza Sandstone consists of a turbidite sequence showing thin-bedded shaly and marly lithofacies, alternated by medium-bedded sandstone lithofacies. This unit was affected by S-verging recumbent folds and gently-dipping detachment faults, crossed by high-angle fault systems: the NE-trending sinistral transpressive faults, the NNE-SSW normal faults and the NW-SE late normal faults.

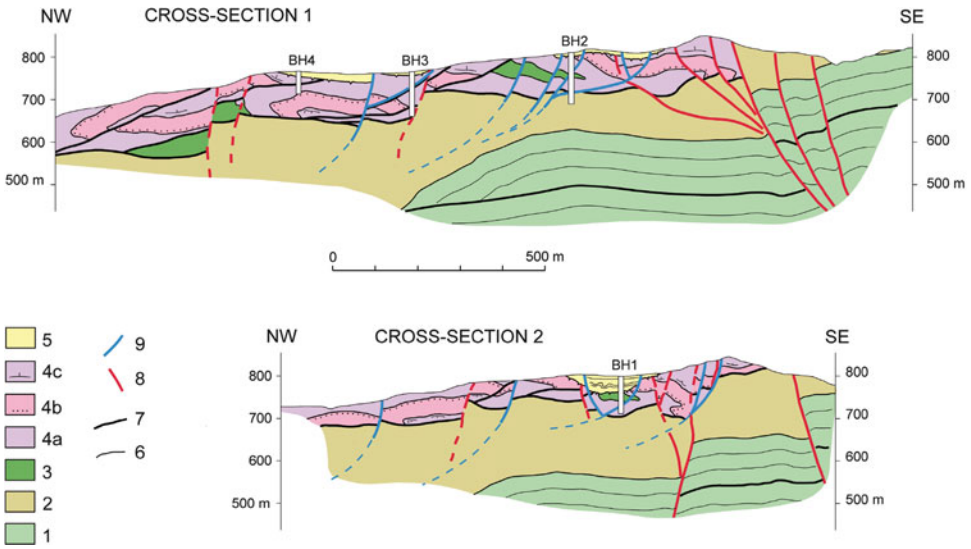


Fig. 2 Geological cross sections 1 and 2. Key to symbols: *1* Mt. Caio Flysch (thick-bedded marlstones), *2* Shaly Chaotic Complex (with ophiolite breccias), *3* Mt. Rizzone Shale and Limestone, *4* Scabiazza Sandstone (*4a* Thin-bedded shale and sandstone lithofacies, *4b* Medium-bedded sandstone lithofacies, *4c* Thin-bedded marls and sandstone lithofacies), *5* Late Pleistocene Lacustrine deposits, *6* stratigraphic boundary, *7* overthrust and low-angle detachment faults, *8* high-angle faults (shifted by gravity where hatched), *9* gravitational faults (inferred where hatched)

This structural framework and the lithological characteristics of the Scabiazza Sandstone are considered responsible for the development of a trench at the top of the Berceto slope.

A 50 m borehole drilled in the village in 2001 found Upper Pleistocene laminated lacustrine sediments about 25 m thick (radiocarbon dating 29,620 ± 290 14C yr B.P.) deposited in the trench (Unit 5 in Bertoldi et al. 2004). The lacustrine sediments overlay a sedimentary breccia containing very weathered clasts of sandstone in silty matrix (Unit 6 in Bertoldi et al. 2004) and passing up into peat (radiocarbon dating 11,150 ± 70 14C yr B.P.). The lacustrine sequence was affected by folding and exhibits shear surfaces, testifying both compressive and, likely, extensive deformation occurred during the Late Pleistocene gravity-induced deformation of the Berceto slope; these deformative phases may have produced either a rotational rockslide (Bertoldi et al. 2004) or sliding over a shear surface gently dipping towards NW (Corsini et al. 2006).

Surface Displacements

In the early 90s the first data on Earth's surface provided by Synthetic Aperture Radar (SAR) mounted on satellites, have imparted a significant breakthrough in the field of Earth Observation. Since then new unthinkable perspectives have been gained on surface deformation phenomena analysis and monitoring. The advanced survey techniques of Earth's superficial displacements from satellite are known as SAR Interferometry (InSAR) (Fig. 2).

SAR data processing techniques have been developed and improved by Radar Group of Electronics Department of the Politecnico of Milano (POLIMI) and after by Tele-Rilevamento Europa (TRE), first spin-off of POLIMI. TRE was granted exclusive license called Permanent Scatterers (PS) technique, or PSInSAR™ (Ferretti et al. 2001). The SqueeSAR™ technique (Ferretti et al. 2011) is a second generation algorithm, an evolution of PSInSAR™ technology, that searches for 'targets' on the ground that return stable radar reflections over time back to the satellite.

As well known, a SAR image is a collection of signals coming from different types of radar targets, either natural (forests, rocks, etc.) or man-made (buildings, bridges, poles, etc.). The signal recorded by the sensor can vary abruptly even in neighbor pixels, depending on the different radar signatures of the illuminated objects and the acquisition geometry. In general, image pixels where InSAR data can be extracted belong to two families of targets: point-wise targets (Permanent Scatterers, PS), where the reflected energy comes from a single or a few connected pixels, and Distributed Targets (DS). A Distributed Scatterer (DS) corresponds to a homogeneous area spread over a group of pixels in a radar image, like for example an agricultural field, a forest, a debris covered area. The characteristics of the radar returns coming from all pixels corresponding to the same DS, are "statistically homogeneous", i.e. the interaction between the radar target on ground and the electromagnetic wave is almost identical and can be modeled by the same probability density function.

While PS typically correspond to point-wise scatterers exhibiting a very high Radar Cross Section (RCS), the

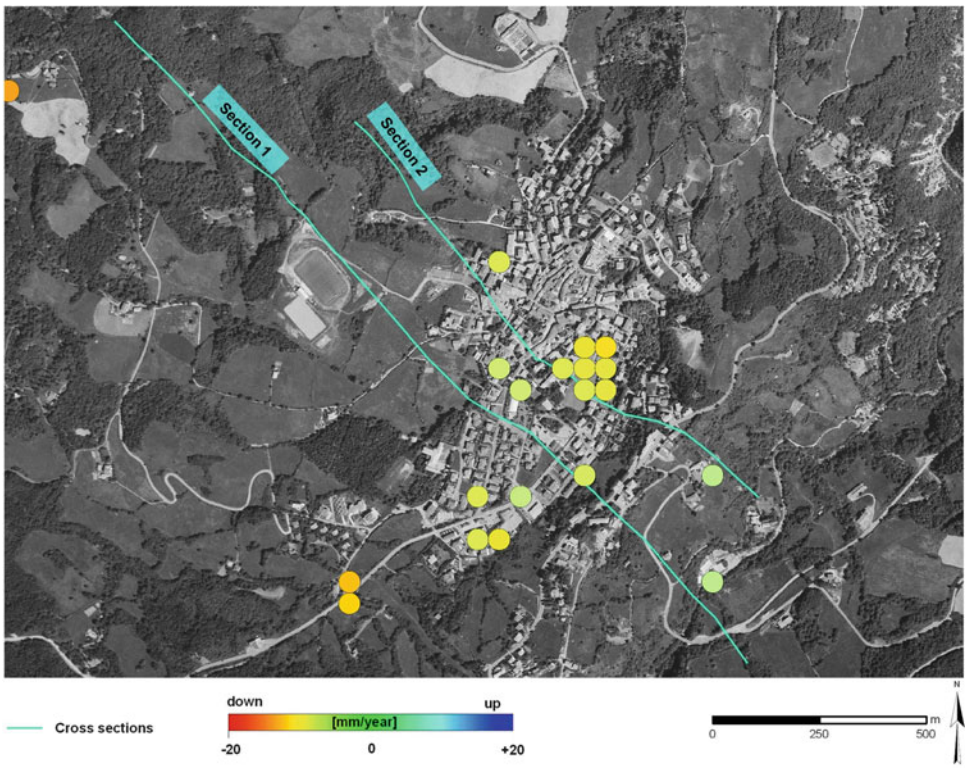


Fig. 3 Vertical average yearly displacement rate provided by SqueeSAR^{TM} analysis

amplitude of the radar return of a pixel belonging to a DS is usually much weaker, due to the lack of a dominant scatterer in the resolution cell, and is characterized by lower SNR. Indeed, if the estimation of displacement rate and elevation values is performed on a pixel-by-pixel basis across a DS, results are very noisy. However, by averaging the signal of all the pixels belonging to the same DS, it is possible to significantly improve the estimation quality, obtaining SNR values similar to the PS, at the cost of a loss of spatial resolution due to the averaging process. Thanks to typical remote sensing characteristic and in particular, the ability of covering vast remote areas of Earth's surface (from a few to thousands of square kilometres) and to the ability of estimating displacement with millimetre accuracy, SqueesAR™ is a very effective tool for high-precision monitoring of surface displacements, and can be applied at different scales, from regional to single building.

The SqueeSARTM analysis provides for each measurement point the average yearly displacement velocity value and a displacement time history. Displacements are measured along the "line of sight" (LOS) of the radar beam. The satellites fly over the Earth along polar orbits, and therefore pass over the area of interest in two possible geometries: ascending, flying from south to north, and descending, from north to south. The availability of displacement data in both ascending and descending geometries over the same area enhances the coverage of the study area and enables the estimation of vertical and E-W horizontal displacement fields (Fig. 3).

Two data sets of 77 descending and 27 ascending SAR scenes acquired by ERS-1 and ERS-2 satellites were processed, covering the period July 1992–January 2001. More than 6,000 measurement points in both acquisition geometries were identified within the study area (Fig. 4).

The main results of the analysis are summarized in the following points:

- The average yearly displacement rate (LOS displacements, descending geometry) is 10–15 mm/year in the urbanized area, 20–30 mm/year near the foot of the slope, with maximum values up to 50 mm/year measured in the mid part of the slope
- The yearly displacement rate distribution evidences the upper limit of the sliding area, corresponding to the eastern limit of the urbanized area
- Within the urbanized area and the upper right part of the Berceto slope, seasonal displacement cycles, sometimes superimposed on the average displacement trend, seem to be present; the amplitude of the seasonal cycles reaches maximum values of about 10 mm;
- In the lower left part of the Berceto slope, the displacement time history seems to show an increase of displacement rate during spring;

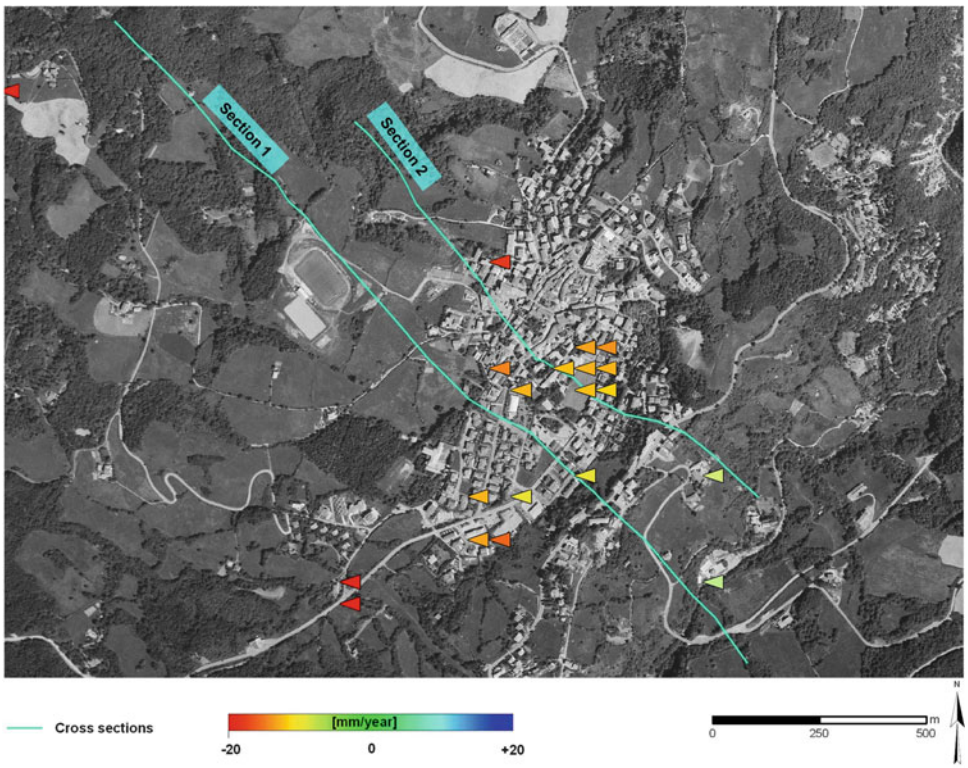


Fig. 4 E-W horizontal average yearly displacement rate provided by SqueeSAR™ analysis

– The estimation of vertical from E-W horizontal components obtained by geometrically combining data acquired in ascending and descending geometries indicates that the vertical component prevails in the upper part of the slope, while the E-W horizontal component in higher than the vertical one in the lower part of the slope.

Subsurface Structure of the Upper Berceto Slope

Eight DC resistivity tomography profiles, with 126 smart electrodes spaced 11.5 m for a total length of 1437.5 m each, crossing the upper part of the Berceto slope including the village were recorded. The investigation depth was about 250 m. According to the lithology of the geological units recognized in the study area, three geoelectric units were recognized: resistive (coherent lithologies), conductive (shaly lithologies) and intermediate (heterogeneous lithologies and/or high water content).

Two resistivity profiles, together with their geological interpretation (Figs. 5 and 2 respectively), have been selected as representative of the geological and structural framework of the Berceto slope. From a general point of view, the following sequence was recognized, from top to bottom: an upper intermediate resistivity unit (IRU), a central conductive unit (CU) and a lower resistive unit (RU). A more detailed description of the selected cross section follows.

The resistivity profile 1 exhibits the IRU (Scabiazza Sandstone) characterized by thin-bedded shales and sandstones, including more resistive medium-bedded sandstones up to 100 m thick in the NW part. The upper IRU is dislocated by discontinuities interpreted both as tectonic faults and/or gravitational sliding surfaces. Such discontinuities are SE-dipping near the Baganza valley, NW dipping on the Berceto slope. The central CU (Shaly Chaotic Complex) even if more continuous than the upper one, with an average thickness of about 100 m, appears stretched in at least three points, one of which corresponding to the deepening of the lower RU in the NW part of the cross section. This lower RU was interpreted as the Mt. Caio Flysch, which exhibits an antiformal geometry faulted in the NW part, where the unit is about 150 m deeper.

The resistivity profile 2 crosses the Berceto village and the trench with the lacustrine sediments previously described, evidenced by high conductivity values. The upper IRU shows higher conductivity values compared to cross section 1, probably related to a higher water content in more fractured and permeable levels. The central CU (Shaly Chaotic Complex) has an average thickness of about 100 m,

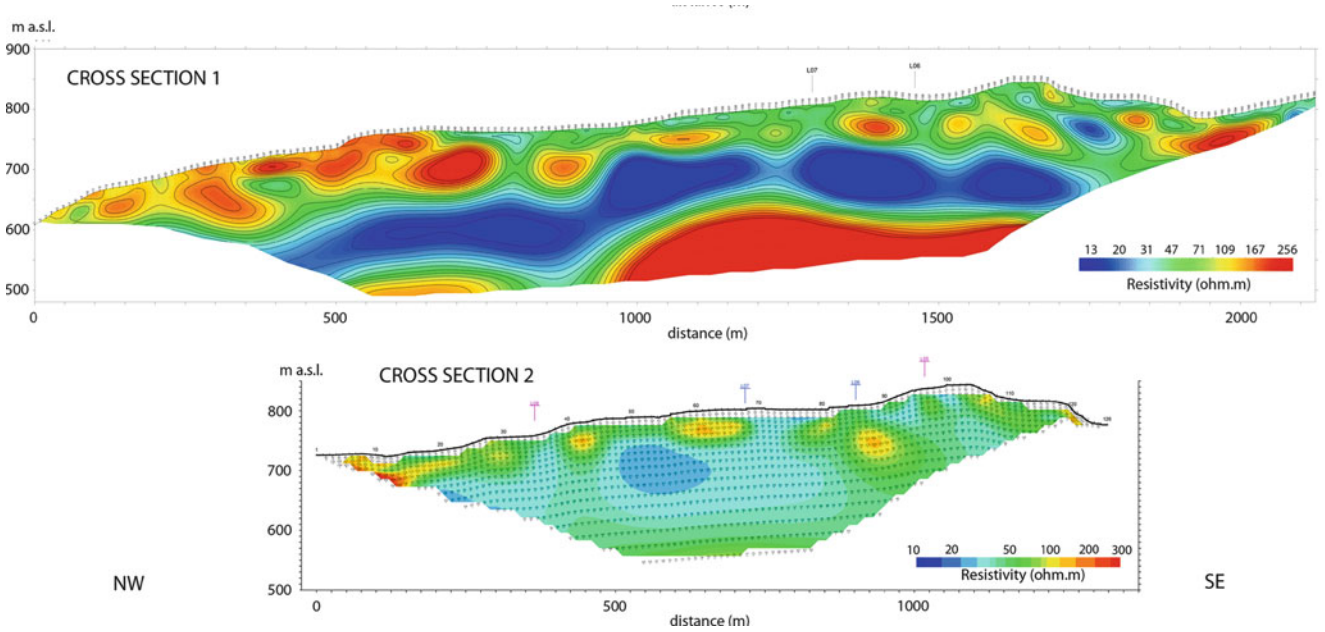


Fig. 5 DC resistivity tomography profiles 1 (by GEOINVEST s.r.l. Piacenza, up) and 2 (by SGG s.r.l. Siena, down)

and is clearly stretched in the NW part of the section. Compared to cross section 1, the lower RU (Mt. Caio Flysch) is less evident but visible at the same depth.

Geoelectrical data were integrated with borehole data and structural data collected on the outcrops close to the village and along Baganza valley, in order to provide a geological interpretation of the subsurface structure of the Berceto slope.

The geological cross section 1 (corresponding to resistivity profile 1) shows in the right part SW-NE high-angle faults affecting the Mt. Caio Flysch; under the Berceto village this unit exhibits an antiformal structure, visible in outcrop along the Baganza river. The Mt. Caio Flysch is overthrusted by the Shaly Chaotic Complex, which is overthrusted by the Scabiazza Sandstone. This last was deformed by a pre-Apennine S-verging folding, detached by N-dipping low angle surfaces and by high angle faults related to Apennine tectonics. The high-angle faults appear shifted by NW-dipping gravitational faults, that could explain the presence of plastic clay-rich breccia with arenaceous blocks levels identified in boreholes BH2 at a depth of 40 and 90 m respectively (Fig. 2). The presence of gravitational faults could explain the stretching observed within the Shaly Chaotic Complex and the higher surface displacement rate pointed out by satellite interferometry. The Berceto lacustrine sequence, recognized in both boreholes BH3 and BH4 could have probably been dislocated by gravitational faults. About 10 m of lacustrine deposits, corresponding to the Unit 6 (Bertoldi et al. 2004), were encountered in Borehole BH3; the same unit, overlain by 4 m thick laminated lacustrine sediments (Unit 5, Bertoldi et al. 2004), deformed by extensional shearing, were found in borehole BH4. Such laminated deposits appear 13° dipping, meaning the occurence of rotational movements.

From a general point of view the geological cross section 2 (corresponding to resistivity profile 2) shows the same geological and structural framework of section 1. About 25 m of laminated lacustrine deposits were encountered in borehole BH1, within the trench delimited by gravitational faults corresponding to the Berceto hollow. A 2 m thick plastic interval was found at a depth of 58 m, and interpreted as the evidence of a gravitational fault.

Discussion and Conclusions

Hypotheses about the evolution of the Berceto slope were advanced after integrating surface and subsurface data and observations with literature data.

The structural framework of the Berceto area indicates that the upper Berceto slope was affected by gravitational faults (Persaud and Pfiffener 2004; Ustaszewski and Pfiffener 2008). One possible mechanism for these gravitational slope processes are the "deep-seated gravitational slope deformations" (DGSD) by Dramis and Sorriso-Valvo (1994), recognised in several parts of the Northern Apennines (D'Amato and Puccinelli 1996; Coltorti et al. 2009).

The uppermost portion of the Berceto slope is characterized by the tectonic uplift related to transpressive tectonics; this structure may be a relevant factor for the development of the DGSD (Dramis and Sorriso-Valvo 1994).

Several gravitational faults developed close to the northwestern side of the antiformal stacking of the buried Mt. Caio Flysch. Within the Scabiazza Sandstone gravitational faults using pre-existing discontinuities such as tectonic faults and foliation planes and the kinematics seems a rotational sliding (Cruden and Varnes 1996). Through the Shaly Chaotic Complex, characterized by lithologies affected by pronounced foliation, the gravitational deformations may develop with more ductile mechanical behaviour, resulting in failure surfaces flattening towards the valley floor or a deep-seated creep with very slow movement rates (Hutchinson 1988).

The evolution of the DGSD was probaly responsible for the formation of a depression larger than the present Berceto hollow, in the upper part of the slope, where the lacustrine sequence was deposited. According to radiocarbon data, this lacustrine sequence was dislocated during the Holocene. The difference in elevation between the bottom of the lacustrine basin encountered in boreholes BH1 and BH4 is about 50 m, which could correspond to an horizontal displacement of more than 100 m, according to the present-day morphology of the slope. Under this hypothesis the average yearly displacement rate is consistent with the present-day surface displacement rate measured from 1992 to 2000 with satellite interferometry.

Surface displacement data are also consistent with the hypothesis of gravitational faults reaching the Shaly Chaotic Complex. The distribution of vertical versus horizontal component ratio indicates the presence of rotational sliding surfaces; moreover the highest displacement rates occurr in the central part of the slope, corresponding to the top of the deep antiformal structure, where the deformation of the slope seems to affect a thicker sequence.

Finally, the interferometric data analysis provided some evidences of correlation between landslide activity and precipitation. Seasonal displacement cycles observed in the urbanized area and the upper right part of the Berceto slope can be explained as the result of swelling-shrinkage deformation cycles, typical of the clayey deposits, i.e. the lacustrine sequence. Moreover displacement rate increase during spring in the lower left part of the Berceto slope could be an evidence of creep phenomena superimposed on the deep deformation trend, related to water circulation.

This first attempt of integration between surface displacements provided by SqueeSARTM analysis and subsurface data provided by geophysical and borehole investigations suggested that the evolutional model proposed for the Berceto DGSD is nevertheless more complex than expected. Further investigations are needed in order to gather more surface and subsurface data. Moreover a new ground based monitoring system is being installed, in order to integrate the results obtained by satellite radar interferometry and improve the knowledge of the slope dynamics.

References

Argnani A, Barbacini G, Bernini M, Camuri F, Ghielmi M, Papani G, Rizzini F, Rogledi S, Torelli L (2003) Gravity tectonics driven by Quaternary uplift in the Northern Apennines: insghts from the La Spezia-Reggio Emilia geo-transect. Quatern Int 101–102:13–26

Bernini M, Papani G (2002) La distensione della fossa tettonica della Lunigiana nord-occidentale (con Carta Geologica alla scala 1: 50.000). Boll Soc Geol It 121:313–341

Bernini M, Vescovi P, Zanzucchi G (1997) Schema strutturale dell'Appennino Nord-Occidentale. L'Ateneo Parmense Acta Naturalia 33:43–54

Bertoldi R, Chelli A, Roma R, Tellini C, Vescovi P (2004) First remarks on Late Pleistocene lacustrine deposits in the Berceto area (Northern Apennines, Italy). Il Quaternario 17:133–143

Coltorti M, Ravani S, Cornamusini G, Ielpi A, Verrazzani F (2009) A sagging along the eastern Chianti Mts., Italy. Geomorphology 112:15–26

Corsini A, Farina P, Antonello G, Barbieri M, Casagli N, Coren F, Guerri L, Ronchetti F, Sterzai P, Tarchi D (2006) Space-borne and ground-based SAR interferometry as tools for landslide hazard management in civil protection. Int J Rem Sens 27:2351–2367

Cruden DM, Varnes DJ (1996) Landslides types and processes. In: Turner AK, Shuster RL (eds) Landslides investigation and mitigation, T.R.B. Spec. Rep. 247, National Research Council, pp 36–75

D'Amato AG, Puccinelli A (1996) Deep-seated gravitational slope deformations in North-Western Tuscany (Italy): remarks on typology, distribution and tectonic connections. Geogr Fis Dinam Quat 19:325–334

Dramis F, Sorriso-Valvo M (1994) Deep-seated gravitational slope deformations, related landslides and tectonics. Eng Geol 38:231–243

Ferretti A, Prati C, Rocca F (2001) Permanent Scatterers in SAR Interferometry. IEEE Trans Geosci Rem Sens 39(1):8–20

Ferretti A, Fumagalli A, Novali F, Prati C, Rocca F, Rucci A (2011) A new algorithm for processing interferometric data-stacks: SqueeSAR. To be published on IEEE Trans Geosci Rem Sens

Hutchinson JN (1988) General report: morphological and geotechnical parameters of landslides in relation to geology and hydrogeology. In: Bonnard C (ed) Landslides, vol 1. Balkema, Rotterdam, pp 3–36

Persaud M, Pfiffener OA (2004) Active deformation in the eastern Swiss Alps: post-glacial faults, seismicity and surface uplift. Tectonophysics 385:59–84

Pini GA (1999) Tectonosomes and olistostromes in the argille scagliose of the Northern Apennines, Italy. Geol Soc Am Spec Pap 335:1–70

Ustaszewski M, Pfiffener OA (2008) Neotectonic faulting, uplift and seismicity in the central and western Swiss Alps. In: Siegesmund S, Fugenschuh B, Froitzheim N (eds) Tectonic aspects of the Alpine-Dinaride-Carpathian System. Geological Society London, Special Publications, vol 298, pp 231–249

Vescovi P (2002) Foglio 216 "Borgo Val di Taro" della Nuova Carta Geologica d'Italia alla scala 1: 50.000 e Note Illustrative. Servizio Geologico d'Italia



Use of the Seismic Dilatometer (SDMT) in Landslide Research and Practice

Sara Amoroso, Ferdinando Totani, and Gianfranco Totani

Abstract

This paper shows the use of the seismic dilatometer (SDMT) testing (Marchetti J Geotech Eng Division, 106:299–321, 1980; Marchetti et al. Proceedings of 2nd international flat dilatometer conference, Washington, DC, pp 7–48, 2001, In Situ tests by Seismic Dilatometer (SDMT), pp 109–138, 2008) in landslide diagnosis and monitoring. The quick K_D-DMT method, developed by Totani et al. (1997) for detecting active or old slip surfaces, was recently applied in a research programme on stability conditions of natural slopes shaped in colluvial cover formations in Abruzzo region (Chieti, Teramo). The paper illustrates the capability of SDMT to identify remoulded zones, symptom of instability, and slip surfaces in the investigated slopes.

Moreover, the paper presents the possibility to use the DMT blade as a piezometer, to monitor rapidly the variation of the ground water level in relation to weather trend.

Keywords

Seismic dilatometer • Horizontal stress index • Colluvial cover formations

Introduction

The study presented in this paper refers to research aiming at quickly identifying the colluvial covers in Abruzzo (Central Italy) through the use of the seismic dilatometer (SDMT) testing (Marchetti et al. 2008), recently introduced to add the measure of the shear wave velocity to the flat dilatometer (Marchetti 1980; Marchetti et al. 2001). In particular, this method allows the detection of very slow movements, that occur frequently on large areas, as a typical feature of the region, and to evaluate the thickness of these formations.

S. Amoroso (✉) • F. Totani • G. Totani
Department of Structural, Water and Geotechnical Engineering, University of L'Aquila, L'Aquila, Italy
e-mail: sara.amoroso@gmail.com

K_D – DMT Method in the Colluvial Cover Formations

As well documented by Totani et al. (1997) and then validated by Leroueil (2001), the K_D – DMT method quickly detects active or old slip surfaces in overconsolidated (OC) clay slopes, based on the inspection of the horizontal stress index K_D profiles. The K_D – DMT method can be summarized as follows:

(a) The sequence of sliding, remolding and reconsolidation generally creates a remolded zone of nearly normally consolidated clay, with loss of structure, aging or cementation;
(b) In NC clays $K_D \approx 2$, if an OC clay slope contains layers where $K_D \approx 2$, these layers are likely to be part of a slip surface (active or quiescent).

In Abruzzo the colluvial covers distributed over the marly clay bedrock (Teramo area) and over the OC clay (Chieti area) could generate both translational and rotational slip surfaces. Thus, the K_D – DMT method could be used to verify the slope stability in these situations, as illustrated in Fig. 1.

C. Margottini et al. (eds.), *Landslide Science and Practice*, Vol. 2,
DOI 10.1007/978-3-642-31445-2_58, © Springer-Verlag Berlin Heidelberg 2013

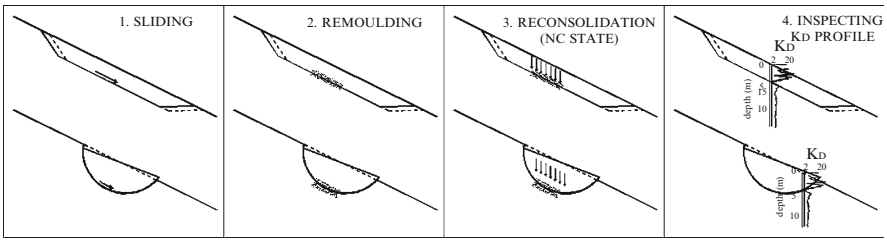


Fig. 1 K_D – DMT method in colluvial covers with translational and rotational slip surfaces

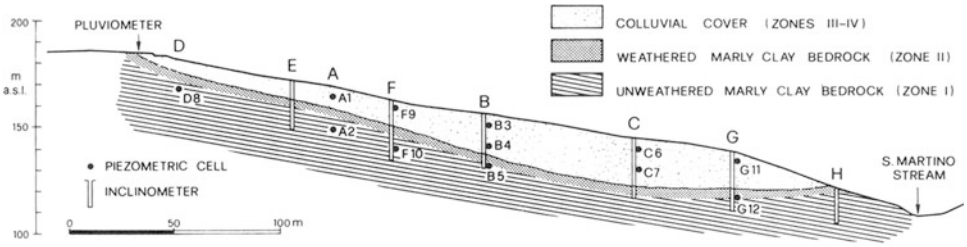


Fig. 2 Geological cross section of a colluvial cover over a marly clay bedrock in Abruzzo (Bertini et al. 1984)

In addition, K_D can identify the thickness of these colluvial covers, even if these formations don't generate a slip surface. In fact, the rapid change of K_D values in a vertical profile locates the contact between the colluvial cover and the layer below.

Use of the DMT in the Abruzzo Colluvial Covers

The case studies illustrated in the following paragraphs concern two different colluvial covers:

- Silty clayey colluvial covers over marly clay bedrock that are potential translational slip surfaces, located in Teramo district;
- Silty clayey colluvial cover over OC clay that are potential rotational slip surfaces, situated along Chieti hill.

Teramo District

Very slow movements (a few cm/year) have been detected with site investigations (Bertini et al. 1980) as occurring on slopes shaped in Pliocenic marine marly clay formations in Teramo district, between Gran Sasso and Laga Mountains and the Adriatic Sea.

The slow translational movements involve the weathered part of these formations and the thick silty clayey colluvial covers overlying them on large portions of the slopes.

Geological and Geotechnical Setting

The region, referred to as the "hilly piedmont belt", is formed by a succession of layered marly clays which sedimented in Lower Pliocene ("Cellino" formation) and Middle-Upper Pliocene ("Argille grigio-azzure" formation).

Thick silty-clayey colluvial deposits suggestive of recent and very intense evolutional phases are widely distributed over marly clays. Due to their areal distribution and great thickness (until 30 m in depth), colluvial covers can be considered as a true geological formation.

Bertini et al. (1984) schematized a typical colluvial cover over a marly clay bedrock as follows (Fig. 2):

- Zone I: saturated overconsolidated very stiff marly clay bedrock;
- Zone II: bedrock band formed by weathered marly clay. Weathering, softening and destructuring increase progressively from the bottom to the top;
- Zone III: saturated slightly overconsolidated medium to stiff silty clayey colluvial cover with constant in depth geotechnical properties;
- Zone IV: oxidized and highly fissured superficial crust of the colluvial cover subjected to drying and wetting cycles following the climatic variations.

A deep monitoring campaign (pluviometric stations, piezometers and inclinometers), realized by Bertini et al. (1984), shows that the equilibrium conditions of these slow translational movements are controlled by the seasonal variations of the pore pressure regime and that the slip surface is placed between the bottom of the colluvial cover (zone III) and the top of the weathered marly clay (zone II).

An immediate and economic alternative is the use of flat dilatometer (DMT). Figure 3 illustrates the results of two seismic dilatometer (SDMT) tests (Marchetti et al. 2008) carried out in a representative area of Teramo district. Even if the profiles of K_D do not identify any layers with $K_D \approx 2$ (absence of slip surfaces), in these vertical profiles the rapid change of the horizontal stress index K_D, as well as the constrained modulus M, identifies different thickness of the colluvial cover (red arrows in Fig. 3).

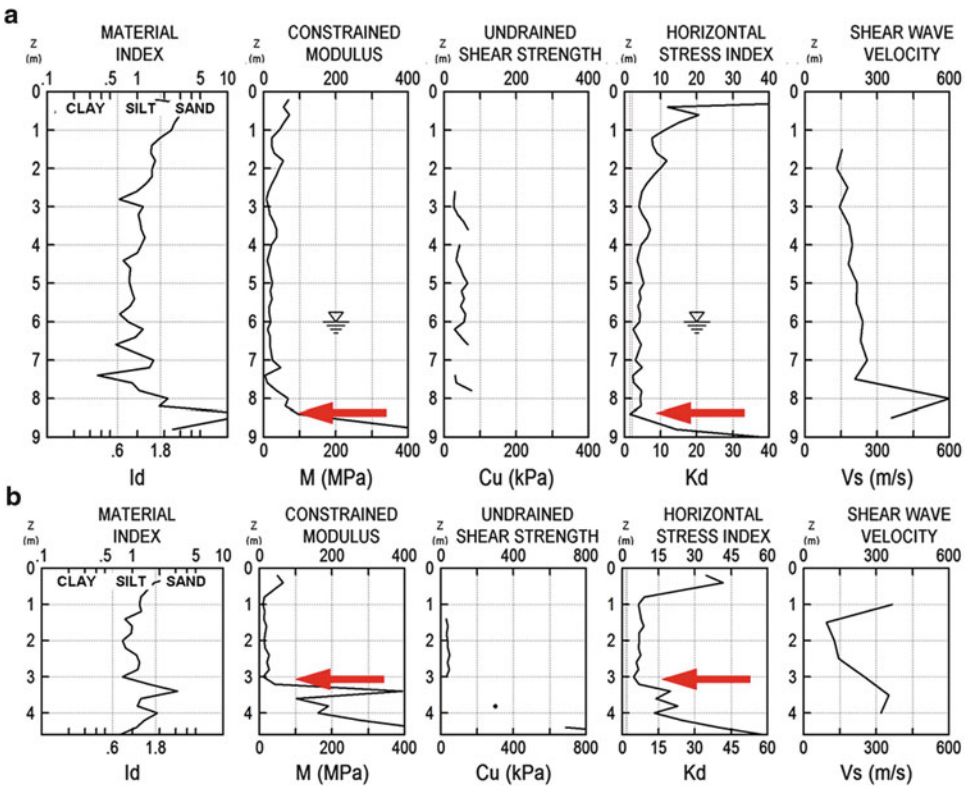


Fig. 3 SDMT profiles of the colluvial cover in Abruzzo

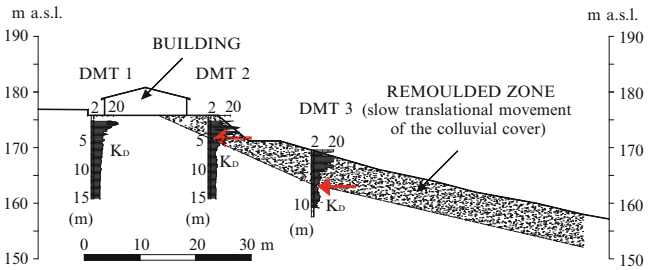


Fig. 4 Horizontal stress index K_D profiles on Atri hill

Even if less evidently than K_D and M, the shear wave velocity V_S feels the change of the profile between the colluvial cover and the below intact unweathered layer.

DMT Testing in Atri

A series of three DMT tests, each 8–15 m in depth, and two boreholes, each 15 m in depth, were carried out in 2002 on Atri hill (Teramo district). The aim of this study was to investigate a building probably damaged by the slow translational movements of a colluvial cover.

An overall systematic description of the observed cracks showed that the structure was damaged only at the bottom, while the construction was safe at the top. The analysis of the surveys demonstrated that the building was realized in part on a stable area (at the top) and in part on an instable zone (at the bottom).

In fact, DMT2 and DMT3 soundings, performed at the bottom of the construction, highlighted layers where $K_D \approx 2$ (red arrows in Fig. 4), respectively at 4 and 6 m in depth. Thus, these layers detected a NC zone constituted by a colluvial cover (K_D decreases gradually with the depth until values $K_D \approx 2$) over a marly clay formation (K_D assumes constant values until 15 m in depth, $K_D \approx 8$–10). Moreover, the high value of K_D in the first few meters of the probe justified the presence of a superficial crust of colluvial cover.

Instead, DMT1 test, carried out at the top of the slope, next to the building, showed a typical profile of an OC clay (K_D decreases gradually with the depth until values $K_D \approx 8$–10).

The profiles of the constrained modulus M (Fig. 5) gave high values, substantially uniform from the colluvial cover to the marly clay formation. Therefore M cannot supply clearly information on the position of the NC zone.

Hence, considering the previous geological and geotechnical studies (Bertini et al. 1984) the DMT investigations, through K_D, provided rapidly the slip surface (the remoulded zone with $K_D \approx 2$) at 4–6 m in depth, typical for the slow translational movements of the colluvial covers in Teramo district.

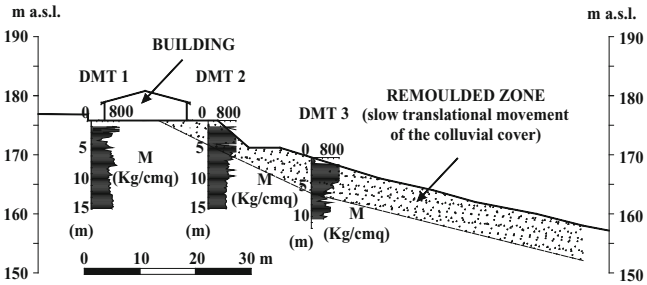


Fig. 5 Constrained modulus M profiles on Atri hill

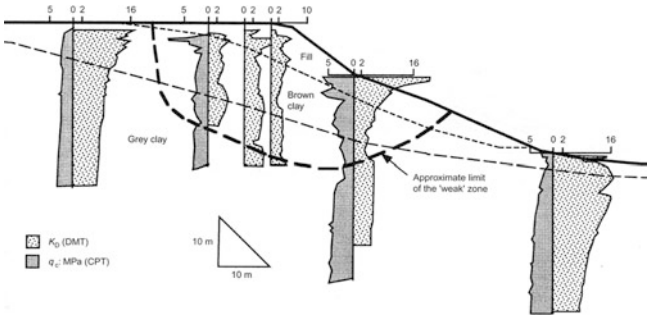


Fig. 6 CPT (q_c) and DMT (K_D) profiles at Chieti, Italy (Leroueil 2001)

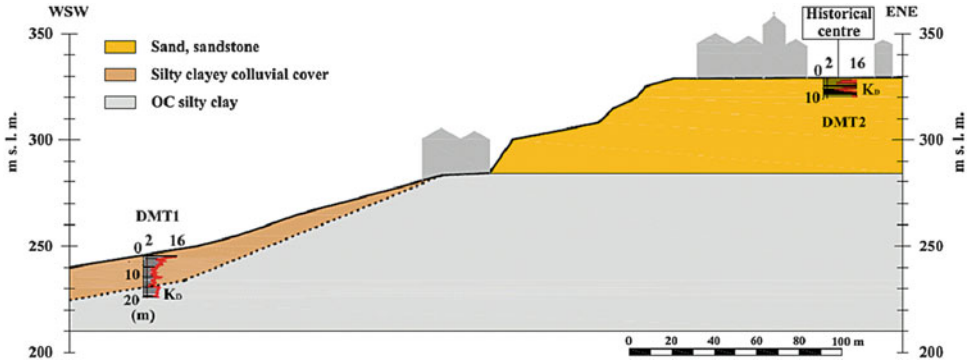


Fig. 7 Fosso S. Chiara: geotechnical cross section with K_D profiles

Chieti Hill

Chieti hill, located between Majella Mountain and the Adriatic Sea, is characterized by Plio-Pleistocenic marine formation and recent continental deposits that could create localized rotational slip surface.

Geological and Geotechnical Setting

The periadriatic region is formed by a Plio-Pleistocenic succession ("Mutignano" formation). It includes silty clays ("Argille grigio-azzure" formation) that change gradually in sandy clays, sands and arenaria on the top of Chieti hill.

Recent continental deposits are widely distributed over the previous mentioned OC clays. They are constituted by silty-clayey colluvial covers and they reach until 20 m in depth, as maximum thickness.

Instability phenomena of localized soil mass are controlled by the seasonal variations of the pore pressure regime, as documented by several monitoring activities concerning the hydrogeologic risk of the Chieti hill.

As well as in the Teramo district, the flat dilatometer can quickly solve the problem of slope stability. In particular, a case history on Chieti hill was examined by Totani et al. (1997) and then validated by Lerouil (2001), using the profiles of the horizontal stress index K_D from the flat dilatometer (DMT) and of the cone resistance q_c from the cone penetration test (CPT). The inspection of K_D profiles clearly highlighted the presence of several layers with $K_D \approx 2$, suggesting that an approximate limit of the "weak" zone (Fig. 6).

DMT Testing in Fosso S. Chiara

A detailed investigation of six SDMT tests, each 10 m (on the top of the hill) and 20 m in depth (on the bottom of the hill) and six boreholes, each 30–50 m in depth, were performed in 2011 on Chieti hill to restore an historical building, damaged by the April 6, 2009 L'Aquila earthquake.

The soundings allowed the construction of a geotechnical cross section of the slope in the area of Fosso S. Chiara (Fig. 7). The historical centre was built on sandy and arenaria deposits (45 m in depth), while moving towards the bottom of the slope the colluvial cover start to emerge over the OC silty clay, as well interpreted by the flat dilatometer. In fact, the SDMT1 profiles (Fig. 8) clearly indicated the contact surface between the colluvial cover and the OC silty clay at 15 m in depth. The constrained modulus M, the undrained shear strength c_u and the horizontal stress index K_D increase rapidly moving from superficial deposits to the OC formation (red arrows in Fig. 8), while the shear wave velocity V_S appears to not recognize this contact surface. In particular, K_D decreases

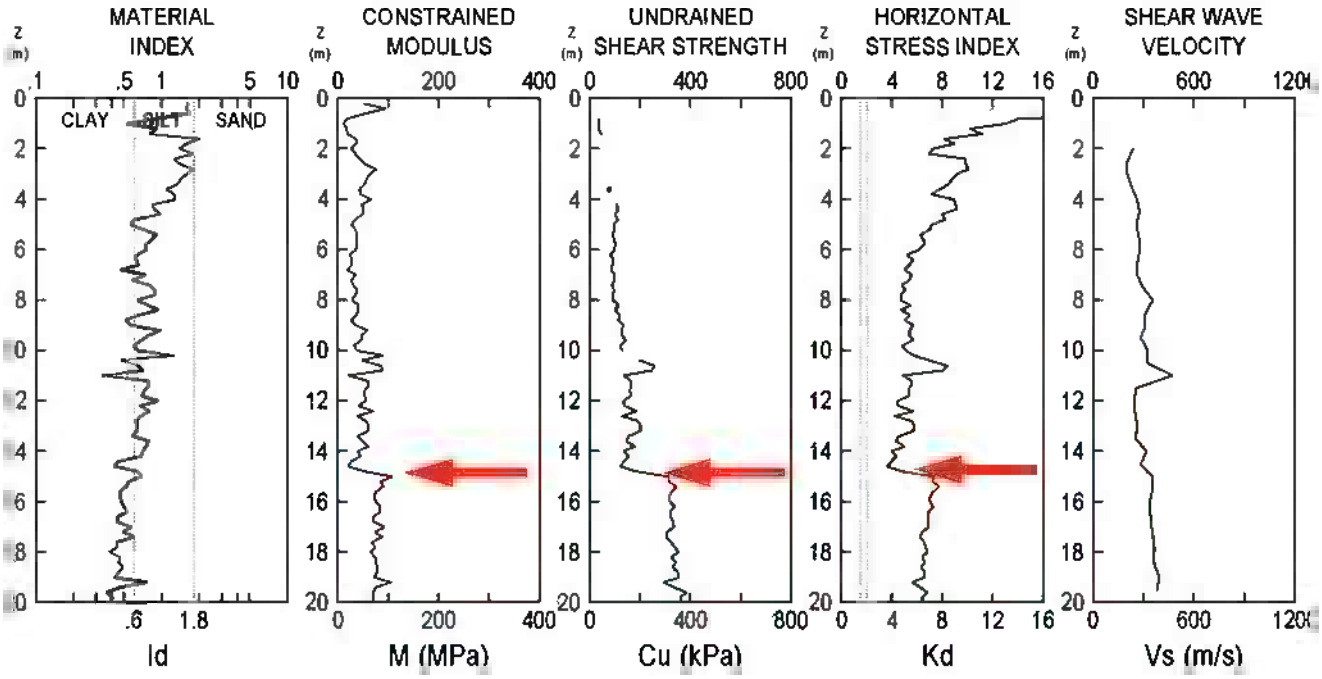


Fig. 8 Fosso S. Chiara: DMT1 profiles

gradually until values $K_D \approx 4$ (15 m in depth) and then the parameter increases quickly in correspondence of this contact surface and it becomes constant ($K_D \approx 6$–8) in the OC silty clayey formation.

Therefore, on the Chieti hill the seismic dilatometer provided to identify the thickness of this colluvial covers, even if this formation doesn't generate a slip surface. In fact, the rapid change of K_D values, as well as M and c_u, in a vertical profile locates the contact between the colluvial cover and the layer below.

Concluding Remarks

The examined case study demonstrated the ability of the seismic dilatometer to detect rapidly and economically the thickness of the colluvial covers.

The rapid change in K_D, M and c_u profile discriminate these formations from the intact unweathered OC clay.

In the Abruzzo colluvial covers, the K_D-DMT method identifies slip surface signalled by layers with $K_D = 2$, as well documented for Atri hill.

Acknowledgments This study was founded by Geo L'Aquila s.a.s., Provincia di Chieti and Studio Prof. Marchetti s.r.l.

References

Bertini T, D'Elia B, Grisolia M, Oliviero S, Rossi-Doria M (1980) Lenti movimenti di coltri colluviali sulle argille marnose della Laga. In: Proceedings of 14th Convegno Nazionale di Geotecnica, Firenze, vol 2, pp 207–218

Bertini T, Cugusi F, D'Elia B (1984) Climatic conditions and slow movements of colluvial covers in Central Italy. In: Proceeding of 4th international symposium on landslides, Toronto, vol 1, pp 367–376

Marchetti S (1980) In Situ tests by flat dilatometer. J Geotech. Engineering Division, ASCE, 106 (GT3):299–321

Marchetti S, Monaco P, Totani G, Calabrese M (2001) The flat dilatometer test (DMT) in soil investigations. A report by the ISSMGE committee TC16. In: Proceedings of 2nd international flat dilatometer conference, Washington, DC, 2–5 April 2006, pp 7–48

Marchetti S, Monaco P, Totani G, Marchetti D (2008). In Situ tests by Seismic Dilatometer (SDMT). From research to practice in geotechnical engineering, ASCE Geotechnical Special Publication honoring Dr. J. H. Schmertmann, GSP n. 170, Geo-Institute Meeting in New Orleans, pp 109–138

Leroueil S (2001) Natural slopes and cuts: movement and failure mechanisms. Géotechnique 51(3):197–243

Totani G, Calabrese M, Marchetti S, Monaco P (1997) Use of in situ flat dilatometer (DMT) for ground characterization in the stability analysis of slopes. In: Proceeding of 14th international conference on soil mechanics and foundation engineering, Hamburg, vol 1, Sept 1997, pp 607–610



Gravitational Instability Analysis of the Prato Carnico Village

Marco Del Fabbro, Roberto Meriggi, and Nicola Stefanelli

Abstract

This paper reports in situ test results and monitoring performed to characterise the development of a gravitational phenomenon. Analysis made it possible to create a 3D subsoil model to identify the main preferential paths of groundwater seepage, the boundaries of the subsidence area and the relationships between rainfall and displacements. The results of seepage and stability analyses highlight some aspects that characterise the kinematical mechanism of the slope. Displacements show a constant increase over time independently from the pluviometric regime. Stratigraphic sections and geophysical investigations highlight that the subsidence basin was formed just above a morphological bedrock depression and was filled with weathered gypseous arenite and sandy silt. The slow and constant sinking of the cover may be ascribed to the progressive collapse of the voids created through karstification within the gypseous rock mass and which attract loose material from above causing vertical and horizontal movements.

Keywords

Monitoring • Gravitational • Stability analyses • Seepage • Karstification • Subsidence • Displacements

Introduction

The alpine village of Prato Carnico (Fig. 1) is located in the Pesarina Valley (northern Friuli region) on the alluvial fan formed by the solid transport of two streams which flow along the sides of the small town and at its southern end it is bordered by a road located on the top of the steep slope that descends towards the Pesarina Torrent.

Gravitational movement has been known about since the 1850s when static problems concerning buildings with damage, cracks and splits were reported; however, the first signs of relevant road settlements were registered in the 1950s. As the road that crosses the village is the only way of communication for the Pesarina Valley, many studies have been performed over the years in order to find the causes of instability, but in spite of the numerous analyses and in situ investigations carried out, certain and shared conclusions have never been reached.

During the period between 2003 and 2008, on behalf of the Civil Defence, the Department of Georesources and Territory of the University of Udine performed a comprehensive analysis of geostatic phenomena for the Prato Carnico town.

Before the end of the geotechnical and stability analyses, the state of road degradation made it necessary to construct a retaining structure created with a double row of micropiles and anchored to the ground with two orders of anchors. Remedial work began in summer 2006 and finished at the beginning of 2007.

M. Del Fabbro (✉) • R. Meriggi
Dipartimento di Chimica Fisica e Ambiente, University of Udine, via del Cotonificio 108, Udine, Italy
e-mail: roberto.meriggi@uniud.it

N. Stefanelli
Civil Defence, via Natisone 43, Palmanova, Italy

C. Margottini et al. (eds.), *Landslide Science and Practice*, Vol. 2,
DOI 10.1007/978-3-642-31445-2_59, © Springer-Verlag Berlin Heidelberg 2013

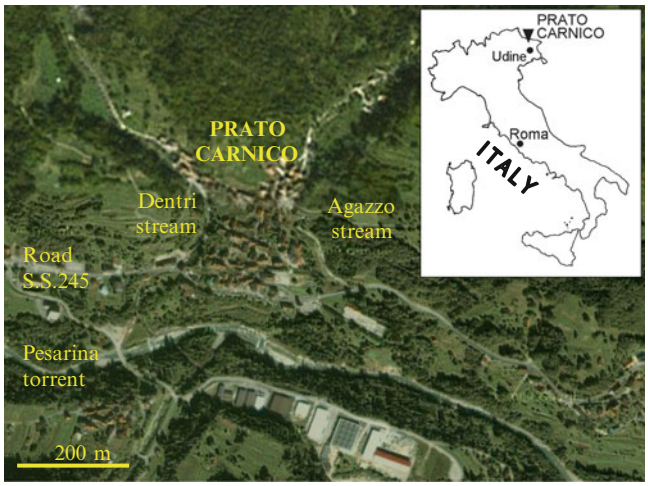


Fig. 1 Area of the gravitational instability

Site Geology

At the base of the Quaternary deposits of the Prato Carnico terrace there is a transitional surface which divides the Val Gardena bedrock in the north-west sector and by the Bellerophon formation of gypseous member (rock) and black dolomite for the other part. Above this second unit a weathered layer is often present which can reach some meters in thickness and which is a sandy silt with angular cobbles.

It is probably a lodgement till related to the maximum expansion of the Val Pesarina glacier during the Last Maximum Glacial Age and it is also retraceable in the outcrop in the terraces along the slopes around Prato Carnico (Venturini 2002).

Above this glacial deposit, gravels and sands 1 m thick or just over a meter thick are present and over them lays a mass of sandy silts with angular gravel that can reach 20 m in thickness. It is likely that they are glacial deposits of the left lateral moraine of the Val Pesarina glacier or a glacial contact; the latter hypothesis would justify the presence of gravels and sands at the base.

Geotechnical Investigations, Geochemical Analyses and Monitoring

The first stage of the analysis was the collection of stratigraphic logs from over 39 boreholes created over the last 32 years, placing them in their correct topographic location (Fig. 2) and carrying out the homogenization of lithological descriptions reviewing the borehole cores. Moreover, as there was no information about the subsoil geological structure near the steep zone of the slope, 25 seismic passive HVSR tests (Horizontal to Vertical Spectral Ratio) were performed.

From some borehole cores, 12 semi-undisturbed samples were collected and submitted for geotechnical laboratory analyses for index property identification and shear strength characterization. Samples collected from the bedrock and from the weathered layer were also submitted for mineralogical and petrographic analyses to verify the presence of sulphate inside. Afterwards, a wide in situ monitoring investigation was carried out for 5 years and several series of data were recorded for deep and superficial displacements, piezometric levels, monitoring of the structural damage and cracks using mechanical crackmeters. After the construction of the retaining structure, two multi-base extensometers were installed, one uphill and one downhill of the sheet pile wall and load cells were also installed on the heads of 5 anchors.

Geochemical Properties

Geochemical analyses performed on the bedrock and weathered (soil) layer have shown that there is no uniform distribution of gypsum values.

The upper part of the bedrock is made up of gypseous dolomite and, inside this, gypsum is present in two different forms.

The first type (A) is more widespread and it is characterized by a succession of fine sediment dark veins and white-transparent gypsum blocks. The rock is compact with a gypsum percentage of 65 %. The second type (B) is less widespread and it is characterized by the presence of more coarse sediment inside the white-opaque gypseous matrix. The rock is less compact with a higher gypsum percentage, 75 %.

Both gypsum types resulted as being soluble in water with a weight loss percentage, measured over two months, of 4.35 % for type A and 2.71 % for type B. The difference is probably due to the mechanical water action and selective gypsum dissolution because the weight loss for type A is caused by fine fraction detachment and dissolution of the rock mass.

The weathered layer that covers the gypseous bedrock is generally present as a loose soil; it is prevalently sandy and silty with a clay fraction which has low plasticity and activity characteristics and which is not more present than 20 %. Inside the weathered layer, or more frequently in direct contact with bedrock, there are coarse horizons where gravel or rock fragments are predominant.

The soluble sulphate percentage present inside the weathered layer is between 0 % and 4 % and may be considered very low when compared to the percentage inside the bedrock (36–42 %). The siltstone is present in the bedrock under the gypseous dolomite.

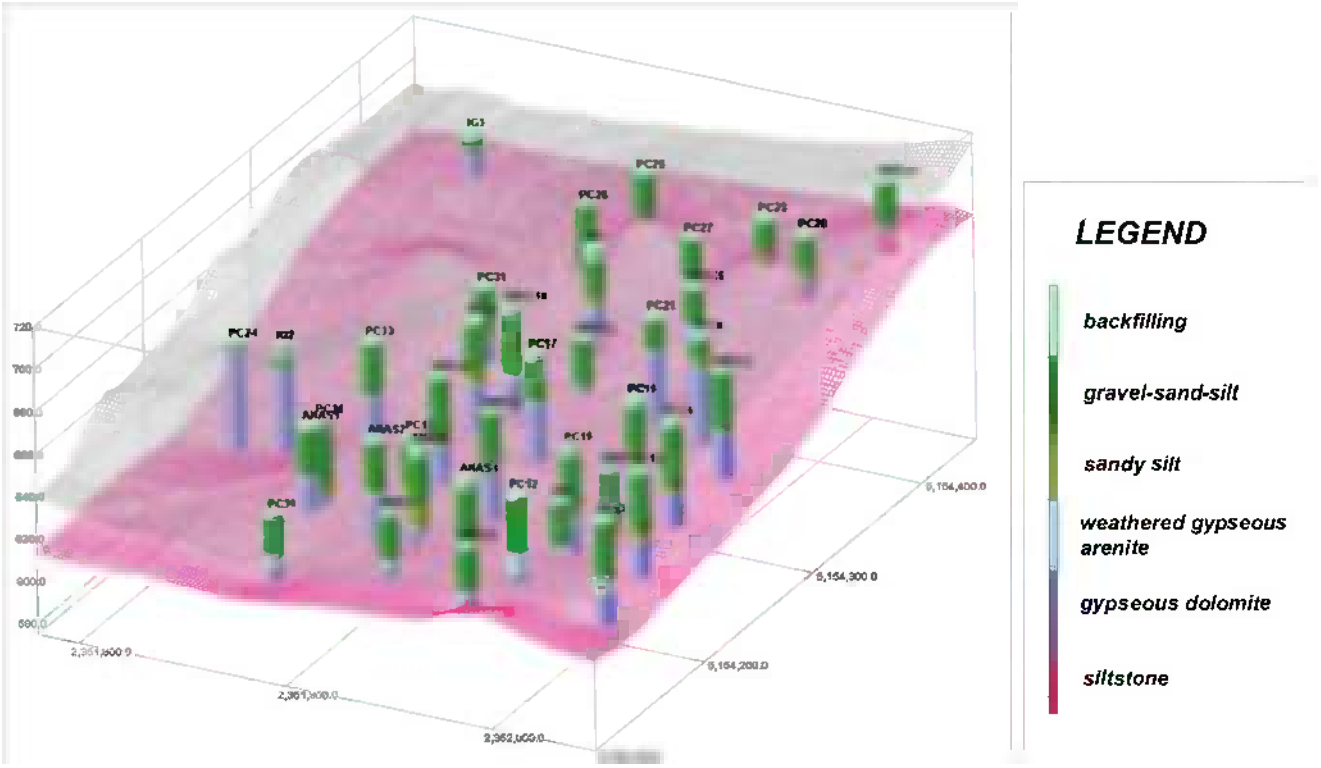


Fig. 2 3D model of Prato Carnico subsoil create by stratigraphic logs

Geotechnical Properties

Index properties of the main lithological units are summarized in Table 1. Three main lithological units are distinguishable under the shallow cover backfilling and are made up of heterogeneous soils, prevalently loose, about 2 m thick, and over the gypseous bedrock. Their names were chosen to clearly distinguish them, highlighting the presence of more or less fine fraction and gravel even if not precisely reflecting their grain size distribution.

The most widespread lithological unit is made up of an irregular succession of coarse deposits about 20 m thick, rock fragments or cobbles and fine deposits prevalently formed by silty and sandy soils. A second lithological unit is present with continuity over the weathered arenite, with a thickness ranging between 2 and 4 m, and it is made up of sandy silt and sometimes with angular cobbles. The third lithological unit is the bedrock weathered layer and it is formed by partially or totally weathered gypseous arenite; often it appears in sandy silt facies with cobbles and rock fragments inside.

Each unit was then divided into sub units to consider the local lithological variability. Shear strength and hydraulic conductivity values for different sub units are reported in Table 2. Shear strength characteristics and their range of statistic variability were deduced from the results of laboratory direct shear tests and from N_{SPT} values measured during borings.

The permeability coefficient values were deducted both from the results of in situ Lefranc tests and from seepage FEM analyses inside the slope: the values of hydraulic conductivity used in the analyses were progressively modified to obtain congruent results with on-site water table measurements.

Groundwater Regime

Groundwater monitoring was performed by DiSGAM (2008) both with automatic water level continuous measurements in 18 electrical piezometers, and with water table velocity and direction measurements through fluorescein injections. Moreover, during boring operations, directional and velocity measurements were carried out with the thermal current meter. The measurements carried out highlighted the following peculiarities of the underground water regime:

- Groundwater flow develops prevalently inside the gravel-sand layer located above silty and clayey materials that covers gypseous bedrock.
- The water table level is subjected to small variations, generally lower than 1.2–1.5 m also in concomitance of heavy and intense rainfalls.

Table 1 Index properties of main lithological units

Lithological unit	Gravel (%)	Sand (%)	Silt (%)	Clay (%)	Plasticity index	Activity index
Gravel, sand, silt	47.9	22.9	22.5	12.5	6.0	0.48
Sandy silt	28.6	31.6	23.6	16.2	7.0	0.43
Weathered arenite	15.5	40.9	28.3	15.3	6.9	0.45

Table 2 Range of shear strength variation used in the probabilistic stability analyses and values of permeability used in the seepage analyses

Material	K (m/s) permeability	γ (kN/m^3) unit weight	c (kPa) cohesion	Ø (°) friction angle
Backfilling	$6.0 \cdot 10^{-4}$	18–20	3÷7	28–32
Gravel and sand upper	$7.5 \cdot 10^{-4}$	19–21	0	36–40
Gravel and sand lower	$2.5 \cdot 10^{-3}$	19–21	0	36–40
Silty sand	$5.0 \cdot 10^{-4}$	19.5–21.5	0	30–34
Sand with gravel	$7.0 \cdot 10^{-4}$	19.5–21.5	0	32–36
Sandy silt upper	$1.9 \cdot 10^{-4}$	20–22	0	25.5–29.5
Sandy silt lower	$5.0 \cdot 10^{-5}$	20–22	0	25.5–29.5
Weathered arenite	$1.0 \cdot 10^{-9}$	20–22	0	25.5–29.5

- The heterogeneity of the backfilling grain size distribution and the type of gypseous dolomite bedrock affect the movement of groundwater along preferential seepage paths; this leads to different values of water table variation even at distances of tens of meters.

Continuous groundwater monitoring was supplemented by the Georesources and Territory Department with some local piezometer measurements located in the area of major subsidence.

Superficial Displacements

The monitoring of slope superficial displacements was performed by means of a bench mark network, variously distributed in the subsidence area and in the surroundings; over the years and after remedial work, some bench marks were updated or remade. Total station and levelling topographical measurements were carried out from year to year for more than a decade and they pointed out the development of important prevalently vertical displacements situated near the southern part of the inhabited village both uphill and downhill of the slope (Fig. 3).

Before remedial work, the bench marks located uphill of the road highlighted vertical displacements characterized by increments between 5 and 12.5 mm/year while bench marks located on the old retaining wall were subjected to more relevant displacements with increment rates between 5 and 21 mm/year. The vertical displacement rate of bench marks, located along a path that runs halfway up the slope, was higher with values between 6.9 and 29.6 mm/year.

The construction of the retaining structure seems to have had a positive effect slowing down the displacement rate both of the uphill road bench marks, which currently move with a rate between 3 and 7.5 mm/year, and new bench marks located on the retaining structure, 2.4–9.2 mm/year.

Vertical displacements of the bench marks located on the path in the middle of the slope still increase with a yearly rate similar to the one previous to the consolidation work. The trend observed is also confirmed by extensometer measurements carried out 3 years after their installation. The first instrument, located downhill of the retaining structure, highlights relevant vertical displacements that develop velocities which decrease with depth and which vary between 5.5 mm/year for the base located at a depth of 4.0 m–1.1 mm/year for the more deep base at a depth of 32 m.

The second extensimeter located uphill of the sheet pile wall highlights significantly lower vertical displacements and which vary between 0.8 mm/year at a depth of 12.0 m to 0.4 mm/year at a depth of 32 m.

The most peculiar aspect shown by the measurements carried out is that the progression of vertical displacements results as almost constant and it is not dependent on a pluviometric regime or by water table variations; these considerations are valid for measurements carried out both before and after remedial work. The cumulated horizontal displacements between 7 and 65 mm and are often characterized by an irregular trend with variable directions but with a final downhill resulting direction.

Deep Displacements

Inclinometer measurements carried out before and after the construction of the retaining structure confirm what was observed with topographical and extensometer measurements. The rate of horizontal displacement of the head inclinometer (Pc11) (Fig. 3), located uphill of the road near the middle of the subsidence area, was equal to 8.4 mm/year before consolidation works and then it went down to 5.3 mm/year after the construction of the retaining structure.

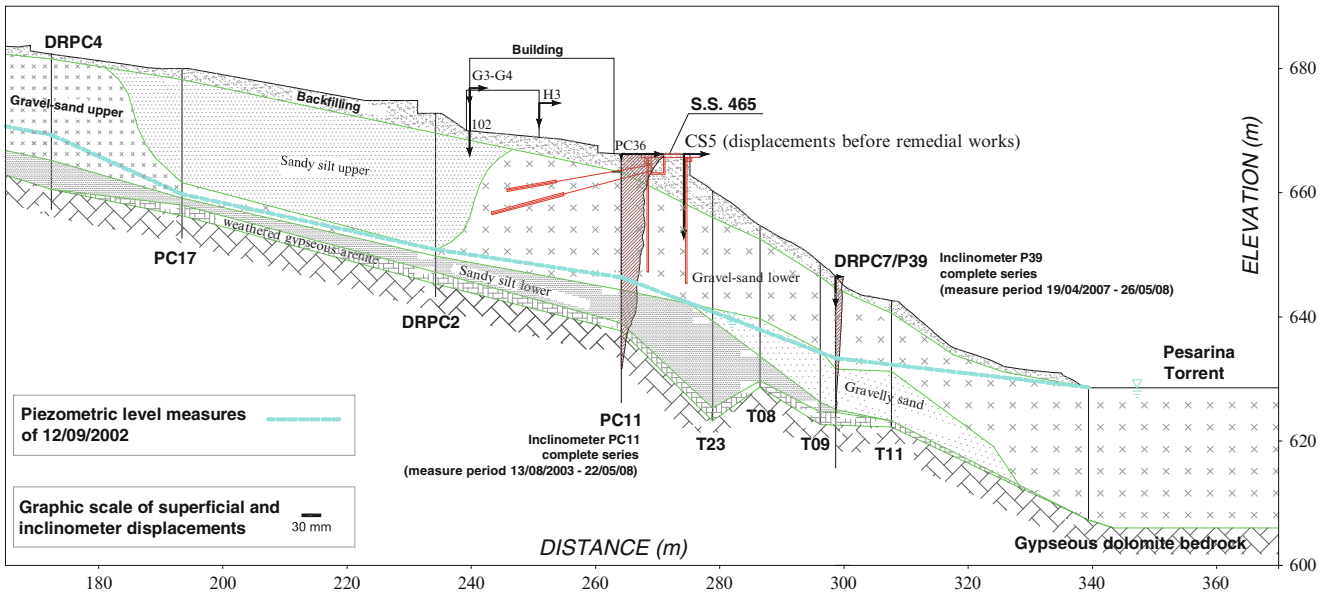


Fig. 3 Stratigraphic section of involved materials, mean water table and displacements

The trend of the displacement profile highlights an increment in horizontal displacement towards the south, until a depth of 26 m and further on there is a steep slope change.

In another inclinometer located near the Pc11, but downhill of the road and the retaining structure, the yearly rate of displacement remained elevated before and after remedial work, measuring from 21.5 to 14.6 mm/year. Currently, the displacement profile seems to show a slope change at about a depth of 27 m and over this the cumulated displacement value is constant until about 34 m depth.

In another inclinometer P39 (Fig. 3), installed after completion of the retaining structure, the mean rate of displacement resulted equal to 9.2 mm/year for about 4 years.

In the displacement graph the most important slope changes are present both near the surface, at 2–3 m of depth, and over at 16–17 m of depth.

Recent monitoring load cell measurements confirm the existence of deep horizontal displacements that are limited and which are not uniform inside the slope.

In the last 3 years the yearly rate of load increment has generally resulted as being reduced for the anchors located in the eastern side of the retaining structure, 0.32–0.36kN/year, but more elevated for those near the western side, 2.26–3.09kN/year.

Interpretation of Geotechnical Investigation and Monitoring

The key monitoring results, from geotechnical and topographical measurements and the structural building damage, highlight that only the area near the road is subjected to



Fig. 4 General view of kinematics mechanism

vertical and horizontal gravitational movements (Fig. 4). The analysis on the measured data has made it possible to create a 3D model of the subsoil to identify the main preferential paths of groundwater seepage, the boundaries of the subsidence area and finally the relationship between rainfall and increments of superficial and deep displacements. The planimetric and altimetric shape of the gypseous dolomite bedrock represented by isohypse (Fig. 5) show the morphological characteristics of the Prato Carnico subsoil.

One of the higher morphological bedrock parts develops from NE to SW and acts as an underground watershed creating two incisions in the bedrock that represent the preferential paths of groundwater seepage.

This hypothesis is in line with the results of tracing tests performed with fluorescein injections. The two underground flows coming from uphill tend to converge and then

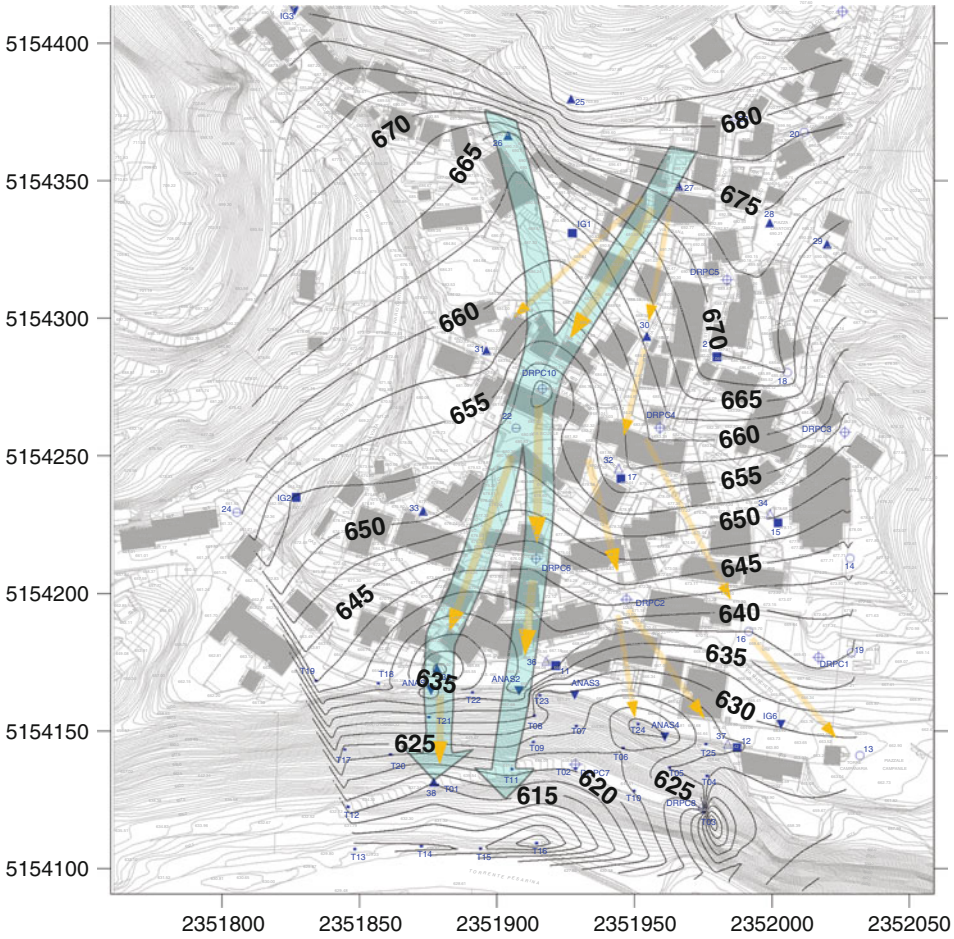


Fig. 5 Hypothesis of the preferential direction of underground water downflows based on bedrock mapping, downflow direction and on tracer tests

follow the two main preferential paths south and follow bedrock features.

The most important characteristic is the presence of a deep morphological bedrock depression, located under the part of the road which experienced the most displacements, and filled with weathered gypseous arenite and sandy silt for about 10 m (Fig. 3). Another less deep morphological depression is to the west of the underground watershed.

Seepage and Stability Analyses

A seepage analysis was performed using FEM software (Geostudio 2004) with the aim of evaluating pore pressure values which were then utilized afterwards in the slope stability analysis. Boundary conditions and soil permeability values were opportunely changed to reach ground water table positions in line with those measured by piezometers.

Slope stability conditions have been carried out on three representative sections crossing the zones where damage was more severe and extended from the Pesarina stream to the end of the alluvial fan.

Stability, deterministic and probabilistic analyses, were performed without taking the resistance of retaining sheet pile wall into account and considering both shallow and deep sliding surfaces and which also pass along discontinuity points of inclinometer curves.

Probabilistic analyses were performed using the Montecarlo method considering the variability of soil geotechnical properties, the oscillations of the Pesarina stream water level and those of pore pressures inside the slope.

The results (Table 3) showed good stability conditions for the western section with minimum safety factors values (FoS) mostly greater than 1.2 and with very low failure probability. The results obtained for section n. 1, located in the eastern part of the slope, showed critical sliding surfaces, both shallow and deep, with FoS values very close to one and with a non-negligible failure probability, $P_f = 16.37–49.37$ %, but with a low reliability index, $\beta = 0.05–1.034$ (Table 3 and Fig. 6).

Nevertheless, the hypotheses that there is sliding along these surfaces is not corroborated by the results of measurements carried out by the inclinometers nearest to this section.

Table 3 Main results of probabilistic stability analyses

Section Type of surface	μ(F) mean value	β reliability index	P_f (%) failure prob.	σ standard dev.	Fs_{min} Fs_{max}
Section 1	1.003	0.050	49.37	0.061	0.863
Shallow-low					1.150
Section 1	1.065	1.034	16.37	0.063	0.916
Shallow-whole					1.219
Section 1	1.015	0.460	33.83	0.035	0.917
Deep					1.110
Section 1	1.028	0.515	33.19	0.053	0.899
Mean value					1.160
Section 2	1.148	2.617	0.07	0.057	0.995
Shallow-high					1.309
Section 2	1.268	3.886	0.00	0.069	1.102
Shallow-whole					1.452
Section 2	1.369	9.174	0.00	0.040	1.245
Deep					1.518
Section 2	1.262	5.226	0.02	0.055	1.114
Mean value					1.426
Section 3	1.099	1.674	4.57	0.059	0.951
Shallow-low					1.273
Section 3	1.177	2.991	0.00	0.059	1.026
Shallow-high					1.329
Section 3	1.299	3.894	0.00	0.077	1.126
Shallow-whole					1.486
Section 3	1.321	5.757	0.00	0.056	1.180
Deep					1.492
Section 3	1.224	3.579	1.14	0.063	1.071
Mean value					1.395

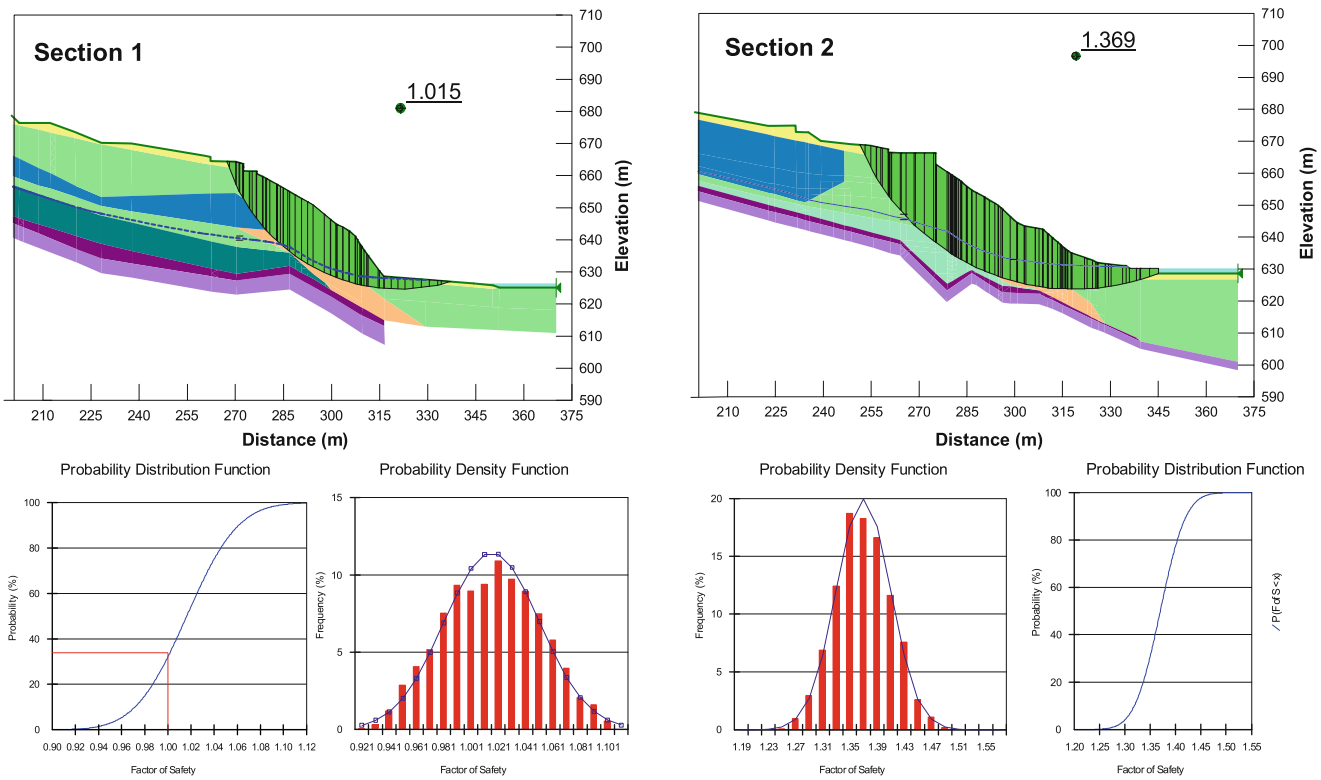


Fig. 6 Results of the probabilistic stability analyses for the Sections 1 and 2 for deep failure surfaces

Monitoring Outstanding Remarks

The damages to the road and the cracks in the buildings located in the southern part of the Prato Carnico village do not strictly appear to be caused by a landslide movement which took place in the past or which still exists. This assertion is justified by the following reasons.

- Pore pressures inside the slope remain almost stationary even during long and heavy rainfall periods and their variations in the range of 10–15kPa cannot lead to soil shear strength reductions sufficient to reactivate any deep sliding movement.
- Topographic and inclinometric measurements show, moreover, that there are no quiescent phases followed by the reactivation of superficial and deep movements that are, on the contrary, subjected to steady increments over time.
- The results of the stability analysis show generally high FoS values and associated with very low probability of failure. The FoS values resulted near to one only for one analyzed section but the shape and the position of the critical surfaces were not in agreement with the results from inclinometric measurements.
- The sheet pile wall has only slowed down the evolution of horizontal and vertical displacements in uphill zones while downhill and along the slope the movements maintain the same intensity. If the cause of damages is a rotational or translational slip movement, the structure should have reduced the driving forces acting on downhill soil mass and then slow down its displacements.

Conclusions

The complexity of the phenomena affecting the southern part of Prato Carnico Village may be explained by considering the horizontal and vertical displacements as caused by a karst sinkage located in the morphological depression found under the road and filled with weathered gypseous arenite and sandy silt.

Buried iperkarst phenomena with formation of sinkholes are very common in the High Tagliamento Valley and were already reported at the end of 1800s by Marinelli (1897, 1916) and later by Gortani (1904, 1965). Recently, Cucchi and Piano (2002) have described and analyzed the causes of karsism in the Prato Carnico territory.

In karst areas, characterized by typical morphologies of outcropping or underlying mainly carbonate rocks, where the water circulation is fast and plentiful, the rocks may undergo progressive dissolution phenomena which may cause subsidence or sinkholes.

Technical literature reports many cases of phenomena of this type (Nicod 1972; White 1988; Lamont-Black et al. 2002; Nisio 2008) as well as several others which even though they don't develop big and wide karst hollows, involve rocky basements in the same way with high gypseous or sulphate contents as well as their weathered layers in which sulphates are present in quantities lower than the native rock.

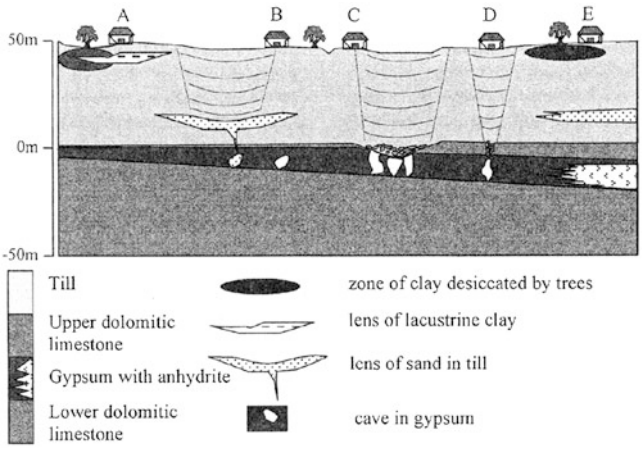


Fig. 7 Conceptual models of subsidence: (*A*) desiccation of lacustrine clays in dry periods; (*B*) downwashing of sand and silt in the till into karstic voids; (*C*) gradual lowering of till and gypsum interface; (*D*) upward migration of karstic voids; (*E*) localised desiccation and shrinking of clays due to large trees (Lamont-Black et al. 2002)

In the case of Prato Carnico, the slow and steady sinkage of the cover soil layer may be explained by a progressive collapse of the karstic voids present inside the gypseous rock which collect the upper loose material inside them, causing vertical and horizontal displacements. It is also possible that progressive loosening of the soil mass could locally cause gravitational movement of the rotational type independently of pore pressure variations or other equilibrium perturbation causes.

The Soil Defense Department of APAT (2004) also reports some of the driving causes of subsidence phenomena due to karsism as in the case of Prato Carnico:

- A carbonate substratum or one formed by soluble rocks (limestone, evaporate or sulphate rocks, exposed to karst phenomena);
- The presence of an uneven bedrock morphology, both on a small and a large scale with karst macroshapes (dolines, uvala, clefts and caves) and with karst hollows in the substratum roof (the interface between soil and rock) as result of corrosive and pedogenic processes;
- The presence of a layer of sediment with very low permeability in the roof of the substratum and formed by silts, clays, sands with different grain size distribution, homo or heterogeneous;
- Poor geotechnical properties of the upper soil layers;
- Underground circulation of plentiful water.

Figure 7 shows some conceptual models (Lamont-Black et al. 2002) which are useful in explaining

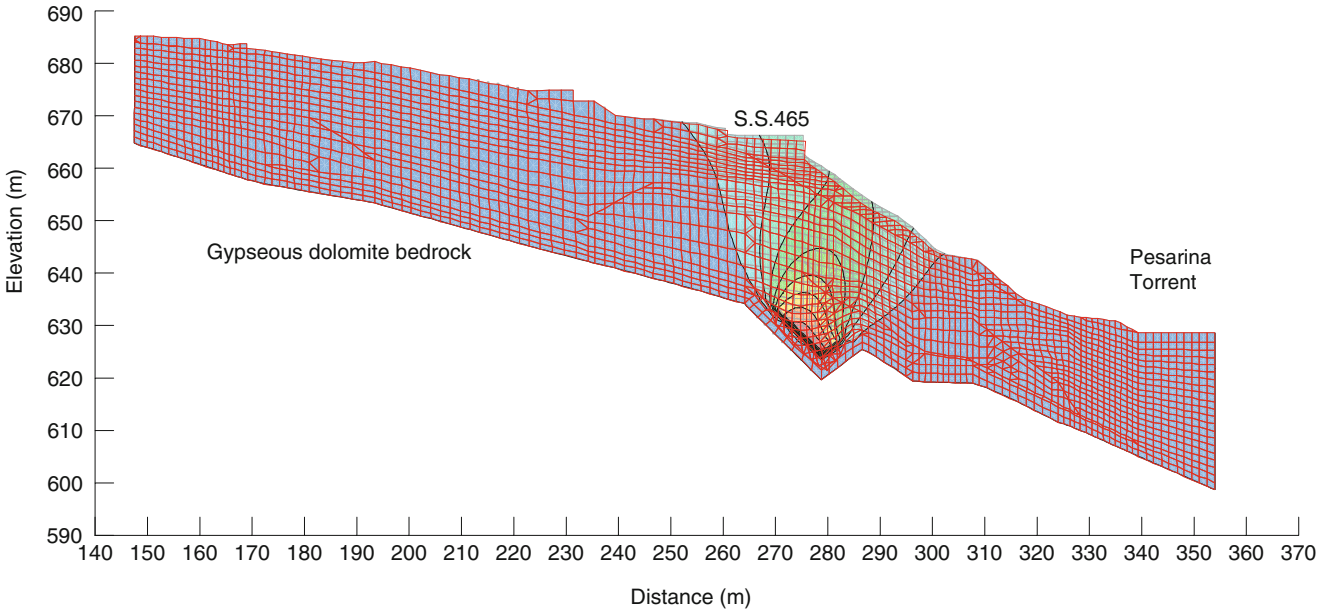


Fig. 8 Preliminary interpretation of the effects due to karstification phenomenon and obtained by FEM method

subsidence causes; excluding model A and E they may describe the origin of the damage occurring in the southern part of the Prato Carnico village. In particular, Model C shows how progressive lowering of bedrock-cover interface may cause a wide superficial subsidence hollow.

A preliminary interpretation of the subsidence due to karst phenomenon (Fig. 8) has been performed using FEM modelling simulating gypseous dissolution and removing some mesh elements which represent the rocky formation under the morphologic hollow.

The results show that this hypothesis may at least explain some of the observed kinematic mechanisms. The deformed mesh and the bulbs of XY displacements (Fig. 8) show that the dolomite gypseous rock dissolution may induce horizontal and vertical displacements that are in line with those observed during monitoring, mainly vertical displacements located over the karst hollow and lower horizontal ones with a downhill direction.

Nevertheless, the results of the FEM analyses in the lower part of the slope, between the path and Pesarina torrent, point out horizontal displacements which are however very limited, in an uphill direction while the latest measurements show the opposite direction.

These displacements could be caused not only by the karst phenomena as modelled but also by shallow slidings. This difference may be also due to the limitations of the models used which did not take into account the real planimetric and volumetric wideness of the area subject to karstification and which is unknown at the moment.

References

APAT: IdeAmbiente (2004) www.apat.gov.it

Cucchi F, Piano C (2002) Ipercarsismo superficiale e sepolto nelle evaporiti del Friuli-Venezia Giulia. Atti del Convegno di Grosseto "Le voragini catastrofiche: un nuovo problema per la Toscana", pp 35–46

DiSGAM (2008) Relazione tecnica illustrativa delle attività svolte e dei risultati conseguiti per l'elaborazione di un modello idrogeologico del sottosuolo dell'area su cui sorge l'abitato di Prato Carnico ai fini della definizione della dinamica del dissesto che lo coinvolge

GeoStudio (2004) Seepage modeling with SEEP/W – stability modeling with SLOPE/W – User's Guide

Gortani M (1904) Una dolina di sprofondamento presso Treppo Carnico. Mondo Sotterraneo, Udine 1(2):40–41

Gortani M (1965) Doline alluvionali in Carnia. Mondo Sotterraneo, Udine, n.u., pp 14–20

Lamont-Black J, Younger PL, Forth RA, Cooper AH, Bonniface JP (2002) A decision-logic framework for investigating subsidence problems potentially attributable to gypsum karstification. Eng Geol 65:205–215

Marinelli O (1897) Fenomeni di tipo carsico nei terrazzi alluvionali della Valle del tagliamento. Studi geografici delle Alpi orientali. Memorie della Società Geografica Italiana, Roma 8(2):415–419

Marinelli O (1916) La nuova dolina di sprofondamento di Auronzo. Mondo Sotterraneo, Udine 13(4/6):112–116

Nicod J (1972) Pays et paysages du calcaire. Presses Universitaires de France, Paris, 242 pp

Nisio S (2008) I fenomeni naturali di sinkhole nelle aree di pianura italiane. Memorie Descrittive della Carta Geologica d'Italia. LXXXV, pp 419–426

Venturini C (2002) Carta Geologica delle Alpi Carniche. S.EL.CA. Ed. Firenze

White WB (1988) Geomorphology and hydrology of karst terrains. Oxford University Press, New York



Rockfall Full Scale Field Tests

Alberto Clerici, Ezio Giuriani, Danilo Cambiaghi, Antonio Isceri, Giorgio Vassena, Egidio Marchina, and Luca Cominoli

Abstract

The phenomenon of rockfall along slopes is an environmental risk that frequently occurs in mountainous regions. In this phenomenon are directly involved infrastructures (railways, ordinary roads or highway) but also residential areas as well as individual structures are also interested in prevention and defense. Among different types of action taken into account to reduce the risk of rockfall, passive defenses are solutions widely adopted. In this field, the most frequently used are the elasto-plastic steel barriers, while greater resistance are offered by reinforced earth. University of Brescia has developed a special "test field" in Pezzaze (near Brescia) and in 2010 started a research activity with the aim of studying the phenomenon of rockfall both on elasto-plastic passive defenses and on reinforced earth.

Keywords

Rockfall • Elastoplastic passive defenses • Reinforced earth barrier

Introduction

Rockfall along slopes represents an environmental risk that occurs frequently in mountainous regions. In this phenomenon, infrastructures (railways, ordinary roads and highway) are directly involved, but also residential areas as well as individual structures are interested in prevention and defense.

Among the different types of action usable to reduce the risk of rockfall, protection defenses are widely adopted. The elasto-plastic steel barriers are the most frequently used, while greater resistances are given by reinforced earth. In any case, these devices have the goal of limiting the effects of rockfall transforming kinetic energy into deformation energy with development of elastic and plastic deformations.

The high performances requested to protective barriers bring to high construction costs. At present, notwithstanding their widespread use and high safety expectancy, there is – especially for reinforced earth – the lack of clear guidelines relevant to their design and to the indication of laboratory tests useful to determine the performance of the components of the barrier. At the same time, the procedures relevant to monitor the different realization phases as well as indications on full-scale tests on the finished structures are still lacking.

As to the elasto-plastic steel barriers, literature reports the results of lab tests carried out on some components (brakes, springs) and of some full scale tests. In the latter, a mass (for instance free falling or launched by a cable car) hits a barrier after a translatory motion. The rotational component of motion, so important in natural falling events both in terms of kinetic energy and of the behaviour of the rolling mass in collision with the defence, is never considered.

Some years ago, the Department of Civil Engineering, Architecture, Land and Environment began a research, granted by Ministry of Education, University of Brescia and Pietro Pisa Laboratory (belonging to the same Department)

A. Clerici (✉) • E. Giuriani • G. Vassena • E. Marchina • L. Cominoli
Department of Civil Engineering and Architecture, Land and Environment, University of Brescia, Brescia, Italy
e-mail: alberto.clerici@ing.unibs.it

D. Cambiaghi • A. Isceri
Mechanical Department, University of Brescia, Brescia, Italy

C. Margottini et al. (eds.), *Landslide Science and Practice*, Vol. 2,
DOI 10.1007/978-3-642-31445-2_60, © Springer-Verlag Berlin Heidelberg 2013



Fig. 1 View of the artificial test channel characterized by constant cross section and regular profile

with the aim of studying the phenomenon of rockfall both on elasto-plastic passive defenses and on reinforced earth.

A test field was located near Pezzaze, a small town in the north of Brescia. After the design and the construction phases, in 2010 the research activity started. Since theoretical studies have demonstrated that rotational energy of rockfall can not be considered negligible (15 % ÷ 20 % of the total energy) with respect to the translational one, the test field allows body rotation.

The tests were carried out on an artificial test channel with constant section, regular profile and a slope of about 100 % (Fig. 1). The rigid body is a reinforced concrete sphere (density equal to 28 kN/m^3, not exceeding the density of natural rocks) with a diameter of 1.5 m, which allows to reach high energies (about 4 MJ). Along the test channel were arranged different release points of the sphere in order to have different energies on reinforced earth. An automatic camera enables to control, step by step, every phase of the launch and of the impact too. This system provides also the speed before and during the impact.

The possibility of considering rotational energy of the falling body underlines the originality of this "field test" that is suitable to test both elastic-plastic barriers and reinforced earth, also with subsequent events and to verify the capacity to maintain performance after more impacts.



Fig. 2 Trolley necessary to host the counter pulley

Test Set-Up Description

The Mechanical Design Group of the University of Brescia has been charged to design a special system to lift and release the sphere necessary to test the reinforced earth.

The environmental conditions were:

- Impossibility to use standard vehicles for recovery and transport of the sphere (no available roads);
- Impossibility to take advantage of any kind of sky lift like facility;
- No electric power available;

To lift the sphere an electric motor operated hoist was foreseen; the motor being fed by way of a diesel generator with a capacity of 12 kW. A counter pulley system was designed to reduce both the pulling force and the wire rope size.

A trolley had been foreseen to host the counter pulley. Such trolley needed to be heavy enough to guarantee the tension of the wire rope when unloaded, especially in descent and recovery phase, after the release had been performed.

To play the role of the trolley a secondary sphere was designed, equipped with an axis linked to the pulley support structure, as shown in Fig. 2.

The mass of such sphere was in the range of 3 tons. The primary sphere was to be linked to the secondary one by way of two tie-rods, ending with bearings. As a consequence the primary sphere needed to be equipped with a couple of protruding shanks located in diametrically opposite positions, such shanks being to be dismantled before the release of the sphere.



Fig. 3 The steel skeleton of the primary sphere

The sphere had consequently to be bored with couples of opposite housings properly shaped to help inserting and dismantling the shanks. To help hooking the sphere in whatever position it may stand, several couples of opposite shank housings were foreseen, located all over the outer surface.

To the purpose a concrete sphere was molded around a steel skeleton shaped as in Fig. 3, so to present to the outside the needed couples of machined housing to host the dismountable shanks.

Figure 4 shows the two spheres linked together and ready for the lifting phase.

The release of the sphere was problematic too. To the purpose a kind of textile hammock has been designed, fit to be linked at the four corners to several couples of hooking points located on the ground aside the roller channel. The linkage was foreseen by way of wire ropes. The hooking points have been located at the foreseen release levels.

The first step to perform the test is to lye the hammock on the roller channel at the foreseen level and to connect it to the linking wire ropes. Then the two spheres are lifted until the primary one is on the hammock (Fig. 5).

The hammock is then rolled-up to wrap the sphere (Fig. 6). Thanks to other wire rope linkages it features a kind of pocket where the sphere can rest. The hoist releases a little so that the weight of the sphere leans completely on the hammock.

Now the tie–rods are no more in tension, and it is possible to manually dismount the shanks after disconnecting the tie-rods themselves (Fig. 7).

The dismounting must be performed by skilled worker, properly instructed and equipped with safety devices. When the primary sphere is free from shanks and cables the upper limb of the hammock can be released and the sphere is left free to roll down.

It is important to release contemporarily the two upper cables retaining the hammock. For this purpose a special



Fig. 4 The two spheres during the lifting phase



Fig. 5 Hammock on the roller channel



Fig. 6 Phase of rolled up of the sphere



Fig. 7 Sphere ready for the test



Fig. 8 Special device designed for release contemporarily the hammock

device has been designed (Fig. 8). It is moved by pneumatic cylinders operated by pressurized gas (dry nitrogen transported in bottles). The cylinders are controlled by way of electric valve properly synchronized.

Experimental Measurements

The measurement of the speed of the falling concrete sphere has been carried out using a high frequency camera (FasteImaging TroubleShotter model) (Fig. 9). The images have been acquired in grey levels at a 500 (fps) with a resolution of 1280 × 512 pixel.

The speed of the falling sphere has been obtained thanks to the MiDS Express for Fastec software, that allows the user to visualize the video and to make exact measurements on the movie itself (Fig. 10).

The geometry of the test site has been measured using a 3D TLS (terrestrial laser scanner) Faro Photon 80 (Fig. 11). The 3D raw data has been managed using the JRC 3D Reconstructor software package. The results of these measurements has been the 3D accurate description of the test site, the starting position of the sphere and the altimetric profile of the test site.

The targets (Fig. 11) has been observed also with total station. The distances has been indipentently verified using linear rods. Figure 12 represents the 3D laser scanner measurement of the site.

The first test has shown a speed of 10.0 m/s while regarding the second test the speed measured at a distance of 2.63 m from the earth dam, was equal to 15.47 m/s (55.69 km/h). A second speed evaluation, in a shorter interval, equal at 0.20 m, have shown a speed of 15.75 m/s (56.69 km/h).



Fig. 9 The high frequency camera used during tests

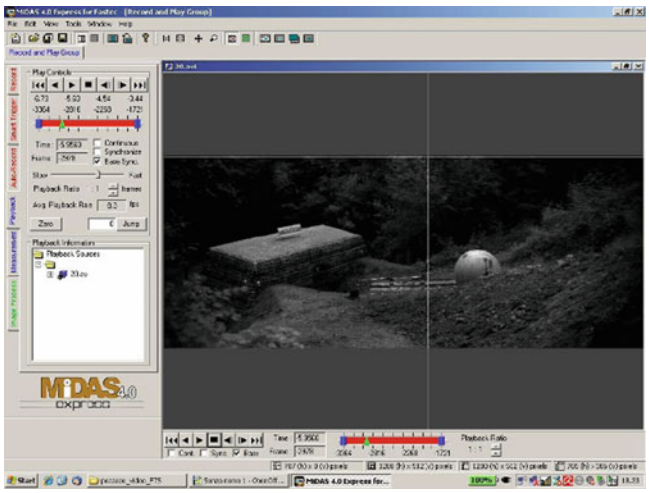


Fig. 10 The "print screen" of the MiDS software

The speed of the sphere at the time of impact can be estimated at about 60 km/h.

Preliminary Experimental Results

In summer 2010 were performed preliminary experimental evidences of "roller channel".

The reinforced earth barrier (Fig. 13) consists of six layers of 50 cm thickness for a total height of 3 m. The width at the base is 4 m while at the top is 1.9 m. The angle of inclination of the walls is about 71°. The trajectory of the primary sphere crosses the barrier at about mid-height in perpendicular direction of the wall.



Fig. 11 3D measurements with laser scanner



Fig. 12 3D image of the dam after the impact with the concrete sphere

In the first test, the sphere was placed at 11.15 m from the point of impact while in the second test the height was equal to 29.45 m (Fig. 14).

The potential energy ($E_p = mgh$) associated with release points (considering the mass of the sphere $m = 4{,}875$ kg and the acceleration of gravity $g = 9.81$ m/s^2) is respectively 0.52 and 1.38 MJ. In both tests the reinforced barrier stopped the rigid body with damage tolerance (Figs. 15 and 16).

The kinetic energy E_c of the sphere in movement can be calculated as:



Fig. 13 Reinforced earth barrier with the imprint caused by the impact of the sphere after the first test



Fig. 15 Imprint of the primary sphere on reinforced earth after first test (0.52 MJ)

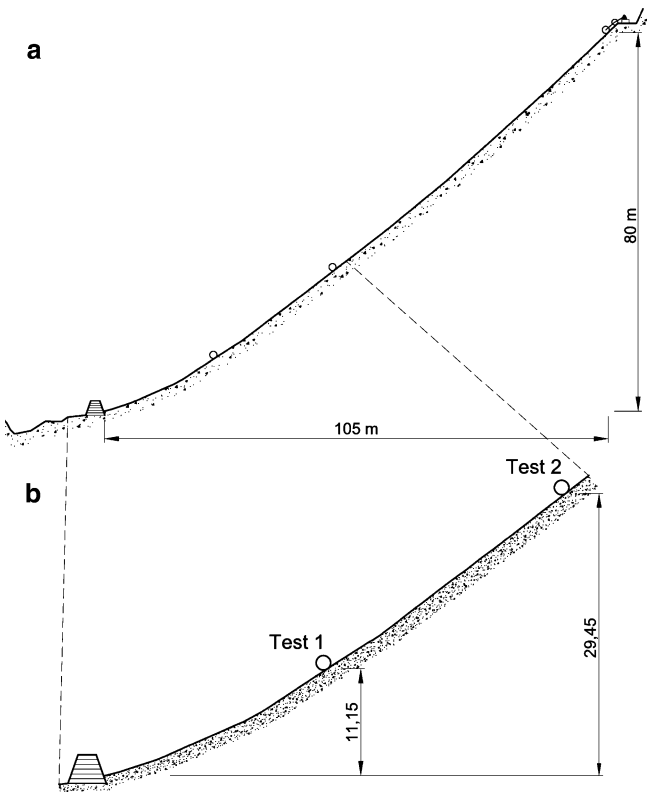


Fig. 14 Section of the artificial roller channel (**a**) and detail of the two release points (**b**)

$$E_c = \frac{1}{2}mv^2 + \frac{1}{2}I\omega^2$$

where the first part of E_c is related to the translatory motion at velocity v while the second part is due to the rotary motion at angular velocity ω. For a sphere of radius r and homogeneous material the mass moment of inertia I can be calculated as:



Fig. 16 Damage of the upper part of reinforced earth after second test (1.38 MJ)

$$I = \frac{2}{5}mr^2$$

In the case of rolling without sliding (no relative movement between the point of contact of the sphere and the support) the two velocities are related by:

$$\omega = \frac{v}{r}$$

In this way:

$$E_c = \left(\frac{1}{2} + \frac{2}{10}\right)mv^2 = \frac{7}{10}mv^2$$

It can be noticed that the energy associated with rotation is almost 30 % of the total energy. The upwelling of the



Fig. 17 The sphere hit the reinforced barrier at the base, but rolling over itself, climbed the upstream slope significantly

sphere along the barrier is significantly even in the first test with limited energy. It can be estimated equal to 1 m height (Fig. 17).

During tests were measured velocity (at the time of impact) of 10.0 and 15.75 m/s corresponding to kinetic energies of 0.33 and 0.83 MJ. The loss of energy, compared with a theoretical calculation, can be attributed to the non perfect rolling of the sphere due to geometrical irregularities of the roller channel which led to a series of inelastic impacts.

In addition, the significant elastic deformations of the roller channel observed during the movement of the sphere increase the losses for rolling friction, especially at points where the trajectory change inclination near the reinforced barrier.

Conclusion

The test field has been completed and first tests (with rolling lengths of 17 and 35 m) have been carried out.

Next tests are planned to make maximum use of the 135 m length of the launch channel. The availability of high energies (considering both the translatory and rotational motion) makes this test site unique.

Current researches on reinforced earth barriers have the goal of investigating the following items: quantification of the rotational energy in terms of different going up heights along the defense structure; quantification of the absorption capacity of the kinetic energy due to deformation resulting from subsequent impacts on the defence; research of innovative solutions on the composition of the reinforced earth with the aim of reducing their volumes maintaining high absorption capacity.

Acknowledgments The Authors wish to express their gratitude to the Ministry of University and Research (MIUR) for financing the research work with the national projects PRIN 2003 "*Previsione, prevenzione e protezione da caduta massi*" and PRIN 2005 "*Prove in vera grandezza della efficienza delle barriere paramassi e dei suoi componeneti*".
A special acknowledgement goes to Mr. Domenico Fiorillo and Mr. Domenico Caravaggi (technicians of the Laboratory Pietro Pisa of the University of Brescia) and to Olli Scavi s.r.l. for their assistance in the experimental work.



Sprinkling Tests to Understand Hydrological Behaviour of Mudslide

Dominika Krzeminska, Thom Bogaard, Taha-Hocine Debieche, Vincent Marc, and Jean-Philippe Malet

Abstract

The unsaturated zone buffers precipitation and controls groundwater recharges. Quantification of groundwater recharges is important for the improvement of hydrogeomorphological hazard analysis. The importance of fast preferential flow is recognized in literature, but its quantification remains difficult.

This paper presents the results from three 1 m^2 sprinkling experiments carried out in highly heterogeneous black marls of the Super-Sauze mudslide, in Southern French Alps. The aim of the experiments was to study the hydrological system within three morphological units characterized by different displacement rates and possible hydrological conditions. Special attention was given to identify and characterise the preferential flow patterns with the attempt for its quantification. The infiltration process was monitored with hydrological observations and hydrochemical tracers (Br^-, Cl^-). Based on the analysis of all available field data, conceptual models of the hydrological responses were proposed.

Keywords

Preferential flow • Sprinkling experiment • Active landslide

Introduction

The importance of understanding the hydrological system within a landslide is commonly accepted, however, including hydrological processes and their variability in landslide modelling is quite difficult and therefore often limited (Bogaard 2001; Lindenmaier 2007). In spite significant research attention given to advanced study of hydrological processes within landslide (e.g. Iverson 2000; Uchida et al. 2001; de Montety et al. 2007; Wienhöfer et al. 2011), their understanding is still limited especially because of the strong heterogeneity of landslide lithology and the spatial and temporal variations of the hydrological properties.

This is particularly true when dealing with highly heterogeneous clay shale slopes such as black marls. Additionally, in slow moving clayey landslides, the continuous opening and closing of fissure apertures by reworked sliding material occur (Bogaard 2001). Fissure networks provide preferential flow paths for infiltration and drainage. This changes the permeability of the soil influencing infiltration rates, saturation processes and groundwater recharges. The quantification of the groundwater recharge processes, in particular taking into account preferential flow, is a natural next step in advanced understanding of hydrological systems in hillslopes and landslides (Savage et al. 2003; Coe et al. 2004; Weiler and McDonnell 2007). Although the complexity of the processes and their high spatial variability make it very difficult to measure preferential flow in the field and to build

D. Krzeminska (✉) • T. Bogaard
Water Resources Section, Delft University of Technology, Stevinweg 1, 2628 CN Delft, Netherlands
e-mail: d.m.krzeminska@tudelft.nl

T.-H. Debieche • V. Marc
Laboratory of Hydrogeology, University of Avignon and Pays de Vaucluse, Avignon, France

J.-P. Malet
Institut de Physique du Globe de Strasbourg, CNRS UMR 7516, Université de Strasbourg, Ecole et Observatoire des Sciences de la Terre, 5 rue Descartes, Strasbourg F-67084, France

C. Margottini et al. (eds.), *Landslide Science and Practice*, Vol. 2,
DOI 10.1007/978-3-642-31445-2_61, © Springer-Verlag Berlin Heidelberg 2013

up process models (van Schaik 2010). Nevertheless, a combination of hydrodynamic and hydrochemical responses observed during infiltration tests can give valuable information about natural preferential water pathways (e.g. Debieche et al. 2011).

This paper focuses on 1 m^2-scale sprinkling tests using hydrochemical tracers (Br^-, Cl^-). The main objective of our research is to identify and measure the dominant hydrological process and its distribution across the mudslide. The sprinkling tests were carried out in three main morphological units of the mudslide in order to observe spatial heterogeneity in hydrological responses, with special attention given to preferential flow processes. The observations are then generalised into a hydrological concept of the behaviour of different hydromorphological areas within the mudslide and linked to the observed spatial distribution of the mudslide movements.

Site Description

The Super-Sauze mudslide (Fig. 1a) is a persistently active mudslide and consists of a heterogeneous clay-rich material containing reworked blocks and panels of marls at various stage of weathering (Malet et al. 2005). Infiltration of rainfall and snow melt is the main source of groundwater, with limited water contribution from deep water sources along the major faults (de Montety et al. 2007).

Malet et al. (2005) divide the morphology of the Super-Sauze mudslide into three hydro-geomorphological units (Fig. 1a):

- Upper unit (HG1)– very active and very wet viscous muddy formation, with variety of crack systems,
- Western part of upper unit (HG2) – the most stable part of the landslide, with dense, compacted texture,
- Lower unit (HG3), which is stiff compact, impervious and stable formation with limited extension of cracked surface system.

The experiment plots were selected to represents morphologically different parts of the landslide: crumbly area near the crown (HG1), compacted stable part of the deposit (HG2) and active area which is muddy formation with width open fissures (HG1).

Methodology

Field Experimental Setup

Three 1 m^2 infiltration experiments were carried out, between 20 and 25 July 2008. For each plot, 2 days of 7–8 h artificial rain was applied with the use of a rain simulator. The rain was applied in time blocks of 15 min rain and 15 min break with

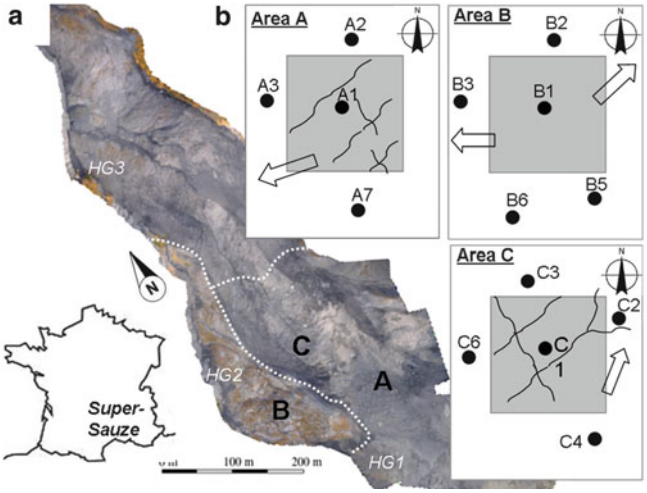


Fig. 1 (**a**) Super-Sauze mudslide with the indicated locations of three sprinkling tests; (**b**) schematic representation of experimental areas (not scaled); *grey squares* represent 1 m^2 *sprinkling plots* and *dots* represent location of the piezometers

average intensity of approximately 50 $mm.h^{-1}$. The tracing was realised with two tracers: Br^- during the first day of experiment and Cl^- during the second day of experiment. In order to protect the experiment from wind disturbances and to minimize evaporation the rainfall infiltration area was covered with a tent (Fig. 2).

Within each plot, 4–5 shallow piezometers were installed: one in the middle of the plot, 2 in the direction of expected (sub-) surface water movement (in the direction of fissures, if they were visible at the surface) and one uphill from the plot as a reference (Fig. 1b).

The depth of the piezometers is different at each area and depends on local hydromorphological conditions:

- Within plot A, all piezometers were installed at around 2 m depth;
- Within plot B, depths of the piezometers were determined by the presence of rocks in the soil and vary from 1.30 to 3 m;
- Within plot C, depths of the piezometers are around 1 m due to the shallow groundwater level.

Groundwater responses were monitored manually every 15 min, and with automatic water pressure devices every 3 min. The water for hydrochemical analyses was sampled every 1 h from all piezometers during the sprinkling experiment and one time per day for two consecutive days after the experiment.

Analysis Methodology

The analyses of the sprinkling experiments were done based on the water balance calculations (1) and mass balance for the tracer (2):

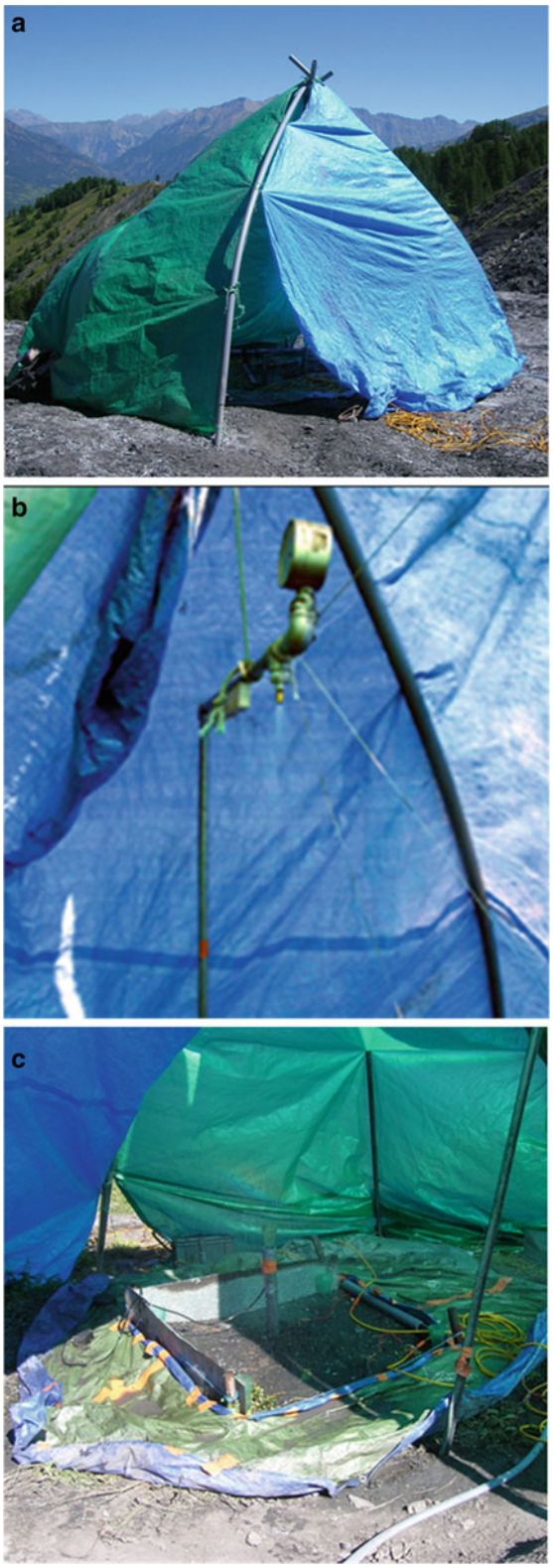


Fig. 2 The photograph of the experimental setup: (**a**) protective tent, (**b**) sprinkler, (**c**) 1 m^2 sprinkling plot

$$P + GW_{in} = GW_{out} + OF + E + SSF + \Delta S \quad (1)$$

where: P is applied rain [m^3], OF is an overland flow [m^3] and ΔS is change in storage over the sprinkling experiment [m^3]; GW_{in} and GW_{out} are groundwater inflow and outflow [m^3] and are assumed to be equal; E is evaporation [m^3] and is neglected as the experimental plots were cover with the tent; SSF is a subsurface flow [m^3] and it comprises exfiltration, vertical and lateral flow.

$$\begin{aligned} V_T &= V_{pre-event} + V_{\inf} \\ C_T \cdot V_T &= C_{pre-event} \cdot V_{pre-event} + C_{\inf} \cdot V_{\inf} \end{aligned} \quad (2)$$

where V_T, $V_{pre\text{-}event}$ and V_{inf} are respectively the total water volume, the estimated volume of pre-event water and the volume of infiltrated water in [m^3]; C is the tracer concentration in [mg m^{-3}] and the indexes are analogical to the one used to determine the water volumes.

Results of Sprinkling Experiments

Table 1 shows measured components of the water balance and applied tracer concentration for each plot. The summary of observed groundwater variation and tracer concentration patterns is presented in Fig. 3. Results of the three sprinkling experiments show large difference in their hydrodynamic and hydrochemical responses which confirm great variation of hydrogeomorphological properties over the landslide. The general behaviour is in agreement with the one presented by Debieche et al. (2011). The rain water infiltrates into the top soil either through the matrix (plot B) or through both matrix and preferential flow paths (plot A and C). The water flow in the subsurface follows the overall slope direction, however, the presence of fissures and macroporosity (plot A and C) strongly influence the exact direction of the flow.

Based on three experimental plots, three conceptual models of the principal water pathways are formulated:

- Fast vertical flow through the matrix and fissures,
- Matrix flow with limited fissures,
- Isolated fissure system.

Plot A

Plot A represents fast input–output type of hydrological response. The system gives very fast response to the rainfall as well as sudden groundwater level drop after rainfall

Table 1 Measured water balance components for each experimental plot and applied tracer concentrations

	Plot A		Plot B		Plot C	
Day of experiment (tracer)	D1 (Br^-)	D2 (Cl^-)	D1 (Br^-)	D2 (Cl^-)	D1 (Br^-)	D2 (Cl^-)
Rain, P [m^3]	0.272	0.332	0.291	0.304	0.364	0.419
Applied tracers [g m^{-3}]						
- Br^-	118.3	461.3	122.5	–	121.5	–
- Cl^-	–	1034.9	–	1,047	–	127.7
Overland flow, OF [m^3]	Not observed		0.217	0.226	Not observed	
Subsurface flow (exfiltration form the fissures) [m^3]	Not observed		Not observed		>165[a]	0.304

[a]Exfiltration started after 2 h of sprinkling but was measured only since the third hour

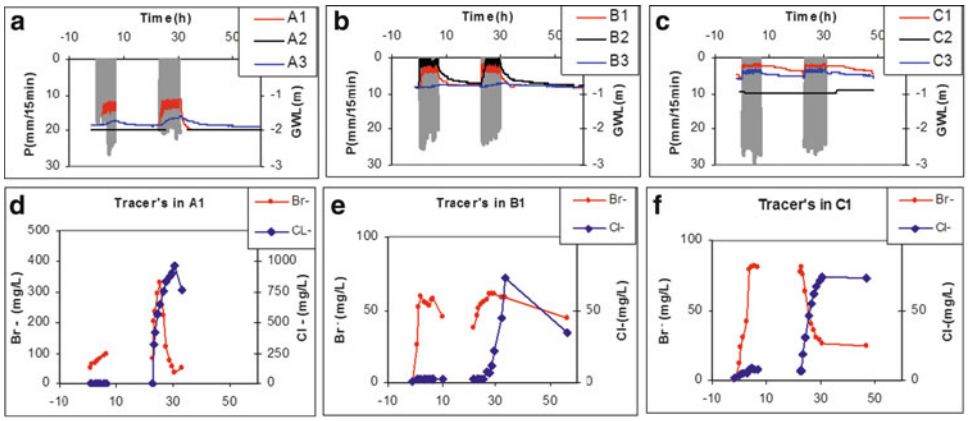


Fig. 3 Results of three sprinkling experiments: panels (**a**),(**b**) and (**c**) show sprinkling intensity (primary Y-axis) and groundwater level (GWL) responses observed in plot A, B and C (secondary Y-axis); panels (**d**),(**e**) and (**f**) examples of tracer concentrations observed in piezometers A1, B1 and C1 respectively

is finished. Groundwater level fluctuation in piezometer A1 during the first rain period shows very fast vertical movement of water: both, matrix flow and preferential flow are rapid. High infiltration capacity of the area (>40 mm. h^{-1}, which is the sprinkling intensity), together with surface area characteristics, confirms presence of highly permeable matrix and well connected fissure network. The groundwater behaviour in piezometers A2 and A3 gives an indication of the importance of preferential flow in the area: they suggest the occurrence of faster later flow in the direction indicated by the fissure network and, much slower, matrix flow in a general slope direction.

The mixing process is very clear on plot A. The Br^- concentration changes with time show that there is pre-event water in the system that can readily move and 'dilute' the infiltrating water. This high capacity of water remobilization indicates that water is stored not only in the matrix but also has to be stored in macropores (e.g. fissures). After the sprinkling experiment, concentration of the Br^- stayed at a high level which confirms that water is (temporarily) stored in the fissures. Within 4 h after the end of the experiment, the system comes back to its initial condition. This clearly indicates that within plot A, hydrological processes are strongly influenced by the system of deep fissures that drains the water out of the experiment area.

Plot B

The general observation of the water balance component (Table 1) indicates that plot B represents matrix behaviour. The relatively low concentration of the tracer in the groundwater can be directly related to the limited infiltration capacity of the area and limited mixing processes. Only 25 % of applied water infiltrates into the soil and the majority of the water leaves the system as overland flow. Moreover, the tracer concentrations are relatively low and they remain constant during and after the experiment. This means that there is limited contribution of pre-event water in mixing processes or that not the entire experiment area is hydrologically active. It also indicates low hydraulic conductivity at the deeper layers in the area.

Plot C

The presence of a largely open (up to 0.14 m) fissure system influences distribution of the infiltrating water in the area. The groundwater response and water balance analysis shows that the storage capacity of the area is limited and that hydrological response of the system is a combination of fast vertical infiltration through fissures (surface infiltration),

fast downslope flow (subsurface flow through the fissures), and slow matrix-like flow.

The behaviour of the tracer concentration indicates complex mixing processes in plot C. The relatively low concentration of tracer in piezometer C1 indicates that the significant amount of pre-event water is stored in the matrix but is not mobilised (only 10 % of mobile water). The tracer concentration in the subsurface flow is almost the same as the applied initial. It demonstrates that the fissure system is isolated and it provides direct drainage for infiltrated water. The preferential flow occurred through this fissures system is around 50–80 % of applied water.

Discussion and Conclusion

This paper presents the analysis of three 1 m^2 sprinkling experiments carried out in the highly heterogeneous mudslide of Super-Sauze. Three hydrological conceptual models of different hydrogeomorphological units are proposed. Presented concepts support the conclusion of Debieche et al. (2011) that landslide body should be seen as double porosity systems, with spatially variable characteristics. They also stress the importance of distributed approaches for forecasting spatio-temporal behaviour of the landslides (e.g.: van Westen et al. 2005; Malet et al. 2005).

In general, the experimental data confirm the advantage of combined hydrological and hydrochemical on-site investigations. They show that small scale sprinkling test can give useful information about the local hydrological system, especially their spatial heterogeneity. As such, they create very good alternative for large scale sprinkling experiments (e.g.: Debieche et al. 2011) that are logistically and financially very demanding and cannot be undertaken on a regular basis.

On going study of the three sprinkling tests include detailed analysis of: tracer mass balance, depletion curve and Darcy's flow. The next step of this study will be to introduce the concept into a spatially-distributed model coupling hydrological and stability dynamics (van Beek 2002)

Acknowledgments

This research is a part of the "Mountain-Risks" project that is Marie Curie Research Training Network within the 6th Framework Program of the European Commission and ANR-ECCO "Ecou-PRef" Programme financially supported by the French Ministry of Research and the French Research Agency.

References

Bogaard TA (2001) Analysis of hydrological processes in unstable clayey slops. Ph.D. thesis, University of Utrecht, Utrecht

Coe JA, Michael JA, Crovelli RA, Savage WZ, Laprade WT, Nashem WD (2004) Probabilistic assessment of precipitation-triggered landslides using historical records of landslide occurrence, Seattle, Washington. Environ Eng Geosci 10:103–122

Debieche T-H, Bogaard TA, Marc V, Emblanch C, Krzeminska DM, Malet J-P (2011) Hydrological and hydrochemical processes observed during large-scale infiltration experiment: Super – Sauze mudslide (France). Hydrol Process. doi:10.1002/hyp. 7843

De Montety V, Marc V, Emblanch C, Malet J-P, Bertrand C, Maquaire O, Bogaard TA (2007) Identifying the origin of groundwater and flow processes in complex landslides affecting black marls: insights from a hydrochemical survey. Earth Surf Process Land 32:32–48

Iverson RM (2000) Landslide triggering by rain infiltration. Water Resour Res 36(7):1897–1910

Malet J-P, van Asch TWJ, van Beek R, Maquaire O (2005) Forecasting the behaviour of complex landslides with a spatially distributed hydrological model. Nat Hazards Ear Syst Sci 5:71–85

Lindenmaier F (2007) Hydrology of a large unstable hillslope at Ebnit, Vorarlberg: identifying dominating processes and structures. Ph.D thesis, Universität Potsdam, Potsdam

Savage WZ, Godt JW, Baum RL (2003) A model for spatially and temporally distributed shallow landslide initiation by rainfall infiltration. In: Proceedings of the third international conference on debris flow hazards mitigation: mechanics, prediction, and assessment. Davos, 10–12 Sept 2003, pp 179–187

Uchida T, Kosugi K, Mizuyama T (2001) Effects of pipeflow on hydrological process and its relation to landslide: a review of pipeflow studies in forested headwater catchments. Hydrol Process 15:2151–2174

Weiler M, McDonnell JJ (2007) Conceptualizing lateral preferential flow and flow networks and simulating the effects on gauged and ungauged hillslopes. Water Resour Res 43:W03403. doi:10.1029/2006WR004867

Wienhöfer J, Lindenmaier F and Zehe E (2011) Challenges in Understanding the Hydrologic Controls on the Mobility of Slow-Moving Landslides. Vadose Zone Journal. 10(2): 496–511, doi:10.2136/vzj2009.0182

Van Beek L PH (2002) Assessment of the influence of changes in land use and climate on landslide activity in a Mediterranean environment. Ph.D. thesis, University of Utrecht, Utrecht

Van Schaik L (2010) The role of macropore flow from plot to catchment scale: a study in a semi-arid area. Ph.D. thesis, Utrecht University, Utrecht

van Westen CJ, van Asch TWJ, Soeters R (2005) Landslide hazard and risk zonation: why is it still so difficult? Bull Eng Geol Environ IAEG 65:167–184



High Resolution InSAR Monitoring of Coastal Landslides

Vernon Singhroy, François Charbonneau, Junhua Li, and Rejean Couture

Abstract

Radar interferometry (InSar) techniques using images from several radar satellites are increasingly being used in slope stability assessment. During the past year there were at least 25 media reports of landslides, some fatal, occurring in various areas in Canada. In this paper, we provide examples of using high resolution (3 m) InSAR techniques from RADARSAT and TerraSAR X to monitor coastal landslide affectiong transportation corridors. The high-resolution InSAR images are very effective in characterizing differential motion within these low velocity coastal landslides. The active wet spring periods are better monitored by the more frequent revisits from TerraSAR X.

Keywords

RADARSAT-2 • TerraSAR X • InSAR • Landslides • Coastal erosion

Introduction

Canada has the longest coastline and largest continental margin in the world. As a result, it is vulnerable to coastal hazards. Coastal landslides represent a specific threat on the coastlines of populated areas in southern British Columbia and the Atlantic provinces because high tsunami potential. In these coastal regions, landslides are triggered by seawater intrusion, coastal scouring, high intensity/frequency rainfall and storm events, land subsidence and human activity. They occur without warning and with little time lag between failures. Along the Canadian coastline, there are various con of topography, geomorphology, and geology conditions, which are conductive to mass failure (Mosher 2008). IN British Columbia, for example, rainfall intensity between 80 and 100 mm in 24 h has resulted in a rapid increase in coastal landslides with increasing precipitation (Guthrie et al. 2010). Along the Oregon coast, landslides are directly correlated with erosion by high winter waves and increased rainfall during the major winter storms (Witter et al. 2009).

Recently, InSAR techniques were increasingly being used in slope stability assessment (Singhroy et al. 1998, 2008; Ferretti et al. 2001, and others). Our research has shown that PS InSAR™ techniques using field corner reflectors are useful to monitor coastal landslides affecting strategic transportation corridors in Eastern Canada. We present the results of high resolution RADARSAT-2 and TerraSAR X images for monitoring several active coastal landslides resulting from high frequency and intensity if storms combined with favourable geological conditions.

Landslisdes on the Western Newfoundland Coastline

In this section, we report on several landslides along the western Newfoundland coast at Corner Brook and Daniels Harbour.

Batterson et al. (1999) reported that three separate landslides occurred within several hours of one another

V. Singhroy (✉) • F. Charbonneau • J. Li
Canada Centre for Remote Sensing, Natural Resources Canada,
588 Booth Street, Ottawa K1A 0Y7, Canada
e-mail: vern.singhroy@Nrcan.gc.ca

R. Couture
Geological Survey of Canada, Natural Resources Canada,
601 Booth Street, Ottawa K1A 0Y7, Canada

C. Margottini et al. (eds.), *Landslide Science and Practice*, Vol. 2,
DOI 10.1007/978-3-642-31445-2_62, © Springer-Verlag Berlin Heidelberg 2013

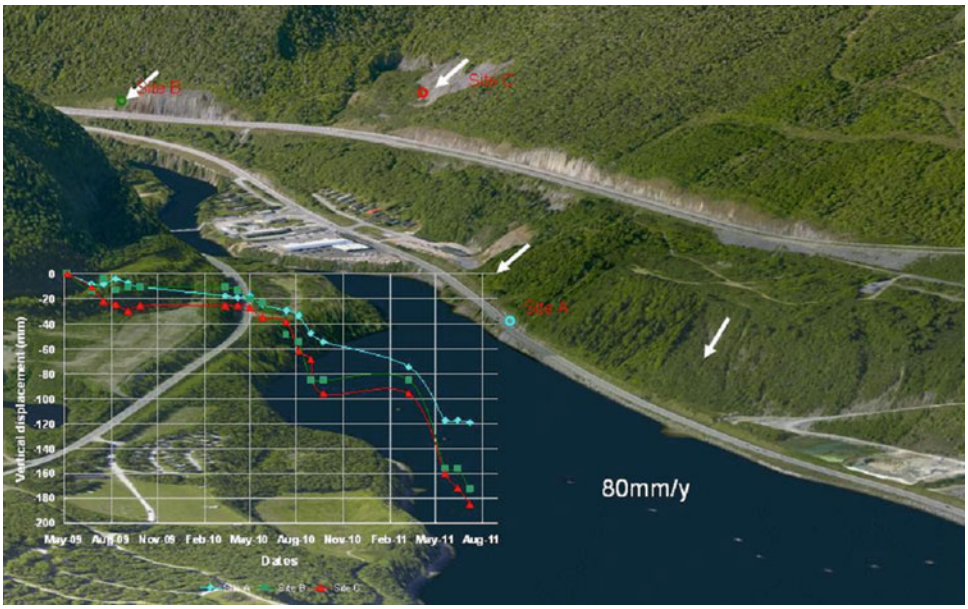


Fig. 1 InSAR monitoring of landslides at Corner Brook, Newfoundland

along Riverside Drive in Corner Brook, Newfoundland, in April 1994. These landslides cause the main highway to close for several months, and are still active. Since May 2009, we acquired monthly high resolution 3 m RADARSAT InSAR images. To date we analysed over 20 images using the Gamma IPTA techniques. Our results show that over the past 2 years all the landslides affecting the coastal highway are still active with an average motion of about 80 mm a year (Fig. 1).

The landslides on the upper steeper slopes are moving more rapidly (90 mm/year) than on the lower coastal slopes, (50 mm/year). As expected, the wet summer months are more active than frozen winter months. At Daniles Harbour, during the spring of 2008, several homes were destroyed and the main highway was re reouted because of the coastal landslides. Our field investigation suggests that this landslide is triggered by erosion from high winter waves combined with groundwater seeps from the nearby reseroir.

Batterson et al. (1999) and others documented the detail geotechnical investigations at this site. Since the landslide in 2008, we started acquiring RADARSAT 2 InSAR omages for every 24 days orbital cycle.

During the spring of 2010, we acquired TerraSAR X InSAR images every 8 days for 2 months. To date our InSAR results show that this landslide is still active with very slow motion of about 15 mm a year. The most active is during the spring and summer months which shows motion about 25 m during these wet periods (Fig. 2).

During the winter, months when the ground is frozen our InSAR data show that the landslide is stable. We also observed additional landslide areas about 2 km south along the same coastline. We believe that the similar conditions of high storm erosion combined with groundwater seeps may also be responsible for these new landslides. Our high-resolution (3 m) TerraSAR X data show that the spring months are particularly active. We measure about 20 mm motion after the spring rains. The more frequent revisit by TerraSAR, compared to the 24-day revisits of RADARSAT 2, are particularly useful to monitor the effects of the spring rains and melting snow. Future satellites such as the RADARSAT Constellation Mission with a 5-day revisit will be more effective to monitor active spring conditions.

During the winter, months when the ground is frozen our InSAR data show that the landslide is stable. We also observed additional landslide areas about 2 km south along the same coastline. We believe that the similar conditions of high storm erosion combined with groundwater seeps may also be responsible for these new landslides. Our high-resolution (3 m) TerraSAR X data show that the spring months are particularly active. We measure about 20 mm motion after the spring rains. The more frequent revisit by TerraSAR, compared to the 24-day revisits of RADARSAT 2, are particularly useful to monitor the effects of the spring rains and melting snow. Future satellites such as the RADARSAT Constellation Mission with a 5-day revisit will be more effective to monitor active spring conditions.

Gascons, Quebec

Our site at Gascon, Quebec is characterised by the presence of numerous large, oper fissures coinciding with the main discontinuity found in the underlying bedrock. Fissures show opening varying from to tens of centimetres to tens of metres indications of significant rock slope movement and instability processes at the site (Locat 2010). Some of these fissures were monitored in the 1990s and are now part of a

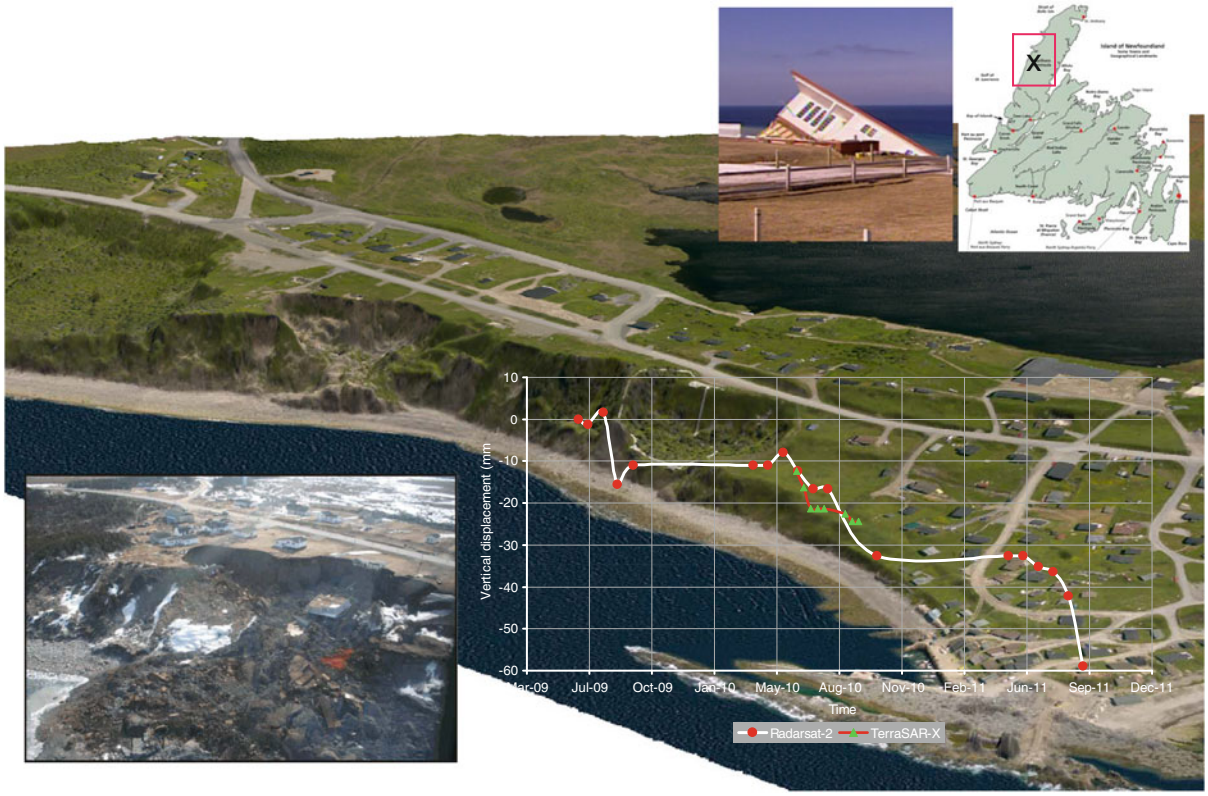


Fig. 2 InSAR monitoring of landslides at Daniels Harbour, Newfoundland

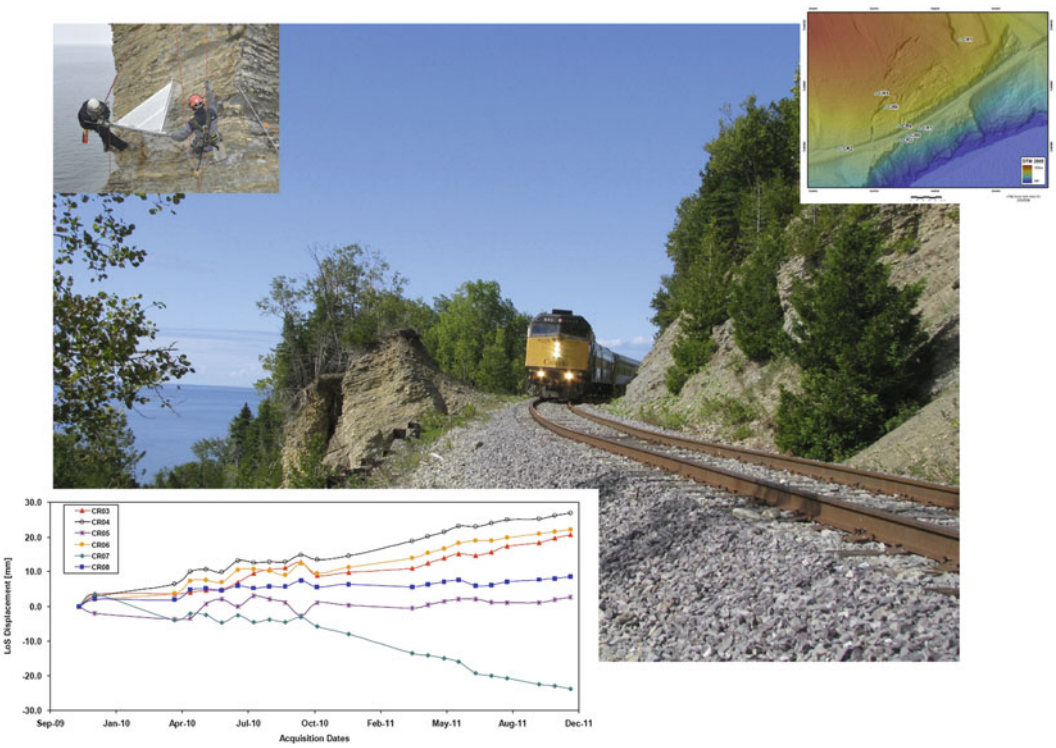


Fig. 3 InSAR monitoring of Gascons Landslide, Quebec

new monitoring program using traditional geotechnical instrumentation.

In summer 1998, a rock failure occurred and the railway line was close for several days. Because the site is vegetated 20 corner reflectors were installed to monitor the landslide motion. To date, our results show a significant motion using both RADARSAT-2 images, taken over a 2-year period. We found similar motion as at Corner Brook were the uooer slopes above the railway is more active (12 mm/year) (Fig. 3). This indicates that favourable geological conditions – fractured bedrock – is more significant than coastal erosion at the Gascons landlside.

Conclusion

From these brief case studies, it is clear that the high-resolution InSAR images are very effective in separatinf differential motion within these low velocity coastal landslides. The Active wet spring periods are better monitored by the more frequent revisits of TerraSAR X.

Acknowledgements We thank Dr. Batterson from the Geological Survey of Newfoundland for leading our field visits at the landslides in Newfoundland. Rick Wheeler from College of North Atlantic provided the lidar images for our InSAR processing at the Corner Brook site. Prof. Locat and his team at Laval University provide the geological interpretation at the Gascons site.

References

Batterson M, Liverman DG, Ryan J, Taylor D (1999) "The assessment if geological hazards and disasters in newfounfland: an update" In Current Research Newfoundland Dept of Mines and Energy Geological Survey Report 99-1 pp 95–123

Ferretti A, Prati C, Rocca F (2001) Permanent scatters in SAR interferometry. IEEE Trans Geosci Rem Sens 39:8–20

Guthrie RH, Mitchell SJ, Lanquaye-Opoku N, Evans SG (2010) Extreme weather and landslide initiation in coastal British Columbia. Q J Eng Geol Hydrogeol 43:417–42

Locat J (2010) "An integrated mass movement system for landslide hazard assessment at Gascons, Quebec". In: Proceedings of the 63rd Canadian geological conference, Calgary, p 8

Mosher DC (2008) "Submarine Mass Movement in Canada: Geohazard with far reaching implications". In: Locat J, Perret D, Turmel D, Demers D, Leroueil S (eds) Proceedings of the 4th Canadian conference on geohazards, Laval, p 12

Singhroy V, Mattar K, Gray L (1998) Landslide characterization in Canada using interferometric SAR and combined SAR and TM images. Adv Space Res 2(3):465–476

Singhroy V (2008) Satellite remote sensing applications for landslide detection and monitoring (chap7). In: Kioji S, Paolo C (eds) Book landslide disaster risk reduction. Springer, Berlin, pp 143–158

Witter RC, Horning T, Allan JC (2009) "Coastal erosion hazard zones in Souhtern clatsop county, Oregon: Seaside to Cape Falcon" Open file Report O-09-06, Oregon, Dept of Geology and Minarals, p 39



Evaluation of Temperature Effects on Strain Measurements with DTSS

Gerhard Kapeller, Rafael P.O. Rocha, Luiz Alkimin de Lacerda, and Markus Aufleger

Abstract

Field measurements are exposed to daily and seasonal temperature variations due to meteorological and hydrological events. This paper presents the obvious influence of temperature on strain measurements with DTSS. Tests with wide range temperature variations inside the reference section and the strained section were performed. Moreover, temperature effects on different system configuration relating reference section types are investigated. Results show temperature compensated as well as uncompensated strain of DTSS measurements. Finally, a manual temperature compensation was accomplished for comparison to DTSS temperature compensated strain.

Keywords

DTSS • temperature compensation • Reference section type

General

Up to now the occurrence of landslides are measured by means of geodetic surveying, geotechnical monitoring, geophysical methods and remote sensing (Climchalp 2008). Depending on the number of installed instruments there is a lack of information concerning an endangered hillside.

In the last century Distributed Fiber Optic Measurements got known as a new innovative monitoring system in many approaches. At the moment there are two measuring systems: Distributed Temperature Sensing (DTS) and Distributed Temperature- and Strain Sensing (DTSS). One advantage of both systems is the high spatial resolution, with measurements in every meter of the optic cable. Depending on the power of the laser cable lengths up to 24 km in DTSS and 30 km in DTS respectively, can be measured. Due to its robustness both systems are applicable for long time monitoring (Sensornet 2009, 2011).

There are several applications of both systems in hydraulic engineering, e.g. Aufleger et al. (2005), Selker et al. (2006), Perzlmaier (2007), geotechnical engineering, e.g. Sayde et al. (2010) and structural engineering, e.g. Lee et al. (2010). A new application of this innovative system is the monitoring of landslides (Hoepffner 2008; Iten et al. 2009). An early warning monitoring for landslides becomes more and more important. With temperature as a perfect tracer, the degree of saturation and changes of hydrological boundary conditions can be investigated by means of DTS (Rocha 2011). Together with DTSS for the investigation of dynamic deformations decisive parameters for land sliding are known. But the temperature dependent strain can be misinterpreted.

This paper deals with the influence of temperature on strain. Therefore the temperature within a strained section but as well as in the reference section, necessary for the system configuration, will be diversified.

G. Kapeller (✉) • M. Aufleger
University of Innsbruck, Unit of Hydraulic Engineering, Technikerstr. 13, Innsbruck A-6020, Austria
e-mail: gerhard.kapeller@uibk.ac.at

R.P.O. Rocha • L.A. de Lacerda
Institute of Technology for Development - LACTEC, Department of Civil Structures – LAME/DPEC, BR-116 – KM 98 – No 8813 – Centro Politécnico da UFPR, Curitiba, Paraná, Brazil

C. Margottini et al. (eds.), *Landslide Science and Practice*, Vol. 2,
DOI 10.1007/978-3-642-31445-2_63, © Springer-Verlag Berlin Heidelberg 2013

Temperature Compensation

The launched optical signal is backscattered at every fiber position. DTSS uses the frequency shift of the backscattered brillouin part to calculate local strain. Beside the strain this part is also sensitive regarding the temperature along the fiber. Thus a temperature change is often misinterpreted as strain. Temperature variations can be a result of rapid change in daily meteorological and hydrological conditions. However, also seasonable temperature changes during long time monitoring will falsify strain measurements. For these reasons a temperature compensation is essential.

The brillouin frequency shift $\Delta\nu_{B(T,\varepsilon)}$ corresponding to the brillouin reference frequency is known as linear related to changes in temperature ΔT and strain $\Delta\varepsilon$. The change in strain can be estimated with (1) by measuring the frequency shift and the temperature change along the fiber. (Parker et al. 1997)

$$\Delta\nu_{B(T,\varepsilon)} = C_{\nu\varepsilon} \bullet \Delta\varepsilon + C_{\upsilon T} \bullet \Delta T \tag{1}$$

Cνε and CνT are dependent coefficients for the strain and temperature responsible frequency shift. For these tests a tight buffered single- and multi-mode fiber for DTS and DTSS measurements were chosen. The related coefficients are displayed in Table 1.

DTSS-Sensornet measures the frequency shift $\Delta\nu_{B(T,\varepsilon)}$ together with the brillouin power P_B at all points along the fiber.

Similar to the frequency shift the power is linear dependent on strain and temperature:

$$\Delta P = \frac{100 \bullet \Delta P_B}{P_B} = C_{P\varepsilon} \bullet \Delta\varepsilon + C_{PT} \bullet \Delta T \tag{2}$$

With $C_{p\varepsilon}$ and C_{PT} the coefficients for a change in brillouin power due to temperature and strain changes (Table 2). P_B in (2) is related to the Rayleigh power to consider input-power fluctuations (Parker et al. 1997).

The brillouin power shows a negligible negative effect on strain compared to frequency shift ($C_{\upsilon\varepsilon}/C_{P\varepsilon} = 35$). In contrast it is significantly dependent on the temperature ($C_{\upsilon T}/C_{PT} = 6$). Therefore the DTSS temperature is calculated based on the power. However DTSS temperature shows with 1 °C a lower resolution than DTS temperature with 0.01 °C (Sensornet 2009, 2011).

With (1) and (2) the temperature dependency can be eliminated. The estimated strain is only dependent on the brillouin power and the frequency shift.

$$\Delta\varepsilon = \frac{\Delta P \bullet C_{\nu T} - \Delta\upsilon_B \bullet C_{PT}}{C_{P\varepsilon} \bullet C_{\nu T} - C_{\nu\varepsilon} \bullet C_{PT}} \tag{3}$$

DTSS measurements output both, temperature compensated and uncompensated strain.

Figure 1 shows the effect of DTSS temperature compensation regarding the spreading of results. It displays results of a strained fiber section without a change in strain and temperature over several hours. The spreading of compensated strain increases to about 400 % compared to uncompensated strain.

Project Description

Test Setup

The measurements were done at LACTECLAME – Department of Civil Structures in Curitiba, Paraná, Brazil in cooperation with University of Innsbruck, Austria.

For all performed tests a tight buffered single- and multi-mode fiber for DTSS and DTS measurements were chosen. Both, DTS and DTSS are from Sensornet. The basic test setup is shown in Fig. 2. For all strain measurements a clear reference section along the fiber is essential to define the zero strain section. Therefore at least 10 m of both fibers were placed loose on a barrel inside a heating oven. The oven allows temperature variations up to about 120 °C and a constant temperature over the measuring time. The fibers in the strained section were placed in a water bath. Again to achieve a constant temperature over the whole measuring time the central water channel is surrounded with at least 5 cm of styrofoam. A flexible foil inside the channel takes care of water-proof conditions.

The total length of the strained section was 3,406 mm. Based on a small pre-strain the single-mode fiber was strained for 24 mm (7,046.4 με) For applying the strain the fiber was slightly pressed in sandwich plates. The multi-mode fiber was placed loose inside the water channel. To verify DTS measurements additional conventional thermometer were placed inside the water channel.

For the system configuration a Pt100 of both systems was placed next to the reference section inside the oven.

Test Procedure

The measuring time for each case study was set to 2 min and five repetitions. In total four test-types were performed:

(a) *Temperature variation in the reference section*

The temperature increase interval in the reference section was set to about 5 °C for each case up to 45 °C (Fig. 3). To assure stable oven conditions for DTSS results the temperature variations were controlled with DTS. The temperature in the strained section was kept constant. This test is based on an external reference DTSS configuration.

Table 1 Cable dependent coefficients for frequency shift (Hoepffner 2008)

Coefficient	Description	Value
$C_{\nu\varepsilon}$	Change in brillouin frequency versus strain	0.0481 MHz/με
$C_{\nu T}$	Change in brillouin frequency versus temperature	2,488 MHz/°C
$C_{\varepsilon T(\nu)}$	Change in strain with temperature	51,726 με/°C

Table 2 Cable dependent coefficients for brillouin power (Hoepffner 2008)

Coefficient	Description	Value
$C_{P\varepsilon}$	Change in brillouin power versus strain	−0.0014 %/με
C_{PT}	Change in brillouin power versus temperature	0. 417 %/°C
$C_{\varepsilon T(P)}$	Change in strain with temperature	−297,857 με/°C

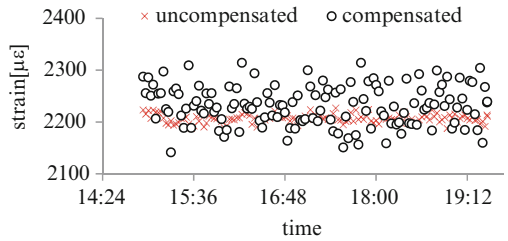


Fig. 1 Spreading of compensated and uncompensated strain

(a) *Temperature variation inside the strained section*

To show the influence of temperature change in the strained section the water was heated up with a heating stick in steps of about 5 °C (Fig. 4).

By reaching the desired temperature the water was filled in the canal and closed with a top styrofoam. For a better contact and thus less heat loss heavy weights were placed on the top. This test is also based on an external reference DTSS configuration.

(c) *Change in DTSS system configuration*

In general, strain measurements are based on a clear reference section which is defined by zero strain. DTSS-Sensornet allows three different ways for the configuration of the reference section (Fig. 5).

With the external reference the temperature around the reference section is continuously measured by means of a Pt100. The fixed reference presumes a constant reference temperature. Therefore a Pt100 is not necessary. For both types it is suggested to place the reference fiber inside a water barrel. Sensornet DTSS also contains an internal reference section. The temperature is measured by means of a system integrated platinum resistor.

(d) *DTS temperature compensation*

DTSS-Sensornet is unique in the field of automatic temperature compensation. For a manual temperature compensation the temperature along the fiber was also measured by DTS. The uncompensated and compensated strain is calculated based on (1). A comparison with DTSS strain will show the efficiency of both temperature compensations.

Experimental Results and Analysis

The accuracy of tight buffered fibers for compensated and uncompensated DTSS strain is dependent on the applied strain. This is shown in Fig. 6, where load steps were applied every 6 min and the data recorded every 2 min. For instance, the accuracy for an applied relative strain of 7,000 με without temperature changes during the measurements about was ± 200 με.

The following graphs show results of the temperature compensated and uncompensated relative strain along the fiber. The constant strain of 7,064.4 με is applied to a pre-strain of about 1,100 με. The strains are average values over three repetitions for each temperature case.

(a) *Temperature variation inside the reference section*

In case of the temperature variation inside the reference section the strain is lowered down to the defined zero strain inside the reference section (Fig. 7). Therefore the uncompensated strain along the whole fiber length shows a decreasing strain with an increasing temperature shift. The strain shift between the lowest and highest temperature is about 750 με and results in about 40 με/°C. The compensated strain shows the same strain development for all temperatures.

Within the strained section the accuracy of compensated strain depends on the applied strain value (Fig. 6).

(b) *Temperature variation inside the strained section*

In case of temperature variation along the strained section the strain difference between the lowest and highest temperature is about 760 με and results in about 26 με/°C. As there is no temperature change in the reference section, the strain only changes within the strained section. Even the compensated strain shows variations of about 500 με and 16 με/°C respectively. In contrast to temperature variation within the reference section the uncompensated strain increases with temperature. The temperature compensation results again in a decreasing strain with increasing temperature.

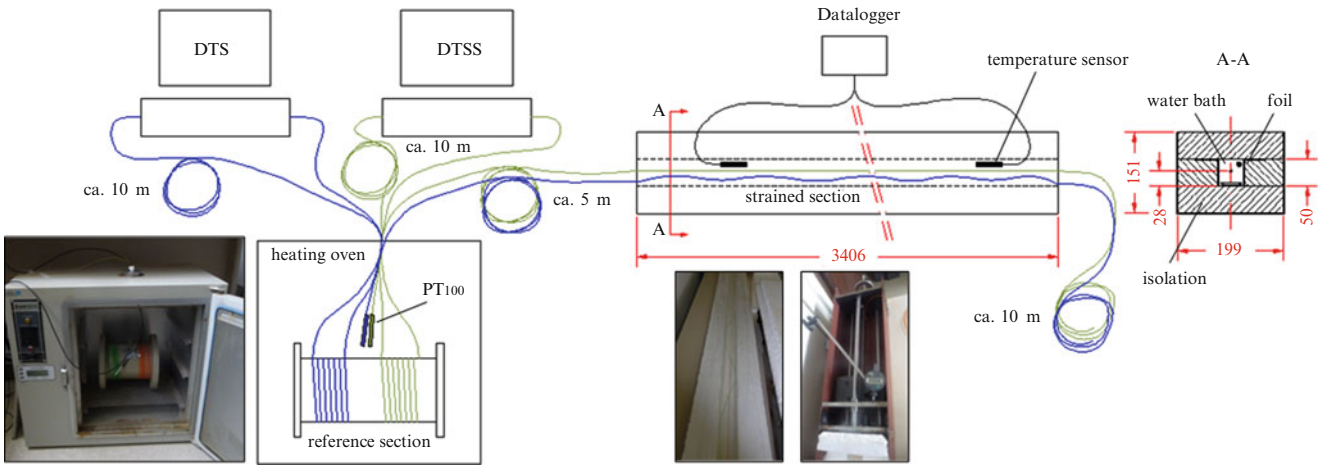


Fig. 2 Setup for temperature effects on strain

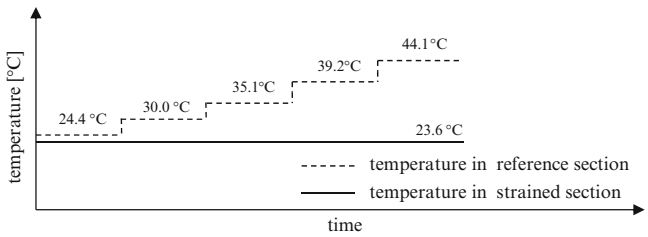


Fig. 3 Temperature change in reference section

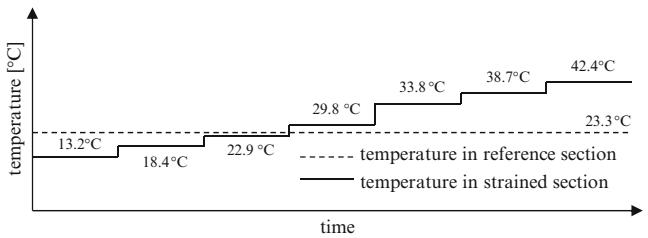


Fig. 4 Temperature change in the strained section

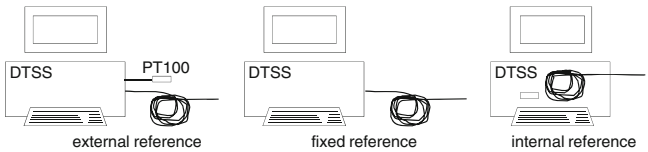


Fig. 5 Types of reference sections for DTSS system configuration

(c) *Change in DTSS system configuration*

For these tests only the temperature inside the reference section was varied. A change in the system configuration to a fixed reference temperature shows almost the same results as in Figs. 7 and 8 for the external reference. The reason is the same temperature over the total measuring duration of 10 min per temperature step. Only a fast temperature change or long measuring interval will result in different strain data.

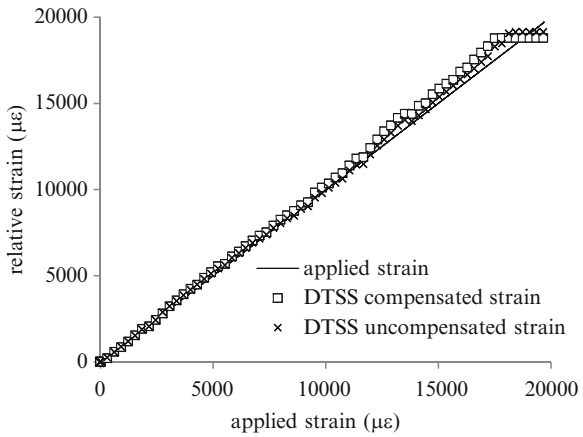


Fig. 6 DTSS accuracy for temperature compensated and uncompensated strain (Lacerda 2011 with changes)

To change the temperature of the internal reference section the room temperature was influenced by means of an air conditioner. Therefore the temperature of the reference section as well as of the fiber along the test was varied. Even the temperature inside the oven and the water filled channel varied. The results for the internal reference section are displayed in Fig. 9. Within the strained section the temperature compensation results in almost the same strain as uncompensated. Also the unstrained fiber section shows similar results comparing compensated and uncompensated strain.

With a strain difference of 370 με a shift of about 44 με/°C is expected. The temperature compensated strain varies with about 32 με/°C.

(d) *DTS temperature compensation*

For the manual temperature compensation the DTS temperature measurements with higher accuracy were used. By neglecting the temperature term in equation [1] the manual calculated uncompensated strain results in the same strain development (Figs. 10 and 11) like DTS uncompensated

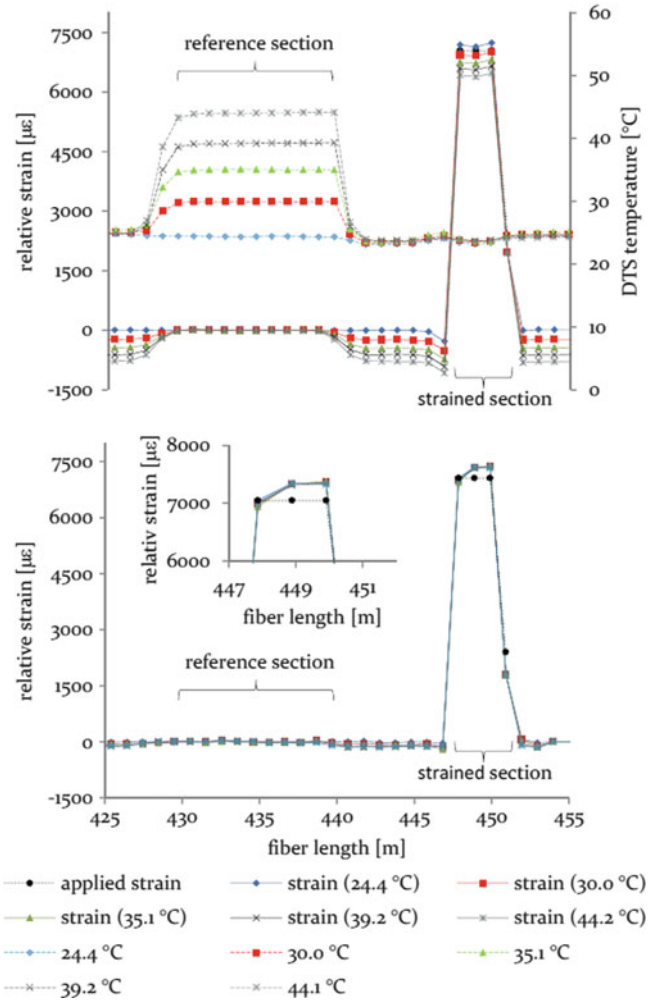


Fig. 7 External reference: uncompensated strain and DTS temperature (*up*) and compensated strain development (*down*) for a temperature variation inside the reference section

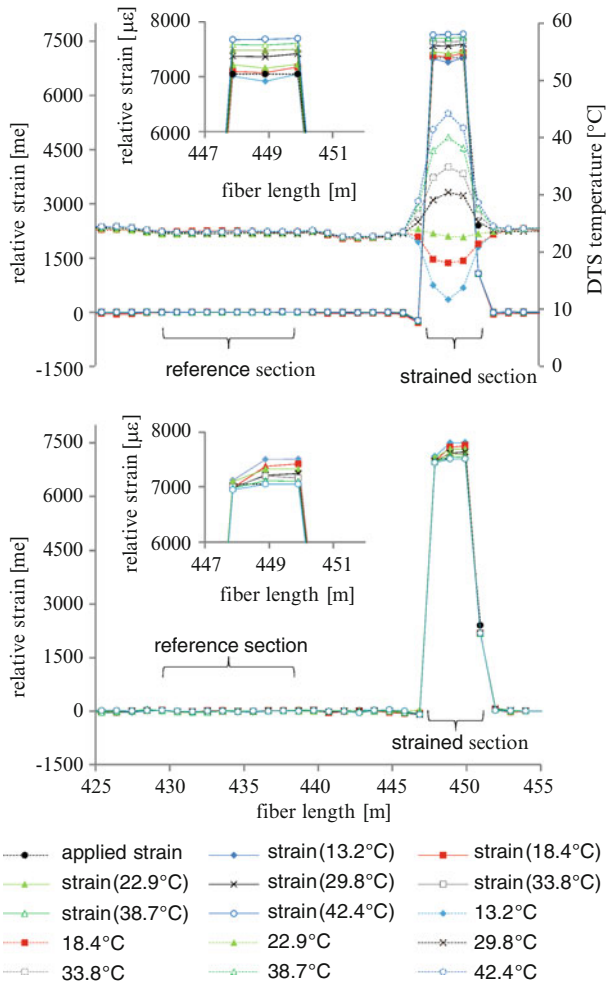


Fig. 8 External reference: uncompensated strain and DTS temperature (*up*) and compensated strain development (*down*) for a temperature variation inside the strained section

strain (Figs. 7 and 8). The manual temperature compensated strain with (1) for a temperature variation in both sections is displayed in Figs. 10 and 11. Both manual temperature compensation show worse results than DTSS compensation.

The integral area below the strain curve corresponds to the total applied strain. Figure 12 illustrates the calculated total deformation and strain, respectively within the strained section. For a comparison the strains of both temperature variation sections and external reference type are displayed. Moreover, it includes the manually calculated strains. The graph clearly indicates the best results by using DTSS compensation relating to the applied strain.

Conclusions

A temperature change along the fiber results in a remarkable change and misinterpretation of measured strain. A temperature change in the reference or strained section results in similar strain development in case of uncompensated strain. For the automatic DTSS temperature compensation the reference section type in the system configuration is essential. The external reference type shows best results. A temperature change inside the reference section can be eliminated.

Therefore for all kind of measurements the reference fiber should be placed inside a temperature controlled box or a water barrel. For outside measurements the box or barrel should be closed and entrenched inside the soil to avoid rapid temperature changes inside the reference section due do meteorological effects. A temperature change inside the strained section results in strain fluctuations even after temperature compensation. Nonetheless, the automatic temperature compensation of DTSS-Sensornet works very well over a wide range of temperates.

The manual temperature compensated strain based on the linear relation of frequency shift and temperature

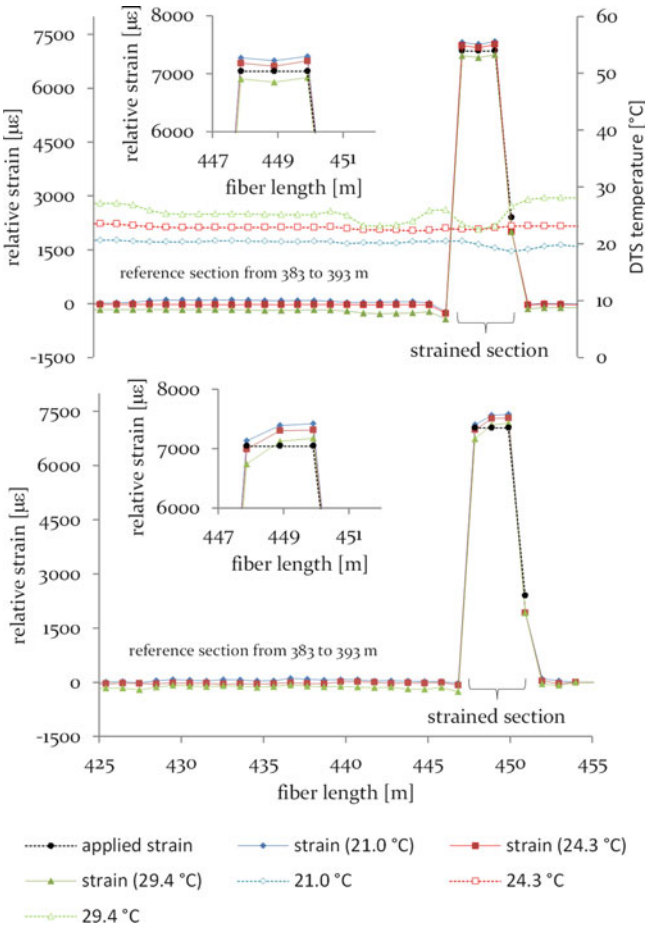


Fig. 9 Internal reference: uncompensated (*up*) and compensated strain development (*down*) for a temperature variation inside the reference section

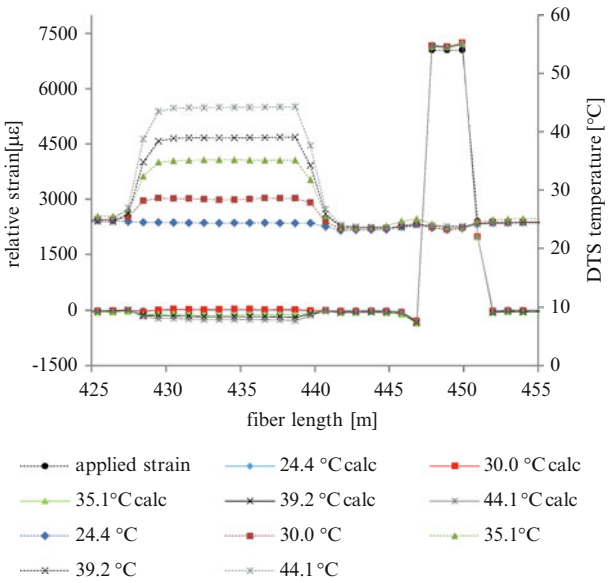


Fig. 10 Manual temperature compensation for temperature variation inside the reference section (external reference)

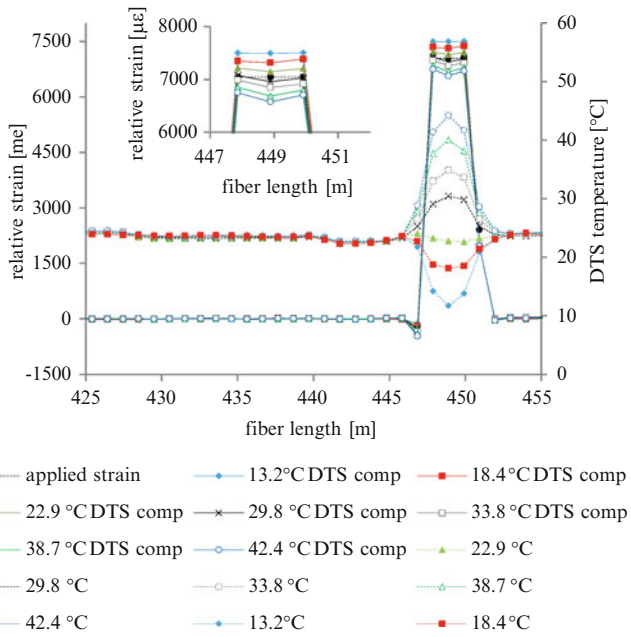


Fig. 11 Manual temperature compensation for temperature variation inside the strained section (external reference)

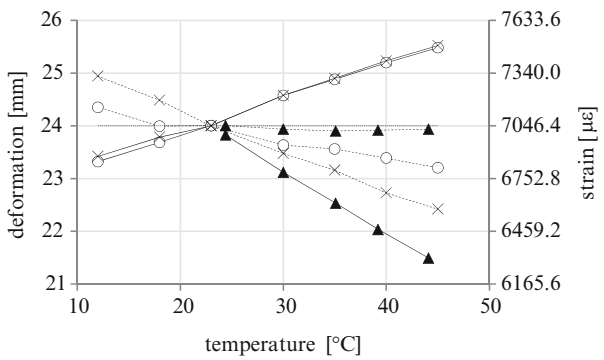


Fig. 12 Summary of DTSS and manually temperature compensated and uncompensated strain results

shows worse results compared to DTSS compensation. A reason of this fact could be the consideration of losses at DTSS temperature compensated strains.

Acknowledgement The authors thank UFPR and LACTEC as scientific research partners for the stay abroad in Curitiba and the great discussions. Moreover, thanks to the University of Innsbruck for the doctoral grant and the funding of the stay in Curitiba.

References

Aufleger M, Conrad M, Perzlmaier S et al (2005) Improving a fibre optics tool for monitoring leakage. Hydro Rev Worldwide 13(4):18–23

ClimChAlp (2008) Slope monitoring methods – a State of the art report. The ClimChAlp partnership, Work Package 6, Munich

Hoepffner R (2008) Distributed fiber optic strain sensing in hydraulic concrete and Earth structures. Berichte Des Lehrstuhls Und Der Versuchsanstalt Für Wasserbau Und Wasserwirtschaft, Technische Universität München, Wasserbau und Wasserwirtschaft, Nr. 121, München

Iten M, Ravet F, Niklés M et al (2009) Soil-embedded fiber optic strain sensors for detection of differential soil displacements. In: 4th international conference on structural health monitoring on intelligent infrastructure, Zurich, 22–24 July 2009

Lee J, Choi K, Huh Y (2010) Damage detection method for large structures using static and dynamic strain data from distributed fiber optic sensor. Int J Steel Struct 10(1):91–97

Parker TR, Farhadiroushan M, Handerek VA et al (1997) Temperature and srain dependence of the power level and frequency of spontaneous Brillouin scattering in optical fibers. Optics Letters, vol 22, No. 11

Perzlmaier S (2007) Verteilte Filtergeschwindigkeitsmessung in Staudämmen. Berichte Des Lehrstuhls Und Der Versuchsanstalt Für Wasserbau Und Wasserwirtschaft, Technische Universität München, Wasserbau und Wasserwirtschaft, Nr. 109, München

Rocha RPO (2011) Instrumentação Geotécnica Com Fibra Ótica: Monitoramento De Frente De Umedecimento E Análise Da Variação Do Grau De Saturação Em Solos Arenosos. Dissertação de Mestrado, Programa de Pós-Graduação em Construção Civil, Setor de Tecnologia, Universidade Federal do Paraná, Curitiba

Sayde C, Gregory C, Gil-Rodriguez M et al (2010) Feasibility of soil moisture monitoring with heated fiber optics. Water Resour Res 46: W06201

Selker JS, Thévenaz L, Huwald H et al (2006) Distributed fiber-optic temperature sensing for hydrologic systems. Water Resour Res 42: W12202

Sensornet (2009) Sentinel Dts – data sheet. Sensornet, United Kingdom

Sensornet (2011) Dtss specifications. Sensornet, United Kingdom



Measurements of Hydraulic Subsurface Processes by Means of Distributed Fiber Optic Temperature Sensing (DTS)

Gerhard Kapeller, Thomas Etzer, and Markus Aufleger

Abstract

Distributed Fibre Optic Temperature sensing (DTS) system allows the monitoring of geo-hydrological changes of boundary conditions due to rainfall. Based on the heat transport in soils the temperature distribution is closely correlated with the presence and movement of water in soils. Therefore rainfall infiltration as well as the degree of saturation as common landslide triggers can be monitored in a distributed way. The advantage of continuous measurements over several kilometers of cable and its robustness allows a long-time and early warning monitoring for landslide occurrence. This paper represents the potential and installation of DTS for monitoring of infiltration processes and degree of saturation in soil. Therefore about 600 m cable were installed at two scientific interesting test sites in Austria. In total an area of about 1,200 m^2 was instrumented. The results are based on natural and artificial rainfalls.

Keywords

DTS • Landslide • Geo-hydraulic parameters • Early warning monitoring

Introduction

During the last decade Distributed Fiber Optic Temperature (DTS) measurements were identified as a very useful instrument for several applications. Especially in the field of hydraulic engineering is an increasing trend visible. Monitoring of embankment dams, dikes and channels by means of leakage detection is only a small scope of applications (Johansson et al. 2000; Aufleger et al. 2005). The technology and its behaviour has been improved and investigated in several research studies and is ready to be transferred into the field of monitoring of groundwater movement and soil processes.

The closer understanding of surface and subsurface processes in hill slopes is still a challenge for engineers due to the complex interactions of hydrological, hydro-geological and soil mechanical processes. Infiltration and seepage processes through and below earth structures were investigated in several studies since they are essential for the stability of structures. Up to now, the actual conditions of endangered hill slopes (e.g. degree of saturation, pore-water pressure) are measured punctually by a single gauge or by a series of single gauges, respectively. The number of required gauges is directly connected with time and cost consuming installation of the instruments. In addition, depending on the number of gauges, there is a serious lack of information considering the variation of soil conditions over the entire hill slope.

In an actual research project funded by the Austrian Academy of Sciences the suitability of distributed fiber optic temperature measurements in the field of subsoil hydraulic investigation is shown for the first time. Therefore two Austrian test sites got instrumented. Based on the high spatial and temporal resolution over long distances DTS could be a serious innovative and efficient monitoring system.

G. Kapeller (✉) • T. Etzer • M. Aufleger
Unit of Hydraulic Engineering, University of Innsbruck,
Technikerstreet 13, Innsbruck 6020, Austria
e-mail: gerhard.kapeller@uibk.ac.at

C. Margottini et al. (eds.), *Landslide Science and Practice*, Vol. 2,
DOI 10.1007/978-3-642-31445-2_64, © Springer-Verlag Berlin Heidelberg 2013

Methodology

The principle of DTS is based on the temperature-sensitive properties of the optical fibre, which is conductor and sensor as well. By means of a powerful laser a intensive, short optical impulse is sent into the fibre. Depending on the frequency shift the backscattered signal can be separated into Rayleigh-, Raman- and Brillouin-Light (Fig. 1).

The anti-Stokes part of the Raman light is correlated with the local temperature. The temperature is determined by the relationship of the frequency shift and the intensities of the Stokes and anti-Stokes parts of the Raman-scattering. The distance from the scattering point to the light source is determined by the runtime. Depending on the lasers power several kilometres can be monitored continuously along the fiber. The main advantages of this technology are the high spatial resolution of 1.0 m, the temperature accuracy of $\pm$ 0.2 °C and its robustness against environmental influences. This innovative technology was well investigated over the last decade and is installed in several international projects (Aufleger et al. 2005).

The heat-up technique additionally allows the monitoring of degree of saturation based on the measured distributed temperature profile along the cable (Perzlmaier 2007). By means of an electrical voltage application on copper wires integrated in a hybrid cable, the cable gets heated up. The temperature depends mostly on the thermal capacity and conductivity of the surrounding material. Heat conduction is dominant in case of dry or partly saturated soil around the cable. The effective convective heat transmission is active by the incidence of passing water.

The local degree of saturation can be estimated based on the heat-up curve. The effective thermal conductivity of a linear heat source can be calculated for a long heating time with (1).

$$\lambda_{eff} = \frac{q}{4 \bullet \pi} \bullet \frac{\ln(t_2) - \ln(t_1)}{T(t_2) - T(t_1)} \tag{1}$$

With q the specific heating power, t different time steps and T the temperature at these time steps.

Johansen (1975) developed an (2) for the effective thermal conductivity of unsaturated soils based on the Kersten number K_e as well as the thermal conductivity of dry λ_{dry} and saturated λ_{sat} soil.

$$\lambda_{eff} = \left(\lambda_{sat} - \lambda_{dry}\right) \bullet K_e + \lambda_{dry} \tag{2}$$

With

$$K_e = a \bullet \log(S) + 1 \tag{3}$$

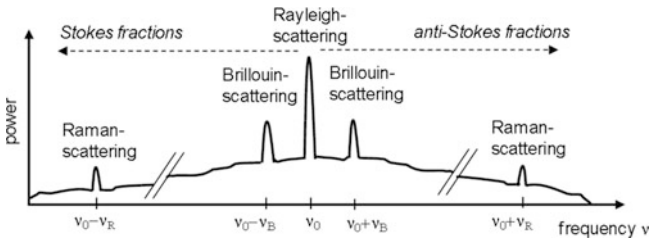


Fig. 1 Spectrum of the backscattered light

the degree of saturation S > 0.1 can be estimated with (1) and (2). The constant a was found to be 0.68 for coarse (fraction of clay < 2 %) and 0.94 for fine materials (fraction of clay > 2 %).

Further theoretic details as well as the confirmation of this monitoring system under perfect conditions in laboratories are summarized in Perzlmaier (2007). Based on these results this innovative technology is ready for transfer to field applications.

Project Description

The main goal of the pilot project is the adequate installation and verification of DTS for the application of landslide monitoring. Therefore fiber optic cables were installed at two Austrian alpine test sites in summer 2009. Both are different in their soil structure characteristics.

The "*Heumöser Slope*", situated in Vorarlberg, has a total length of about 2,000 m and a width of about 500 m. The elevation ranges from 940 to 1,360 m above sea level. Due to the shallow silty, loamy soil layers the hydraulic conductivity is in a range of 10^{-4} to 10^{-6} m/s. The annual average amount of precipitation is about 2,100 mm. The test area is used as pasture in summer and as skiing slope in winter (Lindenmaier 2007) (Fig. 2).

The "*Herzogbauer Alpl*" is part of the creek "Löhnersbach" catchment area near Saalbach in Salzburg. It is situated on the more afforested orographic right side of the Löhnersbach. The slope is characterized with brown soil in the top layer and a hydraulic conductivity of about 10^{-5} m/s. The annual average amount of precipitation is about 1,500 mm. The test area is used as pasture in summer (Kirnbauer et al. 2009).

At both test sites about 600 m of fiber optic cables were installed meandering in shallow depth. The rocky soil in Salzburg requires an walking excavator to dig a cable channel. This procedure results in a heavy encroachment in the natural soil structure. In contrast, the channel in Vorarlberg was excavated using spades. For infiltration monitoring the cables are installed as horizontal as possible in two depths. The upper cable in Salzburg is 20 cm, in Vorarlberg about

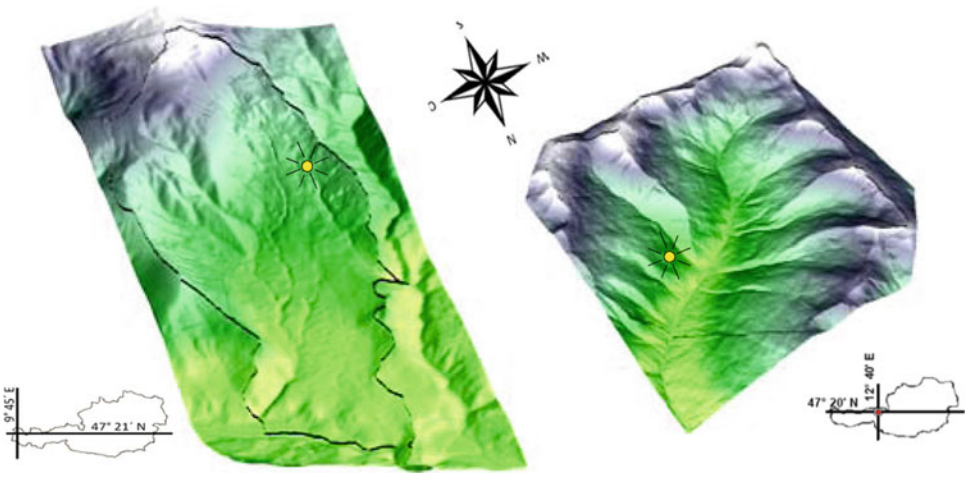


Fig. 2 Topography of Heumöser slope in Vorarlberg and Herzogbachers Alpl in Löhnersbach catchment in Salzburg

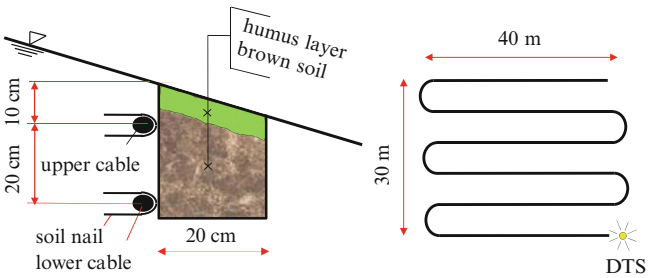


Fig. 3 Conceptional installation of the fiber optic cable in Vorarlberg

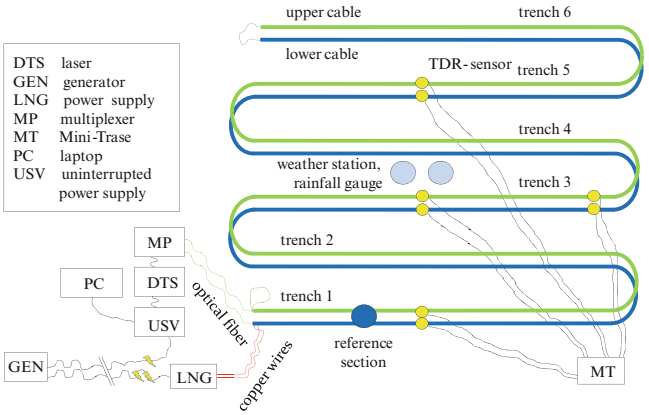


Fig. 4 Conceptional illustration of DTS measuring system

5 cm below surface. The lower cable is placed 20 cm deeper in vertical direction. To achieve as natural soil conditions as possible the cable is installed in a separate small channel at the uphill channel side. The cable position is fixed by earth nails. In total an area of 1,200 m^2 each test site is instrumented (Fig. 3).

Both cable layers are spliced together. Thus, the whole cable system can be measured at the same time from one cable end. Moreover, in case of a cable damage measurements to the breaking point are still possible from both cable ends. About 10 m of both cable ends are placed inside a water filled barrel which defines the reference sections. To avoid meteorological effects the barrel is entrenched into the soil.

For verification of DTS 8 conventional TDR-sensors are installed close to both cable layers at four positions inside the undisturbed natural soil. Moreover, air temperature and relative humidity is as well recorded continuously by a weather station. The rainfall is recorded by a switch gauge equipped with an event based data logger (Fig. 4).

The main measurement activities took place in summer 2010. Measurements during natural as well as artificial rainfall were performed. By varying interval and period a short heavy precipitation and a long-term low precipitation at each test could be simulated successfully. The chronological hydrograph for both test sites is shown in Figs. 5 and 6.

Because of a dry period during the first measuring campaign in Salzburg a second one was performed in order to get natural rainfall conditions. However during this period only little snowfall was recorded.

All measurements are based on the same DTS configuration. The measuring interval was set to two minutes and continuing repetitions. The results are averaged temperatures over this period every meter along the cable. After five reference measurements the cable was heated up by applying a specific power of 12 W/m on the cable integrated copper wires. The specific resistance of copper is linear dependent on temperature and results in a decreasing of the specific power first.

Nonetheless, continuous recordings of actual applied voltage and current enables a scaling up to the initial specific power. The measurements terminated every day after the fuel tank of the generator was empty, i.e. after at least 16 h. Based on the temperate difference between continuous measured and initial reference temperature the results are prepared in post-processing and analyzed. To realize higher temperature differences the cable is surrounded with single-layered fleece.

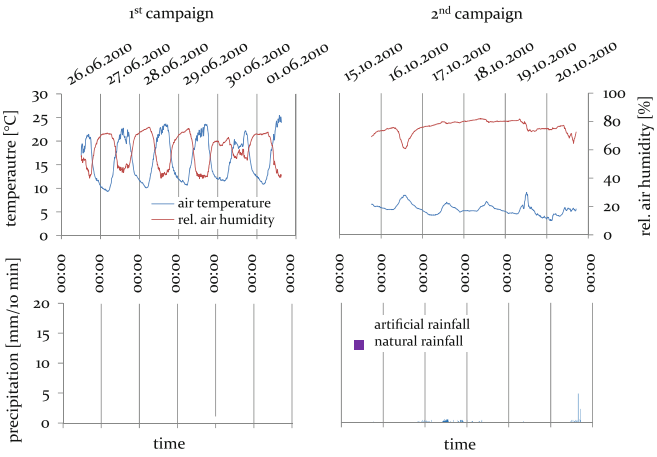


Fig. 5 Hydrographic overview at test site in Salzburg

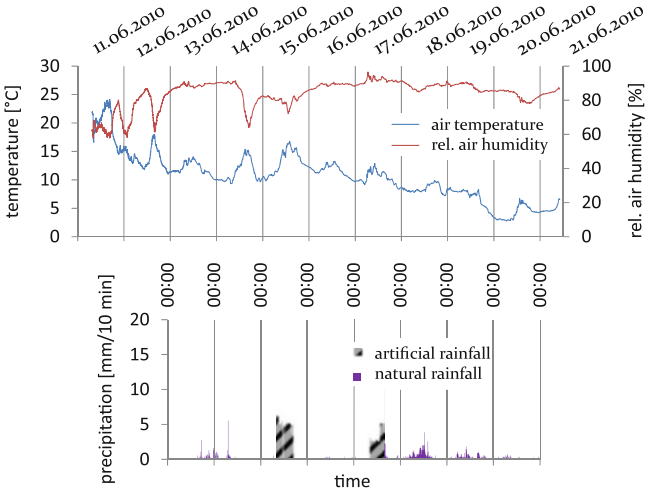


Fig. 6 Hydrographic overview at test site in Vorarlberg

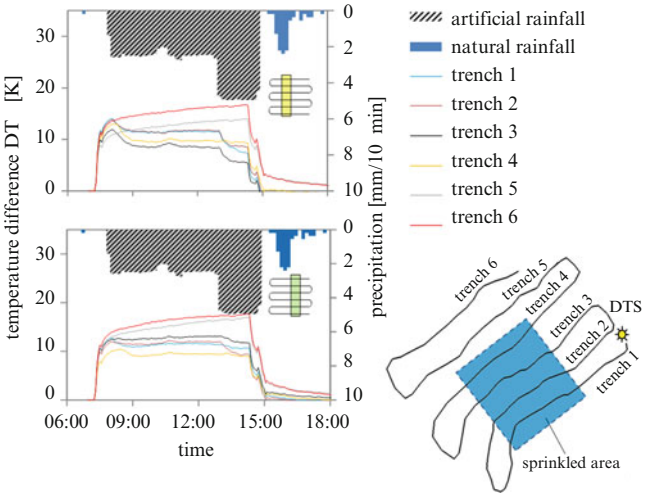


Fig. 7 Heating curves within area of artificial generated rainfall

Experimental Results and Analysis

For the illustration of the main results one characteristic measuring day is chosen in this paper. Thus, the following results belong to the test site in Vorarlberg on June 17th, 2010. This day is characterized by artificial rainfall over 6 h with 18 and 30 mm/h, respectively followed by natural rainfall.

Figure 7 illustrates the development of temperature differences at two site stripes of 7 m width, i.e. the second and third quarter of the test site. This approach results in manual averaged temperature difference in post-processing over this width. After the reference measurement the cable was heated up which results in a temperature increase first. This rapid increase is dominated by the cable design. For soil conditions as stable as possible the artificial rainfall was also started after the reference measurement. In general, the temperature increase is dependent on the surrounding soil material and structure and hydrological soil processes. Moreover, the actual situation of cable installation could influence the results. The cable design only dominates the rapid temperature increase at first. Temperature is a very efficient tracer. Thus, water passing the cable results in an temperature decrease. This effect as well as changes in rainfall intensities are clearly visible in trench 1–4 in Fig. 7. Trench 5 and 6 are outside the irrigated area, therefore the rainfall is not influencing the temperature development. The rapid temperature decrease at 14:28 is a result of generator overloading followed by the turn off of heating.

In general, with an increasing width of the considered site stripes information of local processes get lost due to averaging.

For verification TDR-sensors for soil moisture measurements are installed too. Figure 8 shows results of four TDR-measurements with a temporal resolution of 5 min. For the comparison results of one fiber meter at each layer and sensor (S1 and S2) was chosen.

Both, TDR and DTS results show a clear response at hydrological changes. Furthermore, DTS also indicates temperature changes at small intensity variations. Thus, temperature seems to be more sensitive on passing water.

Up to now there is almost no time delay between the beginning of the rainfall and the response of the temperature cable. Moreover, a time shift in temperature reaction between upper and lower cable based on rainwater infiltration is missing. Thus, effects due to cable installations are expected, but not validated yet.

Nonetheless, as a first conclusion temperature seems to be a powerful tracer to identify hydrological boundary conditions.

In a next step the degree of saturation based on the heating curve is estimated. By means of (1), (2) and (3) the local effective heat conductivity can be calculated and further the degree of saturation. Equation 1 shows that degree of saturation is only dominated by the temperature gradient

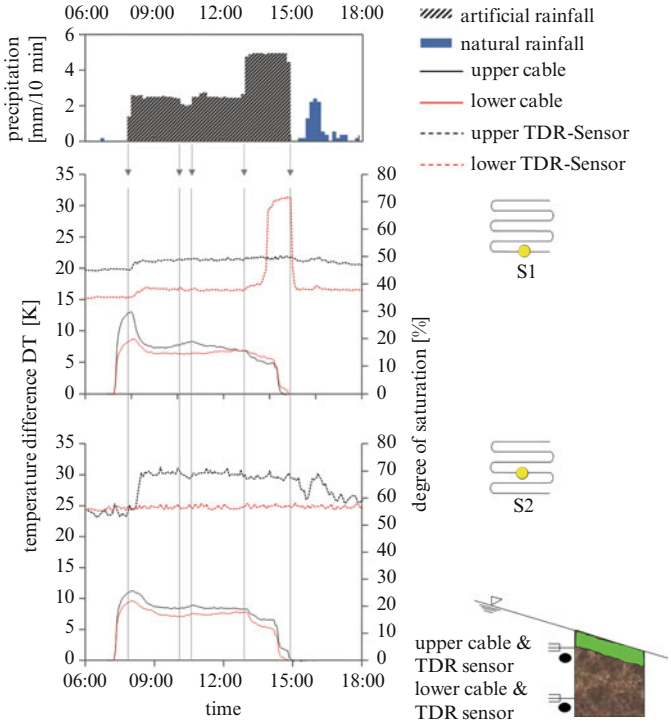


Fig. 8 Comparison of temperature development and four TDR-Sensors at two local positions

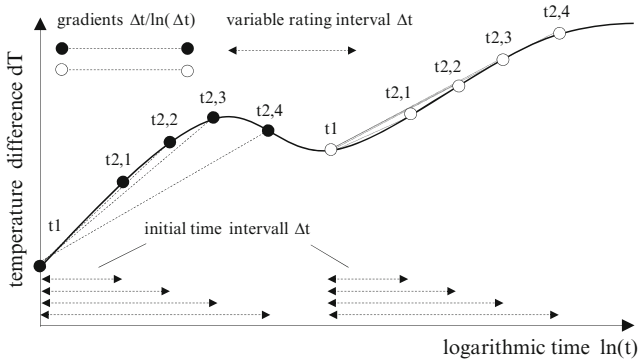


Fig. 9 Method for evaluation of degree of saturation

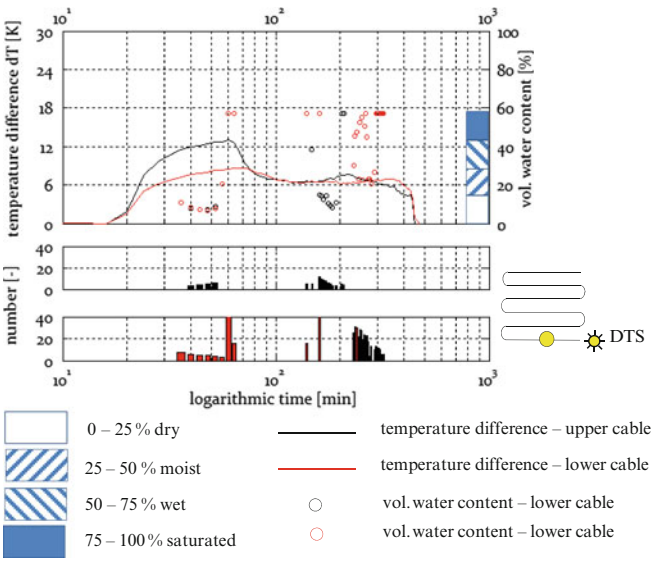


Fig. 10 Estimation of vol. water content based on the heating curve

ΔT/ln(Δt) in the logarithmic scale. However, even small measuring fluctuations within very short time interval Δt results in a change of the temperature gradient. Thus a certain time interval for the evaluation of degree of saturation is necessary. Moreover, also (1) assumes a certain time of constant soil conditions, which will never be existent. For these reasons only a roughly estimation of the degree of saturation is possible.

Nonetheless, for the investigation of degree of saturation a method of evaluation was chosen to eliminate small fluctuations in measuring. Starting with an initial time difference Δt of 60 min the temperature gradient is calculated. In a next step the time difference is increased to the next available temperature measurement $t_{2,1}$, thus to 64 min. The first time t_1 remains the same. The actual gradient is compared with the initial gradient. This step is continued until the difference to the initial gradient is three times in series outside the defined confidence interval of ± 25 % (Fig. 9).

The temperature gradients inside the confidence interval result in an average temperature gradient. Furthermore the effective heat conductivity and degree of saturation is estimated for this average time step. In a next step this method is repeated with t_1 set to the next temperature measurement time.

Figure 10 shows the development of temperature differences and volumetric water content over logarithmic time scale. Both variables are related to one fiber meter close to TDR-sensor in trench 1. A decreasing temperature curve is a result of changing conditions, i.e. rainfall and can't be used for appraising the soils degree of saturation. These data entries are filtered out. The graph also displays the number of involved measurements for the estimation. The total saturated condition at the test site in Vorarlberg is defined by 58 vol% (Markart et al. 2010). The results show a clear difference to conventional TDR sensors (Fig. 8). The main reason is the influence of still disturbed soil conditions around the cable.

However as in Perzlmaier (2007) already mentioned, this method is less accurate to consider degree of saturation compared to conventional instruments (TDR and needle sensors). There is only a classification into dry, moist, wet and saturated soil conditions reasonable. But the main advantage of DTS is again the high spatial and temporal resolution.

For a general overview the temperature differences at every cable meter along the upper and lower cable layer are shown in Fig. 11 for two time steps. The heavy artificial

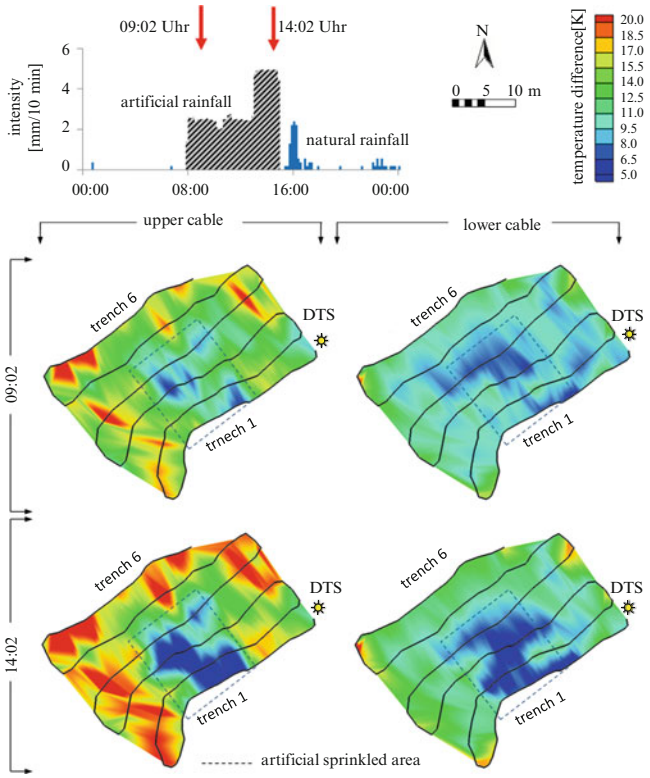


Fig. 11 Temperature plot of upper and lower cable layer with a spatial resolution of 1 m

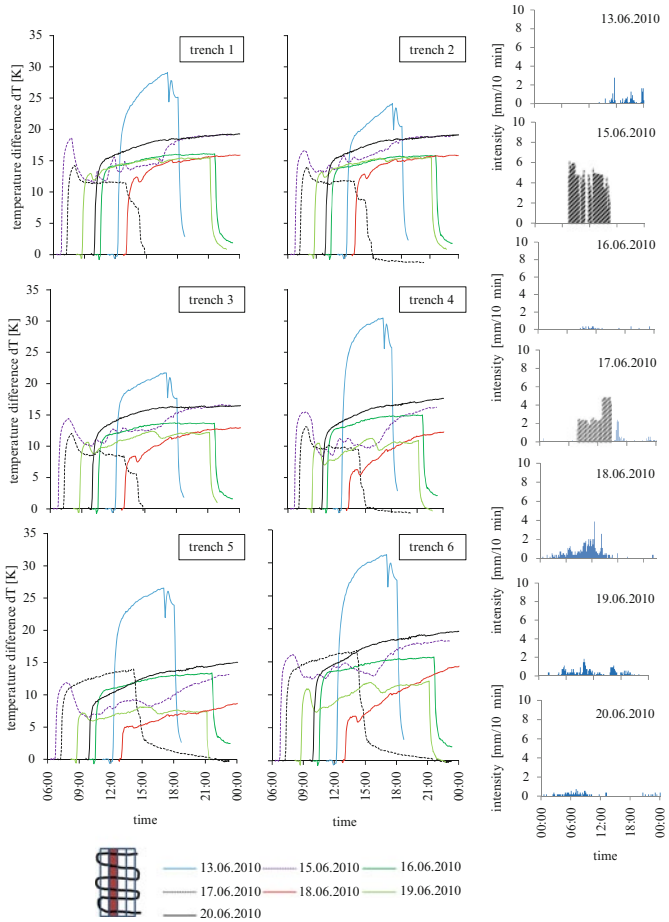


Fig. 12 Temperature progress at the second quarter of the Heumöser slope

rainfall is applied in the middle section of trench 1–4 and clearly visible. While the temperature difference within the sprinkled area decreases due to infiltration of rainfall water, the outer area is getting dryer and warmer. Furthermore, variations in temperature differences over the entire site are results of soils heterogeneities might also be influenced by the installations. When evaluating the temperature plot the different depth of cable coverage might also be factored in. Another effect which was not considered until now is a possible drainage along the fiber optic cable or within the fleece, respectively.

Figure 12 summarizes distributed temperature differences dT and hydrograph curves of all measuring days at the Heumöser slope. For this overview the temperature differences are averaged over a length of 8 m in the second quater of the test site.

Conclusion

This paper represents some fundamentally basics of DTS as a new innovative long time monitoring equipment. After some characteristics of the measuring system and the installed fiber optic cable the investigated test sites are described briefly. The paper closes with some results of the main measurements in summer 2010.

The main goal of the project is the verification of DTS for investigation of subsoil hydraulic processes. Based on the heat up technique a clear variation of boundary conditions, i.e. rainfall duration and intensities can be considered. Soils heterogeneities can be visualized and therefore different hydraulic aspects considering rainfall runoff could be more coherent. By means of the theory of a linear heating source the local degree of saturations can be estimated roughly. However realized tests have also shown, that a certain duration of a condition is necessary for satisfying results. As stated the disturbance of soils conditions due to installation has a big influence on distributed temperature measurements. The degree of influence could not rated up to now. There should be at least two winter periods after installing the cable to get almost realistic soil conditions again. In summary fiber optic measurements are an important and essential tool to identify distributed hydro-geological parameters and soil conditions on a site.

The robustness of the cable allows measurements over years. Based on the high spatial resolution and a possible

cable length up to 24 km DTS approves an adequate monitoring system of landslides. Due to the high temporal resolution and the correlation between rainfall and landslides DTS could also be used as an long-time and early-warning system of earth structures.

Outlook and acknowledge Laboratory tests of Perzlmaier (2007) have proven the correlation between distributed temperature difference and filter velocity at saturated conditions. Nonetheless, there is a need for some more investigations to evaluate the influence of soils compaction and structure. Furthermore, this correlations have to be proved in unsaturated soil conditions as well. Moreover, the effect of drainage along the fleece around the cable has to be considered in a next research step.

The authors would like to thank the Austrian Academy of Sciences for funding this project and the owner of the test sites for acceptance of installing the fiber optic cables.

References

Aufleger M, Perzlmaier S, Dornstädter J et al (2005) A leakage detection system for concrete face rockfill dams. In: CFRD05 symposium, vol, 19, Yichang, 26 Sept 2005

Johansen O (1975) Varmeledningserne Av Jardarter – thermal conductivity of soils. Ph.D. theses, NTH Trondheim, Trondheim, (CRREL Draft Translation 637, 1977)

Johansson S, Dahlin T, Farhadrioushan M et al (2000) New and improved monitoring systems for embankment dams – experience from initial resistivity, Sp, strain and temperature measurements at Sädva Dam. Elforsk rapport 00:14, Sweden

Kirnbauer R, Haas P, Chifflard P et al (2009) Hochwasserentstehung in Der Nördlichen Grauwackenzone. Wiener Mitteilungen, Institut für Wasserbau und Ingenieurhydrologie, TU Wien, Band 213, Wien

Lindenmaier F (2007) Hydrology of a large unstable hillslope at Ebnit, Vorarlberg – identifying dominating processes and structures. Dissertation, Mathematisch-Naturwissenschaftlichen Fakultät, Universität Potsdam, Potsdam

Markart G, Kohl B, Pausch H et al (2010) Bericht Über Beregnungen Und Bodenphysikalische Analysen an Den Testgebieten Heumöserhang (Ebnit, Vlbg.) Und Herzogbauernalm (Löhnersbach, Sbg.). Institut für Naturgefahren und alpine Waldgrenzregionen, Bundesamt und Forschungszentrum für Wald, Innsbruck

Perzlmaier S (2007) Verteilte Filtergeschwindigkeitsmessung in Staudämmen. Berichte Des Lehrstuhls Und Der Versuchsanstalt Für Wasserbau Und Wasserwirtschaft, Technische Universität München, Wasserbau und Wasserwirtschaft, Nr. 109, München



Applying GPR and 2D ERT for Shallow Landslides Characterization: A Case Study

Biljana Abolmasov, Aleksandar Ristić, and Miro Govedarica

Abstract

We present a procedure to estimate the characteristics of small shallow landslides based on the application of ground penetrating radar (GPR) and 2D electrical resistivity tomography (ERT). Existing procedures based on either conventional or non-invasive geophysical methods, observe almost exclusively large and deep landslides. Verification has been done on a small shallow landslide in the village of Vinča, near Belgrade, Serbia. The proposed procedure is realized in two simultaneous steps. First, from high resolution raw data obtained by GPR survey, soil horizons inside and near landslide body are estimated up to 4 m deep. The rupture surface is defined and its depth is estimated at 1.7 m. Second, ERT technology confirmed and integrated the results obtained by GPR survey. Main advantages of proposed procedure are efficiency and applicability for small shallow landslides whose number and impact on environment is dominant.

Keywords

Shallow landslides • Ground penetrating radar • 2D resistivity tomography

Introduction

The conventional methods of landslides investigations are based on engineering geological mapping and in most cases combined with borehole drilling, standard penetration test (SPT) and laboratory methods. Therefore, conventional methods are expensive and relatively slow, whereas the results of analysis are based on processing the limited range of subsurface data (Bichler et al. 2004). These disadvantages may be overcome by combined or independent application of non-invasive geophysical methods whose expansion follows the development of modern techniques and instruments (McGuffey et al. 1996). Simultaneously with the development of these methods, the possibilities of their application in detailed research of landslides were analysed (Hack 2000; Bichler et al. 2004). These analyses were carried out almost exclusively for large landslides with the sliding depth bigger than 20 m, and showed that ERT technology is rather appropriate in these conditions (Godio and Bottino 2001; Lapenna et al. 2003; Xiujun et al. 2005; Friedel et al. 2006; Marescot et al. 2008; Göktürkler et al. 2008). In terms of large deep landslides, GPR technology has been used only to confirm the results of ERT technology, due to maximum penetration depth of electromagnetic (EM) waves and survey site accessibility (Bichler et al. 2004; Bruno and Marillier 2000). Considering that the main goal of the research is to determine characteristics of small shallow landslides with the sliding depth in the range up to 5 m and then the application of GPR technology, which is characterized by swift and completely non-invasive acquisition of high resolution data, becomes very appropriate (Ristić et al. 2009). Taking into account objective possibilities of non-invasive geophysical methods, they are rarely carried out independently.

B. Abolmasov (✉)
Faculty of Mining and Geology, University of Belgrade, Djusina 7, Belgrade, Serbia
e-mail: biljana@rgf.bg.ac.rs

A. Ristić • M. Govedarica
Faculty of Technical Sciences, University of Novi Sad, Novi Sad, Serbia

C. Margottini et al. (eds.), *Landslide Science and Practice*, Vol. 2,
DOI 10.1007/978-3-642-31445-2_65, © Springer-Verlag Berlin Heidelberg 2013

More often, they are used in combination with other methods and then correlation of obtained results is carried out. Such integrated geophysical approach of using different methods combined with traditional methods of research is described in various papers (Sass et al. 2008; Naudet et al. 2008). Advantages and disadvantages of using geophysical methods in geomorphological studies are described on various examples by Schrott and Sass (2008).

On the basis of previously mentioned points, it can be concluded that recent results of landslide analysis point to the integrated approach which involves different technologies of active remote sensing. Also, the analysis of small shallow landslides was rarely tackled in literature, while the GPR technology was not applied significantly.

Since small shallow landslides are numerous and their impact on environment is considerable, this paper aims to represent new procedure for defining their characteristics. The presented procedure involves combined application of GPR and ERT technologies and it has been verified on the given landslide.

During the research the emphasis was put on non-invasive geophysical methods since the landslide has specific position and geometry. Due to capabilities of non-invasive geophysical methods for the landslide research (Bichler et al. 2004) field work was conducted during the summertime (July 2009), in a dry period, after the period of heavy precipitation in the previous winter and spring which reactivated the landslide. Results presented in this paper clearly show that in case of small shallow landslides applied geophysical methods give reliable data on the structure of a landslide body and the spatial disposition of the rupture surface.

Materials and Methods

The integrated geophysical research was carried out on the landslide located 14 km southeast of Belgrade, in the village of Vinča, on the right bank of the Danube (Fig. 1). The right valley bank of the Danube is characterized by hills (altitude of 80–130 m) and numerous deep landslides whose feet reach the Danube (Rokić 1997). The general geological settings of study area includes continual surface layer of diluvium (dl) with the thickness of 0.2–0.5 m and beneath it there is loess (Q) with the thickness of 0.5–2.0 m with traces of secondary carbonate sediments (Jevremović and Kuzmić 2001). The bedrock consists of Sarmatian sand (M_3^1), brownish marls (M_3^1GL) and grey marls (M_3^1L).

The analysed landslide has the dimensions of 50 × 40m and it is situated in the middle of the Danube slope above the local road and three private residential objects that are directly endangered by the landslide (Figs. 1 and 2). The landslide is on the private property and due to the specific terrain configuration and the problems with the owners of nearby properties it is almost impossible to reach the body of the landslide equipped with drill tools and tools for SPT measurements.

The landslide activated in March 2008 was triggered by heavy rainfall and slope indentation. Indentation was done while building residential objects. First reactivation occurred in March 2009, also triggered by heavy rainfall. Second reactivation occurred in late December 2009 and was triggered by instant snow melting (Fig. 2). According to Cruden and Varnes (1996), this landslide can be classified as shallow retrogressive and active landslide, very slow to slow, in the phase of active movement. The main scarp, with the height of 1.7 m is obvious with the visible zone of mass deficit. Lithological composition of the landslide comprises a thin diluvium with the thickness up to 0.3 m, loess with the thickness of 1–1.5 m and bedrock consisted of Sarmatian laminated well-compacted sand with weathered marls (Fig. 3).

Ground Penetration Radar Scanning

The data acquisition was done in July 2009, with GSSI SIR3000 system. The formation of radargram was carried out using antennas with central frequency 200, 400 and 900 MHz and a high scan resolution of 1,024 samples/scan, and 100 scan/m. The maximum scanning depth of 4 m was achieved by antenna with the central frequency 200 MHz taking into consideration soil structure in the landslide body and capabilities of used antenna. GPR calibration, in terms of determining the dielectric constant of soil was done according to known lithological structure of main scarp area (Ristić et al. 2007, 2009). Figure 4 shows the layout and numbering of radargrams in order of acquisition (labels from F029 to F059), with defined acquisition parameters: the direction of antenna motion (marked by arrow), antenna frequency (200, 400 and 900 MHz) and measuring location characteristics. Points used to georeference the radargrams were measured using two Trimble 5800 Global Positioning System (GPS) rovers in Real-Time Kinematic (RTK) mode (first covers the points 01–16, while the second covers the points p001–p011). The set of characteristic points for radargram georeferencing contains start and end point. Radargram post-processing, conducted in software package RADAN, included determination of time zero distance (distance from the antenna centre to the soil surface), and the application of several digital signal processing algorithms for reflected signals processing. It was done to obtain a clear view of all structural characteristics of landslides (Ristić et al. 2007, 2009).

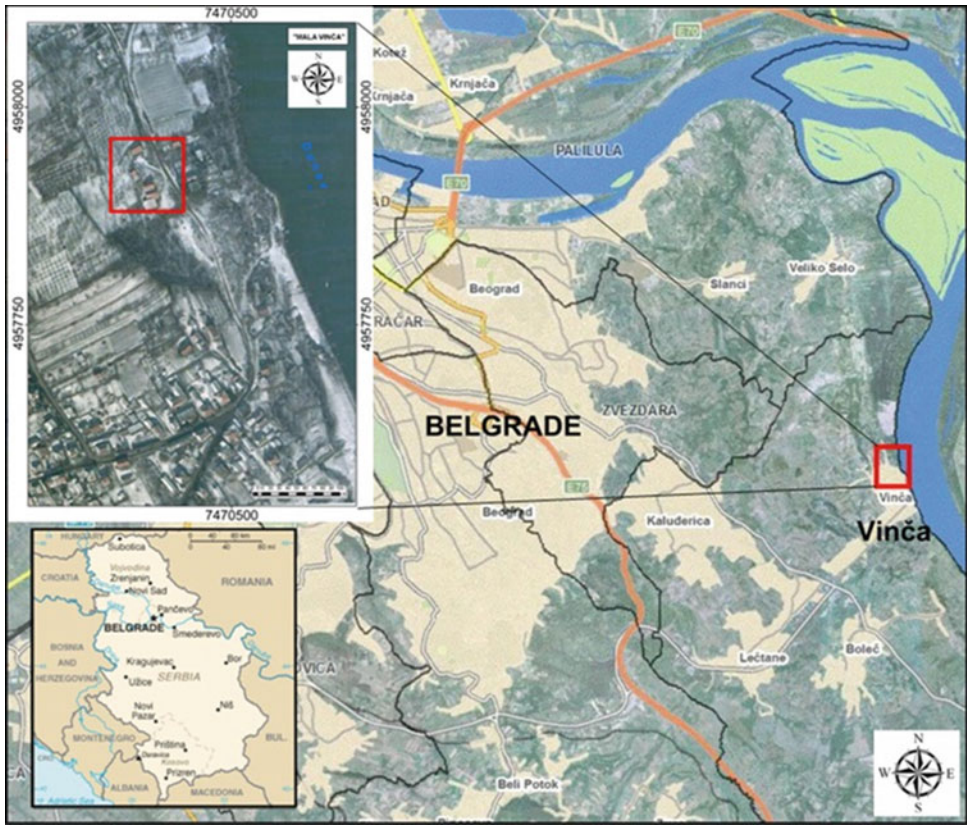


Fig. 1 Geographical position of study area



Fig. 2 Landslide Vinča (Photo December 2009)



Fig. 3 Weathered Sarmatian marls (Photo December 2009)

Electrical Resistivity Tomography

In addition to the acquisition by GPR, another profile of detailed ERT scanning was done and its location is shown by a discontinuous line in Fig. 4. The equipment used for data acquisition was ABEM SAS 300B with sensitivity of 0.01 mV. The length of the profile was 45 m, and there was 113 points at 6 depth levels. The distance between two measuring points (step) was 2 m. The total depth was approximately 4 m. The processing of measured data was conducted by software packet RES2DINV. The complete profile was carried out by the combination of Wenner-Schlumberger array electrodes. The first depth level was done by Wenner array configuration; the distances between A-M-N-B were equal (2 m), whereas A and B are electrodes for introducing electric current J (mA) into the ground, and M and N are electrodes for measuring the difference of electric potential ΔV(mV). From level 2 to level 6 electrode

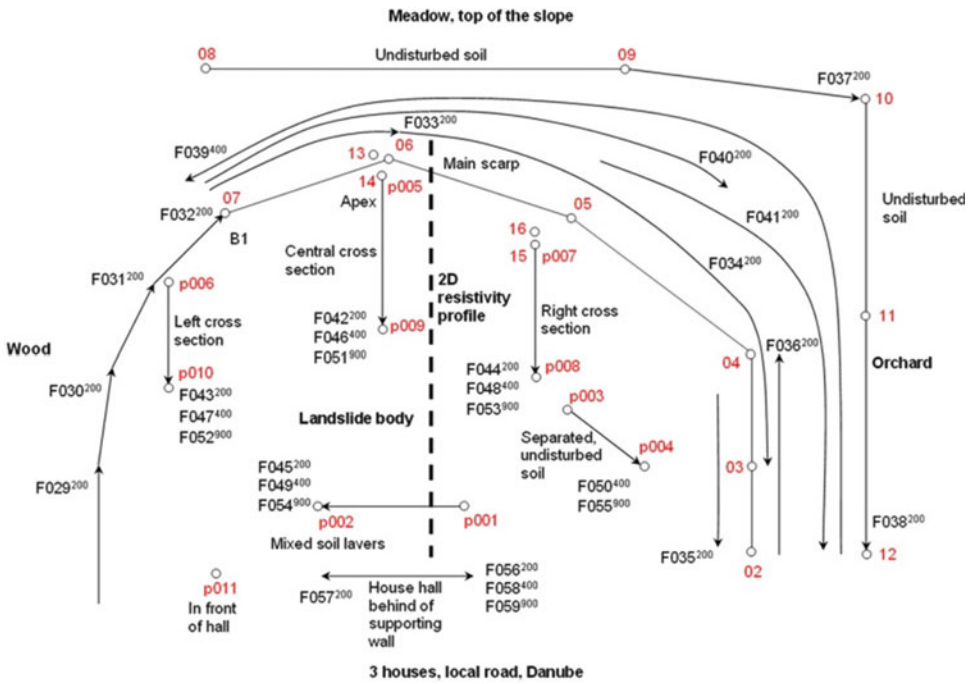


Fig. 4 Disposition of GPR and ERT profiles

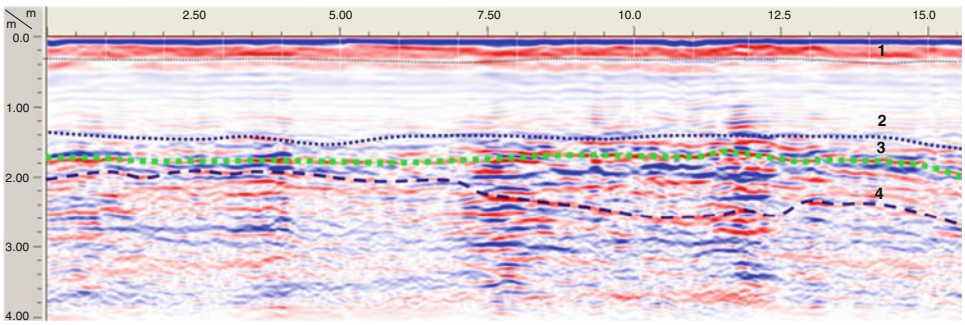


Fig. 5 Interpretation of the radargram F032

configuration. Schlumberger was used where the distance M-N remains the same (2 m) while the distance between current electrodes A-B successively increases (10, 14, 18, 22 and 26 m). The measurements on the points consisted of placing M and N at a 2-m distance, and a series of measuring ΔV/J ratio at the rising distances A and B from 6 m (Wenner, 2-2-2) to 26 m (Schlumberger, 12-2-12, for last sixth level). In case of Schlumberger configuration A-M-N-B, A-M and N-B, the distances between electrodes increased successively (2, 4, 6, 8, 10 and 12 m).

Results and Discussion

Using technologies of GPR and ERT, 31 profiles are generated: 30 GPR and 1 ERT profile. Several GPR profiles that characterize the most important features have been selected for discussion. The interpretation and relation of geophysical data to lithological data are then presented in the following.

The disposition of the radargrams F032, F033 and F034 and its starting and ending points (formed in nearby, undisturbed terrain) is shown in Fig. 4. Lithological elements that can be found in the landslide body are noticed in these radargrams as well. The marks from 1 to 4 define the position of borders between soil horizons in these radargrams.

Ground Penetrating Radar Results (GPR)

Radargram F032, 16 m^1 long, is formed in undisturbed terrain, about 1 m parallel to the edge of the right side scarp (Fig. 4). The coordinates of the beginning of radargram F038 (0 m^1) are not measured by GPS (surrounded by trees), and the end of radargram corresponds to the point 07 (16 m^1). The changes in terms of the phase inversion of reflected signal and disorder of the structure range from 7 m^1 to 16 m^1 (Fig. 5). The changes are especially visible from 7 m^1 to 12 m^1.

Radargram F033, 7 m^1 long, is formed in undisturbed terrain left from the head scarp apex. The beginning of F033

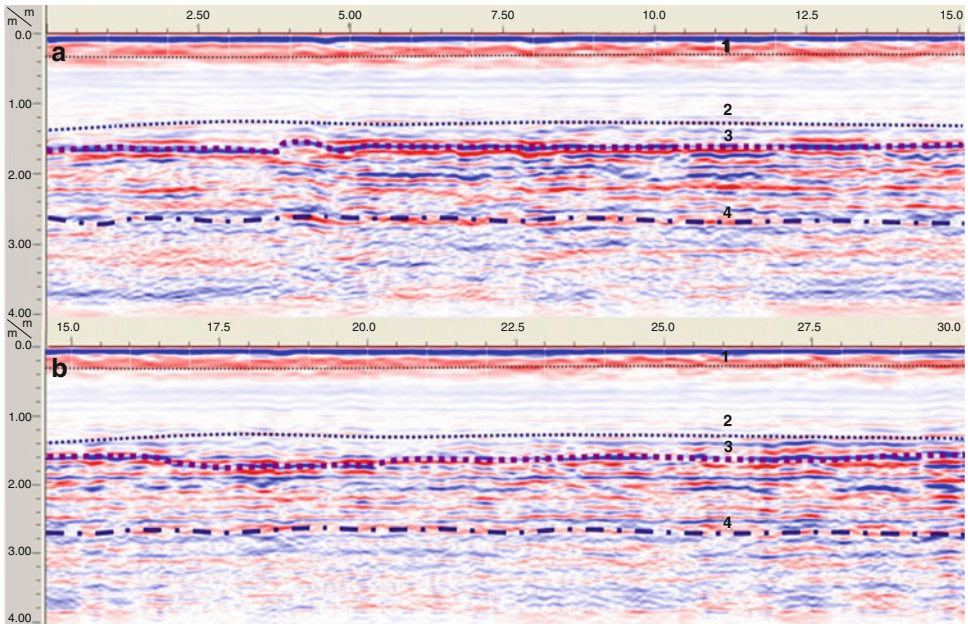


Fig. 6 Interpretation of radargram F034

radargram (0 m^1) corresponds to the coordinates of the point 07 (the position of the scanner B1), and the end of the radargram corresponds to the point 06 (7 m^1) – head scarp apex (Fig. 8a). The abscissa of the radargram F033 defines the resolution of generating scans where the achieved resolution is 1scan/1 cm. The given resolution is the same for all shown radargrams. Scan 390 from radargram F033 is represented with oscilloscope preview of reflected signal with clearly visible borders between soil horizons.

Since it was possible to see a part of soil horizons on the main scarp apex, they served as a solid basis for interpreting geophysical data. Therefore, the radargram F033 is formed directly above the scarp, so geophysical parameters can be defined and correlation between borders in radargram and visible soil horizons is established. Figure 8b shows a visual representation of the borders 2 and 3 which served as a basis for recalibration of a device and defining dielectric constant $\varepsilon_R = 28$ (Saarenketo 1998).

Radargram F034, 33 m^1 long, is formed in undisturbed terrain (in time of acquisition) and involves the entire left side scarp starting from the head scarp apex (Fig. 4). The beginning of F034 (0 m^1) radargram corresponds to the coordinates of the point 06, 8 m^1 corresponds to the point 05, 24 m^1 to the point 04, and the end corresponds to the point 03 (33 m^1). The changes in terms of phase inversion of reflected signal and disorder of the structure can be seen in a complete radargram (Fig. 8a, b). The changes are especially noticeable from 2 m^1 to 20 m^1.

The interpretation of the radargrams F032, F033 and F034 (Fig. 5, 6 and 8)

- Soil horizon from the surface to the border 1 – from 0 to 30 cm – humificated loess diluvium, dark brown, dry
- Soil horizon between borders 1 and 2 – from 30 to 135 cm – loess diluvium, pale brown, dry with variable amount of carbonates
- Soil horizon between borders 2 and 3 – from 135 to 170 cm – incoherent sand, pale brown
- Soil horizon between borders 3 and 4 – from 170 to 210 cm – on F032, that is, 260 cm on F034 – weathered marls; at 170 cm there is maximum reflected amplitude, probably clay sediments but also distorted structures and air-filled fractures, which was confirmed after the second reactivation of landslide in December 2009 (Fig. 9)
- Soil horizon beneath border 4 – high reflection amplitude, probably weak consolidated sand, no phase inversion and a small amount of moisture.

Radargram F046, 13.6 m^1 long, is formed in the landslide body starting from the head scarp apex to the centre of the landslide body. Beginning of radargram F046 (0 m^1) corresponds to the point p005, and the end of radargram corresponds to the point p009 (13.6 m^1). The trace of radargram F046 overlaps the part of ERT profile, where the starting point of radargram p005 corresponds to 37 m^1 of ERT profile, and the ending point of radargram p009 corresponds to 23 m^1 of ERT profile. Since height of the starting point p005 is 113.9 m above mean sea level and the end point p009 is at 109.4 m, then the difference in height of the profile is 4.5 m.

The comparative analysis of geophysical data from common parts of the radargram trace F046 and ERT profile showed an excellent correlation. It is explained in more detail when interpreting the results from ERT profile.

The labels 1 and 2 define the position of interpreted borders on the radargram F046:

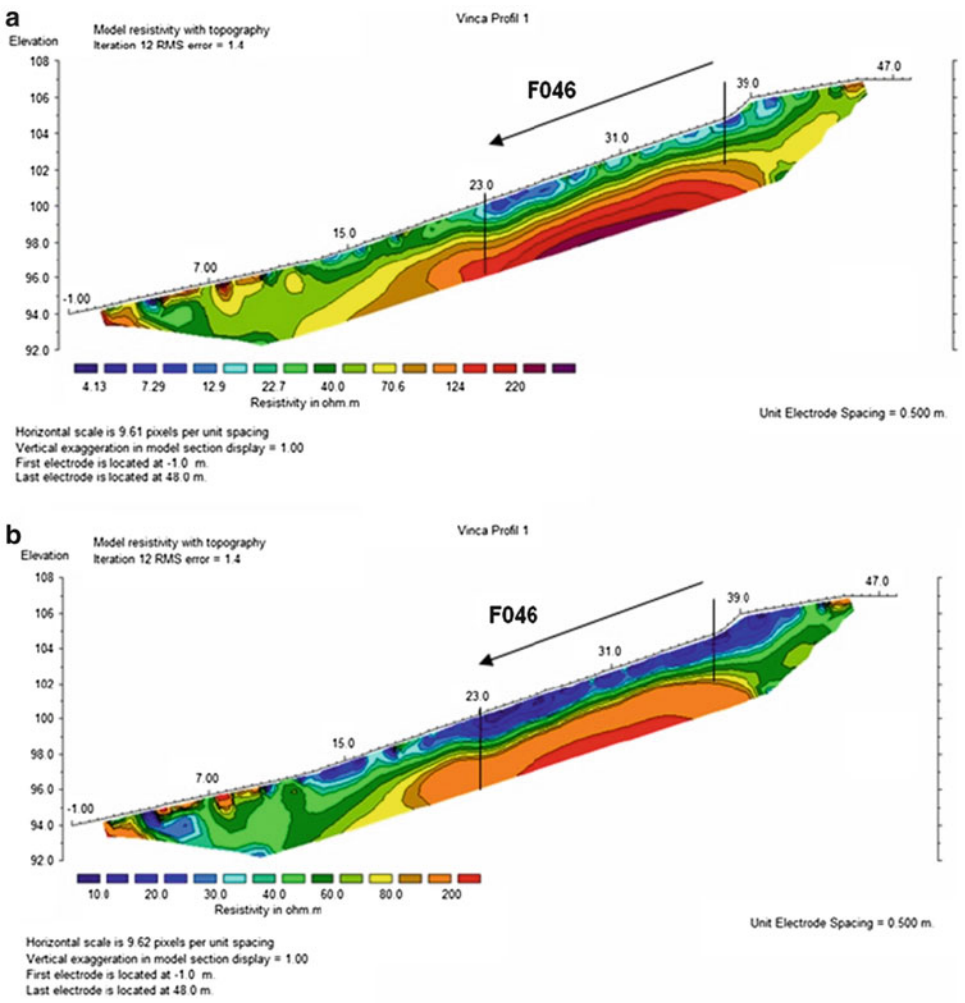


Fig. 7 Interpretation of ERT profile

- Soil horizon from the surface to the border 1 – from 0 to 65 cm – homogenous lithological composition and structure
- Soil horizon between borders 1 and 2 – from 65 to 120 cm – disorder in structure and phase inversion of reflected signal
- Soil horizon beneath border 2 – completely disordered structure with a high percentage of clay and significant attenuation of signal. Possible surface of rupture is expected in this soil horizon, but deeper than maximum penetration depth of EM wave.

ERT Profile: Central Cross Section in Landslide Body

In the raw ERT profile (Fig. 7a) three resistivity units can be identified. First, there is a clearly visible unit with a low specific electrical resistivity with values between 10 and 20Ωm (marked with shades of blue colour). This unit reaches the depth of 65 cm and it can be related to moved diluvium and loess sediments and incoherent sands.

Second, resistivity unit with values between 20 and 70Ωm (in ERT profile marked with shades of green), can be related to the landslide body consisting of moved diluvium, loess and sand, and at the bottom there is weathered marls where, at the depth of maximum 170 cm, the surface of rupture was formed.

The third, clearly identified resistivity unit in ERT profile was coloured in yellow to the nuances of red with corresponding resistivity ranging from 70 to 250 Ωm. This unit most probably corresponds to weak consolidated sand that can be seen in immediate adjacency to the landslide on a smaller vertical cut. Also, there are traces of clay. In ERT profile can be distinguished the debris, that is, the material which is deposited from 0 m^1 to 10 m^1 of the profile length. All the results are defined in the raw ERT profile (Fig. 7a) and they become more visible after re-interpretation considering identified resistivity units (Fig. 7b).

Comparing interpretation results of the radargram F046 and ERT profile it can be noticed that border 1 on radargram corresponds to resistivity unit 1 on ERT profile. Also, border 2 on radargram corresponds to light green colour from

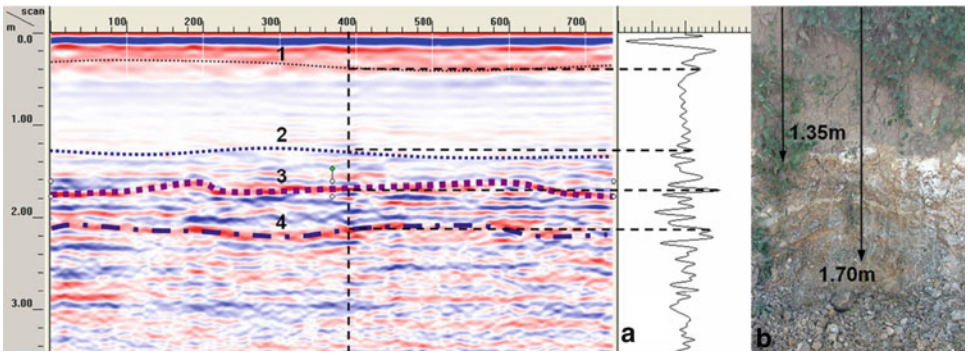


Fig. 8 Interpretation of radargram F033 on the head scarp apex



Fig. 9 Sliding surface (Photo December 2009)

resistivity unit 2 on ERT profile. It means, in this case, these two methods resulted in well correlated data (Fig. 7a, b).

ERT profile is perpendicular to head scarp and crosses radargrams F033 and F034. Since there is overlapping zone above head scarp apex it is possible to compare interpretation results of radargrams and profile. There are overt changes in the soil structure in the length of maximum 3 m^1 (from 39 m^1 to 42 m^1 in ERT profile) and to the depth of maximum 170 cm that can be noticed on the radargrams as well. This leads to conclusion that in this zone it is expected to have a further expansion of the landslide. After landslide reactivation in December 2009 this assumption was confirmed. Reactivation occurred in zones of the left side and head scarp. Surface of rupture was revealed at the depth of 170–180 cm (Fig. 9).

Conclusion

The paper presents the procedure to estimate characteristics of small shallow landslides that, in scientific literature, have not been treated appropriately, regarding their number and impact on environment. Proposed procedure is based on the integrated application of active remote sensing technologies (GPR and ERT) whose characteristics are mostly adequate for analysing the given type of the landslide. The capabilities of the proposed procedure have been successfully verified on a typical example of the landslide in the village of Vinča, near Belgrade, Serbia.

GPR technology was chosen to be the primary one, due to accessibility and dimensions of the landslide, as well as speed and resolution of data acquisition. The comparative analysis of results obtained by GPR and ERT technologies resulted in a more detailed and clearer interpretation of the landslide body structure. GPR scanning enabled the data of high resolution to the maximum depth of 4 m, and the most important results include estimation of the surface of rupture at the depth of 1.70 m, the composition of the landslide body and the prediction of landslide enlargement directions.

The results obtained by proposed procedure may be used as a high-quality input data for shallow landslides mitigation. Due to the widespread presence of this type of landslide, the achieved results can be used as simultaneously as conventional methods.

References

Bichler A, Bobrowsky P, Best M, Douma M, Hunter J, Calvert T, Burns R (2004) Three-dimensional mapping of a landslide using multi-geophysical approach: the Quesnel Forks landslide. Landslides 1:29–40

Bruno F, Marillier F (2000) Test of high-resolution seismic reflection and other geophysical techniques on the Boup landslide in the Swiss Alps. Surveys Geophys 21:333–348

Cruden DM, Varnes DJ (1996) Landslide types and processes. In: Turner KA, Schuster RL (eds) Landslides investigation and mitigation. Special report 247, Transportation Research Board, National Research Council, National Academy Press, Washington DC, pp. 36–75

Friedel S, Thielen A, Springman SM (2006) Investigation of a slope endangered by rainfall-induced landslides using 3D resistivity tomography and geotechnical testing. J Appl Geophys 60:100–114

Godio A, Bottino G (2001) Electrical and electromagnetic investigation for landslide characterisation. Phys Chem Earth Part C: Solar Terrest Planet Sci 26:705–710

Göktürkler G, Balkaya Ç, Erhan Z (2008) Geophysical investigation of a landslide: the Altindağ landslide site, Izmir (western Turkey). J Appl Geophys 65:84–96

Hack R (2000) Geophysics for slope stability. Surv Geophys 21:423–448

Jevremović M, Kuzmić V (2001) Complex geological map of Belgrade KGK 10 (1:10.000). Geozavod, Beograd

Lapenna V, Lorenzo P, Perrone A, Piscitelli S, Sdao F, Rizzo E (2003) High resoution geolectrical tomographies in the study of Giarrossa landslide (southern Italy). Bull Eng Geol Environ 62:259–268

Marescot L, Monnet R, Chapellier D (2008) Resistivity and induced polarization surveys for slope instability studies in the Swiss Alps. Eng Geol 98:18–28

McGuffey VC, Modeer VA, Turner KA (1996) Subsurface exploration. In: Landslides investigation and mitigation. Special report 247, Transportation Research Board, National Research Council, National Academy Press, Washington DC, pp. 231–277

Naudet V, Lazzari M, Perrone A, Loperte A, Piscitelli S, Lapenna V (2008) Integrated geophysical and geomorphological approach to investigate the snowmelt-triggered landslide of Bosco Piccolo village (Basilicata, southern Italy). Eng Geol 98:156–167

Ristić A, Petrovački D, Govedarica M, Popov S (2007) Detection of underground water flows by ground penetrating radar. Vodoprivreda 39:228–230 (in Serbian with English abstract)

Ristić A, Petrovački D, Govedarica M (2009) A new method to simultaneously estimate the radius of a cylindrical object and the wave propagation velocity from GPR data. Comput Geosci 35:1620–1630

Rokić L (1997) Origins of landslides on the right bank of Danube river near Novi Sad. In: International symposium on engineering geology and the environment, Athens, June 23–27, pp 1003–1008

Saarenketo T (1998) Electrical properties of water in clay and silty soils. J Appl Geophys 40:73–88

Sass O, Bell R, Glade T (2008) Comparison of GPR, 2D-resistivity and traditional techniques for the subsurface exploration of the Öschingen landslide, Swabian Alb (Germany). Geomorphology 93:89–103

Schrott L, Sass O (2008) Application of field geophysics in geomorphology: advances and limitations exemplified by case studies. Geomorphology 93:55–73

Xiujun G, Xiaoyu H, Yonggang J (2005) Forward modelling of different types of landslides with multi-electrode electric method. Appl Geophys 2:14–20



Monitoring and Modelling of Rainfall-Induced Landslide in Volcanic Soil Slope

Adrin Tohari, Khori Sugianti, and Katsumi Hattori

Abstract

Reactivated landslides have often posed a significant hazard to human lives and properties in many regions of Indonesia. In order to mitigate the hazard, a better understanding of mechanism leading to the reactivation of landslides is necessary. For this purpose, a long-term monitoring and numerical analysis of an active landslide in a volcanic soil slope in West Java, Indonesia was conducted. Monitoring instruments consisted of jet-fill tensiometers, inclinometers, open stand-pipes, and a tipping-bucket rain-gage. The records of pore-water pressure responses of the soil slope show that a transient perched water table could develop within the shallow soil profile, and the groundwater table could rise significantly in the middle portion of the slope during heavy rainstorms. Meanwhile, the inclinometer records show the existence of a multiple sliding zone at a maximum depth of about 17 m. Based on the monitoring data, a couple analysis of seepage and slope stability was performed to evaluate the effect of rainwater infiltration on long-term stability of the slope. The numerical results indicated that the total rainfall of at least 550 mm, with intensity of more than 80 mm/day was the triggering hydrological condition for reactivation of the landslide.

Keywords

Active landslide • Displacement • Field monitoring • Numerical modelling • Pore-water pressure • Rainfall

Introduction

The role of rainfall in the stability of soil slopes is complex. Besides affecting the hydrological and geotechnical conditions of the slopes, rainfall also affects the properties of the soil itself. The changes in the hydrological condition affect the geotechnical condition of the slope, particularly by increasing the pore-water pressure in the soil. In a steep slope with a deep groundwater table, matric suctions play positive role in affecting the shear strength of the soil and thus the stability of the slopes (Rahardjo 1999).

The strength of residual soil mass may also deteriorate with time as the soil is constantly weathered. The effect of climate on the properties of the soil is not easily quantified in a short period of time. On the other hand, the role of rainfall in affecting the groundwater table, pore-water pressure and the shear strength of the soil can now be assessed with the current knowledge.

Understanding of mechanisms and conditions leading to the initiation of rainfall-induced landslides has been generally gained from field measurements and laboratory strength tests. From the results of field measurements, it is generally accepted that the rapid rise of rainfall-induced pore-water pressure is

A. Tohari (✉) • K. Sugianti
Research Center for Geotechnology, Division of Engineering Geology and Earth Conservation, Jl, Indonesian Institute of Sciences, Sangkuriang, Bandung 40135, Indonesia
e-mail: adrin@cbn.net.id

K. Hattori
Graduate School of Sciences, Department of Earth Sciences, Chiba University, Chiba, Japan

C. Margottini et al. (eds.), *Landslide Science and Practice*, Vol. 2,
DOI 10.1007/978-3-642-31445-2_66, © Springer-Verlag Berlin Heidelberg 2013



Fig. 1 Research slope located above the Cadas Pangeran Provincial Road, Sumedang District, West Java, Indonesia. *Dashed white lines* indicate tension cracks (Photograph was taken on May 2006)

such landslides have caused US$ 1–2 million in damages on average every year. A high occurrence of the landslides can be attributed in part to the lack of understanding of the mechanism of the landslides. As such, it is still difficult to practice an effective measure to mitigate the hazard posed by the landslides.

This paper presents the results of a long-term monitoring and numerical modelling of an active landslide to evaluate the mechanism of the landslide. The research was carried out in a volcanic soil slope in Sumedang District, West Java, Indonesia due to a prolonged landslide hazard to a major provincial road called the Cadas Pangeran road. Despite the completion of geometry correction and slope reinforcement works after a movement in 2005, tension cracks (Fig. 1) were still found to develop across the slope, indicating that the cut-slope was still in an unstable condition.

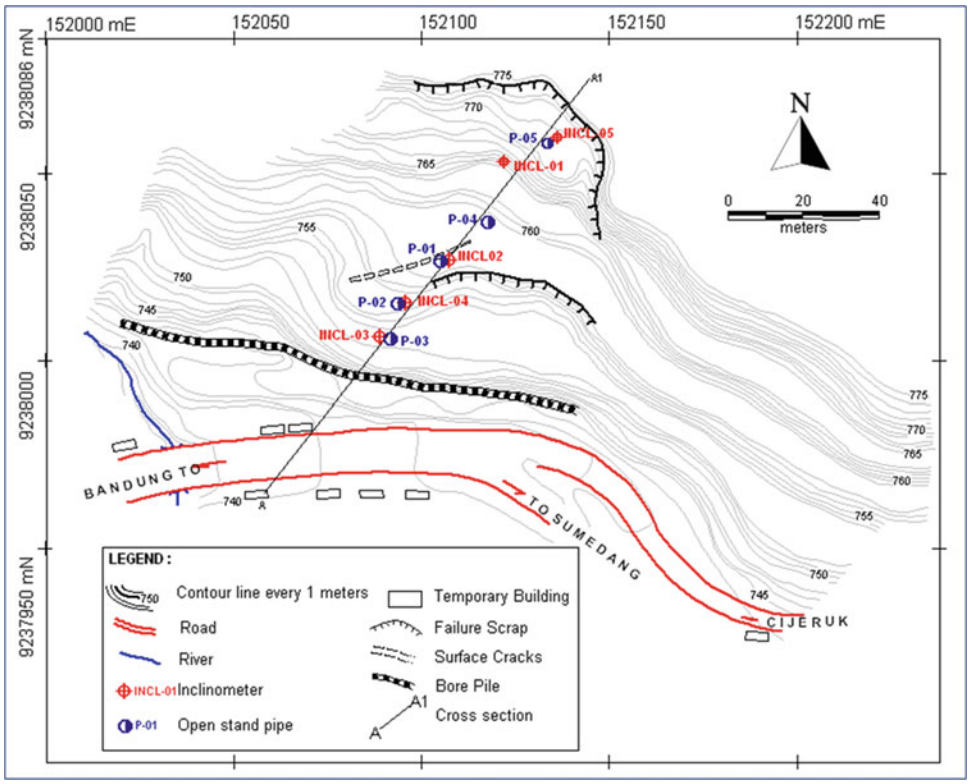


Fig. 2 Topographical map of the research landslide area, showing the locations of geotechnical investigations

critical to the initiation of landslides (Johnson and Sitar 1990). It is typically observed that significant build up in positive pressure heads is generated in an area low on the slope (Sitar and Anderson 1992; Anderson and Thallapally 1996). However, the mechanism of pore-pressure generation differs from site to site, depending on the site hydrology and soil properties (Sitar and Anderson 1992; Tohari et al. 2004).

Reactivation of landslides have affected human lives and properties in many regions of Indonesia. The occurrences of

Methodology

Slope Characterization

Based on the topographical map shown in Fig. 2, and subsurface geotechnical data, the slope profile was constructed as shown in Fig. 3. The slope profile is made up of the following soil layers of volcanic origin:

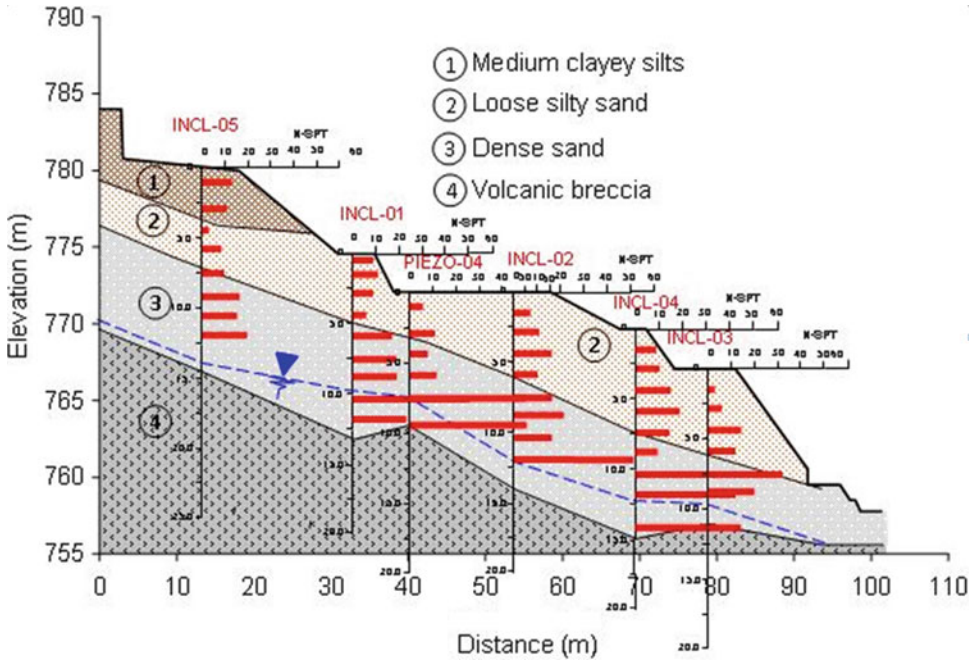


Fig. 3 Geotechnical profile of the research slope along A-A1

Table 1 Geotechnical properties of the soils

Soil properties	Clayey silt	Silty sand	Sand
Plastic limit (%)	50–60	50–60	20–40
Liquid limit (%)	110–120	70–80	40–60
Unit weight (kN/m^3)	16.5	17.6	18.5
Porosity	0.61	0.69	0.51
Saturated coefficient of permeability (m/s)	2.6×10^{-6}	1.4×10^{-6}	5.1×10^{-4}
Effective cohesion (kPa)	19	5	33
Effective friction angle (deg.)	30	20	32

(a) Medium clayey silt layer of 3.0–4.0 m thick, made up of completely decomposed volcanic breccias.
(b) Loose silty sand layer of 2.0–6.5 m thick, derived from highly decomposed volcanic tuff.
(c) Dense sand layer of 4.0–10.0 m thick, as the product of moderately decomposed volcanic breccias.

Soil Properties

A series of laboratory tests was conducted on soil samples obtained from each soil layer to determine the following soil properties: (1) the index properties, (2) the saturated coefficient of permeability, (3) the saturated shear strength parameters (c', ϕ'), and (4) the soil water characteristic (SWC) curves. The saturated properties of the soil samples are summarized in Table 1.

Figure 3 shows the SWC curves for each soil sample measured in the laboratory using the drying path. The curves were fitted using the van Genuchten function (1980). The air-entry value (AEV) for all soil samples is approximately 10 kPa (Fig. 4).

Figure 5 shows the soil permeability functions estimated from the SWC curves using the van Genuchten equation (1980). It can be seen that the estimated soil permeability (k_w) decreases by almost four orders of magnitude over the soil suction range of 100 kPa.

The shear strength functions of each soil layer were estimated from the saturated shear strength parameters and SWC curves using a method the Khalili and Khabbaz's method (1998). The results are shown in Fig. 6. The values of ϕ^b for each soil is approximately 10° for soil suction at the air entry value.

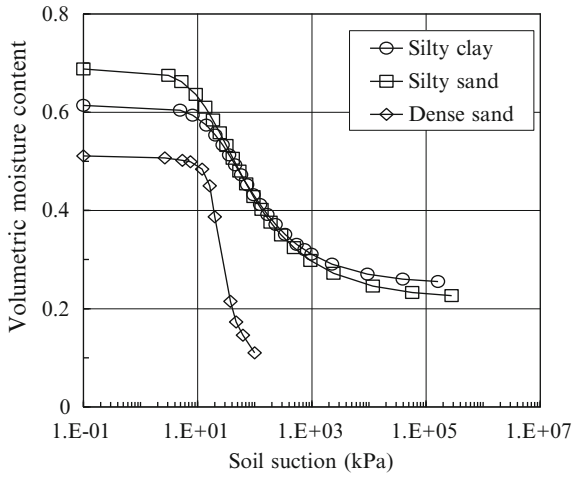


Fig. 4 Soil-water characteristic curves for each soil sample

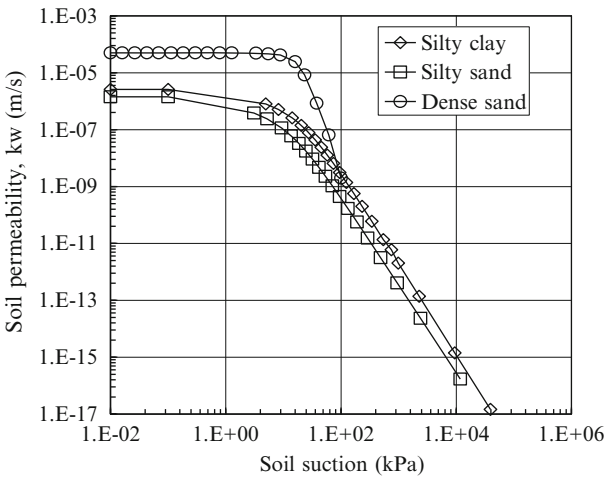


Fig. 5 Permeability functions for each soil sample

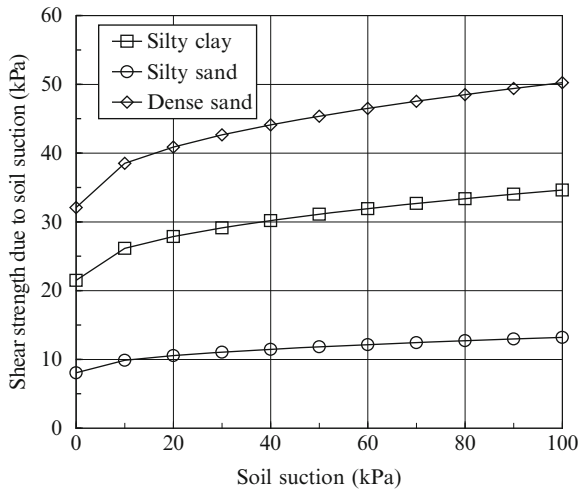


Fig. 6 Shear strength functions for each soil sample

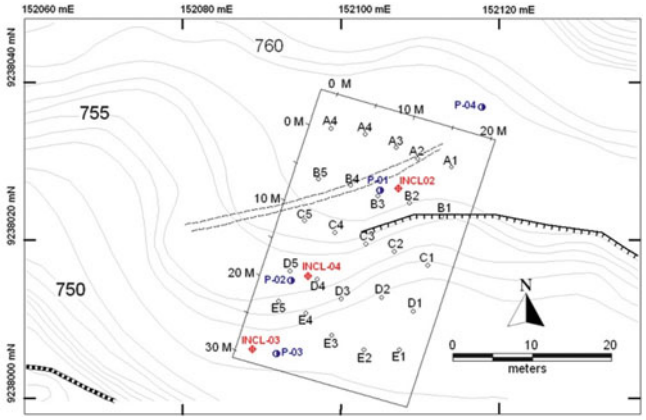


Fig. 7 Lay-out of jet-fill tensiometer nests in the research slope

Field Instrumentation System

Field instruments consisted of 24 jet-fill tensiometers, five open standpipes and five inclinometers and a rain-gauge. All the tensiometers were installed at five closely-spaced nests (A to E) within 5.0 m radius (Fig. 7). Each nest consisted of five tensiometers, installed at depths of 0.5, 1.0, 1.5, 2.0 and 3.0 m. The objective was t0 obtain the spatial variation of pore-water pressure responses of the slope to rainfall infiltration.

Five open standpipes and five inclinometers (see Fig. 2) were installed, up to a maximum depth of 25 m, to monitor groundwater levels and horizontal deformation of the slope, respectively. A dipmeter was used to monitor groundwater levels in the open standpipes. A portabel inclinometer probe was used to measure horizontal displacement in the inclinometers. The monitoring was manually performed every month for 2 years.

A tipping-bucket rain gauge was used to obtain site-specific rainfall data (i.e., rainfall total and intensity). The rain gauge was calibrated to measure rainfall in increment of 0.2 mm.

An automatic data acquisition system was set up to monitor the soil pore-water pressure and rainfall in real time on a continous basis. The data acquisition system consisted of the sensors, cables, data logger, and power supplies. The data logger was configured to collect data at a 5 min interval. The data were collected biweekly or monthly

Numerical Modelling

Seepage Analysis

To understand the effect of rainwater infiltration on the pore-water pressure distribution within the soil slope, the slope profile shown in Fig. 3 was subjected to a transient seepage analysis using the finite element computer program SEEP/W

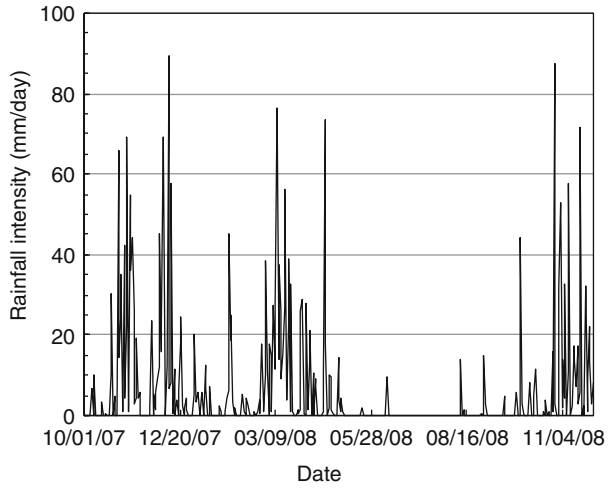


Fig. 8 Daily rainfall used in transient seepage analysis

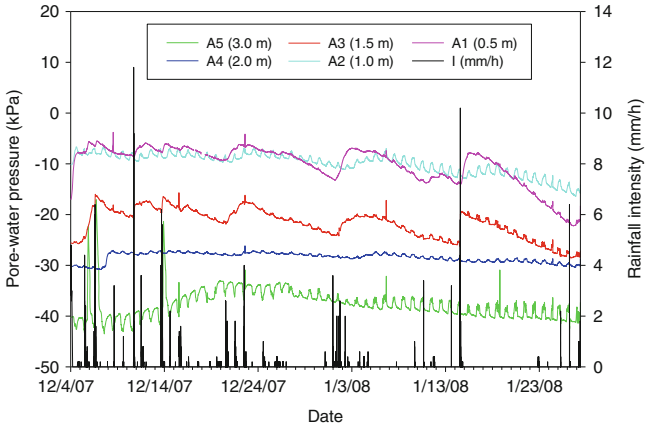


Fig. 9 Variations of pore-water pressure response at Nest A and the daily rainfall from December 2007 to January 2008

(Geo-Slope International Ltd 2002a). The boundary conditions were imposed using the groundwater level data obtained from the open standpipes. Zero flux conditions were assigned to the left, right and lower boundaries. An initial pore-water pressure value of -40 kPa was used. For this analysis, the hydraulic properties of each soil layer are given in Figs. 4 and 5. The transient analysis was then performed using the daily rainfall records of December 2007 to November 2008 (Fig. 8).

Slope Stability Analysis

The computer program SLOPE/W (Geo-Slope International Ltd 2002b) was used to perform a limit equilibrium analysis on the landslide investigated in this study. The stability analysis used the pore-water pressure distributions obtained from the seepage analysis as input data at each time step. The general limit equilibrium (GLE) method was used in this analysis. The shear strength parameters adopted for each soil layer are given in Table 1 and Fig. 6. The depth of critical slip surface was determined from the inclinometer records of INCL-03.

Results

Field Monitoring of Pore-Water Pressure Responses

Figures 9 and 10 show the responses of pore-water pressure at Nests A and D to rainfall events from December 2007 to January 2008, respectively. Generally, the pore-water pressures decreased with depth. Prior to the rainfall events,

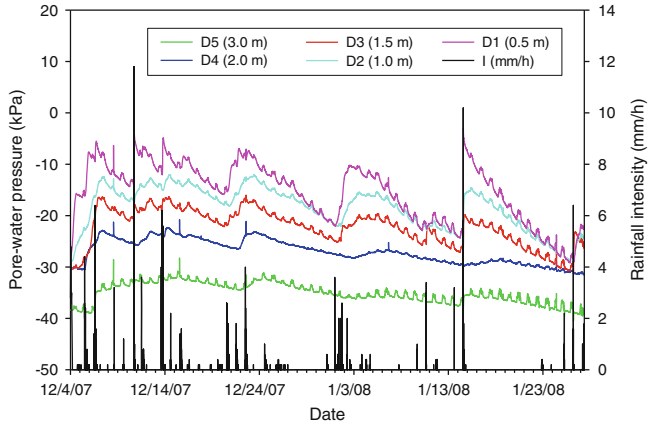


Fig. 10 Variations of pore-water pressure response at Nest D and the daily rainfall from December 2007 to January 2008

a minimum pore-water pressure of -40 kPa was recorded by the deepest tensiometers.

In response to the rainfall events, all tensiometers recorded the increase of pore-water pressures within the slope. However, the pore-water pressure responses in Nest A were less rapid than those in Nest D because the antecedent pore-water pressures of the near-surface soils in Nest A was higher than those in Nest D. The records of shallow tensiometers indicate that the near-surface soil profile was nearly saturated. Meanwhile, the records of deepest tensiometers in Nest A show that the rainwater did not infiltrate to a depth of 3.0 m. In other words, the infiltration of rainwater were confined within the zone of higher saturation that developed near the slope surface in this slope portion.

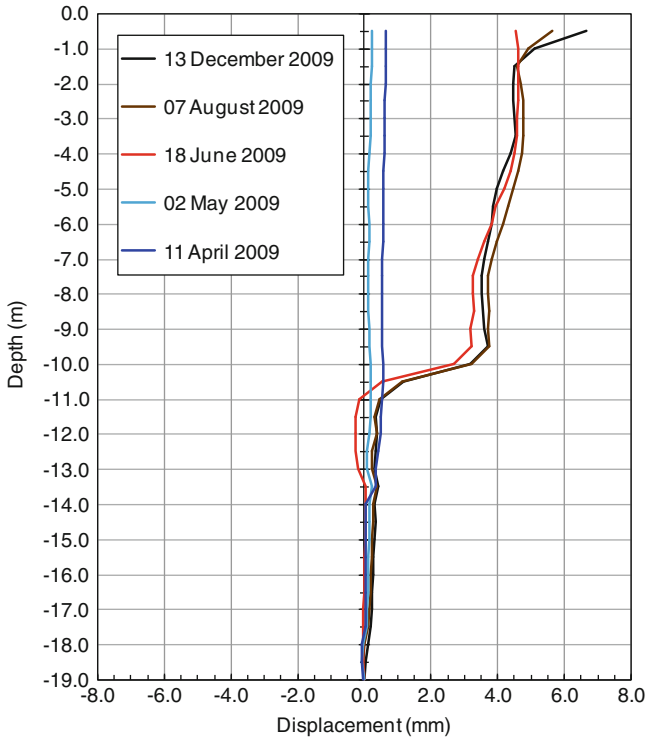


Fig. 11 Displacement records of INCL-05 from April to December 2009

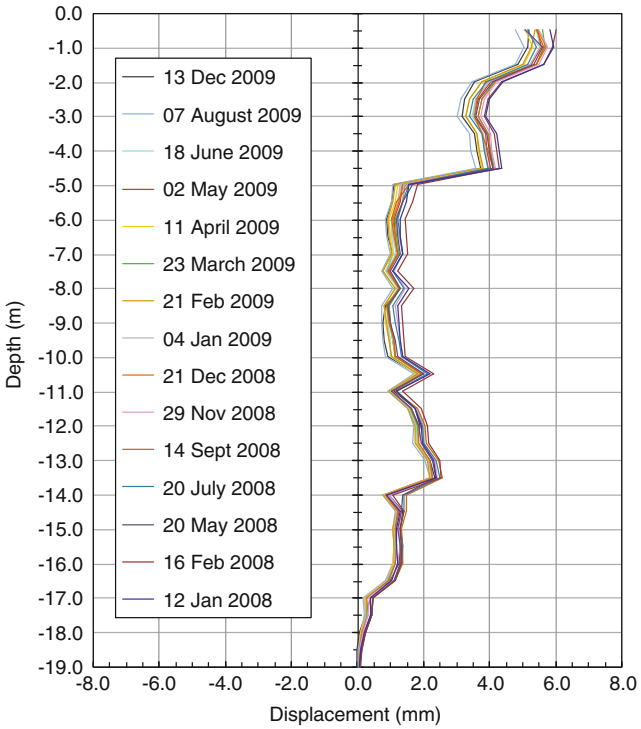


Fig. 12 Displacement records of INCL-03 from January 2008 to December 2009

Field Monitoring of Slope Movement

Displacement records of inclinometer INCL-05 (Fig. 11), located at the upper part of the slope, shows a clear development of a sliding zone at a depth of 11 m, with a cumulative displacement of about 6 mm. Meanwhile, inclinometer INCL-03 (Fig. 12), located at the lower part of the slope, show sliding zones developed at depths of 5 and 17 m. Thus, the monitoring records suggest that the landslide investigated in this study is an active landslide with a multiple sliding zone.

Numerical Analysis

Pore-water pressure distributions within the slope due to rainfall events from October 2007 to November 2008 are shown in Fig. 13 for four selected days. The results show a rise of the groundwater table, especially in the middle and lower portions of the slope, and that the near-surface soils were almost saturated in response to a heavy rainfall period until March 2008 (Fig. 13a). In response to a dry period from May to August 2008, the near-surface soils became more unsaturated. However, the groundwater table still increased within the slope profile (Fig. 13b). As heavy rainfall periods started from October to November 2008, the groundwater level increased significantly, especially in the middle part of the slope. Groundwater seepage also started to develop at the slope toe (Fig. 13c)

Figure 14 shows the evolution of the factor of safety with time during the periode of rainfall infiltration from December 2007 to November 2008. The period of rainfall infiltration of October 2007 to January 2008, with a rainfall total of 710 mm and a maximum intensity of 89.5 mm/day, resulted in a significant decrease of the factor of safety from 2,07 to 1.33. The factor of safety then decreased to 1.28 during a heavy rainfall period from February to March 2008. The factor of safety decreased further to 1.16 due to the heavy rainfall of 553 mm with a maximum intensity of 87.6 mm/day in October-November 2008. This was associated with the development of groundwater seepage at the slope toe area.

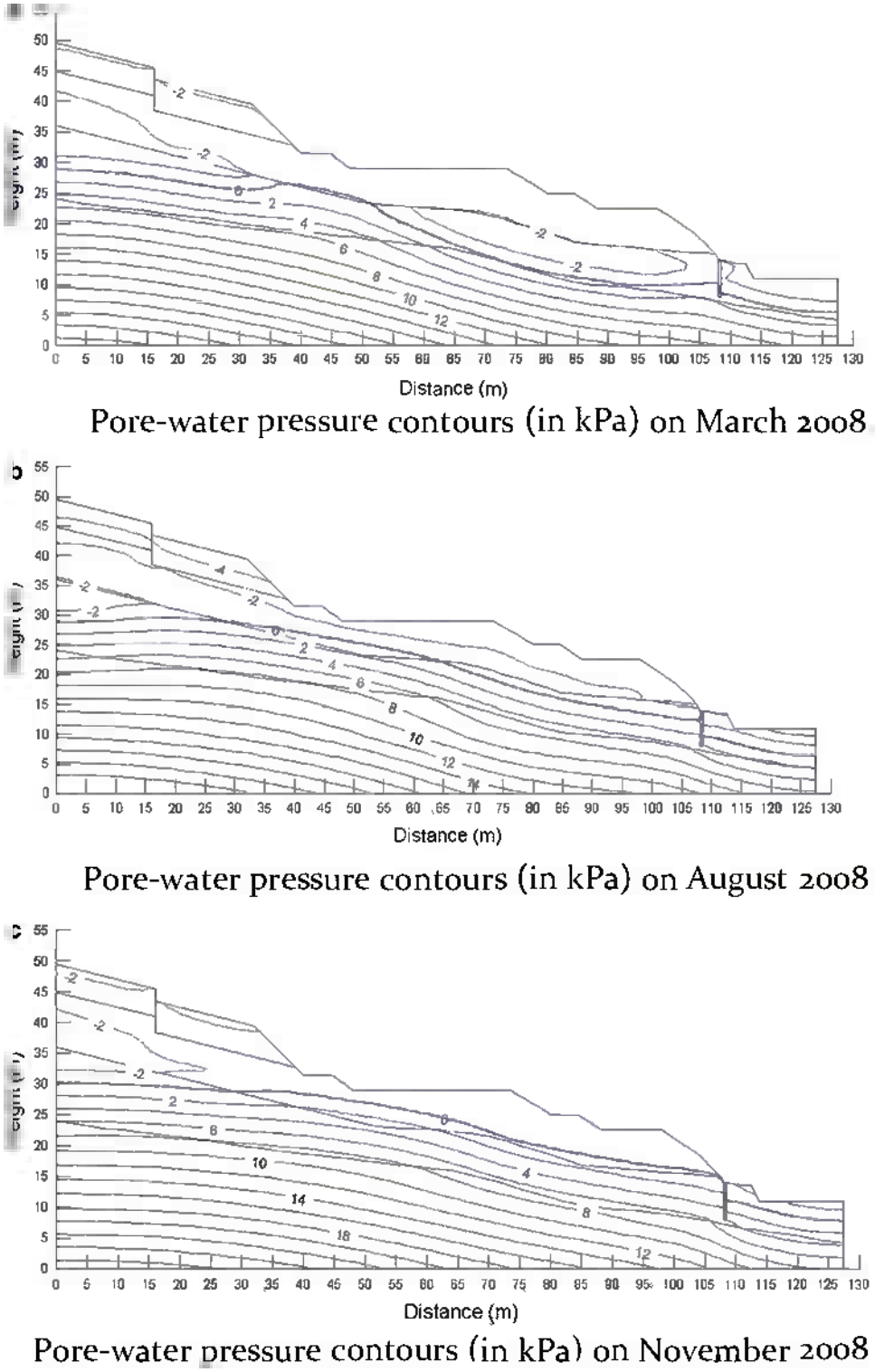


Fig. 13 Pore-water pressure distributions due to rainfall infiltration from October 2007 to November 2008

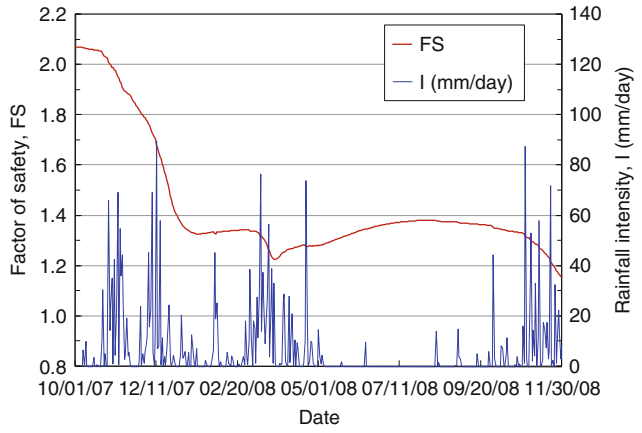


Fig. 14 Factor of safety variations due to rainwater infiltration and evaporation during October 2007 to November 2008

Conclusions

The results of field monitoring and numerical analysis of the landslide lead to the following conclusions:

- During a long period of heavy rainfall, positive pore pressures were observed to increase within the upper 2 m soil.
- The evolution of the factor of safety indicates that the landslide would reactivate during heavy rainfall periods, involving a slow movement with a multiple deep sliding at a maximum depth of 17 m.
- The reactivation of the landslide is associated with the increase of groundwater table within the slope, and the development of seepage in the lower portion of the slope.
- The numerical analysis shows that rainfall of at least 550 mm with an intensity of more than 80 mm/day would be the triggering hydrological condition for reactivation of the landslide.

Acknowledgments The authors would like to acknowledge the project funding from the Indonesian Institute of Sciences, the Ministry of Research and Technology, and the Indonesia Toray Science Foundation (ITSF).

References

Anderson SA, Thallapally LK (1996) Hydrologic response of a steep tropical slope on heavy rainfall. In: Proceedings of 7th international symposium on landslides, Trondheim, 17–21 June 1996, pp 1489–1495

Geo-Slope International Ltd (2002a) SEEP/W Version 5.12 *User Manual*, GEO-SLOPE International Ltd., Calgary

Geo-Slope International Ltd (2002b) SLOPE/W Version 5.12 *User Manual*, GEO-SLOPE International Ltd., Calgary

Johnson KA, Sitar N (1990) Hydrologic conditions leading to debris flow initiation. Can Geotech J 27(6):789–801

Khalili N, Khabbaz MH (1998) A unique relationship for X for the determination of the shear strength of unsaturated soils. Geotechnique 48(5):681–687

Rahardjo H (1999) The effect of rainfall on the slope stability of residual soil in Singapore. Report of Research Project, Nanyang Technology University, Jurong

Sitar N, Anderson SA (1992) Conditions for initiation of rainfall-induced debris flows. In: Geotechnical engineering division specialty conference: stability and performance of slopes and embankments-II, ASCE, New York, pp 834–849

Tohari A, Nishigaki M, Komatsu M, Kankam-Yeboah K, Daimaru S (2004) Field monitoring of hydrologic response of residual soil slope to rainfall. In: Proceedings of the 9th international symposium on landslides, Rio de Janeiro, 28 June–2 July 2004, pp 749–754

van Genuchten MT (1980) A closed-form equation of predicting the hydraulic conductivity of unsaturated soils. Soil SciSoc Am J 44:892–898



Impact Pressure Measurements in Shallow Landslides

Bugnion Louis and Wendeler Corinna

Abstract

We reproduce shallow landslides by releasing 50 m^3 of debris mixture down a 40 m long and 30° steep slope. The slope is instrumented in order to measure front and surface velocities, flow height and impact pressure on small obstacles. The mixture properties are determined from analysis of material samples. The impact process is investigated on the basis of the undisturbed flow properties 4 m upstream of the obstacles. Impact coefficients relating mixture density and surface velocity to the impact pressure are computed from the front to the tail of the flow.

Keywords

Impact pressure • Shallow landslide • Field scale test

Introduction

Among the large family of landslides, shallow landslides or hillslope debris flows make up a particular category that is sparsely documented and studied. They distinguish themselves with small failure depths or equivalently small volumes (up to 2 m or 200 m^3 respectively). They release on steep slopes during intense rainfall and despite their small size they can reach high velocities. The failure process is fast and its location mostly unpredictable. Their evolution from failure to deposition is in the order of dozens of seconds which makes their observation particularly difficult. Runout distances are usually smaller than a hundred meters, while if the slide is channelised by the terrain and is able to entrain material, runout distance may be multiplied several times and the flow will be regarded as a debris flow.

B. Louis (✉)
Debris Flows and Rockfall Research Unit, WSL Institute for Snow and Avalanche Research SLF Avalanches, Flüelastrasse 11, Davos Dorf, Switzerland
e-mail: bugnion@slf.ch

W. Corinna
Geobrugg AG, Protection Systems against Natural Hazards, Romanshorn, Switzerland

Due to their high bulk density and speed, shallow landslides represent a serious hazard to people, buildings and infrastructures such as roads or railway lines. The potential of damage is materialised through the pressure that they exert on objects during impact. The impact pressure results from halting deflecting of flowing material encountered by an object. This pressure is dependent on the kinetics and material properties of the flow as well as the geometry of the flow-object pair. Relationships defining impact pressure as a function of the aforementioned parameters are of great importance in mitigation studies delimitating hazard zones and in the design of protection measures like reinforced buildings, retaining walls or flexible barriers.

Systematic study of full-scale shallow landslides and their interaction with obstacles is carried out at the Veltheim test site in Switzerland. Debris mixtures with volumes of 50 m^3 are released down a 30° degrees steep and 40 m long slope on the hillside of a disused quarry. Mean front velocities between 5 and 10 m/s are measured, while maximum flow heights 25 m downstream of the release mechanism range between 0.3 and 1.0 m. Thirty meters downstream of the release mechanism two square-shape obstacles are installed perpendicular to the flow. They have sides of 12 and 20 cm respectively, with their lower side 5 cm above the ground. Strain-gauge sensors built in the

C. Margottini et al. (eds.), *Landslide Science and Practice*, Vol. 2,
DOI 10.1007/978-3-642-31445-2_67, © Springer-Verlag Berlin Heidelberg 2013

obstacles record the forces experienced during the impact. In addition to the pressure measurements, distance sensors hung above the test slope measure flow depths over time and permit the computation of flow surface velocities through a correlation of the signals from the distance sensors.

More than 20 releases are performed, which with the instrumentation setup in addition to the analysis of mixture samples allow for a detailed characterization of the flows. The dependency of the impact pressures on the flow parameters is evaluated from the flow front to the tail. Likewise the comparison between the pressure signals obtained from the small and the large obstacles provide useful information about the structure of the flow. The impact pressure exerted on rigid obstacles by full-scale shallow landslides can be measured and related to other flow parameters by a simple formula. It is tested for a wide range of flows with surface velocities varying between 2 and 13 m/s and applies only for cases where the flow depth is within the same order of magnitude as the obstacle size.

Test Site

A 41 m long, 8 m wide channel is excavated on the side of a rock quarry in Canton Aargau, Switzerland. It has an average slope inclination of 30°. At the upper channel end, a wall is constructed to create a sloping reservoir with a maximum capacity of 50 m^3 of debris (approximately 100 tons). The lower 0.8 m of the wall operates as a trap door that is released to the spill material down the slope. The material is obtained by mixing up soil and bedrock material with water. The proportion of the raw materials is varied roughly from one test to another and samples of material are taken from the reservoir to assess grain-size distribution and water content. The filling of the reservoir and the release take place within 2 h. Plastic sheets are placed at the bottom of the reservoir to prevent water loss and to ensure evacuation of all material. At the lower end of the channel a flexible barrier is mounted that stops the material, so no runout occurs (Fig. 1).

Upon release the material flows rapidly out of the reservoir. Fast flows deposit little material and accelerate over the entire channel length while slower flows deposit more material and decelerate along the second half of the channel. Vertical velocities are visible in the vicinity of the trap door, but observations of the flow surface from video recordings indicate that they rapidly disappear leading to flows in which the primary velocity component is parallel to the slope. Material at the slope sidewalls lags slightly behind, indicating some sidewall friction. At the end of a test day the channel is cleared out with a pressurized water hose. On tests with successive releases (between two and four), deposited material from the first releases is still present on the channel bed during the consecutive releases.

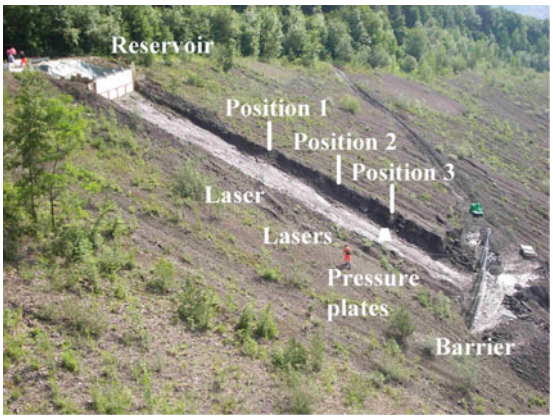


Fig. 1 Test channel with reservoir and flexible barrier at its end

The channel is instrumented with vertically-oriented laser distance sensors located 14 m (position 1) and 26 m (position 2) downstream of the reservoir. The sensors are used to determine the flow heights at the middle of the channel. The flow heights correspond to the height perpendicular to the bed surface. At position 2 two laser distance sensors are spaced 30 cm with their beams parallel. The velocity of the upper flow surface is derived computing the discrete cross correlation function $h_1h_2(t, \Delta t)$ of the two height signals. The time interval Δt that maximizes the function is proportional to the surface velocity.

At 30 m downslope (position 3) two force sensors measuring up to 20 kN are mounted on wedges to measure impact pressures. The smaller wedge is 225 mm high and the larger wedge 295 mm high (height measured above the bed surface). Thus both wedges are submerged in the flow body. The sensors are each surmounted by two square steel plates with side lengths 120 and 200 mm, respectively. The steel plates are separated by an elastomer layer of 20 mm thickness to damp hard contacts. The two sensors are separated laterally by 1 m (see Fig. 2).

The strain-gauge sensors deliver a 2 kHz signal. The oscillations of the force signal due to hard contacts between solid grains and the pressure plates (vibrations of the plates) are replaced by the mean value over 0.05 s time intervals. The choice of the time interval is based on calibration tests and corresponds to the typical duration of the force oscillation consecutive to a hard contact (with a steel ball). From the calibration tests it is shown that the mean force value taken over the duration of the oscillation scales with the momentum exchanged between the steel ball and the pressure plate while the median value is close to zero. The averaging of the pressure signal conserves the momentum exchanged between the encountering material and the plate.



Fig. 2 Two pressure plates 30 m downstream of the reservoir. The measuring surfaces are 12 × 12 cm and 20 × 20 cm respectively

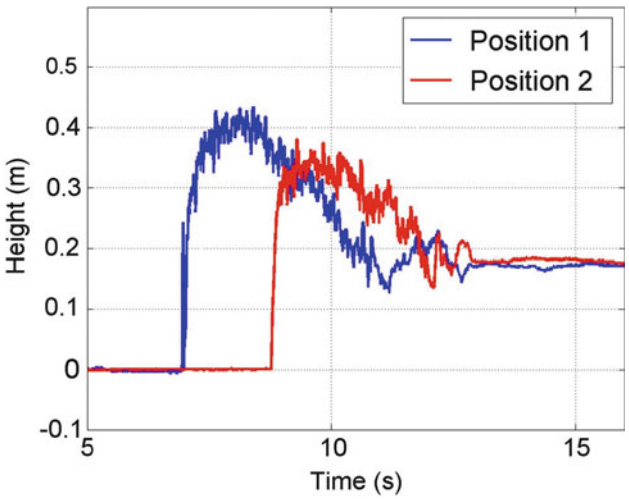


Fig. 3 Flow heights at position 1 and 2 versus time during first release 16.1

Measurements

We perform 16 tests, most of them consisting of one single release of 50 m^3 debris material. On some tests two, three or four successive releases are carried out. During consecutive releases (spaced between 2 and 3 h) deposited material remains on the channel bed surface. Material samples are taken from the top of the reservoir before every first release and are analysed in the laboratory for density, water content, grain-size distribution and consistency limits of the fines content. The volume of the samples (about 30 kg) are large enough to assess the grain-size distribution accurately for grain sizes up to 60 mm. On one release two material samples are collected, one in the reservoir and one in the deposit at the flexible barrier. The properties of the two samples are very close (maximum deviation of 8 % for the clay mass fraction).

The density of the debris mixtures range between 1,760 and 2,110 kg/m^3 and the water content between 14 % and 28 % (percentage of mass). The mass fractions of fines content (grain size $d < 0.063$ mm) and gravel (2 mm $< d <$ 60 mm) vary between 21 % and 48 % and 16 % and 59 % respectively (Fig. 3).

Two main types of flow front can be recognized. Flows in a channel free of deposits have a moderately steep front followed by a body with smoothly varying flow height (maximum flow heights between 0.3 and 0.5 m). Flows in a channel with previously deposited material show steeper fronts and a shorter body (maximum flow heights between 0.6 and 1 m). The peak heights correspond to the aerated upper part of the front region of the flow. The tail of the flow, indicated by decreasing flow heights with time is followed by a constant surface elevation indicating that the material has stopped moving. The deposition heights correlate negatively with the mean front velocity. Mean front velocities between positions 1 and 2 are computed from the front passing times at the laser sensors and range between 5.3 and 10.4 m/s. The passing time of the front is defined as the time when the height is equal to 0.05 m. From the pressure signals it is defined when the pressure attains 10 kPa.

Comparing first releases, we can distinguish a difference in flow behaviour among releases with a large fraction of coarse particles (gravel fraction between 45 % and 50 %) and releases with large fines content (clay and silt fraction larger than 40 %). Releases with a large fraction of coarse particles are fast flows independently of water content or liquidity index. Releases with large fines content have on average lower front velocities which correlate with the liquidity index (Fig. 4).

The maximum impact pressures range between 15 and 200 kPa i.e. over more than one order of magnitude, equivalent to 2–50 times the static pressure values. In Fig. 5, the mean and standard deviation of the pressure signal over 0.05 s intervals measured during release 16.1 by the large pressure plate are plotted. The maximum impact pressure is measured in the front of the flow. In contrast to the flow height time series, no systematic difference is observed between impact pressure of first releases and consecutive releases. Thus, no correlation between maximum impact pressures and maximum flow heights are assessed while correlation between the maximum impact pressure values and the square of the front speed are observed. The standard deviation values of the raw signal computed over the 0.05 s time interval are proportional to the mean impact pressure values. They represent 0.23 and 0.39 of the mean pressure values for the large and small pressure plate respectively. They are related to hard contacts and to density and velocity inhomogeneities (see also Iverson (1997)).

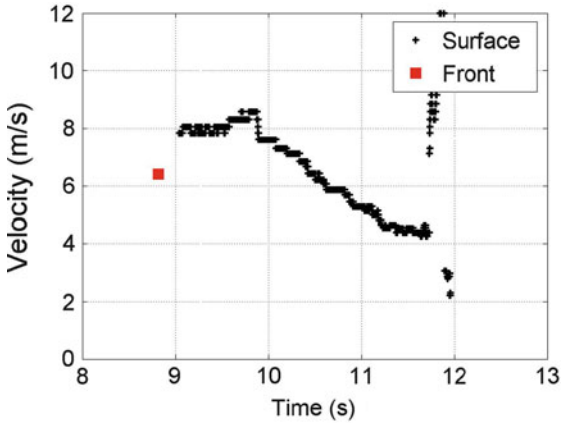


Fig. 4 Surface and front velocitie at position 2 versus time during first release 16.1

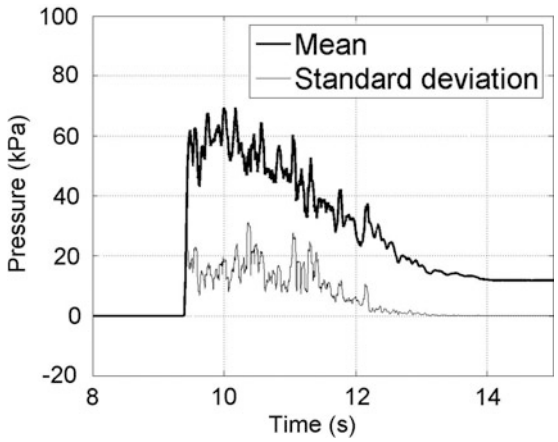


Fig. 5 Mean and standard deviation of the pressure signal over 0.05 s time intervals at position 2 versus time during first release 16.1

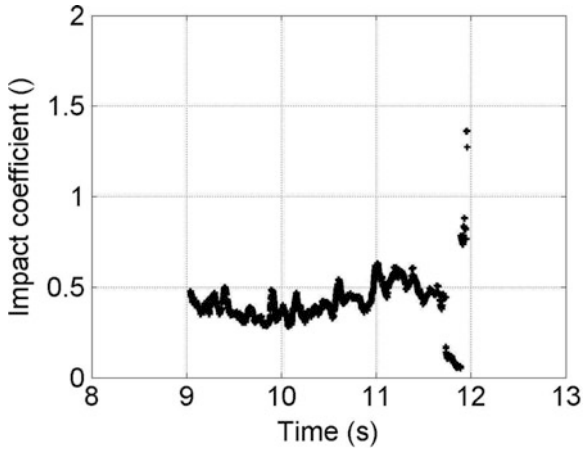


Fig. 6 Impact coefficients at position 2 versus time during first release 16.1

Discussion

The flow heights having the same order of magnitude as the obstacle size, the flow is disturbed over the entire depth. Material impacting the plates is either deflected around the plates or is stopped. The relative importance of theses processes plays a crucial role in the formation of the impact pressure.

We want to quantify the impact pressure with respect to the flow parameters including mixture properties, flow height and flow velocity. Two types of empirical formulas are used to describe the impact pressures. Impact height-dependent pressure $p = k \cdot \rho \cdot g \cdot H$ with ρ the material density, g the gravitational acceleration and H the immersion depth; or velocity-dependent pressure $p = C \cdot \rho \cdot u^2$ with u the impact velocity and C the impact coefficient. The first expression states that the impact pressure is proportional to the static pressure with k a proportionality coefficient. The second expression relates the impact pressure to the momentum rate of material passing the obstacle. If the material is stopped by the obstacle, the force exerted on the obstacle would be $A \cdot \rho \cdot u^2$ with A the surface of the obstacle. In reality not all the material is stopped but part of it is only decelerated or deflected. Likewise, the flow around the cross section of the obstacle may be affected and thus contribute to the pressure measured on the obstacle. The deviation from the pressure $\rho \cdot u^2$ is accounted for by the impact coefficient C.

Impact pressure data from debris flows or landslides are scarce. The Swiss and Hong Kong guidelines (see GEO Report (2000)) recommend the use of the velocity square dependant relationship for the calculation of debris flow impact pressure on obstacle with impact coefficient values of 2 and 3 respectively.

In the majority of the releases, only the front velocity is available. For releases 13.1–16.2, the surface velocity time series are also available. They are used together with the impact pressure time series to compute the impact coefficient time series over the duration of the impact. One difficulty arises as the surface velocity is computed at position 2 and the impact pressure is measured at position 3. The surface velocity time series are thus extrapolated to position 3 by shifting them in time. The shift in time is chosen as twice the difference between the front passing times at positions 2 and 3 (taking into account that the front is faster than the rest of the flow). The impact coefficient values are plotted versus time in Fig. 6 for first release 16.1. In the first two-thirds of the impact, the value of the impact coefficient remains nearly constant. In the last third of the impact, a slight increase of the impact coefficient values is observed. The reason for this effect may lie in the extrapolation of the surface velocities from position 2 to position 3 using a constant time shift. The extrapolation is accurate in

the flow body (where the velocity is about half the front velocity) but it is less precise in the front and in the tail. Note that the first two-thirds of the impact correspond to the time where impact pressures and velocities are the largest.

Conclusion

Guidelines for construction of mitigation measures against shallow landslides require reliable estimates of impact pressures on structures and obstacles. In our investigation using field-scale flows, we find that the pressures depend primarily on the flow speed, which depends on the grain-size distribution and water content. The velocities investigated range between 2 and 13 m/s. Thus, the pressure measurements indicate that if the velocity can be predicted, for example using a computational model, the impact pressures can be estimated using a quadratic velocity-dependent formula. Impact coefficients C in the range between 0.4 and 0.8 appear to be appropriate for objects with size of the same order of magnitude as the flow heights. Stiff obstacles submerged in mudflows have been reported to have C values up to 3; however, we find indication for such high values.

More work is required to investigate other flow-obstacle geometries encountered in landslide problems. Generally, more quantitative data on flow velocity, flow height and impact pressure are needed to increase the confidence in the prediction shallow landslide properties.

References

Geotechnical Engineering Office, The Government of the Hong Kong Special Administrative Region (2000) Review of Natural Terrain Landslide Debris-Resisting Barrier Design. GEO Report No. 104

Iverson RM (1997) The physics of debris flows. Rev Geophys 35(3):245–296



Application of Terrestrial Laser Scanner to the Assessment of the Evolution of Diachronic Landslides

José A. Palenzuela, Clemente Irigaray, Jorge D. Jiménez-Perálvarez, and José Chacón

Abstract

During the diachronic evolution of landslides, slope-morphology changes may be detected and assessed by using high-resolution digital models. Slope deformation is detected by scanning sequences over a given time period. This paper presents the results found combining TLS digital models and Global Navigation Satellite Systems in the detection and assessment of reactivations and differential displacements of two slides located at the SW of Sierra Nevada (Spain) between 2008 and 2010. In the first landslide a maximum downward movement of 1.2 m at the top was measured, whereas below the middle part of the mass, 1.3 m of maximum advance was established with a maximum displacement gradient of 1.04 m/year. In the second landslide, downward displacements with gradients between 0.32 m and 0.56 m/year were found, corresponding to rupture movements in incipient to initial stages of evolution. The combined use of TLS and GNSS enabled a quantification and mapping of complementary terrain features which are considered useful in forecasting further activity and slope evolution of these landslides. The high resolution and accuracy of the techniques applied offer broad possibilities in the spatial location of the slope movement and also in forecasting its diachronic activity.

Keywords

Landslide • Activity • Displacement • TLS • ICP • GIS

Introduction

For the prevention of landslides, spatial data are useful in preparing susceptibility maps; nevertheless, in the case of hazard and risk maps, temporal data and information concerning the destructive capacity of landslides are also necessary (Chacón et al. 2006). For the analysis of the diachronic evolution of slope movements (Chacón et al. 2010) the degree of activity and development, velocity, volume of displaced masses, and the morphological evolution of the slope are quantified, including the scarps and zones of reduction and accumulation of displaced masses (IAEG 1993, 1995; Cruden and Varnes 1996; Fernández et al. 2003; Corominas and Moya 2008; Fell et al. 2008; Fernández et al. 2009).

One of the most powerful tools for monitoring, characterizing, and quantifying the relief evolution, including landslides, is Terrestrial Laser Scanning (TLS) (Teza et al. 2008; Dunning et al. 2009; Abellán et al. 2010; Dunning et al. 2010). This technique provides a high-resolution cloud of points measured in time-of-flight on the slope surface by using an infrared pulse emission in a known direction. The three-dimensional variation of the slope features are detected and quantified by a treatment and analysis of sequences of data gathered over a given time (Lim et al. 2005; Rosser et al. 2005; Oppikofer et al. 2009).

This technique has been applied to the detection of slope deformations prior to rockfall (Abellán et al. 2010), the determination of amount of slope displacement (Teza et al. 2007;

J.A. Palenzuela (✉) • C. Irigaray • J.D. Jiménez-Perálvarez • J. Chacón
Department of Civil Engineering, University of Granada, Avda. Fuentenueva s/n, Granada, Spain

C. Margottini et al. (eds.), *Landslide Science and Practice*, Vol. 2,
DOI 10.1007/978-3-642-31445-2_68, © Springer-Verlag Berlin Heidelberg 2013

Oppikofer et al. 2009), and the gathering of geometrical and morphological features, as well as other objectives (Dunning et al. 2009, 2010).

In this paper the methodology and results on combining TLS and GNSS (Global Navigation Satellite Systems) were applied to detect and assess morphological slope features, movements, reactivations, and differential displacements in the landslides of Almegíjar and Borincho, settled in the SE of Sierra Nevada (Granada, southern Spain), representative of the slope movements in a sector with high landslide susceptibility extensively affected by slope-instability processes (Chacón et al. 2006; Fernández et al. 2009; Jiménez-Perálvarez et al. 2009). In Almegíjar landslide, previous results, by means of photogrammetry techniques (Fernández et al. 2011), suggest non-uniform sliding activity with a diachroneity duration scale of VIII (Chacón et al. 2010) corresponding to slope movements with irregular activity, alternating phases of low activity with reactivations, due mainly to heavy rainfall.

Study Zone

The Almegíjar and Borincho planar slides are settled in the Alpujarride Complex of the Betic Cordillera (Fig. 1), a major tectonic unit composed of widespread phyllite, calcareous schist, and marble of Late Permian to Triassic outcropping from the NE to SW of southern Spain along its Mediterranean border. Both are located in Granada province, on the SW margin of Sierra Nevada in the northern part of the Guadalfeo River basin, in a hilly to mountainous region heavily divided by river channels and abundant landslides (Jiménez-Perálvarez et al. 2009). These two slides affect slopes of between 40 % and 60 % and a rock massif of low strength and very low permeability composed mainly of phyllite, both conditions favouring the instability process.

Methods and Materials

In this research, a TLS Riegl® 420 i system (Riegl 2011) was used for remote sensing by Laser Imaging Detection and Ranging (LIDAR), complemented by a distance explorer of the type Time of Flight (TOF), providing data on distances as well as spherical and Cartesian scales of the measurement positioning in the scanning system. This technology supplies high-density measuring (thousand points per second) with centimetric precision and accuracy, thus permitting the exploration of the entire scanned surface and the detection of small-sized features.

The error or reliability of the measure positioning in a plane perpendicular to the scanning laser beam is determined by the distance to the observation target and the angular divergence of the laser beam (Lichti and Jamtsho 2006; Riegl 2011), which reaches 0.25 mrad/50 m. The linear error in the distance to the target measured reaches 1 cm plus 20 ppm times the range. In the slopes studied, with observation distances of less than 600 m, the distance errors measured were less than 22 mm, and the dispersion in the position of the collimator point less than 125 mm.

Besides distance measurements, a direct geo-referencing in absolute coordinates was implemented, following the static positioning method with GNSS (GPS + GLONAS) of millimetric accuracy, by the correction of measurements gained from two permanent reference surveying stations with pinpointed with exact geodetic coordinates. In this way, minimum accuracies, related to the global position, of 11 and 17 mm were achieved for the horizontal and vertical components, respectively, for the Almegíjar slide, and 37 and 51 mm for the Borincho slide.

The methodology involved the following stages:

Planning

In this stage the landslides to be studied are selected, and the timing and positioning of scanning are determined:

Selection of Landslides Targets

This is based mainly on a review of geomorphological and landslide-susceptibility maps of the region (Jiménez-Perálvarez et al. 2010), where information concerning the activity and potential development of landslides are available.

Determination of Scanning Points

The location of correct scanning points permits measurements to be established over most of the study target, minimising the accumulative error during the alignment of the different scanning and shadow or hole zones.

Scanning Timing

For the Almegíjar slide, three scans were made, on 15/07/2008, 10/03/2009, 11/06/2010. This included an extraordinarily rainy period between the latter two dates, corresponding to the December 2009–March 2010 term, with a record of 500 mm of rain and an average value for this period of 250 mm.

For the Borincho slide, two scannings were made: in 12/03/2009 and 15/06/2010, also including the wet period 2009–2010.

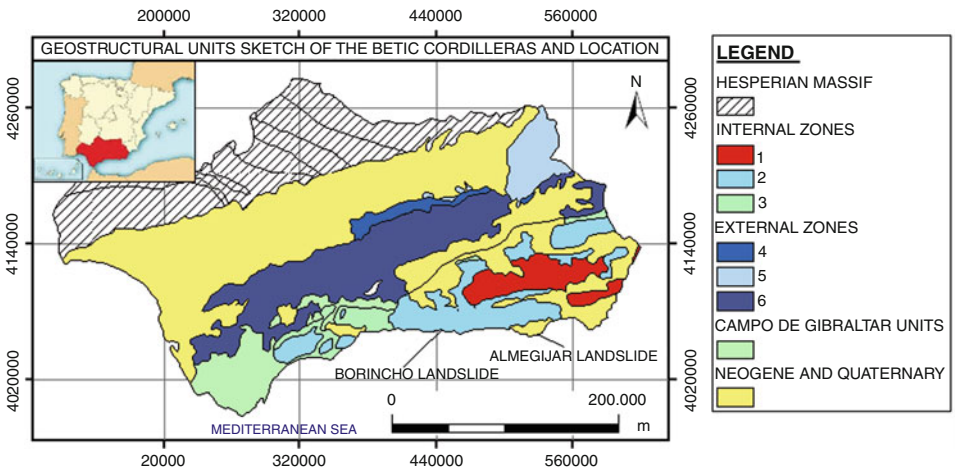


Fig. 1 Tectonic sketch of major geo-structural units of the Betic Cordillera, and setting of the two study zones. (*1* Nevado-Filábride Complex, *2* Alpujárride Complex, *3* Maláguide and Dorsale units, *4* Intermediate units, *5* Prebetic zone, *6* Subbetic and Penibetic zones)

Field Surveying Research

Setting of Control Target Points on Field Sites (GCPs)

With the morphological boundaries of the slide taken into account, external and internal GCPs were used as scattered and misaligned as possible, in order to achieve the main objective of this scanning, which was to find a good correlation for the tie points in the resulting scanned cloud of points. These target control points were made with highly reflective material clearly differentiated from other points in the scanned cloud. In order to facilitate a merging of data sets from different dates, without including those affected by displacements during the time interval, points in the external parts of the slide were intended to acquire a permanent character, despite the difficulties or factors this implies. On the other hand, the alignment of data achieved on the same date may also be supported by the internal tie points. The GCPs were installed seeking the highest intervisibility between them and with the other scanning positions in each study zone.

TLS and GNSS Data Acquisition

In this stage TLS was installed in each scanner coordinate system (SOCSi), with a calibrated GNSS receiver to determine its position. For a direct geo-referencing in the global coordinate system (GLCS), a back-sighting point or BS point was installed with registered geodetic coordinates.

Data Processing

This is the most important stage of the methodology, which includes the preparation of the raw data, the global cloud-point merging, its accuracy and that of the final terrain model depending greatly on the quality of the alignments and adjustments between the different data sets. Finally, it concludes with the information comparison and interpretation.

Reduction of the Point Cloud

The implementing of a filter with Octant Tree Structure (OCTREE) is to minimize the spread of each temporal data set, and to attain a file size manageable by the available computer software and hardware, maintaining the representativeness of the actual surface by the centres of gravity of cubes with a minimum side length of 0.1 mm for the centimetre resolution reached during the site scanning.

Alignment

This is a registration or merging between each specific system for each scanning position ($SOCS_i$) and one of them chosen as Project Control System (PRCS). In a further step, this system is transformed into the global coordinate system (GLCS) by means of direct geo-referencing.

The procedure is carried out by assigning tie points manually (Coarse registration), or automatically if a GCPs (Fine registration) is available.

In the Almegíjar slide, control points (GCPs) were available for all the scanning positions, except for a case in which some difficulties were encountered in detecting a sufficient number of tie points for an automated alignment. Except in that position, where the standard deviation between the tie-point positions of a data set and the PRCS was of 47 cm, the value for the other aligned data sets was between 1 and 7.7 cm.

In the Borincho slide, only the second data-acquisition control points were available, and therefore the cloud of points corresponding to 12/3/2009 was aligned by coarse registration until the GCPs previously installed permitted an automated alignment. In the first case of coarse registration the standard deviation of the values reached between 12 and 20 cm, until in the automated registration the value was 0.8 cm.

Multistation Adjustment (MSA)

When errors in the previous stage over the transform of coordinates reached values of more than 2.5 cm, the parameters were improved in this matrix running the SOCSs multistation adjustment until the errors were below that value. This procedure is generally based on the Iterative Closest Point (ICP), an iterative supervised adjustment by applying an algorithm implemented by most software packages for 3D treatment, such as the Riscan Pro software (Riegl 2010), applied in this research.

The ICP algorithm calculates not only the distance between artificial targets, tie points or tie objects created with a previous filtering of plane surfaces, but also the angles between the normal vectors of the tie objects corresponding to each data set, trying to minimize these values in each iteration.

By means of this adjustment a final standard deviation between 0.5 and 2.5 cm resulted for the Almegíjar slide and between 0.8 and 2.2 cm for the Borincho slide.

Filtering of Features not Acceptable for the Analysis

Consecutively, trees, shrubs, and taller vegetation constituting noise in the analysis of topographic changes of the ground surface are removed. A semiautomatic method is used, consisting of the elimination of "floating points" on site of a metric-width section (2–20 m) which is progressively displaced along the entire scanned surface (Riegl 2010).

Triangulation

Once filtered, all survey data, a mathematical model of reference for comparison of temporal data is built up, creating a triangular irregular network (TIN) using the Delaunay triangulation algorithm.

Information Analysis and Interpretation of Results

At this stage, we have used the Risca Pro software, which provides tools for comparative analysis of multi-temporal data. Given the difficulty of defining a reference plane for calculating orthogonal displacements resulting from the high irregularity of the site topography, a variant of the Surface Comparison algorithm was adopted for assessing the minimum distance (D_i) from the selected surface points (q_i) to the average plane of the triangles adjacent to the nearest point (p_i) of the reference surface in the direction of its normal vector. Starting with these orthogonal displacements to the average plane, the triangles adjacent to q_i were classified depending of their values, resulting in a distribution of the minimum displacement undergone by the modelled surfaces

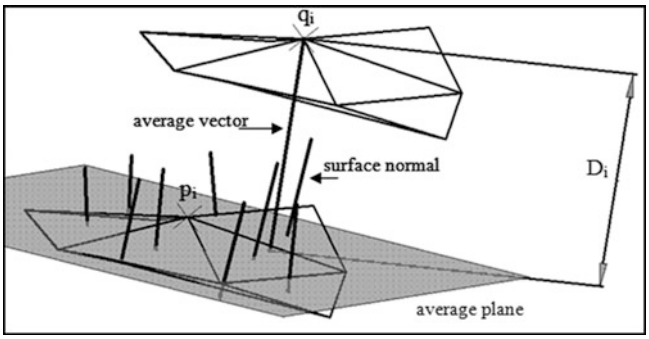


Fig. 2 Determination of distance Di

in each temporal interval. This classification was performed in a supervised way considering the detection and quantification of slope features related to the sliding. The values found were differentiated between positive and negative, when q_i fell above or below the average plane, respectively (Fig. 2). The negative values were interpreted as areas of relief loss either by erosion, subsidence, scarp back warding, etc., whereas to those zones classified with positive values corresponded to depositional zones, slope mass advance, debris accumulation, etc..

Results

The slope features and changes detected following this methodology are described as follows:

Geomorphological Evolution of the Almegíjar Slide

- Period 7/2008–3/2009 (Fig. 3a): only topographical variations derived from erosive processes with values in the range −0.15 to 0.50 m with reference to a TIN from July 2008 were detected. The highest erosion concentrates in the highest part of the scarp, whereas the thickening of the alluvial fan, below a gully, registered the maximum accumulation value.
- Period 3/2009–6/2010 (Fig. 3b): a range of values between −1.30 and 1.80 m was selected, despite that the negative values in the deep incision at the foot of the displaced mass were outside that interval (white non-classified area). This range shows a general advance of the lower half of the mass of a value up to 1.30 m, or whatever it might be, a maximum advance of 1.04 m/year (yellowish green to yellow) while in the top of the mass the orthogonal displacements between surfaces indicated an average subsidence of 0.70 m, with a maximum value of 1.20 m, which corresponds to a maximum subsidence rate of 0.96 m/year. (bluish colours).

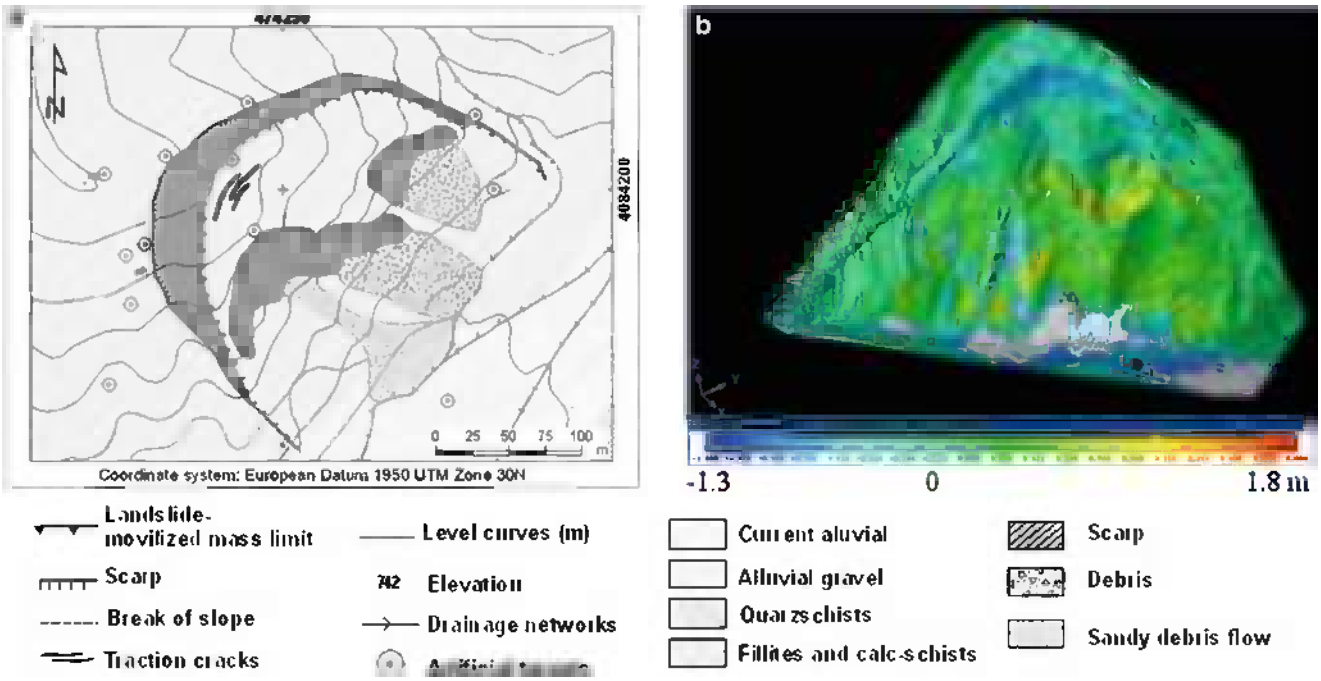


Fig. 3 Almegíjar slide, (**a**) Geomorphological map; (**b**) Classification of orthogonal displacements of the slope surface in March 2010 with regard to its previous position in June 2009, shown in a continuous colour scale

All these results indicate a slide reactivation, with a strain shortening during the last temporal interval similar to a compressive arch-like shape, with its longitudinal length (from bottom to top) shortened, while an advance towards the external part of the displaced mass occurred in the lower half side of the slide (Fig. 4).

Geomorphological Evolution of the Borincho Slide

- Period 3/2009–6/2010: the displacements calculated by comparison of the scanning results of June 2010 and March 2009 range between −3.00 and 0.50 m (Fig. 5b).
- The highest negative values coincide with the collapses affecting the slope mass foot at the border of the River Guadalfeo channel. The area reduction by these collapses has been quantified as 19,345 m^2, with a volume of 49,090 m^3. These features are stored as indirect descriptors useful for assessing the frequency of sliding reactivation based on the amount of reduced mass at the foot of the slide.
- The mass deposits generated during this period are concentrated in zones with a lower slope angle, and in concave zones (small gullies and lower parts of the slide borders in yellowish-green). A neutral zone (white) is established for values between −0.10 and 0.10 m in order to avoid noise produced by changes in vegetation and measuring errors (Fig. 5b).
- Expansion of the scale of negative values in the zone of greatest subsidence located on the right side of the slide foot (Fig. 5a) made it possible to distinguish a zone with values ranging between 8 and 70 cm, composed of semi-elliptical-shaped units interpreted as a set of small incipient planar slides. The zone affected by this subsidence covers 2,610 m^2, with a subsidence rate ranging between 0.32 and 0.56 m/year.

Discussion and Conclusions

The TLS remote monitoring technique has proved to be a rather accurate method for detecting smaller geomorphic features, through the acquisition of slope measurements from scanning positions located about 500 m apart. Thus, this methodology provides information on the temporal evolution of the activity of landslides located in the study area and detects the movement prior to the sudden rupture of the slope without previous access to the displaced mass. The analysis of applying the methodology to these two study areas supports the argument that:

The differential displacements calculated and classified for the Almegíjar slide show that it underwent a reactivation in the period 3/2009–6/2010, and it was in a suspended state between the dates 7/2008 and 3/2009. This reactivation resulted in a slope strain shortening along its longitudinal

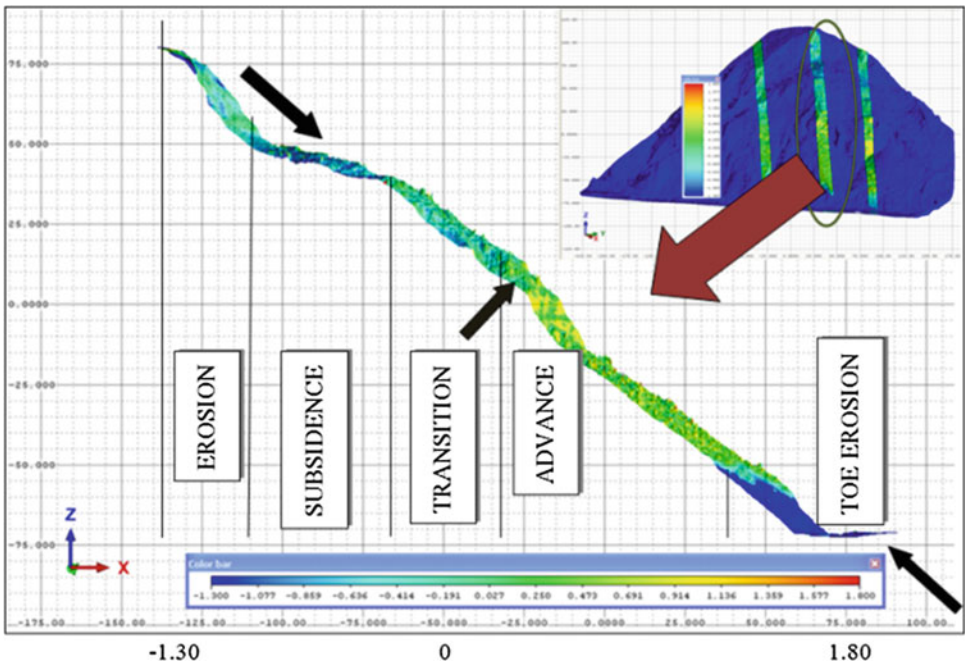


Fig. 4 Lateral view of a metric section in a centred side of the Almegíjar slide showing a classification of displacements between slope surfaces 2010–2009 in the range −1.30 to 1.80 m. From *bottom* to *top* the following processes were observed: erosion-subsidence-transition (very low deformation)-advance-erosion. The *black arrows* indicate the direction of shortening in longitudinal trend, and the extension of the mass perpendicular to the shortening direction

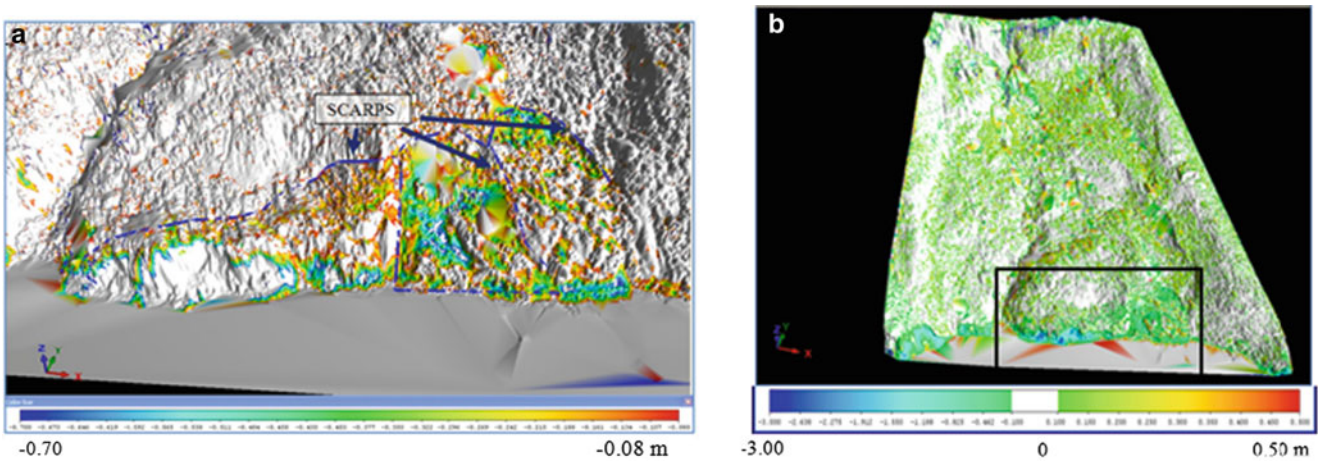


Fig. 5 (**a**) Classification of subsidence zones at the foot of the Borincho slide, shown in Fig. 5b, corresponding to the timing interval March 2009 to June 2010, with enhanced scale in the range −0.70 to −0.08 cm. (**b**) Classification in continuous colour scales of orthogonal displacements in the June 2010 slope surface with regard to the March 2009 slope

axis, and extension perpendicular to this, giving an arch-like shape to the displaced mass.

For the case study of the Borincho slide, a differential slope subsidence located at the foot of the displaced mass in the range from centimeters to decimeters (0.08–0.70 m), associated with 3 new slope ruptures in the incipient to initial stages of activity and semi-elliptical morphology, distinguished by the supervised classification of the displacements measured.

The observed reactivations in both slides coincide with a heavy rainy period between December 2009 and March 2010 (500 mm of rain for this period).

The areas that have undergone a substantial slope alteration in terms of the slide bodies have been mapped digitally and quantified as descriptors of the evolution of the activity of these events, which may be investigated either by techniques of a Geographical Information System (GIS), or by other analytical methods.

Acknowledgements This research was supported by the project CGL200-04854 funded by the Ministry of Science and Innovation of Spain and by the Group RNM 121 of the Andalusian Plan of Research.

References

Abellán A, Calvet J, Vilaplana JM, Blanchard J (2010) Detection and spatial prediction of rockfalls by means of terrestrial laser scanner monitoring. Geomorphology 119(3–4):162–171

Corominas J, Moya J (2008) A review of assessing landslide frequency for hazard zoning purposes. Eng Geol 102(3–4):193–213

Cruden DM, Varnes DJ (1996) Landslide types and processes. Special Report – National Research Council, Transportation Research Board. 247:36–75

Chacón J, Irigaray C, El Hamdouni R, Jiménez-Perálvarez JD (2010) Diachroneity of landslides. Geologically active: proceedings of the 11th IAEG congress. In: Proceedings of the 11th IAEG congress, Auckland, 5-10 Sept 2010, pp 999–1006

Chacón J, Irigaray C, Fernández T, El Hamdouni R (2006) Engineering geology maps: landslides and geographical information systems. Bull Eng Geol Environ 65(4):341–411

Dunning SA, Massey CI, Rosser NJ (2009) Structural and geomorphological features of landslides in the Bhutan Himalaya derived from Terrestrial Laser Scanning. Geomorphology 103(1):17–29

Dunning SA, Rosser NJ, Massey CI (2010) The integration of terrestrial laser scanning and numerical modelling in landslide investigations. Q J Eng Geol Hydrogeol 43(2):233–247

Fell R, Corominas J, Bonnard C, Cascini L, Leroi E, Savage WZ (2008) Guidelines for landslide susceptibility, hazard and risk zoning for land-use planning. Eng Geol 102(3–4):99–111

Fernández P, Irigaray C, Jiménez-Perálvarez J, El Hamdouni R, Crosetto M, Monserrat O, Chacon J (2009) First delimitation of areas affected by ground deformations in the Guadalfeo River Valley and Granada metropolitan area (Spain) using the DInSAR technique. Eng Geol 105(1–2):84–101

Fernández T, Irigaray C, El Hamdouni R, Chacón J (2003) Methodology for landslide susceptibility mapping by means of a GIS. Application to the Contraviesa area (Granada, Spain). Nat Hazards 30(3):297–308

Fernández T, Pérez J L, Delgado J, Cardenal F J, Irigaray C, Chacón J (2011) Evolution of a diachronic landslide by comparison between different DEMs obtained with digital photogrammetry techniques in Las Alpujarras (Granada, Southern Spain). International Symposium on Geo-information for Disaster Management (Gi4DM) Evolution of a diachronic landslide by comparison between different DEMs obtained with digital photogrammetry techniques in Las Alpujarras (Granada, Southern Spain), Antalya, 3–8 Mayo 2011

IAEG (1993) UNESCO Working Party on World Landslide Inventory (WP/WLI). A suggested method for describing the activity of a landslide. Bull Int Assoc Eng Geol París 47(1):453–455

IAEG (1995) UNESCO Working Party on World Landslide Inventory. Working Group on Rate of Movement A suggested method for describing the rate of movement of a landslide. Bull Int Assoc Eng Geol París 47:53–57

Jiménez-Perálvarez JD, Irigaray C, El Hamdouni R, Chacón J (2009) Building models for automatic landslide-susceptibility analysis, mapping and validation in ArcGIS. Nat Hazards 50(3):571–590

Jiménez-Perálvarez JD, Irigaray C, El Hamdouni R, Chacón J (2010) Landslide-susceptibility mapping in a semi-arid mountain environment: an example from the southern slopes of Sierra Nevada (Granada, Spain). Bull Eng Geol Environ. Article in Press (Online First™)

Lichti DD, Jamtsho S (2006) Angular resolution of terrestrial laser scanners. Photogramm Rec 21(114):141–160

Lim M, Petley DN, Rosser NJ, Allison RJ, Long AJ, Pybus D (2005) Combined digital photogrammetry and time-of-flight laser scanning for monitoring cliff evolution. Photogramm Rec 20(110):109–129

Oppikofer T, Jaboyedoff M, Blikra L, Derron MH, Metzger R (2009) Characterization and monitoring of the Åknes rockslide using terrestrial laser scanning. Nat Hazards Ear Syst Sci 9(3):1003–1019

Riegl (2010) Riscan Pro v.1.5.3b10 Operator's manual. Riegl Laser Measurement Systems GmbH, Horn

Riegl (2011) Terrestrial scanning. http://www.riegl.com/nc/products/terrestrial-scanning/produktdetail/product/scanner/4/. Last accessed 8 June 2011

Rosser NJ, Petley DN, Lim M, Dunning SA, Allison RJ (2005) Terrestrial laser scanning for monitoring the process of hard rock coastal cliff erosion. Q J Eng Geol Hydrogeol 38(4):363–375

Teza G, Galgaro A, Zaltron N, Genevois R (2007) Terrestrial laser scanner to detect landslide displacement fields: a new approach. Int J Rem Sens 28(16):3425–3446

Teza G, Pesci A, Genevois R, Galgaro A (2008) Characterization of landslide ground surface kinematics from terrestrial laser scanning and strain field computation. Geomorphology 97(3–4):424–437



Ground-Based Radar for Permanent Monitoring of Landslides

Richard Norland and Rune Gundersen

Abstract

Large uncontrolled avalanches pose a hazard to both people and infrastructure. Timely warning of potential avalanches can save lives and reduce damage to the infrastructure. However, access to the potential landslide area can be difficult and electronic monitoring equipment installed at the site may fail. This paper presents a radar system for remote monitoring using interferometric measurements. The radar can be installed several kilometres away from the potential landslide area and movements in the landslide can be monitored with an accuracy better than 1 mm. The data can be presented remotely in real time and a warning can be issued automatically to the relevant authorities if movements are registered. ISPAS installed the first permanent radar for monitoring a rockslide area in 2006 and the second radar in 2009. The paper presents the technical solution and experiences of the remote monitoring of the landslide areas in Tafjorden and Åknes, Norway.

Keywords

Radar • Interferometric • Monitoring

Introduction

On the west coast of Norway two unstable rock areas are monitored using permanent radar installations under the auspices of the Åknes/Tafjord – project.[1] The first installation was installed by the company ISPAS in February 2006 monitoring two potentially unstable mountain blocks in Hegguraksla in the Norwegian fjord Tafjorden. The rocks pose a possible hazard to people living close to the fjord. The first site is a block estimated to be approximately 0.8 mill. m^3. The second site north of the block also shows sign of instability. This block's volume is approximately 1.0 mill. m^3 (Oppikofer 2010). The Hegguraksla area with the blocks encircled is presented in Fig. 1.

The second permanent radar monitoring is the Åknes rock slide area close to Hellesylt. The rock slide area is presented in Fig. 2 showing the positions of the corner reflectors.

Åknes is known as the most hazardeous rockslide area currently identified in Norway with an estimated volume of 35–40 mill. m^3 Derron et al. (2005). Should the rockslide be triggered, it is estimated that a large floodwave will threaten the neigbouring villages in the fjords.

Background

Interferometric radar measurements take advantage of the phase of the electromagnetic wave, where the phase φ is varying as a function of range (R) and electromagnetic wavelength (λ)

[1] The Åknes/Tafjord – project is a task group organization to assess and monitor rock slide hazard areas in the Stranda and Norddal county on the west coast of Norway.

R. Norland (✉)
ISPAS, 219, Moss NO-1501, Norway
e-mail: Richard.Norland@ispas.no

R. Gundersen
ISPAS, 219, Moss NO-1501, Norway

Norwegian University of Life Sciences, Ås NO-1432, Norway

C. Margottini et al. (eds.), *Landslide Science and Practice*, Vol. 2,
DOI 10.1007/978-3-642-31445-2_69, © Springer-Verlag Berlin Heidelberg 2013

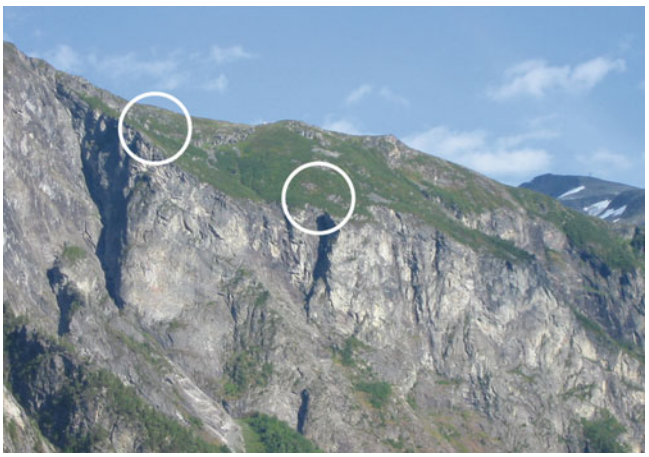


Fig. 1 The unstable blocks at Hegguraksla, Tafjorden, Norway. View from the village Fjørå

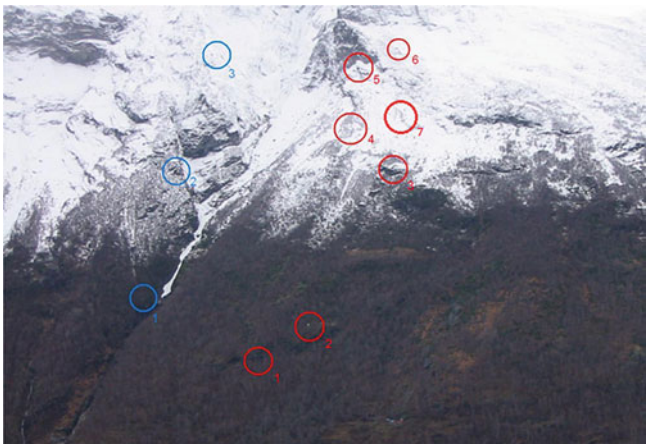


Fig. 2 The corner reflector positions in the Åknes rockslide area. *Red circle* indicates potentially unstable area

$$\varphi = \frac{4\pi \cdot R}{\lambda} \tag{1}$$

where

$$R = \frac{T_0 \cdot C_0}{n(\vec{r}, t)} \tag{2}$$

C_0 = velocity of light in vacuum, T_0 = travel time of the electromagnetic wave from the radar to the reflector and $n(\vec{r}, t)$ is the spatial and temporal index of refraction. The refractive index is presented as the scaled up radio refractivity index N. The scaled up radio refractivity index for radio frequencies in terms of the pressure p (mbar), the temperature T (^oK) and the partial water vapour pressure e (mbar) is (Bean and Dutton 1968):

$$N = (n-1) \cdot 10^6 = 77.6\frac{p}{T} + 3.734 \cdot 10^5 \frac{e}{T^2} \tag{3}$$

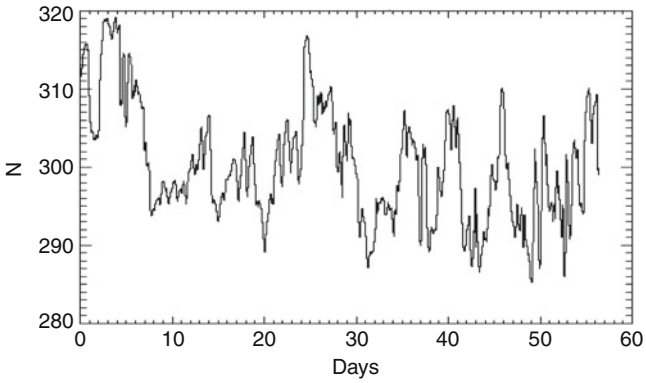


Fig. 3 Variation of the refractivity N over approximately 2.9 km during two winter-months in Norway. The data are 3 h median

where n is the index of refraction. Refractivity N equal to 319 at sea level is standard atmosphere.

The partial water vapour pressure can be estimated using the relative humidity (RH)

$$e = RH\left(\frac{e_S}{100.0}\right) \tag{4}$$

where e_S is the saturation vapour pressure. When the saturation vapour pressure is at equilibrium with respect to water, the saturation vapour pressure becomes a function of the temperature only, i.e.

$$e_S = 6.1 \cdot 10^{\frac{7.45T}{235+T}} \tag{5}$$

where T now is degrees Celsius. An example showing the variation of the refractivity N during two winter-months, over a distance of 2.9 km, is presented in Fig. 3, (Norland 2006)

A variation of one unit in N corresponds approximately to a variation of 5.8 mm at 2.9 km using a frequency 9.65 GHz. The corresponding variation of the range to one reflector is presented in Fig. 4, (Norland 2006).

Due to the variation of the index of refraction, high accuracy instantaneous phase measurements are not possible less the measurements are averaged over a relatively long time span or corrected using meteorological data (Norland 2007). However, by introducing a second reflector, and measuring the differential phase ($\Delta\varphi$) between the two reflectors, the variation of the index of refraction is reduced, see Fig. 5.

The differential movement (Δr) between the two reflectors, where one is on stable ground, can then be calculated as

$$\Delta r = \frac{\lambda \cdot \Delta\varphi}{2\pi} \tag{6}$$

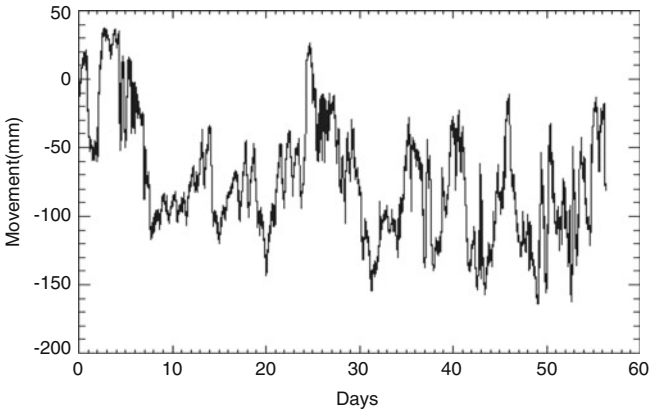


Fig. 4 Variation of the range to a corner reflector at a distance of approximately 2.9 km during two winter-months in Norway. The data are 3 h median

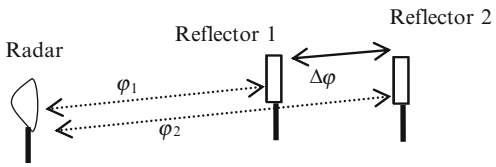


Fig. 5 General arrangement for differential interferometric radar measurements

Table 1 Radar parameters for slide monitoring

Radar parameters	
Frequency	C, X or K – band
TX Power	< 0.001 W
Polarization	Horizontal or vertical
Waveform	Stepped frequency or Frequency modulated
Range resolution	Variable, < 0.5 m
Pulse Repetition Frequency	Variable, from 100 Hz to one every minute

The instantaneous accuracy of the movement is now limited by the variation of the refractive index in the area between the reflectors.

Since natural variations due to the weather conditions are small and continuous, while a physical movement probably will appear as a discontinuous large instantaneous movement, it is possible to distinguish between the two movements. The fluctuations due to the variations in the index of refraction will also over time vary around zero movement while a physical movement will be biasing the data.

The differential interferometric radar is a well proven technique, demonstrated for the first time in 1974 (Graham 1974). An interferometric radar measurement experiment for small relative movements in mountainous area is presented in (Norland and Gundersen 2005).

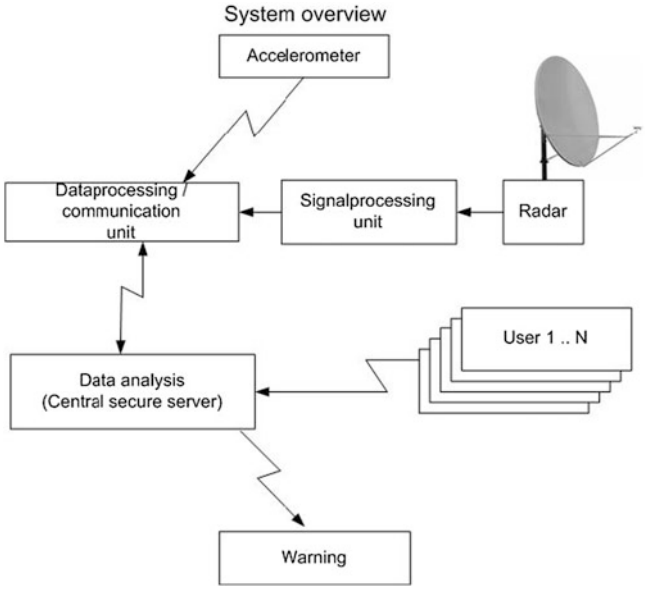


Fig. 6 Installed monitoring system for Hegguraksla, Tafjorden, Norway



Fig. 7 Corner reflector for tracking movements during winter

The advantage of the ground based differential interferometric radar is the high temporal sampling-rate combined with inexpensive spatial sampling using relatively cheap corner-reflectors as compared to other electronic equipment e.g. GPS and extensometers. Depending on the transmitted frequency, the radar can be used during most weather conditions at large distances.

The Monitoring System

The radar is tailored to the monitoring through choice of frequency, polarization and range resolution and is based on more that 20 years experience with measuring small military targets. The radar parameters are presented in Table 1.

The radar measurements are processed on site and the resulting data from both the movement sensors and radar are sent to a remote, secure server for analysis and generation of graphs. If a physical movement is detected, both e-mail

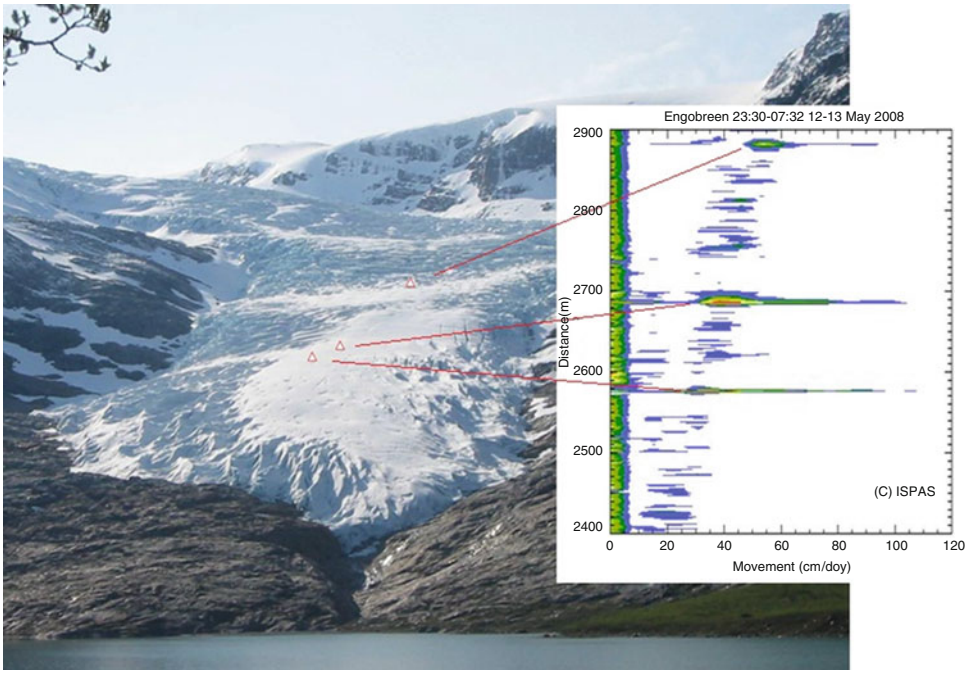


Fig. 8 Natural and artificial reflection points on glacier. The artificial reflection points are indicated by their position on the glacier and corresponding measured velocity

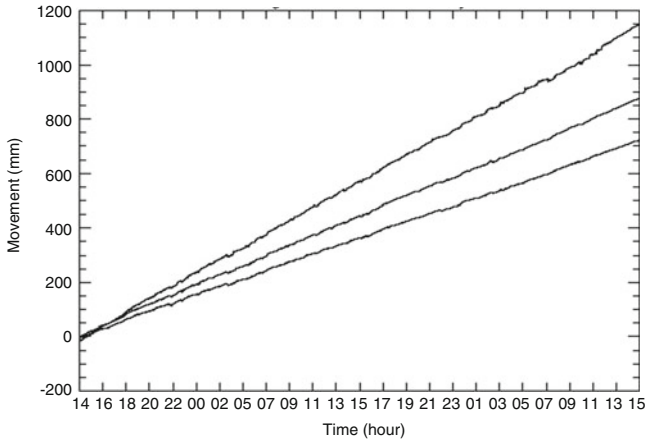


Fig. 9 Interferometric measurements using corner reflectors on glacier

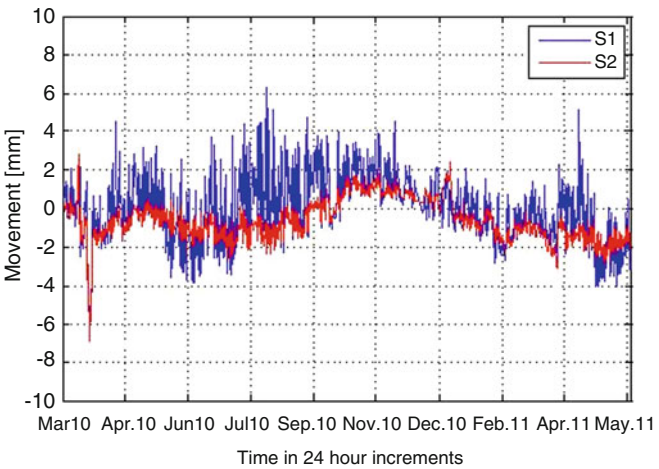


Fig. 10 Results from the monitoring of the two blocks on Hegguraksla. Twenty-four hours moving average data over 14 months

and SMS messages are sent to registered authorities and the data from both the radar and movement sensors can be inspected through a password protected website (http://skredweb.ispas.no). The monitoring system is presented in Fig. 6.

Natural or Artificial Scattering

Beside the atmospheric influence on the refractive index, the accuracy of the method is dependent on the distance between the scatterers in the stable and the unstable area and quality of the scatterers. In general there are two types of scatterers; natural and artificial. The natural scattering points are identified among the stable reflections in the slide area and stable surroundings by observing the scattering behaviour over time while the artificial scattering points are often corner reflectors installed in both the stable and unstable area, but on local stable ground.

The limitations using natural scatterers are mainly due to whether there are reflections in the areas of interest, variations in vegetation, precipitation on the scatterer, i.e. wet/dry surface or wet/dry snow covering the surface and stability of the scatterer over time. The limitation using artificial scattering points is mainly the stability of the

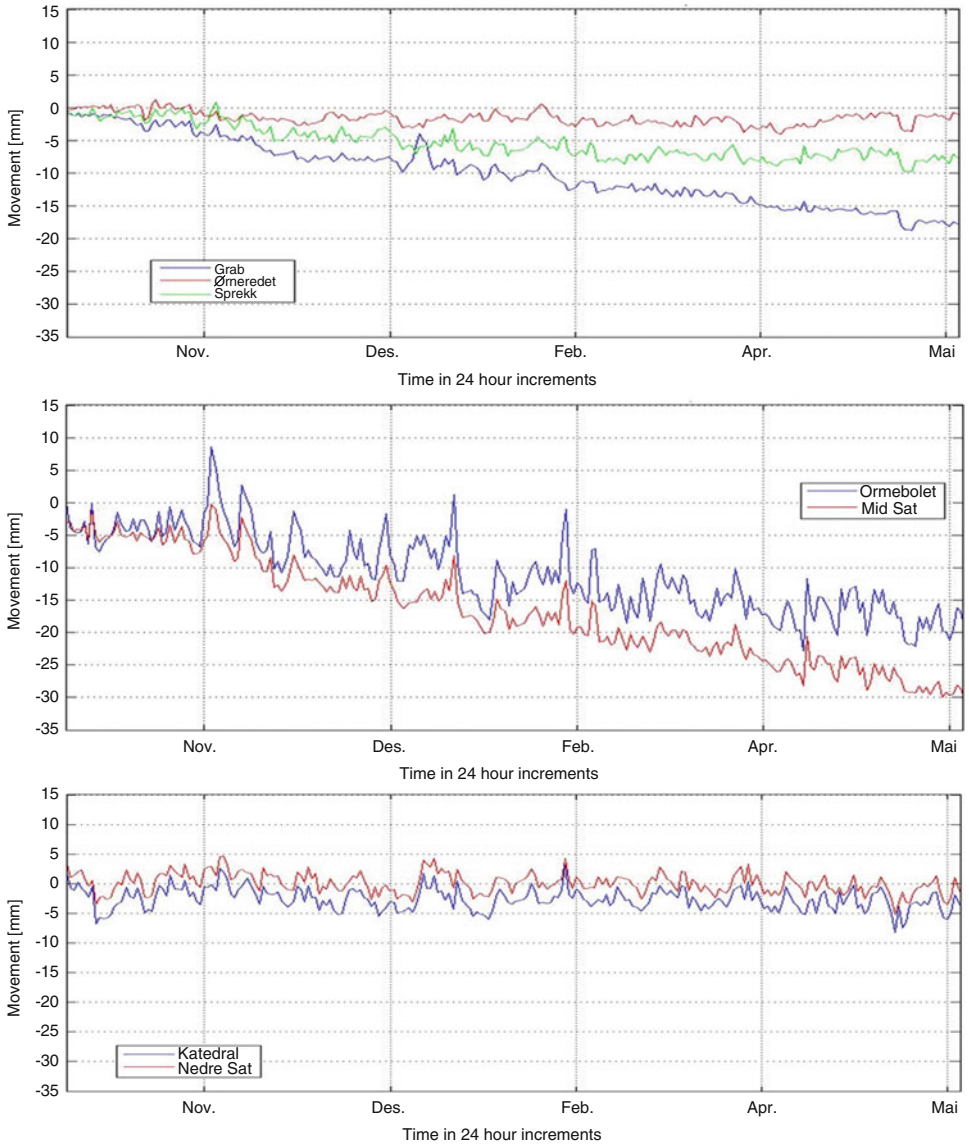


Fig. 11 Results from the monitoring of Åknes rockslide area. Twenty-four hours moving average data over approximately 6 months showing the movment in mm. The plots corresponds with Fig.2, i.e. top plot is top corner reflector in Fig. 2

reference reflector. In our experience there are few other problems using e.g. a corner reflector under very different weather conditions, even through winter. An example showing a corner reflector in heavy snow is presented in Fig. 7.

A comparison using natural and artificial references is presented in Fig. 8. The movement is calculated using traditional Doppler processing. The figure shows how natural scatterers and corner reflectors follow similar velocity patterns, but also lack of reflections from parts of the glacier.

The corresponding interferometric movement of the corner reflections are presented in Fig. 9.

Figure 9 show that the accuracy using interferometric data is much higher than the corresponding Doppler processing presented in Fig. 8.

Monitoring Results

The monitoring of Hegguraksla is performed using differential interferometric radar measurements of the two unstable blocks. The distances to the blocks from the radar are approximately 2,900 m and the heights are 735 and 825 m relative to the radar. The operating frequency is 9.65 GHz with a bandwidth of 200 MHz. One measurement is performed every minute. Optional radar parameters are presented in the appendix.

A measurement set showing approximately 14 months during varying local weather conditions, is presented in Fig. 10.

As the measurements indicate the movements of the blocks are negletable. This is also confirmed by crack meters installed at the sites.

The monitoring of Åknes is done using stable corner reflectors on stable ground, i.e. to the left in Fig. 2, indicated by blue circles, and seven corner reflectors in the rockslide area, indicated by red circles in Fig. 2. The radar is installed on the other side of the fjord and is measuring the corner reflectors once every minute. The distance to the reflectors is between 2,300 and 3,300 m and heights are 176–908 m. The radar frequency is 5.7 GHz with an instantaneous bandwidth of 150 MHz. Figure 11 shows an example presenting data over 6 months through the winter.

As the data show, the large movements are mainly in the centre of the rockslide, up to 60 mm/year. The instantaneous measurement of the corner reflectors can also give insight into the dynamics of the slide by comparing the movements of different reflectors. An example indicating downwards propagating micro movements in glacier is presented in Norland (2008).

Conclusion

Differential interferometric radar measurements has been monitoring the unstable mountain blocks in Tafjorden since 2006 and Åknes landslide area since 2009.

The data show that movements are detected with very high measurement accuracy as compared to traditional Doppler processing by using corner reflectors as reference both in the stable sorroundings and slide area. The use of artificial scatters is of great importance to achieve a high level of precision and to ease the geo-referencing task.

Results from two different scenarios one with a movement of 60 mm/year and one with a 230 m/year movement show the monitoring versatility of the radar system.

Long time monitoring of unstable mountainsides with our high reliability radar system shows that unsurpassed sub millimetre precision is achieved. This performance is weather independent and ideally suited for high risk areas where human life might be at stake.

References

Bean BR, Dutton EJ (1968) Radio Meteorology. Dover Publications, New York

Derron MH, Blikra LH, Jaboyedoff M (2005) High resolution digital elevation model analysis for landslide hazard asessment (Åkerneset, Norway). In: Senneset K, Flaate K, Larsen JO (eds) Landslide and avalanches ICFL 2005 Norway. Taylor & Francis Group, London

Graham LC (1974) Synthetic interferometer radar for topographic mapping. Proc IEEE 62:763

Norland R, Gundersen R (2005) Use of radar for landslide hazard monitoring. In: Proceedings of the 11th international conference and field trip on landslides, ICFL 2005, Norway 2005

Norland R (2006) Differential interferometric radar for mountain rock slide hazard monitoring. In: Proceedings of the IEEE international geoscience and remote sensing symposium 2006, Denver

Norland R (2007) Improving interferometric radar measurement accuracy using local meteorological data. In: Proceedings of the IEEE international geoscience and remote sensing symposium 2007, Barcelona

Norland R (2008) Observations of small deviations in glacier velocity measurements. In: Proceedings of the IEEE international geoscience and remote sensing symposium 2008, Boston

Oppikofer T (2010) Detection, analysis and monitoring of slope movements by high-resolution digital elevation models. Ph.D. thesis, University of Lausanne



The Ganderberg Landslide (South Tyrol, Italy): Mitigation of Residual Risk by Real-Time Monitoring

Martina Stefani, Matteo Mantovani, Volkmar Mair, Gianluca Marcato, Alessandro Pasuto, and Ludwig Nössing

Abstract

The whole flank of Ganderberg western slope (3.75 km^2) (lat. 46°51′12″, long. 11°10′15″) is involved in a Deep Seated Gravitational Slope Deformation phenomenon. The upper part is characterized by several joint surfaces, with possible wedge failure mechanisms. In particular, the northern crown ridge is divided into three sectors with noticeably different indications of subsidence and displacement. The orientation of the joint planes and evidence of vertical movements of a distinct rock block allow a potential rock avalanche to be hypothesized (up to the volume of 4.5×10^5 m^3). On the basis of historical archives analysis it was found that the same slope was involved in a rock avalanche event dating back to 1401. The landslide deposits created a 35 m deep lake, damming the Passer Torrent, creating the Passeirer Wildsee or Kummersee.

Aim of the study is the evaluation of residual risk scenarios and its mitigation by means of monitoring and data interpretation using Saito and Fukuzono techniques.

Keywords

Landslide • Risk management • Monitoring • Prediction • Ganderberg • DSGSD

Introduction

From a geomorphologic point of view South Tyrol is a very active region: several slope instabilities and mass movements occur all over the territory; during particular climatic phenomena (long lasting or high intensity rainfall) these can evolve in paroxystic events.

Therefore, in order to minimize the social impact of landslides with limited amounts of available funds and technologies, sites that need to be preferentially stabilized should be identified in advance, and effective preventive measures as well as efficient retaining works should be carried out. Risk management that involves evaluation and control of existing risks is widely used to solve these problems.

The paper deals with a case of a landslide in Hahnebaum, in the municipality of Moos in Passeier (Moso in Passiria), 40 km north of Bozen (Bolzano) on the orographically left bank of the Passeier Valley (Fig. 1). The mass movement has been known since historical times and can be easily identified in the field and from aerial fotos and lidar data. It can be classified as a deep seated gravitational slope deformation which includes secondary mass movements occurring on the principal scarp and along the main body of the DSGSD. The movements have been identified as rotational sliding along slope changes and translational sliding in the upper part of the main scarp. The latter could evolve in a rock avalanche in case of a collapse harming the existing infrastructure and interfering with the Passer torrent.

The Passeier Valley is an alpine valley with tourist structures operating both in the summer and winter time. During the summer time, many tourists pass the Timmelsjoch

M. Stefani (✉) • V. Mair • L. Nössing
Provincia Autonoma di Bolzano – Alto Adige – Südtirol, Ufficio Geologia e Prove Materiali, Via Val d'Ega 48, Cardano, BZ 39053, Italy
e-mail: martina.stefani@provinz.bz.it

M. Mantovani • G. Marcato • A. Pasuto
IRPI-CNR, U.O.S. di Padova, Corso Stati Uniti, 4, Padova 35127, Italy

C. Margottini et al. (eds.), *Landslide Science and Practice*, Vol. 2,
DOI 10.1007/978-3-642-31445-2_70, © Springer-Verlag Berlin Heidelberg 2013

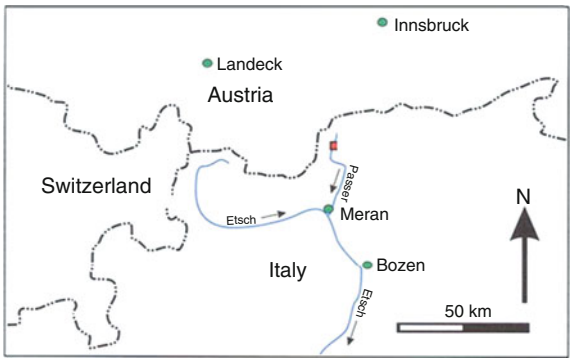


Fig. 1 Location of the studied area (Modified from Egger 2001)

(Passo Rombo) high alpine road connecting South Tyrol with Austria. Also an important hiking trail (European walking route E5) follows the path over this mountain pass.

In order to study the phenomenon and assess the hazard several boreholes were drilled and a real time monitoring system using extensometer was set up for collecting kinematic data.

All the activities, carried out in the framework of the European project MONITOR II financed by the South East Europe Programme 2007–2013 (www.monitor2.org), along with the installed instrumentation allow hazard assessment in order to predict the failure phases. Preparedness is one of the important tasks in the risk management cycle and more effective are these interventions less are the social and economic impacts of the possible phenomenon. The time of failure should be predicted by analyzing the rate of movement.

Regional and Historical Framework

The landslide has been known since 1401 AD (Stampfer 1889): on the basis of an historical analysis it was found that the slope has been involved in a rock avalanche event dating back in 1401 AD. The landslide deposits (Seehofer Bergsturzmasse) dammed the Passer torrent creating a 35 m deep lake (Walcher 1773), the Passeirer Wildsee or Kummersee. This lake, as his second name (lake of grief) suggests, caused trough several dam breaks damages and devastation down the valley reaching even the town of Meran, situated approximately 26 km southwards in the Etsch (Adige) Valley. The disastrous dam breaks happened mostly after heavy rainfall in autumn and are known from 1419, 1503, 1512, 1572, 1721, 1772, 1773 and 1774. According to historic sources there were 400 casualties during the flooding of the town of Meran in 1419 (Stampfer 1889). The other recorded events brought mainly damages to property in the town of Meran and had repercussions to the economic situation of the town.

After the first disastrous outbreaks protection measures were built and the outlet of the lake was regulated. But nevertheless, the inundations continued until 1774 AD when the lake leaked completely out as the control barrier on the dam was opened too much causing again destruction and four fatalities down the valley (Stampfer 1889).

Nowadays only the geomorphology and some place names ("Seehof") reminds of the existence of the Kummerlake.

From a geological point of view the landslide is located in the Austroalpine domain. The Austroalpine basement shows a complex polymetamorphic history and consists of many tectono metamorphic units affected by at least two orogenesis, the variscan and the alpine (Bargossi et al. 2010). The study area lies within the Schneeberger unit (close to its southern boundary), which marginal belt is composed of a variety of rocks as micaschists with well-formed garnets, marbles, amphibolits, quarzites and calc-micaschists (multicolored serie – Bunte Serie). The Schneeberger unit is bordered to the south by the Texel unit, which here mainly consists of garnet and staurolite-mica schist, with marble and calc-scist ("Laas Serie" *Auct.*)

The Passer torrent is characterized by the alpine climate: its catchment basin of about 97 km until the southern border of the Ganderberg mass movement comprises high mountain peaks (Seewerspitz, 3,288 m a.s.l, Schwarzwandspitze, 3,254 m a.s.l) with consistent snow cover in the winter months (Egger 2001). In the spring and summer time heavy rainfall and the snowmelt increase the discharge which can be extremely high.

The erosion potential of the torrent has been regulated by several check dams.

Hazard Assessment

The Ganderberg mass movement (Fig. 2) has been intensely studied from geological and geomorphological point of view (Egger 2001; Tagliavini et al. 2009). There have been found several parts with different behaviour and types of movement. The most important sectors are briefly summarized below.

The first type of movement is assigned to the overall Ganderberg mass movement: the whole area of 3.75 km is involved in a Deep Seated Gravitational Slope Deformation (DSGDS) with an estimated basal sliding/shear surface in 150 m depth. Laterally the landslide is bordered by tectonic features, while in the upper part a huge ridge borders the landslide crown. GPS benchmarks were fixed in 2007 all over the slope and periodic measurements in the past years have shown that the whole slope can be subdivided in different landslide blocks.

One of the secondary landslides is located in the lower part close to the settlement of Hahnebaum and the national road SS44bis (Fig. 2b). Here a rotational landslide has been intensively reactivated in recent times mainly because of heavy rainfall and snowmelt. In 1951, 1962 and 2000 the national road has been damaged and interrupted. The 2000



Fig. 2 View of the studied area: the *dashed line* borders the Ganderberg DSGSD, the *white line* follows the national road SS44bis; *A* indicates the northern monitored crown, *B* the rotational landslide and *C* the location of the former lake (Kummersee)



Fig. 3 View of the monitored area in the northern crown (A from Fig. 2); (**a**) on the left view of the detached area with an estimated volume of 4.5×10^5 m; (**b**) on the right view along the different sectors with evidence of subsidence and displacements, the *red dashed line* indicates the monitored area

event happened in November after heavy snowfall and a vertical displacement of the road of 3 m was recorded in about 18 days. This area has been drained in order to avoid back water.

The northern scarp of the DSDGS crown (Fig. 2a) is characterized by several joint surfaces with possible wedge failure mechanisms. The scarp between an altitude of 2,000–2,200 m a.s.l. is divided into three sectors with noticeably different indications of subsidence and displacement. The orientation of the joint planes and evidence of vertical movements of a distinct rock block allow in case of failure the formation of a rock avalanche comprising a volume up to 4.5×10^5 m. This area is situated aside of that part of the slope which probably failed in 1401 AD (Stampfer 1889) forming the dam and finally the lake.

Mitigation of Residual Risk

The dimension of the Ganderberg DSGDS does not allow a direct intervention with structural measures in order to reduce the potential hazard.

Still it is possible to reduce residual risk by monitoring the different sectors of the mass movement and by developing a forecasting/alerting system usable for civil protection purposes.

The Ganderberg DSGDS has been monitored measuring periodically since 2007 the installed GPS benchmarks and the average displacement rate of 3–5 cm per year.

The rotational landslide in the lower part of the slope is still moving and each year minor interventions along the national road SS44bis have to be carried out. Two boreholes aligned along longitudinal section were equipped with inclinometers in order to get information about the geometry of the sliding plan. When a clear slip surface will be recognized the tubes will be equipped with fixed inclinometers and pressure transducers in order to control the variations of the displacements in correlation with the water level and rainfall data. As this landslide reactivates abrupt due to heavy rainfall or snowmelt water special control of this parameter has to be planned.

The northern scarp (Figs. 3a, b and 4) of the DSGDS with its wedge failure mechanism and possibility to evolve in a rock avalanche crashing down to the Passer torrent probably



Fig. 4 Location of the six extensometers forming the monitoring system with warning device; in *red* the extensometers, in *black* the active tension cracks

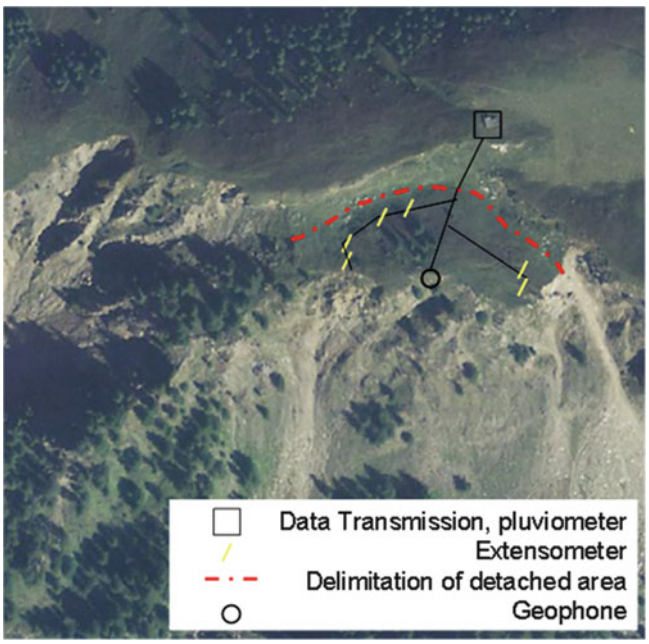


Fig. 5 Design of the monitoring system of the northern scarp; the *red dashed line* shows the detached area, the *yellow lines* indicate the six extensometers and the *circle* the geophone. All data are transferred via cable to the data management and transferring system located outside the active area (*rectangle*)

causing a landslide dam and passing over the national road has been equipped with a monitoring system in order to assess the displacements and velocities of movement. Six extensometers were installed across the widening pre-existing cracks (Fig. 5). The most reliable and accurate monitoring data can be used to forecast the failure time and to evaluate the effectiveness of different equations in order to better assess the resulting risk situation.

There are two practical methods to predict landslide collapse, respectively proposed by Saito and Fukuzono; these methods are not fully inspected so that they are tested by using the displacements recorded here and verifying the range of fluctuation of the predicted failure time.

The application of the model proposed by Saito on the basis of field measurements and laboratory experiments (Saito 1965, 1968, 1969) should be particularly reliable thanks especially to the fact that the kinematic behaviour of the investigated slope movement can be assumed as a typical creep-failure. The simple equation used takes into consideration the close relationship between strain rate in the secondary creep phase and the residual time to failure.

The Fukuzono (1985a, b; 1990) prediction method, further implemented by Voight (1988) and Crosta and Agliardi (2003), is based on the consideration that when velocity becomes high, its inverse tends to zero. Therefore, the intersection of the 1/v curve with the time axis represents the time of maximum velocity or, in other words, the time of failure. This method if applied during the emergency phase should allow to strongly reduce the potential damages.

The data are collected and stored in a safe position outside the detached area and transferred via GPRS (Fig. 5). The managing data software will be set with Saito and Fukuzono equation analysis. In order to verify the accuracy of the prediction as well as the effectiveness of the monitoring system, including the instrumentation installed and the acquisition and continuous processing of data, a comparison of the results obtained by the Saito's equation with the recorded time of failure, will be performed by a custom software. This back analysis takes into account the data recorded by the extensometers which prove to be the most reliable. An automatic notification system to mobile phones of the staff when warning is given, and a real-time automatic monitoring system that enable the headquarter office to follow up the displacements is set up.

Conclusions

Landslide investigation was conducted in order to better understand the characteristics of the Ganderberg DSGSD and connected secondary mass movements. On the basis of these observations and for risk control of one of these secondary movements a monitoring system consisting of a warning device based on extensometers was designed.

The collected data will be analyzed in order to control and forecast the progressive failure by means of widely tested methods.

Monitoring procedures to keep the displacement under constant surveillance seems to be the most effective and practicable method to reduce the risk in case of the Ganderberg landslide.

Acknowledgments This research has been funded by the Interreg project MONITOR II, financed by the South East Europe Programme 2007–2013.

References

Bargossi GM, Bove G, Cucato M, Gregnanin A, Morelli C, Moretti A, Poli S, Zanchetta S, Zanchi A (2010) Note Illustrative della Carta Geologica d'Italia alla scala 1:50.000, foglio 013 "Merano". Servizio Geologico d'Italia – ISPRA, SystemCart, Roma, 320 p

Crosta GB, Agliardi F (2003) Failure forecast for large rock slides by surface displacement measurements. Can Geotech J Rev Can Geotech 40(1):176–191

Egger H (2001) Ingenieurgeologische Untersuchung des Ganderberger Talzuschubs und der Seehofer Bergsturzmasse. Diplomarbeit, Institut für Geologie und Mineralogie, Friedrich-Alexander-Universität Erlangen-Nürnberg

Fukuzono T (1985a) A new method for predicting the failure time of a slope. In: Proceedings of the 4th international conference and field workshop on landslide, Tokyo, pp 145–150

Fukuzono T (1985b) Method for predicting the time of slope failure using rainfall and inverse of surface movement velocity. J Jap Landslide Soc 22(2):8–13 (in Japanese)

Fukuzono T (1990) Recent studies on time prediction of slope failure. Landslide News 4:9–12

Saito M (1965) Forecasting of time of occurrence of slope failure. In: Proceedings of the 6th ICSMFE, Montreal, pp 537–541

Saito M (1968) Study on predicting the time of slope failure. Railway Technical Research Report, No. 626, Railway Technical Research Institute, 53 pp, (in Japanese)

Saito M (1969) Forecasting time of slope failure by tertiary creep. In: Proceedings of the 7th ICSMFE, Mexico City, pp 677–683

Stampfer PC (1889) Geschichte von Meran, der alten Hauptstadt des Landes Tirol. Wagner, Innsbruck

Tagliavini F, Mantovani M, Marcato G, Pasuto A, Silvano S (2009) Relazione di fine progetto: Frana del Monte Ganda, unpublished report for the Autonomous Province of Bolzano in the framework of the Interreg project "Monitor"

Voight B (1988) A relation to describe rate-dependent material failure. Science 243:200–203

Walcher J (1773) Nachrichten von den Eisbergen in Tyrol. Kurzböck, Wien



The Case History of the Bagnaschino Landslide, from Early Warning to Site Specific Rainfall Threshold

Corrado Faletto, Enzo Novello, and Paolo Tible

Abstract

The highway n° 164, in 1994, was struck by a complex composite landslide activated in Bagnaschino (Torre Mondovì, Cuneo) due to flood events. In order to continuously monitor the stability conditions, the Cuneo County established a borehole monitoring plan in 2008 with DMS column 60 m long. DMS (patents CSG Srl Italy) is a multiparametric system for the stability monitoring of slopes, excavation fronts and engineering works; the column is like a spiral cord composed of a sequence of hard tubular modules connected to each other by special flexible junctions. Correlation between DMS column and rain data allowed identifying critical events that have reactivated the landslides, along the sliding surface at 7 m blg, allowing the adoption of preventive interventions (closing the road during the March 2011 rain event). Moreover with the DMS system was possible to calculate the site specific rainfall threshold curve that shows the limit stability condition related to the rain intensity and duration.

Keywords

Complex composite landslide • Early warning • DMS monitoring • Site specific rainfall threshold

Introduction

The study area is in the Municipality of Torre Mondovì, Cuneo County, Piedmont Region. During the flood event occurred in 1994 the highway n. 194 was seriously damaged by a composite landslide activated in Bagnaschino site. In proximity of km 1 + 400 the landslide invaded the carriage way (Fig. 1).

The landslide is a composite type, with a flow area at 5–8 mbgl and a deep creep at 30–40 mbgl. The estimate area is about 150,000 m with a volume of 1.2 M m. The element at risk is the Regional highway S.P. 164 and a potential lake formation.

To monitoring the area was developed an Early warning system composed by one DMS column and surface systems.

Geological Setting

Basic's geological data are summarized in the sheets "Cuneo" (80) and Boves (91) of Italian's Geological Map (1:100,000 scale) and in the sheet "Gap" of French's Geological Map (1:250,000 scale).

On the basis of the mentioned cartography, the test area, affected by the geological instability, implicate materials belonging to the Axial Perm Carboniferous in particular gneissic, sericitic and filladic schists; sericitec quartz, generally paragenesic rocks (Fig. 2).

We observed, during the inspection, wide outcrops of prasinite and ofiolites. Being geomechanically rigid rocks,

C. Faletto (✉) • E. Novello • P. Tible
Cuneo Province, Mobilità e infrastrutture, Corso Nizza, 21, Cuneo, Italy
e-mail: faletto_corrado@provincia.cuneo.it

C. Margottini et al. (eds.), *Landslide Science and Practice*, Vol. 2,
DOI 10.1007/978-3-642-31445-2_71, © Springer-Verlag Berlin Heidelberg 2013



Fig. 1 Aerial photo in 2000



Fig. 2 Photograph of the landslide in 1994

this heaps suffered a tectonics of disjunctive type, resulting in more points very fractured and predisposed to an aggressive action of weathering and to a raising distension.

Geomorphologic Setting

The Geomorphologic structure of the whole valley bottom of T. Casotto and of the underlies slopes, results very conditioned by the litology of the bedrock and especially from his tectonical grade. So in the sector which structure is made by high tectonized rocks and/or high schistose (which appear covered by an abundant debris and soil), the valley bottom is quite large and the form of the reliefs are steep, whereas, in the zones where the bedrock of gneissic rocks or amphibolites rocks is present we have very steep scarps, and the valley bottom is narrow and the riverbed is embedded.

In many areas of these side' sectors we notice evident indications of deep gravitative morphogenesis (crowns and scarps, zone of accumulation of large paleoslides) which lead to suggest that the current slopes are in a condition of limit-equilibrium and are predisposed to slow movements or to run out processes, facilitated or caused by the temporary arise of triggering factors (large water's infiltrations, pronounced river erosion at the foot)

Lito-Stratigraphics Characteristics

On the basis of the geotechnical surveys, the stratigraphy of the landslide area (the upper part) is made by a considerable power (20–30 m) of heterometric and heterogeneous debris in an abundant sandy silt and clayey matrix, with a low permeability primary porosity and endowed a high water retention and imbibition.

These materials lay on bedrock, which is highly weathered, intensely fractured and clayed, given by laminated micaschists, overlapping to metabasites and prasinites, highly weathered and fractured, no mapped in the geological maps. During the drillings several levels of perched water table were found, generally included in the most superficial levels, and the crossing of the bedrock generated a lot of problems because of the lost of the circulation caused by the highly fractured system.

The movement affects the recently reactivated portion, due to an alluvial event, of a biggest deformation of the slope of D.S.S.G.D type. The trigger of these movements is generally due to several factors; for the big Paleoslides of Bagnaschino the glacier decompression, after the withdrawal of the quaternary ices, and the presence of tectonically dislocations and fragile deformation, due to the presence of faults, had a crucial role.

Description of the DMS Analysis

In order to monitor in continuous the stability conditions, the Cuneo County established in 2008 a slope monitoring plan with DMS system.

The monitoring system is composed by n.1 multiparametric DMS column, 60 m long, installed in a borehole conditioned with an inclinometric pipe. The system is linked respectively to a local control unite, with its solar power supply, and a GSM transmission system for the collected data.

The column is composed by a series of 60 modules stainless steel AISI 304 containing transducers and digital electronic, linked by special joints, having the necessary freedom degrees for the type of measurement required, allowing the single unite to adapt to the characteristics of the borehole and to the movements of the landslide, preserving the azimuthal direction compared to an external reference system.

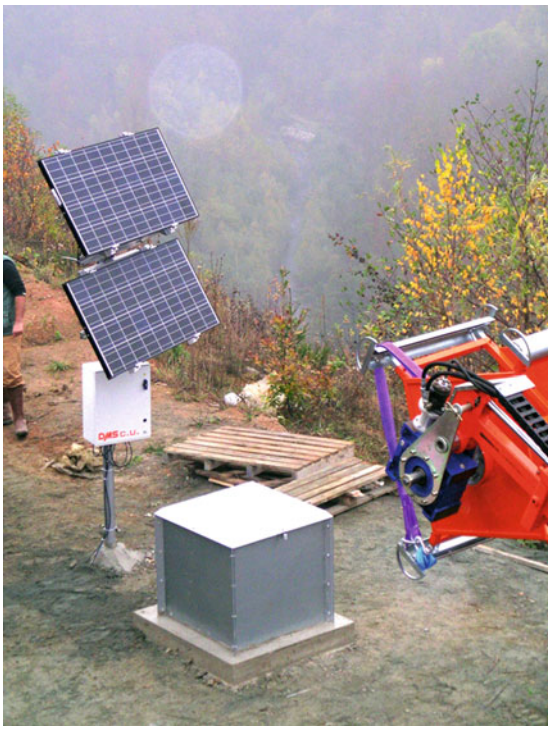


Fig. 3 DMS system installation completed

The instrumentation was installed in 28.10.2008 and in the same day linked to the monitoring centre by the GSM network (Fig. 3).

The modules contain 60 biaxial digital inclinometric sensors (range ± 20°, resolution 0.005°), 1 piezometric sensor (range: 0–100 psi, resolution 1 cm), 60 temperature sensors (resolution 0.1 °C).

Data acquisition is continuous (24/24 h) checking for the warning every minute, and information is recorded in a data base every hour. The remote control station checks the system automatically through G.S.M. remote data transmission.

Correlation between DMS column and precipitation data allowed to identify critical events that have reactivated the landslide on the sliding surface at 7 m blg, with direction 30° NE. During the observation period it was possible to monitor in continuous different kinematics and different weather conditions.

DMS system allowed to investigate five triggering events and their relative period of stasis, with a clear delay time after rain events or snow melting (Figs. 4 and 5).

The following describes the characteristics of each event:

– *First event*: on 28th November 2008 there was the first snowfall (one of the most intense of the last century in the area) that was followed by some rainy days and finally by

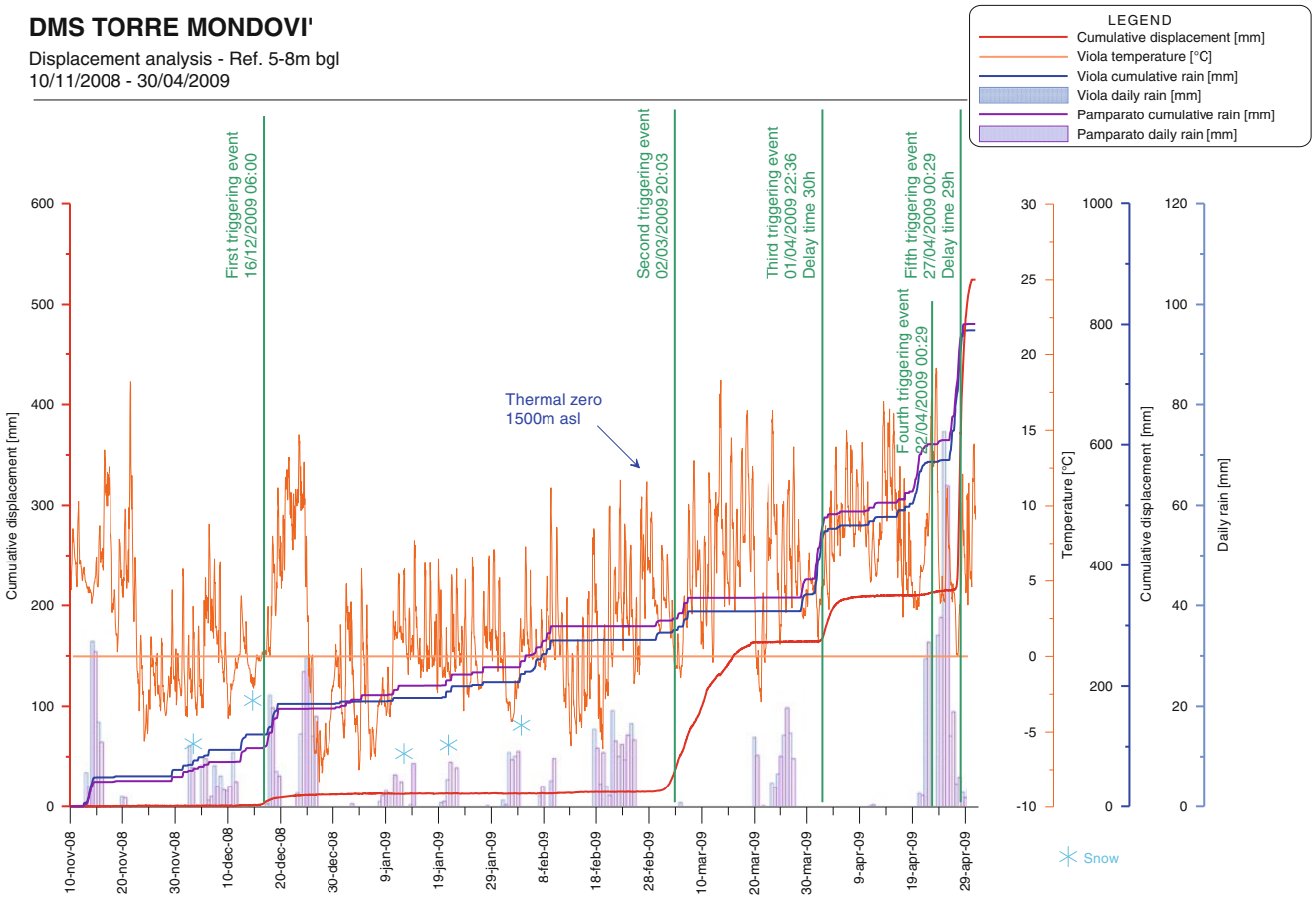


Fig. 4 Triggering events

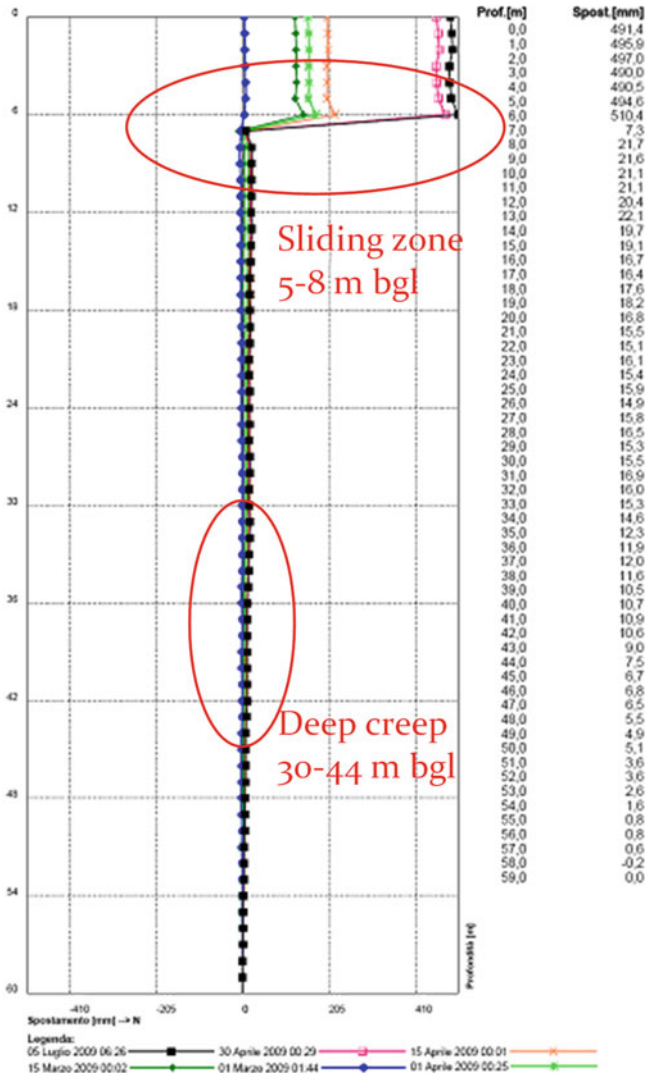


Fig. 5 Displacements during the events

another snowfall on 13–19th December. In the same days there was a temperature rise that caused the partial snow melting and subsequently the first movement read by DMS column.

- *Second event*: on 1st March 2009 there was a light rainfall following by a strong temperature rise (thermal zero at 1,500 m asl) that caused the second landslide activation on 2nd March 2009 at 20:03, 37 h after the rainfall beginning.
- *Third event*: on 31st March 2009 at 06:00 a strong rainfall began and lasted for some days. After 30 h, the landslide moved.
- *Fourth event*: this event is linked to more rainfalls occurred in the days 16th–22nd April 2009 and is different from the previous events because of a lower movement velocity (displacement about 10 mm).
- *Fifth event*: on 26th April 2009 the strongest spring rainfall started and after about 29 h (27th April, 08:00) the landslide moved. This heavy rainfall lasted for some days: the cumulative displacement was 299.7 mm in only 2 days. The roll axis on the involved DMS module reached its saturation angle (tilt $> 20°$): the further displacement is calculated with the interpolation of its pitch axis, still active (Table 1).

In the following table each triggering event has been described in detail considering also rain, cumulative rain, snow events and temperature.

Improvements with Respect to Previous Applications

Data, for the first time, were relating to the overall landslide body (both superficial landslide zone and deep creep zone) and water table at the same time in order to model the

Table 1 Triggering event data

	First event	Second event	Third event	Fourth event	Fifth event
Rainfall start	12/12/200	01/03/2009	31/03/2009	16/04/2009	26/04/2009
	8 0.00	6.00	6.00	6.00	3.00
Displacement start	16/12/2008	02/03/2009	01/04/2009	22/04/2009	27/04/2009
	6.00	20.00	12.00	0.00	8.00
Rainfall type	Snow	Rain/snow	Rain	Rain	Rain
Snow at ground	Yes	Yes	Yes	No	No
Temperature rise	Yes	Yes	No	No	No
Concomitant factors	Snow melting 90 mm	Snow melting 120 mm	–	–	–
Rainfall [mm]	70	44	63	160	77.6
Rainfall duration [h]	84	96	30	138	29
Critical intensity [mm/h]	1.8	1.7	2.1	1.16	2.7
Total cumulative rainfall [mm]	190	354	480	590	800
Cumulative rainfall event [mm]	150	164	180	110	220
Total cumulative displacement [mm]	11.5	160.6	209.0	225.0	524.7
Cumulative displacement event [mm]	11.5	149.1	48.4	10.0	299.7

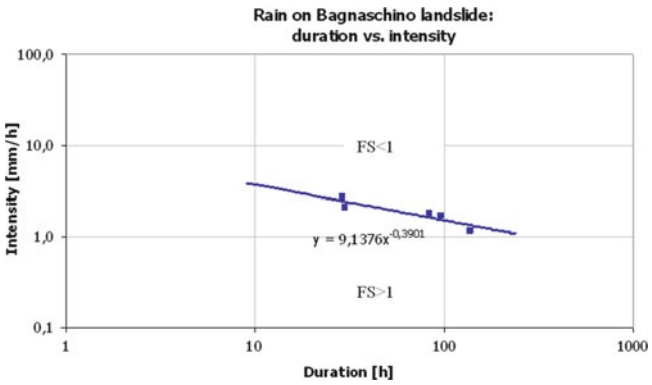


Fig. 6 Rain intensity-duration, Bagnaschino site

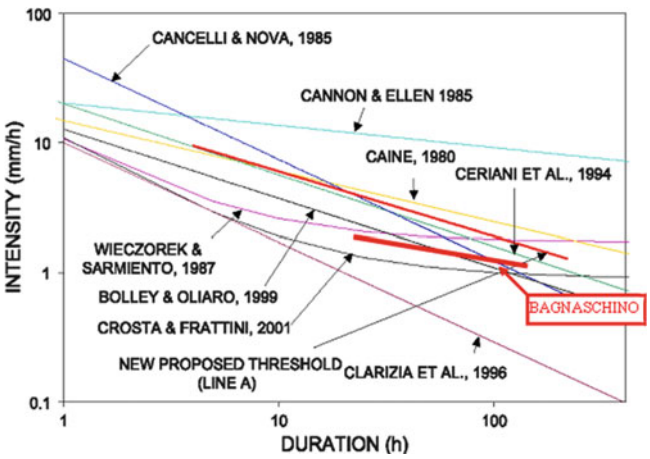


Fig. 7 Rain intensity-duration in literature

complex phenomenon. Thanks to a multiparametric approach it was possible in this way to deepen the knowledge of the geotechnical and kinematic model in a short time.

For each event was calculated moreover a particular value, the critical intensity, that correspond to the ratio between precipitation quantity (calculated in mm) that caused triggering movement and its duration (calculated in hours).

The interpolated line in the bi-logarithmic plot can be considered a site specific deterministic approach to the limit equilibrium threshold that separates the stability and instability field (Fig. 6).

The site specific equation describing the rainfall thresholds for the initiation of the Bagnaschino landslide (rainfall, duration) can be written in the following way:

$$I = c + a^{*}D^{-\beta}$$

Where in the specific site:
c = 0
a = 9.1376
β = 0.3901

The following diagram shows the site specific experimental equation elaborated by the DMS data, compared with the regional analysis available in literature basic on national and international cases (Fig. 7).

DMS column allowed obtaining with continuity the kinematics of the landslide in action, not only limited to the initial stages of trigger, but also during the evolution up to achievement of stasis conditions.

The integrity of DMS column is preserved in spite of the displacement recorded of 600 mm; this is a significant improvement, probably the largest deformation recorded at only one module (length =1 m) considering also that the instrumentation was still active and operating correctly (Fig. 8).

The excavation realized confirmed depth, direction and extent of the displacement, allowing the complete recovery of the instrumentation.



Fig. 8 Recovery of DMS column and displacement control

The activity in Bagnaschino with the cooperation of the Cuneo County allowed also repairing the inclinometer Al pipe that was replaced and protected by another pipe with a larger diameter in the interval of interest reaching the surface. This solution tested specifically in Bagnaschino will allow maintaining a long term monitoring both in the shallow zone and in the lower part of the landslide.

This experience was discussed inside the EU Safeland project 2009–2012 "Living with landslides risk in Europe: assessment, effects of global change and risk management strategies", in which Bagnaschino is a test site, during the Vienna Meeting in 2010.

Continuous monitoring of the landslide allowed noticing weak deep creep in the interval 30–44 m blg in addition to considerable shallow movements. The activation of deep movements is delayed in respect to shallow movements, with a well defined behaviour.

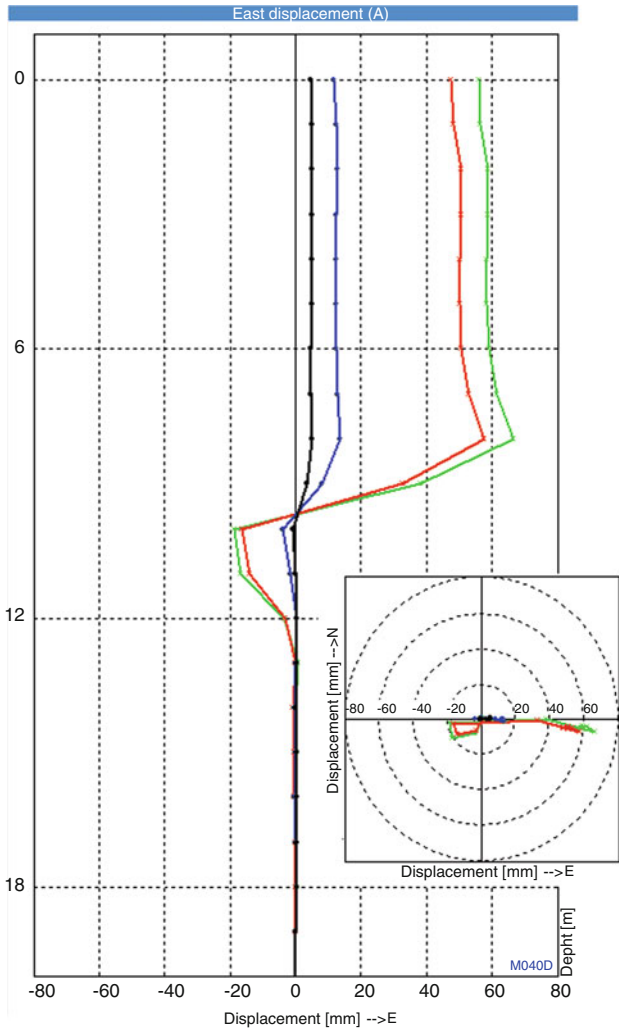


Fig. 9 Displacements in March 2011, cumulative East displacement and polar diagram

A DMS system has been installed permanently in June 2010 for Early Warning function by means of 2 columns (DMS 1–60 and DMS 2–10 active in the intervals depths 20–60 and 0–10 m).

The Integration of the Real Time Monitoring Data in Risk Management Aspects

The Province of Cuneo, using the available data from DMS system and taking into account the values of rain and the identified correlations between these parameters, manage aspects of civil protection related to the safety of the provincial road n° 164.. The remote data access and in real-time, supports the necessary management measures; in fact, on one side, the information in the system of Italian alert for the purposes of civil protection allows the activation of the procedures already being forecast, on the other side monitoring and processing of data of rain and displacement are the basis of decisions taken by the group responsible in order to possible necessary closure of the road. An example of these aspects may refer to the rain event that has affected the Piedmont Region in March 2011.

In fact a relevant triggering event occurs on site with starting the 12th of March since 8:00. At the beginning were recorded only micro-movements, but quickly grow up, reaching the 17/03/2011 a cumulative displacement of 63.3 mm at 8 mbgl. Figure 9 shows the displacements in the interval 15th–18th of March. The event monitored reached a level of stasis and the cinematic stopped on the 21st of March, lasting a total of 9 days for an overall displacement of 71.5 mm.

On the basis of the analysis of these information Province of Cuneo, already in the level of enhanced alert as a result of the forecasts of Meteorological Bulletins, has ordered the closure of the road no. 164 on the day 13/03/2011 with reopening the day 21/03/2011.

References

Baldesi L (2006) Studio cinematico dei dissesti ed analisi dei fattori di innesco nella media ed alta Val Nure (Piacenza). I casi di monitoraggio in continuo di Farini e Casale Colla. Thesis, University of Milan 2006

Dallagiovanna G (1994) Carta tettonica del settore meridionale del Monregalese. Scala 1:50.000 in: Dallagiovanna G. – Rilevamento geologico e analisi strutturale della zona compresa fra le Valli Mongia e Corsaglia (Alpi Liguri). Atti Ticinensi Scienze della Terra, vol. 37, Tav. II

Dunnicliff J (2005) Geotechnical instrumentation for field measurements. Training course, (2005), University of Florida

Giuffredi F, Zanolini L, Foglino L (2003) Application of a new integrated multi-parametric monitoring system for the analysis of micro-movements in the civil protection activities: an example. In: Proceedings of the sixth international symposium on field measurements in geomechanics, Balkema, FMGM Oslo, pp 61–66

Lovisolo M, Della Giusta A (2005) Precision of D.M.S. columns from real time in-place measurements and improvement in micro-movements analysis with early warning function. In: Brebbia CA, Carlomagno GM (eds) Computational methods and experimental measurements XII, WITpress, Southampton/Boston, pp 177–186

Regione Piemonte (2000) Riprese aerofotografiche relative al Volo alluvione 2000. Volo Rossi srl. Aerial photo views digital format

R. Servizio geologico d'Italia (1931) Carta Geologica d'Italia a scala 1:100.000. Foglio 80 – Cuneo. Prima edizione. F. Sacco, S. Franchi, A. Stella

R. Servizio geologico d'Italia (1934) Carta Geologica d'Italia a scala 1:100.000. Foglio 91 – Boves. Prima edizione. Rilevato da D. Zaccagna col concorso di S. Franchi, preparato per la pubblicazione da V. Novarese. Ministero dell'Industria, del Commercio e dell'Artigianato

Studio IG. Ingegneria Geotecnica, Valutazione geologica e geotecnica del movimento franoso Sp 164e definizione a livello di studio di fattibilità degli interventi tecnici da adottare (Technical Report for the Province of Cuneo)



Application of Monitoring Data for the Prediction of the Time to Failure and Risk Management

Ziaoddin Shoaei and Karim Karamsoltani

Abstract

During the past decades, excavation in open mine has been planned based on "more extraction with low cost". This resulted to the poor management of excavation and consequently, slope instability in many open pit mines. Anguran zinc and lead open mine in Zanjan Province, northwestern of Iran is an old mine that has been excavated since 1940 and is one of the examples of improper management that has encountered to several instabilities in its northern and western flanks. The economic importance of the operation of this mine and high risk of landslide occurrence put this mine as of the main concerns of the local governor.

The investigation has been done through detail field study together with high precision monitoring of unstable blocks. It was found that the main landslide in this mine is a creep type of motion that caused by overlying a block of hard limestone on a low strength clay bearing schist. It was also concluded that in a creep type of landslide, independence of the rate of motion from its initial triggering factor such as rain is a good indicator for predicting the time of rapid failure and for controlling the risk by proper evacuation plans.

Keywords

Monitoring • Prediction • Risk control • Anguran mine

Introduction

During the past decades, excavating in open mine was planned based on "the more extraction with lower cost". This resulted in poor management of excavation and consequently slope instability in many open pit mines. Development of engineering geology and geotechnical engineering has drawn the attention of mine managers on re-evaluation of excavation plans and slope stability of open old mines.

Anguran zinc-lead open pit mine is one of the oldest one in Iran that has been excavated since 1950 for several decades. This mine is located in a mining area (47: 00–47:30 E, 36:30–37:00 N), in Zanjan Province, northwestern Iran (Fig. 1). The northern and western flanks of this mine has encountered to a serious instability due to its improper excavation. The economic importance of this mining operation and its effect on the regional job opportunities, made this event as one of the main concerns of the local governor. Moreover, the working of more than 50 workers and about 50 Million $US of machinery, put the risk of landslide occurrence at the highest level.

Study Method

This research works have been planned for investigating the main causes of recent instabilities, interpretation the mechanism of motion and planning the early warning system for evacuation.

Z. Shoaei (✉)
Soil Conservation and Watershed Management Research Institute, 19395–1113, Tehran, Iran
e-mail: z.shoaei@cgiar.org, zshoaei@gmail.com

K. Karamsoltani
Madan Zamin Consultant Co, Tehran, Iran

C. Margottini et al. (eds.), *Landslide Science and Practice*, Vol. 2,
DOI 10.1007/978-3-642-31445-2_72, © Springer-Verlag Berlin Heidelberg 2013

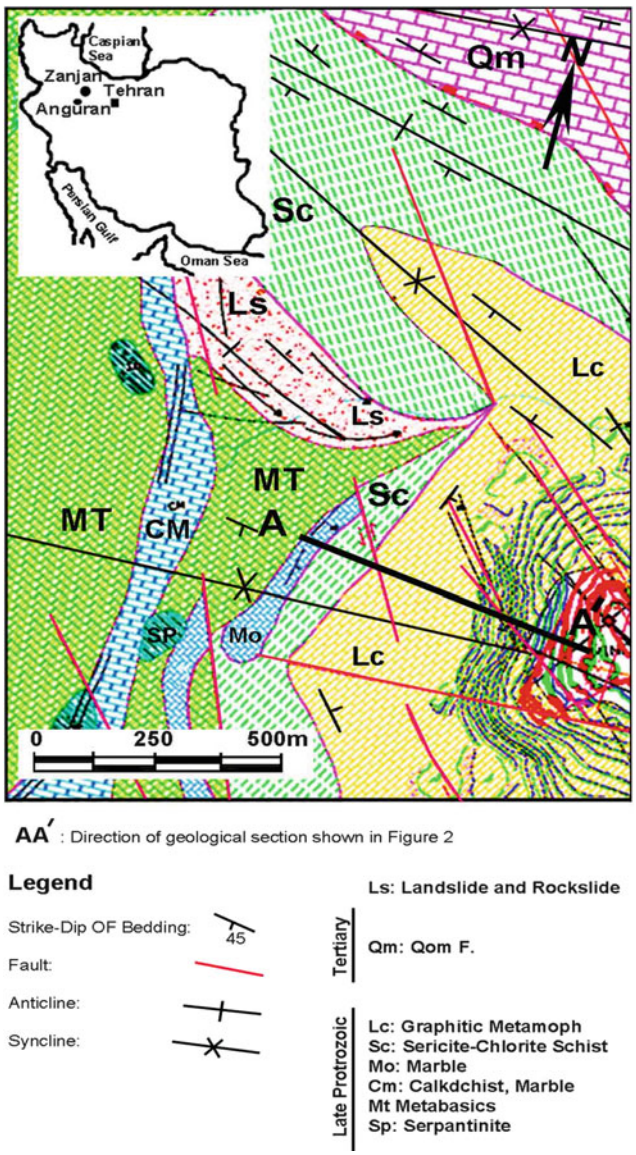


Fig. 1 Geological map of the studied area

This work was composed of the following steps:

- Preparing the engineering geological map of the study area.
- Clarifying the border of the main unstable block/s.
- Monitoring the landslide activity together with the variation of local precipitation.
- Interpretation the mechanism and prediction the time to rapid failure of landslide for early warning and risk control.

Geology

Anguran mine is a part of the Takht-e-Soleiman geology quadrangle map of the Geological Survey Organization of Iran and part of the central Iran geological zone (Fig. 1). The

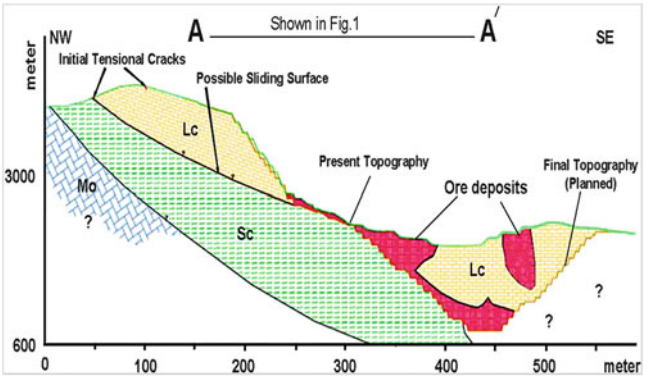


Fig. 2 Cross section of landslide, direction is shown in Figs. 1 and 3

studied area is composed of a series of volcanic, sedimentary and metamorphic rocks. The evidence of plutonic and volcanic activities is predominant in the area. These are the main cases of metamorphism and hydrothermal intrusion that has formed different ore veins as the mines in the region. The well fractured limestone and intrusion of hyrothermal liquid caused the formation of low-strength interlayers. This could be one of the most important factors of slope instability in the region. The most critical instability that was initiated at the northern flank of Anguran mine was selected for this study. As shown in Fig. 2, despite to the complex geology of the region, the geology of the selected site is very simple. It is composed of a block of weathered and well fractured of limestone laying on a series of crystalline carbonate and mineralized schist. This limestone had subjected to a sever weathering and dissolving that appeared as widened discontinuities, hollows and small caves.

Some of the effective factors on the slope instability that has been found through detailed geological field survey are as follows:

- Abundance of schist in the region as a low strength material.
- Alternation of limestone and schist in the most geological formations.
- High permeability of the overlaid limestone due to its various system of fracturing, jointing and faulting that caused rapid infiltration of surface water to the lower schist layers.
- Generation of thin clay layer as the result of weathering and consequently leaching to the lower level.

Landslide

Anguran mine is one of the most important ore resources in Iran. It has been exploited as an open pit mine for several decades. No evidence of instability has been reported until March 2003.

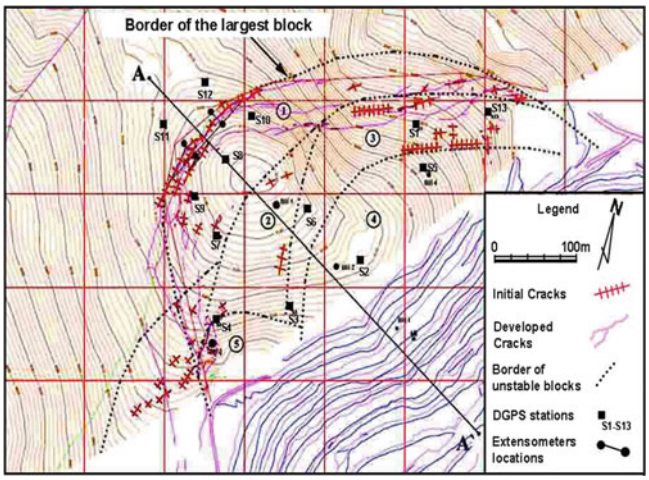


Fig. 3 Engineering geological map of the study area. Borders of unstable blocks, location of extensometers and DGPS stations are shown

The first indicator of instability in Anguran mine was a few tensional cracks appeared at the upper part of its northern flank around March 2003. The field study started on August 2003. At the first step, the geological map of the area was reviewed based on the field data (Fig. 1). Based on the field and well-log data, cross section was prepared along the largest unstable block that is shown in Fig. 2. The approximate border of the main block was drawn that is shown in Fig. 3. Correlation of the appeared initiation cracks on the surface confirmed that this landslide could be a block slide type of landslide (Cruden 1991; Varnes 1978). The unstable block is a massive limestone overlaid on a low strength clay bearing schist. This landslide was initiated from an area on the back slope of the main outcrop with 120 m height from the base of the mine pit. Locations of early initiated cracks on the top of the northern flank are shown in Figs. 2 and 3.

Monitoring

Due to the high risk of this initiative, simultaneously to the field investigation, monitoring systems were planned and were set from September 2004. The monitoring works has started from fall 2004 up to fall 2005. The total duration of monitoring was around one year that covered two periods of dry and rainy seasons of one water year.

DGPS Monitoring System

Dual frequency positioning system (DGPS) is a set of devices capable to detect the position of points on the ground with high precision. This system works by recieving dual frequency signals propagating from the satellites. It consists of a flat antenna, a signal receiver and a simple computer that is capable to locate X, Y, Z coordinations of the ground stations. The employed DGPS in this work was a high qualified system with the precision of 1 mm that can be applied for detecting the positions of stations on an active landslide.

Thirteen stations were set on the largest active block of the Anguran landslide. These stations were selected based on the preliminary prepared border map of the active block. The locations of these stations are shown in Fig. 3 as S1 to S13. A reference station was set in an stable area beside the main office of the mine. For higher precision and avoiding the error coming from the antenna setting on a tripod at each stage, the bolt was set inside the concrete of the stations. The location of the stations were selected all over the bolck in order to find out the amount of motion as well as its distribution in different parts of the block. Two sets of DGPS devices were employed. The static method was used for data collection. The data recording for each station was done from three neighbor stations that made data processing easier and get high precision of the positioning. The subtraction of measured displacement between two consequent readings will be the amount of motion of stations for the time interval. For measuring the real displacement, the amounts of difference between two consequent readings of X, Y, and Z was plotted on the main direction of displacement and along the sliding surface (Z).

The landslide motion was monitored by DGPS every 50 days (six surveys). It has started from November 2004 up to August 2005. Figure 4 shows the vector map including the measured displacements and their directions. Colored vectors show the displacement and direction for every recording surrvey. The displacement of S14 as the reference station was nearly zero for all surveys. Also, Station S11 and S12 that were selected out of the unstable block showed no measurable displacement that support the proper landslide block bordering at the initial stage.

Extensometer Monitoring System

The data collected from DGPS presents the total displacement for about 50 days interval that is not a continued time series data. Thus, for continued monitoring of displacement of landslides across the surface cracks, two extensometers were employed. In this instrument, the generated data is analogue data that is more reliable than those from digital instruments. The location of two wire type-paper recording extensometers on the back slope of the unstable block are shown in Fig. 3. Continued displacement was recorded from September, 2004, to September, 2005. The recorded data.by extensometers were calibrated and the amount of displacement was measured for

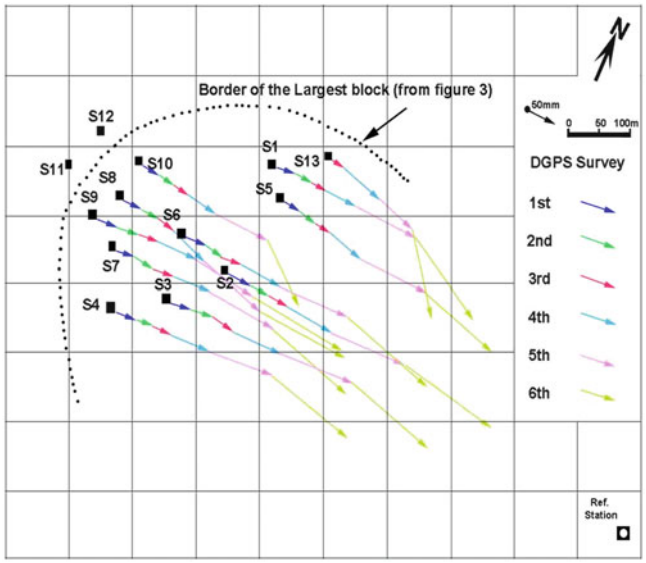


Fig. 4 The result of DGPS monitoring in Anguran open pit mine

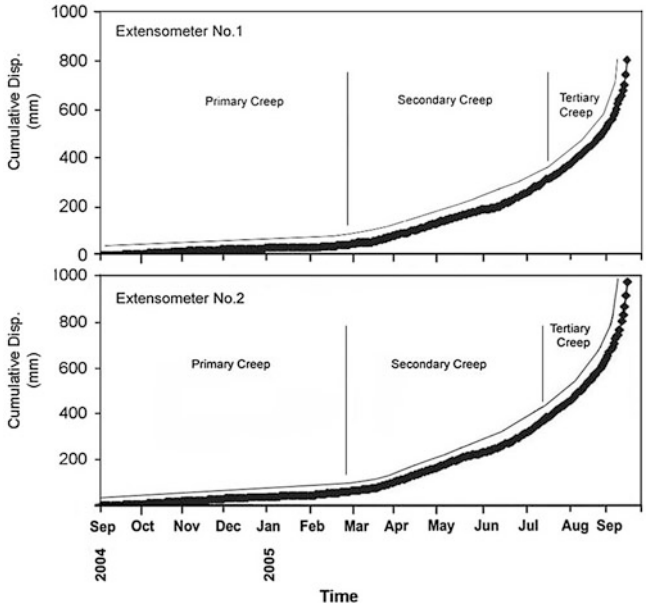


Fig. 5 Cumulative displacements recorded by the extensometers

each day and week to comparable with DGPS data. The results are illustrated in two diagrams in Fig. 5.

Discussion and Conclusion

The movement in both extensometers and DGPS shown in Figs. 4 and 5 confirm the exponentially increase of motion in the main block.

During September and early October, 2004, the amount of precipitation in the region is nearly zero and consequently, the level of underground water droped to the minimum level. The rate of displacement was about 0.4–2.4 mm/week during late October to November period. It was increased to 2.4–3.6 mm/week during November and early December, 2004, which was due to the increase in precipitation. The rate of displacement decreased again due to the low precipitation on the late December, 2004, and January, 2005. During this period, the rate decreased to 1.3 mm/week that could be because of less runoff by the beginning of winter. This low displacement continues to the end of winter (March, 2005).

At the beginning of the spring, 2005, the rate of displacement increased due to the higher precipitations and snow melting. The landslide motion in this period ranged from 3 to 6.2 mm/week that was observed in both extensometers and DGPS. The increase of displacement continued during April and May, 2005, and reached to 11.4–20.0 mm/week. This rate was nearly constant during June and July, 2005, in both DGPS and extensometers data.

The increment of landslide displacement can be divided into two periods. The displacements rates during the first period (September, 2004, to July, 2005) that was directly corresponding to the rainy season,, at the and second period (August to September, 2005), the rate of movement showed an exponential trend that was about 70–80 mm/week (10–12 mm/day). The rate of movement grew increasingly during August 15, to September 15. Consequently, the rapid and main failure with the total of 150–250 m displacement at the head scarp occurred on September 25. This behavior can clearly be observed in the cumulative diagram of extensometers data and vector map of DGPS in Figs. 4 and 5.

The mechanism of landslide motion is closely related to the geological structure, material, and geotechnical properties. Variation of triggering factors such as precipitation and groundwater table, as well as external additional load such as earthquakes and traffic make the reliable interpretation of the landslide very difficult. Also, time to failure is very important for landslide management and risk control that were reported in many works (e.g. Sassa et al. 2009). The possibility of using the variation of precipitation and groundwater table for predicting the time to failure was reported in some works (e.g. Shoaei 1998). It is also reported that enough knowledge about the clays and corresponding geotechnical sensitivity to the degree of saturation can be used to predict the characteristics of a creep type of landslide motion (Skempton 1985).

In Anguran mine, it was observed that the cumulative displacement of this landslide can be a typical creep type of deformation (Fig. 5). The graph of motion is comprised of three phases of primary, secondary, and tertiary creep. The result of monitoring from its early initiation to rapid failure shows that this creep type of landslide was very sensitive to the amount of precipitation. This could be caused by saturation of material on the sliding surface. However, it was found that during July and August, 2005, the amount of precipitation is at the lowest level, the rate of motion not

only did not decrease, but also showed an exponentially increase in rate. In this period, simultaneous with tertiary creep (Fig. 5), it is clearly observed that the landslide motion becomes independent from its triggering factor. It could be concluded that in an active landslide when the curve of displacement-time gets the tertiary creep shape and the motion becomes independent for the triggering factor, the condition would represent a reliable sign of a rapid landslide. This conclusion was employed in Anguran mine; 2 weeks before the rapid failure an early warning for evacuation was sent to the management team of the mine. The main and rapid failure occurred at 18:30 PM on September 24, 2005, and was completed at 5:00 AM on the next day. Total displacement at the head scarp was about 180–240 m. The estimated speed of the landslide is about 7.5–10 m/h. Evacuation was successfully conducted and the risk was controlled to the lowest possible level. Fortunately, no casualty and machinery losses were happened due to the rapid failure of this landslide.

Acknowledgments The authors would like to thank the Soil Conservation and Watershed Management Research Institute (SCWMRI) for logistic and financial support to this project. Also the efforts of Mr. Emam Jomeh from (SCWMRI) for his field instrumentation and data collection are highly appreciated.

References

Cruden DM (1991) A simple definition of a landslide. Bull Int Assoc Eng Geol 43:27–29

Sassa K, Picarelli L, Yuenpin Y (2009) Landslides, disaster risk reduction. In: Sassa K, Canuti P, Springer (ISBN: 978-3-540-69966-8). 649 p

Shoaei Z (1998) The necessity of monitoring of landslide. In: 2nd conference on landslides and measuring works, UNESCO National Committee, Sanandaj, July 1998

Skempton AW (1985) Long term stability of clayey slopes, Fourth Rankine Lecture, Geotechnique

Varnes DJ (1978) Slope movement type and processes. In Special Report 176. Schuster RL, Krizek RJ (eds) Landslide: analysis and control TRB, National research Council, Washington, DC, pp 11–33



Development of WILMS: Well Inform Landslide Monitoring System for USM Healthy Campus

Fauziah Ahmad, Ahmad Shukri Yahaya, Mohd Azam Osman, Wong Poh Lee, and Ahmad Badri Ismail

Abstract

Slope monitoring system was installed for the purpose of monitoring the hill development for student accommodation which houses three main blocks of hostels. This was implemented under a special programme known as Healthy Campus which covers all aspects conducive to student, staff and environment. A full package of pilot study has been conducted by a group of experts in the field to run a monitoring and mitigation system for Universiti Sains Malaysia (USM) hostels. WILMS (Well-Inform Landslides Monitoring System) is a real-time web monitoring system which integrates the use of SMS (Short Messaging Services) and MMS (Multimedia Messaging Services) technology to inform and to alert users of different needs about the presence of a pessimistic change in land stability. The uniqueness of this application is that it makes monitoring job easier, without needing constant human power while maintaining accurate data acquisition cocpyntinuously and reducing human errors. This method is offering cheaper solution as well as sustaining environmental issues.

Keywords

Slope monitoring • Landslide • Instrumentation

Background

The occurrences of slope failures, Sumatran earthquake and Tsunami have an indirect effect in Malaysia and caused concern not only to the nation but also to USM. This has resulted in actions taken to develop a slope monitoring system. The role of USM is to monitor the development of University hostels located at highland area which is considered as an area at risk. A group of experts was formed and formalized the best method in developing the monitoring system together with the analysis which will able to understand the stability and safety of the area (Ahmad et al. 2002; Ab Talib 2003; Mahadzer and Mohd 2002). The experts are from the geotechnical, geological, structural and hydrological fields from several Universities and Agencies in Malaysia such as: University Sains Malaysia (USM), the leading organization, Kuala Lumpur Infrastructure University College (KLIUC), Malaysian Centre for Remote Sensing (MACRES), University Technology Malaysia (UiTM), Public Works Department (JKR), Penang State Government, Soil Instrument Sdn Bhd and other related state government agencies.

From the proposal presented, a Healthy Campus project for USM Hostels Monitoring System was approved by the Vice Chancellor with an allocation given for the instrumentation installed by phases. This project is also supported by MACRES in giving satellite data and other related sources.

F. Ahmad (✉) • A.S. Yahaya
Disaster Research Nexus, School of Civil Engineering, Universiti Sains Malaysia, Engineering Campus, NibongTebal, Seberang Perai Selatan, Penang 14300, Malaysia
e-mail: cefahmad@eng.usm.my

M.A. Osman • W.P. Lee
School of Computer Science, Universiti Sains Malaysia, 11800 USM, Seberang Perai Selatan, Penang, Malaysia

A.B. Ismail
School of Material and Mineral Resources, Universiti Sains Malaysia, Nibong Tebal, Seberang Perai Selatan 14300, Malaysia

C. Margottini et al. (eds.), *Landslide Science and Practice*, Vol. 2,
DOI 10.1007/978-3-642-31445-2_73, © Springer-Verlag Berlin Heidelberg 2013

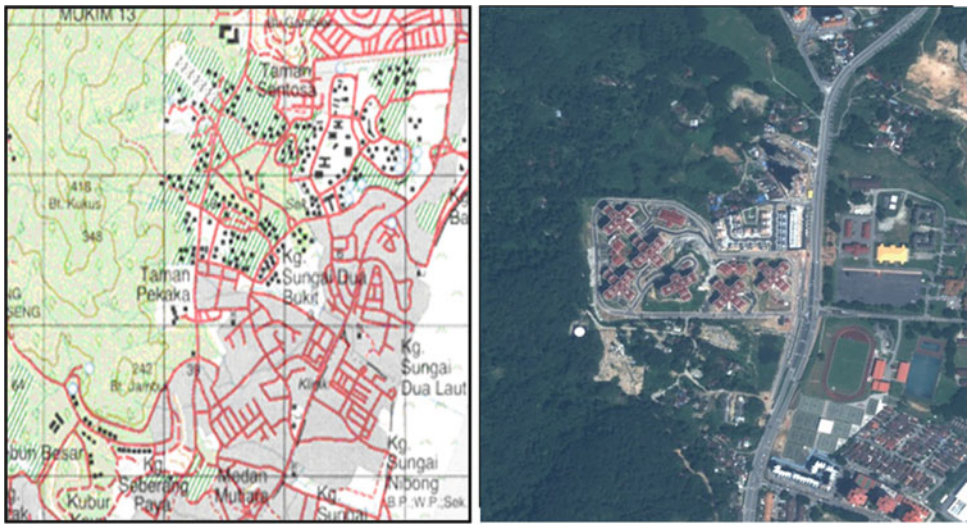


Fig. 1 The study area with satellite image

Based on the collected data, WILMS is able to intelligently forecast future results and to give early notifications which indirectly minimize the risk taken as early measures. On the other hand, this method is another way of offering a cheaper solution as well as to attain and maintain the sustainable land. WILMS also establishes a secure communication while preserving proper data transfer between data acquisition tools, servers, computers and mobile devices via wired and wireless.

Objectives

The main objectives of the monitoring are;

- To developed an alert warning system as a pilot study to monitor the critical area for USM slope
- To monitor the soil/rock behaviour which comprises of water pressure in soil, movement and rain intensity
- To create a database of USM hilly area.

The Location

Figures 1 and 2, show the study areas for the remote monitoring system being installed, which comprises of three blocks of hostel for USM student named as Restu, Saujana and Tekun. The area is situated at the hilly area within the university compound.



Fig. 2 The USM hostels

The Remote Monitoring System

The configuration of the instrumentation scheme consist of a small number of strategically placed electronic water pressure sensors, in-place inclinometers and an electronic/automatic rainfall measuring gauge. These devices are linked as one system of architecture as a real-time web monitoring system that integrates the data logger and all other instrumentation as shown in Figs. 3 and 4.

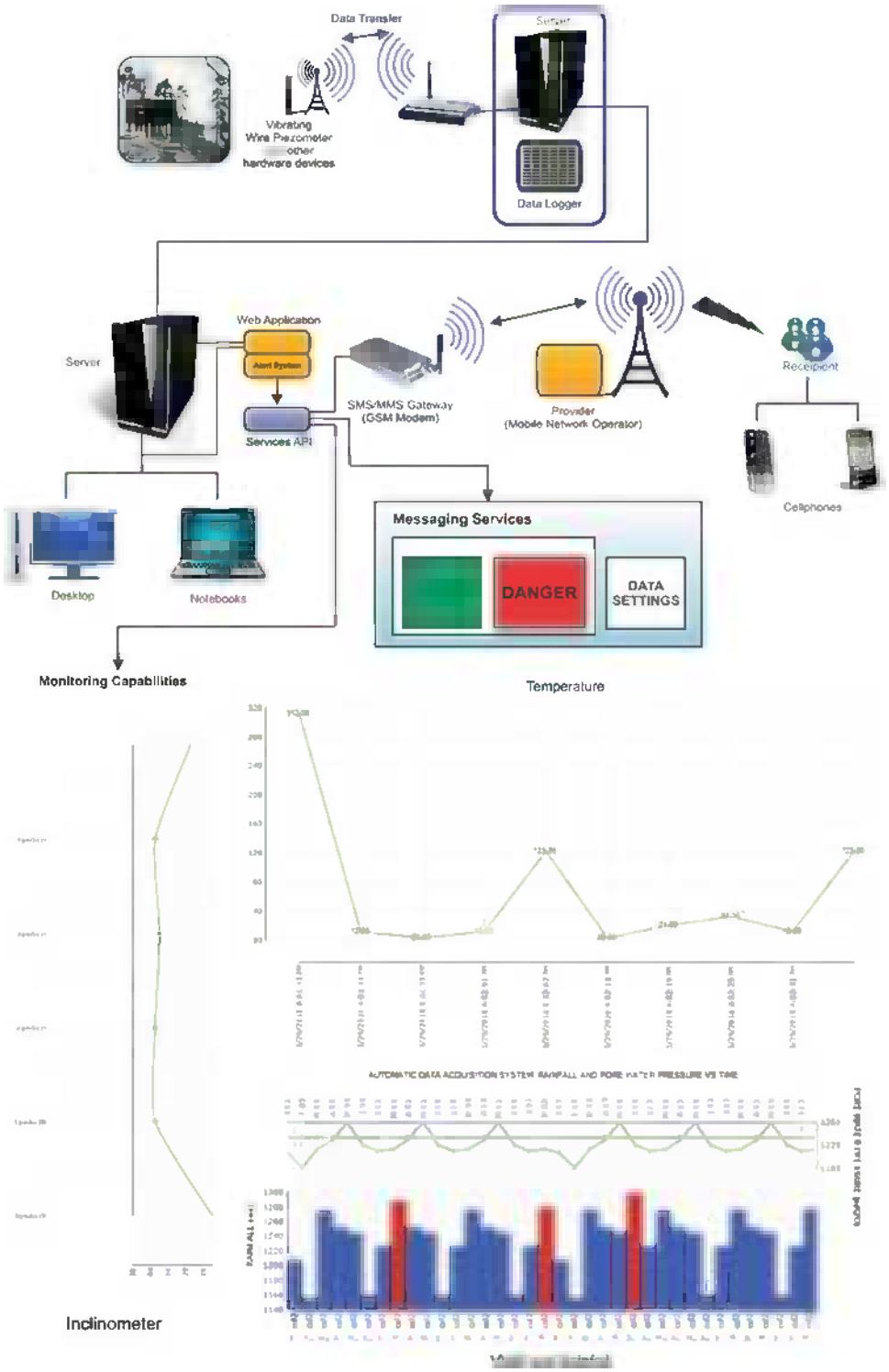


Fig. 3 The system architecture

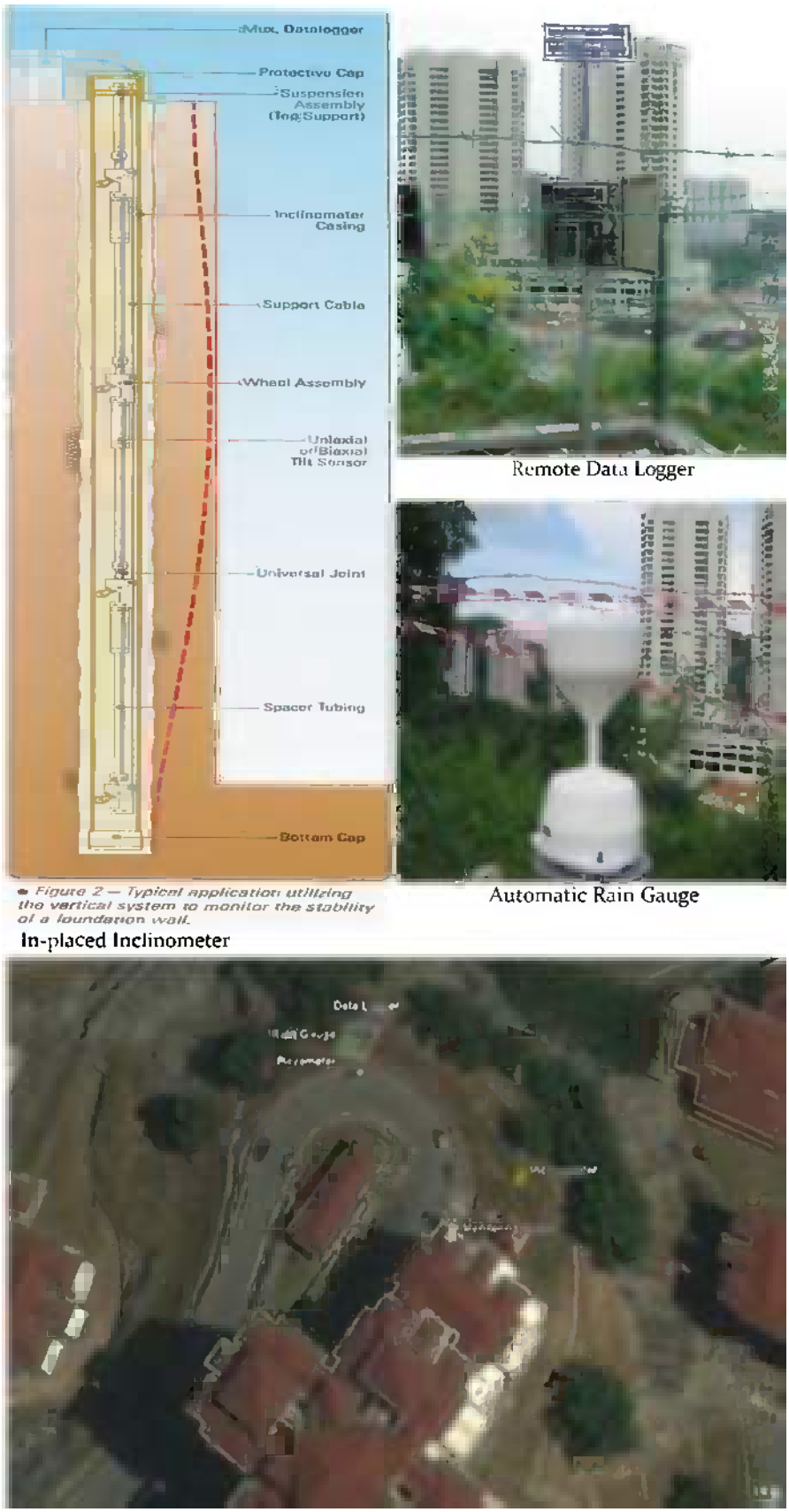


Fig. 4 The instrumentation of remote monitoring and location of the system used at USM hostel

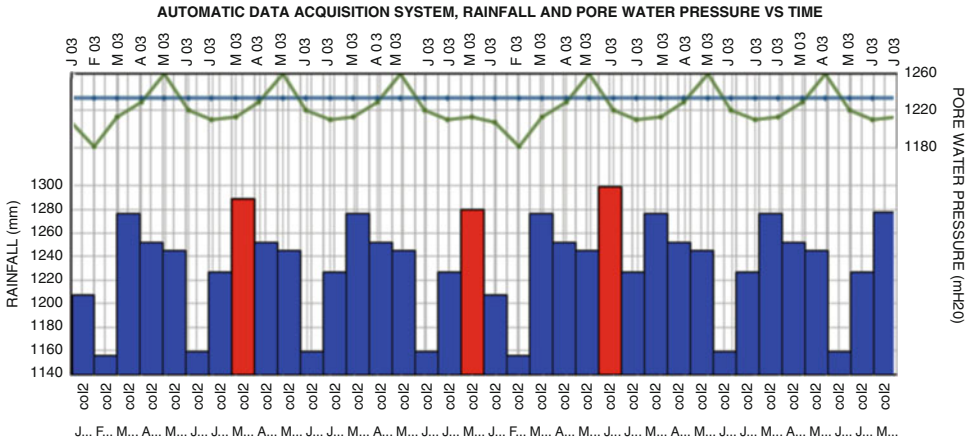


Fig. 5 Typical rain intensity and pore pressure reading

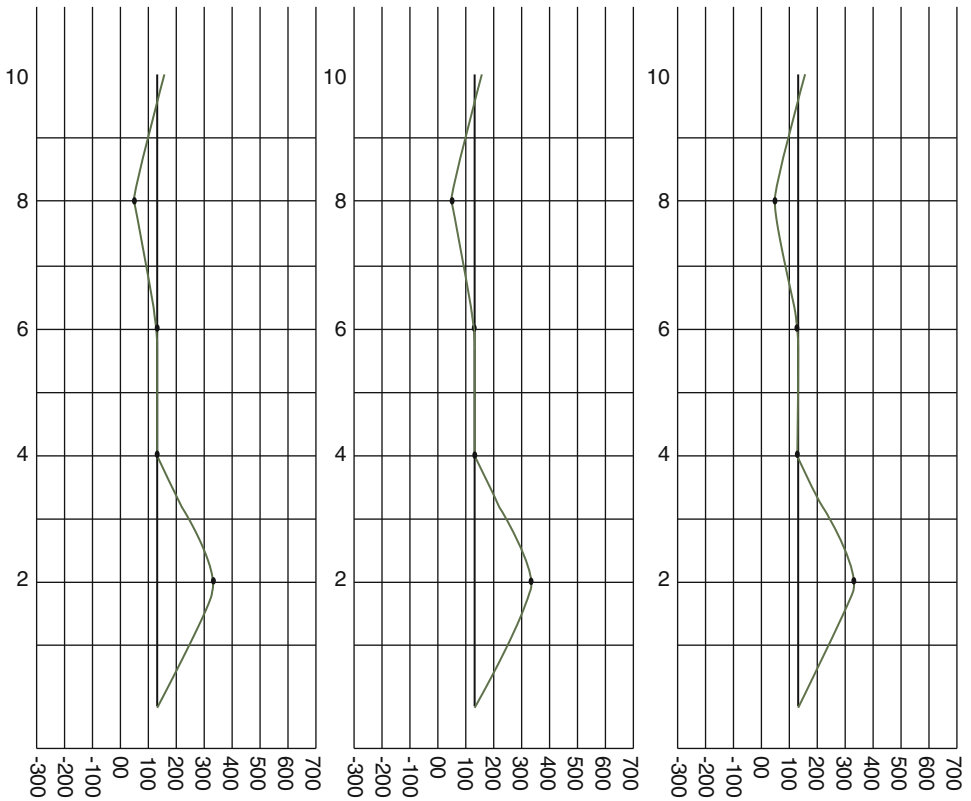


Fig. 6 Typical piezometer readings every time frame

The system is intended to provide an automatic recording facility to create a data base of the measured geotechnical parameters which would be used in any geotechnical assessment of the long term safety of the slope. The logging system is also able to generate an alarm signal if it detects significant changes in the geotechnical parameters of the slope being measured. This could be used to alert engineers if thresholds have been crossed and further attention is required.

Should remedial measures, such as slope stabilising, be deemed necessary, data from the instruments could be used

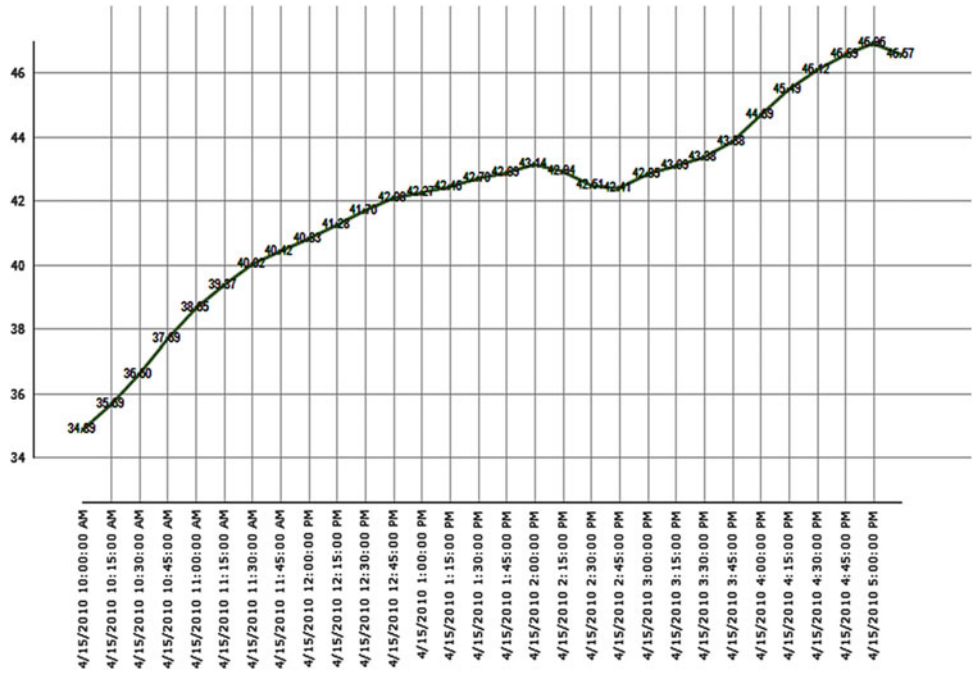


Fig. 7 Typical temperature reading every 15 min

to verify the effectiveness of the work that was carried out. The instrumentation sensors installed on site were as follows;

(a) Vibrating Wire Transducer based PIEZOMETERS were installed in the investigation boreholes to register changes of the pore water pressures within the slope. These pore water pressures often form the critical indicator with regard to the stability of a slope and are generally considered the primary indicator. Any increase in the pore pressures will generally be triggered by increased rainfall and changes in the flow of surface and sub-surface water courses can also have a significant effect on pore water pressures. The threshold value were taken as more than 10 % of usual reading.

(b) An automatic rain measuring gauge is, therefore, installed close to the main data logger enclosure and was linked to the data logger. It will send pulse to the central logger each time an accumulation of 0.2 mm of rain has fallen, making it a suitably sensitive instrument. If rain falls continuosly for more than 2 h then the system will alert the user and further action will be taken.

(c) An in-placed inclinometer sensor system was installed to form part of the remote monitoring system. The sensors were installed inside the access tubes and would comprise interconnected and articulated solid state Tilt Sensors suspended from the top cap assembly.

The sensors were linked to the central data logger thereby recording any deflection of the access tubes, on a regular basis. They were installed in the investigation boreholes located in key areas where the slopes are considered most critical. The data can then be used to generate graphical profiles of the access tubes which will then be compared with previously recorded and base data. The resulting information will provide long term slope movement data that can be used to assess the stability of the remaining slopes. In this form, these inclinometers will form part of the in-place warning system since they were interrogated automatically, it can be monitored at the request of an Engineer, if an alarm threshold from another

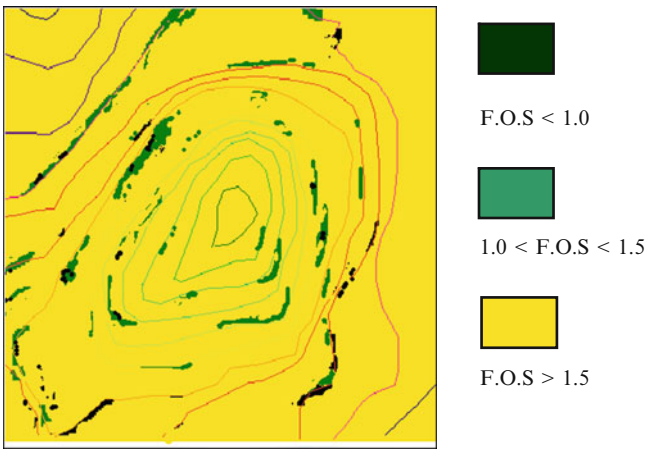


Fig. 8 Analysis of slope stability using GIS techniques

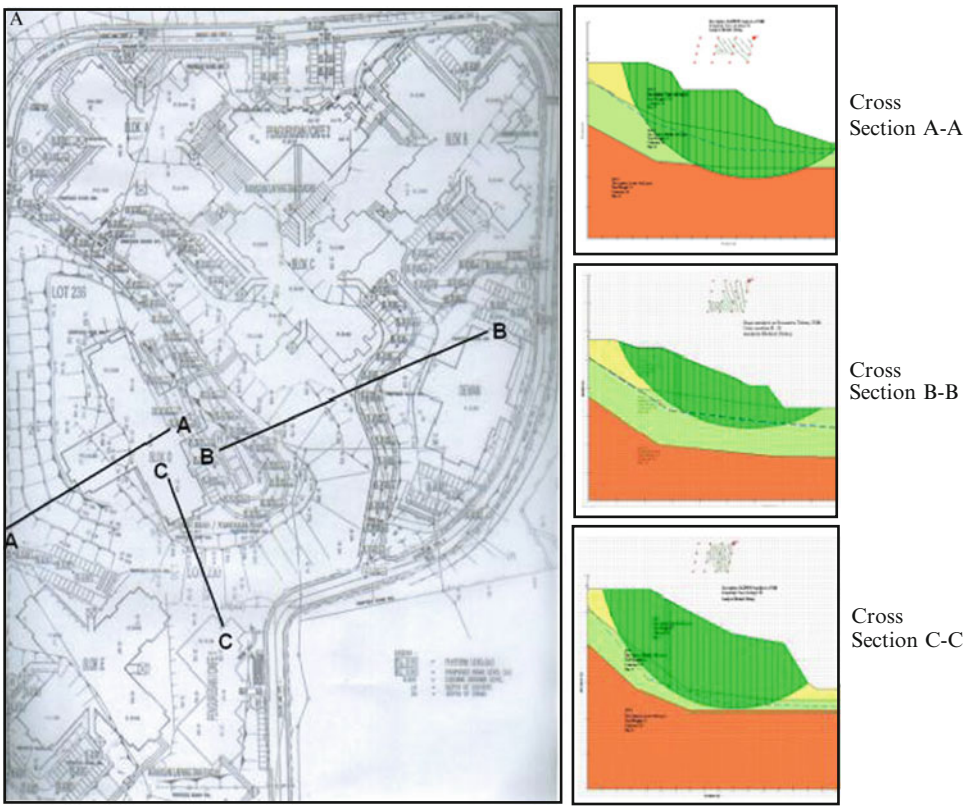


Fig. 9 Analysis using Geo-Slope software to calculate factor of safety

sensor is exceeded. If the deflection exceeds more than 25 mm than it will be alerted throught the system.

Data Handling Routines

Each time the instruments are interrogated by the logger, the results are initially recorded in the primary memory of the logger for analysis. The internal software then compares the recorded values with pre-defined threshold values to test for unusual readings. This operation would normally be carried out on a regular basis at any required time intervals.

The rain gauge forms a critical element of the data gathering and the logger can be configured to change its monitoring routines if a significant (pre-defined) rainfall occurs. It could be set to interrogate the instruments on a more regular basis, hourly for example.

In any routine, if the thresholds have not been exceeded the logger will store readings in its 'final' memory only once for a 24 h period, thereby saving both memory capacity/ download time and sending an excess of data to the engineer for analysis. If thresholds have been exceeded, more data will be saved to the 'final' storage memory. If the software has been configured to issue warnings via the web data base, it will dial the pre-defined numbers and transmit pre-defined messages when any sensor reaches a particular threshold. A number of thresholds can be set for each transducer and the rain gauge.

Monitoring and Analysis of Results

Two types of result were produced, the plotted result from Figs. 5, 6 and 7 are the data from the piezometers, rain gauges and inclinometer readings retrieved from the data logger by remote monitoring system.

The results obtained from the borehole data previously done during initial site investigation were used to develope the GIS technique and to calculate factor of safety using Geo-Slope software. These data were used to analyse the slope stability of the surrounding area as to verify that the area are safe. These are shown in Fig. 8 for the GIS techniques and Fig. 9 using the Geo-Slope. From the Slope stability analysis it was found that the safety factor calculated are more than 1.5 and can be considered stable and safe, which is shown in Table 1.

Table 1 Calculated factor of safety for USM slope

Critical area	Factor of safety		
At USM	Ordinary	Bishop	Janbu
A-A 	2.694	3.367	2.718
B-B 	2.943	3.325	2.906
C-C 	2.858	3.394	2.810

Conclusion

The setting up of WILMS well inform remote monitoring system which can be monitored, analysed and alert remotely via internet connection on real time are cost effective. The video camera is able to control and alert any major events if found necessary to notify residents of the hostels. As for the analysis we can actually analyse the result and identify the critical threshold for the ground water pressure and stability calculated from time to time. Any effect of earthquake or tsunami encountered can be monitored and measured immediately via the system.

WILMS has established a secure communication while preserving proper data transfer between data acquisition tools, servers, computers and mobile devices via wired and wireless conditions.

Acknowledgments Special thanks to USM Healthy Campus, USM Short term and Sciencefund under Ministry of Science and Technology (MOSTE) grants in financing the project. Also to all the collaborative partners and the working group committee especially to all the academicians, technical officers from other organization and technicians who have work closely in this projects.

References

Ab Talib J (2003) Probabilistic landslide susceptibility analysis and verification using GIS and remote sensing data at Penang, Malaysia. Geol Soc Malay 46:173–179

Ahmad F, Hamir R, Mohd S, Yahaya AS (2002) GIS application on slope stability. In: Proceedings of the 2nd IKRAM international geotechnical conference, Kuala Lumpur, Malaysia, pp 159–165

Mahadzer M, Mohd FB (2002) Application of aerial photos, GIS and GPS in slope management. In: Proceedings of the 2nd IKRAM international geotechnical conference, Kuala Lumpur, Malaysia, pp 125–138



Integrating Landslide Monitoring into Multi-Hazard Monitoring Systems

Guido Bernardi and Fabio Procopio

Abstract

Civil Protection of Regione Calabria, in cooperation with the regional Multi-Risk Functional Centre, chose CAE to carry out the implementation of a landslide real-time monitoring solution. The landslide happened during February 2011 at Cirò, located within the Crotone Province. In June 2011 CAE completed the installation of the real-time landslide remote monitoring system. Data measured by a number of geotechnical sensors placed in relevant points are received at the regional Multi-Risk Functional Centre, located in Catanzaro Province. Among the strengths of this innovative solution developed by CAE, the leading Italian provider of multi-hazard monitoring systems, there is the opportunity to use traditional geotechnical sensors in a new and innovative manner. Their wireless and remote usage in real-time proved to make easier the implementation without affecting reliability of data measurement and collection. Three months after the activation of the system, data are nearly 100 % collected and transmitted in real time, with no interruption in data availability.

Keywords

Landslide • Wireless Sensor Network • MHEWS • Monitoring • Multi-hazard early warning system • Real time • Remote monitoring

Need for Technology to Put Science into Practice

According to IFFI Project, a National landslide database updated to 2007, in Italy there are at least 460,000 observed landslides. Rock-falls, deep failure of slopes, shallow debris flows and other phenomena threat transport infrastructures, cultivated fields, industrial facilities and unfortunately population in most of the national municipalities.

Italian institutions set local majors to be responsible for the implementation of Civil Protection practices in case of emergency due to natural hazards with local effects, including those caused by landslides. A strong support to majors' decision making process comes from the regional Multi-Hazard Functional Centres. These institutions collect data in real time about phenomena, elaborate forecasts and transmit official bulletins before, during and after each extreme event.

Since few decades ago technology for remote monitoring in real time has substantially evolved and widespread networks have been implemented. These networks in Italy operate mostly on regional bases and include hundreds of Automatic Weather Stations (AWSs) for meteorological and hydrological purposes, among others. Data make possible to calibrate and operate forecasting models to predict floods or other catastrophic events. After a forecast is made, then a bulleting can be issued to facilitate emergency response.

Notwithstanding geological science improved the capability of geologists to understand and analyse landslides, yet

G. Bernardi (✉)
Bernardi Guido c/o CAE S.p.A - Via Colunga, 20 400068 S.Lazzaro di Savena (BO) - Italy
e-mail: guido.bernardi@cae.it

F. Procopio
Studio Geologico Procopio - Via, Cosenza 36 - Catanzaro

C. Margottini et al. (eds.), *Landslide Science and Practice*, Vol. 2,
DOI 10.1007/978-3-642-31445-2_74, © Springer-Verlag Berlin Heidelberg 2013

remote data collection and real time interpretation (especially for civil protection scopes) still proves a hard task. According to CAE preliminary researches to understand the "state of the art technology", carried out before starting the development of this solution, remote monitoring technology can seldom be in real time and vice-versa. Anytime these two features are coupled, then accuracy in measurement and/or reliability in data transmission are missing.

CAE invested to combine geotechnical traditional sensing with remote monitoring in real time. Two practices individually supported by well-established technologies, but unsuccessfully joined in a unique reliable solution at that time. This solution finally came out to be a practical and robust local Wireless Sensor Network (WSN) to collect data from standard geotechnical sensors and a master rain gauge station, to input data into existing networks.

CAE WSN Monitoring Solution

CAE started research activities about WSN solutions for landslide monitoring in 2008, getting ready to begin a test to verify in-field reliability and develop some accessory parts in 2010. In order to carry out this test CAE took part in a joint project with University of Bologna, Department of Earth and Geologic-Environmental Sciences. WISELAND research project (Integrated Airborne and Wireless Sensor Network Systems for Landslide Monitoring; Italian Ministry of Education, 2007) made possible to test the newly developed solution on a real landslide, though moving slowly, and realize some modifications to make it more practical, more efficient in energy consumption and adaptable to different conditions and sensors.

The landslide was at Porretta Terme (BO), in Italy, specifically in the Silla district. The system was installed on 19th April 2010 and worked properly for the whole period of 1 year, with some minor maintenance and testing interventions. Results were also presented at EGU General Assembly 2011 (Berti et al., 2011).

Hereinafter the description of the WSN refers to the last developed technology, applied in June 2011 at Cirò (KR), Italy.

Robust WSN Communication Technology

CAE developed its WSN solution according to the firm's philosophy: first of all at reliability and efficiency of the data collection system. Redundancy of communication, robustness of each component and a long independency from external sources of electric power had to be obtained.

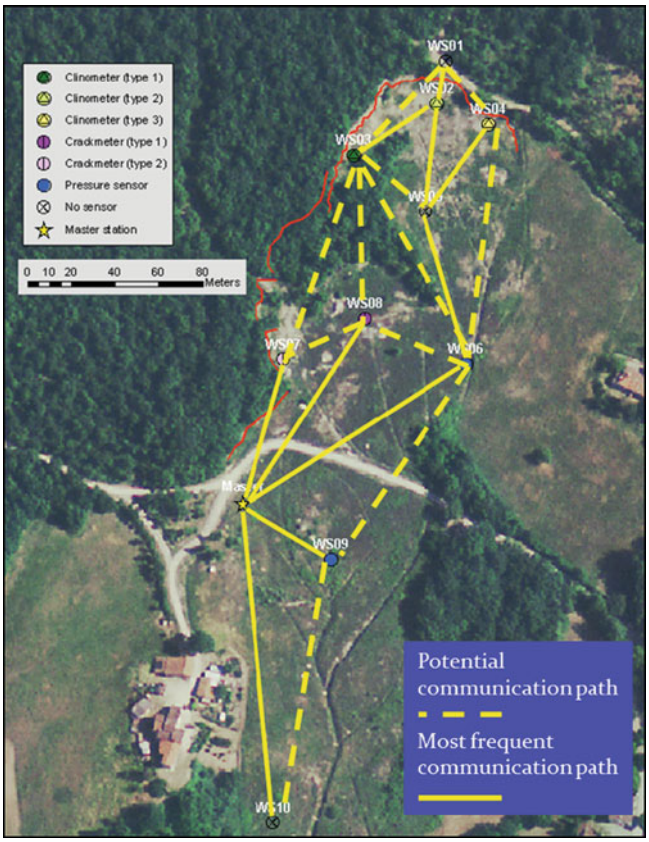


Fig. 1 Layout of the landslide test site at Porretta Terme (BO), Italy. It shows the potential communication paths between nodes, due to the "mesh network" structure, and the path most frequently used for communications in normal conditions

Redundancy of communication has been obtained by using ZigBee protocol. It allowed forming a "mesh network" made up of self-healing and route discovering modules. As represented in Fig. 1 data may follow numerous different paths to be transferred from a node to the master module. Actual path is self-adapting depending on the availability of the intermediate "repeating" nodes. Nodes must be "visible" between each other to transmit effectively data, which may mean some "bridge nodes" may be required and suitable supports should be designed to keep antennas free.

Communication proved to work well, in real circumstances, even when the distance between two nodes exceeds 200 m. Multiple "bridge nodes" can be connected sequentially to each other to cover much longer distances. Atmospheric conditions and growth of vegetation do not significantly affect the system operations. Even multiple networks can work in the same area, having the chance to let simultaneously transmit through 12 different channels without interferences.

Transmission of data collected in the period happens at certain established time, being possible to modify the interval

between each transmission remotely at any time, even depending on thresholds set for parameters measured by other sensors within the network (Example: rain gauge/rain intensity). An important safety measure, in case the communication should fail, consists of saving data on each node, until the transmission activity recovers or data are manually retrieved.

The long experience in installing and maintaining hydro-meteorological networks let CAE developers pay much attention to the consumption issue. A safe and reliable tool for Civil Protection operations must be independent from any source of electricity, but internal lithium batteries or little solar packs. In fact, apart from the communication functioning, sensors within the WSN usually rely on node batteries for their operations. This is why each node absorbs 600 μA at 3.3 V in stand-by mode and 80 mA at 3.3 V while transmitting data. Waking-up time is nearly zero, so that energy is not wasted in the process. It has been tested that, with one sensor connected and a 30 min interval, batteries with no solar pack last more than 9 months.

Interoperability with Standard Geotechnical Sensors

Once reliability and efficiency of the data collection system were obtained, another important objective was to give users the chance to integrate any standard sensor for geotechnical measurements. CAE wanted to give professionals a tool to leverage their competences and experiences, for example about the free choice and free placement of sensors along a landslide. Interoperability of standard geotechnical sensors, possibility to connect multiple sensors to each node and a sounding transmission capacity had to be obtained (Fig. 2).

Each node is provided with 12 analogic inputs, 2 digital input/outputs and 2 RS232/RS485. It makes possible for a single module to connect a wide range of different sensors, including multi-clinometric chains, biaxial clinometers, piezometers and others. In this respect CAE tested a selection of sensors produced by the leading manufacturers in the world, but still the WSN can go along with preferences of local geologists by interoperating with sensors by specific producers. Each node, for reference only, is also internally equipped with sensors to measure battery status, internal temperature, biaxial inclination and collisions.

Integration of WSN Network into MHEWS

Once the WSN works properly and traditional sensors available in the market interoperate with it, then it becomes important to ensure a good communication between the landslide area and the monitoring centre. This is the basic condition to allow data transmission from each sensor to the control unit and to facilitate remote management and maintenance of the system.



Fig. 2 Wireless communication module installed at Cirò. The box at the *bottom* hosts numerous plugs to connect geotechnical sensors, in this case a piezometer

In the last decades the core business of CAE has always been to design, produce, install and maintain hydro-meteorological networks, made up of hundreds of AWS and water level measurement stations. Since few years ago the company decided to move its offering from meteorological and hydrologic applications to multi-hazard monitoring systems. The main concept is to use the data acquisition system (data loggers, communication network and central unit) to collect data through many different localized "solutions" engineered by the company itself. The landslide monitoring WSN is one of these solutions.

The first step consists of collecting data from each salve node of the WSN into the automatic station, where the master node is placed. Then the data-logger puts together all the different data measured by any sensor of the station, for example rain gauge for rain intensity measurement and thermometer for air temperature, and transmits them all (Fig. 3).

There are three main ways to transmit data from remote areas to central units: radio, GPRS/GSM and satellite



Fig. 3 Master automatic station with rain gauge for rainfall and rain intensity measurement, complete with thermometer. It collects all data from the whole WSN and transmits them into the regional network

communication. Any of these ways, even combined in a redundant system, can be successfully used to compose a network with a nearly 100 % efficiency in data transmission. Each of them is characterized by pros and cons but, for Civil Protection scopes, it is certainly the UHF radio to ensure the best results. In fact: it is a dedicated network, so that doesn't risk getting busy in case of emergency; it can be extended depending on specific needs, so to reach the most remote areas; and allows a two way exchange of information, making possible a remote maintenance. By the way, whenever the remote solution requires transmission of images in real time, though still possible by radio, it may be considered also a redundant GPRS link.

Radio networks can retrieve data from stations all at once, for example every a certain period of time or upon request, or they can selectively call a specific station and its sensors. This flexibility makes the system suitable for managing specific localized events, such as landslides triggered by rainfall or snow melting. Whenever certain parameters are about their thresholds in a specific area, then the system can give the priority to selected stations. According to CAE statistics about real in-field applications, a network made up of 200 stations with standard mixed hydrological or meteorological configurations, is expected to complete retrieval operations of a minimum 99 % data within three polling cycles. All of these cycles can be completed, depending on system optimization, within 30 min from the measurement of the event.

Once data reach the monitoring centre, CAE software can display them in real time. An open source database can also be organized, where historical series can be either navigated and validated by proprietary software or transmitted through web-service in standard formats to any other non-proprietary application. Complete interoperability and diffusion of data are ensured.

Case History

In the night between the 1st and the 2nd February 2011 a massive landslide seriously affected the only road to Cirò town, in Crotone Province, and forced citizens to evacuate five houses. Fire-brigades, Civil Protection officers, local major and technicians from the gas and electric companies had to work hard for many hours before opening again the road.

It was a rainy night and, despite of previous civil works in the area, yet people risked their lives in a potentially catastrophic event. From that time on, as Calabria Regional Civil Protection stated, a remote monitoring system operating in real time had to be installed. Once the regional Multi-Hazard Functional Centre was identified as the competent authority and the place where data should be collected, a new solution should have been integrated within the existing hydro-meteorological monitoring system.

Data began to flow from Cirò to the Multi-Hazard Functional Centre in June 2011 and currently there are no failures to be reported.

Landslide Description

The urban area of Cirò is located on the hills of Crotone province, where a prominent rock exposed at NE-SW hosts the urban historical centre. Being its surface made up of sandstone and calcareous materials, it is possible to observe sub-vertical slopes. These slopes often break and several rock-falls and rotational slides happened through the years, as sediments at landslide toes and scarp shapes demonstrate (Fig. 4).

The Cirò landslide occurred in 2011 takes around 30,000 m^2 along the south-western slope aside the city. It caused the collapse of a municipal road and the evacuation of five houses. Via De Gasperi, affected by the landslide,

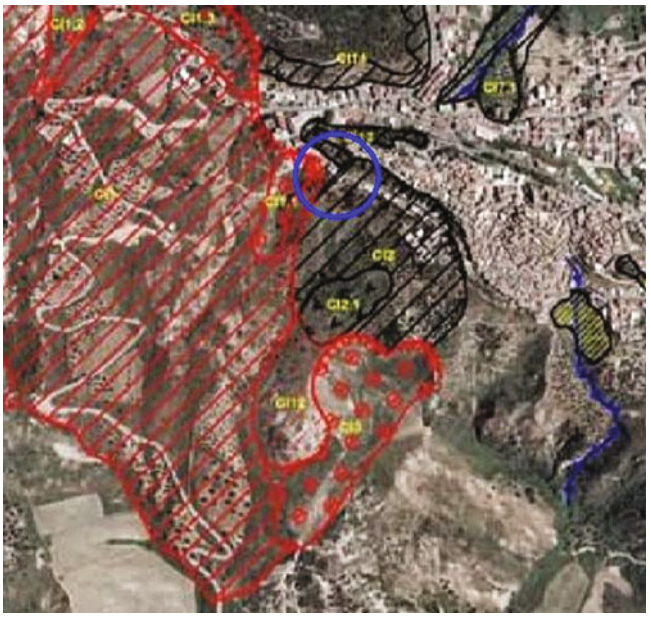


Fig. 4 *Blue circle* highlights the area hit in February 2011. Parts colored in *red* are active landslides, while *black* colored areas are dormant landslides (PAI Regione Calabria)

runs along the south-west slope of the rock and it is the only road from the valley to the historical centre. This slope is characterized by several landslides. This macroscopic phenomenon, together with many others in the area, is clearly highlighted in the previous regional "Piano stralcio per l'assetto idrogeologico", an official document about hydrogeologic risks and mitigation plans.

The lithology emerging in the collapsed area is made up of sandstone of Scandale (Piacenzian, 3.4 Ma), characterized by stratifications of submerged yellow sand and bioclastic levels made up of shellfish. These strata run counter to the slope and they are basically permeable. In normal conditions sandstone is a resistant material, but constant water flows can dramatically affect its original geo-mechanic responsiveness, downgrading its resistance to middle and middle-low.

Below the emerging sandstone there is a clay layer, called clay of Ponda. It was formed during Miocene period (Serravallian-Tortonian, 10.4 Ma) and it is characterized by low permeability. Difference in permeability between the two levels, together with the presence of two water springs in the area, generates considerable water flows through the sandstone layer along the landslide (Fig. 5).

At the beginning of 2011 the area has been hit by a constant and abundant rain. This natural phenomenon, jointly with non-effective retaining works or erroneous maintenance, made the underground water level increase constantly for some days until sandstone degraded and the ground collapsed.

The landslide developed on the ridge of the rock hill, along the slope where the Palombelli torrent originates. It has a curve and sub-vertical crown of rupture at 300 m AMSL, it is 120 m wide and approximately 250 m long. Up to now, notwithstanding in situ analysis, it has not been possible to find out a clear end of the toe or the place for natural retaining morphologies (Fig. 6).

Existing Network of AWSs Throughout Regione Calabria

The hydro-meteorological monitoring network operating throughout Regione Calabria is made up of 147 automatic stations connected in real time to two control centres: one at Catanzaro and one at Germaneto. In order to ensure this connection there are 27 radio repeaters working throughout the region.

The Multi-Hazard Functional Centre operates it, hosting the main monitoring centre and contracting the maintenance program – including planned, corrective, remote and in-field maintenance – to CAE. The constant presidium of technicians makes this network efficient in data measurement and collection. Statistics about the overall operating efficiency rate during the first 6 months of year 2011 are reported in Table 1. This performance depends also on settings, such as the "polling interval" of the radio network, which is decided by network administrators based also on needs other than efficiency. These data do not represent the best possible performance, but the actual situation.

The efficiency of the network and the institutional setting made convenient, safe and cost effective for Civil Protection of Regione Calabria to use this platform for landslide monitoring purposes.

Sensor Type and Position

The monitoring program proposed by the geologist to Civil Protection and Multi-Risk Functional Centre officers, is firstly concentrated on keeping under control water table level. That's why S2 and S4 piezometers were installed. Another relevant risk to be monitored is the possible enlargement of the landslide area back toward Via De Gasperi, affecting the stability of the whole rock sustaining the historic centre of Cirò. This is the reason for installing two chains of inclinometers S1 and S3 down to a depth of 30 m, placed upstream the landslide.

Furthermore the monitoring system includes four clinometers (P1, P3, P4, P5) and one accelerometer (P2) located along the structures and buildings mostly affected by the landslide in order to assess the possible evolution of the phenomenon.



Fig. 5 Aerial image of the collapsed area, close to the main road located right beyond the houses



Fig. 6 The sub-vertical crown of rupture and the collapsed area

The system also includes the thermometric and rain gauge master station for data collection and transmission (Fig. 7).

Data Collection, Analysis and Diffusion

During the first 3 months monitoring activities proceeded without any interruption, collecting nearly 100 % data to the Functional Centre in real time.

In the period no relevant rainfalls have been registered in the area. Inclinometers didn't report horizontal movements at the ground, as well as clinometers and accelerometers didn't reveal structural movements. Soon after the landslide piezometers registered a dramatic drop in the water table level, while in the period between June and September the value decreased steadily.

Data confirm geologic analysis of the slope: landslide movements are strongly related to rainfalls, as the sandstone permeable lithology quickly changes its characteristics depending on water flows.

Table 1 Overall efficiency of the monitoring network of Regione Calabria. Percentages are calculated as retrieved data out of the total number of measured data every month. All stations are included. "Real Time" means data are displayed within 30 min from the event measurement

2011	Data measured	Real time (%)	Within the end of the day (24:00) (%)
Jan.	2,173,787	96.3	99.5
Feb.	3,150,696	95.8	99.6
Mar.	3,654,624	96.7	99.7
Apr.	3,550,560	98.3	99.9
May	3,643,632	96.3	97.7
Jun.	3,563,688	98.2	100.0
Tot.	19,736,987	97.0	99.4



Fig. 7 Layout of geotechnical sensors located along the collapsed area. In *blue* the position of the master automatic station

References

APAT (2007) Rapporto sulle frane in Italia. Il progetto IFFI: metodologia, risultati e rapporti regionali, APAT, Rapporti 78/2007, Roma. (ISBN 978-88-448-0310-0)

Autorità di Bacino Regione Calabria (2001) Piano Stralcio per l'Assetto Idrogeologico (PAI) Regione Calabria: Relazione Generale. Catanzaro

Berti M, Corsini A, Ronchetti F, Bernardi G, Bertocchi F, Rosi A, Zambonelli F (2011) Use of wireless sensor networks for landslide monitoring. Geophys Res Abstr 13:EGU2011–10549, 2011, EGU General Assembly 2011

Cassa per il mezzogiorno (1961) I consolidamenti degli abitati in Calabria. Officine Grafiche Calderini, Bologna

Procopio F (2011) Relazione geomorfologica per il monitoraggio della frana di Via De Gasperi di Cirò

Part II

Early Warnings and Emergency Plans

Introduction by Nicola Casagli[1] and Yin Yuepin[2]

1) University of Florence, Florence, Italy
2) China Geological Survey, Beijing, China

Introduction

The Session L16 of the 2nd World Landslide Forum address technical and operational aspects related to the implementation of early warning systems and emergency plans for reducing landslide risk at local, regional and national levels.

These aspects involve technological development, landslide impact scenarios, capacity building, planning mitigation, preparedness and recovery actions.

Critical issues of early warning systems are discussed, such as the understanding of critical factors of landslide triggering, the rapid identification of precursors and anomalies, the correlation among different indicators, the multi-parameteric monitoring, the definition of thresholds and alert levels.

Moreover the session embraces the technical and scientific requirements of emergency plans associated to early warning systems, such as the modeling of risk scenarios, the implementation of fast risk reduction measures, the planning of civil rescue actions and their scheduling for the different alert levels.

Special consideration has been given to those papers reporting innovative methods, new technologies, remote sensing and best practices of scientific and technological transfer.

Eighteen contributions have been submitted to this session. They can be divided into the following broad topics:

- Early warning systems based on rainfall thresholds and hydrological models
- Early warning systems based on measurements of soil properties
- Emergency management
- Capacity building
- Technological development

Early Warning Systems Based on Rainfall Thresholds and Hydrological Models

Bai et al. present a study on rainfall threshold analysis and landslide susceptibility mapping in Wudu county (China). Rainfall thresholds are calculated using an antecedent daily rainfall model based on the landslides induced by multi-temporal rainfall events in the region. Three susceptibility maps of the region were produced based on historic, earthquake and rainfall data. An integrated landslide susceptibility score is computed considering the maximum landslide probability of the three factors.

Jamaludin and Hj Ali present a review of some empirical methods to correlate rainfall and shallow landslide triggering at national level in Malaysia. This national early warning system is based on three types of empirical rainfall thresholds: (1) intensity versus duration thresholds, (2) intensity versus working rainfall and (3) intensity versus antecedent thresholds.

A group of presentations is focused on the National Early Warning System established in 2004 in Italy by the Government and implemented by the National Civil Protection and by the Regions. This system is based on rainfall forecasting and nowcasting as input of threshold models for the forecasting of landslide triggering at regional scale.

Basile and Panebianco describe the experience in the Sicily region where warning models are based on the combination of precipitation intensity and antecedent rainfall of the previous 15 days. The warning model is associated to specific procedures to activate the regional civil protection system and on-site assessment carried out by geologists.

Lazzari et al. present a study on local rainfall thresholds for landslide triggering in the Basilicata region (Southern Italy). The authors set up a database of historical landslides and climatic data with more than 300 well-dated landslides. For each recorded landslide, the daily rainfall and the previous cumulate rainfalls on 2, 3, 5, 10, 15 and 30 days are calculated in order to identify precipitation thresholds. Moreover the use of a standardized precipitation index is investigated.

Martelloni et al. describe an operational warning system for forecasting landslide occurrence at regional scale in the Emilia-Romagna region (Northern Italy). The system, named SIGMA, combines rain gauges measurements and rainfall forecasts and compares them with a series of statistical rainfall thresholds based on the total amount of rainfall, which was cumulated considering different time intervals from 1 up to 365 days. The model is integrated into the regional warning system of Emilia Romagna for civil protection purposes. For its simplicity, the proposed model seems particularly appropriate for developing countries that have no systematic information on landslide distribution.

Ratto et al. illustrate the operational procedures for hydrogeological warning system in the Aosta region (Norhern Italy). They define multi-parametric thresholds based on previous precipitations, current precipitations (maximum and average) and snow level. The associated operational procedures are based on alert levels defined taking into account monitoring results and actual scenarios. The result is given in terms of probability (low, medium or high). For the mountainous range a new network of soil moisture sensors has been installed for feeding a specific hydrological model.

Ponziani et al. present the Landwarn model, an operative early warning system for landslides forecasting based on rainfall thresholds and soil moisture of the Umbria region (Central Italy). The authors developed and tested a continuous physically based soil water balance model, addressed to the estimation of soil moisture conditions over the whole region. Landslide triggering thresholds are defined by coupling the computed soil moisture conditions with rainfall intensity thresholds.

Salciarini et al. propose a method for defining physically-based rainfall thresholds for early warning systems. The authors combine short-time rainfall forecasts with a GIS-based code which evaluates the spatial distribution of the minimum rainfall intensity, which triggers shallow landslides and debris flows over a given area, based on the rainfall duration and the local geometric, hydrologic and mechanical characteristics of the slopes. An example of application to a study area of the Umbria Region in Central Italy is presented, describing the capability of the model of providing site-specific thresholds for different rainfall scenarios and issuing different levels of hazard warning.

Early Warning Systems Based on Measurements of Soil Properties

Raj Bhat et al. stress the importance of a residual-state creep test to understand the creeping behavior of landslide soils. This can improve the prediction performance of warning models based on the analysis of time series of landslide displacements or velocities. A residual - state creep test procedure was developed by the authors with a modified torsional ring shear

machine, which is capable of measuring the displacement with respect to time under the application of constant creep load.

Chae et al. propose an innovative method of landslide early warning based on measurements of the gradient of volumetric water content. Their study is based on a real time monitoring system to observe physical property changes in soil during rainfall events. According to the authors, the response of volumetric water content is faster than pore water pressure, and volumetric water content maintains the maximum value for some time before slope failure. The results show that a large rainfall amount and a high gradient of volumetric water content induce slope failures. Based on these results, it is possible to suggest a threshold of the gradient of volumetric water for early warning of landslides related to rainfall.

Emergency Management

Dell'Acqua et al. describe a case study of successful emergency management carried out by the Italian Civil Protection with the support of research institutes. The case is the reactivation of the Montaguto earth flow, which on March 2010 caused the interruption of both a railway and a route of national relevance. A real-time monitoring system was deployed, combining real-time total stations with ground-based radar interferometry. The continuos real-time monitoring system was employed for the design and the implementation of stabilization measures, based on the observational method. The landslide stabilization was achieved with drainage and engineering solutions at low environmental impact.

Fischer Gramani presents a successful case study for the identification of processes and risk scenarios during the emergency actions and field works undertaken in the Vale do Itajai in 2008 (Brazil). Several mass movements were triggered by heavy rains in the month of November, affecting the region of Santa Catarina State, South of Brazil, causing 135 deaths, 2 missing, nearly 80,000 displaced and homeless people. The recognition of the different scenarios and understanding of their evolution allowed local authorities to define the preventive actions and to establish the procedures for the safety of persons and of teams working in rescue operations. Technical inspections and geotechnical safety procedures were adopted during the post disaster operations in the affected area.

Capacity Building

Bandara et al. and Billedo et al. present a joint regional project of the Asian Disaster Preparedness Center (ADPC) and the Norwegian Geotechnical Institute (NGI) for documenting and sharing good practices for early warning of landslides in Bangladesh, Bhutan, China, India, Indonesia, Nepal, Pakistan, Philippines, Sri Lanka, Thailand, and Vietnam. This ongoing project aims to promote cost effective practices for monitoring and early warning of landslides for sustainable development. This is currently being achieved through data gathering from existing approaches and through the formation of joint working groups to identify critical factors. The project expects to disseminate knowledge on good practices of landslide monitoring to promote landslide early warning among participating countries.

Fathani et al. describe the early warning system for debris flows in the region of the volcano Merapi in Indonesia. This system was set up after the 2010 major volcanic eruption, in order to monitor the triggering of debris flow along the Boyong/Code River and to protect the city of Yogyakarta. The debris flows are affected by the presence of accumulated sediment in the upstream sectors of the rivers and are triggered by rainfall. The early warning system is based on the most adaptive, least cost, and collaborative-based technology. The system was developed by considering the community aspiration in determining the types and placement of monitoring equipment, and maintaining its sustainability.

Technological Development

Towhata et al. present the validation and interpretation of slope monitoring provided by low-cost multi-sensor devices installed on unstable slopes. The employed sensor can monitor slope deformation by means of tiltmeters during heavy rainfalls. A wireless network periodically collects signals from the sensors and warns local authorities through cellular phones, sending an alert signal or an emergency evacuation order, depending upon the progress of tilting of sensors. The developed equipment has been deployed in several slopes in the recent times for validation of field performance.

Tapete et al. describe an early warning system for monuments at risk based on ground-based radar interferometry (GB-InSAR) and Permanent Scatterers (PSInSAR) technique, presenting case studies in the archaeological areas of Rome (Italy). The high sampling frequency and spatial resolution of Ground-Based InSAR (GB-InSAR) instrumentation allowed the authors to perform real-time monitoring of the displacements and of the structural behaviour of Roman monuments. An automatic data analysis was exploited for the real-time detection of displacement anomalies as deviations from the normal trend, while PS time series were used to warn about actual instability of monuments.

Pascal et al. stress the importance of data fusion for effective early warning systems based on real-time multi-parameter monitoring technologies. They propose the use of the term "cloud monitoring" as an innovative approach which includes heterogeneous clustered field instrumentation, smart data acquisition protocols and sophisticated transmission technologies, as well as on-line processing routines and multiple levels alarm capabilities. Cloud monitoring also involves datawarehouse capacities with data redundancy and secured long-term interactive accessibility to data and metadata.

References

Bandara MS, Bhasin RK, Kjekstad O, Arambepola NMSI. Cost effective practices for landslide monitoring for early warning in selected countries in Asia

Pascal B, Emmanuelle K, Yves G, Thierry V. Cloud monitoring: an innovative approach for the prevention of landslide risks

Billedo EB, Bhasin RK, Kjekstad O, Arambepola NMSI. An appraisal on ongoing practices for landslide early warning systems in selected South and East Asian countries

Chae B, Choi J, Seo Y. An alternative method of landslide early warning by gradient of volumetric water content

Bhat DR, Bhandary NP, Yatabe R. Method of residual-state creep test to understand the creeping behavior of landslide soils

Tapete D, Casagli N, Fanti R. Radar interferometry for early stage warning on monuments at risk

Salciarini D, Tamagnini C, Ponziani F, Berni N. Defining physically-based rainfall thresholds for early warning systems

Ponziani F, Berni N, Stelluti M, Zauri R, Brocca L, Moramarco T, Salciarini D, Tamagnini C. Landwarn: an operative early warning system for landslides forecasting based on rainfall thresholds and soil moisture

Martelloni G, Segoni S, Fanti R, Catani F. An operational warning system for the forecasting of landslide occurrence at regional scale

Basile G, Panebianco M. Experimental alert modelling in hydrogeological risk and related procedures to activate civil protection systems: a real case study in Sicily

Towhata I, Uchimura T, Wang L, Qiao J. Validation and interpretation of monitored behavior of slopes vulnerable to failure

Gramani MF. Processes and risk scenarios identified during the emergency actions undertaken in the Vale do Itajai (Brazil) in 2008

Lazzari M, Piccarreta M, Capolongo D. Landslide triggering and local rainfall thresholds in Bradanic foredeep, Basilicata region (southern Italy)

Dell'Acqua N, Albanese V, Corazza A, Pagliara P, Casagli N, Moretti S, Proietti C, Lollino G, Guzzetti F, Guadagno F. Integration of technological development and civil protection activities during a landslide emergency phase

Ratto SM, Stevenin H, Navillod E, Cauduro M. Operational procedure for hydrogeological warning system in Aosta Valley

Bai S, Wang J, Glade T, Bell R, Thiebes B. Rainfall threshold analysis and integrated landslide susceptibility mapping: application to landslide management in Wudu, China

Jamaludin S, Hj Ali F. Review of some empirical methods to correlate rainfall and shallow landslide and applications in Malaysia

Fathani TF, Legono D, Rahardjo AP, Karnawati D, Prabowo I. Development of debris flow early warning system for volcanic rivers at Mt. Merapi area



An Appraisal on Ongoing Practices for Landslide Early Warning Systems in Selected South and East Asian Countries

Elmer B. Billedo, Rajinder K. Bhasin, Oddvar Kjekstad, and N.M.S.I. Arambepola

Abstract

It is widely acknowledged that Asia is the world's most disaster prone region, with nearly two-thirds of global disaster mortality and morbidity occurring within the region. The IPCC Working Group II noted that heavy precipitation events are very likely to increase in frequency and will augment the multi-hazard risk scenario in most of the countries. Extreme weather events, such as cloud bursts and heavy concentrated rainfall, especially in some parts of Asia, have been blamed for loss of life and property in the region. Landslides have been triggered during these events causing further casualties.

In consideration of the aforementioned events, the Asian Disaster Preparedness Center (ADPC) in collaboration with the Norwegian Geotechnical Institute (NGI) in Oslo, Norway is implementing a "Regional Project" on sharing best practices for early warning of landslides with participation from 11 countries. The project, which is financed by the government of Norway, includes the countries Bangladesh, Bhutan, China, India, Indonesia, Nepal, Pakistan, the Philippine, Sri Lanka, Thailand, and Vietnam.

This ongoing project aims to document, share, enhance and develop sound practices for early warning of landslides for sustainable development in affected areas. This is currently being achieved through gathering of data from existing approaches and through formation of joint working groups to identify critical factors and disseminate knowledge from participating countries.

This paper describes the current status of landslide early warning systems in the participating countries with emphasis on the identification of critical elements for an effective early warning approach.

Keywords

Landslides • Early warning • Best practices

Introduction

The Asian Disaster Preparedness Center (ADPC) and the Norwegian Geo-Technical Institute (NGI), in collaboration with the Ministry of Foreign Affairs of Norway, conceptualized an Asian program called the "Regional Capacity Enhancement for Landslide Impact Mitigation" (RECLAIM). The RECLAIM program was initiated in seven countries in South and East Asia. This has now been expanded to cover, at present, eleven (11) countries namely

E.B. Billedo (✉)
Mines and Geosciences Bureau, Quezon City 1101, Philippines
e-mail: docebb@hotmail.com

R.K. Bhasin • O. Kjekstad
Norwegian Geotechnical Institute, Norway

N.M.S.I. Arambepola
Asian Disaster Preparedness Center, Thailand

C. Margottini et al. (eds.), *Landslide Science and Practice*, Vol. 2,
DOI 10.1007/978-3-642-31445-2_75, © Springer-Verlag Berlin Heidelberg 2013

Bangladesh, Bhutan, China, India, Indonesia, Nepal, Pakistan, Philippines, Sri Lanka, Vietnam and Thailand.

The RECLAIM program is on its Phase III (thus the appellation RECLAIM III), having been implemented by the Urban Disaster Risk Management (UDRM) team of ADPC since early 2004. The main goal of the RECLAIM III project is to share, enhance and develop sound practices for early warning of landslides for sustainable development in areas affected by landslides. The negative impact of landslides is expected to increase, given the current environmental degradation worldwide. The situation in East and Southeast Asia is particularly alarming, as the number of storms/cyclones/tropical depressions per year and abnormal precipitation with high intensity level, both being preludes to landslide occurrence, is noted. As such, it is imperative that countries within the said region develop good practices for early warning of landslides.

This paper presents an appraisal on the ongoing practices for landslide early warning systems in selected South and East Asian countries.

Definition of a Good or Sound Practice for LS-EWS

A good or sound practice for landslide early warning should have the following components and/or mechanisms: regulatory framework or institutional mechanism and linkages; stakeholders involvement and public awareness; upgraded observation equipments and data communication facilities; numerical prediction capability using rainfall threshold limits; skilled human resource; and capacitating local community on response to disaster.

Community response plays an active role in Landslide-EWS. Programs on disaster awareness, mitigation and actual rescue operations should be established in the community.

Guidance by a Responsible Mandated Institution

In any risk reduction programme, it is important that a government institutionalizes Landslide -EWS as part of its mandate. Success stories relating to this aspect include those of China, Sri Lanka, Philippines, Thailand, Indonesia and Pakistan. In China, for instance, a practical landslide risk mitigation strategy was set up, from investigation, to landslide monitoring and to landslide preparedness (including installation of warning system) and slope stabilization. Such move resulted to far less casualties due to landslides, having been reduced to about half of the peak value in 1998. On the other hand, in the Philippines, the Congress has passed into law the Republic Act No. 10121 which aims to strengthen the Philippine Disaster Risk Reduction and Management System. Among the strategies being adopted under this law is to institutionalize the disaster risk programs and management from the local up to the national level and to integrate disaster risk reduction education into the school curricula, the youth council (locally called "Sangguniang Kabataan") program and the mandatory training program for the Public Sector Employees

Cost Effectiveness for Establishment and Continuity

The effectiveness of Landslide-EWS relies on its economic feasibility. Cheap monitoring tools and equipment are readily available in countries such as Thailand, Philippines and Sri Lanka.

Accuracy

The Landslide-EWS must provide accurate data which in turn is dependent on the economic feasibility as well as the availability of cheap monitoring tools and equipment in countries concerned (e.g., Thailand, Philippines and Sri Lanka).

Acceptability by Beneficiaries

The beneficiaries should be involved response planning including evacuation planning and provided with hands-on training in first aid and rescue operations. Upon doing so, they will be capacitated in terms enhancement of Knowledge on the technical and scientific explanations and know-how and skills in responding to events. The Landslide-EWS should form part of the local communities' social-economic programs.

Sustainability

Landslide Early warning system could use simple monitoring weather equipments (ex. Use of local and simple rain gauges) that can be easily maintained and sustained.

The sustainability of the Landslide -EWS should be based on the low maintenance costs and availability of funds. Budgets for disaster preparedness must be included in the annual work and financial plans and programs of each community, as has been practiced successfully in countries such as China, India, Indonesia, Pakistan, Philippines, Sri Lanka, and Thailand.

Programs Which Can be Qualified to be Sound Practices

The programs which could be included to be qualified as sound practices are: (1) landslide hazard mapping (ex. landslide mapping programs aimed at identifying communities or most vulnerable settlements) (2) geological and geotechnical data acquisition and/or monitoring; (3) weather and climate analysis and forecasting together with real time data acquiring mechanisms such as automated weather stations, locally, installation of several rain gauges to monitor thresholds should be in place or on a national level, satellite-based real-time monitoring weather stations; (4) warning dissemination- weather bureaus and other monitoring stations which posses efficient communication networks ; and lastly, (5) response and preparedness mechanisms in place at community level to respond to EW messages – this should include preparedness and response planning, Search and rescue (S&R), procedure for conducting simulations and drills periodically.

A number of countries have demonstrated sound practices for landslide preparedness. This includes China, where its Ministry of Land Resources (MLR) and Meteorological Administration (CMA) have implemented a real-time weather-based geohazards warning program since 2003 (Yin et al. 2010) (Fig. 1). Such program requires the CMA to provide rainfall data to MLR. The MLR, in turn, issues geo-hazards occurrence warning through the China Central Television CCTV.

In the Philippines, the Mines & Geosciences Bureau (MGB) – Department of Environment and Natural Resources (DENR) implemented its geohazards assessment and mapping programme. Crucial activities under this program include 1:50,000 scale and 1:10,000 scale landslide mapping, the conduct of Information, Education Campaign (IEC) throughout the country with the cooperation of local government units (LGUs) and the Office of Civil Defence, and the installation of landslide sign boards. Bilateral agreements (e.g., the READY project) have been arranged with foreign countries (e.g., Australia) for capacity building, and also to facilitate experience sharing in hazard mapping activities.

Member countries like Bhutan, Bangladesh, Indonesia, etc have already started their landslide mapping programs.

Department of Mineral Resources (DMR) of Thailand is the mandated institution in Thailand for landslide risk management and make great efforts to solve the landslide problem by launching many projects dealing landslide and flash floods. The aim of all projects is to decrease life lose number in each year.

DMR has already identified vulnerable villages to landslides through mapping. The DMR now maintains a network of volunteers in Landslide prone villages. All the local volunteers in the network have gone through the DMR training course to obtain knowledge on the landslide hazards, symptoms, rainfall monitoring, landslide warning etc. They are supposed to prepare a village landslide prevention and mitigation plan under supervision of DMR experts. Local knowledge is also integrated into the plan and the network members will follow the plan when heavy rainfall is approaching their respective areas. The village heads in vulnerable locations activate the plan in such situations and network volunteers in the village start vigilance on vulnerable slopes assigned to them as per the plan. They will monitor rainfall more frequently and provide warning to villages utilizing the following criteria (Table 1).

If the volunteers notify landslide symptoms such as rainfall higher than 150 m, tension cracks on slopes, rumble sound in the forest, water color change or appetence of springs etc, they will inform the head of village. The head of village will obtain permission from Tambon (Municipality) Administration Office (TAO) for warning and evacuation of villagers from vulnerable locations.

To support the network, DMR has established the Geohazards Operation Center (GOC) in the head office to monitor weather conditions especially heavy rain by using data from Thai Meteorological Department. GOC will inform the network volunteers about heavy rain in their respective area and inform the real time forecasts to the villages. GOC will also disseminate watch bulletin if heavy rain is longer than 3 h or rainstorm is approaching. In case of critical situation the center will inform the network volunteers the forecasts in advance via short mobile phone massages (SMS). After establishing the network in the villages, the landslide early warning system is running automatically and no need for outside help for landslide warning.

Several such initiatives have been taken in Sri Lanka by National Building Research Organization (NBRO) which is the mandated institution of the country for landslides studies and services. The NBRO operates under the Ministry of Disaster Management and implements a comprehensive programme funded by the government to manage the risk from landslides events. The Program includes activities such as hazard mapping (scale 1:10,000 at local government level and 1:50,000 at District level) for identification of most vulnerable settlements, Awareness creation, Early warning based on precipitation thresholds, response planning, and issuing landslide clearance reports for new constructions in landslide prone areas.

Landslide Hazard Zonation Mapping Project (LHMP) culminated as an aftermath to the Government Cabinet Paper 116 of 16th June 1986 and extended after the May 2003 catastrophic landslide and flood events as per the Cabinet Paper 03/1372/111/061 dated 17.07.2003. This

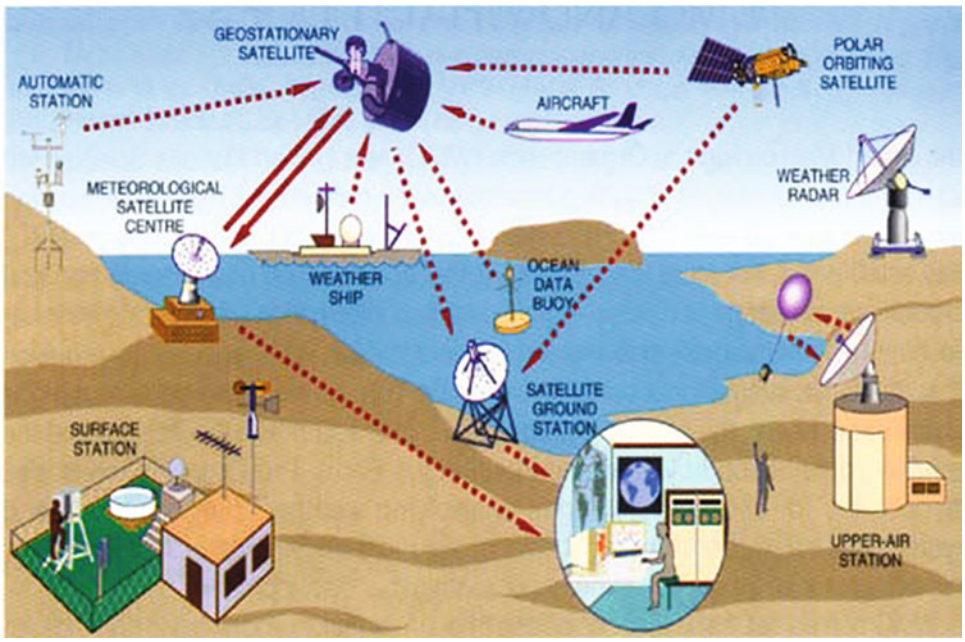


Fig. 1 The diagram shows the important components of EWS for hazard events (Adapted from "Landslide Early Warning and Forecasting in China" – National Meteorological Center (NMC), China Meteorological Administration (CMA), China)

Table 1 Warning criteria for landslide

Rainfall (mm)	Situation
0–50	Normal
50–100	Watch
100–150	Alert to evacuate
>150	Warning for evacuation

mapping programme cover ten landslide prone districts. Mapping in 05 districts have already been completed at the movement and the preparation of LHMPs of the other districts is underway (districs are shown in Fig. 2). NBRO also has developed a trained volunteer network for monitoring rainfall thresholds and mobilize their support for evacuation of people from vulnerable locations. They use simple instrumentation for monitoring of critical slopes for taking appropriate mesuers in davance.

Limitations and Challenges Pertaining to Landslide EW of Member Countries

Limitations of Existing Mandatory Agencies to Provide Necessary Assistance to Vulnerable Communities Living in Landslide-Prone Areas

Bangladesh – At present, there is no well-established landslide warning system (e.g., relating rainfall threshold value to landslide occurrence) in the country. Part of the problem lies on the lack of a network of meteorological and radar stations which could provide crucial data for landslide prediction. Comprehensive Disaster Managament programme has initiated a pilot project for landslid EW based on two highly vulnerable cities of Cox's Bazar and Tecknaf.

Bhutan – The pre-landslide activities/mapping is not a priority in the country. Although the Department of Geology and Mines is beginning to compile its landslide inventory map, it does not have the capacity to set up a community level landslide early warning systems, owing to the lack of manpower and scarce monitoring tools and equipment.

China – Although the country, through its Ministry of Land Resources, has had some significant achievements in its efforts to mitigate landslides, it still faces tremendous challenges particularly with regards to meteorological observation data applications, disaster monitoring, forecasting techniques and risk assessment among others. Strong cooperation and communication with other member countries (especially those affected by monsoonal rains) are necessary to address such limitations.

Indonesia – Despite the tremendous efforts made by concerned agencies in Indonesia, the country acknowledges that improvements still has to be made on the following: (1) Inclusion of hazard maps and risk zone maps in contingency planning; (2) Building of community awareness through training and need for simulations and drills related to hazard response to increase community participation in landslide preparedness ; (3) Increase capacity building of government officials and community through education and information dissemination; (4) Preparation of construction guideline and detail landslide risk maps for high hazard areas and; (5) Building good coordination amongst institutions related to landslide hazard risk management.

Nepal – Nepal still does not have any early warning system in place, despite the relatively large number of casualties brought about by landslides. Establishment of a

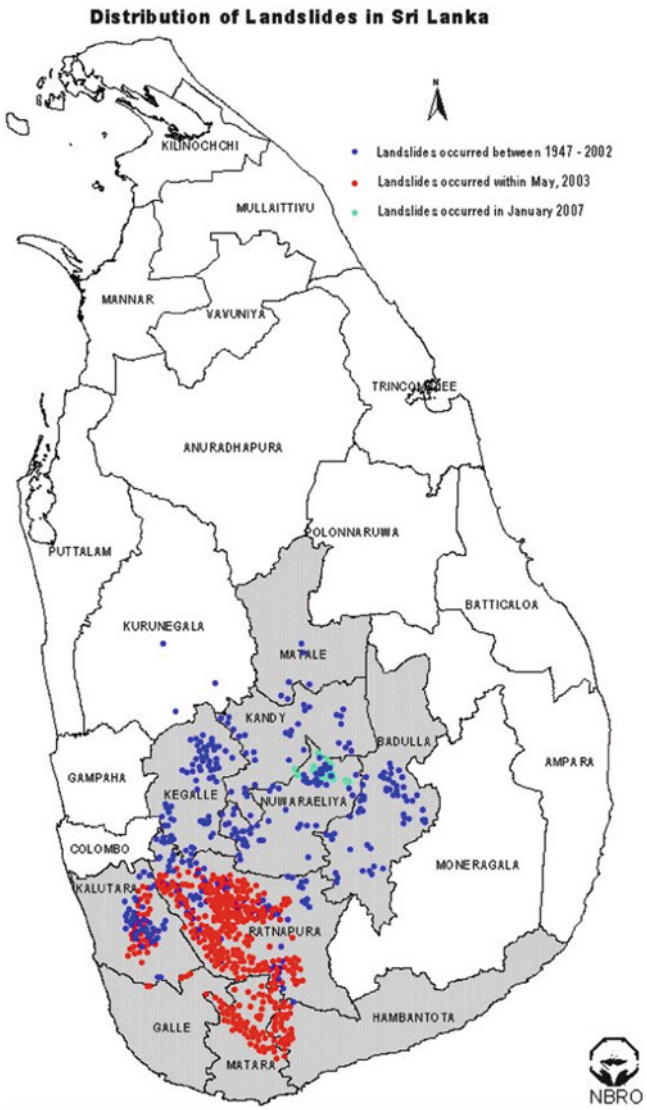


Fig. 2 Past landslide locations and the landslide prone districts of Sri Lanka

Landslide-EWS (including landslide and rainfall data correlation) is therefore a priority.

Philippines – The country, through the Mines & Geosciences Bureau (MGB) – Department of Environment and Natural Resources (DENR), has considerable set of accomplishments in its efforts to mitigate landslide risk. The landslide mapping being implemented recognizes generally the community-local knowledge on the subject. This starts with a detailed landslide hazards assessment being conducted by DENR-MGB with the community living in respective vulnerable slopes. An example of a completed 1:50,000 scale landslide maps are shown in Fig. 3. This is followed by the sharing of this information through provision of landslide threat advisories on areas that are highly susceptible to landslides. The communities are also being advised on the possible signs of an impending

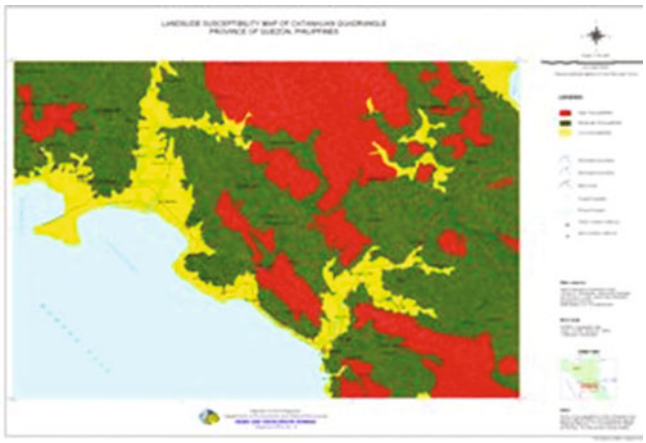


Fig. 3 Example of a Landslide susceptibility map published in the Philippines by the Mines & Geosciences Bureau

landslide and for them to consider particularly during the heavy rainfall.

On selected areas, DENR-MGB in collaboration with the local government units/communities and the local disaster risk reduction and management council is installing landslide warning sign boards in areas that are highly susceptible to landslides as part of their early warning system.

A crucial input, however, that is yet to be realized is the integration of geotechnical/engineering geological data in their assessment of landslide susceptibility. Training (especially that focused on landslide modeling) and capacity building are needed for this to be attained.

Pakistan – Mountain areas of Pakistan are vulnerable to landslides and wet and dry movements are very frequent phenomena. During the recent flood events as well as during last major earthquake disaster occurrence of massive landslide events have been observed. Geological survey of Pakistan in implementing a hazard mapping program but coverage is yet not sufficient for community level landslide early warning.

Sri Lanka – The primary agency that is involved in landslide mapping and assessment is the Landslide Studies and Services Division of the National Building Research Organization (NBRO) under the Ministry of Disaster Management. The scientists in the NBRO have a solid group geologist that regularly conducts hazard zonation mapping. However, Sri Lanka has to strengthen the current programme on landslide Instrumentation and Monitoring of critical slopes and development of Warning based on instrumentation technology in highly vulnerable urban areas (NRBO 1992). In addition they need to provide automatic rain gauges in more prone areas to augment the present rain gauge station network to strengthen the present EWS for landslides.

Vietnam – The country is yet to institutionalize geohazards assessment and mapping and consequently, to develop

warning and information system. Other activities (e.g., search and rescue capacity, dissemination and education programme, forecasting methods which also involve a close cooperation with neighboring countries) are to be enhanced.

Other Problems and Challenges

As much as disaster preparedness has been an utmost concern of the member countries (e.g., in Bangladesh, Nepal, the Philippines, Thailand and Vietnam), their aim to enhance and to capacitate their government agencies to implement disaster prevention and mitigation programs are often hampered by limitation and due to budgetary constraints. The lack of manpower and training opportunities have also contributed in the countries' efforts to improve their capabilities, including the creation of quick study teams and mobilization their support to vulnerable communities when there is a need.

In the landslide mitigation and preparedness programs itself, challenges are realized in relocating communities living in unstable slopes, not to mention the considerable efforts spent in convincing people to relocate or to heed the warning made by concerned government agencies. In view of this, it is crucial that a close cooperation with the community and an active participation of local or village officials are pursued for the successful implementation of the disaster preparedness and mitigation programs implemented in respective countries.

To demonstrate the effectiveness of landslide early warning, in the Philippines, the Mines & Geosciences Bureau- Department of Environment and Natural Resources (MGB-DENR) has embarked on simple approaches. The MGB-DENR endeavours to make the people in the vulnerable communities and other stakeholders actively involved in assessing their vulnerability in respective areas and in coming up with viable options to address the immediate concerns. Provision of direct advisories, warnings and community level meetings in critical areas/villages are held during or immediately after the conduct of the geohazard assessment. Province-wide geo-hazards seminar-workshops are being organized with the participation of all village representatives and local government officials as well as teachers from the primary and secondary level schools in respective areas. The workshops include training on landslide susceptibility map interpretation. MGB-DENR conduct lecture series on geohazards and land use management and planning, and distribute awareness materials on geo-hazards (e.g., posters, flyers, CDs) among the vulnerable communities and other stakeholders. Regular drills are also being held in most vulnerable communities, with the help and participation of other government agencies.

Institutionalization of Lanslide Disaster Preparedness Programmes in Partner Countries

Landslide Early Warning System Design Using Rainfall Thresholds

A review of available literature emphasizes the role of precipitation as an important control on the initiation of slope failures and provides evidence that landslides are often triggered by meteo-climatic events that are in excess of some thresholds. Therefore, it is indeed necessary to investigate the possibility of interpreting landslide events in terms of rainfall patterns immediately preceding a landslide event. This can be further enhanced by taking the geological formation into account.

Opportunities for Implementation of Pilot Projects

Considering that a number of approaches, which can otherwise be varied, are being adopted, it is essential that sharing of information (e.g., rainfall threshold value) and experiences (e.g., in information and education campaign) through regular consultative meeting (both within and outside the context of RECLAIM III project as proposed by ADPC) be made among the member countries for the initiation of Landslide-EWS.

Capacity Building (National to Local)

Capacity building for landslide disaster preparedness should be done from national down to the local level. Based on the experiences of member agencies (e.g., China, India, Pakistan, the Philippines and Thailand), the creation of awareness on all aspects of landslide risk management is essential involving community members as well as local government level officials, teachers, school children etc. They have to be involved in the conduct of geohazards mapping at various scales and the information and education campaign (IEC) should be made a component of all such geo-hazard mapping programs.

Another crucial factor following the geo-hazards mapping is preparation of hazard preparedness plans at community level including an assessment of evacuation

sites, particularly intended for the benefit of potential affected communities. Along with this information dissemination on the location of escape routes and evacuation sites is very essential. Sign boards pinpointing to the direction of these strategic areas should be displayed as a part of the "best practices" of an effective Landslide-EWS as what had been done in countries such as in China, India, the Philippines, Sri Lanka and Thailand.

As part of landslide disaster preparedness programmes, monitoring of critical slopes should be undertaken. In China, Sri Lanka and Thailand, automated rain gauges, sensors and other monitoring equipment are put in place in most critical slopes. To note, Sri Lanka has devised a simple, yet innovative way for landslide monitoring systems involving community members to monitor development of tension cracks on walls, on the ground so that community vigilance can be increased in prone areas. This includes community watching of symptoms of slow moving landslides of those such as tilted trees, as well as rapid moving slopes observations on the presence of slicken-sides on shear plans within the moved mass among others. China, on the other hand, has established a nationwide network for Landslide-EWS and is based on the information from Real-Time monitoring system (RTM). The RTM means that the landslide monitoring data is acquired remotely, and disseminated to vulnerable areas soon after such information is collected after analysis and assessment. The acquisition process is an automated system, requiring no on-site technicians.

Conclusions and Recommendations

Owing to its geographic and geologic setting, South and South-East Asian countries have had a bulk share of geohazards events, including landslides, which is documented worldwide. Through the efforts of the Asian Disaster Prepardness Center (ADPC) Thailand and Norwegian Geotechnical Institute (NGI), the RECLAIM III project was initiated aiming at sharing, enhancing and developing sound practices for early warning of landslides. For these to be realized, key components for effective landslide disaster preparedness must be promoted and for sustainability of such action the the patronage of the respective governments is essential. Based on the experiences and discussion made among the member countries, the essential componenets of EW can be generally categorized as follows: (a) Detection of critical slopes which involves data collection (e.g., slope conditions and rainfall data) and analysis as well as assessment and mapping of areas at risk; (b) Risk communication; entailing communicating the "risk" (results of risk assessment) to the affected community; and (c) Response planning including identification of evacuation and relocation sites and installation of monitoring/early warning devices and sign boards; (d) awaness creation which involves the conduct of information and education campaigns,conduct of drills,simulations at local levels etc.

A crucial aspect for the success and sustainability of any landslide disaster preparedness programme, however, is the institutionalization of activities related to such programme from the local to the national level. In line with this, establishement of mandated national level institutions for landslide risk management, inter-agency collaboration, development of close linkage between agencies involved in disaster management and local government units, and active participation of affected communities play a vital role among others. Information sharing through regular consultative meetings among the affected countries could provide significant inputs in improving the EW practice and this can be achived in establishing RECLAIM network as a newtwork of institutions involved in landslide disaster preparedness within Asia.

References

Alam MK, Hasan AKM, Khan MR, Whitney JW (1990) Geological map of Bangladesh. Geological Survey of Bangladesh, Dhaka

Bandara RMS (2008) Landslide early warning in Sri Lanka. Regional seminar on experience of geotechnical investigations and mitigation for landslides, Bangkok, 13–14 Oct 2008

Huat BBK, Jamaludin S (2005) Evaluation of slope assessment system in predicting landslides along roads underlain by granitic formation. 1. Faculty of Engineering, University Putra Malaysia, Malaysia; 2. Public Works Department, Malaysia

Coates DR (1981) Environmental geology. Wiley, New York

Cruden DM (1991) A simple definition of a landslide. Bull Int Assoc Eng Geol 43:27–29

Dai FC, Lee CF, Ngai YY (2002) Landslide risk assessment and management: an overview. Eng Geol 64:65–87

David S, Billedo E, Montero A, Beroya T (1999) Cherryhills landslide event of August 3, 1999. Geologists from the Mines & Geosciences Bureau. Int J Geol Soc Philippines

Ekram Ali RM, Khan MMH, Uddin MZ (2007) Preliminary report on the deadliest landslides of 11 June 2007 in and around Chittagong City Corporation Area, Chittagong, (unpublished)

Environmental Geology Division (2003) a. A manual of landslide geohazard prevention and list of landslide risk villages of the north region of Thailand (a), Department of Mineral Resources, Bangkok, Thailand, 113pp (in Thai)

Gerath R, Hungr O, van Dine D (1997) Terrain stability mapping in British Columbia. Resources Inventory Committee, Province of British Columbia. (http://srmwww.gov.bc.ca/risc/pubs/earthsci/terrain2)

Jotisankasa A, Vathananukij H (2008) Investigation of soil moisture characteristics of landslide-prone slopes in Thailand. In: International conference on management of landslide hazards in the Asia-Pacific region, Sendai, 11h–15 Nov 2008, 12pp

Karim MF, Ahmed S, Olsen HW (1990) Engineering geology of Chittagong City Bangladesh. Geological Survey of Bangladesh (unpublished)

Muminullah M (1974) Geology of Northern part of Chittagong District Bangladesh. Records of the Geological Survey of Bangladesh, vol 11, Part-3, Dhaka

National Building Research Organization (NRBO) Internal Publication (for restricted circulation) (1992) Complexities of landslide forecasting, Document no. 24, 1–11

National Building Research Organization (NRBO) Internal Publication (for restricted circulation) (1995) Landslide instrumentation – general consideration and measurement of landslide activity, Landslide Hazard Mapping Project, SRL 89/001, 1–93

Pioquinto WP, Caranto JA, Bayrante LF, Zarco M, Catane S (2009) Mitigating a deep seated landslide hazard – the case of 105 Mahiao slide area. Leyte Geothermal Production Field, Philippines

Republic Act 10121 (2010) An act strengthening the Philippine disaster risk reduction and management system, providing for the National disaster risk reduction and management framework and institutionalizing the National disaster risk reduction and management plan, appropriating funds therefor and for other purposes. Republic of the Philippines, Congress of the Philippines, 14th Congress, Third Regular Session, pp 1–29

Ringenbach JC (1992) La faille Philippine et les chaines en decrochment associes (centre et nord de Luzon): Evolution cenozoique et cinematiques des deformations quaternaires. These de doctorat: Univ de Nice, 316pp

Shuster SRL (1995) Reducing landslide risk in urban areas- experience in the United States. In: Cheng FY, Sheu MS (eds) Urban disaster mitigation – the role of engineering and technology. Elsevier, Burlington, pp 217–230

Soralump S, Chotikasathien W (2007) Integration of geotechnical engineering and rainfall data into landslide hazard map in Thailand. In: Proceedings of GEOTHAI'07 international conference on geology of Thailand: towards sustainable development and sufficiency economy, pp 125–131

Sri Lanka Urban Multi-Hazard Disaster Mitigation Project (SLUMDMP) (2003) Guidelines for construction in landslide prone areas, pp 1–22

Tantiwanit W (2005) Landslide risk area management. Environmental Geology Division, Department of Mineral Resources, 57pp

Tinnakorn T (2009) The best practices for landslide early warning system in Thailand. In: Proceedings of RECLAIM partner meeting

Yin Y, Wang H, Gao Y, Li X (2010) Real-time monitoring and early warning of landslides at relocated Wushan Town, the three gorges reservoir. In: Sassa K, Yueping Y (eds) China in early warning of landslides, Geological Publising House, Beijing



Examples of Cost Effective Practices for Landslide Monitoring for Early Warning in Developing Countries of Asia

R.M.S. Bandara, Rajinder K. Bhasin, Oddvar Kjekstad, and N.M.S.I. Arambepola

Abstract

In recent times landslides and mass movements have become widespread events, posing great problems and serious challenges to development process especially in mountainous areas of developing nations in Asia. They have increased both in frequency and intensity and have assumed catastrophic and disastrous proportions in number of countries such as China, Indonesia, Pakistan, Sri Lanka, causing extensive damage to life and property. Mass movements occur as a result of heavy precipitation or as a secondary hazard triggered by geological events such as earthquakes, volcanic eruptions etc. In addition to its triggering factors, increase in landslide occurrence has been associated with a combination of factors and several attributes such as geological, topographic, morpho-metric, climatic and anthropogenesis nature that directly or indirectly contribute to the phenomena of slope instability.

A review of available literature emphasizes the role of landslide monitoring as an important controlling factor if the observation of initiation of slope failures can be introduced as a preparedness measure. Landslides are often triggered in areas with past landslide history and monitoring of landslides using community based approaches is considered as an effective measure for limiting the damages from landslides. In most areas development activities seems to be responsible for reactivation of dormant landslides. Hence communities living in areas with landslide history should be warned in time through constant monitoring and early warning of potential reactivation. In addition, slow moving slides on hill slopes need constant monitoring as many of developing countries in Asia cannot afford to undertake mitigation measures or to resettle people to safer areas after identification of the potential threat.

Realizing the importance of recording sound and cost effective practices of landslide monitoring for early warning, the Asian Disaster Preparedness Center (ADPC) in collaboration with the Norwegian Geotechnical Institute (NGI), Norway is implementing a "Regional Programme (RECLAIM)" for documenting and sharing good practices for early warning of landslides with the participation of mandated national institutions for landslide related activities from Bangladesh, Bhutan, China, India, Indonesia, Nepal,

R.M.S. Bandara (✉)
National Building Research Organization, 99/1, Jawatthe Road,
Colombo 5, Sri Lanka
e-mail: senarath_bndr@yahoo.com

R.K. Bhasin • O. Kjekstad
Norwegian Geotechnical Institute, Oslo, Norway
e-mail: rajinder.kumar.bhasin@ngi.no; oddvar.kjekstad@ngi.no

N.M.S.I. Arambepola
Asian Disaster Preparedness Center, SM Tower, 24th Floor 979/69
Paholyothin Road, Samsen Nai Phayathai, Bangkok 10400, Thailand

C. Margottini et al. (eds.), *Landslide Science and Practice*, Vol. 2,
DOI 10.1007/978-3-642-31445-2_76, © Springer-Verlag Berlin Heidelberg 2013

Pakistan, Philippines, Sri Lanka, Thailand, and Vietnam. The Programme receives financial assistance from the government of Norway. This paper presents some of the examples of landslide monitoring initiatives from Sri Lanka implemented by the project partner National Building Research Organization (NBRO).

Keywords
Landslide instrumentation • Monitoring of landslides • Community ownership

Introduction

Landslides are extremely complex phenomena, governed by a multitude of factors. Due to the same reason, predicting landslide movement is difficult and a wide gap exists between predictions and the actual field performance. In many cases it is difficult to convince the communities living in landslide prone areas to resettle in to a safe place due to various reasons. If they are not ready to move away from a vulnerable location the only options available are either implementing a mitigation program which can increase the stability of slope or execute a program of instrumentation which can help in monitoring the movements. If we as scientists cannot build the confidence of vulnerable communities on the reliability of performance of both options it will be difficult to implement such options. There are records of both failures and successes in both options. Due to high expenditure involved in mitigation solutions, vulnerable communities cannot afford to undertake mitigation measures. Therefore, there is a clear need for executing an elaborate, carefully planned, and conscientiously executed program of instrumentation in landslide prone areas. It is necessary to include sufficient investigations and field observations in the program to come with the diagnostics of the factors responsible for the trigger and then carefully execute it.

Instrumentation involves a chain of operations such as selection of type, number and location of instruments, purchase, transportation, calibration, installation, monitoring and maintenance, data processing and reporting. The cost effectiveness, simplicity, reliability of the system and developing a mechanism of monitoring are equally important in the same way as the selection of right kind of instruments and locating it in a right place. Community involvement in the chain of actions mentioned above is important to build the confidence of beneficiary communities and also to build ownership of the above system.

Causative Factors Observed in the Region

The phenomena of landslides depend on the interplay of diverse factors such as geology, geomorphology, ground water dynamics, and change of weather conditions including rainfall. Most significant among factors is the way slopes are exploited, for a great variety of purposes, some time in tune and most of the time hopelessly out of tune with the nature, in the name of development. Such factors operate within and across the time space. It is no wonder therefore that slopes which stood safe for centuries are unsafe today and those which are safe today might not remain so safe even tomorrow or the day after, not to speak of centuries (Bandari 1984). The global climate change also creates extreme events of precipitation, more inconsistent and intense, which has not been witnessed so often in the recent history. Out of all, the human interventions can be controlled though it may be difficult in developing Asian countries. The dominance of natural forces and variation of weather conditions in a combination will become always a challenge for landslide professionals as these are the key factors to consider in providing reliable forecasts.

Why Monitoring of Slope Movement Is Significant?

The communities living in landslide prone areas have difficulties to conceptualize why only certain slopes fail when safe and unsafe slopes are subjected to similar conditions. They continue to live in landslide prone areas with the assumption that slopes which did not fail for a considerable time in the past will never fail. It has been experienced that in certain cases the communities build houses adjacent to a cutting or creates a high cutting just behind the house and they have a perception that the slope will not fail.

Landslide professionals face difficulties in forecasting the instability to the extent to define the moment of failure. They do not have a hold on factors controlling the stability due to lack of reliable information and the resources to obtain such information. It is not easy to understand the moves of nature as it is triggered due to chain of events and underlying factors. Usually several simplifying assumptions can be made in forecasting as well extrapolation of the past events. A study of factors associated with forecasting is useful. Since many of the options available to us for forecasting landslide accurately cannot guarantee the safety of communities living

in areas already known to be landslide prone, there is a need to have instrumentation and monitoring as a measure for observing the movement so that at a critical juncture we should be able to evacuate the affected people. The results of monitoring, if it shows a clear movement, can also be used for undertaking necessary slope stabilization measures in order to reduce the impacts eventually.

The Objectives of Monitoring of Slopes

The uncertainties associated with various factors make the precise prediction of the behavior of a slope a difficult task. In the same way the possibility of a slope having marginal safety to become unstable is high in areas known to be landslide prone. In both cases monitoring can help in detecting the changes and the state of stability or instability so as to serve as a premonition against the incipient slope failure.

As per the landslide instrumentation handbook developed by NBRO under UNDP Project Landslide Hazard mapping SLR/89/001 Instrumentation usually helps in

- Determining the in-situ state of stress and pore water pressure within a slope or a sliding mass, for figuring out initial ground conditions at any point of time
- Elucidation of death and shape of the surface of sliding for an old landslide
- Establishment of boundaries of most probable plane of sliding for an incipient one
- Monitoring the behavior of an existing structure-foundation-slope system or of an unstable slope itself, with a view to evaluating the need or otherwise of control measures. (When the need is established instrumentation, inter alia, aids planning of control measures and evaluation of the efficacy and assessing the risk potential at every stage)
- Measuring surface and sub-slope lateral and vertical movements, which may usually fall in a very wide band
- Serve as evidence for law suits

Factors Governing the Choice

The selection of the scheme of instrumentation should be done carefully to fulfill the purpose for which the monitoring has been designed. Possibility to obtain range of measurements within a specified response time is an important factor to be considered in designing monitoring systems for landslides. In developing countries cost factor is a very significant challenge to be addressed unless there is an opportunity for external donor assistance. In addition, low installation skills, problems of upkeep and maintenance, capacity building of professionals to be able to design, obtain readings, analysis of data etc. are other key problems. Often due to those factors the developing countries are used to design systems optimizing the cost factor not to compromise too much with accuracy of data that will be used in analysis.



Fig. 1 Landslide at Munwatta, Walapane – Jan 2007



Fig. 2 Landslide at Beragala – 2008

Recent Landslide Events and Impacts in Sri Lanka and Role of NBRO

Sri Lanka is one of the partner countries of RECLAIM, where landslides are a recurrent problem. The central region of Sri Lanka is hilly and mountainous with highly fractured and folded basement rock overlain by residual soil and colluvium. Ten administrative districts out of 23 have been identified as Landslide prone areas. Those are Badulla, Nuwara-Eliya, Rathnapura, Kegalle, Kandy, Matale, Matara, Galle, Hambanthota and Kaluthara which cover more than

Table 1 The landslides reported in Sri Lanka during November 2010 to January 2011

District	Type of landslides					
	Debris-flows	Cutting failures	Rock-fall	Earth-flows	Others	Total
Nuwara Eliya	23	7	2	3	2	27
Matale	11	3	9	1	6	30
Badulla	16	4	0	0	1	21
Kandy	17	12	2	9	1	50
Kegalle	8	7	0	0	1	16
Total	75	43	13	13	10	154

20,000 km^2 of land area. Most of the landslides reported in Sri Lanka are debris flows, rock falls and cutting failures and occur annually in the central highland of the country (some samples are given in Figs. 1 and 2). Most of them are triggered by the heavy and intense precipitation. The escalation in number and severity in the recent years can be attributed to urbanization, population growth as well as to the global climate change. Major Landslides which have occurred during the past two decades have caused loss of around thousands deaths and about 175,000 people have become homeless.

During the last N-E Monsoon season from November to 2010 to February 2011, around 150 landslide events have been reported (Please see Table 1) from above districts.

Few Pilot Initiatives for Monitoring of Landslides from Sri Lanka

The National Building Research Organization (NBRO) is the mandated institution for landslide studies and services in Sri Lanka. NBRO carries out number of programs aiming at landslide risk management in hill country districts of the country. NBRO considers landslide monitoring as an important controlling mechanism as the regular observations on the initiation of slope failures can help to design measurers for reducing the impacts and losses. Like many other developing countries in Asia, Sri Lanka cannot afford to undertake mitigation measures in all cases of reported slope movement. Resettlement of people to safer areas after identification of the potential threat cannot be effective due to various reasons. Therefore landslide monitoring, emergency response planning, awareness creation etc. are taken as alternative short term measures for minimizing the risk in areas known to be landslide prone. Although monitoring cannot reduce material losses and damages to property, it has helped to reduce the death toll to a considerable level in recent years.

Landslide Hazard Zonation Mapping Program

Landslide Hazard Zonation mapping was initiated in Sri Lanka by NBRO after catastrophic landslide events in 1986 with technical and financial assistance from UNDP. The Programme extended after escalation of events in May 2003 through the Government funding. The mapping programme covers ten landslide prone districts of Nuwara eliya, Badulla, Kandy, Matale, Kegalle, Ratnapura, Kalutara, Matara, Galle, and Hambantota. Landslide Hazard Zonation maps of 07 districts have already been completed and maps of the other districts are being prepared in the scales of 1:10000 and 1:50000 (Fig. 3).

Early Warning in Landslide Prone Areas

Almost all Sri Lankan landslides that have been investigated to date are known to be rain induced. Therefore "Early Warning System" needs to be developed using the threshold limits of precipitation based on the data of past historic events. NBRO has developed landslide monitoring schemes for areas with landslide hazard to monitor

(a) Possible re-activation of old landslides or development of new landslides in areas identified as landslide prone
(b) Occurrences of fresh landslides in areas without any significant previous landslide history or without any early symptoms.

After critical evaluation of signs of potential landslide occurrence verified with the landslide zonation maps, NBRO has established early warning systems to cover most critical and vulnerable areas and provides following type of warnings during monsoon periods.

Warning Part 1 (Alert) – 75 mm rainfall for 24 h – Alert for Landslides

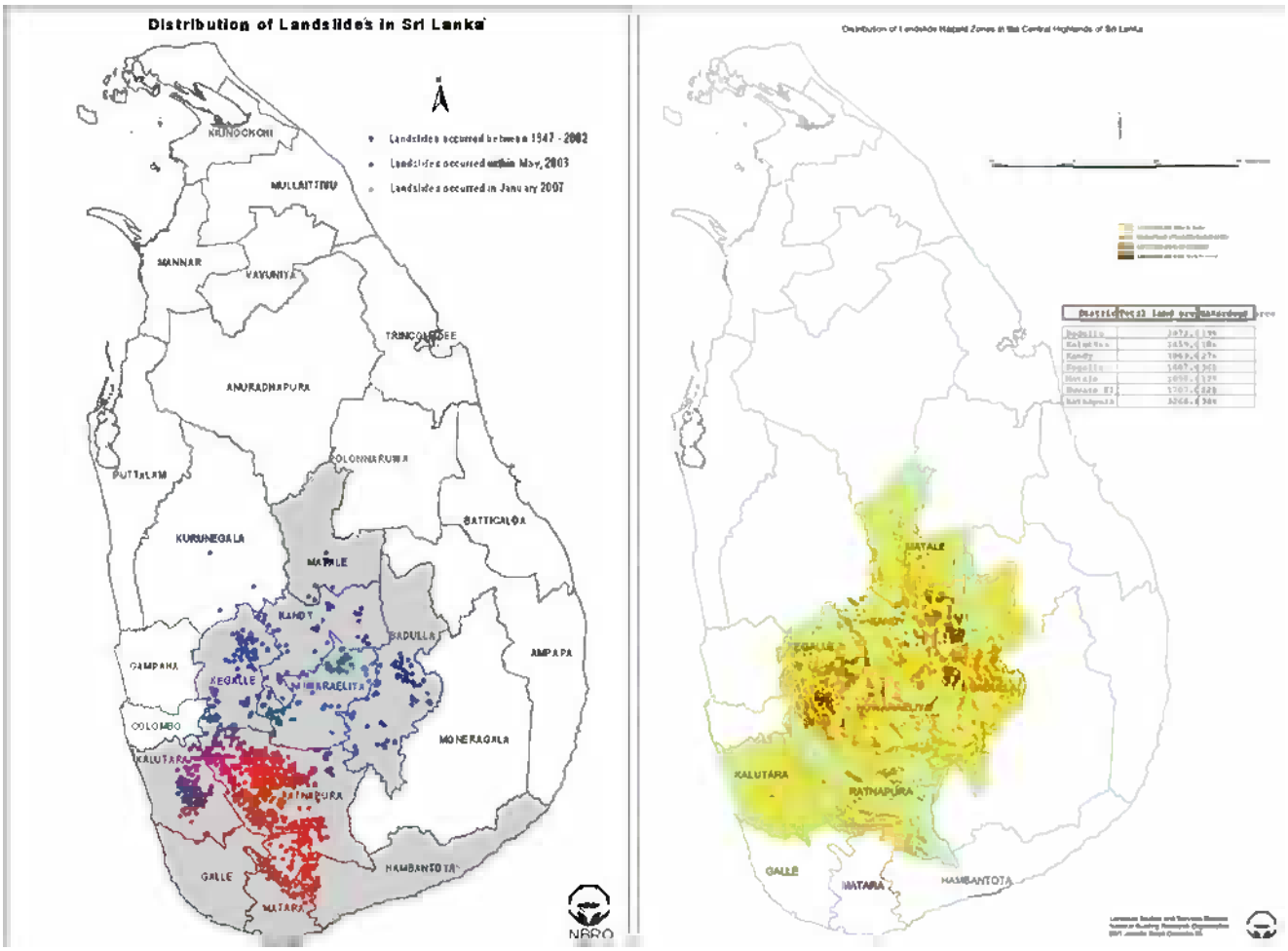


Fig. 3 Past landslide locations and the landslide prone districts of Sri Lanka

Warning Part 2 (Warning) – 100 mm rainfall for 24 h – Get ready for evacuation, under short notice

Warning Part 3 (Evacuation) – 150 mm rainfall for 24 h – Evacuation or 70 mm rainfall per hour – Warning for evacuation

In order to increase the effectiveness, NBRO conducts regular community awareness programs. In addition, critical locations and most vulnerable communities are provided with landslide monitoring schemes to facilitate monitoring of slope movements. The instrumentation selected in monitoring the slopes is a combination of simple techniques and sophisticated measures depending on the circumstances considering the cost effectiveness and possibility for involvement of trained man-power. Some of such cost effective practices for landslide monitoring are briefly explained below.

Locally Developed Crack Monitoring Gauges

In landslide prone areas, usual indication of movement is reflected from the cracks appearing in buildings and such cracks develop rapidly and extend in length. Since such tension cracks can be developed due to various other reasons too, the community members have to find a way to identify the cracks on houses which are connected with landslide movement and settlements. Such cracks are usually found on walls and the floor of houses. Crack monitoring inside houses is essential in giving warnings against potential failures and community members are themselves trained to monitor crack developments. The crack-gauge developed by NBRO as a monitoring device can measure extension of tension cracks, progress of development on the walls of the

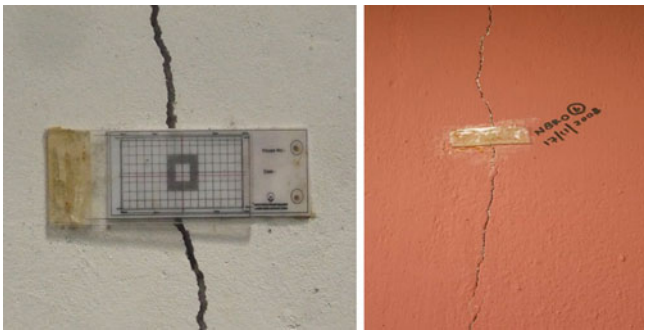


Fig. 4 Locally developed crack monitoring gauges for monitoring cracks on walls

house in active landslide as given in Figs. 4 and 5. It has confirmed its reliability for measuring displacements. The instruments can be easily installed and require minimum maintenance and are reasonably priced.

Measurements with Reference Survey Grids

For delineating the slide boundaries, and for following the growth of area involved in landslide movement, grid surveys offer a simple and rather inexpensive approach. The pattern of movement, the area and extent of bulge and subsidence, development of scars, ground cracks and seepage, and the successive locations of surface landmarks with the passage of time can all be found by simple surveying operations. In the process, well established old trees, rocky outcrops etc. do serve as targets of reference. The vector sum of the components of slope movement enables estimates of the magnitude and direction of the actual movement.

Figure 6a, b, c shows one of such monitoring schemes set up by NBRO where the simple pegs are used for measurement of movement with the Electronic Distance Meter (EDM). Several grid lines have been laid out falling within the slide to take measurements. The grid lines are perpendicular to one another and oriented in such a way that the grid line is perpendicular to the direction of slope movement. The reference line is located outside the sliding area. The pegs have been placed on a grid to indicate the movement horizontally and vertically. The surface movements in most parts of the earth slide were found to fall in tune with the rainfall measurements.



Fig. 5 Use of two nails to measure the movement of the concrete road located on a landslide

Use of Extensometers

Wire extensometers are useful for monitoring large movements. Substantial movements generally occur before a failure. The movement of any soil mass is measured using a simple device developed by connecting a wire to wire. This is shown in Fig. 7 below.

Monitoring Tension Cracks Using Crack Gauges

The land slides are often identified by the resulting cracks and bulges in the slope. The mapping of landslides always involves a full survey of tension cracks on the ground as well as survey of bulging mass. When such cracks are obscured by vegetation, these cracks need to be uncovered and their width and the vertical shifts are to be recorded. The behavior of the slide whether a landslide is accelerating or it is slowing down would be seen from the movement of pegs set up along the slide as shown in Fig. 8. The measurements consist of recording the changes of width and extent of cracks and noting down the change of elevations across the cracks (Fig. 9).

Lessons Learned

Experiences from monitoring for early warning of landslides in some developing countries of Asia indicate that simple and cost effective instruments, which can be easily installed and maintained by local people, are highly useful for predicting the behavior of landslides. There may be number of alternative instruments types competing with one another

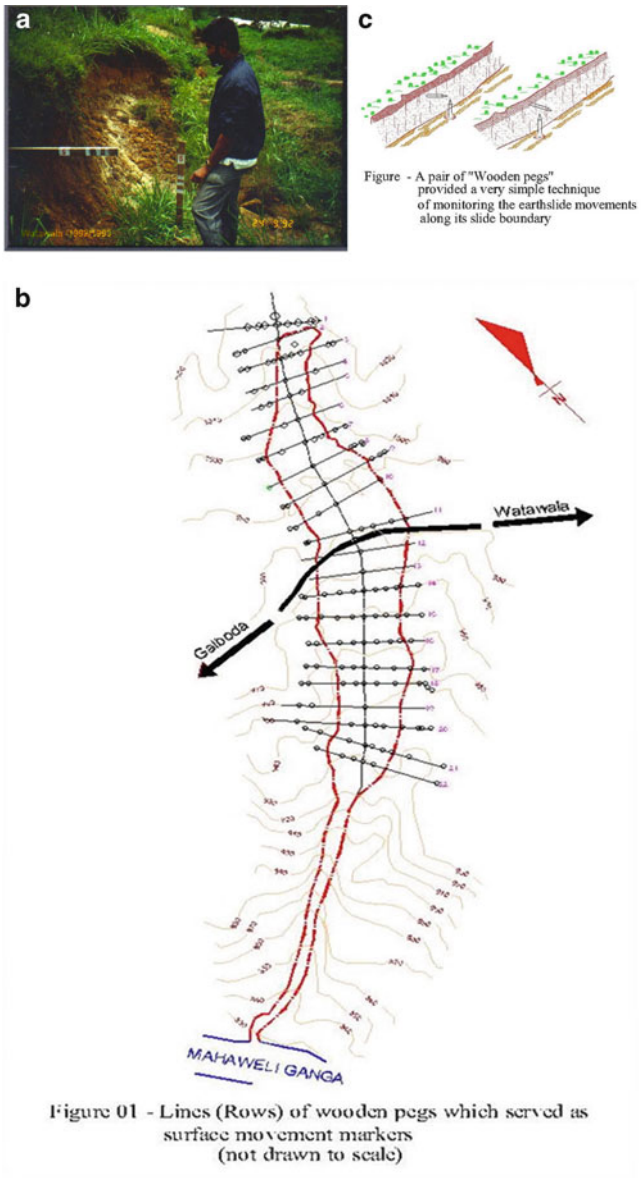


Fig. 6 (**a**, **b**, **c**) Example for measurements with reference Survey grids

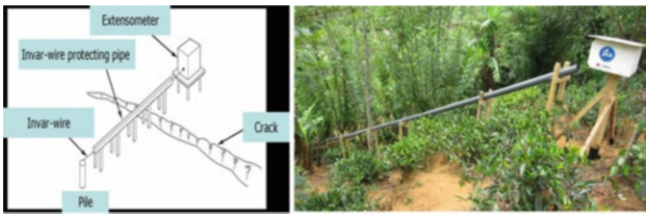


Fig. 7 Extensor meters with wire (Some of the extensor meter measurements against rainfall measurements in Mahaoya site is given in Fig. 9)

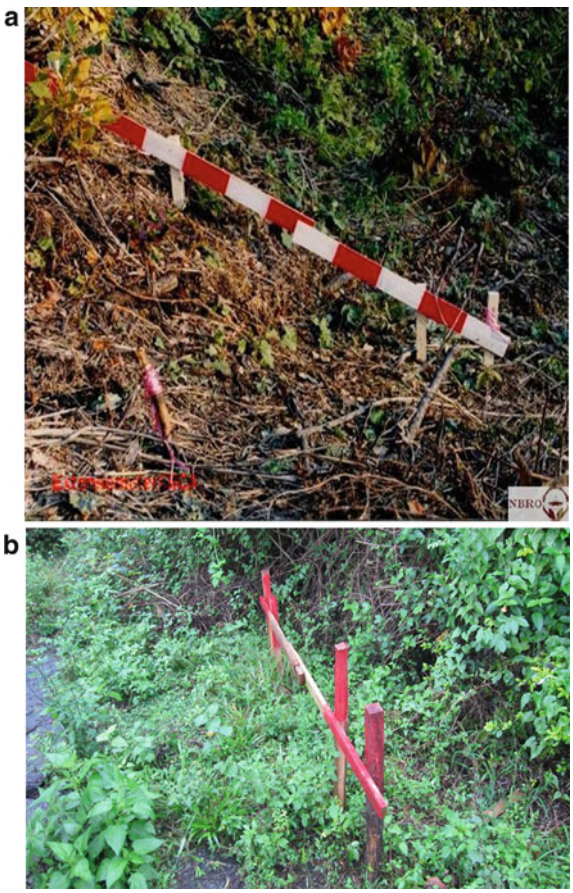


Fig. 8 (**a**, **b**) Wooden pegs used in monitoring the slope behavior at Mahaoya site

to meet specific demands. However, attempts of higher orders of accuracy generally require higher cost, higher handling skills and higher maintenance. In situations where measurement levels are extremely low and the phenomena are short lived, transient, intermittent or highly time dependent, there exists no substitute for sophistication and automation.

Similarly, if simple instruments may serve the purpose, there is no justification for sophistication as one is then faced with the problem of what to do with the precision data faced with semi empirical tools of design and attendant uncertainties.

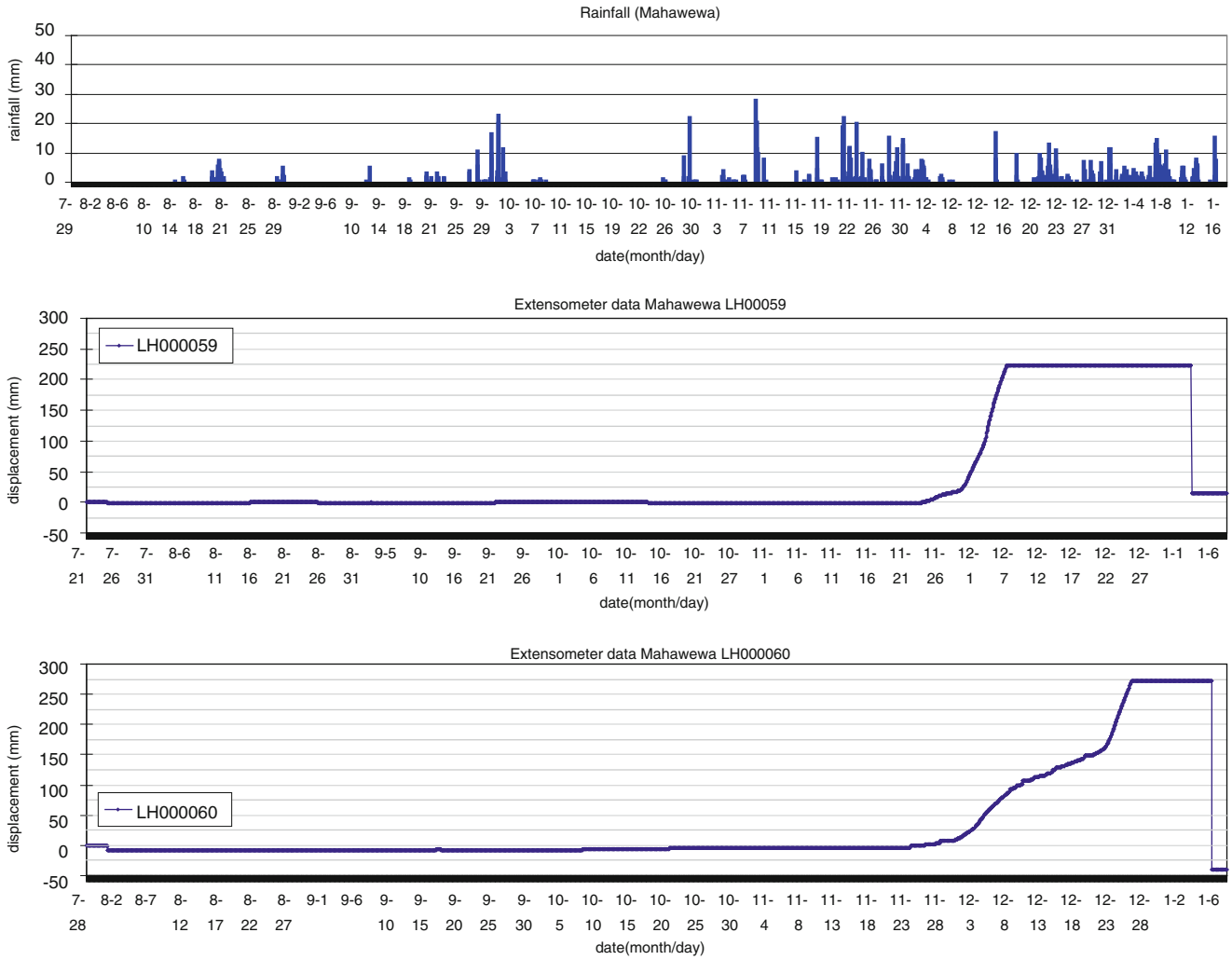


Fig. 9 Extensometer changes with the rainfall variation at Mahawewa from July 2010 to January 2011, NBRO – JICA study

Acknowledgments The authors would like to express their gratitude to the management of National Building Research Organization (NBRO) and funding agencies such as UNDP, JICA etc. for granting permission to use data related to landslide monitoring activities in Sri Lanka for this paper.

Reference

Bandari RK (1984) A state-of-the-art report on simple & economical instrumentation and warning systems for landslides and other mass movements. In: Proceedings of the fourth international symposium on landslides, Totento, 16–21 Sep 1984



Validation and Interpretation of Monitored Behavior of Slopes Vulnerable to Failure

Taro Uchimura, Ikuo Towhata, Lin Wang, and Jianping Qiao

Abstract

Monitoring and early warning is one of the most promising ways toward reduction of disasters induced by landslides and slope instabilities. Although less costly than construction of retaining walls and other mechanical measures, early warning has several problems to be overcome. First, it is often the case that the exact location of an unstable soil mass is not defined and hence the location of monitoring sensors cannot be decided. This problem can be solved by installing many low-cost sensors within a possibly unstable slope. The second problem concerns what information of slope should be monitored. The present study has developed a low-cost MEM sensor unit that can monitor slope deformation during heavy rainfall. A wireless network collects signals from the sensors periodically and helps the local government issuing an alert signal or emergency evacuation order, depending upon the progress of tilting. It is further important that the low cost of the sensors allow individuals to purchase personally and installs them in order to protect themselves from slope disasters. The developed equipments have been deployed in several slopes in the recent times for validation of their field performances. The present text reviews the obtained records and discusses their use for practice.

Keywords

Slope failure • Monitoring • Early warning • Tilt sensors

Introduction: Proposed Wireless Monitoring System

The authors have proposed an early warning system for slope disasters, as one of feasible countermeasures for small-scale slope disasters (Towhata et al. 2005; Uchimura et al. 2010). The system watches the behaviours of subsoil at minimum number of points on a slope with inexpensive and sophisticated sensors, and the data is transferred through wireless network. Thus, the system is low-cost and simple enough so that the residents in hazardous areas can use it to protect themselves from slope disasters.

It is reported from model tests that gradual displacement and high saturation ratio (80–90 %) are observed at the toe of model slopes before failure (Orense et al. 2003, 2004). Ochiai et al. (2004) also reported gradual and accelerating displacement on a slope surface observed before failure in an artificial rainfall-induced landslide test conducted at Mt. Kaba-san, Tsukuba City, Japan. Thus, it is useful to monitor the displacement and the water contents on the slope for early warning of landslides.

Figure 1 shows the basic concept of the wireless monitoring and early warning system proposed by the authors. A group of low-cost and simple sensor units (Fig. 2) are placed on the slope. The system is designed to be wireless, that is,

T. Uchimura (✉) • I. Towhata
Department of Civil Engineering, University of Tokyo, Hongo 7-3-1, Tokyo, Bunkyo-ku, Japan
e-mail: uchimura@civil.t.u-tokyo.ac.jp

L. Wang
Chuo Kaihatsu Corporation, Tokyo, Japan

J. Qiao
Institute of Mountain Hazards and Environment, Chengdu, China

C. Margottini et al. (eds.), *Landslide Science and Practice*, Vol. 2,
DOI 10.1007/978-3-642-31445-2_77, © Springer-Verlag Berlin Heidelberg 2013

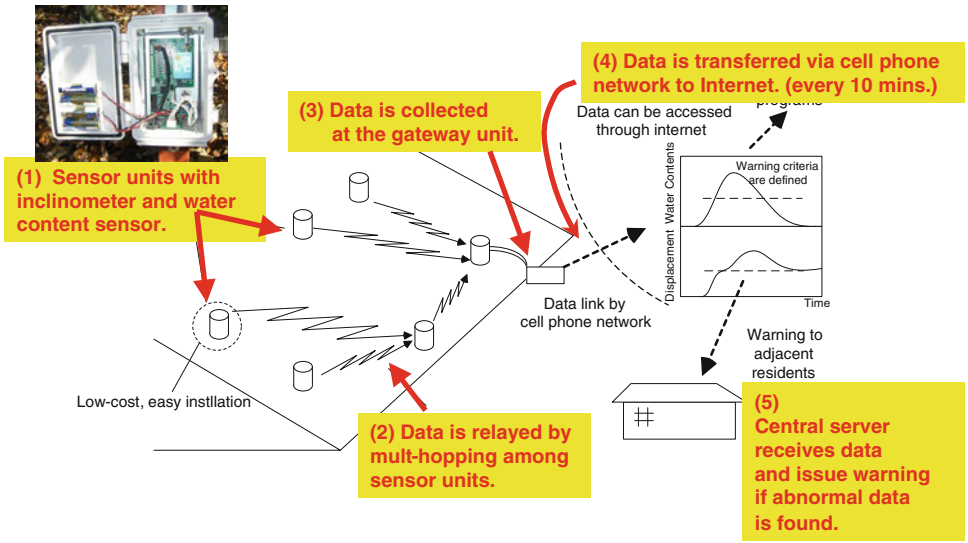


Fig. 1 Outline of wireless monitoring and early warning system for slope failure

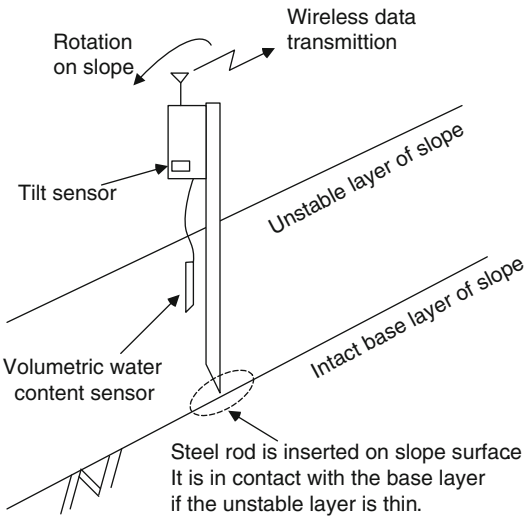


Fig. 2 Wireless sensor unit with tilt and water content sensors on a slope

each unit works autonomously with micro computer with independent power supply by batteries or solar cells. The sensor units measure the condition of the slope periodically, every 10 min for example. The data is transferred to a gateway unit, which is also placed near the slope, by using low power radio communication modules. Its communication distance is 300 m under typical conditions in the field. The gateway unit collects the data from all the sensor units, and sends them to a data server on internet through a cell phone network. Thus, the data can be browsed anywhere and anytime on Web site. The data is processed by the server, and any abnormal behaviour of the slope can be detected as a precaution of failure, and then warning is issued. Each sensor unit works for duration of more than 1 year with 4 AA Alkaline batteries.

The proposed system watches the rotation on the slope surface and the volumetric water content in the slope. A MEMS tilt sensor (nominal resolution = 0.04 mm/m = 0.0025°) is installed in each sensor unit. At each monitored point, a steel rod is installed through the thickness of unstable soil layer on the slope surface. If the unstable layer is too thick, the rod is installed for 50–100 cm-deep. Then, the wireless sensor unit is attached at the top of the rod. Consequently, the tilt sensor detects the average shear deformation of the slope surface layer as the deformation of the slope. Extensometer is commonly used for monitoring the displacement of slopes, but the advantage of using tilt sensor is that a long wire of an extensometer is not required, and therefore, the installation and maintenance is simple and inexpensive.

The water content is measured at a shallow position (typically 30 cm-deep) of slope by using a volumetric water contents sensor. This sensor measures the dielectric constant of the surrounding soil, which corresponds to the water contents. The soil mechanics theories say that the slope stability directly depends on the suction, or pore water pressure, rather than water content. But, measurement of suction of unsaturated soils is usually difficult, and careful maintenance of the sensors is required. Therefore, use of volumetric water content sensors is more suitable for low-cost monitoring.

Monitoring of a Slope Failure Site During Remedy Work

Prototypes of the developed monitoring system have been deployed at various sites by the authors. One of them, a slope failure site along a highway, is shown in Fig. 3. This slope consists of strongly weathered granite, and it was failed due to a heavy rainfall in July of 2009. The slope was excavated to have a gradient of 45° for remedy work, and was

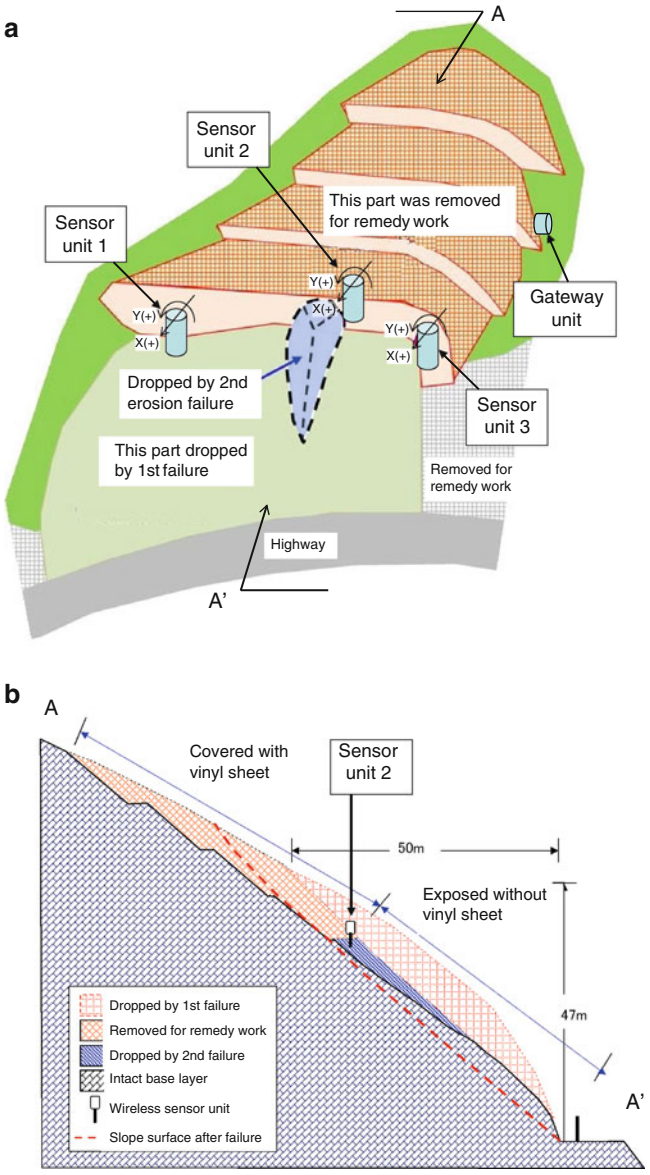


Fig. 3 (**a**) Sketch of failed slope along highway and arrangement of deployed sensor unit; (**b**) cross-section of the slope including the second failure part

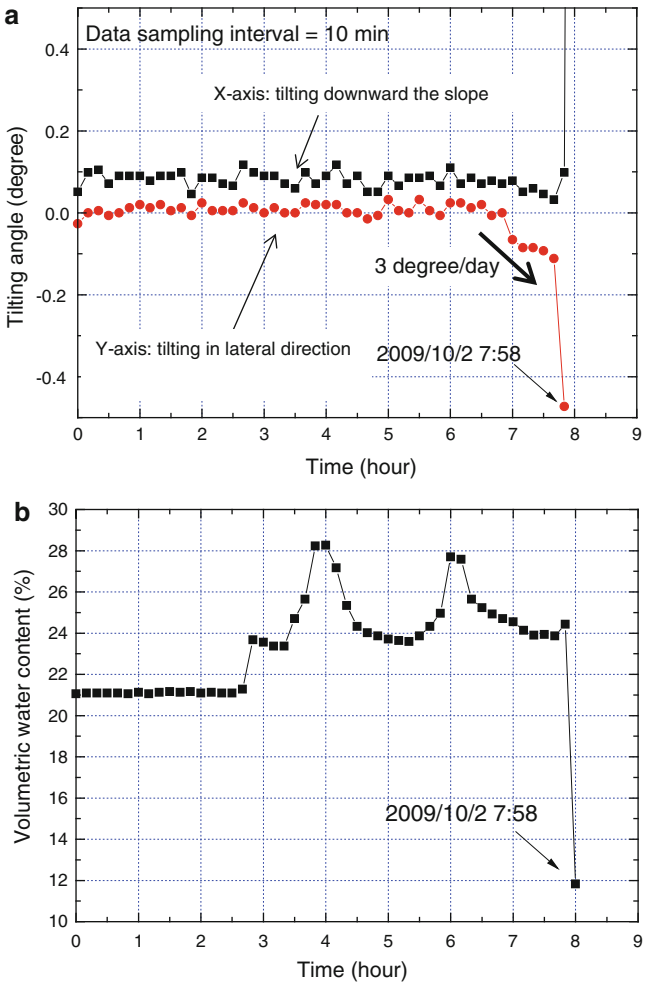


Fig. 4 Tilting angle and volumetric water content obtained by sensor unit 2 on the slope site along highway just before the second failure

monitored with three sensor units. After 2 months during the remedy work, another heavy rainfall caused a second failure, and a local part of slope including the sensor unit fallen down. As this second failure took place adjacent to the location of the sensor unit 2, the behaviours of the slope before and after the failure was detected by the monitoring system. The site manager got aware of the extraordinary behaviours of the data from sensor unit 2, and he stopped the remedy work and the highway service successfully.

Figure 4a shows the records of tilt sensor of the unit, in directions toward and lateral to the slope, respectively. Specially, the tilting in Y-axis (lateral direction) showed extraordinary behaviours 50 min before the second failure. Its tilting rate was around 3° per day (0.12° per hour). Figure 3a also shows the directions of the sensor units. The negative changes in Y-axis mean that the sensor unit 2 tilted in the backward direction to the second failure part. It suggests a failure mode with a slip surface in the slope.

Figure 4b shows the behaviours of volumetric water contents at the unit. The slope did not failed when the water content recorded its peak value, but it failed after 2 h of drainage stage. This may be because the distribution of water in a slope is quite non-uniform, and the measured value of volumetric water content depends on the position of the sensor. Thus, it is difficult to detect a precaution of slope failure only watching the water content.

Considering the data obtained from the slope mentioned herein, the followings issues are concluded:

(a) Monitoring of tilting (rotation) on slope surface is effective to detect the precaution of failure preceding by 30 min or more;

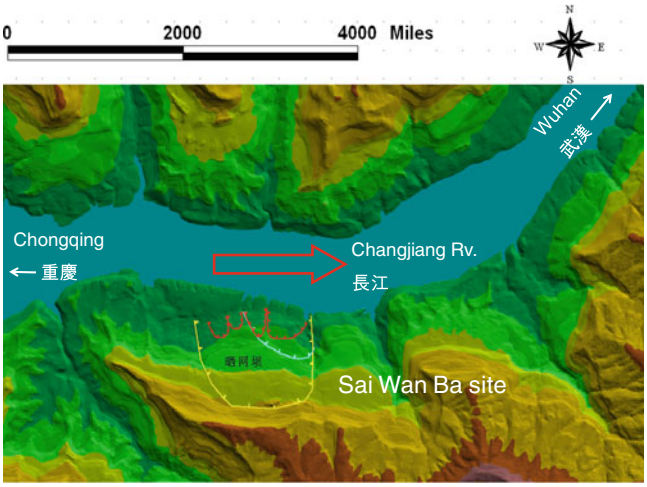


Fig. 5 Location of Sai Wan Ba landslide site

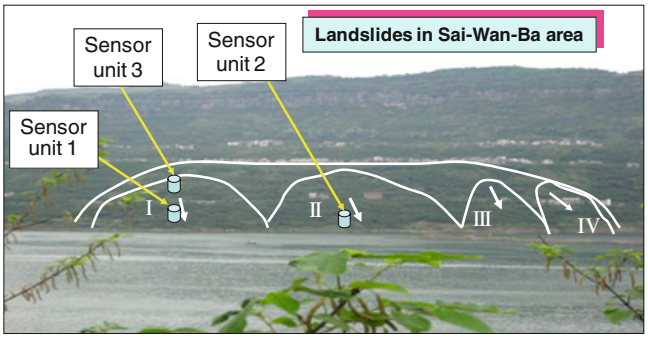


Fig. 6 Panoramic view of Sai Wan Ba landslide site

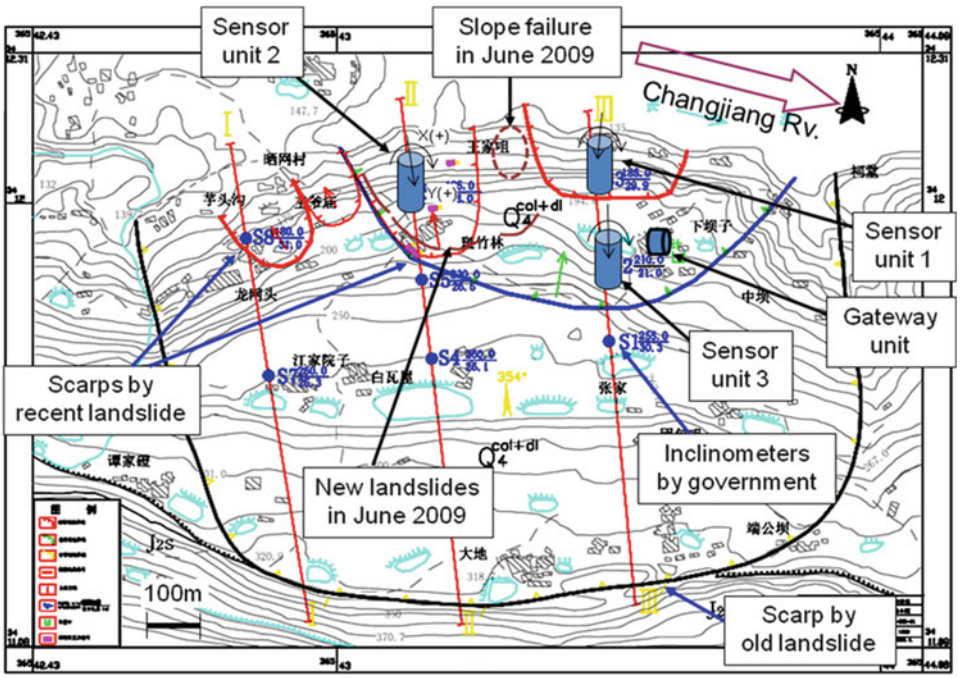


Fig. 7 Plan view of Sai Wan Ba landslide site and locations of sensor units

(b) It is difficult to detect a precaution of slope failure only by watching the water content; and
(c) Record of water content is very sensitive to rainfall events. It can be used to detect heavy rainfall which may cause slope failure.

Monitoring of a Slope by Three Gorges Dam

Prototype of the developed monitoring system has been installed on a side slope by Three Gorge Dam, the world largest dam in China, since 2008.

The site, Sai-Wan-Ba area, is located on the right side of the dam lake, near Wanzhou Ward, 80 km eastward from Chongqing City (Fig. 5). Several landslide blocks, are found by geological investigations as shown in Figs. 6 and 7. The locations of three sensor units deployed by the authors are also shown in Fig. 7. They are responsible for each recent landslide blocks respectively.

Figure 8 show the cross-section of slope passing the position of "sensor unit 2" shown in Fig. 7. The slope mainly consists of mad stone or sandy mad stone layers, and a deposit layer of clayey soil with some crushed mad stone covers the slope surface with an average depth of 15 m.

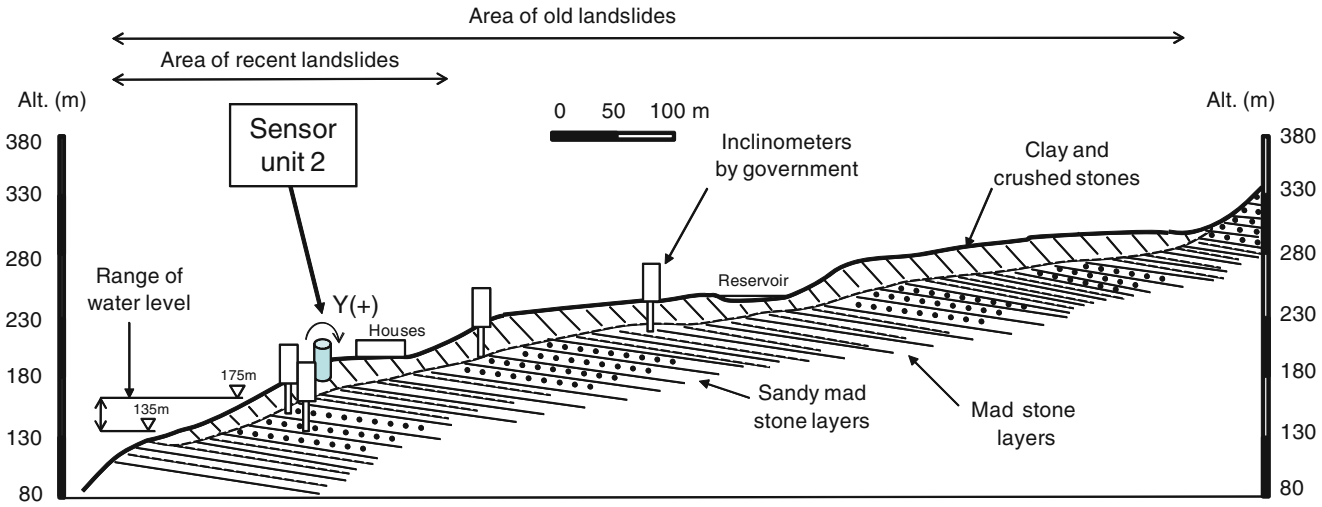


Fig. 8 Cross sectional view of Sai Wan Ba landslide site passing the position of sensor unit 2

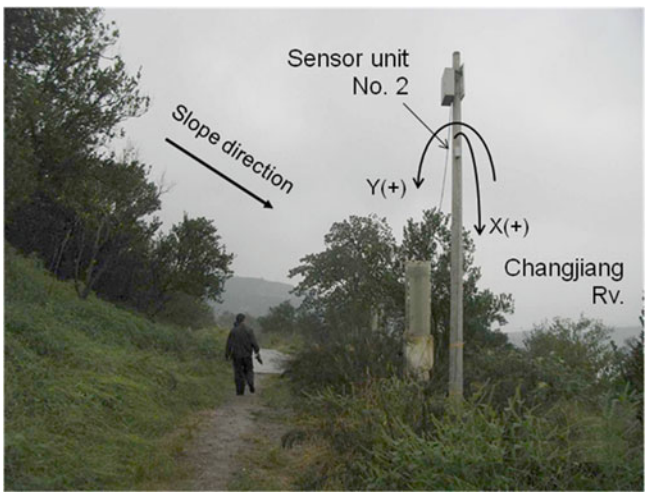


Fig. 9 Installation of a sensor unit



Fig. 10 Installation of a gateway unit

The length of the recent landslide block is around 350 m, with slope angle of 5–15°.

The dam has been in service since 2008, and 30 m of periodical changes in the water level of dam-lake (Changjiang River) are scheduled every year for dam operation. Besides, the site is located in a subtropical region where heavy rainfall events are expected, and some displacement on the slope surface was reported in summer of 2008. Therefore, the government also observes this area continuously by using borehole inclinometers, ground water level sensors, and a rain gage.

The sensor unit by authors are attached to a pole installed on the slope (Fig. 9). Each sensor unit has a MEMS tilt sensor attached on the pole and a volumetric water content sensor buried into the ground at a depth of around 30 cm. The data was obtained every 10 min, and transferred to a gateway unit (Fig. 10), which is placed on a roof of a private house nearby, by radio communication. The gateway unit collects the data from all the sensor units, and sends them to a data server on internet through a cell phone network.

The monitoring system has been in practice since October of 2008. Meanwhile, a heavy rainfall event on June 7 and 8, 2009, caused significant displacements in landslide blocks including the position of the sensor unit 2. The locations of the landslides are shown in Fig. 7. It includes a slope failure at 150 m eastward of the sensor unit 2 as shown in Fig. 11, where more than 10 m of displacement was observed in the sliding block.



Fig. 11 New landslide on June 7, 2009

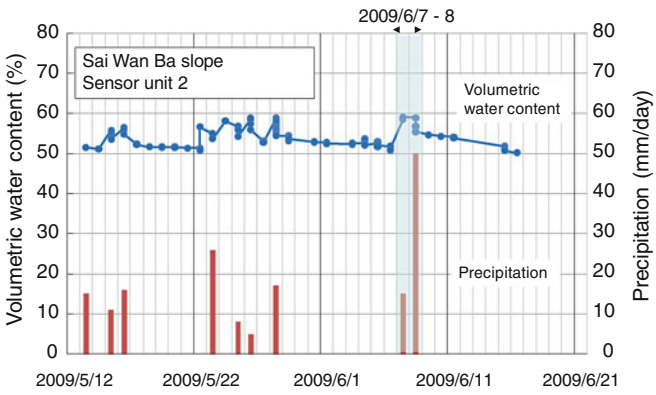


Fig. 13 Time history of volumetric water content transducer at sensor unit 2, and records of rainfall intensity

The time histories of the tilting angles of the pole in X-axis and Y-axis, the volumetric water content at a depth of 30 cm on the ground surface, and the record of precipitation are shown in Figs. 12 and 13 respectively. While receiving frequent rainfall events, the tilting angles showed gradual progress, and the tilting angle in Y-axis reached around 5° at the beginning of June 2009. As shown in Fig. 9, positive values of tilting angle in Y-axis means that the pole tilted upward the slope. Correspondingly, the tilting angle in X-axis in lateral direction on the slope, showed relatively smaller values.

A quick increase in the tilting angle in Y-axis, and a small increase in the X-axis are recorded on June 7 and 8. The precipitation for these 2 days was 65 mm, while the criteria for heavy rain warning was decided to be 30 mm per day in this area. The increasing rate of the tilting angle in Y-axis was 3° per day during this event, while the rate just before

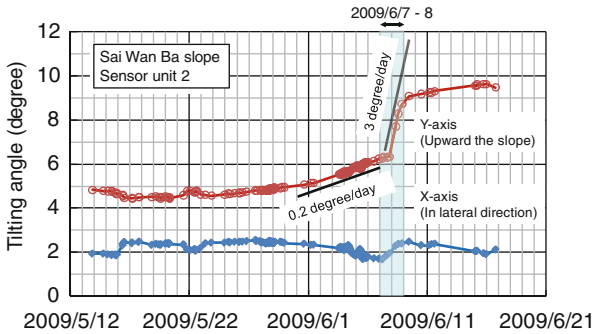


Fig. 12 Time histories of tilting angle obtained by sensor unit 2

this event was around 0.2° per day. This quick behaviour should be corresponding to the landslide event in this period. According to village people in this area, the slope failure near the sensor unit 2 took place at noon of June 8, while the quick increase in Y-axis started in late night of June 7. Therefore, there was a time margin sufficient for issuing early warning in this area.

As the slope surface consists of clayey soil deposit, the volumetric water contents showed high values between 50 % and 60 % throughout the monitoring period. It responded to every rainfall events, but no extraordinary response was recorded at the time of the landslide on June 7 and 8. As the volumetric water contents sensor was buried at a shallow part of the slope, only 30 cm from the ground surface, the obtained values are not corresponding to the conditions at the depth of slip surfaces. So it is not relevant to define the criteria of early warning based on use these values only.

Conclusions

A low-cost and simple monitoring method for precaution of rainfall-induced landslides is proposed, which uses tilt sensors on the slope surface to detect abnormal deformation. A wireless sensor unit with a MEMS tilt sensor and a volumetric water content sensor was developed and installed on several real slopes in Japan and China, and a long-term monitoring was attempted.

At a slope failure site along a highway, the slope surface showed abnormal tilting behaviours 30–50 min before failure. The tilting rate was around 3° per day, although it continued for only 50 min before failure. Such behaviours could be used as a signal for early warning.

At a side slope of Three Gorge Dam in China, consecutive movement of a sliding block was observed for a long period. A quick movement was detected at a heavy rainfall event, in which a tilting rate of around 3° per day was continued for 2 days. This event includes a slope

failure and significant displacement in a wide area including the position of the sensor unit.

Considering the behaviours of tilting monitored on the surfaces of these two slopes, a tilting rate of 3° per day, or 1° per day for conservative decision, could be a criteria to presume a significant sliding or failure of slopes.

It is difficult to evaluate the probability of slope failure quantitatively based on the values of water content. Conversely, it is easy to detect rainfall events from the water content data.

Acknowledgments These researches are supported by Grants-in-Aid for Scientific Research of Japan Society for the Promotion of Science (JSPS), Construction Technology Research and Development Subsidy Program of Ministry of Land, Infrastructure, Transport and Tourism of Japan, Joint Research Projects/Seminars by JSPS, and International Cooperate Project of Chinese Ministry of Science and Technology (projects #: 07(2007DFA21150) and 09(2009DFB20190)).

References

Ochiai H, Okada Y, Furuya G, Okura Y, Matsui T, Sammori T, Terajima T, Sassa K (2004) A fluidized landslide on a natural slope by artificial rainfall. Landslides 1(3):211–219

Orense RP, Towhata I, Farooq K (2003) Investigation of failure of sandy slopes caused by heavy rainfall. In: Proceedings of international conferecne on fast slope movement-prediction and prevention for risk mitigation (FSM2003), Sorrento

Orense RP, Farooq K, Towhata I (2004) Deformation behavior of sandy slopes during rainwater infiltration. Soils Found 44(2):15–30

Towhata I, Uchimura T, Gallage CPK (2005) On early detection and warning against rainfall-induced landslide. In: Proceedings of the first general assembly and the fourth session of Board of Representatives of the International Consortium on Landslides (ICL). Springer, Washington, DC, pp 133–139

Uchimura T, Towhata I, Trinh TLA, Fukuda J, Bautista CJB, Wang L, Seko I, Uchida T, Matsuoka A, Ito Y, Onda Y, Iwagami S, Kim MS, Sakai N (2010) Simple monitoring method for precaution of landslides watching tilting and water contents on slopes surface. Landslides (Published online: 17 Oct 2009)



Overview of Some Empirical Methods to Correlate Rainfall and Shallow Landslide and Applications in Malaysia

Suhaimi Jamaludin and Faisal Hj Ali

Abstract

Malaysia is located in a tropical region, known to have an extremely high annual rainfall which frequently triggered a landslide. If a landslide early warning system to be developed in Malaysia, it should be implemented based on empirical correlation of rainfall data and landslide cases. The proposed method is more economical compared to physically based approach. In this paper, two types of empirical rainfall thresholds were discussed i.e. (1) Intensity versus Duration (ID) and (2) Intensity versus Working Rainfall. Three efforts in correlating rainfall and landslides empirically in Malaysia were also been discussed. Intensity versus Duration (ID) method was used for works in Ampang/Hulu Kelang and Penang areas whereas Intensity versus Working Rainfall method was used for Cameron Highland area.

Keywords

Landslide • Rainfall • Empirical correlation • Working rainfall • Thresholds

Introduction

Malaysia is located in a tropical region with an average annual rainfall of about 2,000–2,500 mm. With such amount of rainfall, landslides are one of the most destructive natural disasters in Malaysia besides floods. Most landslides in Malaysia are shallow landslides whereby it is defined based on the maximum depth over length of the scar (D/L) ratio of less than 0.1 (Casadei et al. 2003).

These shallow landslides mostly triggered by heavy rainfall in wet seasons due to loss of matrix suction or loss of negative pore-water pressure. In some other places, it was due to development of perched water table near to the soil surface (Van Asch Th and Sukmantalya 1993; Haneberg and Onder Gocke 1994; Terlien 1996; Corominas and Moya 1996; Tsaparas et al. 2002; Chen et al. 2006). To fully apply this knowledge for the development of landslide warning system based on rainfall monitoring, it will involved a significant effort and budget for installation of related instruments and sensors in order to measure matrix suction and ground water level, thus it was quite impossible to implement it at regional level.

Due to this difficulty, empirical correlation between rainfall and shallow landslide can be developed and used. Empirical correlation can be developed by simply based on analysis of historical data of rainfall and landslides occurrences (Caine 1980; Crozier and Glade 1999). Using this empirical correlation, rainfall thresholds can be developed and used in the development of landslide early warning system for either localises or regional level.

Overview of Some Empirical Rainfall Thresholds for Landslide Triggering

Empirical thresholds for critical rainfall, either daily or hourly and antecedent rainfall which trigger the landslide, can be developed when the date, time and rainfall data prior

S. Jamaludin (✉)
Public Works Department, Slope Engineering Branch, Kuala Lumpur, Malaysia

Faculty of Engineering, University of Malaya, Kuala Lumpur, Malaysia
e-mail: suhaimij@jkr.gov.my

F.H. Ali
Faculty of Engineering, National Defence University of Malaysia, Kuala Lumpur, Malaysia

C. Margottini et al. (eds.), *Landslide Science and Practice*, Vol. 2,
DOI 10.1007/978-3-642-31445-2_78, © Springer-Verlag Berlin Heidelberg 2013

to the occurrence are available. The term "threshold" can be defined as the minimum or maximum (critical) level of some quantity needed for a process to take place (Reichenbach et al. 1998). When related to a rainfall threshold with practical applications in landslide warning systems, thresholds of interest are the minimum ones, i.e. thresholds that define the lowest level above which one or more than one landslide can be triggered. This threshold can be used as a warning signal for personnel who manage the monitoring system (Bacchini and Zannoni 2003).

A review of the relevant literature has shown various works and methods to define rainfall thresholds can be found. However, in this paper, only two types of empirical rainfall thresholds were discussed: i.e. (1) Intensity versus Duration (ID) Thresholds and (2) Intensity versus Working Rainfall Thresholds.

Intensity Versus Duration Thresholds

One of the earliest works in developing rainfall and shallow landslide relationship based on intensity-duration (ID) thresholds was carried out by Caine (1980) using a total of 73 shallow (<3 m deep) landslides on slopes that were unaffected by artificial disturbance or undercutting by streams. Using local precipitation records, he defined an upper threshold for landslide initiation as $I = 14.82D^{-0.39}$ where I is rainfall intensity (mm/h) and D is rainfall duration (h). The data were compiled from a variety of climatic and geologic conditions, and as a result, the rainfall intensity-duration estimates are no-homogenous.

Caine's dataset does not include an equally important dataset and climatic events that did not trigger landslides as pointed out by Crozier (1997). As reported by Jakob and Weatherly (2003), storm events that did not trigger debris flows were included in the analysis of climatic thresholds for debris flow initiation at Moscardo Torrent in the northern Italian Alps. Caine also noted a reasonable fit for precipitation data between 10 min and 10 days in duration, and a poor fit for longer or shorter durations. He suggested that the lack of fit for a very short durations resulted from insufficient depths of water to change pore water pressure.

Since Caine (1980) works, there are many researchers follow the same method and among them are Cancelli and Nova (1985), Crosta and Frattini (2001), Aleotti (2004) and the most recent works are reported by Dahl and Hasegawa (2008) and Guzzeti et al. (2008). In Guzzeti et al. (2008) works, intensity-duration (ID) thresholds for different climate regions (humid subtropical east coast, mild marine west coast, Mediterranean warm, Mediterranean cool, warm humid subtropical and mountain climate) was developed based on 2,626 landslides covering the 89-year period between 1917 and 2005. Figure 1 shows global ID thresholds developed by various researchers as reported by Guzzeti et al. (2008).

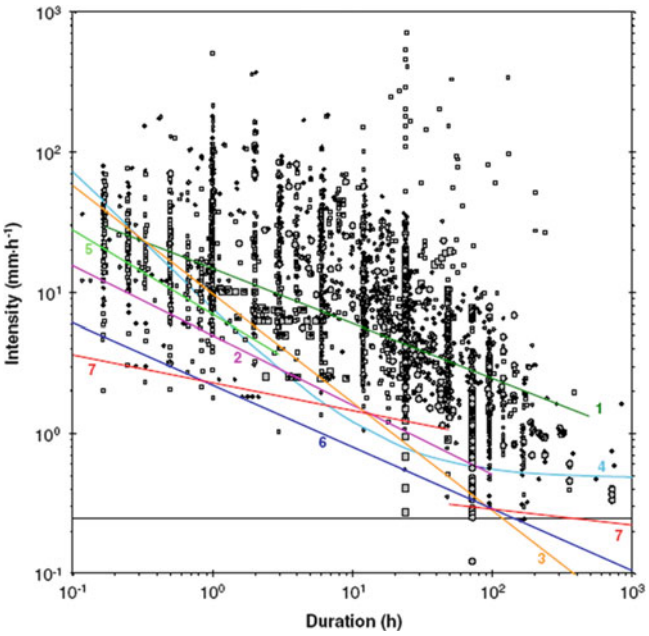


Fig. 1 Global ID thresholds developed by various researchers as reported by Guzzeti et al. (2008): *1* Caine (1980), *2* Innes (1983), *3* Clarizia et al. (1996), *4* Crosta and Frattini (2001), *5* Cannon and Gartner (2005), *6* Guzzeti et al. (2008) and *7* Guzzeti et al. (2008)

Intensity Versus Working Rainfall Thresholds

The working rainfall is a cumulative rainfall that takes into account the effect of an antecedent rainfall (MILT 2004). In general, shallow landslides occur under the influence of not only a landslide-causing rain events but also antecedent rainfall. The degree of influence of an antecedent rainfall normally reduces as time becomes distant from a landslide-causing rain. To derive the effect of an antecedent rainfall, similar method proposed by Crozier (1986) was used by MILT (2004) with value of K of 0.5. Calibrated Antecedent Rainfall (CAR) named by Crozier (1986) was also called the Antecedent Working Rainfall (R_{WA}) in the MILT (2004).

Working Rainfall (WR) was derived as the sum of the Absolute Cumulative Rainfall (R_{AC}) produced by a series of rain prior to the occurrence of landslide and the Antecedent Working Rainfall (normally R_{WA} of 14 days). A series of rain was defined as a continuous rain prior to the occurrence and it was terminated when there is presence of 24 h non-rain.

Working rainfall (WR) = Absolute Cumulative Rainfall (R_{AC}) + Antecedent Working Rainfall (R_{WA})

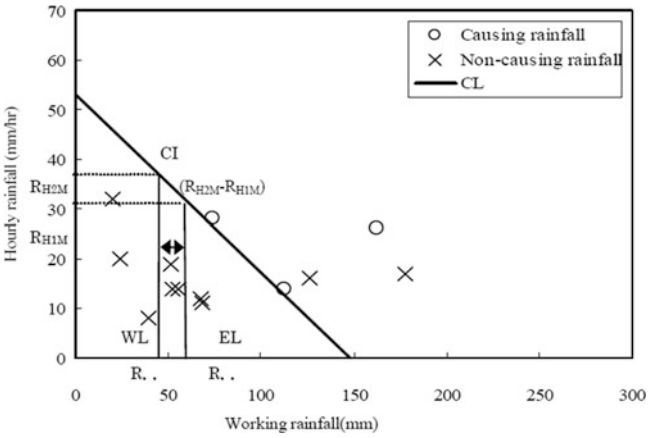


Fig. 2 Example of warning based on intensity – Working Rainfall (MLIT 2004)

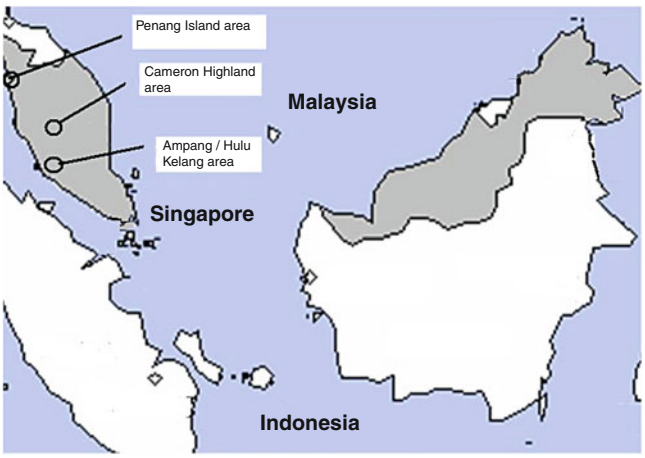


Fig. 3 Locations of the Ampang/Hulu Kelang and Cameron Highland areas

Figure 2 shows an example of critical line (CL) produced from Working Rainfall versus Hourly Rainfall graph (MLIT 2004).

Empirical Rainfall and Landslides Correlation Developed in Malaysian

There are few efforts in Malaysia in attempts to develop landslides and rainfall correlation for the purpose to be used in the landslide early warning system for regional basis. Three of the said efforts that will be addressed briefly here are for Ampang/Hulu Kelang and Penang Island areas which were developed by the Public Works Department of Malaysia (PWD) and another one for Cameron Highland area, developed by the Drainage and Irrigation Department of Malaysia (DID) as reported by Norlida et al. (2006). All three sites have a similarity in term of geological factor: located mostly on granitic residual soil. Coverage areas of the developed thresholds are quite small but stands as a good starting point. With existing data and with anticipation of more data will come in the future, wider coverage of thresholds can be developed.

Figure 3 shows the locations of the Ampang/Hulu Kelang, Penang Island and Cameron Highland areas.

Rainfall Thresholds for Ampang/Hulu Kelang Area

The Ampang/Hulu Kelang area is located at the suburb of Kuala Lumpur; capital city of Malaysia. This area, covering about 100 km^2 is a highly landslide prone area within the country due to the hilly terrain as well as intense rainfall pattern. In term of elevation, this area cannot be considered as a mountainous area where it is only at 50–250 m above mean sea level (MSL). This is the first area selected for developing of landslide and rainfall relationship in the country by the PWD Malaysia through the National Slope Master Plan Study (NSMP) which was carried out from 2006 to 2009 (PWD 2009). Its high socio-economic impact also justifies the selection of Ampang/Hulu Kelang as a pilot study area in the NSMP.

There were 40 landslides recorded since 1984. Amongst them, 16 landslides were identified as rainfall-induced landslides. The rainfall intensity during the event dates were determined using rainfall data obtained from DID. The DID daily rainfall data since 1984 were also been analysed in order to obtain the number and intensity of the rainfall that did not trigger landslides by adopting the methodology introduced by Caine (1980) but with some improvement where the non-occurrence rainfall data were included as suggested by Crozier (1997). However, the shorter time of rainfall data, for example every 15 min interval was unavailable for this area. Therefore in the events less than 24 h, hourly rainfalls that exceed 3 mm were used in the analysis. It was found that there were 228 rainfall events that did not trigger landslides. Of the 228 rainfall events, 22 storms were found to be above the landslide threshold relation that may lead to false alarms. Since the threshold line is defined based on the lower boundary of landslide events, the warning line adopted will be conservative and in a warning system such a conservatives approach may be justified to prevent any casualties even at the expense of few false alarms. But if later it was found that false alarm are too frequent, the warning line can be modified.

A landslide threshold relation was derived by fitting the lower boundary of the landslide triggered rainfall events (Fig. 4), as express as

$$\mathbf{I = 11D^{-0.5317}}$$

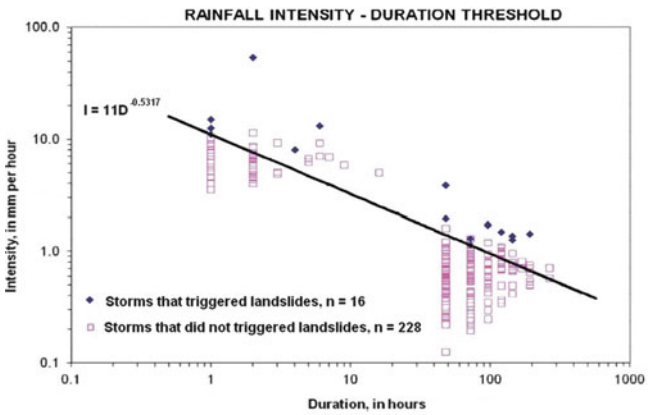


Fig. 4 Rainfall – landslide thresholds for Ampang/Hulu Kelamg area (PWD 2009)

Where I is the rainfall intensity in millimetres per hour, and D is duration in hours.

It has to be emphasized that this first attempt produced only a crude correlations. The Ampang/Hulu Kelang landslide-rainfall correlation has its limitations that may affect the accuracy of the derived curve, due to the following factors:

1. Reported landslide: Only limited cases of landslides have been investigated and reported in developing areas that had damaged the properties or poses a greater risk to life. Therefore, the total number of landslides over a given years, percentages and probabilities were only referred on those reported cases.
2. Rainfall data: only limited numbers of rain gauges were installed in specific locations. Therefore, the exact total amount of rainfall at the Ampang (specifically Bukit Antarabangsa) landslides site can only be estimated using the nearest rain gauge data which is in Klang Gates area and DID Ampang office.

Rainfall Thresholds for Penang Island

Penang Island is located at the northern part of peninsular Malaysia, about 400 km north of Kuala Lumpur. Penang Island is a highly populated historical city covering 293 km^2 with populations of 678,000. In term of elevation, similar to Kuala Lumpur, Penang Island can't be considered as a mountainous area where the highest elevation is 735 m above mean sea level (MSL). Penang Island is the second area selected by the PWD Malaysia for developing of landslide and rainfall relationship in the country through the NSMP (PWD 2009).

There were 23 landslides recorded since 1984. Fifteen of them were rainfall-induced landslides. The majority of these landslides occurred in the Paya Terubong residential area and along the road at Balik Pulau area. Both areas are located mainly along steep terrain of granitic residual soil. The nearest DID rain stations are located at the peak of Bukit Bendera; the highest elevation of Penang Island which is about 6 km from most of the landslide sites.

Using landslides and rainfall data since 1984, intensity-duration graph was developed based on similar method as the Ampang/Hulu Kelang area. It was found that quite difficult to draw critical line because there is no clear separation between non-occurrences and occurrences points on the plotting. The line finally made based on the minimum level of rainfall those triggered landslides in the past. The correlation for the line is as express as

$$\mathbf{I = 15.64D^{-0.81}}$$

There were many non-occurrence rainfall events appeared above the landslide threshold line as shown in Fig. 5. With this line, higher false alarm will be expected compared to Ampang/Hulu Kelang area. To improve the warning line or to get more reliable landslide threshold in the future, more rain gauges stations need to be installed at or near to the landslide prone area.

Rainfall Thresholds for Cameron Highland Area

Cameron Highland is a highland resort town in the state of Pahang. Cameron Highland, covering area of 712 km^2, located on the main range of Peninsular Malaysia with an elevation ranging between 1,050 and 1,500 m above MSL. The main activities of the 50,000 local populations are agricultural, mostly vegetables farming.

The DID, in response to two major mudflow incidences in Cameron Highland in 2000 and 2004, had established a rainfall-landslide (in this case mudflow) correlation in 2005 as a mudflow prediction tools (Norlida et al. 2006). The correlation is shown in Fig. 6, and was adapted from the guidelines published by the Ministry of Land, Infrastructure and Transportation of Japan (MLIT 2004). Using the rainfall data from their Cameron Highland rain gauges stations, the correlation was developed and evaluated (Norlida et al. 2006). According to Norlida et al. (2006), since its development, there has been no significant incidence of mudflow that can be directly predicted by the threshold model. However an occurrence of high rainfall in 2006 provided an opportunity for them to test the model by following the rainfall pattern on the correlation graph but no mudflow was reported. The DID planned to further improve the model so that it can be applied to other areas in the country and subsequently introduced it to National Disaster Committee at the federal, state and district levels.

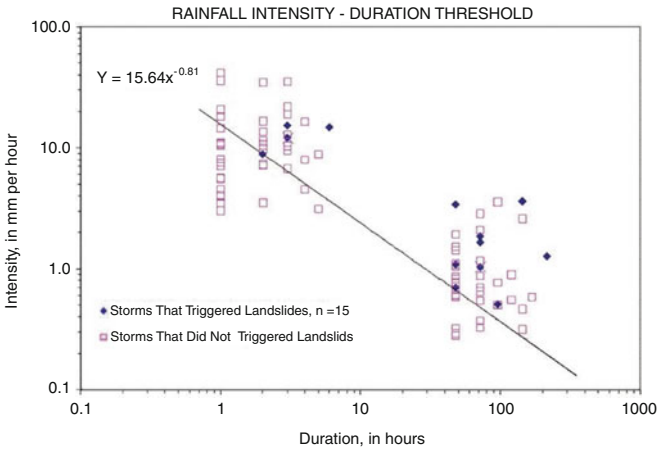


Fig. 5 Landslide threshold relations for Penang (PWD 2009)

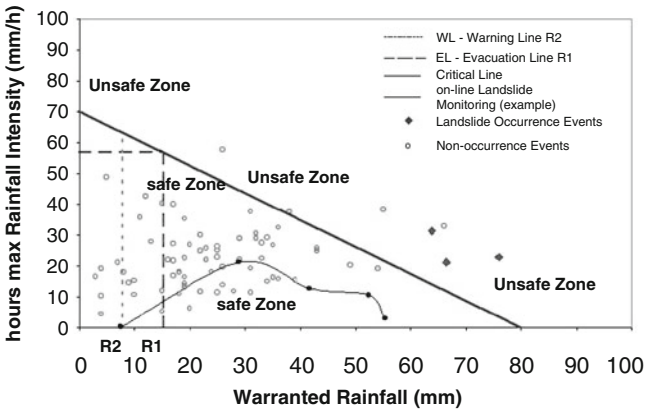


Fig. 6 Warning model for Cameron Highland area (Norlida et al. 2006)

Currently, PWD Malaysia in the midst of developing correlation between landslides occurrence and rainfall for various sites with the main aim to be used as an early warning. The thresholds will be verified using physically based approach before it will be applied as a mechanisms of warning system. Utilising existing national rain gauge networks owned by DID with some additional PWD new monitoring stations coupled with radar forecasting by Malaysian Meteorological Services (MMS), the more accurate and economical landslide early warning system can be developed.

Summary

Landslides are one of the most destructive natural disasters in Malaysia besides floods and mostly triggered by heavy rainfall in wet season. Therefore, the most economical way to develop landslide early warning system in Malaysia should be based on empirical correlation of rainfall and landslide.

There are various works and methods to correlate landslide and rainfall, and defining rainfall thresholds can be found in the literature. Two types of it were discussed in this paper: i.e. (1) Intensity versus Duration (ID) Thresholds and (2) Intensity versus Working Rainfall.

When date and time of landslide occurrences and rainfall data prior to the occurrence are available, thresholds for critical rainfall, either daily or hourly and antecedent rainfall which trigger the landslide, can be examined empirically.

Three efforts in Malaysia trying to develop landslides and rainfall correlation for the purpose to be used in the landslide early warning system were presented in this paper; for Ampang/Hulu Kelang, Penang and for Cameron Highland areas. Intensity versus Duration (ID) thresholds method was used for the Ampang/Hulu Kelang and Penang areas whereas Intensity versus Working Rainfall were used for the Cameron Highland area.

References

Aleotti P (2004) A warning system for rainfall-induced shallow failures. Eng Geol 73:247–265

Bacchini M, Zannoni A (2003) Relations between rainfall and triggering of debris-flow: case study of Cancia (Dolomites, Northeastern Italy). Nat Hazards Earth Syst Sci 3:71–79

Caine N (1980) The rainfall intensity-duration control of shallow landslides and debris flows. Geogr Ann 62A:23–27

Cancelli A, Nova R (1985) Landslides in soil debris cover triggered by rainstorm in Valtellina (Central Alps, Italy). In: Proceedings of the IVth international conference on landslides, Tokyo, vol 1, Balkema, Rotterdam, pp 267–272

Cannon SH, Gartner JE (2005) Wildfire-related debris flow from a hazards perspective: Chapter 15. In: Jakob M, Hungr O (eds) Debris flow hazards and related phenomena. Praxis/Springer, Berlin/Heidelberg, pp 363–385

Casadei M, Dietrich WE, Miller NL (2003) Testing a model for predicting the timing and location of shallow landslide initiation in soil-mantled landscapes. Earth Surf Landforms 28:925–950

Chen H, Dadson S, Chi YG (2006) Recent rainfall-induced landslides and debris flow in northern Taiwan. Geomorphology 77:112–125

Clarizia M, Gulla' G, Sorbino G (1996) Sui meccanismi di innesco dei soil slip. Atti del Convegno Internazionale "La prevenzione delle catastofi idrogeologiche: il contributo della ricerca scientificia", Alba (Italy), vol 1, pp 585–597

Corominas J, Moya J (1996) Historical landslide in the Eastern Pyrenees and their relation to rainy event. In: Chacon I-F, Balkema AA (eds) Landslides. Brookfield, Rotterdam, pp 125–132

Crosta G, Frattini P (2001) Rainfall thresholds for triggering soil slips and debris flow. In: Proceedings of EGS 2nd Plinius conference 2000, Mediterranean Storms, Siena, pp 463–488

Crozier MJ (1986) Landslides: causes consequences and environment. Croom Helm, UK, p 245

Crozier MJ (1997) The climate-landslide couple: a southern hemisphere perspective. In: Matthews JA, Brunsden D, Frenzel B, Glaeser B, Weiss MM (eds) Rapid mass movement as a source of climatic evidence for the Holocene. Gustav Fischer Verlag, Stuttgart, pp 333–354

Crozier MJ, Glade T (1999) Frequency and magnitude of landsliding: fundamental research issues. Z Geomorphol NF 15:141–155

Dahal RK, Hasegawa S (2008) Representative rainfall thresholds for landslides in the Nepal Himalaya. Geomorphology 100:429–443

Guzzeti F, Peruccacci S, Rossi M, Stark CP (2008) The rainfall intensity-duration control of shallow landslides and debris flows: an update. Landslides 5:3–17

Haneberg WC, Onder Gocke A (1994) Rapid water level fluctuations in a thin colluvium landslide west of Cincinnati, Ohio. US Geological Survey Bulletin 2059 C, pp 1–16

Innes JL (1983) Debris flows. Prog Phys Geogr 7:469–501

Jakob M, Weatherly H (2003) A hydroclimatic threshold for landslide initiation on the North Shore Mountains of Vancouver, British Columbia. Geomorphology 54:137–156

Ministry of Land, Infrastructure and Transport (MLIT) Infrastructure Development Institute, Japan (2004) Guidelines for development of warning and evacuation system against sediment disaster in developing countries

Norlida MD, Nasehir K, Yahya EM (2006) Development and evaluation of debris and mudflow warning model in high risk hilly slopes in Malaysia. In: Proceedings of the national conference on water for sustainable development towards a developed nation by 2020, Port Dickson, Malaysia

Public Works Department (PWD) (2009) Early warning and real-time monitoring systems. In: Sectoral report of national slope master, vol 2, Government of Malaysia, 186pp

Reichenbach P, Cardinali M, De Vita P, Guzzetti F (1998) Regional hydrological thresholds for landslides and floods in the Tiber River Basin (central Italy). Environ Geol 35(2–3):146–159

Terlien MTJ (1996) Modeling spatial and temporal variations in rainfall-triggered landslides. International Institute for Aerospace and Earth Sciences, JTC Publ. No. 31, Enschede, 254pp

Tsaparas I, Rahardjo H, Toll DG, Leong EC (2002) Controlling parameters for rainfall-induced landslides. Comput Geotechn 29:1–27

Van Asch Th WJ, Sukmantalya IN (1993) The modeling of soil slip erosion in the upper Komering area, South Sumatra Province. Indonesia Geogr Fis Din Quat 16:81–86



Experimental Alert Model for Hydrogeological Risk: A Case Study in Sicily

Giuseppe Basile and Marinella Panebianco

Abstract

The north-eastern part of Sicily (Messina district) is often hit by violent storms that cause great damage resulting from flash floods and debris flows. On 1st October 2009 there were 37 victims and on other occasions events have led to serious risks to both public and private safety.

The environment is characterized by the presence of high slopes, clay terrains deriving from mainly metamorphic rocks, and intensely inhabited territories: conditions that make risk mitigation measures particularly difficult.

Since there is very little time between the event of rainfall and the subsequent need for preventive intervention, the preparation of a civil protection system is a fundamental requirement.

For these reasons the Sicilian Department of Civil Protection has an ongoing series of initiatives that seek to reduce response times: instrument installation (rain and temperature sensors, X-band meteorological radar), development of an alert model based on critical rainfall thresholds, and the development of a plan for activating civil protection procedures.

Keywords

Hydrogeological risk • Soil slip • Debris flow • Rain thresholds • Civil protection plan

The Geographical and Meteorological Context

On 1st October 2009 a violent storm hit the northeast coast of Sicily in a restricted area from Pezzolo Village to Giampilieri Village, and from Scaletta Zanclea to Itala (about 25 km^2). The event was recorded by a single rain-gauge in Santo Stefano di Briga, a few kilometres north of the affected area (Fig. 1).

In 7 h about 225 mm of rain fell with a peak intensity of about 53 mm/h and an average intensity of about 32 mm/h (Fig. 2). The ground-effects in the affected areas were widespread and very severe: 37 victims due to mudflows and floods and more than 600 shallow landslides (Ardizzone et al. 2009; Basile 2009).

G. Basile (✉) • M. Panebianco
Sicilian Department of Civil Protection, via Abela, 5, Palermo 90141, Italy

Since in the rain gauge area there was no corresponding damage of any significance, it is possible to estimate that the amount of precipitation in the affected area at considerably more than 225 mm.

After the event the Sicilian Department of Civil Protection set up six real-time weather stations (data transmitted by radio signals) to measure the amount and the intensity of precipitation, the air temperature and the humidity in the affected area. Even more recently an X-band micro radar was installed.

The Determination of Rainfall Thresholds

Historical and Statistical Analysis

The question under consideration is how to assign rainfall thresholds and associated alert levels and how to decide what the civil protection system must do in order to mitigate hydraulic and geomorphic risks.

C. Margottini et al. (eds.), *Landslide Science and Practice*, Vol. 2,
DOI 10.1007/978-3-642-31445-2_79, © Springer-Verlag Berlin Heidelberg 2013

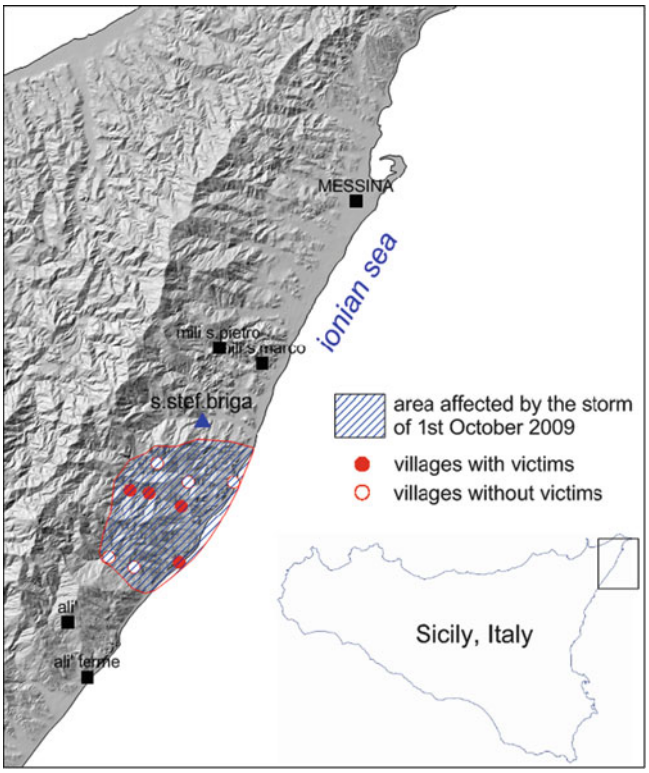


Fig. 1 The area affected by the storm of 1st October 2009

Several authors have examined the issue using approaches based on physical or empirical models. Most common empirical models study historic rainfall and their ground effects (Aleotti 2004; Brunetti et al. 2010; Caine 1980; Cannon et al. 2008; Cevasco et al. 2010; Chleborad et al. 2006; Corominas et al. 2002; Guzzetti et al. 2005; Iverson 2000; Luino 2008; Zêzere et al. 2008).

From these studies it is evident that the meteorological, morphological and geological characteristics of each geographic area induce different results with regard to the determination of rainfall thresholds for mudslides. For this reason threshold values may have only a local validity.

In the case in question we have only one rain gauge (the one at S. Stefano Briga) to study previous events, but its historical data does not include hourly rainfall intensity values.

The analysis of cumulative rainfall from 1 to 15 rainy days shows some relevant events with total amounts greater than in October 2009 (Fig. 3).

From data examination it is possible to conclude that:

- Very critical situations occurred often with P(1d) > 100 mm, P(5dd) > 150 mm, P(15dd) > 200 mm;
- Critical situations occurred occasionally with P (1d) > 70 mm, P(5dd) > 100 mm, P(15dd) > 150 mm;
- Sometimes critical situations occurred with sudden intense rainfall events > = 100 mm in a day without significant previous rainfall.

Filtering the entire data-set (from 1924 to 2009) we obtain 196 events with P(1d) > 50 mm and we consider the average of these values to represent the most critical situation for the pre-conditional factors leading to hydrogeological risk.

The exponential fitting of these values is shown in Table 1:

Criteria for Threshold Evaluation

The value of the 'd' parameter (rainy days before the generic event) in the previous equation is not of secondary importance because the alert levels depend on this value.

We may only assume that physical phenomenon induces soil slips and debris flows, but we do not know with precision the total amount of water required. Other unknown factors are the physical and mechanical constitution of the soil (mineralogy, density, porosity, permeability, cohesion, friction angle), the contribution of air temperature to evaporation, and the quantitative role of vegetation and burrowing animals.

Thus, although the system is influenced by many unknown variables, the only data of which we are sure is the amount of rainfall.

However, even if we know with certainty the exact physical process that causes the debris flows, in order to establish the threshold level we must also take into account human inertia factors.

The population's "practice" to alerts is another unknown element that we must consider: while avoiding too many false alarms, we must not overlook the possibility of unexpected phenomena.

In addition, the software used by the weather stations has two kinds of alarms: for cumulative and for intense rainfall.

For these reasons, the thresholds are based on two indicators: the pre-conditional factors with cumulative rainfall and the triggering factors with rainfall intensity.

The above formula (1) shows the maximum level for pre-conditional factors while the lower levels are a fraction of the 'd' coefficient. Thus we have the following expressions (as shown in Fig. 4):

$$K3 = 69.91^{*}d^{0.307} \quad (1)$$

$$K2 = 46.61^{*}d^{0.307} \quad (2)$$

$$K1 = 23.30^{*}d^{0.307} \quad (3)$$

Triggering factors caused by rainfall intensity (mm/h) are unknown because of inexistent historical data. However, based on only a few events (October 25, 2007; November 15, 2008;

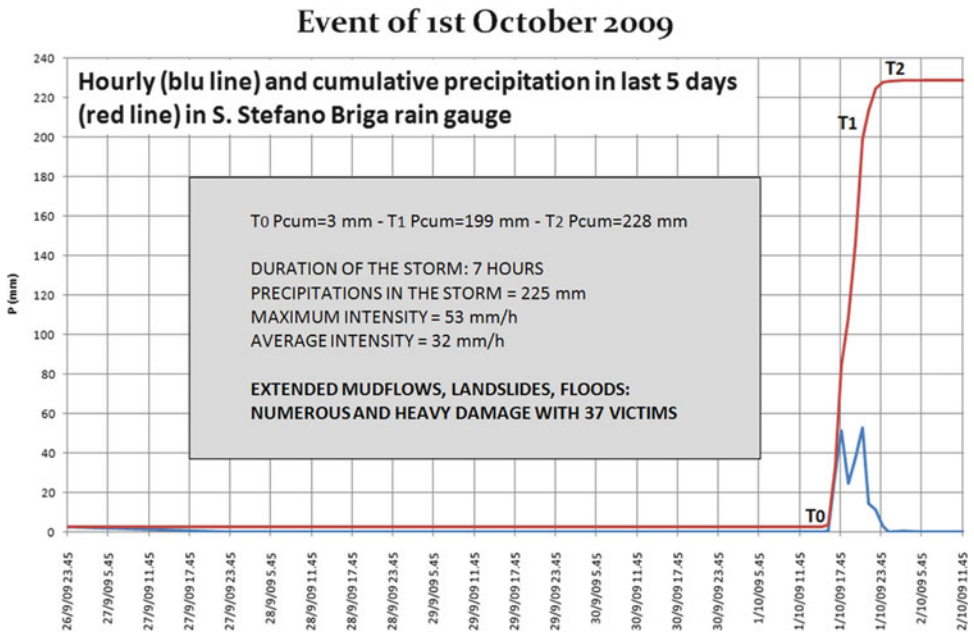


Fig. 2 Diagram of event of 1st October 2009

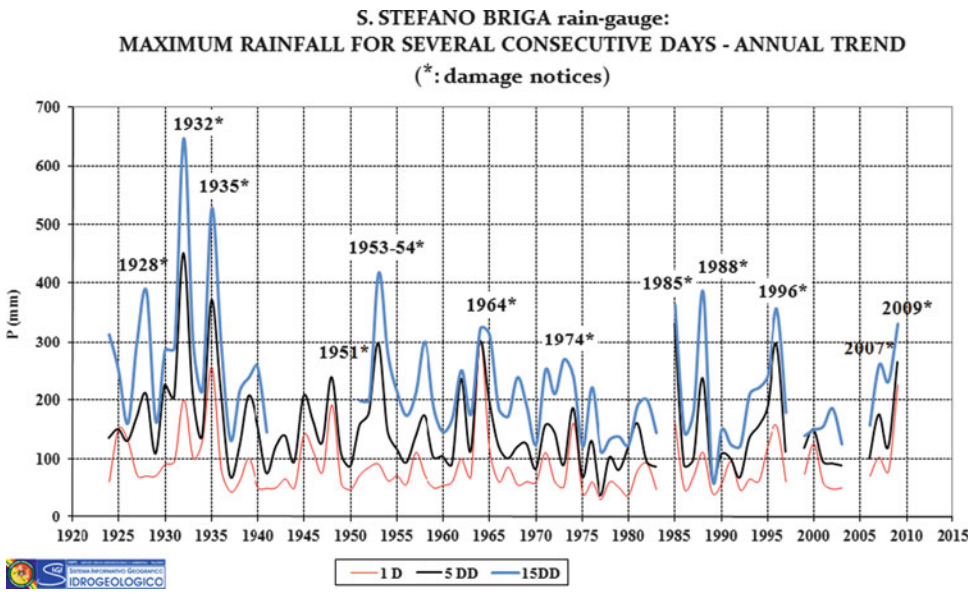


Fig. 3 Annual trend of S. Stefano Briga rain-gauge

Table 1 Average values for cumulative rainfall from 1 to 20 consecutive days (1924–2009 years) and best fit equation

P1d	P2d	P3d	P4d	P5d	P10d	P15d	P20d
72	87	97	105	110	139	164	181
	[1] K3 = 69.91*d$^{0.307}$		**linear form**				
	[1'] K3 = 8.89*d$^{-3.12}$		**logarithmic form**				

October 1, 2009; March 1, 2011) we can assign the following levels (Fig. 5):

I1 = 10 mm/h
I2 = 25 mm/h
I3 = 40 mm/h

To avoid alarm activation caused by a series of abrupt changes in rainfall intensity, the minimum duration of the intense event must be half an hour.

Respectively, the three thresholds identified four alert levels (LEV0, LEV1, LEV2, LEV3), as shown in Table 2:

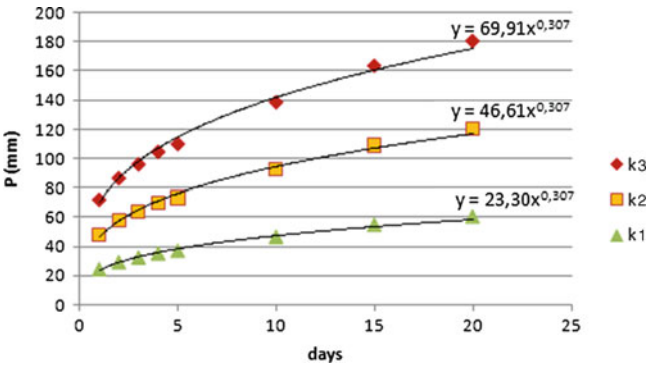


Fig. 4 Threshold equations related to cumulative rainfall

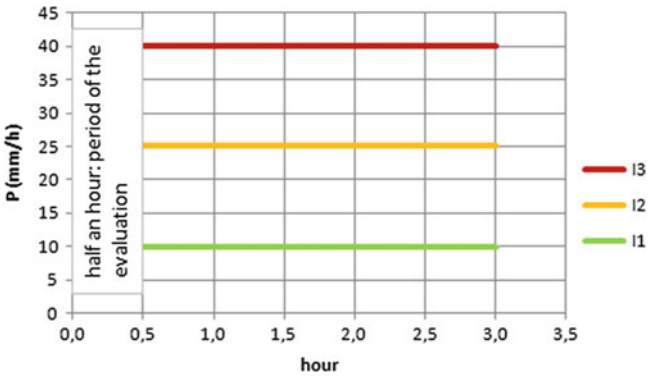


Fig. 5 Thresholds related to rain intensity

Table 2 Relations among thresholds and alert levels

Alert levels for cumulative rainfall				
Thresholds		**K1**	**K2**	**K3**
Levels	C_LEV0	C_LEV1	C_LEV2	C_LEV3
Alert levels for rainfall intensity				
Thresholds		**I1**	**I2**	**I3**
Levels	I_LEV0	I_LEV1	I_LEV2	I_LEV3

Cumulative rainfall

$$C_LEV0 < K1$$
$$K1 \leq C_LEV1 < K2$$
$$K2 \leq C_LEV2 < K3$$
$$C_LEV3 \geq K3$$

Rainfall intensity

$$I_LEV0 < I1$$
$$I1 \leq I_LEV1 < I2$$
$$I2 \leq I_LEV2 < I3$$
$$I_LEV3 \geq I3$$

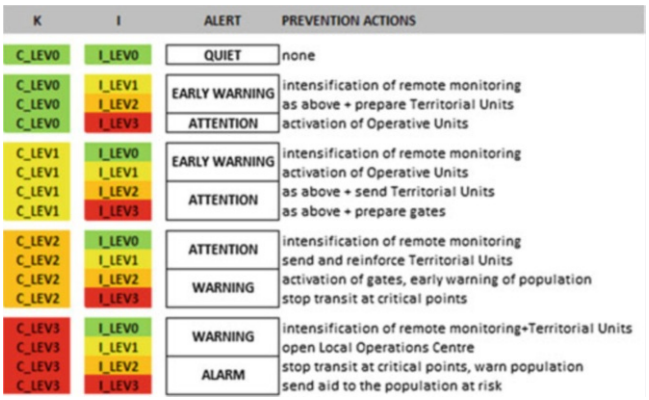


Fig. 6 Combination of threshold and alert levels

Criteria for Alert Level Evaluation

Thresholds for both cumulative rainfall and rain intensity have to combine to assign alert levels and relative preventive actions (Fig. 6). The alert levels (Quiet, Early Warning, Attention, Warning and Alarm) are related to those of the national and regional systems.

In order to understand what is indicated in Fig. 6, it should be noted that the Italian system of civil protection is organized as follows:

1. The "Functional Centre" (state or regional) issues the warning messages,
2. The Municipalities predispose all preventive activities by the Operative Units and the Territorial Units, and open a Local Operation Center during critical situations,
3. The regional and national system provides aid to Municipalities with men and equipment.

Obviously the preventive actions indicated are to be considered as a hypothetical model which needs to be developed according to the role and responsibility that each institution has within the civil protection plan.

The preventive actions represent a plan for the development of related roles and responsibilities of each institution within the civil protection plan.

All activities must be planned and discussed by the institutions involved and require repeated checks to ensure that the system works efficiently.

A Retrospective Analysis

With reference to the Santo Stefano di Briga rain-gauge, simulations were carried out to determine the most appropriate 'd' value in formulas (1), (2) and (3) in order to prepare the civil protection system.

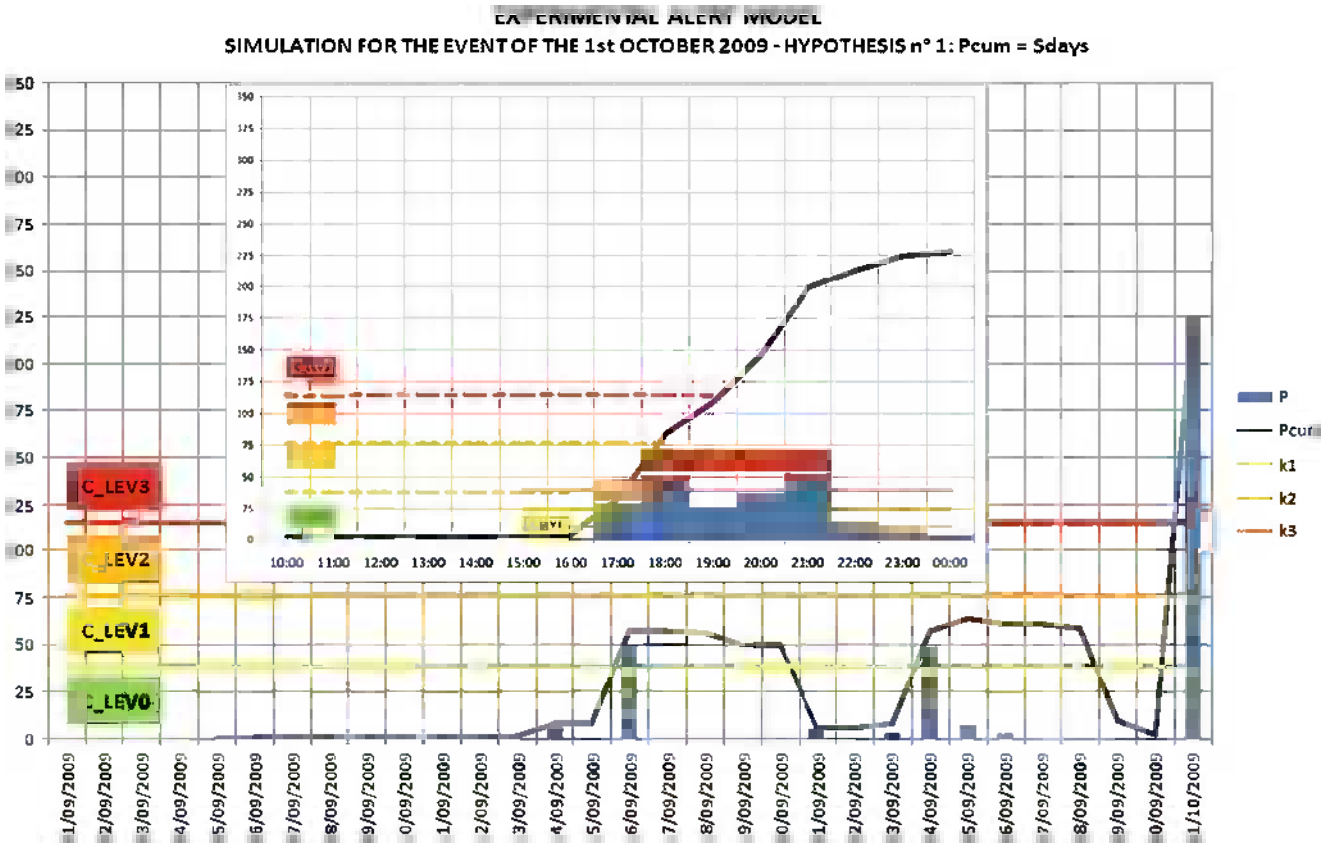


Fig. 7 Comparison between the accumulated rainfall in 5 days, the intensity of precipitation and alert thresholds

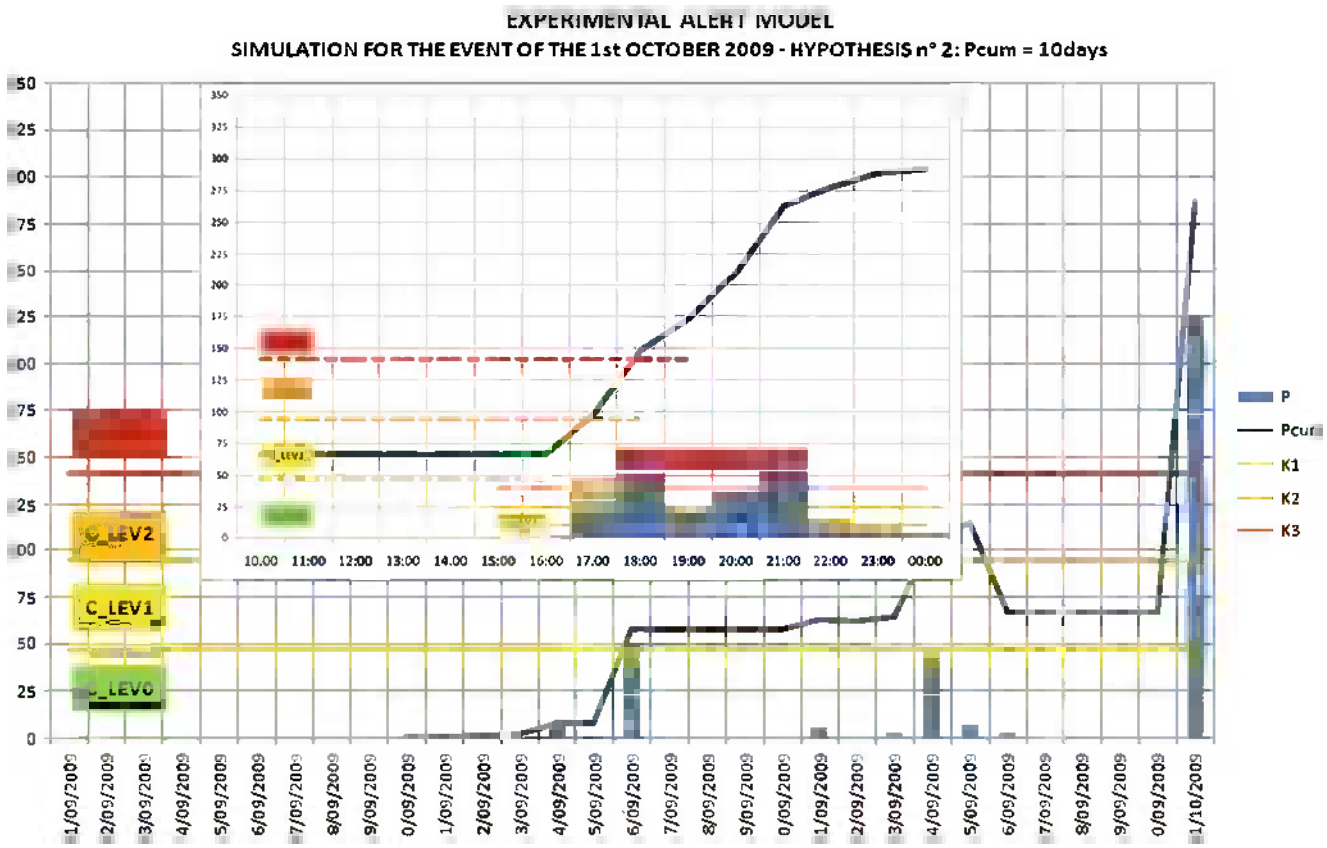


Fig. 8 Comparison between the accumulated rainfall in 10 days, the intensity of precipitation and alert thresholds

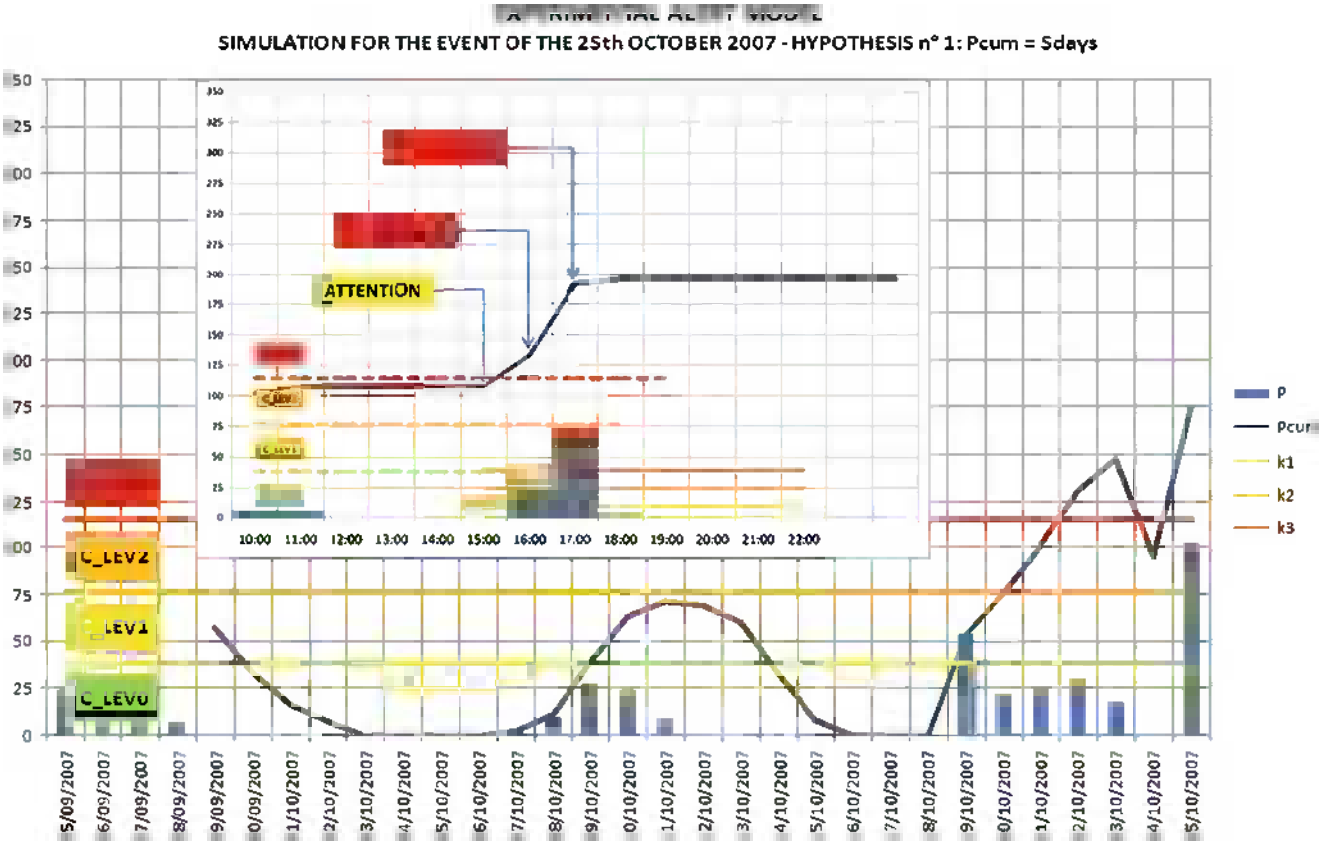


Fig. 9 Comparison between the accumulated rainfalls in 5 days, the intensity of precipitation and alert thresholds

As shown in Fig. 7, if 'd' = 5 (days) the model would not alert the civil protection system: up to 16.00 h on 1st October the alert level would be on QUIET (C_LEV0 + I_LEV0); from 17.00 to 18.00 h the system would pass to an ATTENTION level (C_LEV1 + I_LEV2/I_LEV3); and only at 19.00 h would the system pass to an ALARM level (C_LEV3 + I_LEV3). In this case it would be too late to safeguard the population.

If 'd' = 10 (days), at 16.00 h the alert level would be on EARLY WARNING (C_LEV1 + I_LEV0); at 17:30 h the system would pass to a WARNING level (C_LEV2 + I_LEV2); and at 18.00 h to an ALARM level (C_LEV3 + I_LEV3) (Fig. 8).

We cannot ascertain if this would be sufficient to save lives, but it would at least guarantee the presence of civil protection experts in the affected area who would be able to ascertain the seriousness of the situation.

We also analyzed another event that occurred in 2007 where there were similar ground-effects but different meteorological characteristics.

On 25th October 2007, the same area was affected by a severe storm that caused a lot of debris flows and considerable damage, but no casualties.

In the Santo Stefano di Briga rain-gauge, the storm was preceded by a fair amount of rain; so, if the experimental model had been active we would have had the following conditions (Figs. 9 and 10).

'd' = 5 (days)
15 o'clock: ATTENTION level (C_LEV2 + I_LEV0)
16 o'clock: ALARM level (C_LEV3 + I_LEV2)
17 o'clock: ALARM level (C_LEV3 + I_LEV3)

'd' = 10 (days)
15 o'clock: WARNING level (C_LEV3 + I_LEV0)
16 o'clock: ALARM level (C_LEV3 + I_LEV2)
17 o'clock: ALARM level (C_LEV3 + I_LEV3)

In this case, there is no substantial difference between the two positions (d = 5, d = 10) in alert messages. Probably, in a real-time system with d = 10 position the ALARM level would have taken half an hour before reaching d = 5.

Other simulations were made for similar events in the same area (October 2010, March 2011). In all cases, it seems that the most representative 'd' value is 10 days for a balanced activation of the civil protection system. However, the

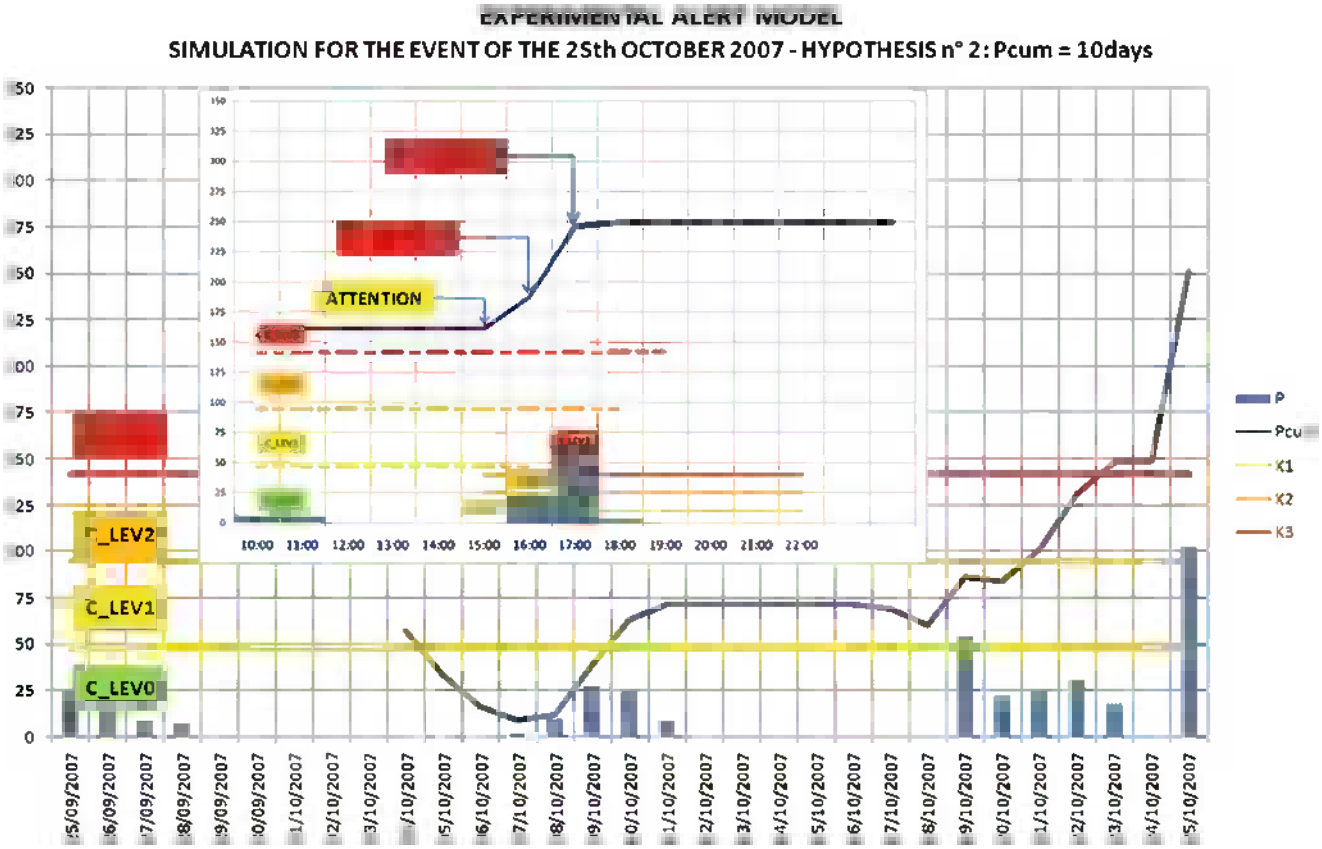


Fig. 10 Comparison between the accumulated rainfall in 10 days, the intensity of precipitation and alert thresholds

frequency of unexpected (and so far unpredictable) storms requires constant attention because of the rapid evolution of meteorological phenomena in the Straits of Messina district.

Conclusions

The proposed experimental alert model regards a restricted area of north-eastern Sicily that is frequently hit by extreme rainfall events that cause serious damage.

After the disastrous event of the 1st October 2009, six rain-gauges were installed in this area with real-time data transmission. The monitoring system's on-board software can establish three thresholds for cumulative precipitations and for rain intensity.

In order to determine the rain thresholds that could trigger the phenomenon of hydrogeological instability, the historical rainfall archives of the station at Santo Stefano di Briga (Osservatroio delle Acque), the only useful nearby reference point, were analyzed and compared with other damage-related data deriving from further archival research.

The elaboration of the data has allowed for the identification of two types of numeric expression:

$k_i = a_i * d^n$ for accumulated rainfall

(k_i = critical threshold, a_i,n = parameters depending on the law of distribution, d = in days)

Ii = m for intense rainfall

(Ii = critical threshold, m = rainfall value in mm/h)

The analyses carried out after a number of significant rainfall events have allowed for the identification of a 'd' value that provides greater guarantees in terms of prevention.

In the assigning of threshold and relative alert levels, the time required for the activation of civil protection procedures has been taken into account. In fact, thanks to the direct experience of the Regional Department of the Civil Protection together with other local organizations (town and county), it has been possible to ascertain that the amount of time needed to activate risk prevention actions – checking and verifying data, communicating with local organizations, activating operative and territorial centres, activating other system components – is a critical factor considering the speed with which the phenomenon of hydrogeological instability generally progresses.

The calculated thresholds and relative procedures would appear to be sufficient for the correct activation of preventive measures. However, the uncertainty of the

working model, together with the poor correlation between rainfall and mudslides, is considerable and as a consequence "false alarms" and "missed alarms" are possible during the inevitable initial calibration period. These, however, will help to make the necessary corrections to the system.

In the current absence of more sophisticated procedures that take into account other parameters (for example: the air temperature and the consequent variations of the quantity of water held in the soil) which could have an effect on the development of mudflows and debris flows, the only other currently available instruments of preventive analysis are those which observe rainfall in real time. Only relatively recently has a band X meteorological micro radar been installed in the area which could help the real time monitoring of rainfall distribution.

Nonetheless, bearing in mind the predisposition to hydrogeological instability of the area concerned and the high level of urbanization, a suitable emergency plan that is able to activate a timely risk prevention action is of fundamental importance.

Acknowledgments Many thanks to Tony Lawson for the translation of this document into English.

References

Aleotti P (2004) A warning system for rainfall-induced shallow failures. Eng Geol 73:247–265

Ardizzone F, Basile G, Cardinali M, Del Conte S, Fiorucci F, Iovine G, Mondini A, Moretti S, Panebianco M, Raspini F, Reichenbach P, Rossi M, Terranova O, Casagli N, Guzzetti F (2009) Mapping rainfall-induced landslides and inundated areas using remote sensing technology and field surveys: the 1 Oct 2009, Messina, Sicily, event. European Geosciences Union, General Assembly, Vienna, 19–24 Apr 2009

Basile G (2009) Rapporto sugli eventi meteo che hanno colpito la provincia di Messina il 1 ottobre 2009. Department document: www.protezionecivilesicilia.it

Brunetti MT, Peruccacci S, Rossi M, Luciano S, Valigi D, Guzzetti F (2010) Rainfall thresholds for the possible occurrence of landslides in Italy. Nat Hazards Earth Syst Sci 10:447–458

Caine N (1980) The rainfall intensity-duration control of shallow landslides and debris flows. Geogr Ann 62A:23–27

Cannon SH, Gartner JE, Wilson RC, Bowers JC, Laber JL (2008) Storm rainfall conditions for floods and debris flows from recently areas in Southwestern Colorado and southern California. Geomorphology 96:250–269

Cevasco A, Sacchini A, Robbiano A, Vincenzi E (2010) Evaluation of rainfall thresholds for triggering shallow landslides on the Genoa municipality area (Italy): the case study of the Bisagno Valley. Italian J Eng Geol Environ 1:35–50

Chleborad AF, Baum RL, Godt JW (2006) Rainfall thresholds for forecasting landslides in the Seattle, Washington, area – exceedance and probability. U.S. Geological Survey Open-File Report 2006-1064

Corominas J, Moya J, Hürlimann M (2002) Landslide rainfall triggers in the Spanish Eastern Pyrenees. Mediterranean Storms. In: Proceedings of the 4th EGS Plinius conference, Mallorca, Oct 2002

Guzzetti F, Stark CP, Salvati P (2005) Evaluation of flood and landslide risk to the opulation in Italy. Environ Manage 36(1):15–36

Iverson RM (2000) Landslide triggering by rain infiltration. Water Resour Res 36:1897–1910

Luino F (2008) Definizione delle soglie pluviometriche d'innesco di frane superficiali e colate torrentizie: accorpamento per aree omogenee. Istituto Regionale di Ricerca della Lombardia. Rapporto finale, Milano

Zêzere JL, Trigo RM, Fragoso M, Oliveira SC, Garcia AC (2008) Rainfall-triggered landslides in the Lisbon region over 2006 and relationships with the North Atlantic Oscillation. Nat Hazards Ear Syst Sci 8:483–499



An Operational Warning System for the Forecasting of Landslide Occurrence at Regional Scale

Samuele Segoni, Gianluca Martelloni, Daniela Lagomarsino, Riccardo Fanti, and Filippo Catani

Abstract

In this work we present a regional scale warning system (named SIGMA) for rainfall induced landslides. The system combines rain gauges measurements and rainfall forecasts and compares them with a series of statistical rainfall thresholds based on the total amount of rainfall. The system was specifically built to take into account both shallow and deep seated landslides. A decisional algorithm integrated in the warning system automatically provides a criticality level depending on which thresholds are exceeded. The model was integrated in the regional warning system of the Emilia Romagna region (Italy) for civil protection purposes. This paper accounts also for the main modifications that the model had during its development, passing form a base version relying on thresholds defined by means of a statistical analysis on rainfall data, to an advanced version in which thresholds were calibrated using a landslide database. The passage from a system to another was straightforward and for its flexibility and versatility, the proposed methodology seems particularly appropriate for emerging countries that have not yet gathered extensive and complete information on the location and time of occurrence of landslides.

Keywords

Landslide • Rainfall • Threshold • Calibration • Warning system • Emilia Romagna • SIGMA

Introduction

Landslides are a recurrent phenomenon responsible for casualties and damages. In Italy the main triggering factor is constituted by rainfall, therefore Civil Protection agencies are interested in setting up warning systems to monitor and possibly to forecast the occurrence of landslides over very large areas (e.g. thousands of squared kilometres). At such scales, the most common approach is based on empirical or statistical rainfall thresholds. This methodology is based on the analysis of the rainfall characteristics that in the past have lead to landslides initiation, with the aim of defining a mathematical expression (threshold) that separates the stability and the instability conditions (Caine 1980; Wieczorek 1996; Aleotti 2004; Guzzetti et al. 2008).

The most diffuse thresholds are based on intensity and duration of the critical precipitation (Caine 1980; Aleotti 2004; Guzzetti et al. 2008; Rosi et al. in press), but also cumulative rain is widely used (Innes 1983; Terlien 1998; Hong et al. 2005; Cardinali et al. 2006).

Once a rainfall threshold has been established, an early warning system can be easily set up because only a single parameter needs to be monitored (rainfall) in order to forecast the occurrence of landslides.

This paper summarizes the developments and the outcomes of the research activities carried out at Earth Science Department – University of Firenze on behalf of the Civil Protection agency of the Emilia Romagna region, aimed at developing an

S. Segoni (✉) • G. Martelloni • D. Lagomarsino • R. Fanti • F. Catani
Earth Sciences Department, University of Firenze, via La Pira 4, Florence 52021, Italy
e-mail: samuele.segoni@unifi.it

C. Margottini et al. (eds.), *Landslide Science and Practice*, Vol. 2,
DOI 10.1007/978-3-642-31445-2_80, © Springer-Verlag Berlin Heidelberg 2013

operative regional scale warning system for rainfall induced landslides.

The Emilia Romagna region (Northern Italy) is recurrently threatened by both shallow and deep seated landslides. While the first are mainly triggered by short and intense rainfalls (Campbell 1974; Crosta 1998), the latter are activated (or reactivated) preferably by less intense but prolonged precipitations (Bonnard and Noverraz 2001). This peculiarity required the adoption of a flexible warning system able to correctly take into account both kinds of rainfalls in order to consider both kinds of landslides.

We therefore built a decisional algorithm based on the overcoming of statistical thresholds: the algorithm considers two different periods of cumulative rainfall: daily checks of the 1 day, 2 days and 3 days cumulative rainfall (short period) are aimed at detecting shallow landslides; a series of daily checks over a longer time window (ranging from 4 to 243 days) is instead aimed at detecting deep seated landslides in low-permeability terrains.

Both the statistical model used to define the rainfall thresholds and the monitoring system which is based upon them are called SIGMA (*Sistema Integrato Gestione Monitoraggio Allerta* – Integrated system for alert monitoring management) (Martelloni et al. under review). This paper in particular emphasizes one of the main constraints of this kind of models: the quantity and quality of input data. The SIGMA model was progressively updated from a base version (calibrated only with historical rainfall data) to an advanced formulation, in which a database of dated and georegistered landslides was used to better calibrate the model. A validation procedure was carried out to quantify the improvements from a version to the other.

The proposed scheme is very flexible, and easily applicable everywhere. If a landslide inventory is not available, the base version could be applied and the switching to the final version could happen easily when a sufficient number of landslide data are collected for a more robust calibration.

Materials and Methods

Study Area

Emilia Romagna is a 22,446 km^2 wide Italian region. The northern and eastern part of its territory is occupied by a wide flat area (the River Po alluvial plain), which was excluded from the analyses. The study in fact was carried out only in the landslide prone areas, which correspond to the hilly and mountainous reliefs of the Apennine fold and trust belt (Fig. 1).

The study area is characterized by a very complex tectonic and geological setting (Vai and Martini 2001) and by the outcropping of a variety of different lithologies, some of

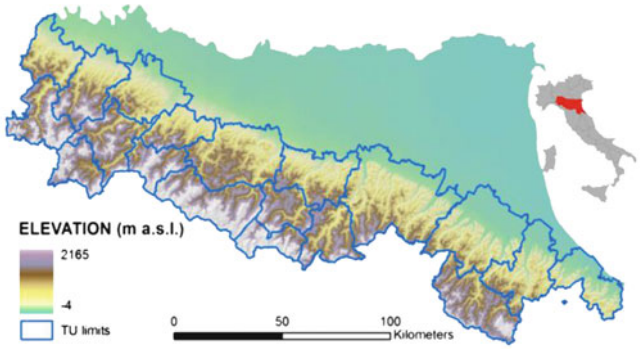


Fig. 1 The Emilia Romagna region

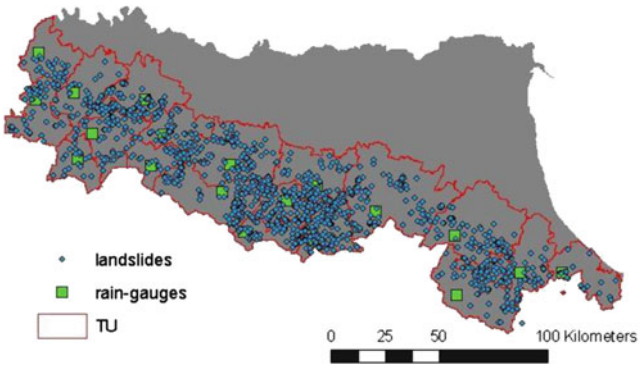


Fig. 2 Territorial Units (TU) (*red*), landslide dataset (*blue*) and rain-gauges (*green*)

which very susceptible to shallow and deep seated landslides (such as flysches, evaporites and argillaceous formations).

The most recurrent landslides typologies are rotational-translational slides, slow earth flows and complex movements (typically rotational failures at the head progressively changing into flows or translational movements throughout the body and toe) (Bertolini and Pellegrini 2001; Bianchi and Catani 2002). Shallow rapid slides are common as well. All those kinds of movements are mainly triggered by rainfall and, to a lesser extent, snowmelt.

The rainfall regime of the study area is characterized by a wet period (from November to April) and a dry period (from May to October).

Territorial Units (TU)

Instead of devising a single regional threshold, the study area was partitioned into 19 Territorial Units (TU) (Figs. 1 and 2), and each of them was analyzed separately in order to set up local thresholds with increased predictive efficiency. TUs represent the basic spatial unit both for the modelling and the SIGMA warning system. The latter in facts provides as a final output a distinct warning level for each TU.

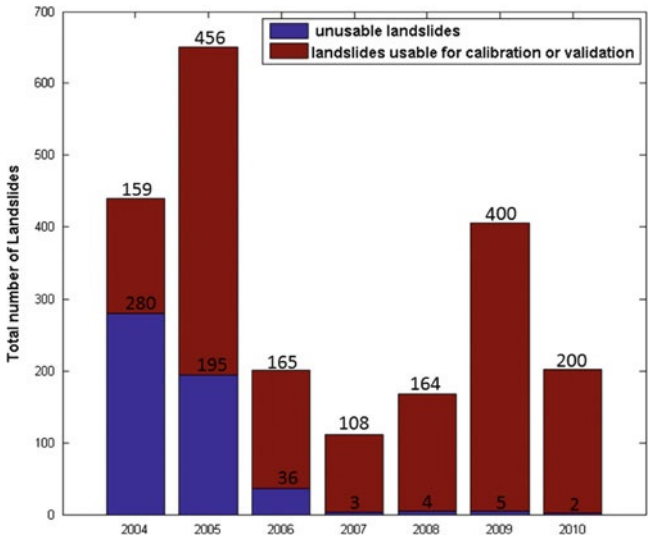


Fig. 3 High- and low-quality data in the landslide database

The Territorial Units were delimitated on the basis of meteorological and lithological characteristics and their boundaries match as much as possible the main regional and local mountain divides.

Landslide Data

Landslide data were fundamental in the development of the model, as they were used to calibrate and validate the rainfall thresholds. Landslide data were collected from the records of the regional Civil Protection Department, then landslides with accurate spatial and temporal location were selected and organized in a geographical database in shapefile format.

The database was constantly expanded during the years, starting from 2004, when regional Civil Protection agency first started to systematically collect accurate reports of landslides. In fact, to be used for calibration, the location and time of occurrence of the landslides must be known with the highest possible detail.

The quality of the collected data showed a marked increase with time (Fig. 3). Due to imprecision in temporal or spatial localization, almost no landslide before 2004 could be used, in 2004 only the 36 % of landslides met the requisites to be included in the database, while the percentage rose to 70 % in 2005 and 82 % in 2006. Since 2007, the reports began to be so reliable that almost the totality of the landslides could be used for the model calibration or validation.

Rainfall Data and Sigma Curves

The Emilia Romagna region is equipped with a network of 504 rain-gauges which automatically measure and transmit rainfall data. Among these, we selected a reference rain gauge for each TU, choosing the measuring station which best matched the following requisites: (1) presence of a long historical series of rainfall recordings; (2) hourly automatic recording; (3) central position among the TU; (4) elevation close to the mean elevation of the TU.

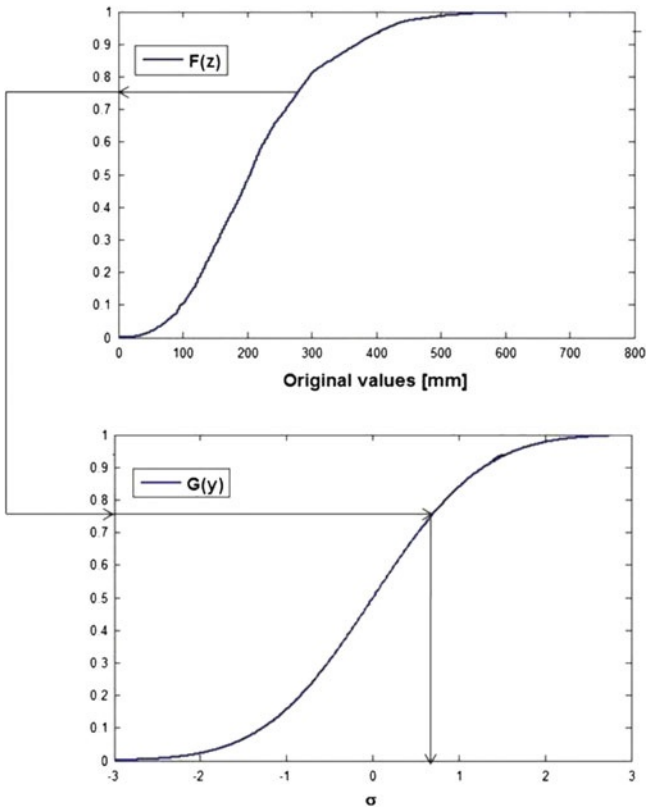


Fig. 4 Graphic procedure to transform the original values of cumulative rainfall in sigma values

For every reference rain gauge, the historical daily recordings were collected and used to build the time series of rainfall cumulates from 1 to 365 days.

All cumulated rainfall series were characterized by an asymmetric distribution (Benedetti et al. 2005), therefore, to obtain probability values of not exceeding a given rainfall value, the data of the original distributions were adapted to a standard Gaussian distribution chosen as a target function (Goovaerts 1997).

This transformation is represented in the graphic of Fig. 4 and basically allowed to express a given amount of rain fallen in a given period as a multiple of the standard deviation (σ) characterizing the time series.

Applying the procedure in reverse, from a particular multiple of σ, corresponding to a certain probability of not overcoming, it was possible to calculate the rainfall amount expressed in mm.

By means of a semi-automatic procedure implemented in Matlab, the procedure was repeated for different periods of accumulation (from 1 day to 1 year, at 1 day intervals) and for several σ multiples.

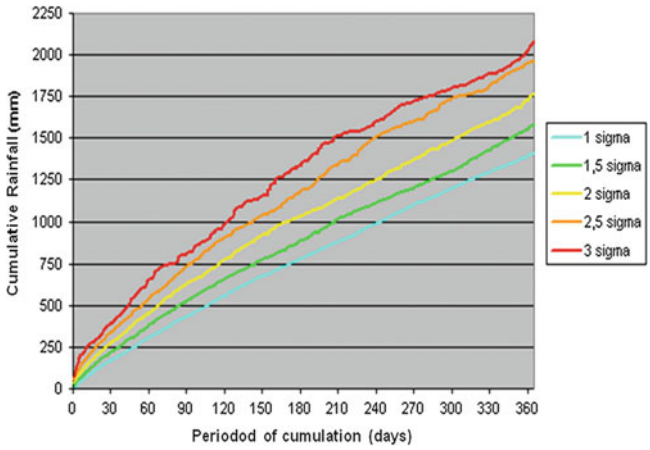


Fig. 5 Example of σ curves for a reference rain gauge

As a result, for each rain gauge, rainfall probability curves (σ curves), were set up (Fig. 5). A σ curve expresses which rainfall amount has a given probability of not being overcome for periods of 1, 2, 3, . . ., 365 days.

Base SIGMA Warning System

As discussed in the previous section, in the first years of the research, a statistically significant amount of information about location and time of occurrence of landslides was not available.

Therefore a base version of the SIGMA warning system was set up defining warning threshold based only on the statistical study of present and historical rainfall data (Benedetti et al. 2005). On the hypothesis that anomalous or extreme values of rainfall are responsible of landslide triggering, multiples of the standard deviation (σ) are used as thresholds to discriminate between ordinary and extraordinary rainfall events.

The warning system was implemented in a server which collects rainfall measurements and forecasts from the reference rain gauge of every Territorial Unit. For each of them, rainfall data are cumulated at increasing time intervals ranging from 1 to 245 days. A decisional algorithm compares all these cumulates with various sigma curves: depending on which of them are overcome, the decisional algorithm provides a warning level.

In order to detect short and very intense precipitations (for the triggering of shallow landslides), the decisional algorithm was set up to compare the 1, 2 and 3 days cumulates with the 1.5σ, 2σ, 2.5σ and 3σ curves.

To forecast the occurrence of deep seated landslides, the algorithm analyzes longer periods of rainfall in search of anomalous (but not necessarily "extreme") values: the algorithm checks if the 1.5σ and 2σ curves are exceeded by one or more of the cumulative rainfalls from 4 days up to 63 days. In addition, during the wet season (1st of November–30th of April), the maximum period of accumulation of rainfall is increased by one each day, up to a maximum cumulate of 245 days on the 30th of April. This variable time window was introduced to consider the influence of antecedent autumnal rainfall on early spring.

On the basis of which σ curves are exceeded (if any), the decisional algorithm provides one of the four criticality levels adopted in the Civil Protection procedures: "absent", "ordinary", "moderate" and "high" (Fig. 6).

Advanced SIGMA Warning System

Over the years, the quantity and quality of landslide data increased, and it became possible to use them to calibrate the model, as to better constrain the correspondence between σ thresholds and expected number of landslides.

We developed an optimization algorithm to compare the daily model outputs with the corresponding number of occurred landslides. By means of a trial and error procedure, the algorithm identifies the σ curves that minimize the occurrence of threshold overcoming in days for which landslides were not reported in the calibration database, without affecting the number of correctly detected landslides. This procedure was repeated separately for every TU over a calibration period spanning from 2004 to 2007 (included).

As an outcome of the calibration procedure, each TU was provided with a customized set of sigma curves instead of the predefined values 1.5σ, 2σ, 2.5σ, 3σ (Fig. 6). Some TU had marked modifications (the most relevant increase of the σ thresholds occurred in TU 2, which was optimized with the values 1.9σ, 2.15σ, 2.7σ, 3.5σ), while some σ levels remained untouched because rising them would have lead to reduce the number of detected landslides.

Upgrading and Updating SIGMA Warning System

Once the customized values of σ curves were defined for each TU, the passage from the base to the advanced version of the warning system was very rapid, since it basically needed only the adjustment of the σ values in the decisional algorithm.

In perspective, an update of the decisional algorithm is planned at regular intervals. New landslide data are constantly included in the database as events are reported to the Civil Protection agency, and every couple of years the updated database will be used to calibrate the thresholds with respect to an increased (thus statistically more significant) number of landslide events.

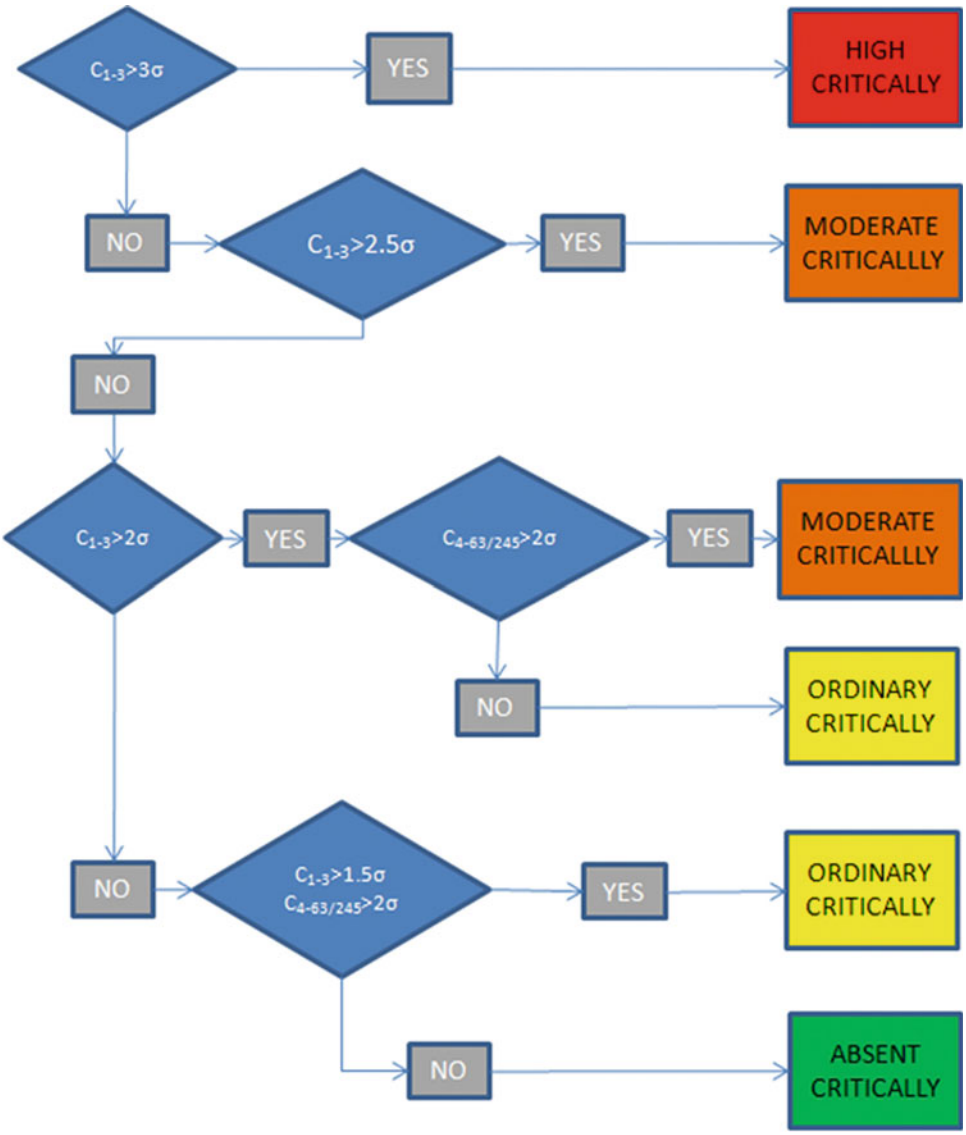


Fig. 6 Decisional algorithm of the SIGMA warning system. C1-3 is the cumulative rainfall from 1 to 3 days, C4-63/245 is the cumulative rainfall from 4 to 63 days (or 245 in the variable time window). 1.5σ, 2σ, 2.5σ, 3σ are the thresholds expressed in terms of standard deviation

Results

Validation of the Base Version of the SIGMA Warning System

The base version of the SIGMA warning system, with thresholds defined by means of a statistical analysis of rainfall time series, was used on a test phase during the years in which information on landslides was not sufficient to calibrate the model with respect to past events. Contemporarily to the test phase, official reports of landslides were collected and organized in a constantly updated geodatabase. For each TU, they were compared to the daily alert levels provided by the SIGMA warning system.

This validation procedure covered the period 2004–2007, and results showed that the model was capable of correctly detect a relevant number of landslides (Table 1). At the same time, validation highlighted a pronounced tendency to overestimate the criticality level (Table 1): in many TU the model produced a very high number of false alarms and in many cases the highest level of criticality was reached without the triggering of any landslide.

Validation of the Advanced Version of the SIGMA Warning System

The landslide dataset of the years 2008–2010 was used to validate the advanced version of the SIGMA model

Table 1 Results obtained by sigma base version for the period 2004–2007

		SIGMA base version
False alarms	Ordinary	1057
	Moderate	251
	High	41
Missed alarms	Days	109
	Landslides	210
Correct predictions (landslides number)	Ordinary	175 (98 days)
	Moderate	217 (65 days)
	High	286 (39 days)
	Total	678 (202 days)

Table 2 Results obtained by SIGMA base version and SIGMA advanced version for the period 2008–2010

		SIGMA base version	SIGMA advanced version	(%)
False alarms	Ordinary	1403	679	−51
	Moderate	401	223	−44
	High	47	12	−74
Missed alarms	Days	62	68	+9
	Landslides	117	127	+8
Correct predictions (landslides number)	Ordinary	161	202	+25
	Moderate	311	301	−3
	High	175	134	−23
Correct predictions (days with landslides)	Ordinary	76	83	+9
	Moderate	79	80	+1
	High	35	21	−40

In the last column the variation between the two methods is reported

(Table 2). During this period 764 landslides occurred and 84 % of them were correctly predicted.

An analysis carried out on the main missed alarms revealed that for the most part they correspond to landslides triggered by snowmelt. To solve this problem an integrated module to account for snow accumulation – snowmelt phenomena has been implemented (Martelloni et al. 2011).

Comparison Between the Versions

Comparing the two versions of the model, it can be clearly seen that the calibration of the decisional algorithm with respect to past landslide events improves the results (Table 2).

If the period 2008–2010 is used for comparison, in the advanced version of the model false alarms are dramatically reduced: highly critical alarms dropped by the 74 %, while ordinarily and moderately critical alarms were almost halved. Switching from the base version to the advanced one, we can observe an increase in the correct predictions of landslides in ordinary and moderate alert and an almost equivalent decrease in landslides corresponding to a highly critical level. This is due to the fact that the model calibration with respect to past landslides allowed to better constrain the criticality level with the number of occurred landslides: as a consequence many events characterized by few landslides were correctly associated to a lower criticality level.

Discussion and Conclusions

In this work we present a regional scale warning system (named SIGMA) which combines rain gauges measurements and rainfall forecasts and compares them with a series of statistical rainfall thresholds. Such thresholds were based on the total amount of rainfall, which was cumulated considering different time intervals: 1, 2 and 3-days cumulates took into account the critical rainfall influencing shallow movements, while a variable time interval cumulate (up to 243 days) was used to consider the triggering of deep seated landslides in low-permeability terrains. A decisional algorithm integrated in the warning system automatically provides a criticality level depending on which thresholds are exceeded. The model was integrated in the regional warning system of the Emilia Romagna region (Italy) for civil protection purposes.

Most part of the statistical or empirical models require a database of dated landslides, which is not always and everywhere available. The basic version of the SIGMA model was not affected by this limitation because the thresholds were calibrated only with a statistical analysis on historical rainfall data. The name itself of the model, SIGMA, reflects the central role of the standard deviations in the proposed methodology. The standard sigma curves considered by the algorithm (1.5σ; 2σ; 2.5σ; 3σ) delineate exceptional rainfalls with respect to the meteorological characteristics of each TU, and the decisional algorithm is organized to provide increasing criticality levels with increasing rainfall amounts.

The proposed model has therefore the advantage of being easily and rapidly exportable to other contexts, since it requires only rainfall data from a sufficiently organized network to be implemented in operational warning systems.

Consequently, if during the first years of activity data are collected about landslide occurrence, model errors and correct predictions, an additional empirical calibration procedure can be performed with respect to dated and georegistered landslides. In our test case this calibration highly improved the performance of the model and the advanced version of the SIGMA warning system provided satisfactory results during a 3 years validation period. The passage from a system to another was very easy from a technical point of view as it required only the adjustment of a few parameters in the decisional algorithm of the early warning system. For its flexibility and versatility, the proposed methodology seems particularly appropriate for emerging countries that have not yet gathered extensive and complete information on the location and time of occurrence of landslides.

References

Aleotti P (2004) A warning system for rainfall-induced shallow failures. Eng Geol 73:247–265

Benedetti A, Casagli N, Bosi V, Dapporto S, Ciolli S, Palmieri M, Zinoni F (2005) Modello statistico per la previsione operativa dei fenomeni franosi nella regione Emilia-Romagna. Boll Soc Geol Italy 124:333–344

Bertolini G, Pellegrini M (2001) The landslides of the Emilia Apennines (Northern Italy) with reference to those which resumed activity in the 1994–1999 period and required Civil Protection interventions. Quaderni Geolo Appl 8(1):27–74

Bianchi F, Catani F (2002) Landscape dynamics risk management in Northern Apennines (Italy). Environ Stud 7:319–328

Bonnard CH, Noverraz F (2001) Influence of climate change on large landslides: assessment of long term movements and trends. In: Proceedings of the international conference on landslides causes impact and countermeasures. Gluckauf, Essen/Davos, pp 121–138

Caine N (1980) The rainfall intensity–duration control of shallow landslides and debris flows. Geogr Ann A 62:23–27

Campbell RH (1974) Debris flows originating from soil slips during rainstorms in Southern California. Quart J Eng Geol 7:339–349

Cardinali M, Galli M, Guzzetti F, Ardizzone F, Reichenbach P, Bartoccini P (2006) Rainfall induced landslides in December 2004 in Southwestern Umbria, Central Italy. Nat Hazard Earth Sys Sci 6:237–260

Crosta GB (1998) Regionalization of rainfall thresholds: an aid to landslide hazard evaluation. Environ Geol 35(2–3):131–145

Goovaerts P (1997) Geostatistics for natural resources evaluation. Oxford University Press, New York

Guzzetti F, Peruccacci S, Rossi M, Stark CP (2008) The rainfall-intensity-duration control of shallow landslides and debris flows: an update. Landslides 5(1):3–17. doi:10.1007/s10346-007-0112-1

Hong Y, Hiura H, Shino K, Sassa K, Suemine A, Fukuoka H, Wang G (2005) The influence of intense rainfall on the activity of large-scale crystalline schist landslides in Shikoku Island, Japan. Landslides 2 (2):97–105

Innes JL (1983) Debris flows. Prog Phys Geog 7:469–501

Martelloni G, Segoni S, Catani F, Fanti R (WLF2-2011-0392) Snow melt modelling for improving the forecasts of rainfall threshold-based landslide triggering

Martelloni G, Segoni S, Fanti R, Catani F (under review) Rainfall thresholds for the forecasting of landslide occurrence at regional scale. Landslides

Rosi A, Segoni S, Catani F, Casagli N. Statistical and environmental analyses for the definition of a regional rainfall thresholds system for landslide triggering in Tuscany (Italy). J Geogr Sci (in press)

Terlien MTJ (1998) The determination of statistical and deterministic hydrological landslide-triggering thresholds. Environ Geol 35:125–130

Vai GB, Martini IP (2001) Anatomy of an Orogen: the Apennines and adjacents Mediterranean basins. Kluwer, Dordrecht/Boston/London, 636pp

Wieczorek GF (1996) Landslide triggering mechanism. In: Turner AK, Schuster RL (eds) Landslides investigation and mitigation, Special Report 247(4):76–89, Transportation Research Board. National Academy Press, Washington, DC



Radar Interferometry for Early Stage Warning on Monuments at Risk

Deodato Tapete, Nicola Casagli, and Riccardo Fanti

Abstract

Prevention measures on monuments affected by landslides and instability processes can effectively avoid damages to the elements at risk if the warning phase takes place at an 'early stage', i.e. when the phenomena are not completely triggered and developed. To realize this warning approach, satellite and ground-based radar interferometry techniques were tested, exploring their capabilities for detection and monitoring of structural deformation on the monuments of archaeological areas in Rome (Italy). Thanks to a procedure shared with the local conservators, fully involved in both investigation and feedback phases, early stage warning was carried out. Updated mapping products were obtained, identifying the most critical sectors to be stabilized. The recognition of definite deformation patterns allowed a high level of alert to be activated because of the significant threat for the monument conservation and public safety. Temporal series analysis highlighted the onset of probable instability processes, suggesting appropriate mitigation countermeasures.

Keywords

SAR interferometry • Permanent scatterers • Ground-based SAR • Monitoring • Warning • Archaeological heritage • Rome

Introduction

The preservation of both the material integrity and intrinsic cultural value of the monuments implies the adoption of all those measures aimed at the prevention of the occurrence of severe events which could produce permanent and irreversible deterioration effects, avoiding partial or total loss of the historic artefacts.

Innovative and shared procedures allowing a preventive warning undoubtedly represent one of the major actions of risk-reduction, especially in cases when the elements at risk cannot be removed and/or mitigation interventions are not cost-effective and sustainable. Nowadays warning is the most economical risk-reduction measure and its effectiveness depends on the combination with wider capacity development including public awareness and close collaboration with local managers (Sassa and Picarelli 2010).

According to the criteria of the preventive diagnosis, an early analysis of the temporal and spatial evolution of the ongoing instability phenomena can help to avoid reaching the critical phase, when an effective protection of the artefact is not longer possible. It means to think a different concept of 'early warning', trying to detect the local conservation criticalities at an 'early stage', i.e. at a stage when the instability process has not yet fully developed and it is possible to plan appropriate countermeasures for the safeguard of the exposed elements.

Among the most innovative remote sensing technologies increasingly used in environmental applications, radar interferometry techniques are quite suitable for archaeological investigations and cultural heritage preservation (Evans and

D. Tapete (✉) • N. Casagli • R. Fanti
Earth Sciences Department, University of Firenze, Largo E. Fermi 2, Firenze I-50125, Italy
e-mail: deodato.tapete@gmail.com

C. Margottini et al. (eds.), *Landslide Science and Practice*, Vol. 2,
DOI 10.1007/978-3-642-31445-2_81, © Springer-Verlag Berlin Heidelberg 2013

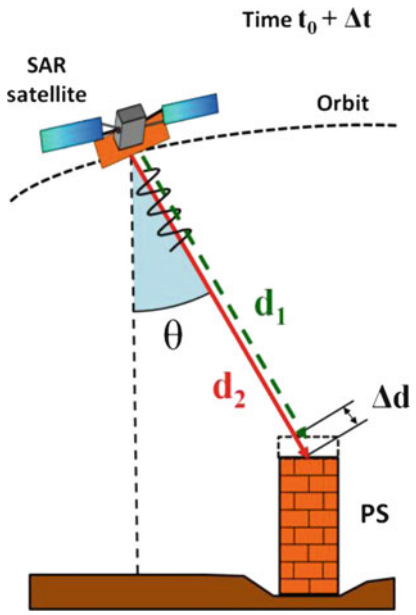


Fig. 1 Displacements (Δd) occurred during the monitoring time (Δt) are measured under an observation angle (θ) along the satellite LOS for the masonry structures recognized as radar targets (*PS*) within the processed SAR image. The scheme is referred to superficial deformation due to ground collapse, detectable as a displacement of the monitored structure

Farr 2007). The integrated exploitation of satellite and terrestrial radar instrumentations has recently showed interesting potentials for stability analysis in archaeological contexts at different spatial and temporal scales (Tapete et al. 2011, 2013).

Reporting the results of the most recent research, the paper extends the experimentations carried out on the archaeological heritage of Rome (Italy) Tapete et al. (2012), to demonstrate the capabilities of Interferometric Synthetic Aperture Radar (InSAR) technologies to support the daily management of monuments affected by ground and/or structural instability. Shared warning procedures were also established with the local conservators, activating alert systems and receiving prompt feedback.

Radar Interferometry Techniques

The radar interferometric techniques tested in this work exploit the *Synthetic Aperture Radar* principle, synthesizing a wider antenna while traversing a definite path during the acquisition phase (an orbit for satellite sensors; a linear rail for terrestrial instrumentations) (Rosen et al. 2000). Cigna et al. (2011) and Casagli et al. (2010) summarize all the benefits and shortcomings of satellite radar interferometry and ground-based radar techniques, respectively. In terms of potentials for applications on cultural heritage, it is to be mentioned the feature of non-invasiveness, jointly to the capability to perform monitoring campaigns at different spatial and temporal scales.

Satellite Radar Interferometry

Satellite techniques are specifically suitable to execute monitoring at 'archaeological site scale', covering at the same time large areas up to few square kilometres. Such technical feature encouraged the employment in the field of conservation science, especially in case of monuments spread over wide sites or huge archaeological systems (e.g., aqueducts and military fortifications).

Among the multi-interferogram approaches, we selected *Permanent Scatterers* technique – PSInSAR (Ferretti et al. 2001). It takes advantage of long temporal series of SAR data, recognizing, within the processed SAR images, high density of radar targets whose displacements along the LOS (Line Of Sight) direction of the satellite can be measured and plotted vs. time (*PS deformation time series*). Historical deformation of the monitored area are reconstructed with millimetre precision on single measures, with reference to the LOS components of the real displacement vectors associated to the detected ground motions (Fig. 1). The roughly monthly sampling frequency of the satellite acquisition (revisiting time generally of 24–35 days for the satellites here exploited) does not allow a real-time monitoring to be performed. Conversely, it is possible to activate *back monitoring* analyses to retrieve recent deformation occurred in the observed area, facilitating up-to-date detection and mapping of the sectors affected by recent/ongoing local instability.

Ground-Based Radar Interferometry

Based on the same principle as space-borne InSAR, the Ground-Based Interferometric SAR (GB-InSAR) instrumentation acquires SAR images of a single slope or entire monument with maximum extent up to 1–2 km^2. The higher sampling frequency (up to 1 image every few minutes) configures real-time monitoring of the displacement field, to constantly evaluate the structural behaviour of a monument.

Thanks to the adaptability of such terrestrial approach, effective implementation can be easily achieved in both urban and suburban areas, adjusting the acquisition geometry in relation to the orientation of the monument and to the assumed directions of the vectors associated to the ongoing displacements. Processing of GB-InSAR data generates displacement maps with a millimetre accuracy of the measurements along the LOS (Fig. 2).

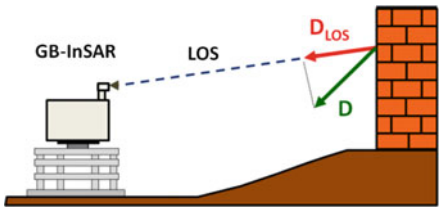


Fig. 2 Scheme of the GB-InSAR measurement of the LOS component (D_{LOS}) of the displacement (D) which affects the monitored monument

Test Sites: Roman Archaeological Areas

The wide-spectrum applicability of radar interferometry was explored on different archaeological areas in Rome (Italy), monitoring single monuments (Domus Tiberiana in the Roman Forum, Fig. 3a), entire sites (Oppian Hill, NE from the Colosseum, Fig. 3b) and huge linear archaeological systems (Southern Aurelian Walls, Fig. 3c; Roman Aqueducts, Fig. 3d).

The PSInSAR techniques were implemented for 'archaeological site scale' analyses, whereas the GB-InSAR technique was used for 'single monument scale' monitoring campaigns (Table 1). The selection between the satellite and terrestrial radar configurations was justified in relation to the typology of the instability processes and the extent of the monuments to monitor.

The recent collapse occurred on 30th March 2010 in the Oppian Hill, near the hypogean structures of the famous Nero's Golden House, interested about 60–80 m^2 of vault ceiling of a gallery, located beneath the garden usually frequented by tourists and passers-by (BBC News 2010). This event highlighted the urgency to verify the stability of the entire site, to avoid future damages to the exposed and subterranean cultural heritage, and to guarantee the public safety.

Same civil protection and conservation needs raise for the long systems of the Southern Aurelian Walls around the city centre and the Roman Aqueducts located in suburban public areas. In the last decades several collapses and masonry falls damaged sparse sectors of the Aurelian Walls (BBC News 2001), while diffuse structural instability and deterioration patterns were mapped on the exposed surfaces of the Roman Aqueducts. Ashby (1935) already reported the historical interventions carried out for structural reinforcement in correspondence of probable weak points, presumably related to instability of the local geological substratum.

Domus Tiberiana (i.e. the former imperial residence of the Roman emperor Tiberius), sited along the NW corner of the Palatino Hill, was selected for the experimentation of a 'single monument scale' monitoring by GB-InSAR. The local ground instability are chronically linked to the non-homogeneity of the underlying soil layers, constituted by

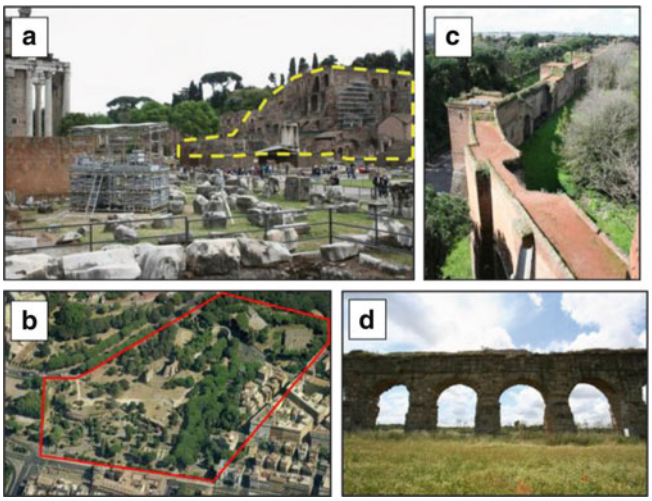


Fig. 3 Views of the test sites in Rome (Italy): (**a**) GB-InSAR monitoring the Domus Tiberiana (*yellow dashed line*) in Roman Forum; (**b**) aerial view of Oppian Hill (*red line*) with the Nero's Golden House; (**c**) towers and wall-walks of the Southern Aurelian Walls; (**d**) arches of the Roman Aqueducts

tuff strata superimposed, at the base of the slope, by alluvial soft cover. According to the topographical records acquired in 1985–1994 which clarified the directions of the structural deformation (Scarpelli et al. 1997), the GB-InSAR was installed in the Roman Forum to monitor the substruction arcades in the period Apr'09–Mar'10 (Fig. 3a).

Early Stage Warning Procedure

All the experimentations were carried out adopting a common warning procedure, specifically established during the planning of the monitoring campaigns and shared with the local conservators. The involvement of the latter was intentionally foreseen to define a joint path between the monitoring unit and the local bodies responsible for the conservation of the monitored monuments (Fig. 4).

Following this three-step procedure, the co-operation starts from the background phase (first step), during the initial overview of the conservation issues interesting the studied monuments. All the historical and literature data are collected and reviewed, and first surveys are executed to properly design the radar monitoring campaign.

During the investigation phase (second step), the monitoring activities combined with the necessary field validation allow a continuous surveillance to be performed, at the spatial and temporal scales related to the specific type of radar configuration (satellite and/or ground-based) employed for the monitoring. The prompt communication of any anomaly or potential criticality to the local conservators activates immediate on site inspections. The real condition of the monuments is directly verified and the confirmation of

Table 1 Summary of the InSAR experimentations carried out on the test sites selected in Rome (Italy)

Test site	Spatial scale	InSAR technique	Monitoring period
Oppian Hill	Entire site	PSInSAR	Mar'03 –June'10
Roman Aqueducts	Entire site	PSInSAR	Mar'03 –Feb'10
Aurelian Walls	Entire site	PSInSAR	Mar'03 –Feb'10
Domus Tiberiana	Single monument	GB-InSAR	Apr'09 –Mar'10

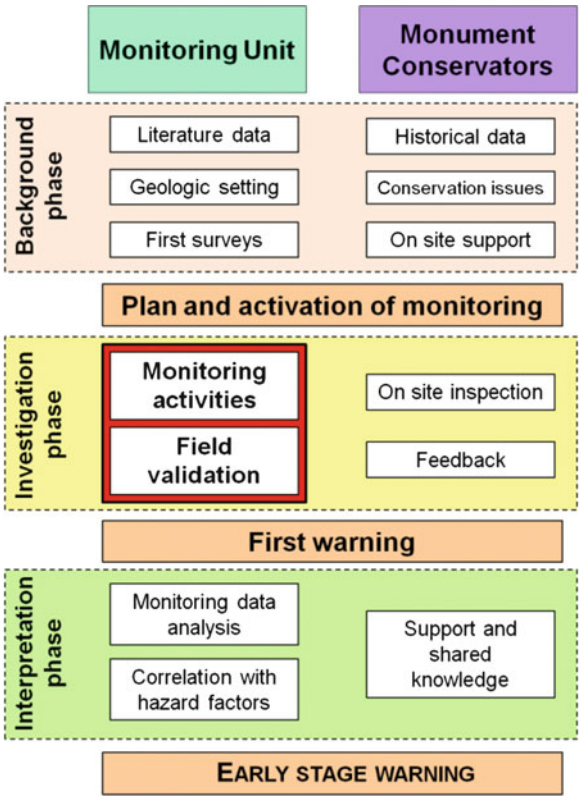


Fig. 4 Flow chart of the 'early stage warning' procedure tested for radar monitoring of archaeological monuments/sites

existing damages (*feedback*) can produce a first warning which contributes to guide the subsequent interpretation phase (third step).

At this level, the complete analysis of the monitoring data is integrated with the geologic setting and the local hazard factors. The local conservators with additional information on the monuments and related conservation issues can further contribute to the final assessment of the alert level. Ground and structural displacements are finally mapped and the most critical sectors are identified.

In relation to the magnitude of the detected criticalities and the related alert level assigned to the single area/monument, early stage warning can be activated, providing a proper classification of the exposed element(s) in terms of risk level.

Warning Activities on Monuments at Risk

Detection of Deformation Patterns

Multi-interferogram processing by PSInSAR techniques, included the most recent algorithm SqueeSAR (Ferretti et al. 2011), can reveal past/recent ground and structure motions. Thanks to the capability of distinguishing unstable sectors from stable ones, deformation patterns can be discovered by analyzing the distribution of the mean LOS deformation rates over the monitored area.

The concentration, in correspondence of a monument or a portion of soil, of different PS with homogeneous LOS deformation rates indicates the presence of localized instability. Based on the magnitude of the deformation velocity, the persistence of the ongoing deformation over the monitoring period can be immediately perceived.

The analysis of RADARSAT1 F3 ascending images acquired in 2003–2010 for the entire extent of the Roman Aqueducts, south of Rome, highlighted significant displacements for *Torre del Fiscale*, a medieval tower built over the ancient structures of two aqueducts crossing each other (Fig. 5a). All the detected displacements reach mean LOS deformation rates around −5.0 mm/year calculated over the entire period (Mar'03–Feb'10), with acceleration phases up to −9.6 mm/year away from the satellite (Fig. 5b).

The comparison with the general stability detected for the neighbouring areas (Fig. 5a) and the similar trend observed within the PS time series (Fig. 5b) confirmed the high level of criticality for the tower, as hypothesized from the crack pattern survey of the masonry (Fig. 5c). The height values associated to the PS demonstrated that the displacements interested the lower part of the tower and the surrounding ground, suggesting that the movements could be related to local ground instability, besides to a structural weakening due to the extended cracks.

The alert report about the existing high risk for the tower, sent to the Superintendances responsible for the monument, was recently confirmed by the opening of wide fissures on the ground, not so far from the building, and by the presence of subterranean caves running for kilometres underneath the

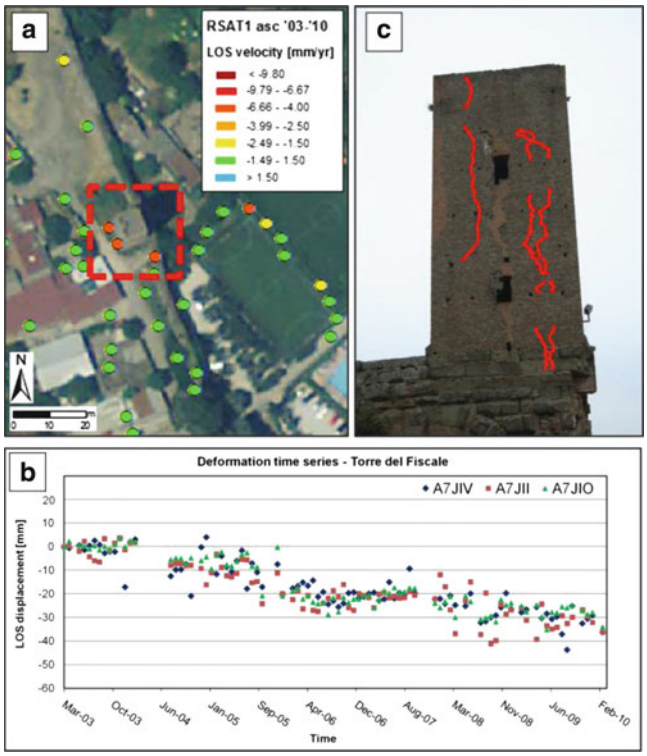


Fig. 5 PSInSAR results for *Torre del Fiscale*, Roman Aqueducts, Rome (*dashed red line*), with: (**a**) spatial distribution of the PS deformation rates from RADARSAT1 F3 2003–2010; and (**b**) the corresponding deformation time series. The satellite evidences confirm the structural criticality observed on the masonry, interested by an extended crack pattern on the exposed surfaces (**c**)

entire archaeological area. This early stage warning encouraged the local conservators to start urgent works on the tower and, at the same time, to verify the condition of the foundations.

Similar effectiveness of the PSInSAR analysis was demonstrated for the back monitoring of the Oppian Hill, identifying a worsening of the structural instability for the *Cisterna delle Sette Sale*, the massive cistern of the Baths of Trajan, for which the local conservators had supposed the occurrence of recent structural damages.

The comparison of three different PS stacks (RADARSAT1 F3 ascending 2003–2010; RADARSAT1 S3 descending 2003–2009; RADARSAT2 S3 descending 2008–2010) clarified the situation and an immediate procedure of early stage warning was activated for the monument. As summarized in Fig. 6, a definite deformation pattern with negative displacements away from the satellite was clearly detected for the period Jun'08–Jun'10. The mean LOS deformation rates range from −2.5 up to −4.1 mm/yr, affecting both the southern and northern parts of the cistern (Fig. 6b). The acceleration of the displacements in the last monitoring period is emphasized if compared with the roughly stable condition observed in 2003–2010 (Fig. 6a).

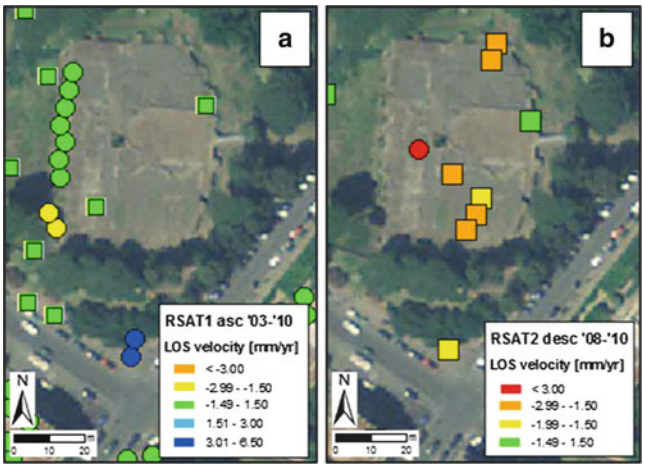


Fig. 6 Comparison between: (**a**) PS RADARSAT1 F3 ascending 2003–2010 and (**b**) PS RADARSAT2 S3 descending 2008–2010, for the *Cisterna delle Sette Sale*, Oppian Hill, Rome

Such satellite evidences convinced the local conservators to keep the monument close to the public and carry out terrestrial surveys and deep investigations.

Time Series Analysis for Warning

Besides the distribution of LOS deformation rates (first level of analysis), the second level of the satellite radar-interpretation consists in the recognition of differential displacement phases within the PS deformation time series. Acceleration/deceleration can be referred to a specific instability event or can testify a change of the structural behaviour of the detected radar target. Any discontinuity from the previous linear trend or appreciable deviation from the expected trend has to be verified in relation to the conservation history of the interested area. Cigna et al. (2011) recognized, for several PS time series, rapid displacements with temporary or permanent modification of the trend, associable to the fracture reactivation of a landslide.

Time series analysis for some PS identified on the NW corner of the Nero's Golden House in the Oppian Hill (apparently classifiable as 'stable' based on the low value of the mean LOS rate calculated over the entire monitoring period) revealed sensible deviations from the previous trend, concentrated in the final months of the satellite monitoring. Such accelerations, frequently with movements away from the satellite, reach mean LOS rates of about −5.1 mm/year in the period Jul'08–Aug'09 (Fig. 7a). The linear progression of these displacements does not exclude a near future evolution into severe deformation of the radar targets. The alert level for these areas is quite high, especially considering the typology of the structures interested by the displacements. The ancient masonry partially outcrops from

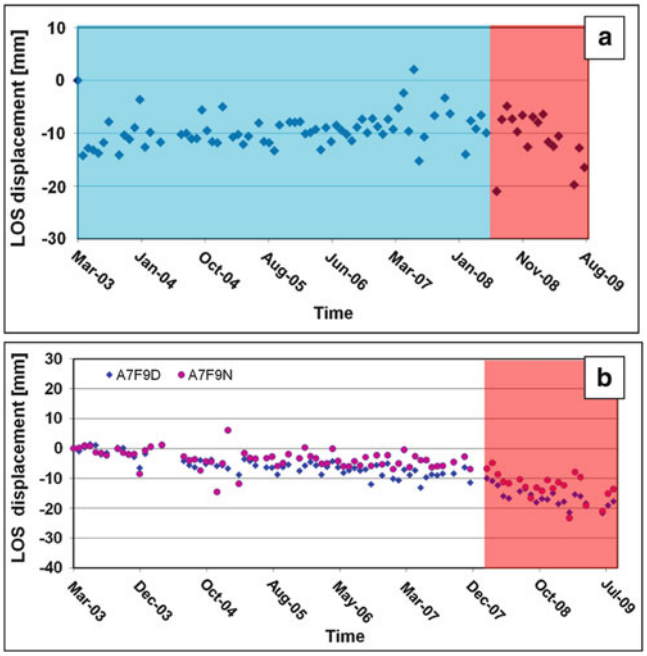


Fig. 7 Time series of PS RADARSAT1 S3 descending 2003–2009 identified in the areas of: (**a**) the NW corner of the Nero's Golden House, Oppian Hill, and (**b**) the sector of the Aurelian Walls, Via del Campo Boario, Rome

the covering terrain and is subjected to both superficial deterioration and hydrostatic pressure from the rear terrain. Such condition is very similar to the former geo-archaeological configuration of the gallery collapsed during the event of 30th March 2010.

The usefulness of the time series analysis for the prediction of potential instability events damaging the cultural heritage is also demonstrated by the results obtained from the satellite monitoring of the Aurelian Walls. RADARSAT1 descending images acquired in 2003–2009 showed for a sector of the Walls a definite trend to progressive movements away from the satellite, with two acceleration phases for the periods Jul'04–Dec'07 and Feb'08–Aug'09, with mean LOS rates of −1.4 and −4.9 mm/year, respectively (Fig. 7b). The latter constitutes a relevant deviation from the previous trend, assumable as an alerting signal (*precursor*) of upcoming deformation.

Based on these satellite evidences, the first warning suggested the execution of specific on site inspections. A collapse of the external brick curtain of the wall was found in the correspondence of the interested area, with irreversible loss of huge portion of the masonry structure. The event is thought to have occurred between Feb'10 and Mar'10, as the previous on site surveys did not record any damages. In this case the acceleration phase characterizing the PS time series until Aug'09 can be properly assumed as precursor of the instability event that subsequently occurred.

Real-Time Monitoring for Warning

The higher sampling frequency provided by GB-InSAR technique can be effectively exploited for real-time monitoring of single monuments, not achievable by satellite radar interferometry. Constantly updated deformation time series can be extracted for some control points properly selected within the observed scene. Hence the evolution of the LOS displacements can be continuously monitored for the exposed surfaces. Such surveillance activity configures the possibility of real-time detection of anomalies and suspicious movements, allowing the activation of early warning procedure, similar to the early stage one illustrated in Fig. 4.

The 'single monument scale' monitoring of the substruction arcades of Domus Tiberiana (Fig. 3a) confirmed a general stability for the period Apr'09–March'10, without significant or permanent deformation measured along the GB-InSAR LOS. The cumulative LOS displacement maps showed very low values, estimated for the entire monitoring period, ranging from +1.0 mm away from the sensor to −2.0 mm towards the GB-InSAR position (Fig. 8a).

Although this first level of analysis did not reveal any particular conservation criticalities for the monument, some anomalies from the expected trend were identified during the monitoring, as illustrated in Fig. 8b with the recognition of sudden displacements on the upper arcades, that were initially thought to be a localized collapse. The prompt alert sent to the local conservators and the immediate execution of on site checks demonstrated the absence of any damages, referring the detected movements to the effects of borehole drilling in the monitored masonry carried out exactly at that time.

Conclusions

The experimentations of radar monitoring and radar-interpretation on the archaeological areas of Rome have demonstrated the potentials of the radar interferometry for multi-temporal and multi-scale analysis on monuments threatened by ground and/or structural instability, as diagnostic tool for early stage warning. The exploitation of the technical features specific for the two configurations currently available (satellite and ground-based) confirmed the high analytical capability to perform 'entire site'/'single monument' monitoring and 'early stage'/'real time' warning.

The success of the present research consisted in carrying out monitoring activities within the framework of shared early stage warning procedure, which foresees the direct participation of the monument conservators, starting from the background phase until the interpretation phase. Following the step-sequence of the radar analysis (from the detection of deformation patterns to the series analysis and from the cumulative LOS displacement maps to the

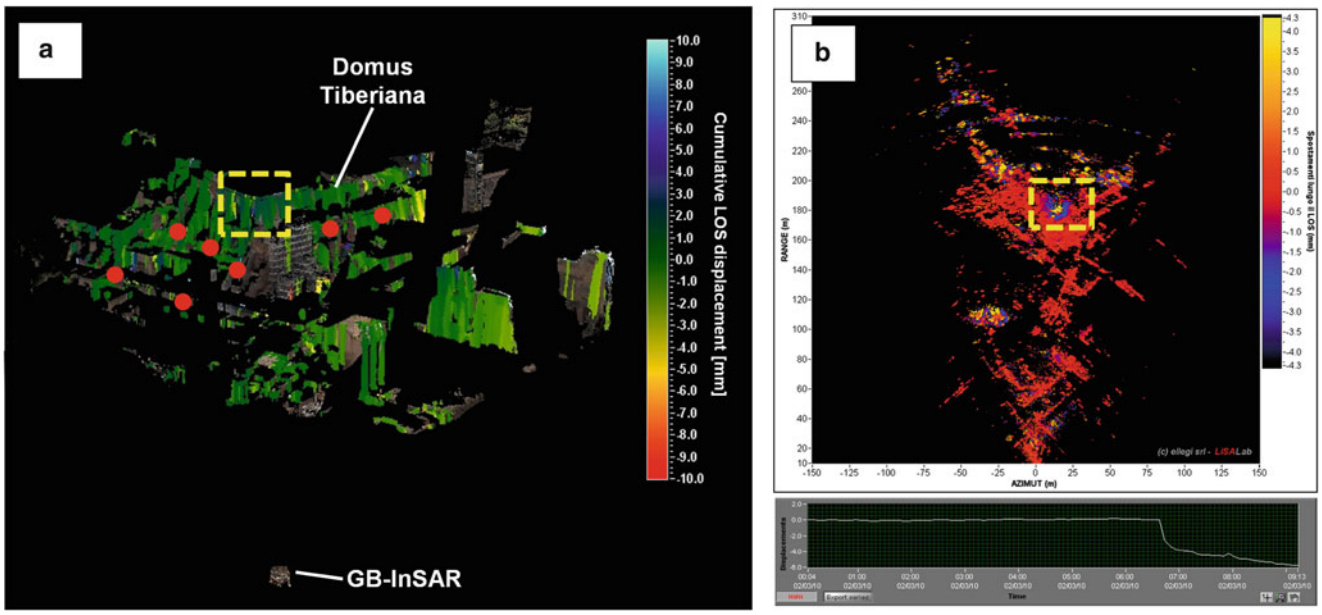


Fig. 8 Summary of the GB-InSAR results for Domus Tiberiana, Roman Forum, Rome, with: (**a**) cumulative LOS displacement map for the entire monitoring period Apr'09–Mar'10. *Red* points indicate the location of some of the control points used for the extraction and analysis of deformation time series; and (**b**) the 2D interferogram which shows a sudden movement occurring on the upper substruction arcades (*dashed yellow square*) with the related time series reported above

real-time time series analysis), prompt warning activities can be performed, at an 'early stage', prior to the occurrence of not remediable damages for the monuments.

Acknowledgments The results here presented were obtained from the research projects funded by the Italian Ministry of Cultural Heritage and Activities. The authors would like to thank the Commissioner for the archaeological areas of Rome and Ancient Ostia, arch. Pia Petrangeli and all the staff of the local Superintendances for their co-operation and support to the monitoring activities.

References

Asbhy T (1935) In: Richmond IA (ed) The aqueducts of ancient Rome. Clarendon Press, Oxford

Casagli N, Catani F, Del Ventisette C, Luzi G (2010) Monitoring, prediction and early warning using ground-based interferometry. Landslides 7(3):291–301

Cigna F, Del Ventisette C, Liguori V, Casagli N (2011) Advanced radar-interpretation of InSAR time series for mapping and characterization of geological processes. Nat Hazards Earth Syst Sci 11 (3):865–881

Evans D, Farr T (2007) The use of Interferometric Synthetic Aperture Radar (InSAR) in Archaeological Investigation and cultural heritage preservation. In: Wiseman J, El-Baz F (eds) Remote sensing in archaeology. Springer, New York, pp 89–102

Ferretti A, Prati C, Rocca F (2001) Permanent scatterers in SAR interferometry. IEEE Trans Geosci Remote Sens 39(1):8–20

Ferretti A, Fumagalli A, Novali F, Prati C, Rocca F, Rucci A (2011) A new algorithm for processing interferometric data-stacks: SqueeSAR. IEEE Trans Geosci Remote Sens 49(9):3460–3470

BBC News (2001) Ancient Roman wall collapses. http://news.bbc.co.uk/2/hi/europe/1280611.stm. Last accessed 6 June 2011

BBC News (2010) Ceiling collapse at Nero's golden palace in Rome. http://news.bbc.co.uk/2/hi/8595660.stm. Last accessed 6 June 2011

Rosen PA, Hensley S, Joughin IR, Li FK, Madsen SN, Rodriguez E, Goldstein RM (2000) Synthetic aperture radar interferometry. Proc IEEE 88(3):333–382

Sassa K, Picarelli L (2010) Preface for the thematic issue "Early Warning of Landslides". Landslides 7(3):217

Scarpelli G, Sakellariadi E, Cittadini M (1997) History and geotechnics of the Domus Tiberii on the Palatine Hill in Rome. In: Viggiani C (ed) Proceedings of geotechnical engineering for the preservation of monuments and historic sites, Naples, 3–4 Oct 1996, Balkema, pp 293–303

Tapete D, Casagli N, Fanti R, Del Ventisette C, Cecchi R, Petrangeli P (2011) Satellite and ground-based radar interferometry for detection and monitoring of structural instability in archaeological sites. Geophys Res Abstr 13, EGU2011-8387

Tapete D, Fanti R, Cecchi R, Petrangeli P, Casagli N (2012) Satellite radar interferometry for monitoring and early-stage warning of structural instability in archaeological sites. J Geophys Eng 9: S10–S25

Tapete D, Casagli N, Luzi G, Fanti R, Gigli G, Leva D (2013) Integrating radar and laser-based remote sensing techniques for monitoring structural deformation of archaeological monuments. J Archaeol Sci 40(1):176–189



Landwarn: An Operative Early Warning System for Landslides Forecasting Based on Rainfall Thresholds and Soil Moisture

Francesco Ponziani, Nicola Berni, Marco Stelluti, Renato Zauri, Claudia Pandolfo, Luca Brocca, Tommaso Moramarco, Diana Salciarini, and Claudio Tamagnini

Abstract

The Umbria Region is one of the Italian areas that are most prone to landslides and floods. For early-warning procedures aimed at the reduction of the hydrogeological risk, the rainfall thresholds represent the main component of the Italian Civil Protection System. To improve the performances of the alert system for landslide risk, the Umbria Region CFD, in cooperation with the Research Institute for Geo-Hydrological Protection (IRPI-CNR), developed and tested a continuous physically-based soil water balance model, addressed to the estimation of soil moisture conditions over the whole regional territory prior to severe landslide events. The relationship established between the maximum cumulative rainfall values and the soil moisture preceding the triggering of landslides allows to dynamically adjust the rainfall thresholds as a function of the estimated soil moisture values. The main components of the new early-warning system (named LANDWARN) for landslide risk prevention operating at the CFD are: (1) the observed and 72 h-predicted cumulative rainfall from the dense regional hydrometeorological network; (2) a local area meteorological model, known as COSMO ME; (3) the soil water balance model by Brocca et al. 2008; and (4) a web-based Information System. All these elements are arranged in a MATLAB-based flux of operations. Nowadays, the system is still under development and implemented at three different scales: (1) for a specific rockslide site, where a real-time extensometer network is available; (2) for 110 high-risk landslide sites located across the whole regional territory; and (3) for the whole regional territory over a regular grid. Further steps of the implementation are currently in progress. In particular, a GIS-based physically-based model that combines the hydrological information with a simple slope stability analysis is being validated in a test-area of the Umbria Region (Salciarini et al. Nat Hazards 9739–9742, 2011), with the aim of evaluating the possibility of developing an early-warning system capable to take into account the mechanical and physical characteristics of the slopes, besides rainfall and soil moisture.

Keywords

Hydrogeological risk • Alert states • Shallow landslides • Remote sensing • Soil water balance model

F. Ponziani (✉) • N. Berni • M. Stelluti • R. Zauri • C. Pandolfo
Regione Umbria, Civil Protection, Foligno, Italy
e-mail: fponziani@regione.umbria.it

L. Brocca • T. Moramarco
Research Institute for Geo-Hydrological Protection, CNR, Perugia, Italy

D. Salciarini • C. Tamagnini
Department of Civil and Environmental Engineering, University of Perugia, Perugia, Italy

Introduction

Predicting the spatial and temporal occurrence of rainfall-triggered shallow landslides represents an important scientific and practical issue due to their high threats to human lives and properties (Ray et al. 2011; Ren et al. 2011).

C. Margottini et al. (eds.), *Landslide Science and Practice*, Vol. 2,
DOI 10.1007/978-3-642-31445-2_82, © Springer-Verlag Berlin Heidelberg 2013

The Umbria Region, located in central Italy, is one of the most prone areas to landslide risk in Italy, being almost yearly affected by landslides and flood events at different spatial and temporal scales. For the early-warning procedures of the Italian Civil Protection System, aimed at the reduction of the hydrogeological risk, the rainfall thresholds represent the main element of evaluation. A more accurate and reliable methodology for the landslide risk assessment and management is one of the main objectives of the Umbria Region Civil Protection Centre (where the "Decentralized Functional Centre" – CFD is the operative early warning office). It is well known that the application of rainfall thresholds based only on the intensity/duration information is not sufficient for the risk assessment, as the initial soil moisture conditions play a crucial role (Baum and Godt, 2009). By affecting the pore water pressure value, the soil moisture can change the strength-stress ratio of the soils, up to constitute a crucial precondition for the triggering of landslides. This insight was already pointed out in former studies by Ponziani et al. (2010, 2012) who experimentally shown the relationship between the triggering of several large landslide events occurred in the Umbria Region and the initial soil moisture conditions. On this basis, in order to improve the performances of the alert system for landslide risk, the Umbria Region CFD, in cooperation with the Research Institute for Geo-Hydrological Protection (IRPI-CNR), developed and tested a continuous physically-based soil water balance model, addressed to the estimation of soil moisture conditions over the whole regional territory (Brocca et al. 2008).

The soil water balance model is hence used in combination with rainfall thresholds in the new early-warning system for landslide risk prevention of the CFD, named LANDWARN, that is under development and applied to:

1. The known high-risk landslides across the whole Umbria Region territory (110 in total);
2. The Torgiovannetto Rockslide, for which a real-time extensometer network allows to record the movement of the rock wedge; note that this site is also used to test the reliability of the system itself;
3. The whole regional territory, by a dense regular grid, aimed at the development of a real time landslide risk scenario.

The LANDWARN system runs in real-time and uses rainfall and temperature observations coming from the dense regional hydrometeorological network. Moreover, 72 h-in-advance rainfall and temperature forecasts, derived by the local scale meteorological model COSMO ME, are also used to issue landslide risk warnings up to 2 days in advance.

However, to issue effective warnings, the emergency operators need to better define which areas are included in the warning. Probabilistic rainfall thresholds compiled on correlations between recorded data show that precipitation amounts and durations required to trigger shallow landslides vary with climatic, geotechnical and topographic conditions; consequently, thresholds exhibit a high degree of spatial variability, even across relatively small geographic areas (Guzzetti et al. 2007, 2008). For rapid analysis of intensity/duration rainfall thresholds at the local scale, GIS-based modeling techniques have been developed and successfully applied starting from Iverson's theory (Baum et al. 2008; Godt et al. 2008; Iverson 2000; Salciarini et al. 2008). Here a GIS-based modeling system is going to be implemented in a test area, in order to build a system capable to improve the overall performances, taking in account rainfall, soil moisture, geometric, hydrologic and mechanical characteristic of the slopes.

Study Area

The Umbria Region (8,456 km^2) is located in the central Italy and is characterized by complex topography. The geology is constituted of post-orogenics marine and continental facies, flysch deposits consisting of clay-schist and clay-marl sediments, well-bedded limestones and volcanic rocks. In Umbria Region all municipalities are prone to hydrogeological risk areas and about 9 % of the territory (650 km^2) is affected by active landslides. More than 70 % of the inventoried landslides are of dormant type, subject to reactivation with strong precipitations. The analysis of the landslides type shows that most of them (more than 70 %) are of translational-rotational slow-moving type, about 4 % are fast-moving slides, and 10 % are deep-seated landslides. The precipitation regime can be classified as Mediterranean, with distinct dry and wet seasons. Higher monthly precipitation values generally occur during the autumn-winter period when landslides and floods, caused by widespread rainfall, normally occur. As an example, during a rainfall event that occurred in December 2008, 300 mm of rainfall in 12 days was registered (the mean of maximum monthly rainfall is around 240 mm), with 120 landslides reported to the Regional Civil Protection Office. Mean annual precipitation is about 1,000 mm; mean annual temperature is 11 °C; snowfalls at altitude below 500 m a.s.l. are unusual.

The territory is covered by a near real-time hydrometeorological network (1 station every 80 km^2 approximately with a data transmission time interval 30 min), operating from more than 20 years (see Fig. 1). The historical rainfall database used for this analysis is composed by records from 56 rain-gauges characterized by continuous and high quality data during the period from 1989 to 2001. The temperature database is composed of records from 30 thermometers operating over the same area.

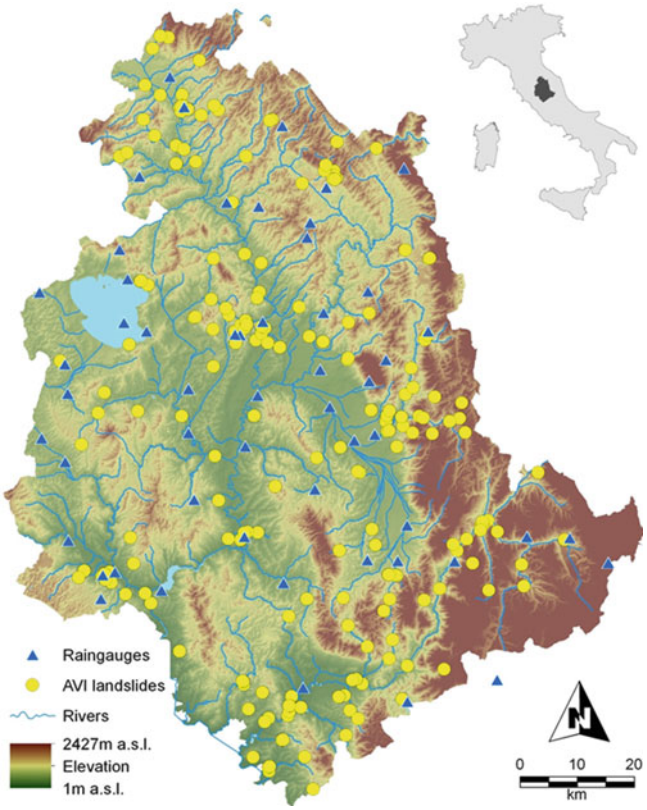


Fig. 1 Morphology and hydrometeorological network of the Umbria Region. The location of the landslides reported in the AVI (Italian Vulnerable Areas) inventory are also shown

Methodology

Soil Water Balance Model

The physically-based soil water balance model applied here was developed using soil moisture observations carried out in experimental catchments located in the Umbria Region (Brocca et al. 2008). In particular, different expressions were considered for the different components of the model, such as infiltration, percolation and evapotranspiration. The analysis allowed the selection of the simple soil water balance model employed in this study and briefly described in the sequel.

The surface soil layer is assumed as a spatially lumped system described by a water content balance equation. The infiltration rate is estimated by using the Green-Ampt equation while for the drainage component a non-linear relationship as a function of soil saturation is adopted. The evapotranspiration is represented by a linear relation depending on the potential evapotranspiration and the soil saturation.

As forcing data, the model uses as meteorological variables the rainfall and air temperature that are routinely measured by standard hydrometeorological networks. Five parameters are involved in the model calibration. As these parameters are physically based and their values range is limited, the model was found consistent even when the calibration is done through a limited number of observations (Brocca et al. 2008). These characteristics allow to confidently use the model over large areas and for periods different from those employed for calibration. In this study, the model parameters were kept the same for the whole area and equal to the average value obtained by outcomes of previous studies (Brocca et al. 2008, 2010). Therefore, the output of the model should be seen as a soil moisture index allowing us to estimate the relative wetness conditions of the soil before a severe event, not as the actual soil moisture value.

LANDWARN

The LANDWARN system developed by the CFD performs the following main steps:

1. Estimation (using spatial interpolation algorithms) of the 20-days past rainfall and temperature together with the 72 h forecast data for the calculation grid points. This is done by using real-time data from the regional hydrometeorological monitoring network and the results of quantitative weather forecast COSMO ME models on a local scale for Umbria;
2. Computation of the soil moisture index through the physically-based soil water balance model;
3. Comparison of observed and forecasted rainfall data with the rainfall thresholds that take into account a correction factor linked to the soil moisture index;
4. Definition of four early-warning indicators for each grid point (normal, caution, warning, alarm), in compliance with national and regional law.

Further actions are performed for every step. As an example, in the step no. 3 rainfall data are combined with a susceptibility layer and a vulnerability layer over a regular grid of the Umbria territory (100 × 100 m), to allow the construction of a dynamic risk scenario that is published on a WEB GIS platform.

More specifically, the susceptibility layer consists of a 100 × 100 m raster which contains a number of classes

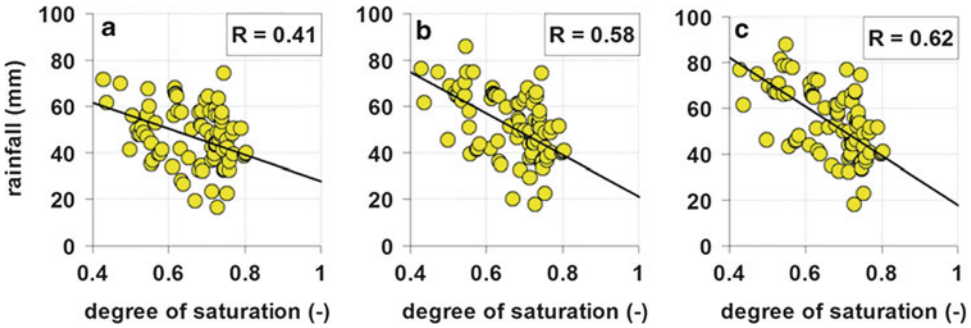


Fig. 2 Cumulated rainfall values over 24 (**a**), 36 (**b**) and 48 (**c**) hours versus the simulated initial degree of saturation (soil moisture index) for the landslide events reported in the AVI database and considering the period 1991–2001

of indicators of landslide susceptibility from elaboration of the most significant variables such as slope, presence of landslides, lithology, etc. The state of the susceptibility layer is constantly changing due to the complexity of the problem and the large number of data and information needed, with the involvement of various Departments, Regional Offices and Research Centres, such as the National Research Council (CNR), Universities, etc. The Vulnerability layer is constituted by the overlapping of different levels, each divided into classes: roads, ordinary and strategic buildings, infrastructure network, etc.

The Role of the Soil Moisture in Rainfall Thresholds Assessment

Based on the analysis of the widespread landslide events available within the Italian AVI ("Aree Vulnerate Italiane") Landslide database, a linear relation between the rainfall values triggering landslides and the initial soil moisture conditions, as estimated by the soil water balance model, was found (Fig. 2) with correlation coefficients up to 0.60 (Ponziani et al. 2012) showing the key role of initial soil moisture conditions on landslide triggering.

Therefore, the relation established between the maximum cumulative rainfall values and the soil moisture prior to the triggering of landslides allows to dynamically adjust the rainfall thresholds which is of paramount interest for warning activities. Indeed, these results provided a significant contribution to the real-time landslides risk assessment for the regional territory, decreasing the uncertainties tied to the application of the rainfall thresholds only.

Moreover, collected data can be used both for the effective calibration of physically-based models of infiltration and for establishing correlations for empirical models of landslides triggering.

Applications

High Risk Landslides

This section of the early-warning system (Fig. 3) is aimed to the monitoring of 110 landslides at high risk in the Umbria territory: the choice of the sites comes from a preliminary work in which all the known situations at hydrogeological risk were classified. It must be pointed out that the system, up to now calibrated on the landslide dataset recorded during the main rainfall events occurred in the last 20 years in the Umbria territory, works also as a monitoring system able to evaluate the landslide hazard in larger areasaround the landslide sites, so with a higher detail with respect to the 6 territorial zones of the current alert system.

The diagram in Fig. 4 shows the operational flux.

The Torgiovannetto Landslide

The Torgiovannetto landslide originated from a dismissed stone quarry near the town of Assisi, in Central Italy. The stratigraphy is constituted by stratified limestone with intercalation of thin weak clay layers: the dip of the front of the quarry is about 30−38°, similar of that of the limestones

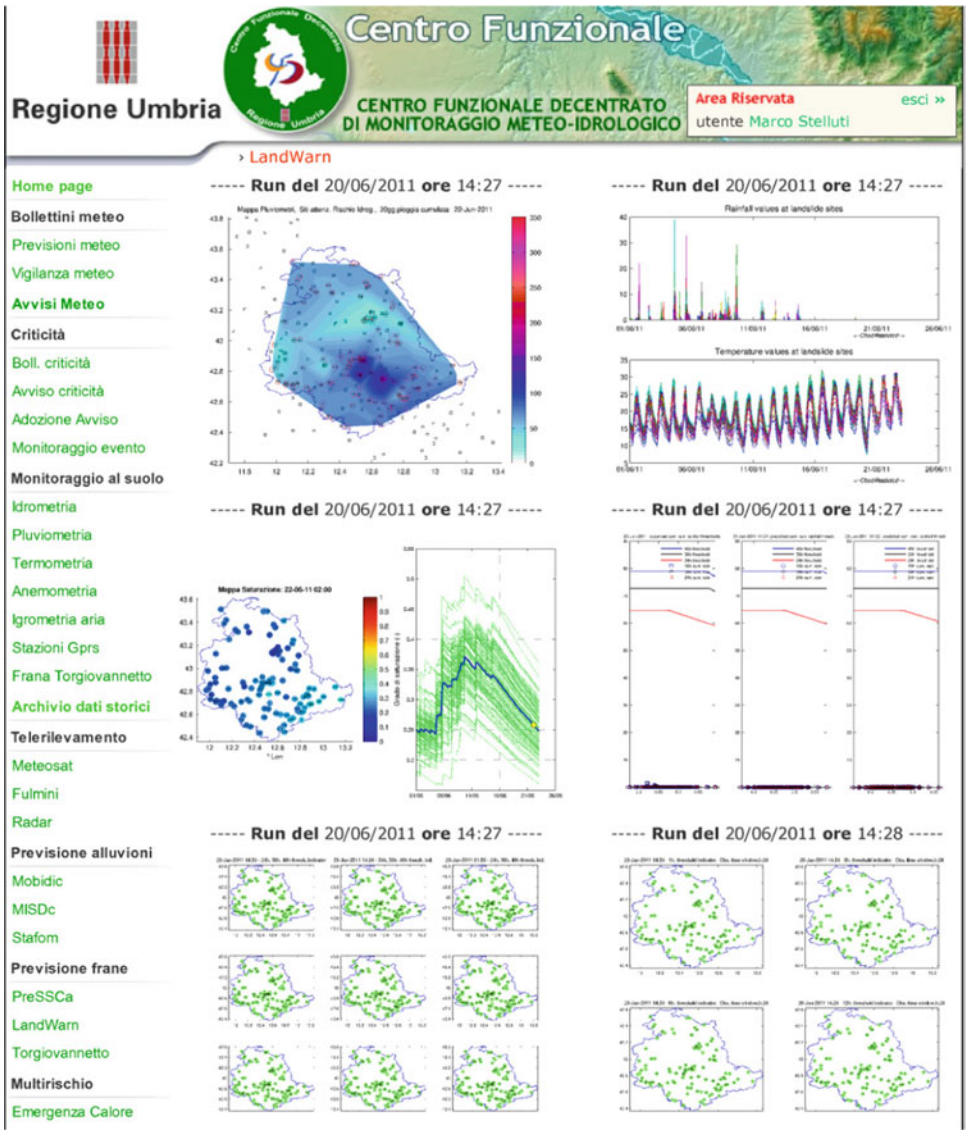


Fig. 3 CFD Web page of the early-warning system, section 1

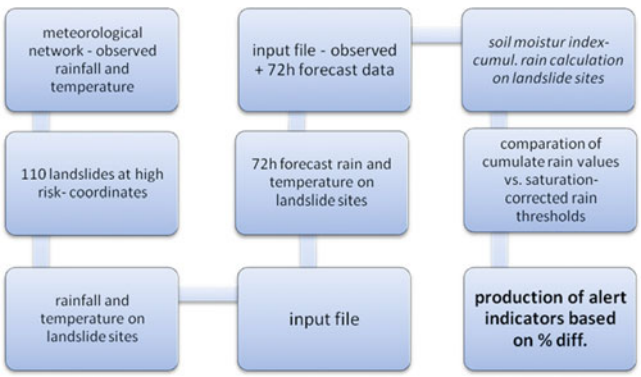


Fig. 4 Operational Flux for the application of LANDWARN to the 110 high risk landslides

bedding planes. A huge sliding rock wedge in the upper part of the quarry has formed, delimited by a big tension crack up to one meter wide and over 100 m long, shoving slow movements after heavy rainfalls, relating the raising of the pore pressure to the reduction of the shear strength on the stratification planes.

The rock wedge threatens two roads at the base of the slope: the landslide is monitored by a meteorological station, an extensometer network and, recently, by a high dynamic accelerometer. The dataset collected up to now demonstrated the clear influence of the rainfall on the rock slide movements.

Due to the potentiality of a catastrophic failure that could affect the suburban road passing close to the quarry,

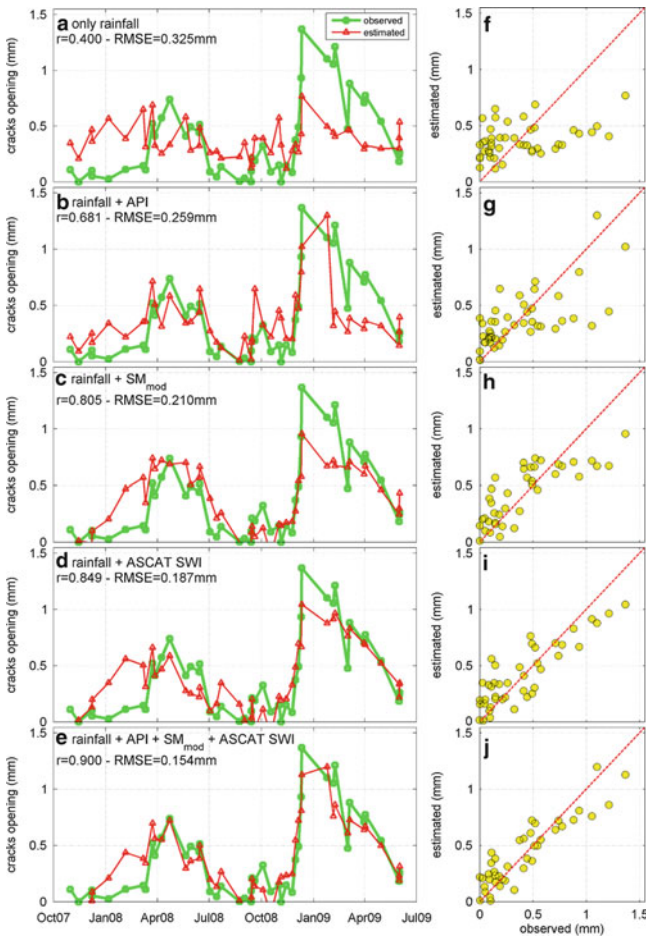


Fig. 5 Comparison between observed and estimated cracks opening from the beginning to the end of the selected rainfall events in the study period: (**a**–**e**) time series, and (**f**–**j**) scatter plots (*r* correlation coefficient, *RMSE* root mean square error). The predictors are: (**a**–**f**) rainfall variables (i.e., total rainfall, maximum rainfall for durations of 1, 3 and 12 h); (**b**, **g**) rainfall (the same as before) and Antecedent Precipitation Index, API (cumulated on 20 days); (**c**–**h**) rainfall and modelled soil moisture, SM_{mod}; (**d**–**i**) rainfall and the ASCAT Soil Water Index, SWI; (**e**–**j**) rainfall, API, SM_{mod} and SWI

the CFD is in charge of an alert procedure based upon the observation and prediction of the overtopping of cracks opening velocity (equal to 0.5 or 1 mm/day depending on the location of the different extensometer). The procedure developed for the forecast of the cracks opening velocity is based on the following tasks:

- The calculation of the accumulate rain measured by the in-situ meteorological station, and the predicted ones for the three following days using the COSMO-ME local scale prevision models;
- The calculation of the soil moisture content by the soil water balance model;
- The estimation of the cracks opening velocity through a multiple regression analysis that takes rainfall and soil moisture conditions into account.

The system result is constituted by the real-time evaluation of rainfall and soil moisture conditions for the Torgiovannetto site and the forecast for three following days of cracks opening.

The multiple linear regression equation used for the estimation of cracks opening has been calibrated by analyzing a series of rainfall events that occurred in the period 2007–2009 for which the opening of the tension cracks (as recorded by extensometers) is available (Brocca et al. 2012). Specifically, besides via the soil water balance model, soil moisture estimates are also retrieved by satellite sensor. The Soil Water Index product obtained by the Advances SCATterometer (ASCAT) on board MetOp (Meteorological Operational) satellite is used for this purpose. Results (Fig. 5c) indicate that the ASCAT SWI can be effectively used for the prediction of the cracks opening of the investigated Torgiovannetto landslide because of the good agreement between the observed and estimated cracks opening. The multiple regression performance decreases if modelled soil moisture data and Antecedent Precipitation Indices are used instead of the ASCAT SWI. The derived relationships are hence used for the alert procedure of Torgiovannetto landslide.

Risk Scenario: Early-Warning from Regional Level to Specific Site

The section is based on the same methodology used for the 110 high risk landslides, but using a dense regular grid, in order to spatially extend the analysis and the monitoring to the whole regional territory.

A WebGis platform is used to build near real-time dynamic scenarios combining the rainfall forecasts (at 24 and 72-h) with landslide susceptibility and vulnerability data. The main result of the analysis is a spatial information on landslide risk, highlighting the areas where local risk situations can emerge due to the interaction of the rainfall-induced landslides with the presence of vulnerability elements. This scenario has a dynamic character because of the re-computation of the rainfalls that are likely to trigger landslides on every dataset updating (Fig. 6).

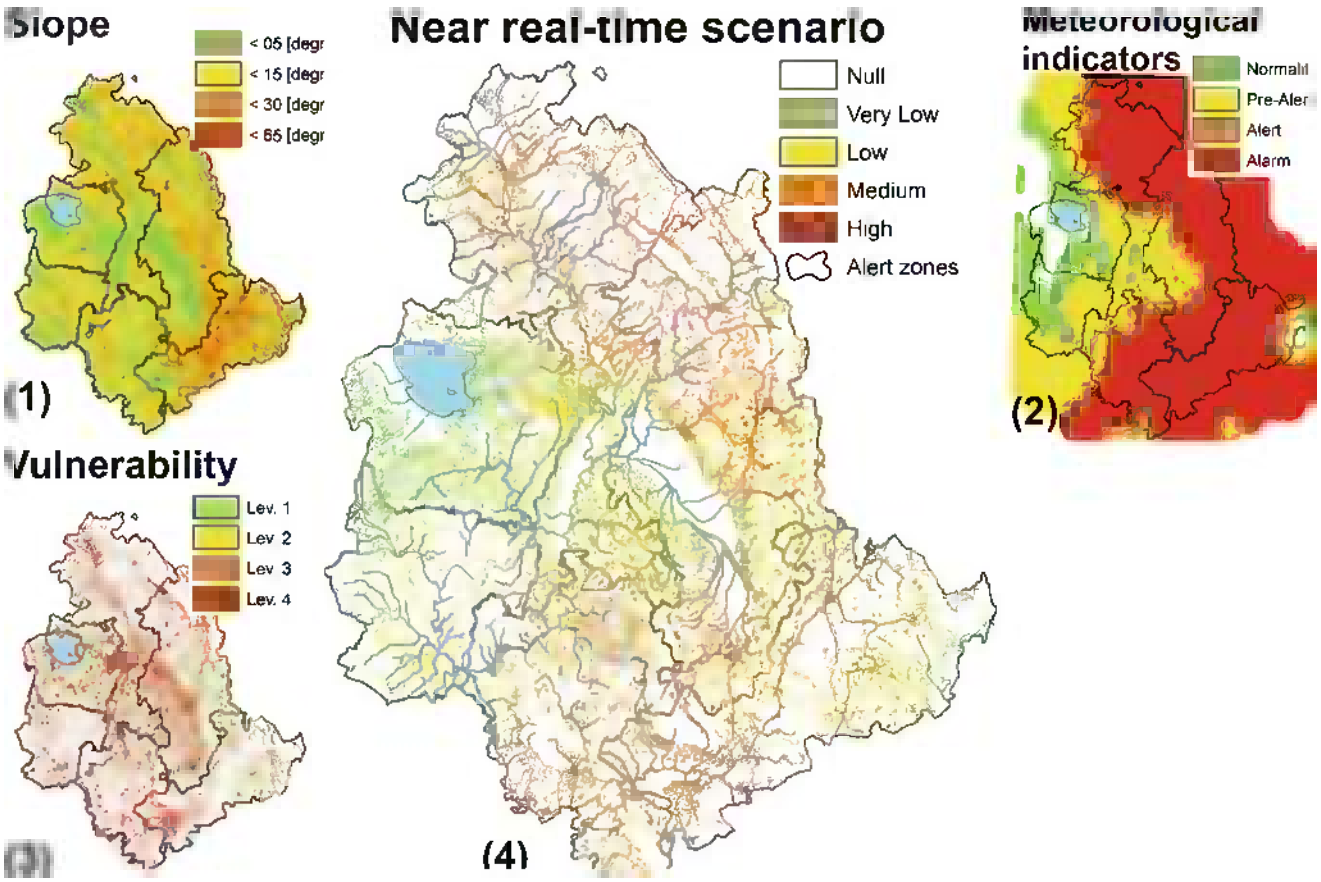


Fig. 6 Landslide susceptibility (here only slope contribution is shown) (1), meteorological indicators (2) and vulnerability (3), producing the dynamic, near real time scenario (4)

Moreover, a under-development GIS-based code permits the prediction of the spatial distribution of the minimum rainfall intensity which is likely to trigger shallow landslides and debris flows over a given study area, based on the rainfall duration and the local geometric, hydrologic and mechanical characteristics of the slopes. Once validated, such an approach can be combined with short-time predictions of rainfall data, derived from the CFD real-time meteorological network, with the aim of implementing a new section of the early-warning system.

Conclusions

In this paper, the early-warning system LANDWARN for landslides forecast based on rainfall thresholds operating at the Decentralized Functional Centre – CFD, in the Umbria regional Civil Protection Centre, is shown. Three different applications are illustrated.

Nowadays the system provides reliable and robust warnings. However it is continuously under developing and, in particular, with the following task:

- Definition of landslide-specific rainfall thresholds data using more complete reactivation date information;
- Calibration of the soil water balance model parameters for each landslide site using detailed soil stratigraphy and geological-geotechnical maps;
- Building specific physically-based slope stability models on a number of landslides for which sufficient geological-geotechnical data are available;
- Use of the ASCAT Soil Water Index product for the whole regional territory, not only for the Torgiovannetto landslide, in order to reduce the uncertainties linked to soil moisture estimation.

Moreover, the GIS-based modelling technique is shown fundamental for an application during emergency phases.

References

Baum RL, Savage WZ, Godt JW (2008) TRIGRS – a Fortran program for transient rainfall infiltration and grid–based regional slope–stability analysis, version 2.0. USGS Open File Report 08-1159. http://pubs.usgs.gov/of/2008/ofr-08-1159/

Guzzetti F, Peruccacci S, Rossi M, Stark C (2008) The rainfall intensity–duration control of shallow landslides and debris flows: an update. Landslides 5:3–17

Baum RL, Godt JW (2009) Early warning of rainfall-induced shallow landslides and debris flows in the USA. Landslides 7(3):259–272

Brocca L, Melone F, Moramarco T (2008) On the estimation of antecedent wetness condition in rainfall-runoff modeling. Hydrol Process 22:629–642

Brocca L, Melone F, Moramarco T, Wagner W, Hasenauer S (2010) ASCAT Soil Wetness Index validation through in-situ and modeled soil moisture data in central Italy. Remote Sens Environ 114 (11):2745–2755

Brocca L, Ponziani F, Moramarco T, Melone F, Berni N, Wagner W (2012) Improving landslide forecasting using ASCAT-derived soil moisture data: A case study of the torgiovannetto landslide in central Italy. Remote Sensing 4(5):1232–1244

Godt JW, Schultz WH, Baum RL, Savage WZ (2008) Modeling rainfall conditions for shallow landsliding in Seattle, Washington. Rev Eng Geol 20:137–152

Guzzetti F, Peruccacci S, Rossi M, Stark CP (2007) Rainfall thresholds for the initiation of landslides in central and southern Europe. Meteorol Atmos Phys 98:239–267

Iverson RM (2000) Landslide triggering by rain infiltration. Water Resour Res 36:1897–1910

Ponziani F, Pandolfo C, Stelluti M, Berni N, Brocca L, Moramarco T (2012) Assessment of rainfall thresholds and soil moisture modeling for operational hydrogeological risk prevention in the Umbria region (central Italy). Landslides 9(2):229–237

Ponziani F, Berni N, Pandolfo C, Stelluti M, Brocca L (2010) An integrated approach for the real-time monitoring of a high risk landslide by a regional civil protection office. In: Proceedings of international conference EGU Leonardo topical conference series on the hydrological cycle 2010, Luxembourg, 10–12 Nov 2010

Ray RL, Jacobs JM, Ballestero TP (2011) Regional landslide susceptibility: spatiotemporal variations under dynamic soil moisture conditions. Nat Hazards, doi:10.1007/s11069-011-9834-4 (in press)

Ren D, Fu R, Leslie LM, Dickinson RE (2011) Predicting storm-triggered landslides. Bull Am Meteorol Soc 92:129–139

Salciarini D, Godt JW, Savage WZ, Baum RL, Conversini P (2008) Modeling landslide recurrence in Seattle, Washington, USA. Eng Geol 102:227–237



Method of Residual-State Creep Test to Understand the Creeping Behaviour of Landslide Soils

Deepak Raj Bhat, Netra P. Bhandary, and Ryuichi Yatabe

Abstract

Many researchers have studied creeping behaviour of landslide soils in the laboratory using both odometer and triaxial tests; however in most cases, they have only concentrated on the pre-peak creep behaviour of soil, which does not adequately explain the creep movement of landslides that undergo large displacements at close-to-residual state of shear. This necessitates the importance of further studying creep behaviour of clayey soils in residual-state of shear. In order to investigate creep behaviour of clayey soils, a method of residual-state creep test in a modified torsional ring shear machine is developed in laboratory, which can simulate the creeping behaviour of a large-scale landslide. This paper discusses on the typical results obtained from four representative landslide soils, i.e., commercially available Kaolin clay and three other samples from the landslide area in Japan and Nepal which have higher percentage of smectite, chlorite, and mica. Finally, possibilities towards displacement prediction are discussed.

Keywords

Landslide soils • Residual-state creep test • Creep behaviours

Introduction

Clayey soils exhibit creep behavior, in which the deformation of soil depends on time under any applied constant effective pressure or self weight. Clay soils show all the rheological properties, where the creep is the most typical, pronounced and readily observed. To understand the creeping behavior of landslide soils, the ideal creep curve is divided into three sections: (1) primary creep (damping or unsteady), (2) secondary creep (steady, at a constant rate), and (3) tertiary creep (undammed or progressive flow). In primary creep, rate of acceleration decrease and after a certain period of time, rate of acceleration becomes constant which is known as secondary creep. In tertiary creep, the rate of acceleration is sharply increases leading to failure.

D.R. Bhat (✉) • N.P. Bhandary • R. Yatabe
Graduate school of Science and Engineering, Ehime University,
3 Bunkyo, Matsuyama, 790-8577, Japan
e-mail: deepakrajbhat@yahoo.com

Special soil properties such as strength parameters, physical parameters, mineralogical composition, and many others are required to evaluate mechanism and prediction of large-scale landslides. Field tests for these properties may be time consuming, expensive, tedious, and a difficult task, but laboratory investigation in most cases is affordable and convenient. The application of a ring shear apparatus to estimate the strength of a soil is preferred especially when the soil strength is governed by higher shear deformation. Creeping landslides, for example, possess very high shear strain at very low rate of deformation along the slip surface. The strength of slip surface soils in case of a slow-moving landslide is thus governed by the state of extremely slow rate of shear. Such a state of soil, when its strength is governed by shear deformation resulting in no change in volume is often known as residual state, at which the strength of a clayey soil is always less than its peak strength. Creeping landslides usually move with extremely slow rate of displacement, and they often undergo cumulative displacement of several meters. Theoretically, under similar

C. Margottini et al. (eds.), *Landslide Science and Practice*, Vol. 2,
DOI 10.1007/978-3-642-31445-2_83, © Springer-Verlag Berlin Heidelberg 2013

conditions the residual strength for landslide clay in its field residual state measured in the laboratory must be equal to that in the field. Skempton (1985) has mentioned that the field residual strength value for the slip surface soil of landslide should be the same as the strength calculated from the back analysis of the landslide in which movement has been reactivated along a pre-existing slip surface. It means the back analyzed and lab-determined strength parameters must be the same that the lab tests are carried out under precisely similar in-situ conditions. Bromhead and Curtis (1983), Stark and Eid (1994), Mesri and Shahien (2003), Stark et al. (2005), and Tiwari and Marui (2005) have concluded that the drained residual shear strength measured in a ring shear machine is in agreement with the back-calculated drained residual shear strength for a landslide slip surface. Hence, laboratory investigated shear strength can be useful for the study of creep landslide mechanisms and further possibilities toward displacement predictions.

Most of large-scale landslides show the creeping behaviour due to the presence of greater composition of clayey minerals such as smectites, chlorites, and micas and illites. The past works are confined to pre-peak creep study; however, landslide mass is supposed to reach residual state which naturally demands post-peak creep study, especially residual-state creep study. The residual-state creep test set-up is developed in the laboratory using a modified torsional ring shear machine, which is adequately capable of measuring the displacement with respect to time under the application of constant creep load. In this study, four representative landslide soils, i.e., commercially available Kaolin clay and three other samples, which have higher percentage of smectite, chlorite, and mica are tested using newly developed residual-state creep testing procedures. To understand the creeping behaviour of clayey soils, creep load is varied until the specimen fails keeping the effective normal stress constant. A series of residual-state creep test (i.e. seven tests) for each sample are conducted, and the results thus obtained are interpreted in terms of Residual-State Creep Stress Ratio (RCSR), at which the soil samples fail at their residual state. The term RCSR is the ratio of applied constant shear stress to residual strength. The test results show that when RCSR ≤ 1, the soil does not show creeping behaviour where as the soil undergo creeping behaviour when RCSR > 1. This paper mainly focuses on the residual-state creep behaviour of landslide soils and further possibilities towards displacement prediction based on experimental findings.

Materials and Methods

In this study, four representative landslide soil samples consisting of commercially available Kaolin clay and three other samples from the landslide areas in Japan and Nepal

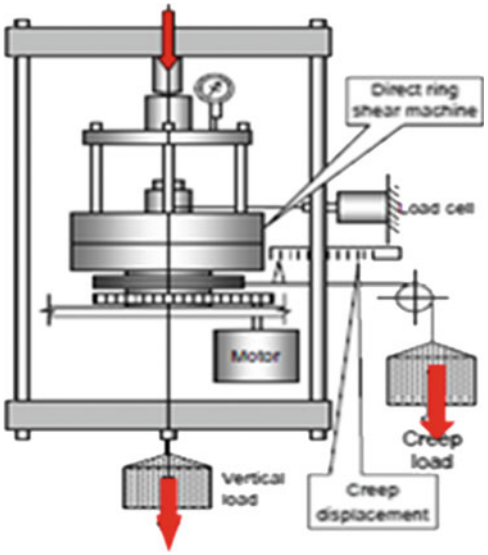


Fig. 1 Modification of torsional ring shear machine

are taken. The landslide soil from Shikoku area in Japan is confirmed to have comparatively high amount of chlorite, and is named "Chlorite-rich sample" and the landslide soil from Kobe area in Japan is confirmed to have high amount of smectite, which is named "Smectite-rich sample". Similarly, the landslide soil from Krishnabhir landslide area in Nepal is confirmed to have high amount of mica, and is named "Mica-rich sample". All test samples are prepared with over consolidated under the effective normal stress 196.20 kN/m^2, and effective normal stress (98.10 kN/m^2) is uniformly applied to the entire specimen during shear and creep test.

Bishop et al. (1971) type ring shear machine is modified based on transitional change of strain-controlled motor-driven shear into creep load shearing without completely releasing the applied shear stress as shown in Fig. 1. In residual-state creep test, there are mainly two steps: (1) ring shear test, and (2) residual-state creep test. Ring shear test is done to determine the peak and residual shear strength of clayey soils under the fully saturated state. This state is confirmed when the shearing has reached the residual state indicating the constant values in load-cell reading and dial gauge reading after a large displacement; then, the specimen is ready for the residual-state creep test. The lower part of ring shear has developed in such a way that the overall effect of creep load is directly acting on the slip surface of test specimen and the small displacement due to the application of constant creep load is recorded in displacement recorder unit. The deformation of the specimen with respect to time and the corresponding changes in volume if any during creep tests recorded automatically. The controlled shearing of the specimen is done until the specimen reaches to the residual state after the large

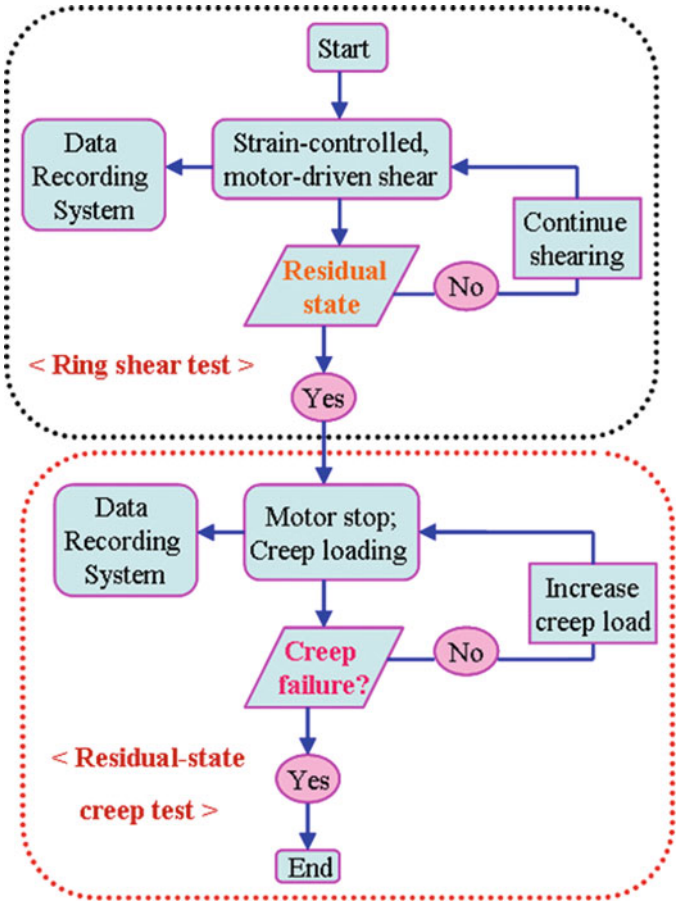


Fig. 2 Overall experimental flow of creep test

displacement of shearing; then, shearing process is stopped to start the residual-state creep test. Initially, the creep load is applied 85 % of its residual state which is equivalent to RCSR, 0.8500. Then, it is left for a couple of hours in the same condition to check the significant effect of creeping behaviour or not. Similarly, creep load is applied accordingly with RCSR values 0.9000, 0.9500, 1.000, 1.0025, 1.0050, 1.0100, 1.0125, 1.01500, 1.0200 until the specimen reach to fail. Figure 2 shows the overall experimental flow of residual-state creep test.

Results and Discussion

Typical ring shear test results on Kaolin clay, Smectite-rich sample, Chlorite-rich sample, and Mica-rich sample are presented in terms of variation of shear stress and specimen depth with the shear displacement (as shown in Fig. 3). Residual state of shear in each case has obtained after 10.0 cm of shear displacement except in Smectite-rich sample. For the being of this confirmation, residual-state creep tests of Smectite-rich soil specimen are preceded up to 20.0 cm of shear displacement and up to

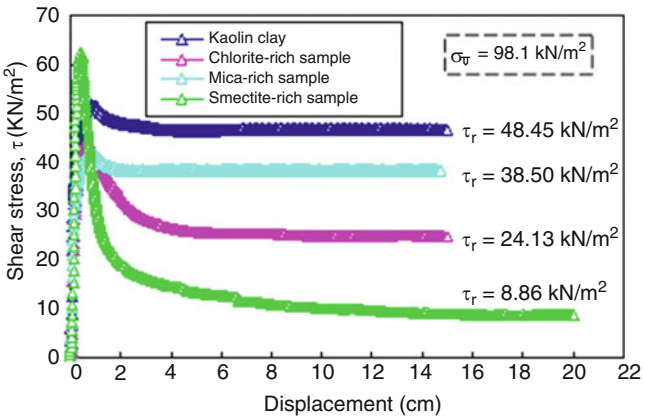


Fig. 3 Ring shear test on trepresentative landslide soil samples

15.0 cm for remaining soil specimens. Since the sample preparation and test procedures are conducted in certain set procedure, the residual strength of each samples are found in close agreement. Result shows that Kaolin clay has higher value of residual shear strength and followed respectively by other soils specimen such as Mica-rich sample, Chlorite-rich sample, and Smectite-rich sample as shown in Fig. 3.

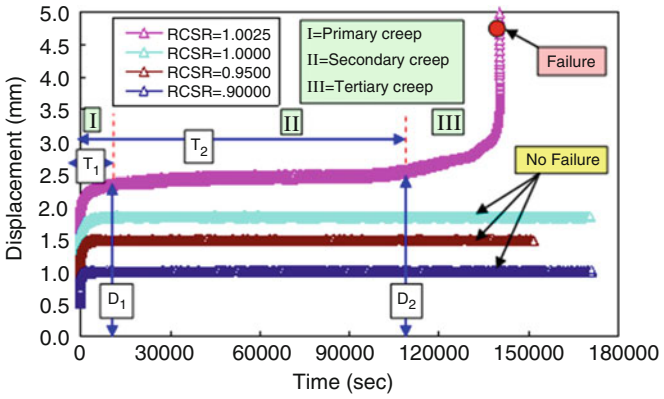


Fig. 4 Typical residual-state creep test on Kaolin clay

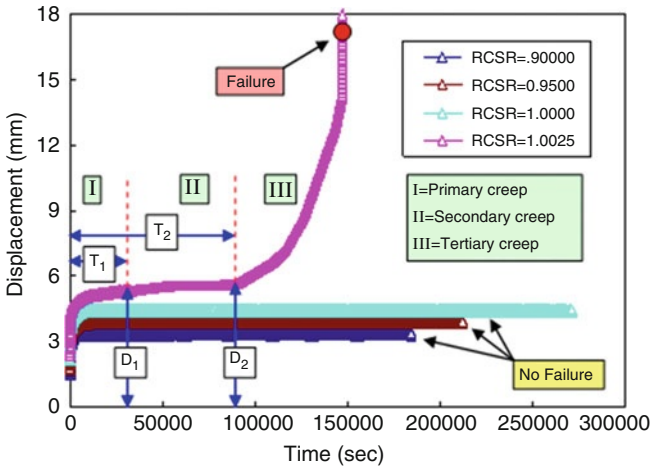


Fig. 5 Typical residual-state creep test on Smectite-rich sample

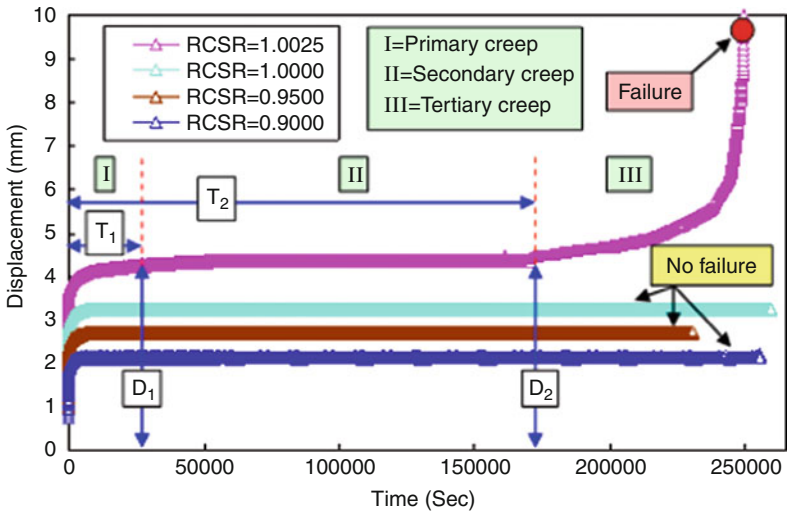


Fig. 6 Typical residual-state creep test on Chlorite-rich sample

Figures 4, 5, 6 and 7 show the typical residual-state creep test on Kaolin clay, Smectite-rich sample, Chlorite-rich sample, and Mica-rich sample respectively. Similarly, six more tests for each sample are conducted with vary applied constant creep load. The results thus obtained are summarised in tabular form as shown in Tables 1, 2, 3 and 4 below. Tables 1, 2, 3 and 4 show the summary of residual-state creep tests on Kaolin clay, Smectite-rich sample, Chlorite-rich sample, and Mica-rich sample respectively. Test results show that the creeping process is initiated from the residual state and there is no significant creeping effect on and below the residual state. That means when RCSR $\leq$ 1, the soil does not show creeping behaviour, and the soil undergo creeping behaviour when RCSR $>$ 1. When the application of constant creep load is higher, the clayey soils begun to fail immediately with small

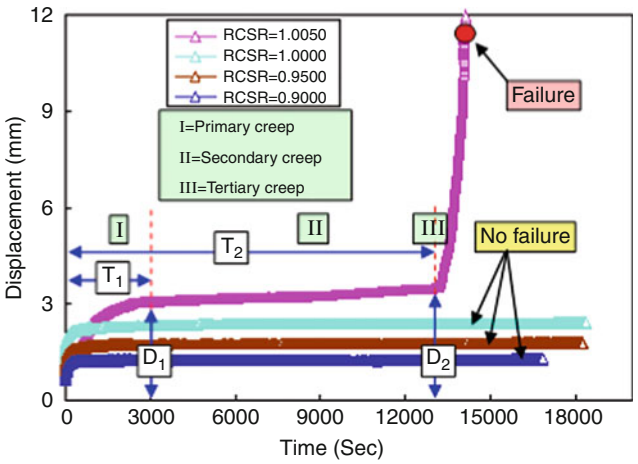


Fig. 7 Typical residual-state creep test on Mica-rich sample

Table 1 Summary of residual-state creep test on Kaolin clay

Test no.	RCSR	T1 (s)	D1 (mm)	T2 (s)	D2 (mm)	Remarks
7	1.0200	14	1.42	62	2.09	Failure
6	1.0150	24	0.68	182	1.07	Failure
5	1.0125	72	0.81	786	1.14	Failure
4	1.0100	164	0.97	1,502	1.26	Failure
3	1.0075	458	1.06	3,306	1.29	Failure
2	1.0050	1,376	1.48	14,010	1.67	Failure
1	1.0025	13,036	1.63	110,420	2.00	Failure
1	1.0000	7,034	0.51	170,110	0.51	No failure
1	0.9500	6,662	0.83	151,840	0.83	No failure
1	0.9000	7,034	0.51	170,110	0.51	No failure

Table 2 Summary of residual-state creep test on Smectite-rich sample

Test no.	RCSR	T1 (s)	D1 (mm)	T2 (s)	D2 (mm)	Remarks
7	1.0200	10	0.90	22	1.50	Failure
6	1.0150	16	1.37	58	1.80	Failure
5	1.0125	32	1.60	100	2.21	Failure
4	1.0100	144	1.96	322	3.04	Failure
3	1.0075	318	2.65	926	3.61	Failure
2	1.0050	1,122	2.61	3,962	4.08	Failure
1	1.0025	32,584	2.98	89,948	4.15	Failure
1	1.0000	6,054	2.36	207,552	2.36	No failure
1	0.9500	5,700	2.17	212,500	2.17	No failure
1	0.9000	5,420	1.86	184,520	1.86	No failure

Table 3 Summary of residual-state creep test on Chlorite-rich sample

Test no.	RCSR	T1 (s)	D1 (mm)	T2 (s)	D2 (mm)	Remarks
7	1.0200	18	0.70	42	1.20	Failure
6	1.0150	28	1.07	110	1.39	Failure
5	1.0125	58	1.36	190	1.51	Failure
4	1.0100	250	1.76	802	2.07	Failure
3	1.0075	554	2.56	1,758	2.79	Failure
2	1.0050	1,964	2.59	7,528	2.97	Failure
1	1.0025	57,020	2.90	170,900	2.99	Failure
1	1.0000	7,398	1.89	259,440	1.89	No failure
1	0.9500	6,850	1.81	255,050	1.81	No failure
1	0.9000	6,950	1.37	230,880	1.37	No failure

Table 4 Summary of residual-state creep test on Mica-rich sample

Test No.	RCSR	T1 (s)	D1 (mm)	T2 (s)	D2 (mm)	Remarks
7	1.0200	22	1.53	72		Failure
6	1.0150	36	0.56	190		Failure
5	1.0125	66	0.60	330		Failure
4	1.0100	260	1.23	1,390		Failure
3	1.0075	570	1.39	3,060		Failure
2	1.0050	2,402	1.95	13,174		Failure
1	1.0025	54,840	0.54	300,784		Failure
1	1.0000	8,440	0.95	204,132		No failure
1	0.9500	7,990	0.65	182,208		No failure
1	0.9000	6,840	0.59	16,840		No failure

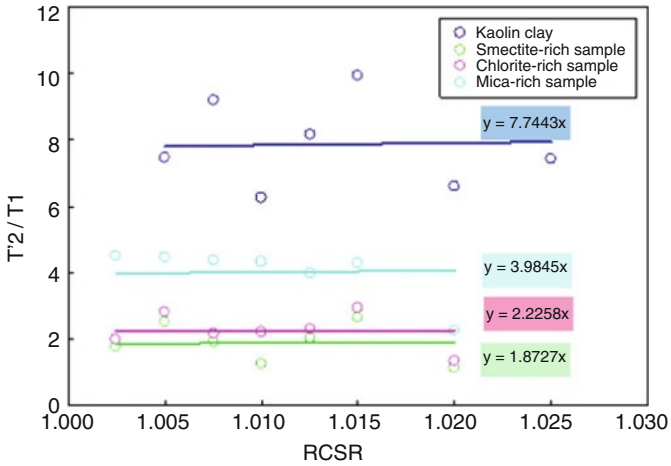


Fig. 8 Correlation between primary and secondary creep

displacement, but with lower value of applied constant stress, it takes long time to reach the failure state. For the same applied constant creep load, Smectite-rich sample is failed in short time and Chlorite-rich sample, Mica-rich sample, and Kaolin clay are taken some longer time reach to fail respectively.

In this study, different stages of creep are defined based on the change in displacement. When the change in displacement is continuously decreased, such range is named primary creep. In secondary creep, the change in displacement is constant, and when the change in displacement suddenly increased, and which reach to fail the specimen, is named tertiary creep

The nature of curve in primary stage of creep consists of logarithmic curves, secondary stage of creep shows linear, and in tertiary creep of parabolas. In primary creep, Smectite-rich sample shows the smooth curve nature and Chlorite-rich sample, Mica-rich sample, and Kaolin clay are followed it. Mica-rich sample shows the steep curve nature in the stage of tertiary creep. The nature of secondary creep for all tested samples is almost similar pattern; however, Smectite-rich sample and Chlorite-rich sample show slightly steep slope than Mica-rich sample and Kaolin clay. In tertiary creep, Smectite-rich sample shows the smooth parabolic curve with higher radius of curvature, and chlorite-rich sample and mica-rich sample are followed it. Smectite-rich sample and Chlorite-rich sample show tertiary creeping behaviour in long period of time with maximum displacement with compare to Mica-rich sample before leading failure, that means range of tertiary creep in Smectite-rich sample and Chlorite-rich sample are higher than Mica-rich sample.

Correlation between primary creep and secondary creep is presented in Fig. 8. $Y = 1.8727\times$ indicates that the total duration of secondary creep is 1.8727 times higher than the total duration in primary creep. The test results show that the ratio of total duration of secondary creep, T2 to the total duration of primary creep, T1 depends up on its residual strength. The residual shear strength of Chlorite-rich sample is nearly three times higher than the residual shear strength of Smectite-rich sample. The average total duration ratio of secondary creep to primary creep in case of Chlorite-rich sample is 2.2258, which is greater than Smectite-rich sample. The residual shear strength of Mica-rich sample and Kaolin clay are about four times and six times higher than the Smectite-rich sample respectively. In case of Mica-rich sample, the average total duration ratio of secondary creep to primary creep is 2.12 times higher than the Smectite-rich sample. Similarly, the average total time period ratio of secondary creep to primary creep is 4.13 times higher than the Smectite-rich sample in case of Kaolin clay as shown in Fig. 8. Comparative study shows that there is close relation between the ratio of residual strength to the total duration ratio of secondary creep to primary creep.

The prediction curves (time vs. RCSR) based on the tertiary creep is presented in Fig. 9. This curve can predict the failure time (sec) with corresponding to RCSR value. For example, if RCSR is 1.0025, Smectite-rich sample will reach to fail after 89,948 s but, Kaolin clay takes 110,420 s. In case of Chlorite-rich sample, test specimen resists the applied constant creep load up to 170,900 s and up to 300,784 s in case of Mica-rich sample. Failure trends show that Smectite-rich sample is failed in short time with respect to other tested sample. Kaolin clay need more time reach to fail. The range of failure time with varying RCSR; 1.0025–1.0200, are 22–89,948 s, 42–259,440 s, 72–300,784 s, and 62–110,420 s on Smectite-rich sample, Chlorite-rich sample, Mica-rich sample, and Kaolin clay respectively. This graph shows that a soil mass which have minimum residual strength shows the significant creeping behaviour. Hence, Smectite-rich test sample is failed first in short time; then, Chlorite-rich sample, Mica-rich sample, and Kaolin clay are failed respectively.

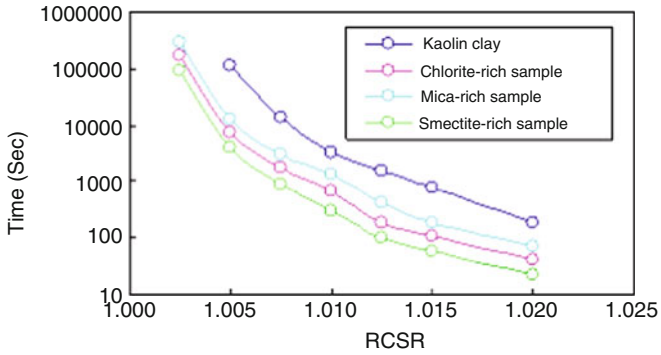


Fig. 9 Prediction curve (time vs. RCSR)

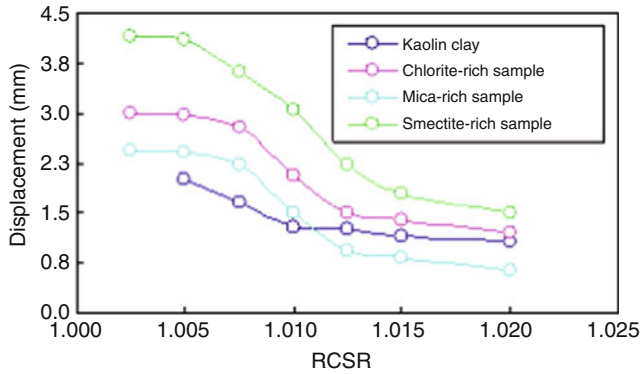


Fig. 10 Prediction curve (displacement vs. RCSR)

Similarly, the prediction curve (displacement with respect to RCSR) is purposed based on test results as shown in Fig. 10. In this prediction curve, Smectite-rich sample has maximum displacement before failure and Chlorite-rich sample, Mica-rich sample, and Kaolin clay is followed it respectively. The range of displacement is 1.5–4.16 mm, 1.20–2.99 mm, 3.67–2.44 mm, and 2.09–2.00 mm with varying RCSR; 1.0025–1.0200, on Smectite-rich sample, Chlorite-rich sample, Mica-rich sample, and Kaolin clay respectively. It can be concluded that the clayey soil which has higher percentage of weak clayey minerals such as smectite and chlorite show the significant creeping behaviour in the large-scale landslides.

The prediction curves have a potential to predict the failure initiated time period and its corresponding displacement for any value of RCSR. Although, the prediction curves are obtained from the lab test results of representative landslide soils, it certainly gives the possible direction toward deformation prediction of a clayey soils mass with respect to time under any applied constant effective pressure or self weight. In this residual-state creep test, the increment of the creep load is done by directly increasing the applied creep load, but in real field, the effective stress is being changed with the fluctuation of ground water table by rainfall or seismic event. If some relationships between this experiment results and real field scenario can be established, displacement prediction is analytically possible.

Chandler (1977) has indicated that the shear strength of the slip-surface zone was recovered in a stable period before re-sliding. Gibo et al. (2002) has observed the recovery of the shear strength for the clayey soil under the normal stress below 100 kPa. He has concluded that the soil containing the large amount of clay particles and dominated by Smectite, there was a large fall in shear strength to the residual state, but the strength recovery was negligible for the whole range of normal stress. Strength recovery is not considered in this study.

Conclusions

Based on test results, the main findings of this study are as: (1) the residual-state creep test set up is developed in the laboratory using a modified tortional ring shear machine, which is adequately capable of evaluating the residual-state creep behavior of clayey soils, (2) new concept of residual-state creep test and its testing procedures are developed, (3) ideal creep curve is experimentally verified, (4) when RCSR ≤ 1, there is no significant creeping effect but specimen shows the creeping behaviour when RCSR > 1, (5) the total duration ratio of secondary creep to primary creep on Smectite-rich sample, Chlorite-rich sample, Mica- rich sample, and Kaolin clay are found 1.87, 2.22, 3.98, and 7.74 respectively, (6) prediction curves (time vs. RCSR and displacement vs. RCSR) are purposed which have potential towards displacement prediction.

Acknowledgments The authors wish to thank Assistant Professor Jinghe Tan of the College of Civil and Construction Engineering, Guilin University of Technology, China for his valuable support and advice during the experiments. We also wish to Technical Assistant Mr. Osamu Futagami, for his regular support during the set up, repair and maintenance of the apparatus. Research was funded by Special Graduate Course on Disaster Mitigation Study for Asian Students, Graduate School of Science and Engineering, Ehime University, Matsuyama, Japan.

References

Bishop AW, Green GE, Garga VK, Andersen A, Browns JD (1971) A new ring shear apparatus and its application to the measurement of residual strength. Geotechnique 21(4):73–328

Bromhead EN, Curtis RD (1983) A comparison of alternative methods of measuring the residual strength of London clay. J Ground Eng 16(4):39–40

Chandler RJ (1977) Back analysis techniques for slope stabilization works: a case record. Geotechnique 27(4):479–495

Gibo S, Egashira K, Ohtsubo M, Nakamura S (2002) Strength recovery from residual state in reactivated landslides. Geotechnique 52(9): 683–686

Mesri G, Shahien M (2003) Residual shear strength mobilized in first-time slope failures. J Geotech Geoenviron Eng 129(1):12–31
Skempton AW (1985) Residual strength of clays in landslides, folded strata and the laboratory. Geotechnique 35(1):3–18
Stark TD, Choi H, McCone S (2005) Drained shear strength parameters for analysis of landslides. J Geotech Geoenviron Eng 131(5): 575–588
Stark TD, Eid HT (1994) Drained residual strength of cohesive soils. J Geotech Geoenviron Eng 120(5):856–871
Tiwari B, Marui H (2005) A new method for the correlation of residual shear strength of the soil with mineralogical composition. ASCE 131(9):1139–1150



Operational Procedure for a Hydrogeological Warning System in Aosta Valley

Sara Maria Ratto, Hervé Stevenin, Evelyne Navillod, and Marco Cauduro

Abstract

The main mission of a Functional Centre consists in the daily issuing of the "criticality bulletin" defining the alert level for hydrogeological and hydraulic risk at regional scale. The forecast system of the hydrogeological risk in the Aosta Valley used to be based on a threshold system, developed by the Italian Civil Protection Department. The operator was used to decide the alert level on the basis of his experience, using the maximum precipitation threshold as the only indicator for landslide triggering processes. A new operational multi-parametric threshold system has been developed, taking into account the maximum precipitation and the snow level too, calibrated through a back analysis of the previous 10 years. At the same time a new procedure has been drafted in order to take advantage of the experience acquired by operators and to uniformize the warning selection criteria. A new method to predict criticality scenarios has been developed and it is now being tested.

Keywords

Operational procedure • Early warning • Multi-parametric threshold • Hydrogeological risk

Introduction

The Regional Functional Centre (RFC) of the Aosta Valley (NW – Italy), during these past years, used to issue a hydrogeological alert level (for landslide prediction) using a threshold system proposed by the National Department of Civil Protection (DPCN), based on a sole indicator related to past and expected maximum precipitation. Operators were used to decide the alert level on the basis of both the result of this indicator and their experience.

After a thorough analysis of the results obtained by the application of this system, it became apparent that there was a serious necessity to uniformize choice criteria, by translating, when possible, operator's experience (and intuition?) into a guideline with the aim of increasing reliability of the alert system.

S.M. Ratto (✉) • H. Stevenin • E. Navillod • M. Cauduro
Centro Funzionale Regionale, Regione Autonoma Valle d'Aosta, Aosta, Italy
e-mail: centrofunzionale@regione.vda.it

At the same time, feedbacks resulting from interaction with local communities demonstrated a loss of credibility of the early warning system. This was also a consequence of the ambiguity due to the alerts issued both at regional and national level at the same time and these were terminated on November 2009 with the official acknowledgement of the RFC competences by DPCN. The impression that there were an excessive number of false alerts was dealt with by trying to work both on changing the communication policy with the local communities, in order to better understanding of reciprocal tasks and responsibilities, and on designing new procedures in order to reduce the false alerts.

Hence, a new procedure has been drafted with a check-list explaining the actions to be followed by the operator and with the development of two different, more performing technical instruments. The first procedure is ready to be operative and it uses old maximum precipitation threshold coupled with new threshold regarding average precipitation and snow level calibrated on back-analysis. The second, of an experimental nature, is based on new multi-parametric

C. Margottini et al. (eds.), *Landslide Science and Practice*, Vol. 2,
DOI 10.1007/978-3-642-31445-2_84, © Springer-Verlag Berlin Heidelberg 2013

threshold and is calibrated on meteorological events with "moderate" criticality scenario (second degree of alerting level on a scale that goes from one to three levels).

Materials and Methods

During 2004, operational guidelines were issued by DPCN defining the tasks, responsibilities and organisation of the National Early Warning System, and the development of the Functional Centres and Competences Centres network - Presidenza del Consiglio dei Ministri (2004).

DPCN and regions work together through the national network of Functional Centres to provide the national Early Warning System, which produces forecast and conducts surveillance for floods, landslides, forest fires, volcanoes and hydro-meteorological risk - OECD (2010).

Early warning system has to be based on a threshold approach, used as an indicator to issue three alert levels ("ordinary", "moderate" and "high" criticality) related to different scenarios expected on an "alert" area, a geographic zone with homogeneous hydro-meteorological features.

In this paper we will look into hydrogeological risks (landslides and floods only in small drainage basins), not considering criticality related to storm and scattered showers.

Old Procedure

The RFC of the Aosta Valley adopted, as technical instrument for the Early Warning System, an empirical precipitation threshold system designed by "ARPA Piemonte" and approved by DPCN - ARPA PIEMONTE (2004).

Regarding "moderate" and "high" criticality, maximum precipitation thresholds used for different duration (6, 12, 24, 36 and 48 h) were related to previous soil saturation condition. These soil saturation parameters were simply defined by exceeding a cumulated rainfall threshold over the previous 30 days according to the "Cancelli and Nova" Curve (1985). This curve is calibrated on the precipitation in the Aosta Valley Region.

The thresholds were obtained correlating the damage caused by individual landslides with the precipitation recorded in the nearest rain gauges and using a logical function based on the number of false alarms and missed detects. The calibration of the method was performed using landslides and precipitations regional data.

This system revealed the following main flaws:

- The thresholds have been calculated using individual landslides, while they are used to predict areal scenarios;
- Other important indicators are not taken into account: the snow level is very important in a mountain region (average altitude of about 2,100 m a.s.l.) where the precipitation can be often solid (snow) over a large area of the region; the average precipitations play a fundamental role in meteorological events that can be critical over an area of about 1,000 km^2 (average size of alert area).

Hence, the operator was used to issue the alert level not only on the basis of the threshold method but also on the basis of his personal experience.

Concerning "ordinary" criticality, the threshold was established in 45 mm average precipitation during 24 h, even if, as stated above, the operator's experience was the real decision process.

Considering the importance of each operator's personal experience, it is clear that the absence of a codified procedure could lead to non – homogeneous choice criterion and to excessive caution.

New Procedure

To deal with the problems listed above, the drafting of the new procedures has been carried out in order to reach the following goals:

- Resilience of the Early Warning System, trying to reduce the diversity of choices depending on an operator;
- The need to bring into the procedure the experience gained by the Functional Centre;
- Ensuring that the procedure was the basis for criticism and improvement of the system after each event;
- Making the logical path of choice recognizable (as based on indications of the judiciary);
- Improving the performance of Early Warnings System following the impression that the high number of false alarms were due to the use of thresholds.

Two main modifications have been introduced to reach these goals: the definition of new multi-parametric thresholds and the draft of new operational guidelines.

New Multi-Parametric Thresholds

The criterion followed to figure out new thresholds was to use and optimize existing data and instruments in order to succeed in producing an operational tool in a relatively short time.

In this first phase the maximum precipitation thresholds were maintained while new thresholds were calibrated for the other parameters (average precipitation and snow level) through a back analysis.

Another constraint was to exploit the quantitative data provided by the weather forecaster: average and maximum precipitation (mm/12 h and mm/24 h) and highest snow level every 12 h.

The source data used are briefly listed below:

- Regional landslide inventory: landslides which had occurred during 2000–2008 were analyzed;
- Real scenarios: list of "ordinary", "moderate" and "high" criticality scenarios as defined on the basis of landslide analysis;
- Weather forecast: quantitative data (precipitation, freezing and snow level values) during 2002–2008;
- Weather Data: precipitation and temperature database from regional hydrometeorological monitoring network during 2000–2008;
- Criticality Bulletins: list of "ordinary", "moderate" and "high" criticality scenarios issued by the RFC.

Data Processing

The rainfall data (from rain gauges) were aggregated in order to get, for each alert area, maximum and average values of rainfall every 12 h ("perfect weather forecast") and in order easily compare them with the weather forecast quantitative data. The cumulated rainfall curve was then calculated for the previous 30 days for each rain gauge and the exceeding of the "Cancelli and Nova" curve was then verified (soil saturation condition). The exceeding defines the set of thresholds to be used. Temperature data were processed by calculating, with a simple linear regression, freezing level in steps of 12 h. The snow level was estimated in a simplified way by subtracting 300 m to freezing level. This work has been done for the years between 2000 and 2008 and the data were organized and stored in a specific database.

The processing was carried out in this way in order to be compatible with the current system of thresholds and to be easy compared with the Aosta Valley weather forecast quantitative data.

At the same time, landslides which had occurred in the last 10 years were analyzed to identify "ordinary", "moderate" and "high" criticality scenarios (Table 1). A scenario of "high" criticality took place only during October 2000; considering each alert area, "moderate" criticality occurred 10 times, while "ordinary" criticality 19 times. This analysis was also included in the same database.

"Ordinary" criticality scenarios that are consequences of storms and showers were not considered in this study.

In general, the definition of criticality scenarios was carried out in conservative terms, by defining "ordinary" criticality scenarios events characterized by a small number of landslides.

Every criticality scenario was related to a condition of soil saturation, to maximum and average precipitation values and to maximum snow level, allowing the definition of new multi-parametric thresholds (maximum and average precipitation, snow level) on the basis of the number of false alarms and missed detects. Concerning each criticality scenario, the following assumptions were done:

Table 1 List of dates, for each alert area (A, B, C and D), with real criticality scenarios

Date	A	B	C	D
28/04/00	Ordinary	Ordinary	Ordinary	Ordinary
29/09/00	Ordinary	Ordinary		
12/10/00		Moderate	Moderate	
13/10/00	Moderate	Moderate	Moderate	Moderate
14/10/00	High	High	High	High
01/05/01			Ordinary	
14/07/01		Ordinary		
15/07/01		Ordinary	Ordinary	Ordinary
02/05/02		Ordinary		
08/05/02		Ordinary		
04/06/02	Ordinary	Moderate	Ordinary	Ordinary
05/06/02		Moderate	Ordinary	Ordinary
01/11/04	Moderate	Moderate	Moderate	
02/11/04		Moderate		
01/08/05		Ordinary		
14/09/06	Moderate	Moderate		
27/05/08			Moderate	Moderate
28/05/08	Moderate	Moderate	Moderate	Moderate
29/05/08	Moderate	Moderate	Moderate	Moderate
04/11/08	Moderate	Ordinary		Ordinary
14/12/08		Ordinary		

The date refers to the moment (12.00 GMT) of issue of criticality bulletin, considering that criticality is related to what will happen within next 36 h

(a) "High" criticality: it was not possible to make any analysis because since 2000, the Aosta Valley Region was affected by just 1 event (October 2000);
(b) "Moderate" criticality: the goal was to have no missed detects, minimizing false alarms;
(c) "Ordinary" criticality: the analysis looked for a favourable ratio of false alarms to missed detects. The existence of critical events related to low values of precipitation (caused probably by particularly anomalous temperature conditions which affected snow melting and soil saturation) didn't allow to pursue the absence of missed detects.

Then, a similar analysis was carried out using digitalized weather forecast data (since summer of 2005) and the criticality issued since 2002, data included in the database above described.

This analysis is useful to test the reliability and resilience of the entire Early Warning System, in order to understand its sensitivity related to the weather forecast uncertainty, especially with regard to the potential increase in false alarms. At the same time, the comparison with the criticality issued by operators is necessary in order to understand if the new procedure could really improve the performance of the system.

Table 2 Extract of the thresholds proposed in the new procedures, considering that the numeric values are just illustrative and are not the operative ones

	Ordinary			
	Av. prec. (mm)	Max prec. 12 h (mm)	Max prec. 24 h (mm)	Snow level (m a.s.l.)
Area	50	70/100[a]	95/130[a]	1,800
Condition: (Av. Prec. or Max 12 h or Max 24 h) and snow level				
	Moderate			
	Av. prec. (mm)	Max prec. 12 h (mm)	Max prec. 24 h (mm)	Snow level (m a.s.l.)
Area	50	70/100[a]	95/130[a]	2,200
Condition: (Av. Prec. and (Max 12 h or Max 24 h)) and snow level				

[a]Depending on the soil saturation level

Table 3 Synthetic results of the back analysis applying old and new thresholds with perfect forecast (real precipitation observed)

	Old thresholds	New thresholds
False	42	28
Missed	3	6
Hits	26	3

Table 4 Synthetic results of the back analysis applying old and new thresholds with perfect forecast (real precipitation observed) in terms of "ordinary" and "moderate" criticality

	Ordinary		Moderate	
	Old thresholds	New thresholds	Old thresholds	New thresholds
False	19	20	23	8
Missed	2	3	1	3
Hits	12	13	14	10

Operational Procedure

The new operational procedure was drafted in order to take advantage of the experience acquired by operators and in order to uniformize, as far as possible, the warning selection criteria.

First, the operator's main activities, required for a comprehensive overview of the situation, were organised according to a chronological process and linked to a specific software. Furthermore, in case of threshold exceeding, the associated alert level was defined taking into account monitoring results and actual scenario, too.

And moreover, instruments were calibrated on the system architecture and on the timing of the choice, which must be done in a short period time.

Results

In the first part of the following chapter, the results of multi-parametric thresholds calculation and of the tests, carried out using digitalized weather forecast data and criticality issued, will be described. In the second part, the guidelines of the new procedure will be pointed out.

New Method

For each alert area, the calculations described above led to threshold values (Table 2) for the following parameters:

1. Maximum precipitation during 12 and 24 h;
2. Average precipitation during 24 h;
3. Snow level.

Maximum precipitation consists in two different values for each time limit (12 and 24 h) depending on the soil saturation level ("Cancelli and Nova" exceeding/not exceeding). Snow level threshold has different values for "ordinary" and "moderate" criticality, while maximum and average precipitations threshold don't change.

A "moderate" criticality will be issued in the case of exceeding of all three threshold (maximum and average precipitation, snow level); an "ordinary" criticality in case of exceeding of snow level threshold and of just one threshold between maximum and average precipitations.

As described above, concerning "moderate" criticality thresholds, the goal was to obtain no missed detects from back analysis, minimizing false alarms. That was always possible excluding the May 27, 2008 event, when the south west area of the Aosta Valley was interested by significant damages, the consequence of debris flows and bank erosions. Both weather forecast and perfect forecast (rain gauges measurement) highlight low values of maximum and average precipitations; a local temperature anomaly, not significant if considering an average snow level over all the Aosta Valley, which led to an important 207 snow melting, could be considered the main cause for the 208 critical event.

Application of the new threshold has lead to a significant 209 decrease in false alarms, which refers mainly to "moderate" 210 criticality (Tables 3 and 4). The increase in missed detects refers to May 27, 211 2008 event (described above) and to December 14, 2008 event ("ordinary" criticality), when some instabilities were reported in south east area

Table 5 Synthetic results of the back analysis with real weather forecast

	Old thresholds	Old system	New thresholds
False	41	42	21
Missed	2	3	3
Hits	4	2	4

Table 6 Synthetic results of the back analysis with real weather forecast in terms of "ordinary" and "moderate" criticality

	Ordinary			Moderate		
	Old thresholds	Old system	New thresholds	Old thresholds	Old system	New thresholds
False	10	31	11	31	11	10
Missed	0	1	1	2	2	2
Hits	1	0	0	3	2	4

of the Aosta Valley even if snow level was at about 1,000 m a.s.l. However, using similar values as snow level threshold would lead to a significant increase in false alarms.

The second step of this study was a back analysis carried out using digitalized weather forecast data and the criticality level issued. In particular, using as input data the real weather forecast, the following results have been pointed out:

- Alerts issued in case of applying only the maximum precipitation thresholds (old thresholds);
- Alerts issued in case of applying the old warning system, consisting in the alerts actually issued (old system);
- Alerts issued in case of applying new multi-parametric thresholds (new thresholds).

The analyses have been carried out since summer of 2005 (availability of digitalized weather forecast data). In Table 1 the real criticality scenarios which affected the Aosta Valley after 2005 are listed.

The most remarkable result concerns the significant decrease in false alarms (Table 5).

Analyzing "moderate" criticality, it appears very interesting that with the application of the new thresholds, it was possible to get the same performance of the application of the old system (alerts actually issued) (Table 6). It means that the experience of operators could give a great contribution in correcting the problems related to the application of maximum precipitation threshold. At the same time, new multi-parametric threshold has succeeded in bringing to the procedure the experience gained by the Functional Centre.

As regards missed detects, the performance remains the same.

New Procedure

The definition of specific guidelines, organized in a new procedure, allows:

- A more organised, and consequently repeatable, decision-making process;
- The possibility of improving the procedure itself taking into account the experience acquired by new events;
- The operator to remember every essential step during the short period time of the decision-making process.

All the information is organized in a specific software platform called "Criticality Bulletin".

First, all the tools available for the operators are listed following a chronological process and linked to the corresponding software.

The main activities, required for a comprehensive overview of the situation, are the following:

- Monitoring of the meteorological data (temperature, precipitations, snow and hydrometric levels);
- Acquisition of the information related to the latest landslides;
- Briefing with the weather forecaster in order to obtain a good understanding of present and future weather conditions;
- Comparison between weather forecast quantitative data and the multi-parametric thresholds.

Information about landslides (type, position, time of occurrence, pictures, etc.) is mostly gathered by the Aosta Valley Regional Forest Corp and sent in real time to the RFC server to be used by operators.

If landslides analysis and meteorological data monitoring assesses the existence of a current criticality scenario, the issue of the criticality level has to take into consideration the operator's personal experience. In this case, the new procedure does not give fixed choices, but helps the operator with different suggestions depending on the current scenario, on the monitoring values and on the weather forecast quantitative data. In this case, the alert level has to be chosen by a team of geologists and hydrologists.

The other relevant points of the procedure are listed below:

- The logical path that led to the alert level choice have to be explained in the operator's note;
- The issue of an "high" scenario criticality is expected only in case of an actual scenario existence;
- A derogation from the procedure is always possible. The choice must be agreed with a group of technicians, while the reasons and logical path which have led to the derogation must be transcribed in a synthetic report.

Work in Progress

As described above, in order to design a new procedure, it was established to use, as starting point, methods and threshold values already used and tested in the past in order to issue new operative guidelines.

At the same time, the RFC of the Aosta Valley is developing a new system, called "Indicators", to estimate the probability of the occurrence of a "moderate" criticality scenario.

The system is no longer based on the analysis of individual landslides, but on a detailed back analysis study concerning events of "moderate" criticality scenarios. This approach allows to reduce statistical noise, not taking into account landslides not directly related to the meteorological events.

The Aosta Valley, since 2002, has been affected by "moderate" criticality scenario five times (see Table 1). Considering each alert area, A and B areas have been affected four times, C area two times and D area only once.

In the study the considered parameters (precipitations, temperature field and soil saturation) were analysed both as previous and as forecast data. In particular, for each alert area, eight indicators were finally chosen:

- Four indicators regarding precipitations: maximum and average expected precipitations, during 12 and 24 h;
- Two indicators regarding temperature field: freezing level during last 48 h and freezing level expected;
- Two indicators regarding soil saturation: "Cancelli and Nova" curve exceeding and actual river discharge values.

For each indicator two different thresholds were established, related to high and medium probability of occurrence of a "moderate" criticality scenario, respectively called red and yellow thresholds. If the indicator value is below the yellow threshold, a green condition is defined, corresponding to a low probability regarding that parameter (Fig. 1).

The following criteria were used to calculate the red and yellow threshold for each indicator and each alert area:

- Previous precipitation (related to soil saturation): exceeding the "Cancelli and Nova" curve by cumulated mean precipitation during last 30 days establishes the red threshold; exceeding the "Cancelli and Nova" curve by cumulated mean precipitation plus its mean square deviation during the last 30 days establishes the yellow threshold;
- Other indicators: the red threshold value is the one that has been exceeded only once considering all the "moderate" criticality scenario events; the yellow threshold value is the one that has always been exceeded;
- River discharge (related to soil saturation): the different values for each alert area have been synthesized in an unique value taking into account geographic position and type of the river of each hydrometric station.

The first step for the calibration of the new system was to test it on important past critical events (September 22, 1993, September 28, 2000 and October 14, 2000); a good pattern corresponding to major events was confirmed.

INDICATORS

	PREVIOUS			FORECAST				
AREA	Prec. Cancelli&Nova	Freezing level	Discharge	Aver. Prec. 12h	Aver. Prec. 24h	Max Prec. 12h	Max Prec. 24h	Freezing level
A	LOW	HIGH	MEDIUM	LOW	LOW	MEDIUM	MEDIUM	HIGH
B	MEDIUM	HIGH	MEDIUM	LOW	LOW	LOW	LOW	MEDIUM
C	LOW	HIGH	HIGH	HIGH	MEDIUM	MEDIUM	MEDIUM	MEDIUM
D	MEDIUM	HIGH	HIGH	LOW	LOW	LOW	LOW	MEDIUM

Fig. 1 Example output of the new system called "Indicators"

The small number of past events does not allow the method to be considered statistically significant; so a test period to allow the new system "Indicators" become an operative system began during 2010. The aim is to have a new tool, useful for a comprehensive overview of the situation, picking out the most critical aspects of present and future conditions. At the moment, there is no intention of calculating a synthetic value able to give a unique probability of occurrence of a "moderate" criticality scenario.

During the test period (January 2010–June 2011), the Aosta Valley was interested by two main events: June 15–17, 2010 and June 1, 2011.

June 2010: the RFC issued "moderate" criticality scenario in A, B and C alert areas. The real scenario corresponded to a "ordinary" criticality in B alert area. Taking into account the weather forecast, the new procedure scenario would have been of "moderate" criticality in B alert area for June 15 (for June 16th and 17th the decision would have been based on the operator's experience), while the result of the system "Indicators" (valid for June 15–17) would have been of a dominant yellow condition on B alert area and of a dominant red condition on C alert area. Considering the perfect forecast, neither the application of the new procedure nor the system "Indicators" would have issued a "moderate" criticality scenario.

June 2011: the RFC issued "moderate" criticality scenario in A alert area. The real scenario corresponded to the absence of criticality. Considering both the weather forecast and the perfect forecast, the new procedure scenario would have been of "moderate" criticality in A alert area while the result of the system "Indicators" would have been of a dominant green condition.

The back analysis related to the definition of multi-parametric thresholds (new procedure and system "Indicators") led to the conclusion that the most important parameter to understand the scenario evolution of an event is the soil saturation indicator.

This parameter is very hard to estimate just by using previous precipitations, especially in a mountain area with significant snow precipitations. Indicators are trying to relate the soil saturation with the river discharge, but the results are not good considering the complexity of the Aosta Valley orographic context. Hence the next goal is to better estimate the soil saturation.

The RFC is now studying the possibility of using an intermediate product of hydrologic model used to issue hydraulic criticality. It produces a map containing a water quantity (expressed in mm) exchanged between the soil and the atmosphere, which is now studied in order to correlate this parameter to the soil saturation. At the same time, in five test sites three soil temperature sensors and three soil moisture sensors were installed at different depths.

Conclusions

One of the main goal of the RFC of the Aosta Valley during these last few years has been to develop new procedures and new methods to increase the reliability and the resilience of the alert system.

First, a new procedure has been drafted: a check-list explains the actions to be followed by the operator and a multi-parametric threshold using snow level, maximum and average precipitation helps in deciding the criticality level to issue. The criterion followed was to use and to optimize the existing data and the instruments in order to succeed in producing an operational tool in a relatively short time.

A calibration conducted using meteorological measurement (perfect forecast), weather forecast quantitative data and criticality levels issued allowed one to verify that the application of a new procedure can lead to better performances (mainly in reducing number of false alarms).

At the present time the procedure is being tested by every operator to verify its real applicability and to find possible corrections. The RFC is carrying on the dialogue with judiciary to understand the reciprocal tasks and duties, aiming to translate the remarks in the procedure.

Second, a new system called "Indicators" is being developed to estimate the probability of a "moderate" criticality scenario happening. The system is based on a back analysis regarding significant events (and not individual landslides) which led to the definition of eight different indicators. For each indicator two different thresholds were calculated, defining three different conditions of low, medium and high probability.

The system is now being tested; in the last 2 years it has obtained encouraging results in term of very low number of false alarms. Future significant events will allow us to perform a complete calibration of the method.

The most important parameter that has to be investigated is the soil saturation. To reach this goal, the RFC is trying to use intermediary results of hydrologic models, calibrated for flood prediction. At the same time, five test sites were instrumented by soil moisture and temperature sensors.

The synergy of the activities described above is the basis expectation to have a new and more resilient soil saturation indicator, in order to progressively continue assisting the operator's activities.

References

ARPA Piemonte (2004) Convenzione tra il Dipartimento per la Protezione Civile e l'ARPA Piemonte per l'assistenza alla gestione delle situazioni di rischio idro-meteorologico sul territorio nazionale – SOGLIE PLUVIOMETRICHE

Cancelli A, Nova R (1985) Landslides in soil and debris cover triggered by rainfall in Valtellina (Central Alps – Italy). In: Proceedings of the4th international conference and field workshop on landslides, vol 1, Tokyo, pp 267–272

OECD Reviews of Risk Management Policies (2010) Review of the Italian National Civil Protection System. OECD Publishing

Presidenza del Consiglio dei Ministri (2004) D.P.C.M. 27 febbraio 2004 – Indirizzi operativi per la gestione organizzativa e funzionale del sistema di allertamento nazionale, statale e regionale per il rischio idrogeologico ed idraulico ai fini di protezione civile. Supplemento ordinario alla "Gazzetta Ufficiale" n. 59 dell'11 marzo 2004



Defining Physically-Based Rainfall Thresholds for Early Warning Systems

Diana Salciarini, Claudio Tamagnini, Francesco Ponziani, and Nicola Berni

Abstract

Empirical rainfall thresholds compiled on correlations between recorded data show that precipitation intensities and durations required to trigger shallow landslides vary with climatic, geotechnical and topographic conditions; consequently, thresholds exhibit a high degree of spatial variability, even across relatively small geographic areas (see, e.g., Baum and Godt (Landslides 7:259–272, 2010; Guzzetti et al. Landslides 5:3–17, 2008). In order to define intensity/duration rainfall thresholds capable of considering the site-specific hillslope characteristics, GIS-based modelling techniques have been developed and successfully applied starting from Iverson's theory (Baum et al. TRIGRS – a Fortran program for transient rainfall infiltration and grid–based regional slope–stability analysis, version 2.0, 2008; Godt et al. Rev Eng Geol 20:137–152, 2008; Salciarini et al. Eng Geol 102:227–237, 2008). In this work A GIS-based code is presented which permits the assessment of the spatial distribution of the minimum rainfall intensity that triggers shallow landslides and debris flows over a given study area, based on the rainfall duration and the local geometric, hydrologic and mechanical characteristics of the slopes. Such an approach is used for predicting landslide scenarios produced by short-duration rainfalls. An example of application to a study area of the Umbria Region in central Italy is presented, describing the capability of the model of providing site-specific thresholds for different rainfall scenarios and issuing different levels of hazard warning. The application illustrates some challenges on the technically feasibility of shallow-landslide early warning systems, capable of including specific information on the affected areas, probability of landslide occurrence and expected timing.

Keywords

Physically-based models • Rainfall thresholds • Early-warning systems

Introduction and Motivations

In general, the triggering of rainfall-induced shallow landslides is influenced both by the physical and mechanical behaviour of the soil, and by the hydrological processes induced by the rainfall that hits the ground surface.

The analysis of the relationships existing between precipitation and landslides has suggested the use of rainfall thresholds, i.e., critical values of rainfall intensity for which the probability of landslide occurrence becomes very high. Improvements in understanding these relationships have

D. Salciarini (✉) • C. Tamagnini
Department of Civil and Environmental Engineering, University of Perugia, via G. Duranti 93, Perugia, Italy
e-mail: diana@unipg.it

F. Ponziani • N. Berni
Umbria Region, Department of Civil Protection, Decentred Functional Office, Foligno, Italy

C. Margottini et al. (eds.), *Landslide Science and Practice*, Vol. 2,
DOI 10.1007/978-3-642-31445-2_85, © Springer-Verlag Berlin Heidelberg 2013

a great interest from both scientific and practical point of view, especially for possible application in implementing early-warning systems. Indeed, the models that describe the rainfall-landslide correlations are the essential component of the Italian Civil Protection System. The aim is to predict landslides induced by rainstorm events with sufficient confidence to alert agencies that can draw up emergency plans. Such an approach is being done for flooding, but the challenge is much greater in the case of landslide hazard, above all because the potential landslide locations are harder to delineate for the strong influence of local conditions (e.g., soil thicknesses, root strength, localized seepage, bedding fractures, etc.).

Currently, two main approaches for defining rainfall thresholds are used: (1) empirical and (2) physically-based methods. Empirical rainfall thresholds are identified from databases of landslides actually occurred as consequence of rainfalls with known duration and intensity. In such approach, the rainfall thresholds are defined as the line that separates rainfalls that are likely to cause landslides, from those which are not (see, e.g., Caine 1980; Crosta and Frattini 2001; Cannon and Gartner 2005; Guzzetti et al. 2008). However, the empirical nature of this approach does not allow taking into account a number of factors that play a key role in the slope stability conditions, such as:

- The local physical and mechanical characteristics of the soil;
- The local morphology of the slope;
- The ratio between the rainfall duration and the characteristic time of the transient infiltration process.

The second approach (see, e.g., Montgomery and Dietrich 1994; Crosta 1998; Frattini et al. 2009; Salciarini et al. 2011) permits to overcome these limitations, being able to consider: (1) the specific site conditions, in terms of: mechanical, hydraulic and physical soil properties; (2) the local seepage conditions; and (3) their contribution to soil strength.

In particular, to assess the local transient infiltration of rainfall over a hillslope, and the corresponding effects on the stability conditions, Baum et al. (2002, 2008) developed a code, called TRIGRS (*Transient Rainfall Infiltration and GRid-based Slope-stability*), that combines an analytic solution for the evaluation of the pore pressure variation in response to complex rainfall patterns with a stability analysis based on the simplified assumption of infinite slope. Salciarini et al. (2008, 2011) extended the TRIGRS capabilities by adding a new module, called CRF (*Critical RainFall*) that provides physically-based rainfall thresholds that lead a given slope to limiting equilibrium conditions.

A first application of CRF was carried out over a large territory in the Seattle area (Washington, USA), where high-resolution data for the inputs required by the model were available. The performance of the model was proven to be very good (Salciarini et al. 2008). Also, a one-dimensional validation of the same model, incorporating some improvements in order to provide more accurate predictions for short-duration rainfalls, was given in Salciarini et al. (2011), by comparing the thresholds provided by the model with available empirical thresholds. Encouraging results were obtained from the qualitative and quantitative point of view.

In what follow we describe the theoretical basis of the model, and discuss the challenges in its application to a central Italy case study, for the planned integration of the code in the early-warning system of the Umbria Region Civil Protection.

Theoretical Basis of the Model

Main Hypotheses

The CRF model is based on the following main hypotheses:

1. The loose soil cover thickness is small compared to the slope length;
2. The failure surface is parallel to the topographic surface and is localized at the contact between the loose cover and the underlying bedrock;
3. The bedrock is much less permeable than the loose cover, so that it can be considered impervious;
4. In the initial condition (before the rainfall event) the slope is fully saturated;
5. The rainfall inducing the failure is uniform in space and time.

Hypotheses (1) to (3) are largely acceptable in most real cases of shallow landslides. The hypothesis (4) is consistent for fine-grained soils, where the tension at the air-water interface allows maintaining full saturation of the solid skeleton, even in presence of negative pore pressures. As for the hypothesis (5), Iverson (2000) and D'Odorico et al. (2005) demonstrated that the pore pressure variation in response to a constant rainfall is 20–25 % higher than the pore pressure variation in response to a non-uniform rainfall. Thus the hypothesis is on the safe-side.

Slope Stability Model

In general, the limiting equilibrium conditions along the potential failure surface are reached when the mobilized shear stress – function of the weight per unit volume of the soil, depth of the soil cover, and slope angle – is equal to the available shear resistance (given by the Mohr-Coulomb criterion). Expressing the pore pressure u at the failure surface in terms of pressure head, $\psi = u/\gamma_w$, where γ_w is the water unit weight, the limiting equilibrium conditions are reached when:

$$\frac{\tan\phi'}{\tan\alpha}+\frac{c'-\gamma_w\psi\tan\phi'}{\gamma d_b\sin\alpha\cos\alpha}=1 \tag{1}$$

where c' and ϕ' are the effective cohesion and the effective friction angle, d_b is the depth of the failure surface, α is the slope angle, and γ is the soil unit weight.

The limiting value of the pressure head leading the hillslope to instability is determined from (1) as:

$$\psi_{\lim}=\frac{c'}{\gamma_w\tan\phi'}+\frac{\gamma}{\gamma_w}d_b\cos^2\alpha\left(1-\frac{\tan\alpha}{\tan\phi'}\right) \tag{2}$$

Hydrological Model

For a fully saturated cover, the pressure head variation with time and space along the vertical direction is governed by the following one-dimensional diffusion equation (Iverson 2000):

$$\frac{\partial\psi}{\partial t}=D\frac{\partial^2\psi}{\partial Z^2} \tag{3}$$

where Z is measured in the vertical direction; $D=D_0\cos^2\alpha$, and D_0 is the vertical coefficient of consolidation of the soil cover.

Iverson (2000) first derived a closed-form solution of (3) for a permeable layer of infinite depth. Baum et al. (2002, 2008) extended this solution including the possibility of having an impervious lower boundary at finite depth, d_b, from the topographic surface. For a constant rainfall of intensity I_Z and duration t_{end}, their solution yields the following expression for the pressure head at the failure surface, for $t > t_{\text{end}}$:

$$\psi(d_b,t)=(d_b-d_w)\beta+4\left(\frac{I_Z}{k_Z}\right)\times\left[S(d_b,t)-S(d_b,t-t_{end})\right] \tag{4}$$

where d_w is the initial depth of the water table, measured in the Z-direction, k_Z is the hydraulic conductivity in the Z-direction, and:

$$S(d_b,t)=\sqrt{D(t-t_{\text{end}})}\sum_{m=1}^{\infty}\text{ierfc}\left[\frac{(2\text{m}-1)\text{d}_\text{b}}{2\sqrt{\text{D}(\text{t}-\text{t}_{\text{end}})}}\right] \tag{5}$$

In (5), the function ierfc is expressed in terms of the complementary error function erfc(x).

The time t_p at which ψ reaches its maximum value is obtained by maximizing the expression given by (4):

$$\frac{\partial\psi}{\partial t}=4\frac{I_Z}{k_Z}\left[\frac{\partial S}{\partial t}(d_b,t)-\frac{\partial S}{\partial t}(d_b,t_{\text{end}})\right]=0 \tag{6}$$

Equation (6) can be numerically solved by using Newton's method to determine t_p. Then, the peak of pressure head $\psi_p=\psi(d_b, t_p)$ is computer from (4).

Physically-Based Rainfall Thresholds

For a rainfall of given duration, t_{end}, the critical rainfall intensity, I_{Zf}, is defined as the particular value of I_Z that yields $\psi_p=\psi_{\lim}$, at $t=t_p$, and $Z=d_b$.

By putting $\psi(d_b, t_p)=\psi_{\lim}$ in (4), taking into account (2) and solving for $I_Z=I_{Zf}$, we obtain:

$$I_{Zf}(d_b,t_{\text{end}})=F_1(d_b,t_{\text{end}})F_2(d_b,t_{\text{end}}) \tag{7}$$

where:

$$F_1=\frac{k_Z}{4\left[S(d_b,t_p)-S(d_b,t_p-t_{\text{end}})\right]}$$

and

$$F_2=\left\{\frac{c'}{\gamma_w\tan\phi'}+\frac{\gamma}{\gamma_w}d_b\cos^2\alpha\left(1-\frac{\tan\alpha}{\tan\phi'}\right)-(d_b-d_w)\beta\right\}$$

In (7), I_{Zf} is a function of the depth of the impervious boundary, d_b, and of the rainfall duration t_{end}, since $t_p=t_p(d_b, t_{\text{end}})$.

Validation of the Model

For a first validation of the model, one-dimensional simulations have been carried out using data from an instrumented area located in Seattle (see, e.g., Godt et al. 2008). The reliability of the model has been assessed by comparing the physically based thresholds provided by the CRF model with empirical rainfall thresholds available from literature. Table 1 shows the values of the parameters adopted in the analyses.

As for the slope geometry and initial conditions, a slope angle of 32°, a lower bedrock depth of 2.0 m and a water table depth of 1.0 m, have been assumed for all the slope types.

Figure 1 shows the comparison between the empirical thresholds from literature (black lines) and the physically-based thresholds provided by CRF (green lines) for the three slope-types of Table 1. In the log-log plane, the thresholds provided by the model decrease linearly with increasing

Table 1 Mechanical and hydraulic properties of the soil for the three slope types in which the area has been subdivided

	Slope-type A	Slope-type B	Slope-type C
k_V (m/s)	5.0e-5	2.5e-5	1.0e-5
γ (kN/m^3)	19.0	19.0	19.0
c' (kPa)	4.0	4.0	4.0
ϕ' (deg)	33.6	33.6	33.6

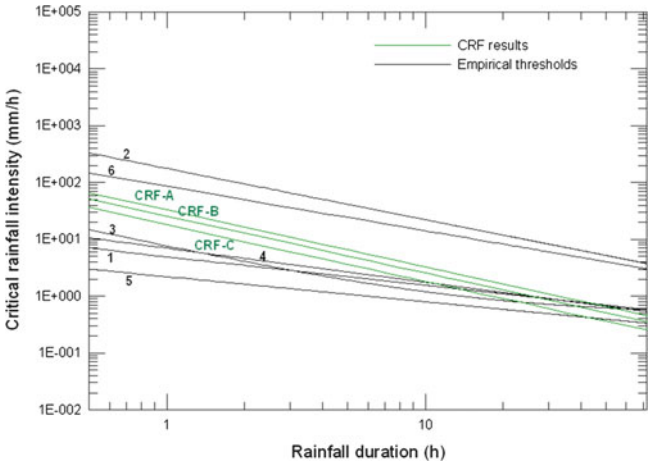


Fig. 1 Comparison between the physically-based thresholds provided by CRF and empirical thresholds provided by: (*1*) Innes (1993); (*2*) Crosta and Frattini (2001); (*3*) Cannon and Gartner (2005); (*4*) Guzzetti et al. (2008); (*5*) Giannecchini (2005); (*6*) Aleotti (2004)

rainfall duration – consistently with the definition of rainfall threshold – and show the same trend of the empirical ones. Further details concerning this validation phase can be found in Salciarini et al. (2011).

Application of the Model to a Real Case Study

Study Area

A first attempt to explore the potentialities of the code at the territorial scale has been done by considering a portion of a study-area located in the Apennine mountains of Umbria region (central Italy), where previous studies related to shallow landslides hazard assessment have been carried out (see, e.g., Salciarini et al. 2006).

Within this area, both the villages on alluvial fans and the transportation corridors crossing the toes of unstable slopes have been periodically exposed to hazards from shallow landslides and debris flows (see, e.g., Guzzetti and Cardinali 1991; Salciarini et al. 2006). The surficial hillslope materials found in this area are the result of the erosion of highly fractured rock masses. These deposits are characterized by variable grain size distribution and thickness and generally accumulate on the lower parts of hillslopes or in erosion gullies associated with dissected weathered rocks.

The Italian National Research Council (CNR) has inventoried historical landslides in the Umbria Region and produced a landslide inventory map that delineates the main areas prone to instability in the region (Guzzetti and Cardinali 1990). Historical landslide records are available, together with technical notes from the landslide archives and relevant bibliography, on the SICI (Information System on Hydrogeologic Catastrophes) website. These data provide the records of landslide location. However, accurate timing of landslide occurrences is not available.

Input Data Collection

The CRF model requires the following input data: local slope inclination ⟨, mechanical and hydraulic properties of the soil cover (c', ⟩, k_Z, D_0), bedrock depth d_b, initial position of the water table d_w, and rainfall duration t_{end}. This last quantity is assigned depending on the scenario that the analysis is intended to reproduce, and in this case has been set to 6 h, to reproduce a landslide scenario produced by short-duration rainfalls.

The slope angle information has been computed applying the Spatial Analyst function of ArcGIS to the available 10 × 10 m DEM of the study area.

As for the initial hydraulic conditions, since very limited piezometric measurements are available in the study area, an initial depth of the water table equal to the 25 % of the soil cover thickness has been assumed, following Salciarini et al. (2006).

The spatial distribution of the soil cover thickness, represents a key input data for the critical rainfall assessment, because of its effects on both the local stability conditions of the hillslope, and the initial water table level. The spatial distribution of the soil cover depth is typically dependent on topography (for example, Godt et al. 2008; Schulz et al. 2008). In this study, the following empirical relation between the local slope angle and soil cover thickness has been used:

$$d_b = 14 \exp(-0.07\alpha) \tag{8}$$

which has been obtained by Salciarini et al. (2006) by interpolating available measurements in the study area.

As for the physical and mechanical properties of the soil, broad classes of soil materials with homogeneous behavior can be identified based on the data obtained from the digital Regional Geological Map (Fig. 2). More specifically, for the purposes of this study, the Regional Geological Map can be subdivided into three zones based on lithology and engineering properties:

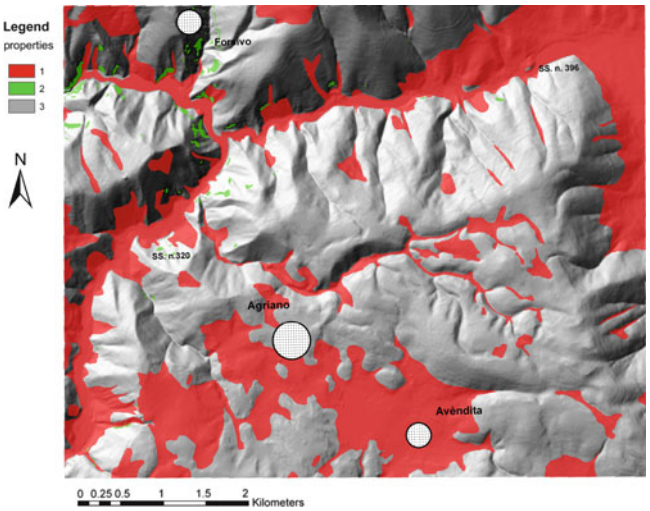


Fig. 2 Spatial distribution of the physical and hydro-mechanical properties of the soil, subdivided into three classes of homogeneous behaviour

Table 2 Mechanical and hydraulic properties of the soil for the three classes in which the territory has been subdivided

	Zone 1	Zone 2	Zone 3
k_V (m/s)	1e-4	1e-6	1e-8
γ (kN/m^3)	18.0	22.0	20.0
c' (kPa)	4.0	100.0	30.0
ϕ' (deg)	30.0	40.0	30.0

- Alluvial and colluvial soils: surficial, loose, variably sorted soil deposits of varying thickness that are primarily products of erosion and weathering (zone 1);
- Competent calcareous rocks (Calcare Massiccio Formation) (zone 2);
- Layered rocks dominated by marl-clay formations (Scaglia Cinerea Formation, Marne a Fucoidi Formation, and Bisciaro Formation) (zone 3).

The mechanical and hydraulic properties of the different classes of geomaterials considered have been assumed to be homogeneous within each class, and have been determined from published data and a limited amount of laboratory tests carried out on undisturbed samples (Salciarini et al. 2006), see Table 2.

Results of the Analysis

Figure 3 shows the landslide scenario predicted by CRF, imposing a 6-h rainfall. The map provides the corresponding critical rainfall intensity I_{Zf} that may cause instability.

The first outcome of the simulations is the locations of possible unstable slopes within the area (i.e., a susceptibility map). In particular, the map shows, for a given rainfall duration, the shallow hillslopes that reach the limit equilibrium conditions. This result can be validated by overlying the digital landslide inventory map by Guzzetti and Cardinali (1990), as shown in Fig. 3. A good agreement is observed between the inventory and the location of potentially unstable slopes.

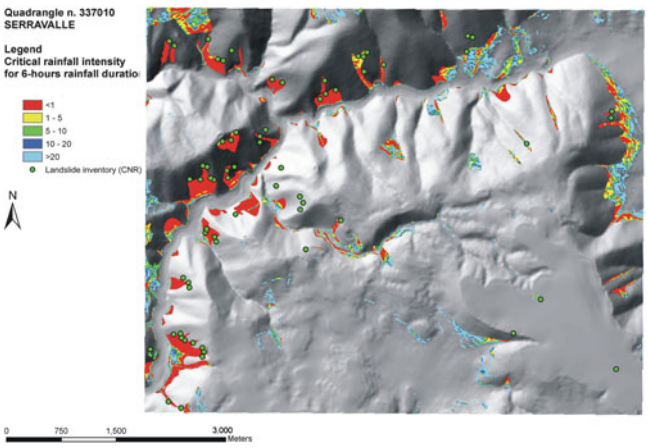


Fig. 3 Spatial distribution of the critical rainfall thresholds. In the figure the shallow landslide inventory by CNR is overlaid

However, the most interesting result of the simulation is that the critical rainfall intensity assumes a rather wide range of values (from less than 1 mm/h to more than 20 mm/h), depending on the local morphological conditions of the slope and the mechanical properties of the soil cover. It is worth remarking that the empirical thresholds would have provided just a single value of I_{Zf} for the specific scenario without any spatial information.

By repeating the analysis for different values of t_{end}, CRF allows producing spatially–based intensity/duration thresholds which are able to reflect the effects of local conditions.

Perspectives and Challenges

The physically-based susceptibility maps obtained with the proposed approach agree well with the digital landslide inventory map compiled by Guzzetti and Cardinali (1990), and show that alluvial and colluvial soils are prone to landslides in the study area. Moreover, the maps clearly indicate that the critical rainfall intensity associated with each duration can vary over a wide range of values, depending on the local morphological conditions of the slope and the mechanical properties of the soil cover. This allows extending the concept of rainfall intensity/duration threshold to the spatial dimension, in order to take properly into account the effects of the local hillslope conditions.

Such kind of thresholds is especially useful for predicting landslide occurrence at the regional scale. If coupled with reliable rainfall forecasts, they can be embedded into real-time early-warning systems for the management of landslide risk. Early-warning systems are still largely based on empirical methods relating rainfall intensity/duration with landslide occurrence. However, although the applicability of physically based models to real cases needs to be tested further, the preliminary results obtained encourage their application in this particular field.

The Department of Civil Protection of the Umbria Region has recently implemented a new early-warning system (named LANDWARN) for landslide risk prevention (Ponziani et al. 2010) that is based on the following main components: (1) the observed and 72 h-predicted cumulative rainfall from the dense regional hydro-meteorological network; (2) a local area meteorological model, known as COSMO ME; (3) a soil water balance model (Brocca et al. 2008); and (4) a web-based Information System. All these elements are arranged in a MATLAB-based flux of operations.

Nowadays, the system is still under development and implemented at three different scales: (1) for a specific rockslide site, where a real-time extensometer network is available; (2) for 110 high-risk landslide sites located across the whole regional territory; and (3) for the whole regional territory over a regular grid. Further steps of the implementation are currently in progress. In particular, the results of the GIS-based physically-based model of CRF, that combines the hydrological information with a simple slope stability analysis are under evaluation.

The potentiality of developing an early-warning system capable to take into account the mechanical and physical characteristics of the slopes, besides rainfall and soil moisture is of great interest, despite some challenges that arise.

The main reasons of the difficulties related to the shallow landslides forecasting by means of physically-based models are the following:

- The large extension and high heterogeneity of the territory (the Civil Protection System typically operates at the regional scale);
- The complexity in collecting available data to properly characterize the mechanical and hydraulic properties of the soil;
- The complexity in finding appropriate laws for the spatial distribution of the mechanical and hydraulic parameters (some authors suggested probabilistic laws to generalized some sparse, local measurements to a wider study area);
- The time and spatial variability of rainfall over the territory under study.

Since the beginning of their introduction, physically based modelling techniques are applied with different simplifying hypothesis (see, e.g., Montgomery and Dietrich 1994; Wu and Sidle 1995; Baum et al. 2002, 2008; Salciarini et al. 2006) with very good results. As general comments, although these models require a quite high resolution for the input data to have a reliable prediction of the shallow landslides over a broad region, some reasonable assumptions on the lacking data allow a good understanding of the observed events, both in terms of triggering time and position.

References

Aleotti P (2004) A warning system for rainfall-induced shallow failures. Eng Geol 73(3–4):247–265

Baum RL, Savage WZ, Godt JW (2002) TRIGRS – a Fortran program for transient rainfall infiltration and grid-based regional slope–stability analysis. USGS Open File Report 02-0424. http://pubs.usgs.gov/of/2002/ofr-02-424/

Baum RL, Savage WZ, Godt JW (2008) TRIGRS – a Fortran program for transient rainfall infiltration and grid-based regional slope-stability analysis, version 2.0. USGS Open File Report 08-1159. http://pubs.usgs.gov/of/2008/ofr-08-1159/

Brocca L, Melone F, Moramarco T (2008) On the estimation of antecedent wetness condition in rainfall-runoff modeling. Hydrol Process 22:629–642

Caine N (1980) The rainfall intensity–duration control of shallow landslides and debris flows. Geogr Ann 62:23–27

Cannon SH, Gartner JE (2005) Wildfire-related debris flow from hazards perspective. In: Jacob M, Hungr O (eds) Debris flow hazards and related phenomena. Springer, Berlin, pp 363–385

Crosta G (1998) Regionalization of rainfall thresholds: an aid to landslide hazard evaluation. Environ Geol 35:131–145

Crosta GB, Frattini P (2001) Rainfall thresholds for triggering soil slips and debris flows. Mediterranean storms. In: Proceedings of the 3rd EGS Plinius conference on Mediterranean storms, vol 1, pp 463–487

D'Odorico P, Fagherazzi S, Rigon R (2005) Potential for landsliding: dependence on hyetograph characteristics. J Geophys Res 110:1–10

Frattini P, Crosta G, Sosio R (2009) Approach for defining thresholds and return periods for rainfall–triggered shallow landslides. Hydrol Process 23:1444–1460

Giannecchini R (2005) Rainfall triggering soil slips in the southern apuane alps (tuscany, italy). Adv Geosci 2:21

Godt JW, Schultz WH, Baum RL, Savage WZ (2008) Modeling rainfall conditions for shallow landsliding in Seattle, Washington. Rev Eng Geol 20:137–152

Guzzetti F, Cardinali M (1990) Landslide inventory map of the Umbria region, central Italy. In: Proceedings of the 6th ICFL-ALPS 90, vol 1, pp 273–284

Guzzetti F, Cardinali M (1991) Debris-flow phenomena in the Central Apennines of Italy. Terra Nova 3:619–627

Guzzetti F, Peruccacci S, Rossi M, Stark C (2008) The rainfall intensity–duration control of shallow landslides and debris flows: an update. Landslides 5:3–17

Innes JL (1993) Debris flows. Prog Phys Geogr 7:469–501

Iverson RM (2000) Landslide triggering by rain infiltration. Water Resour Res 36(7):1897–1910

Montgomery DR, Dietrich WE (1994) A physically-based model for the topographic control on shallow landsliding. Water Resour Res 30:1153–1171

Ponziani F, Berni N, Pandolfo C, Stelluti M, Brocca L (2010) An integrated approach for the real-time monitoring of a high risk landslide by a regional civil protection office. In: Proceedings of the international conference EGU Leonardo topical conference

series on the hydrological cycle 2010, Luxembourg, 10–12 Nov 2010

Salciarini D, Godt JW, Savage WZ, Baum RL, Conversini P (2008) Modeling landslide recurrence in Seattle, Washington, USA. Eng Geol 102:227–237

Salciarini D, Godt JW, Savage WZ, Conversini P, Baum RL, Michael J (2006) Modeling regional initiation of rainfall–induced shallow landslides in eastern Umbria region of central Italy. Landslides 3(3):181–194

Salciarini D, Tamagnini C, Conversini P, Rapinesi S (2011) Spatially distributed rainfall thresholds for the initiation of shallow landslides. Nat Hazard. doi:10.1007/s11069-011-9739-2

Schulz WH, Lidke DJ, Godt JW (2008) Modeling the spatial distribution of landslide-prone colluvium and shallow groundwater on hillslopes in Seattle, WA. Earth Surf Process Landforms 33:123–141

Wu W, Sidle RC (1995) A distributed slope stability model for steep forested hillslopes. Water Resour Res 31:2097–2110



Rainfall Threshold Analysis and Landslide Susceptibility Mapping in Wudu County

Shibiao Bai, Jian Wang, Thomas Glade, Rainer Bell, and Benni Thiebes

Abstract

The main purpose of this study is the analysis of rainfall thresholds and landslide susceptibility mapping in order to assist the prediction, mitigation and management of slope instability in the Wudu county in China. Firstly, the rainfall thresholds were assessed using the Antecedent soil water status (ASWS) model based on landslides induced by multi-temporal rainfall events in the Wudu county. Secondly, three separate susceptibility maps were produced using historic landslide inventories, and inventories reflecting single landslide triggering events, i.e. the 2008 Wenchuan earthquake and heavy rain storms. The separate maps were combined to illustrate the maximum landslide probability of all three landslide susceptibility maps. The results show that rainfall thresholds could be applied to forecast rainfall-induced landslides, and the integrated landslide susceptibility map could be used for planning of spatial development as well as emergency response actions.

Keywords

Landslides • Susceptibility mapping • Rainfall thresholds • GIS • China

Introduction

China is possibly the country with the world's most serious geological disasters. Each year the direct economic losses of geologic disasters accounts for over 20 % of the total losses from all natural disasters. Hereby, landslides are the most important sudden processes of all geological hazards in China's mountains. Nationwide the landslide related direct and indirect economic losses account for more than 20 billion Yuan (approximately two billion EUR) every year (Hu and Tang 2005). According to the inventories of the China Institute of Geo-Environment Monitoring, there were a total number of 102,804 geological disasters nationwide in 2006, of which 88,523 (86 %) were landslides. In 2007 there were 25,364 entries nationwide, of which 15,478 (61 %) were landslide events. In 2008, 14,350 landslides were recorded from a total number of 26,580 geological disasters, which accounts for 54 %.

These numbers underline the importance of disaster prevention and relief for the reduction of economic losses. Therefore, landslide risk mapping and scientific predictions are important tools. Furthermore, 90 % of landslides and debris flows in China are directly induced by or related to rainfall as the triggering or a preconditioning factor (Li et al. 2004). Landslides induced by rainfall occur frequently and cause great harm to human beings. As in numerous countries in the world, also in China landslides are a serious

S. Bai (✉) • J. Wang
College of Geographical Sciences, Key Laboratory of Virtual Geographical Environment (Ministry of Education), Nanjing Normal University, Nanjing 210046, China
e-mail: shibiaobai21@163.com

T. Glade • R. Bell
Department of Geography and Regional Research, University of Vienna, Universitaetsstr.7, Vienna 1010, Austria

B. Thiebes
College of Geographical Sciences, Key Laboratory of Virtual Geographical Environment (Ministry of Education), Nanjing Normal University, Nanjing 210046, China

Department of Geography and Regional Research, University of Vienna, Universitaetsstr.7, Vienna 1010, Austria

C. Margottini et al. (eds.), *Landslide Science and Practice*, Vol. 2,
DOI 10.1007/978-3-642-31445-2_86, © Springer-Verlag Berlin Heidelberg 2013

geological disasters which have to be addressed by various organizations and institutions including also national, regional and local governments (Keefer et al. 1987; Brabb and Harrod 1989; Guzzetti 2000; Keefer and Larsen 2007).

The empirically determined rainfall-induced landslide threshold is a very important methodology in reducing the risk posed by the landslide hazard (Guzzetti 1998. Aleotti 2004; Wieczorek and Glade 2005). Therefore, great efforts have been made on the study of regional rainfall induced landslides forecasting models in recent years. The relationship between rainfall characteristics and landslide occurrence is very complex and is affected by, for example, slope conditions and the type of vegetation, but also by precipitation type, total rainfall amounts and the antecedent rainfall conditions.

The Wudu county covers 4,683 km^2 and is located in the Qinling Mountains and is surrounded by the Qinghai-Tibet Plateau, the Loess Plateau and the Sichuan Basin as the three major geomorphic units. Due to its geophysical conditions, the area is one of China's most severely landslide affected regions (Scheidegger and Ai 1987). In addition to the soft and erodible lithologic formations, the area is tectonically active and frequently experiences earthquakes. Moreover, the increase of urbanization and the reconstructions following the Wenchuan earthquake increased the landslide frequency, and also amplified the impact of landslides occurrences on society. In the past 10 years, several large landslide disasters occurred. For example, the Gansu mudslide which took place on August 8th 2010 only 30 km away from the Wudu study area, was caused by heavy rainfall and killed more than 1,478 people (Fig. 1).

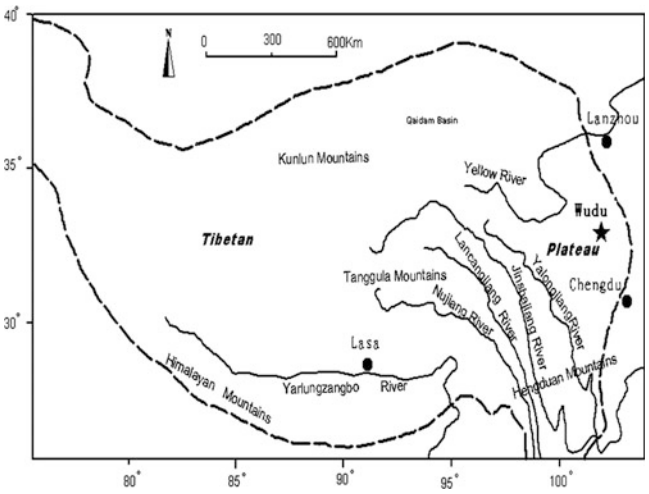


Fig. 1 Location of the Wudu study area

Landslide Inventory and Landslide Triggering Factors

In the Wudu region, landslide triggering factors include high magnitude earthquakes, high intensity rainfall events and human activities such as construction works. The combination of geophysical susceptibility and potential triggering conditions cause a frequent occurrence of landslides and debris flows. Landslide inventories were constructed by a combination of field investigation and SPOT 5 and ALOS remote-sensing image data analysed by visual interpretation, image classification and texture analysis.

The historical rainfall-induced landslide database of the Wudu region has its basis in survey documents of the two former government departments, which has been working on geo-hazard survey plan since 1999; one being the Ministry of Land and Resources of the People's Republic of China; another being the Longnan First Station for Landslide and Debris Flow Forecasting and Warning System of the Upper Reaches of the Yangtze River, which was constructed in 1991. Within this period of 1995–2003, a total number of 826 rainfall landslides have been reported. In 2003, seven successive rainfall events induced 290 landslides and 360 debris flows. The inventories of the Ministry of Land and Resources list 187 historic landslides, and additional 374 landslides which were triggered by the Wenchuan earthquake.

In China, the landslide classification differs from the categorisation by Cruden and Varnes (1996) and primarily differs landslide based on material composition (Liu and Yan 2002). Within the Chinese classification, the landslides in the Wudu region are divided into the four types, i.e. colluvial landslides, loess landslides, loess – mudstone landslides and bedrock landslides.

A database of landslide predisposing factors was constructed accounting for landslides before and after the Wenchuan earthquake. Data were stored in a resolution of 30 × 30 m and include digital orthophoto maps (DOM), digital elevation model (DEM) and derived topographical parameters (e.g. altitude, slope, aspect, profile curvature, plan curvature), geology (the map scale of lithological properties and fault characteristics is 1:200,000), land use (1:100,000) and further layers including road network and rivers. The triggering factors of the Wenchuan earthquake were collected from the USGS database and include the Peak Ground Acceleration (PGA), Peak Ground Velocity (PGV), and the Modified Mercalli Intensity (MMI). The triggering factors of the rainfall dataset were extracted from the daily precipitation records from several rain stations in the region.

Calculation of the Landslide-Inducing Rainfall Threshold

Antecedent Daily Rainfall Model and the Threshold Approach

The calculation of rainfall threshold is one of the methods being adapted to aid the mitigation of the effects caused by landslides (Glade et al. 2000; Jakob and Weatherly 2003). The probability of landslide occurrences for different rainfall events is useful for landslide risk management and important information for organisations which have to deal with landslides. Institutions such as insurance companies or regional governmental bodies can use these landslide probability figures to define the appropriate level of either preparedness or, combined with risk analysis, estimated possible average costs resulting from landslide damage (Glade et al. 2000).

Landslide triggering rainfall threshold models can be divided into three categories: approaches assessing the triggering rainfall characteristics based on for example rainfall intensity and duration conditions, approaches incorporating antecedent soil water conditions (e.g. the ASWM), and models also reflecting geological factors in addition to rainfall characteristics.

The study on rainfall models aims to analyse and determine the relation between landslide occurrence and triggering rainfall characteristics. Earlier threshold studies mainly focussed on the establishment of an empirical formula between landslide occurrence and the total rainfall (Lumb 1975; Brand et al. 1984; Fukuzono 1985; Keefer et al. 1987). Glade et al. (2000) summarised three models for determining landslide thresholds: daily rainfall model, antecedent daily rainfall model, and antecedent soil water content model. These approaches and consequent advancements are the major models that are currently adopted to determine landslide inducing rainfall thresholds (Glade et al. 2000).

Caine (1980) analyzed the available data and presented equations for landslides as a combination of intensity and cumulative precipitation for different areas. Guidicini and Iwasa (1987) developed the statistic relation between landslide events and rainfall for nine areas of Brazil. Ayalew (1999) analyzed 64 landslides and rainfall characteristics in Ethiopia, and worked out the relation between landslide occurrence probability and rainfall in Ethiopia. Crozier and Eyles (1980), Crozier (1999), and Glade et al. (2000) attempted an approach to link soil moisture conditions to the occurrence of landslides. These authors developed the antecedent soil water status (ASWS) model, a conceptual model that estimates soil moisture on a daily basis. This requires detailed soil characteristics data and meteorological information including rainfall, air temperature and potential evaporation. This model calculates the landslide occurrence probability, named the soil water content index, considering a variety of parameters (Glade 2000b). The ASWS model analyses the soil water balance including a drainage factor to account for the excess precipitation over a period of days prior to the day of the landslide event. A decay function for the loss of water through drainage and evapotranspiration is obtained by analysing hydrograph recession curves (Glade et al. 2000). Crozier (1999) calibrated the ASWS model in the Wellington area, New Zealand, using rainfall and landslide information for a severe landslide event occurred in 1974, and successfully predicted days with landslides and days without landslides for an 8-month period in 1996. Despite its proven capability, the model has not been implemented in a landslide warning system (Wieczorek and Glade 2005). Glade et al. (2000) applied probability determination to refine landslide-triggering rainfall thresholds using an empirical "Antecedent Daily Rainfall Model". Based on the study of the antecedent soil water content model, the landslide stability distribution model has been developed as a substitution (Borga et al. 1998; Crosta et al. 2004).

Liu et al. (2004) divided China into 7 major areas and 28 warning areas on the basis of geological and climatic conditions. Based on a statistic analysis of the amount and distribution of rainfall 15 days prior to the landslide occurrence, the forecast and warning criteria for each area were determined. Zhang et al. (2005) based the statistical analysis on 153 landslides and related precipitation in the Chongqing region. They determined a significant relation between landslide occurrence, daily rainfall and accumulated antecedent rainfall. Li and Yang (2006) selected data on 28 landslides triggered by a rainfall event in August 2003 in Yucheng District of Ya'An city. The established rainfall threshold considered both the daily precipitation at day of landslide occurrence and the three days accumulated rainfall before. Wang and Sassa (2006) combined static variables and rainfall conditions (e.g. cumulative precipitation, maximum daily precipitation in of 6 or 7 days) and performed a landslide hazard assessment.

Glade (2000a) used the parameter of daily rainfall for the analysis of landslide triggering and non-triggering conditions. Minimum rainfall threshold below which never landslides were recorded and maximum threshold above which always landslide were observed, were identified. It was confirmed that the antecedent rainfall is of major importance for landslide initiation in many areas. It is argued that the daily rainfall model can not accurately reflect the relation between landslides and rainfall for some regions. Instead the cumulative precipitation, the intensity and the duration of rainfall should be used to determine respective thresholds.

Correlation of Landslides and Daily Precipitation

The Antecedent Daily Rainfall model was applied to the landslides induced by the 2003 rainfall events in the Wudu county. All daily precipitation records of the year 2003 were combined with the available landslide information. Due to missing local soil information, the decay constant k (representing the outflow of the regolith) was set as 0.84 and the rn (maximum regional precipitation on the nth day before landslide occurrence) is 10 days. By applying the ordinary logistic regression model, the relation between landslide occurrence and daily rainfall was determined. Both datasets were used as input for the logistic regression algorithm to calculate the correlation of landslides to daily precipitation ($r0$) and antecedent daily precipitation (ra). The probability between landslide occurrence and rainfall magnitude was obtained in the Wudu county by the following equation:

$$\log\left(\frac{p}{1-p}\right) = -5.257 + 0.222r_0 + 0.314r_a$$

where p is the landslide occurrence probability at day 0, $r0$ and the antecedent days ra with r0 is the daily precipitation at day of landslide occurrence and ra is the antecedent daily precipitation for a specified period prior to day of landslide occurrence.

Combination of Daily and Antecedent Rainfall

Applying the equation to the Wudu county resulted in figures which illustrate how the combination of decayed 10 day antecedent daily rainfall and the magnitude of daily rainfall at day 0 influence landslide initiation. The resulting regional figures are presented in Fig. 2 and give a generally negative relationship between antecedent conditions and daily rainfall, indicating that with increasingly wet antecedent conditions, less rainfall is required to trigger landslides on a given day. After exceeding a given threshold, the soil is so saturated from antecedent rainfall, that no rainfall is required to trigger landslides. Thus, such an initiation is purely based on internal factors (such as positive pore water pressures) and not on external forces (such as additional precipitation). In contrast, exceeding a daily rainfall of 20 mm always leads to landslides; this is independent for the antecedent rainfall conditions.

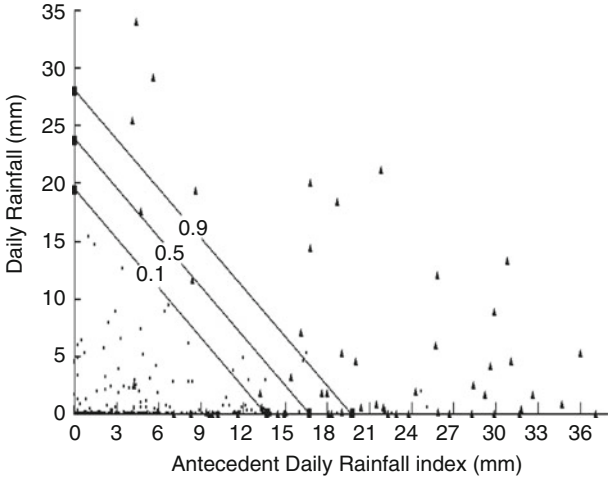


Fig. 2 The Antecedent Daily Rainfall Model applied to rainfall-triggered landslides and precipitation in 2003 (*Large triangle dots* relate to rainfall which triggered landslides, and *small square dots* relate to rainfalls which did not trigger landslides)

Integrated Landslide Susceptibility Mapping

Logical Regression (OLR) Model

Due to the complex nature of rainfall or earthquake triggers, current technologies cannot accurately predict the time of slope failures. Therefore, most local and regional authorities and land use planners rely on landslide inventory and susceptibility maps to develop emergency rescue plans and land use assessment (Fell et al. 2008). Both qualitative and quantitative methods have been used in the process of creating landslide susceptibility maps (Aleotti and Chowdhury 1999; Guzzetti et al. 1999). The qualitative method was widely used during the late 1970s by engineering geologists and geomorphologists. The quantitative methods, however, became popular in the last few decades largely because of its numerical expressions of the relationship between controlling factors and landslides, assisted by the advances in computer and geographic information system (GIS) technology (Chung et al. 2002; Van Westen and Getahun 2003; Bell and Glade 2004; Glade 2005; Guzzetti et al. 2005; Van Westen et al. 2008; Bai et al. 2008, 2009, 2010a, b, 2011).

The Ordinary Logical Regression (OLR) has been applied for landslide susceptibility mapping extensively (Atkinson and Massari 1998; Bai et al. 2010a, b). The algorithm of logistic regression applied maximum likelihood

estimation after transforming the dependent variable into a logic variable representing the natural log of the odds of the dependent occurring or not. In this way, the logistic regression estimates the probability of a certain event occurring (Atkinson and Massari 1998).

The landslide susceptibility analysis using the logical regression model includes four main steps: (1) splitting the dataset and resampling; (2) multi-collinearity diagnosis; (3) implementation of LR models; and (4) validation and evaluation of the model results. In the study, the continuous data like average annual precipitation and the distance were not categorized into binary format, and directly input to the logistic regression for the analysis. The categorized parameters such as lithology, land use and aspect were applied as a dummy variable in the logistic regression model with respect to each class of the respective categorized parameter. The last category is used as the default reference category.

Integrated Landslide Susceptibility Mapping

In this study, for rainfall event based landslide susceptibility mapping, variables such as the average annual precipitation during 1971–2009, aspect, lithological units, elevation, distance to river and land use were selected for statistical significance.

For Wenchuan earthquake landslide susceptibility mapping, variables such as aspect, plan curvature, elevation, land use and peak ground acceleration were selected for statistical significance.

For historic landslide susceptibility mapping, variables such as the average annual precipitation during 1971–2009, aspect, elevation and land use were selected for statistical significance.

In this study, an equal interval method to generate the different classes was applied. The three types spatial susceptibility map was divided into the four classes level 1 (very low), level 2 (low), level 3 (medium) and level 4 (high) respectively. The integrated landslide susceptibility score in this pixel is maximum landslide probability of three landslide susceptibility at that pixel (Fig. 3).

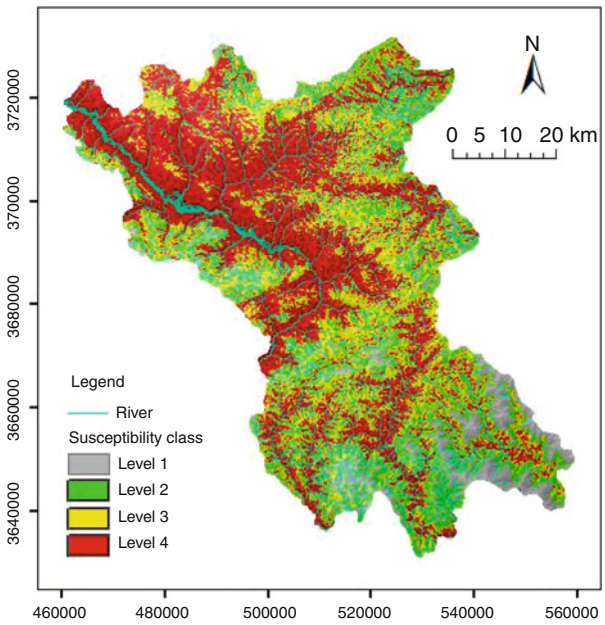


Fig. 3 The integrated landslide susceptibility score mapping

Conclusions

In order to facilitate landslide prediction, mitigation and management, we propose the combined use of susceptibility mapping and rainfall threshold analysis.

GIS-based logistic regression analysis of rainfall and earthquake triggered landslides provided the basis for the assessment of landslide prone areas. The combination of three separate susceptibility maps resulted in a maximum landslide probability map.

A quantitative method based on ASWS and logistic regression analysis including effective antecedent rainfall was used. Preliminary results show, that rainfall thresholds have the potential to be applied within forecasting systems.

The combination of landslide susceptibility maps and rainfall thresholds are of great value for local authorities responsible for spatial planning, landslide hazard management and emergency planning.

Acknowledgements This study was supported by the National Natural Science Foundation of China (Nos. 40801212 and 40871010).

References

Aleotti P (2004) A warning system for rainfall-induced shallow failures. Eng Geol 73:247–265

Aleotti P, Chowdhury R (1999) Landslide hazard assessment: summary review and new perspectives. Bull Eng Geol Environ 58:21–44

Atkinson PM, Massari R (1998) Generalized linear modeling of susceptibility to landsliding in the central Apennines. Italy Comput Geosci 24:373–385

Ayalew L (1999) The effect of seasonal rainfall on landslides in the highland of Ethiopia. Bull Eng Geol Environ 58(1):9–19

Bai SB, Wang J, Glade T, Bell R (2010a) Comparison on landslide susceptibility assessments before and after 5.12 WenChuan Earthquake at Lognan in China. In: Malet JP, Glade T, Casagli N (eds) Proceedings of the international conference 'Mountain risks: bringing science to society', Firenze, 24–26 Nov 2010, pp 87–94

Bai SB, Wang J, Lu GN, Zhou PG, Hou SS, Xu SN (2010b) GIS-based and logistic regression for landslide susceptibility mapping of Zhongxian segment in the Three Gorge area, China. Geomorphology 115:23–31

Bai SB, Wang J, Lü GN, Zhou PG, Hou SS, Xu SN (2009) GIS-based and data-driven bivariate landslide-susceptibility mapping in the Three Gorges Area, China. Pedosphere 19(1):14–20

Bai SB, Lu GN, Wang J, Ding L, Zhou PG (2011) GIS-based rare events logistic regression for landslide susceptibility mapping of Lianyungang, China. Environ Earth Sci 62:139–149

Bai SB, Wang J, Lu GN, Kanevski M, Pozdnoukhov A (2008) Validation of spatial prediction models for landslide susceptibility Maps. In: The eighth international symposium on spatial accuracy assessment in natural resources and environmental sciences, World Academic Union Press, Shanghai, 25–27 June 2008

Bell R, Glade T (2004) Quantitative risk analysis for landslides – examples from Bdudalur, NW-Iceland. Nat Hazard Earth Syst Sci 4(1):117–131

Borga M, Dalla FG, de Ros ML (1998) Shallow landslide hazard assessment using a physically based model and digital elevation data. Environ Geol 35(2–3):81–88

Brabb EE, Harrod BL (eds) (1989) Landslides: extent and economic significance. A.A. Balkema, Rotterdam, 85

Brand EW, Premchitt J, Phillipson HB (1984) Relationship between rainfall and landslide in Hong Kong. In: Proceedings of the 4th international symposium on landslides, Thomas Telford, Toronto, pp 377–384

Caine N (1980) The rainfall intensity duration control of shallow landslides and debris flows. Geogr Ann 62:23–27

Chung CF, Kojima H, Fabbri AG (2002) Stability analysis of prediction models for landslide hazard mapping. In: Allison RJ (ed) Applied geomorphology: theory and practice. Wiley, London, pp 1–19

Crosta GB, Dal Negro P, Frattini P (2004) Distributed modeling of shallow landsliding in volcanoclastic soils. Eng Geol 73(3–4):277–295

Crozier MJ, Eyles RJ (1980) Assessing the probability of rapid mass movement. In: Proceedings of the 3rd Australian New Zealand conference on geomechanics, New Zealand Institute of Engineers, Wellington, pp 247–251

Crozier MJ (1999) Prediction of rainfall-triggered landslides: a test of the antecedent water status model. Earth Surf Proc Land 24:825–833

Cruden DM, Varnes DJ (1996) Landslide types and processes. In: Turner AK, Shuster RL (eds) Landslides: investigation and mitigation. Transportation Research Board, Special Report 247, pp 36–75

Fell R, Corominas J, Bonnard C, Cascini L, Leroi E, Savage WZ (2008) Guidelines for landslide susceptibility, hazard and risk-zoning for land use planning. Eng Geol 102:85–98

Fukuzono T (1985) A new method for predicting the failure time of a slope. In: Proceedings of the 4th international conference field workship landslide, Japan Landslide Society, Tokyo, pp 145–150

Glade T (2000a) Modelling landslide triggering rainfall thresholds at a range of complexities. In: Proceedings of the 8th international symposium on landslides, Thomas Telford, Cardiff, pp 633–640

Glade T (2000b) Modelling landslide-triggering rainfalls in different regions of New Zealand-the soil water status model. Z Geomorphol NF 122:63–84

Glade T (2005) Linking debris-flow hazard assessments with geomorphology. Geomorphology 66:189–213

Glade T, Crozier MJ, Smith P (2000) Applying probability determination to refine landslide-triggering rainfall thresholds using an empirical "Antecedent Daily Rainfall Model". Pure Appl Geophys 157(6–8):1059–1079

Guidicini G, Iwasa OY (1987) Tentative correlation between rainfall and landslides in a humid tropical environment. Bull Eng Geol Environ 16(1):13–20

Guzzetti F (1998) Hydrological triggers of diffused landsliding. Environ Geol 35(2–3):79–80

Guzzetti F, Carrara A, Cardinali M, Reichenbach P (1999) Landslide hazard evaluation: a review of current techniques and their application in a multi-scale study, central Italy. Geomorphology 31:181–216

Guzzetti F (2000) Landslide fatalities and evaluation of landslide risk in Italy. Eng Geol 58:89–107

Guzzetti P, Reichenbach M, Cardinali M, Galli F, Ardizzone F (2005) Landslide hazard assessment in the Staffora basin, northern Italian Apennines. Geomorphology 72:272–299

Hu XL, Tang HM (2005) Research on the GIS system of slope engineering GIS and its application. China University of Geosciences Press, pp 1–36

Jakob M, Weatherly H (2003) A hydroclimatic threshold for landslide initiation on North Shore mountains of Vancouver, British Columbia. Geomorphology 54(3–5):137–156, 920

Keefer DK, Wilson RC, Mark RK (1987) Real time landslide warning system during heavy rainfall. Science 238(4829):921–925

Keefer DK, Larsen MC (2007) Assessing landslide hazards. Science 25:1136–1138

Li Y, Meng H, Dong Y, Hu SE (2004) Main types and characteristics of geo-hazard in China-based on the results of geo-hazard survey in 290 counties (in Chinese). Chinese J Geol Hazard Contr 15(2):29–34

Li Y, Yang XD (2006) Research on the forecasting and early warning of the regional precipitation-induced landslide (in Chinese). Hydrogeol Eng Geol 33(2):101–103

Liu CZ, Wen MS, Tang C (2004) Meteorological early warning of geo-hazard in China based on raining forecast (in Chinese). Geol Bull China 23(4):303–307

Liu GR, Yan EC (2002) Discussion on classification of landslides (in Chinese). J Eng Geol 10(4):339–342

Lumb P (1975) Slope failures in Hong Kong. Q J Eng Geol Hydrogeol 81(1):31–65

Scheidegger AE, Ai NS (1987) Clay slides and debris flow in Wudu region. J Soil Water Conserv 1(2):19–27

Wang HB, Sassa K (2006) Rainfall-induced landslide hazard assessment using artificial neural networks. Earth Surf Proc Land 31:235–247

Wieczorek GF, Glade T (2005) Climatic factors influencing occurrence of debris flows. In: Jakob M, Hungr O (eds) Debris flow hazards and related phenomena. Springer, Berlin, pp 325–362

Van Westen CJ, Getahun FL (2003) Analyzing the evolution of the Tessina landslide using aerial photographs and digital elevation models. Geomorphology 54:77–89

Van Westen CJ, Castellanos E, Kuriakose SL (2008) Spatial data for landslide susceptibility, hazard, and vulnerability assessment: an overview. Eng Geol 102:112–131

Zhang Z, Li SH, Ma L (2005) Probability analysis of relationship between landslide and rainfall in chongqing area (in Chinese). Chinese J Rock Mech Eng 24(17):3185–3191



Cloud Monitoring: An Innovative Approach for the Prevention of Landslide Risks

Bigarré Pascal, Verdel Thierry, Klein Emmanuelle, and Gueniffey Yves

Abstract

Early warning systems (EWS) applied to geohazards and landslides should rely increasingly on cutting edge multi-parameter monitoring systems. These aim to provide both the best insight in the physics and then reach the best time delay required by decision makers. In addition, monitoring geohazard on the long term is becoming an increasingly multi-stakeholder process, involving various interacting actors with different roles. Seamless access to dataset, easy-to-read advanced results and technical information of interest to be shared between numerous actors is becoming all the more important. Then, in the same manner as in the computing field, cloud monitoring technologies and solutions may pace rapidly the next generation of monitoring services. The paper intends to give a brief overview of this prospect, focusing on recent information technology breakthroughs and considerations on the cost benefit of such a network centric approach. The e.cenaris cloud monitoring data center developed by INERIS, France, is evocated along with further linked prospects related to the research undertaken by the authors.

Keywords

Monitoring • Internet • Forecast • Crisis

EWS: A Major Component in the Prevention of Landslides Risks

The pervasive nature of landslides, rock fall and cliff hazards in extensive hilly and mountainous territories, or along shorelines and rivers, combines unpredictability and infrequency of disasters. These favor clearly a cautious investment strategy from decision makers since in numerous situations, hazard mitigation or vulnerability reduction unveils a high socio-economic cost for an uncertain far-off benefit.

B. Pascal (✉) • K. Emmanuelle
National Institute of Environment and Industrial Risks, School of Mines of Nancy, Nancy, France
e-mail: pascal.bigarre@ineris.fr

V. Thierry • G. Yves
Laboratory of Environment, Geomechanics and Structures, School of Mines of Nancy, Nancy, France

Therefore, for some of those situations rated at risks, early warning systems may appear as a very solution in the prevention plan. Monitoring offers a temporary strategy to ensure public safety prior to more definitive remediation or vulnerability reduction works. It provides at least delay for appropriate decision making, timely action and important investments to be planned. It also produces observation data enabling eventually to improve the expertise of the geohazard and to answer more accurately to some relevant issues not clearly quantified from the hazard assessment study.

The deployment of a reliable early warning solution means first to ensure the capabilities to detect both early signs of large scale failure as well as potential worsening or triggering factors such as heavy rain-falls or floods, seismic or volcanic triggering, when not human induced (Lollino et al. 2006; Dünner et al. 2007). Recall that relying on a monitoring solution signifies to have a good confidence in the forecasted kinetic of failure mechanism potentially driving the

C. Margottini et al. (eds.), *Landslide Science and Practice*, Vol. 2,
DOI 10.1007/978-3-642-31445-2_87, © Springer-Verlag Berlin Heidelberg 2013

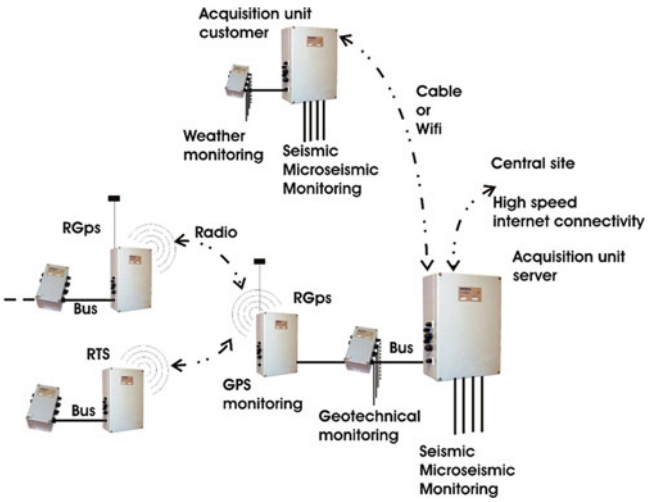


Fig. 1 Block diagram of the SYTGEM multi-parameter EWS installed on the Ruines de Séchilienne landslide. Clusters of sensors are cable or radio linked to a unique acquisition unit with 3D high speed connection to distant data center

instability. The answer is expected to be much lower than the time delay required activating countermeasures. Secondly, it implies a low false alarm rate.

Scalable Multi-Parameter EWS: A Key Innovation Laying the Ground

Multi-parameter monitoring is recognized as essential when looking for forecasting landslide occurrence. Up to now, it is usually undertaken through the deployment of different off-the-shelf specialized field equipments with no or very limited operating connections. This usually results in a tedious, resource intensive and failure-prone monitoring process.

Nowadays, fully integrated real-time multi-parameter monitoring technologies are gradually imposing appearance of new higher standards. These feature clustered field instrumentation capabilities to guarantee flexibility and scalability, smart self-adaptive data acquisition protocols and sophisticated multi-level radio transmission technologies, as well as on-line preprocessing routines and multiple levels alarm capabilities.

For instance, such a system combining and pairing geotechnical, passive microseismic and GPS RTK monitoring has been set up on the Ruines de Séchilienne landslide site, located in the French Alps (Fig. 1, Dünner et al. 2010). It permits to monitor numerous different variables (Fig. 2), including hydrology and weather, usually field monitored independently. In this case, a unique 3G mobile high speed



Fig. 2 Photo of a small size cluster of sensors composed of the GPS-RTK reference module and a weather station. This is radio-linked to a GPS-RTK and microseismic monitoring clustered network located on the distant facing flank affected by the Ruines de Séchilienne landslide, France

connection permits remote control of the overall system on the field as well as a fast data transmission rate.

Integrating a concentration of technologies on the field is aiming to enhance performance, i.e. higher quality in raw data and time series, better flexibility in field deployment and seamless data management and organization capabilities, in order to improve the prevention, based on the expertise and decision making. It also introduces new layers for self-monitoring, i.e. enabling malfunctioning detection along with some auto-fixing capabilities.

However, this overall high-tech trend means much higher complexity in the deployed systems, more sensitive procedures to operate them and then higher levels in technical skills and scientific competences uneasy to acquire. Moreover, processing, validation and interpretation of the data on a routine basis means also to embrace not only geology and geomechanics, but hydrology, geodesy and geophysics. Gathering periodically a multidisciplinary team of specialists and experts is not economically feasible, unless gathering them virtually through the internet, provided all of them have easy and fast access to the same unique and complete dataset.

Fast Information Sharing: An Increasingly Pregnant Requirement

In addition to remote experts and distant specialists, monitoring geohazard is becoming an increasingly multi-stakeholder process, involving various interacting actors with different roles and interests, ranging from risk manager to local experts, local authorities, private contractors and public services, civil protection when not the public itself through residents associations engaged in outreach activities.

Seamless real-time access to easy-to-read advanced results and various type of technical information of interest to be shared between some or all actors is gaining importance in nowadays projects. Here again, sharing the same unique database of information with fast updating rate capabilities towards different distant groups of end-users calls for reliable infrastructures and resources.

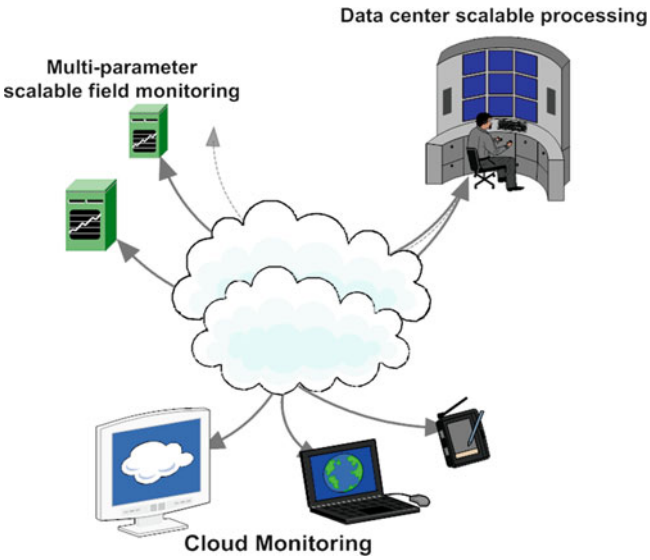


Fig. 3 Schematic view of the cloud monitoring concept: Multiple end-user profiles access effortlessly to the database hosted in a highly specialized data center. This is also in charge of real-time processing, routine and advanced analysis, as well as remote management of the field monitoring system

Cloud Monitoring: An Innovative Approach

This last years, virtualization technologies and web applications have introduced new capabilities to manage critical applications, to store and process important amount of data, while ensuring seamless access to the data whenever and wherever needed, to all persons involved in the collaborative work. This horizon calls nevertheless for higher specialized resources and competences creating new profiles of services.

Based on this recent trend, the Cloud monitoring concept seems now ready to emerge. This means the apparition of new parties able to scope not with a unique national or regional monitoring network, as for seismic or meteorological monitoring national centers, but with numerous independent and different local size monitoring geotechnical projects. The Cloud monitoring concept calls for fully integrated monitoring services based on cost effective verticalization. This ranges from the field installation of a modular scalable early warning system to a web-based scalable package of applications tailored to offer to multiple end-users an appropriate insight to the monitoring project, from raw dataset reviewing to technical reports, documentation and media supports (Fig. 3).

Of course, such an approach is expected to favor significantly technical and scientific discussions and development of ideas between different distant experts, working on the same high quality plotted time series, customized lists and tables, charts, maps and other pre-defined graphics, relevant statistics, forecasting indicators and customized reports.

Eventually, cloud data center offers time-shared access to scientific processing capabilities and warehouse capacities based on servers featuring high level computing resources, redundancy and high availability along with guarantees on a secured long-term interactive accessibility to data and metadata. Finally, cloud monitoring is expected to offer in the close future a significant cost benefit of the monitoring solutions compared to what they are at present (see Table 1).

INERIS is currently developing the e.cenaris cloud monitoring platform, dedicated to geohazards. The objective of this platform is first and above all to provide a breakthrough in the management of numerous geotechnical and geophysical observational and monitoring projects that are currently going on. With more than 40 distinct monitoring sites spread all over the French national territory, feedback experience shows quite clearly that the main advantage of the cloud monitoring concept is its important cost benefit, i.e. the opportunity to introduce new advanced monitoring services at a reasonable cost, which is of importance when dealing with public safety.

As regards the main drawbacks of such an approach, first is the well-known limitation of all geotechnical monitoring projects, a still rather non standardized engineering field, dealing with numerous gaps as regards general technical specifications, norms, compatibility and recommendations. In brief, most data coming from monitoring projects exchanged between specialists and experts in 2011 are still basically formatted for spreadsheet software. Openness and interoperability of the uncountable monitoring solutions available worldwide on the market by the whole branch of companies and services related to this field is still lacking.

Table 1 A short list of the advantages of the Cloud monitoring approach

	Advantages/drawbacks
Field monitoring	Flexibility, uniformity, scalability
	Smart self-adaptive data acquisition protocols
	Self monitoring capabilities
	Built-in remote control and maintenance procedures
Data center processing	Flexibility, scalability, reliability of computing resources based on virtualization tech
	Access to advanced data processing: correction, GPS, seismic, . . .
	3D mapping and graphic facilities
	Automated advanced graphics and tool analysis
	Minimize data losses
Aid to analysis and interpretation	Easy access to multiple types of information
	Customized access to data anywhere – whenever
	Web access to latest data at periodic rate up to real-time
	Applications available for off-line analysis

It is also noteworthy that if cloud monitoring solutions and services are expected to develop, they should be difficult to evaluate in terms of effective cost benefit performances.

If cloud monitoring solutions are emerging with clear high potential to enhance prevention, it opens also to new perspectives to enhance in the future the global services introducing new tools made available by important computing resources at much low cost. First, faster relevant time series analysis capabilities should be developed and implemented on a quasi real time basis to help specialists and experts to better understand the physical model of the geostructure they are monitoring, thus improving time predictability. Second, the internet capabilities could be developed both to help training decision makers and to manage a natural disaster induced crisis.

Further Need for Statistical Modelling of Time Series

Landslides are complex geological instabilities to model through pure physics considerations alone. Since early warning systems generate numerous time series such as displacements, strains, tilts, pluviometry, temperatures, snow levels and microseismic activity, statistical modeling and data analysis methods are supposed to help a lot. Any advanced interpretation of time series aims at least one of the following objectives: to analyze and understand the evolution of the different variables versus time, to detect any significant abnormal change and then to identify and quantify relationships and time delays between those variables (Fig. 4).

These objectives call for the use of proven statistical analysis methods and tools enabling to determine probabilistic laws for occurrences of the dreaded phenomena. If this is usually impossible when dealing with landslide risks, another more reasonable objective is to help in reliable

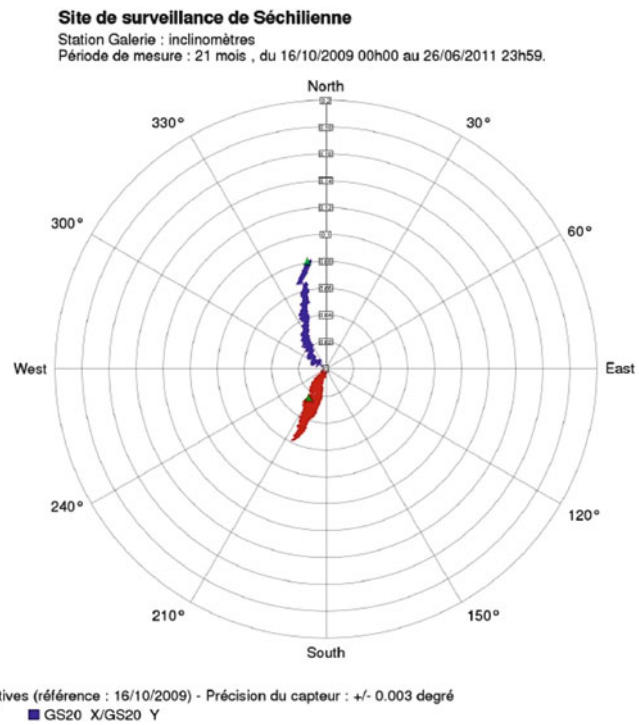


Fig. 4 Time series may be represented following different representations to help the expert. Here the case example of the real time web monitoring of two tilt meters set up on Sechilienne landslide site. Tilt trajectories are computed and plotted on a semi hemisphere projection to provide fast easy intepretation of the mass mouvement

detection and alarm generation based on statistical short term forecasting capabilities.

But beyond basic statistics related to moving average filtering, dispersion, and linear trends, in-depth processing and analysis of multi-parameter time series remains a tedious task, still irrelevant for automated analysis on a routine basis. It requires a tailored approach strongly dependent of the dataset, i.e. the type, accuracy and frequencies of the different field measurements as well as the associated

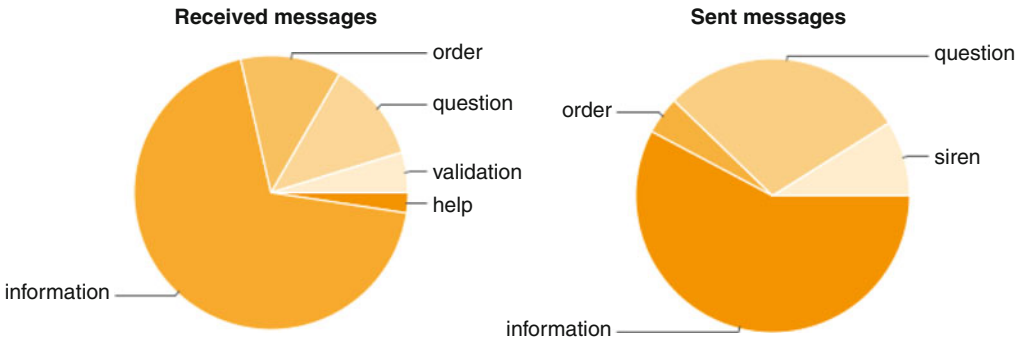


Fig. 5 Example of statistics about the types of messages received or sent by a group after a crisis simulation with iCrisis™

errors and uncertainties. As regards landslide hazards, the data analysis may have to consider non-stationary process as climate change for example. To deal with such issues statistical modeling is required, calling usually for a thorough judicious transformation of the raw data to enhance the performance of the analysis. From there, some of the most current techniques are the principal component analysis, to reconstruct missing data, the time series segmentation to determine uniform characteristics over few intervals easier to model, or to model the time series for appropriate classification of the signals.

This preliminary process of the raw data makes easier the next statistical modeling stage to back-analyze trends, seasonal effects, various dispersion factors as well as possible ruptures and singularities (Verbesselt et al. 2010). In most situations, the end-user is neither a developer nor a statistician, it is thus of utmost importance to build up easy-to-read interpretation tools pairing numerical results and graphics. There is here a clear urgent field for research and development for new tools enabling automated statistical modeling and analysis helping scientists and experts when having a close look to dataset (Chun-houh et al. 2008).

iCrisis: A Research Tool to Help Simulate and Train to Crisis Management

Within the concept of full integration of monitoring services, the Cloud monitoring approach may also include services for real-time disaster management as well as for crisis management training. This idea has been developed within the iCrisis™ project developed at the School of Mines of Nancy at the Laego laboratory (Verdel et al. 2010).

iCrisis™ is first an organizational structure to conduct simulations between several groups of decision makers (or crisis cells) usually involved in the management of post-accident crisis. Most often there are three groups playing respectively: the organization directly in charge of the accident, the local authorities and the national authorities. iCrisis™ is also a technical web-based application to manage such simulations and more particularly to facilitate, record, store and track all exchanges between these groups and each decision maker.

When used as a training system, iCrisis™ provides to the animation team, a copy of all messages exchanged between the decisions makers during a crisis simulation (Fig. 1), as well as a real-time statistical analysis of the number and the type (action, question, information, observation and so one) of the messages exchanged between the groups (Fig. 2). These dynamic analyses then help the simulation team to adapt the scenario of the crisis simulation to the actions taken by the decision makers. It makes the simulations very responsive and very adaptive. Because iCrisis™ is web-based, it can also be used with decision makers groups physically far from each other, even in different countries if necessary.

iCrisis™ has been developed to train to technological catastrophic events as well as to natural disasters. It can help assessing the efficiency and resilience of the organizations in charge of public safety in the case of an accidental landslide event. Furthermore, because it is web-based, it can also make use of or interact with any web-based monitoring platform to take into account real-time monitored data about the involved landslide.

iCrisis is currently being implemented in the e.cenaris platform. This implementation is intended to used first as a collective chat system between the specialists of INERIS to share instant text information about the monitoring projects. Apart to the shared documents and monitored data, shared instant messages will help keeping track of spontaneous ideas, analysis and information without the need to upload a formatted document. Such an approach is expected to be fully beneficiary during an accidental event when time delay is usually very short (Fig. 5).

Conclusions

Early warning systems are an important component in the prevention of landslide disasters. They are also the first source of dataset for in-depth studies of these geohazards.

Cloud monitoring solutions, based on similar design and technologies as fast growing cloud computing services made available nowadays by information technology industries, may pace rapidly the next generation of cutting-edge monitoring services. This approach should offer a very breakthrough with respect to the state-of-the-art in the field of geotechnical and geostructural monitoring, with a significant if not an important cost benefit to stakeholders and local consulting offices. Moreover, development of cloud monitoring tools and services could most likely favour the progressive emergence of new accessible databases to the engineering and scientific communities working in the field of ground failure hazards and, possibly, the beginnings of an e.science infrastructure specifically dedicated to these geohazards.

Acknowledgments Many colleagues contributed to the research and development work underlying the ground to this publication. We thank all of them for their multi-faceted contribution. The authors thank also the French Ministry of Ecology and Environment as well as the French National Agency of Research for their support.

References

Chun-houh C, Antony U, Wolfgang H (2008) Handbook of data visualization, Series: Springer Handbooks of Computational Statistics (eds)

Dünner C, Klein E, Charmoille A, Bigarré P (2010) Multi-parameter monitoring strategy applied to unstable rock slopes: the example of the Ruines de Séchilienne. In: RSS 2010 symposium, INERIS, Paris

Dünner C, Bigarré P, Clément C, Merrien-Soukatchoff V, Gunzburger Y (2007) Natural and thermomechanical stress field measurements at the Rochers de Valabres Pilot Site Laboratory in France. In: Proceedings of the 11th congress international society for rock mechanics. Taylor & Francis, Lisbon, pp 69–72

Lollino G, Arattano M, Allasia P, Giordan D (2006) Time response of a landslide to meteorological events. Nat Hazards Earth Syst Sci 6(2):179–184

Verbesselt J, Hyndman R, Newnham G, Culvenor D (2010) Detecting trend and seasonal changes in satellite image time series. Rem Sens Environ 114(1):106–115

Verdel T, Tardy A, Lopez P, Hansen C, Deschanels JL, Abdel-Aziz S (2010) iCrisis™: un dispositif original de simulation de gestion de crise, communication n°162, Congrès Lambda-mu 17 (Innovation et Maîtrise des Risques), La Rochelle



Landslide Triggering and Local Rainfall Thresholds in Bradanic Foredeep, Basilicata Region (Southern Italy)

Maurizio Lazzari, Marco Piccarreta, and Domenico Capolongo

Abstract

It is recognised that a lot of the landslides occurred in the Mediterranean region are triggered by short intense storms. Due to its geological, geomorphological and climatic settings, the Bradanic Foredeep (Basilicata region) is affected by the widespread presence of landslides. The main objective of this paper is to identify the empirical triggering thresholds in Bradanic Foredeep and to investigate the role of antecedent rainfall. Using a variety of information sources, we have compiled a catalogue listing 97 rainfall events linked to landslides triggering in the investigated area. For each event in the catalogue, the exact or approximate location of the landslide and the time or period of initiation of the slope failure is known, together with information on the rainfall duration D, and the rainfall mean intensity I , that have resulted in the slope failure. The local rainfall threshold for the study area has been established using the statistical Frequentist approach. The comparison with regional thresholds proposed for other Italian regions has revealed that the Bradanic Foredeep thresholds are lower; which is probably due to the different quality of rainfall dataset. In fact, all the previous threshold have been evaluated starting from hourly data, while for the Basilicata region only daily data are available. Throughout this study we could not identify a significant correlation between antecedent rainfall and critical rainfall.

Keywords

Rainfall-induced landslides • I-D relation • Bradanic Foredeep • Southern Italy

Introduction

The Mediterranean region is particularly sensitive to changes in the frequency and intensity of extreme rainfall events, which are often related with disastrous geo-hydrological events, such as floods and landslides (Luino 2005). Italy is one of the most vulnerable countries in terms of exposure to natural hazards within the Mediterranean (Guzzetti et al. 2005). The area affected by hydrogeological risk is 21,505 km^2, which corresponds to the 7.1 % of the whole territory. From 1991 to 2001 more than 1,000 flood events occurred (Ministero dell'Ambiente 2003). In only 1 year, 2003, major floods affected more than 300,000 people and caused damage up to 2,184 million euro.

In this paper we analyze the record of extreme rainfall events and landslides in Bradanic Foredeep, an eastern sector of southern Italian region Basilicata. In Basilicata the area affected by flood risk is 260 km^2 (2.6 % of the whole territory) and 58 % of the 114 municipalities are classified at high risk and a further 13 % at very high risk of landsliding (Clarke and Rendell 2006). In the investigated area slide surfaces are often associated with contacts between unconfined aquifers in sandy-conglomerate layers and underlying impermeable clays and shales (Gostelow et al. 1997).

M. Lazzari (✉)
Institute of Archaeological and Monumental Heritage, National Research Council, 85050 Tto Scalo (PZ), C.da S, Loja, Italy
e-mail: m.lazzari@ibam.cnr.it

M. Piccarreta • D. Capolongo
Department of Geology and Geophysics, University of Bari, Via Orabona, 4, Bari, Italy

C. Margottini et al. (eds.), *Landslide Science and Practice*, Vol. 2,
DOI 10.1007/978-3-642-31445-2_88, © Springer-Verlag Berlin Heidelberg 2013

Large landslides, which have caused structural damages at Pisticci, Ferrandina and Grassano towns, have been linked to extreme rainfall triggers. Lazzari et al. (2006), investigating the relationship between antecedent rainfalls and landslides at Tursi, have used the Standardized Precipitation Index (McKee et al. 1993) as an useful tool to predict rainfall-induced landslides.

This study focused on the compilation and analysis of historical landslides and climatic data to explore the observed relationship between rainfall and landslides. We exploit a catalogue of rainfall events that have resulted in all type of landslides in Bradanic Foredeep, Basilicata region (southern Italy), to define local thresholds for the possible occurrence of rainfall-induced landslides. An intensity-duration (ID) threshold linked to landslide occurrence has been derived by adopting the same approaches proposed by Brunetti et al. (2010). The new local threshold has been compared to similar thresholds proposed for other region of Italy.

We also investigate the role of antecedent rainfall (Crozier 1999) evaluating the relationship between normalized critical rainfall and normalized antecedent rainfall, such as proposed by Aleotti (2004).

Definition of Rainfall Thresholds Based on Literature Review

For rainfall-induced landslides, a threshold may define the rainfall, soil moisture, or hydrological conditions that when reached or exceeded, are likely to trigger landslides (Aleotti 2004). Several types of empirical rainfall thresholds for the possible initiation of landslides have been proposed in the literature.

In this section we report a brief review of the definition of rainfall threshold based on the very exhaustive papers of Wieczorek and Guzzetti (1999) and of Guzzetti et al. (2007, 2008).

Guzzetti et al. (2007, 2008) classify the published thresholds by: (1) the extent of the geographical area for which they were defined, and (2) the type of rainfall measurement used to establish the thresholds. Rainfall thresholds can be further subdivided as global, regional, or local thresholds on the base of their geographical extent. A global threshold refers to a general minimum level below which landslides do not occur, independently of local morphological, lithological, and land-use conditions and of local or regional rainfall pattern and history. Regional thresholds are defined for areas extending from a few to several thousand square kilometers of similar meteorological, climatic, physiographic, and soil characteristics, and are potentially suited for landslide warning systems based on quantitative spatial rainfall forecasts, estimates, or measurements. Local thresholds consider the local climatic regime and geomorphological setting and are applicable to single or to groups of landslides in areas extending from a few to some hundreds of square kilometers.

Two types of landslide-triggering rainfall thresholds can be established:

1. Empirical thresholds, based on historic analysis of relationship rainfall/landslide occurrence (Caine 1980; Crozier and Glade 1999);
2. Physical thresholds, based on numeric models that take into account the relationship between rainfall, pore pressure and slope stability by coupling hydrologic and stability models (Montgomery and Dietrich 1994; Wilson and Wieczorek 1995; Crosta 1998; Terlien 1998).

Empirical rainfall thresholds can be grouped in (1) thresholds that combine precipitation measurements obtained for specific rainfall events, (2) thresholds including antecedent rainfalls (Crozier 1999; Glade et al. 2000; Crosta and Frattini 2003; Aleotti 2004), and (3) other thresholds, including hydrological thresholds (Reichenbach et al. 1998).

Thresholds established using precipitation measurements obtained from individual or multiple rainfall events can be further subdivided in: intensity–duration (ID) thresholds, thresholds based on the total event rainfall (E), rainfall event–duration thresholds (ED), and rainfall event–intensity (EI) thresholds.

Case of Study

The study area is located in the Bradanic Foredeep, (Basilicata region, southern Italy) a Pliocene and Pleistocene sedimentary basin portion of the post-Messinian Apennines foredeep (Adriatic foredeep), which migrated towards east with several deformative phases during the Pliocene and early Pleistocene (Fig. 1). Together with the Murge peripheral bulge (Apulian Foreland) the Bradanic foredeep is the shallow crustal expression of the Apulian or Adria lithosphere subduction (Pieri et al. 1996; Lazzari and Pieri 2002; Lazzari 2008). Two main successions can be recognized, which are composed of clay and sandy-conglomerates, respectively. The former is the basal unit and corresponds to the more than 1,000 m of thick clayey *Argille Subappennine Formation*, while the latter, about 50 m thick, is the closing unit of the Bradanic Foredeep sedimentary cycle. This formation gradually pass, in continuity of sedimentation, to the *Sandy-gravelly Regressive Deposits*, characterized from sandy and gravely bodies (or mixed), defined like a informal lithostratigraphic units of lower rank, including marine and/or continental litofacies, reportable to depositional delta and coastal systems and continental systems (plain alluvial), places among them in relationship of continuity (gradual passage)

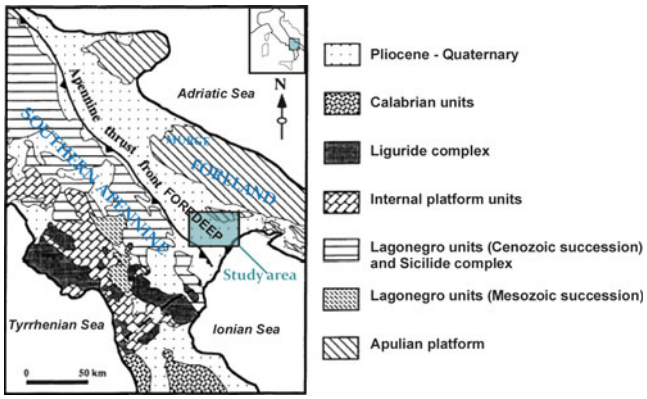


Fig. 1 Geographic location of the study area

and/or disconformity (erosive contact). Their thickness changes between 20 and 130 m. They constitute progradational bodies toward NE, E and SE in relation to their position in the basin. In the Middle Pleistocene the Bradanic Foredeep began to uplift, allowing both the ancestral rivers (Bradano, Basento and Cavone) to cut deep valleys perpendicularly to the coast and the lateral erosion to attack the hillslopes. The hillslopes are cut by deep gullies, which often erode up to their upper parts making them susceptible to landsliding (Boenzi et al. 2008). In the area landslides of all types developed on the clayey hillslopes.

Rainfall and Landslide Information

To determine the new global rainfall ID thresholds for the all type of landslides in Bradanic Foredeep (Basilicata), a database of rainfall events that have resulted in slope failures was compiled. The rainfall and landslide information was obtained through a thorough literature search, including national journals, national project (AVI project, Guzzetti et al. 1994), conference proceedings, and event and technical reports describing single or multiple rainfall-induced landslides. The collected information was organized in a catalogue listing 97 landslide events covering the 85-year period between 1924 and 2009, with the majority of the events (97 %) in the period from 1952 to 2009. For each rainfall event, the information collected and stored in the catalogue includes: (1) the precise or approximate location of the area affected by the rainfall and the landslides, (2) the precise or approximate time, date, or period of the failures, (3) the rainfall conditions that resulted in slope failures, including the total event rainfall, the rainfall duration, the mean rainfall intensity, and the antecedent rainfall for different periods, (4) the landslide type, (5) a generic description of the main rock types and (6) the mean annual precipitation (MAP). Not all the information is available for all the events listed in the catalogue.

Every municipality considered is provided of a rain gauge. Unfortunately, only daily rainfall data was available. The rainfall duration D was determined measuring the time between the moment, or period, of initiation of the failure(s) (rainfall ending time) and the time when the rainfall event started (rainfall starting time). The rainfall ending time was taken to coincide with the time of the last rainfall measurement of the day when the landslide occurred.

As suggested by Brunetti et al. (2010), for the identification of the starting time has been considered a minimum period without rain (a 2-day period without rainfall was selected for late spring and summer, May–September, and a 4-day period without rainfall was selected for the other seasons, October–April) to separate two rainfall events. Once the duration of the event was established, the corresponding rainfall mean intensity I (in mm h^{-1}) was calculated dividing the cumulated (total) rainfall in the considered period (in mm) by the length of the rainfall period (in hours). Using this method, the rainfall mean intensity for the event was determined (Guzzetti et al. 2007, 2008).

Definition of Objective Local Rainfall Thresholds for Bradanic Foredeep (Basilicata, Southern Italy)

In this paper we have considered the rainfall intensity-duration (ID) relationships adopting the statistical frequentist approach for the definition of objective threshold as proposed by Brunetti et al. (2010). The methods assume a threshold curve of the form:

$$I = \alpha D^{-\beta} \quad (1)$$

i.e., a simple power law, where I is the rainfall mean intensity (in mm h^{-1}), D is the duration of the rainfall event (in hr), α is a scaling constant (the intercept), and β is the shape parameter that defines the slope of the power law curve.

As clearly described by Brunetti et al. (2010), the method is based on a frequency analysis of the empirical rainfall conditions that have resulted in known landslides. The empirical data are first log-transformed and then are plotted in a single graph (Fig. 2a), and the distribution of the rainfall conditions, log(I) versus log(D), that have resulted in landslides is fitted (least square method) with a linear equation of the type $\log(I) = \log(\alpha) - \beta \log(D)$ (continuous red line in Fig. 2a), which is entirely equivalent to the power law of equation (1) in linear coordinates. Next, for each rainfall event, the difference $\delta(D)$ between the logarithm of the event intensity log[I (D)] and the corresponding intensity value of the fit log[If(D)] is calculated, $\delta(D) = \log[I(D)] - \log[If(D)]$.

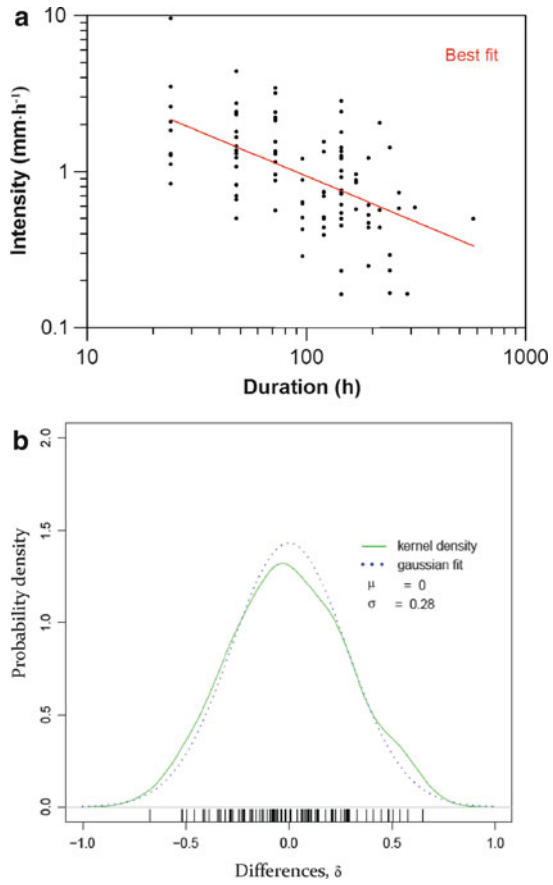


Fig. 2 (**a**) Ninety-seven rainfall events that have resulted in landslides in Bradanic Foredeep, in the period 1923–2009, for which the rainfall duration D (in hr) and the rainfall mean intensity I (in mm h^{-1}) are known. The *red line* is a fit (least square method) of the empirical rainfall (D, I) conditions. (**b**) Kernel Density Estimation of the differences δ(D), fitted with a Gaussian function, for the distribution of the empirical data points (D, I)

Then, the probability density function (pdf) of the distribution of δ(D) is determined through Kernel Density Estimation, and the result fitted (least square method) with a Gaussian function,

$$f(x) = a \exp\left(-\frac{(x-b)^2}{2c^2}\right)$$

where a > 0, c > 0, and a, b, c > R.

Figure 2b portrays the Gaussian fit of the pdf for the 97 empirical data points (D, I) shown in Fig. 2a. Lastly, thresholds corresponding to different exceedance probabilities are defined based on the modelled (fitted) distribution of δ (D).

Empirical Thresholds for Landslide Occurrence in Bradanic Foredeep (Basilicata, Southern Italy)

We exploited the catalogue of 97 rainfall events that have resulted in landslides in Bradanic Foredeep in the 85-year period 1924–2009 to determine rainfall thresholds for the possible occurrence of slope failures in Bradanic Foredeep, Basilicata Region, southern Italy. To determine the thresholds, we adopted the Frequentist method. Figure 3 shows the distribution of 97 rainfall conditions (D, I) that have resulted in all type landslides. Three local, ID thresholds are shown, T50, T10 and T5, which correspond, respectively, to the 50 %, 10 % and 5 % exceedance probability. Rainfall events that have resulted in landslides in the Bradanic Foredeep considered for the determination of the thresholds are in the range of duration 24 h < D < 576 h, and in the range of mean intensity 0.2 mm h^{-1} < I < 9.6 mm h^{-1}, with the 75 % of the events in the range 0.5 mm h^{-1} < I < 2.5 mm h^{-1}, really similar with the range observed for the Abruzzo region (Brunetti et al. 2010).

When the new thresholds are compared with those available in literature (Fig. 4), they appear quite similar to those proposed for several Italian region (Ceriani et al. 1994). The difference is a slightly lower exponent. Probably it is due to the different rainfall dataset, which does not present hourly data.

The "intensity–duration" approach can be further refined by normalizing the intensity value with the mean annual rainfall (MAP), thus emphasizing the regionalization of the thresholds, since the calculation takes into account the climatic regimes of the study area (Cannon 1988; Wieczorek et al. 2000).

This is important because, as suggested by Guzzetti et al. (2008), landscapes adjust to climate and that climate affects the meteorological conditions that can result in landslides. To cope with the observed climate differences, the rainfall measurements were normalized to proxy for regional climate conditions. Therefore, by using the MAP data from Piccarreta et al. (2004), the relationship between I and MAP in Bradanic Foredeep has been performed (Fig. 5). We obtained the normalized I threshold:

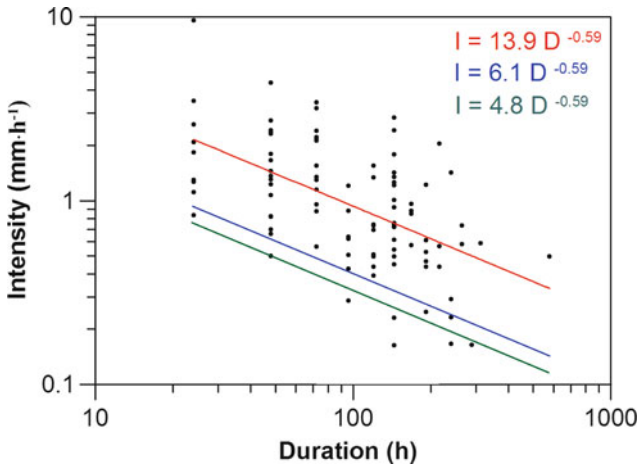


Fig. 3 Rainfall thresholds obtained using the Frequentist method (*green line* is the 5 % threshold, T5; *blue line* is the 10 % threshold, T10; *red line* is the 50 % threshold T50) methods

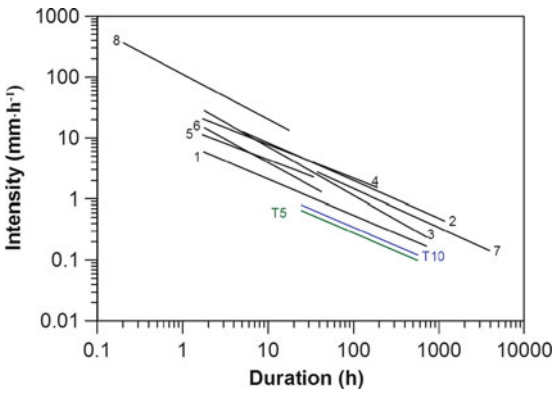


Fig. 4 Comparison of rainfall thresholds for possible landslide occurrence in Italy. New local thresholds are in colour: *green*, T5 5 %; *light blue*, T10 10 % (Source: 1, Brunetti et al. (2010), 2, Ceriani et al. (1994); 3, Calcaterra et al. (2000); 4, Aleotti (2004); 5, Bolley and Olliaro (1999); 6, Marchi et al. (2002); 7, Floris et al. (2004); 8, Giannecchini (2005))

$$\mathrm{IMAP} = 0.02\mathrm{D}^{-0.57}$$

Relationship Between Antecedent and Critical Rainfall

It has been recognized in the literature that antecedent rainfall can be a predisposing factor in the activation of soil slips (Wieczorek 1987). The influence of antecedent rainfall is difficult to quantify as it depends on several factors, including the heterogeneity of soils (strength and permeability properties) and the regional climate. In particular, in low-permeability soils like those of Bradanic Foredeep, antecedent rainfall can be an important factor

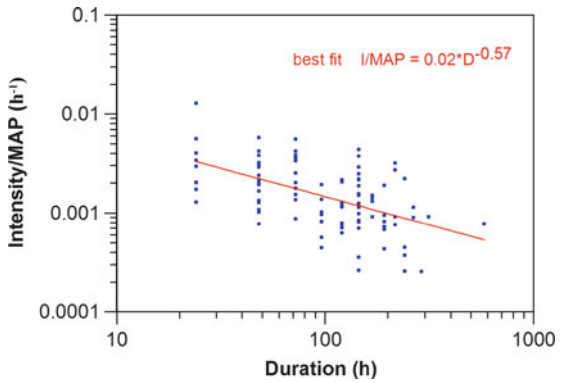


Fig. 5 Rainfall thresholds obtained using the normalized intensity with mean annual rainfall

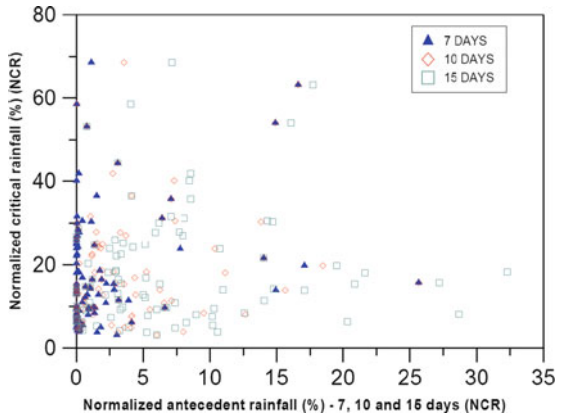


Fig. 6 Relation between normalized antecedent rainfalls (NAR) and normalized critical rainfalls (NCR) for 7-, 10- and 15-day intervals

because it reduces soil suction and increases the pore-water pressures in soils. However, the time interval established as significant by the various authors differs considerably: 5 days (Wieczorek et al. 2000), 10 days (Crozier 1999; Glade et al. 2000), 15 days (Govi et al. 1985).

The time intervals taken into consideration for the events examined in this paper were 7, 10 and 15 days. However, results (Fig. 6) show that not significant correlation exist between antecedent and critical rainfall: the scattering of the population sample, in fact, is very high and the relevant correlation coefficients, based on Pearson test, are $r = 0.22$, $r = 0.21$ and $r = 0.11$ for the 7-, 10- and 15-day intervals, respectively. The data are very similar to those found by Aleotti for the Piemonte region, northern Italy, showing that antecedent rainfall conditions do not play a main role in the landslide triggering.

Conclusion

Using a variety of sources of information, we have compiled a catalogue that lists 97 rainfall events that have resulted in all type landslides in Bradanic Foredeep,

Basilicata region, southern Italy. We have exploited the catalogue to determine new rainfall intensity-duration (ID) thresholds for the possible occurrence of landslides in the study area. Moreover the relationship between critical rainfall and antecedent rainfall has been investigated.

To establish the thresholds, we experimented the independent Frequentist statistical approach (Brunetti et al. 2010), whose application has been found more useful in other Italian regions. Comparison of the thresholds revealed that the Bradanic Foredeep thresholds are lower than regional thresholds proposed for Piedmont (Aleotti 2004), Lombardy (Ceriani et al. 1994), Abruzzo (Brunetti et al. 2010) and the Campania Region (Calcaterra et al. 2000). Probably it is due to the different quality of rainfall dataset. The threshold kown in literature have been evaluated starting from hourly data, while for the Basilicata region only daily data were available. Throughout this study we could not identify a significant correlation between antecedent rainfall and critical rainfall.

Acknowledgments We would like to thank M.T. Brunetti of C.N.R. IRPI, Perugia (Italy), for her fundamental assistance in the statistical analyses.

References

Aleotti P (2004) A warning system for rainfall-induced shallow failures. Eng Geol 73:247–265

Bolley S, Oliaro P (1999) Analisi dei debris flows in alcuni bacini campione dell'Alta Val Susa, Geoingegneria Ambientale e Mineraria, pp 69–74, (in Italian)

Boenzi F, Caldara M, Capolongo D, Dellino P, Piccarreta M, Simone O (2008) Late Pleistocene–Holocene landscape evolution in Bradanic Foredeep, Basilicata (Southern Italy). Geomorphology 102:297–306

Brunetti MT, Peruccacci S, Rossi M, Luciani S, Valigi D, Guzzetti F (2010) Rainfall thresholds for the possible occurrence of landslides in Italy. Nat Hazards Earth Syst Sci 10:447–458

Caine N (1980) The rainfall intensity-duration control of shallow landslides and debris flow. Geogr Ann A 62:23–27

Calcaterra D, Parise M, Palma B, Pelella L. (2000) The influence of meteoric events in triggering shallow landslides in pyroclastic deposits of Campania, Italy. In: Bromhead E (ed) Proceedings of the 8th international symposium on landslides

Cannon SH (1988) Regional rainfall-threshold conditions for abundant debris-flow activity. In: Ellen SD, Wieczorek GF (eds) Landslides, floods and marine effects of the storm of 3–5 January, 1982 in the San Francisco Bay Region, California, pp 35–42. USGS Prof. Paper 1434, 1988

Ceriani M, Lauzi S, Padovan N (1994) Rainfall thresholds triggering debris-flows in the alpine area of Lombardia Region, central Alps – Italy. In: Proceedings man and mountain, I Conv. Intern. per la Protezione e lo Sviluppo dell'ambiente montano, Ponte di Legno (BS), pp 123–139, 1994

Clarke ML, Rendell HM (2006) Hindcasting extreme events: the occurrence and expression of damaging floods and landslides in Southern Italy. Land Degrad Dev 17:365–380

Crosta G (1998) Regionalization of rainfall thresholds: an aid to landslide hazard evaluation. Environ Geol 35(2–3):131–145

Crosta GB, Frattini P (2003) Distributed modelling of shallow landslides triggered by intense rainfall. Nat Hazards Earth Syst Sci 3:81–93

Crozier MJ (1999) Prediction of rainfall triggered landslides: a test of the antecedent water status model. Earth Sur Proc Land 24:825–833

Crozier MJ, Glade T (1999) Frequency and magnitude of landsliding: fundamental research issues. Zeitschrift für Geomorphologie N.F. 15, 141–155

Floris M, Mari M, Romeo RW, Gori U (2004) Modelling of landslide-triggering factors – a case study in the northern Apennines, Italy. Lect Notes Earth Sci 104:745–753

Giannecchini R (2005) Rainfall triggering soil slips in the southern Apuan Alps (Tuscany, Italy). Adv Geosci 2:21–24

Glade T, Crozier M, Smith P (2000) Applying probability determination to refine landslide-triggering rainfall thresholds using empirical "antecedent daily rainfall model". Pure Appl Geophy 157:1059–1079

Gostelow TP, Del Prete M, Simoni A (1997) Slope instability in historic hilltops of Basilicata, southern Italy. Q J Eng Geol 30:3–26

Govi M, Mortara G, Sorzana P (1985) Eventi idrologici e frane. Geologia Applicata e Idrogeologia 20(2):395–401

Guzzetti F, Cardinali M, Reichenbach P (1994) The AVI Project: a bibliographical and archive inventory of landslides and floods in Italy. Environ Manage 18:623–633

Guzzetti F, Peruccacci S, Rossi M, Stark CP (2007) Rainfall thresholds for the initiation of landslides in central and southern Europe. Meteorol Atmos Phys 98:239–267

Guzzetti F, Peruccacci S, Rossi M, Stark CP (2008) The rainfall intensity-duration control of shallow landslides and debris flows: an update. Landslides 5(1):3–17

Guzzetti F, Salvati P, Stark CP (2005) Evaluation of risk to the population posed by natural hazards in Italy. In: Hungr O, Fell R, Couture R, Eberhardt E (eds) Landslide risk management. Taylor & Francis Group, London, pp 381–389

Lazzari M, Pieri P (2002) Modello stratigrafico-deposizionale della successione regressiva infrapleistocenica della Fossa bradanica nell'area compresa tra Lavello, Genzano e Spinazzola. Mem Soc Geol It 57(1):231–237

Lazzari M, Geraldi E, Lapenna V, Loperte A (2006) Natural hazards vs. human impact: an integrated methodological approach in geomorphological risk assessing on Tursi historical site, southern Italy. Landslides 3(4):275–287

Lazzari M (2008) Il comportamento tettonico e sedimentario del bacino d'avanfossa Bradanica durante il Pleistocene inferiore. Volume in memoria di ALFREDO JACOBACCI "Evoluzione delle conoscenze geologiche dell'Appennino Apulo-Campano e Tosco-Umbro-Marchigiano. Mem Descr Carta Geol It, LXXVII, 61–76

Marchi L, Arattano M, Deganutti AM (2002) Ten years of debris-flow monitoring in the Moscardo Torrent (Italian Alps). Geomorphology 46: 1–17

McKee TB, Doesken NJ, Kleist J (1993) The relationship of drought frequency and duration to time scales. In preprints, 8th conference on applied climatology, Anaheim, 17–22 Jan, pp 179–184

Ministero dell'Ambiente e della Tutela del Territorio – Unione Province Italiane (2003) – Pianificazione territoriale provinciale e rischio idrogeologico. Previsione e tutela. Report aprile 2003

Montgomery DR, Dietrich WE (1994) A physically-based model for the topographic control on shallow landsliding. Water Res Res 30:1153–1171

Luino F (2005) Sequence of instability processes triggered by heavy rainfall in north-western Italy. Geomorphology 66:13–39

Piccarreta M, Capolongo D, Boenzi F (2004) Trend analysis of precipitation and drought in Basilicata from 1923 to 2000 within southern Italy context. Int J Climatol 24:907–922

Pieri P, Sabato L, Tropeano M (1996) Significato geodinamico dei caratteri deposizionali e strutturali della Bradanic Foredeep nel Pleistocene. Memorie della Società Geologica Italiana 51:501–515

Reichenbach P, Cardinali M, De Vita P, Guzzetti F (1998) Regional hydrological thresholds for landslides and floods in the Tiber River Basin (central Italy). Environ Geol 35(2–3):146–159

Terlien MTJ (1998) The determination of statistical and deterministic hydrological landslide-triggering thresholds. Environ Geol 35(2–3): 124–130

Wieczorek GF (1987) Effect of rainfall intensity and duration on debris flows in central Santa Cruz Mountains, California. In: Costa W (ed) Debris flows/avalanches: processes, recognition and mitigation. Rev Eng Geol, vol 7, Geological Society of America, pp 23–104

Wieczorek GF, Guzzetti F (1999) A review of rainfall thresholds for triggering landslides. In: Proceedings of the EGS Plinius conference, Maratea, Oct 1999, pp 407–414

Wieczorek GF, Morgan BA, Campbell RH (2000) Debris flow hazards in the Blue Ridge of Central Virginia. Environ Eng Geosci VI(1): 3–23

Wilson RC, Wieczorek GF (1995) Rainfall thresholds for the initiation of debris flow at La Honda, California. Environ Eng Geosci 1(1):11–27



Development of Debris Flow Early Warning System for Volcanic Rivers at Mt. Merapi Area

Teuku Faisal Fathani, Djoko Legono, Adam Pamudji Rahardjo, Dwikorita Karnawati, and Irawan Eko Prabowo

Abstract

The 2010 Mt. Merapi eruption has produced approximately 140 million m^3 of pyroclastic deposit, in which more than ten million m^3 deposits are potential to move downstream through Boyong/Code River towards Yogyakarta City. The flow behavior of Code River may be affected by the presence of accumulated sediment at the upstream of the river (namely Boyong River). By rainfall trigger, this potential source can cause debris flow disaster that may contribute damage to the settlement areas in Yogyakarta City. This paper presents the development of early warning system to mitigate the impact of debris flow disaster along Boyong/Code River as revealed by most adaptive, least cost, and collaborative-based technology. The system was developed by considering the community aspiration in determining the types and placement of monitoring equipment, and maintaining its sustainability.

Keywords

Volcanic debris flow • Real-time monitoring • Early warning system • Community preparedness

Introduction

Mt. Merapi is one of the most active volcanoes in Indonesia. It has a long history of frequent eruptions with avalanche type pyroclastic flows caused by collapsing lava mass. Mt. Merapi eruption induced pyroclastic, tephra, laharic flow and debris flooding have often occurred with a cycle of approximately 9–16 years for larger scale flows and 1–3 years for smaller scale ones. During eruption period, Mt. Merapi produces a large number of sediment volume which could move downstream in various mechanisms, such as through natural flow by bed load transports and debris flows, and flow through human-related activities by sand mining (Wardoyo et al. 2010). Such sediment material and water mixture flow downstream through the steep slope torrential streams in what is called debris flow (Takahashi 2007).

It was reported that the 2006 Mt. Merapi eruption (from April through October 2006), had produced approximately eight million m^3 of sediment, potentially to move downstream towards the southern part of the mountain (Legono et al. 2008). Meanwhile, the 2010 Mt. Merapi eruption (25 October through 2 December 2010) has produced approximately 140 million m^3 of pyroclastic deposit toward the southern and western part of the mountain (Legono et al. 2011a). Since then, the volcanic debris flow has caused severe damage to the inhabitants and residents living on the footslopes.

Due to 2010 Mt. Merapi eruption, a large number of sediment is deposited at the upstream of several volcanic

T.F. Fathani (✉) • D. Legono • A.P. Rahardjo
Department of Civil and Environmental Engineering, Universitas Gadjah Mada, Jalan Grafika 2 (55281), Yogyakarta, Indonesia
e-mail: tfathani@gmail.com

D. Karnawati
Department of Geological Engineering, Universitas Gadjah Mada, Yogyakarta, Indonesia

I.E. Prabowo
Center for Energy Studies, Universitas Gadjah Mada, Yogyakarta, Indonesia

C. Margottini et al. (eds.), *Landslide Science and Practice*, Vol. 2,
DOI 10.1007/978-3-642-31445-2_89, © Springer-Verlag Berlin Heidelberg 2013

rivers, hence the secondary disaster in term of rainfall-induced debris flow may occur in a long period. The presence of river bends will also increase the possibility of inundation in some river flood plain in the city area or may create a new stream, causing significant damage to various infrastructures and settlements. Considering the large deposit accumulation in the upstream part of volcanic rivers, there is a necessity to monitor the hydraulic and hydrology parameters, which may predict the occurrence of debris flow. The monitoring results can be used for both anticipating the debris flow disaster and developing the criteria of rainfall characteristics induced debris flow for early warning system. Therefore, both types of monitoring, i.e. historical and real-time are very much needed.

Debris Flow at Boyong/Code River

The distribution of pyroclastic flow towards the southern part of Mt. Merapi appears dominantly in Boyong/Code River in which in 1994 Mt. Merapi eruption hit the upstream part of the river severely. Since then, several numbers of sediment control structures were built to ensure that Yogyakarta City would be sufficiently safe from debris flow disaster. There are 41 sabo dams provided with river training structures such as groundsills and retaining walls along Boyong River.

The 2010 Mt. Merapi eruption has been predicted to contribute more than ten million m^3 pyroclastic deposits on the upstream (Legono et al. 2011a). By rainfall trigger, this potential source can cause debris flow occurrence that may contribute damage to the settlement areas at the surrounding Boyong/Code River in Yogyakarta City (Fig. 1). Although local communities in this area have been experiencing various flood disasters, such preparedness of flood disaster by means of debris flow is far beyond sufficient because such debris flow phenomena is a very rare case. Such insufficient preparedness was found on 29 November 2010 afternoon, where the first flood after the 2010 Mt. Merapi eruption occurred. The flood carried various materials, from fine sediment to coarse sand, but no boulder was found. The sediment was assumed to be originated from dust particles fallen in the catchment area of Boyong/Code River and accumulation of sediment in the upstream of Boyong/Code River (Fig. 2a). In fact, local communities have initiatives to anticipate the debris flow disaster by identifying the debris occurrence at the upstream part of the river.

Apparently, days after 29 November 2010 showed that the increase in rainfall intensity occurred, triggering a more intensive debris flow that caused significant damages in several infrastructures at some rivers (Pabelan River and Putih River). Fortunately, no casualty was reported. However, the damage of important infrastructures such as roads, bridges, paddy fields, and settlements was very significant. A hyper-concentrated flow in Boyong/Code River occurred several times that made the local people evacuate themselves (Fig. 2b).

The Characteristic of Rainfall-Induced Debris Flow

Rainfall plays an important role in contributing the possibility of massive soil mass movement both in the form of debris flow and landslide. In many occurrences of debris flow or landslide, rain contribution can be in the form of heavy rain (commonly expressed in rain intensity, in mm/h), or relatively long rain (which is expressed in time unit of hour). Depending on the characteristic of soil mass movement, usually defined as soil mass stability (function of mass density, shear strength characteristic, soil water content, soil embankment shape, etc.), the rain intensity and duration will trigger the process of debris flow occurrence.

Three different approaches might be used to develop criteria of debris flow occurrence as described by MLIT (2004), i.e. based on the information of relationship between the rainfall intensity and rainfall accumulation, rainfall intensity and antecedent rainfall, and rainfall intensity and the soil moisture. As an illustration, before 2010 Mt. Merapi eruption, the criterion used as a sign of possibility of debris flow occurrence in the upstream of volcanic rivers at Mt. Merapi area was rainfall with intensity of 25 mm per hour (Takahashi 1991) or 50 mm per hour with the duration of more than 2 h (Legono, et al. 2008). However, at the present, after the 2010 Mt. Merapi eruption, the criterion changes due to the position of the sediment, in which instability increases significantly due to a large number of very loose granular materials forming a very steep slope formation upstream. Such condition may cause debris flow occurrence even in rainfall intensity of less than 50 mm/h and duration of less than 2 h. Based on two events on lahar flow occurrence at Kali Putih on 9 January and 23 January 2011, the rainfall intensities at upstream were 9 mm/h for 2 h duration and 40.9 mm/h for 2 h duration.

In order to obtain historical and real-time information, the rainfall monitoring should show rainfall intensity value in mm/h. Similarly for debris flow, as the wave propagation of debris flow is very fast (e.g. 3–5 m/s order), the monitoring of water elevation in stream should have very high accuracy, e.g. at 1.00 cm, with a reliably short frequency, e.g. every 10 s, particularly if such equipment is dedicated for the development of early warning system.

As the flow monitoring system will be transferred into discharge information (in volume units per unit time), the rating curve establishment, which represents the correlation between the water depth and the discharge, should be

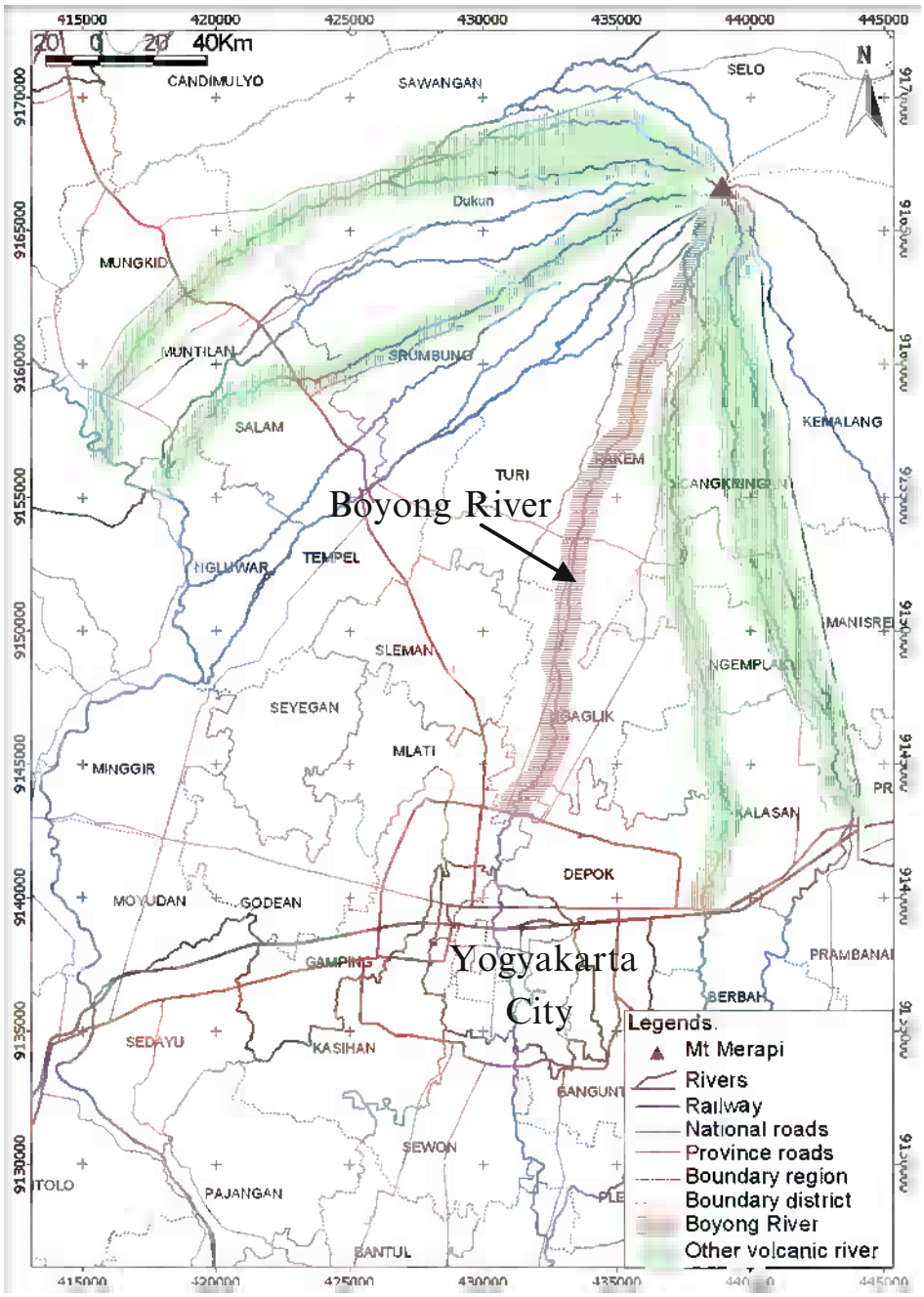


Fig. 1 Volcanic rivers toward southern and western part of Mt. Merapi which have potential impact of debris flow. Boyong River is directed toward Yogyakarta City and change the name to Code River

conducted and updated periodically. The necessary calibration is a part of "rule of thumb" of each system development; therefore, it is an obligatory requirement.

Early Warning System Against Debris Flow

At the moment, the development process which considers reliable sustainability is the involvement of community participation in a form of highly local self-assessment, planning and action (Wisner 2006). In this development of debris flow early warning system, a collaborative-based process is introduced (Legono et al. 2011b). Although it is similar to community involvement process, the term "collaborative" is used to emphasize that community, together with local government should be involved in solving a problem, i.e. debris flow early warning.

The collaborative-based debris flow early warning system of Boyong/Code River was developed with the following process.



Fig. 2 Upstream and downstream condition of Boyong/Code River; (**a**) Sabo dam BOD4 on 14 January 2011; (**b**) Jogoyudan area in the Yogyakarta City on 30 November 2010

(a) Public consultation meeting on Boyong/Code River debris flow (the people living along the Code River requested information on debris flow occurrence).
(b) Determination of key persons (hereinafter referred as focal point: FP) whose task is to receive the earliest news on debris flow phenomenon by SMS blasting.
(c) Construction and installation of integrated monitoring equipment (water elevation sensor, pendulum, camera interval) and its socialization to focal points.

Figure 3 shows the proposed location of the instrument for debris flow monitoring and early warning, i.e. one real-time Automatic Rainfall Recorder (ARR) at Turgo, four sets cross-sectional monitoring system (comprising one real-time Automatic Water Level Recorder-AWLR, one real-time debris sensor, one logger camera) at Donoharjo, Rejodani, Krikilan, and Gemawang. A central station was set up in the Hydraulics Laboratory, Department of Civil and Environmental Engineering of Universitas Gadjah Mada which further addresses in maintaining the sustainability of the system.

Figure 4 shows the information flow of the proposed early warning system. Rainfall station in Turgo and cross-sectional monitoring system in four locations along Boyong River will transmit the result of real-time monitoring to the central station. In addition, the central station also receives information through radio communication from the focal points who monitor debris flow visually. After analyzing the received data, the central station then sends warning alert to focal points located along Boyong/Code River and to the debris flow monitoring radio of 149.940 MHz. This warning can be sent automatically by the system or trigged manually by the operator. The system built in Boyong/Code River is expected to be integrated with the monitoring system of other volcanic rivers at Mt. Merapi area.

Figure 5 shows the current warning system pursued by the community at surrounding Code River. The community living near the river has tried to carry out debris flow monitoring with the simplest way. Based on the previous experience, "caution" and "evacuation" elevation are marked on the river slope protection; hence, they can decide the right time to evacuate. The presence of integrated debris flow early warning system indeed helps the community to increase awareness and preparedness in facing the disaster.

As shown in Figs. 3 and 4, the ideal version of early warning system against debris flow in Boyong/Code Rivers may comprise water level monitoring system at four locations, i.e. Donoharjo, Rejodani, Krikilan, and Gemawang, provided with the pendulum type sensor to confirm the high degree of flow, i.e. the flow depth equal to 1.50 m; 2.25 m; and 3.00 m. Besides, one additional interval camera was also installed to confirm the flow occurrence visually. The sequence of alert should be arranged in such that the debris flow propagation time is sufficiently long to issue the warning that gives significant benefit to community, so that they have sufficient time to take necessary actions for evacuation.

Furthermore, the establishment of collaborative-based debris flow early warning system consists of the following process:

(a) Installation of interval camera on the river side, accompanied by the local people (the installation was witnessed by the local people which are also members of an NGO, Jalin Merapi, at the same time, local people awareness and aspirations were studied).
(b) After the installation, the data on the river flow was collected for several days, a collaborative review of the data was then conducted (the local people saw the benefits and asked for a higher specification, not the historical/logger type, but the real-time one).
(c) The development and installation of equipment were carried out taking into account community aspiration, at least types and locations (the local people showed the best location for the installation, also, due to the necessity on the early debris flow monitoring, the local people avail facilities such as electricity accessibility and key-persons for the socialization of the equipment function and their maintenance).

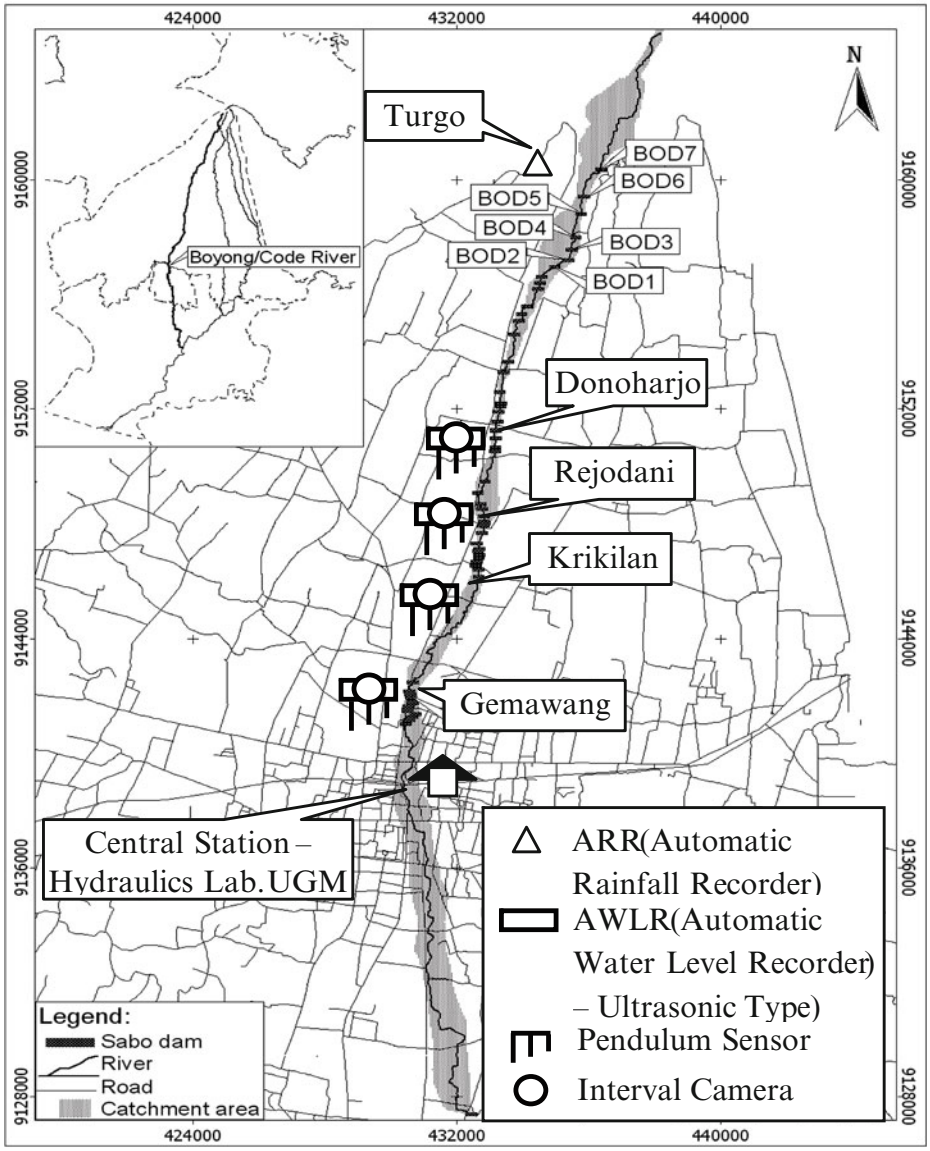


Fig. 3 The proposed location of the instrument for debris flow monitoring and warning system at Boyong/Code River

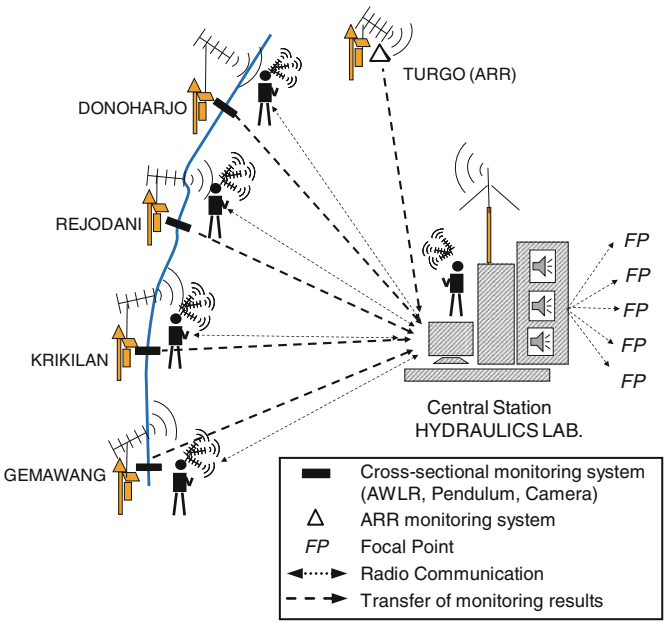


Fig. 4 Proposed information flow for monitoring and early warning of debris flow at Boyong/Code River



Fig. 5 Existing community warning alert in anticipating debris flow

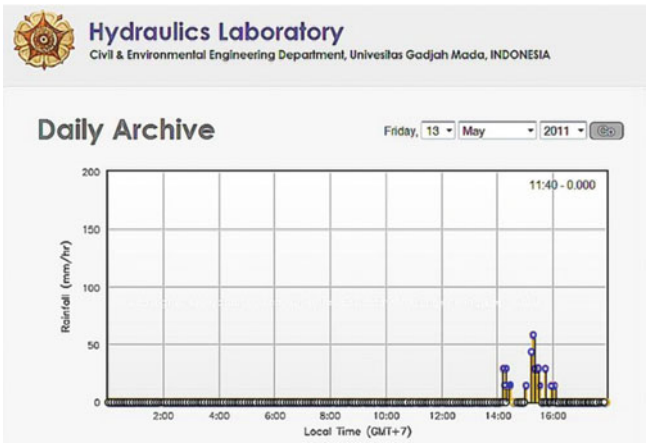


Fig. 6 Example of online reading obtained from Turgo ARR monitoring system

Due to the insufficient budget, only the Automatic Rainfall Recorder (ARR) in Turgo and the Automatic Water Level Recorder (AWLR) in Rejodani were then established in the beginning of year 2011. Figures 6 and 7 show some readings obtained from the installed ARR in Turgo and AWLR in Rejodani, respectively.

Automatic Rainfall Recorder (ARR) in Turgo recorded rainfall intensity every 6 min in the logger and then sent the data to the central station by radio telemetry. Rainfall intensity over 50 mm/h occurring between 14.00 and 16.00 PM on 13 May 2011 can be monitored from the website (Fig. 6). With this information, focal points should increase their awareness on the possibility of debris flow occurrence in the downstream.

In Fig. 7, the rising of the flow monitored by the ultrasonic equipment every 15 s is shown real-time on the website. On 9 January 2011, the water elevation to dam crest rose from 39 to 130 cm in only 20 s. Further study should be carried out to determine the time needed for the debris to reach Yogyakarta City and the elevation of the flow in the downstream.

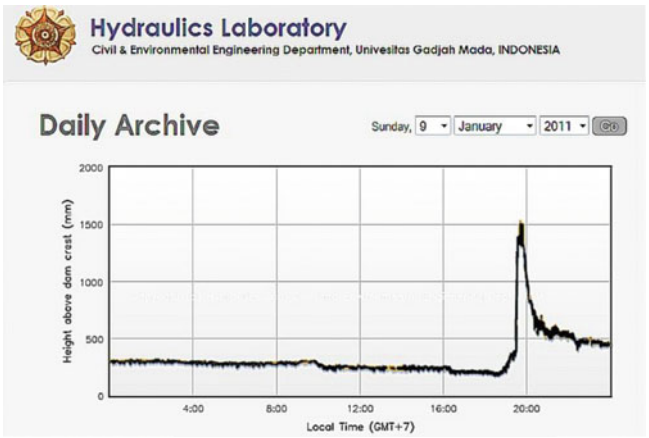


Fig. 7 Example of online reading obtained from Rejodani AWLR monitoring system

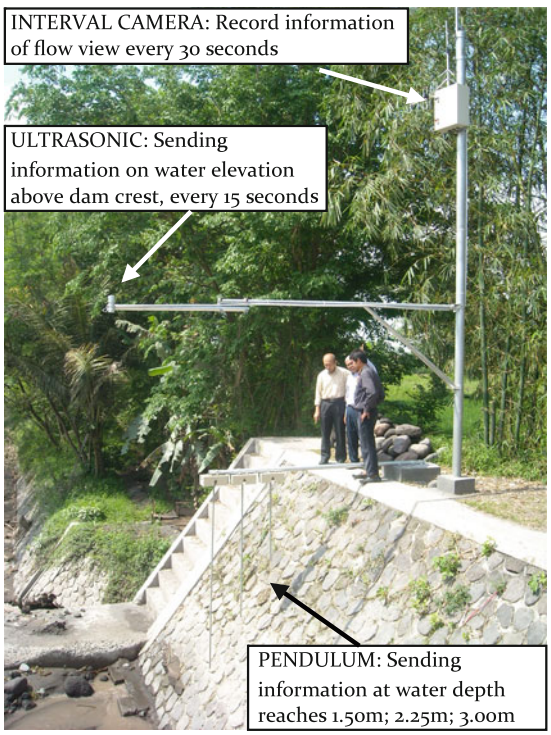


Fig. 8 Cross-sectional monitoring system at Rejodani

Figure 8 shows the cross-sectional monitoring system at Rejodani. Ultrasonic monitoring equipment, interval camera, and three different levels of pendulum are placed in one river cross-section. This system transfers the monitoring results regularly to the central station. The whole system was built by prioritizing most adaptive and least cost technology. Through this system, a debris flow monitoring system of Boyong/Code River for community at Yogyakarta City is implemented. This monitoring system is easy to replicate for rivers threatened by debris flow disaster at the surrounding of Mt. Merapi area.

Conclusions

The monitoring on hydrology and hydraulic parameters (including debris flow and rainfall characteristic) should be carried out with consideration to the physical phenomenon laws of the parameters. Information from the monitoring results should be quantitative and complimentary to the existing system. Both the historical logger type and the real-time monitoring system are necessary for further study in determining rainfall and debris flow characteristic for warning criteria. Collaborative-based debris flow early warning system is considered more sustainable as community understands the value of the information they receive. However, support from the local government is still required. More integrated and effective application in the future is still vastly needed, including completion of monitoring system along Boyong/Code River and also the integration of this system to the others debris flow monitoring at Mt. Merapi area. Further establishment of Standard Operating Procedure utilizing the established early warning system in collaboration with the local community is considered important. By this mechanism, such effort in maintaining its sustainability will be gained.

Acknowledgments The establishment of debris flow warning system against debris flow was supported by the SATGAS-SMBM, a task force established by the Faculty of Engineering, Universitas Gadjah Mada during the emergency response of 2010 Mt. Merapi eruption. The supports from all colleagues, the local governments and local community are highly appreciated.

References

Legono D, Prabowo IE, Karnawati D, Fathani TF, Rahardjo AP (2011a) Lahar flow disaster monitoring and mitigation based on community collaboration. In: Proceedings of symposium Merapi, 21 Feb 2011, Yogyakarta, pp 11–16

Legono D, Prabowo IE, Fathani TF, Karnawati D, Rahardjo AP (2011b) Development of collaborative-based lahar flow early warning system for Code River at Yogyakarta City. In: Proceedings of international seminar on water related risk management, 15–17 July 2011, Jakarta

Legono D, Rahardjo AP, Fathani TF, Prabowo IE (2008) Development of community-based early warning system against debris flow at Mt. Merapi Indonesia. In: Proceedings of the first World landslide forum. Tokyo, 18–21 Nov 2008. pp 404–406

Ministry of Land, Infrastructure and Transport – MLIT (2004) Development of warning and evacuation system against sediment disasters in developing countries, Guidelines for construction technology transfer, Infrastructure Development Institute, Japan

Takahashi T (1991) Lahar flow – Monograph, IAHR, AA Balkema, Rotterdam

Takahashi T (2007) Debris flow: mechanics, prediction and countermeasures. Taylor & Francis, London

Wardoyo W, Legono D, Fathani TF, Jayadi R (2010) Pyroclastic deposit characteristics of volcanic rivers and its affect to the transport mechanism. In: Proceedings of IAHR-APD international seminar, 21–24 Feb 2010, Auckland

Wisner B (2006) Self-assessment of coping capacity: participatory, proactive and qualitative engagement of communities in their own risk management, measuring vulnerability to natural hazard, United Nations University Press, Tokyo, pp 316–328